

Insulation Materials, Testing and Applications

McElroy/Kimpflen editors



STP 1030

STP 1030

Insulation Materials, Testing, and Applications

D. L. McElroy and J. F. Kimpflen, editors



ASTM
1916 Race Street
Philadelphia, PA 19103

Library of Congress Cataloging-in-Publication Data

Insulation materials, testing, and applications/McElroy/Kimpflen,
editors.

(STP: 1030)

Materials from the ASTM Symposium on Insulation Materials,
Testing, and Applications.

"ASTM publication code number (PCN) 84-010300-61"—CIP t.p. verso.

Includes bibliographical references.

ISBN 0-8031-1278-5

1. Insulating materials—Testing—Congresses. 2. Insulation
(Heat)—Testing—Congresses. I. McElroy, D. L. II. Kimpflen,
Joseph F. III. ASTM Symposium on Insulation Materials, Testing, and
Applications (1987: Bal Harbour, Fla.) IV. Series: ASTM special
technical publication; 1030.

TA410.I76 1990

89-17743

620.1'95—dc20

CIP

Copyright © by AMERICAN SOCIETY FOR TESTING AND MATERIALS 1990

NOTE

The Society is not responsible, as a body,
for the statements and opinions
advanced in this publication.

Peer Review Policy

Each paper published in this volume was evaluated by three peer reviewers. The authors addressed all of the reviewers' comments to the satisfaction of both the technical editor(s) and the ASTM Committee on Publications.

The quality of the papers in this publication reflects not only the obvious efforts of the authors and the technical editor(s), but also the work of these peer reviewers. The ASTM Committee on Publications acknowledges with appreciation their dedication and contribution of time and effort on behalf of ASTM.

Foreword

The ASTM Symposium on Insulation Materials, Testing, and Applications was held in Bal Harbour, Florida, on December 6–9, 1987. The event was sponsored by ASTM Committee C-16 on Thermal Insulation, the Department of Energy (DOE), the Building Thermal Envelope Coordinating Council (BTECC), and the Oak Ridge National Laboratory (ORNL).

The Symposium was co-chaired by J. F. Kimpflen, Certain-Teed Corporation, and I. S. Seigler, Ralph M. Parsons Company. Mr. Kimpflen has co-edited the present volume with D. L. McElroy, Oak Ridge National Laboratory.

Contents

Overview

ix

NEW MATERIALS

Evaluation of Fumed-Silica Insulation for a Thermal Conductivity Standard

Reference Material—B. G. RENNEX, T. A. SOMERS, T. K. FAISON, AND
R. R. ZARR

3

A Summary of the Manufacture, Uses, and Properties of Autoclaved Aerated Concrete—R. G. MATHEY AND W. J. ROSSITER, JR.

15

Magnesium Oxychloride-Based Foam Thermal Insulation: An Initial Investigation—

W. J. ROSSITER, JR. AND P. W. BROWN

38

Thermal Resistance of Fine Powders at Atmospheric Pressure and under Vacuum—

D. L. MCELROY, F. J. WEAVER, D. W. YARBROUGH, AND R. S. GRAVES

52

Solid Conductivity of Loaded Fibrous Insulations—J. FRICKE, D. BÜTTNER, R. CAPS,

J. GROSS, AND O. NILSSON

66

Discussion

78

Radiant Heat Transfer in Extremely Low Density Fibrous Assemblies—R. W. DENT,

J. SKELTON, AND J. G. DONOVAN

79

ASSESSMENTS AND PROPERTIES OF FOAMS

Variation of Insulating Properties of Closed-Cell Foam Insulation—

A. G. OSTROGORSKY AND L. R. GLICKSMAN

109

Overview of Physical Properties of Cellular Thermal Insulations—W. R. STRZEPEK

121

Technical Assessment of Foam-in-Place Cellular Plastics for Building Envelope Applications—R. P. TYE

141

Evaluation of Long-Term Thermal Resistance of Gas-Filled Foams: State of the Art—

M. BOMBERG AND D. A. BRANDRETH

156

Measurement of Gas Diffusion in Closed-Cell Foams— I. R. SHANKLAND

174

Foam Insulation Aging: Historical Perspective and Outstanding Problems—

L. M. ZWOLINSKI

189

Deterioration of Thermal Insulation Properties of Extruded Polystyrene: Classification and Quality Control System in Sweden—P. I. SANDBERG	197
Long-Term R-Values and Thermal Testing Requirements for Rigid Insulating Foams—J. R. HAGAN AND R. G. MILLER	205
Discussion	217

LOOSE-FILL BEHAVIOR

Comparison of Gas and Electric Radiant Panels for Measuring the Flammability of Loose-Fill Cellulose Insulation—S. A. SIDDIQUI, R. L. HILLIER, G. H. DAMANT, AND H. L. NEEDLES	221
Field Data on Settling in Loose-Fill Thermal Insulation—B. SVENNERSTEDT	231
An <i>In Situ</i> Evaluation of the Settling of Loose-Fill Rock Wool Insulation in the Attics of Two Manufactured Home Units—R. S. GRAVES AND D. W. YARBROUGH	237
Apparent Thermal Conductivity versus Density as a Function of Blown Thickness for Pneumatically Applied Insulations: Continuing Studies—R. C. MATHIS AND H. D. ANGLETON	244
New Developments Toward Accurate Assessment of Material Density for ASTM C 687 Testing of Pneumatically Applied Insulations—R. C. MATHIS AND T. M. KENNEY	253
A Round Robin on Apparent Thermal Conductivity of Several Loose-Fill Insulations—R. D. ADAMS AND J. G. HUST	263
A Theoretical and Experimental Study of Convective Effects in Loose-Fill Thermal Insulation—C. LANGLAIS, E. ARQUIS, AND D. J. MCCAA	290
An Acoustic Technique for Evaluation of Thermal Insulation—D. R. FLYNN, D. J. EVANS, AND T. W. BARTEL	319

SYSTEM PERFORMANCE TESTING

A Dynamic Test Method for Determining Transfer Function Coefficients for a Wall Specimen Using a Calibrated Hot Box—D. M. BURCH, R. R. ZARR, AND B. A. LICITRA	345
Discussion	361
Thermal Resistances of Metal Frame Wall Constructions Incorporating Various Combinations of Insulating Materials—W. R. STRZEPEK	362
Discussion	377

Methods for Determining the Thermal Performance of Reflective Insulation Systems —R. G. MILLER, D. S. OSCAR, F. SEIFAEI, AND W. P. GOSS	378
Influence of Natural Convection in an Insulated Cavity on the Thermal Performance of a Wall —J. G. N. LECOMPTE	397
A Survey of Window <i>U</i>-Value Measurements in Sweden (1977–1987) —P. STAELENS	421
Heat Transfer Characteristics of a Recently Developed Lightweight Structural Concrete —M. G. VAN GEEM	437
The Northwest Wall Moisture Study: A Field Study of Moisture in the Exterior Walls of New Northwest Energy-Efficient Homes —G. A. TSONGAS	464
A Comparison of Two Techniques for Monitoring the Field Thermal Performance of Roof Systems —G. E. COURVILLE, P. W. CHILDS, A. R. MOAZED, G. D. DERDERIAN, G. D. STEWART, AND L. S. SHU	483
A Comparison of Two Independent Techniques for the Determination of <i>In Situ</i> Thermal Performance —G. E. COURVILLE, A. O. DESJARLAIS, R. P. TYE, AND C. R. MCINTYRE	496
Discussion	509
Use of Two Heat Flow Transducers for Transient Thermal Measurements on Porous Insulating Materials —C. LANGLAIS AND J. BOULANT	510

PROPERTIES AND MODELS

Modeling of Thermal Resistance Test Configurations That Use Thin Heaters —D. W. YARBROUGH, D. L. MCELROY, AND R. S. GRAVES	525
Importance of Radiation in Transient Tests of Fibrous Insulations —J. R. THOMAS, JR.	537
Transient Coupled Conduction and Radiation Heat Transfer Through Ceiling Fiberglass/Gypsum Board Composite —H. Y. YEH AND J. A. ROUX	545
Spectral Radiative Properties and Apparent Thermal Conductivity of Expanded Polystyrene Foam Insulation —S. J. YAJNIK AND J. A. ROUX	561
Optically Thin Fibrous Insulations —J. FRICKE, R. CAPS, E. HÜMMER, G. DÖLL, M. C. ARDUINI, AND F. DE PONTE	575
Minimum Life-Cycle Cost Analysis of Residential Buildings for PC-Based Energy Conservation Standards —A. TULUCA AND J. HEIDELL	587

BUILDING APPLICATIONS AND USER INTERESTS

Computer Modeling of Climates—C. G. CASH	599
Factors Influencing Consumer Insulation Activities—C. B. MEEKS	612
Implementing Thermal Insulation Product Standards—B. D. NELSON	626
Corrosiveness of Residential Thermal Insulation Materials under Simulated Service Conditions—K. SHEPPARD, R. WEIL, AND A. DESJARLAIS	634
The Most Needed Building Foundations Research Products—J. E. CHRISTIAN	655

INDUSTRIAL APPLICATIONS AND TESTS

Case Histories of Underground Heat Distribution Systems: 1959-1986—F. A. GOVAN AND D. R. BAHNFLETH	665
Review of ASTM Guide for Removable Insulation Covers (C 1094)—G. HART	675
New Developments in Test Technology for ASTM C 692 (Preproduction Corrosion Test for Insulation To Be Used on Austenitic Stainless Steel)—T. E. WHITAKER, K. M. WHORLOW, AND F. B. HUTTO, JR.	688
High-Temperature Calorimeter Performance Variable Study—R. L. TROYER	699
An Automated High-Temperature Guarded-Hot-Plate Apparatus for Measuring Apparent Thermal Conductivity of Insulations Between 300 and 750 K—J. G. HUST, B. J. FILLA, J. A. HURLEY, AND D. R. SMITH	710
On the Thermal Insulation of Outdoor Electronic Cabinets—G. GUGLIELMINI AND G. MILANO	723
Heat-Insulating, High-Temperature Materials on Cenosphere Base—Z. IGNASZAK, A. BARANOWSKI, J. HYNAR, AND M. ŻAK	741
Author Index	749
Subject Index	751

Introduction

Since ASTM Committee C-16 on Thermal Insulation was founded in March 1938, its policy has been to sponsor programs periodically that provide the latest information regarding test methods and insulation materials. As a result of these programs, more than a dozen ASTM Special Technical Publications have been published on thermal insulation materials and technology, most of them in the last decade, based on symposia sponsored by the committee.

Activity and interest in thermal insulation have increased as a result of the space program in the 1960s and energy conservation in the 1980s. In 1978, over 500 people participated in a symposium when the topic was enlarged to include not only technical measurement but also all the parameters related to thermal insulation for energy conservation. The trend has continued with sponsorship of conferences and symposia alternating between ASTM and the American Society of Heating, Refrigerating, and Air-Conditioning Engineers (ASHRAE), with additional sponsorship by both the U.S. Department of Energy and Oak Ridge National Laboratory. Proceedings of the ASHRAE-sponsored conferences are available as ASHRAE Special Publications. The ASTM-sponsored conferences and symposia continue to be published as ASTM Special Technical Publications.

A public awareness of rising energy prices has continued to focus attention on the use of thermal insulation as an effective energy-conserving measure. Research and development in thermal insulation materials, testing methods and apparatus, and innovative applications provide the basis for obtaining substantially improved thermal performance. This volume presents the insulation community with an update on the technical database in residential, commercial, and industrial applications.

ASTM Committee C-16 on Thermal Insulation is pleased to continue to provide the format for discussion and documentation of this complex subject. Also, this conference provides excellent input to Committee C-16 in discharging its responsibility for promulgating standards for insulation materials, systems, and test methods.

D. L. McElroy

Oak Ridge National Laboratory, Oak Ridge,
Tennessee; editor

J. F. Kimpflen

Certain-Teed Corporation, Valley Forge,
Pennsylvania; symposium co-chairman and
editor

New Materials

B. G. Rennex,¹ T. A. Somers,² T. K. Faison,³ and R. R. Zarr²

Evaluation of Fumed-Silica Insulation for a Thermal Conductivity Standard Reference Material

REFERENCE: Rennex, B. G., Somers, T. A., Faison, T. K., and Zarr, R. R., "Evaluation of Fumed-Silica Insulation for a Thermal Conductivity Standard Reference Material," *Insulation Materials, Testing, and Applications, ASTM STP 1030*, D. L. McElroy and J. F. Kimpflen, Eds., American Society for Testing and Materials, Philadelphia, 1990, pp. 3-14.

ABSTRACT: Standard Reference Materials (SRMs) used for thermal conductivity measurements are required by industry, academic, and government laboratories for calibrating heat-flux-meter apparatus or checking the accuracy of guarded-hot-plate apparatus. New thermal conductivity SRMs are sought to improve the accuracy and extend the operational range of these apparatus. An advisory panel recommended the development of a low thermal conductivity SRM having approximately the same thermal conductivity as blown fluorocarbon foams, suitable for a temperature range of -175 to 900°C . Fumed-silica insulation was recommended by the advisory panel as the most suitable material.

The National Bureau of Standards (NBS) examined four lots of fumed-silica insulation and recommended one candidate for further development as a low thermal conductivity SRM. The four lots of fumed-silica insulation were examined for their relative handleability, material uniformity, variability of thermal conductivity measurements, and effect of heat treatment on the measured thermal conductivity of the materials. Thermal conductivity measurements were conducted using the NBS 1-m Guarded Hot Plate for each lot of fumed-silica insulation at a mean specimen temperature of 24°C . Analysis of the thermal conductivity data was performed using the NBS statistical analysis program, Dataplot.

KEY WORDS: standard reference material, fumed-silica insulation, thermal conductivity measurements

Thermal conductivity Standard Reference Materials (SRMs) are used by private and government laboratories for calibrating or verifying the accuracy of thermal conductivity apparatus. Materials of known thermal properties are required for calibration of relative heat-flux devices such as the heat-flow-meter apparatus (ASTM C 518). Recent SRM requirements have emphasized a material which is stable over time, capable of withstanding high temperature, and has a thermal conductivity similar to blown fluorocarbon foams.

Previous work identified the need for a Standard Reference Material having a low thermal conductivity of approximately $0.023 \text{ W/m} \cdot \text{K}$ ($0.16 \text{ Btu} \cdot \text{in.}/\text{h} \cdot \text{ft}^2 \cdot ^{\circ}\text{F}$) and suitable for a temperature range of -175 to 900°C (-280°F to 1700°F) [1,2]. An advisory panel consisting of representatives of the Mineral Insulation Manufacturers Association, the Department of Energy, Oak Ridge National Laboratory, and ASTM decided that a fumed-silica insulation product was the most promising material. This study evaluates four fumed-silica insulation products and recommends a candidate for further development as a low thermal conductivity SRM.

¹Falls Church, VA 22043.

²Heat Transfer Group, Building Environment Division, Center for Building Technology, National Bureau of Standards, Gaithersburg, MD 20899.

³Mechanical Engineer, NBS (retired), Damascus, MD 20872.

Four different fumed-silica insulation products were obtained and tested at the National Bureau of Standards (NBS) using the 1-m Guarded Hot Plate. The insulation products were obtained from the following manufacturers: Manville Services Corporation (U.S.), Micropore International LTD (U.K.), Grunzwick & Hartman und Glasfaser Ag (FRG), and Wacker-Chemie GmbH (FRG).⁴ Addresses for the manufacturers are provided in the Appendix.

Evaluation of the four products is based on the following criteria: (1) relative handleability of each material, (2) variability of the material's physical properties, (3) variability of the apparent thermal conductivity measurements for each lot of material, (4) material stability under heat treatment, and (5) economic considerations. Test data for each product are presented anonymously. Hereafter, references to each insulation product are identified simply as Product A, B, C, and D. One of these products is selected based on the overall results of the evaluation criteria. This product is now a candidate material for further SRM development.

Sample Description

The fumed-silica insulation products were manufactured in the form of square insulation boards. The material obtained from three of the manufacturers was 600 by 600 mm, 25 mm thick (24 by 24 by 1 in.). Material from the fourth manufacturer was 680 by 680 mm, 25 mm thick (27 by 27 by 1 in.). All specimens from each manufacturer were from the same lot of material. A total of 33 specimens was obtained.

Fumed-silica insulation is a silica-aerogel composite. The material is micro-porous, comprised primarily of submicron particles of amorphous silica bonded together in a cellular structure. The submicron distance between silica particles effectively reduces gas conduction by inhibiting molecular collisions of gases within the cell walls. Manufacturer's literature states the distance to be less than 0.1 μm , which is less than the mean-free-path length for O_2 and N_2 molecules at standard temperature and pressure. Due to the micro-porous nature of the material, the apparent thermal conductivity depends not only on the type of gas within the interstices of the material but also on the gas pressure.

The composite material contains additional materials for other desirable properties. Metallic opacifiers are added to reduce radiative heat-transmission at high temperatures. Structural support for the material is enhanced by strengthening fibers such as quartz.

Handleability

All specimens were extremely fragile and required care when handling. The size of the specimens handled ranged from 600 mm (24 in.) square to 680 mm (27 in.) square. With careful handling, most of the specimens could be lifted by the edges without the material breaking. The specimens were transported by first lifting one edge of the specimen and then sliding a flat support board underneath the material. The support board was then used to transport the specimen.

The material itself was friable. Abrasion from sliding the support board under the specimen produced a thin layer of "dust" material on the support board. A residual layer of dust material was also deposited on the individual's hands working with the material.

As part of the overall evaluation, the specimens were heat-treated in a gas-fired oven. For testing the specimens in the oven, a stainless steel support-rack that encased the edges of the specimens was used. The support-rack was designed to transport the specimens in either a horizontal or vertical orientation. The support-rack held specimens 600 by 600 mm (24 by 24 in.),

⁴Because the products are potential candidates for SRMs, it is necessary to identify the manufacturers so that other laboratories may obtain the materials. This in no way represents an endorsement of these products by NBS.

requiring the larger size specimens to be cut. Manufacturers recommend following normal precautions associated with nuisance dusts when machining the material. Further information on the health issues concerning fumed-silica is available in Ref 3.

An index rating the relative durability of each material is presented in Table 1. Each specimen was rated for its ability to withstand movement when lifted and transferred onto a support board. The relative durability of the material was rated before and after the heat treatment. Overall, Product B was considered the most durable product, with C and D a close second. Even before heat treatment, the edges of Product A crumbled easily when lifted.

Variability of Physical Properties

Prior to heat treatment, measurements of thickness and density were made on all specimens. The specimen thickness was measured at ten locations using a special thickness caliper capable of 0.1 mm resolution. Mass measurements were made with a digital laboratory scale, uncertain by $\pm 0.1\%$. The density measurements were estimated to be uncertain by $\pm 0.5\%$. The average thickness and density for Products B, C, and D are presented in Table 2. Each average includes the standard deviation. For Product A, the lot size was too small for statistical evaluation and only the measured values are given. Product C was found to be the most uniform.

TABLE 1—Durability of specimens.^a

Product	Room Temperature (21°C)	After Heat Treatment			
		550°C 7.6 h	+ 600°C 6.7 h	+ 625°C 5.3 h	+ 650°C 5.8 h
A	3	3	3	3	3
B	1	1	1	1	1
C	1	1	1	2	2
D	1	1	1	2	2

^aDurability Index:

- (1) Specimen(s) did not crack when transferred to support board; however, a support board is still advised.
- (2) Specimen(s) cracked when transferred to support board; support always required.
- (3) Specimen edge(s) crumbled easily when transferred to support board; support always required and extra-careful handling necessary.

TABLE 2—Material uniformity prior to heat-treatment.

Product	Lot Size	Average Lot Thickness, mm	Average Lot Density, kg/m ³	Range of Density, kg/m ³
A	2	24.7 26.3	361.2 330.1	361.2 330.1
B	10	25.7 \pm 0.2 ^a	379.3 \pm 3.8 ^a	\pm 6.2
C	10	25.5 \pm 0.1	301.4 \pm 2.0	\pm 2.8
D	11	26.4 \pm 0.8	280.4 \pm 9.5	\pm 16.4

^aStandard deviation of average. For Product A, the standard deviation and range of density are not provided due to the statistically small lot size. Measured values are given instead.

Variability of Specimen Apparent Thermal Conductivity

Test Method

The apparent thermal conductivity of the fumed-silica specimens was measured using the NBS 1-m Guarded Hot Plate. The guarded hot plate was operated in a one-sided mode at a mean-specimen temperature of 23.9°C (75°F). Tests were performed in accordance with procedures described in ASTM Test Method C 177 and ASTM Practice C 1044. The apparent thermal conductivity (λ) of the specimen was determined by the equation

$$\lambda = \frac{L}{R} \quad (1)$$

where L is the specimen thickness (m), and R is the thermal resistance of the specimen ($\text{K} \cdot \text{m}^2/\text{W}$). The average thickness for each specimen was computed by averaging ten thickness measurements made within a 400 mm (16 in.) diameter circle corresponding to the metering-area of the guarded hot plate. An uncertainty of $\pm 0.8\%$ was estimated for the thickness measurement. The uncertainty in the thermal resistance measurement was estimated to be $\pm 0.5\%$ [4]. Assuming the two uncertainties to be equally probable in both directions, an overall uncertainty of $\pm 0.9\%$ was determined for the thermal conductivity measurement.

Pressure Dependence

Early work on fumed-silica material by Tye [5] showed that the apparent thermal conductivity of the material depends on the pressure of the gas and the type of gas used in the hot plate measurement. For tests reported here, the apparent thermal conductivity measurements were conducted with air at atmospheric pressure. Variations in atmospheric pressure occurred throughout the test period. The apparent thermal conductivity of the material varied linearly with these variations of barometric pressure. A variation of 15 mbar (0.44 in. Hg) produced an approximate change of 0.7% in the specimen apparent thermal conductivity. The specimen apparent thermal conductivity was determined by averaging measurements taken over several hours when the barometric pressure was stable within ± 1 mbar (± 0.03 in. Hg). Pressure measurements were made with a barometric stripchart recorder calibrated at NBS to within ± 0.4 mbar (± 0.01 in. Hg). A summary of individual apparent thermal conductivity measurements, as well as material density, average thickness of the metered area, and barometric pressure, is presented in Table 3.

Analysis of Data

For comparison purposes, all apparent thermal conductivity measurements were conducted at a mean-specimen temperature of 23.9°C (75°F). The apparent thermal conductivity measurements of the fumed-silica material were found to depend on two independent parameters: material density (ρ) and barometric pressure (P). A linear regression equation dependent on these two parameters was used to predict the thermal conductivity for each lot of material. For the initial analysis the following form was used:

$$\lambda(\rho, P) = a_0 + a_1 \cdot (\rho - \rho_{\text{ref}}) + a_2 \cdot (P - P_{\text{ref}}) \quad (2)$$

The term a_0 is the thermal conductivity at the reference value of material density, standard pressure, and ambient temperature application. The two coefficients a_1 and a_2 are regression coefficients for the material density and barometric pressure, respectively. The following values

TABLE 3—Summary of specimen measurements at a mean temperature of 23.9°C.

Product & Sample No.		Material Density, kg/m ³	Average Thickness of Metered Area, mm	Barometric Pressure, mbar	Measured Thermal Conductivity, W/m · K	Predicted Thermal Conductivity, W/m · K
A	A21	361.2	25.0	1011	0.02267	"
	A22	330.1	26.0	1005	0.02342	
B	A11	381.9	25.5	998	0.02153	0.02158
	A12	384.0	25.8	1019	0.02159	0.02192
	A13	371.6	25.9	1003	0.02191	0.02196
	A14	377.1	26.3	1004	0.02206	0.02183
	A15	381.5	26.0	999	0.02116	0.02161
	A16	383.0	26.1	1000	0.02148	0.02159
	A17	377.7	25.4	1007	0.02135	0.02187
	A18	380.2	25.6	1002	0.02261	0.02170
	A19	375.4	26.1	998	0.02160	0.02176
	A20	380.9	26.0	1012	0.02241	0.02187
C	A1	299.0	25.5	997	0.02173	0.02171
	A2	298.9	25.4	993	0.02172	0.02166
	A3	300.9	25.5	1012	0.02200	0.02191
	A4	300.7	25.7	1002	0.02173	0.02181
	A5	300.6	25.6	1008	0.02186	0.02187
	A6	302.3	25.5	1000	0.02182	0.02184
	A7	299.7	25.5	1005	0.02172	0.02181
	A8	303.4	25.7	1002	0.02191	0.02189
	A9	304.4	25.7	994	0.02179	0.02185
	A10	304.0	25.5	996	0.02192	0.02185
D	A31	290.6	26.2	1012	0.02093	0.02114
	A32	286.8	25.6	1006	0.02148	0.02103
	A33	282.4	26.0	1008	0.02102	0.02098
	A34	299.6	25.2	986	0.02101	0.02107
	A35	281.7	25.9	999	0.02078	0.02091
	A36	274.1	27.3	1016	0.02105	0.02092
	A37	280.5	25.9	1016	0.02087	0.02102
	A38	266.9	27.0	1007	0.02066	0.02075
	A39	275.7	26.9	994	0.02084	0.02078
	A40	269.5	27.9	1010	0.02078	0.02081
	A41	276.9	27.0	988	0.02074	0.02075

"The analysis of measurements for Product A was not done due to the statistically small lot size.

for the reference parameters were used in the analysis: ρ_{ref} = average density of the lot of material (kg/m³) (see Table 2), and P_{ref} = standard pressure of 1013.25 mbar (29.921 in. Hg) [6].

The regression analysis was accomplished using the NBS statistical analysis program, Dataplot [7]. The measured data were fit to Eq 2 using the method of least squares. The material density and barometric pressure coefficients computed using Dataplot are presented in Table 4. An insufficient sample number precluded analysis of the measurements of Product A.

The residual standard deviation (δ_{res}) in units W/m · K is shown as the last line in Table 4. The value is the smallest for Product C, indicating the curve fit is best for these measurements. The calculated regression coefficients in Table 4 are preliminary, based on small ranges of the independent parameters, ρ and P . The negative sign for the density coefficient of Product B is attributed to the large variation in thermal conductivity within the lot of material for a small range in material density.

TABLE 4—Regression coefficients for the thermal conductivity model.

Regression Coefficients	Product B	Product C	Product D
a_0	0.02194	0.02194	0.02100
a_1	-0.2783E-04	0.3076E-04	0.1473E-04
a_2	0.1889E-04	0.9936E-05	0.7621E-05
δ_{res}	0.506E-03	0.069E-03	0.197E-03

Measured values of apparent thermal conductivity are presented in Table 3. Using the regression coefficients in Table 4, predicted thermal conductivity values were calculated using Eq 2 and are also presented in Table 3. The percent deviation for each apparent thermal conductivity data point was calculated from the equation

$$\% \text{ deviation} = \frac{(\lambda_{\text{meas}} - \lambda_{(\rho,p)})}{\lambda_{(\rho,p)}} \cdot 100 \tag{3}$$

where

λ_{meas} = apparent thermal conductivity of measured data point (W/m · K), and
 $\lambda_{(\rho,p)}$ = predicted thermal conductivity at the same density and barometric pressure (W/m · K).

Percent deviation versus material density, barometric pressure, and apparent thermal conductivity are shown in Figs. 1, 2, and 3, respectively. Each plot indicates the percent deviation of the measurement point with the product letter. In the worst case, Eq 1 is able to predict the thermal conductivity of Product B within $\pm 2.1\%$, Product C within $\pm 0.2\%$, and Product D within $\pm 1.0\%$. The percent deviation for Product C is extremely low and within the uncertainty of the measurement. The plots show the smallest scatter for Product C.

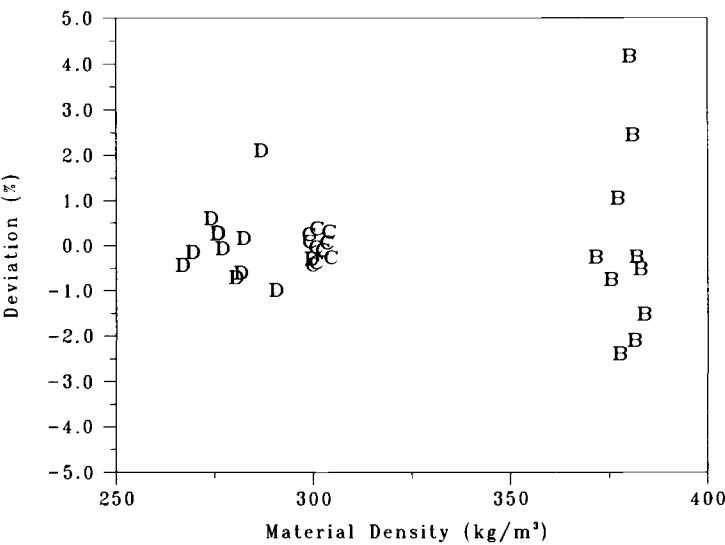


FIG. 1—Deviation (%) as a function of material density.

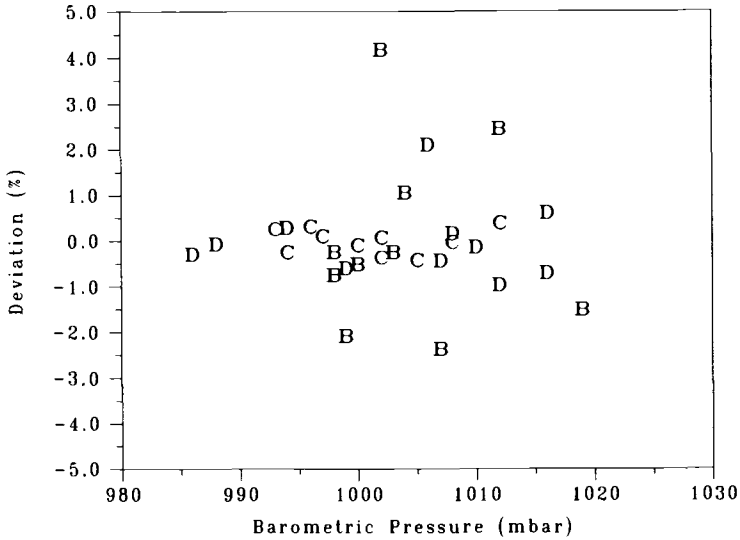


FIG. 2—Deviation (%) as a function of barometric pressure.

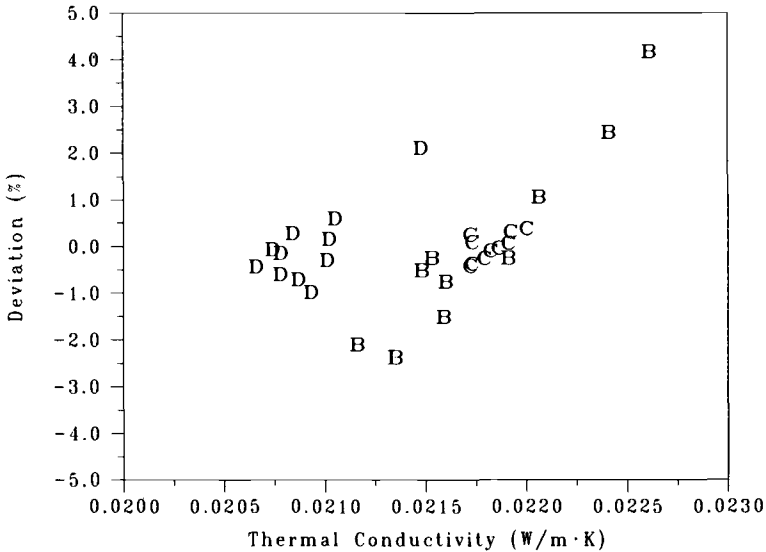


FIG. 3—Deviation (%) as a function of thermal conductivity.

Material Stability under Heat-Treatment

The effect of heat-treatment on the room-temperature apparent thermal conductivity of the fumed-silica material was investigated. One specimen from each manufacturer was selected and together the four specimens were heated in a high-temperature gas furnace. The heat treatment was applied in a cyclic manner. The four specimens were heated to an elevated temperature for approximately 5 to 8 h, removed after cooling, and the thermal conductivity remea-

sured in the NBS 1-m Guarded Hot Plate at a mean-specimen temperature of 23.9°C (75°F). The heat treatment was applied four times at a temperature range from 500 to 650°C (900 to 1200°F). The specimen thickness and density were also remeasured after each heat treatment.

Description of Heat-Treatment Tests

Using two of the stainless steel support racks previously described, four specimens were supported vertically within the gas furnace. Each rack held two specimens 13 cm (5 in.) apart and 10 cm (4 in.) from the furnace walls. The racks were supported 5 cm (2 in.) above the furnace floor on ceramic bricks. Hot gas from two combustion chambers entered the furnace from opposite inlet ports located 46 cm (18 in.) from the bottom of the furnace. The specimens were orientated so that supply hot gas flowed parallel to the specimens. Stainless steel shields were placed in front of each rack to keep the hot gas from directly impinging on the specimens. Temperature control of the furnace was accomplished by manually controlling the inlet flow of hot gas with a servo-valve. Under steady-state conditions, the air temperature was controlled within ± 2 K ($\pm 4^\circ$ F).

Specimen temperature measurements were made with Type K, 24 gage, glass-insulated thermocouples. The thermocouple wire was certified by the Temperature and Pressure Division of NBS to within ± 1 K at 1000°C ($\pm 2^\circ$ F at 1800°F). Oxidation of the wire limited the lifetime of the thermocouples to one heat treatment. Three thermocouples were located along a center line at the top edge, center, and bottom edge of the specimen. Each thermocouple was force-fit into a small hole, approximately 1.6 mm ($1/16$ in.) diameter, drilled about 6.4 mm ($1/4$ in.) deep in the specimen. The specimen was considered to be at a steady-state temperature when the center thermocouple was within 10°C (20°F) of the top edge thermocouple. Generally, the center thermocouple obtained steady-state temperature within 1 to 2 h. The average steady-state temperature of the specimen was computed using the center thermocouple.

Results of Heat Treatment

The results of the sequentially applied heat treatment for the four insulation products are summarized in Table 5. For each elevated conditioning temperature, the percent change in three material properties (mass, volume, density) is presented. In general, the elevated temperature caused all materials to experience a loss of mass and undergo some shrinkage. With the exception of Product D, the density of the materials also decreased. The increase in the density of Product D may have been the result of a sintering process occurring within the material. Product D also changed color in the heat-treatment process.

The percent change in apparent thermal conductivity (k -factor) for the four materials is also presented in Table 5. Products A and D experienced an increase in thermal conductivity, while Products B and C experienced a decrease in thermal conductivity. The change in conductivity for three of the materials (B, C, and D) was in the same direction as the change in the material density. Only Product A did not follow this trend. The reason is not evident from the existing data.

Economic Considerations

The cost of the four products varied over a wide range. Two specimens of Product A were purchased at \$900.00 per specimen. Products B and D were purchased at \$23.20 per specimen (10 specimens) and \$20.70 per specimen (11 specimens), respectively. Product C (10 specimens) was obtained at no cost. However, the commercial cost per specimen would be comparable to Products B and D.

The number of specimens available from a single batch of material is another consideration. It is more efficient to characterize a large lot of material than several smaller size lots. Product

TABLE 5—*Effects of high-temperature conditioning.*

Product	Parameter	% Change of Parameter after Heat Treatment			
		550°C 7.6 h	+ 600°C 6.7 h	+ 625°C 5.3 h	+ 650°C 5.8 h
A	Mass	−6%	−6%	−6%	−6%
	Volume	−2%	−2%	−2%	−2%
	Density	−5%	−5%	−5%	−4%
	<i>k</i> -factor	+0.3%	+0.4%	+0.1%	+1.6%
B	Mass	−2%	−2%	−2%	−2%
	Volume	−0.4%	−1%	−2%	−1%
	Density	−1%	−0.3%	−0.3%	−1%
	<i>k</i> -factor	−1.5%	−1.4%	−0.4%	+0.1%
C	Mass	−1%	−1%	−1%	−4%
	Volume	−0.4%	−1%	−0.4%	−2%
	Density	−1%	−1%	−1%	−2%
	<i>k</i> -factor	−0.8%	−0.9%	−0.8%	−1.1%
D	Mass	−1%	−1%	−1%	−1%
	Volume	−1%	−2%	−2%	−4%
	Density	+1%	+1%	+2%	+3%
	<i>k</i> -factor	+0.9%	+1.0%	+0.4%	+2.2%

A is available in lot sizes of 20 specimens. Products B and C are available in lot sizes of 40 and 45 specimens, respectively. The lot size for Product D is unavailable.

Overall Evaluation

Based on the results of the evaluation, Product C was selected as the material most suitable for further development as a SRM. The results of the evaluation are summarized in order of importance below:

1. The primary item of the evaluation criteria is the variability of the thermal conductivity of a lot of material. For Product C the variation in the thermal conductivity was the smallest among the materials tested at 24°C (75°F). In the worst case, predicted values of thermal conductivity were within $\pm 0.2\%$ of the measured values. The percent deviation is within the uncertainty of the apparatus measurement, $\pm 0.9\%$.
2. Product C had the smallest variation in thickness and material density within the four lots of materials. For the ten specimens measured, the standard deviation for thickness and material density was ± 0.1 mm (± 0.03 in.) and ± 2.0 kg/m³ (± 0.13 lb/ft³), respectively.
3. The effect of sequentially applied heat treatment on the material properties of Product C was minimal until the fourth heat treatment at 650°C (1200°F). The percent change in specimen thermal conductivity was less than 1.0% for the first three heat treatments. The material was also among the most durable until 650°C (1200°F).
4. The lot size available for Product C is the largest.

Additional Tests on SRM Candidate (Product C)

Effects of High Humidity

Three small cubes, approximately 25 by 25 by 25 mm (1 by 1 by 1 in.), of the candidate material (Product C) were cut and placed in high-humidity environments to qualitatively exam-

ine the effect of moisture on the material. A fixed-point humidity was obtained by using aqueous solutions in closed containers [8]. One cube was placed in a relative humidity (RH) of 50%, the second in 75% RH, and the third in 98% RH. The samples were observed and weighed over a period of one month. Visually, the sample placed in the container at 50% RH changed very little; however, the mass of the sample decreased 2%. At 75% RH the sample changed from its original rust color to white. The mass increased 3%. The sample at 98% RH also changed to a white color and its mass increased 58%. In addition, a crack formed in the middle of the sample. Results of the moisture study indicate the material should be stored at a relative humidity below 50%.

Temperature Dependence

The apparent thermal conductivity of one specimen of the candidate material (Product C) was measured to a mean temperature of 48°C (118°F) to examine the temperature effect on the material. For a change of 24 K (43°F) the apparent thermal conductivity increased 2.6%. This value included the small variation due to differences in barometric pressure.

Conclusions and Recommendations

Four lots of fumed-silica insulation products were evaluated as prospective candidates as a low thermal conductivity Standard Reference Material capable of withstanding elevated temperature. Thermal conductivity measurements were conducted on each lot of material using the NBS 1-m Guarded Hot Plate. Measurements were made at atmospheric pressure and at a mean specimen temperature of 23.9°C (75°F). Using the results, a linear regression model dependent on material density and barometric pressure was developed for each lot of material. Predicted thermal conductivity values were calculated at the same values of density and pressure as the measured thermal conductivity values. The thermal conductivity for the lot of material of Product C was predicted within $\pm 0.2\%$ in the worst case. This material is recommended for further development as a low thermal conductivity SRM.

The thermal conductivity model presented in the text is based on preliminary data covering a very small range of temperature and pressure. Further development of the candidate SRM requires characterizing the thermal conductivity over a larger range of temperature and pressure. The NBS Guarded Hot Plate can provide a mean specimen temperature range from approximately 0 to 50°C (32 to 120°F). Characterizing the thermal properties of the material at higher and lower temperatures would be done at NBS Boulder if necessary [9].

Development of the SRM also requires characterizing the fumed-silica material over a range of pressure corresponding to barometric pressures anticipated at test locations within the United States. For example, from sea level to an elevation of 2000 m (6600 ft) the barometric pressure decreases by approximately 220 mbar (6.5 in. Hg) [6]. Under such conditions, the apparent thermal conductivity of the fumed-silica material would decrease by several percent. Extending the pressure range capability of the NBS 1-m Guarded Hot Plate is necessary to characterize the fumed-silica material at lower barometric pressure. Modifications necessary to extend the pressure range of the apparatus are currently being implemented.

The candidate SRM is recommended for temperatures below 600°C. For applications in the building insulation temperature range, heat treatment of the material is not thought necessary. Although the material was among the most durable of the four products, a method to protect the edges of the material from crumbling when handled should be developed. Furthermore, the specimens should not be stored at relative humidities greater than 50%. As part of acceptance of this material, the candidate SRM material is now being reviewed in a small industry round-robin test.

Acknowledgments

The authors express appreciation to the Department of Energy whose sponsorship made this effort possible. Programmatic and technical coordination was provided by Bill Gerken, Program Manager, Materials Program, Building Systems Division, Office of Energy R & D, Department of Energy, and Dr. David McElroy of the Oak Ridge National Laboratory. The authors thank Steve Nabinger and Joan Langseth for their help in gathering and presenting data.

APPENDIX

The manufacturers' addresses are provided below for the reader's information:

1. **Manville Services Corporation**
Post Office Box 5108
Denver, Colorado 80217
United States
2. **Micropore International Limited**
Hadzor Hall, Hadzor
Droitwich, Worcestershire, WR9-7DJ
United Kingdom
3. **Grunzweig & Hartman und Glasfaser Ag**
Abt Te-Fp
D-6802 Ladenburg
Federal Republic of Germany
4. **Wacker Chemie GmbH**
Verkauf LC-HDK
Prinzregentenstrasse 22
D-8000 Munich
Federal Republic of Germany

References

- [1] ASTM Subcommittee C16.30, "Reference Materials for Insulation Measurement Comparisons," in *Thermal Transmission Measurements of Insulation*. ASTM STP 660, R. P. Tye, Ed., American Society for Testing and Materials, Philadelphia, 1978, pp. 7-29.
- [2] Rennex, B. G., "An Assessment of Needs for New Thermal Reference Materials," National Bureau of Standards Interagency Report NBSIR 85-3146, Washington, D.C., 1985.
- [3] *Health Effects of Synthetic Silica Particulates*. ASTM STP 732, D. D. Dunnom, Ed., American Society for Testing and Materials, Philadelphia, 1979.
- [4] Rennex, B., "Error Analysis for the NBS 1016 mm Guarded Hot Plate," *Journal of Thermal Insulation*, Vol. 7, July 1983, pp. 18-51.
- [5] Tye, R. P., "The Thermal Conductivity of MinK-200 Thermal Insulation in Different Environments to High Temperatures," CONF-691002, in *Proceedings*, 9th Conference on Thermal Conductivity, Howard R. Shanks, Ed., U.S. Atomic Energy Commission, March 1970, pp. 341-351.
- [6] List, R. J., *Smithsonian Meteorological Tables*, 6th rev. ed., Smithsonian Institution, Washington, D.C., 1966, p. 13, pp. 265-267.

- [7] Filliben, J. J., "Dataplot: Introduction and Overview," National Bureau of Standards Special Publication 667, Washington, D.C., June 1984.
- [8] Greenspan, L., "Humidity Fixed Points of Binary Saturated Aqueous Solutions," *Journal of Research of the National Bureau of Standards*, Vol. 81A, No. 1, Jan.-Feb. 1977, pp. 89-95.
- [9] Hust, J. G., Filla, B. J., Hurley, J. A., and Smith, D. R., "An Automated High Temperature Guarded Hot-Plate Apparatus for Measuring Apparent Thermal Conductivity of Insulations Between 300 and 750 K," this publication, pp. 710-722.

A Summary of the Manufacture, Uses, and Properties of Autoclaved Aerated Concrete

REFERENCE: Mathey, R. G. and Rossiter, W. J., Jr., "A Summary of the Manufacture, Uses, and Properties of Autoclaved Aerated Concrete," *Insulation Materials, Testing, and Applications, ASTM STP 1030*, D. L. McElroy and J. F. Kimpflen, Eds., American Society for Testing and Materials, Philadelphia, 1990, pp. 15-37.

ABSTRACT: This report is a review of the properties and performance of autoclaved aerated concrete. The material has a relatively low thermal conductivity combined with load-bearing capacity for use in structural and non-structural applications. This feature may make its use attractive for energy-conserving applications.

The review addressed an overview of the manufacturing process, uses of autoclaved aerated concrete in building constructions, properties, energy considerations, the availability of code-related documents, and standards. Uses include block and panel construction in load-bearing and non-load-bearing applications for walls, floors, and roofs. Many properties are reviewed including density, fire resistance, moisture expansion and shrinkage, strength, structure, and thermal conductivity. With regard to energy considerations, the review points out that, for energy-efficient applications under severe climatic conditions, the autoclaved aerated concrete unit alone may be insufficient to provide the targeted minimum value of thermal resistance. In these cases, autoclaved aerated concrete has to be used together with additional thermal insulation. In contrast, autoclaved aerated concrete alone may satisfy insulation needs in areas having mild climates.

KEY WORDS: aerated, autoclaved, cellular, concrete, insulating concrete, lightweight, manufacture, properties, review, standards, uses

Introduction

Autoclaved aerated concrete (AAC) is a factory-made construction material that is available to the user in blocks and precast units for walls, floors, and roofs [1]. It has gained widespread use in many areas of the world including Europe, South America, the Middle East, and the Far East. In brief, autoclaved aerated concrete is a porous lightweight concrete whose cellular structure is generally obtained through an *in situ* gas-producing chemical reaction of a sand and cement slurry. It generally contains no coarse material. Subsequent autoclaving of the material at high temperature and pressure imparts strength, dimensional stability, and other properties to the hardened final product. The autoclaved aerated concrete building material is obtained as the result of a reaction between the binder containing calcium oxide and a silica component cured in an autoclave [2], and a cellular structure producing ingredient. Autoclaved aerated concrete is at times referred to as *aerated concrete*, *gasbeton*, and *autoclaved lightweight concrete (ALC)*. This paper presents a summary of the manufacture, uses, and properties of autoclaved aerated concrete.

Autoclaved aerated concrete is a type of cellular concrete. Another type, using preformed foam and cast in place, is commonly used in the United States for floor and roof fills. The

¹Building Materials Division, Center for Building Technology, National Institute of Standards and Technology, Gaithersburg, MD 20899.

important properties of autoclaved aerated concrete are present to a large degree in cellular concretes which have not been autoclaved [3]. An oft-reported advantage [4–7] of autoclaved aerated concrete is the combination of relatively low thermal conductivity and load-bearing capacity for use in structural applications. Other advantages include relatively low density, high strength-to-weight ratio, nailability, fire resistance, good thermal resistance, and high sound insulation value [8, 9]. Its low density permits use of large building units, which is a reported advantage in prefabrication. The thermal conductivity properties offer potential to conserve energy by reducing building heating and cooling fuel consumption.

Background

Autoclaved aerated concrete was first introduced commercially over 50 years ago [6, 10]. Bessey [4, 11, 12] has described its early development and use in some detail. Initial development of the products including autoclave curing occurred in the 1920s in Scandinavia, with commercial use commencing in the early 1930s. However, little growth was experienced in commercial applications until the mid-1940s and the end of World War II. At this time, its use began to spread in some areas of Europe, in connection with post-war building efforts. In subsequent years, expansion continued to many regions of the world. Use in the expansion years of the 1950s did not result in U.S. production [13]. During the period 1955 to 1972, an autoclaved aerated concrete plant operated in Montreal, Canada, exporting some of its products to the United States.² In the mid-1960s, autoclaved aerated concrete represented a major portion of all structural materials used in some countries; for example, 20 to 40% in the USSR, Germany, Holland, and Sweden [4]. A 1987 estimate placed the amount of autoclaved aerated concrete used annually worldwide at about $8.1 \times 10^8 \text{ ft}^3$ ($23 \times 10^6 \text{ m}^3$).³ Table 1 provides recent estimates of the annual production of the material for some countries. In 1987, autoclaved aerated concrete was produced in 35 countries.³

Figure 1 depicts those countries where autoclaved aerated concrete was produced as of 1983 [6]. A notable feature in Fig. 1 is the lack of use of autoclaved aerated concrete in Canada and the United States. Reasons for this lack of use have received little documentation in the archival literature. Most of the reasons for lack of use, uncovered during the present study, are anecdotal, coming from individuals who are familiar with the production and use of the material. In general, the lack of use is attributed to factors associated with production costs and to tradition in the use of conventional building materials. For example, the costs of building a plant to manufacture hollow core concrete blocks may be 20 to 25% of the large initial investment to construct an autoclaved aerated concrete plant. In 1968, Bessey [12] indicated that the spread of the use of the material into the United States and Canada was marginal. He described the reasons for lack of growth as follows:

The factors involved are many. Except in dense urban areas, timber still plays a large part in the construction industry in these countries. The concrete block industry is well organized and efficient, and the lightweight-aggregate block is highly competitive in cost and is generally of good quality. An aerated concrete plant must be of good size and have a market which will utilize it at nearly full capacity in order to be economic, for the capital costs and fixed overheads together constitute a high proportion of costs.

Bessey [11] also indicated that general factors affecting global development of autoclaved aerated concrete were partly climatic, partly economic, and partly psychological. Specific factors which he has discussed on this point include: the local building regulations or codes affecting building construction, availability of raw materials, climatic conditions, fuel and energy requirements, and costs due to production, transportation, erection and maintenance [4, 12].

Interest in autoclaved aerated concrete use has recently increased in the United States. For

²Samuel Aroni, University of California at Los Angeles, personal communication.

³Gunnar Bave, Sipotex, personal communication.

TABLE 1—*Estimated 1987 production of autoclaved aerated concrete in some countries.^a*

Country	ft ³	m ³
Belgium	8.8×10^6	250×10^3
Czechoslovakia	105.9×10^6	3000×10^3
Denmark	10.6×10^6	300×10^3
Finland	7.1×10^6	200×10^3
France	17.6×10^6	500×10^3
Federal Republic of Germany	97.1×10^6	2750×10^3
Japan	105.9×10^6	3000×10^3
Netherlands	10.6×10^6	300×10^3
Poland	141.3×10^6	4000×10^3
Sweden	8.8×10^6	250×10^3
Soviet Union	187.2×10^6	5300×10^3
United Kingdom	100.6×10^6	2850×10^3
Yugoslavia	35.3×10^6	1000×10^3

^aGunnar Bave, Siporex, personal communication.

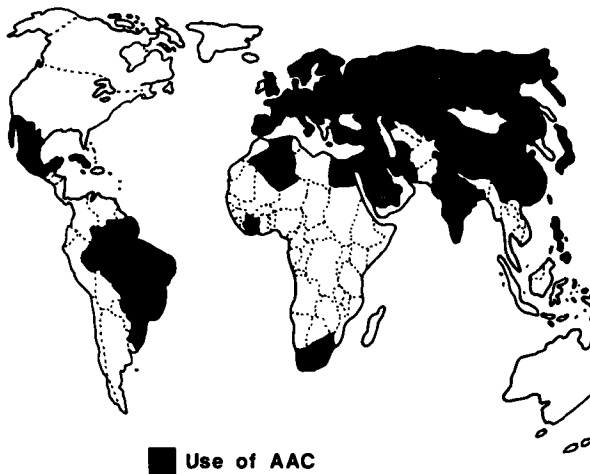


FIG. 1—Countries where autoclaved aerated concrete is used, as described by Bave in 1983 [6].

example, a news item indicated that a 42 000 ft² (3900 m²) facility was completed in 1986 in Florida [14]. The building had autoclaved aerated concrete precast wall and roof panels which were imported from Sweden. The columns and beams consisted of conventional, precast, prestressed concrete. The autoclaved aerated concrete products were not covered by the building code, and therefore a special permit was needed before the material could be used in Orange County, Florida [14].

Scope of the Study

The present study was limited to reviewing existing information, primarily the archival literature. No laboratory or field tests were conducted. As a construction material which has achieved worldwide use, the body of technical information on autoclaved aerated concrete including re-

search reports, standards, design criteria, codes of practice, and related documents is extensive. A bibliography of archival literature having 492 citations was published in 1983 [15]. The bibliography is included in a Proceedings of an International Symposium on Autoclaved Aerated Concrete: Moisture and Properties [16]. In 1954, Valore [13,17] gave a review of methods of preparation and physical properties of moist-cured and high-pressure steam-cured cellular concretes, ranging in density from 10 to 100 lbm/ft³ (160 to 1600 kg/m³). Valore's review covered three decades beginning in the mid-1920s. The present paper is based on a National Bureau of Standards report [18] that presented a state-of-the-art review of autoclaved aerate concrete products and reprinted a listing of applicable standards and related documents.

Manufacture of Autoclaved Aerated Concrete

The manufacture of autoclaved aerated concrete products has been described in the archival literature [1,19–24] and in manufacturers' publications. Although the processes used by different manufacturers are proprietary and have differences between them, the overall procedures of each are considered comparable. The manufacture of autoclaved aerated concrete products is carried out in factories where quality control measures can be implemented regarding materials and handling as well as the individual steps involved in the overall process.

Production is a continuous process which may be envisioned as having four stages (Fig. 2). The four stages are depicted as: (1) raw materials, (2) molding and cutting, (3) autoclaving, and (4) stocking and shipping.

Raw Materials

The major raw materials are, in many processes, sand and portland cement. In place of sand, other siliceous materials such as sandstone, shale ash, fly ash, and mixtures are often used. For example, fly ash has been substituted for ground sand to the extent of 100%.⁴ Lime or cement/lime mixtures are at times used instead of portland cement. The raw materials are used as fine powders which are normally obtained through grinding. Grinding may be done either through a wet or dry procedure.

Accurately proportioned quantities of the raw materials form the mix. In many cases, a slurry of the siliceous component is made in heated water whose temperature is controlled. The slurry is placed in a mixer into which the cement and/or lime are added. Admixtures such as surfactants and compounds for controlling the rate of cure may also be added.

Generation of the cellular structure is normally done through the addition of aluminum powder as the mixing procedure is ending. The aluminum powder in the alkaline medium (due to the cement or lime) produces hydrogen gas which, in turn, generates the cells. The addition of the aluminum powder is controlled so that gassing does not begin during mixing but during the molding stage. For example, one control technique uses aluminum powder surfaced with a layer to delay the reaction with the alkalis. Other methods for producing the cellular structure are the introduction of a preformed foam into the mix or the incorporation of air by whipping [1].

Molding and Cutting

The mixture (from Stage 1) is put into steel molds where the production of hydrogen begins and the mass expands, creating the aerated cellular structure. The expanded mass is allowed to set to a soft cake under controlled temperature and humidity conditions. The reaction time for expansion and setting is 30 min to a few hours (about 1 to 4) depending upon the raw materials. After setting, the cake is cut into the dimensions of the final product (e.g., block or panel units) using highly strung wires (piano wires) or multiple circular saws.

⁴Poul Nerenst, H + H Industri, personal communication.

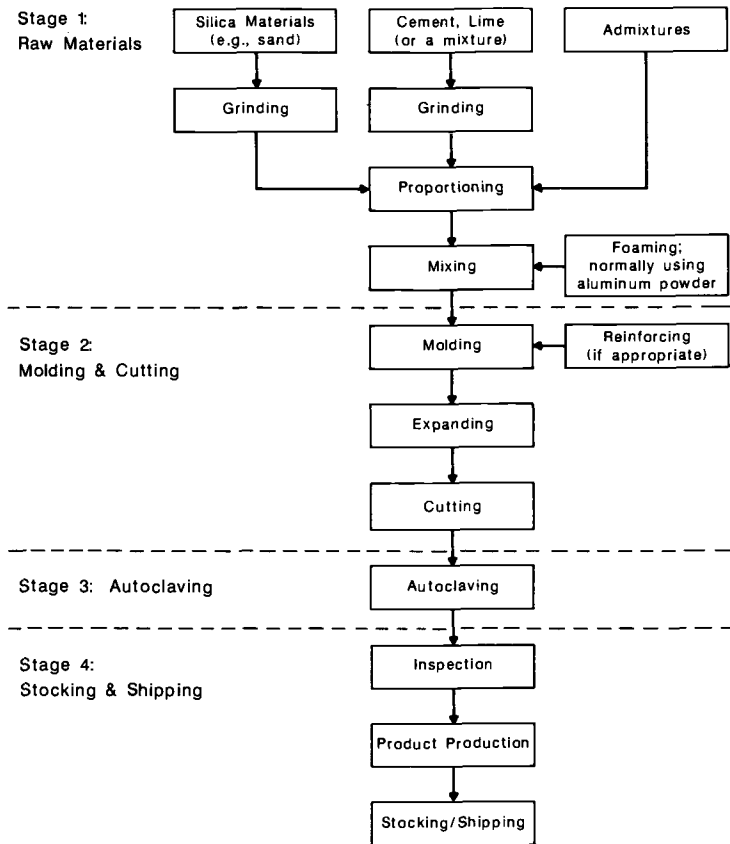


FIG. 2—Production of autoclaved aerated concrete products.

If the final product is to be used for structural applications, steel reinforcement is placed in the mold before casting the autoclaved aerated concrete. The factory procedure allows accurate placement of the reinforcement in the molds so that the set cake may be cut into the intended dimensions without damage. The steel reinforcement is protected from corrosion, normally by coating [25]. For example, one process uses a coating based on portland cement, latex, and finely ground sand. Another process uses a bituminous compound.

Autoclaving

The third stage of the process is the autoclaving whereby the aerated concrete cures to its final strength and dimensions. Autoclaving changes the physical-chemical nature of the hydrated cement materials and produces a material with lower drying shrinkage [26]. The conditions for autoclaving vary somewhat for different proprietary products. In general, the temperature is about 356°F (180°C) at a pressure of about 10 to 12 atm (1.0 to 1.2 MPa). The time varies depending on the size and density of the products, and may range from about 10 to 20 h. Storage of the uncured cake, even through moist and warm, for more than 2 or 3 days prior to autoclaving may be detrimental [27].

Stocking and Shipping

After the cured units are removed from the autoclave, quality assurance tests are normally conducted. Also, if desired, additional shaping through milling or related means may be carried out and a surface finish may also be applied. After autoclaving and cooling the units are ready for use without storage. If not needed immediately after production, the units are stored at the factory site and then delivered to the job site for installation.

Uses of Autoclaved Aerated Concrete

The types of autoclaved aerated concrete units most commonly produced are blocks and pre-cast panels for floors, walls, and roofs. Less often, complete modular room units are produced in the factory from wall, floor, and roof panels. The blocks and panels are used in load-bearing and non-load-bearing constructions for residential and commercial/industrial buildings. As a consequence, autoclaved aerated units are found in single and multi-story constructions oriented both horizontally and vertically. Larger units are reinforced with steel bars or welded mats to resist damage due to superimposed loads and from transportation and handling [8]. It also has been used as an extra layer of insulation for other components of the building envelope [28].

Blocks and panel units are manufactured to very close dimensional tolerances [29]. For example, the French standard (NF P 14-306) for autoclaved aerated concrete blocks for walls requires that the dimensional tolerance of the length be ± 0.1 in. (± 3 mm) for a minimum block length of 30 in. (760 mm). Close dimensional tolerance is important with regard to modular construction to assure that individual units fit together properly. Literature references point out that the modular construction concept provides for simple and fast construction, comparatively low costs, and good architectural possibilities [30,31]. Any deviation from the standard sizes of units could lead to extra costs. Construction time is shortened and building costs reduced by increasing the size of panels [32].

Blocks

Blocks are available in standard sizes and generally do not contain reinforcement [21]. They have been widely used for side cladding and as "in filling" for external walls as well as for external and internal load-bearing walls in low and multi-story construction. Construction techniques include blocks laid using mortar joints and thin glue joints (0.08 to 0.1 in. [2 to 3 mm]) in place of mortar [33]. Since autoclaved aerated concrete blocks are of relatively low weight, they are often somewhat larger than concrete masonry units manufactured in the United States. Due to the cutting process during manufacture, the blocks may have an architectural surface (often referred to as a *wire cut* or *scratched surface*) [34]. This surface allows the use of the blocks without a decorative rendering or parging, but external surfaces should be protected from exposure to water.

Panels

Autoclaved aerated concrete panels are manufactured in various sizes for use in vertical and horizontal applications. Vertical wall panels are available in "story-height" increments and have been used in load-bearing applications up to three or four stories high [1,10]. Wall panels are also laid up horizontally. These panels normally do not carry any load other than their own dead weight.

Another common use of autoclaved aerated concrete is for roof and floor slabs. During erection, the slabs are commonly placed, direct from a truck, on load-bearing walls or a structural frame without use of a mortar bed. Bituminous roofing membranes have been applied directly

to assembled roof panels [1,34]. Regarding this practice, it has been reported that the autoclaved aerated concrete panels fit closely together and serve as thermal insulation [34]. The design of the roof should consider movement between adjacent panels to prevent splitting of the roofing membrane [1,35].

Autoclaved aerated concrete panels are also accepted in several countries for basement walls below ground level [1]. For this application, precautions must be taken to allow moisture present during manufacturing to dry from the walls. One method involves the application of impermeable protection on the outside of the wall below ground level.

In concluding the remarks on autoclaved aerated concrete in panel construction, it is pointed out that this practice in the 1960s involved the use of large-sized panels [36,37]. However, as far back as the late 1960s, it was recognized that excessively large panels could have a serious drawback, with cracking sometimes occurring during manufacture or in service [32]. Recently, in 1980, Bave [38] noted that the trend of using large panels, such as occurred in the 1960s, seems to be broken, at least in the countries in Western Europe. The demand for large panels decreased due to architectural preferences and cost considerations. At present, the use of large panels is mainly in industrial constructions.

Limitations

Although autoclaved aerated concrete has been a long-accepted construction material, the literature is not without reference to limitations in its use. For example, some limitations have been reported by Tietz [39], including: the material chips easily; the face tends to get damaged easily (e.g., from scaffolding); dowels are required between units; the external face is hygroscopic and needs a protective coating which can breathe and should be protected from standing water; the bottom units should be protected from splash-back; the units absorb enormous quantities of paint; the anchorage of units needs careful planning to prevent pullout, especially for dynamic loads; and the face is weak and any tough surface may pull away due to the interface pulling off the parent material. Finally, it should be mentioned that caution should be exercised in transporting and handling the units to avoid damage [30,40].

Design Considerations

The European Experience—A manual, "Autoclaved Aerated Concrete-Design and Technology," was produced by the Euro-International Committee for Concrete (CEB) [1]. The manual addresses the manufacture and properties of aerated concrete, design considerations, and economic considerations. Many typical construction details and application photographs are presented. The manual also advises a check of the design principles for autoclaved aerated concrete structural units with full-scale tests.

Results of testing of autoclaved aerated concrete under dynamic repeated loads indicate that the fields of application of this material must be chosen carefully [41]. Briesemann [42] in his paper concerning criteria for the design of structural elements of autoclaved aerated concrete indicated that knowledge relating to their design is not yet complete. He stated that structural elements of this material have been used in buildings for over 50 years and they have proved to be satisfactory in practice. Briesemann stated further that known design rules have not been verified by scientific experiments like those for reinforced concrete structures and may allow for excessively large safety coefficients.

The U.S. Experience—As previously noted, autoclaved aerated concrete precast units are not presently produced in the United States or Canada. The American Concrete Institute (ACI) has a publication entitled "Guide for Low Density Precast Concrete Floor, Roof, and Wall Units" [43]. This guide outlines provisions and practices of design and fabrication of low density, 50 lbm/ft³ (800 kg/m³) and under, precast reinforced concrete floor, roof, and wall units. Both cellular and low density aggregate precast concrete are included in the guide. The compressive

strength of the low density concrete used in precast units should be a minimum of 300 lbf/in.² (2.1 MPa). The design allowable stresses in the concrete should conform to the requirements of ACI 318 [44], except for shear stress permitted in an unreinforced web and the compressive stress allowed in low density precast concrete load-bearing walls.

The Council of American Building Officials (CABO) and the U.S. Department of Housing and Urban Development (HUD) have issued a report [45] and a Materials Release [46], respectively, for the use of a proprietary autoclaved aerated concrete. The CABO report defines allowable uses for roof, floor, curtain wall, and partition panels and blocks. The HUD Materials Release is for a thin-joint block wall system.

Moisture Considerations—Autoclaved aerated concrete contains moisture from the manufacturing process. The moisture content at the time of delivery to the building site may be 20 to 35% by weight (10 to 18% by volume) [1]. The moisture dries out gradually in normally one to two years and reaches equilibrium in external constructions of about 4 to 6% by weight (2 to 3% by volume) [1]. Moisture may also accumulate in the material during construction and after the building is completed (e.g., from rain and condensation). It is necessary to assure that the design provides for drying out of the initial moisture as well as maintaining low moisture content in the building under service conditions. In general, autoclaved aerated concrete in equilibrium with a normal environment (65% R.H. and 68°F [20°C]) tends to have a moisture content of about 3% by volume [47].

As indicated in the ACI Guide 515.1R-79, concrete masonry walls above grade should normally be painted on the exterior for damp-proofing purposes [48]. Because of the higher porosity and moisture absorption of autoclaved aerated concrete, as compared to dense concrete, a surface treatment should be considered for exterior surfaces of autoclaved aerated concrete masonry and wall panels. The external treatments currently used are mortar for masonry walls and paints for wall panels [1]. The paint should be nearly impermeable to water, but should have some permeability to water vapor so that, if moisture should become trapped or condensed within the wall, it can slowly escape to the exterior. Protections for masonry have included one to three coats of mortar (not exceeding 0.8 in. [20 mm]) for external application and, for internal use, a thin application of resin or gypsum plaster, lime mortar, or paint [1,49].

For decorative purposes, ceramic tiles, colored sand or granite, marble chips, broken glass, and other materials can be used on wall panels [37]. External walls may also have a prefinished surface [50].

Properties of Autoclaved Aerated Concrete

The physical and mechanical properties of autoclaved aerated concrete may be made to vary over a considerable range, depending on the quantities of the raw materials used, the mix design, and curing conditions [17,18]. It is important to note that many properties of cellular concrete can be given as functions of bulk density and thickness [24,51]. This section of the report presents a brief summary of the most often reported properties of autoclaved aerated concrete. Additional information on the properties of this material is presented in a National Bureau of Standards report [18]. The properties summarized herein are based essentially on the list given in the CEB Manual [1].

Capillarity

Capillarity is important for wetting and drying out the materials. The capillary suction is slow in aerated concrete compared with some other porous materials such as clay bricks [1]. Capillary suction takes place almost exclusively through the micropores in the cell walls and is negligible for the macropores [1].

Coefficient of Thermal Expansion

The coefficient of linear thermal expansion for autoclaved aerated concrete is 4.5×10^{-6} per °F (8×10^{-6} per °C) compared to 6.8×10^{-6} per °F (12×10^{-6} per °C) for mild steel reinforcement [6,21,28]. Dense concrete and steel have about the same value of coefficient of linear thermal expansion.

Cracking

One of the major concerns with autoclaved aerated concrete is that of cracking, both externally and internally [28]. Cracking may be caused by shrinkage, creep, temperature, moisture effects, or by deformation and settlement of foundations. It is not always possible to separate the causes and effects of cracking.

The repair of cracks in occupied houses and apartments can be difficult and expensive. In a study by Cividini [52], it was reported that prestress of autoclaved aerated concrete slabs, due to differential drying and cooling after autoclaving, may in some cases increase crack resistance to such an extent that the slab cross section may remain without cracks during its service life.

Creep

For all autoclaved materials, creep is low in relation to the elastic deformation [18]. Factors affecting creep of autoclaved aerated concrete are stress level, moisture content, ambient temperature, and relative humidity. A creep coefficient (creep strain divided by the momentary deformation) is indicated as 0.8 to 1.2 for autoclaved aerated concrete having a density of 31 lbm/ft³ (500 kg/m³) [1]. According to Kruml [53], factors influencing the quantitative value of creep have not been sufficiently defined and evaluated. For this reason, he noted that the creep coefficient often differs in the literature.

In creep studies by Nielson [54] using unreinforced beams, he reported creep coefficients, after one year for dry material at 43% R.H., that ranged from 0.2 to 0.3. For water-saturated material, the creep coefficients ranged from 0.2 to 0.6. These values are somewhat less than those found for normal concrete.

In a study by Houst, Alou, and Wittmann [55], larger creep deformations for moist specimens were reported than for dry ones.

Density

Density for autoclaved aerated concrete generally refers to oven-dry material. When delivered to the building site, the practical density is higher because of the moisture content and presence of any reinforcement. The density of autoclaved aerated concrete is normally reported in the range of 19 to 62 lbm/ft³ (300 to 1000 kg/m³), with 31 lbm/ft³ (500 kg/m³) or more being the most common density for load-bearing products and reinforced flexural members [1,56].

Deterioration Resistance

Autoclaved aerated concrete, because of its porosity and relatively low alkalinity (pH = 9 to 10.5), does not provide the same corrosion protection of reinforcement as that provided by dense concrete [1]. Thus it is recommended that reinforcement should be protected against corrosion by adequate surface treatment [1]. In areas of relative humidity less than 50% at equilibrium moisture content, corrosion of reinforcement is reported likely to be negligible [1].

There also may be a risk of corrosion of nails and steel anchors because of the initial moisture content of the material, or moisture from condensation or rain penetration [1]. Acids in the

form of liquid and gases penetrate aerated concrete more easily than dense concrete and their deteriorating effect is more rapid than for dense concrete. Autoclaved aerated concrete should therefore be protected from acidic liquids or fumes. The porous structure of autoclaved aerated concrete allows air to penetrate the material readily and, depending on the availability of carbon dioxide and atmospheric humidity, a decrease in alkalinity of the material occurs [25]. It was found that 10 in. (24 cm) thick autoclaved aerated concrete members had been carbonated throughout after only two years of service [25]. The CEB Manual [1] indicates that carbonation of autoclaved aerated concrete is generally not of concern if the carbon dioxide content of the air is as normally expected (0.03%). Manufacturer's recommendations should be followed if autoclaved aerated concrete is to be exposed to carbon dioxide concentration above about 0.2%.

Fire Resistance

Autoclaved aerated concrete is non-combustible [1]. Because of its low thermal conductivity, heat migration takes place at a much lower rate than in dense concrete. Consequently, the fire ratings for autoclaved aerated concrete units issued in some countries in Europe indicate that this material provides for very good fire resistance compared with other building materials [1,28]. One reference [21] indicated that, for the same thickness, the use of cellular concrete in place of normal concrete has been reported to increase the fire resistance by 30 to 40%.

The fire rating of load-bearing roof and floor flexural units depends upon density and the thickness of the cover of the reinforcement. Autoclaved aerated concrete may be used as a cladding to protect other materials such as steel members or to increase the fire rating of normal concrete walls [1].

In the early 1960s, the U.S. National Bureau of Standards conducted fire tests of lightweight, cellular precast concrete (reportedly of the *in-situ* gas-forming type) panels for floors and roofs [57]. It was found that fire endurance was up to 2 h for 6 in. (15 cm) thick slabs tested under load, and up to 4 h for other slabs not loaded. The use of greater cover for the reinforcing bars, in the range of $3/4$ to $1\frac{1}{4}$ in. (19 to 32 mm), even without increasing the total thickness of the cellular concrete, will result in longer fire endurance.

Frost Resistance

The extensive use of aerated concrete in countries with cold climates indicates that the material has resistance to frost. Nevertheless, a risk of frost damage exists if the moisture content in any part of the construction unit exceeds the critical moisture content of the autoclaved aerated concrete. The critical moisture content can be considered as the moisture content of the material at which, upon freezing and thawing, a loss in strength properties or damage occurs. The critical moisture is, for example, about 40% by volume for aerated concrete manufactured in Sweden with a density of 31 lbm/ft³ (500 kg/m³) [1]. However, the moisture content is usually highest during construction, rarely exceeding 15 to 20% by volume, before drying out takes place [1]. Under extreme conditions, higher moisture contents may occur close to the surface of the unit, which increases the risk of frost damage. Edlind [28] reported that heavier autoclaved aerated concretes are satisfactory with regard to frost resistance, but at densities below about 31 lbm/ft³ (500 kg/m³) liability to frost damage increases.

From tests of 30 cycles of freezing for 5 h and thawing for 3 h, Purins [58] concluded that the critical moisture content was between 50 to 70% by volume and is dependent on the bulk density. Critical moisture content was 50% by volume for density of 25 lbm/ft³ (400 kg/m³) and 65 to 70% by volume for density of 40 lbm/ft³ (650 kg/m³). Tensile strength after the tests decreased considerably, from 60 to 70 lbf/in.² (0.41 to 0.48 MPa) to 4 to 20 lbf/in.² (0.03 to 0.14 MPa). This decrease was attributed to internal damage occurring during the test, although reportably not visible from the outside [58].

In a similar study, Roulet [59] reported on the resistance to frost action of three different

densities of autoclaved aerated concrete. The densities were 19, 25, and 31 lbm/ft³ (300, 400, and 500 kg/m³). The frost expansion upon cooling to -4°F (-20°C) and their length during thawing were measured. With dry samples, there was linear thermal expansion. For samples with low water content (degree of saturation: 20 to 40% by weight), they exhibited contraction on freezing, and after thawing no significant permanent expansion was measurable. Specimens having a critical water content (60 to 70% by weight), which is low compared to the total porosity or the zero pressure capillary water content, exhibited a large expansion while freezing to about -4°F (-20°C). After thawing, the sample with critical water content showed a permanent expansion. If the samples were nearly saturated with water, they became very brittle after one freeze-thaw cycle. Roulet [59] also reported that samples with a high degree of saturation upon freezing became brittle and cracked. However, scanning electron micrographs gave no evidence of a structure change due to freezing.

In a related study, tests carried out on factors such as loss of weight on freezing, tensile strength after freezing, and changes in length and volume after repeated cycles indicated that the critical degree of saturation was about 35 to 40% of pore saturation [60]. Pore saturation denotes that the total pore volume is filled with moisture. The dynamic modulus of elasticity was determined for each cycle for samples in the thawed condition. Damage occurred at a degree of pore saturation of 38 to 45% [60]. However, a measure of the critical degree of moisture was also obtained by studying the moisture-dependent deformation of samples. It varied to some extent due to the quality of the material and seemed to be in the range of 50 to 60% [60].

Moisture Expansion and Shrinkage

Autoclaved aerated concrete is similar to dense concrete in that it expands on wetting and shrinks on drying [28]. Drying shrinkage varies with density and method of manufacture. Values of drying shrinkage range from 0.1 to 0.5% when measured from saturated condition to a condition of equilibrium at 45% R.H. [28]. The low drying shrinkage of an autoclaved product compared with that for air-cured cellular concrete has been attributed to chemical reactions that take place during autoclaving [21].

Moisture Migration

Autoclaved aerated concrete, due to its higher porosity, has higher moisture absorption than dense concrete. Moisture may migrate through capillarity or through diffusion or both. For normal moisture content conditions, the moisture migration is mainly by diffusion; with increasing moisture content, it is due more to capillarity [1]. Moisture migration is due almost entirely to capillarity when the moisture content is above 40% by mass (20% by volume). The moisture migration is also influenced by the pore structure, the dimensions of the unit, the thermal conductivity of the material, temperature, vapor pressure, and movements of the air to which the surfaces of the construction units are exposed.

Permeability

The permeability of autoclaved aerated concrete to air varies with the moisture content of the material. It decreases with an increase in moisture content in the pores [6]. Nevertheless, the CEB Manual [1] has indicated that the permeability of dry material at normal pressure differences, such as caused by wind, is very low and may be considered negligible. It is noted that significant penetration can take place through improperly formed joints and other connections in the building.

The water vapor permeability by diffusion also decreases with an increase in the moisture content of the material. The diffusion factor of aerated concrete (ratio between the diffusion of water vapor through a layer of air to that through a layer of material of the same thickness) has

been determined to be 5 to 7 under air dry conditions for material having a density of 31 to 38 lbm/ft³ (500 to 600 kg/m³) [1].

Shaping and Working

During construction, autoclaved aerated concrete can be easily cut, nailed, drilled, milled, or shaped to accommodate building needs such as utilities or other construction requirements [1,28,61]. In most cases, ordinary woodworking tools can be used. Reinforced flexural members should not be cut on the construction site without authorization of the manufacture, since anchorage of reinforcement may be affected [1].

Attachment of other buildings units, materials, or accessories to autoclaved aerated concrete is more critical than those in denser materials such as brick or normal concrete, since ultimate failure loads (pullout) are lower [62].

Specific Heat

Specific heat of a material is the heat required to raise the temperature of unit mass of the material one degree. It is a measure of the capacity of a material to store heat. For autoclaved aerated concrete the value of specific heat is about 0.24 to 0.26 Btu/lbm°F (1.0 to 1.1 kJ/kg°C) for material of normal moisture content (2 to 3% by volume or 4 to 6% by weight) [1].

Solubility in Water

The strength-related components of autoclaved aerated concrete have only very low solubilities in water. However, depending on the raw material and mix proportions, the product may contain small quantities of soluble salts which, under certain climatic conditions such as those resulting in slow evaporation, may crystallize on the surface to form efflorescence [1].

Sound Absorption

Autoclaved aerated concrete is considered to provide good sound insulation, having sound absorption properties somewhat better than that for smooth dense concrete [1,21,28]. The sound absorption coefficient of untreated autoclaved aerated concrete was reported to be 0.00, 0.15, 0.25, 0.20, 0.20, and 0.20 for frequencies (Hz) of 125, 250, 500, 1000, 2000, and 4000, respectively [1]. If the aerated concrete is painted or coated, its sound insulation effectiveness is reduced. In general, for solid construction, sound transmission depends on the mass of the structure. Cavity wall construction gives greater sound reduction than solid construction for the same total mass [20].

Strength

Considerable data have been generated regarding the strength of autoclaved aerated concrete including compression, tension, shear and bond strength, and modulus of elasticity. Strength tends to increase with an increase in density (Table 2), while thermal resistance tends to increase with a decrease in density [28]. According to Shrivastava [21], there is a straight-line relationship between strength and density. Grimer and Brewer [63] tested four aerated concretes of varying density, 33 to 43 lbm/ft³ (530 to 690 kg/m³), and found that there was a slight systematic increase in strength with depth. The strength increases were accompanied by increase in specific gravity. The moisture content of autoclaved aerated concrete also has an influence on its strength. Svanholm [64] reported that strength decreases with an increase in moisture content. This was found for compressive and tensile strength and modulus of elasticity.

TABLE 2—Examples of values of compressive strength and modulus of elasticity [28].

Density		Compressive Strength		Modulus of Elasticity	
kg/m ³	lbm/ft ³	MPa	lbf/in. ²	MPa	lbf/in. ²
400	25	1.5	215	1000	142 230
500	31	3.0	430	1400	199 130
650	41	6.5	924	2600	369 810

Compressive Strength—The compressive strength of autoclaved aerated concrete increases with an increase in density [1,8]. The average value of compressive strength measured using cubes for a dry density of 25 lbm/ft³ (400 kg/m³) was reported to be about 290 lbf/in.² (2 MPa); for a dry density of 44 lbm/ft³ (700 kg/m³), it was reported to be about 870 lbf/in.² (6 MPa) [1]. Another report showed that for a density range of 31 to 44 lbm/ft³ (500 to 700 kg/m³), the compressive strength was 290 to 580 lbf/in.² (2 to 4 MPa) [8]. The relationship between the cube compressive strength and the density of autoclaved aerated concrete is shown in Fig. 3 [1].

The compressive strength decreases with an increase in moisture content of the material. The relationship between the compressive strength and the moisture content of autoclaved aerated concrete is shown in Fig. 4 [1]. With moisture contents of 5 and 10%, the compressive strength is reduced about 20 and 25%, respectively. In another study, by Dworjadkin and Malinowski [65], it was reported that the compressive strength of an autoclaved aerated concrete with maxi-

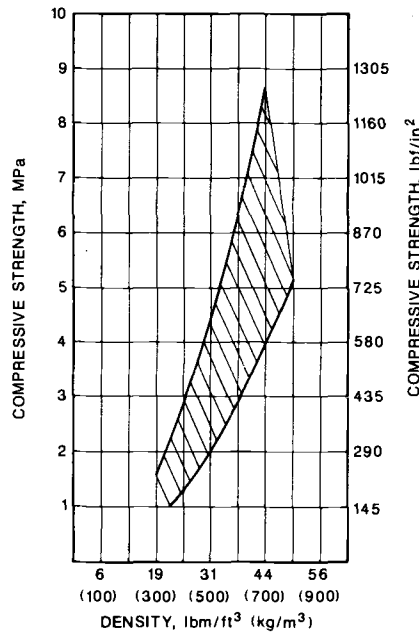


FIG. 3—Relationship between cube compressive strength and density of autoclaved aerated concrete (from CEB Manual [1], courtesy of CEB and the Construction Press).

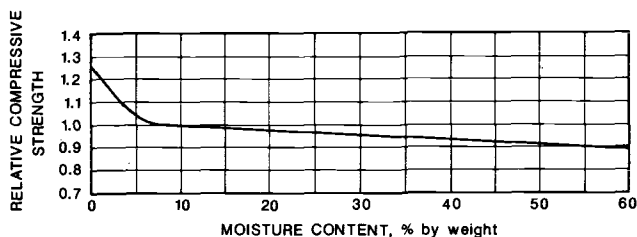


FIG. 4—Relationship between compressive strength and moisture content of autoclaved aerated concrete (from CEB Manual [1], courtesy of CEB and the Construction Press).

imum water saturation (40 to 42% by volume) was 40 to 50% less than that of the air-dried material.

Compressive strength has, in at least one case, been found to decrease with time of exposure. For example, block samples exposed outdoors up to one year were tested by Grimer and Brewer [66], who found changes in strength (as indicated by compressive strength, as well as splitting strength, and modulus of rupture) with time. The decrease ranged from 10 to 15% for these properties.

Tensile Strength—The tensile strength of autoclaved aerated concrete is normally one quarter to one sixth of the compressive strength [1]. Edlind [28] reported the tensile strength to be about 20% of the compressive strength. A moisture gradient within the test specimen has a large effect on the tensile strength test result. The measurement of this property is even more sensitive to test conditions than the measurement of the compressive strength.

The tensile strength in bending is normally somewhat higher than when measured in direct tension. A moisture gradient in the specimen also affects this property.

Grimer and Brewer [67] reported that the modulus of rupture of specimens uncovered and stored outdoors changed considerably (up to 50% decrease) from one month to one year. For specimens covered and also exposed outdoors, no significant change in strength occurred as compared to specimens stored indoors.

The modulus of rupture for a density range of 31 to 47 lbm/ft³ (500 to 750 kg/m³) was about 100 to 190 lbf/in.² (0.7 to 1.3 MPa) [8]. Cracking in reinforced flexural members was observed to occur between 1.5 and 2.0 times the working load, under which condition the tensile stress can approach 50% of the compressive strength of the material.

Shear and Bond Strength—The shear rupture strength, based on pure punching shear, can be assumed to be 25 to 30% of the compressive strength [1]. The value for pure shear can be taken as that for direct tension, if information about shear strength is not available. The shear strength was also reported to be about one eighth of the compressive strength and to range from 36 to 72 lbf/in.² (0.25 to 0.5 MPa) [8].

In tests reported by Regan [67], the nominal shear stresses in reinforced autoclaved aerated concrete beams at the cracking stage were in the range 51 to 58 lbf/in.² (0.35 to 0.4 MPa). This corresponds to the upper limit of values obtained from unreinforced (shear) slabs. The test results suggest that once shear cracking occurs in an autoclaved aerated concrete member, the truss action of the stirrups has to support the full shear with practically no separate contribution from the concrete.

Based on a statistical evaluation of previously published test results, Briesemann [68] developed semi-empirical methods of calculating the ultimate shearing strength of autoclaved aerated concrete slabs without web reinforcement, as well as the loads resulting in diagonal cracks and shear failure in beams with shear reinforcement. This design method was reported as being useful for components of autoclaved aerated concrete, because the test specimens and the components used in practice were identical.

The bond of reinforcement in autoclaved aerated concrete is normally a fairly plastic phenomenon with the peak stress attained at a slip of about 0.0004 in. (0.01 mm) and maintained for movements up to about 0.008 in. (0.2 mm) [67]. Because of the relatively low bond strength, the reinforcement in autoclaved aerated concrete members often relies on welded cross-bars or stirrups which transfer load by bearing [8, 26, 43, 67]. Regan [67] suggests from pullout tests a limiting value of bond stress for coated plain (smooth round) bars of 180 lbf/in.² (1.25 MPa) based on the perimeter of the bar not including the coating. The bond strength of plain bars embedded in autoclaved aerated concrete may differ depending on the type of protective coating used. Other pullout tests [26] on small diameter plain bars coated with a cement-latex coating embedded in autoclaved aerated concrete having a compressive strength of 500 lbf/in.² (3.4 MPa) yielded bond stresses of 150 to 200 lbf/in.² (1.0 to 1.4 MPa) at a slip of 0.001 in. (0.03 mm) at the free end. Dunn [26] stated that these values are generally greater than those calculated at design load, and actual load tests on precast units confirm that while the bond is adequate for design loads, slip can occur at about 1.25 times design load.

Modulus of Elasticity—The modulus of elasticity is about one tenth that of dense concrete [24]. It has been given as a function of the density and compressive strength of the material. As an example, the modulus of elasticity for autoclaved aerated concrete having a density range of 31 to 44 lbm/ft³ (500 to 700 kg/m³) was reported to be $200 \text{ to } 400 \times 10^3 \text{ lbf/in.}^2$ ($1.4 \text{ to } 2.8 \times 10^3 \text{ MPa}$) [8]. The moisture content also affects the modulus value. The modulus decreases with an increase in moisture content, similar to the way it affects the compressive strength.

Structure

The structure of autoclaved aerated concrete is characterized by pores or cells which are formed by the hydrogen gas, air, and water during the molding and expanding phases of production [1]. The micro-cellular structure of autoclaved aerated concrete is shown in Fig. 5.

Scanning electron microscopy (SEM) micrographs of the cell structure of the hardened material, which is generally considered to be uniform, have been reported [1, 58, 59, 69, 70]. The pore structure is important with regard to physical properties of the material such as strength, thermal conductivity, capillarity, and frost resistance. Depending on the pore size and their physical characteristics, they can be divided into micropores and macropores. An example of the distribution of pore sizes in autoclaved aerated concrete is shown in Fig. 6 [1]. Larsson and Purins [60] reported pore size for various kinds of autoclaved aerated concrete investigated in freezing tests. The macropores were determined to have radii of between 64 000 and 550 000 Å and micropores to have radii of between 40 and 64 000 Å. They also reported that the pore size distribution was different for the various autoclaved aerated concretes investigated. Micropores may be considered to be capillary active, and the distribution of cell sizes within the micropore range is important with regard to properties such as freezing and moisture migration [1]. The macropores are usually almost spherical in shape; however, for cases where they are more oval in shape, it may be assumed that the physical characteristics of the autoclaved aerated concrete may differ somewhat in the directions of the major and minor axes [1]. If the cells are irregularly shaped rather than being spherical, excessive reduction in strength occurs [21].

In a study by Schwiete and Ludwig [71], the porosities of some autoclaved aerated concrete specimens were found to be about 70 to 80%. They considered the concept of effective porosity to assess the micropore content of the specimens. They reported that the effective porosities ranged from 4 to 13%. Moisture contents of the specimens were about 2% by volume, and the bulk densities were 44 lbm/in.² (700 kg/m³).

Purins [58] conducted an examination of pore structure and reported no entirely closed pores in autoclaved aerated concrete. His evidence was electron micrographs of the material with magnifications of up to $\times 26\,000$. He observed that the structure was capillary, both at the bottom and in the walls of the pores, and concluded that no closed pores existed in the material.

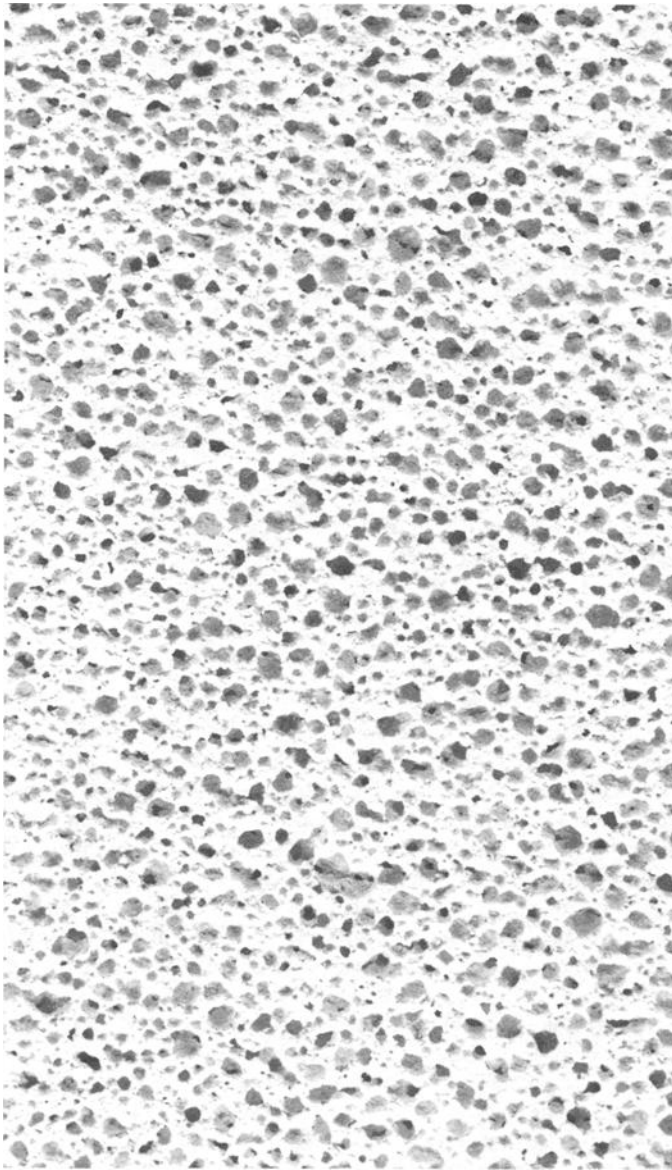


FIG. 5—Micro-cellular structure of autoclaved aerated concrete (about $\times 3$).

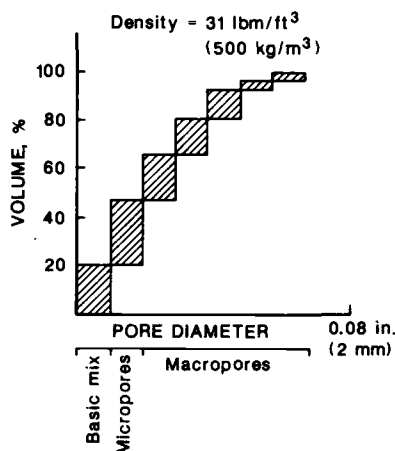


FIG. 6—Example of distribution of pore sizes in autoclaved aerated concrete (from CEB Manual [1], courtesy of CEB and the Construction Press).

Temperature Resistance

Shrinkage cracking will result if autoclaved aerated concrete is exposed to dry air at a high temperature for a long time and excessive drying eventually takes place. For this reason, structural aerated concrete should not be used in constructions that are continuously exposed to dry air at a temperature above 122 to 158°F (50 to 70°C) without protection against excessive drying [1]. For non-structural applications, aerated concrete can be exposed to much higher temperatures, up to 1300°F (700°C), if appropriate precautions are taken against excessive drying. The CEB Manual [1] indicates that, for such high temperature use, manufacturers' design considerations must be strictly followed. The melting point of aerated concrete is 1800 to 2200°F (1000 to 1200°C), depending on the materials used [1].

Thermal Conductivity

The relatively low thermal conductivity of any cellular concrete is due to air-filled pores [26]. The thermal conductivity, k -value, of aerated concrete depends primarily on its density. Other factors such as moisture content, temperature level, pore structure, and raw materials also effect the thermal conductivity [1]. The relationship between the thermal conductivity and the density of dry specimens of autoclaved aerated concrete is given in Fig. 7 [1].

As expected, thermal conductivity increases with an increase in moisture content [1, 10, 64, 72, 73]. Data in the CEB Manual [1] indicate that this relationship is linear for moisture contents up to 20% by weight. As an illustration of the relationship, the average value of thermal conductivity for a material with a dry density of 31 lbm/ft³ (500 kg/m³) was shown to be about 0.76 Btu in./ft² h °F (0.11 W/mK) at zero moisture content, whereas it was shown to be 1.1 Btu in./ft² h °F (0.15 W/mK) at 10% moisture content by weight [1].

For lightweight concretes in general, Valore [74] suggested a single moisture factor that consists of a 6% increase in thermal conductivity for each 1% of moisture, by weight, relative to oven dry density. A constant moisture content of 4% by volume was proposed for lightweight concrete walls having a density of 25 lbm/ft³ (400 kg/m³), protected from rain penetration.

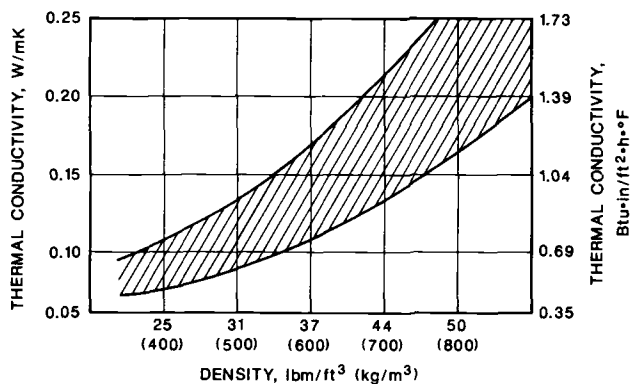


FIG. 7—Relationship between thermal conductivity and density of dry specimens of autoclaved aerated concrete (from CEB Manual [1], courtesy of CEB and the Construction Press).

Energy Considerations

As stated in the introduction to this report, a major advantage influencing the use of autoclaved aerated concrete products has been the relatively low thermal conductivity combined with load-carrying capacity. This factor has been noted by numerous authors who have reported on the properties and performance of autoclaved aerated concretes [e.g., 1,5-7, 10,19,21,24,28,38].

Bave [6,10,38] has summarized the development and growth in use of autoclaved aerated concrete, particularly noting the factors affecting energy conservation. The use of this material originated in northern European countries where thermal insulation has been a long-time concern due to cold climates and a dependency on imported fuel. Subsequently, its use expanded to warm climates where its low thermal conductivity offered advantages for energy savings in cooling buildings. Bave [6] has indicated that autoclaved aerated concrete, in many geographic locations, satisfies both thermal and load-bearing requirements while offering an overall energy saving. He did not indicate the details of these requirements.

In addition to energy considerations associated with use of a low thermal conductivity material, Bave [6,10] also pointed out qualitatively other factors regarding energy savings in the use of autoclaved aerated concrete. These factors included raw materials, the production process, and transportation and erection of the manufactured units. As an example, he stated that the relatively low weight of aerated concrete building units allows cuts in the energy consumption due to handling and erection on site.

Kohler [7] has presented the results of a study on the energy costs for the production and use of autoclaved aerated concrete, taking into account direct and indirect energy costs. He compared the energy costs for production of different types of walls having equivalent thermal and load-bearing properties. Among his findings, he reported that the separation of the thermal and load-bearing functions (i.e., composite wall with thermal insulation and structural element) leads generally to lower overall energy costs. For example, he found that the energy costs for a composite autoclaved aerated concrete wall with expanded polystyrene insulation were about 8% less than those for the equivalent wall comprised only of autoclaved aerated concrete.

Kohler [7] also modeled the energy performance of complete buildings whereby the use of autoclaved aerated concrete floors, walls, and ceilings was compared with the same elements of conventional materials. A significant finding was that, in the case of energy-efficient houses, "... it was not possible to reach the insulation requirements by aerated concrete only even by using very large sections." He indicated that, in these cases, autoclaved aerated concrete has to be used together with a material which is specifically a thermal insulation.

In this regard, Kohler's findings may be related to current practice (as recommended by ASHRAE) in the United States for opaque walls and roofs of new buildings except low-rise residential. For relatively severe climatic locations having 6500 heating degree days or more, the minimum total thermal resistance (R-value) of walls is about 20, whereas for roofs it is about 30 [75]. An autoclaved aerated concrete wall, 8 in. (20 cm) thick and having a density of 31 lbm/ft³ (500 kg/m³) may have an R-value about 11 [28]. A 6 in. (15 cm) roof slab of similar density material would have an R-value of about 8. Obviously, for both the wall and the roof, additional thermal insulation would be needed to attain an R-value of 20 to 30. In contrast, in areas of the United States having mild climates, autoclaved aerated concrete alone may satisfy insulation needs.

Recently Frey and Briesemann [5] studied the factors affecting the primary energy costs to produce autoclaved aerated concrete. They found that, for the plants studied, raw materials production, raw materials transportation, and actual factory production accounted for 60%, 5%, and 35% of the energy costs, respectively. They indicated that the process is currently very energy efficient and consequently substantial energy savings cannot be expected in the future. Where reductions are accomplished, they will be associated with improvements in cementitious binder technology.

Standards and Related Documents

Since autoclaved aerated concrete has been used extensively worldwide, standards and related documents have been developed in many countries. With the exception of the previously mentioned CABO [45] and HUD [46] documents, no standards and codes have been developed in the United States. Recently, RILEM⁵ Technical Committee 78-MCA on Model Code for Aerated Concrete Based on RILEM Testing Methods [76] has compiled, as a working document, a list of "Standards and Regulations Concerning Building and Buildings Constructed with Autoclaved Aerated Concrete." The titles of these documents, as listed by the RILEM committee, are given in a National Bureau of Standards report [18].

Summary

This report is a review of the properties and performance of autoclaved aerated concrete. This is a construction material that has gained widespread use in many areas of the world. Little use has occurred in Canada and the United States. It is a lightweight porous concrete whose cellular structure is generally obtained through an *in-situ* gas-producing reaction. Subsequent autoclaving in the factory provides strength, dimensional stability, and other properties of the finished product. These materials combine a relatively low thermal conductivity with a load-bearing capacity suitable for use in structural applications. This combination of properties might make them attractive for energy-conserving applications.

The review addressed an overview of the manufacturing process, uses of autoclaved aerated concrete in building constructions, properties, energy considerations, the availability of code-related documents, and standards. Uses include block and panel construction in load-bearing and non-load-bearing applications for walls, floors, and roofs. With regard to energy considerations, the review pointed out that, for energy-efficient applications under severe climate conditions, the autoclaved aerated concrete unit alone may be insufficient to provide the targeted minimum value of thermal resistance. In these cases, autoclaved aerated concrete has to be used together with additional thermal insulation. In contrast, in areas of the United States having mild climates, autoclaved aerated concrete alone may satisfy insulation needs.

⁵RILEM is a French acronym for International Union of Testing and Research Laboratories for Materials and Structures.

Acknowledgments

This study was sponsored by the U.S. Department of Energy, Office of Conservation and Renewable Energy. The authors appreciate the support and assistance of William Gerken (DOE) and David McElroy (ORNL), who both provided liaison between DOE and NBS. The authors also thank their NBS colleagues, James Pielert, James Clifton, Geoffrey Frohnsdorff, and Daniel Gross, who gave important review comments on this report. The authors acknowledge the excellent support of Denise Herbert for typing the manuscript. Finally, special thanks are expressed to Samuel Aroni, University of California at Los Angeles, Poul Nerenst, H + H Industri, Denmark, and Gunnar Bave, Siporex, Sweden, who visited NBS to discuss their experiences regarding the properties and performance of autoclaved aerated concretes. Their valuable review comments on this report are appreciated.

References

- [1] "Autoclaved Aerated Concrete: CEB Manual of Design and Technology," Comité Euro-International du Béton (CEB), The Construction Press, New York, 1978, 90 pages.
- [2] Tabak, R., "Differential Thermogravimetric Analysis in Autoclaved Cellular Concrete Research," in *Thermal Analysis*, Vol. 3, Proceedings of 4th ICTA, Budapest, 1974, pp. 525-532.
- [3] Leitch, F. N., "The Properties of Aerated Concrete in Service," in *Proceedings*, Second International Congress on Lightweight Concrete, The Concrete Society, London, 14-15 April 1980, pp. 97-113.
- [4] Bessey, G. E., "The History and Present Day Development of the Autoclaved Calcium Silicate Building Products Industries," in *Proceedings*, Symposium on Autoclaved Calcium Silicate Building Products, University of London, Society of the Chemical Industry, 18-21 May 1965, pp. 3-6.
- [5] Frey, E. and Briesemann, D., "More Recent Calculations of the Primary Energy Costs of Autoclaved Aerated Concrete," *Betonwerk und Fertigteil-Technik*, No. 7, 1985, pp. 468-472.
- [6] Bave, G., "Climatic Conditions and Energy," in *Autoclaved Aerated Concrete: Moisture and Properties*, F. H. Wittmann, Ed., Elsevier, Amsterdam, 1983, pp. 1-12.
- [7] Kohler, N., "Global Energetic Budget of Aerated Concrete," in *Autoclaved Aerated Concrete: Moisture and Properties*, F. H. Wittmann, Ed., Elsevier, Amsterdam, 1983, pp. 13-26.
- [8] "Autoclaved Aerated Concrete," *Building Digest*, Central Building Research Institute, India, No. 86, Dec. 1970, 3 pages.
- [9] Korovkevich, V. V., "The Use of Low-Density Aerated Concrete in Load-Bearing Structures for Residential and Public Buildings in the U.S.S.R.," in *Proceedings*, 1st International Congress on Lightweight Concrete, Vol. 2, Cement and Concrete Association, London, May 1968, p. 179.
- [10] Bave, G., "Aerated Concrete—How it Conserves Energy," *Housing Science*, Vol. 5, No. 1, 1981, pp. 73-81.
- [11] Bessey, G. E., "Author's Introduction," in *Proceedings*, 1st International Congress on Lightweight Concrete, Vol. 2, Cement and Concrete Association, London, May 1968, p. 161.
- [12] Bessey, G. E., "The World Development and Economic Significance of the Aerated Concrete Industry," in *Proceedings*, 1st International Congress on Lightweight Concrete, Vol. 1, Cement and Concrete Association, London, May 1968, pp. 203-212.
- [13] Valore, R. C., Jr., "Cellular Concretes: Part 1—Composition and Methods of Preparation," *ACI Journal*, Vol. 25, May 1954, pp. 773-796.
- [14] "Concrete Product Gets First U.S. Use," *Building Design and Construction*, Vol. 27, No. 6, June 1986, p. 26.
- [15] Houst, Y. and Wittmann, F. H., "Bibliography on Autoclaved Aerated Concrete," in *Autoclaved Aerated Concrete: Moisture and Properties*, F. H. Wittmann, Ed., Elsevier, Amsterdam, 1983, pp. 325-369.
- [16] *Autoclaved Aerated Concrete: Moisture and Properties*, F. H. Wittmann, Ed., Developments in Civil Engineering, No. 6, Elsevier, Amsterdam, 1983, 380 pages.
- [17] Valore, R. C., Jr., "Cellular Concretes: Part 2—Physical Properties," *ACI Journal*, Vol. 25, June 1954, pp. 817-836.
- [18] Mathey, R. G. and Rossiter, W. J., Jr., "A Review of Autoclaved Aerated Concrete Products," NBSIR 87-3670, National Bureau of Standards, March 1988, 79 pages.
- [19] Merlet, J.-D., "Cellular Autoclaved Concrete," *CSTB Magazine*, No. 23, Jan.-Feb. 1984, p. 2.
- [20] Ironman, R., "Cellular Concrete Gains Worldwide Strength," *Concrete Products*, July 1977.
- [21] Shrivastava, O. P., "Lightweight Aerated or Cellular Concrete—A Review," *Indian Concrete Journal*, Jan. 1977, pp. 18-23.

- [22] Kritov, V. A., Skatynsky, V. I., Chikota, E. I., and Udachkin, I. B., "Building Enclosing Structures Made of Energy Saving Autoclave Concrete," in *Proceedings*, CIB 83, 1983, pp. 145-152.
- [23] Bennett, R. P., Furgeaud, R., and Paljak, I., "Le Beton Cellulaire Autoclave: Propriétés et Utilisations," *Annales de l'Institut Technique du Batiment et des Travaux Public*, No. 376, Oct. 1979, pp. 74-102.
- [24] "Autoclaved Aerated Concrete," Building Research Establishment Digest, Digest 178, Building Research Station, Garston, Watford, England, June 1975, 4 pages.
- [25] Schulze, W. and Gunzler, J., "Corrosion Protection of the Reinforcement in Lightweight Concrete," in *Proceedings*, 1st International Congress on Lightweight Concrete, Vol. 1, Cement and Concrete Association, London, May 1968, pp. 111-122.
- [26] Dunn, R. H., "Precast Low Density Concrete Units," Paper SP 29.9, in *Lightweight Concrete*, Publication SP 29, American Concrete Institute, Detroit, 1971, pp. 147-159.
- [27] Crosier, C. M., "Effects of Variations in Curing Factors on the Strength of Autoclaved Aerated Concrete," Paper SP 32-10, in *Menzel Symposium on High Pressure Steam Curing*, Publication SP-32, American Concrete Institute, Detroit, 1972, pp. 193-219.
- [28] Edlind, O., "Some Properties and Practical Aspects of Hardened Aerated Concrete: Swedish Experience," in *Proceedings*, 1st International Congress on Lightweight Concrete, Vol. 1, Cement and Concrete Association, London, May 1968, pp. 77-87.
- [29] Svanholm, G., "The Use of Storey High Units of Aerated Concrete for External Walls and for Cellars," in *Proceedings*, 1st International Congress on Lightweight Concrete, Vol. 2, Cement and Concrete Association, London, May 1968, pp. 76-82.
- [30] Wennstrom, I., "The Use of Aerated Concrete Units for Low-Rise Housing: Planning and Design, Architectural Properties and Some Experience with Completed Houses," in *Proceedings*, 1st International Congress on Lightweight Concrete, Vol. 1, Cement and Concrete Association, London, May 1968, pp. 65-75.
- [31] Nettleton, C. N., "Advantages and Limitations of Large Aerated Concrete Units," in *Proceedings*, 1st International Congress on Lightweight Concrete, Vol. 2, Cement and Concrete Association, London, May 1968, pp. 164-165.
- [32] Makarichev, A. A., "Author's Introduction," in *Proceedings*, 1st International Congress on Lightweight Concrete, Vol. 2, Cement and Concrete Association, London, May 1968, pp. 161-163.
- [33] Gemmel, C., "Developments in the Use of Aerated Concrete in Sweden," in *Proceedings*, 1st International Congress on Lightweight Concrete, Vol. 2, Cement and Concrete Association, London, May 1968, pp. 90-91.
- [34] Purvis, J. F., "Finishes on Aerated Concrete," in *Proceedings*, Symposium on Autoclaved Calcium Silicate Building Products, University of London, Society of the Chemical Industry, 18-21 May 1965, pp. 252-258.
- [35] Stromberg, J., "Some Technical Data Concerning a New Type of Tongue-and-Groove Joints for Roof Slabs of Cellular Concrete," in *Proceedings*, Symposium on Autoclaved Calcium Silicate Building Products, University of London, Society of the Chemical Industry, 18-21 May 1965, pp. 234-238.
- [36] Bave, G., "New Applications of Siporex Large Size Aerated Concrete Units," in *Proceedings*, Symposium on Autoclaved Calcium Silicate Building Products, University of London, Society of the Chemical Industry, 18-21 May 1965, pp. 230-233.
- [37] Ulanichev, P. V., "The Various Products of an Aerated Concrete Factory in the U.S.S.R.," in *Proceedings*, 1st International Congress on Lightweight Concrete, Vol. 2, Cement and Concrete Association, London, May 1968, pp. 165-166.
- [38] Bave, G., "Aerated Lightweight Concrete—Current Technology," in *Proceedings*, Second International Congress on Lightweight Concrete, The Concrete Society, London, 14-15 April 1980, pp. 28-35.
- [39] Tietz, S. B., "Some Problems with Aerated Concrete," in *Proceedings*, 1st International Congress on Lightweight Concrete, Vol. 2, Cement and Concrete Association, London, May 1968, pp. 188-189.
- [40] Eden, N. B., Manthorpe, A. R., Miell, S. A., Szymanek, P. H., and Watson, K. L., "Autoclaved Aerated Concrete From Slate Waste: Part 1—Some Property/Density Relationships," *International Journal of Lightweight Concrete*, Vol. 2, No. 2, June 1980, pp. 95-100.
- [41] Polyakov, S. V. and Kotov, Y. I., "The Strength and Deformation of Aerated and Lightweight-Aggregate Concrete under Repeated Dynamic Loads," in *Proceedings*, 1st International Congress on Lightweight Concrete, Vol. 2, Cement and Concrete Association, London, May 1968, pp. 113-118.
- [42] Briesemann, D., "Structural Elements and Masonry of Autoclaved Aerated Concrete," in *Autoclaved Aerated Concrete: Moisture and Properties*, F. H. Wittmann, Ed., Elsevier, Amsterdam, 1983, pp. 257-266.
- [43] "Guide for Low Density Precast Concrete Floor, Roof, and Wall Units," ACI 523.2R68, Report by ACI Committee 523, American Concrete Institute, Detroit, rev. 1982, 6 pages.
- [44] "Building Code Requirements for Reinforced Concrete (ACI 318-83)," ACI 318-83, American Concrete Institute, Detroit, Sept. 1984, 111 pages.

- [45] Council of American Building Officials, Report NRB-192, April 1984, 4 pages.
- [46] U.S. Department of Housing and Urban Development, Materials Release No. 1062a, 19 March 1984, 5 pages.
- [47] Kinniburgh, W., "Moisture Content and Moisture Migration in Aerated Concrete," in *Proceedings*, Symposium on Autoclaved Calcium Silicate Building Products, University of London, Society of the Chemical Industry, 18-21 May 1965, pp. 174-181.
- [48] "A Guide to the Use of Waterproofing, Dampproofing, Protective and Decorative Barrier Systems for Concrete," ACI 515.1R-79, Report by ACI Committee 515, American Concrete Institute, Detroit, Sept. 1984, 41 pages.
- [49] Ahlstedt, E. T., "The Quality of Aerated Concrete Products in Sweden," in *Proceedings*, 1st International Congress on Lightweight Concrete, Vol. 2, Cement and Concrete Association, London, May 1968, pp. 103-104.
- [50] Aldrin, L., "Dimensional Accuracy of Aerated Concrete Wall Units," in *Proceedings*, 1st International Congress on Lightweight Concrete, Vol. 2, Cement and Concrete Association, London, May 1968, pp. 82-84.
- [51] Nakano, S. and Tada, S., "Optimum Performance Design for Cellular Concrete Outer Wall," in *Proceedings*, 3rd ASTM/CIB/RILEM Symposium, Performance Concept in Building, 29,30,31 March-1,2 April 1982, pp. 373-385.
- [52] Cividini, B., "Investigation of Long Time Deflection on Reinforced Aerated Concrete Slabs," in *Autoclaved Aerated Concrete: Moisture and Properties*, F. H. Wittmann, Ed., Elsevier, Amsterdam, 1983, pp. 267-282.
- [53] Kruml, R., "Influence of Saturation Degree on Autoclaved Aerated Concretes on Their Creep," in *Autoclaved Aerated Concrete: Moisture and Properties*, F. H. Wittmann, Ed., Elsevier, Amsterdam, 1983, pp. 249-256.
- [54] Nielsen, A., "Some Experiments on the Creep of Aerated Concrete," in *Proceedings*, 1st International Congress on Lightweight Concrete, Vol. 2, Cement and Concrete Association, London, May 1968, pp. 105-106.
- [55] Houst, Y., Alou, F., and Wittmann, F. H., "Influence of Moisture Content on Mechanical Properties of Autoclaved Aerated Concrete," in *Autoclaved Aerated Concrete: Moisture and Properties*, F. H. Wittmann, Ed., Elsevier, Amsterdam, 1983, pp. 219-234.
- [56] Nakano, S. and Tada, S., "Durability Criteria for Cellular Concrete Outer Wall," in *Proceedings*, 2nd International Conference on the Durability of Building Materials and Components, National Bureau of Standards, 14-16 Sept. 1981, pp. 232-241.
- [57] Ryan, J. V. and Bender, E. W., "Fire Tests of Precast Cellular Concrete Floors and Roofs," NBS Monograph 45, 12 April 1962, 12 pages.
- [58] Purins, E., "The Frost Resistance of Aerated Concrete," in *Proceedings*, 1st International Congress on Lightweight Concrete, Vol. 2, Cement and Concrete Association, London, May 1968, pp. 94-100.
- [59] Roulet, C. A., "Expansion of Aerated Concrete Due to Frost-Determination of Critical Saturation," in *Autoclaved Aerated Concrete: Moisture and Properties*, F. H. Wittmann, Ed., Elsevier, Amsterdam, 1983, pp. 157-170.
- [60] Larsson, L. and Purins, E., "Determination of the Critical Degree of Saturation for Autoclaved Lightweight Aerated Concrete by Studying Deformations in Single-Cycle Freezing Tests," *International Journal of Lightweight Concrete*, Vol. 2, No. 1, 1980, pp. 33-41.
- [61] Jennings, B. M., "Versatility and Serviceability of Aerated Concrete Units," in *Proceedings*, 1st International Congress on Lightweight Concrete, Vol. 2, Cement and Concrete Association, London, May 1968, pp. 82-86.
- [62] Custance, R. M., "Fixings to Autoclaved Aerated Concrete Building Elements," in *Proceedings*, Symposium on Autoclaved Calcium Silicate Building Products, University of London, Society of the Chemical Industry, 18-21 May 1965, pp. 216-219.
- [63] Grimer, F. J. and Brewer, R. S., "The Within Cake Variation of Autoclaved Aerated Concrete," in *Proceedings*, Symposium on Autoclaved Calcium Silicate Building Products, University of London, Society of the Chemical Industry, 18-21 May 1965, pp. 163-170.
- [64] Svanholm, G., "Influence of Water Content on Properties," in *Autoclaved Aerated Concrete: Moisture and Properties*, F. H. Wittmann, Ed., Elsevier, Amsterdam, 1983, pp. 119-130.
- [65] Dworjadkin, A. and Maalinowski, R., "Porosity, Compressive Strength and Volume Changes of Autoclaved Aerated Concrete," in *Proceedings*, Symposium on Autoclaved Calcium Silicate Building Products, University of London, Society of the Chemical Industry, 18-21 May 1965, pp. 174-181.
- [66] Grimer, F. J. and Brewer, R. S., "The Effect of the Environment on the Strength of Autoclaved Aerated Concrete," in *Proceedings*, Symposium on Autoclaved Calcium Silicate Building Products, University of London, Society of the Chemical Industry, 18-21 May 1965, pp. 182-187.
- [67] Regan, P. E., "Shear in Reinforced Aerated Concrete," *International Journal of Lightweight Concrete*, Vol. 1, No. 2, 1979, pp. 47-61.

- [68] Briesemann, D., "A Method of Calculating the Shear Resistance of Reinforced Slabs and Beams of Autoclaved Aerated Concrete," *International Journal of Lightweight Concrete*, Vol. 2, No. 1, 1980, pp. 21-31.
- [69] Tada, S. and Nakano, S., "Microstructural Approach to Properties of Moist Cellular Concrete," in *Autoclaved Aerated Concrete: Moisture and Properties*, F. H. Wittmann, Ed., Elsevier, Amsterdam, 1983, pp. 71-90.
- [70] Prim, P. and Wittmann, F. H., "Structure and Water Absorption of Aerated Concrete," in *Autoclaved Aerated Concrete: Moisture and Properties*, F. H. Wittmann, Ed., Elsevier, Amsterdam, 1983, pp. 55-69.
- [71] Schwiete, H. E. and Ludwig, U., "The Porosity and Gas Permeability of Aerated Concrete," in *Proceedings, Symposium on Autoclaved Calcium Silicate Building Products*, University of London, Society of the Chemical Industry, 18-21 May 1965, pp. 188-194.
- [72] Loudon, A. G., "The Effect of Moisture Content on Thermal Conductivity," in *Autoclaved Aerated Concrete: Moisture and Properties*, F. H. Wittmann, Ed., Elsevier, Amsterdam, 1983, pp. 131-142.
- [73] Hums, D., "Relation Between Humidity and Heat Conductivity in Aerated Concrete," in *Autoclaved Aerated Concrete: Moisture and Properties*, F. H. Wittmann, Ed., Elsevier, Amsterdam, 1983, pp. 143-152.
- [74] Valore, R. C., Jr., "Calculation of U-Values of Hollow Concrete Masonry," *Concrete International - Design & Construction*, Vol. 2, No. 2, Feb. 1980, pp. 40-63.
- [75] ASHRAE Standard ANSI/ASHRAE/IES 90.1 P, "Proposed American National Standard for Energy Efficient Design of New Buildings Except Low-Rise Residential Buildings," Chapter 8, 22 Aug. 1986, p. 8-58.
- [76] Wittmann, F. H. and Houst, Y., "Standards and Regulations Concerning Building and Buildings Constructed with Autoclaved Aerated Concrete," 2nd rev. version, Working Document, RILEM Technical Committee 78-MCA.

Magnesium Oxychloride-Based Foam Thermal Insulation: An Initial Investigation

REFERENCE: Rossiter, W. J., Jr., and Brown, P. W., "Magnesium Oxychloride-Based Foam Thermal Insulation: An Initial Investigation," *Insulation Materials, Testing, and Applications, ASTM STP 1030*, D. L. McElroy and J. F. Kimpflen, Eds., American Society for Testing and Materials, Philadelphia, 1990, pp. 38-51.

ABSTRACT: This study is an initial investigation of the properties and performance of magnesium oxychloride-based foam thermal insulation. Tests and observations were performed on samples prepared in the laboratory and also removed from one cavity of a wall of a wood-frame house. The tests to characterize the foam included measurements of density, moisture content, shrinkage, and thermal conductivity, and were combined with analysis using X-ray diffraction, scanning electron microscopy, and thermogravimetry techniques.

It was found that the foam had a thermal conductivity comparable to that of other insulations used to retrofit walls of houses. Shrinkage could not be quantified, but was seen to be generally small. The moisture content of the foam removed from the house was about 2%. The results of the analytical measurements indicated that the laboratory-prepared samples and some of those removed from the house were not identical. It was suggested that further analysis be conducted to continue characterization of the foam.

KEY WORDS: characterization, density, foam, insulation, magnesium oxychloride cement, moisture content, SEM, shrinkage, thermal analysis, thermal conductivity, X-ray diffraction

Introduction

Background

For the past decade, the Building Materials Division of the National Bureau of Standards (NBS) has provided technical assistance to the U.S. Department of Energy (DOE) in assessing the properties and performance of insulation materials. This has included new or non-conventional insulation materials used for retrofitting uninsulated cavities in walls of buildings. Some of these studies have summarized available technical data on the insulation and recommended research to fill in gaps in the information data base [1].

About five years ago, a new low-density (about 32 kg/m³ or 2.0 lbm/ft³) inorganic foam insulation, based on magnesium oxychloride cement technology, became available in the United States [2]. The chemical composition has not been described in the archival literature, but the manufacturer has indicated that it is described as a calcium magnesium oxychloride silicate composition [2]. The insulation has been used in constructions such as new and existing wood-frame, steel-stud and masonry cavity walls, curtain walls, and for filling hollow-cores in masonry block walls.

The insulation is foamed-in-place from aqueous solutions at the building site in a manner

¹Building Materials Division, Center for Building Technology, National Bureau of Standards, Gaithersburg, MD 20899.

similar to some plastic foams. The unset foam insulation may be pumped under pressure into closed cavities where access is obstructed and which may be difficult to fill with loose-fill insulation. After application, the foam hardens in place to a self-supporting material.

A review report on available data on the properties and performance indicated the characterization of the foam as thermal insulation was not complete, and research was needed to provide data [2]. Properties for which the available data were limited included composition and structure, durability, effect on other building materials, shrinkage, and water absorption.

This paper presents data on the properties and performance of the oxychloride cement-based foam insulation. Foam samples, prepared in the laboratory and removed from a wood-frame house, were included in the study. Measurements of density, moisture content, thermal conductivity, and shrinkage were combined with X-ray diffraction (XRD), scanning electron microscopy (SEM), and thermogravimetric (TG) analyses.

Manufacture of Magnesium Oxychloride Cement-Based Foam

The manufacture of the low-density foam insulation involves: an aqueous cementitious slurry (based on magnesium oxychloride technology), a surfactant (or foaming agent) solution for cell generation, compressed air, and a mixing (or foaming) gun [2]. The foaming agent is first pumped into the gun, where the compressed air mixes with it in an expansion chamber, and expands it into foam bubbles. Just before the bubbles exit from the nozzle of the gun, they are mixed with the cementitious slurry, which has been pumped through a separate line into the gun. The foam is then pumped from the gun. Expansion of the foam is complete at this point, and no expansion occurs after installation. Initial hardening of the foam proceeds to an extent sufficient for it to be self-supporting as it exits the gun. Complete hardening reportedly occurs a few weeks after application. When it exits from the nozzle of the foaming gun, the unset low-density foam reportedly contains about 50 to 60% water by mass [2].

Experimental Procedure

Laboratory foam samples were prepared in wooden boxes and, periodically, the boxes were opened to observe shrinkage. Foam specimens were removed from the opened boxes, and the selected properties were determined. In addition, a section of a exterior wall of a house was opened to observe the foam in service and to obtain a specimen for laboratory testing.

Laboratory-Preparation of Foam Samples

A commercially available foam was prepared by manufacturer representatives according to their prescribed application techniques. The formulation of the foam was proprietary. Boxes, with interior dimensions of 610 × 610 × 90 mm (24 × 24 × 3.5 in.) and constructed from exterior-grade plywood and nominal 2 × 4 wooden studs, were filled with foam. After filling, the boxes were maintained with a long dimension in a vertical position at 23 ± 3°C (73 ± 5°F) and 45 ± 5% relative humidity. Periodically, the boxes were opened for shrinkage observations and removal of test specimens. These specimens are subsequently referred to as *laboratory specimens*.

Foam Samples from the Field

Foam specimens were obtained from a wood-frame house located in a rural northwest suburb of Washington, D.C. The wall construction consisted of nominal 2 × 4 wooden stud framing with a lath and plaster interior facing, and a rough-sawn wooden plank sheathing and painted wooden siding as the exterior facing. No membrane-type vapor retarder was found in the wall

cavity. The foam had been installed in the walls of the house about one year before the sampling. Specimens removed from the house are subsequently referred to as *field specimens*.

In October 1986, an exterior wall section, about 0.2 m² (2 ft²) in area, was opened across one cavity (space between adjacent studs) to observe the *in situ* foam insulation and to remove samples. Some of the samples were sealed in glass jars for subsequent determination of density and moisture content. After removal of the foam, the empty cavity space was filled with fibrous glass insulation and the wall was closed using the original sheathing and siding.

Measurement of Linear Shrinkage and Density

Linear shrinkage of the foam samples in the wooden boxes was measured using a rule or calipers graduated in millimetres in accordance with a procedure that had been previously developed for cellular plastic insulation [3]. The boxes were opened for each measurement and then closed until the next determination. Shrinkage measurements were made 28, 96, and 195 days after foaming.

For purposes of this report, *wet density* is the density at installation when the foam contains the water present during formation and application. Wet density was calculated from the mass of wet foam applied in tared 1-gal metallic (to avoid moisture absorption) paint cans and the volume of the cans. Weighing was performed using an analytical balance with a sensitivity of 0.01 g.

To determine the amount of water present during application, the filled cans without lids were allowed to remain at ambient laboratory conditions and periodically reweighed. No provisions were made to avoid exposure to atmospheric carbon dioxide. Weighing was continued until a constant mass ($\pm 1\%$ difference between consecutive weighings over at least 24 h) was reached.

Dry density indicates the density of the foam insulation after it releases moisture present during application and it reaches equilibrium under normal laboratory environmental conditions. The foam in this condition is thus not totally "dry" in that no absorbed moisture is present. The dry density of foam was determined using samples removed from the wooden boxes. The procedure was according to that described in ASTM Test Method for Apparent Density of Rigid Cellular Plastics (D 1622).

Moisture Content

Percent moisture content (MC) of the foam specimens was determined by measuring mass changes occurring during heating for 16 h at $98 \pm 2^\circ\text{C}$ ($208 \pm 4^\circ\text{F}$) in a laboratory oven without mechanical convection:

$$\text{MC}\% = [(M_w - M_d)/M_d] \times 100$$

where

M_w = mass of wet foam before heating, and

M_d = mass of dry foam after heating.

Mass of the specimens was determined using an analytical balance having a sensitivity of 0.01 g.

Measurement of Thermal Conductivity

Thermal conductivity measurements were carried out in accordance with ASTM Test Method for Steady-State Heat Flux Measurements and Thermal Transmission Properties by Means of the Guarded-Hot-Plate Apparatus (C 177). The metering area of the hot plate used

was circular with a diameter of 400 mm (16 in.). The insulation specimen, having dimensions of $584 \times 584 \times 69$ mm ($23 \times 23 \times 2.7$ in.) was placed in a wooden frame with a thin non-metallic bottom screen to hold the specimen during testing. The specimen was cut to the frame size with a wire to avoid damage. The thickness of the specimen was slightly greater than the wooden frame so that the top surface of the specimen was in contact with the cold plate of the guarded hot plate. The bottom screen surface of the wooden frame was placed directly on the hot plate. The thermal conductivity measurements were at 12, 24, and 38°C (44, 75, and 100°F), with a temperature differential across the specimen of 28°C (50°F). The hot plate apparatus was operated in a one-sided mode, as described in ASTM Practice for Using the Guarded-Hot-Plate Apparatus in the One-Sided Mode to Measure Steady-State Heat Flux and Thermal Transmission Properties (C 1044).

X-Ray Diffraction Analysis

X-ray diffraction (XRD) provides a means for identifying the crystalline phases in a sample [4]. Specimens were prepared for X-ray diffraction analysis by grinding samples of the foam insulation in an agate mortar and pestle. The resultant powders were back loaded into specimen holders to minimize preferred orientation. Specimens were step scanned from 4° to 65° 2θ (specific angle) at a scan rate of 0.02°/s.

SEM Specimen Preparation and Analysis

Scanning electron microscopy (SEM) analyses were conducted to characterize the cellular structure of the foam specimens. The SEM technique provides good depth of field at high magnification [5]. The foam specimens for SEM analysis were cut into cylinders of about 10 to 15 mm (0.4 to 0.6 in.) length and with 10 to 12 mm (0.4 to 0.5 in.) diameters. Two SEM specimen mounting stubs with 12 mm (0.5 in.) diameters were bonded to the ends of the cut specimens with an epoxy adhesive. When the adhesive had cured, the mounting stubs were pulled in opposite directions, breaking the single cut specimen into two mounted specimens with fractured surfaces.

The mounted specimens were sputter coated with a nominal 20 nm (8×10^{-7} in.) gold conductive film to prevent surface electron charging during SEM analysis. The fractured surfaces were examined in the SEM using an acceleration voltage of 30 kV and photographed at magnifications from $\times 20$ to $\times 2000$.

Thermogravimetric Analysis

The thermogravimetry (TG) technique determines the mass change of a sample as a function of temperature [6]. Foam specimens for thermogravimetric analysis were cut from large samples using a laboratory scalpel. The specimens (about 2.6 to 3.8 mg) were heated from 40 to 490°C (104 to 914°F) in nitrogen gas at a rate of 1°C/min (1.8°F/min). The nitrogen flow rate was 40 mL/min. The analyzer instrument was evacuated and then filled with nitrogen prior to each run.

Results and Discussion of Laboratory Measurements

Density and Moisture Content

Wet Density—The average wet density of the foam was 89 kg/m³ (5.6 lbm/ft³) (Table 1). Thirty-eight (38) days were required for the wet foam in the metal cans to dry to constant mass. During this time, the foam samples in the cans lost about 135 g (0.30 lbm) of water or 40% of their initial wet mass. The dry density of the samples in the cans was not determined.

TABLE 1—Results of density measurements.

Specimen	No. of Determinations	Density		COV, ^a %
		kg/m ³	lbm/ft ³	
Lab, wet	3	89	5.6	1.0
Lab, dry (28 days)	4	44	2.8	4.4
Lab, dry (96 days)	4	46	2.9	3.5
House, dry	3	48	3.0	3.3

^aCoefficient of Variation.

Dry Density—The first specimens removed from the boxes were found to contain moisture, indicating that the foams applied in the wooden boxes had not dried in 28 days. These specimens were placed on an open shelf in the laboratory to dry under normal conditions. Nine days were required for equilibrium mass to be reached under normal laboratory conditions. During that time, about 25% of the initial mass was lost, which provided evidence that some of the initial moisture in the laboratory samples was lost in the wooden boxes. The average dry density of the foam was 44 kg/m³ (2.8 lbm/ft³) (Table 1). When they were heated for 16 h at 98 ± 2°C (208 ± 4°F), they lost, on the average, an additional 1.7% of their mass. Heating for another 16-h period produced no significant additional change in mass. The mass lost on heating was taken to be moisture.

Density specimens were again removed from the wooden boxes 96 days after foaming. In this case, the average value of dry density was 46 kg/m³ (2.9 lbm/ft³) (Table 1). In contrast to the specimens removed from the wooden boxes after 28 days, the 96-day specimens were essentially at equilibrium moisture content.

The dry density of three specimens removed from the house was also determined. The average value was 48 kg/m³ (3.0 lbm/ft³) (Table 1). This density was comparable to the value for the laboratory specimens. The average mass loss on heating for the field specimens was 2.2%.

Shrinkage

Shrinkage of a foam insulation may cause air gaps that result in unwanted heat flow paths and thus lower the thermal efficiency of the insulated wall [7,8]. It was intended to measure the percent shrinkage of samples prepared in the wooden boxes. However, the shrinkage measurements on the laboratory samples could not be quantified, but were found to be generally small (see the paragraphs that follow). Quantification of shrinkage was precluded because, where cracks attributed to shrinkage were present, they were narrow in width and randomly located across the bulk of the foam. Under such conditions, it was not possible to determine the accumulated gap space (necessary for a shrinkage calculation) created by the shrinkage cracks.

All wooden boxes were opened by removing a plywood face 28 days after filling, and again after 96 and 195 days. The initial (28 day) observations showed that the boxes were essentially full. A few small gaps, penetrating through the foam from the front face of the box to the back face, were found in two foam samples. In all cases, the foam had adhered to the inner surfaces of the box. A narrow crack was visible near the box sides and near the perimeter of the foam samples. For each box, the width of the crack was immeasurably small using a rule or calipers graduated in millimetres. One box also had a narrow crack in the center of the foam. The presence of the cracks was attributed to minor shrinkage of the foam over the 28-day period. It was considered that the adhesion of the foam to the inner surface of the boxes was greater than the cohesive strength of the foam, resulting in the narrow shrinkage cracks near the perimeter of

the foam samples, and not between the foam and the sides of the box. After 96 and 195 days, the cracks were more readily apparent than during the first opening. In addition to the cracks near the perimeter of the foam, a number of cracks were found randomly throughout the bulk of the foam. The width of the cracks were variable, with many being about 1 to 2 mm (0.04 to 0.08 in.) wide. The narrowest were considered immeasurably small, whereas the largest were found to be about 5 to 7 mm (0.2 to 0.3 in.) wide. It is noted that a single gap of 7 mm (0.3 in.) over a distance of 610 mm (24 in.) would represent slightly greater than 1% shrinkage.

After six months exposure in the laboratory, the foam samples in the cans were observed to have shrunk more than (4.5 to 6%) those in the wooden boxes. Although the significance of this observation, particularly as related to the use of foams in wood-frame construction, is not defined, this finding is reported since it raises concerns that the factors affecting foam shrinkage are not completely understood.

Thermal Conductivity

The study plan was to perform thermal conductivity measurements on two specimens removed from the wooden boxes 28 days after foaming. These specimens would be allowed to remain at ambient laboratory conditions for one week before measurement. In this way, some residual moisture would remain in the foam, as would be considered typical of the foam in service where it would not be expected to be absolutely dry. The plan was to determine the thermal conductivity first on the "wet" specimens at a 24°C (75°F) mean temperature. Then, the specimens would be dried in an oven and, subsequently, additional thermal conductivity measurements would be made over a range of mean temperatures. However, it was found that specimens large enough for thermal conductivity measurements were difficult to handle due to the inherent friability of the insulation. This precluded carrying out the proposed measurement procedure. The first specimen was damaged during drying in an oven after the initial thermal conductivity measurement at 24°C (75°F). Thus, upon removal of the second specimen from the application box, it was placed in the hot plate apparatus after remaining at ambient laboratory conditions for a week. Thermal conductivity measurements were made at three mean temperatures without oven drying of the specimen.

The results of the thermal conductivity measurements are given in Table 2. The values are comparable to those measured for other retrofit insulations such as mineral fiber or cellulose [9]. The foam specimens used for thermal conductivity measurement contained two or three narrow (< 1 mm) random cracks which formed while they remained at ambient temperature upon removal from the wooden boxes. The thermal conductivity values for the specimens with

TABLE 2—Results of thermal conductivity measurements.

Specimen No.	Density	Mean Temp.	Thermal Conductivity
	kg/m ³ (lbm/ft ³)	°C (°F)	W/m · °C (Btu · in./h · ft ² · °F)
1	47 (2.9)	24 (75)	0.0430 (0.298)
2	46 (2.9)	12 (44)	0.0408 (0.283)
2	46 (2.9)	24 (75)	0.0425 (0.294)
2	46 (2.9)	38 (100)	0.0450 (0.312)

^aDensity was determined after the thermal conductivity was measured.

narrow cracks are reported, since cracks were observed in the foam sample examined in the house during the field phase of the study. The laboratory specimens for thermal conductivity were thus considered typical of that examined in the field. Also, as given in Table 2, the density of the laboratory specimens was comparable to that of the foam removed from the house. The extent to which the cracks in the laboratory specimens contributed to unwanted heat flow during the thermal measurements was not determined and requires further investigation.

Thermal conductivity values for Specimen 2 increased linearly with temperature, with a correlation coefficient of 0.997. After completion of the thermal conductivity tests, a section of the specimen was dried in a laboratory oven. It lost 1.8% of its mass during heating, which was comparable to the heating mass loss for other specimens in the present study.

The thermal conductivity value of $0.0430 \text{ W/m} \cdot ^\circ\text{C}$ ($0.298 \text{ Btu} \cdot \text{in.}/\text{h} \cdot \text{ft}^2 \cdot ^\circ\text{F}$) determined in the present study at 24°C (75°F) for a foam density of 47 kg/m^3 (2.9 lbm/ft^3) may be compared with a previously reported value. The literature reported value was $0.0371 \text{ W/m} \cdot ^\circ\text{C}$ ($0.257 \text{ Btu} \cdot \text{in.}/\text{h} \cdot \text{ft}^2 \cdot ^\circ\text{F}$) for a density of 33 kg/m^3 (2.1 lbm/ft^3) [2]. The literature reference did not specify the mean temperature of the test. The foam in the present study was found to have a thermal conductivity about 15% greater than that previously reported. The difference may possibly be attributed to the higher density of the foam in the present study, with perhaps some contribution due to the cracks in the specimens. This, of course, assumes that the mean temperature of the literature test was about ambient laboratory temperature.

X-Ray Diffraction

X-ray diffraction (XRD) analyses were carried out on two laboratory specimens and two field specimens. One of the field specimens was taken from the vicinity of the outer side of the wall cavity, and the other was the vicinity of the inner side of the cavity.

Analysis of the X-ray diffraction patterns obtained from the two laboratory specimens indicated that the two were identical. The field specimen obtained from the outer side wall cavity gave a diffraction pattern which was also found to be virtually identical to those of the laboratory specimens. These three specimens were characterized by strong diffraction peaks at 2.37 ($I/I_0 \approx 100$), 3.19 ($I/I_0 \approx 60$), and $1.57^\circ 2\theta$ ($I/I_0 \approx 50$).² Cole and Demediuk [10] have published X-ray diffraction data for magnesium oxychloride cements including the 3-form, $3\text{Mg}(\text{OH})_2 \cdot \text{MgCl}_2 \cdot 8\text{H}_2\text{O}$, and 5-form, $5\text{Mg}(\text{OH})_2 \cdot \text{MgCl}_2 \cdot 8\text{H}_2\text{O}$. A comparison of the positions and relative intensities of the above peaks from the present study with the Cole and Demediuk data [10] indicated that the foams contained some magnesium oxychloride material, but the percentage was not ascertained. The comparison also did not provide determination as to whether the oxychloride present was the 3-form or the 5-form or, if a mixture were present, the relative percentages of both.

Analysis of the field specimen from the vicinity of the inner side of the wall cavity also showed the presence of the above peaks. However, their intensities were significantly diminished. Rather, in this instance the following strong peaks were observed: 2.99 ($I/I_0 \approx 100$), 3.19 ($I/I_0 \approx 86$), 11.5 ($I/I_0 \approx 86$), and $3.02^\circ 2\theta$ ($I/I_0 \approx 79$). The presence of strong 11.5 and $3.01^\circ 2\theta$ peaks is suggestive of the presence of the chlorocarbonate phase, $\text{Mg}(\text{OH})_2 \cdot \text{MgCl}_2 \cdot 2\text{MgCO}_3 \cdot 6\text{H}_2\text{O}$, which forms as a result of the carbonation of the magnesium oxychloride cement. The reaction of carbon dioxide in air with magnesium oxychloride cements to form a carbonation product has been previously described [10, 11]. Sorrell and Armstrong [11] have reported that the carbonation reaction can be beneficial and have a stabilizing effect on the magnesium oxychloride cements.

² I/I_0 is the ratio of the given peak intensity to that of the most intense peak.

Scanning Electron Microscopy

SEM analysis was conducted on two laboratory specimens. The results indicated that the microstructures of the two were generally the same. Figure 1 shows a SEM photomicrograph taken of a laboratory specimen at $\times 20$ magnification. It is evident that the structure of the foam consists of cells that have a large variability in size. Each of the cells was seen to have a number of thin windows and ribs connecting the windows. Some of the windows were open in that no membrane was present, whereas others had membranes in place.

Figure 2 is a SEM photomicrograph at $\times 200$ magnification. Cell windows both with and without membranes are apparent. This figure also shows that the surface of the cells between the windows has a rough or pockmarked texture. In general, this surface roughness was typical of the cellular structure of the laboratory specimens. One exception was a limited area of one specimen in which a cell wall was found to have the appearance of needles.

SEM analysis were also performed on two field specimens for comparison with the photomicrographs of the laboratory specimens. As with X-ray diffraction, one field specimen was taken from the vicinity of the outer side of the wall cavity, and the other was taken near the inner side of the wall cavity. At low magnification (e.g., $\times 20$ – $\times 100$), the microstructure of the field specimens appeared to be the same as that of the laboratory specimens. However, higher magnification observations (e.g., $\times 500$) of the surfaces of the cells indicated a marked difference between the two field specimens. The microstructure of the specimen from the outer side of the cavity was comparable to that of the laboratory specimens. In contrast, in the case of the field specimen taken from the inner side of the cavity, needles were observed on the surface of many of the cells (Fig. 3).

The difference of surface characteristics of the microstructure of the two field specimens,

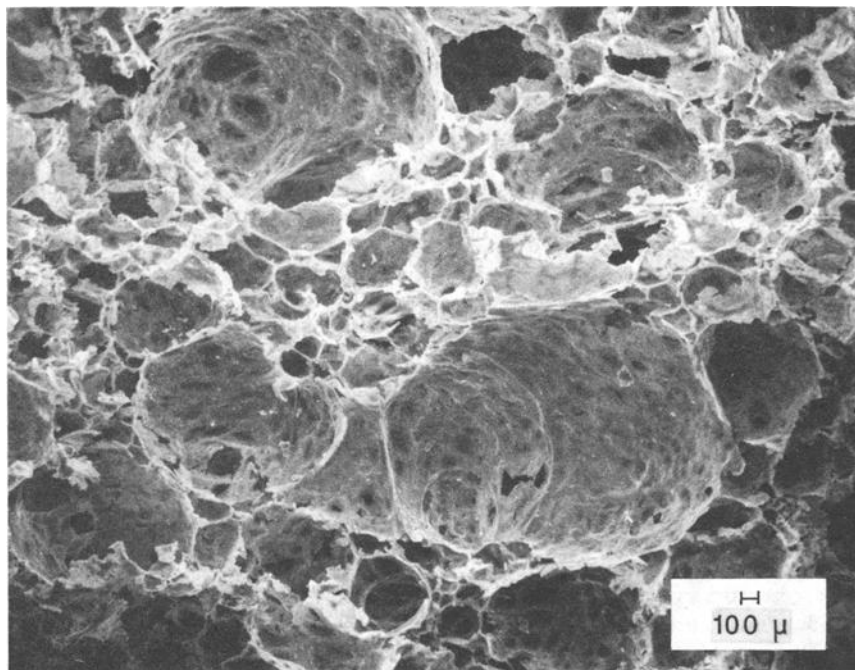


FIG. 1—SEM photomicrograph of a laboratory foam specimen at ($\times 20$ magnification).

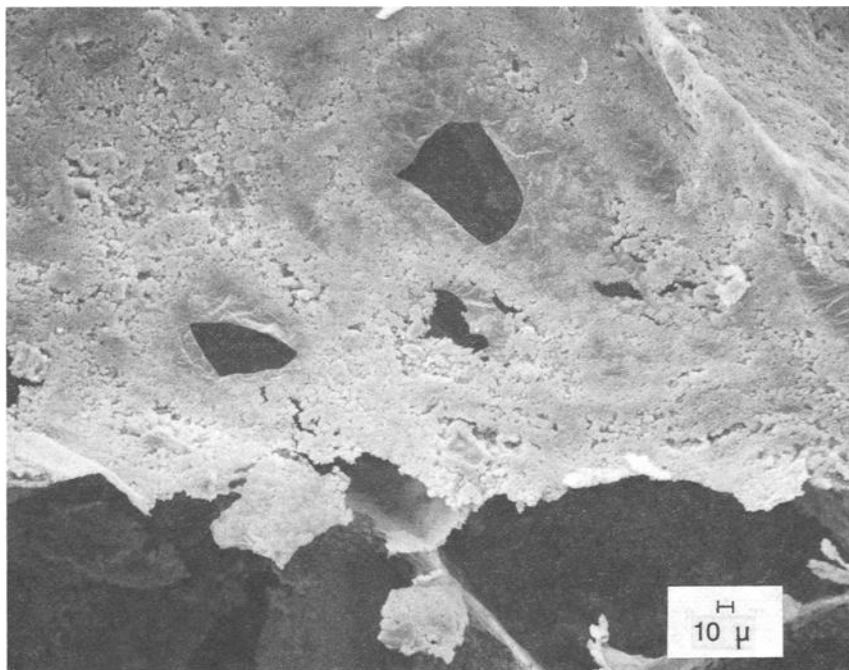


FIG. 2—SEM photomicrograph of a laboratory foam specimen at ($\times 200$ magnification).

observed by SEM analysis, was consistent with the results of the X-ray diffraction analysis. As discussed, X-ray analysis also showed the laboratory specimens to be essentially identical to the field specimen from the outer side of the cavity; on the other hand, the field specimen from the inner side was different, possibly having formed some chlorocarbonate. The formation of a chlorocarbonate may produce a change in the microstructure that was observed in the SEM analysis.

It is of interest to determine whether the needles observed in the limited section of cell wall of one laboratory specimen was due to incipient formation of the chlorocarbonate or other reaction product. Further investigation is required to examine this question.

Thermogravimetric Analysis

Thermogravimetric (TG) analyses were performed on foam specimens prepared in the laboratory and obtained from the field. As was the case of the SEM analyses, the field foam specimens were taken from locations near the outer and inner sides of the wall cavity. The results are presented in Fig. 4 and summarized in Table 3. In Table 3 the mass loss results are given for three temperature ranges: a low range between 40 to 175°C (104 to 347°F), a medium range between 175 to 300°C (347 to 572°F), and a high range from 300 to 450°C (572 to 914°F). The ranges were selected so that comparisons could be made (see below) with data for magnesium oxychloride cements presented by Cole and Demediuk [10].

A notable feature in Fig. 4 is that the mass loss curves for the laboratory specimens and field specimens are not the same. In particular, the laboratory-prepared specimens underwent about 30% total mass loss over the heating range, whereas the field specimens lost about 40% of their

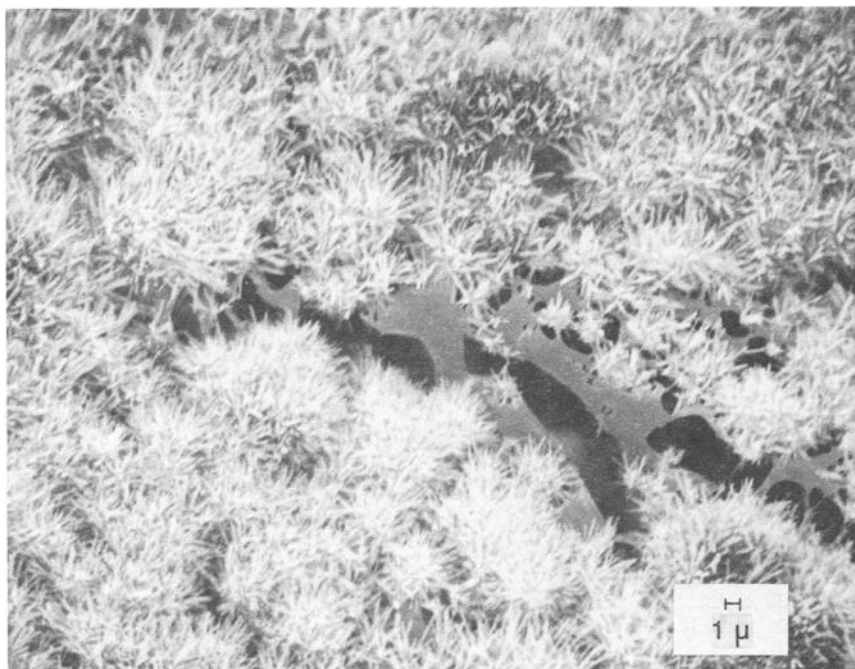


FIG. 3—SEM photomicrograph of a field foam specimen ($\times 2000$ magnification). The specimen was removed from the inner side of the wall cavity.

mass. The increased mass loss for the field specimens is accounted for by greater mass losses in all three temperature ranges as compared to the laboratory specimens (Table 3). These mass loss results cannot, at this time, be related to the chemical composition of the foam, since its formulation is proprietary.

The TG evidence regarding relative mass loss for the three temperature ranges suggests that the composition of the laboratory specimens and both field specimens may be different. This finding contrasts sharply with the results of the X-ray diffraction and SEM analyses which indicated the field specimen from the outer side of the cavity was essentially the same as the two laboratory specimens.

It is also evident from Fig. 4 that the mass loss curves for the replicate laboratory specimens are comparable. The shapes of the curves have marked similarity and the total mass loss over the heating range is closely the same (29% versus 32%). This result supports those of the X-ray diffraction and SEM analyses which indicated that the replicate laboratory specimens were generally the same.

In agreement with the results of the X-ray diffraction and SEM analyses, the TG evidence also suggests that two field specimens may be different from each other. In particular, the curves in the low temperature range have different slopes. The total weight loss during heating for the outside and inside field specimens was 39% and 44%, respectively.

The results of the thermogravimetric analyses in the present study can be compared to those reported by Cole and Demediuk [10] for the 3-form and 5-form magnesium oxychloride cements. Their data (included in Table 3) may be categorized into two major temperature regimes over which mass loss occurred: a low range from about 100°C (212°F) to about 175°C (347°F), and a high range of about 300 to 460°C (572 to 860°F).

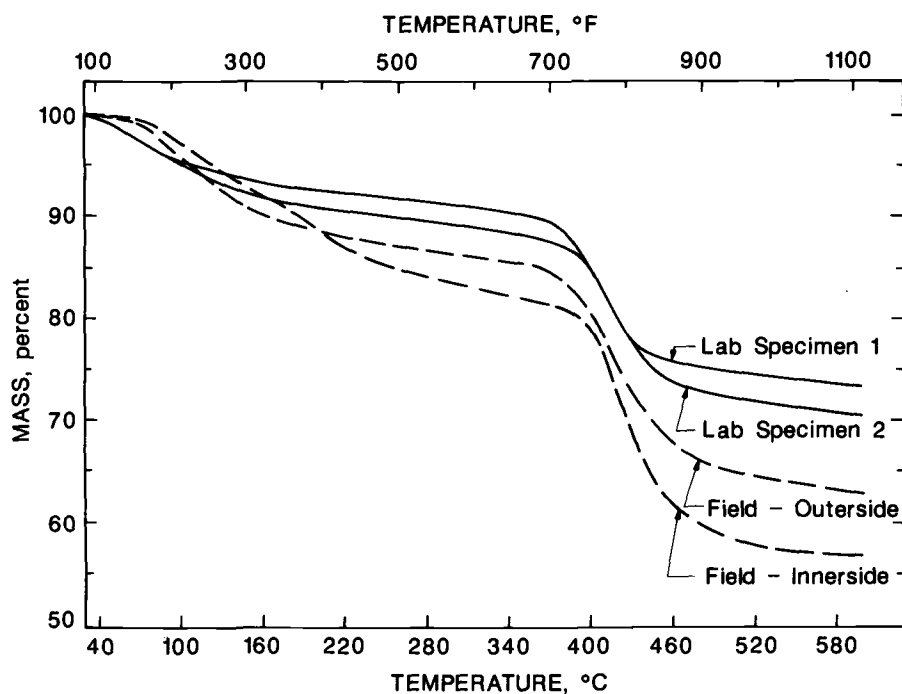


FIG. 4—Results of TG analysis. Specimens were heated in nitrogen gas at $1^{\circ}\text{C}/\text{min}$ ($1.8^{\circ}\text{F}/\text{min}$).

TABLE 3—Results of thermogravimetric analyses.

Specimen No.	Temperature Range		
	Low	Medium	High
	40–175°C (104–347°F)	175–300°C (347–572°F)	300–450°C (572–842°F)
	Mass Loss, %	Mass Loss, %	Mass Loss, %
Lab. 1	11	2	16
Lab. 2	11	2	19
Field	15	3	21
(Outer) ^a			
Field	16	4	24
(Inner) ^b			
3-form	34	negligible	26
MgOCl ^c			
5-form	27	negligible	26
MgOCl ^c			

^aSpecimen was taken from the vicinity of the outer side of the cavity.

^bSpecimen was taken from the vicinity of the inner side of the cavity.

^cData are taken from Cole and Demediuk [10].

In the low range, the magnesium oxychloride cements underwent dehydration to the same anhydrous phase [10]. The 3-form and 5-form lost about 34% and 27% of their mass, respectively, when heated to about 175°C (347°F). These percents were essentially equal to the theoretical percentage of water of hydration present in each form. At higher temperatures, thermal degradation of the anhydrous phase occurred. The additional loss of mass by heating from about 300 to 460°C (572 to 860°F) was about 26% for the 3-form and the 5-form.

A comparison of the TG results of the present study (Table 3) with those of Cole and Demediuk [10] suggests that the foam insulation is not a pure 3-form or 5-form magnesium oxychloride cement or a combination of the two. In particular, the percent loss in mass of the insulation specimens in the present study was considerably less, particularly over the low temperature range, than reported by Cole and Demediuk for the magnesium oxychlorides. Over the low temperature range, the mass loss in the present study was 16% or less (Table 3), whereas that from Cole and Demediuk was about 30%. The TG finding that the foam insulation is not a pure 3-form or 5-form magnesium oxychloride cement is not considered surprising, since the insulation is prepared with fillers [2]. Fillers would be expected to alter the mass loss curves of the foam in relation to the pure magnesium oxychloride cements. Moreover, the manufacturer has indicated that the foam may be more aptly described as a calcium magnesium oxychloride silicate composition [2]. Further research is needed to continue characterization of the foam insulation and to resolve the apparent inconsistencies between the present X-ray diffraction and TG results.

Results and Discussion of Field Observations

The wall was opened from the exterior to provide access to the foam insulation. The oak plank sheathing had been installed diagonally to the studs, which did not allow opening more than one cavity without removing many pieces of siding board. Consequently, the observations of the *in situ* foam from the house were limited. It cannot be overemphasized that the observations reported here apply only to the house in question, because of their limited extent.

Upon removing the sheathing from the house, it was apparent that the installed foam had not completely filled the cavity space. The foam was in the center of the cavity, with unfilled cavity areas along the left and right studs. The opening of an incompletely filled cavity filled was unfortunate, for it precluded taking measurements on shrinkage of the foam insulation. Shrinkage is normally estimated by determining the width of gaps created between the studs and the completely installed insulation.

The foam was found to be intact in the cavity. There was no evidence of crumbling, although the foam was friable to handle. Horizontal and vertical cracks of varying widths were observed in the foam. Most cracks were estimated to be no greater than 1 to 2 mm (0.04 to 0.08 in.) in width. In some cases, the cracks were considered immeasurably narrow; in one case, the largest crack was found to be about 5 mm (0.2 in.) in width. Some of the cracks completely traversed the thickness of the insulation. Consequently, only relatively small pieces of the foam could be removed.

Four of the pieces of foam were weighed immediately in the field upon removal from the wall. They were again weighed periodically in the laboratory over a two-week period during which they remained unsealed and exposed to normal room conditions. The samples showed no significant change in mass between the initial and final weighing, indicating that these foam samples removed from the wall contained no excessive accumulated moisture.

Upon removal of the foam from the cavity, a metal-sheathed electrical cable was found in the cavity mounted along the right stud. The foam had been in contact with the metal. No evidence of corrosion was visually observed. Finally, no indications of moisture problems (e.g., wet sheathing, water staining) in the cavity were seen. Measurements of moisture contents of the wooden members of the wall were not made.

Summary and Recommendations

This initial investigation of the properties and performance of magnesium oxychloride-based foam thermal insulation was performed on samples prepared in the laboratory and also removed from one cavity of a wall of a wood-frame house. The tests to characterize the foam included measurements of density, moisture content, shrinkage, and thermal conductivity, combined with analysis using X-ray diffraction, scanning electron microscopy, and thermogravimetric techniques. It is again emphasized that, because of the limited extent of the field observations and laboratory testing, the information reported herein applies only to the samples in the study.

Because of the limited scope of the study and inconsistencies in some of the analytical data, recommendations are made that the X-ray diffraction, SEM, and thermogravimetric analyses be extended to provide further characterization of the foam. Investigations should include studies to quantify the composition of the cement-based insulation, and to evaluate the potential of the cement to undergo carbonation and the effect of carbonation on insulation performance.

Acknowledgments

This study was sponsored by the U.S. Department of Energy, Office of Conservation and Renewable Energy. The authors gratefully acknowledge the support of William Gerken, DOE, and David McElroy, ORNL, for their encouragement and assistance during the study. Thanks are also extended to their NBS colleagues who assisted in the laboratory testing and report preparation: Jack Lee and Ned Embree for sample preparation and density and moisture measurements; Thomas Somers and Thomas Faison for thermal conductivity measurements; Paul Stutzman for X-ray diffraction and SEM analyses; Willard Roberts for thermogravimetric analysis; and Douglas Burch and Stephen Treado for valuable review of a draft of the report.

Thanks and appreciation are also expressed to Douglas and Carmen Palmer (Palmer Industries, Frederick, Maryland) who provided laboratory samples and made arrangements for obtaining field samples from the house. Mr. Palmer also performed the necessary carpentry to remove the foam from the house and restore its wall.

References

- [1] Rossiter, W. J., Jr., and Mathey, R. G., "Urea-Formaldehyde Foam Insulations: A Review of Their Properties and Performance," National Bureau of Standards, Technical Note 1210, March 1985, 70 pages.
- [2] Rossiter, W. J., Jr., and Mathey, R. G., "Magnesium Oxychloride Cement-Based Foam Insulation: A Review of Available Information and Identification of Research Needs," National Bureau of Standards, NBSIR 86-3326, June 1986, 40 pages.
- [3] Rossiter, W. J., Jr., Ballard, D. B., and Sleater, G. A., "Elevated Temperature Effects on Urea-Formaldehyde Foam Insulations Observed by Scanning Electron Microscopy," in *Thermal Insulation, Materials, and Systems for Energy Conservation in the '80s*, ASTM STP 789, F. A. Govan, D. M. Greason, and J. D. McAllister, Eds., American Society for Testing and Materials, Philadelphia, 1983, pp. 665-687.
- [4] Klug, H. P. and Alexander, L. E., *X-Ray Diffraction Procedures*, 2nd ed., Wiley, New York, 1974.
- [5] Goldstein, J. I. et al., *Scanning Electron Microscopy and X-Ray Microanalysis*, Plenum Press, New York, 1981.
- [6] Turi, E. A., Ed., *Thermal Characterization of Polymeric Materials*, Academic Press, New York, 1981.
- [7] Tye, R. P. and Desjarlais, A. O., "Performance Characteristics of Foamed-in Place Urea-Formaldehyde Insulation," Oak Ridge National Laboratory, ORNL-Sub-78/86993/1, June 1981, 36 pages.
- [8] McFadden, P. W., Azar, K., and Zebrowski, T. J., "The Thermal Resistance of In Situ Urea-Formaldehyde Foam Insulation," *Journal of Thermal Insulation*, Vol. 6, Oct. 1982, pp. 63-74.

- [9] Weidt, J., Saxler, R. J., and Rossiter, W. J., Jr., "Field Investigation of the Performance of Residential Retrofit Insulation," National Bureau of Standards Technical Note 1131, Sept. 1980, 67 pages.
- [10] Cole, W. F. and Demediuk, T., "X-Ray, Thermal, and Dehydration Studies on Magnesium Oxychlorides," *Australian Journal of Chemistry*, Vol. 8, No. 2, 1955, pp. 231-251.
- [11] Sorrell, C. A. and Armstrong, C. R., "Reactions and Equilibria in Magnesium Oxychloride Cements," *Journal of the American Ceramic Society*, Vol. 59, No. 1-2, 1976, pp. 51-54.

Thermal Resistance of Fine Powders at Atmospheric Pressure and under Vacuum

REFERENCE: McElroy, D. L., Weaver, F. J., Yarbrough, D. W., and Graves, R. S., "Thermal Resistance of Fine Powders at Atmospheric Pressure and under Vacuum," *Insulation Materials, Testing, and Applications, ASTM STP 1030*, D. L. McElroy and J. F. Kimpflen, Eds., American Society for Testing and Materials, Philadelphia, 1990, pp. 52-65.

ABSTRACT: Heat transport measurements are reported on candidate insulation systems with relatively high thermal resistances for use in appliances. The thermal resistances of small diameter silica powders at atmospheric pressure and under vacuum were measured from 295 to 340 K using unguarded radial heat flow techniques. The thermal resistances of rectangular panels containing perlite or silica powder at reduced pressure were determined using an unguarded linear heat flow technique.

Values of $1.2 \text{ m}^2 \cdot \text{K/W}$ for 0.0254 m (R-7 per inch) were obtained at atmospheric pressure for powders of pure, fumed, amorphous ($0.01 \text{ } \mu\text{m}$ diameter) silica particles compacted to about 10% of theoretical density. Values of $0.7 \text{ m}^2 \cdot \text{K/W}$ for 0.0254 m (R-4 per inch) were obtained at atmospheric pressure for powders of impure, amorphous ($0.3 \text{ } \mu\text{m}$ diameter) silica particles. Under vacuum these particle systems yielded thermal resistances as high as $6 \text{ m}^2 \cdot \text{K/W}$ for 0.0254 m (R-34 per inch), and mixtures with the pure silica particles yielded over $9 \text{ m}^2 \cdot \text{K/W}$ for 0.0254 m (R-50 per inch). Evacuated panels of pure silica particles yielded thermal resistance values over $3 \text{ m}^2 \cdot \text{K/W}$ for 0.0254 m (R-17 per inch) and decreased about 5% in resistance in 39 months. Evacuated panels of a perlite powder yielded similar values.

KEY WORDS: thermal resistance, amorphous silica powders, evacuated panels of powders, unguarded radial heat flow apparatus, unguarded linear heat flow apparatus, appliance insulation

Nomenclature

- A Material parameter associated with particle contact resistance (Eqs 2 and 3)
- A_0 Screen wire metering area (Eqs 7 and 8)
- D Density, lb/ft^3
- d Particle diameter, m
- E Extinction coefficient, a function of λ , m^{-1}
- \bar{E} Average value of E , m^{-1} , $F_{\lambda_1-\lambda_2}$ for interval $\lambda_1 - \lambda_2$
- F_s Fraction solid
- I Current
- k Thermal conductivity, $\text{W/m} \cdot \text{K}$
- k apparent
- k_c of composite
- k_g° of bulk gas at 1 atm
- k_r radiative

¹Metals and Ceramics Division, Oak Ridge National Laboratory, Oak Ridge, TN 37831.

k_s	of solid at contact between spheres
ℓ	Plate to screen spacing
L	Voltage tap spacing
L°	Thickness
ℓ_g	Mean free path in gas phase
R	Thermal resistance, $\text{m}^2 \text{ K/W}$ or $\text{ft}^2 \text{ h } ^\circ\text{F/Btu}$
r_0	outside radius
r_i	inside radius
T	Temperature, K
T_C	cold surface
T_H	hot surface
T_m	Modified mean absolute temperature defined by Eq 5
ΔT	Temperature difference
V	Voltage drop
ϵ	Emissivity or emittance
ϵ_C	of cold surface
ϵ_H	of hot surface
λ	Wavelength, μm
ρ	Density, kg/m^3
σ	Stefan-Boltzmann constant, $5.6697 \times 10^{-8} \text{ W/m}^2 \text{ K}^4$

Introduction

This paper reviews the status of a research project on materials properties sponsored by the U.S. Department of Energy at the Oak Ridge National Laboratory (ORNL). The project goal is to develop insulations for appliances with a thermal resistance at 24°C (75°F) of at least $3.5 \text{ m}^2 \cdot \text{K/W}$ for a thickness of 0.0254 m ($\text{R-20 h} \cdot \text{ft}^2 \cdot ^\circ\text{F/Btu}$ for an inch). This goal corresponds to a material or system with an apparent thermal conductivity (k) of $0.0072 \text{ W/m} \cdot \text{K}$ ($0.05 \text{ Btu} \cdot \text{in.}/\text{h} \cdot \text{ft}^2 \cdot ^\circ\text{F}$). The k -value target is about 30% of the thermal conductivity of air and less than 40% of the k of commercially available high thermal resistance insulations such as organic foams containing chlorofluorocarbon gases.

The starting point for this research was a technical assessment of the feasibility of developing high thermal resistance materials for advanced insulations for appliances by Lawrence and Ruccia [1]. Their assessment yielded three important observations: (1) an annual energy savings of about 10^{18} J ($0.947 \times 10^{15} \text{ Btu}$) would result if an insulation with a k of $0.0072 \text{ W/m} \cdot \text{K}$ were used in appliances; (2) theoretical analyses of twelve candidates indicated that either evacuated or gas-filled insulation systems could meet the k -value target; and (3) materials property information was not available to verify these promising candidate systems. In addition, their report identified U.S. Patent 4,159,359 issued to L'Air Liquide, France [2], which showed k -values below $0.005 \text{ W/m} \cdot \text{K}$ for evacuated panels containing fumed silica particles when tested at low temperatures. The patent reports data for hot surfaces of 300 K and cold surfaces of 77 K , which corresponds to a mean temperature of 188 K (-85°C , -120°F).

Recently two U.S. patents [3,4] were issued to the General Electric Company for evacuated panels containing precipitated silica or fly ash that achieved high thermal resistance at room temperature. These systems achieve high thermal resistance by using small diameter powders to produce available void spaces having dimensions much less than the mean free path of the interstitial gas. This reduces the contribution of gas conduction to the k -value of the system.

The use of evacuated powders to achieve high thermal resistances has been described in several reports [5-9]. These have shown that high thermal resistance depends on decreasing gas-phase conduction and decreasing radiative transport in the system without significantly increasing the contribution due to solid-phase conduction. For example, particulate thermal

insulations containing air at atmospheric pressure as the gas phase will have the k of air as a limiting value unless the effective pore size can be reduced to less than the mean free path in the gas phase. Since the k for air at 298 K and one atmosphere pressure is $0.026 \text{ W/m} \cdot \text{K}$, this limits practical R -values to $0.98 \text{ m}^2 \cdot \text{K/W}$ for 0.0254 m of material ($5.5 \text{ h} \cdot \text{ft}^2 \cdot ^\circ\text{F/Btu}$ for one inch thickness).

Assuming convective transport to be negligible, the heat transport through fine particle systems has been modeled [5,10,11] as the sum of two independent heat transfer mechanisms: the net radiative contribution, k_r , and the net conductive contribution, k_c :

$$k = k_r + k_c \quad (1)$$

Models for k_c and k_r have been derived and show that these can be described in terms of the powder system properties with

$$k_c = \frac{0.33F_s k_s}{1 + 0.33AF_s} + \frac{(1 + 0.33F_s)k_g^\circ}{1 + 1.5F_s(\ell_g/d)} \quad (2)$$

$$\lim_{(\ell_g/d) \rightarrow \infty} (k_c) = \frac{0.33F_s k_s}{1 + 0.33AF_s} \quad (3)$$

$$k_r = \frac{4F_{\lambda_1-\lambda_2} \sigma T_m^3 L^\circ}{1/\epsilon_H + 1/\epsilon_C - 1} + \frac{4(1 - F_{\lambda_1-\lambda_2}) \sigma T_m^3 L^\circ}{3\bar{E}L^\circ/4 + 1/\epsilon_H + 1/\epsilon_C - 1} \quad (4)$$

$$T_m = [T_H^4 - T_C^4]/4(T_H - T_C)]^{1/3} \quad (5)$$

where the individual terms are as defined in the Nomenclature section. The interpretation of these equations in achieving a low k for a particulate system includes:

1. Large values of the ratio of the mean free path, ℓ_g , of the gas relative to the particle diameter, d , will minimize k_c for fixed values of A , F_s , and k_s by eliminating the second term in Eq 2.
2. Small values of fraction solid, F_s , and solid thermal conductivity, k_s , are required to decrease k_c .
3. The optimum density cannot be determined mathematically because A is an unknown function of F_s and particle characteristics, so k for a given powder must be determined experimentally.
4. Because k_r is independent of pressure, k_c will decrease as the pressure decreases. The value of k_r will be decreased by a high extinction coefficient and low boundary emittances.

These considerations show that systems with high thermal resistance can be obtained using small diameter particles and reduced gas pressures.

Experimental Apparatus

The apparent thermal conductivity of candidate insulation systems composed of small diameter particles was measured at steady-state with an unguarded radial-heat-flow apparatus and an unguarded linear-heat-flow apparatus that are described below.

Unguarded Radial Heat Flow Apparatus

Figure 1 depicts the unguarded radial-heat-flow apparatus (ORNL-7) that evolved from its predecessors (ORNL-3, -4, and -5) described in Refs 5 to 9. ORNL-7 consists of an unguarded, axially positioned, thin-walled stainless steel core heater that is instrumented with three small

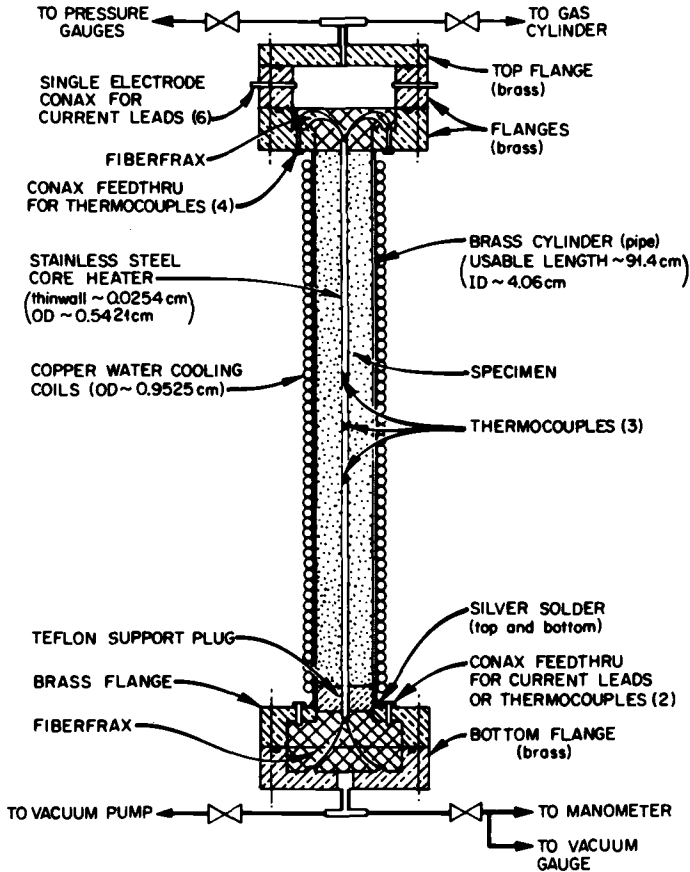


FIG. 1—Unguarded radial-heat-flow apparatus (ORNL-7). The apparent thermal conductivity has been measured for silica powder systems near room temperature with void spaces filled with air or evacuated using unguarded radial heat flow techniques. The techniques have had various length-to-diameter ratios to minimize axial heat flow. ORNL-7 has a length-to-diameter ratio of 22.

diameter chromel P-constantan thermocouples welded to holes in the tube wall. These span a distance (L) of 20 cm, serve as voltage taps (V) for power determination, and yield the tube temperature at its diameter (T_H). The powder specimen is contained in the annulus between the core heater and a concentric brass cylinder covered with copper tubing over its length. Water from a Braun controlled-temperature bath is circulated through this copper coil, and the temperature (T_C) is measured with chromel P-constantan thermocouples joined to the copper coil with thermally conducting epoxy. The brass cylinder is joined to end flanges and caps that form the outer perimeter of the cell. Power leads exit through these ends to a d-c power supply and standard resistor for measuring the current (I) to the core heater. Thermocouples also exit through these ends to join copper wires in an ice bath reference junction. The copper wires extend to a switching system and a Guideline Model 9578 8 $\frac{1}{2}$ Digit Precision Digital Voltmeter for measuring all thermal emfs. The end flanges connect to the gas pressure system, vacuum pumps, and gages to read the pressure or vacuum in the cell.

Steady-state k determinations are based on the temperature difference, ΔT , across the specimen in the radial direction, ($\Delta T = T_H - T_C$); the electrical power dissipated in the stainless steel core heater, $V \cdot I/L$; and the radial dimensions of the annular space, r_0 and r_i ;

$$k = \frac{VI}{2\pi L} \cdot \frac{\ln r_0/r_i}{\Delta T} \quad (6)$$

If axial heat flow occurs in the measurement section of ORNL-7, a correction to k calculated from Eq 6 is necessary. The length-to-diameter ratio of ORNL-7 is 22.5, which minimizes the correction to k due to axial heat flow. The effect of axial heat flow for an unguarded radial measurement apparatus becomes increasingly important as the specimen k decreases. Thermal modeling with the HEATING5 computer code [12] was performed; Table 1 indicates the corrections required for a range of specimen k -values. A determinate error analysis for ORNL-7 indicated a total error in k of $\pm 3\%$.

Unguarded Linear Heat Flow Apparatus

The k of evacuated panels containing small diameter particles was measured from 300 to 330 K using the unguarded thin heater technique that has been previously described [13-17]. The apparatus is an absolute, longitudinal heat flow technique and consists of an unguarded, electrically heated, flat, large-area nichrome screen wire heat source sandwiched between two horizontal layers of insulation with flat isothermal bounding surfaces. The wire screen heat source has a low thermal conductance which reduces unwanted lateral heat flow and minimizes the need for active edge guarding. Figure 2 is a schematic drawing of the unguarded thin heater apparatus.

The heat source provides vertical heat flow in its central region across the subject insulation to two temperature-controlled, water-cooled copper plates. The screen is large, 0.9 by 1.6 m, and is instrumented with eleven thermocouples for temperature measurement and voltage taps for power measurements. A measured direct current passes through the screen, and the heat generated passes through the two layers of insulation. When steady-state is reached, standard potentiometric equipment is used to measure the thermocouple outputs, the current, and the voltage. These quantities and the spacing between the plates allows the apparent thermal conductivity to be calculated for two-sided heat flow:

$$k = \frac{I \cdot V}{2} \cdot \frac{\ell}{A_0 \Delta T} \quad (7)$$

By changing the screen power and the plate temperatures, mean temperatures from 30 to 50°C can be achieved. The independent temperature control for each copper plate allows one-

TABLE 1—Results of thermal modeling of ORNL-7 with HEATING5.

Sample k -value, W/m · K	% Error in k Due to Axial Heat Flow	Distance from Center for Error in k to be Less Than 1%, cm
5.0	0.20	42
2.0	0.20	41
1.0	0.20	41
0.2	0.22	39
0.1	0.20	37
0.05	0.20	33
0.007	0.70	15

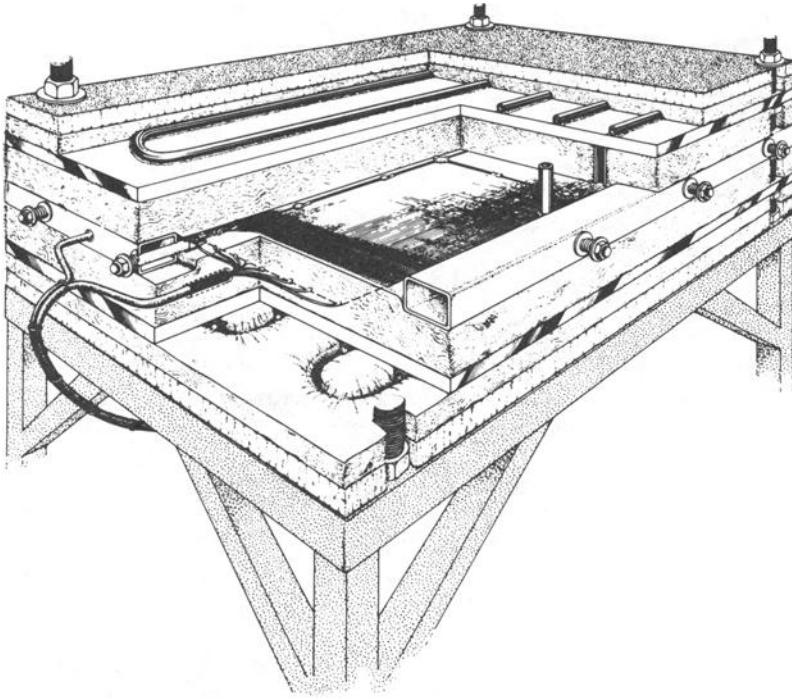


FIG. 2—Unguarded thin-heater apparatus.

sided heat flow tests. If one plate is controlled to the temperature of the screen wire heater, the thermal conductivity of the insulating specimen with an imposed temperature difference is calculated from

$$k = \left[I \cdot \Delta V - \frac{k(B) \cdot \Delta T(B) \cdot A_0}{\ell(B)} \right] \cdot \frac{\ell}{A_0 \Delta T} \quad (8)$$

The B -terms provide a heat flow correction for the small temperature difference mismatch. This one-sided feature was used for the evacuated panels.

The measurement errors of the thin heater apparatus have been assessed. A determinate error analysis of the quantities in Eq 7 predicts a maximum uncertainty of 1.7% if ΔT is 5 K and 0.7% if ΔT is 30 K. The most probable uncertainty is 1.2% and 0.4%, respectively, for these ΔT values.

Materials

Because the modeling of Eqs 2 to 5 indicates that powder systems composed of small diameter particles could yield high thermal resistance insulations, thermal conductivity measurements included commercially available small diameter amorphous silica powders and evacuated panels containing small diameter silica particles. The relatively small specimen volumes of the unguarded radial heat flow systems described above allowed k measurements on limited quantities of specimen materials as a function of powder bed density at atmospheric pressure and at reduced pressures.

One set of specimens included pure, amorphous fumed silica powder bed densities from 80 to 350 kg/m³. These powders had nominal particle diameters from 0.005 to 0.120 μm . Figure 3a is a photomicrograph of one such powder that shows powder clusters much larger than the nominal particle diameters due to linking together of individual particles. The clusters are at least ten times the mean free path of N_2 at STP, 0.07 μm .

A second set of specimens was formed from commercially available, impure amorphous silica particles. Powder beds of these impure particles were tested in the density range 100 to 450 kg/m³; the nominal particle diameters range from 0.300 to 3 μm . Figure 3b is a photomicrograph of one such powder that shows a few even larger clusters that approach 50 μm diameter. A third set of specimens that was tested involved mixtures of pure and impure powders and with other selected types of powders.

Three sets of evacuated panels filled with different types of small diameter particles were tested in the unguarded thin heater apparatus. Table 2 lists the dimensions, bulk density, and content of these panels. The panels from France were encased in two individually sealed laminates of aluminized plastic and were evacuated to about 130 Pa (1 mm of Hg) when initially produced.

The panels from the United States were a set of prototypical panels with two sealed laminates. An inner microporous pouch holds the powder during fabrication processing and a metallized polymeric impermeable laminate forms the outer gas barrier. Panels 1 to 4 were evacuated for 2 to 7 min to achieve various internal gas pressures for panels of nearly the same density.

Two of the panels from Japan (P1 and P2) were foamed-in-place side walls of refrigerators and one (P3) was a bare panel without foam. Panel P1 was punctured during removal from the refrigerator and its contents examined after testing. This revealed a two-package assembly, the inner package being a porous paper bag containing milled perlite. This envelope allowed evacuation prior to heat sealing the outer package composed of multilayer polyester metallized film.

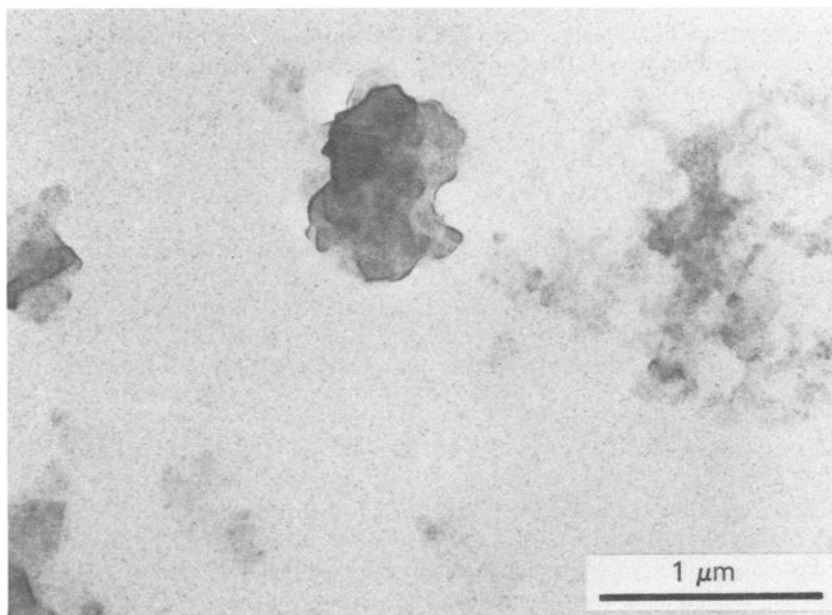


FIG. 3a—Photomicrograph of small-diameter, pure amorphous, fumed silica particle clusters (30 000 \times).

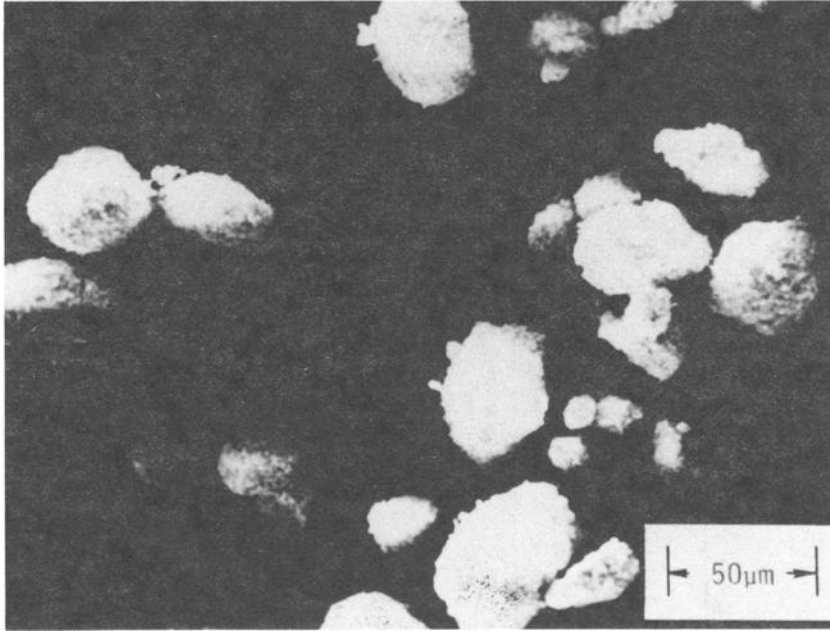


FIG. 3b—Photomicrograph of small-diameter, impure amorphous silica particle clusters (400 \times).

Results

One purpose of this paper is to summarize the results of the project publications [5–9] which contain the data base of candidate insulation systems with relatively high thermal resistances for use in appliances. The emphasis will be on reporting the data trends; more complete descriptions are given in the references.

Air at One Atmosphere

Figure 4 shows the k -values from the radial heat flow apparatus obtained for beds composed of small-diameter, pure, amorphous fumed silica particles at 300 K, atmospheric pressure, and for densities in the range 80 to 350 kg/m³. The results show a minimum k of 0.021 W/m · K (0.146 Btu · in./h · ft² · °F) near 160 kg/m³, which is about 7% of the theoretical density of SiO₂ (2300 kg/m³). Thus, when as-received powders from two companies (Cabot and DeGussa) are compacted, a k value is obtained in air at one atmosphere that is only 80% of the thermal conductivity of air. This shows that k is being determined by an assembly of particles that changes two heat transfer components: reduced gas conduction by a mean free path effect and reduced radiative transport by increased density.

The results in Fig. 4 are described to better than $\pm 3\%$ by a least-squares fit as

$$k(\text{W/m} \cdot \text{K}) = 0.148 \times 10^{-2} + 0.514 \times 10^{-4} \rho + \frac{1.795}{\rho}, \quad \rho \frac{\text{kg}}{\text{m}^3} \quad (9)$$

$$k\left(\frac{\text{Btu} \cdot \text{in.}}{\text{h} \cdot \text{ft}^2 \cdot ^\circ\text{F}}\right) = 0.01087 + 0.00567 D + \frac{0.775}{D}, \quad D \frac{\text{lb}}{\text{ft}^3} \quad (10)$$

TABLE 2—*Characteristics of evacuated panels containing small diameter particles.*

Source	Nominal Dimensions, m	Density, kg/m ³	Content	Age, months	Apparent Thermal Conductivity, W/m · K	Cubic Term (C × 10 ⁶)	Apparent Thermal Resistance (R-value at 75°F for one inch), h · ft ² · °F/Btu
France-12	0.96 × 0.48 × 0.053	174	0.007 μm pure fumed silica	15	0.00988	0.38 ^a	14.6
France-22	0.97 × 0.48 × 0.057	183	0.007 μm pure fumed silica	15	0.01202	0.46	12.0
France-20a	0.97 × 0.48 × 0.055	190	0.007 μm pure fumed silica	15	0.00859	0.32	16.8
France-20b				25	0.00860		16.77
France-20c				39	0.00911		15.84
USA-1	0.6 × 0.33 × 0.012	235	Precipitated silica	1	0.01442		10.0
USA-2	0.6 × 0.33 × 0.013	221	Precipitated silica	1	0.00931		15.5
USA-3	0.6 × 0.33 × 0.012	226	Precipitated silica	1	0.00902		16.0
USA-4	0.6 × 0.33 × 0.012	227	Precipitated silica	1	0.00747		19.3
Japan-P1	0.5 × 0.56 × 0.038 ^a	...	Perlite, 13 μm dia	6	0.0401		3.6
Japan-P2	0.4 × 0.7 × 0.038 ^a	...	Perlite	6	0.0105		13.8
Japan-P3	0.73 × 0.38 × 0.012	270	Perlite	1	0.0080		18.0

^aSize of foamed-in-place refrigerator side panel.^bCoefficient of T³ term; see text.

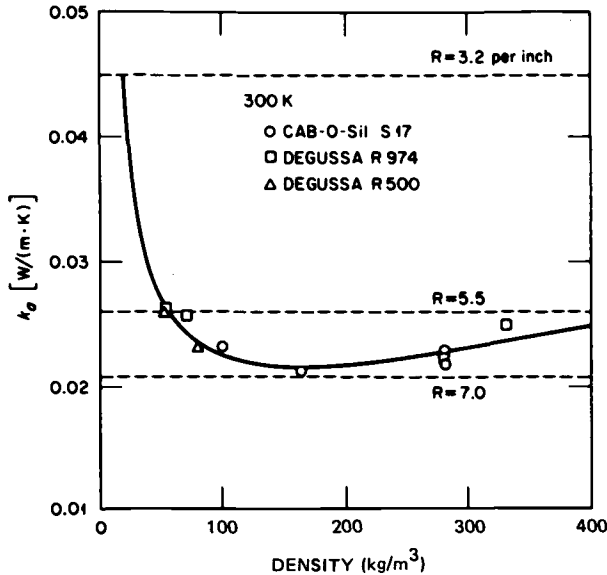


FIG. 4—Apparent thermal conductivity at 300 K as a function of density for three pure amorphous silica powders at atmospheric pressure.

If the magnitude of these terms are associated with gas conduction, solid conduction, and radiative transport, respectively, then comparing these to values for air and fiberglass insulations, one notes: the gas term is 5% that of still air; the solid conduction term is within 15% of the value for fiberglass; and the radiative transport coefficient is eleven times that of fiberglass. Equation 9 suggests that the powders formed from these pure amorphous silica particles are not as effective in reducing the radiative term as are small diameter fibers, but they are effective in reducing the gas phase transport.

Figure 5 shows the k -results obtained for beds composed of small-diameter, impure amorphous silica particles at 300 K, atmospheric pressure, and for densities in the range 100 to 500 kg/m^3 . These low-cost commercially available powders with moderately large nominal particle diameters show k data 0.01 to 0.02 $\text{W/m} \cdot \text{K}$ greater than the pure, amorphous, fumed silica. A minimum k of 0.034 $\text{W/m} \cdot \text{K}$ occurs near 200 kg/m^3 . These data are described by a least-squares fit

$$k(\text{W/m} \cdot \text{K}) = 0.135 \times 10^{-1} + 0.56 \times 10^{-4} \rho + \frac{1.81}{\rho}, \quad \rho (\text{kg/m}^3) \quad (11)$$

The leading term suggests these larger particles reduced the gas conduction to about 50% that of air; the other two terms agree closely with Eq 9.

Figure 6 shows that the k -value for mixtures of pure and impure amorphous silica particles decreases as the density decreases. The amount of pure amorphous fumed silica was increased to 20 wt% for the mixtures showing the lowest k and density values. The resulting k -values are between those given in Figs. 4 and 5, which indicates existence of mean free path effects.

Reduced Pressures

Table 2 gives thermal conductivity values obtained using a one-sided mode of operation in the unguarded thin heater apparatus for evacuated panels from France, Japan, and the United

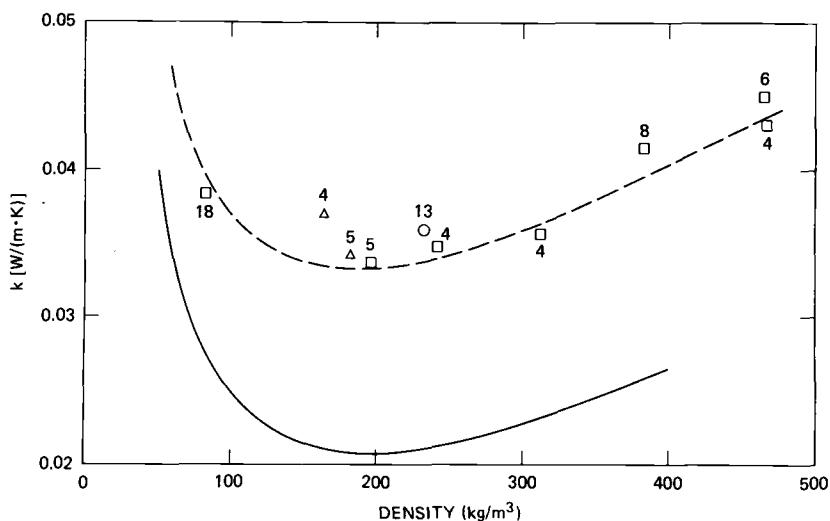


FIG. 5—Apparent thermal conductivity at 300 K as a function of density for impure amorphous silica powders at atmospheric pressure. Code numbers from Ref S. Solid line is Eq 9. Dashed line is Eq 11.

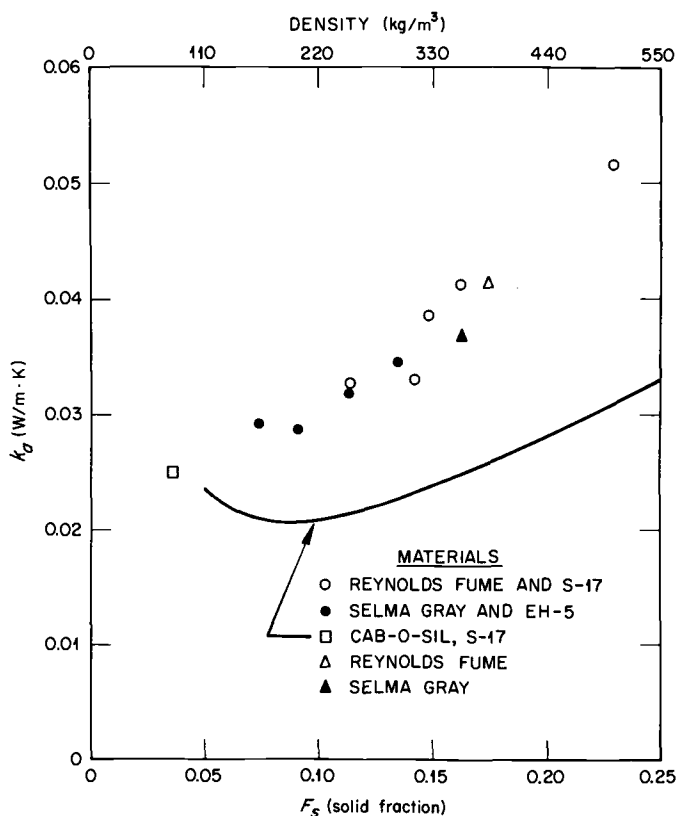


FIG. 6—Apparent thermal conductivity of silica powders at 300 K as a function of fraction solid or density. The curve was calculated from $k_a = 0.1484 \times 10^{-2} + 0.5140 \times 10^{-4} \rho + 1.795/\rho$ (Eq 9).

States. The initial tests on three panels from France were conducted about 15 months after these had been produced and yielded k -values at 24°C in the range 0.0086 to $0.012 \text{ W/m} \cdot \text{K}$ (R -values for an inch from 12 to $16.8 \text{ h} \cdot \text{ft}^2 \cdot ^{\circ}\text{F/Btu}$). These k -values increased with temperature from 297 to 320 K and can be described by a linear or a cubic function of temperature. The CT^3 term for Panel 20 yields an extinction coefficient of 944 m^{-1} using the Rosseland approximation [18]. This agrees remarkably well with the extinction coefficient of 864 m^{-1} predicted by Eq 9 for pure, amorphous SiO_2 powders in air. The data on Panel 20 as aged at room temperature show that the k -value increased about 6% from 15 months to 39 months; this is probably due to an increase in internal gas pressure. Data presented below suggest an internal pressure near 2000 Pa existed during the last test of Panel 20.

The prototypical evacuated panels produced in the United States were tested by placing these panels in a picture frame of a polyisocyanurate board. This procedure yields a thermal resistance for the composite of panel and board. An iterative analysis yielded the evacuated panel k -values using measured k -values for the polyisocyanurate board. The time of exposure to the vacuum pumping during fabrication of the panels increased from 2 to 7 min for Panels 1 to 4. Panel 4 is within 5% of the target R -value for this project, but the value is less than that presented in Ref 3.

The composites and evacuated panels made in Japan were tested using the aforementioned picture frame technique. The k -value for the one-month-old evacuated panel P-3, $0.0080 \text{ W/m} \cdot \text{K}$, was derived by the same iterative analysis described above. The k -values derived for Panels P-1 and P-2 involved a double composite that included the refrigerator side panel and the foam surrounding the evacuated panels. The k -value for the foam had to be estimated to derive the evacuated panel k -values. Even though derived values for Panels P-1 and P-2 are uncertain to $\pm 25\%$, it is clear from the k -value of Panel P-1 that it had been punctured during removal from the refrigerator. Nevertheless, the k -values for the evacuated panels containing perlite provide an alternative material for obtaining high thermal resistance insulation systems.

Figure 7 shows the R -values obtained at 24°C for three powder systems at reduced pressure

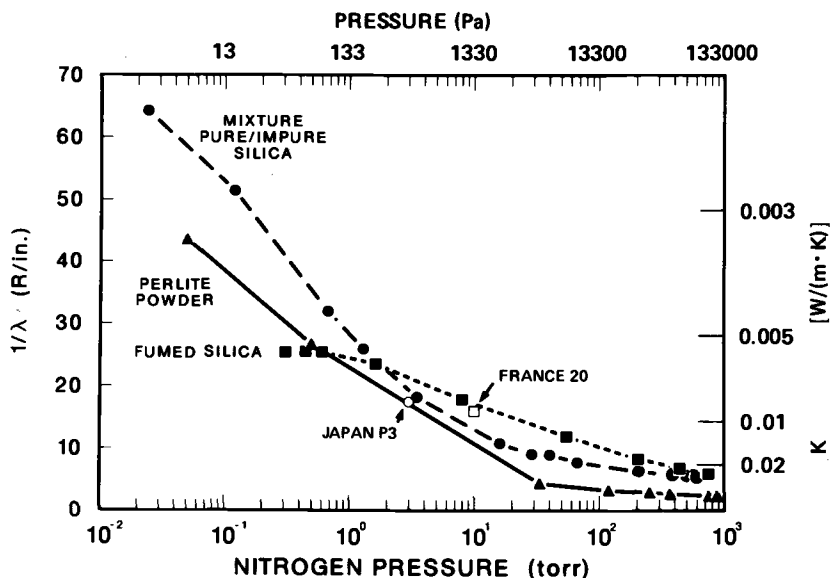


FIG. 7— R -value per inch at 24°C (75°F) versus reduced gas pressure for three powder systems and two evacuated panels.

and two of the evacuated panels, France-20 and Japan-P3. The R-values for the powder systems increase as the gas pressure in the voids is decreased, as expected for a reduced gas conduction contribution to the apparent thermal conductivity. The results for pure, amorphous fumed silica reach a plateau k -value below 133 Pa of $0.0058 \text{ W/m} \cdot \text{K}$. A powder mixture of 20 wt% pure and 80 wt% impure amorphous silica particles show the highest R-values below 133 Pa and near 13 Pa has a k -value below $0.003 \text{ W/m} \cdot \text{K}$. The perlite powder removed from Japan-P1 was found to have a k -value below $0.004 \text{ W/m} \cdot \text{K}$ near 13 Pa. The pressure dependence of the k of these powders was used with the k determinations for France-20 and Japan-P3 to estimate the internal pressures of these panels as near 2000 Pa and 400 Pa, respectively.

Conclusions and Recommendations

The described material property results indicate that insulation systems with k -values of $0.007 \text{ W/m} \cdot \text{K}$ or less can be achieved by the use of several different filler materials and enclosure materials for evacuated panels. An optimum combination has not been established. A loss of thermal resistance with time has been observed for one type of evacuated panel; this effect probably depends both on filler material and enclosure material properties. Additional materials research is needed to address the aging behavior, the measurement of internal pressures, development of thermal property models that incorporate filler material morphology, on enclosure material permeability and seal quality, and on low cost evacuated panel production techniques to yield high thermal resistance composites for use in appliances and other building applications.

Acknowledgments

The authors are grateful for reviews by V. D. Baxter and R. E. Pawel. This research was sponsored by the Office of Buildings and Community Systems, Building Equipment Division, U.S. Department of Energy, under Contract DE-AC05-84OR21400 with Martin Marietta Energy Systems, Inc.

References

- [1] Lawrence, W. T. and Ruccia, F. E., "Development of Advanced Insulation for Appliances, Task I Report," ORNL/Sub-81/13800/1, Oak Ridge National Laboratory, Oak Ridge, Tenn., June 1981.
- [2] Pellaux-Gervais, P. and Goumy, D., "Insulating Material with Low Thermal Conductivity, Formed of a Compacted Granular Structure," U.S. Patent 4,159,359 (assigned to L'Air Liquide, Paris, France), 26 June 1979.
- [3] Barito, R. W. and Downs, K. L., "Precipitated Silica Insulator," U.S. Patent 4,636,415 (assigned to General Electric Company, Louisville, Ky.) 13 Jan. 1987.
- [4] Barito, R. W. and Downs, K. L., "Insulation Formed of Precipitated Silica and Fly Ash," U.S. Patent 4,681,788 (assigned to General Electric Company, Louisville, Ky.) 21 July 1987.
- [5] McElroy, D. L., Yarbrough, D. W., Copeland, G. L., Weaver, F. J., Graves, R. S., Tong, T. W., and Fine, H. A., "Development of Advanced Thermal Insulation for Appliances," ORNL/CON-159, Oak Ridge National Laboratory, Oak Ridge, Tenn., June 1984.
- [6] Yarbrough, D. W., Weaver, F. J., Graves, R. S., and McElroy, D. L., "Development of Advanced Thermal Insulation for Appliances," ORNL/CON-199, Oak Ridge National Laboratory, Oak Ridge, Tenn., May 1986.
- [7] Yarbrough, D. W., Graves, R. S., Weaver, F. J., and McElroy, D. L., "The Thermal Resistance of Perlite-Based Evacuated Insulations for Refrigerators," ORNL/CON-215, Oak Ridge National Laboratory, Oak Ridge, Tenn., Sept. 1986.
- [8] Copeland, G. L., McElroy, D. L., Graves, R. S., Weaver, F. J., Fine, H. A., and Tong, T. W., "Insulations with Low Thermal Conductivity," 18th Thermal Conductivity Conference, Rapid City, S.D., 3-5 Oct. 1983.
- [9] Yarbrough, D. W., Tong, T. W., and McElroy, D. L., "Use of Fine Powders for High Thermal Resistance," *High Temperature Science*, Vol. 19, 1985, pp. 213-225.

- [10] Crane, R. A., Vachon, R. I., and Khader, M. S., "Thermal Conductivity of Granular Materials—A Review," in *Proceedings, 7th Symposium on Thermophysical Properties*, American Society of Mechanical Engineers, New York, 1977, pp. 109–123.
- [11] Luikov, A. V. et al., "Thermal Conductivity of Porous Systems," *International Journal of Heat Mass Transfer*, Vol. 11, 1968, pp. 117–140.
- [12] Turner, W. D., Elrod, D. C., and Siman-Tov, I. I., "Heating 5—An IBM 360 Heat Conduction Program," ORNL/CSD/TM-15, Oak Ridge National Laboratory, Oak Ridge, Tenn., March 1977.
- [13] Moore, J. P., McElroy, D. L., and Jury, S. H., "A Technique for Measuring the Apparent Thermal Conductivity of Flat Insulations," ORNL/TM-6494, Oak Ridge National Laboratory, Oak Ridge, Tenn., Oct. 1979.
- [14] Moore, J. P., McElroy, D. L., and Jury, S. H., "A Technique for Measuring the Apparent Thermal Conductivity of Flat Insulations," in *Thermal Conductivity 17*, J. G. Hust, Ed., Plenum Press, New York, 1983, pp. 727–735.
- [15] McElroy, D. L., Graves, R. S., Yarbrough, D. W., and Moore, J. P., "A Flat Insulation Tester That Uses an Unguarded Nichrome Screen Wire Heater," in *Guarded Hot Plate and Heat Flow Meter Methodology, ASTM STP 879*, C. J. Shirliffe and R. P. Tye, Eds., American Society for Testing and Materials, Philadelphia, 1985, pp. 121–139.
- [16] Graves, R. S., Yarbrough, D. W., and McElroy, D. L., "Apparent Thermal Conductivity Measurements by an Unguarded Technique," in *Thermal Conductivity 18*, T. Ashworth and D. R. Smith, Eds., Plenum Press, New York, 1985, pp. 339–355.
- [17] Yarbrough, D. W., McElroy, D. L., and Graves, R. S., "Thermal Resistance of Roof Panels and In-Situ Calibration of Heat-Flux Transducers," in *Thermal Performance of the Exterior Envelopes of Buildings III*, ASHRAE, 1985, pp. 794–800.
- [18] Siegel, R. and Howell, J. R., *Thermal Radiation Heat Transfer*, 2nd ed., McGraw-Hill, New York, 1972, pp. 739–746.

Solid Conductivity of Loaded Fibrous Insulations

REFERENCE: Fricke, J., Büttner, D., Caps, R., Gross, J., and Nilsson, O., "Solid Conductivity of Loaded Fibrous Insulations," *Insulation Materials, Testing, and Applications, ASTM STP 1030*, D. L. McElroy and J. F. Kimpflen, Eds., American Society for Testing and Materials, Philadelphia, 1990, pp. 66-78.

ABSTRACT: The thermal conductivity and the elasto-mechanical behavior of a fibrous glass paper insulation and of a fibrous alumina fleece were investigated as a function of external pressure load. The main findings are: (1) at an external load $p_{\text{ext}} = 1$ bar the solid thermal conductivity λ_s of the glass fiber paper is about $1.5 \cdot 10^{-3} \text{ W/(m} \cdot \text{K)}$ and for the fleece is $3 \cdot 10^{-3} \text{ W/(m} \cdot \text{K)}$; and (2) the variation of λ_s with p_{ext} is weak for the paper and pronounced for the fleece.

Three models were employed to study the correlation between λ_s and the elasto-mechanical behavior: Kaganer's model, percolation theory, and the phonon diffusion model.

KEY WORDS: fiber insulation, thermal conductivity, solid conduction, radiative heat transfer, elasto-mechanical behavior, disperse systems

In evacuated load-bearing thermal superinsulations heat transfer is governed by infrared (IR) radiative transport and solid conduction processes within the porous spacer. Extinction of IR radiation in the wavelength region 1 to 50 μm is caused either by absorption or by scattering within the fibrous insulation. In order to further reduce the radiative conductivity λ_r , an opacifier is generally added. In such systems, with large optical thickness in the IR throughout the range of the thermal spectrum, radiative transport proceeds via diffusion of photons. The radiative heat flux (or the effective extinction coefficient E) can be derived from the variation of total thermal flux with mean radiative temperature, which is usually determined in an evacuable guarded hot plate machine [1]. Another way is to derive extinction coefficients from spectral IR optical transmission/reflection measurements or from *ab initio* Mie-scattering calculations, starting with the complex index of refraction. Properly scaled extinction coefficients are fed into a radiative transport equation or, more simply, into a diffusion approximation. All these techniques have been successfully employed by our research group [2]. Though, in principle, it is now possible to accurately calculate the radiative flux through a fibrous insulation, the search for optimal opacifiers with large specific extinction coefficients

$$e = E/\rho \quad (1)$$

(with ρ = density of the fibrous layer) goes on [3]. Typical values of e for a variety of materials are given in Table 1.

On the other hand, the suppression of the solid conduction through a disperse system has relied more or less upon trial and error. Recall that fiber systems have large porosities of about 90% even under external atmospheric pressure load. Thermal resistance is provided by the many point contacts between crossing fibers and by the length of the fibers themselves. The

¹Physikalisches Institut der Universität Würzburg, Am Hubland, D-8700 Würzburg, West Germany.

TABLE 1—Mean specific extinction coefficients e for fiber layers and opacifiers in the wavelength region 1 to 50 μm at $T_r = 300\text{ K}$.

Material	Particle or Fiber ϕ (μm)	e ($\text{m}^2 \text{kg}^{-1}$)
5% Fe_3O_4 in fumed silica	2	40
5% TiO_2 in fumed silica	2.5	40
Soot	< 0.1	600
Glass fiber	5	50
SiO_2 fiber	10	30
Al_2O_3 fiber	4	50

preferred orientation of the fibers is perpendicular to the temperature gradient. A simple model for the solid conduction in fiber systems was proposed nearly 20 years ago [4]. Though this model gives important hints, a detailed understanding of conductive heat transfer through a fibrous layer has not yet been reached. One reason is the difficulty of modelling the heat flow through a more or less random arrangement of partially contacting fibers. A second reason is that investigation of the solid conduction in fibrous insulations under a controlled external pressure load has been initiated only recently [5].

Solid Conduction

The total conductivity λ in evacuated insulations with large optical thickness $\tau_o = E \cdot d \gg 1$ (d = thickness of insulation) is given by

$$\lambda = \lambda_s + \lambda_r \quad (2)$$

where λ_s and λ_r are the solid and the radiative conductivity of the fibrous layer, respectively. λ_r is a "true" conductivity for $\tau_o \gg 1$. In this case radiative transport occurs via diffusion of IR photons and thus is a local phenomenon—as is conduction, too. Therefore λ_r is independent of specimen thickness and boundary emissivity. The same additive superposition as in Eq 2 holds for the thermal loss coefficients ($k = \lambda/d$):

$$k = k_s + k_r \quad (3)$$

Especially for amorphous fibers λ_s is only weakly temperature dependent, whereas λ_r varies with the third power of the mean radiative temperature T_r :

$$\lambda_r = \frac{16}{3} \cdot \frac{n^2 \sigma T_r^3}{E} \quad (4)$$

with T_r defined by

$$T_r^3 = (T_1 + T_2)(T_1^2 + T_2^2)/4 \quad (5)$$

The extinction coefficient E of the specimen is an average over all participating infrared wavelengths. It generally may depend on temperature. The mean index of refraction of the porous layer is represented by n , σ is the Stefan-Boltzmann constant, and T_1 and T_2 are the temperatures of the hot and cold boundaries, respectively. Here n is calculated from $n = 1 +$

$(n_o - 1)\rho/\rho_o$, with n_o being the index of refraction of the fibers and ρ_o their density, where ρ is the density of the fibrous layers.

A typical value for λ_r in Eq 4 is $4 \cdot 10^{-3} \text{ W}/(\text{m} \cdot \text{K})$ at $T_r = 500 \text{ K}$, if $n^2 \approx 1$ and $E \approx 10^4 \text{ m}^{-1}$, corresponding to $e = 50 \text{ m}^2/\text{kg}$ and $\rho \approx 200 \text{ kg}/\text{m}^3$. In accordance with Eq 4 measured conductivities or loss coefficients are normally plotted against T_r^3 . If a straight slope results, the extinction coefficient E can be assumed to be independent of T_r .

In a zeroth-order approach, we extrapolate the data set towards $T_r = 0$. From the ordinate intersection, we extract k_s , which we then subtract from k to obtain the radiative loss coefficient k_r as a function of T_r . Neither specific extinction coefficient e nor k_r changes upon compression of the specimen as long as the variation of n^2 with density is neglected and the scattering character remains "multiple independent scattering" in the fleece. Thus k_r can be subtracted from k for any temperature T_r , regardless of the state of compression, in order to derive k_s (or λ_s), which is assumed to be independent of T_r in this zeroth-order approach.

The solid conductivity of the insulating layer λ_s has been considered as depending on a number of parameters:

- Solid conductivity λ_o of the fiber material.
- Young's modulus Y_o of the fiber material.
- Porosity Π (or density ρ) of the layer.
- Pressure imposed upon the layer p_{ext} .
- Fiber orientation etc.:

$$\lambda_s = \lambda_o f(\Pi, Y_o, p_{\text{ext}}, \dots) \quad (6)$$

From measurements on λ_s and λ_o typical values for f on the order of 10^{-3} result.

In Kaganer's "lattice" model [4] of crossing fibers arranged regularly in planes perpendicular to the heat flow the number of contacts is unchanged upon compression. Only the area of each single contact increases. Thermal insulation is provided by the resistances of the contacts and the sections of fiber lying between two neighboring contacts.

In this case one obtains

$$f = \frac{16}{\pi^2} \left[\frac{Y_o^{1/3}}{\{3 \cdot \pi^2(1 - \mu^2)(1 - \Pi)^4 p_{\text{ext}}\}^{1/3}} + \frac{1}{4 \cdot (1 - \Pi)^3} \right]^{-1} \quad (7)$$

where μ is the Poisson's ratio of the fiber material. From Eqs 6 and 7 we learn that for efficient superinsulations λ_o ought to be as small as possible, while Y_o is required to be large and Π should approach 1. For typical values like $Y_o \approx 10^{10} \text{ N}/\text{m}^2$, $\Pi \approx 0.9$, $\mu^2 \ll 1$, $p_{\text{ext}} = 1 \text{ bar} = 10^5 \text{ N}/\text{m}^2$, one gets $f \approx 3 \cdot 10^{-3}$. Thus λ_s can be roughly a factor 10^3 smaller than λ_o .

In Kaganer's model, with the fibers being arranged in a regular state and the number of contacts being fixed, the porosity is assumed not to change upon compression. As especially in fleece-type fibrous insulations the porosity does change considerably, one has to modify Eq 7 to account for the compression of the insulating layer. The porosity Π now is considered as a function of p_{ext} . It can be determined from the insulation fiber mass per unit area m'' and the thickness d :

$$\Pi = 1 - \rho/\rho_o = 1 - m''/(d \cdot \rho_o) \quad (8)$$

A completely different view of insulating systems comes from percolation theory. In a percolating system at low densities (e.g., a tenuous layer of randomly oriented criss-crossing fibers), no conductivity at all occurs. Above a critical density ρ_c the conductivity λ_s (and thus also f) is said to "scale":

$$f = \begin{cases} 0 & \text{for } \rho < \rho_c \\ \text{const} \cdot (\rho - \rho_c)^\beta & \text{for } \rho \geq \rho_c \end{cases} \quad (9)$$

The increase of f with ρ in this statistical model is caused by the increasing probability of closed contacts between adjacent fibers. (The contacts are either "on" or "off.")

For highly porous aerogels, values of $\beta \approx 1.6$ and $\rho_c \approx 0$ have been derived [6].

According to the phonon diffusion model, the solid thermal conduction of nondisperse systems is

$$\lambda_s = (1/3) \cdot c_v \cdot \ell \cdot \rho \cdot v \quad (10)$$

where c_v is the specific heat at constant volume, ℓ is the phonon mean free path (on the order of 1 nm at ambient temperatures), and v is the sound velocity. We want to discuss whether this model can also be applied to a fiber layer. The relation

$$v = (Y/\rho)^{1/2} \quad (11)$$

holds approximately, where Y is the Young's modulus of the system (in our case = the fiber layer). Both c_v and ℓ are assumed to be independent of density ρ . From Eqs 10 and 11 we would expect

$$\lambda_s \propto (Y \cdot \rho)^{1/2} \quad (12)$$

Y can either be determined from static compression experiments by

$$Y(\rho) = \rho \frac{\partial p_{\text{ext}}}{\partial \rho} \quad (13)$$

or from ultrasonic propagation and use of Eq 11.

The density dependence of the thermal conductivity may conveniently be described by the g -value, defined [7] as

$$g = \frac{\partial \ln \lambda_s}{\partial \ln \rho} \quad (14)$$

We further introduce the following logarithmic derivatives:

$$h = \frac{\partial \ln Y}{\partial \ln \rho} \quad (15)$$

$$\varphi = \frac{\partial \ln \lambda_s}{\partial \ln Y} = \frac{g}{h} \quad (16)$$

$$\psi = \frac{\partial \ln \lambda_s}{\partial \ln(Y\rho)} = \frac{g \cdot \varphi}{g + \varphi} = \frac{g}{1 + h} \quad (17)$$

If the approximations in the phonon diffusion model hold (Eq 12), we have $g = (1 + h)/2$ and $\psi = 1/2$.

Thermal and Elasto-Mechanical Measurements

The apparatus used for the current investigation was the evacuable guarded hot plate device LOLA II [8]. It carries a piston system which allows us to apply a variable pressure load p_{ext} onto the evacuated sample. We record the thermal loss coefficient k and the thickness d of the specimens as a function of p_{ext} . From the various measurements we performed, we want to present data for two types of fiber insulations with comparable radiative heat transfer (i.e., with similar specific extinction coefficient e):

- Borosilicate glass fiber paper, consisting of amorphous fibers with diameters $\phi \approx 1$ to $7 \mu\text{m}$ and a solid conductivity λ_0 about $1 \text{ W}/(\text{m} \cdot \text{K})$; each fiber paper layer is 0.25 mm thick under a load of 1 bar , and the specific extinction coefficient is $e \approx 45 \text{ m}^2/\text{kg}$.
- Alumina fiber fleece consisting of fibers with at least some degree of crystallinity and diameters $\phi \approx 2$ to $4 \mu\text{m}$; the solid conductivity of the fibers is estimated to be $\lambda_0 \approx 10$ to $20 \text{ W}/(\text{m} \cdot \text{K})$, and the specific extinction coefficient is $e \approx 40 \text{ m}^2/\text{kg}$.

In Figs. 1a and 1b, the total thermal loss coefficient k as a function of T_1^3 is depicted for the two insulations. In both cases, the data fall on straight lines, underscoring the validity of the approximations described above. For the alumina fiber fleece, the loss coefficient is shown for $p_{\text{ext}} \approx 1 \text{ bar}$ and 0 bar . As the slopes and thus the specific extinction coefficients are comparable for the two pressures, the radiative heat transfer obviously is not altered significantly, though the geometrical conditions (6.5 mm versus 25 mm thickness) are drastically changed. A small decrease of the specific extinction upon compression from $e = 44$ to $41 \text{ m}^2/\text{kg}$ can be explained by a trend towards more dependent scattering in a compacted system and the increase of n^2 with density.

The major reason for the strongly increased thermal losses with rising pressure load is the increase in solid thermal conduction.

The total thermal losses of the two insulations as a function of p_{ext} are displayed in Figs. 2a and 2b. The temperatures are chosen low ($T_1 = 328 \text{ K}$, $T_2 = 298 \text{ K}$, $T_r = 313 \text{ K}$) in order to have as little contribution from k_r as possible. As indicated in the previous section, k_r is taken from Fig. 1 and subtracted from k in order to obtain k_s . In Figs. 3a and 3b, the thickness d of the insulation upon loading is depicted. Cycling leads to smaller thicknesses (i.e., larger densities). The data in Figs. 1 to 3 allow us to derive the solid conductivity λ_s as a function of p_{ext} (see Figs. 4a and 4b).

We observe the following features:

- $\lambda_s(p_{\text{ext}} \rightarrow 0)$ is decisively different for the two insulations. For the fleece, λ_s tends to vanish for $p_{\text{ext}} \rightarrow 0$; this is not observed for the fiber paper.
- At $p_{\text{ext}} = 1 \text{ bar}$, the conductivities are larger for the fleece ($\lambda_s \approx 2.8$ to $3 \text{ W}/(\text{m} \cdot \text{K})$) than for the fiber paper ($\lambda_s \approx 1.3$ to $1.7 \text{ W}/(\text{m} \cdot \text{K})$).

Both findings are plausible. In the paper insulation, even without external load, the paper layers touch and therefore $\lambda_s(p_{\text{ext}} \rightarrow 0) \neq 0$ results. For the fleece, on the other hand, we expect a vanishing conductivity, as fewer and fewer fibers touch each other for $p_{\text{ext}} \rightarrow 0$. The overall larger conductivity λ_s for the fleece is caused by the partial crystallinity of the alumina fibers (i.e., their large conductivity λ_0).

The logarithmic derivatives g , h , φ , and ψ determined from Figs. 5 to 7 are compiled in Table 2. The g -value was found to be about 2 for the two runs on alumina fleece (Fig. 5b) and for the uncompacted glass fiber paper (Fig. 5a). In the later cycles with the paper, however, a much steeper slope occurs. The difference is most pronounced in the variation of Young's modulus with density (Fig. 6a). We believe that the differences in λ_s and Y between the first run and the later cycles originates from the layered structure. In the uncompacted material one has the paper layers from which single, rather stiff fibers protrude. After compaction these fibers are "ironed" out. For a given load, then, an increased density and Young's modulus result, causing

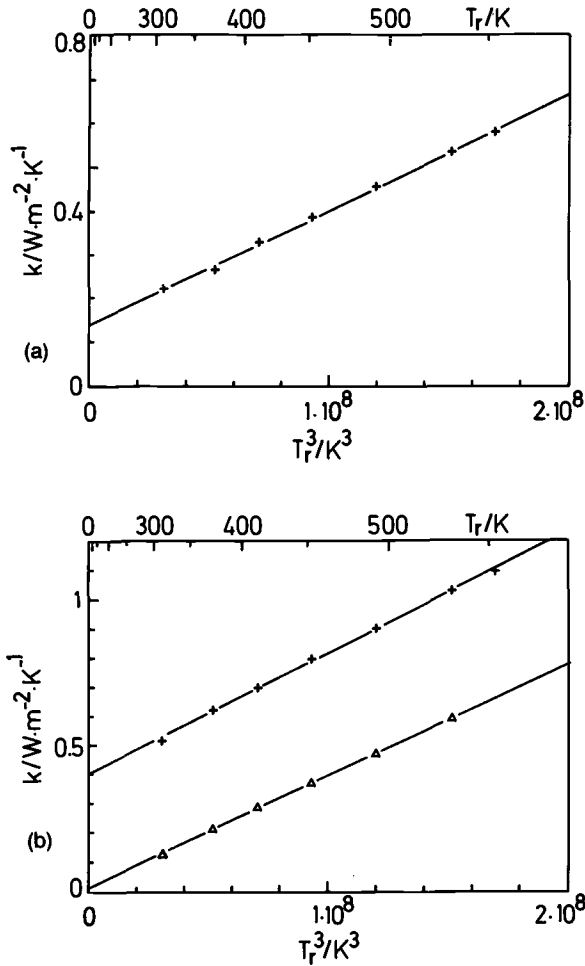


FIG. 1—Loss coefficient k of evacuated fibrous insulations with comparable specific extinction. (a) Boro-silicate fiber glass paper, mass per unit area $m'' \approx 2.5 \text{ kg/m}^2$, $e \approx 45 \text{ m}^2/\text{kg}$, $d \approx 10.3 \text{ mm}$ at $p_{\text{ext}} \approx 1 \text{ bar}$. (b) Alumina fiber fleece, $m'' \approx 1.8 \text{ kg/m}^2$, $d \approx 6.5 \text{ mm}$ and $e \approx 41 \text{ m}^2/\text{kg}$ at 1 bar [+], $d \approx 25 \text{ mm}$ and $e \approx 44 \text{ m}^2/\text{kg}$ at $p_{\text{ext}} = 0 \text{ bar}$ [Δ].

a higher solid conductivity (Fig. 4a). However, at a given density the laminar structure with the empty space in between has a smaller Young's modulus (Fig. 6a) and also a smaller solid conductivity (Fig. 5a).

Ultrasonic Investigation

The elasto-mechanical behavior of the alumina fleece was also studied by measuring the sound velocity v at ultrasonic frequencies (70 kHz). The measurements were performed under vacuum and with external pressure loads up to 0.6 bar. Typical values for v were 50 to 60 m/s. From v the Young's modulus Y can be derived according to Eq 11. As seen in Fig. 6b the values for Y determined by ultrasonic measurements are about 2 to 10 times larger than the values derived from static compression measurements. On the other hand, the logarithmic derivative h

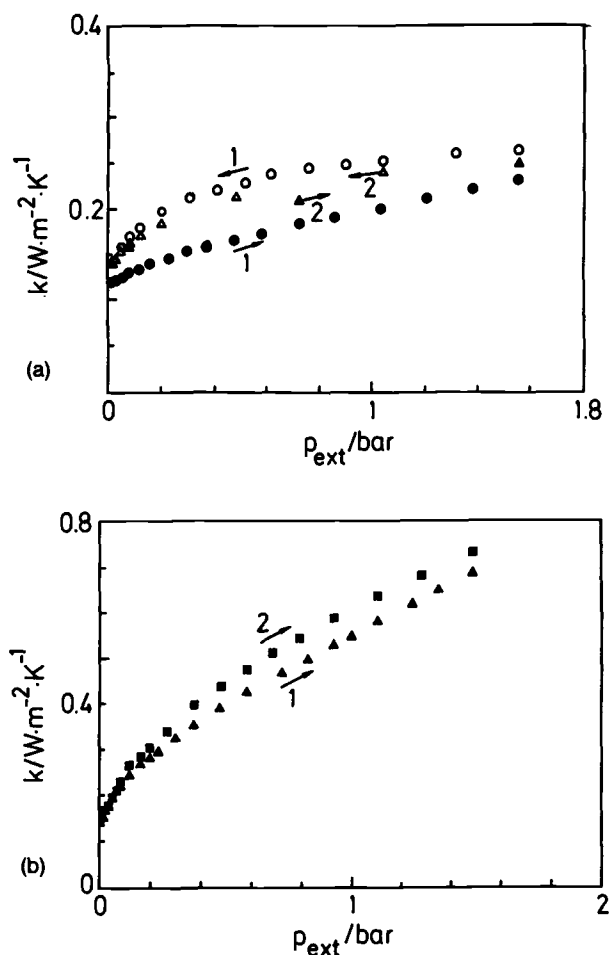


FIG. 2—Loss coefficient k versus external pressure load p_{ext} . (a) Borosilicate glass fiber paper. (b) Alumina fiber fleece. The successive loading/unloading cycles are indicated by numbers, the directions by arrows.

(Eq 15) is lower for the ultrasonic measurements ($h = 2.1$ compared to 3 to 4 for the static experiments).

The large difference can be explained by the visco-elastic behavior of the fleece. In the static measurements the material creeps for a few minutes after a change of external load. At ultrasonic frequencies no time is available for relaxation effects; thus the higher Young's modulus results.

Discussion of Models

Starting with Kaganer's model, using either a fixed porosity or a varying porosity according to Eq 8 with λ_0 as a fit parameter, $\lambda_s(p_{\text{ext}})$ for both insulation systems could be reproduced to within 30%. λ_0 was derived to be about $0.5 \text{ W}/(\text{m} \cdot \text{K})$ for the paper and $3 \text{ W}/(\text{m} \cdot \text{K})$ for the

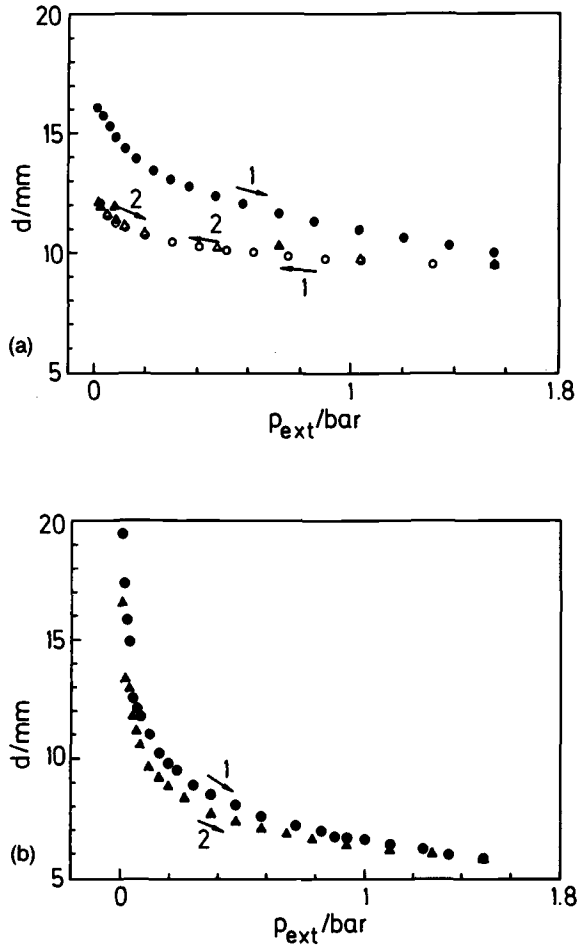


FIG. 3—Thickness d versus external pressure load p_{ext} . (a) Borosilicate glass fiber paper. (b) Alumina fiber fleece. Successive loading/unloading cycles are indicated by numbers and arrows.

fleece. The result for λ_0 in the paper is close to the anticipated value of about $1 \text{ W}/(\text{m} \cdot \text{K})$. However, the result for λ_0 in the fleece drastically deviates from the literature value $\lambda_0 \approx 30 \text{ W}/(\text{m} \cdot \text{K})$ for polycrystalline Al_2O_3 . Thus the degree of crystallinity in the fibers has to be small.

An attempt was made to fit the conductivity data also to the percolation model (Eq 9). For the alumina fleece, where one would expect percolation to occur, we obtained a critical density $\rho_c \approx 70 \pm 10 \text{ kg}/\text{m}^3$ for both runs. The derived exponent β was 1.2 ± 0.2 . For the paper in the first run $\rho_c \approx 90 \text{ kg}/\text{m}^3$ and $\beta \approx 1.1$ was derived. For the second run $\rho_c \approx 170 \text{ kg}/\text{m}^3$ and $\beta \approx 0.9$ occurred. Though the representation of data by the percolation model is much better than by Kaganer's model, one certainly would prefer the latter one, as it allows us to calculate absolute conductivity values from the known properties of the fiber material, while the former only provides a proportionality.

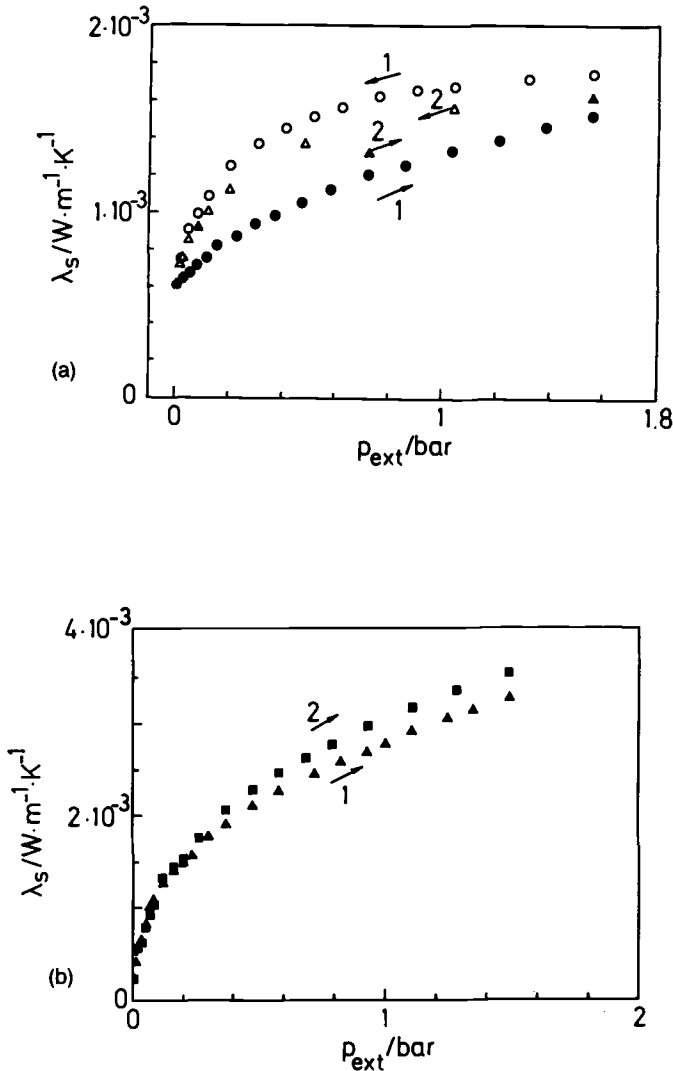


FIG. 4—Solid thermal conductivity λ_s versus p_{ext} . (a) Borosilicate glass fiber paper. (b) Alumina fiber fleece. The successive loading/unloading cycles are indicated by numbers and arrows.

From the phonon diffusion model we would expect λ_s to scale with $(\rho Y)^\psi$, with $\psi = 0.5$ (Eq 12). If Y is taken from the static compression measurements, the obtained values of ψ are lower than the predicted value. For the fleece and the first compression on the paper ψ is about 0.35, whereas the second cycle for the paper yields a value as low as 0.2 (Table 2).

If Y is taken from the ultrasonic data we have $h = 2.1$. Using an average g -value from both thermal measurements ($g = 1.9$), $\varphi = 0.9$ and $\psi = 0.6$ result. Obviously the latter data are more representative for high frequency phonon transport. Thus an eventual substitution of

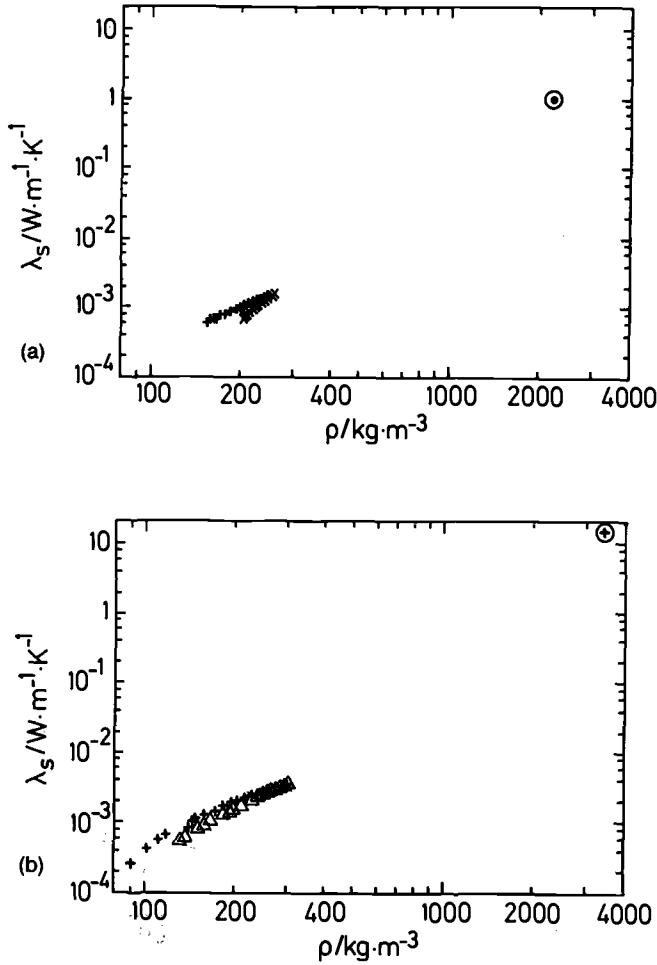


FIG. 5—Double log plot of solid conductivity λ_s versus density ρ of (a) borosilicate and (b) alumina system (+ corresponds to the first run in both cases); data for the largest conductivity/density combinations ($\lambda_s = \lambda_o$, $\rho = \rho_o$) represent massive borosilicate/alumina material.

time-consuming thermal measurements by elasto-mechanical investigations according to Eq 10 requires measurements of sound velocity at the highest possible frequencies.

The experimental data depicted in Figs. 5 to 7 are rather scarce with respect to the range of the variables shown. Data are only provided for the massive materials (ρ_o , Y_o and λ_o) and for low densities with $\rho \leq \rho_o/10$. Further measurements will have to show whether the derived slopes for small densities will persist upon further compression or whether a change of slopes (g , h and φ) occurs. Such a change was found upon compression of silica aerogel [6]. The derived g -values were 1.6 for $\rho < 900 \text{ kg/m}^3$ and 2.6 above. It is our goal to extend the pressure range to a few kilobars in order to investigate the region between the highly porous and the non-porous materials.

Finally a remark with respect to the optimization of fibrous superinsulations seems oppor-

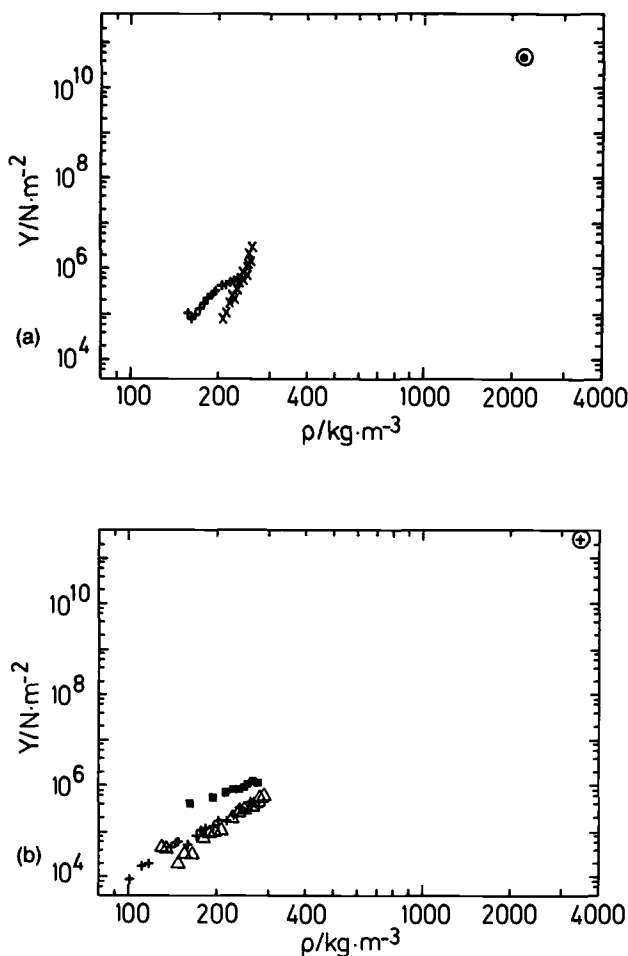


FIG. 6—Young's modulus Y versus density ρ for (a) borosilicate fiber paper (+: first run; X: second run) and (b) alumina fiber fleece (+: first run; Δ : second run; ■ data obtained by ultrasonic measurements). The encircled points indicate the values for the non-porous solids.

tune. From Figs. 4a and 4b we learn that in fleece systems small conductivities occur for low pressures, which, however, rapidly increase with p_{ext} . For paper insulations the conductivity at low pressures is much larger, but the increase with p_{ext} is smaller than for the fleece. Which of the systems is superior for thermal superinsulations thus depends on the pressure range it is to be used in. As the alumina fibers of the fleece show at least some degree of crystallinity and the material of the glass fiber paper is amorphous, we cannot decide whether a wool, fleece, or paper system made of the *same* material shows the lowest solid conductivity.

Acknowledgments

This work was supported by the German Bundesministerium für Forschung und Technologie (BMFT). One of us (O. N.) is indebted to the Deutsche Forschungsgemeinschaft (DFG).

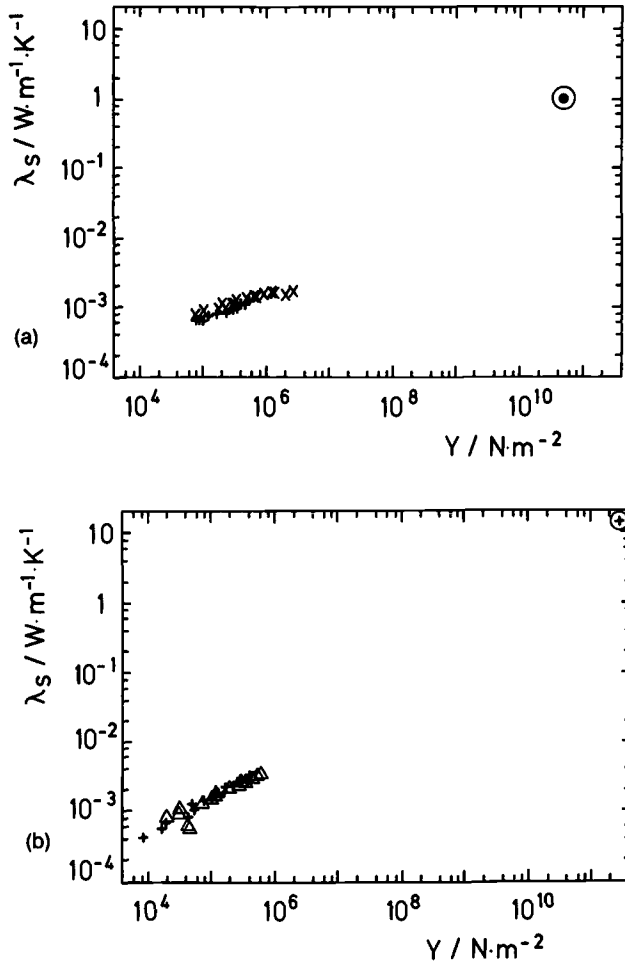


FIG. 7—Solid thermal conductivity λ_s versus Young's modulus for (a) borosilicate glass fiber paper and (b) alumina fiber fleece. The encircled points indicate the values for the non-porous solids (+ refers to the first run in both figures).

TABLE 2—Logarithmic derivatives defined in Eqs 14 to 17 for the borosilicate glass fiber paper and the alumina fleece, derived from thermal and static compression measurements.

	Glass Fiber Paper		Alumina Fleece		
	First Run	Second Run	First Run	Second Run	Ultrasonic Measurements
g	2.0	3.3	1.7	2.1	1.9 ^a
h	3.9	17.5	3.0	4.6	2.1
φ	0.40	0.22	0.49	0.45	0.9
ψ	0.33	0.20	0.38	0.37	0.6

^aAverage of g -values from thermal measurements.

References

- [1] Büttner, D., Fricke, J., and Reiss, H., "Analysis of the Radiative and Solid Conduction Components of the Thermal Conductivity of an Evacuated Glass Fiber Insulation: Measurements with a 700×700 mm² Variable Load Guarded Hot Plate Device," in *Proceedings, 20th AIAA Thermophysics Conference*, Williamsburg, Va., 1985, Paper 85-1019.
- [2] Fricke, J., Caps, R., Hümmer, E., Döll, G., Arduini, M. C., and De Ponte, F., "Optically Thin Fibrous Insulations," this publication, pp. 575-586.
- [3] Fricke, J., Büttner, D., Caps, R., Döll, G., Hümmer, E., Kreh, A., and Reiss, H., "Load-Bearing Evacuated Fibrous Superinsulations," presented to 20th International Thermal Conductivity Conference, Blacksburg, Va., Oct. 1987.
- [4] Kaganer, M. G., "Thermal Insulation in Cryogenic Engineering," Israel Program for Scientific Translations, Jerusalem, 1969, p. 24.
- [5] Büttner, D., Löffler, G., Caps, R., and Fricke, J., "Investigation of Solid Thermal Conduction in Evacuated Load-Bearing Fibrous Insulations," *High Temperatures - High Pressures*, Vol. 18, 1986, pp. 537-543.
- [6] Nilsson, O., Fransson, Å., and Sandberg, O., "Thermal Properties of Silica Aerogel," in *Aerogels*, Springer Proc. in *Physics*, Vol. 6, J. Fricke, Ed., Springer Verlag, Heidelberg, 1986, pp. 121-126.
- [7] Slack, G. A. in *Solid-State Physics*, H. Ehrenreich, F. Seitz, and D. Turnbull, Eds., Academic Press, New York, 1979, pp. 1-71.
- [8] Scheuerpflug, P., Caps, R., Büttner, D., and Fricke, J., *International Journal of Heat and Mass Transfer*, Vol. 28, 1985, pp. 2299-2306.

DISCUSSION

*Francesco De Ponte*¹ (written discussion)—Are your results valid only in vacuum or can they be extended to solid conduction for insulations in air?

J. Fricke et al. (authors' response)—In general it is not possible to calculate the total conductivity, λ_{total} , from the data for evacuated insulations, λ_{evac} , by just adding the thermal conductivity of air, λ_{air} . λ_{total} may be larger or smaller than $\lambda_{\text{evac}} + \lambda_{\text{air}}$. For granular fills consisting of massive, hard, and well-conducting grains, one has $\lambda_{\text{total}} = \lambda_{\text{evac}} + C \cdot \lambda_{\text{air}}$, with $C > 1$. For highly porous, spongy, and weak-conducting grains (e.g., aerogels), C could be as low as 0.5. We are currently investigating this coupling effect in our laboratory.

¹Istituto di Fisica Tecnica, Via Marzolo, 9, I-35131 Padova, Italy.

Radiant Heat Transfer in Extremely Low Density Fibrous Assemblies

REFERENCE: Dent, R. W., Skelton, J., and Donovan, J. G., "Radiant Heat Transfer in Extremely Low Density Fibrous Assemblies," *Insulation Materials, Testing, and Applications, ASTM STP 1030*, D. L. McElroy and J. F. Kimpflen, Eds., American Society for Testing and Materials, Philadelphia, 1990, pp. 79-105.

ABSTRACT: In very low density insulating assemblies, heat transfer occurs mainly by gas phase conduction, by convention, and by radiation. Many attempts have been made to analyze the parameters that control the radiant component of this heat transfer using electromagnetic theory based on the Maxwell equations. Extensive solutions are available in the literature for spheres but few results have been calculated for cylinders (which would model fibrous insulations), although the relevant equations have been given by Van de Hulst and by Larkin and Churchill. Larkin and Churchill give appropriate values for "real" refractive indices only, with zero absorption.

We have now obtained complete "complex" solutions as functions of fiber diameter and the fiber optical properties of refractive index and absorption coefficient (or dielectric constant). These solutions allow a full understanding of the roles of scattering and absorption in radiant energy transfer and show how these can be optimized for various materials as a function of wavelength (or temperature).

Once the radiant heat transfer is minimized for single isolated cylinders, we consider how this translates to a low density assembly of many such cylinders or fibers. The results show that radiant heat transfer can be minimized by the selection of an optimum fiber diameter and that this optimum differs for each material and for different absorption coefficients (as these affect the real and imaginary parts of the refractive index which determine the heat transfer).

KEY WORDS: radiant heat transfer, fibrous assemblies, density, insulation, cylinders, fiber diameter, optical properties, refractive index, absorption coefficient

Nomenclature

L	Assembly thickness
ΔT	Temperature difference across assembly
k_o	"Effective" overall thermal conductivity
k_a	Air thermal conductivity
k_R	Radiant conductivity
k_{Ro}	Radiant conductivity of an air gap
σ	Boltzmann's constant
T_m	Effective mean temperature
ϵ_0, ϵ_L	Plate emissivities at $x = 0$ and $x = L$
T_0, T_L	Plate temperatures at $x = 0$ and $x = L$
ϕ_e	Radiation extinction efficiency factor
K_s	Scattering coefficient (or cross section)
K_a	Absorption coefficient (or cross section)
K_e	Extinction coefficient (or cross section)

¹Albany International Research Company, Mansfield, MA 02048-9114.

ρ_F	Fabric (or fibrous assembly) packing density
d	Fiber diameter
E_i, E_s, E_c	Incident, scattered, and internal electric vectors
$J_j(\)$	j th-order Bessel function of first kind
α	Normalized diameter = $\pi d/\lambda$
$H_j(\)$	j th-order Hankel function of second kind
$Y_j(\)$	j th-order Bessel function of second kind
A_j, B_j	Wave amplitude coefficients for parallel polarization
P_j	Wave amplitude coefficients for perpendicular polarization
t	Time
ω	Angular speed
c	Speed of light
λ, λ_m	Median wavelength
B	Back-scattered fraction
H	Magnetic field strength vector
$J'_j(\), H'_j(\)$	Differentials of $J_j(\)$ and $H_j(\)$ with respect to α
$ A_j $	Absolute value of amplitude
$\text{Re}(\)$	Real part
$\text{Im}(\)$	Imaginary part
m	Refractive index (complex)
n	Refractive index (real part)
k	Refractive index (imaginary part)
ϕ_s, ϕ_a	Scattering and absorption efficiencies
χ	$= \alpha - j\pi/2 - \pi/4$
β, γ	Angles dependent on m, α , and χ
M	Electron mass
E	Electric field
e	Electron charge
β	Damping constant per unit mass
ω_0	Natural angular speed
N	Number of free electrons/unit volume
P	Polarization
$\bar{\epsilon}, \epsilon$	Dielectric constant (complex and real parts)
A	$= 4\pi Ne^2/M$
σ_E	Conductivity
ν	Frequency
$\ell, \bar{\ell}$	Typical and average fiber lengths
δ	Slice dimension
D, \bar{D}	Typical and average value of $d \sec \theta$
θ	Fiber inclination in slice
n_ℓ	Number of fibers/unit length
n_a	Number of fibers/unit area
n_v	Number of fibers/unit volume
t_1, t_L	Fractional transmissions for thickness of 1 cm and L cm
ρ_f	Fiber density

Introduction

It has been shown by Pelanne [1] and others [2] that the main heat transfer mechanisms in extremely low density insulators of the fibrous type are gas conduction, natural convection, and radiation. The gas phase conduction cannot really be altered, except by sealing and evacuating

the system, while the convective component is controlled [3] by the structural geometry (density and fiber diameter) and the Rayleigh number ($\propto L^3 \Delta T$) where L is the assembly thickness and ΔT is the temperature difference across the insulator.

Often the major cause of energy transfer is the radiative component. We need to fully understand the factors which control this heat transfer mechanism in order to control and minimize its contribution. Such an understanding is the objective of this paper where we try to define the optimum fiber size (diameter) for a given web density and fiber optical properties, etc., in order to minimize the radiative heat transfer.

Various workers [4-6] have interpreted the radiant heat transfer between two horizontal plates in terms of forward and backward radiant fluxes. In very low density structures this is inappropriate since the radiant flux depends on the interference of scattered radiation, which cannot be resolved into only these two directions and whose true effects are mostly lost if this is done.

Thus, if the plates are horizontal with the hotter one uppermost so that convection is suppressed and negligible even at quite large Rayleigh numbers, then the overall "effective" thermal conductivity k_o is given approximately by

$$k_o = k_a + k_R$$

where k_a is the thermal conductivity of air and k_R is the "effective" radiant conductivity. If we consider an air gap alone, then the classical result for the radiant conductivity is

$$k_{Ro} = \frac{4\sigma T_m^3 L}{\left(\frac{1}{\epsilon_L} + \frac{1}{\epsilon_0} - 1\right)}$$

where σ is Boltzmann's constant, L is the plate spacing, ϵ_L and ϵ_0 are the plate emissivities, and T_m is an effective temperature such that

$$4T_m^3(T_L - T_0) = T_L^4 - T_0^4$$

and T_L and T_0 are the plate temperatures (absolute) at $x = 0$ and $x = L$.

When some fibers are added to this air gap, they absorb the radiation as well as scattering it in *all* directions. This means that the net radiant flux

$$\sigma(\epsilon_L T_L^4 - \epsilon_0 T_0^4)$$

now decreases with distance x . Hence the "effective" radiant conductivity k_R is reduced to

$$k_R = k_{Ro}[1 - \phi_e(K_s, K_a, d, \rho_F, L)]$$

where ϕ_e is the radiation extinction efficiency factor that depends on K_s and K_a which are the scattering and absorption coefficients (or cross sections) obtained from basic, classical, electromagnetic theory for single cylinders. This dependency can also be written in terms of the total extinction cross section or coefficient K_e , where $K_e = K_s + K_a$. The factor ϕ_e also depends on d , the cylinder (or fiber) diameter, on L , the plate separation, and on ρ_F , the fabric or fibrous assembly packing density, assuming the plate separation corresponds to the natural uncompressed thickness of the fibrous assembly. In this paper, we will try to define the function ϕ_e in general for *absorbing* as well as for scattering fibers and for assemblies of such fibers. We will consider single cylinders first.

A Single Cylinder

The use of the Maxwell equations to predict the polar scattering of electromagnetic waves is fully described by Van de Hulst [7] and Stratton [8]. The theory was initially developed by Mie [9] for spheres, and Van de Hulst gives many calculated results. Unfortunately, comparable results for cylinders are not available and these differ by the use of cylindrical rather than spherical functions.

Scattering Theory with Absorption

The relevant equations are given by Larkin and Churchill [10] and so we will summarize their results with a brief explanation. Essentially, the wave equations for the incident radiation and the scattered wave are written as Fourier series (for both the parallel and perpendicularly polarized components for perpendicular incidence), and these are expressed in terms of either Bessel functions J_j or Hankel functions H_j . The Bessel functions are used for plane waves and Hankel functions for radial waves. The results for the incident wave vector E_i and the scattered wave vector E_s (at the cylinder surface) are

$$E_i = e^{i\omega t} \left[J_0(\alpha) + 2 \sum_{j=1}^{\infty} i^j J_j(\alpha) \cos j\theta \right] \quad (1)$$

and

$$E_s = e^{i\omega t} \left[A_0 H_0(\alpha) + 2 \sum_{j=1}^{\infty} i^j A_j H_j(\alpha) \cos j\theta \right] \quad (2)$$

The corresponding result *inside* the cylinder E_c (at its surface) is

$$E_c = e^{i\omega t} \left[B_0 J_0(m\alpha) + 2 \sum_{j=1}^{\infty} i^j B_j J_j(m\alpha) \cos j\theta \right] \quad (3)$$

where m is the refractive index which is complex for an absorbing cylinder such that $m = n - ik$, with n and k the real and imaginary parts, while α is the normalized diameter such that

$$\alpha = \frac{\pi d}{\lambda}$$

where λ is the appropriate wavelength and d is the cylinder or fiber diameter.

In these equations, E is the electric field strength vector and the subscripts "i," "s" and "c" refer to the incident, scattered and cylinder (internal) waves. The angular speed is

$$\omega = \frac{2\pi}{\lambda} c$$

where c is the speed of light and λ is the wavelength, while t is time, $i = \sqrt{-1}$, and θ is the angle relative to the direction of incidence. J_j is a Bessel function of the first kind (which is appropriate for a plane wave) and H_j is the Hankel function of the second kind (appropriate for an outward-going cylindrical wave, as in scattering) such that

$$H_j = J_j - iY_j \quad (4)$$

where Y_j is the Bessel function of the second kind (or N_j , the Neumann function).

The wave amplitudes are determined by the coefficients A_j and B_j , with that of the incident wave being taken as unity. The value of A_j determines the final scattering and absorption. A_j is complex and is obtained from the boundary condition at the cylinder surface. This requires that the electric field E strength be continuous, so that the external field, given by Eqs 1 and 2, must equal the field inside the cylinder, given by Eq 3. Thus

$$J_j(\alpha) - A_j H_j(\alpha) = B_j J_j(m\alpha)$$

Also, the magnetic field strength vector

$$H = \frac{\partial E}{\partial \alpha}$$

must also be continuous, so that

$$J'_j(\alpha) - A_j H'_j(\alpha) = m B_j J'_j(m\alpha)$$

where

$$J'_j(\alpha) = \frac{dJ_j(\alpha)}{d\alpha} \quad \text{etc.}$$

From these boundary conditions, we can eliminate B_j and obtain

$$A_j = \frac{m J_j(\alpha) J'_j(m\alpha) - J_j(m\alpha) J'_j(\alpha)}{m H_j(\alpha) J'_j(m\alpha) - J_j(m\alpha) H'_j(\alpha)} \quad (5)$$

This is the result when the electric vector is parallel to the cylinder axis. We similarly obtain the corresponding result for the vector perpendicular to the cylinder axis:

$$P_j = \frac{J_j(\alpha) J'_j(m\alpha) - m J_j(m\alpha) J'_j(\alpha)}{H_j(\alpha) J'_j(m\alpha) - m J_j(m\alpha) H'_j(\alpha)} \quad (6)$$

We assume that our cylinders (fibers) are perpendicular to the incident beam but randomly oriented in this plane. In this case, the arithmetic average of A_j and P_j is then the wave amplitude for *randomly* polarized radiation.

From the amplitudes A_j and P_j , we then calculate the scattering coefficient K_s from

$$K_s = \frac{1}{\alpha} \left[\sum_{j=-\infty}^{\infty} |A_j|^2 + \sum_{j=-\infty}^{\infty} |P_j|^2 \right] \quad (7)$$

and the total "extinction" coefficient K_e from

$$K_e = \frac{1}{\alpha} \left[\sum_{j=-\infty}^{\infty} \text{Re}(A_j) + \sum_{j=-\infty}^{\infty} \text{Re}(P_j) \right] \quad (8)$$

while the absorption coefficient is obtained from

$$K_a = K_e - K_s \quad (9)$$

In these equations, $|A_j|^2$ is the absolute value of the amplitude such that

$$|A_j|^2 = \text{Re}^2(A_j) + \text{Im}^2(A_j)$$

where $\text{Re}(A_j)$ and $\text{Im}(A_j)$ are the real and imaginary parts of the complex amplitude A_j (and similarly for P_j).

It is seen from Eqs 7 and 8 that all the results follow from the calculation of the real and imaginary parts of A_j and P_j . Equations 5 and 6 show that these are somewhat awkward functions of $J_j(\alpha)$ and $H_j(\alpha)$. As these values depend on α , we will first consider the limiting cases of small α and then large α , since we can obtain analytical (rather than graphical) results in these cases. Subsequently, we consider general values of α .

Small Diameter Cylinders

Equations 7, 8, and 9 show that all the results are obtained from A_j and P_j given in Eqs 5 and 6. These are not simple functions, but the expansions of $J_j(\alpha)$, $J'_j(\alpha)$, $H_j(\alpha)$, etc., are available in standard tables. Hence we can obtain A_j and P_j approximately when $\alpha \rightarrow 0$ or for the case of small diameters. It turns out that the dominant terms are A_0 and P_1 and that all other terms are negligible.

Expansion and calculation then give

$$K_e = \frac{\pi \alpha n k}{2} \left[1 + \frac{4}{(n^2 - k^2 + 1)^2 + (2nk)^2} \right] + \frac{\pi^2 \alpha^3}{16} [(n^2 - k^2 - 1)^2 - (2nk)^2 - \dots]$$

$$K_s = \frac{\pi^2 \alpha^3}{16} \left[(n^2 - k^2 - 1)^2 + (2nk)^2 + 2 \frac{\{(n^2 + k^2) - 1\}^2 + (4nk)^2}{\{(n^2 - k^2 + 1)^2 + (2nk)^2\}^2} \right] + \dots$$

and

$$K_a = \frac{\pi \alpha n k}{2} \left[1 + \frac{4}{(n^2 - k^2 + 1)^2 + (2nk)^2} \right] - \frac{\pi^2 \alpha^3 n^2 k^2}{2} [1 + \dots]$$

We see that if $k = 0$ (so that the refractive index is real), then

$$K_a = 0 \quad \text{and} \quad K_e \equiv K_s \propto \alpha^3$$

It will be shown later that extinction, scattering, and absorption efficiencies are defined such that $\phi_e \propto K_e/\alpha$, $\phi_s \propto K_s/\alpha$, and $\phi_a \propto K_a/\alpha$, so that from above, when $k = 0$, $\phi_e = \phi_s$ and both are functions of α^2 . However, when $k \neq 0$, the value of ϕ_s is unaltered but ϕ_e is now increased by the value ϕ_a , which in this case is now not zero but is roughly proportional to nk and independent of α .

Large Diameter Cylinders ($\alpha \rightarrow \infty$)

The calculation of the upper limit for large values of α is more difficult, since the sums in Eqs 7 and 8 have to be taken out to $n = \alpha$ terms before further terms become negligible. In fact:

$$J_{\alpha}(\alpha) = 0.45\alpha^{-1/3}$$

$$J'_{\alpha}(\alpha) = 0.41\alpha^{-2/3}$$

$$H_{\alpha}(\alpha) = 0.45\sqrt{3}\alpha^{-1/3}$$

and

$$H'_{\alpha}(\alpha) = 0.41\sqrt{3}\alpha^{-2/3}$$

so that

$$A_{\alpha} = -\frac{1}{\sqrt{3}} \left(\frac{m^{2/3} - 1}{m^{2/3} + 1} \right)$$

which is already quite small. When $j > \alpha$,

$$J_j(\alpha) = \frac{1}{\sqrt{2\pi j}} \left(\frac{e\alpha}{2j} \right)^j \rightarrow 0$$

and all the other terms similarly vanish.

However, when $\alpha \rightarrow \infty$ and $j < \alpha$, then

$$J_j(\alpha) = \sqrt{\frac{2}{\pi\alpha}} \cos \chi$$

where

$$\chi = \alpha - \frac{j\pi}{2} - \frac{\pi}{4}$$

so that eventually we find

$$\text{Re}(A_j) = \sin^2(\beta - \chi)$$

where

$$\tan \beta = m \tan((m-1)\alpha + \chi)$$

and similarly

$$\text{Re}(P_j) = \sin^2(\gamma - \chi)$$

where

$$\tan \gamma = \frac{1}{m} \tan((m-1)\alpha + \chi)$$

and

$$\text{Im}(A_j) = \sin 2(\beta - \chi) \quad \text{and} \quad \text{Im}(P_j) = \sin 2(\gamma - \chi)$$

Now the mean value of $\sin^2(\beta - \chi)$ is $1/2$ when taken over multiples of $\beta - \chi = \ell\pi$, where ℓ is an integer. From Eq 8, we see that

$$K_e = \frac{1}{\alpha} \left[\text{Re}(A_0) + 2 \sum_{j=1}^{\infty} \text{Re}(A_j) + \text{Re}(P_0) + 2 \sum_{j=1}^{\infty} \text{Re}(P_j) \right]$$

Now, as the sums must be taken to $j \approx \alpha$ and $\text{Re}(A_j) \approx 1/2$ for all n , we see that $K_e \rightarrow 2$. This is a very important result and is discussed a little later.

Thus, we find that ϕ_e (which is proportional to K_e/α) increases with α^2 when $\alpha \ll 1$, but the fact that $K_e \rightarrow 2$ when $\alpha \gg 1$ means that ϕ_e decreases inversely as α at large α . Hence it is clear that there should be an optimum value for α where the extinction is maximized and the radiative heat transfer is minimized. This implication was previously noted by Larkin and Churchill [4] and by Aronson [11], and they quote experimental data that tend to confirm this suggestion. Larkin and Churchill found a maximum diameter for fiberglass somewhere between 2.5 and 10 μm at 93°C (200°F) with a shift to lower diameters at higher temperatures. Aronson shows a calculated optimum between 2 and 8 μm for polypropylene.

The fact that $K_e \rightarrow 2$ at large diameters d means that the fiber removes twice its own projected area from the incident wave. At first glance, this appears to be impossible and the effect is called the Extinction Paradox [7]. The extra removal, above that scattered or absorbed, is due to interference or diffraction by the light incident on the cylinder edges which doubles the energy lost by the incident flux [12].

The General Solution

So far we have been considering the issue of a system optimized for minimum radiation transfer in qualitative terms only. Equations 7 to 9 give us the means to obtain rigorous information from which to calculate quantitative results for such optima. Unfortunately, these equations have only been thoroughly solved (over the entire range of α) for a scattering, nonabsorbing cylinder (or fiber), although Larkin and Churchill [10] give some calculated results for refractive indices of $m = 1.5$, 2.0, and 2.5.

In practice, most polymeric materials absorb radiation as well as scattering it. This means that the refractive index of the material is complex, such that

$$m = n - ik$$

where n is the "real" part and k is the "imaginary" part of the refractive index. Larkin and Churchill point out that in this case, the equations are identical, but with m now being complex, as above. However, this requires the availability of tables or graphs of the Bessel functions (real and imaginary parts) of *complex* arguments. These have previously been unavailable so that results could only be calculated with difficulty. Van de Hulst [7] does report a few results specifically for $m = 1.414 - 1.414i$ and for $m = 1.25 - 0.10i$ and $m = 1.50 - 0.10i$.

The trends shown by these cases are similar to those for spheres but differ quantitatively. Also, the foregoing results give too little data to obtain the accurate trends we require in our task of looking for optimum diameters. Accordingly, we have now calculated the required Bessel functions for complex arguments.

Results

Armed with these values, we can now exactly evaluate Eqs 5 and 6 as functions of α for any selected values of n and k where the refractive index m is defined by

$$m = n - ik$$

and hence calculate the coefficients K_s , K_a and K_e for specific combinations, corresponding to any material of interest. A typical result is given in Fig. 1 for a fixed value of 1.50 for the real part, n , of the refractive index and for various values of k from 0 to 0.50. The corresponding contributions of the scattering K_s and absorption K_a terms to the total extinction K_e are shown for the same case where $m = 1.50 - ik$ in Figs. 2 and 3. The relative contributions of K_s and K_a to K_e are shown in Fig. 4, where $m = 1.50 - 0.50i$. If we plot the scattering results for different n against $y = \alpha(m - 1)$ as abscissa, then the results largely coincide for a wide range of values of n (for zero absorption) as shown in Fig. 5. This clearly shows the role of n , the real part of the refractive index. Some corresponding results of the backscattering fraction defined by Larkin and Churchill [10] are given in Fig. 6, again for zero absorption.

These typical results clearly show that a single cylinder which only scatters (i.e., has a real refractive index) gives a series of maxima and minima in the extinction curve $K_e(\alpha)$ and that any concurrent absorption tends to dampen out this cyclic behavior. This means that for a single cylinder there are a series of optimum diameters of decreasing magnitude at values close to $y = \alpha(m - 1) = 1.8, 5.0, 8.0$, etc., with the initial value causing the most extinction of all. These maxima are caused by reinforcing interference. In between these optima are minima such that the extinction at that diameter may be only a quarter as much as that at the first maximum for scattering alone. This shows that the choice of diameter can have an extremely important effect on the resulting system behavior. However, it will be shown later that the optimum diameter for an assembly may differ significantly from that for a single cylinder (or fiber).

Before examining this assembly effect, we need to consider how to obtain values for the real and imaginary parts n and k of the refractive index m . Unfortunately, in many cases, this information is not immediately available. A value for the real part of the refractive index is often known but is generally measured at the wavelength of a sodium lamp, which is $0.59 \mu\text{m}$. In our calculations, we are dealing with wavelengths up to the order of $10 \mu\text{m}$ (when $T \approx 300 \text{ K}$), this value being obtained from Wein's displacement law for radiation which shows that the peak wavelength λ_m for any absolute temperature T is given by

$$\lambda_m T = 2897.8 \mu\text{m K} \quad (10)$$

Thus we next consider how to convert n and k data from the wavelength of measurement to the wavelength of interest.

Complex Refractive Indices and Wavelength

Borne and Wolf [13] give the result for a damped electron, but this is inadequate for our needs, so we must extend their result to the more general case of the electron which is also undergoing simple harmonic motion.

In an electric field E , the motion of an electron (of charge e) is given by

$$M\ddot{x} = Ee - M\beta\dot{x} - M\omega_0^2 x$$

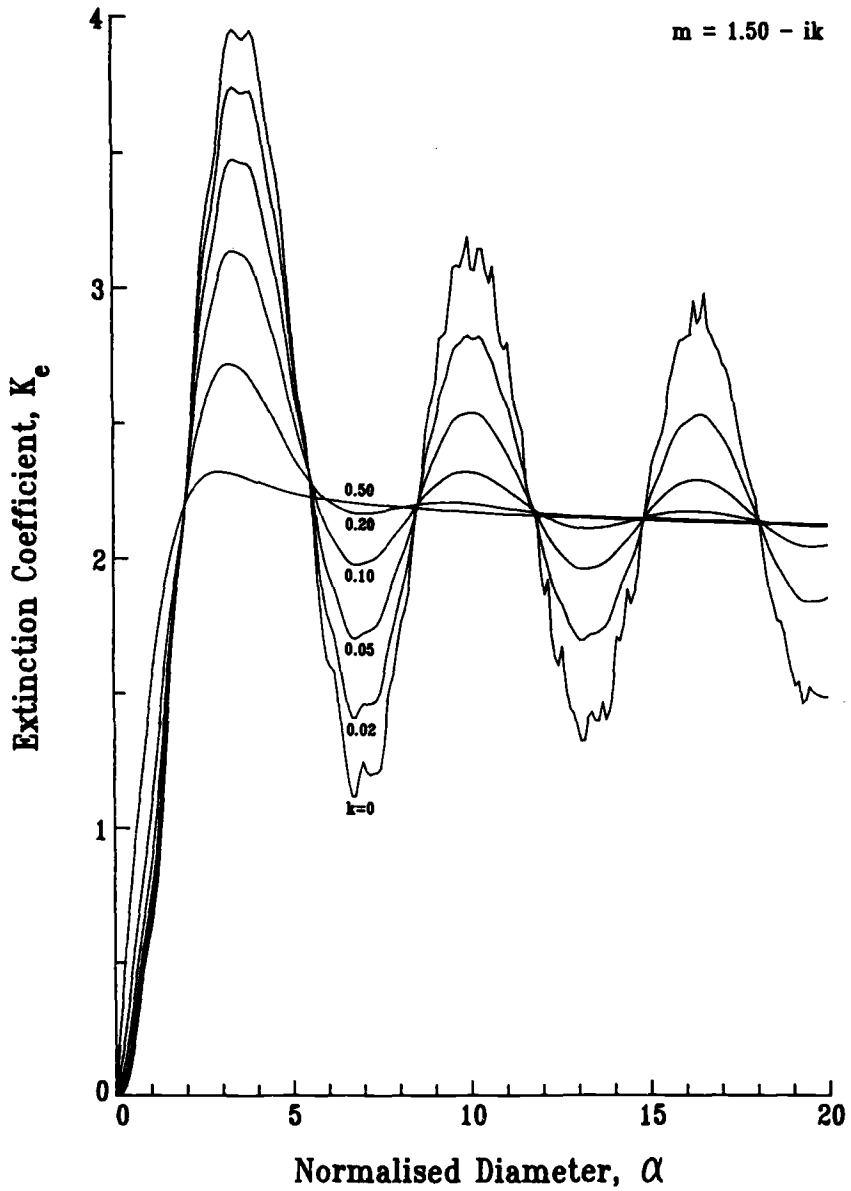


FIG. 1—Extinction coefficient K_e shown as a function of x for $n = 1.50$ and various values of k from 0 to 0.5.

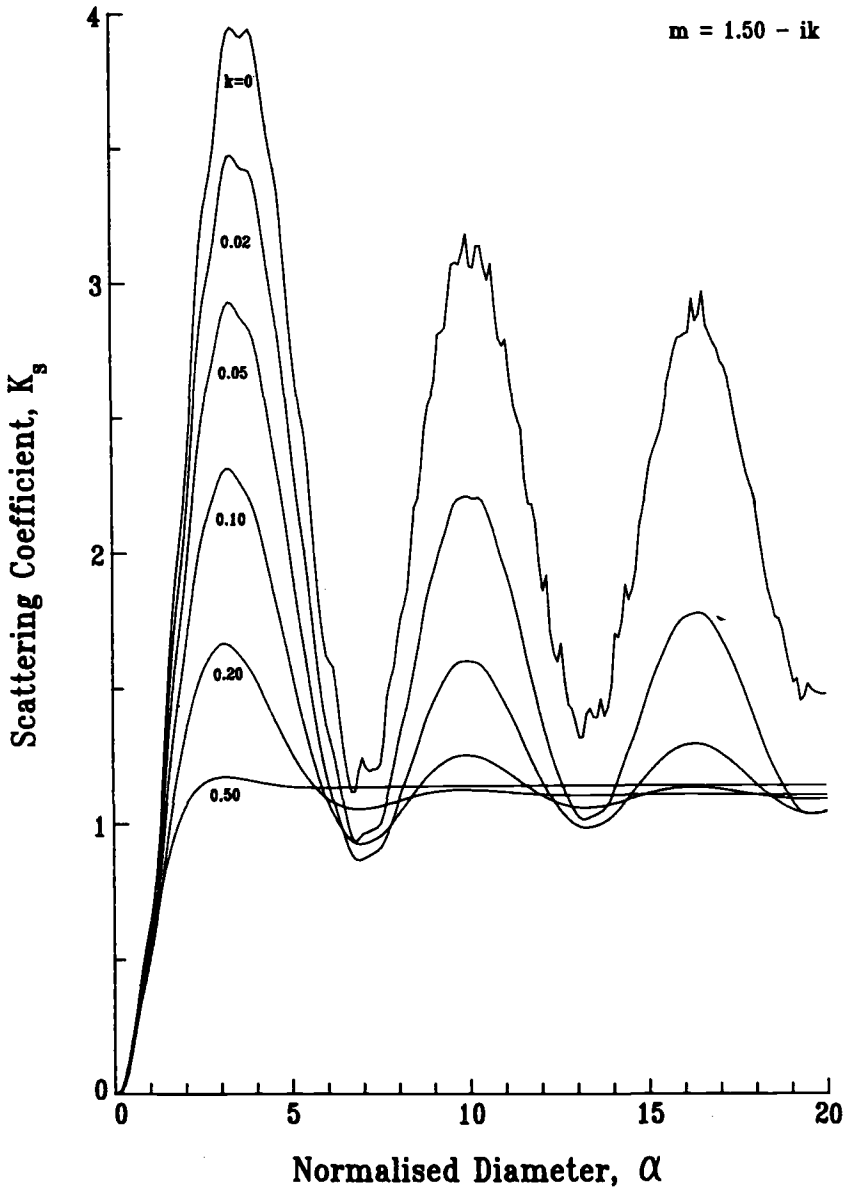


FIG. 2—Scattering coefficient K_s shown as a function of x for $n = 1.50$ and various values of k from 0 to 0.5.

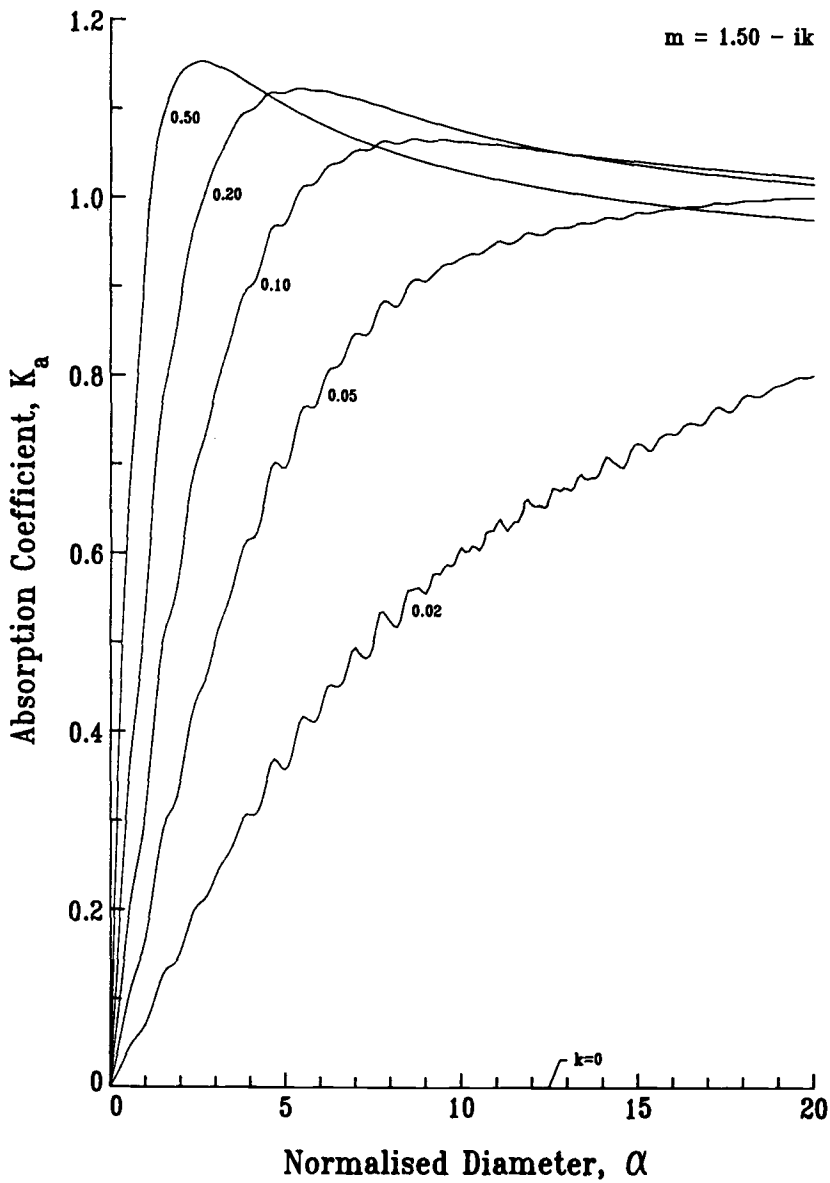


FIG. 3—Absorption coefficient K_a shown as a function of x for $n = 1.50$ and various values of k from 0 to 0.5.

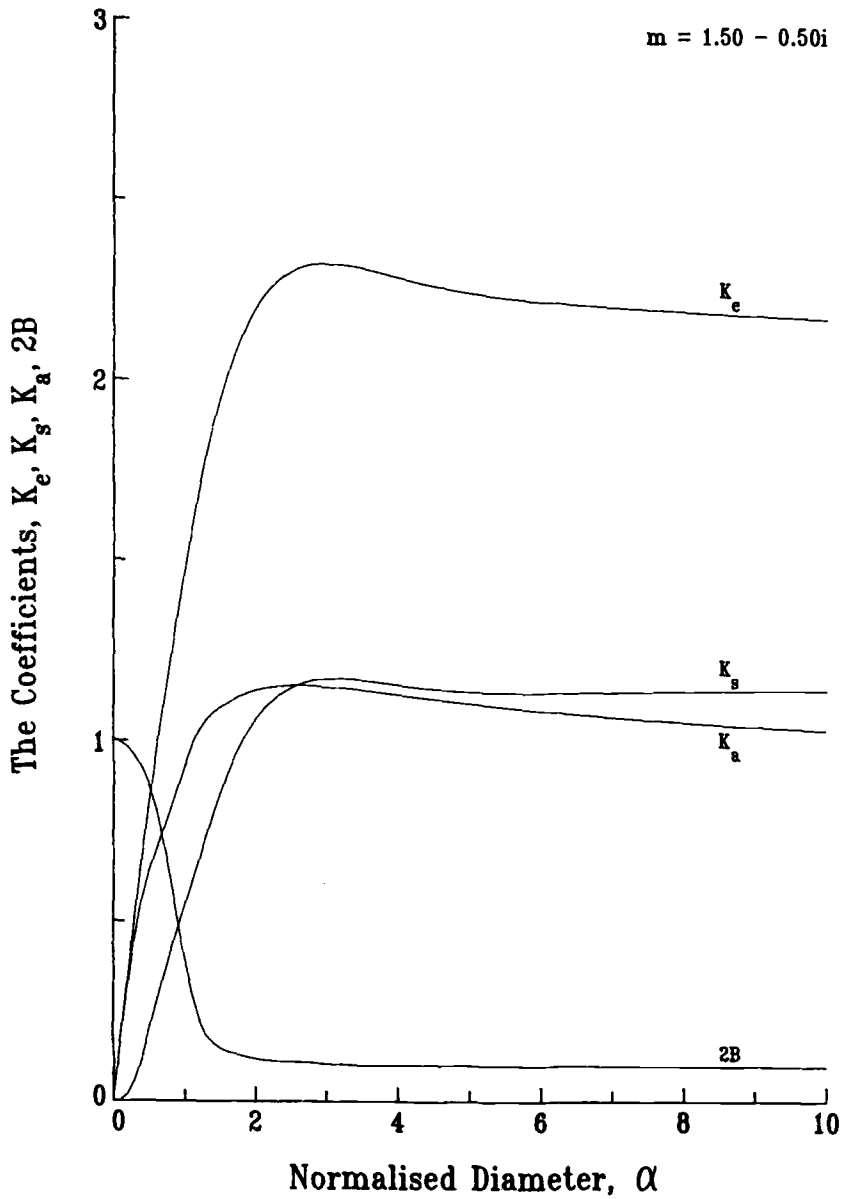


FIG. 4—Scattering, absorption, and extinction coefficients compared in one case where $m = 1.50 - 0.50i$ which shows their relative contributions. Also shown is $2B$, where B is the back-scattered fraction [10].

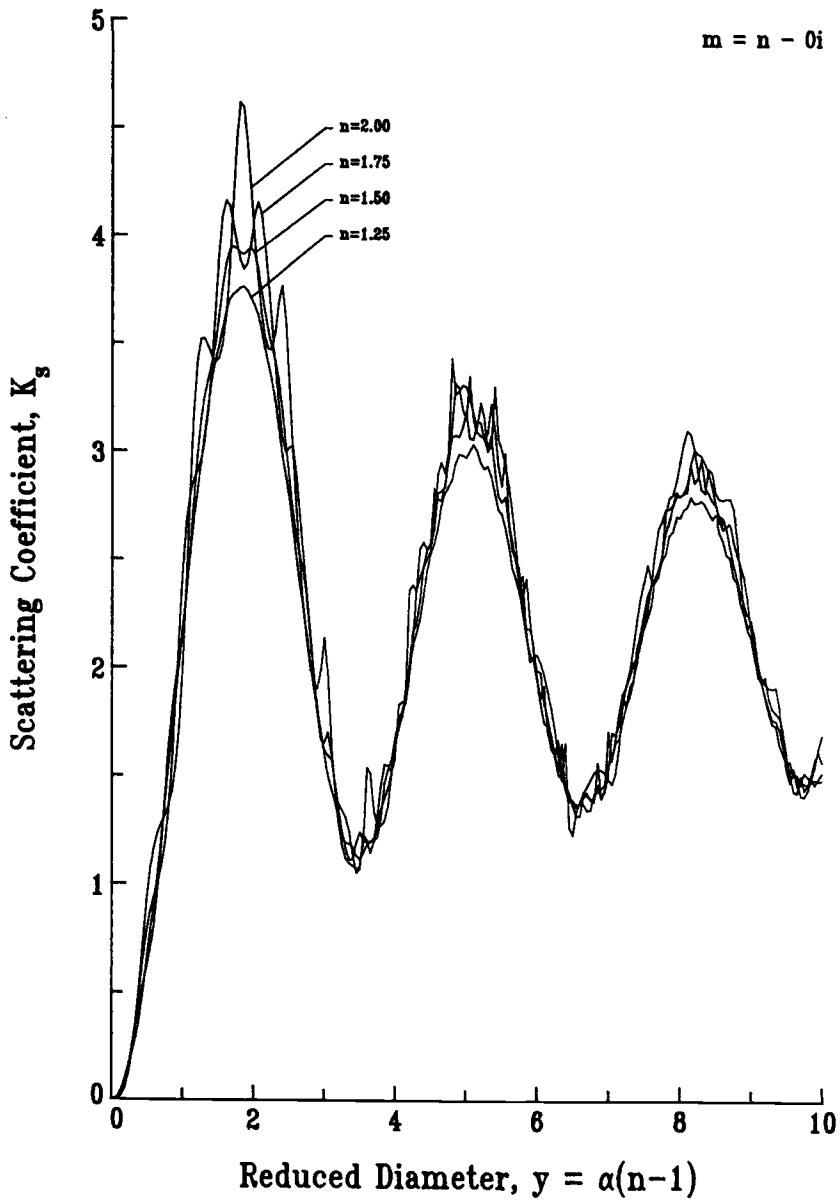


FIG. 5—Values of K_s plotted against $y = \alpha(m - 1)$ when $k = 0$, for values of n from 1.25 to 2.00. There is considerable normalization in this case.

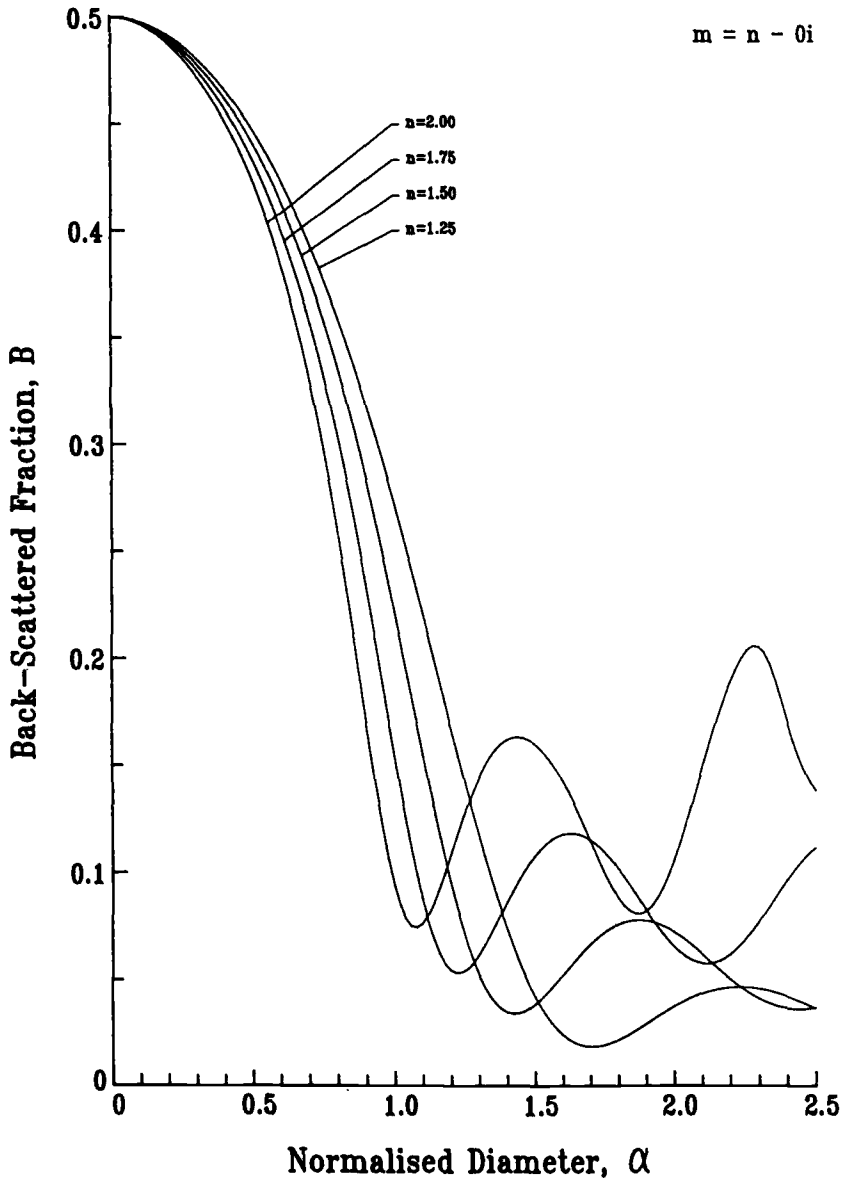


FIG. 6—Values of the back-scattered fraction B defined by Larkin and Churchill [10] shown as a function of α when $k = 0$, shown for $n = 1.25$ to 2.00 .

where M is the mass of an electron, β is the damping constant per unit mass, $\omega_0/2\pi$ is the natural frequency of the harmonic motion, and x is the displacement. Solving this differential equation gives

$$x = \frac{Ee/M}{(\omega_0^2 - \omega^2) + i\omega\beta}$$

from which the polarization P is

$$P = \frac{NEe^2/M}{(\omega_0^2 - \omega^2) + i\omega\beta}$$

where N is the number of free electrons/cm³. From this the complex dielectric constant (for permeability $\mu_m = 1$) is

$$\epsilon = 1 + \frac{4\pi Ne^2/M}{(\omega_0^2 - \omega^2) + i\omega\beta}$$

It is also known that $\bar{\epsilon} = m^2 = (n - ik)^2$ so that equating the real and imaginary parts gives

$$n^2 - k^2 = \epsilon = 1 + \frac{A(\omega_0^2 - \omega^2)}{[(\omega_0^2 - \omega^2)^2 + (\beta\omega)^2]}$$

where ϵ is the real part of the dielectric constant, and where A is given by

$$A = \frac{4\pi Ne^2}{M}$$

while

$$nk = \frac{\sigma_E}{\nu} = \frac{A\beta\omega/2}{[(\omega_0^2 - \omega^2)^2 + (\beta\omega)^2]}$$

where σ_E is the conductivity and ν is the frequency. From these two equations, we can obtain the approximate first-term dependence of n , the real part, and k , the imaginary part, on wavelength. These are (when $\omega \ll \omega_0$ and $\beta \ll \omega_0$)

$$n^2 = \left(1 + \frac{A}{\omega_0^2}\right) + \frac{A(2\pi c)^2}{\omega_0^4 \lambda^2} \quad (11)$$

which is the Cauchy equation, where

$$\omega = \frac{2\pi c}{\lambda}$$

the wavelength is λ , and c is the speed of light. The corresponding relationship for k is

$$k^2 = \left(\frac{\pi c A \beta}{\omega_0^2 \lambda}\right)^2 \left(1 + \frac{A}{\omega_0^2}\right) \quad (12)$$

Thus, in principle, if we have two measured values of n at different wavelengths λ , we can find A and ω_0 (as c is known), and with one value of k at any wavelength, we can then find β so that values of n^2 and k^2 can be calculated for any desired wavelength or temperature as from Eq 10:

$$\lambda_m = 2897.8/T$$

Actually

$$A = \frac{4\pi N e^2}{M}$$

should be independently calculable so that only one value of n would be required. We see from Eqs 11 and 12 that k^2 is more wavelength dependent than is n^2 . Alternatively, if the real part of the refractive index n and the dielectric constant ϵ are known, then simply

$$k = \sqrt{n^2 - \epsilon}$$

and as Eq 12 shows that $k\lambda$ is a constant, then we can find k at the appropriate wavelength.

Unfortunately, most polymers have many groups of bound electrons, each having its own characteristic natural frequency so that there are a large number of absorption bands such as discussed above. The formulae become correspondingly complicated, and n and k must be obtained from the experimental absorption spectrum. McKay and co-workers [14] give a method for doing this. We summarize some values we have found in the literature [15, 16] in Table 1 for the materials of interest to us: Keratin (Down), glass, polyester (PET), and polypropylene (PP). These give us an order of magnitude for k and n until we obtain more accurate values using the method of McKay.

We see that at optical frequencies $n^2 \approx \epsilon$, so that we cannot use these data to obtain k with any accuracy. Thus, we presently have to simply consider k to be small, but not necessarily negligible. More accurate data will be calculated in our further investigations.

Assembly of Cylinders

Many materials used as thermal insulators are made from fibrous materials and these can generally be assumed to be comprised of randomly oriented fibers in planes perpendicular to the heat flow direction. Very few fibers (or fiber segments) are oriented in the thickness direction and these few can be ignored, although McKay et al. [14] have considered the case where the fibers are oriented obliquely relative to the heat flow direction. Also, most fibers are very long compared to their diameter and so, from an analytical point of view, they can be assumed to be infinitely long, or so long that fiber ends can be ignored.

TABLE 1—*Relevant properties* [15,16].

	ρ	n	n^2	ϵ
Keratin	1.30	1.55	2.40	2.38
Glass	2.54	1.55	2.40	2.40
PET	1.38	1.60	2.56	2.57
PP	0.91	1.40	2.22	2.2–2.3

Assembly Effects

If we look down on such an assembly as shown in Fig. 7, then on the plan view, we only see randomly oriented fibers of diameter d and of various lengths ℓ . If the dimensions of the top area are δ by L , the mean chord length $\bar{\ell}$ of the projected fibers is found to be

$$\frac{\bar{\ell}}{\delta} = \frac{2}{\pi\sqrt{1 + (\delta/L)^2}} \ln \left[\frac{1 - \delta/L + \sqrt{1 + (\delta/L)^2}}{\sqrt{1 + (\delta/L)^2} - \delta/L} \frac{1 + \delta/L - \sqrt{1 + (\delta/L)^2}}{\delta/L} \right] \quad (13)$$

When $\delta = L$, this gives

$$\frac{\bar{\ell}}{\delta} = \frac{2\sqrt{2}}{\pi} \ln(\sqrt{2} + 1) = 0.7935$$

or when $\delta \ll L$,

$$\frac{\bar{\ell}}{\delta} = \frac{2}{\pi} \ln \left(\frac{2L}{\delta} \right)$$

If we now consider the corresponding vertical face shown in Fig. 8, the cut fibers are all ellipses which have the same vertical dimension d but their horizontal dimensions D are dependent on their inclination to the face, so that

$$D = d \sec \theta$$

where θ is the inclination to the δ direction. Integration gives the mean dimension

$$\frac{\bar{D}}{d} = \frac{2}{\pi} \int_0^{\cos^{-1}(d/L)} \sec \theta d\theta$$

or

$$\frac{\bar{D}}{d} = \frac{2}{\pi} \ln \left(\frac{1 + \sqrt{1 - (d/L)^2}}{1 - \sqrt{1 - (d/L)^2}} \right) \quad (14)$$

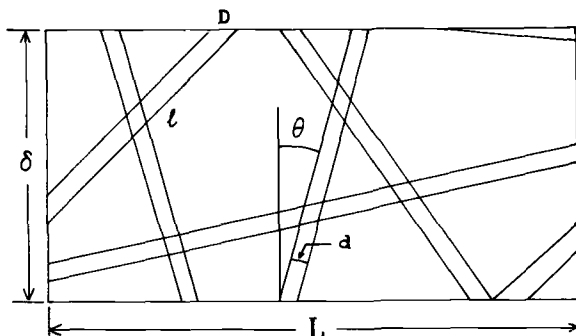


FIG. 7—Plan view of an area $\delta \times L$ of the fibrous insulator with all the fibers projected onto a plane.

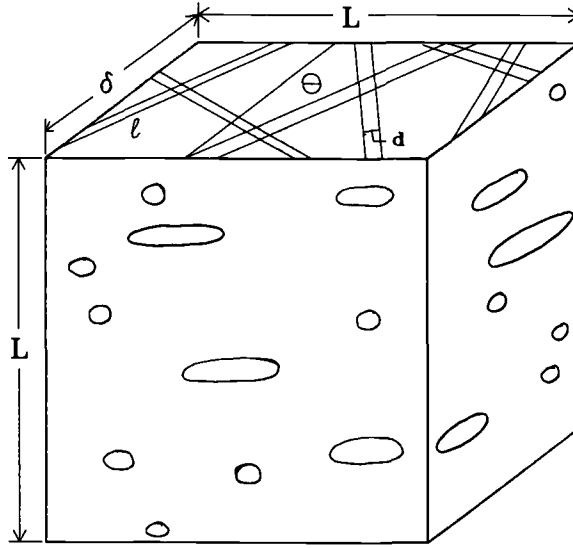


FIG. 8—Isometric view showing the corresponding side view of the insulator. The fibers cut the sides as ellipses of varying eccentricity.

When $d \ll L$,

$$\frac{\bar{D}}{d} = \frac{4}{\pi} \ln \left(\frac{2L}{d} \right)$$

From the average fiber projection, we see that

$$\sec \theta = \frac{\bar{\ell}}{\delta} = \frac{\bar{D}}{d}$$

so that when $\delta \ll L$ and $d \ll L$,

$$\frac{\delta}{L} = \frac{1}{2} \left(\frac{d}{L} \right)^2$$

Now, knowing the web assembly density ρ_F and the fiber density ρ_t , we can calculate the number of fibers in a thin vertical slice from

$$L^2 \delta \rho_F = n_a \frac{\pi d^2}{4} \bar{\ell} \rho_t = n_a \frac{\pi d \bar{D}}{4} \delta \rho_t$$

so that

$$n_a = \frac{4 \rho_F / \rho_t}{\pi (d/L)^2 (\bar{\ell}/\delta)} = \frac{4 \rho_F / \rho_t}{\pi (d/L)^2 (\bar{D}/d)}$$

If we first consider such a slice, where $L = 1$, then if we take $\rho_F = 0.008 \text{ g/cm}^3$ (0.5 lb/ft^3) and $\rho_t = 1.38 \text{ g/cm}^3$ (polyester) and $d = 10 \mu\text{m}$, and if we consider the thin slice such that $\delta = d^2/2$, then for the above values we find

$$n_a = 763 \text{ fibers/cm}^2$$

The square root of this gives $n_t = \sqrt{763} = 27.6 \text{ fibers/cm}$, as $n_a = n_t^2$.

Thus, in this vertical section when δ is small, we may consider this as 27.6 layers, each $1/27.6d = 36$ diameters deep so that in each layer there are approximately 27.6 fiber ends spaced 36 fiber diameters apart. This gives the average fiber end spacing.

Before we try to calculate the assembly extinction, we must discuss the assumptions to be made in the derivation. Firstly, the flux between the hot and cold plates is assumed to be planar as it is the integrated sum of the fluxes from an infinite number of radiant point sources on the plate surface. This is consistent with scattering theory where the incident wave is always taken to be planar.

Secondly, the scattering from each cylinder causes a radial scattered wave and interference (or diffraction) between the waves scattered by each edge of the same cylinder. However, because the distances between cylinders is so large and the intensity of the scattered wave decreases linearly, we assume that there is no interference between pairs of cylinders. Further, although each cylinder changes the field intensity locally in its neighborhood, this is assumed to have averaged out at large distances such as at the cold plate or at a neighboring cylinder, this average being a small but net decrease in flux for each interception or individual cylinder extinction. For denser structures, this is no longer true and the applicability of electromagnetic scattering theory becomes more questionable.

Thus the incident flux crosses the first of the 27.6 layers, its energy loss/fiber end is $K_e d$, where K_e is the extinction coefficient/cm calculated earlier. In this layer of the slice of Fig. 6 there are (on average) n_t such fibers and so the transmission per layer is $1 - n_t K_e d$.

The energy is reduced exactly the same in each of the n_t layers, so that the fractional transmission/cm of thickness is ($L = 1$)

$$t_1 = (1 - n_t K_e d)^{n_t}$$

For a thickness of L , the result becomes

$$t_L = (1 - n_t K_e d)^{n_t L}$$

Now as $n_t K_e d \ll 1$, this gives approximately (as $n_a = n_t^2$)

$$t_L = e^{-n_t^2 d K_e L} = e^{-n_a d K_e L} \quad (15)$$

and the corresponding extinguished fraction is $\phi_e = 1 - t_L$ or

$$\phi_e = 1 - (1 - n_t K_e d)^{n_t L} \approx 1 - e^{-n_a d K_e L} \quad (16)$$

which is the Lambert/Bouguer/Beer law. Further, if $n_a d K_e L \ll 1$, then

$$\phi_e \approx n_a d K_e L = n_a d (K_a + K_s) L \quad (17)$$

If we consider a cubic volume element with sides of length 1 cm rather than the 1 cm square slice, then the number of fibers/cm³ is given by

$$n_v = \frac{4\rho_F/\rho_t}{\pi d^2 \bar{\ell}}$$

and, in this case, $\bar{\ell} = 0.7935$, from Eq 13, so that

$$n_v = 9302$$

This compares to the number in our thin slice of

$$n_a = \frac{\rho_F/\rho_t}{d^2 \ln(2/d)} = 763 = (27.6)^2$$

Hence we write

$$\phi_e = 1 - e^{-\frac{\rho_F/\rho_t K_e L}{d \ln(2/d)}} \quad (18)$$

as an alternative to Eq 16. There are equivalent equations in terms of K_a and K_s which give the components of K_e .

Results

In this way, we have calculated the assembly radiation extinction efficiency term ϕ_e for the four materials listed in Table 1, assuming that k , the imaginary part of the refractive index, can take values from 0 to 0.2, approximately.

The results for ϕ_e for polyester (PET) are shown in Fig. 9 for $m = 1.60-0i$ and $1.60-0.20i$ which spans this range of k . Note that the single fiber maxima corresponding to these curves taken from Fig. 1 occur at larger values of α . Also, note that the ϕ_e curve has an intercept at ~ 0.40 , when the fiber is absorbent with $k = 0.20$. This effect at small α was discussed previously. In Figs. 10 to 12, we show corresponding results for polypropylene (PP), glass, and Keratin (Down) fibers.

From these calculated values for all four fiber types, we can plot the results in Fig. 13, where we have read off from the curves such as in Fig. 9 the values of α which make ϕ_e a maximum. From this value of α , we can calculate the corresponding diameter d_{\max} . Figure 13 shows that the optimum value of d_{\max} is larger for PP than for glass or Keratin (Down), while the optimum for PET is finer still. Values vary between 7 and 8 μm , depending on whether the fibers are absorbent or not. If the fibers are absorbent (due to molecular structure, pigment, roughness, etc.), the optimum diameters decrease dramatically between $k = 0.15$ and 0.20. The maximum values of extinction efficiency are roughly 65% with PP, 57% with PET, and 56% for Keratin, but only 34% for glass. The low result for glass fibers is due to its large density and resultant low covering power and show the effect of material specific gravity. Experimental measurements have confirmed that the optimum diameter for PET is 7 to 8 μm .

Conclusions

These results show that for a given insulating problem, and hence for a specific effective temperature and wavelength, an insulation material can be engineered to provide maximum insulation to radiative heat transfer. This requires a particular fiber diameter and this diameter depends on the material optical properties such as the refractive index and dielectric constant. These determine the balance between scattering (and interference) and absorption for those specific conditions and so require different optima.

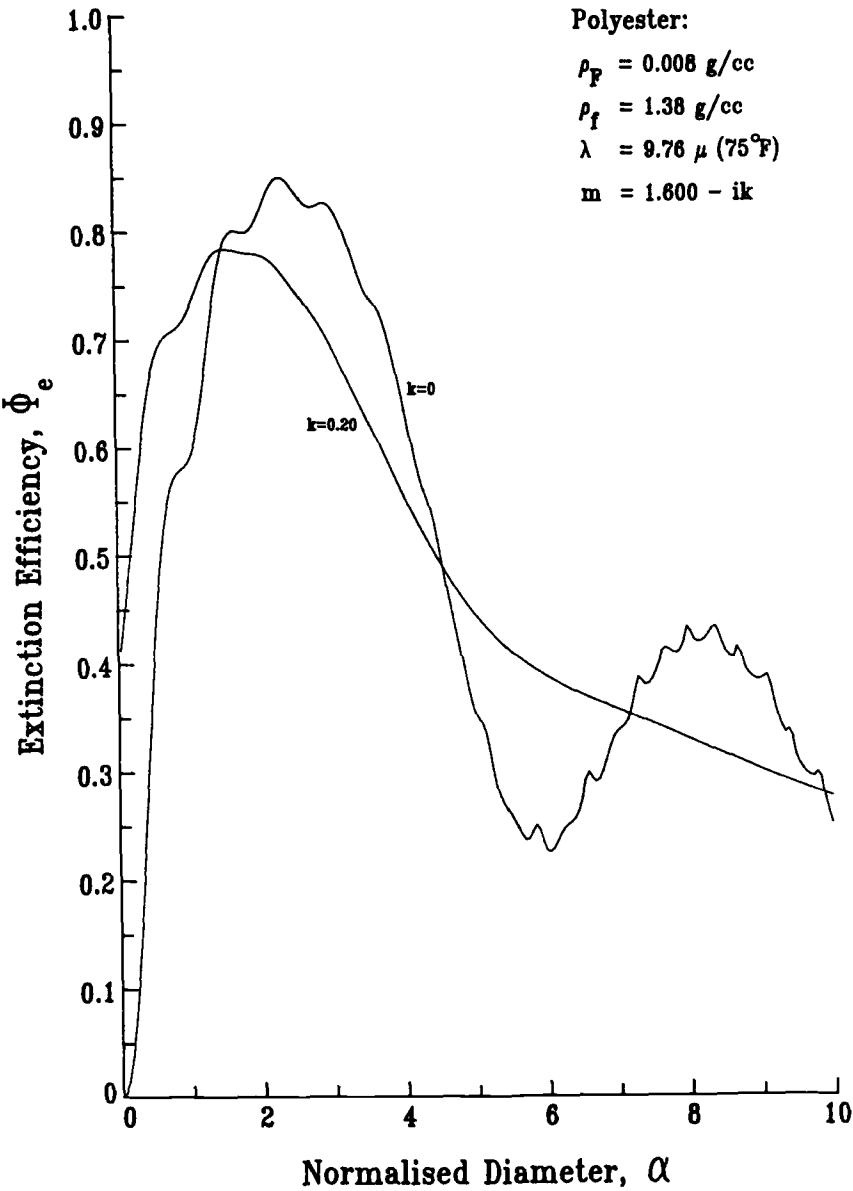


FIG. 9—Plot showing the optimum extinction ϕ_e for a polyester fibrous assembly for $k = 0$ and $k = 0.2$.

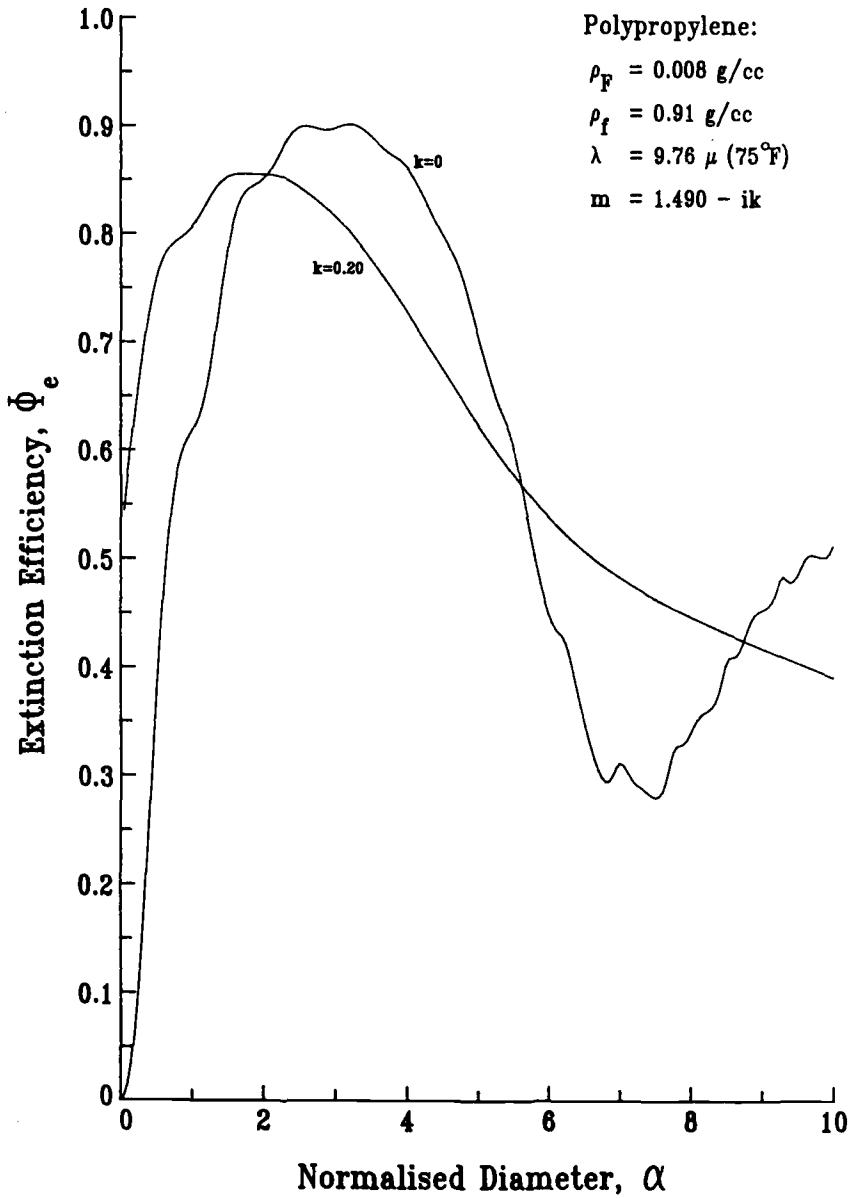


FIG. 10—Plot showing the optimum extinction Φ_e for a polypropylene fibrous assembly for $k = 0$ and $k = 0.2$.

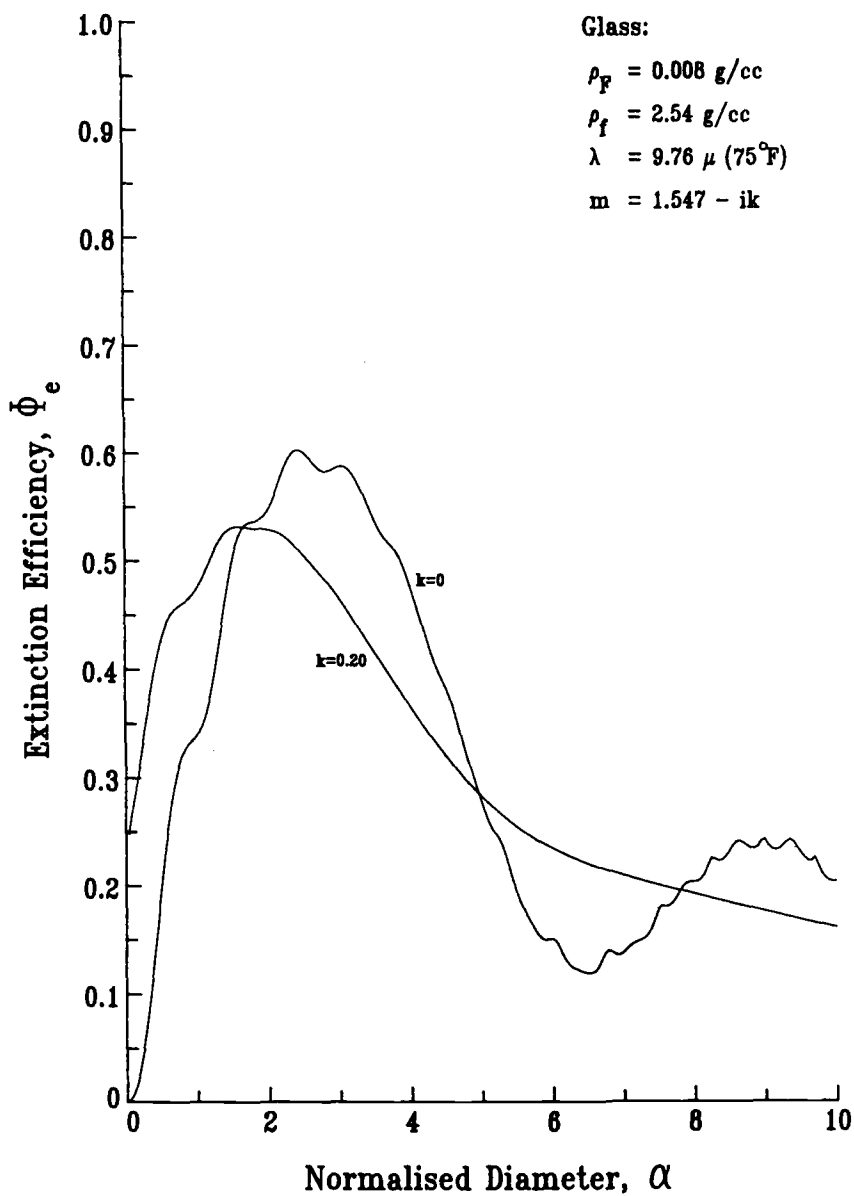


FIG. 11—Plot showing the optimum extinction Φ_e for a glass fibrous assembly for $k = 0$ and $k = 0.2$.

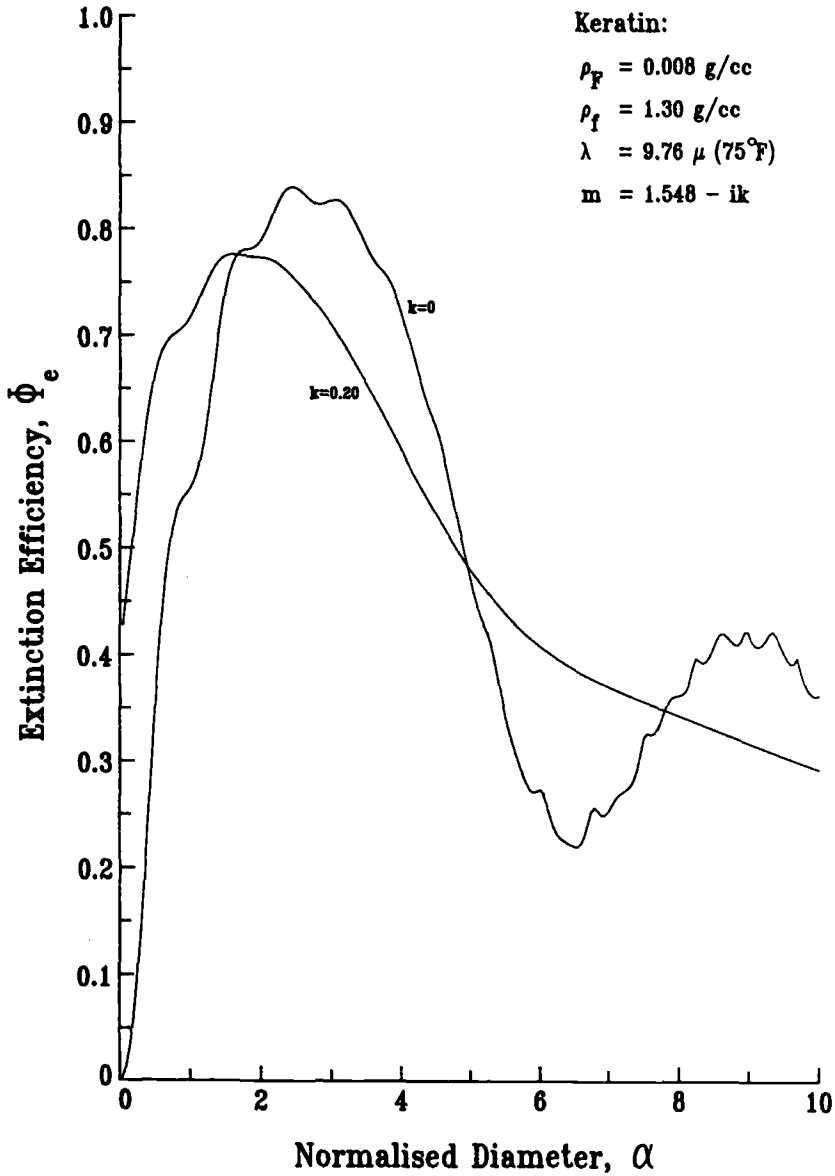


FIG. 12—Plot showing the optimum extinction ϕ_e for a Down (Keratin) fibrous assembly for $k = 0$ and $k = 0.2$.

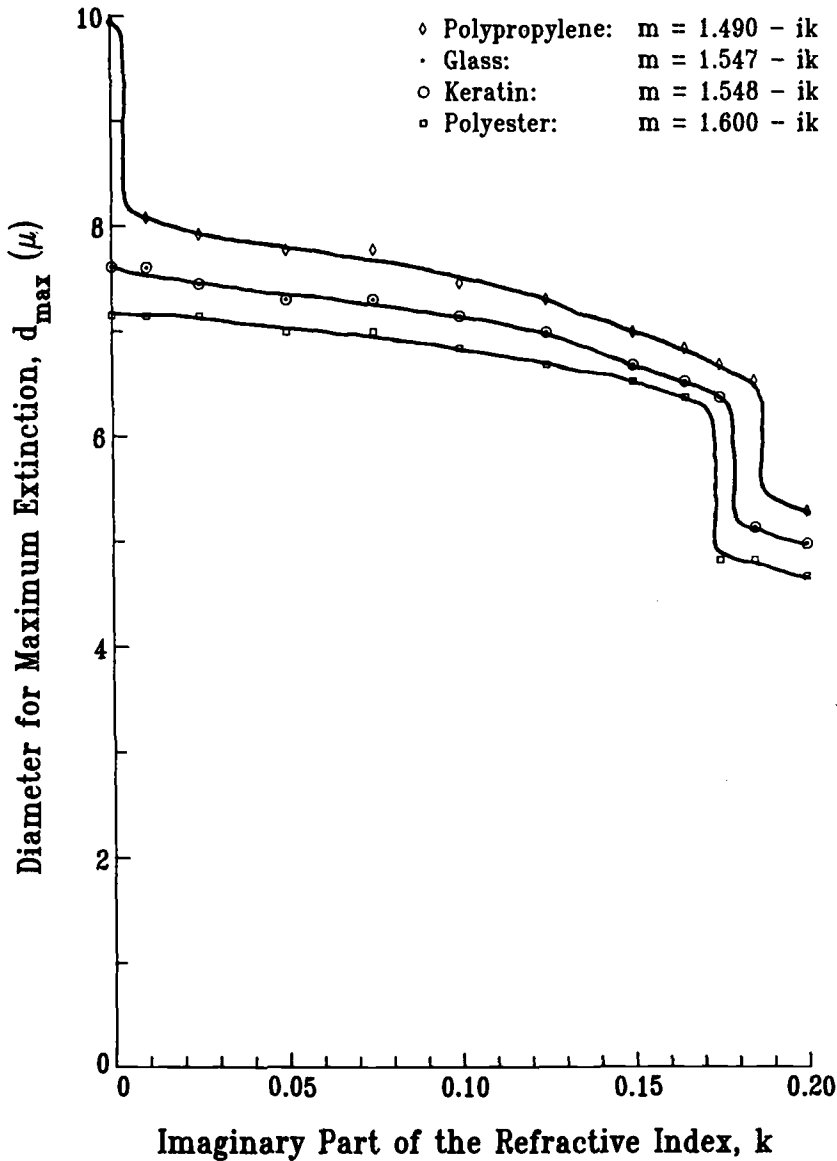


FIG. 13—Optimum diameter d_{\max} for extinction for polypropylene, glass, Keratin, and polyester obtained from the value of α in Figs. 9 to 12 corresponding to the maximum ϕ_e values, for various k 's.

The relevance of the classical results for the scattering and absorption of electromagnetic radiation by cylinders is clarified and new general results are calculated. It is also shown that it is inappropriate to consider only forward and backward fluxes in low density assemblies of finite thickness as interference effects are then ignored.

We have shown then that optimum diameters occur and have calculated some values for several materials for an assembly density of 0.008 g/cm^3 (0.5 lb/ft^3) and a mean temperature of 24°C (75°F).

The results given here are not final, however, because two effects have been ignored in this paper. These are (1) the detailed frequency dependency of n and k , the real and imaginary parts of the refractive index, and (2) the fact that any temperature T corresponds to a spectrum of wavelengths distributed about the maximum value λ_m discussed here. We hope to include both of these modifications in a further paper, and these may somewhat modify the present conclusions.

References

- [1] Pelanne, C. M., "Experiments on the Separation of Heat Transfer Mechanisms in Low Density Fibrous Insulation," in *Thermal Conductivity*, Plenum Press, New York, 1969, p. 897.
- [2] Bomberg, M. and Klarsfeld, S., "Semi-Empirical Model of Heat Transfer in Dry Mineral Fiber Insulation," *Journal of Thermal Insulation*, Vol. 6, No. 1, 1983, p. 156.
- [3] Dent, R. W., Donovan, J. G., Skelton, J., and Fossey, S., "Development of Synthetic Down Alternatives," Natick Report AD, 1984.
- [4] Larkin, B. K. and Churchill, S. W., "Heat Transfer Through Porous Insulations," *AIChE Journal*, Vol. 5, No. 4, Dec. 1959, p. 467.
- [5] Schuster, A., "Radiation Through a Foggy Atmosphere," *Astrophysical Journal*, Vol. 21, No. 1, 1905, p. 1.
- [6] Hamaker, H. C., "Radiation and Heat Conduction in Light Scattering Material," *Phillips Research Reports*, Vol. 2, 1947, pp. 55, 103, 112, 420.
- [7] Van de Hulst, H. C., *Light Scattering by Small Particles*, Dover, New York, 1981.
- [8] Stratton, J. A., *Electromagnetic Theory*, McGraw-Hill, New York, 1941.
- [9] Mie, G., "Beitrage zur Optik trüber Medien, Speziell Kolloidaler Metallösungen," *Annalen der Physik*, Vol. 3.4, No. 25, 1908, p. 377.
- [10] Larkin, B. K. and Churchill, S. W., "Scattering and Absorption of Electromagnetic Radiation by Infinite Cylinders," *Journal of the Optical Society of America*, Vol. 49, No. 2, 1959, p. 188.
- [11] Aronson, J. R. et al., "Infrared Emittance of Fibrous Materials," *Applied Optics*, Vol. 18, No. 15, 1979, p. 2622.
- [12] Brillouin, L., "The Scattering Cross-Section of Spheres for Electromagnetic Waves," *Journal of Applied Physics*, Vol. 20, No. 11, 1949, p. 1110.
- [13] Borne, M. and Wolf, E., *Principles of Optics*, 4th ed., Pergamon Press, Oxford, 1970.
- [14] McKay, N. L., Timusk, T., and Farnworth, B., "Determination of Optical Properties of Fibrous Thermal Insulation," *Journal of Applied Physics*, Vol. 55, No. 11, 1984, p. 4064.
- [15] Morton, W. E. and Hearle, J. W. S., *Physical Properties of Textile Fibres*, Butterworths, London, 1962.
- [16] Brandrup, J. and Immergut, E. H., *Polymer Handbook*, Wiley Interscience, New York, 1975.

Assessments and Properties of Foams

Variation of Insulating Properties of Closed-Cell Foam Insulation

REFERENCE: Ostrogorsky, A. G. and Glicksman, L. R., "Variation of Insulating Properties of Closed-Cell Foam Insulation," *Insulation Materials, Testing, and Applications, ASTM STP 1030*, D. L. McElroy and J. F. Kimpflen, Eds., American Society for Testing and Materials, Philadelphia, 1990, pp. 109-120.

ABSTRACT: Heat is transferred through closed-cell foam insulation by conduction through the solid polymer making up the cell structure, conduction through the low conductivity gas (blowing agent) inside the cells, and radiation. The effective thermal conductivity of closed-cell foam panels changes with the foam age due to diffusion of air components into the foam and diffusion of the blowing agent out from the foam. The change in the composition and thermal conductivity of the gas mixture was modeled as a function of the aging time. The change in the composition is computed by solving the transient diffusion equations for each gas species in the foam. The thermal conductivity of the gas mixture is computed from an empirical correlation proposed by Lindsay and Bromley.

A computer program was developed to numerically solve the governing equations. The effective diffusion coefficients of the air components and the blowing agent are the main code inputs. The numerical prediction of the change of the effective conductivity of foam panels for a given age is within 6% or better of the conductivity obtained in long-term tests under three different thermal environments.

KEY WORDS: aging, closed-cell foam, insulation, diffusion, permeability

Nomenclature

- A* Area, cm²
- D* Diffusion coefficient, cm²/s
- E* Energy of activation, J
- f_p* Fraction of the polymer in the cell walls
- J_m* Mass flux, g/cm²-s
- K* Conductivity, W/m-K
- L* Length, cm
- p* Gas pressure or gas partial pressure, atm
- Pe* Permeability coefficient, cm³_{STP}/cm-s-atm
- Pe₀* Reference value of *Pe*
- R* Gas constant, J/kg-K
- S* Solubility, cm³_{STP}/cm-atm
- T* Temperature, K
- t* Thickness, cm
- V* Volume, cm³
- x* Molar fraction

¹Department of Mechanical Engineering, Massachusetts Institute of Technology, Cambridge, MA 02139. Dr. Ostrogorsky is presently at Department of Mechanical Engineering, Columbia University, New York, NY 10027.

Subscripts

eff Effective
STP Standard temperature and pressure

Greek Letters

α Porosity (void fraction)
 ϵ Enhancement parameter
 μ Dynamic viscosity
 ρ Density

Introduction

Closed-cell foams made of polymers such as polyurethane have the lowest conductivity of any currently available insulation material other than vacuum insulation systems. The total conductivity of new closed-cell polyurethane foam is only two thirds of the conductivity of stagnant air. It is one half the conductivity of glass fiber insulation, allowing buildings with conventional construction practices to approach super-insulation values.

Heat is transferred through closed cell foam insulation by conduction and radiation. Because of the small cell size, there is no convective heat transfer. Thermal radiation and conduction through the solid polymer making up the cell structure account each for approximately 25% of the heat transferred through a fresh foam panel [1]. At least 50% of the total heat is transferred by conduction through the gas, so it is advantageous to have a low conductivity gas inside of the foam—for example, Fluorocarbon 11 (R 11).

The increase of foam conductivity with age is caused by the diffusion of air components into the foam and the diffusion of Fluorocarbon 11 out from the foam. Because of diffusion, the composition and thermal conductivity of the gas mixture change with time. This effect is known as the *aging effect*. Air components diffuse much faster than fluorocarbon vapor, so that the aging process can be divided into two stages: (1) the diffusion of the air components, which lasts typically 1 year for a 2.5 cm thick unfaced sample, and (2) the diffusion of Fluorocarbon 11, which lasts one or two orders of magnitudes longer.

To quantify the aging rate of closed-cell foam, a test, called the *accelerated aging test*, is presently performed by industry [2]. A fresh foam sample is kept for 90 to 180 days at 60°C (140°F). This temperature increases the rate of diffusion, although the exact increase for different gas components is not well known. The overall foam thermal conductivity is measured before and after the accelerated aging. Foams having a smaller increase in the thermal conductivity in this test are assumed to age more slowly over their entire life. The accelerated aging test quantifies the foam resistance to aging and therefore enables industry to distinguish foams with good and bad aging properties. Still, it has several major disadvantages:

- It does not give any insight into the physics of the aging process.
- It is unclear whether the foams have reached their ultimate aged values at the end of the accelerated aging test.
- The increase of the diffusion rate with temperature is different for N₂, O₂, CO₂ and R11. Consequently, it is difficult to relate the aging that occurred during the accelerated test to the aging that would occur under different operating conditions. Accelerated aging is done at isothermal conditions; in actual practice, foams are subjected to temperature gradients.
- During accelerated aging tests the composition and conductivity of the gas mixture inside the foam are not known. Therefore it is impossible to extrapolate the results of an accelerated aging test if the foam has not completely aged.
- It is too lengthy to enable fast feed-back between production conditions and foam quality.

Because of these deficiencies of the accelerated aging tests, industry at present is not able to determine and guarantee the properties of closed-cell foams over their lifetime.

The change in the effective thermal conductivity of the foam panels can be computed based on a prediction of the change of thermal conductivity of the gas mixture inside the foam. The thermal conductivity of the solid polymer and the apparent conductivity due to radiation remain constant.

In the present paper, the transient diffusion inside closed-cell foam panels is modeled. The effective diffusion coefficients of Fluorocarbon 11 and air components obtained from measurement or by modeling are used in the transient diffusion equation to predict the composition of the gas mixture inside the foam cells. The thermal conductivity of the gas mixture is then computed and added to the effective conductivity due to conduction through the solid polymer and apparent conductivity due to thermal radiation.

Conductivity of Gas Mixtures

A review of models of the thermal conductivity of the gas mixtures is given in Ref 3. An equation with empirical corrections proposed by Lindsay and Bromley was selected as the most accurate to be used in our model. The equation has the form

$$K_{\text{mix}} = \sum_{i=1}^4 K_i \left/ \left(1 + 1/x_j \sum_{\substack{j=1 \\ i \neq j}}^4 A_{ij} x_j \right) \right. \quad (1)$$

where subscript $i = 1, 2, 3$ denotes the air components N_2 , O_2 and CO_2 ; $i = 4$ denotes Fluorocarbon 11; K_i are the thermal conductivities of the gasses in the mixture; and x_i are the molar fractions of the gasses. The coefficients A_{ij} are computed as

$$A_{ij} = 0.25[1 + [(\mu_i/\mu_j)(M_j/M_i)^{0.75}(T + s_i)/(T + s_j)]^{0.5}](T + s_{ij})/(T + s_i) \quad (2)$$

where μ_i is the dynamic viscosity of the i th component, and M_i is the molar mass. The constants s_i and s_{ij} are computed from the equations

$$s_i = 1.5T_{bi} \quad (3)$$

and

$$s_{ij} = (s_i s_j)^{0.5} \quad (4)$$

where T_{bi} is the absolute boiling temperature of the gas component i at atmospheric pressure. When the molecules of one of the gasses are strongly polar, the geometric average (Eq 4) is multiplied by 0.773.

The molar fractions of a gas component, x_i , are equal to the partial pressure of the component divided by the total pressure of the mixture:

$$x_i = p_i / \sum_{i=1}^4 p_i \quad (5)$$

Prediction of Gas Composition

In order to use Eq 1 to calculate the gas conductivity, the gas composition must be predicted throughout the foam. The length and width of a foam panel are much larger than the thickness

of the panel. Therefore a one-dimensional model of gas diffusion can be applied. (The influence of diffusion along the length and the width of the panel can be neglected.) For typical foam applications the thickness of a foam slab is much larger than the average cell diameter so that a continuum model of the gas diffusion within the foam can be employed. It is assumed that different gas species diffuse independently: gas molecules present negligible resistance to diffusion of other gas molecules when compared to the diffusion resistance of the solid polymer. The concentration of gas species inside the cells is not affected by the presence of other gasses.

The one-dimensional transient diffusion of each of the air components and Fluorocarbon 11 inside the foam panel is described by the set of partial differential equations equating accumulation to net transport for each gas component:

$$\partial p_i / \partial t = (\partial / \partial x)(D_{\text{eff},i} \partial p_i / \partial x) \quad (i = 1, 2, 3, 4) \quad (6)$$

where p_i is the partial pressure of one gas component, and $D_{\text{eff},i}$ is the effective diffusion coefficient of that gas.

Assuming that initially only Fluorocarbon 11 is present inside the foam panel, the initial conditions within the foam are: $p_i(x, 0) = 0$ for $i = 1, 2, 3$, the air components N_2 , O_2 and CO_2 ; and $p_i(x, 0) = 1$ for $i = 4$, the fluorocarbon gas used to blow the foam.

With the foam exposed to air on both boundaries (without facing materials or with facings with negligible gas diffusion resistance) the boundary conditions are:

$$p_i(0, t) = p_i(L, t) = 0.7808 \quad \text{for } i = 1 (\text{N}_2)$$

$$p_i(0, t) = p_i(L, t) = 0.2095 \quad \text{for } i = 2 (\text{O}_2)$$

$$p_i(0, t) = p_i(L, t) = 0.000314 \quad \text{for } i = 3 (\text{CO}_2)$$

$$p_i(0, t) = p_i(L, t) = 0.0 \quad \text{for } i = 4 (\text{R11})$$

Equations 6 are taken to be uncoupled (i.e., for low gas pressures the transient diffusion of one gas component through the polyurethane membranes of the foam does not affect the transient diffusion of any of the other gas components).

In most situations of practical interest, foam panels are exposed to a temperature gradient. To be able to compute the values of the temperature-dependent properties, such as the effective diffusion coefficient or the gas conductivity, the temperature profile must be known at each location within the foam. Since the thermal diffusivity is much larger than the effective diffusivity for mass transfer, the response to temperature changes is much faster than the response to the concentration changes at the foam surface. Therefore, for purposes of calculating diffusion within the foam, it can be assumed that the temperature profile inside the foam has a steady-state distribution given by

$$T(x, t) = T(0, t) + [T(0, t) - T(L, t)](x/L) \quad (7)$$

where $T(0, t)$ and $T(L, t)$ are temperatures imposed on the foam boundaries at a given time.

Foam Effective Diffusion Coefficient

The effective foam diffusion coefficient can be measured or it can be modeled based on knowledge of the foam geometry and the permeability of the solid polymer cell walls [4]. The diffusion coefficients of gasses in closed-cell polyurethane foams are strongly temperature dependent. The foam permeability coefficient was found to follow an Arrhenius-type equation [5,6]:

$$Pe_{\text{eff}} = Pe_0 \exp(-E/RT) \quad (8)$$

where Pe_0 is a reference value of Pe , R is the gas constant, T is the absolute temperature, and E is the energy of activation. The effective solubility has an inverse linear temperature dependence which comes from the ideal gas law [4]:

$$S_{\text{eff}} = T_{\text{STP}}/T[\text{cm}^3_{\text{STP}}/\text{cm}^3\text{-atm}] \quad (9)$$

where T_{STP} is the standard temperature, 298 K. Since, by definition,

$$D_{\text{eff}} = Pe_{\text{eff}}/S_{\text{eff}} \quad (10)$$

combining Eqs 8, 9, and 10 yields

$$D_{\text{eff},i} = Pe_{0i} \exp(-E_i/RT)(T/T_{\text{STP}}) \quad (i = 1, 2, \dots, 4) \quad (11)$$

Measured effective diffusion coefficient of the air components and Fluorocarbon 11 for an MDI foam sample are given in Table 1 [6]. Table 2 gives values of the constants for Eq 11 [6]. The constants are computed based on the data in Table 1.

Reference 4 gives the following model for the effective diffusion coefficient of foam. It combines the cell wall permeability and the foam geometry to yield

$$Pe_{\text{eff}} = (A_{\text{SM}}/A_{x-s})L_{\text{av}}/t Pe_c = \epsilon L_{\text{av}}/t Pe_c \quad (12)$$

where ϵ is a parameter, equal to two, which accounts for the enhancement of permeation due to random orientation of the cell walls; t is the cell wall thickness; Pe_c is the permeability of the cell

TABLE 1—Measured effective foam diffusion coefficient ($\times 10^{-8} \text{ cm}^2/\text{s}$) (polyurethane, MDI-type foam sample, density = 25.2 kg/m³) [6].

Temp.	D_{CO_2}	D_{O_2}	D_{N_2}	D_{R11}
25°C	202.0	46.8	7.6	0.23 to 0.57*
50°C	529.0	145.0	26.3	1.7
75°C	82.7	11.2
90°C	202.0	29.6

*Range of data at 25°C. Extrapolation of data at 50°C and 90°C to 25°C yields the value $D_{\text{eff}} = 0.20 \times 10^{-8} \text{ cm}^2/\text{s}$.

TABLE 2—Coefficients for the equation $Pe_{\text{eff}} = Pe_0 \exp(-E/RT)$ (polyurethane, MDI-type foam sample, density = 25.2 kg/m³) [6].

Gas	Pe_0 ($\text{cm}^3_{\text{STP}}/\text{cm-s-atm}$)	E/R (K)
CO ₂	0.1797	3396.
O ₂	0.3737	4050.
N ₂	0.2535	4476.
R11	842.715	7974.

walls;² A_{SM} is the surface area of a cell wall; and A_{x-s} is the area of a cell wall projected normal to the concentration gradient. Here L_{av} is the average distance between the cell walls measured by drawing N random lines parallel to the flow direction and counting the number of intersections, n , with cell walls:

$$L_{av} = (NL)/(Nn) = L/n \quad (13)$$

where L is the length of each random line.

Equation 12 can be further simplified to avoid measurements of the cell wall thickness and the average distance between cell walls. The ratio of the cell wall volume to the entire foam volume is equal to

$$V_{c.w.}/V_{foam} = ntA_{SM}/(A_{x-s}L) = \epsilon t/L_{av} \quad (14)$$

The foam density is equal to

$$\rho_{foam} = \rho_{gas} + (1 - \alpha)\rho_{poly} \quad (15)$$

where α is the foam void fraction or porosity. Rearranging, the volumetric fraction of the solid polymer becomes

$$1 - \alpha = V_{poly}/V_{foam} = (\rho_{foam} - \rho_{gas})/(\rho_{poly} - \rho_{gas}) \quad (16)$$

The polymer can be in the cell walls or in the struts, the thickened regions formed at the intersections of the cell wall. The struts do not contribute to the permeation resistance of the material. The fraction of the polymer in the cell walls is defined as

$$fp = V_{c.w.}/V_{poly} \quad (17)$$

Combining Eqs 12, 16, and 17 yields

$$Pe_{eff} = (\epsilon^2/fp)(\rho_{poly} - \rho_{gas})/(\rho_{foam} - \rho_{gas})Pe_{c.w.} \quad (18)$$

Note that foams with many thin walls and foams with a few thick walls have the same effective permeability if the foam density and the fraction of polymer in the cell walls are the same.

Reference 5 describes a technique of measuring the fraction of the polymer in the cell walls. For a variety of foams, fp was found to be in the range 0.15 to 0.25. Therefore one can assume that fp is approximately equal to 0.20 and replace the measurement of the cell wall thickness and the average distance between the cell wall with a measurement of the foam density. Note that Eq 18 assumes that the foam is isotropic.

Besides the conduction through the gas mixture, heat is transferred through closed-cell foam by conduction through the solid and by radiation. However, conductivity of the solid and the amount of heat transferred by radiation do not change with time. These two components of heat transfer can be modeled or measured separately and added to the mixture conductivity computed from Eq 1:

$$K_{eff} = K_{mix} + K_{solid} + K_{rad} \quad (19)$$

²Room temperature data on the cell wall permeability are given in Ref 4.

Numerical Solution

A computer code was developed to solve Eqs 1 to 19. A number of quantities that do not change with time are computed first. These quantities include the partial pressure of the air components at standard pressure, $S(I)$, $S(I, J)$.

The initial temperature profile inside the foam is computed from the boundary conditions and Eq 7. It is assumed that the initial pressure of the gas mixture (usually only R11) inside the foam cells is equal to 1 atm at 25°C. If temperature inside the foam changes, the partial pressure of the mixture components also changes. From the computed initial temperature distribution, the initial partial pressure of the gas inside the axial nodes is computed by the ideal gas law.

At each time step, the partial pressure of the air components and Fluorocarbon 11 inside the axial nodes is computed. Equations 6 are approximated by the Crank-Nicolson finite difference scheme. To avoid the stability limits on the time step, the implicit Crank-Nicolson finite difference scheme was used. Diffusion coefficients of N_2 , O_2 , CO_2 and R11 are computed for all axial nodes as a function of temperature at each time step.

From the partial pressures, the molar fractions are computed. Next, temperature-dependent properties like viscosity and conductivity of the gasses are computed as a function of the local temperature in the axial nodes.

The conductivity of the mixture is computed from Eq 1 for each axial node using the local values of temperature and mole fraction. The conductivity of the mixture in the nodes is averaged to obtain an average conductivity of the gas mixture in the foam panel. The thermal conductivity of the solid and the apparent conductivity due to radiation are added to the average conductivity of the gas mixture to give the effective conductivity of the foam panel.

Results

Figures 1 to 3 show the comparison between the effective thermal conductivity as predicted by the computer program and the data [7] obtained in long-term aging tests. The foam samples were aged under three different thermal environments:

- A uniform temperature of 24°C.
- A uniform temperature of 60°C.
- A linear temperature gradient between 60 and 24°C on the sides of the panel.

The data shown in Figs. 1 to 3 represent the average values of measurements performed on four samples. There is a rapid initial increase in conductivity as the air components begin to diffuse into the foam. The rate of increase is complicated because of the three different diffusion rates for the three main air components. The gradual rise in conductivity after approximately one year results from an equilibrium composition of air within the foam and an almost steady loss of refrigerant vapor. The numerical predictions follow the measurements closely. Starting by matching the initial conductivity, the predicted conductivity at any later time is within 6% of the measured values.

Figures 4 and 5 show the code prediction of the change of the partial pressure of N_2 , O_2 , CO_2 and Fluorocarbon 11 with the aging time at the center line and at the surface of a 2.54 cm thick sample held at room temperature. It can be seen that the partial pressures change much faster for the foam cells near the surface than for the foam cells at the center line. After 10 000 days only a small amount of Fluorocarbon 11 is left in the foam sample. The numerical prediction is made using the assumption that the amount of fluorocarbon dissolved in the polymer is negligible compared to that in the vapor phase.

Figure 6 shows the change of the effective conductivity of 2.54 cm thick foam panel exposed to room temperature for 10 000 days. The data given in Fig. 6 are the average values of mea-

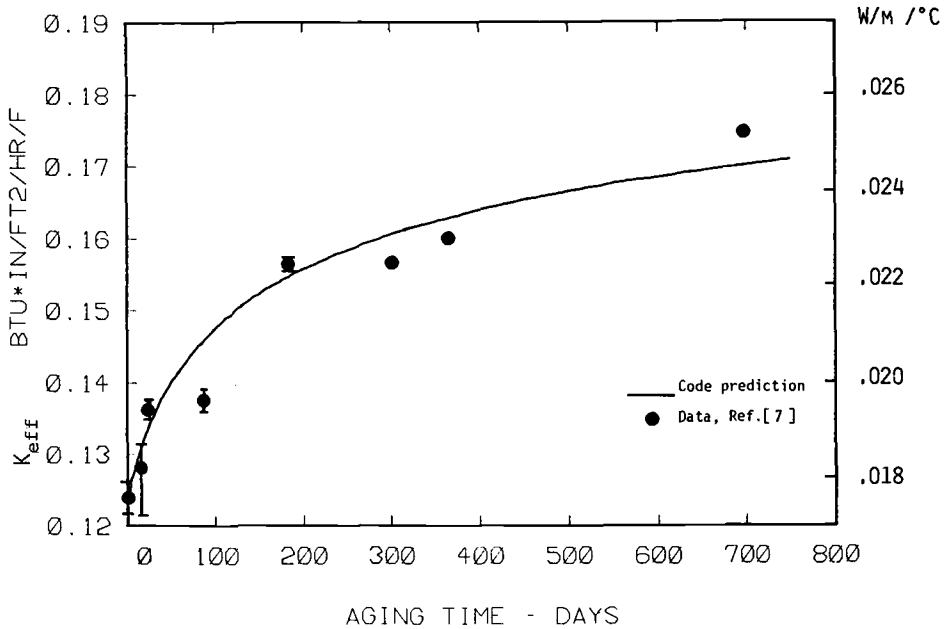


FIG. 1—Effective thermal conductivity of closed-cell polyurethane foam as a function of aging time ($T_1 = T_2 = 24^\circ\text{C}$; $= 28.35 \text{ kg/m}^3$; specimen thickness = 5.1 cm).

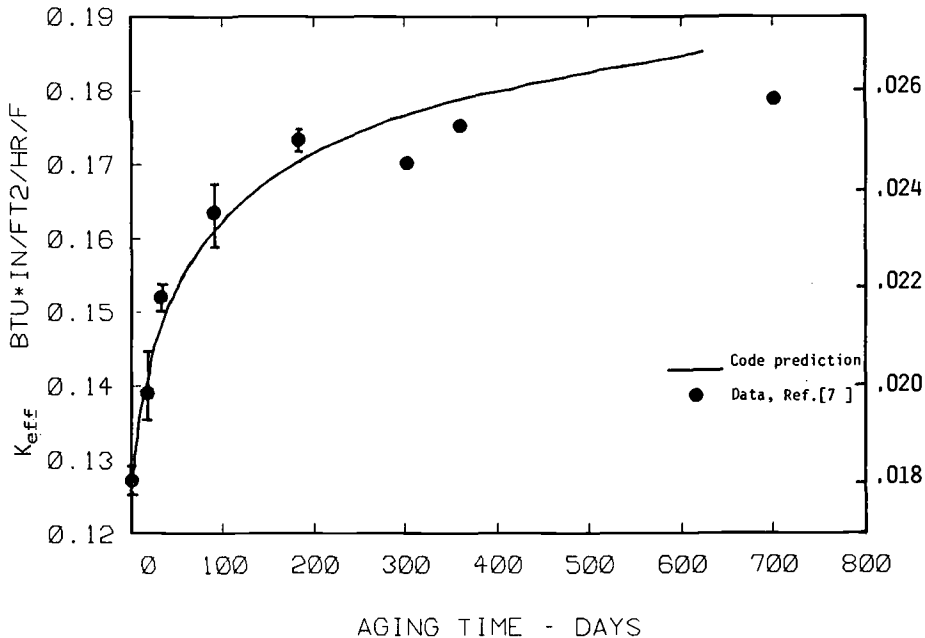


FIG. 2—Effective thermal conductivity of closed-cell polyurethane foam as a function of aging time ($T_1 = T_2 = 60^\circ\text{C}$; $= 28.35 \text{ kg/m}^3$; specimen thickness = 5.1 cm).

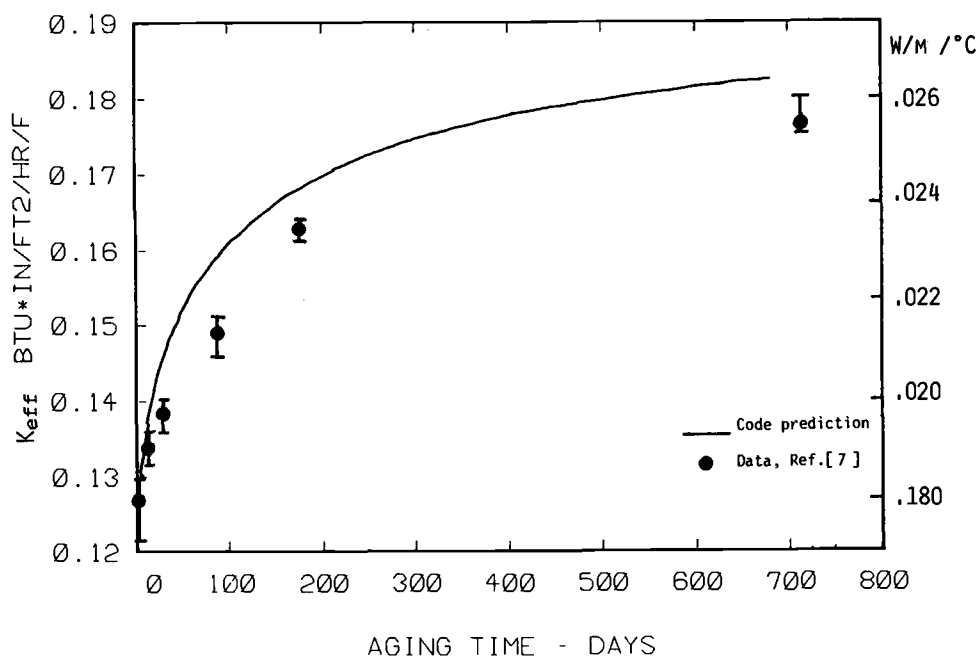


FIG. 3—Effective thermal conductivity of closed-cell polyurethane foam as a function of aging time ($T_1 = 24^\circ\text{C}$, $T_2 = 60^\circ\text{C}$; $= 28.35 \text{ kg/m}^3$; specimen thickness = 5.1 cm).

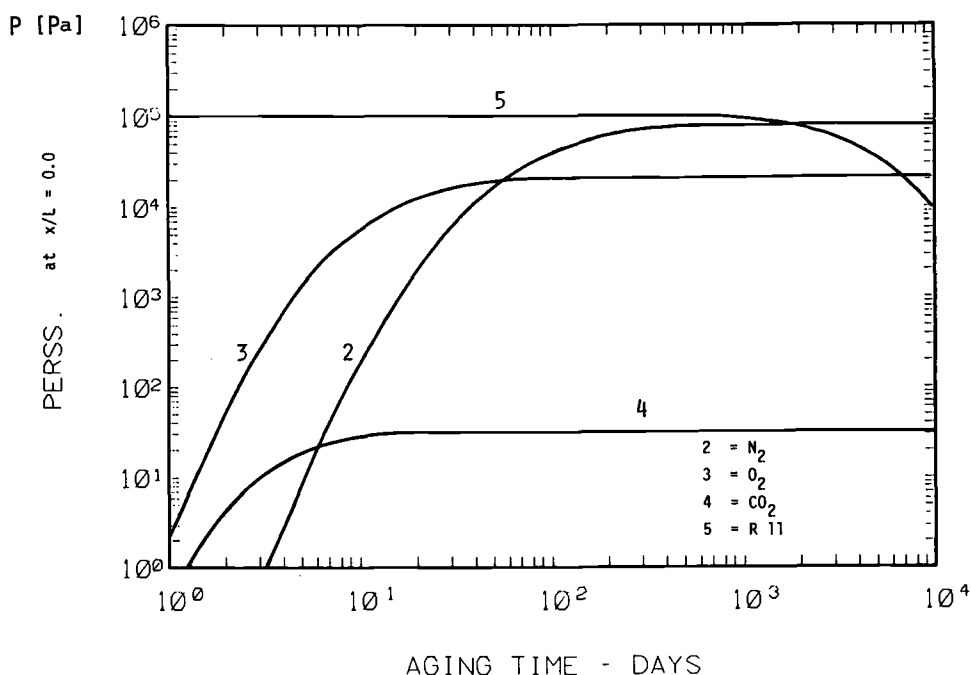


FIG. 4—Partial pressure of N_2 , O_2 , CO_2 and Fluorocarbon 11 as a function of aging time ($T_1 = T_2 = 24^\circ\text{C}$; $= 28.35 \text{ kg/m}^3$; specimen thickness = 5.1 cm; center line node).

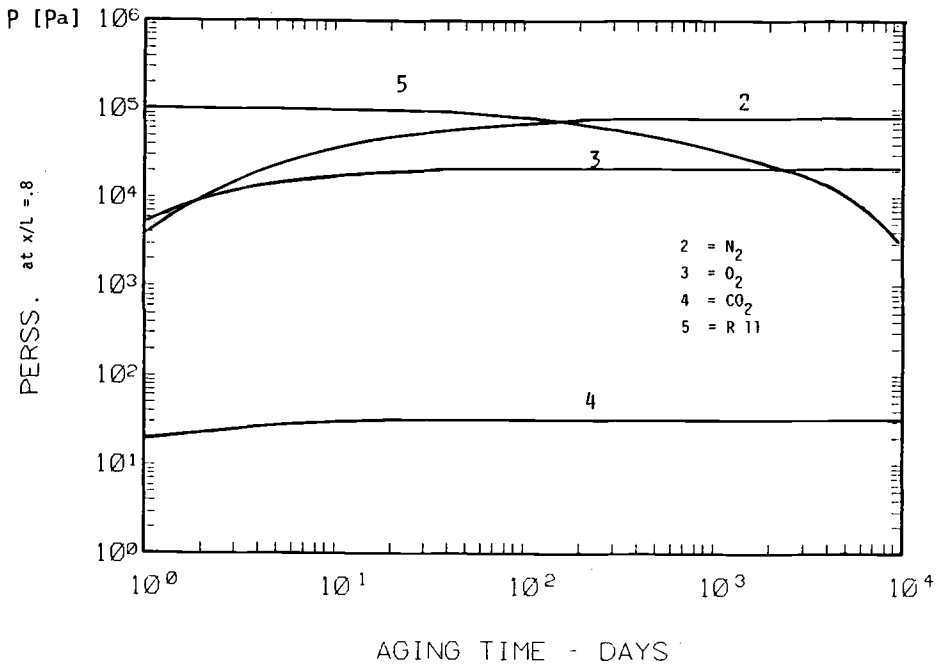


FIG. 5—Partial pressure of N_2 , O_2 , CO_2 and Fluorocarbon 11 as a function of aging time ($T_1 = T_2 = 24^\circ C$; $= 28.35 \text{ kg/m}^3$; specimen thickness = 5.1 cm; next to surface node).

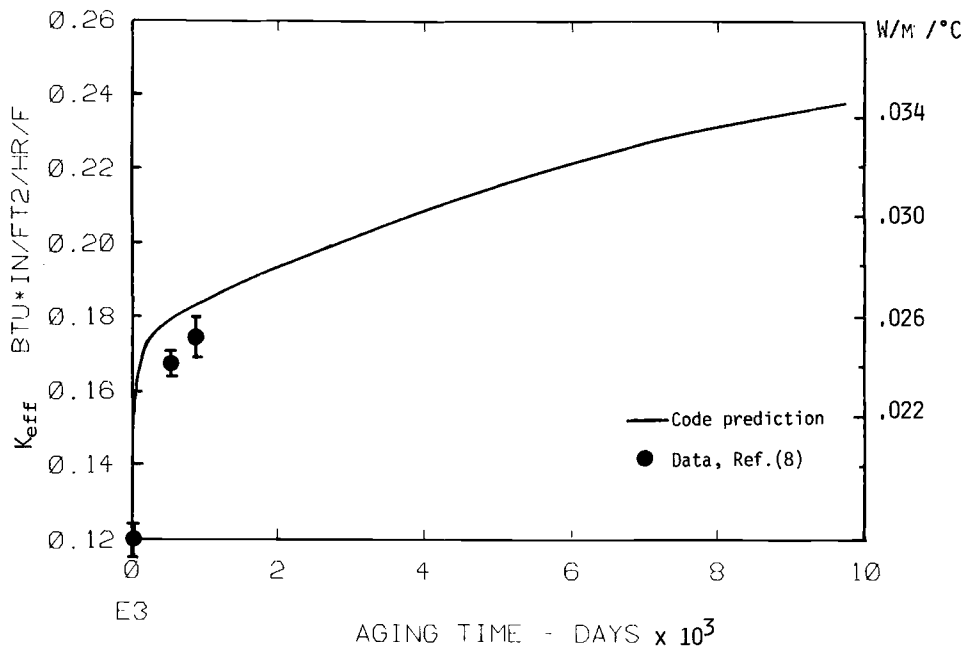


FIG. 6—Effective thermal conductivity of closed-cell polyurethane foam as a function of aging time ($T_1 = T_2 = 24^\circ C$; $= 28.35 \text{ kg/m}^3$; specimen thickness = 2.54 cm).

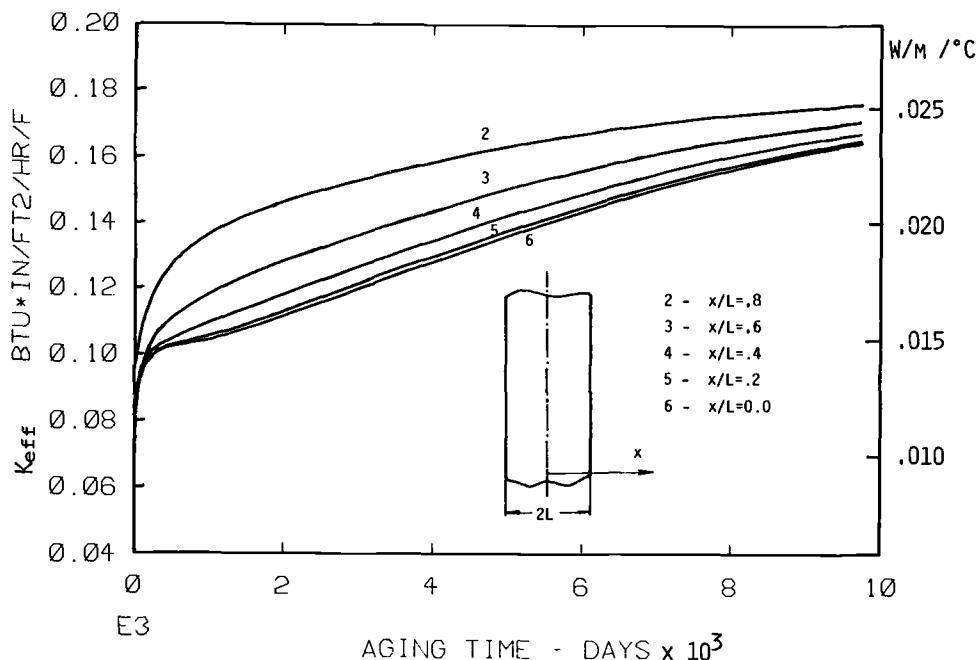


FIG. 7—Effective thermal conductivity of closed-cell polyurethane foam as a function of aging time ($T_1 = T_2 = 24^\circ\text{C}$; $= 28.35 \text{ kg/m}^3$; specimen thickness $= 2.54 \text{ cm}$).

sured effective conductivity of five MDI-type foam samples having densities in the range 25.6 to 30.6 kg/m^3 (1.6 to 1.91 lb/ft^3) [8, 9]. The data were taken after 1.5 and 2.5 years of aging.

Figure 7 shows the increase in the conductivity of the gas mixture inside the 2.54 cm thick foam panel at different axial locations.

Conclusions

The value of the foam effective thermal conductivity can be predicted rapidly and accurately by the developed computer program when the main program inputs, the diffusion coefficients of N_2 , O_2 , CO_2 and Fluorocarbon 11, are known. Accurate predictions were obtained for the aging rate in different thermal environments. Therefore, if accurate data on the foam effective diffusion coefficients are available, for specific operating conditions the foam aging rate can be estimated more accurately by use of the code than by extrapolation of the data obtained in long-term or accelerated aging tests that are at present performed by industry.

References

- [1] Schuetz, M. A. and Glicksman, L. R., "Basic Study of Heat Transfer Through Foam Insulation," *Journal of Cellular Plastics*, Vol. 20, 1984, pp. 114-121.
- [2] *Federal Register*, Part III, Vol. 44, No. 167, 27 Aug. 1979, pp. 50218-50245.
- [3] Tsederberg, N. V., *Thermal Conductivity of Gases and Liquids*, The M.I.T. Press, Cambridge, Mass., 1965.
- [4] Ostrogorsky, A. G., Glicksman, L. R., and Reitz, D., "Aging of Polyurethane Foams," *International Journal of Heat and Mass Transfer*, Vol. 29, 1986, pp. 1169-1175.
- [5] Reitz, D. W., "A Basic Study of Gas Diffusion in Foam Insulation," S.M. thesis, Department of Mechanical Engineering, Massachusetts Institute of Technology, Cambridge, Mass., 1983.

- [6] Ostrogorsky, A. G., "Aging of Polyurethane Foams," Sc.D. thesis, Department of Mechanical Engineering, Massachusetts Institute of Technology, Cambridge, Mass., 1985.
- [7] Bauman, G., "R-Value Study of Rigid Polyurethane Foam: An S.P.I. Research Project," presented to S.P.I. Annual Conference, 1982.
- [8] Booth, L. D. and Lee, W. M., "Effects of Polymer Structure on K-Factor Aging of Rigid Polyurethane Foam," *Journal of Cellular Plastics*, Vol. 21, pp. 6-30.
- [9] Booth, L. D., The Dow Chemical Company, personal communication, 1987.

Overview of Physical Properties of Cellular Thermal Insulations

REFERENCE: Strzepek, W. R., "Overview of Physical Properties of Cellular Thermal Insulations," *Insulation Materials, Testing, and Applications, ASTM STP 1030*, D. L. McElroy and J. F. Kimpflen, Eds., American Society for Testing and Materials, Philadelphia, 1990, pp. 121-140.

ABSTRACT: A comprehensive overview of the physical properties of cellular thermal insulations commonly used in the insulation industry has been developed. The insulations addressed are molded, expanded polystyrene (MEPS) and extruded, expanded polystyrene (XEPS) foams, polyurethane (PUR) and polyisocyanurate (PIR) foams, urea-formaldehyde (U-F) foams, phenolic foams, and cellular glass. Information was compiled primarily from manufacturers' literature, published documents, and private communications.

In addition to a general listing of typical physical properties, three areas are given special emphasis. The effects of aging and mean temperature on thermal transmission properties are discussed. Moisture absorption values measured using several different methods are presented, and a tabulation of typical mechanical strength properties is included.

The information presented is intended to serve as a general guide for comparing the physical properties of the various cellular insulations commonly used. The values are intended to be conservative; however, this may not be true for some commercially available products. Therefore it is recommended that the insulation manufacturer be contacted to obtain values for use in design.

KEY WORDS: aging, cellular glass, cellular plastic, foam, mechanical properties, mechanical strength, moisture content, moisture effects, permeance, phenolic, polyisocyanurate, polystyrene, polyurethane, temperature effects, thermal conductivity, thermal insulation, thermal properties, thermal resistance, urea-formaldehyde, wet insulation

The use of cellular materials as thermal insulations has become popular due to the good thermal insulating properties and high strength-to-weight ratio exhibited by these materials. Also, cellular materials generally are reasonable in cost when compared with their energy-saving potential.

There are many organic and inorganic substances that are capable of being processed to form stable foams. Basically the substance must have the capability of being processed as a fluid, foamed or expanded by a gas or mechanically while in that state, and then solidified while maintaining the cellular matrix established during the foaming process. Cellular materials can be produced with varying degrees of rigidity depending primarily on the chemical composition and rigidity of the substance used to form the cellular matrix. For example, flexible, semiflexible (or semirigid) and rigid materials are available; however, in general only rigid cellular materials are used as thermal insulations. The most common types of organic, cellular thermal insulations are manufactured using polystyrene resins, polyurethane and polyisocyanurate chemistry, urea-formaldehyde resins, and phenol-formaldehyde resins (which are used in the manufacture of phenolic foams). The most common inorganic, cellular insulation is produced from glass. (Perlite and vermiculite are also common expanded inorganic products, but they are not addressed in this paper.)

¹Dow Chemical U.S.A., Granville, OH 43023.

General Characteristics

Cellular materials consist of a gas phase, which is made up of a multitude of fine gas bubbles, dispersed in a solid phase, which is the cellular matrix. The physical properties of these materials are determined by both the gas and solid phases. The gas phase consists of the cell gas atmosphere, which can be air, chlorofluorocarbons, carbon dioxide, or other blowing agents used to foam or expand the solid substance. Some blowing or foaming agents are fugitive in that they readily diffuse through the cellular matrix and remain a component of the cell gas atmosphere for only a short period of time—that is, less than six months. The solid phase consists of the cellular matrix. It is composed of the organic or inorganic substance of which the matrix is formed and other ingredients added for a variety of reasons, such as foaming agents, fire retardants, and dyes or pigments. In low-density cellular materials such as those used as thermal insulations, the gas phase accounts for the majority of the volume of the material, whereas the solid phase accounts for virtually all of the weight.

The fine cells or bubbles, which constitute the gas phase, may be interconnected so that gas can pass readily from one cell to another. Materials with this characteristic are called *open-celled*. If cells are not interconnected and the gas phase of each cell is relatively independent of that of the surrounding cells, the material is *closed-celled*. In practice, no material is entirely open- or closed-celled; the terms imply that the material is predominately one or the other. Cellular thermal insulations are primarily closed-celled, but some phenolic and urea-formaldehyde foams are notable exceptions.

The base resin constituting the solid phase of foamed plastics may be either thermoplastic or thermosetting. Foam insulations made using thermoplastic resins such as polystyrene will soften or melt (if exposed to a sufficiently high temperature) before undergoing pyrolysis. Thermosetting foams, such as polyurethane and polyisocyanurate, urea-formaldehyde, and phenolic, will not. These materials generally will form a char as they pyrolyze depending on the conditions. This and some of the other differences between these two classes of foams can be important considerations in some end uses.

Materials and Manufacturing Processes

The processes for manufacturing cellular thermal insulations are similar in a general sense regardless of which substance is being foamed. However, there are specific differences in the processes which are worth noting.

Polystyrene

Expanded polystyrene (EPS) can be produced in either a molding process or an extrusion process. In the molding process small polystyrene beads, which have been impregnated with a blowing agent (typically pentane), are expanded in two stages. In the first stage the expandable beads are exposed to pressurized steam and the blowing agent vaporizes, which causes the beads to expand. The second steam expansion is done in a large mold. The partially expanded beads are expanded fully and fused together to form a billet, which can then be cut into board-stock or various shapes.

Polystyrene is also commonly expanded in an extrusion process. A solution of molten polymer, pressurized blowing agent in a liquid state, and other additives is extruded at elevated temperature and pressure through a slot-shaped orifice onto a conveyor system at ambient temperature and atmospheric pressure (or in some cases at a partial vacuum). As the polymer solution passes through the orifice, the blowing agent vaporizes because of the reduction in pressure, and the polymer is expanded into a foam. The material is extruded continuously as boards or billets with naturally occurring, high-density skins.

Polyurethane and Polyisocyanurate

Polyurethane (PUR) and polyisocyanurate (PIR) foams are produced by reacting two main ingredients, a polyol and a polyisocyanate (both in a liquid state) in the presence of a catalyst, a blowing agent, and other additives. The physical properties of the resultant foam can vary greatly depending on the specific type and amount of ingredients selected as well as the particular foaming process used. Since the foaming process occurs at the same time the polyurethane or polyisocyanurate polymer is being produced, the material can be foamed on site, which may be advantageous in some situations. PUR and PIR foams can be produced using a spray-applied technique, a pour-in-place process, a slabstock process, and a free-rise or restrained-rise continuous lamination process.

In the spraying process the ingredients are mixed and dispersed as a spray; the surface being insulated generally must be clean and dry to ensure good adhesion of the foam. In the pour-in-place process, the chemical components are mixed and the resulting blend is poured into a mold or cavity in which the expansion takes place. Billets are occasionally made using this process as well. To make boardstock and billets, reactants are mixed and deposited on a conveyor in a continuous process. After the foam cures, billets can be cut into boardstock and various shapes. In the free-rise or restrained-rise continuous lamination process, the components are poured or sprayed between two facing materials, and the mixture adheres to the facings as it expands. The restrained-rise process uses top and bottom conveyors to maintain thickness.

Polyisocyanurate foams are closely related to polyurethane products. In general, the same basic ingredients are used, but the specific formulations are different. Different reaction conditions are established which result in the production of the PIR polymer. There are differences in some of the physical properties: polyisocyanurate foams typically have improved thermal stability and flammability characteristics compared with polyurethane foams.

Urea-Formaldehyde

Urea-formaldehyde (U-F) foams are typically poured-in-place on site. To produce these foams, compressed air is mechanically dispersed into an aqueous solution of a catalyst and a foaming agent in a mixing gun, and a foam is generated. A second aqueous solution of partially cured urea-formaldehyde resin is then mechanically blended into the foam and the bubbles are coated with the resin. The mixture is then poured under pressure and the foam cures in place over time as the resin reacts with the catalyst.

Phenolic

Phenolic foams used as thermal insulations are typically produced in a continuous slabstock or double-band-lamination process similar to that used for the manufacture of PUR and PIR foams discussed previously. A phenol-formaldehyde resin, produced by reacting phenol and formaldehyde, is mixed with a catalyst, a blowing agent, and a foaming agent to generate the foam. Either open-celled or closed-celled materials can be obtained, depending on the formulation used and the foaming conditions selected.

Cellular Glass

Cellular glass insulation is generally manufactured from a mixture of silicates and alkali oxides which is fused at high temperatures and cellulated as a result of a high-temperature reaction between carbon and oxygen. The product is available in blocks, boards, and various shapes.

Physical Properties

Typical physical properties for cellular thermal insulations are shown in Tables 1 to 4 and Figs. 1 to 3. The data are taken primarily from general references such as technical sales literature, material specifications, and published articles and papers; however, some data are included from private communications with insulation manufacturers and proprietary research reports. The data reported are for the purposes of general comparison, and the values may not be representative of every product available in the marketplace. For any given entry in the tables the range in values may be considerable due to the variability between specific products within a given material type and other factors relating to the testing of the products. Also, the data represent typical properties, not minimum values or specification limits. To obtain appropriate values for use in design and information concerning the test methods followed, the insulation manufacturer should be consulted.

Thermal Transmission

Perhaps the most important physical property of cellular thermal insulations is thermal transmission. Typical thermal transmission data for the common cellular insulations are listed in Tables 1 and 2. In cellular insulations thermal energy is transferred by three different mechanisms: conduction through the solid portion of the foam, conduction through the gaseous portion, and radiation through the cellular matrix from cell wall to cell wall [1]. Convection heat transfer within the cells is generally not considered, because the cell size is usually too small to support convective movement [1].

For many products measures are taken to minimize the heat transfer contribution from one or more of these mechanisms. For example, chlorofluorocarbon blowing agents are commonly introduced not only to help foam the fluid but also to reduce conduction through the gaseous portion of the foam. The use of facings laminated or bonded in some way to chlorofluorocarbon-blown foams also can help improve thermal performance. These measures are discussed further in the Aging Effects section.

To minimize radiation through the cellular matrix, density can be increased to provide more material in the cell walls to absorb infrared radiation. Although an increase in density can reduce the radiation component of heat transfer, it simultaneously increases the conduction through the solid portion of the foam. For example, the optimum balance point for radiation and conduction effects is generally 1.8 to 2.5 lb/ft³ (28.8 to 40.0 kg/m³) for cellular plastics [1-3].² However, because other factors generally need to be considered, such as raw material costs and mechanical strength requirements, the density of cellular plastics typically ranges from less than 1.0 to 4.0 lb/ft³ (16.0 to 64.0 kg/m³).

Radiation transfer can also be reduced by decreasing the cell size so that more cell walls are provided to absorb the radiation. However, in some cases cell size can be reduced only to a certain point before the product becomes difficult or uneconomical to produce. It can also be difficult to control cell size or produce a uniform cellular matrix.

Aging Effects

The thermal resistance, commonly termed *R*-value, of some cellular insulations decreases with time, as shown in Fig. 1. This phenomenon is termed *aging*. Aging can occur only with those closed-celled materials expanded with agents other than air, such as chlorofluorocarbons, and reflects a change in composition of the cell gas atmosphere. Products containing only air, such as molded bead polystyrene (MEPS), do not age in this way. However, *R*-value can also decrease as a result of environmental factors relating to a particular end use, such as physical

²For easier comparison with the tables, data in the body of the paper are presented in standard U.S. units first with metric equivalents following in parentheses.

deterioration and water absorption. Aging occurs in addition to these other mechanisms of *R*-value degradation and in some cases can be accelerated by them. Regardless of the mechanism at work, aging effects and *R*-value degradation are important to consider when designing or selecting an insulation system.

The decrease in *R*-value of chlorofluorocarbon-blown foams can be most easily comprehended by recognizing that the phenomenon is the result of two independent mechanisms which take place simultaneously. At the time of manufacture, the cells of these materials contain virtually no air, only the chlorofluorocarbon and perhaps some other fugitive blowing agents, such as carbon dioxide, which readily diffuse out of the product. Because of the difference between the partial pressure of the air in the ambient atmosphere and that in the cell gas atmosphere, air immediately begins to enter the cells. The diffusion of air into the product continues until the partial pressure of the air in the foam equals the ambient air pressure. The chlorofluorocarbons have a lower thermal conductivity than that of air, so the net effect of the entry of air into the foam is the reduction of the *R*-value of the product. Air intrusion constitutes one of the two mechanisms involved in aging. It is reflected in the curves in Fig. 1. For most products and applications this mechanism of aging occurs early enough in the service life of the product that it is significant and needs to be taken into account. However, the presence of well-bonded, low-permeance facings, such as some aluminum foils, can significantly retard this air influx.

The second mechanism of aging involves the diffusion of the chlorofluorocarbon blowing agent out of the foam and occurs because of the difference between the partial pressure of the chlorofluorocarbon gas in the cell gas atmosphere and that in the ambient atmosphere. This mechanism also begins immediately after manufacture but generally proceeds very slowly compared with air intrusion. It is completed when there is virtually no chlorofluorocarbon remaining in the cellular matrix, only air. Diffusion of the chlorofluorocarbon is generally so slow that it is of no consequence in most applications. For example, for an unfaced, 1.0-in. (2.54-cm) sample of extruded polystyrene (XEPS) the second mechanism takes approximately 100 years to complete [4]. For thicker products and those with well-bonded, low-permeance facings, diffusion of the chlorofluorocarbon out of the product can involve a much longer time frame.

The rate at which each mechanism occurs for a given product depends on the rates of diffusion of air and chlorofluorocarbons into and out of the product. The diffusion rates through the various types of cellular materials are different. For example, in general the diffusion of air and chlorofluorocarbons through PUR and PIR foams proceeds at a slower rate than diffusion through extruded polystyrene (XEPS) foams, as illustrated in Fig. 1, and diffusion through closed-celled phenolic foams is slower than that through polyurethane and polyisocyanurate foams. To effectively retard diffusion, the percentage of open cells in the product must be very low. If the cells are not completely closed, the aging phenomenon can take place much more rapidly [5].

The timing of each mechanism also depends on the gas-permeation resistance of any facings attached to the foam core, the quality of the bond between the facings and the core, and the thickness of the product. If a chlorofluorocarbon-blown foam is totally encapsulated with an effective gas-diffusion barrier during or immediately following manufacture, then air cannot enter the product and the chlorofluorocarbon cannot exit. The *R*-value of such a product could be as great as 9.00 F ft² h/Btu in. (62.5 K m/W). However, in practice most products are not totally encapsulated and aging does occur. Even for those products in which the major surfaces are protected by aluminum foil or foil-composite facings, aging can be significant [6, 7].

In most cases the aluminum foils used on such products are too thin to be totally free of pinholes. As a result diffusion of gases is only impeded to some degree depending on the thickness of the foil. Generally a foil must be at least 1.0 mil in thickness before it can be considered pinhole-free and hence a true diffusion barrier [8]. However, some foil or foil-composite facings may act as diffusion barriers at lower thicknesses, and in some cases the 1.0 mil thickness may not provide a pinhole-free barrier. Most foil products used in facings range between 0.3 and 1.0 mil in thickness. Generally facings of this type should be considered retarders, not barriers.

TABLE 1—Typical physical properties of cellular thermal insulations. ^(a)

Property	Expanded Poly- styrene (Molded)	Expanded Poly- styrene (Extruded)	Polyurethane and Polyisocyanurate	Urea-Formaldehyde	Phenolic	Cellular Glass
Apparent Density, lb/ft ³ ^(b)	0.8-2.0	1.4-4.0	1.7-3.0	0.8-1.2	2.0-3.0	8.5-12.0
Open Cell Content, %	5-40	1-7	2-10	30-95	5-90	0-1
Apparent Thermal Conductivity ^(c) , Btu in./h ft ² °F ^(d)	0.23-0.30	0.20	0.13-0.18	0.24	0.12-0.23	0.35-0.57
Heat Capacity, Btu/lb °F ^(e)	0.27-0.31	0.27-0.31	0.20-0.25	0.36	0.38	0.20
Apparent Water Vapor Permeability ^(f) , perm in. ^(g)	0.6-5.0	0.4-1.4	2.0-4.0	4.5-100	1.4-3.5	0.0
Water Absorption ^(h) , vol %	<2.5	<0.3	2-5	Very high	<10	Nonabsorptive
Compressive Strength, lb/in. ⁽ⁱ⁾	5-33	15-125	20-60	5	10-35	100-210
Coefficient of Linear Thermal Expansion, in./in. °F ^(j) ($\times 10^{-6}$)	25-40	25-40	30-60	50	10-20	1.6-4.6
Dimensional Stability ^(k) , % linear change	<2	<2	2-10	30	<2	Very low

Maximum Use Temperature, °F ⁽¹⁾	165	165	250 PUR 250-300 PIR	120	300	900
Combustibility	Combustible	Combustible	Combustible	Combustible	Combustible	Noncombustible
Flame Spread ^(m)	5 ⁽ⁿ⁾	5 ⁽ⁿ⁾	25-50 PUR 20-25 PIR	10-25	20-25	5
Smoke Developed ^(m)	45-200 ⁽ⁿ⁾	45-200 ⁽ⁿ⁾	150-500 PUR 50-200 PIR	5-70	5-15	0

^(a)The data reported are for the purposes of general comparison, and the values may not be representative of every product available in the marketplace. The range in values may be considerable due to the variability between specific products within a given material type and other factors relating to the testing of the products.

^(b)To convert from lb/ft³ to kg/m³, multiply by 16.0.

^(c)Materials are measured at a 75°F (24°C) mean temperature. In general, values are intended to be representative of long-term performance. However, values may not be appropriate for all products in the marketplace due to lack of long-term data and uncertainties regarding product quality and aging conditions.

^(d)To convert from Btu in./h ft² °F to W/m K, multiply by 0.144.

^(e)To convert from Btu/lb °F to kJ/kg K, multiply by 4.19.

^(f)Values are based on the cellular material only. The effects of facings are not included. Values are determined using the Desiccant Method as described in ASTM E 96.

^(g)To convert from perm in. to ng/Pa s m, multiply by 1.46.

^(h)Materials are immersed for 24 h in accordance with ASTM C 272.

⁽ⁱ⁾To convert from lb/in.² to MPa, multiply by 0.006895.

^(j)To convert from in./in. °F to m/m °C, multiply by 1.8.

^(k)Values are representative of materials conditioned at approximately 158°F (70°C) and 97% relative humidity for 7 days. See ASTM D 2126.

^(l)To convert from °F to °C, use the following equation: $T_{(C)} = (T_{(F)} - 32)/1.8$.

^(m)Values are indicative of the response of these materials to heat and flame under controlled laboratory conditions. To describe or appraise the fire hazard or fire risk under actual fire conditions, other factors need to be considered as well. Values may vary with thickness. See ASTM E 84.

⁽ⁿ⁾Ignition of molten residue on the floor of the furnace is not considered.

TABLE 2—Typical thermal transmission properties^(a) (1.0-in. [2.54-cm] thickness).

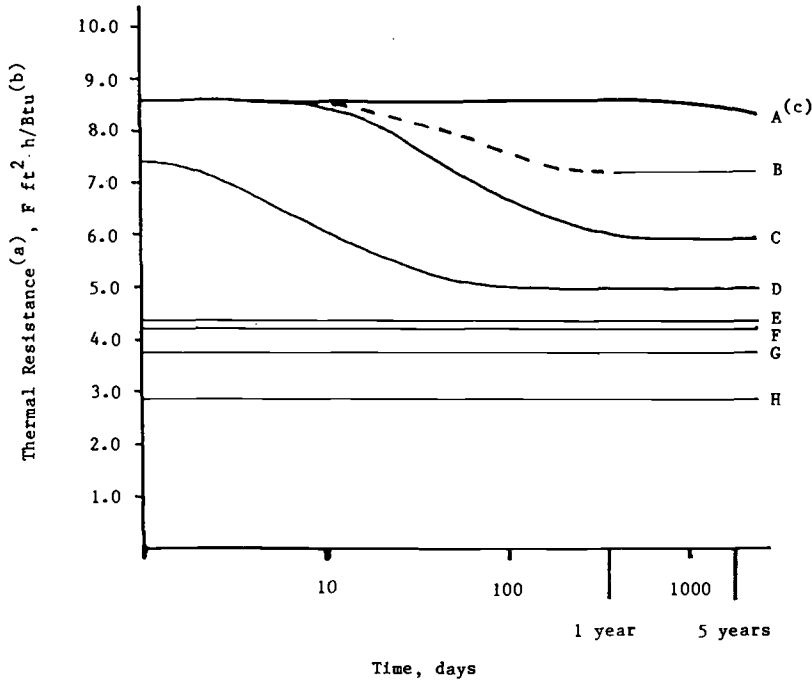
Property	Polyurethane and Polyisocyanurate										Cellular Glass	
	Expanded Polystyrene (Molded)		Expanded Polystyrene (Extruded)	$\rho = 1.7-3.0$ lb/ft ³			Urea-Formaldehyde		Phenolic		$\rho = 8.5$ lb/ft ³	$\rho = 12.0$ lb/ft ³
	$\rho = 1.0$ lb/ft ³ (b)	$\rho = 2.0$ lb/ft ³	$\rho = 1.4-4.0$ lb/ft ³	Unfaced or High-Permeance Facings	Low-Permeance Facings	$\rho = 0.8-1.2$ lb/ft ³	Open-Cellled	Closed-Cellled				
Apparent Thermal Conductivity, Btu in./h ft ² °F(c)												
Mean Temperature	25°F	0.23	0.20	0.18	0.16-0.18	0.13-0.15	0.21	0.20	0.115	0.31	0.54	
	40°F	0.24	0.21	0.19	0.15-0.17	0.12-0.14	0.22	0.21	0.116	0.32	0.55	
	75°F	0.26	0.23	0.20	0.16-0.18	0.13-0.15	0.24	0.23	0.12	0.35	0.57	
	110°F	0.28	0.25	0.22	0.17-0.19	0.14-0.16	0.26	0.25	0.126	0.38	0.59	
Thermal Resistance, °F ft ² h/Btu(d)												
Mean Temperature	25°F	4.3	5.0	5.6	5.6-6.2	6.7-7.7	4.8	5.0	8.7	3.2	1.9	
	40°F	4.2	4.8	5.4	5.9-6.7	7.1-8.3	4.5	4.8	8.6	3.1	1.8	
	75°F	3.8	4.3	5.0	5.6-6.2	6.7-7.7	4.2	4.3	8.3	2.9	1.8	
	110°F	3.6	4.0	4.7	5.3-5.9	6.3-7.1	3.8	4.0	7.9	2.6	1.7	

^(a)The data reported are for the purposes of general comparison, and the values may not be representative of every product available in the marketplace. The range in values may be considerable due to the variability between specific products within a given material type and other factors relating to the testing of the products. In general, values are intended to be representative of long-term performance. However, values may not be appropriate for all products in the marketplace due to lack of long-term data and uncertainties regarding product quality and aging conditions.

^(b)To convert from lb/ft³ to kg/m³, multiply by 16.0.

^(c)To convert from Btu in./h ft² °F to W/m K, multiply by 0.144.

^(d)To convert from °F ft² h/Btu to K m²/W, multiply by 0.176.



- A - Phenolic; 2.0 - 3.0 lb/ft³ (32.0 - 48.0 kg/m³); closed-celled
 B - Polyurethane and polyisocyanurate; 1.7 - 3.0 lb/ft³ (27.2 - 48.0 kg/m³); low-permeance facings
 C - Polyurethane and polyisocyanurate; 1.7 - 3.0 lb/ft³ (27.2 - 48.0 kg/m³); unfaced or high-permeance facings
 D - Expanded polystyrene (extruded); 1.4 - 4.0 lb/ft³ (22.4 - 64.0 kg/m³)
 E - Phenolic; 2.0 - 3.0 lb/ft³ (32.0 - 48.0 kg/m³); open-celled
 F - Urea-formaldehyde; 0.8 - 1.2 lb/ft³ (12.8 - 19.2 kg/m³)
 G - Expanded polystyrene (molded); 1.0 lb/ft³ (16.0 kg/m³)
 H - Cellular glass; 8.5 lb/ft³ (136 kg/m³)

(a) The data reported are for the purposes of general comparison and the values may not be representative of every product available in the marketplace. The range in values may be considerable due to the variability between specific products within a given material type and other factors relating to the testing of the products.

(b) To convert from F ft² h/Btu to K m²/W, multiply by 0.176.

(c) The curve is based on limited measured data from Reference 14.

FIG. 1—Thermal resistance versus time for 1.0-in. (2.54-cm) materials aged at ambient conditions and measured at a 75°F (24°C) mean temperature.

Also, in some cases facings are made of materials which are not effective barriers, such as kraft paper and thin polyethylene film. Such facings should not be considered barriers either. The impact of the barrier properties of a facing on the R -value of PUR and PIR foams is indicated in Table 2.

The quality of the bond between the facing and the core material is also important. If the facing is not properly laminated to the core or the bond is in some way broken, diffusion can

take place, which can increase the rate at which aging occurs [8,9]. In addition, product thickness also has an effect on aging: thicker products age more slowly. Diffusion of air into the cellular matrix and chlorofluorocarbons out of the product takes longer for thicker products because there is more material through which the gases must diffuse.

Mean Temperature Effects

The thermal resistance of all cellular insulations changes with mean temperature. Generally speaking, at lower mean temperatures the R -value is greater, as indicated in Table 2 and Fig. 2. The thermal performance of the insulations generally improves as the mean temperature decreases because the thermal conductivities of the cell gases decrease with temperature. Like aging effects, mean temperature effects should also be considered in the design or selection of insulation systems.

As shown in Fig. 2, the curves for extruded polystyrene (XEPS), unfaced PUR and PIR, and phenolic foam products have inflection points which occur around -75 and -150°F (-60 and -100°C), 50 and -25°F (10 and -30°C), and 25 and -100°F (-5 and -75°C), respectively. The occurrence of inflection points in a curve indicates the presence of a chlorofluorocarbon (which explains why there is no peak in the curve for the molded polystyrene [MEPS] product, for example). The specific location of the inflection points is characteristic of the particular chlorofluorocarbon that is contained in the foam. For example, Refrigerant-11 is generally used with polyurethane and polyisocyanurate foams and Refrigerant-12 with extruded polystyrene foams, so it is not surprising that the inflection points occur at different locations for these products.

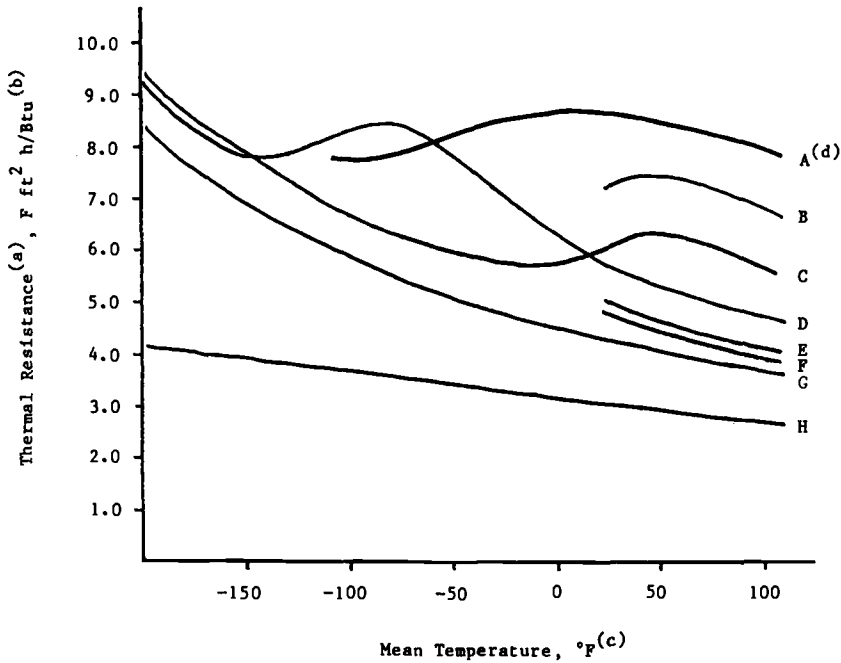
Over the mean temperature range bounded by the inflection points, the R -value decreases as mean temperature decreases. This phenomenon is observed because the chlorofluorocarbons condense from a vapor to a liquid over this range of mean temperatures. As the condensation continues the cell gas atmosphere becomes increasingly rich in air, which is a poor insulator relative to the chlorofluorocarbons. Therefore the R -value of the product decreases. Once all the chlorofluorocarbon has condensed, then the R -value again increases with decreasing mean temperature.

Thickness Effects

For low-density cellular insulations the R -value per inch of a given material may be lower for products of greater thickness. In other words, the thermal resistance of a 3.0-in. (7.62-cm) product, for example, may not be as great as the resistance of a similar 1.0-in. (2.54-cm) product multiplied by three. The effect is primarily caused by the fact that the radiation component of thermal transmission can be different for similar products of different thickness. The transfer of heat by radiation through cellular thermal insulations is influenced by several factors including the material that constitutes the solid phase; the product thickness, density, and cell size; and the mean temperature. For cellular insulations, the reduction in R -value attributable to the thickness effect can be as great as 5% of the thermal resistance of the product (or perhaps even greater in some cases) [10-12]. For more information contact the insulation manufacturer.

Other Considerations

When deciding which cellular thermal insulation is most appropriate for a particular application, it is important to compare products on an equal basis. As far as product aging is concerned, the comparison should generally be made with R -values that reflect the first mechanism of aging, that is, intrusion of air. Several sample conditioning procedures have been used in the industry in an attempt to represent this aging condition: 180-day aging at 75°F (24°C) and 50%



- A - Phenolic; 2.0 - 3.0 lb/ft³ (32.0 - 48.0 kg/m³); closed-celled
 B - Polyurethane and polyisocyanurate; 1.7 - 3.0 lb/ft³ (27.2 - 48.0 kg/m³); low-permeance facings
 C - Polyurethane and polyisocyanurate; 1.7 - 3.0 lb/ft³ (27.2 - 48.0 kg/m³); unfaced or high-permeance facings
 D - Expanded polystyrene (extruded); 1.4 - 4.0 lb/ft³ (22.4 - 64.0 kg/m³)
 E - Phenolic; 2.0 - 3.0 lb/ft³ (32.0 - 48.0 kg/m³); open-celled
 F - Urea-formaldehyde; 0.8 - 1.2 lb/ft³ (12.8 - 19.2 kg/m³)
 G - Expanded polystyrene (molded); 1.0 lb/ft³ (16.0 kg/m³)
 H - Cellular glass; 8.5 lb/ft³ (136 kg/m³)

(a) The data reported are for the purposes of general comparison, and the values may not be representative of every product available in the marketplace. The range in values may be considerable due to the variability between specific products within a given material type and other factors relating to the testing of the products. In general, values are intended to be representative of long-term performance. However, values may not be appropriate for all products in the marketplace due to lack of long-term data and uncertainties regarding product quality and aging conditions.

(b) To convert from F ft² h/Btu to K m²/W, multiply by 0.176.

(c) To convert from °F to °C, use the following equation:
 $T(^{\circ}\text{C}) = (T(^{\circ}\text{F}) - 32)/1.8$.

(d) The curve is based on limited measured data from Reference 14. There is uncertainty regarding the reason for the large temperature range between the inflection points for the phenolic foam product (at approximately 25 and -100°F) compared with the corresponding ranges shown in Curves C and D. The differences in the relative magnitudes of the temperature ranges shown in Curve A and Curves C and D may be the result of differences in experimental procedure.

FIG. 2—Thermal resistance versus mean temperature for 1.0-in. (2.54-cm) materials aged at ambient conditions.

relative humidity, 90-day aging at 140°F (60°C), and 5-year aging (or longer) at 75°F (24°C). Whether or not these procedures accurately represent the first mechanism of aging depends on many factors which relate to the rate at which air and chlorofluorocarbons pass into and out of the products. In general, *R*-values based on conditioning procedures involving long time periods or high temperatures are more indicative of long-term performance.

It is also important to compare the thermal resistances of the insulations at the same mean temperature. The particular mean temperature selected should be representative of the particular end use in question. This affects the comparison because the thermal performance of one product with respect to another can change over a given range of mean temperatures. For example, the *R*-value per inch of extruded polystyrene at a mean temperature of approximately 10°F (−12°C) is equivalent to that of unfaced polyurethane and polyisocyanurate. This is not the case at a mean temperature of 75°F (24°C), as shown in Fig. 2. The particular mean temperature selected also establishes the *R*-value per inch that is used to determine the thickness of insulation required. To simplify matters somewhat a mean temperature of 75°F (24°C) is often used for purposes of comparison because it is widely accepted as a standard within the industry. For some end uses the Federal Trade Commission requires that *R*-values be reported at a mean temperature of 75°F (24°C). Therefore most manufacturers report *R*-values for their products at this mean temperature, even though it is not representative for many applications.

Moisture Transmission and Absorption

Moisture can have an adverse affect on the thermal transmission (and perhaps mechanical strength) properties of cellular thermal insulations. In most applications, good system design and proper installation of vapor retarders minimize the danger of moisture accumulation in insulating materials. Despite these precautions it is still possible (and in some applications expected) that insulations will be exposed to moisture. Therefore it is important to consider the moisture transmission and absorption characteristics of insulating materials. These properties are given in Tables 1 and 3 for cellular thermal insulations. Compared with other common insulating materials, such as fibrous and granular insulations, cellular insulations exhibit good resistance to moisture intrusion.

The values for apparent water vapor permeability shown in the tables apply to unfaced materials. When facings are added, which is the case with many products, they may be rendered essentially impermeable depending on the barrier qualities of the facings or laminates. In general, products with a water vapor permance of 0.5 to 1.0 perm (28.7 to 57.4 ng/Pa s m²) or less are considered vapor retarders, so some cellular insulations may be installed in certain applications without any moisture protection. For a given product type, higher density materials generally have lower permeability and absorption values. However, this is not always true because these properties are also dependent on other factors such as the integrity of the cellular matrix. For example, some closed-celled foams often contain interstitial spaces or voids between the cells. As a result, these products can exhibit some of the characteristics of open-celled foams, such as relatively high water absorption values, depending on the number and size of the voids.

It is important to consider the severity of the moisture exposure expected for a given application. The severity of the exposure to which the insulation is to be subjected is a major factor in determining which material is selected and what protective measures are appropriate, if any. Various moisture transmission and absorption tests are available to help assess the moisture resistance of various insulations. Some of these tests are listed in Table 3. Results from such tests should not be used indiscriminately, however. The tests differ greatly with regard to the severity of the moisture exposure involved, so care should be taken to ensure that the method or methods in question relate to the intended end use.

As mentioned previously, the thermal performance of insulations can be adversely affected by the presence of moisture depending on the amount present and its location. This is because the thermal conductivities of liquid water and especially ice are significantly greater than that of the

TABLE 3—Typical moisture transmission and absorption properties^(a).

Property	Expanded Polystyrene (Molded)		Expanded Polystyrene (Extruded)		Polyurethane and Polyisocyanurate		Phenolic		Cellular Glass	
	$\rho = 1.0 \text{ lb/ft}^3$ ^(b)	$\rho = 2.0 \text{ lb/ft}^3$	$\rho = 1.4\text{--}4.0 \text{ lb/ft}^3$	$\rho = 1.4\text{--}4.0 \text{ lb/ft}^3$	$\rho = 1.7\text{--}3.0 \text{ lb/ft}^3$	$\rho = 2.0\text{--}3.0 \text{ lb/ft}^3$	$\rho = 2.0\text{--}3.0 \text{ lb/ft}^3$	$\rho = 2.0\text{--}3.0 \text{ lb/ft}^3$	$\rho = 8.5 \text{ lb/ft}^3$	$\rho = 8.5 \text{ lb/ft}^3$
Apparent Water Vapor Permeability, ^(c) perm in. ^(d)	1.2–3.0	0.6–1.5	0.4–1.4	0.4–1.4	2.0–4.0	1.4–3.5	1.4–3.5	1.4–3.5	0.0	0.0
Water Absorption, vol%										
ASTM C 272 (24-h immersion)	<2.5	<1.0	<0.3	<0.3	2–5	5–10	5–10	5–10	Nonabsorptive. Only moisture retained is that adhering to surface cells after immersion.	Nonabsorptive. Only moisture retained is that adhering to surface cells after immersion.
ASTM D 2842 (96-h immersion)	1–6	1–4	1	1	0–2	5–20	5–20	5–20		
ASTM D 2842 (500-h immersion)	4–7	1–5	1	1	1–4	15–40	15–40	15–40		
Water Vapor Diffusion ^(e) (28-day exposure)	8–25	4–25	1–4	1–4	5–40	10–60	10–60	10–60		
Freeze Thaw Cycling ^(f) (1000-cycle exposure)	15–80	15–50	2–10	2–10	4–90 ^(g)	50–70	50–70	50–70	70 ^(h)	70 ^(h)

^(a)The data reported are for the purposes of general comparison, and the values may not be representative of every product available in the marketplace. The range in values may be considerable due to the variability between specific products within a given material type and other factors relating to the testing of the products.

^(b)To convert from lb/ft³ to kg/m³, multiply by 16.0.

^(c)Values are based on the cellular material only. The effects of facings are not included. Values are determined using the Desiccant Method as described in ASTM E 96.

^(d)To convert from perm in. to ng/Pa s m, multiply by 1.46.

^(e)Materials are subjected to both thermal and water vapor pressure gradients. Specimens are placed between a cooling plate at 34°F (1°C) and a water bath in which the temperature is regulated to maintain a temperature gradient of 46°F/in. (10°C/cm) thickness. See Swiss Standard SIA 279.

^(f)Materials are subjected to freeze-thaw cycling by freezing in air at 0°F (–18°C) followed by thawing in water at 40°F (4°C). See ASTM C 666.

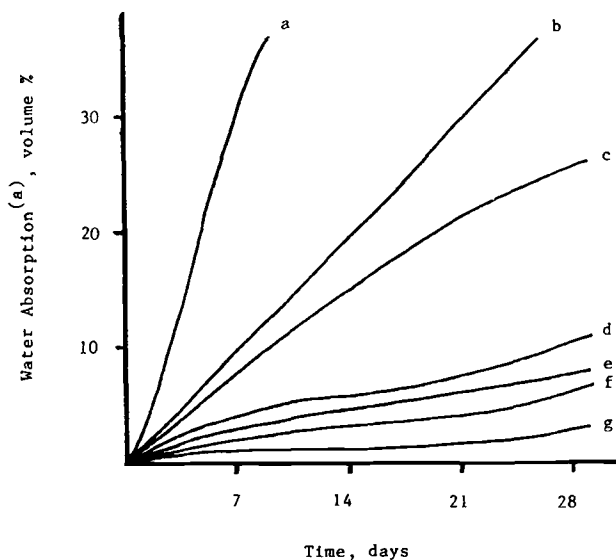
^(g)The higher water absorption levels are representative of materials with glass-fiber reinforcement; in many cases the test must be terminated prematurely because of excessive damage to the specimens.

^(h)Generally the test must be terminated prematurely because of excessive damage to the specimens.

insulation. Figures 3a and 3b show the water absorption and *R*-value retention of several cellular insulations following a 14-day exposure in a conditioning apparatus where specimens were subjected to both water vapor pressure and thermal gradients.

Mechanical Strength

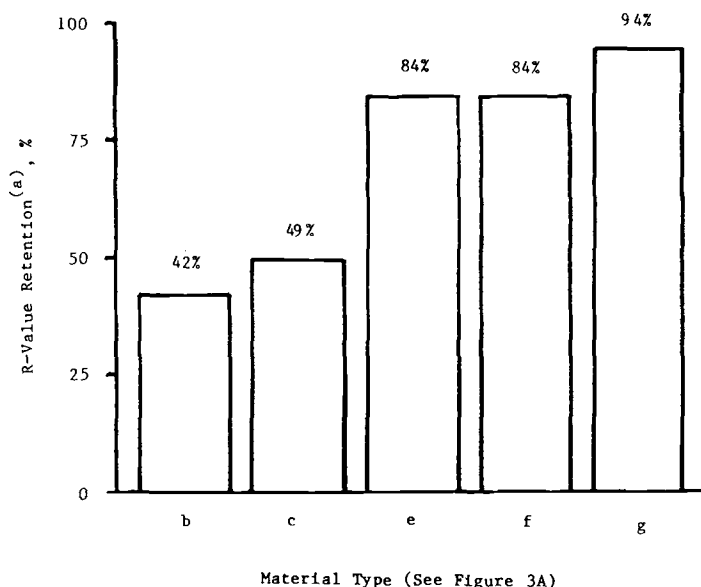
Approximate mechanical strength properties for cellular thermal insulations are presented in Table 4. As mentioned previously, the range in the values for a given property may be considerable due to variability between specific products and differences in test procedures and test specimen dimensions. As a result, the data reported may not be representative of all the materials available. Some materials, extruded polystyrene and polyurethane and polyisocyanurate products, for example, exhibit anisotropic behavior—that is, the mechanical properties differ according to the direction of measurement. Hence the direction of measurement, either parallel



- a - Phenolic; 2.5 - 3.0 lb/ft³ (40.0 - 48.0 kg/m³); open-celled; perforated and corrugated kraft paper/aluminum foil facings
- b - Polyurethane; 2.4 lb/ft³ (38.4 kg/m³); kraft paper facings
- c - Expanded polystyrene (molded); 1.6 lb/ft³ (25.6 kg/m³)
- d - Phenolic; 3.0 lb/ft³ (48.0 kg/m³); closed-celled; corrugated kraft paper/aluminum foil facing on one surface, flat kraft paper facing on the other
- e - Expanded polystyrene (molded); 0.9 lb/ft³ (14.4 kg/m³)
- f - Polyisocyanurate; 2.0 lb/ft³ (32.0 kg/m³); aluminum foil facings
- g - Expanded polystyrene (extruded); 1.4 - 4.0 lb/ft³ (22.4 - 64.0 kg/m³)

- (a) The data reported are for the purposes of general comparison, and the values may not be representative of every product available in the marketplace. The range in values may be considerable due to the variability between specific products within a given material type and other factors relating to the testing of the products. Water absorption data for Materials "b" and "c" are taken from Reference 15. Other data are taken from internal reports of The Dow Chemical Company.

FIG. 3a—Water absorption versus time for 2.0-in. (5.08-cm) materials subjected to thermal and water vapor pressure gradients in a water vapor diffusion test (Modified Swiss Standard SIA 279).



- (a) The data reported are for the purposes of general comparison and the values may not be representative of every product available in the marketplace. The range in values may be considerable due to the variability between specific products within a given material type and other factors relating to the testing of the products. R-value retention is calculated using equations developed by Dechow and Epstein, which are given in Reference 15. Data for Materials "a" and "d" are not shown because equations for predicting the thermal transmission properties of phenolic foam materials containing moisture are not included in Reference 15.

FIG. 3b—R-Value retention for 2.0-in. (5.08-cm) materials subjected to thermal and water vapor pressure gradients for 14 days in a water vapor diffusion test (Modified Swiss Standard SIA 279).

or perpendicular to rise, is indicated in the table. Generally speaking, both the length and width directions are perpendicular to rise. (Rise is the thickness direction, which is generally the principal direction of expansion.) In some cases there may be differences in the values measured in the length and width directions. Such differences have not been identified to keep the table as simple as possible.

The facings that are laminated or bonded to some materials can increase the strength of the products significantly as well as help prevent the foam core from being damaged. For some properties such as tensile strength, the strength of the composite can be reduced if the bond between the facing and the core is poor. The values shown in Table 4 apply to unfaced materials. For data on faced products consult the insulation manufacturer. In addition to the obvious variation in properties with density and product type, the manufacturing process and related factors can also be important. At similar densities extruded polystyrene (XEPS) products are stronger than molded bead (MEPS) products; and the strength properties of rigid PUR and PIR boards and buns, which are reflected in Table 4, may be different than those of spray-in-place and pour-in-place products. The strengths and moduli also generally increase with decreasing temperature. For data at other temperatures within the ranges shown, consult Ref 13 and contact the insulation manufacturer.

TABLE 4—Typical mechanical strength properties^(a), lb./in.²(b),

Property	Expanded Polystyrene (Extruded)										Polyurethane and Polyisocyanurate		Urea-Formaldehyde		Phenolic		Cellular Glass			
	Expanded Polystyrene (Molded)										$\rho = 2.0$ lb/ft ³ $\rho = 4.0$ lb/ft ³		$\rho = 2.0$ lb/ft ³ $\rho = 6.0$ lb/ft ³		$\rho = 0.8-1.2$ lb/ft ³		$\rho = 2.0-3.0$ lb/ft ³		$\rho = 8.5$ lb/ft ³ $\rho = 12.0$ lb/ft ³	
	$\rho = 1.0$ lb/ft ³ (c) @ 75°F (d)	$\rho = 2.0$ lb/ft ³ @ 75°F	$\rho = 1.4$ lb/ft ³ @ 75°F	$\rho = 2.0$ lb/ft ³ @ 75°F	$\rho = 4.0$ lb/ft ³ @ 75°F	$\rho = 2.0$ lb/ft ³ @ -325°F	$\rho = 4.0$ lb/ft ³ @ 75°F	$\rho = 2.0$ lb/ft ³ @ -325°F	$\rho = 6.0$ lb/ft ³ @ 75°F	$\rho = 12.0$ lb/ft ³ @ -325°F	$\rho = 2.0$ lb/ft ³ @ -325°F	$\rho = 6.0$ lb/ft ³ @ 75°F	$\rho = 0.8-1.2$ lb/ft ³ @ 75°F	$\rho = 2.0-3.0$ lb/ft ³ @ 75°F	$\rho = 8.5$ lb/ft ³ @ 75°F	$\rho = 12.0$ lb/ft ³ @ 75°F				
Compressive Strength, parallel to rise (thickness)	10-14	25-33	15-25	25-50	45-65	115-125	25-35	40-50	100	190	5	10-35	100	210						
Compressive Modulus, parallel to rise (thickness), ($\times 10^3$)	0.2	0.5	...	1.3	2.5	3.0	0.9	2.0	2.6	10.5	...	1.0	150	180						
Flexural Strength, perpendicular to rise	25-30	50-75	40-70	50-100	...	100-140	50	...	210	...	15	25	80	110						
Shear Strength, perpendicular to rise	20	35	...	35	30	70	20	20	100	175	...	12	50	...						
Tensile Strength, parallel to rise (thickness)	18	25	25	50	25	125	45	25	140	200	1	20	50	...						
Tensile Modulus, parallel to rise (thickness), ($\times 10^3$)	0.2	0.5	...	3.2	4.2	4.7	1.6	3.0	4.0	10	...	0.2						

^(a)The data reported are for the purposes of general comparison, and the values may not be representative of every product available in the marketplace. The range in values may be considerable due to the variability between specific products within a given material type and other factors relating to the testing of the products.

^(b)To convert from lb./in.² to MPa, multiply by 0.006895.

^(c)To convert from lb./ft³ to kg/m³, multiply by 16.0.

^(d)To convert from °F to °C, use the following equation: $T(^{\circ}\text{C}) = (T(^{\circ}\text{F}) - 32)/1.8$.

Miscellaneous

Maximum use temperature and solvent resistance must be considered for many applications. In general, thermosetting foams can be used at higher temperatures and exhibit greater solvent resistance than thermoplastic foams. Cellular glass products can be used at higher temperatures than other cellular insulations, and they also have excellent solvent-resistant properties. Dimensional stability may also be a significant factor, especially if the materials are exposed to high temperatures and humidities. Urea-formaldehyde foams generally exhibit considerable shrinkage as they cure; this should be taken into account when these products are used. Polyisocyanurate foams typically exhibit improved dimensional stability at high temperatures compared with polyurethane foamed plastics. In certain applications corrosivity may also be a concern with some phenolic foams because of the acid catalyst used in the reaction to produce the polymer.

In regard to product handleability, friability should also be taken into consideration. In general, thermosetting foamed plastics are more friable than thermoplastic foams, which is one of the reasons many of the thermosetting products are offered with facings. Also, prolonged exposure to solar radiation will result in the deterioration of the surface of unfaced foamed plastics. The severity of the degradation will vary depending on the foam type and specific formulation, and the intensity of the solar exposure. The surface degradation will not have a measurable effect on the insulating value of the products unless deterioration is allowed to continue until the thickness of the foam is measurably reduced. All products, faced and unfaced, should be protected during storage and after installation with a covering or coating that is opaque to ultraviolet radiation.

Applications

The largest markets for cellular thermal insulations are building construction applications involving both new and retrofit construction in residential, commercial, agricultural, and industrial structures. Cellular insulations in board form are routinely installed in conventional built-up roofs and beneath single-ply membranes; some products, namely, extruded EPS, are installed above the membrane in protected membrane roof applications. Insulating boards are also used in cathedral ceilings in residential and light-commercial construction. They are often used as sheathing on wood-frame, metal-frame, and masonry walls in a variety of systems, which are installed on both the interior and exterior of the structures. They are also widely used as core materials in a variety of sandwich-panel constructions. In addition, these products are used as foundation insulations in basement, crawlspace, and slab-on-grade applications. Cellular insulating boards are the predominant insulations used in the walls, roofs, and floors of low-temperature storage and processing facilities; in these applications they are installed as boards individually or incorporated in various sandwich-panel systems. These products are also widely used as insulation in metal buildings and agricultural buildings.

Polyurethane and urea-formaldehyde foams are poured into wood-frame, metal-frame, and masonry wall cavities, and they are also used as core-fill insulation for concrete masonry units. Spray-applied polyurethane and polyisocyanurate foams are used as roof insulation and are often used to insulate irregularly shaped building envelope components, which would be difficult to insulate with rigid boardstock. Polyurethane foam, sprayed or poured in place, is sometimes used as an air infiltration barrier. Rigid-board and spray-applied cellular insulating materials are also widely used in industrial applications as tank, vessel, and pipe insulation in a great variety of systems and processes. In addition, fabricated products for insulating pipes and pipe fittings are routinely prepared from large billets.

Cellular insulating boards have been used to insulate highways, airport runways, and railroad embankments to prevent the earth from freezing and thereby eliminate damage from frost heaving. In some cases these materials are installed to prevent the earth from thawing in order to

avoid large seasonal changes in the load-bearing capacity of the underlying soils. Cellular insulations are also occasionally used to insulate water and sewage utility lines and oil and gas pipelines. These products are often used in appliances such as refrigerators and freezers as well as in vehicles used to transport foods and other goods that require refrigeration. They are also typically incorporated in structural panels which are used in the manufacture of recreational vehicles.

The various cellular insulations each present a unique combination of physical properties and cost. They all can be used in many applications, although no one material is recommended for use in every application. The appropriateness of a material for a given application can only be determined after the physical properties of the product and the demands of the end use have been carefully reviewed.

Health and Safety Considerations

With the exception of cellular glass, the cellular thermal insulations discussed in this paper are combustible, as indicated in Table 1, and may constitute a fire hazard if improperly used or installed. The combustibility characteristics for the various types of foamed plastics are different, and the presence of various facings can influence these characteristics. Phenolic foams are recognized for their superior fire-resistance properties, and polyisocyanurate foam insulations also exhibit improved flammability characteristics. Polystyrene foams typically melt when exposed to a fire, which helps account for the low flame-spread and smoke-developed ratings for these materials. Many of these materials contain flame-retardant additives to inhibit accidental ignition during storage and after installation. Those that do not are inherently fire resistant, such as phenolic foams.

The use of cellular thermal insulations in construction applications is regulated by the various building codes. Various small-scale and large-scale fire tests on products and systems incorporating these materials may be required depending on the application, and in most cases a thermal barrier must be installed to protect the foamed plastics. Maximum limits for the flame-spread and smoke-developed ratings of cellular insulations are also included in the codes. The numerical flame-spread and smoke-developed ratings presented in Table 1 are not intended to reflect hazards presented by cellular thermal insulations under actual fire conditions. The values are indicative of the response of these materials to heat and flame under controlled laboratory conditions. To describe or appraise the hazard under actual fire conditions, several other factors should also be considered.

The products of combustion for cellular plastic insulations are also important. Toxicity of combustion products is an extremely complex issue, and at the present time there is no universally accepted test for toxicity. Most experts agree, however, that the foamed plastics used as thermal insulations are no more toxic than other commonly used combustible materials. The production of carbon monoxide and the generation of smoke during fires are the two issues of primary concern. For some cellular plastic insulations relatively small amounts of other toxic gases are generated during the course of combustion, but they are not believed to have a major impact on overall toxicity.

Some products contain additives or unreacted components that may be a concern in applications where direct contact with food is anticipated. Also, formaldehyde vapor may be emitted from urea-formaldehyde foams as a result of a variety of factors relating to the formulation, foaming process, and end-use conditions. (Formaldehyde vapor can also be emitted from many common building materials.) Above a certain level the vapor is a strong irritant and can cause illness.

Conclusions

This paper presents a comprehensive overview of the physical properties of cellular thermal insulations with special emphasis on thermal transmission properties, moisture absorption

properties, and mechanical strength properties. The information presented was compiled for the most part from manufacturers' literature and other published documents available to the public. It is intended to serve as a general guide for comparing the physical properties of various cellular insulations. However, the values may not be representative of every product available in the marketplace, and the range in values may be considerable due to the variability between specific products within a given material type and factors relating to the testing of the products. The various cellular insulations each present a unique combination of physical properties and cost. They all can be used safely and effectively in many applications, although no one material is recommended for use in every application. The appropriateness of a material for a given application can only be determined after the physical properties of the product and the demands of the end use have been carefully reviewed.

All organic cellular insulations discussed in this paper are combustible and may constitute a fire hazard if improperly used or installed. These materials will pyrolyze at elevated temperatures and will burn when exposed to a sufficiently intense heat source.

Acknowledgments

Dale Keeler of Dow Chemical U.S.A. deserves special recognition for his guidance in the preparation of this paper and his careful review of the document. The author would also like to thank those folks within Dow Chemical U.S.A. and other operating units of The Dow Chemical Company that took the time to review and comment on the paper. Finally all the friends and colleagues associated with insulation manufacturers, test laboratories, research organizations, and universities deserve special thanks for their contributions in the preparation and review of this document.

References

- [1] Skochdopole, R. E., "Thermal Conductivity of Foamed Plastics," *Chemical Engineering Progress*, Vol. 57, No. 10, Oct. 1961, pp. 55-59.
- [2] Booth, L. D. and Lee, W. M., "Effects of Polymer Structure on *K*-Factor Aging of Rigid Polyurethane Foam," *Journal of Cellular Plastics*, Jan.-Feb. 1985, pp. 26-30.
- [3] Norton, F. J., "Thermal Conductivity and Life of Polymer Foams," *Journal of Cellular Plastics*, Vol. 3, Jan. 1967, pp. 23-37.
- [4] Proprietary computer model developed by The Dow Chemical Company to study thermal transmission characteristics of cellular plastic insulations.
- [5] Johnson, S. E. and Muhlenkamp, S. P., "In-Place Thermal Aging of Polyurethane Foam Roof Insulations," in *Proceedings*, Seventh Conference on Roofing Technology, National Bureau of Standards/National Roofing Contractors Association, April 1983, pp. 49-55.
- [6] Baumann, G. F., "R-Value of Rigid Polyurethane Foam—An SPI Research Project," *Journal of Thermal Insulation*, Vol. 6, July 1982, pp. 39-47.
- [7] Desjarlais, A. O. and Tye, R. P., "Experimental Methods of Determining the Thermal Performance of Cellular Plastic Insulation Materials Used in Roofs," in *Proceedings*, Eighth Conference on Roofing Technology, National Bureau of Standards/National Roofing Contractors Association, April 1987, pp. 12-22.
- [8] Ascough, M. R., Baitinger, S. A., and Dishart, K. T., "Barrier Packaging Technology—A New Approach to the Thermal Aging Problem of Rigid Foam Insulation," in *Proceedings*, Thirtieth Annual Polyurethane Technical/Marketing Conference/Society of the Plastics Industry, Oct. 1986, pp. 388-392.
- [9] Glicksman, L. R. and Ostrogorsky, A. G., "Laboratory Tests of the Effectiveness of Diffusion Barriers," *Journal of Cellular Plastics*, Vol. 22, July 1986, pp. 303-313.
- [10] Cammerer, W. F., "Thermal Conductivity as a Function of the Thickness of Insulating Materials," *International Institute of Refrigeration Bulletin (Annexe)*, Issue No. 4, 1973, pp. 189-200.
- [11] Jones, T. T., "The Effect of Thickness and Temperature on Heat Transfer through Foamed Polymers," in *Proceedings*, Seventh Conference on Thermal Conductivity, National Bureau of Standards, Washington, D.C., Sept. 1968, pp. 737-748.
- [12] Shirliffe, C. J., "Effect of Thickness on the Thermal Properties of Thick Specimens of Low Density Thermal Insulation," in *Thermal Insulation Performance*, ASTM STP 718, D. L. McElroy and R. P. Tye, Eds., American Society for Testing and Materials, Philadelphia, 1980, pp. 36-50.

- [13] Sparks, L. L., "Low-Temperature Properties of Expanded Polyurethane and Polystyrene," in *Thermal Insulation Performance, ASTM STP 718*, D. L. McElroy and R. P. Tye, Eds., American Society for Testing and Materials, Philadelphia, 1980, pp. 431-452.
- [14] Private communication from E. W. Kifer, Koppers Company, Inc., 5 Oct. 1987.
- [15] Dechow, F. J. and Epstein, K. A., "Laboratory and Field Investigations of Moisture Absorption and Its Effect on Thermal Performance of Various Insulations," in *Thermal Transmission Measurements of Insulation, ASTM STP 660*, R. P. Tye, Ed., American Society for Testing and Materials, Philadelphia, 1978, pp. 234-260.

Technical Assessment of Foam-in-Place Cellular Plastics for Building Envelope Applications

REFERENCE: Tye, R. P., "Technical Assessment of Foam-in-Place Cellular Plastics for Building Envelope Applications," *Insulation Materials, Testing, and Applications, ASTM STP 1030*, D. L. McElroy and J. F. Kimpflen, Eds., American Society for Testing and Materials, Philadelphia, 1990, pp. 141-155.

ABSTRACT: Foam-in-place urethane and other cellular plastic materials, in conjunction with appropriate protective coatings and facings, have been used successfully for insulating industrial systems, including tanks and pipelines, and are becoming more widely used for insulating roofs of large buildings. Because of their relatively high strength-to-weight ratio, coupled with potential higher thermal efficiency, they present attractive alternatives to current insulation materials and systems.

A technical assessment of foam-in-place materials and systems for use as thermal insulations in buildings has been undertaken to evaluate their overall potential. The assessment (ORNL/Sub/86-56525/1) discusses the following major topics:

- Definition of various materials, their compositions and costs, and associated coatings and barriers, including variability between geographical regions.
- Production and installation procedures, including variability between production lots and geographical regions.
- Application areas in buildings and identification of relevant standards and codes that describe these products and their properties, compositions, configurations, and methods of joining to envelope assemblies.
- Existing mechanical, physical, and thermal property data and other relevant properties, including property dependencies due to environmental parameters.
- Identification of specific property data not presently available or known to the degree of reliability and/or accuracy required for optimal thermal design and analysis of assemblies.
- Identification of recent advances and newer developments now in the research stage that are likely to be used within the next five years and areas requiring research for future use and application.

KEY WORDS: adhesion, aging, anomalies, building codes, building envelope, coatings, costs, injection, International Standards Organization markets, performance, polycarbonilide, polyisocyanurate, polyurea, polyurethane, properties, research program, robotics, spray applied

Since their development during the 1950s [1], polyurethane and polyisocyanurate rigid and semi-rigid foams (urethane) have been used increasingly as thermal insulations. These materials are manufactured in three different ways: bun stock (to provide cut boards), continuous board stock (often laminated between facers), and foam-in-place systems (a more recently developed form).

Foam-in-place urethanes have been used extensively for a number of industrial, space, and appliance applications [1,2] and are now increasingly used for, or proposed for use for, building

¹Manager - Market Development, Thermatest Division of Holometrix, Inc., Cambridge, MA 02139.

envelope components, especially roofs. Currently, three major types of such foam-in-place insulations are used:

1. *Spray applied, essentially closed-cell systems*, used extensively for large area roofs and other buildings envelope components and for tanks, piping, and other industrial applications.
2. *Injected, essentially closed-cell materials*, used extensively for pre-insulated wall panels and other building components, refrigerators, freezers, and transportation vehicles.
3. *Injected, essentially open-cell materials*, used particularly for retrofit of walls and other building envelope components.

Apart from considerations of initial cost and uncertainty of performance characteristics with time, foam-in-place insulations have a number of potentially desirable attributes as insulations for all buildings, including various types of residential structures [3,4]. A growth of 10% per year is forecast for foam-in-place materials with emphasis on new applications in walls and other areas of the building envelope [5]. Major growth in building envelope applications, especially for external wall insulation, is projected for the southern regions of the United States. Accordingly, a technical assessment has been carried out to provide the Department of Energy (DoE) with information on which a more informed basis for decision making as it applies to future needs for material-related research and development within the program can be made.

The information needed for the assessment was obtained by means of a literature search through over 60 publications, including a significant number of government and industry studies and reviews relating specifically to the use of these materials for roofs. Literature from raw materials suppliers, systems formulators, application machinery developers, protective coating suppliers, and major applicators was also reviewed. In addition, interviews or discussions were held with over 50 informed members of industry, government, and academia involved internationally in the development, application, and performance evaluation of these materials in buildings.

The assessment provided much information on present and future applications. This paper outlines the existing building envelope uses of this type of thermal insulation and discusses the potential future promise, together with many of the research needs required to realize this potential. It does not address the very recent needs for alternative blowing agents required for all urethane-type cellular insulations.

Collection of Information

Individuals Involved in Manufacturing and Use

Foam-in-place insulations, by their nature, are fabricated *in situ*. This fabrication involves the mixing of liquid chemicals with other liquid and solid materials, including fluorocarbon blowing agents, and spraying or pouring the resultant reacting mixture onto a surface or into a cavity. The resultant closed-cell foam-in-place thermal insulations are a hardened cellular plastic material containing a low thermal conductivity gas which provides the high thermal efficiency. Final protection of any exposed surfaces of the foam is attained by spraying or otherwise applying a resilient, well-adhered coating to the surface.

While the ultimate integrity and performance of the resultant insulation system is dependent on the applicator, it has been found that four basic contributors are involved in the production of a satisfactory material:

- Manufacturers of the isocyanates, polyols, catalysts, surfactants, additives, flame retardants, and blowing agents.
- Systems developers who blend or otherwise formulate the above components and materials into an insulation system for a specific application.

- Manufacturers of spray equipment.
- Contractors who utilize the system and the spray equipment to fabricate the foam-in-place insulation.

Much is known about the basic chemistry and effects of various parameters, including components additives, viscosity, temperature, etc. However, the subject still contains a significant amount of "art" over technology.

Foam-in-place insulations have been in wide use for roofs of large buildings. In particular, various agencies within the U.S. Government, including the Departments of Defense, Commerce, and Interior, have had much experience in the application to, and subsequent performance of, new and retrofitted foam-in-place insulated roofs.

Literature

There are a number of technical papers in the literature relating specifically to the basic chemistry, production processes, and applications of urethane and isocyanurate materials. Much of this is contained in Ref 1. However, in the particular case of foam-in-place, a more limited number of very specific, informative, general papers and technical reports are available, particularly from the Department of Defense [6-10] and the Urethane Foam Contractors Association [11-14].

Organizations, Specifications, and Codes

As a result of projected growth and the issues relating to installation and performance, the Urethane Foam Contractors Association (UFCA) was formed in 1973. It was disbanded in 1986 and its members advised to join the new Polyurethane Foam Contractors Division of the Society of the Plastics Industry. Similar associations responsible for foam-in-place systems exist in the United Kingdom, France, and the Federal Republic of Germany.

The prime purposes of the associations are to promote the use of foamed-in-place materials for all applications, including buildings, and to make available reliable technical information in order to ensure that membership is well informed and provides a good product and system.

There are three applicable ASTM standards:

- *C 1029, "Spray Applied Rigid Cellular Polyurethane Thermal Insulation"*—This Committee C-16 Specification covers the types and physical properties of spray-applied cellular material for all uses, including buildings, over the range of -33 to 120°C . Four classifications are included, some of which are applicable to those used for walls (Types I or II) and roofs (Type III).
- *C 945, "Design Considerations and Spray Application of Rigid Cellular Polyurethane Insulation System on Outdoor Service Vessels"*—This Committee C-16 Practice does not deal specifically with building applications but does contain information which is applicable to this type of use; it is cited as an Applicable Document in ASTM C 1029.
- *DXXX, "Spray-Application of Urethane Foam Roofing Systems"*—This Committee D-8 Practice is in the course of preparation and covers the application of the insulation systems over a structural deck or over an existing built-up roofing membrane.

At the international level, ISO/DIS 8873, "Cellular Plastics, Rigid-Spray-Applied Urethane Foam for Thermal Insulation of Buildings-Specification," is currently in ballot. This document, prepared by TC 61 on Plastics, is similar in content to ASTM C 1029, the major difference being the more stringent requirements for dimensional stability in the former. Finally, both ISO TC 163 on Thermal Insulation, together with TC 61, and the European Economic Community are working on descriptive documents relating to minimum requirements for all thermal insulation materials used in buildings, including foam-in-place urethanes.

The principal issue addressed in the three model building codes under BOCA, SBCCI, and ICBO is fire safety. In all cases, all forms and types of urethanes are considered to be the same and they are covered by the provisions relating to foamed plastics in general. By means of suitable additives, all current foam-in-place materials are available with the appropriate upper limit in flame spread classification. Furthermore, there are combined foam and coating systems which have the lower flame spread classification so that they can be used in buildings without additional protection.

To conform to additional requirements for roofs, all foam-in-place urethane insulated systems, with or without an additional fire barrier, must be designated as Class A, B, or C, in accordance with Underwriters Laboratories Standard 790, "Tests for Fire Resistance of Roof Covering Materials." This test is similar to ASTM E 108, "Fire Tests for Roof Coverings," whereby three separate tests are carried out to evaluate the fire resistance characteristics of the roof insulation systems. These involve intermittent fire exposure, burning board, and flame spread. The systems are then rated in one of the three categories, depending on the total performance in the three tests.

Applications

All cellular plastics, particularly board materials, have been used for built-up and single-ply insulated roof systems. However, the thermal and related performance of some of these roofs was often not as good as expected [15]. Problems also developed due to moisture intrusion at joints in the boards or at the areas where insulation was attached to protrusions through the roof.

These issues led to the consideration of using the sprayed-applied form of urethane. Essentially, this would eliminate the joint problem since the roof could be insulated with a continuous, monolithic covering of the material. Furthermore, since urethanes have extremely good adherence properties to most materials, provided the surfaces are clean and dry, the problems at protrusions are less likely to occur. Finally, repairs could be more easily carried out on small areas. As a result, during the past 15 to 20 years, spray-applied urethanes have become widely used for roofs.

A separate but smaller concurrent development was the manufacture, by spraying or foaming, of prefabricated, insulated wall and ceiling panels for buildings. The advantage here is that the material can flow and foam into joints and spaces which would otherwise be difficult to insulate if board stock was utilized. More recently, open-cell forms have been developed, particularly as a replacement for urea-formaldehyde and for use in cavity wall retrofit applications.

The major uses of foam-in-place cellular plastics are given in the following sections.

Roofs

Foam-in-place cellular plastics are used nationwide for insulating new roofs (predominantly single-ply), for the complete retrofit of built-up and single-ply systems [12,13], and for repairing and patching of small areas.

Walls

External and Internal—Foam-in-place cellular plastics can be sprayed directly to the surfaces of cavity and masonry wall systems. This type of insulated system is used predominantly in the southern parts of the United States. There are increasing amounts used for retrofit applications, as well as for new buildings, including below-grade applications.

Cavity—There is increasing use of the material for new walls by direct spraying into the cavities prior to the attachment of the dry wall. In addition, foam-in-place is being used for the retrofit of empty cavities by the careful injection of successive small amounts of the material.

This practice has been used extensively in Europe for a number of years for insulating the cavity between the two masonry courses which form the exterior envelope. It has the significant advantage of sealing cracks and voids and thus minimizing air movement within the exterior envelope.

Prefabricated—This was an original application and one that is growing as more highly insulated, specialized buildings are required. Another prefabricated form, used more extensively in Europe, is foam-in-place urethane to pre-insulate masonry blocks. The use of insulated block reduces the overall number of building operations required, thereby saving time, labor, and costs, and the final well insulated, high heat capacity structure is also cost competitive with conventional types.

Other Uses

Cathedral ceilings is one area where the material is starting to be used. Other suggested applications where foam-in-place urethane has attractions are the transition areas between floors and floors/walls. These include band joists, places where insulation changes from attic floor to attic wall, and around all service conduits, pipes, trusses, etc. Pre-insulated cavity doors is another potentially large application. Finally, foam-in-place materials are ideal for the small caulking and sealing operations necessary around windows and doors to reduce air movement.

A novel use is the field production of small (4.6 to 6.1 m [15 to 20 ft] diameter), stable, durable, insulated emergency structures or igloos such as may be required after a natural disaster. They are fabricated easily by spraying on a large, inflated, PVC-reinforced fabric hemispherical balloon fastened to a rotating turntable. Once the foam has hardened, the balloon is deflated, leaving the igloo free and allowing the openings for windows and doors to be cut.

Markets and Costs

Growth of the foam-in-place materials is predicted to continue with that of general plastics growth of some 8 to 9% per year for the next five-year period [5]. Since the raw materials are used for all spray, pour-in-place, and board production applications, it is difficult to obtain precise figures of raw materials use only for the foam-in-place form for buildings. However, a recent estimate by Skowronski [16] showed that in 1982 the total raw materials production for all applications was approximately 220×10^6 kg. Approximately 50×10^6 kg was used for all spray applications in the field and, of this, 30×10^6 kg was for buildings purposes. In addition, some 100×10^6 kg were used for all other foam-in-place applications and, of this, approximately 10% was used for building-oriented applications. The projected use for buildings in 1986 is 40×10^6 kg for spray applied and 14×10^6 kg for other foam-in-place types. Of the total use for buildings, some 70% will be used for roofing and the remainder for walls and other purposes. These estimates are summarized in Table 1.

Similarly, it is difficult to obtain precise costs since the final cost is for the installed product. This is governed by a number of factors, including raw materials, transportation (often involving large distances) from contractor to site, and the fact that for roofing applications a protective coating must be used.

Currently, the best available estimate for directly installed, spray-applied roof systems is \$21.00 ($\pm 20\%$) per m^2 for a 25 to 50 mm thick urethane including a 0.5 to 1 mm thick protective coating. For the poured or injected-in-place systems, mostly for walls and ceiling applications, the cost is $\$6.00 \pm \1.00 per m^2 . See Table 2.

The material has significant potential for growth in all existing areas and for new and retrofit wall applications, prefabricated building components, and preformed constructional materials. Reduction of air and moisture movement by sealing holes, cracks, and other imperfections with foam-in-place materials is a further beneficial application. Finally, areas in various buildings where thermal bridges are present need detailed examination in order to evaluate potential new

TABLE 1—*Growth of urethane raw materials production in the United States, kg $\times 10^6$ (lb $\times 10^6$).*

Year	Total Production	Total Foam-in-Place		Spray-Applied Buildings
		All Uses	Buildings	
1982	220 (500)	150 (300)	50 (110)	30 (65)
1986	300 (659)	200 (450)	64 (130)	40 (80)

TABLE 2—*Cost of foam-in-place insulation systems.*

Application	Average per m ² (ft ²)	Range per m ² (ft ²)	Cost per R of 1 h \cdot ft ² \cdot °F/Btu
Roofs	\$21 \pm 2.8 (\$2 \pm 0.2)	13–48 (1.20–4.50)	\$0.15–0.30
Walls and ceilings	\$6 \pm 1 (\$0.55 \pm 0.2)	...	\$0.04–0.60

or modified designs where the foam-in-place material could provide significant reductions in the thermal bridge effect. While these materials cannot be classed as structural in the building sense, the fact that they can provide a monolithic layer having some structural integrity around or over, for example, a basic frame structure suggests that some of the framing members providing thermal bridges can be eliminated.

Systems

Materials

The basic chemistry has been well documented for the generic-type, closed-cell polyurethane materials [1,6]. The material is the result of a controlled exothermic reaction between a polyisocyanate, usually referred to as Component A, and a modified hydroxyl compound (alcohol), Component B. Other components and additives, including blowing agents, catalysts, surfactants, flame retardants, antioxidants, and fillers are used. Depending upon the functionality of the initial compounds, a cross-linked polyurethane foam is developed with properties dependent on the amount of cross-linking and the effects of different additives.

The materials and the mixture must be kept at an accurately controlled temperature between 20 to 40°C, depending on the type of foam required for a particular application and geographical area. This is important because the viscosity versus temperature relationship has an extremely sharp slope in this range. Large divergencies in temperature will have significant effects on various factors, such as pressure, density, aeration, and reactivity. All of these affect the properties of the resultant material. Absence of moisture is also necessary to inhibit the formation of polyurea materials having much poorer properties.

The blowing agent, surfactant, and catalysts are important in determining the properties of the final product. In most materials, monofluorotrichloromethane (R11), boiling point 24°C, or difluorodichloromethane (R12), -33.5°C , are the most commonly used blowing agents. These provide the low thermal conductivity gas in the predominantly closed-cell system.

The catalysts, usually tertiary amines or organotin compounds, determine the reaction time and rate which control the chain propagation and extension, the cross-linking, and "cure" time. The last parameter controls the final properties and the extent to which they are retained with time.

The fillers are usually inorganic materials and pigments added to provide specific colors, help reduce cost, alter a physical property, and assist in reducing the degrading effects of ultraviolet

light. Finally, flame retardants and inhibitors are added to reduce flammability and other fire property characteristics. These are typically stabilized, brominating compounds which do not oxidize so readily as the earlier non-stabilized forms.

The whole objective is to obtain close to a 100%, uniform, closed-cell system with "ideal" pentagonal-dodecahedron (near spherical) cell structure with a cell diameter of < 1 mm and having equal distribution of solid material disposed within the cell wall.

The chemistry of these materials is similar, although not identical, to that of board or bunstock. The actual formulation has to start at the applicator gun and be completed relatively quickly once the reaction has started. In addition, if applied to a vertical surface, it must not have time to flow due to gravity. Finally, it has to be foamed in various geographical areas and is thus subject to a range of environmental conditions of different temperatures and relative humidities.

In order to attain such a foam-in-place system:

1. Proprietary formulations are available to provide resultant closed-cell foams having densities of 32 to 48 kg/m³ and specific mechanical strengths on the order of 0.14 to 0.28 MPa for wall and roof applications, respectively. These are governed, in the main, by variation of final density and closed-cell content.
2. Specific formulations are developed which, when used with an appropriate blowing agent, will provide foams at various temperatures within the overall range expected for the various hot and cold geographical areas.
3. The formulations are generally much more reactive in order to provide greater nucleation. In addition, special catalysts are employed in order to ensure a faster and more complete cure.
4. Special spray-applied protective coatings compatible with the foam-in-place urethanes have been developed.
5. Current systems are applied with modern guns designed to operate at air pressures of 14 to 21 MPa, thus enabling the applicator to obtain a much better yield and a more uniform product with optimum properties.

Protective Coatings

A closed-cell, foam-in-place insulation material cannot be totally effective without some sort of surface protection. For the cavity fill, the surfaces bounding the cavity offer some protection. However, for exposed surfaces, an applied coating is necessary. The subject has been discussed fully in the UFCA Guideline document [13]. However, relevant details are included in this section.

A coating is necessary for protection in order to:

- Increase the resistance to mechanical damage and physical abuse.
- Provide added protection against the gaseous exchange which reduces the thermal efficiency.
- Reduce moisture pickup.
- Reduce effects of intensity and exposure time of sunlight, particularly ultraviolet light.

In addition, if the coating is appropriately formulated, it can also assist in allowing the resultant insulation system to achieve the desired fire rating and pass appropriate code requirements.

Very large numbers and types of coatings compatible with urethane foam are manufactured for application over spray-applied materials. These coatings must be flexible and have appropriate tensile, elongation, and tear strengths to allow them to accommodate the normal movement of the high expansion foam systems. In addition, good adhesive strength combined with low moisture absorption and water vapor permeance are required. Finally, it must be resistant to effects of heat and cold, $\sim 90^{\circ}\text{C}$ to -40°C , and cyclic behavior between the two, and to the effects of weathering.

Basically, the available generic elastomeric coatings are: acrylic latex, butyls, hypalons, neoprenes, silicones, and synthetic rubbers; urethane elastomers; and vinyls. These are supplemented with asphalt and cementitious, non-elastomeric types for external surfaces. All of these may be combined with the application of different mineral granules into the coating while it is still wet in order to reduce damage from hail and wind, foot traffic, and animals.

Coatings should be applied within one day of applying the foam by the appropriate spray (air or airless) power, brush, or paint techniques recommended by the manufacturers. In general, the recommended dry cured thickness is at least 0.5 mm (0.020 in.), preferably greater.

Problem areas with coatings are similar to those for insulation:

- *Pinholing* is a major concern only avoided completely by ensuring that the foam itself has a virtual pinhole-free surface and that correct multi-thin coat application procedures are followed.
- *Cracking* is caused by the coarse surface finish of the foam and applying the coating at too great a thickness at improper temperature conditions or where there is excessive moisture which will not allow the coating to cure properly.
- *Blistering* is due essentially to poorly prepared surface conditions of the foam.

Properties

The basic physical, mechanical, and thermal properties of these three types of materials for use as insulations in buildings are shown in Table 3. The table also contains values of the same properties for a typical boardstock material. It can be seen that the values for the different types are similar when compared at the same density. In general, values of strength for the bun and boardstock show small but significant differences for the parallel (\parallel) and perpendicular (\perp) directions, respectively. However, the differences for the foam-in-place materials are usually within the spread of the experimental results, and values for each direction are not quoted separately.

Thermal Properties

Typical thermal resistance is shown in Table 4. It is similar to bun and boardstock. For example, in an R-11 blown foam, the inflections in the curve occur in the same range due to the same refrigerant gas being used as the blowing agent.

While these materials, in general, have similar properties to bun and boardstock, due to the particular method of production involving relatively faster rise times, there are some differences which can affect certain properties. The foam-in-place fabrication tends to produce smaller, more uniform cells which more closely resemble the "ideal" shape; in consequence, this form will tend to exhibit slightly better thermal and mechanical properties. Furthermore, anisotropy in these properties, although still present, will be less. Finally, since the solid polymer is more equally distributed in the wall of the basic cell, the effects of aging should be reduced.

These factors have been discussed in two recent papers [17,18]. These describe laboratory studies carried out on different urethane materials and building envelope components containing these materials. One also refers to an earlier field study for the U.S. Navy [19] which covers spray-applied insulation specimens cut from a large number of types of insulated roofs in different climate areas.

The results of the laboratory studies are shown in Tables 5 and 6. For the spray-applied system, under the three laboratory exposures, they show an overall aging effect of approximately 20% over two years. Comparable aging of 30% or more was found for bun, board, and laminated materials, but aging of 10% or less was found for a foam-in-place system sandwiched between steel sheets. Furthermore, the rate of change was found to be somewhat less than for the other materials. The spray-applied systems also appeared to "stabilize" at the two-plus

TABLE 3—*Properties of typical foam-in-place urethane.^a*

Property	Roofs	Walls	One Component for Cavities and Patching	Typical Board Stock	ASTM Test Method
Density, kg/m ³	45-51	29-35	19-32	32	D 1622
Closed-Cell Content, %	90-95	>90	70-80	90-92	D 2856
Compressive Strength at Yield or at 10% Deflection, MPa	0.28-0.34	0.14-0.21	0.03-0.15	0.17 0.14 ⊥	D 1621
Tensile Strength, MPa	0.28-0.34	0.17-0.24	0.10-0.14	0.24	D 1623
Shear Strength, MPa	0.28	0.21	0.14	0.17	C 273
Apparent Thermal Conductivity at 297 K					C 518
Initial	0.020	0.020	0.021	0.020	or
Aged	0.025	0.025	0.029	0.026	C 177
R-Value m ² · K/W for 25.4 mm at 297 K					C 518
Initial	1.25	1.25	1.23	1.25	or
Aged	0.98	0.98	0.88	0.97	C 177
Specific Heat, J/kg · K	1590	1590	1590	1590	C 351
Coefficient of Expansion per K × 10 ⁻⁶	55-90	55-90	72-90	45-72 63-100 ⊥	D 696
Thermal Diffusivity, m ² /s × 10 ⁻⁷	2.5	4.0	7.0	5.0	
Water Vapor Permeability, 10 ¹² (kg/Pa · s · m)	3.7	3.7-4.4	5.1-7.3	3.7-4.4	E 96
Water Absorption, vol% maximum	5	5	5	5	D 2842
Dimensional Stability, % 80°C/100% RH/7 Days	<10	<12	<12	<5	D 2126
-26°C/7 Days	<2	<2	<2	<0.5	D 2126

^aAll materials affected by ultraviolet light are dependent on intensity and time. All materials may be manufactured to have specific flame spread properties required to satisfy regulatory and code requirements.

TABLE 4—*Typical results for apparent thermal conductivity of spray urethane versus temperature.*

Temperature, K	Apparent Thermal Conductivity, W/m · K
200	0.019
230	0.022
250	0.020
260	0.019
275	0.020
300	0.022
325	0.024

TABLE 5—Measured thermal performance of two urethane materials [17].

Conditioning	Time, days	Apparent Thermal Conductivity, W/m · K at 24°C (297 K)	
		Spray Applied	Foam-in-Place
Exposed at 24°C	0	0.0178	0.0152
	90	0.0206	0.0170
	180	0.0217	0.0173
	360	0.0220	0.0165
	720	0.0228	0.0167
Exposed at 60°C	0	0.0178	0.0152
	90	0.0205	0.0173
	180	0.0205	0.0176
	360	0.0218	0.0170
	> 720	0.0221	0.0166
Exposed at 60/24°C Gradient	0	0.0178	0.0152
	90	0.0199	0.0170
	180	0.0205	0.0162
	> 360	0.0212	0.0170
	720	0.0210	...

years time period with a λ value on the order of 0.0228 W/m · K or less. The overall changes were slower over two years and are seen to average 17%; the absolute values ranged from 0.0203 to 0.0239 W/m · K with an average of 0.0217 W/m · K.

In the U.S. Navy field study [19], covering roofs up to ten years old in six different geographical and climatic regions of the United States and including Guam, the results, as may be expected, showed considerable variability. Measured apparent thermal conductivity values at four years or greater ranged from a low of 0.0195 to a high of 0.0291 W/m · K for a 25 mm or greater thickness monolithic layer of the insulation material. In a number of cases, sufficient information was available on the condition and form of the material and/or the protective coating to explain adequately why the value of λ was high. For example, a few were less than 25 mm thick, on average, some contained excessively large cells, while various coatings had degraded under the environmental and operational conditions of the roof in particular areas. However, in the majority of cases, the final λ_{app} value was less than 0.0231 W/m · K.

As a result of their observations and measurements, the authors were able to show general effects of age, type of environment, thickness of specimen, and the efficacy of coating type and thickness. Their conclusions were all in line with the general accepted behavior expected of this type of system in the respective climates. Their overall quantitative conclusion was that a design value of 0.0231 W/m · K (0.16 Btu · in./h · ft² · °F) could be established for spray-applied material having a density in the range of 32 to 48 kg/m³ when properly installed and where protected by an adequate coating.

Little information is available on the specific heat or thermal expansion of these materials. In general, the former property is the same for all types since they are all essentially the same material. For the case of thermal expansion, most published results indicate values in the 55 to $72 \times 10^{-6}/K$ (30 to $40 \times 10^{-6}/^{\circ}F$) ranges. However, reports of abnormal behavior in some roofing application materials suggest that the expansion may be above $90 \times 10^{-6}/K$ ($50 \times 10^{-6}/^{\circ}F$). With the above variations in these two properties, derived thermal diffusivity values, as shown in Table 3, cover a wide range, dependent particularly on the density and age of the material. Furthermore, since for many spray-applied applications the material and its protective coating are an integral system, the thickness, density, and specific heat of the coating will affect the thermal diffusivity significantly. Similarly, the behavior versus temperature will be affected by the thermal expansion of the particular material or system.

TABLE 6—*Measured thermal performance of four foam-in-place cellular plastic systems [17].*

Conditioning	Time (days)	Apparent Thermal Conductivity, W/m · K at 24°C (297 K)											
		32 kg/m ³ Spray PU			48 kg/m ³ Spray PU			48 kg/m ³ Spray PU			Poly- carbanilide		
		M ^a	D ^a	M	D	M	D	M	D	M	D	M	D
24°C	0	0.0195	...	0.0182	...	0.0177
	180	0.0189	0.0202	0.0209	0.0191	0.0210	0.0179	0.0179	0.0179
	360	0.0219	0.0228	0.0209	0.0197	0.0200	0.0180	0.0180	0.0180
	>540	0.0218	0.0239	0.0203	0.0195	0.0212	0.0189	0.0189	0.0189
33°C/24°C	0	0.0185	...	0.0198	...	0.0186	...	0.0424	...	0.0424
	180	0.0196	0.0194	0.0196	0.0210	0.0193	0.0199	0.0403	0.0199	0.0403	0.0408	0.0408	0.0408
	360	0.0233	0.0226	0.0210	0.0213	0.0213	0.0206	0.0377	0.0206	0.0377	0.0411	0.0411	0.0411
	>540	0.0231	0.0246	0.0208	0.0218	0.0227	0.0216	0.0385	0.0216	0.0385	0.0404	0.0404	0.0404
-1.5°C/24°C	0	0.0182	...	0.0185	...	0.0199	...	0.0421	...	0.0421
	180	0.0180	0.0197	0.0186	0.0192	0.0193	0.0214	0.0407	0.0214	0.0407	0.0446	0.0446	0.0446
	360	0.0206	0.0210	0.0203	0.0194	0.0227	0.0216	0.0438	0.0216	0.0438	0.0446	0.0446	0.0446
	540	0.0212	0.0210	0.0203	0.0194	0.0213	0.0224	0.0411	0.0224	0.0411	0.0413	0.0413	0.0413

^aM = Measured on individual specimens.

D = Derived from measurements on system, assuming initial λ is the same as that for the individual specimen.

The dimensional stability values in Table 3 are those obtained from results of laboratory tests. Many reports of past roofing problems or failures suggest that unstable behavior is a contributory cause. In actual application, the materials are subjected to a wide variety of environmental conditions over long times, and the behavior may be different to that seen under limited laboratory conditions of isothermal temperature and invariant relative humidity.

Water and Water Vapor Transmission

Since these materials are, in general, closed cell, they are resistant to water and water penetration. However, they can transmit water vapor and, thus, both the need for and the position of a vapor retarder must be considered for use in a particular building application for a specific climate.

Mechanical Properties

As shown in Table 3, the mechanical strengths are dependent mainly upon the density. To some extent, the degree of anisotropy also affects the strengths. Compressive and adhesive strengths are important properties for foam-in-place materials, particularly those used for roofing application. In general, adhesive strengths are more than adequate, especially so as failure due to "uplift" has not been reported. However, effects of real environmental conditions on the various properties have not been evaluated, particularly for long-term applications such as the 20 to 25 year expected lifetime of an insulated roof.

All mechanical strengths decrease as the temperature increases up to ~ 135 to 200°C where the materials become soft and have no load bearing capacity. The decrease is not linear and the most significant changes take place above 75°C , which is generally above the normal building environment except for hot, dry desert climates.

Mechanical strength may be affected by water and water vapor, provided the fluid can penetrate into the cell. Laboratory tests for short-term exposure at isothermal conditions do not provide sufficient evidence to show the long-term effects on these properties.

Areas of Research

Current Research

Existing formulations and installation criteria provide good insulations systems, but the ultimate responsibility still lies with the installers and their individual knowledge. Some less-than-adequate insulations are still produced, and there is a need to eliminate much of the current "art".

An effort towards this goal is currently in the early planning stage in Canada [20]. A comprehensive research program is being developed by the Division of Research in Construction of the National Research Council and the Society of the Plastics Industry of Canada, Inc. This program will involve a study of the various parameters which control production and affect performance of the material.

Part of this program will also be oriented towards the understanding of the basic performance characteristics and especially the aging phenomenon. In this area, modeling and experimental work are planned on the insulations and protective coverings, with the goal being to separate individual effects.

Research on foam-in-place materials is oriented towards relatively small changes but continual improvement by raw materials suppliers and systems developers. The basic objective is to provide systems that can be applied at lower and higher temperatures than the approximate 5 to 55°C (40 and 120°F) limits which are the current norms.

While most of the current foam-in-place materials are urethanes, newer, modified polyisocyanurates, polyureas, and polycarbanilide materials are under development. These materials are being developed for easier application, particularly for foaming and injecting in place into cavities. Pressure build up is lower; thus larger enclosed volumes can be insulated at each application without blowoff problems of the internal wall board. Some have better fire resistance characteristics, but all have a higher open-cell content than the urethanes and the thermal, mechanical, and water absorption and transmission characteristics are not as good.

A third material area relates specifically to development of a new range of compatible coatings. These are single-component, fast-drying urethanes which can be applied in one single layer up to 1 mm (0.040 in.) thick. They are chemically cured in contrast to most of the current longer time moisture cured one- and two-component urethane systems.

In the application area, there are two major areas of research. First, there is growing use of computer control of the basic mixing and spraying processes and machines involved in the production in order to provide more uniformity in the end product. This is now being augmented by the use of robotics where the complete application procedure is automated. This development will eliminate the human judgement factor currently involved in producing a uniform insulation system. Machines exist in the United States and Japan for spraying spherical and flat surfaces, and their application to roofs and other building structures is quite conceivable.

Necessary Research

A particularly important area of research, as identified by a Roof Systems Research Committee of the UFCA (now PFCA), is the development of more appropriate and adequate test methods for these materials and systems. In particular, the subject of adhesion and cohesion of the protective facings with the basic materials, especially with respect to temperature, needs to be evaluated, as well as the dimensional stability, the water vapor, and air permeance characteristics and the water absorption resistance of the separate and combined materials. These materials can, in some circumstances, act as both moisture and air barriers, but there is uncertainty in their use in particular climatic areas. This is compounded by the problem that adequate materials standards and requirements for air barriers do not exist.

These materials and systems are produced and perform over a range of temperatures; thus temperature or temperature gradient is particularly pertinent in the determination of properties. Currently, many of the standard tests to determine physical and mechanical properties are carried out at only one set of isothermal conditions, usually 24°C (75°F) and 50% RH. In addition, since different temperatures and conditions are used for similar but different ASTM tests, particularly for flexible barriers, there is uncertainty in evaluating the comparability of resultant performance.

Since adhesion, mechanical strengths, flexibility, and permeance characteristics are all temperature dependent, measurements taken at one temperature are insufficient, especially where this temperature is not representative of the conditions at which the materials are manufactured or will perform. "Standardized" testing criteria are needed for these materials. Any attempts to undertake and validate modeling of actual performance of buildings and building components containing these materials will need information on these temperature-dependent parameters.

In the building envelope components area, there is a need for evaluating the overall efficacy and particularly the thermal performance of new designs of wall, roof, and other systems. In particular, structural performance, as well as reduction of air and moisture movement, are necessary criteria to add to the thermal performance in order to establish the overall performance characteristics. Information on the contributions of these various parameters to the overall performance is essential in order to determine the cost effectiveness of foamed-in-place systems.

Thermal performance of foamed-in-place urethanes is dominated by the subject of aging and

the extent to which it can be minimized. There has been a great deal of experimental and modeling work in this subject, most of it relating to materials and facings. In general, the process and the extents of the effects are well known and documented.

However, measurements of thermal performance of typical envelope systems aged for different times are required in order to establish that system performance can be determined from information on the materials alone. As mentioned earlier, foamed-in-place materials do appear to age at a significantly slower rate than comparable board and bun stock materials. It is also interesting that in a recent study of some urethane insulated systems [17] the measured thermal resistance values were significantly higher than those calculated using the current ASHRAE models.

Finally, in the envelope components area, there is a need not only for information to be developed in the laboratory on the thermal performance of identical systems under steady-state, simulated, and actual typical environmental conditions but also in the field. This information is required both for the validation of existing field measurement techniques and to enable studies of the factors such as workmanship which can affect performance significantly but cannot always be identified or quantified. A well-planned coordinated approach is necessary therefore in order to attain the above goals.

Summary

An assessment has been carried out on foam-in-place urethanes. The results illustrate that they have some potentially significant advantages for insulating building envelope components, provided that they can be fabricated reproducibly and in a cost-effective manner. The potential of insulation systems based on these types of materials has been realized, especially by sectors of industry and by some governments. While various research efforts on the materials and systems have been identified, there are several relevant issues which have not been addressed fully. These relate to the subject of long-term performance. They involve, both for the materials and envelope components, the selection of relevant test criteria together with development of test methods which will supply performance parameters under real conditions. In some cases, test methods that will provide this information under accelerated conditions are required. It should also be pointed out that such test methods and criteria are required for other materials and the overall subject is thus more general in application. This subject is multifaceted and requires a coordinated approach involving the various industry and other groups currently addressing the issues, including the search for alternative blowing agents.

Acknowledgments

This work was carried out for Martin Marietta Energy Systems, Inc., Oak Ridge National Laboratory, with Dr. D. L. McElroy as Project Manager, under Subcontract 41X-56525V, on behalf of the U.S. Department of Energy as part of the National Program Plan for Building Thermal Envelope Systems and Materials.

References

- [1] *Polyurethane Handbook*, Gunther Oertel, Ed., Hanse Publishers, Munich, Federal Republic of Germany (distributed in the United States by Macmillan, New York), 1984.
- [2] Sparks, L. L., "Low Temperature Properties of Expanded Polyurethane and Polystyrene," in *Thermal Insulation Performance, ASTM STP 718*, D. L. McElroy and R. P. Tye, Eds., American Society for Testing and Materials, Philadelphia, 1980, pp. 431-452.
- [3] Tye, R. P., "Future Trends and Needs in Performance Evaluation of Cellular Plastic Thermal Insulation Materials," ROC 2425, *SPI Annual Urethane Division Technical Conference: Key to the Future of Urethane*, Atlanta, Ga., Oct. 1978, pp. 129-134.
- [4] "An Assessment of Thermal Insulation Materials and Systems for Building Applications," Report BNL-50862, United States Department of Energy, June 1978. See also Tye, R. P., et al. in *Thermal*

- Insulation Performance, ASTM STP 718*, D. L. McElroy and R. P. Tye, Eds., American Society for Testing and Materials, Philadelphia, 1980, pp. 9-26.
- [5] Tye, R. P., "Cellular Plastics as Insulations," *Encyclopedia of Polymer Science and Engineering*, Mark-Bikales-Overberger-Henges, Vol. 6, 2nd ed., Wiley, New York, 1986, pp. 52-64.
 - [6] Cullen, W. C. and Rossiter, W. J., Jr., "Guidelines for Selection of and Use of Foam Polyurethane Roofing Systems," NBS Technical Note 778, May 1973.
 - [7] Coultrap, K. H., "Principles of Urethane Foam Roof Application," U.S. Navy Civil Engineering Laboratory Report, 79 MR 461, June 1980.
 - [8] Rosenfield, M. J., "Evaluation of Spray Polyurethane Foam Roofing and Protective Coatings," Technical Report M-297, U.S. Army Corporation of Engineers, Nov. 1981.
 - [9] Kashiwagi, D. T., "The Economic Feasibility of the Polyurethane Foam Roof System," Master's thesis, Arizona State University, Tempe, Feb. 1984.
 - [10] Alumbaugh, R. L., Keaton, J. R., and Humm, E. F., "Experimental Polyurethane Foam Roofing Systems—II," U.S. Navy Civil Engineering Laboratory, Port Hueneme, Calif., Technical Note N1656, Jan. 1983.
 - [11] "Design Considerations and Guide Specifications: The Application of Sprayed Urethane Foam Insulation Systems for New Roofing," Urethane Foam Contractors Association, 28 pp.
 - [12] "Design Considerations and Guide Specifications: The Application of Sprayed Urethane Foam Insulation Systems for Remedial Roofing," Urethane Foam Contractors Association, 26 pp.
 - [13] "Guidelines for Selection of Protective Coatings over Sprayed Polyurethane Foam Roofing Systems," Urethane Foam Contractors Association, 65 pp.
 - [14] "Performance Criteria for New and Aged Polyurethane Roofs," Urethane Foam Contractors Association, 19 pp.
 - [15] Kugler, W. E., McCorkle, J., and Morris, L. B., "In-Service Thermal Performance of Polyurethane and Polyisocyanurate Roof Board Insulations," presented at 6th International Conference on Roofing and Waterproofing Worldwide, London, 30 April-2 May 1986, International Waterproofing Association, Brussels, Belgium. See also "Are 'Aged' Values Adequate for Rating Foam Thermal Insulation Board?" *Roofing, Siding, Insulation*, Vol. 62, 1986, p. 38.
 - [16] Skowronski, M., Jim Walter Research Corporation, private communication, April 1986.
 - [17] Tye, R. P. and Desjarlais, A. O., "Aging Characteristics of Cellular Plastic Insulation Materials and Insulated Building Envelope Components," in *Polyurethane World Congress 1987: 50 Years of Polyurethanes*, Fachverband Schaumkunststoffe e.V. Frankfurt, FRG, Society of the Plastics Industry, New York, 1987, pp. 91-98.
 - [18] Tye, R. P., "Assessment of Aging of Cellular Plastics with Particular Reference to Field Performance of Building Envelope Systems," *Journal of Thermal Insulation*, Vol. 12, 1988, p. 28.
 - [19] Zarate, D. A. and Alumbaugh, R. L., "Thermal Conductivity of Weathered Polyurethane Foam Roofing," Report TN-1643, U.S. Naval Civil Engineering Laboratory, Port Hueneme, Calif., 1982.
 - [20] Bomberg, M., National Research Council, Ottawa, private communication. See also *Proceedings*, SPI Urethane Division Annual Meeting, Toronto, Canada, Oct. 1986.

Evaluation of Long-Term Thermal Resistance of Gas-Filled Foams: State of the Art

REFERENCE: Bomberg, M. and Brandreth, D. A., "Evaluation of Long-Term Thermal Resistance of Gas-Filled Foams: State of the Art," *Insulation Materials, Testing, and Applications, ASTM STP 1030*, D. L. McElroy and J. F. Kimpflen, Eds., American Society for Testing and Materials, Philadelphia, 1990, pp. 156-173.

ABSTRACT: Some cellular plastics (foams) incorporate a chlorofluorocarbon (CFC) to improve their thermal insulating properties. During the service life of this type of insulation air diffuses into the foam cells and the CFC gas diffuses out, each at a rate that depends on type of polymer and temperature, eventually reducing the effectiveness of insulation. This effect is known as aging. Although literature on the aging process is extensive, there are no generally accepted procedures for evaluating long-term thermal resistance of new gas-filled foams. The mechanisms of the aging process are reviewed, and integrated approach to the evaluation of aging of gas-filled foams is proposed.

KEY WORDS: thermal conductivity, thermal resistance, thermal resistivity, polyurethane, gas-filled foams, thermal insulation, foam insulation, cellular plastics, aging, models of aging

Although the mechanisms of aging of gas-filled foams (GFF) have been understood for at least 20 years [1], it has not been easy to develop methods of evaluating the long-term thermal performance. This is largely because many variables affect aging and not all the interactions are fully understood. Research on foam aging requires a multipronged attack on the problem [2,3].

This paper reviews the aging process with a view to developing procedures for evaluating the long-term thermal resistivity of GFF under four sections. The first discusses the practical difficulties encountered in evaluating the performance of gas-filled foams. Not only are there large differences in the long-term thermal resistance of commercial GFF products, but even within the same product there may be significant differences from batch to batch. In addition, traditional experimental evaluation of the aging process has so far failed to provide satisfactory ratings. This deficiency, the uncertainty of thermal tests, and the limitations of accelerated laboratory testing are discussed in the second section.

The third section presents an overview of models of the aging process, focusing on the limitations of the models and impediments to their use. As the key material characteristics used in these models are effective diffusion coefficients for oxygen, nitrogen, and CFC, the concept of effective diffusion coefficients and its limitations and application to a material with significant spatial variability are also discussed.

¹Institute for Research in Construction, National Research Council of Canada, Ottawa, Ontario, Canada K1A 0R6.

²Widener University, Chester, PA 19013.

The fourth section highlights the need for integration of modelling and experimental work in evaluating the long-term performance of these materials. Differences in thermal resistance, measured under field and laboratory conditions, combined with statistical evaluation of measurements, lead to the conclusion that a link is required among the various elements of evaluation. A model of aging describing thermal resistance *as a function of time and of testing conditions* may provide that link. This paper will introduce a concept of integrated evaluation, but will not discuss details of the evaluation procedure itself.

The Problem

Evaluation of the long-term thermal performance of GFF is difficult because it must recognize:

1. Changes in the overall thermal resistance of a material slab as a function of time (overall rate of aging).
2. Differences in the initial thermal properties and rate of aging at various locations of any one product which are caused by material variability; this includes batch variability (differences in the average properties of materials manufactured at different times) and material spatial variability (differences in the local properties of material produced at the same time). One should further distinguish between two kinds of material spatial variability: board variability (differences in the properties of full thickness specimens cut from different locations of the same board) and cross-sectional variability (differences in properties of thin material layers cut from different locations of the same specimen [e.g., adjacent to a surface] or at the center of the cross section).

To understand the reasons for these differences in initial properties and aging rate of various GFF products, as well as the reasons for spatial variability, one must recognize the large number of variables that can affect the aging process. These variables may be listed in the following categories [2]:

1. *Chemical Variables*—Formulation, mixing, reaction profile (particularly cream time), conditions of storage of the foam components (temperature and period), solubility of chloro-fluorocarbon in the polymer matrix.
2. *Manufacturing Variables*—Temperature and ambient gas pressure during the foaming process, distance of the nozzle from the foam plane, traverse speed, thickness of the foam layer (pass thickness in the spray systems), conditions of foam rise (free or restrained), including the presence of shear stress during the foam lamination process, initial partial pressure of CFC, presence or absence of free water (from manufacturing process).
3. *System Variables*—Presence of skins, diffusion barriers, or facing materials and their effectiveness in retarding the aging processes and in controlling the ingress of water vapor.
4. *Environmental Variables*—Ambient temperature and humidity (particularly for unfaced foams) and stress/strain transferred from adjacent structural components (sprayed foams).

Changes in chemical and manufacturing variables affect material structure (cell size and shape, thickness of cell-walls, fraction of struts, etc.) and may result in products with very different physical properties. Since material structure may be quantified by means of microscopic examinations [4], it may be correlated with differences in thermal performance of the foam. This approach, however, cannot be used in the product evaluation performed by an independent testing laboratory, because chemical and manufacturing variables are usually unknown to the testing agency and the evaluation must be limited to the information generated during testing. To define the problems encountered by such testing agencies, the next section discusses the aging process and material variability (batch and spatial variability) of commercial PUR products.

Aging Process

A plastic foam with chlorofluorocarbon (CFC) gas introduced during manufacture [5,6] is an effective thermal insulation. The CFC gas not only produces uniform cell size but, because of its high thermal resistivity (the inverse of thermal conductivity), is also responsible for the good insulating properties of the foam product. Thermal resistivity of trichlorofluoromethane (CFC-11) gas is rated at about 290% of that of air at room temperature [7].

During the service life of gas-filled foams, air components diffuse into the cells and the CFC gas diffuses out, each at a rate that depends on the type of polymer matrix and temperature. Moreover, a fraction of the CFC enters and saturates the polymer matrix, again with a dependence on the polymer type and temperature. The net effect is a gradual loss of thermal resistivity, often termed "aging" [8].

As the inward diffusion of nitrogen and oxygen is much faster than outward diffusion of CFC [9], the aging process may be said to comprise two stages:

1. A thermal drift stage when composition of the cell-gas changes at a significant rate, caused mainly by the influx of air.
2. A plateau stage when air diffusion is almost complete and the lower-rate efflux of CFC causes a very slow decrease in thermal resistivity with time.

This slow but uninterrupted decrease in thermal resistivity continues until all CFC has been replaced by air [10], predicted by laboratory aging of some foam to be as long as 100 to 250 years. All commercially produced GFF exhibits the same order of magnitude of thermal resistivity at initial and final stages. The initial thermal resistivity varies from 65 to 73 $\text{m} \cdot \text{K}/\text{W}$ [1,11,12]. The final equilibrium of air-filled foam varies from 30 to 33 $\text{m} \cdot \text{K}/\text{W}$ [9,13-15], depending on such material characteristics as the mean cell size and the extinction coefficient of radiation. Because of this it has often been questioned whether each product must be tested or whether one value could be quoted for long-term thermal properties. Practice, however, does not support one value for a generic class of materials [16-18].

To illustrate this point further, some results of tests performed at the National Research Council of Canada (NRCC) on commercial polyurethane (PUR) specimen products are shown in Fig. 1. In addition to these (denoted LAB), there are two specimens recovered from field applications: one from the roof of an industrial plant, the other from an underground application. Figure 1 displays differences in both initial thermal conductivity and rate of aging. It is clear that the initial thermal properties and the aging rate are not always correlated. For instance, the material that shows the best initial thermal properties (the lowest thermal conductivity) shows the worst thermal properties after long-term exposure of four years or more, indicating that one cannot predict long-term thermal resistance of GFF from initial values alone.

Finally, some GFF showed worse thermal resistance under laboratory conditions than GFF that had been aged for the same period under service conditions, indicating that the differences in commercial PUR products may affect the results more than the conditions of aging. Whereas Fig. 1 reports thermal conductivity of different products, significant differences were also found between different batches of the same polyurethane products, as will be discussed next.

Batch Variability of Commercial PUR Products

Until recently [19], batch variability has not been addressed in the literature. In a study at the NRCC three batches of three materials were first exposed at each of three Canadian sites (Halifax, Ottawa, and Saskatoon) [20] for ten years and then stored in the laboratory.

Specimens for testing were cut from the exposed batches and sent to the testing laboratory, so that the test results relate to different specimens taken from the same material batch. Table 1 shows the thermal resistivity of the three materials, measured after one, two, and three years. In addition, the values of thermal resistivity retained after five and fourteen years (ten years of outdoor exposure plus four years in the laboratory) are included.

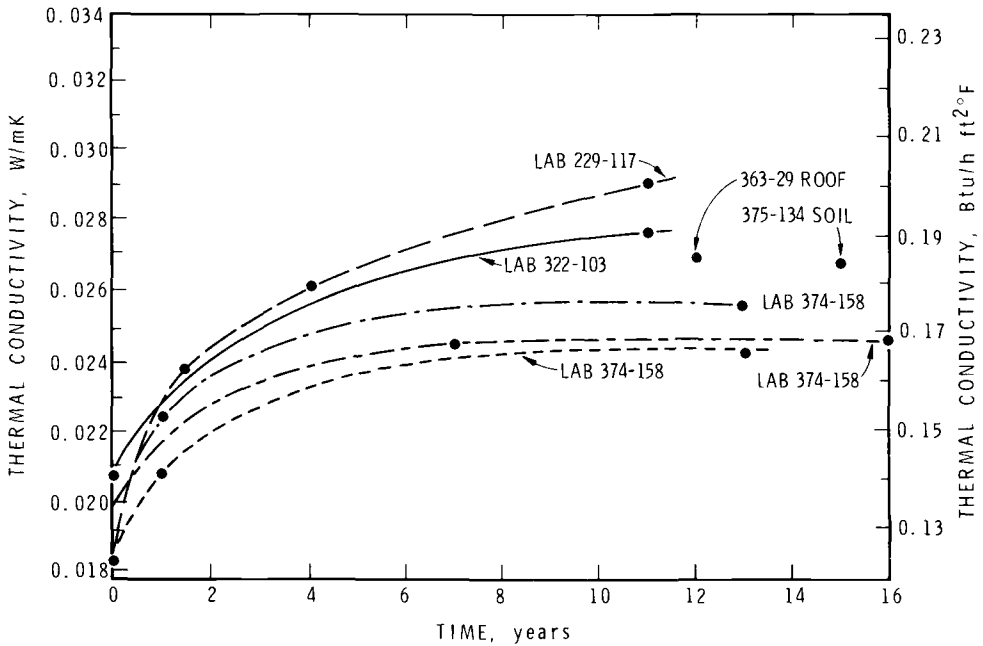


FIG. 1—Thermal conductivity versus aging time: NRCC tests on commercial polyurethane products.

The following points may be highlighted from the results shown in Table 1:

1. There was scatter in the experimental data. The variability between material batches delivered to the three locations was perhaps more significant than the reduction of thermal resistance of the same material batch over one to three years. As different specimens were tested, the differences in the results of thermal tests appeared as variability in the aging rate. For instance, after two years in Ottawa and Saskatoon, Material B had a higher thermal resistance than after only one year.

2. Initially, and for a period of either two or three years, materials showed significant differences in thermal resistivity, but the differences eventually disappeared in the plateau-stage of the aging process, and the long-term thermal resistivity (five or fourteen years) approached the same value for all samples from Materials A and C. It was about $38 \text{ m} \cdot \text{K}/\text{W}$ for Material A and approximately $40 \text{ m} \cdot \text{K}/\text{W}$ for Materials C and B (Halifax, Saskatoon). The samples of Material B exposed in Ottawa, however, retained higher thermal resistivity. After fourteen years of exposure, it was about $45 \text{ m} \cdot \text{K}/\text{W}$ ($6.4 \text{ ft}^2 \cdot \text{h}^\circ\text{F}/\text{Btu} \cdot \text{in.}$).

Although materials produced fifteen years ago may not be representative of the products currently on the market, the relative trends shown in Table 1 are characteristic of GFF produced today, and the large batch variability of GFF remains an important factor in evaluation of field performance.

Board Variability of Commercial PUR Products

In addition to differences in properties of materials manufactured at different times (batch variability), differences have been observed in properties of GFF specimens cut from various parts of the same product (board variability). This issue was discussed by Sherman [21,22], who demonstrated that using a single point of R-value is much too imprecise for characterization of

TABLE 1—*Thermal resistivity mK/W, of polyurethane foam from different exposure sites. (British units in parentheses).*

Material/Location	As-Received (Moist)				10 Years Outdoors + 4 Years in Laboratory (Dry)
	1 Year	2 Years	3 Years	5 Years	
Material A					
Ottawa	43.2 (6.23)	43.3 (6.25)	41.0 (5.92)	38.1 (5.49)	...
Halifax	43.6 (6.29)	41.0 (5.91)	40.4 (5.83)
Saskatoon	37.1 (5.35)	36.5 (5.26)	35.4 (5.11)	...	37.7 (5.44)
Material B					
Ottawa	49.1 (7.08)	52.5 (7.57)	48.5 (6.99)	45.8 (6.60)	45.1 (6.40)
Halifax	47.4 (6.83)	43.7 (6.30)	41.5 (5.99)
Saskatoon	42.9 (6.19)	46.5 (6.70)	39.0 (5.63)	...	39.3 (5.67)
Material C					
Ottawa	40.9 (5.90)	39.8 (5.74)	38.76 (5.59)	40.1 (5.78)	...
Halifax	37.9 (5.47)	37.1 (5.35)	37.02 (5.34)
Saskatoon	42.2 (6.09)	37.5 (5.41)	36.19 (5.22)	...	39.3 (5.67)

the 1.2 by 2.4 m polyisocyanurate (PIR) boards; he showed that use of the average R-value determined on eight 30 by 30 cm specimens is more appropriate. Following this research, the Canadian General Standards Board adopted a standard for faced polyurethanes [23] requiring either six 30 by 30 cm specimens or, preferably, four larger 60 by 60 cm specimens, cut from the board according to a pattern shown in Fig. 2.

More recently, a similar study of board variability was conducted at NRCC using eight 60 by 60 cm specimens randomly selected from adjacent PUR boards selected from the production line. The results (Table 2) display a standard deviation in thermal resistivity of 6.3%. Thus board variability as well as batch variability must be taken into consideration when evaluating long-term thermal performance of GFF products.

Cross-Sectional Variability of Commercial PUR Products

In previous testing at NRCC, differences were observed not only in specimens cut from different locations of the board but also in slices cut from the same specimen. To pursue this issue, a GFF material perceived to be highly homogeneous (sprayed PUR foam) was examined. Two specimens were prepared by spraying PUR foam on different substrates. From each of these, one slice was cut from the layer adjacent to the substrate and one slice from the core. The four slices were then placed together in the heat flow meter (HFM) apparatus. Thermal resistivity

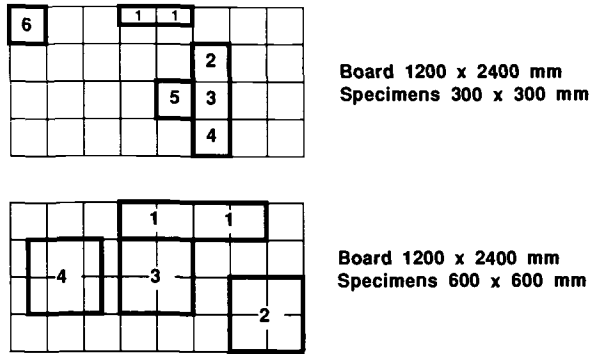


FIG. 2—Pattern for selecting specimens from boards for thermal resistance determination [23].

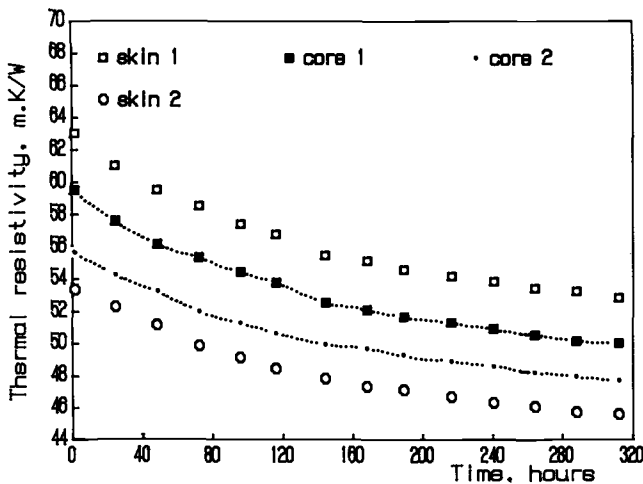


FIG. 3—Aging of 6-mm layers of polyurethane spray at temperature of 24°C.

changes as a function of time (Fig. 3) displayed large differences, which are particularly significant for the material adjacent to different substrates. One of the surface layers showed better thermal performance than the core material, the other worse, indicating that surface properties of substrate can affect foam structure. From results shown in Fig. 3 one can infer that both type of substrate and application technique can affect thermal resistance of the spray-applied PUR foam.

Given the large number of chemical and manufacturing variables, resulting in batch, board, and cross-sectional variabilities of GFF, it is not surprising that large differences were found in the long-term thermal resistivity of various commercial products [15,20,24–26]. It is evident that the use of a single thermal resistivity value for all (unfaced) materials of one kind (e.g., all polyurethanes) is not appropriate and that the products must be individually evaluated [16,17]. Such an evaluation may be done on an entirely experimental basis, as discussed in the next section, or with testing supplemented by the model of aging, as will be discussed in the section on Integrated Evaluation of Aging.

Experimental Evaluation of Aging

There are two key aspects of an experimental evaluation of the aging process:

1. Use of accelerated laboratory aging tests.
2. Uncertainty of thermal tests.

These aspects are discussed next.

Accelerated Laboratory Aging Tests

In experimental evaluations an attempt is made to accelerate the aging process by use of elevated temperature, temperature gradient, temperature and high humidity cycling, etc. Most common is exposure to elevated temperature, believed to increase the rate of gas diffusion in a very significant manner.

Conditioning at 60 or 100°C for a specified period has been recommended in some material specifications [23]. However, the possibility of cell breakage, introduced by the 100°C conditioning exposure for PUR, has been indicated previously [10]. Experiments performed at NRCC clearly illustrate the discriminatory character of 100°C exposure for another GFF product.

Two types of GFF were examined: one manufactured with process water and the other without. Thermal resistivity was periodically determined for all samples exposed to either 60 or 100°C (Figs. 4 and 5). For all practical purposes there was no significant difference between the results obtained from both aging exposures for GFF manufactured without process water (Fig. 4), but the situation was entirely different for the batch of foam denoted "GFF with process water" (Fig. 5). The thermal resistivity determined during three months' exposure to 60°C remained practically constant or even showed a slight increase due to drying of the process water. The thermal resistivity of the material exposed to 100°C, however, showed a significant reduction.

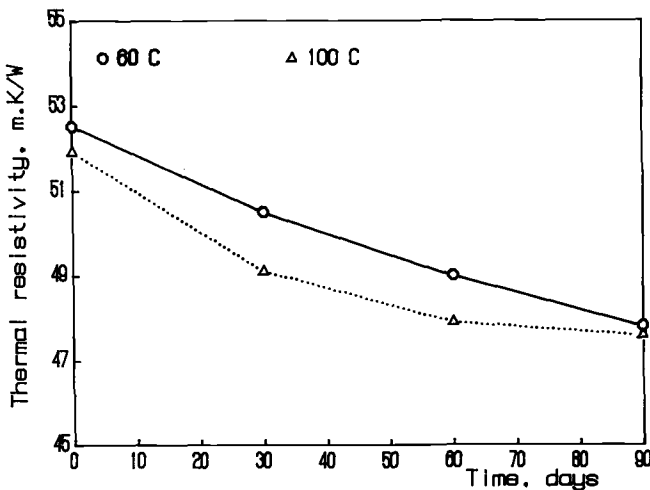


FIG. 4—Aging of full-board of GFF manufactured without water at temperature of 60 and 100°C.

³This observation relates to a specific batch of GFF product. We do not believe that foams containing process water are less stable than foams produced without water. This observation is included, however, to illustrate the risk of laboratory testing under conditions beyond those encountered during service life.

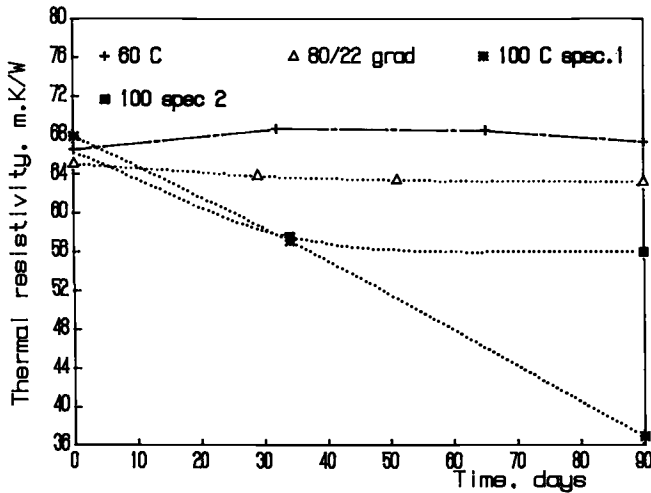


FIG. 5—Aging of full-board of GFF manufactured with process water at three conditions: isothermal 60 to 100°C and under thermal gradient.

Two cases are shown in Fig. 5. In one, aging at 100°C caused a reduction continuing through the 90-day test period; in the other, the reduction occurred only in the first 30 days. No further reduction of thermal resistance could be seen for the remaining test period. A third type of exposure was introduced when testing GFF with process water. The specimen was placed between two environments: 80 and 22°C (both at ambient air humidity). The thermal resistance of this specimen showed minor reduction that continued through the whole test period.

Two observations can be made from Fig. 5:

1. Aging at 100°C may indicate a possible cell-breaking phenomenon in the tested batch of GFF containing process water.³
2. The differences in aging rate for the same material are large, and the interpretation of results obtained under high temperature exposure is difficult.

Kabayama [16] also has stated: "After critically reviewing the literature, the group (CGSB Task Force) agreed that there appears to be no generally accepted method to accelerate aging of test samples." Another general approach should be sought. One based on slicing of the material in thin layers and determination of their thermal resistance as a function of time is discussed later. There is, however, one more difficulty in the experimental evaluation of aging, namely, uncertainty regarding the results of thermal tests performed on GFF products.

Uncertainty of Results of Thermal Tests

For an ideal specimen (isotropic and homogeneous in all three directions, with conductive mode prevailing and negligible contribution of convective and radiative heat flows) the uncertainty of actual test results should be identical to the uncertainty of the test method. Uncertainty in testing actual thermal insulating materials will always be higher than the uncertainty of the test method alone because of feedback between material non-uniformity and instrument response. This fact is, however, often forgotten and users expect ASTM Methods C 177 and C 518 to yield the same precision and bias for different materials. This is the case in testing of GFF products. For example, Smith et al. [27] have stated with regard to the precision of ASTM C 518:

A Round Robin series of tests was run to estimate the precision of ASTM Method C 518, when used to measure the k-factor (thermal conductivity) of rigid polyisocyanurate foam boardstock. The test results show that k-factors of similar products, measured in different laboratories, should differ by more than 12% ($0.022 \text{ Btu} \cdot \text{in.}/^\circ\text{F} \cdot \text{hr} \cdot \text{ft}^2$; 0.003 W/mK) before they are judged to be different. Results obtained within laboratories, if their procedures are similar to this Round Robin's, should differ by about 7% ($0.013 \text{ Btu} \cdot \text{in.}/^\circ\text{F} \cdot \text{hr} \cdot \text{ft}^2$; 0.002 W/mK) before being called different. The levels of the between- and within-laboratory uncertainty which were measured have a high degree of validity, owing to the large number of laboratories (16) participating in the Round Robin. Both levels of uncertainty are much higher than the 2% that most people in the polyurethane industry expect from C 518 results.

The above estimates appear to agree with other estimates of the precision of thermal measurements performed on GFF boards. Sherman [21] performed 275 single-specimen measurements of thermal conductivity and found that 94.2% were within 7% of the average value for the whole-board from which the specimen was cut. Using a standard deviation of 6.3% determined for the tests shown in Table 2 and four specimens, one would obtain uncertainty of 8.5% for 95% probability level.

Recently a review of the uncertainties in the results obtained with a particular test method and those attaching to the method itself (ASTM C 518) was undertaken by the manufacturers of mineral fiber insulation (MFI) products. Round-robin tests showed that, while MFI batts and blankets can be measured to within $\pm 3.5\%$ uncertainty, for MFI loose-fill specimens values ranged between 10 and 16% [28]. Thus the results of both round robins [27,28] indicate that the uncertainties of thermal testing are much more affected by the non-uniformity of the specimens than had been anticipated.

So far, we have discussed the inherent uncertainty of individual test methods. When a comparison is made between results obtained with different test methods, however, the uncertainty is even larger. It depends on the geometry of the test specimen, the applied temperature difference, and the dynamics of the aging process during the test [16]. As these factors are quite different in four ASTM laboratory test methods used to determine thermal resistance of GFF (C 177, C 518, C 236, C 976), the experimental-only evaluation of long-term thermal resistance is difficult.

Modelling of the Aging Process

This section will address the following areas: an overview of the models, limitations in the use of the models, and discussion of the key material characteristic, namely the effective diffusion coefficient.

TABLE 2—Initial thermal resistivity of polyurethane board.

Specimen	mk/W ($\text{ft}^2\text{h}^\circ\text{F}/\text{Btu} \cdot \text{in.}$)
1	50.8 (7.33)
2	47.7 (6.88)
3	49.3 (7.12)
4	53.2 (7.68)
5	56.4 (8.14)
6	53.1 (7.66)
7	57.7 (8.32)
8	52.6 (7.59)
Avg.	52.6 (7.59)
Std. Dev.	= 6.3%

Review of Aging Models

The development of aging models was initiated by Norton [1], who treated the problem as a case of isothermal, multicomponent Fick's diffusion. Given the initial and boundary conditions for rectangular slabs, the gas composition at any time and in any location in the foam can be calculated from the analytical solution. Assuming that the polymer matrix remains unchanged in time and that the thermal resistance of the gas mixture, $R(t)$, is proportional to the molar fraction of chlorofluorocarbon (CFC), Norton introduced the equation

$$R(t) = R_0 + C \cdot f(t) \quad (1)$$

where R_0 is the thermal resistance of air-filled foam, the coefficient C is proportional to the difference between thermal resistance in the initial stage of aging (CFC-filled) and the final stage (air-filled), and f is the molar fraction of CFC in the cell-gas. Norton's model explains and describes many aspects of foam aging. For example, predictions of CFC diffusion made using Norton's model, with minor corrections, relate well to the directly measured CFC release rates for similar foams [29,30].

The drawbacks of Norton's model are as follows:

1. It requires knowledge of thermal resistance at the final stage (air-filled), which usually is not available.
2. It approximates the effect of CFC concentration on thermal resistance of GFF in a linear fashion.
3. It disregards the effects of temperature gradients on cell-gas composition.
4. It disregards differences in cell-gas composition and uses average values for the slab.

Norton's model did not relate to the material structure. The intricacy of the foam structure was subsequently better described by a series of research papers at MIT [31–38] that led to development of another model based on the following assumptions:

1. Heat transfers by radiation and conduction are separate and independent.
2. Radiative heat transfer is described by the Rosseland approximation.
3. Solid-phase conduction depends on material porosity, conduction of the polymer film, and distribution of polymer between material in the cell-walls (membranes or windows) and material deposited at interstices of cells (struts).
4. Conduction of a gas mixture may be calculated in terms of viscosity, thermal conductivity, and the relative amounts of each component.

Thermal conductivity of the foam at any time may be calculated from the equation

$$\lambda = \lambda_g + 0.8 \left(\frac{2}{3} - \frac{f_s}{3} \right) (1 - \delta) \lambda_p + \frac{16\sigma}{3K} \cdot T_m^3 \quad (2)$$

where λ_g is thermal conductivity of a gas mixture, $W/(m \cdot K)$; λ_p is the solid phase conductivity, $W/(m \cdot K)$; f_s is the fraction of struts; δ is the foam porosity; σ is the Steffan-Boltzman constant, $5.67 \times 10^{-8} W/(m^2 K^4)$; K is the extinction coefficient, $1/m$; and T_m is the mean temperature of the specimen, K .

Thermal conductivity of the mixture of oxygen, nitrogen, and CFC may be calculated from an equation for a mixture of polyatomic gases—for example, those of Wassiljewa (discussed by Reitz [38]) or Mason and Saxena [39]. Table 3 shows good agreement between results of calculations [39] for nitrogen/CFC 11 mixtures at 292 K and the measured values reported by Peters et al. [40]. The agreement between linear approximation used in Norton's model [1] and measured values is poor. As may be seen in Table 3, thermal conductivity of a gas mixture can be calculated precisely if the relative amounts (partial pressures) of each component are known. In

TABLE 3—*Thermal conductivity of gas mixtures, $(W/m \cdot K) \times 10^{-3}$, measured and calculated.*

Molar Fraction CFC	Thermal Conductivity				
	Measured [40]	Calculated [39]		Calculated [1]	
	λ	λ	% Difference	λ	% Difference
0.00	25.40	24.97	2.3	25.40	0
0.25	16.99	16.62	2.2	21.00	23.5
0.50	12.28	12.15	1.1	16.59	35.2
0.75	9.54	9.44	1.1	12.18	27.7
1.00	7.77	7.64	1.0	7.77	0

turn, to estimate partial pressures at a given time one must know the initial partial pressure for each gaseous component as well as the factors governing diffusion of gases into and out of the foam cells (i.e., effective diffusion coefficients). These factors affect the aging process much more than an incorrect approximation of the solid phase conduction or the radiative heat transfer in Eq 2. As will be discussed in the next section, the lack of this information limits the usefulness of the models.

Errors introduced into the MIT model by assuming specific formulas for solid phase and radiative heat transfer can be estimated from other analytic research by Boetes [41], Schuetz [32], Sparks and Arvidson [42], Booth [43], and Cunningham and Sparrow [44] to be in the 1 to 3% range. Errors introduced into the MIT model by assuming that coupling between conductive and radiative heat fluxes is negligible can be estimated from studies of Kumaran and Stephenson [45] to be in the 2 to 5% range. The last category of errors appears to be of somewhat higher significance than errors caused by inaccurate estimates of fraction of struts or thermal conductivity of the solid polymer. For a density range of 20 to 80 kg/m³ both types of error are small when compared with batch or board variabilities of GFF products. None of these errors, however, affects the dependence of thermal conductivity on time if it is determined for individual specimens.

The MIT model, while an improvement on Norton's linear approximation, failed to recognize that the composition of cell-gas and therefore its thermal conductivity is strongly affected by the phase change of CFC (condensation and evaporation).

Moreover, heat release or extraction involved in condensation and evaporation processes may affect the apparent thermal conductivity of the foam. Nevertheless, even if all these corrections were introduced into the MIT model (as will be explained in the next section), the application of the model would still be limited by the lack of proper input parameters (initial CFC pressure and diffusion coefficients).

Limitations in Use of Models

As previously stated, to calculate the thermal conductivity of the gas mixture in Eq 2 one needs information on the initial conditions of CFC partial pressure and effective diffusion coefficient.

The CFC pressure reached during the foaming process is equal to approximately 1 atm. When the foam cools from the high temperature caused by exothermic reactions, the CFC pressure is reduced. An estimate of this reduction put it between 0.3 and 0.4 atm [8, 29]. Moreover, a part of the CFC gas enters and saturates the polymer matrix. The CFC solubility in the polymer matrix is, however, subject to controversy. Norton [1] assumed much lower solubility than was found by Steinle [46] or Brandreth and Ingersoll [29]. While Steinle et al. [47] and Boetes [41] reported that the reduction of gaseous phase of CFC-11 and CFC-12 occurs primarily within a one to three month period, Brandreth and Ingersoll [29] found that it takes much

longer. Results of tests performed at NRCC are shown in Table 4. The mean chlorine content of the cell gas was obtained by subtracting the cell-wall chlorine content from the total chlorine content of each foam. The cell-wall chlorine content, shown for different foams in Table 4, varies from 3 to 30% of the total chlorine content.

Such a large variability in CFC solubility in different polymers, coupled with large differences in the initial CFC pressure caused by foam cooling, once more emphasizes the need for experimental determination of the factors affecting initial CFC pressure. The model must therefore be improved to incorporate a better description of factors affecting initial CFC pressure and subsequent changes in the gas composition, as described by the effective diffusion coefficients of oxygen, nitrogen, and CFC gases. The concept of the effective diffusion coefficient will be discussed next.

Effective Diffusion Coefficient

The concept of effective diffusion coefficient was derived from studies of the permeability of plastic films. According to Fick's law of diffusion, the proportionality constant relating mass flux to the gas concentration gradient causing this diffusion process is called the *diffusion coefficient* (often denoted D). If D is independent of the gas concentration and Henry's law holds (mass of the substance dissolved in the polymer is proportional to the partial pressure of this substance), then from Fick's law one obtains:

$$P = D \cdot S \quad (3)$$

where P is gas permeability through the film, D is the diffusion coefficient, and S is Henry's law constant or solubility of the gas in the polymer. Henry's law, however, holds only for dilute solutions such as nitrogen in polymers and not for many vapors. Moreover, absorbed vapors can act as plasticizers enhancing the passage of another gas, and some organic vapours exhibit a diffusion coefficient dependent on concentration [48].

The rate of diffusion and the solubility of a gas in the polymer are normally described by an Arrhenius relation leading to a temperature dependence of the diffusion coefficient of the following character:

$$\ln D = a - b/T \quad (4)$$

As diffusion coefficients and solubilities normally increase with temperature rise, the permeability of a single polymer film will also increase at a rate depending on the type of gas and the polymer.

TABLE 4—*Thermal resistivity and total chlorine content as well as that of the cell walls alone, as determined by NRCC, Division of Chemistry.*

Specimen Code	Age (Years)	Thermal Resistivity (m · K/W)	Total Cl (%)	Cell Wall Cl (%)	Cell Gas Cl (%) (Mean)
375-245	0	48.5	7.5	2.4	5.0
355-37	6	41.6	9.5	0.3	9.2
375-131	14	44.4	7.5	0.2	7.3
374-158	18	40.9	10.6	3.4	7.2
293-173	11	42.3	9.4	2.8	6.6
375-134	14	37.4	10.4	2.3	8.0
396-85	1 ¹ / ₂	41.5	6.6	4.0	2.6
396-89	0	48.7	5.4	2.5	2.9

Although the permeability of a plastic film is affected by a number of factors (e.g., nature of the gas and polymer, temperature and pressure conditions, presence of condensable vapors and their interaction, particularly in causing swelling or plasticization of the polymer [48]), the permeation rate of gases through plastic films may be evaluated with an accuracy usually higher than the permeation rate for many of the cellular plastics.

This is possible because in most commercially produced cellular plastics two interlinked diffusion processes occur simultaneously: (1) diffusion through polymer films and (2) diffusion through cracks, tears, pinholes, ultra-thin windows, and other imperfections in the polymer films. Depending on the incidence of the imperfections and even on the material anisotropy, the rate of diffusion may vary between the rate of diffusion through polymer only (no holes) and the rate of diffusion through the imperfections only (high fraction of holes).

To preserve the simplicity of the $P = D \cdot S$ relation, the effective permeability P_{eff} , solubility, S_{eff} , and diffusivity, D_{eff} , were introduced [37,49]. While this relation appears to be simple, it comprises a mixture of two different physical phenomena. For "ideal" materials with no imperfections, the temperature dependence is described by an Arrhenius equation. For material with a high fraction of holes, the temperature dependence may be calculated from Boyle-Mariotte's law for an ideal gas. In the actual case, depending on the incidence of imperfections, the temperature dependence is an unknown mixture of both cases. For example, an increase from 25 to 90°C increases CFC-11 diffusion by a factor of 25 [29,36], but N₂ permeability by a factor of 12 [36].

Study of diffusion coefficients of different types of polymers has always been the central point of development of thermal insulating foams. As Ingersoll and Brandreth showed [8,29], there are large differences in the diffusion coefficients of different foam compositions and, therefore, in their thermal performance. Whether, in fact, the differences in the "effective" foam diffusion coefficients reported by Ingersoll and Brandreth were primarily caused by differences in the properties of the films or by holes and ultra-thin windows in the cells is not known. Defects are the more likely cause, because the effective foam diffusion coefficients are appreciably larger than those found from single film experiments. As defects may to a great extent be process dependent, the necessity of evaluating each foam product on an individual basis is once more highlighted. Notwithstanding advances in correlating film and foam diffusion rates (e.g., those by Shankland [49]), the actual evaluation of GFF performance must be based on the effective foam diffusion coefficients and these coefficients must be determined by careful consideration of batch and of spatial and chemical variability of materials.

To incorporate material variability into the evaluation of long-term thermal resistance of GFF, one should ideally determine the effective diffusion coefficient for thin layers cut from various locations in the board. When measuring the diffusion or permeance with conventional "flow through" experiments, however, the use of thin layers increases the probability of erroneous results caused by cracks and imperfections spanning the whole thickness of the specimen. To avoid these errors the only approach currently available is to calculate the gas diffusion coefficients from the measured change in thermal resistance of the layer as a function of time (Fig. 3). This approach requires the simultaneous use of a model and aging experiments.

Integrated Evaluation of Aging

The main elements of the proposed integrated approach for evaluation of aging of GFF are:

1. Testing of *thin layers* combined with a diffusion model to determine material characteristics (initial CFC concentration and diffusion coefficients).
2. Use of a *model of aging* to calculate aging performance of full boards.

Use of thin layers helps to reduce the duration of the aging experiments. One may reduce test duration either by increasing temperature, which leads to increase in diffusion coefficient, or by reducing the thickness of the tested layer. Increased temperature, as discussed previously, in-

creases diffusion through material imperfections in a manner different from solubility of the gas in a polymer matrix. Since gas solubility governs transport through cell walls, use of increased temperature becomes questionable as a technique for accelerating the aging process in *different* foams.

At NRCC the following approach is being developed. Several thin layers, 40 to 80 mean cell-diameters thick, are cut from different locations to permit examination of the extent of material spatial variability and establish sampling procedure. The layers are placed in a heat flow meter (HFM) apparatus immediately after slicing. During a 10 to 14 day period their thermal resistivity is continuously recorded. They are then stored in the laboratory and periodically tested to determine when the plateau stage has been reached. Testing of the layers continues, but at less frequent intervals, for a period of several months. From thermal resistance changes measured on the thin specimens and use of the model of aging, one can calculate the effective diffusion coefficients. Diffusion of air components is calculated from the first stage of aging (thermal drift) and diffusion of CFC is calculated from the second stage (plateau stage) of aging.

After 4 to 6 weeks of aging, some of these layers are used to determine gaseous fraction of CFC measuring chlorine (fluorine) content twice: once on undisturbed foam, and the second time after crushing the foam and off-gassing the polymer powder. (The technique has been described elsewhere [10, 50].) After correcting for chlorine content of the fire retardant agents (fluorine is used if such correction is not possible), the fraction of gaseous CFC is calculated. This value determines initial CFC pressure and contains both the effect of foam cooling and the effect of CFC solubility in the polymer matrix. Normally, one may assume that CFC diffusion over 4 to 6 weeks is insignificant, but the correction for CFC loss may be easily introduced if CFC diffusion coefficient is known.

Thermal resistivity measured at the beginning of the plateau stage is used to check whether the extinction coefficient (determined independently) and the initial CFC pressure are correct. Knowing these parameters and assuming oxygen and nitrogen pressures equal to those of the ambient air (plateau stage) one can calculate thermal resistivity from Eq 2. By comparing this value with the measured value, one can verify the two parameters of the model. This is another feature of the integrated approach.

The use of thin layers in the integrated evaluation of aging has many benefits:

1. It increases the precision of the thermal resistivity test by increasing the uniformity of the test specimen.
2. It reduces the duration of the aging tests while avoiding adverse effects of increased temperature.
3. It helps in determining initial CFC concentration and effective diffusion coefficients.
4. It provides for a check of the initial CFC concentration and extinction coefficient versus thermal resistivity at the beginning of the plateau stage.
5. It helps in evaluation of material variability, cross-sectional variability in particular.

The use of thin layers has a serious drawback, however, in that it increases the number of measurements to be performed. These may be reduced, however, by the application of another two elements of the integrated approach: the model of aging and the method of material characterization. The aging model estimates the effect of differences in material characteristics on long-term thermal performance. It therefore permits testing of a small number of specimens so long as their properties represent either the mean or extreme case, as required. To select such specimens, one needs a method of material characterization (fingerprinting). This method must correlate well with the most important factor affecting aging, the effective diffusion coefficient for nitrogen. Originally, the use of nitrogen diffusion itself was tried at NRCC, but it proved to be impractical since nitrogen concentration was difficult to establish in GFF purchased on the market. A transient diffusion of an inert gas (e.g., helium) is now being examined as a means of characterizing the material. The helium diffusion must be correlated with the nitrogen diffusion coefficient for the GFF.

The benefits of material characterization are evident in:

1. Assessing effects of material variability on estimated long-term R-value.
2. Selecting representative specimens for long-term aging tests.
3. Ensuring uniform quality in the manufacturing process.
4. Comparing aging characteristics of specimens exposed to different environmental conditions.
5. Checking whether the specific environmental exposure causes significant cell-breakage.

The last aspect (No. 5) is particularly important, since the significance of environmental factors affecting aging rate [51–54] is unknown. When established, one may incorporate the effect of the environmental factors in the aging model, expanding it to evaluate the field performance of GFF. One may, alternatively, establish a correction for aging under field conditions. Until one of these approaches is developed, thermal resistivity must, on an interim basis, be measured on specimens selected from a field exposure. Use of the model and the fingerprinting method may become a link connecting the laboratory and field evaluation of GFF.

Concluding Remarks

Current laboratory accelerated aging test procedures give comparative ratings that are applicable *only* to those materials for which comparative studies have been performed. As evaluation must also include materials of unknown field performance, it is therefore necessary to develop a method of evaluation on an absolute basis.

Experimental evaluation alone is not a sufficient basis because of the large uncertainty of results from thermal testing. In spite of the high precision of ASTM C 177 and C 518, the spatial variability of the specimens has caused uncertainty of measurements so large that the number necessary for the requisite precision becomes impractical.

As accurate and statistically valid determinations of the thermal resistivity of gas-filled foams is very expensive, in terms of both time and effort, one must strive to construct a mathematical model that can yield, if realistic enough, more economical solutions to practical problems. A review of existing models has indicated that insufficient attention has been paid to the initial cell-gas composition or to changes in it, as defined by effective diffusion coefficients. This review has also revealed that high temperature affects diffusion and solubility phenomena in different ways, leading to questionable results.

Another approach to evaluation of long-term thermal performance is proposed. It involves use of thin material layers cut from different locations in the plane and in the cross section of the board. Use of the thin layer is much more effective in reducing the length of the experiment while at the same time avoiding the adverse effects of high temperature level. It permits increasing the number of tests. These may, however, be reduced if each of the specimens has been “fingerprinted” with a material characterization method. Development of such a method as well as modification of the MIT model to include phase changes of CFC is currently on the research agenda at NRCC. With the two elements completed, the integrated approach may be used for evaluating long-term thermal resistance of gas-filled foams with *different* blowing agents.

Acknowledgments

The authors wish to express deep gratitude to Dr. S. Berman, Mr. M. Bednas, and Mr. V. Clancy, Division of Chemistry, NRCC, for determination of CFC solubility and cell-gas composition on several specimens; to colleagues at the Institute for Research in Construction, NRCC, Drs. M. K. Kumaran, N. V. Schwartz, and S. A. Barakat for assistance and discussion; to Mr. R. G. Marchand and Mr. J. G. Theriault for constructing the instruments and performing all the reported experiments.

Thanks are also offered to all the manufacturers of GFF who supplied materials for NRCC research and who shared information regarding laboratory and field performance of their materials. This assistance is extremely valuable, since the consensus of industry is needed to develop better means of evaluating field performance of GFF products.

References

- [1] Norton, F. J., "Thermal Conductivity and Life of Polymer Foams," *Journal of Cellular Plastics*, Jan. 1967, pp. 23-37.
- [2] Brandreth, D. A., "Prospects for Improved Insulation Foams," in *Advances in Foam Aging*, Vol. 1, D. A. Brandreth, Ed., Caissa Editions, Yorklyn, Del., 1986, pp. 4-11.
- [3] *Advances in Foam Aging*, Vol. 1, D. A. Brandreth, Ed., Caissa Editions, Yorklyn, Del., 1986.
- [4] Rhodes, M. B., "Applicable Technique of Optical Microscopy for Polyurethane Investigations," *Cellular and Non-Cellular Polyurethanes*, Carl Hausen Verlag, 1980, p. 803.
- [5] Knox, R. E., "Insulation Properties of Fluorocarbon Expanded Rigid Urethane Foam," presented to ASHRAE Semi-Annual Meeting, New York, 11-14 Feb. 1963.
- [6] Ball, W. G., Hurd, R., and Walker, M. G., "Urethane Rigid Foams: A Review of Factors Affecting the Attainment and Retention of Optimum Thermal Conductivity and Their Significance in Service Applications," in *Proceedings*, Heat Transfer, Current Applications of Air Conditioning, International Institute of Refrigeration, Commissions II and VI, 1969, pp. 261-269.
- [7] "Thermal Conductivity of Rigid Urethane Foam," *Journal of Cellular Plastics*, Vol. 6, No. 2, 1970.
- [8] Brandreth, D. A., "Factors Influencing the Aging of Rigid Polyurethane Foam," *Journal of Thermal Insulation*, Vol. 5, July 1981, pp. 31-39; also in *Advances in Foam Aging*, D. A. Brandreth, Ed., Caissa Editions, Yorklyn, Del., 1986.
- [9] Norton, F. J., "Diffusion of Chlorofluorocarbon Gases in Polymer Films and Foams," *Journal of Cellular Plastics*, Sept./Oct. 1982, pp. 300-318.
- [10] Bomberg, M., "Problems in Predicting the Thermal Properties of Faced Polyurethane Foams," in *Thermal Insulation Performance, ASTM STP 718*, American Society for Testing and Materials, Philadelphia, 1980, pp. 412-428.
- [11] Ball, G. S., Healay, G. W., and Partington, J. B., "The Thermal Conductivity of Isocyanate-Based Rigid Cellular Plastics: Performance in Practice," *European Journal of Cellular Plastics*, Jan. 1978, pp. 50-62.
- [12] Dixon, R. R., Edelman, L. E., and McLain, K. D., "Effect of Aging on Thermal Conductivity of Cellular Materials," *Journal of Cellular Plastics*, Jan./Feb. 1967, pp. 44-47.
- [13] Kuester, W., "Thermal Conductivity of Plastic Foam," translation from *Kunststoffe*, Vol. 60, No. 4, 1970, pp. 249-255.
- [14] Zehendner, H., "Wärmeleitfähigkeit von Schaumkunststoffen mit hochmolekularen Zellgasen" [Thermal Conductivity of Foam Plastics with High Molecular Gas], *Bauphysik*, Vol. 5, No. 5, Oct. 1983, pp. 169-173 (translation available).
- [15] Zehendner, H., "Results of 15 Years of Rigid Polyurethane Foam Quality Supervision," *Cellular Polymers*, Vol. 1, 1982, pp. 211-220.
- [16] Kabayama, M. A., "Long-Term Thermal Resistance Values of Cellular Plastic Insulations," *Journal of Thermal Insulation*, Vol. 10, April 1987, pp. 286-300.
- [17] Kugler, L. B. and McCorkle, J., "Are 'Aged' Values Adequate for Rating Roof Insulations?" *Roofing, Siding, Insulation*, July 1986, pp. 38-43, 62.
- [18] Baumann, G. F., "R-Value of Rigid Polyurethane Foam: An SPI Research Project," *Journal of Thermal Insulation*, Vol. 6, July 1982, pp. 39-47.
- [19] Zehendner, H., "Untersuchungen au PUR-Hartschaum im Rahmen von GSH-Forschungsvorhaben," *GSH-Mitteilungen*, No. 5, May 1987.
- [20] Bomberg, M., "Thermal Resistance of Polyurethane Cellular Plastic Insulations Following Outdoor Aging," Internal Report 514, IRC/NRCC, 1987.
- [21] Sherman, M., "Sampling Faced Foam Insulation Board for Heat Flow Meter Thermal Performance Testing," in *Thermal Insulation Performance, ASTM STP 718*, American Society for Testing and Materials, Philadelphia, 1980, pp. 298-306.
- [22] Sherman, M., "Aged Thermal Resistance (R-Value) of Foil-Faced Polyisocyanurate Foam Thermal Insulation Board," in *Proceedings*, ASHRAE/DOE-ORNL Conference on Thermal Performance of Exterior Envelopes of Buildings, 1981, pp. 952-964.
- [23] National Standard of Canada CAN/CGSB-51.26-M86, "Thermal Insulation Urethane and Isocyanurate, Boards, Faced."
- [24] Zarate, D. and Alumbaugh, R., "Thermal Conductivity of Weathered Polyurethane Foam Roofing," in *Advances in Foam Aging*, D. A. Brandreth, Ed., Caissa Editions, Yorklyn, Del., 1986.

- [25] Mullenkamp, S. P. and Johnson, S. E., "In-Place Thermal Aging of Polyurethane Foam Roof Insulations," in *Proceedings*, 7th Conference on Roofing Technology, NBS/NRCA, 14-15 April 1983, pp. 49-55.
- [26] Larsson, L. E., "Determination in Long-Term Tests of the Thermal Conductivity of Foamed Polyurethane Used as Thermal Insulation in Sandwich Panels," Publication No. 78:3, 1978, and "Sandwich Panels with Foamed Polyurethane Insulation," Publication No. 79:9, 1979, Chalmers Institute of Technology, Gothenburg, Sweden; see also *Proceedings*, ASHRAE/DOE-ORNL Conference on Thermal Performance of the External Envelopes of Buildings, 3-5 Dec. 1979, pp. 638-650.
- [27] Smith, S. A., Galbraith, C. J., Carmell, M. J., Moore, M. L., and Brown, R. K., "A Round Robin Testing Program to Estimate the Precision of ASTM C 518 for Measuring the k -Factor of Rigid Foam Products," in *Proceedings*, Polyurethanes World Congress, 29 Sept.-2 Oct. 1987, pp. 74-79, or report from ICI Polyurethanes, West Depford, N.J.
- [28] Adams, R. D. and Hust, J. G., "A Round Robin on Apparent Thermal Conductivity of Several Loose-Fill Insulations," this publication, pp. 263-283.
- [29] Brandreth, D. A. and Ingersoll, H. G., "Accelerated Aging of Rigid Polyurethane Foam," *European Journal of Cellular Plastics*, Oct. 1980, pp. 134-143; also in *Advances in Foam Aging*, D. A. Brandreth, Ed., Caissa Editions, Yorklyn, Del., 1986.
- [30] Khalil, M. A. K. and Rasmussen, R. A., "The Release of Trichlorofluoromethane from Rigid Polyurethane Foams" and "The Resistance Time of Trichlorofluoromethane in Polyurethane Foams," in *Advances in Foam Aging*, Vol. 1, Caissa Editions, Yorklyn, Del., 1986, pp. 190-215.
- [31] Valenzuela, J. A. and Glicksman, L. R., "Thermal Resistance and Aging of Rigid Urethane Foam Insulation," in *Thermal Insulation, Materials, and Systems for Energy Conservation in the '80s*, ASTM STP 789, American Society for Testing and Materials, Philadelphia, 1983, pp. 688-702.
- [32] Schuetz, M. A., "Heat Transfer in Foam Insulation," M.Sc. thesis, MIT, Cambridge, Mass., 1982.
- [33] Schuetz, M. A. and Glicksman, L. R., "A Basic Study of Heat Transfer Through Foam Insulation," in *Proceedings*, Sixth International Polyurethane Conference, San Diego, Calif., 1983, pp. 341-347.
- [34] Sinofsky, M., "Property Measurement and Thermal Performance Prediction of Foam Insulations," M.Sc. thesis, MIT, Cambridge, Mass., 1984.
- [35] Ostrogorsky, A. G., "Aging of Polyurethane Foams," D.Sc. thesis at MIT, L. R. Glicksman, Supervisor, Cambridge, Mass., 1985, 185 pages.
- [36] Ostrogorsky, A. G. and Glicksman, L. R., "Aging of Polyurethane Foams: The Influence of Gas Diffusion on Thermal Conductivity," ORNL/SUB/84-9009/2, Aug. 1986.
- [37] Ostrogorsky, A. G., Glicksman, L. R., and Chiappetta, S., "Effective Conductivity of Aging Polyurethane Foam," ORNL/SUB/84-9009/1, March 1986.
- [38] Reitz, D. W., "Heat Transfer and Aging of Closed-Cell Foam Insulation," in *Advances in Foam Aging*, Vol. 1, D. A. Brandreth, Ed., Caissa Editions, Yorklyn, Del., 1986, pp. 110-130.
- [39] Mason, E. A. and Saxena, S. C., *Physics of Fluids*, Vol. 1, 1958, p. 361.
- [40] Peters, H. C., Breunese, J. N., and Hermans, L. J. F., "Thermal Conductivity of Gaseous CFC11 (Freon 11) and CFC12 (Freon 12) and Their Mixtures with N₂ at 292 K," *International Journal of Thermophysics*, Vol. 3, No. 1, 1982, pp. 27-34.
- [41] Boetes, R., "Heat Transfer Reduction in Closed-Cell Polyurethane Foams," D.Sc. Thesis, Technische Hogeschool Delft, The Netherlands, 1984, p. 293.
- [42] Sparks, L. L. and Arvidson, J. M., "Thermal and Mechanical Properties of Polyurethane Foams at Cryogenic Temperatures," *Journal of Thermal Insulation*, Vol. 8, Jan. 1985, pp. 198-232.
- [43] Booth, L. D., "Radiation Contribution as an Element of Thermal Conductivity," in *Proceedings*, Polyurethanes World Congress, 1987, pp. 85-90.
- [44] Cunningham, A. and Sparrow, D. C., "Rigid Polyurethane Foam: What Makes It the Most Effective Insulant," *Cellular Polymers*, Vol. 5, 1986, pp. 327-342.
- [45] Kumaran, M. K. and Stephenson, D. G., "Heat Transport Through Thermal Insulation: An Application of the Principles of Thermodynamics of Irreversible Processes," ASME, 86-WA/HT-70, pp. 1-4.
- [46] Steinle, H., "Prog. Refrig. Sci. Technical," in *Proceedings*, 13th Int. Congr. Refrig., Vol. 47, 1971.
- [47] Steinle, H., Brodsky, J., and Ilgner, U., *Kaltetechnik-Klimatisierung*, Vol. 24, No. 6, 1972, pp. 153-4, 157, 158, 161.
- [48] Hennessy, B. J., Mead, J. A., and Stering, T. C., "The Permeability of Plastic Films," The Plastics Institute, London, 1966, pp. 1-61.
- [49] Shankland, I. R., "Gas Transport in Closed-Cell Foams," in *Advances in Foam Aging*, D. A. Brandreth, Ed., Caissa Editions, Yorklyn, Del., 1986.
- [50] Nadeau, H. G., Waszeciak, P. H., and Sayigh, A. R. R. in *Proceedings*, Conference on Cellular Plastics, 13-15 April 1966, Publication 1462, National Academy of Science, National Research Council, Washington, D.C., 1967.
- [51] Levy, M. M., "Moisture Vapor Transmission and Its Effect on Thermal Efficiency of Foam Plastics," *Journal of Cellular Plastics*, Vol. 2, No. 1, 1966, pp. 37-45.

- [52] Patten, G. A. and Skochdopole, R. E., "Environmental Factors in Thermal Conductivity of Plastic Foams," *Modern Plastics*, 1962, pp. 149-152, 191.
- [53] Hilado, C. J., "Effect of Accelerated and Environmental Aging on Rigid Polyurethane Foams," *Journal of Cellular Plastics*, April 1967, pp. 161-167.
- [54] Skochdopole, R. E., "The Thermal Conductivity of Foamed Plastics," *Chemical Engineering Progress*, Vol. 57, No. 10, Oct. 1961, pp. 55-59.

Measurement of Gas Diffusion in Closed-Cell Foams

REFERENCE: Shankland, I. R., "Measurement of Gas Diffusion in Closed-Cell Foams," *Insulation Materials, Testing, and Applications, ASTM STP 1030*, D. L. McElroy and J. F. Kimpflen, Eds., American Society for Testing and Materials, Philadelphia, 1990, pp. 174-188.

ABSTRACT: The aging process in closed-cell thermal insulation foams refers to that phenomenon which results in a degradation of insulation value of the foam over a period of time and is generally attributed to diffusion of atmospheric components into the foam and diffusion of expansion agent out of the foam. In this paper an apparatus is described for measuring the effective or apparent diffusion coefficient of atmospheric and other rapidly permeating gases in closed-cell polymeric foams. The technique is based on a solution of the transient diffusion equation, which is outlined along with the method of data reduction. The diffusion cell is designed to accommodate cylindrical foam specimens of varying sizes up to 7.6 cm (3 in.) in diameter and up to 5.1 cm (2 in.) thick. Other features of the apparatus include quick and convenient interchange of foam samples as well as automatic data acquisition. Major sources of experimental error are discussed; those aspects of the experimental technique designed to reduce the magnitude of the experimental uncertainty are also mentioned.

Results obtained with the apparatus for a number of different foams are presented and discussed in terms of various foam diffusion models described in the literature. Interpretation of the data in this manner gives some insight into the cellular structure of the foam and also provides a correlation for estimating the diffusion coefficient of other gases in the foam sample.

KEY WORDS: foam aging, thermal insulation, diffusion, permeability, chlorofluorocarbons

Low density polymeric foams have found wide application as thermal insulation materials in the building, construction and appliance industries owing to their unique combination of properties which range from excellent insulation efficiency to ease of manufacture and installation. The insulation efficiency or low thermal conductivity of these materials arises from the entrapment of a very low thermal conductivity vapor (generally a fluorocarbon) in a matrix of closed cells which are sufficiently small in size as to essentially inhibit convective heat transfer. The mechanisms of heat transfer through the foam are thence relegated to conduction through the continuous but tortuous polymer network, to gas phase conduction across the cell, and to radiative energy transfer. The thermal conductivity of the gas or vapor trapped in the cells represents an important contribution to the overall foam thermal conductivity, because about 50% of the heat transfer through the foam occurs by conduction through the gas phase. However, as the polymer cell wall is permeable to atmospheric gases, the low thermal conductivity fluorocarbon contained in the foam cells will become diluted with higher thermal conductivity air as it diffuses into the foam. The fluorocarbon expansion agent also permeates the cell walls and escapes from the foam, although generally at a much lower rate than the air influx. The foam aging phenomenon is therefore characterized by a relatively rapid increase in thermal conductivity due to the influx of air followed by a much slower asymptotic approach to the fully aged thermal conductivity attained when the foam is completely depleted of fluorocarbon.

¹Allied Signal Inc., Buffalo Research Laboratory, Buffalo, NY 14210.

It has been demonstrated [1,2] that it is possible to reliably estimate the aged foam thermal conductivity if the apparent or effective diffusion coefficients of the atmospheric gases and the fluorocarbon blowing agent are known. Furthermore, recent work by Glicksman et al. [2,3] has demonstrated that the effective diffusion coefficient can be related to both the polymer wall permeability and an accurate description of the foam geometry. This ability to predict aging rates from the basic polymer permeability and from measurements of the foam structure represents a very powerful tool which can be used to investigate and understand the effects of foam structure and polymer chemistry on the aging rate. At Allied-Signal we have employed a similar foam aging model to investigate the aging characteristics of insulation foams expanded with stratospherically safe fluorocarbons such as R-123 (CHCl_2CF_3), R-123a (CHClFCClF_2), R-141b (CFCl_2CH_3), R-134a ($\text{CF}_3\text{CH}_2\text{F}$) and R-124 (CClHFCF_3). As these fluorocarbons possess different vapor thermal conductivities and different polymer permeabilities than the conventional chlorofluorocarbon blowing agents, R-11 (CCl_3F) and R-12 (CCl_2F_2), it would be expected that foams expanded with these fluids would possess different initial thermal conductivities as well as different long term aging characteristics.

The purpose of this paper is to describe an apparatus which has been used to measure the effective diffusion coefficients of gases such as CO_2 , N_2 , O_2 , or other rapidly diffusing gases in polymeric foams. Experimental data obtained with this apparatus are correlated in a form suggested by published foam diffusion models. These correlations can be used to estimate the effective diffusion coefficients of other gases (e.g., the much slower diffusing fluorocarbons) for use in the foam aging model. Diffusion data are presented for some of the common thermoset and extruded thermoplastic foams. These results suggest that the two types of closed-cell foam possess differences in cell geometry, a conclusion supported by earlier foam morphology studies.

Experimental Method

Published techniques for measuring the diffusion of gases in foams can be divided into three general classes: (1) gas transmission methods [1,3-6], where a pressure gradient is imposed across a foam sample and the quantity of gas passing through the foam is measured; (2) quantitative analysis of cell gas compositions [7] present in the foam at a known foam age; and (3) measurement of out-gassing rates [8,9] from foam samples as a function of time. The method discussed in this paper belongs to the first category, being a gas transmission technique. It assumes that the foam behaves as a continuum and that the diffusion process can be characterized through use of an effective or apparent diffusion coefficient, D_{eff} .

Two types of gas transmission technique are possible: (1) the steady-state method such as that employed by Lee and Brown [4], Mehta and Colombo [6], and Ostrogorsky et al. [3], and (2) a transient technique as described in this paper. Although the latter technique is somewhat more complicated to implement, it can provide diffusion coefficient data in a shorter time span than the steady-state method.

The diffusion cell is shown schematically in Fig. 1. One surface of the foam sample, at $X = 0$, is exposed to a constant pressure of the diffusing gas, P_0 , while the other surface, at $X = L$, opens into a finite volume, V . As the gas diffuses through the foam it collects in this exit volume causing the pressure, $P(t)$, to increase until it attains the value P_0 . If we assume that the foam obeys Henry's law (i.e., the concentration of gas, C , dissolved in the foam is proportional to the applied pressure), then the boundary conditions are

$$C(0, t) = (k_{\text{eff}}/RT)P_0 \quad (1)$$

$$C(L, t) = (k_{\text{eff}}/RT)P(t) \quad (2)$$

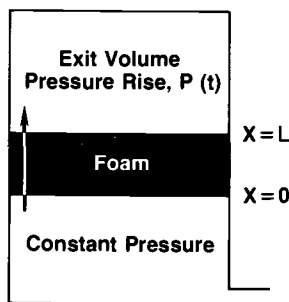


FIG. 1—Diffusion cell schematic.

where k_{eff} denotes the effective Henry's law (or solubility) coefficient for the foam, R denotes the gas constant and T the absolute temperature. When the gas is ideal this definition of solubility reduces to $k_{\text{eff}} = C_{\text{foam}}/C_{\text{gas}}$, the ratio of the concentration of gas in the foam to its concentration in the gas phase (for an ideal gas $C_{\text{gas}} = P/RT$); k_{eff} is more correctly the Bunsen absorption coefficient [12] rather than the Henry's law coefficient. If the foam initially contains none of the diffusing gas, then the initial condition is given by

$$C(X, 0) = 0 \quad (3)$$

The rate of change of pressure in the exit compartment is related to the flux at $X = L$ according to

$$\frac{dP}{dt} = -RT \left(\frac{D_{\text{eff}} A}{V} \right) \left(\frac{\partial C}{\partial X} \right)_{X=L} \quad (4)$$

where A denotes the surface area of the foam. The solution of the diffusion equation:

$$\frac{\partial C}{\partial t} = D_{\text{eff}} \left(\frac{\partial^2 C}{\partial X^2} \right) \quad (5)$$

subject to the above conditions is readily obtained by taking the Laplace transform. The exit compartment pressure rise, $P(t)$:

$$\frac{P(t)}{P_0} = 1 - \sum_{r=1}^{\infty} B_r \exp[-q_r^2 D_{\text{eff}} t / L^2] \quad (6)$$

is obtained from Eq 4 using the solution for $C(X, t)$ [10, 11]. The coefficients, B_r , in this equation are given by

$$B_r = \frac{2\alpha(-1)^{r+1} \sqrt{q_r^2 + \alpha^2}}{q_r[\alpha(\alpha + 1) + q_r^2]} \quad (7)$$

where q_r are the successive roots of

$$q_r \tan q_r = \alpha \quad (8)$$

$$\alpha = k_{\text{eff}} AL / V \quad (9)$$

This treatment of gas diffusion in a closed-foam, as do all others which employ an apparent or effective diffusion coefficient, assumes that the foam behaves as a hypothetical continuous solid where the effective diffusion coefficient is independent of concentration of the diffusing species. However, diffusion through the polymer phase of the foam can be strongly influenced by the concentration of the diffusing species especially where the solubility in the polymer is great. Foam diffusion measurements reported here were performed for gases like O_2 , N_2 and CO_2 which are only sparingly soluble in polystyrene, polyethylene or polyurethane under the measurement conditions; in the case of the fluorocarbon blowing agent this need not be the case. The extent to which the polymer phase diffusion coefficient (and permeability) for fluorocarbons in these types of foams is affected by concentration has not been studied to our knowledge.

In order to measure D_{eff} it is necessary to measure the exit compartment pressure rise, $P(t)$, versus time. These data are fitted to Eq 6 using a nonlinear regression technique to obtain the optimum value of D_{eff} . Before this curve fitting can be performed, the area and thickness of the foam specimen, the volume of the exit compartment, and the effective solubility of the gas in the foam must be specified. The physical dimensions are readily measured, while the effective solubility can be estimated using

$$k_{\text{eff}} = \phi_g + (1 - \phi_g)k/RT \quad (10)$$

where ϕ_g is the gas phase volume fraction of the foam and k is the solubility coefficient for the polymer which is defined in a manner analogous to k_{eff} . In deriving this expression it is assumed that the gas behaves ideally. For low density foams $\phi_g \approx 1$ and, unless the gas is very soluble in the polymer, $k_{\text{eff}} \approx 1$.

This particular solution of the diffusion equation was derived for the initial condition corresponding to zero concentration in the foam. It can be easily modified to account for the situation where the foam initially contains a uniform concentration of the diffusing gas or if the exit volume already contains some of the diffusing gas at time zero. These particular initial conditions may apply when the diffusing gas is an atmospheric component and the foam is already saturated with air.

Apparatus and Technique

The foam diffusion apparatus employed in this work is illustrated in Fig. 2. The cell consists of a cylindrical foam specimen mounted in an annular shaped sample holder which is clamped between two circular metal plates. The volume defined by the top surface of the foam and the top plate (including the internal volume of the attached pressure transducer) is the exit volume. The foam is sealed into the aluminum holder using a slow curing epoxy resin (Hobypoxy H52, Pettit Paint Co.), completely filling the gap between the cylindrical foam surface and the inside surface of the holder. Care is exercised when filling this gap so as not to overflow the epoxy onto the end surfaces of the foam. Measurements of the foam diameter and thickness are made prior to sealing it into the sample holder. Foam samples up to 5.1 cm (2 in.) thick and 7.6 cm (3 in.) in diameter can be accommodated in the current diffusion cell. The sample holder is inserted into the cell by clamping it between the two plates; O-ring seals which contact the aluminum surface of the holder provide a positive and pressure tight seal. This sample holder construction allows for quick, convenient interchange of foam specimens. Foam samples were allowed to reach equilibrium with the atmospheric gases before being used, ensuring the foam cells contained one atmosphere of air in addition to residual fluorocarbon vapor. The exit compartment volume was measured using a gas burette before the start of each experiment. For 2.54 cm (1 in.) diameter foam samples this volume was typically 27.3 cm³. The smaller this volume the more rapid is the exit pressure rise; however, a compromise must be struck between using a very small volume and the relative error with which the volume can be measured. Uncertainty in the vol-

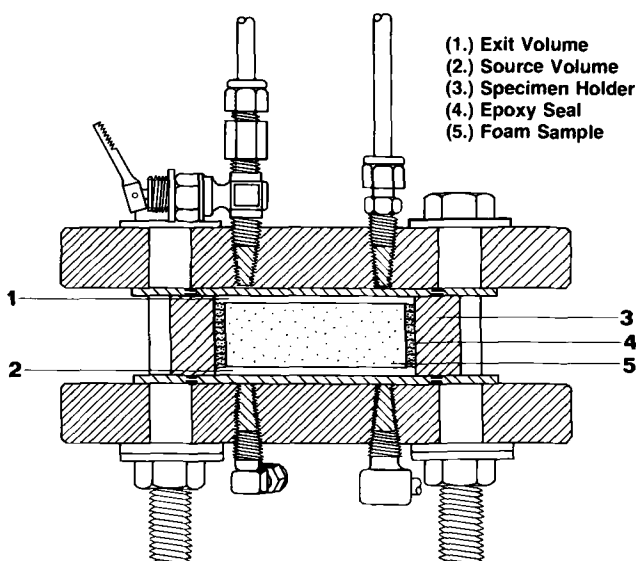


FIG. 2—Diffusion cell construction.

ume measurement is believed to be less than $\pm 0.2 \text{ cm}^3$. A similar compromise must be reached in the choice of specimen thickness. A smaller value of L facilitates a more rapid experiment; however, there must be a minimum thickness below which the assumption that the foam behaves as continuum becomes suspect and below which the foam may not be physically strong enough to support the imposed pressure gradient. Effects arising from the layer of ruptured cells at the foam surface may also become significant for small thicknesses. The continuum assumption is reasonable for foams 20 or more cells thick [5], and in practice thicknesses in the range 12 to 25 mm (0.5 to 1.0 in.) were employed.

The source compartment of the diffusion cell is connected to a regulated supply of test gas and a 0 to 207 kPa (30 psia) pressure transducer. A small bleed of test gas is maintained through the source compartment using a needle valve. The 0 to 5 V output of the pressure transducer, in addition to providing a measure of the source pressure P_0 , is used to control a solenoid valve for regulating the flow of test gas into the compartment. This mechanism provides source pressure control to within $\pm 0.2 \text{ kPa}$ ($\pm 0.03 \text{ psi}$). The source compartment is evacuated prior to admitting the test gas to initiate an experiment. Source pressures of 55 to 200 kPa (8 to 30 psia) were typically used.

The exit pressure rise is monitored using a 0 to 35 kPa (0 to 5 psi) transducer which measures relative to atmospheric pressure; only the first 35 kPa (5 psi) pressure rise is measured in each experiment. The exit volume is not evacuated before starting a run, rather it contains air at the barometric pressure prevailing at the start of the run. Use of a relative gage pressure transducer requires measurement of the barometric pressure each time the exit pressure is measured during an experiment. One of the reasons for adopting this practice was to minimize the pressure difference between the exit volume and the environment, thus minimizing the effect of a leak in the exit compartment. If the exit compartment were evacuated at the start and only the first 35 kPa (5 psi) pressure rise is monitored, the exit pressure would be less than the atmospheric pressure by at least 67 kPa (9.5 psi). This is almost double the difference between the exit pressure and the atmosphere experienced when the compartment is not evacuated at the start.

An experiment is initiated by imposing the test gas pressure gradient across the foam and isolating the exit compartment from the atmosphere. If the test gas is not an atmospheric com-

ponent, or is only present as a trace in the atmosphere, then the foam and the exit compartment contain essentially no test gas, which is consistent with the initial conditions assumed in deriving the working equation (Eq 6). At the start of the experiment the atmospheric gases in the exit compartment are in equilibrium with the atmospheric gases contained in the foam; however, as the source compartment does not contain any air there is a partial pressure or concentration gradient causing diffusion of air towards the source compartment, in the opposite direction to the diffusion of test gas. Back diffusion of air could be eliminated if the source compartment contained 1 atm of air in addition to the test gas. This was not feasible in the present setup, since a slow bleed of test gas was maintained through the source compartment to effect pressure control. For most of the work reported in this paper the back-diffusion of air was neglected because the test gas diffused significantly faster than the atmospheric gases. When measuring the diffusion coefficient of O_2 or N_2 the measured pressure rise may have to be corrected for the back-diffusion of the other species. In this instance the diffusion coefficient of O_2 , which generally diffuses faster than N_2 , would be measured first, neglecting the back-diffusion of N_2 . A N_2 diffusion experiment could then be performed correcting the data for O_2 back-diffusion using the previously measured diffusion coefficient. The corrections are applied using an equation analogous to Eq 6 but modified to reflect the appropriate boundary conditions.

The diffusion cell is submerged in a thermostat bath controlled to within $\pm 0.02^\circ C$. Pressure transducer outputs (source pressure, exit pressure and barometric pressure) are recorded at regular intervals (5 min–1 h) using an automated data acquisition system. The duration of a typical experiment can vary from two days to four weeks depending on the particular choice of foam, test gas, sample size and source pressure. Pressure versus time data are stored in a computer file and are readily accessible for on-line analysis by the non-linear regression software. Typical pressure rise data for a three-day duration experiment are shown in Fig. 3. The data exhibit a time-lag of about 7 h before the pressure starts to increase. This time-lag arises when the test gas must diffuse through the foam before it begins to collect in the exit compartment. Data were collected about every 15 min during this experiment and were fitted to Eq 6 to obtain the optimum value for D_{eff} ; the inset graph in Fig. 3 depicts the deviations between the measured and fitted pressure rise data. Large, systematic deviations are indicative of a leak or some other source of experimental error. The standard deviation of the fit to Eq 6 is typically 0.13 to 0.25 kPa (0.02 to 0.04 psi).

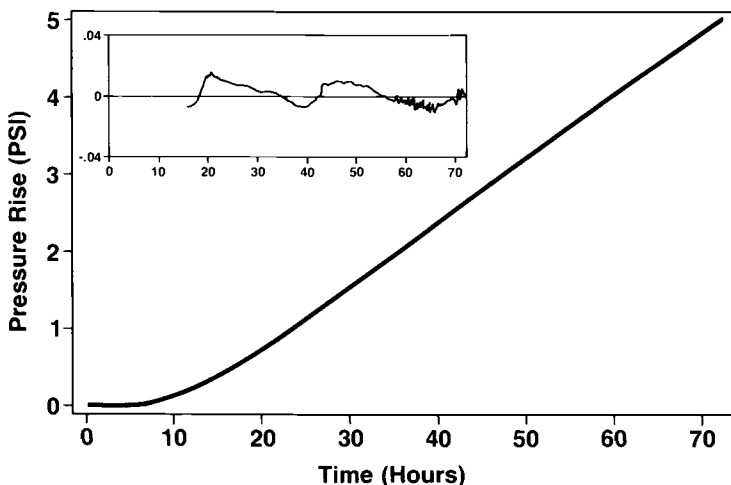


FIG. 3—Typical exit pressure rise versus time. Inset plot depicts the deviations between the measured pressure rise and values fitted to Eq 6. (Multiply 1 psia by 6.8947 to obtain kPa.)

When an experiment is completed the sample holder is removed from the cell and another inserted to begin a new run. The removed sample now contains test gas in addition to blowing agent and atmospheric gases; it may be re-used after an appropriate interval of time during which the test gas diffuses out of the foam and equilibrium with the atmosphere is re-attained.

Precision and Accuracy

The experimental precision attainable with the present technique is typically $\pm 2\%$ for measurements using the same foam specimen. This estimate was obtained from the reproducibility of repeated measurements on the same foam sample (Table 1). Sample-to-sample precision is estimated at $\pm 5\%$ from the reproducibility of measurements on different foam samples. The difference between the two precisions arises principally because diffusion measurements on different foam specimens are burdened with a systematic errors stemming from the uncertainties associated with the measurements of L , A and V . Another, more subtle, reason for the difference is due to the fact that each foam sample, although cut from the same board, may have a slightly different cell structure (e.g., there may be more open cells in one specimen than another). This type of difference is minimized when foam specimens consist of a sufficiently large number of cells, another reason for using thicker foam samples.

Other sources of experimental error are more difficult to quantify. One source of uncertainty which must be guarded against in the present technique is the presence of a leak in the exit compartment or a gas leak through the epoxy seal around the foam. The exit compartment was tested for leaks by inserting a solid aluminum disk into the cell rather than a conventional sample holder and increasing the pressure in the compartment to about 35 kPa (5 psi) above atmospheric pressure, the maximum achieved in any experiment. This pressure was monitored for eight to nine days and showed no significant decrease through leakage (Fig. 4). Excursions of ± 0.21 kPa (± 0.03 psi) caused by the effect of 110 V line variations on the electronic transducers were evident during the test (we have an electrically very noisy laboratory). The epoxy seal material was evaluated by sealing a solid aluminum cylinder into a sample holder instead of a foam specimen and performing a typical experiment using the maximum source pressure, 207 kPa (30 psi). Figure 4 shows that the exit pressure did not rise during the seven-day test period, indicating that the epoxy was impervious to the test gas (helium in this case).

The possibility that the pressure gradient imposed across the foam could damage the cell structure by rupturing cell walls leading to an erroneously high diffusion coefficient must also be admitted. Pressures routinely employed varied from 55 to 207 kPa (15 to 30 psi) on the source side to 103 to 138 kPa (15 to 20 psi) total pressure on the exit side. The effect of source pressure

TABLE 1—*Experimental precision of helium diffusion in 34.8 kg m^{-3} extruded polystyrene foam.*

Foam Sample	T (°C)	$10^5 D_{\text{eff}}$ ($\text{cm}^2 \text{ s}^{-1}$)
3	25.07	1.65
3	25.07	1.72
3	25.07	1.66
3	25.00	1.70
Single sample precision = $\pm 2\%$		
1	50.07	3.52
2	50.05	3.62
7	50.00	3.23
Sample-to-sample precision = $\pm 5\%$		

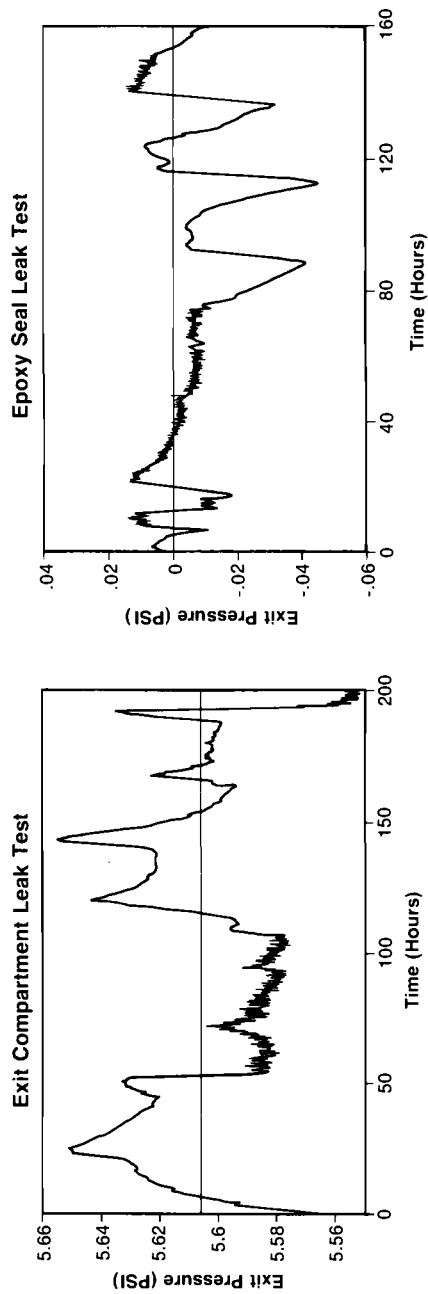


FIG. 4—(left) Pressure maintained in the exit compartment during a leak test. (right) Leak test of epoxy seal material. No significant pressure rise is detected, which implies that the epoxy material is impervious to the test gas. (Multiply 1 psia by 6.8947 to obtain kPa.)

on the measured diffusion coefficient was determined by performing experiments with source pressures varying from 55.2 kPa (8 psi) to 207 kPa (30 psi) using the same test gas (in this case helium) and the same sample of foam taken from a 2.54 cm (1 in.) thick, 25.6 kg m⁻³ (1.6 lb/ft³) polyisocyanurate board. Experiments were performed in increasing order of source pressure. The results, depicted in Fig. 5, show that D_{eff} was independent of the source pressure over this range, implying negligible cell damage due to the pressure gradient.

The overall accuracy of the effective diffusion coefficient measurement is difficult to define, although we believe that $\pm 10\%$ is a conservative estimation for the present method.

Treatment of Data

Before discussing the experimental data it is appropriate to give a brief summary of some of the theoretical treatments of gas diffusion in closed-cell foams. Perhaps the simplest physical model of a low density closed-cell foam is a three-dimensional array of identical cubic cells. The effective diffusion coefficient for a gas diffusing through this type of structure was first derived by Barrer and Petropoulos in 1961 [13] and re-derived in a variety of forms [1,5,8] since then. The cubic cell result can be written as

$$D_{\text{eff}} = \left(\frac{d}{\ell} \right) \left[\frac{P_{\text{stp}} T}{T_{\text{stp}}} \right] P_e \quad (11)$$

where d denotes the distance between opposite cell faces, ℓ denotes the cell wall thickness, P_e the polymer wall permeability expressed in cm³(STP)cm/cm² s cmHg, P_{stp} denotes the pressure at STP conditions (76 cmHg), T denotes the absolute temperature, and $T_{\text{stp}} = 273.15$ K. The ratio, (d/ℓ) , for a lattice consisting of a large number of cells is given by

$$(d/\ell) = \left[\phi_g^{-1/3} - 1 \right]^{-1} \quad (12)$$

where the gas phase volume fraction can be computed from the polymer density ρ_p , the foam density ρ_f , and the gas phase density ρ_g :

$$\phi_g = \frac{\rho_p - \rho_f}{\rho_p - \rho_g} \quad (13)$$

Equation 13 is applicable to all foams, not only to a hypothetical lattice of cubes.

A modification of the cubic cell expression which attempts to account for the actual distribution of polymer material between the struts and windows has been suggested by Reitz et al. [1]:

$$D_{\text{eff}} = 3.46\beta \frac{100}{w} \frac{\rho_p - \rho_f}{\rho_f - \rho_g} \left[\frac{P_{\text{stp}} T}{T_{\text{stp}}} \right] P_e \quad (14)$$

Here w denotes the percentage of polymer present in the cell windows (which must be measured) and β is the cell stagger factor ($1 \leq \beta \leq 2$). A more recent result due to Ostrogorsky, Glicksman and Reitz [3] states that

$$D_{\text{eff}} = \frac{2\langle d \rangle}{\ell} \left[\frac{P_{\text{stp}} T}{P_{\text{stp}}} \right] P_e \quad (15)$$

where $\langle d \rangle$ is the average distance between successive cell windows and ℓ is the average wall thickness. Both quantities are derived from accurate cell geometry measurements.

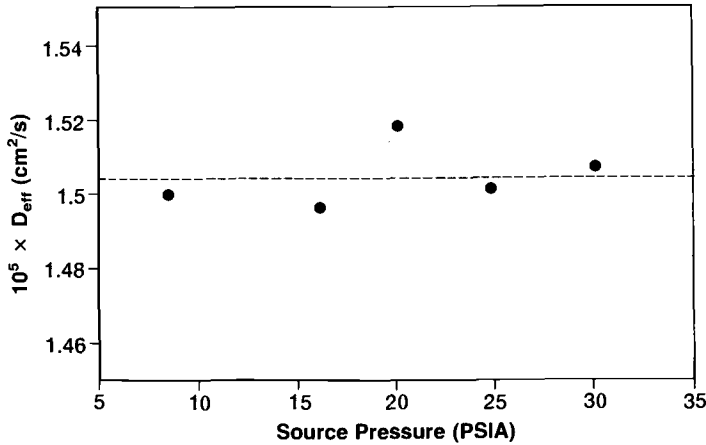


FIG. 5—Effect of source pressure on the measured diffusion coefficient for a 2.54 cm thick, 25.6 kg m^{-3} polyisocyanurate foam sample. (Multiply 1 psia by 6.8947 to obtain kPa.)

The three results for D_{eff} (Eqs 12, 14 and 15) have in common that they can be expressed in the form

$$D_{\text{eff}} = G \left[\frac{P_{\text{stp}} T}{T_{\text{stp}}} \right] P_e \quad (16)$$

where G is a quantity related to cell geometry or structure. This equation represents a convenient way to summarize experimental foam diffusion coefficient data, since a plot of \bar{D}_{eff} for a number of gases in the same foam versus $[P_{\text{stp}} T / T_{\text{stp}}] P_e$ should be linear with the slope being a measure of G . This value could be compared with the hypothetical cubic cell result $G = d/\ell$ or, if morphological data are available, with the result of Ostrogorsky et al., $G = 2\langle d \rangle/\ell$.

Results and Discussion

Effective diffusion coefficient data for two extruded polystyrene foams, an extruded low density polyethylene foam and a rigid polyurethane foam, are summarized in Tables 2 to 5 and Figs. 6 to 8. Each of the diffusion coefficients reported in these tables is the average of at least

TABLE 2—2.54 cm thick, 34.8 kg m^{-3} extruded polystyrene results.

Test Gas	T (°C)	$10^{10} P_e^*$ ($\text{cm}^3(\text{STP})\text{cm}/\text{cm}^2 \text{ s cmHg}$)	$10^5 D_{\text{eff}}$ ($\text{cm}^2 \text{ s}^{-1}$)
He	25.05	19.6	1.68
	30.12	21.6	2.10
	40.05	25.7	2.72
	50.05	30.3	3.46
CO ₂	25.07	11.8	0.91
	50.04	14.1	1.54
O ₂	50.10	4.21	0.45

*Multiply by 29.86×10^{-3} to convert to $\text{fmol}/\text{m}^2 \text{ s Pa}$.

TABLE 3—1.65 mm thick, 87.5 kg m⁻³ extruded polystyrene results.

Test Gas	<i>T</i> (°C)	10 ¹⁰ <i>P_e</i> * (cm ³ (STP)cm/cm ² s cmHg)	10 ⁵ <i>D_{eff}</i> (cm ² s ⁻¹)
He	25.15	19.6	0.623
	40.05	25.7	0.808
	49.98	30.3	0.986
CO ₂	25.01	11.8	0.276
	50.00	14.1	0.490

*Multiply by 29.86 × 10⁻³ to convert to fmol/m² s Pa.TABLE 4—2.54 cm thick, 24.0 kg m⁻³ extruded polyethylene results.

Test Gas	<i>T</i> (°C)	10 ¹⁰ <i>P_e</i> * (cm ³ (STP)cm/cm ² s cmHg)	10 ⁵ <i>D_{eff}</i> (cm ² s ⁻¹)
He	25.00	7.66	1.04
	39.91	14.6	2.31
CO ₂	25.01	18.8	2.06
	29.89	22.8	3.46
	34.92	27.5	4.52
	39.96	33.0	6.05
	45.02	39.4	6.15
	50.06	46.8	9.20

*Multiply by 29.86 × 10⁻³ to convert to fmol/m² s Pa.TABLE 5—2.54 cm thick, 27.2 kg m⁻³ rigid urethane results.

Test Gas	<i>T</i> (°C)	10 ¹⁰ <i>P_e</i> * (cm ³ (STP)cm/cm ² s cmHg)	10 ⁵ <i>D_{eff}</i> (cm ² s ⁻¹)
He	25.13	2.32	1.78
	30.14	2.71	2.16
	40.16	3.62	2.97
	50.03	4.74	4.10
CO ₂	25.20	0.36	0.135
Ne	50.09	1.01	0.561

*Multiply by 29.86 × 10⁻³ to convert to fmol/m² s Pa.

two measurements. All experiments were performed using approximately 2.5 cm (1 in.) thick samples, except for one of the polystyrene foams which was 1.65 mm (0.065 in.) thick. The 27.2 kg m⁻³ (1.7 lb/ft³) rigid urethane foam was based on an MDI formulation and was expanded with R-11. The polystyrene foams were expanded with R-12 and possessed densities of 34.8 kg m⁻³ (2.7 lb/ft³) and 87.5 kg m⁻³ (5.5 lb/ft³). Both foams were used with the naturally occurring surface densification intact. The polyethylene foam was blown with a mixture of R-12 and R-114 and had a density of 24.0 kg m⁻³ (1.5 lb/ft³). The test gases used in this work consisted of CO₂, O₂, He and Ne, which were chosen for their ability to diffuse rapidly through the various polymers.

Tables 2 to 5 also include the test gas permeability in the different polymers; these were measured using a conventional variable pressure gas transmission cell (ASTM D 1434). The operation of this instrument was verified using the National Bureau of Standards (NBS) Reference

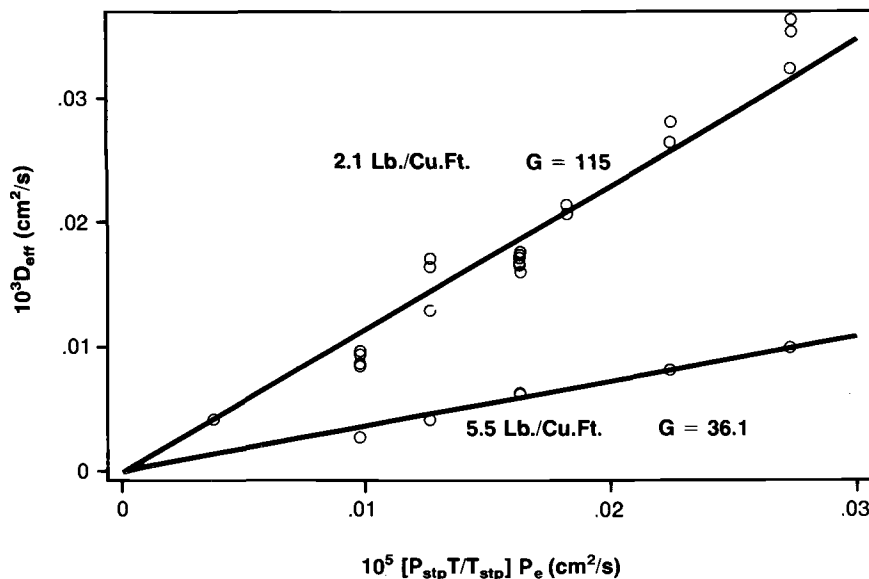


FIG. 6—Effective diffusion coefficient data versus polymer permeability for two extruded polystyrene foams.

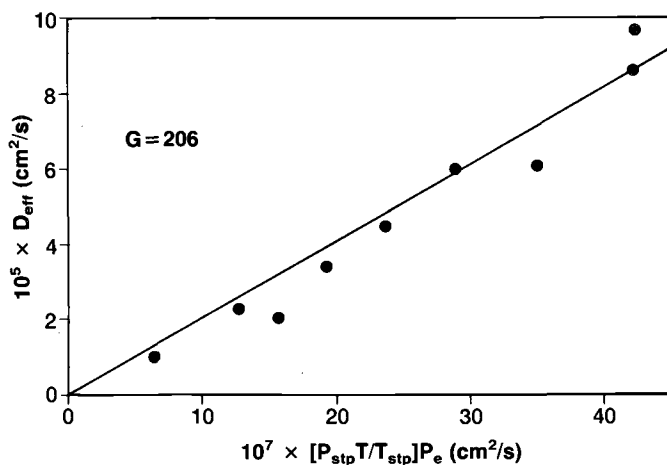


FIG. 7—Effective diffusion coefficient data versus polymer permeability for an extruded polyethylene foam.

Material 1470, a standardized polyester material of well defined permeance [14]. We were able to reproduce the NBS data to within $\pm 2\%$. Diffusion measurements on the 1.65 mm polystyrene sheet foam were performed using the polymer film gas transmission apparatus rather than the foam diffusion cell.

In order to test Eq 16 with experimental data we have assumed that polymer film material used to determine P_e in the film permeation experiment is substantially the same as the polymer window material in the foam. This assumption is reasonable for the thermoplastics like polysty-

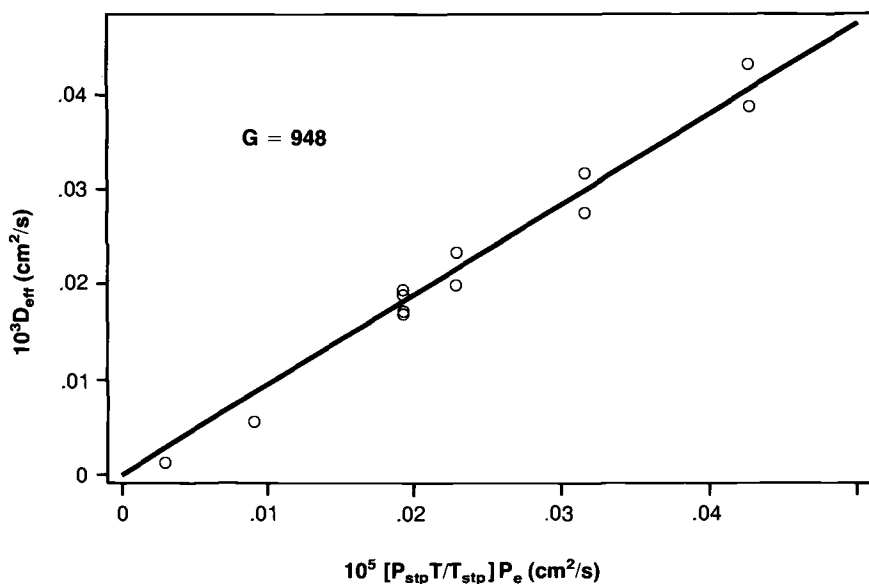


FIG. 8—Effective diffusion coefficient data versus polymer permeability for a rigid urethane foam.

rene where the Dow Chemical T-1000 film was supplied as being representative of the polystyrene resin used in extruded foam manufacture. It must be recognized, however, that there could be differences in orientation due to the different mechanisms of film and foam manufacture. The problem is more serious for the rigid urethane film which was made from the same formulation as the foam except for the presence of blowing agent. The thermal history of the film and foam material is different, and it must be admitted that there may be differences in the polyurethane chemistry. Infrared spectra of the polyurethane foam and film polymers were very similar except for slightly more unreacted isocyanate present in the film.

Inspection of Figs. 6 to 8 shows that the plot of D_{eff} versus $[P_{\text{stp}} T/T_{\text{stp}}] P_e$ is linear within the experimental precision as implied by Eq 16; values of G obtained from these plots are listed in Table 6. These linear relationships confirm the general form of the foam diffusion model and also constitute a correlation for each of the foams which can be used to estimate D_{eff} for other gases using polymer permeability data. Although the correlations based on these G values are specific to the foams studied here, the overall procedure can be simplified and applied to any closed-cell foam. One approach would be to use a foam diffusion apparatus to measure D_{eff} for a rapidly diffusing gas such as CO_2 or He, measure its permeability in the polymer material, and then compute G according to Eq 16. Diffusion coefficients of other gases in the foam are estimated using this value of G and the polymer permeability. This estimation procedure is an

TABLE 6—Cell geometry factors.

Foam	Density (kg m^{-3})	ϕ_g	G (Cubic Cell)	G (Measured)
Polystyrene	34.8	0.974	113.4	115.
Polystyrene	87.5	0.917	34.1	36.1
Polyurethane	27.2	0.983	174.5	948.
Polyethylene	24.0	0.979	140.9	206.

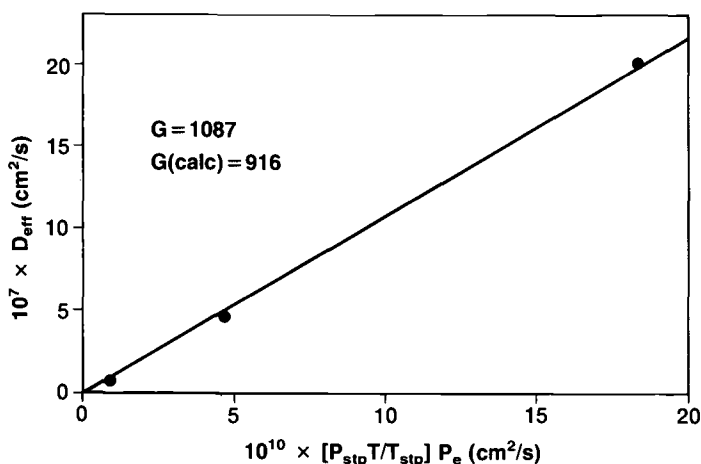


FIG. 9—Effective diffusion coefficient data for a rigid polyurethane foam. Data reported by Ostrogorsky *et al.* [3] are plotted and evaluated according to Eq 16. $G(\text{calc})$ is computed using the scheme reported by the same authors.

alternative to that of Ostrogorsky *et al.* [3] and can be used when detailed foam morphology data are unavailable.

We are presently unable to compare the measured foam geometry factors with the calculations based on the more realistic foam diffusion models of Glicksman and co-workers [1,3] due to a lack of reliable morphology data. Nevertheless, it is interesting to compare the measured G values with those calculated from the albeit, unrealistic cubic cell result. Table 6 lists both sets of data for the foams studied here. Agreement between the measured and calculated results is reasonable for the thermoplastic foams (polystyrene and polyethylene); however, there is a significant difference in the case of the polyurethane foam. This comparison suggests a difference in cell structure between thermoplastic and thermoset foams, a conclusion supported by earlier cell structure studies. Reitz [1] has shown that the cell windows in a typical rigid urethane foam contain only 10 to 20% of the total polymer material; the rest is concentrated in the struts. Consequently, the cell windows will be thinner than the simplistic cubic cell calculation would imply and the real G value would be greater than the cubic cell result which agrees with the data of Table 6. In the case of thermoplastic foams the cell structure has been characterized by Throne and Progelhof [15] and Benning [16] as a principally window-like structure as opposed to the principally strut-like structure of rigid urethane foams. The more even distribution of polymer between windows and struts in thermoplastic foams is perhaps the reason for the seemingly better agreement between calculated and measured values seen in Table 6.

Comparison of the present measurements with other work is difficult given the dearth of reliable foam diffusion data. However, data for a 25.2 kg m^{-3} density urethane foam reported by Ostrogorsky, Glicksman and Reitz [3] can also be represented in a manner similar to the present results (Fig. 9). The value of G obtained from this plot is 1087, very similar to the value of 948 obtained for the urethane foam studied here. Although indirect, this evidence supports the experimental methods employed in each case.

References

- [1] Reitz, D. W., Schuetz, M. A., and Glicksman, L. R., *Journal of Cellular Plastics*, Vol. 20, March/April 1984, pp. 104-113.
- [2] Schuetz, M. A., "Heat Transfer in Foam Insulations," M.S. thesis, Dept. of Mechanical Engineering, Massachusetts Institute of Technology, Cambridge, 1982.

- [3] Ostrogorsky, A. G., Glicksman, L. R., and Reitz, D. W., *International Journal of Heat Mass Transfer*, Vol. 29, No. 8, 1986, pp. 1169-1176.
- [4] Lee, W. M. and Brown, C. N. in *Proceedings*, SPI 27th Annual Technical/Marketing Conference, 1982, pp. 285-289.
- [5] Shankland, I. R. in *Advances in Foam Aging*, D. A. Brandreth, Ed., Caissa Editions, 1986, pp. 60-88.
- [6] Mehta, B. S. and Colombo, E. A., *Society of Plastics Engineers, Technical Papers*, Vol. 24, 1978, pp. 689-692.
- [7] Brandreth, D. A. and Ingersoll, H. G., *European Journal of Cellular Plastics*, Vol. 3, Oct. 1980, pp. 134-143.
- [8] Cuddihy, E. F. and Moacanin, J., *Journal of Cellular Plastics*, Vol. 3, 1967, pp. 73-80.
- [9] Khalil, M. A. K. and Rasmussen, *Journal of the Air Pollution Control Association*, Vol. 36, 1986, pp. 159-163.
- [10] Jenkins, R. C., Nelson, P. M., and Spierer, L., *Transactions of the Faraday Society*, Vol. 66, 1970, pp. 1391-1401.
- [11] Barrie, J. A., Spencer, H. G., and Quig, A., *Transactions of the Faraday Society*, Vol. 71, 1975, pp. 2459-2467.
- [12] Hildebrand, J. H., *Solubility of Non-Electrolytes*, 2nd ed., Reinhold, New York, 1936, p. 16.
- [13] Barrer, R. M., *Diffusion in Polymers*, J. Crank and G. S. Park, Eds., Academic Press, New York, 1978, pp. 165-217.
- [14] NBS Standard Reference Material 1470, available from the National Bureau of Standards, Washington, D.C.
- [15] Throne, J. L. and Progelhof, R. C., *Journal of Cellular Plastics*, Vol. 20, Nov./Dec. 1984, pp. 437-441.
- [16] Benning, C. J., *Plastic Foams*, Vol. 1, Wiley-Interscience, New York, 1969, p. 54, p. 129, p. 327.

Foam Insulation Aging: Historical Perspective and Outstanding Problems

REFERENCE: Zwolinski, L. M., "Foam Insulation Aging: Historical Perspective and Outstanding Problems," *Insulation Materials, Testing, and Applications, ASTM STP 1030*, D. L. McElroy and J. F. Kimpflen, Eds., American Society for Testing and Materials, Philadelphia, 1990, pp. 189-196.

ABSTRACT: Rigid polyurethane foam originated in the World War II era. This material, the reaction product of polyisocyanates and hydroxyl-terminated polyols, was originally expanded by *in situ* generation of carbon dioxide during the polyurethane polymerization process. A major improvement in the insulation value of polyurethane foam was effected in the early 1950s by the development of technology to use chlorofluorocarbons (CFCs) as the blowing agent.

This paper presents a historical perspective on the development of rigid polyurethane foam as a superior insulation material. The role of CFC expansion agent will be examined with a review of the early concerns of aging of foam and the accompanying change in insulating property. The effects of blowing agent diffusion, humidity during foam aging, and the aging environment gas on the thermal conductivity of cellular material are detailed. Early attempts to explain heat transfer through rigid cellular structures in terms of conduction, convection and radiation factors are cited.

Attention is focused on problems outstanding to a complete understanding of foam aging. These factors include test methodology, the role of gas diffusion, polymer distribution in a cellular structure, effects of barrier materials, in-service moisture influences, foam structure features, and total insulation-containing structural design.

KEY WORDS: thermal conductivity, polyurethane foam, thermal insulation, chlorofluorocarbon, insulating gases, foam gas diffusion

Rigid polyurethane foams have been important commercial thermal insulating materials for about 40 years. More recently, modified rigid polyisocyanurate foams, prepared by trimerizing polyfunctional isocyanates, have been developed with improved dimensional stability and resistance to flammability. From a modest post-World War II beginning, production volume of these rigid foams now totals about 317 to 341 thousand metric tons (700 to 750 million pounds) per year. However, there is still much to be learned about the insulation properties of these useful materials, particularly as these properties relate to foam aging in in-field situations.

Historical Perspective

While today we have advanced theories on changes in thermal conductivity of aging rigid foams and sophisticated methodology for studying this phenomenon, it is interesting that early investigators had identified many of the causes of thermal conductivity change.

Ball [1] reviewed the components associated with heat transfer of porous materials as previ-

¹Technical Supervisor, Allied-Signal Corporation, Buffalo, NY 14127.

ously established by McIntire and Kennedy in 1948. The general equation for such heat transfer is

$$\lambda = \lambda_G + \lambda_S + \lambda_R + \lambda_C$$

where

- λ = conductivity of the foam,
- λ_G = conductivity through the gaseous phase (conduction),
- λ_S = conductivity through the solid phase (conduction),
- λ_R = radiative transfer through the pores, and
- λ_C = convective transfer through the gaseous phase.

It was shown that convection is a negligible component of heat transfer where foam cell size is small [2-4]. With rigid polyurethane foams mostly in the 0.3 to 1.0 mm range, Ball concluded that convection contributions to heat transfer in such foams is zero. It followed that the principal path of heat transfer in foams was through gas and solid polymer conductance with a smaller, but important, radiative transfer component. This analysis highlights the importance of the original blowing agent used to make the foam and the make-up of the gases in the cells as the foam ages.

Initially, rigid polyurethane foams were based on the reaction of polyester polyols, toluene diisocyanate, and water. Carbon dioxide (CO_2), generated during the polyurethane polymerization, expanded the polymeric mass to a cellular structure. In the late 1950s the utility of chlorofluorocarbons (CFCs), particularly trichlorofluoromethane (CFC-11), as blowing agents accelerated the growth of the rigid polyurethane foam insulation industry. Margedant [5] demonstrated the superior insulating characteristics of CFC-11 versus CO_2 blown foams over the 24 to 64 kg/m^3 (1.5 to 4.0 lb/ft^3) density range (Fig. 1). He also cited the increase in thermal conductivity for CFC-11 expanded foam when aged for 16 weeks at 50°C (Fig. 2). The identifi-

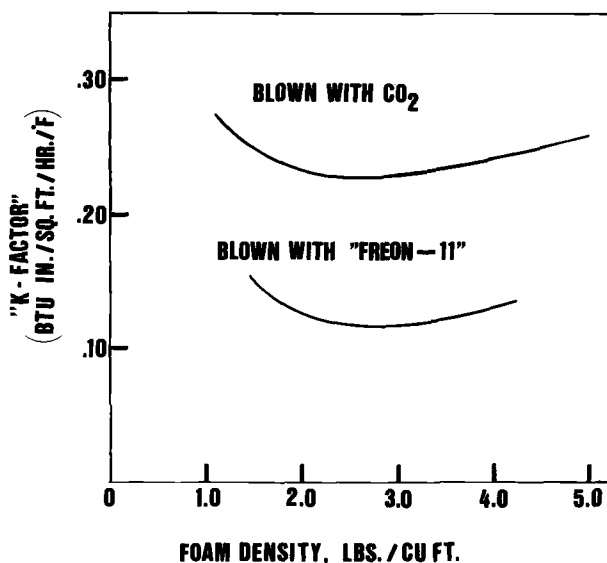


FIG. 1—Comparison of *K*-factors of Freon-blown and conventional carbon dioxide-blown rigid polyester urethane foams [5].

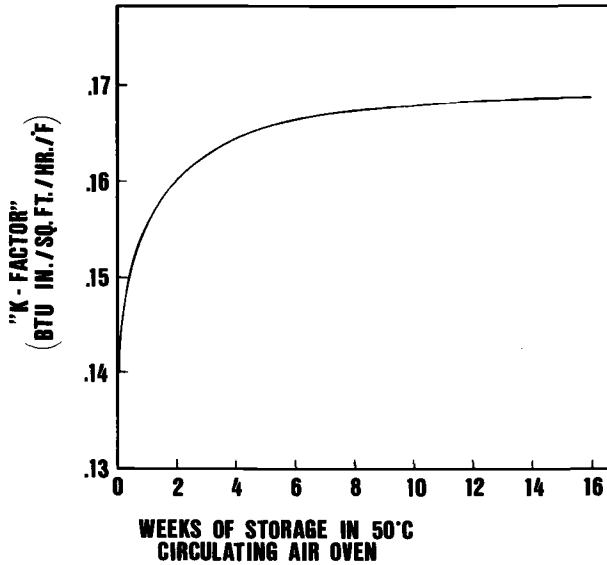


FIG. 2—Effect of accelerated aging on *K*-factor of Freon-expanded rigid urethane foams [5].

cation of the phenomenon of changing insulating properties as foam ages caused a great deal of attention be paid to the nature of the blowing agent choice and to gas diffusion processes.

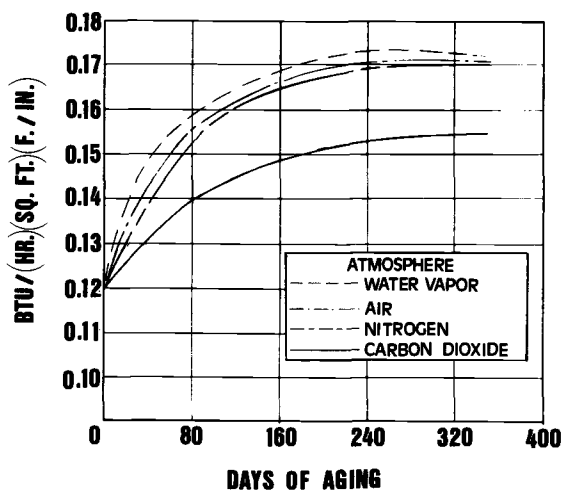
Kaplan [6], Doherty [2], Norton [7], and others showed that the upward drift of the closed-cell rigid polyurethane foam *K*-factor, $\text{btu}/(\text{h})(\text{ft}^2)(^\circ\text{F}/\text{in.})$, was primarily caused by infusion of atmospheric gases (N_2 , O_2 , CO_2 , H_2O) into the foam over time. A study of gas permeation through a model polyurethane film showed great differences in the rates of CFC-11 and atmospheric gases (Table 1). The high permeation rates of the atmospheric gases coupled with their high thermal conductivity offered a sound explanation for observed *K*-factor increase in CFC-11 expanded foams (Table 2). This aging process was experimentally confirmed by Kaplan [6], where CFC-11 blown foams were exposed to different atmospheric gases. The thermal conductivity drift of these foams correlated well with the thermal conductivity of the test gases (Fig. 3). Norton extended this work with an elegant theoretical treatment using diffusion and solubility factors with experimental verifications [7]. More recently a number of investigators have refined this approach to improve on the ability to predict thermal conductivity change as foam ages.

TABLE 1—Permeability of gases through urethane films [6].

	Gas Permeability
	$\frac{\text{cm}^3 \text{ gas (STP)} \times \text{mm}}{\text{s} \times \text{cm}^2 \times \text{cm Hg}}$
Trichlorofluoromethane	0.029×10^{-10}
Nitrogen	0.27×10^{-10}
Air (calc.)	0.43×10^{-10}
Oxygen	1.07×10^{-10}
Carbon dioxide	4.0×10^{-10}
Water vapor	1100×10^{-10}

TABLE 2—*Thermal conductivity of gases and vapors [6].*

$K = \text{btu}/(\text{h})(\text{ft}^2)(^\circ\text{F}/\text{in.})$		
	$^\circ\text{F}$	K
Nitrogen	32	0.168
Air	32	0.168
Oxygen	32	0.170
Carbon dioxide	32	0.102
Water vapor	115	0.144
Trichlorofluoromethane	32	0.068

FIG. 3—*Effect of various atmospheres at 43°C (110°F) on thermal conductivity of one-shot rigid urethane foam [6].*

In addition to simple gas permeation considerations, other factors such as those cited by Varland [8] and Buist [9] are also important in controlling K-factor drift. These factors include cell size, extent of open-cell content, natural or applied skin, temperature during aging, and dimensions of the foam insulation. For example, Varland showed that refrigerators and freezers in which the poured-in-place foam was surrounded by a positive gas barrier (outside metal skin, inside plastic liner) had no foam thermal conductivity change after 40 months because the foam was essentially hermetically sealed. Similarly, it has been shown that small-celled foam retains its original thermal conductivity better than large-celled foam of the same density (Table 3). It may be that polymer distribution is significantly different in a small-celled foam with more polymer in the cell membrane than in a large-celled foam.

CFC Blowing Agents

As mentioned previously, the emergence of rigid polyurethane and polyisocyanurate foams as superior insulation materials took place when CFC blowing agents came into use. Trichlorofluoromethane (CFC-11) and, in some specialty froth foams, dichlorodifluoromethane (CFC-

TABLE 3—Effect of cell size on *K*-factor [9].

Foam No.	Cell Diameter, mm	K-Factor btu/(h)(ft ²)(°F/in.)
1	0.4	0.110
2	0.8	0.120
3	1.2	0.130
4	1.6	0.140

12), not only possessed low vapor thermal conductivity values but had other desirable features. These chemicals have low-order toxicity, low boiling points, and are nonflammable, nonreactive, compatible with liquid foam ingredients, and readily available. The low thermal conductivity of these CFCs is explained, in part, by their high molecular weight. Ball [1] has cited the excellent correlation of thermal conductivity with molecular weight (Fig. 4).

In recent years, there has been concern that the fully-halogenated CFCs may contribute to a decrease in the earth's protective ozone layer. It is theorized that, because these chemicals are so stable, the CFCs slowly migrate into the stratosphere (15 to 40 km above the earth). In the stratosphere the CFCs could then be photolytically decomposed, with the liberated chlorine radical reacting with ozone to destroy this species. Because of concern that reduction of the ozone layer could allow more ultraviolet radiation (UV-B) to reach the earth with possible consequences to human health, aquatic and plant life, and climate, the United States and several other countries have already banned the use of CFCs in most aerosol products. In September 1987 a global agreement was reached to limit, and then reduce, the production of fully-halogenated CFCs for all end uses, including rigid insulating foams. Such action could severely limit

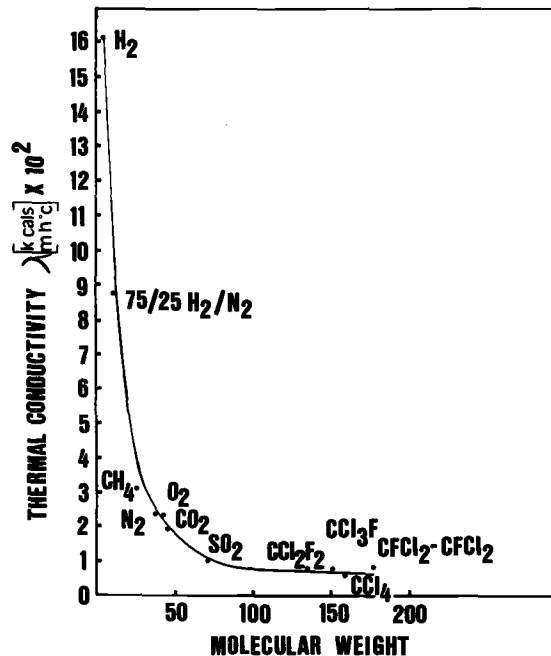


FIG. 4—Thermal conductivity of gases at 24°C: crude relationship between thermal conductivity and molecular weight [1].

the growth of the rigid foam industry, now dependent on CFC-11 and CFC-12 as the blowing agents of choice.

Since the CFC-ozone theory was first published in 1974, the CFC producers have carried out research programs to develop environmentally acceptable substitutes. It is generally agreed that partially-halogenated CFCs, having a carbon-hydrogen bond in the molecular structure, have a short atmospheric lifetime and decompose in the troposphere by reaction with hydroxyl radical. Most work to develop substitutes for rigid foam blowing agents and other applications has been concentrated on species with such a feature. Of course, all the other requirements of an efficient, safe product should also be met. A number of potential replacements for CFC-11 and CFC-12 have been identified and are being evaluated. CFC-123, 1,1,-dichloro-2,2,2-trifluoroethane, boiling point 27.9°C, is one such candidate. Figure 5 shows the vapor thermal conductivity of this species and its position isomer, CFC-123a, 1,2-dichloro-1,2,2-trifluoroethane, compared to CFC-11.

The future need to have environmentally acceptable, low thermal conductivity substitutes for the currently used CFCs is the most pressing problem facing the polyurethane foam insulation industry. Not only must new blowing agents be qualified and produced commercially but the polyurethane and polyisocyanurate polymer, foam structure, and insulation covering (e.g., barrier coverings, coating) must be optimized for these expansion agents.

Test Methodology

The guarded hot plate (ASTM C 177) and the heat flow meter (ASTM C 518) methods have become the most commonly used techniques for measuring insulation thermal conductivity under controlled laboratory conditions. These methods require sample conditioning at prescribed temperature and humidity prior to testing. Because of ease of operation and short testing time, most production operations making rigid polyurethane foam insulation use a commercial heat flow meter apparatus for making quality control thermal conductivity measurements.

Because the heat flow meter method is not a primary measurement technique, a calibration standard is necessary. This standard is National Bureau of Standards (NBS)-supplied fiberglass with a K-factor of about 0.230. For some years it has been questioned whether such a calibration standard is appropriate where rigid polyurethane foam insulation with a K-factor in the

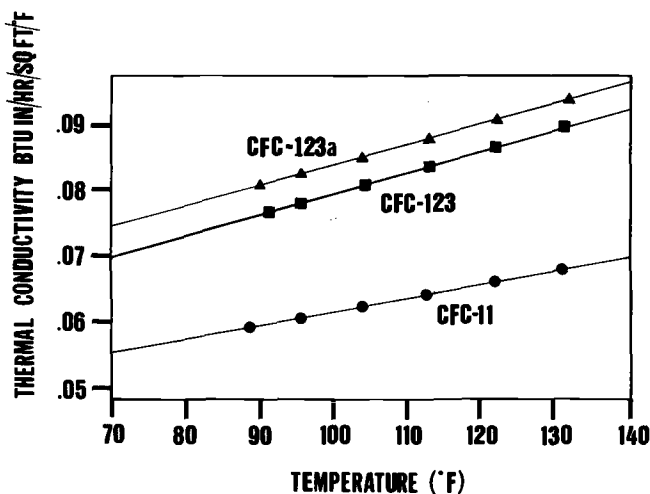


FIG. 5—Vapor thermal conductivity for CFC-11, CFC-123, and CFC-123a.

0.110 to 0.160 range needs to be measured. Thus far; there has been no success in establishing a stable, low K-factor standard as a reference for heat flow meter equipment.

Commercial manufacturers of all home insulation, including rigid polyurethane foam, are obligated by a 1979 Federal Trade Commission (FTC) regulation to label products with a representative thermal resistance value (R-value, $(h)(ft^2)(^{\circ}F)/btu$, at product thickness). ASTM C 518 is a recognized way to measure foam R-value by the FTC. Because of the competition between producers of other insulation (e.g., fiberglass, mineral wool) and the heavy fines possible for misrepresentation of R-values, foam producers are sensitive to the accuracy of measured K-factor (R-value) of their products. Obviously, each insulation manufacturer wants to label his product with the highest possible R-value.

Heat flow meter apparatus, depending on individual design, can be subject to measurement errors due to edge losses as recognized by Bomberg [10] and Coumou [11]. ASTM C 518 procedures call for testing of a homogeneous insulation. In practice, however, the commercial heat flow meter units are used by foam producers to measure thermal insulation values of complete products, including laminated foam insulation with facer sheets. (The 1979 FTC regulation required that foil-faced insulation have the facing removed and R-values obtained on the insulation alone.) The effect of non-foil facer sheets and foam densification at the insulation surfaces may facilitate lateral heat flow during foam testing in a way that could influence thermal resistance values obtained.

In-Field Insulation Performance

Although laboratory thermal conductivity testing of insulating materials provides useful information about the nature of such materials, the resulting data may be misleading in characterizing in-service performance. In construction installations, insulation continues to function under a variety of temperature, humidity, and total assembly conditions. It is of questionable value, for example, to compare the insulation value of different insulating materials under conditioned, laboratory procedures, when such materials may behave very differently when subjected to high-humidity or water environments, or even cold temperatures. In high-humidity conditions, unfaced fiberglass can become quickly saturated while foil-faced foam insulation may remain dry. The practical consequence of such a situation is that wet fiberglass loses a substantial part of its dry insulation property. Similarly, the total insulation-building construction assembly is important to control and predict the long-term temperature conditioning characteristics of a structure. In this regard, for example, protective membranes for roof insulation, ship-lap joints for individual insulation panels, and fastening methods that preserve the integrity of the insulation are all important in insuring that the insulation performs to design specifications. The same insulation can give greatly different total structure insulation performance depending on installation practices.

The Polyisocyanurate Insulation Manufacturers Association (PIMA), a group of former members of the Roofing Insulation Committee/Thermal Insulation Manufacturers Association (RIC/TIMA), has recognized the problem of actual in-service insulation performance versus laboratory thermal conductivity testing. This organization is planning to continue to monitor two field roof insulation programs to evaluate the installed performance of several materials. The studies were designed to use heat flow measuring elements to determine insulation behavior in normal use over a period of several years. The results should provide a useful guide to understanding long-term, installed insulation properties.

Summary

Since the early pioneering work on long-term aging properties of rigid polyurethane foam, great progress has been made. However, there is still much to be learned about gas permeation through a cellular structure, the distribution of polymer in a closed-cell low-density foam (i.e.,

the polymer in the cell walls and struts), the influence of positive gas barriers on preventing gas transport in laminated foam products, and the role of environmentally acceptable, partially-halogenated CFCs as new blowing agents.

Acknowledgment

The vapor thermal conductivity measurements of CFC-11, 123, and 123a were obtained by Dr. I. R. Shankland of the Allied-Signal Corporation, Buffalo Research Laboratory.

References

- [1] Ball, G. W. et al., *Journal of Cellular Plastics*, Vol. 6, No. 2, March-April 1970, pp. 66-78.
- [2] Doherty, D. J. et al., *Chemistry and Industry*, Vol. 30, No. 7, July 1962, pp. 1340-1356.
- [3] Stevenson, M. E. and Mark, M., *ASHRAE Journal*, Vol. 3, No. 2, Feb. 1961.
- [4] Scochdopole, R. E., *Chemical Engineering Progress*, Vol. 57, No. 10, 1961, p. 55.
- [5] Margedant, J. A., *Freon Blown Rigid Foams*, E. I. duPont de Nemours, 1958.
- [6] Kaplan, M. et al. in *Proceedings*, Society of Plastics Engineers, 18th ANTEC, Feb. 1962.
- [7] Norton, F. J., *Journal of Cellular Plastics*, Vol. 3, No. 1, 1967, pp. 23-37.
- [8] Varland, R. N., *SPE Journal*, Vol. 22, No. 11, 1966, pp. 34-36.
- [9] Buist, J. M., *Advances in Polyurethane Technology*, Wiley, New York, 1968, pp. 212-214.
- [10] Bomberg, M. and Solvason, K. R. in *Guarded Hot Plate and Heat Flow Meter Methodology*, ASTM STP 879, American Society for Testing and Materials, Philadelphia, 1985, pp. 140-153.
- [11] Coumou, K. G., in *Guarded Hot Plate and Heat Flow Meter Methodology*, ASTM STP 879, American Society for Testing and Materials, Philadelphia, 1985, pp. 161-170.

Deterioration of Thermal Insulation Properties of Extruded Polystyrene: Classification and Quality Control System in Sweden

REFERENCE: Sandberg, P. I., "Deterioration of Thermal Insulation Properties of Extruded Polystyrene: Classification and Quality Control System in Sweden," *Insulation Materials, Testing, and Applications, ASTM STP 1030*, D. L. McElroy and J. F. Kimpflen, Eds., American Society for Testing and Materials, Philadelphia, 1990, pp. 197-204.

ABSTRACT: In the process of assessing design values for thermal conductivity of insulating materials, knowledge of the time-dependent deterioration of the insulation performance is important. Extruded polystyrene is affected by changes in the composition of the gas mixture in the cells (normally referred to as *ageing*) and in some applications by moisture accumulation, both mechanisms resulting in a higher thermal conductivity.

In the Swedish quality control system the determination of thermal conductivity is carried out 91 ± 7 days after manufacture. Part of the ageing has by then already taken place, and the rest of the ageing during the life span of a building is taken care of by a specified addition ($\Delta\lambda_a$) to the laboratory value in the assessment of the design value. The more ageing that takes place before the determination of the thermal conductivity, the more accurate the design value will be. Different ways of accelerating the ageing have been discussed. This paper describes a method of acceleration by cutting the specimens into thin slices. It is shown that, by making use of this method, no extra addition allowing for the ageing under service conditions is needed (i.e., $\Delta\lambda_a = 0$).

The paper also deals with moisture accumulation in soil insulation and inverted roofs. The moisture corrections ($\Delta\lambda_m$) in the classification system are given. A method for acceleration of the moisture pickup and correlation to *in situ* measurements as well as a theoretical model for predicting moisture accumulation are described. Finally, effects of moisture on thermal conductivity are discussed.

KEY WORDS: thermal conductivity, ageing, moisture, extruded polystyrene, classification, quality control

The current Swedish system for classification of thermal insulation materials was introduced in the middle of the 1960s. Since then far-reaching developments have taken place, but the system has not been adapted to these changes.

A new classification system has therefore been worked out with the aim of guaranteeing impartial rules for all insulation materials. The new system will probably be adopted by the end of 1987. This paper describes how the new system will handle the adverse effects of moisture and change in gas composition on the thermal conductivity in extruded polystyrene (XPS).

The thermal conductivity applicable in practice (design value) is in principle calculated according to

$$\lambda_p = \lambda_{i0} + \Delta\lambda_s + \Delta\lambda_m + \Delta\lambda_1 + \Delta\lambda_a$$

¹Head of Division of Building Physics, Swedish National Testing Institute, P.O. Box 857, S-501 15 Borås, Sweden.

where

- λ_p = practical thermal conductivity,
- λ_{10} = laboratory measurement on dry material at 10°C mean temperature,
- $\Delta\lambda_s$ = correction for dispersion in the manufacturing process,
- $\Delta\lambda_m$ = correction for moisture,
- $\Delta\lambda_1$ = correction for air movements in the material, and
- $\Delta\lambda_a$ = correction for ageing.

In addition to these material corrections, there are corrections of the thermal transmittance of building elements (ΔU) for environmental factors and workmanship.

Change of Gas Composition in Cells

Assessment of $\Delta\lambda_a$ in the Classification System

After manufacture, extruded polystyrene contains a certain amount of chlorofluorocarbon (CFC) in the cells. CFC has a lower thermal conductivity (λ) than air, and the presence of CFC is favorable for the material's λ -value. Gradually, however, air diffuses into the material and CFC diffuses slowly out of the material. The composition of the gas mixture will change and the thermal conductivity will rise. This process is usually referred to as *ageing*.

A difficult problem in a classification system is the prediction of the deterioration of the thermal conductivity during the service life of the building. For such a prediction it is necessary to know the duration and exposure conditions during the period between manufacture and the determination of λ_{10} . There is obviously a relation between what has happened before the test of λ_{10} and the further deterioration of the thermal conductivity, $\Delta\lambda_a$ (Fig. 1). This fact has in some cases been overlooked and classification systems have been operating with identical values of $\Delta\lambda_a$ but different rules for the conditioning of test specimens.

As regards the length of the period between manufacture and test of λ_{10} , there are two conflicting needs. On the one hand, measurements should be made as soon as possible after manufacture so that indications regarding defects in manufacture may be obtained. On the other hand, enough time should be allowed for the major part of the ageing to have taken place, so that the extrapolated value $\Delta\lambda_a$ is sufficiently small to be reliable. Both needs should be ad-

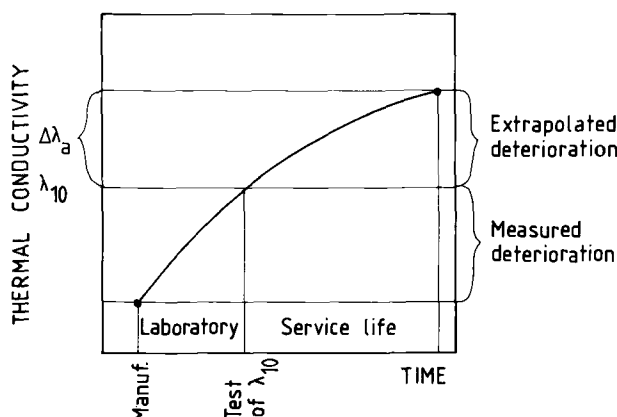


FIG. 1—Thermal conductivity versus time during laboratory conditioning and service life.

dressed, the internal control of the manufacturer being carried out on fresh material and the supervisory control of the testing institute being applied to aged material.

Acceleration Methods

The desire to achieve as much ageing as possible during a short period of time makes one consider ways of accelerating the ageing process. An accelerated laboratory method may be an acceptable solution, provided that one (1) establishes an acceleration factor that correlates time in laboratory with time in service, and (2) ensures that the acceleration does not result in effects that would not be found in practice.

When solving diffusion problems, we often make use of a nondimensional "time", the Fourier number:

$$Fo = (D \cdot t)/d^2$$

where

D = gas diffusivity, m^2/s ,
 t = time, s, and
 d = thickness of material, m.

The gas diffusivity may be concentration dependent.

The value of the Fourier number indicates how far a diffusion process has advanced. An acceleration can consequently be achieved by increasing D or by decreasing d .

A rise in temperature will cause increased gas diffusivity, and this method is used in many countries to accelerate ageing. Unfortunately the different gases involved react differently to increased temperature. The diffusivity and consequently the magnitude of acceleration for the different diffusion processes will therefore vary and the gas composition achieved will never be equal to the composition during natural ageing. Thus the second condition for a sound acceleration method as mentioned above is not fulfilled.

In Sweden we have investigated the technique of accelerating the aging by cutting the material to small thicknesses. This should be a powerful means of acceleration, since the rate of ageing should be proportional to $1/d^2$; compare the expression for Fo above.

Figure 2 shows thermal conductivity versus time for laboratory XPS specimens 10, 30, and 50 mm thick. The 50 mm slab had mould skin on both sides; the other two had no skin. If the time scales for the 30 and 50 mm materials are recalculated according to

$$t_e = t \cdot (0.01/d)^2$$

where

t_e = equivalent time,
 t = (real) time (= time for 10 mm material), and
 d = thickness of material, m.

all the data points should, according to theory, fall on one curve. This is almost true; compare Fig. 3.

Experience has shown that the mould skin has the effect of retarding the diffusion and roughly corresponds to 0.01 m material. The thickness of the 50 mm slab was consequently set to 0.07 m in the formula above.

The acceleration factor can be calculated according to

$$\text{acceleration factor} = (d_{\text{service}}/d_{\text{lab}})^2$$

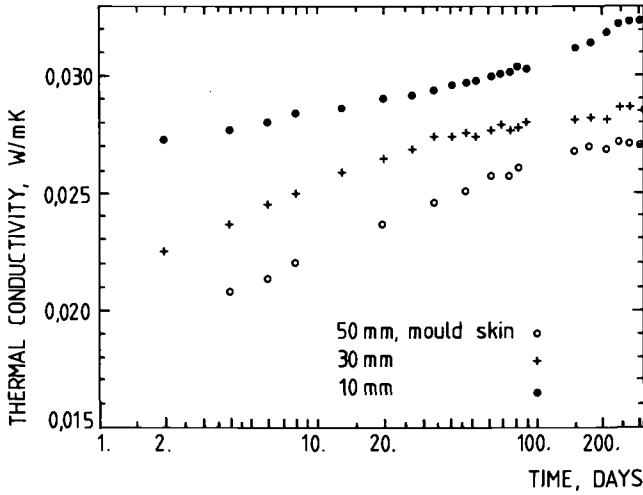


FIG. 2—Thermal conductivity versus time in laboratory conditions for three thicknesses of XPS.

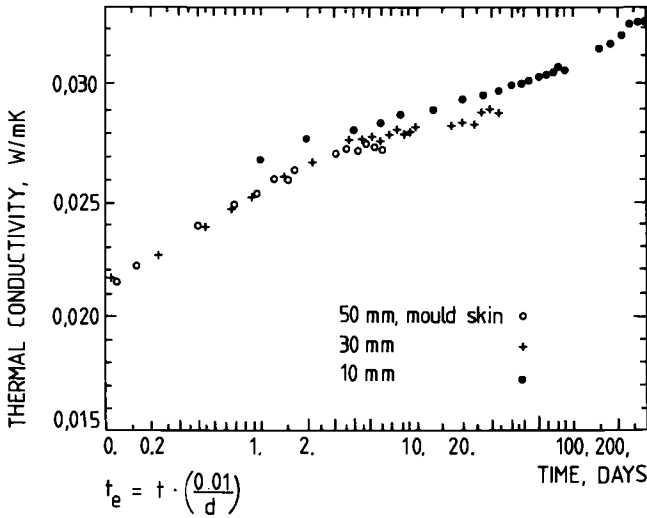


FIG. 3—Thermal conductivity versus time in laboratory conditions for three thicknesses of XPS. The time scale for each thickness is recalculated to "equivalent time"; see text.

where

d_{service} = thickness under service conditions, and
 d_{lab} = thickness during laboratory conditioning.

There are no effects of the acceleration we can think of, deviating from the natural behavior, except that a layer of cells at each surface is destroyed by slicing the sample. The influence of this is probably small.

Conditioning Rules and $\Delta\lambda_a$

The rules laid down in the Swedish classification system prescribe conditioning of the material at 10 mm thickness for 91 days in an atmosphere of 20°C and 50% relative humidity before determining λ_{10} . By conditioning the material according to these rules, the thermal conductivity attained is the same as that of 100 mm thick sheets after 25 years and no correction for ageing is needed.

For sheets less than 100 mm thick, the method gives too low values of the thermal conductivity, while for sheets more than 100 mm thick the value measured is too high. The calculated deviation from correct value (25-year value) is given in Fig. 4 according to Isberg [1]. If an error of 5% can be allowed, the method can be applied to extruded polystyrene of 50 to 200 mm thickness. If the mould skin is retained on the sheets in practice, the method can be applied down to 30 mm thick sheets. Thus it is applicable to all thicknesses encountered in practice and no correction for ageing is needed (i.e., $\Delta\lambda_a = 0$). (For products with surface layers other than mould skin, special rules depending on the diffusion resistance of the surface layer are applicable.)

Acceleration by cutting specimens to thin thicknesses is also being studied by ISO Working Group on Effects of Ageing on Thermal Properties. A test method is under preparation.

Moisture Accumulation

$\Delta\lambda_m$ in the Classification System

Moisture accumulation in the material will cause an increase of thermal conductivity. In the proposed classification system, the moisture correction, $\Delta\lambda_m$, depends on the field of application for the material. Six different moisture environments are defined:

1. Internal use; in equilibrium with 30 to 70% relative humidity (RH).
2. External use, protected from precipitation; in equilibrium with 70 to 98% RH.

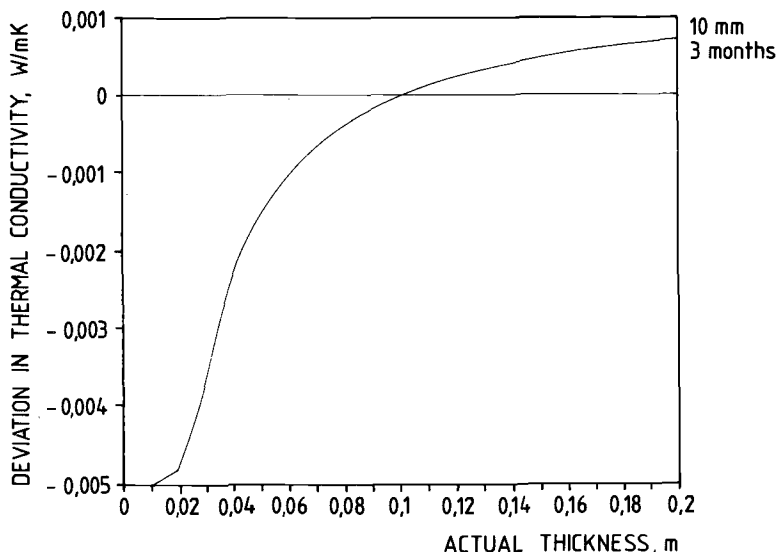


FIG. 4—Calculated deviation from the correct 25 year value if tests for all product thicknesses are made on 10 mm thick test specimens stored for 3 months.

3. External use, unprotected; periodically in equilibrium with 100% RH.
4. External insulation on building elements below ground level (e.g., external basement insulation).
5. Soil insulation, ground on both sides.
6. Inverted roofs.

For extruded polystyrene in Categories 1 to 4, $\Delta\lambda_m = 0$. In Category 5, $\Delta\lambda_m = 0.004 \text{ W/m} \cdot \text{K}$; in Category 6, $\Delta\lambda_m = 0.001$ to $0.008 \text{ W/m} \cdot \text{K}$, depending on the construction. For inverted roofs there is, in addition to $\Delta\lambda_m$, a correction of the thermal transmittance $\Delta U = 0.00$ to $0.04 \text{ W/m}^2 \cdot \text{K}$ to allow for the effects of rainwater movements in the joints and between insulation and roofing membrane. Lower values of $\Delta\lambda_m$ than these nominal values of correction may be accepted if the manufacturer can show that the material performs better than what is stated in the rules.

Both laboratory methods, in which the natural moisture accumulation is accelerated, and calculation methods, simulating the natural behavior, can be used to predict moisture accumulation under service conditions and form a basis for the assessment of $\Delta\lambda_m$.

Accelerated Moisture Accumulation

A detailed analysis of moisture transfer in extruded polystyrene shows that an increase in temperature level and temperature gradient accelerates moisture accumulation. This is achieved in a method originally developed by the Norwegian Road Research Laboratory. The material is exposed to an atmosphere of $+60^\circ\text{C}$ and 100% RH on the warm side and $+10^\circ\text{C}$ and 100% RH on the cold side. The method is primarily suitable for acceleration of moisture accumulation in soil insulation (Category 5), but may also yield valuable knowledge for the inverted roof application (Category 6).

Results from laboratory tests on 50 mm XPS show a moisture accumulation rate in the laboratory apparatus that is 60 to 70 times the value found in specimens which have been exposed to natural conditions in Scandinavian test roads [2]. The acceleration factor of 60 to 70 applies to the mean moisture content. It may be important to point out that normally there is a considerable difference in moisture distribution between laboratory and service conditions. In this respect the acceleration method is not quite reliable and the discrepancy may have to be taken into consideration when the moisture effects are evaluated.

Calculation of Moisture Accumulation

A computer program solving the nonstationary temperature and moisture fields has been developed at the National Testing Institute. The moisture content is calculated by

$$\partial w / \partial t = \partial / \partial x (\delta \cdot \partial v / \partial x)$$

where

w = moisture content, kg/m^3 ,

δ = water vapor permeability, m^2/s ,

x = coordinate in moisture flow direction, m ,

t = time, s , and

v = water vapor content (vapor concentration), kg/m^3 .

In this equation it is assumed that all moisture transfer is due to a gradient in vapor content. This is a reasonable simplification for XPS considering that the moisture transfer ability in liquid phase is poor.

The material properties needed for the calculation are: thermal conductivity, specific heat capacity, and vapor permeability as functions of moisture content, and also the relationship

between moisture content and relative humidity in the material (hygroscopic sorption curve). For products with mould skin, the skin's vapor resistance must be known. Results from computer modeling show reasonably good agreement between calculated and measured moisture contents and distributions in soil insulation (Fig. 5). The scatter in the measured values depends primarily on variations in material properties (e.g., vapor resistance of mould skin) and different relative humidities in the ground at different locations.

An example from a calculation of an inverted roof is given in Fig. 6. The results, showing that the lower slab has the highest moisture content, are confirmed by field measurements in Sweden and Norway; see, for example, Petersson [3], Nilsson [4], and NBI [5]. The results also indicate the crucial effect of a water film between the upper and lower slab. Results from field measurements are essentially in agreement with the calculated alternative with a water film between the slabs.

Moisture Effects on Heat Transfer

The moisture content itself is seldom of primary interest no matter how it is estimated: by experience, by laboratory acceleration, or by computer modelling. More important are the effects of moisture on the material's performance, in this paper the effects on the heat transfer.

Generally there are two effects of moisture on heat transfer: (1) one is related to the presence of moisture in the material, the other is related to moisture movements and phase changes. The latter effect can normally be neglected in XPS since the material is fairly impermeable and the moisture transfer slow. Note, however, the effect mentioned above of moving rainwater in inverted roofs; this must be considered.

The effect of moisture in the material's pores may be regarded as an addition to the thermal conductivity of the dry material. This addition is normally assumed to be a linear function of the moisture content:

$$\Delta\lambda_m = K \cdot w$$

where

K = constant, and

w = moisture content, kg/m^3 .

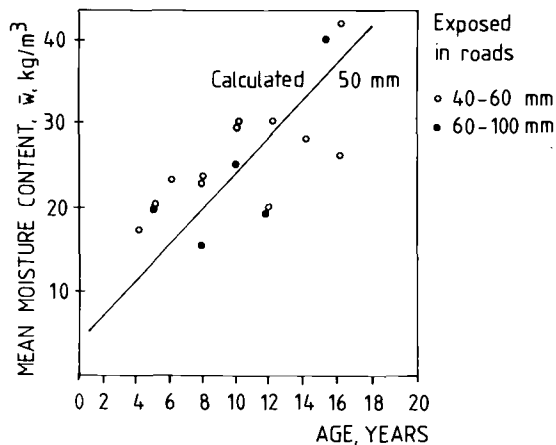


FIG. 5—Mean moisture content versus age for specimens of XPS exposed to natural ageing in Scandinavian roads. The straight line indicates results from computer calculations.

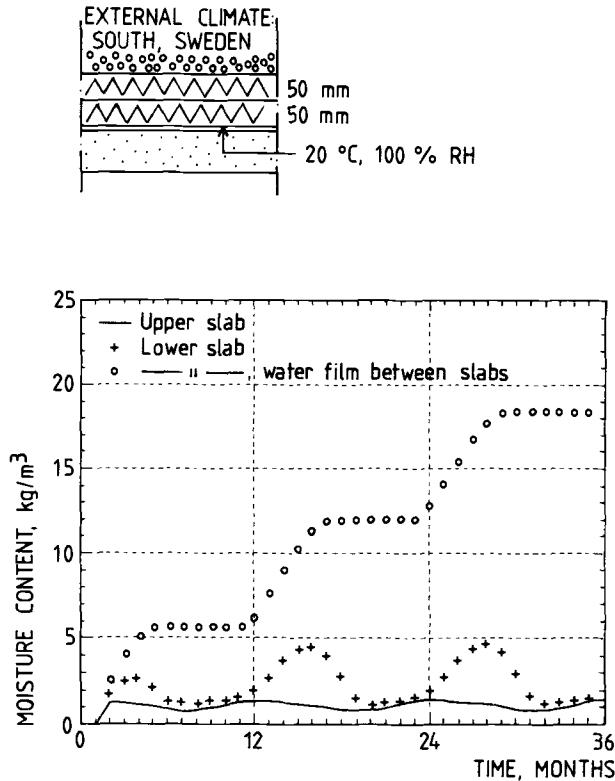


FIG. 6—Calculated moisture content in the upper and lower slab of XPS on an inverted roof. Two alternatives: with and without water film between the slabs.

Typical values of K found in the literature are ~ 0.0001 for XPS. Our test results are the same, although there is some scattering.

The value of K is only slightly dependent on the moisture distribution. In most cases when the thermal conductivity is determined, only the mean moisture content and not the distribution is known. This is in many cases acceptable. A material with a distribution where, for example, all the moisture is concentrated to 25% of the material's thickness, has a thermal resistance only about 5% higher than the same material with an even moisture distribution.

References

- [1] Isberg, J., "Rules Regarding the Conditioning of Specimens for Determination of Thermal Conductivity," Preliminary Report, Chalmers Institute of Technology, Gothenburg, Sweden, 1987.
- [2] Sandberg, P. I., "Moisture Content and Thermal Conductivity in Soil Insulation," *Journal of Thermal Insulation*, Vol. 10, Oct. 1986.
- [3] Petersson, B.-A., "The Upside-Down Roof," Chalmers Institute of Technology, Gothenburg, Sweden, 1980.
- [4] Nilsson, S., "Rapport över provningar av omvända tak med isoleringsskivor i två lag," Sune Nilssons ingenjörbyrå, Malmö, Sweden, 1986.
- [5] "Omvendte tak," Norwegian Building Research Institute, Trondheim, 1983.

Long-Term *R*-Values and Thermal Testing Requirements for Rigid Insulating Foams

REFERENCE: Hagan, J. R. and Miller, R. G., "Long-Term *R*-Values and Thermal Testing Requirements for Rigid Insulating Foams," *Insulation Materials, Testing, and Applications, ASTM STP 1030*, D. L. McElroy and J. F. Kimpflen, Eds., American Society for Testing and Materials, Philadelphia, 1990, pp. 205-217.

ABSTRACT: This paper presents the results of two experimental studies. The first was a continuation of a 5-year aging study on foil-faced polyisocyanurate thermal insulation boards. These boards were retested in the guarded hot box and represent 11-year aged data. The results indicated excellent agreement with the plateaued *R*-values established on the 5-year aged samples.

The second effort is an ongoing correlation study between the large-scale guarded hot box and small-scale heat flow meter tests using permeable faced polyisocyanurate foam thermal insulation boards. Thicknesses tested ranged from 2.5 to 8.1 cm (1 to 3.2 in.). The results to date show that, in general, with proper sampling of large-scale boards, good agreement can be expected between guarded hot box and heat flow meter test results.

KEY WORDS: aging study, foil-faced polyisocyanurate, *R*-value, guarded hot box, heat flow meter, guarded hot box/heat flow meter correlation, rigid foam sampling techniques

Chlorofluorocarbon blown rigid foam plastic thermal insulation products, for use as building insulation, are manufactured from a variety of resins: polystyrene, phenolic, polyurethane, and polyisocyanurate. As shown in Table 1, these resins are utilized in various processes.

These thermal insulation materials can be covered with facing membranes during production or produced unfaced. Generally, polystyrene boardstock products are produced unfaced, while phenolics, polyurethane, and polyisocyanurate boardstock products are faced. Bunstock, spray, and foam-in-place polyurethane and polyisocyanurate products are basically unfaced. Some examples of facing membranes utilized on these products are shown in Table 2. These thermal insulation products are usually contained in the exterior building envelope, including sidewalls, roofs, underslab, foundation, and other specialized applications.

The development of chlorofluorocarbon blown rigid polyurethane/polyisocyanurate foam plastic thermal insulation materials occurred over 30 years ago. Since that time considerable information has been reported in the literature [1] on the theory of aging or aging effect on the thermal insulation characteristics of these products. The generally advanced theory of aging is that it is due to ambient or surrounding air diffusing into, and to a much lesser extent the chlorofluorocarbon gas diffusing out of, the foam cells, resulting in poorer thermal resistance characteristics. It is also widely accepted that this change occurs more rapidly and to a greater extent for unfaced foams versus those faced with a gas-barrier impermeable facer, such as a metallic facing membrane, during manufacture.

The performance of polyurethane and polyisocyanurate thermal insulation board faced with gas-barrier quality aluminum foil has been reported by Sherman [2,3]. In Ref 2, he discusses the results of a 5-year aging study conducted using the ASTM C 236 Guarded Hot Box at three

¹Research Associate, Jim Walter Research Corp., St. Petersburg, FL 33716.

TABLE 1—*Foam thermal insulation products.*

Resins	Process or Product
• Polystyrene	• Extruded Boardstock
• Phenolic	• Restrained-Rise Boardstock
• Polyurethane/Polyisocyanurate	• Bunstock
	• Restrained-Rise Boardstock
	• Free-Rise Boardstock
	• Spray
	• Foam-in-Place

TABLE 2—*Typical facing membranes.*

Metallic Facing Membranes
• Aluminum Foil
• Aluminum Sheet
• Laminated (supported) Aluminum Foil
Bonded Fiber Facing Membranes
• Asphalt/Organic Felt
• Asphalt/Glass Fiber Felt
• Polymer/Glass Fiber Mat
Rigid Board Facing Membranes
• Perlite Insulation Board
• Gypsum Board
• Cellulosic Fiber Insulation Board
• Wood-Based Boards

accredited testing laboratories on full sized, commercially available polyisocyanurate boardstock. The boardstock samples were stored in an unregulated ambient temperature, weather-sheltered, storage area in St. Petersburg, Florida. Sherman summarized the results:

1. Essentially no change in R per inch thickness over this extended (15 through 68 months) period of time after product manufacture with or without glass fiber reinforcement.
2. Demonstrated low order magnitude of change in average R per inch from one month after manufacture (8.34) to time-aged plateau (7.04): approximately 15%.
3. The linearity of aged R value with product thickness at three mean temperatures:
 - (a) 7.81 R /inch at 40°F mean temperature
 - (b) 7.04 R /inch at 75°F mean temperature
 - (c) 6.39 R /inch at 110°F mean temperature
4. A linear relationship between R /inch and insulation mean temperature; an increase of 0.021 R /inch with each °F decrease in mean temperature in the temperature range investigated.

5. Confirmation of the precision capability of the ASTM C 236 Guarded Hot Box test method conducted in three NVLAP-accredited testing facilities; individual laboratory averages within 5% of three-laboratory averages; three-laboratory averages with coefficients of variation within 2.5 to 3.6%.

In Ref 3, Sherman provides data on the effect of protective foil facers for an aging period of over ten years on a commercially (at the time) available polyurethane boardstock.

The question of aging of polyurethane/polyisocyanurate foam thermal insulations and other chlorofluorocarbon gas-filled foams continues. Bomberg [4] pointed out the considerably complex nature of the situation existing on the determination of aged thermal properties of foams. Bomberg also discussed proposed accelerated laboratory testing procedures and included the novel concept of monitoring and determining cell gas content as part of a proposed laboratory test method to determine the aged thermal resistance of chlorofluorocarbon gas-filled foams.

Recently, a working group of the Canadian Government Standards Board Preformed Plastic Thermal Insulation Committee No. 51/GP/9 issued a report [5] on the long-term *R*-value of cellular plastic insulations. This group suggested the selection of "*R*-value after five years of ambient aging as an appropriate criterion for design purposes" and assigned recommended five-year aged *R*-values to specific classes of materials and products. For chlorofluorocarbon blown polyurethane/polyisocyanurates, with impermeable (gas-barrier) facing membranes, it was suggested that each product should be evaluated individually and a specific five-year aged *R*-value be determined. Suggestions of the group are shown in Table 3.

The report [5] recommends the development of a test method to establish the "design thermal resistance (five-year laboratory aged)" of gas-filled foam plastic thermal insulation, particularly faced products, and to allow evaluation of this property within a three-month period following production. The report concludes: "The only true aged *R*-value will be that determined by using appropriate test methods after the sample has been aged for five years under *Standard Laboratory Conditions* [emphasis added] . . ."

This paper presents the results of two studies. One is a continuation of the aging program reported in Ref 2; the second is an on-going correlation study between large- and small-scale testing.

Experimental Method

Aging Test Program

Six different foil-faced polyisocyanurate foam thermal insulation boards, manufactured during 1973 through 1975, were tested in accordance with ASTM Test Method for Steady-State

TABLE 3—CGSB Working Group suggested *R*-values [5].

Material/Product	5-Year Aged <i>R</i> -Value
Moulded Polystyrenes	3.7 to 4.3 per inch
Extruded Polystyrenes	5.0 per inch
Open Cell Phenolics	4.3 per inch
Closed Cell Phenolics	None (lack of data)
PUR/PIR (Permeable Membrane)	5.8 per inch
PUR/PIR (Impermeable Membrane)	Established on an individual product basis

Thermal Performance of Building Assemblies by Means of a Guarded Hot Box (C 236) in the Jim Walter Research Corp. (JWRC) guarded hot box test facility. This facility is accredited under the National Voluntary Laboratory Accreditation Program (NVLAP) and has been fully described by Miller et al. [6]. The boards tested were full-dimension 1.2×2.4 m (4×8 ft) \times thickness and were stored in an uncontrolled enclosed storage area in St. Petersburg, Florida. These boards were the same as tested in Ref 2.

Two boards were required to fill the 2.4×2.4 m (8×8 ft) guarded hot box opening, in which the central 1.8×1.8 m (6×6 ft) was the metered area. All tests were conducted at a mean temperature of 24°C (75°F). All test assemblies were taped along the perimeter and center joint with aluminum foil tape to eliminate possible air leakage paths between the hot and cold chambers.

Correlation Test Program

A correlation study between a large-scale guarded hot box test facility and a small-scale heat flow meter apparatus was conducted. The guarded hot box facility was the same as reported above in the Aging Test Program section. The small-scale tests were conducted per ASTM Test Method for Steady-State Heat Flux Measurements and Thermal Transmission Properties by Means of the Heat Flow Meter Apparatus (C 518) in two different size heat flow meters. JWRC is accredited for both ASTM C 236 and C 518 under the National Voluntary Laboratory Accreditation Program. One heat flow meter (R-Matic) required a 0.6×0.6 m (2×2 ft) sample; the other (Rapid-k) required a 0.3×0.3 m (1×1 ft) sample. The R-Matic had a meter area of 20.3×20.3 cm (8×8 in.); the Rapid-k had a 10.2×10.2 cm (4×4 in.) meter area. All tests in the guarded hot box and heat flow meters were conducted at a mean temperature of 24°C (75°F). Samples consisted of nominal 2.5 cm (1 in.) to 8.1 cm (3.2 in.) permeable faced polyisocyanurate foam thermal insulation boards. The testing sequence was such that the two 1.2×2.4 m (4×8 ft) boards were first tested in the guarded hot box, then cut down and tested in the R-Matic, and then cut down again and retested in the Rapid-k. Figure 1 shows a schematic of a full 1.2×2.4 m (4×8 ft) board and the locations of the 2- and 4-sample traverses for the R-Matic and Rapid-k, respectively. Two full boards were tested in the guarded hot box; therefore two 2-sample traverses were cut from the quarter points of each board (Fig. 1) for testing in the R-Matic, for a total of 8 samples. Each R-Matic sample was then cut into two Rapid-k samples, for a total of 16 samples. Therefore the *R*-value from the guarded hot box test was compared to the 8-test *R*-value average from the R-Matic and the 16-test *R*-value average from the Rapid-k. Six boards have been tested to date. Plans are to continue development of this data base for correlation between large- and small-scale testing.

Results

Aging Test Program

Table 4, excerpted from Sherman [2], summarizes the results of the 5-year aged study on chlorofluorocarbon blown polyisocyanurate thermal insulation boards faced with impermeable, gas-barrier quality aluminum foil. These data were obtained from guarded hot box tests from three NVLAP accredited laboratories and were conducted at a mean temperature of 24°C (75°F). The results of the continuation of this study, at one original laboratory, are shown in Table 5. These data represent *11-year aged R-values* on the identical boards as tested at 5 years.

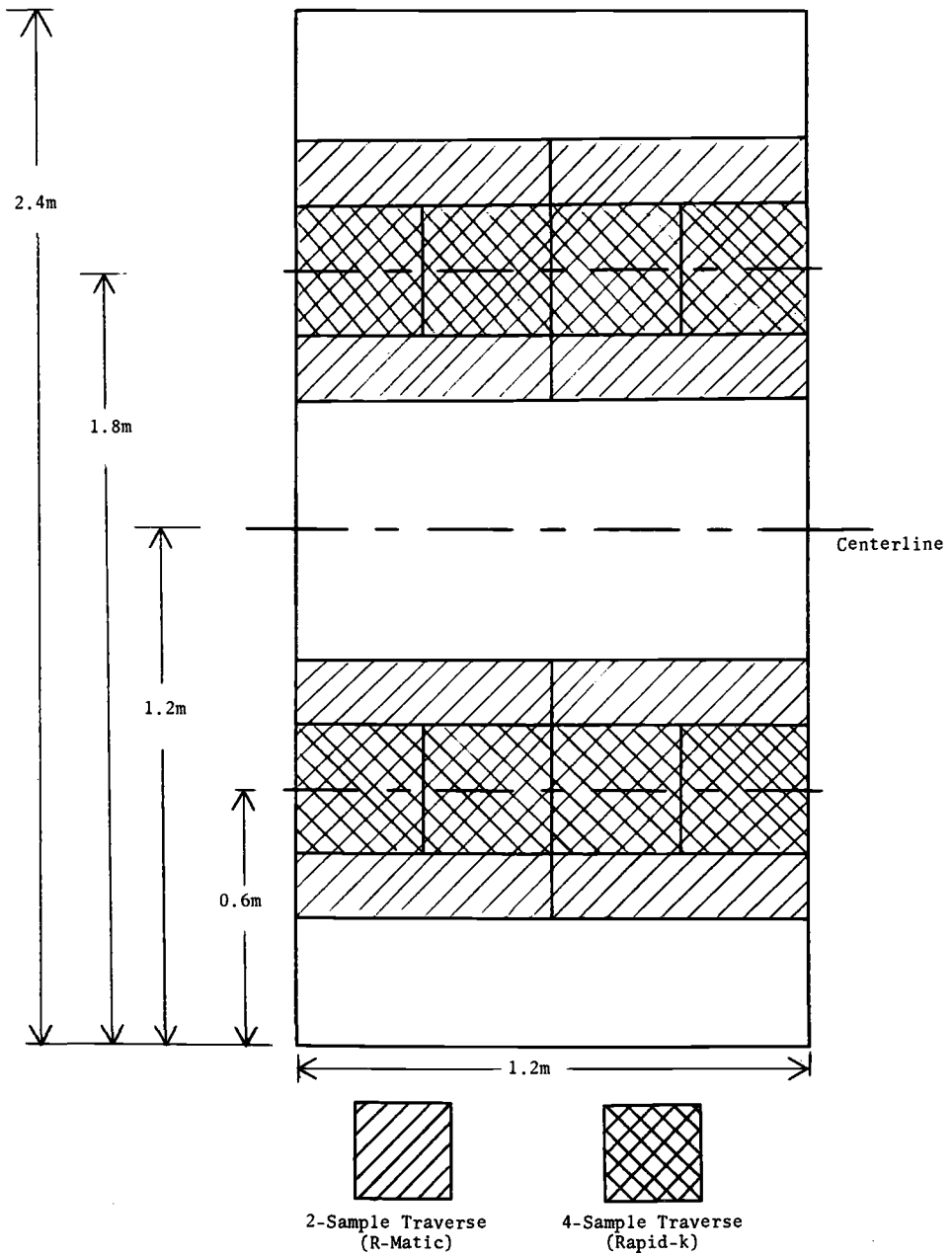


FIG. 1—Test sample locations.

TABLE 4—*Summary of 5-year aged data [2].*

Test Lab. & Product	Mean Temperature, °F	Average Thickness, in.	Measured R, h ft ² °F/Btu	Calculated R/Inch Thickness	Age of Board Tested, months
Dynatherm					
0.5" TF200	75.1	0.46	3.19	6.93	63
	73.4	0.46	3.22	7.00	32
0.6" TF200	74.7	0.55	3.97	7.22	57
	72.4	0.55	3.88	7.05	27
0.6" TF400	75.1	0.53	3.83	7.23	47
	75.1	0.53	3.64	6.88	16
0.6" TF600	76.0	0.57	3.97	6.96	47
	74.5	0.57	3.79	6.65	16
1.0" TF600	75.1	1.09	7.63	7.00	48
	74.6	1.09	7.25	6.65	17
1.5" TF600	74.7	1.48	10.61	7.17	47
	75.1	1.48	9.86	6.66	16
Dynatech					
0.5" TF200	74.7	0.46	3.15	6.85	68
0.6" TF600	74.8	0.55	3.91	7.11	52
1.0" TF600	74.8	1.10	7.31	6.65	52
1.5" TF600	75.4	1.48	9.90	6.69	52
	75.3	1.48	10.10	6.82	52
JWRC					
0.5" TF200	74.4	0.48	3.46	7.21	63
	71.5	0.48	3.60	7.50	32
0.6" TF200	71.1	0.57	4.02	7.05	57
	75.1	0.57	4.00	7.02	27
0.6" TF400	75.2	0.53	3.76	7.09	49
	76.4	0.53	3.80	7.17	15
0.6" TF600	75.0	0.58	4.19	7.22	48
	72.4	0.58	4.10	7.07	16
1.0" TF600	74.9	1.09	7.99	7.33	48
	73.4	1.09	7.81	7.17	17
1.5" TF600	75.2	1.49	11.38	7.64	50
	73.6	1.49	10.64	7.14	16
3 Lab. Avgs.	74.6			7.04	
3 Lab. St. Dev.	1.08			0.247	
% of X	1.44%			3.51%	

The 5-year average calculated R /inch was 7.04. For the 11-year aged data, the average calculated R /inch was 6.91, a difference of less than 2%. This shows excellent correlation with the plateaued R -values established on the 5-year aged samples.

Correlation Test Program

Six tests on permeable faced polyisocyanurate foam thermal insulation boards have been conducted to date in this correlation study. Two tests were run on 2.5 cm (1 in.) boards, two on 5.1 cm (2 in.) boards, one on 7.6 cm (3 in.) boards, and one on 8.1 cm (3.2 in.) boards. The 2.5 cm boards were only tested in the guarded hot box and Rapid-k; the remaining boards were tested in the guarded hot box, R-Matic, and Rapid-k.

Tables 6 to 11 summarize the correlation data. Each table contains the hot box R -value, the heat flow meter R -value for individual samples, 2- or 4-sample traverse averages, single board averages, and the overall (2-board) average; the latter R -value is comparable to the hot box R -value.

As this is a continuing study, the results obtained should be considered interim results and trends could change as additional data are added to the data base. The data show that the use of *individual* heat flow meter R -values to represent a full-dimension board could yield errors of up to 16%. However, the use of two 2- or 4-sample traverses could improve the agreement to about 9%. This agreement is better at thicknesses of 5.1 cm or less, being 2% or less. Additional testing will concentrate on thicknesses greater than 5.1 cm.

Conclusions

Two experimental programs were discussed in this paper, the 11-year aged program and the correlation between large- and small-scale testing. The results of tests on 11-year-aged foil-faced polyisocyanurate foam thermal insulation boards showed excellent agreement with the plateaued R -values from the same boards tested at 5 years. The correlation study showed that good agreement could be expected between large-scale and small-scale testing *if proper sampling techniques are followed*.

Acceptable ASTM test methods are available to measure the thermal resistance of the various chlorofluorocarbon blown foam plastic thermal insulations with various types of facing membranes. The challenge is to incorporate these methods into a standard test protocol which will produce a design thermal resistance truly representative of full-dimension aged material. This method must be applicable to all gas filled foams, regardless of chemical composition and final product characteristics.

TABLE 5—Summary of 11-year aged data.

Sample Identification	Average Thickness, cm (in.)	Measured R , m^2K/W (h ft ² ° F/Btu)	Calculated R/cm ($R/inch$)
0.5" TF200	1.30 (0.512)	0.55 (3.14)	0.42 (6.13)
0.6" TF200	1.46 (0.574)	0.66 (3.76)	0.45 (6.55)
0.6" TF400	1.39 (0.548)	0.59 (3.37)	0.42 (6.15)
0.6" TF600	1.41 (0.554)	0.67 (3.78)	0.48 (6.82)
1.0" TF600	2.84 (1.120)	1.39 (7.92)	0.49 (7.07)
1.5" TF600	3.73 (1.470)	1.88 (10.67)	0.50 (7.26)
Overall Average			0.46 (6.91)

TABLE 6—R-values for nominal 2.5 cm (1 in.) insulation boards (Specimen 1-A).

• Hot Box: $1.05 \frac{\text{m}^2\text{K}}{\text{W}} \left(5.97 \frac{\text{h ft}^2 \text{ }^\circ\text{F}}{\text{Btu}} \right)$						
• Rapid-k: $\frac{\text{m}^2\text{K}}{\text{W}} \left(\frac{\text{h ft}^2 \text{ }^\circ\text{F}}{\text{Btu}} \right)$						
Board A	0.92 (5.22)	0.88 (5.02)	0.90 (5.11)	0.91 (5.17)	0.90 (5.13)	0.93 (5.28)
	0.89 (5.06)	0.88 (5.02)	0.92 (5.21)	0.90 (5.09)	0.90 (5.10)	
Board B	1.01 (5.74)	1.00 (5.65)	0.95 (5.38)	1.00 (5.70)	0.99 (5.62)	0.96 (5.44)
	0.94 (5.33)	0.92 (5.22)	0.90 (5.13)	0.94 (5.33)	0.92 (5.25)	

TABLE 7—R-values for nominal 2.5 cm (1 in.) insulation boards (Specimen 1-B).

• Hot Box: $1.04 \frac{\text{m}^2\text{K}}{\text{W}} \left(5.90 \frac{\text{h ft}^2 \text{ }^\circ\text{F}}{\text{Btu}} \right)$						
• Rapid-k: $\frac{\text{m}^2\text{K}}{\text{W}} \left(\frac{\text{h ft}^2 \text{ }^\circ\text{F}}{\text{Btu}} \right)$						
Board A	1.08 (6.12)	1.01 (5.73)	0.99 (5.63)	1.08 (6.16)	1.04 (5.91)	1.05 (5.94)
	1.04 (5.89)	1.04 (5.88)	0.98 (5.58)	1.09 (6.17)	1.04 (5.88)	
Board B	1.12 (6.35)	1.02 (5.80)	1.02 (5.79)	1.06 (6.04)	1.06 (6.00)	1.05 (5.98)
	1.03 (5.83)	1.04 (5.90)	1.06 (6.01)	1.07 (6.08)	1.05 (5.96)	

TABLE 8—R-values for nominal 5.1 cm (2 in.) insulation boards (Specimen 2-A).

• Hot Box: $2.09 \frac{\text{m}^2\text{K}}{\text{W}} \left(\frac{11.89 \text{ h ft}^2 \text{ }^\circ\text{F}}{\text{Btu}} \right)$					
• R-Matic: $\frac{\text{m}^2\text{K}}{\text{W}} \left(\frac{\text{h ft}^2 \text{ }^\circ\text{F}}{\text{Btu}} \right)$					
Board A	Avg. of 2-Sample Traverse		Board Average	Overall Average	
Board B					
• Rapid-k: $\frac{\text{m}^2\text{K}}{\text{W}} \left(\frac{\text{h ft}^2 \text{ }^\circ\text{F}}{\text{Btu}} \right)$					
Board A	Avg. of 4-Sample Traverse		Board Average	Overall Average	
Board B					

TABLE 9—R-values for nominal 5.1 cm (2 in.) insulation boards (Specimen 2-B).

• Hot Box: $2.46 \frac{\text{m}^2\text{K}}{W} \left(\frac{13.98}{\text{h ft}^2 \text{ } ^\circ\text{F}} \frac{\text{Btu}}{\text{Btu}} \right)$					
• R-Matic: $\frac{\text{m}^2\text{K}}{W} \left(\frac{\text{h ft}^2 \text{ } ^\circ\text{F}}{\text{Btu}} \right)$					
		Avg. of 2-Sample Traverse		Board Average	
				Overall Average	
Board A	2.45 (13.92)	2.58 (14.67)	2.52 (14.30)	2.45 (13.94)	2.45 (13.91)
	2.38 (13.54)	2.40 (13.62)	2.39 (13.58)		
Board B	2.45 (13.92)	2.43 (13.79)	2.44 (13.86)	2.44 (13.88)	
	2.48 (14.09)	2.41 (13.70)	2.45 (13.90)		
• Rapid-k: $\frac{\text{m}^2\text{K}}{W} \left(\frac{\text{h ft}^2 \text{ } ^\circ\text{F}}{\text{Btu}} \right)$					
		Avg. of 4-Sample Traverse		Board Average	
				Overall Average	
Board A	2.43 (13.80)	2.38 (13.51)	2.43 (13.80)	2.45 (13.94)	2.41 (13.70)
	2.25 (12.80)	2.42 (13.73)	2.40 (13.64)	2.38 (13.54)	
Board B	2.60 (14.77)	2.32 (13.20)	2.38 (13.51)	2.40 (13.60)	2.41 (13.67)
	2.57 (14.57)	2.35 (13.36)	2.48 (14.07)	2.42 (13.74)	

TABLE 10—R-values for nominal 7.6 cm (3 in.) insulation boards (Specimen 3-A).

• Hot Box: $3.40 \frac{\text{m}^2\text{K}}{\text{W}} \left(\frac{19.29 \text{ h ft}^2 \text{ }^\circ\text{F}}{\text{Btu}} \right)$					
• R-Matic: $\frac{\text{m}^2\text{K}}{\text{W}} \left(\frac{\text{h ft}^2 \text{ }^\circ\text{F}}{\text{Btu}} \right)$					
		Avg. of 2-Sample Traverse		Board Average	
				Overall Average	
Board A	3.13 (17.75)	3.15 (17.90)	3.14 (17.82)	3.18 (18.07)	3.22 (18.31)
	3.22 (18.31)	3.23 (18.33)	3.23 (18.32)		
Board B	3.35 (19.05)	3.34 (18.98)	3.35 (19.02)	3.27 (18.55)	
	3.16 (17.95)	3.21 (18.22)	3.18 (18.08)		
• Rapid-k: $\frac{\text{m}^2\text{K}}{\text{W}} \left(\frac{\text{h ft}^2 \text{ }^\circ\text{F}}{\text{Btu}} \right)$					
		Avg. of 4-Sample Traverse		Board Average	
				Overall Average	
Board A	3.12 (17.71)	3.01 (17.07)	3.07 (17.42)	3.04 (17.26)	3.08 (17.49)
	3.20 (18.18)	3.05 (17.32)	3.08 (17.49)	3.09 (17.53)	
Board B	3.35 (19.00)	3.07 (17.43)	3.26 (18.53)	3.19 (18.14)	3.10 (17.58)
	3.01 (17.08)	2.94 (16.67)	3.07 (17.44)	3.00 (17.03)	

TABLE 11—R-values for nominal 8.1 cm (3.2 in.) insulation boards (Specimen 3.2-A).

• Hot Box: $4.12 \frac{\text{m}^2\text{K}}{\text{W}} \left(\frac{\text{h ft}^2 \text{ }^\circ\text{F}}{\text{Btu}} \right)$						
• R-Matic: $\frac{\text{m}^2\text{K}}{\text{W}} \left(\frac{\text{h ft}^2 \text{ }^\circ\text{F}}{\text{Btu}} \right)$						
Board A	3.97 (22.56) 3.87 (21.99)	3.91 (22.18) 3.94 (22.36)	Avg. of 2-Sample Traverse		Overall Average	
			3.94 (22.37) 3.91 (22.18)	3.92 (22.28)		
Board B	3.89 (22.07) 3.88 (22.05)	3.97 (22.54) 3.94 (22.40)	Avg. of 2-Sample Traverse		Overall Average	
			3.93 (22.30) 3.91 (22.22)	3.92 (22.26)		
• Rapid-k: $\frac{\text{m}^2\text{K}}{\text{W}} \left(\frac{\text{h ft}^2 \text{ }^\circ\text{F}}{\text{Btu}} \right)$						
Board A	3.70 (20.99) 3.88 (22.05)	3.84 (21.78) 3.87 (21.97)	4.14 (23.53) 3.64 (20.66)	Avg. of 4-Sample Traverse		Overall Average
				3.68 (20.87) 3.93 (22.31)	3.84 (21.79) 3.83 (21.75)	
Board B	3.93 (22.34) 3.92 (22.26)	3.81 (21.62) 3.93 (22.31)	3.98 (22.58) 3.93 (22.31)	Avg. of 4-Sample Traverse		Overall Average
				3.75 (21.30) 3.88 (22.05)	3.87 (21.96) 3.91 (22.23)	
					3.86 (21.94)	
					3.89 (22.10)	

References

- [1] Tye, R. P., "Literature Search and Recommended Procedure for Determining 'Aged' Thermal Value of Polyisocyanurate and Polyurethane Roof Insulations," submitted to: National Roofing Contractors Association, Midwest Roofing Contractors Association, Roofing Insulation Committee of Thermal Insulation Manufacturers Association, 19 March 1987.
- [2] Sherman, M., "Aged Thermal Resistance (R-Value) of Foil-Faced Polyisocyanurate Foam Thermal Insulation Board," in *Proceedings, ASHRAE/DOE-ORNL Conference on Thermal Performance of the Exterior Envelopes of Buildings*, 1979, pp. 952-964.
- [3] Sherman, M., "Sampling Faced Foam Insulation Board for Heat Flow Meter Thermal Performance Testing," in *Thermal Insulation Performance, ASTM STP 718*, D. L. McElroy and R. P. Tye, Eds., American Society for Testing and Materials, Philadelphia, 1980, pp. 298-306.
- [4] Bomberg, M., "Problems in Predicting the Thermal Properties of Faced Polyurethane Foams," in *Thermal Insulation Performance, ASTM STP 718*, D. L. McElroy and R. P. Tye, Eds., American Society for Testing and Materials, Philadelphia, 1980, pp. 412-428.
- [5] Kabayama, M. A., "Long-Term Thermal Resistance Values of Cellular Plastic Insulations," *Journal of Thermal Insulation*, Vol. 10, 1987, pp. 286-300.
- [6] Miller, R. G., Perrine, E. L., and Linehan, P. W., "A Calibrated/Guarded Hot-Box Test Facility," in *Thermal Transmission Measurements of Insulation, ASTM STP 660*, R. P. Tye, Ed., American Society for Testing and Materials, Philadelphia, 1978, pp. 329-341.

DISCUSSION

*R. P. Tye*¹ (*written discussion*)—Results are presented for different thickness specimens using hot box, large heat flow meter, and small heat flow meter apparatus. Results were discussed in terms of "a variability and indicated that this increased as the thickness was increased above 2." It must be pointed out that "small" 30 cm square heat flow meter equipment is not designed to be in conformance with ASTM C 518 for thicknesses above 2 in. *unless* specially calibrated with thicker transfer standards or if smaller meter areas are monitored. Thus some obvious differences in the results could be removed had the small apparatus been calibrated with higher transfer standards. It is recommended that the authors draw attention to this factor in order to avoid misunderstanding by the reader that the smaller area apparatus is less accurate for all thicknesses.

J. R. Hagan and R. G. Miller (authors' closure)—The large heat flow meter was calibrated over a thickness range of 2 to 6 in. with expanded polystyrene boards that had been tested in the large guarded hot plate (ASTM C 177) at the National Bureau of Standards. The small heat flow meter was calibrated over a thickness range of 1 to 3 in. by stacking the 1-in. NBS 1450b Standard Reference Materials.

¹Dynatech Scientific, Inc., Cambridge, MA 02139.

Loose-Fill Behavior

Sarfraz A. Siddiqui,¹ Ray L. Hillier,¹ Gordon H. Damant,¹ and Howard L. Needles²

Comparison of Gas and Electric Radiant Panels for Measuring the Flammability of Loose-Fill Cellulose Insulation

REFERENCE: Siddiqui, S. A., Hillier, R. L., Damant, G. H., and Needles, H. L., "Comparison of Gas and Electric Radiant Panels for Measuring the Flammability of Loose-Fill Cellulose Insulation," *Insulation Materials, Testing, and Applications*, ASTM STP 1030, D. L. McElroy and J. F. Kimpflen, Eds., American Society for Testing and Materials, Philadelphia, 1990, pp. 221-230.

ABSTRACT: Two types of radiant panel apparatus are available for fire-related testing of cellulose insulation. One is the Flooring Radiant Panel (gas-fired radiant panel), an expensive piece of equipment that requires high operational and maintenance costs. The second type is the Veri-Flux "100" (electric radiant panel), also known as the Small-Scale Radiant Panel, which is currently being used as a quality control instrument in the cellulose insulation industry.

There have been few data published comparing the relative performance of the two instruments. This paper analyzes the performance of 53 samples of insulation when tested by these instruments. The analysis attempts to establish whether a direct comparison between the two instruments is feasible. The results of this study will be useful to an ASTM task group that is presently investigating the replacement of the larger gas-fired panel with the electric, small-scale panel.

KEY WORDS: loose-fill cellulose thermal insulation, electric radiant panel, gas radiant panel, critical radiant flux, State of California Thermal Insulation Program

In September 1981 California Energy Commission Insulation Quality Standards became effective, requiring the certification of insulation manufacturers of 13 commonly used insulation materials (including cellulose). These standards, issued pursuant to California Senate Bill 459 (1977), govern the quality of all insulation products installed or sold within the state. The qualities of most concern are those which affect the safety and thermal properties of the insulation material.

Jurisdiction for the insulation program was legislatively transferred to the California Bureau of Home Furnishings in January 1985 by Assembly Bill 3497. In accordance with the Bureau's insulation testing program, every insulation manufacturer is required to have a quality assurance program. Most manufacturers of cellulose insulation conduct small-scale fire tests using a small electric radiant panel as part of quality control requirements. During testing workshops conducted by the Bureau in 1985, 1986, and 1987, cellulose manufacturers expressed concern regarding the calibration of their small-scale radiant panels and correlation of this equipment with the critical radiant flux test [*I*] specified by California State Law.

The critical radiant flux for a given material is the minimum heat flux required to continue

¹California Bureau of Home Furnishings and Thermal Insulation, North Highlands, CA 95660-5595.

²University of California at Davis, Textiles Division, Davis, CA 95616.

the propagation of a flame burning across the material. Hence the higher the critical radiant flux, the more fire retardant the material.

Two types of instrumentation are used to measure the critical radiant flux of cellulose loose-fill insulation. One of these is the Flooring Radiant Panel, which uses a gas-fired panel to create the heat source. The second type, a Small-Scale Radiant Panel, uses an electric radiant heater as heat source.

There have been few published data that establish a direct correlation in performance between the two types of apparatus. This study presents an analysis of the relative performance of the two testing procedures through an evaluation of 53 samples of loose-fill cellulose insulation.

Objective

1. Numerous manufacturers throughout the cellulose insulation industry use an Electric Radiant Panel in an attempt to establish in-house quality control conformance to critical radiant flux criteria of insulation sold in the State of California. The Gas-Fired Radiant Panel test for insulation is a federal standard used by the State of California to determine the critical radiant flux of loose-fill cellulose insulation. The objective of this study is to establish an acceptable correlation between the performance of the Electric Radiant Panel and the Gas-Fired Radiant Panel.

2. ASTM Subcommittee C16.23 on Blanket and Loose-Fill Insulation, responsible for ASTM Specification for Cellulosic Fiber (Wood-Base) Loose-Fill Thermal Insulation (C 739), has also requested that the Bureau of Home Furnishings attempt to establish a correlation between the performance of the two types of apparatus. ASTM C 739 suggests that an Electric Radiant Panel (which is not a standard machine) may be used for the purpose of establishing in-house quality control conformance in correlation with the Gas-Fired Radiant Panel.

Test Material

The 53 cellulose insulation samples tested in this study were manufactured by licensees of the State of California Insulation Program. Approximately one third of these manufacturers are located outside the state of California. The samples were secured from various locations within California by Bureau of Home Furnishings inspectors.

Critical Radiant Panel Test

Two types of test equipment are used for the Critical Radiant Panel Test:

1. Flooring Radiant Panel (Gas-Fired Radiant Panel) [1].
2. Electric Radiant Panel Veri-Flux "100" (Small-Scale Radiant Panel).

Flooring Radiant Panel (Gas-Fired Radiant Panel)

The Flooring Radiant Panel (Gas-Fired Radiant Panel) was developed between 1966 and 1974 at the Research & Development Laboratories of Armstrong Cork Company (now Armstrong World Industries) and further refined at the National Bureau of Standards (NBS). The manufacturer of the NBS Standard Flooring Radiant Panel used by the Bureau of Home Furnishings was Custom Scientific Instruments, Inc., of New Jersey (Fig. 1). The basic elements of this equipment are shown in Fig. 2. In this test a horizontally blown 100 cm insulation test specimen receives radiant energy from an air/gas fuel (propane) radiant panel mounted above the specimen and inclined at an angle 30 deg to horizontal. A pilot burner is used to initiate the test by open-flame ignition of the pre-heated specimen. The gas panel generates a flux profile along the length of the specimen ranging from 0.1 to 1.1 W/cm².

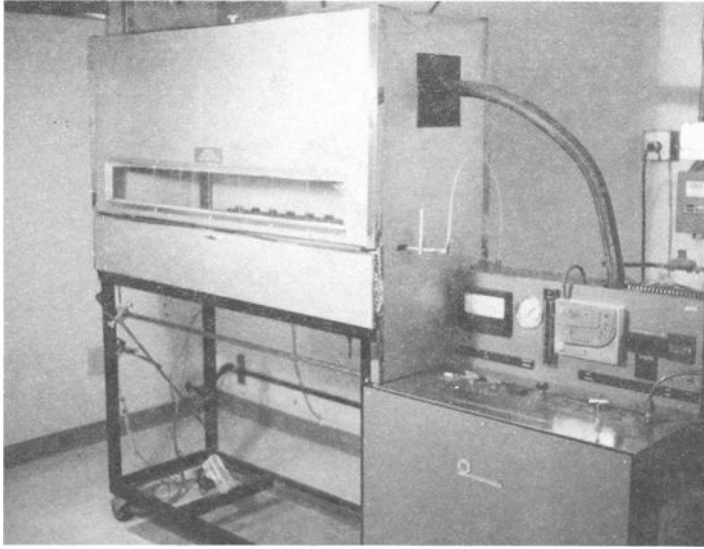


FIG. 1—Flooring Radiant Panel (Gas Radiant Panel).

Calibration of the Apparatus—To ensure that the heat flux profile is both accurate and adequate, the panel must be periodically calibrated. (The panel should be calibrated once a month, whenever a new propane tank is used, or when the black body temperature varies by more than 5°C from the calibrated black body temperature.) During the calibration process the radiant panel is stabilized at a black body temperature of 500 to 510°C . If the black body temperature does not stabilize within approximately 2 h, adjustment of the “panel gas adjust” is required. A dummy specimen board (calibration board) is placed on the sliding platform, positioned with stud bolts, slid into the chamber, and the door closed. Approximately 1 h is required for the chamber to reach equilibrium. Cooling water is turned on to maintain the temperature of the calibrated heat flux transducer. A precision digital millivolt meter or recorder should be used to document readings at all calibration points. The transducer is placed in bored holes (insuring that the transducer face is parallel with the face of the calibration board and at fixed positions). The heat fluxes at 20 , 40 , and 60 cm are measured and compared to standard fluxes in order to determine whether the profile will be satisfactory.

The allowable heat fluxes are: at 20 cm, 0.87 to 0.95 W/cm^2 ; at 40 cm, 0.48 to 0.52 W/cm^2 ; and at 60 cm, 0.22 to 0.26 W/cm^2 . (The conversion from mV to W/cm^2 is made by multiplying the applicable transducer calibration constant by the voltage.)

If the heat flux at any of the aforementioned distances is unsatisfactory, the gas flow is adjusted accordingly. Approximately 30 min to 1 h is allowed for the chamber to reach equilibrium before measuring heat fluxes again at 20 , 40 , and 60 cm. When acceptable heat fluxes are established at these distances, heat flux profile data are collected by measuring the heat fluxes in the following order: 10 , 20 , 30 , 40 , 50 , 60 , 70 , 80 , 90 , 98 , 10 , and 40 cm. (The 98 cm hole is added to obtain a better heat flux profile; the 10 and 40 cm holes are remeasured to insure that the previous data are reproducible.) The panel black body temperature, gas flow, air flow, room temperature, panel gas regulator pressure, static panel pressure, and chamber temperature are recorded. A graph is constructed by plotting the heat flux (W/cm^2) versus distance (cm) as measured from the panel's zero end, and the best smooth curve is drawn through the data points, to produce a heat flux profile.

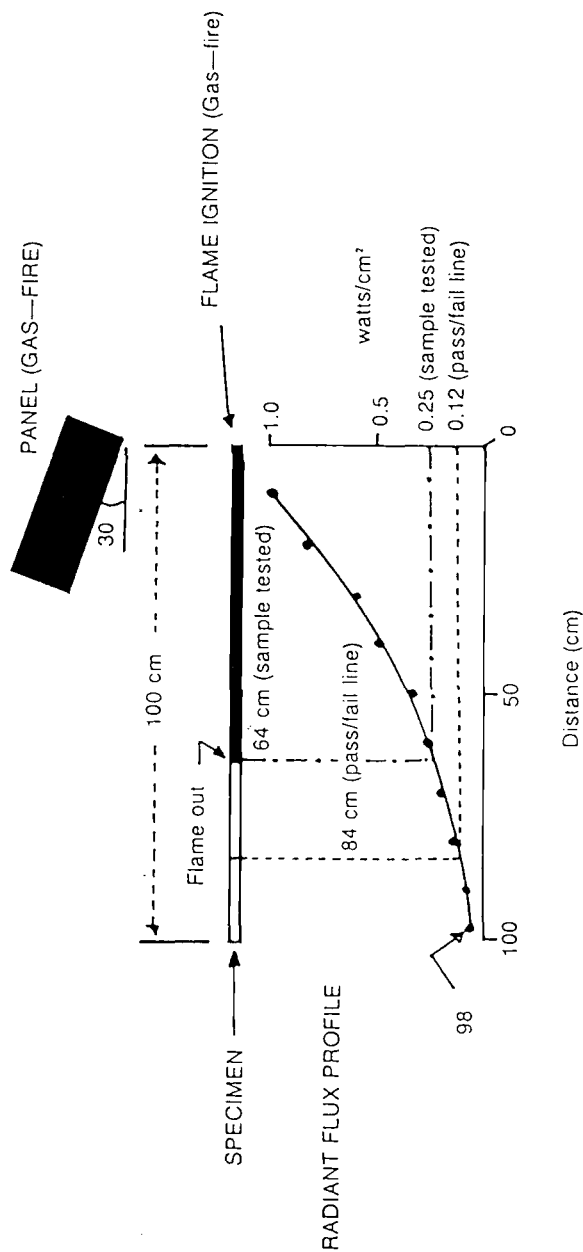


FIG. 2.—Basic elements and radiant flux profile of Flooring Radiant Panel.

Test Procedure—The prepared specimen tray of insulation is placed on the sliding platform and positioned with stud bolts. The pilot burner is ignited, the tray is moved into the chamber, and the door is closed. Following a 2 min preheat, the pilot burner flame is brought into contact with the center of the specimen at the 0 cm mark. The test is continued until all specimen flaming ceases. Then the door is opened and the sliding platform removed. The distance burned is measured and converted into W/cm^2 from the calibrated heat flux profile graph. The result is reported as a critical radiant flux of the insulation material in W/cm^2 (this value is the minimum flux necessary to sustain flame propagation). Samples which have a critical radiant flux of less than $0.12 \text{ W}/\text{cm}^2$, the minimum allowable critical radiant flux value, are normally photographed to maintain a permanent record of the test.

Veri-Flux "100" (Small-Scale Electric Radiant Panel)

The Small-Scale Radiant Panel (Electric Panel) was developed by Johnson Products, Inc., Sheffield, Alabama. The manufacturer of the panel used by the Bureau of Home Furnishings and Thermal Insulation was Insul Chem of Lehi, Utah. The basic elements of this equipment are shown in Fig. 3. In this test a horizontally blown 60 cm insulation specimen receives radiant energy from an electric radiant heater mounted above the specimen and inclined at an angle 30 deg to horizontal. A fireplace match is used to initiate the test by open-flame ignition of the preheated specimen.

Modifications of Electric Radiant Panel Machine—It has been found by extensive testing that the electric radiant panel apparatus in its present state (Fig. 4a) is not able to produce results that correlate with the results obtained on the gas radiant panel. Controls were added to the apparatus to stabilize the internal environment and help obtain reproducible results. In order to create a stable steady-state testing chamber temperature, two variable autotransformers were added to the apparatus (Fig. 4b). These autotransformers are individually used to control the fan speed as well as the radiant heater temperature. Voltmeters are used to monitor the amount of voltage supplied from each transformer. With these additional elements, reproducible results have been obtained.

Modifications of Calibration Board—The calibration board produced by Insul Chem has flux measurement points at 10, 20, 30, 40, and 50 cm. In order to obtain a more precise heat flux profile at the point of greatest concern, two extra measurement points were added at 45 and 55 cm.

Calibration of Apparatus—To insure that the heat flux profile is both accurate and adequate, the panel must be periodically calibrated. The panel should be calibrated once a month, whenever the radiant heater voltage or fan voltage is adjusted, or when there is a change in surrounding room conditions. The radiant panel is turned on and allowed to preheat to a stable, steady-state chamber temperature (i.e., 120°F [49°C]). This procedure takes approximately 30 min, since the panel temperature is very dependent on the room temperature; therefore its control is beneficial. If the temperature does not stabilize at approximately 120°F (49°C), adjustment of the fan speed or radiant heater through the use of the variable autotransformers is necessary. The dummy specimen is mounted on the slide rails and placed in the chamber. It is then allowed to preheat for approximately 30 min. It is suggested that the room temperature be controlled between 70 and 80°F (22 and 27°C); otherwise calibration will be constantly affected. The cooling water is turned on at the rate of 5 gal/h (300 mL/min) and allowed to circulate through the heat flux transducer for 10 to 15 min or until the temperature of the water stabilizes between 40 and 80°F (5 and 27°C). The heat flux transducer is placed in the bored holes (insuring that the transducer face is parallel with the face of the calibration board).

Heat flux profile data are measured in the following order: 10, 40, 10, 20, 30, 40, 45, 50, 55, 10, and 40 cm. Heat fluxes at 10 and 40 cm are measured before and after recording the flux at different distances (cm) in order to insure consistent readings. (The value on the heat flux meter is in W/cm^2 .)

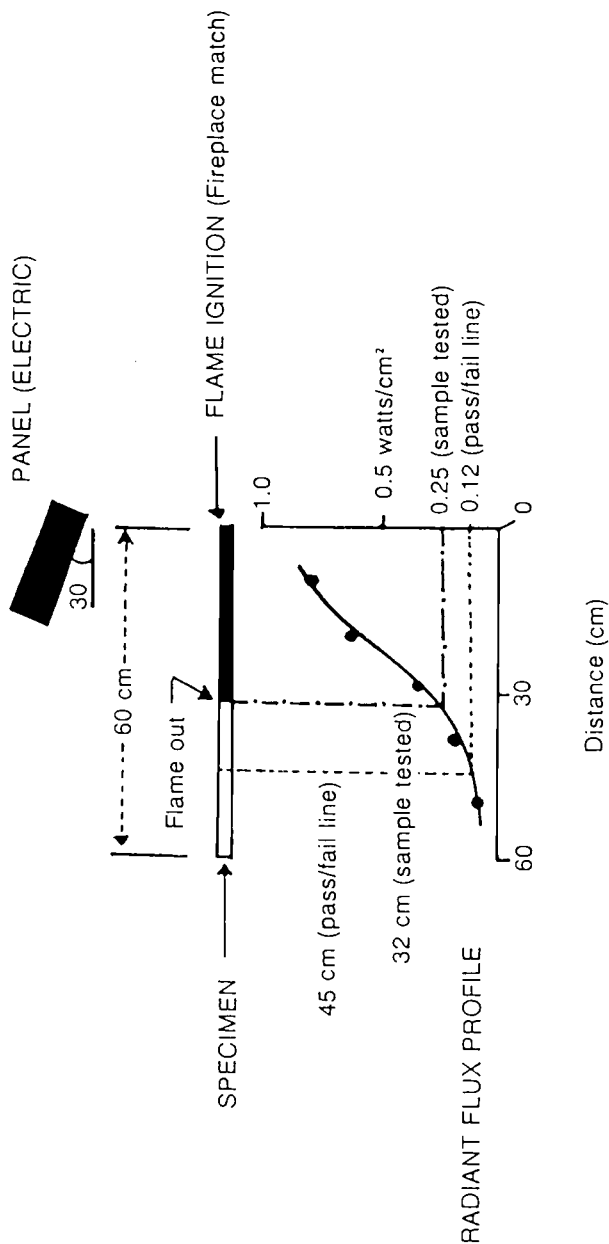


FIG. 3—Basic elements and radiant flux profile of Veri-Flux "100" Radiant Panel (Electric Radiant Panel).

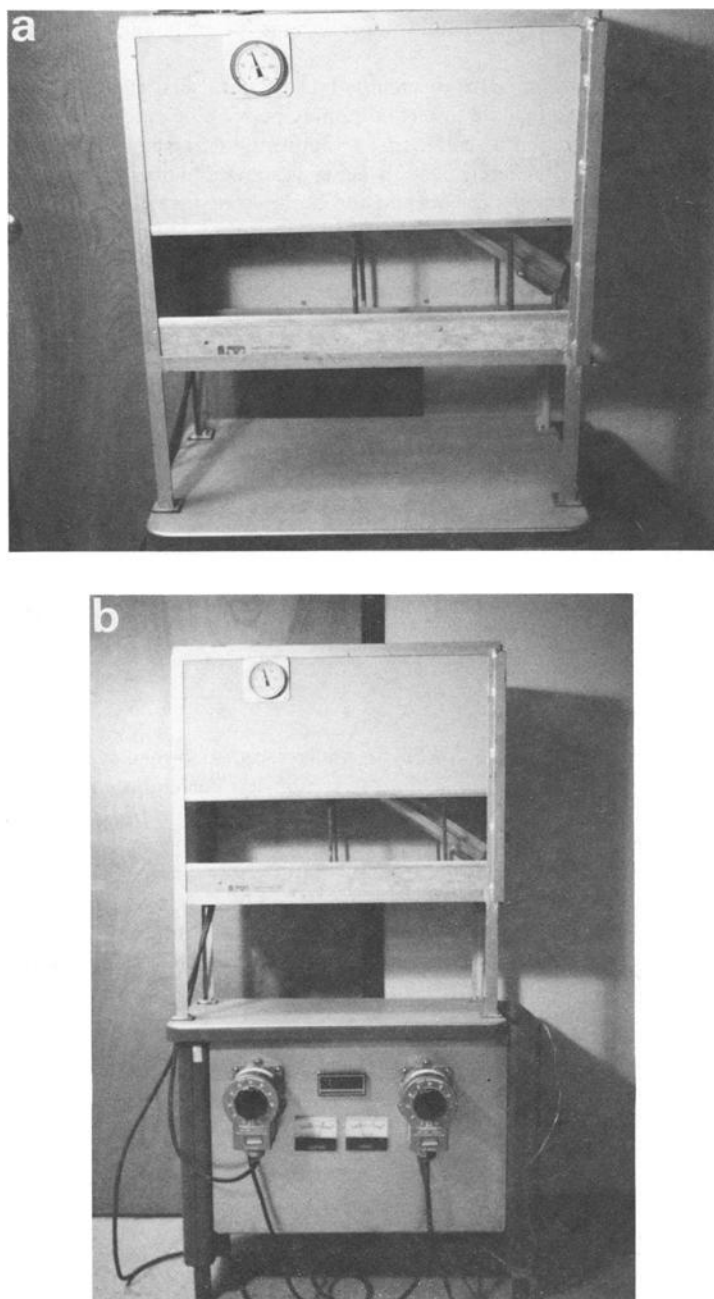


FIG. 4—Veri-Flux "100" Radiant Panel. (a) Present. (b) Modified.

A graph is constructed by plotting the heat flux values (W/cm^2) for each point (10, 20, 30, 40, 45, 50, and 55) versus distance (cm) from the panel end, and the best smooth curve is drawn by connecting all points, to produce a heat flux profile for the small-scale radiant panel. Room temperature, chamber temperature, and voltage settings for the fan and electric radiant heater are also recorded.

Test Procedure—The specimen tray is mounted on the slide rails, placed in the chamber, and the door is closed. At the end of a 3 min conditioning period, the entry door is opened and the specimen is ignited at the high flux end, using an appropriate flame source (a fireplace match). The door is closed again immediately. The specimen is allowed to burn until the flaming ceases. When the flame goes out, the door is opened and the specimen tray removed. The burned distance is measured (from the ignited end to the maximum burn point) and converted into W/cm^2 from the calibrated heat flux profile graph. To meet test criteria, a specimen should have a critical radiant flux of $0.12 \text{ W}/\text{cm}^2$ or greater.

The chamber temperature should be consistent for all tests. An operator must wait for the chamber temperature to return to $120 \pm 2^\circ\text{F}$ (49°C) before beginning a new test.

Preparing the Specimen Tray (Both Apparatus)

Before testing the 53 specimens, they were conditioned in a controlled temperature and humidity environment (72°F [22°C] and 50% relative humidity) in accordance with procedures in the Federal Register [1]. The conditioned specimen was blown into a cyclone apparatus by gently feeding the material into the intake. When sufficient material had been blown, the blowers were turned off and the trays removed from the collection chamber. Excess insulation was carefully screeded off with a flat ruler so that the level of insulation was flush with the top edges of the tray.

Results and Discussion

The Critical Radiant Flux testing of 53 specimens was performed on two types (Gas and Electric) of Critical Radiant Panel machines to establish a correlation between them. It was difficult to use the Electric Radiant Panel machine in its present form. When the unmodified Electric Radiant Panel was first used by the Bureau no consistency in the surface burning of the specimens was found. The assumption was made that this was due to lack of control of the fan speed and radiant heater temperature. As explained, modifications were carried out to the instrument and its calibration board. After modifications it was observed that the operator had much better control of the machine in obtaining and maintaining the panel temperature.

To minimize human error in testing the samples the following precautions were taken:

1. For each sample, six specimens were prepared and tested on both apparatus.
2. The same technician prepared the specimen trays for both apparatus.
3. Specimen trays for each sample were prepared at the same humidity and temperature (same day).
4. The same technician performed the test on all specimen trays for each apparatus.

The 53 cellulose insulation samples tested during this study fell into one of the following categories:

- Severe failure on Gas Radiant Panel.
- Pass on Gas Radiant Panel.
- Borderline samples (pass/fail).

Gas Radiant Panel and Electric Radiant Panel test results were tabulated (Table 1) in the following categories on the basis of their pass/fail test results:

- Passing or failing on both Gas and the Electric Radiant Panels.
- Failure on the Gas Radiant Panel and passing on the Electric Radiant Panel.
- Passing the Gas Radiant Panel and failing the Electric Radiant Panel.

(Failure means radiant flux of less than 0.12 W/cm^2 , pass means radiant flux of 0.12 W/cm^2 or more.)

Table 1 shows that in Category 1, 37 samples of 53 tested were identical in terms of pass/fail. (Of 37 samples tested, 19 passed and 18 failed on both machines.) In Category 2, 14 of 53 samples failed the Gas Radiant Panel but passed the Electric Radiant Panel. This could be due to the following sources of error:

- Insufficient control of the Electric Radiant Panel.
- Slight variations in preparation of specimen trays.
- Fire-retardant chemicals not homogeneously distributed.
- Quality of fire-retardant chemicals.

In Category 3, it was difficult to explain why 2 of 53 samples passed the Gas Radiant Panel and failed the Electric Radiant Panel. It was observed in this category that all specimens for each sample behaved inconsistently (i.e., there was no consistency between the six specimens).

The Pearson Product Moment Correlation Coefficient (r) was calculated to determine the degree of correlation between the Gas Radiant Panel and the Electric Radiant Panel. The calculated correlation coefficient was 0.774 and was based on the mean numeric value for each of the six test specimens on the two apparatus. This correlation coefficient indicates a high degree of correlation between the Gas Radiant Panel and the Electric Radiant Panel.

Conclusions

1. Based on the results of this study, after some modifications in the Electric Radiant Panel apparatus, a high degree of correlation between Gas Radiant Panel and Electric Radiant Panel can be obtained.

2. Approximately 70% of the samples had a direct correlation between these two apparatus in terms of pass/fail.

3. Of the samples passing the Electric Radiant Panel, 60% passed and 40% failed the Gas Radiant Panel, based on this population of samples.

4. Although the overall numeric correlation between the Gas Radiant Panel and Electric Radiant Panel was high, caution should be used in allowing the Electric Radiant Panel to predict the pass/fail outcome of the Gas Radiant Panel. Twenty samples tested on the Electric Radiant Panel failed, and the corresponding results of the Gas Radiant Panel showed 18 failed samples. If a sample failed on the Electric Radiant Panel, it was concluded that it would also fail on the Gas Radiant Panel. However, 33 samples passed the Electric Radiant Panel and the

TABLE 1—*Gas Radiant Panel and Electric Radiant Panel test results.*

	No. of Samples	Identical Pass/Fail Results	Same Sample Contradictory Pass/Fail Results	
			Gas Radiant Panel	Electric Radiant Panel
Category 1	37	Pass & Fail in both machines
Category 2	14	...	Fail	Pass
Category 3	2	...	Pass	Fail
Total	53			

corresponding results had 19 passes and 14 failures on the Gas Radiant Panel. The predictive ability of the Electric Radiant Panel was not as good when the sample passed on the Electric Radiant Panel.

5. This study will aid the ASTM C 739 jurisdiction subcommittee in the development of new recommended testing procedures for the Electric Radiant Panel.

Further Recommendations

The following improvements are recommended for the Electric Radiant Panel to better correlate with Gas Radiant Panel:

- Changing the black body (test chamber) temperature.
- Changing or modifying the radiant heater.
- Establishing a standard air flow (velocity) through the apparatus.

Reference

- [1] Interim Safety Standards for Cellulose Insulation, Consumer Product Safety Commission, *Federal Register*, Vol. 44, No. 131, 6 July 1979, pp. 39966–39973 (State of California – Insulation Program Standard).

Field Data on Settling in Loose-Fill Thermal Insulation

REFERENCE: Svennerstedt, B., "Field Data on Settling in Loose-Fill Thermal Insulation," *Insulation Materials, Testing, and Applications, ASTM STP 1030*, D. L. McElroy and J. F. Kimpflen, Eds., American Society for Testing and Materials, Philadelphia, 1990, pp. 231-236.

ABSTRACT: Blown loose-fill thermal insulation was introduced to Sweden in the late 1970s and has become more common since then. Today loose-fill insulation is used especially for attics, both as insulation in new building production and as additional insulation in older buildings. Loose-fill insulation is mainly manufactured from mineral wool and cellulosic materials.

As users of loose-fill thermal insulation know, this insulation type can settle, which means that it will compress. It is of great importance to know the long-term behavior of the insulation thickness, so as to be able to estimate the insulation capacity during the lifetime of the structure.

This paper reviews a field study of settling in loose-fill thermal insulation performed by the National Swedish Institute for Building Research. The study is confined to the use of loose-fill insulation for horizontal structures and formed part of a wider project in which a laboratory study also was performed.

In the field study both mineral wool and cellulosic loose-fill materials were investigated. The loose-fill materials were blown on several test attics, and settling was measured during one year within the project. The paper presents results of settling after three years in practice.

KEY WORDS: loose-fill insulation, settling, attics

Loose-fill thermal insulation materials like slag and different kinds of shavings have been used in Sweden for several years. Wall and floor structures of older buildings were insulated by hand-filling their cavities.

Since the late 1970s, blown loose-fill thermal insulation has been available on the Swedish market. Today a considerable part of the thermal insulation manufactured in Sweden is loose-fill material. The main types of loose-fill insulation are mineral wool and cellulosic materials. The blown loose-fill materials are especially used for attics, both as additional insulation in older buildings and as insulation in new building production.

As users of loose-fill thermal insulation know, this type of insulation can settle, which means that the insulation layer will compress. It is of great importance to know the long-term behavior of the insulation thickness, so as to be able to estimate its insulation capacity (thermal resistance) during the lifetime of the structure.

In 1984 a project for the purpose of studying settling of loose-fill thermal insulation was started at the National Swedish Institute for Building Research. The survey was initiated by the Swedish thermal insulation manufacturing industry and was partly financed by that industry. The investigation was confined to the use of loose-fill insulation for horizontal structures, primarily attics, and was divided into a field study and a laboratory study. The settling project was completed at the beginning of 1986.

¹Civil Engineer, Materials and Structures Division, The National Swedish Institute for Building Research, Box 785, S-801 29 Gävle, Sweden.

Purpose of the Field Study

The purpose of the field study was to investigate the long-term settling development of loose-fill materials under practical conditions.

Loose-Fill Materials Investigated

Table 1 shows standard values of thermal conductivity, moisture ratio, and density for the four different types of loose-fill materials that were investigated. The data in Table 1 are taken from the Swedish standard approval certificate for each material.

The λ_{10} -value is the thermal conductivity test value measured in the laboratory with a mean temperature of 10°C. The λ_n -value is the thermal conductivity value, which is used for calculations. The nominal density value is the value at which the Swedish contractors have to blow their loose-fill material. Below the minimum density the contractors should not blow any material.

Both cellulosic and mineral wool loose-fill materials were studied in the field investigation. The cellulosic materials consisted of cut newspaper and were treated with different kinds of chemicals in order to prevent fire, moisture, and fungus attack. Cellulosic 1 was treated with boron compounds; Cellulosic 2 was treated with aluminum compounds. In general the newspapers were cut into smaller fibers for Cellulosic 1 than for Cellulosic 2. The mineral wool material consisted of one rockwool material and one glass fiber material.

Performance

In the field study four test buildings were chosen: two stone houses and two wooden houses. Each test building was more than 30 years old.

The attic floor structure of the stone houses was made of concrete; on top there was a 10 to 15 cm thick slag insulation layer. The wooden houses had roof structures of wood trusses. Between the roof trusses there was a 15 to 20 cm thick insulation layer of cutter shavings.

The attic areas of the test buildings were divided into four areas, one for each loose-fill material tested. Each test area was 100 m² in the stone houses and 50 m² in the wood houses.

Each test area was prepared with a number of measuring sticks (Fig. 1). The greater test areas were allotted five sticks, the smaller areas three sticks. The zero level of each measuring stick was calibrated to the upper level of the old insulation. The height scale of the measuring stick was graduated in millimetres.

The loose-fill materials were installed in each attic area as additional thermal insulation. In the stone houses the installed thickness varied between 23.5 and 44.5 cm. In the wood houses the additional insulation thickness varied between 16.0 and 36.0 cm.

During the test period, which originally was limited to one year but was extended to three years, the thickness of the insulation layer was read manually. The reading time intervals were

TABLE 1—Standard values of different properties for the loose-fill materials investigated.^a

Loose-Fill Materials	Thermal Conductivity (W/m K)		Density (kg/m ³)		Moisture Ratio (wt. %)
	λ_{10}	λ_n	Nom.	Min.	
Cellulosic 1	0.037	0.045	35	31	10
Cellulosic 2	0.038	0.045	35	32	10
Glass fiber	0.040	0.051	17	14	0
Rock wool	0.039	0.051	29	26	0

^a λ_{10} = thermal conductivity, tested at 10°C mean temperature (W/m K).

^b λ_n = calculating thermal conductivity (W/m K).

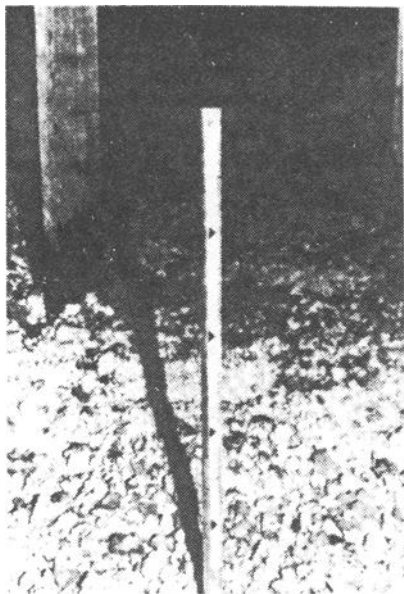


FIG. 1—Measuring stick used for settling measurements of loose-fill materials.

rather short during the first year of the test period (after one day, one week, one month, three months, six months, nine months, and twelve months). During the rest of the test period the readings were performed every six months. The accuracy of the readings was ± 5 mm.

Results

Settling

The field study has shown that there is a great difference in settling between cellulosic and mineral wool materials. Figures 2 and 3 show the settling for each material group. The results are expressed in percentages of the end-height of the insulation layer after a test period of three years. In the figures the settling is shown as an average settling value. The average values for each material group are calculated from 16 measuring points.

Figure 2 shows the settling of cellulosic loose-fill materials. After one year the average value for cellulosic materials is about 15%. The variation between the two tested cellulosic material types is about 5%. The settling after three years shows an average value of 19%, still with a variation of 5% between the two cellulosic materials. After three years the average settling of cellulosic materials expressed in absolute values is about 4.6 cm.

The settling of the mineral wool materials occupies a lower average level compared with the cellulosic materials. After one year the average value for mineral wool materials is about 5%. The variation between glass fiber and rock wool materials is negligible. The glass fiber material showed a generally somewhat higher value than the rock wool material, but the difference was less than 2% (Fig. 3). After the three-year test period the settling had only marginally changed compared with the one-year value and was still on a 5% level. In absolute values the average settling is about 1.3 cm.

The large difference in settling between the two material groups is due to several factors. One concerns the insulation materials and their way of forming an insulation layer. The cellulosic loose-fill materials consist of small material fibers that are laid loosely on each other without any

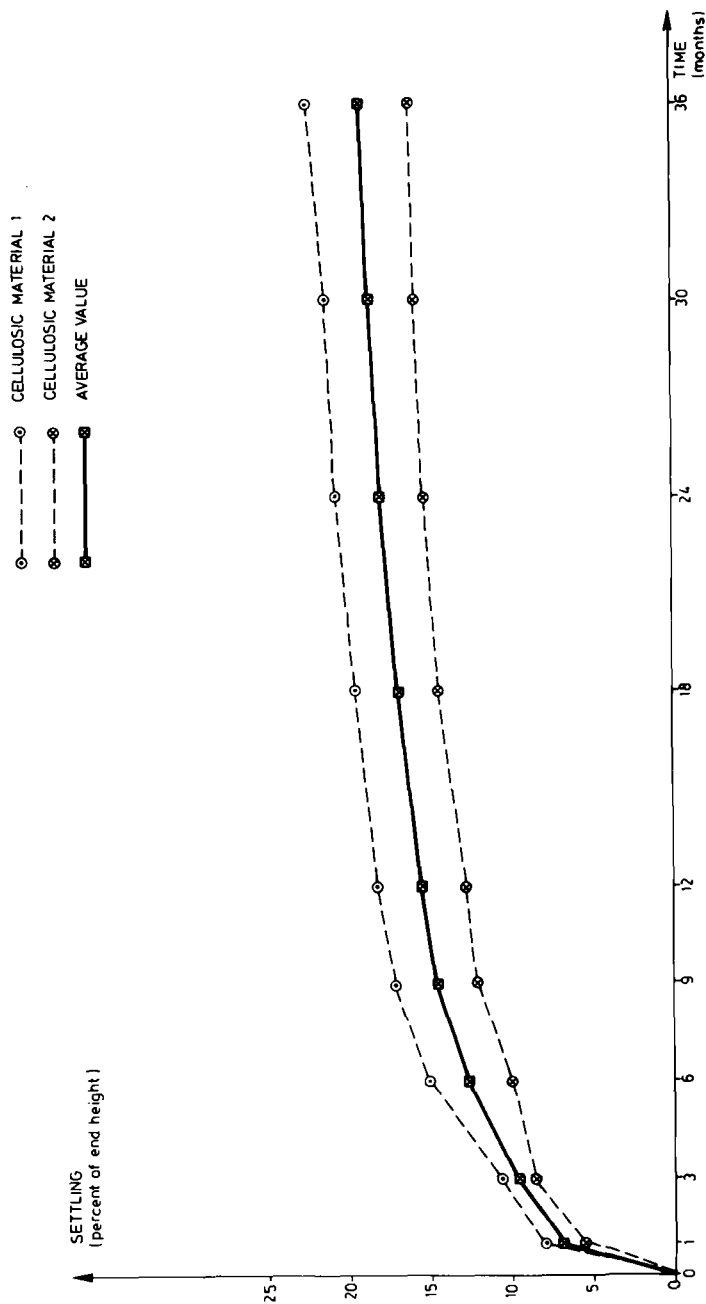


FIG. 2.—Settling versus time for cellulose materials (field objects).

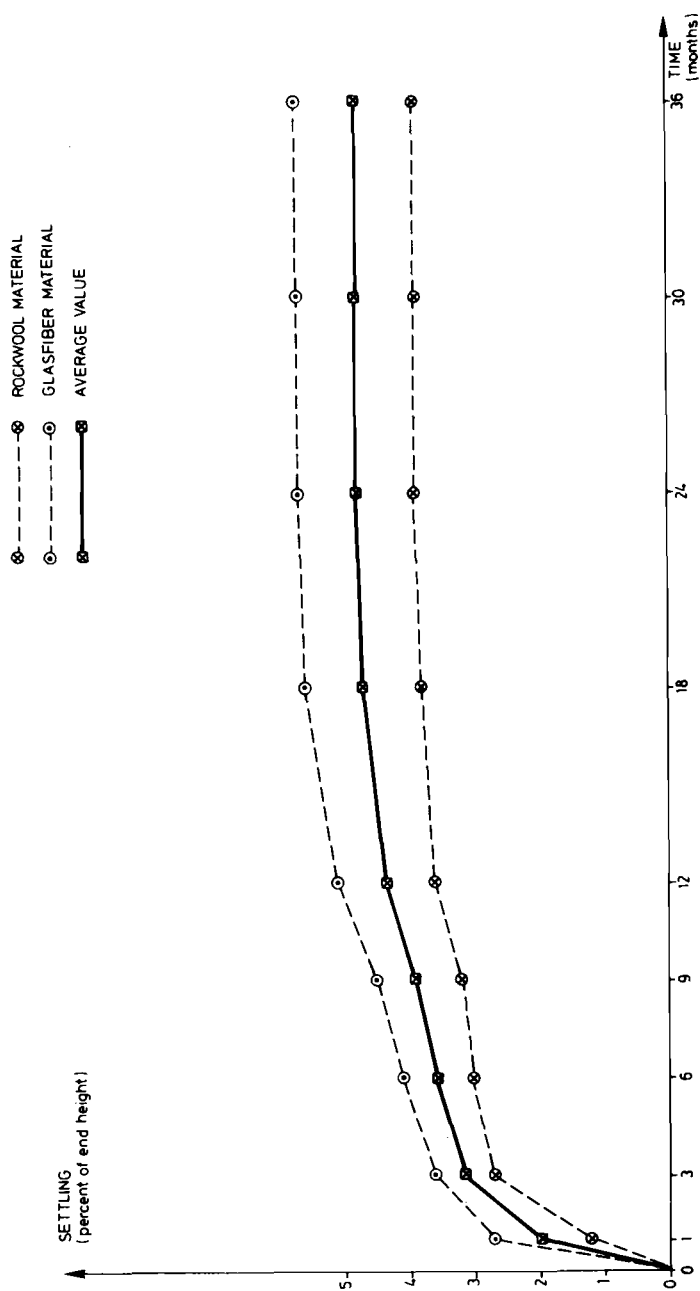


FIG. 3—Settling versus time for mineral wool materials (field objects).

anchorage between them. The mineral wool materials consist of long, thin fibers which are connected to each other. Thus the mineral wool materials are less affected by external factors than the cellulosic materials.

Densities

For Cellulosic 1 the densities installed varied between 46 and 30 kg/m³; for Cellulosic 2 the densities varied between 43 and 34 kg/m³. The densities of the rock wool material installed were between 30 and 26 kg/m³; for glass fiber the densities installed were between 21 and 16 kg/m³.

Conclusions

In order to calculate the thermal insulation resistance of loose-fill materials it is important to know the long-term behavior of the insulation thickness. Thickness changes concurrently with the settling of the loose-fill materials.

The settling of loose-fill insulation materials has been investigated in a Swedish study performed by the National Swedish Institute for Building Research. Cellulosic and mineral-wool materials for horizontal application were studied in the field and laboratory.

An important finding of the field study is that there is a large difference between cellulosic and mineral-wool materials. After a three-year test period the cellulosic loose-fill materials show an average settling value of 19%. The settling of mineral wool materials occupies a much lower average level compared with the cellulosic materials. After the same test period the settling of mineral wool materials is about 5%. Settling is expressed in percentages of the end-height of the insulation layer after the test period.

References

- [1] Svennerstedt, B., "Settling of Loose-Fill Thermal Insulation," Bulletin M85:31, National Swedish Institute for Building Research, Gävle, Sweden, 1986.

An *In Situ* Evaluation of the Settling of Loose-Fill Rock Wool Insulation in the Attics of Two Manufactured Home Units

REFERENCE: Graves, R. S. and Yarbrough, D. W., "An *In Situ* Evaluation of the Settling of Loose-Fill Rock Wool Insulation in the Attics of Two Manufactured Home Units," *Insulation Materials, Testing, and Applications, ASTM STP 1030*, D. L. McElroy and J. F. Kimpflen, Eds., American Society for Testing and Materials, Philadelphia, 1990, pp. 237-243.

ABSTRACT: The effect of vibrations due to manufacturing and transport on the thickness, density, and calculated thermal resistance (R-value) of loose-fill rock wool insulation installed in two manufactured home units has been determined. Thickness and density measurements on blown attic insulation were made after installation, at the end of the manufacturing process, and after the units were towed 426.5 km (265 miles). These measurements were used to calculate R-values for the attic insulation. The end sections of the two units showed an overall insulation thickness decrease of about 16% and an average R-value change from 5.50 to $5.08 \text{ K} \cdot \text{m}^2/\text{W}$ (31.2 to $28.8 \text{ ft}^2 \cdot \text{h} \cdot ^\circ\text{F}/\text{Btu}$). An estimated R-value greater than $5.29 \text{ K} \cdot \text{m}^2/\text{W}$ ($30 \text{ ft}^2 \cdot \text{h} \cdot ^\circ\text{F}/\text{Btu}$) resulted from averaging the end and middle sections of the two units. The effect of reduced thickness along the edges of the attic space was not included in the estimate.

KEY WORDS: thermal insulation, manufactured homes, settling, loose-fill insulation, thermal resistance, insulation density

The thermal resistance at 23.89°C (75°F) of a loose-fill thermal insulation installed in an attic depends on thickness and density for a specific type of fiber. A test method for predicting the settled density of loose-fill cellulosic insulation has been in use for several years [1], and efforts have been under way to collect data that define the extent of settling of loose-fill mineral fiber products in attics [2-5]. Thickness and density measurements are used to quantify settling, but thermal resistance (R-value) is the most important property and must be considered. Field examination of loose-fill attic insulation involves long-term monitoring of materials installed in accordance with label specifications and amounts. Observed settling of above-label-density materials, such as loose-fill fiberglass at densities above $16.0 \text{ kg}/\text{m}^3$ ($1.0 \text{ lb}/\text{ft}^3$) or loose-fill rock wool above $46.5 \text{ kg}/\text{m}^3$ ($2.9 \text{ lb}/\text{ft}^3$), has been negligible [2].

The manufactured housing industry is providing an increasing percentage of new houses, but available data on the behavior of insulation in their structures are scarce. The study reported here was undertaken to add to the data available for attic insulation in manufactured houses [6, 7].

A limited study of the potential settlement of insulation blown into attics in manufactured houses was undertaken in cooperation with a manufacturer who builds single- and double-wide houses in a manufacturing plant. The manufactured units are then highway transported to buyers.

This manufacturer utilizes rock wool blowing wool product and advertises an R-value of $5.29 \text{ K} \cdot \text{m}^2/\text{W}$ ($30 \text{ ft}^2 \cdot \text{h} \cdot ^\circ\text{F}/\text{Btu}$) in the attics of its manufactured houses. This insulation is used as

¹Metals and Ceramics Division, Oak Ridge National Laboratory, Oak Ridge, TN 37831.

one feature to satisfy the heat transmission resistance requirements related to manufactured housing [8]. The information on the insulation manufacturer's label indicates that the material should be installed at a density of 27.2 kg/m^3 (1.7 lb/ft^3). At this density an insulation thickness of 0.2466 m (9.71 in.) is specified for the above R-value.

Normally, the number of bags of insulation blown into an attic is calculated on the basis of the area of the attic. The objective of the test reported here was to determine the extent of settling of the blown-in insulation in the attics of two units (1) after witnessing the installation at 27.2 kg/m^3 (1.7 lb/ft^3) density, (2) after completion of the manufacturing process, and (3) after the units had been towed to the buyer.

Description of the Test

The test house consisted of two units identified by Serial Numbers 2125A and B. Each unit was 19.54 m (64.1 ft) long and 3.597 m (11.8 ft) wide. The total attic area was 70.23 m^2 (756 ft^2), and the insulation label showed that 36 twenty-nine-pound bags of insulation per unit would be required for an R-30 installation. There were 49 trusses that formed 48 bays in each attic (Figs. 1a and 1b). The trusses were numbered from 1 to 49 starting from the front of the structure. Only seven bays at the front and eleven bays at the rear could be examined at the end of the test because of the way the attic is enclosed. Those accessible attic areas were designated as the primary test sites. Wooden rulers 0.4572 m (18 in.) long were attached to trusses as shown in Fig. 1b to measure the depth of insulation at the time of installation and later.

The insulation was blown into the attics on 15 August 1985 with a commercial blowing machine. The machine was equipped with 39.62 m (130 ft) of 0.1016 m (4 in.) diameter hose. The

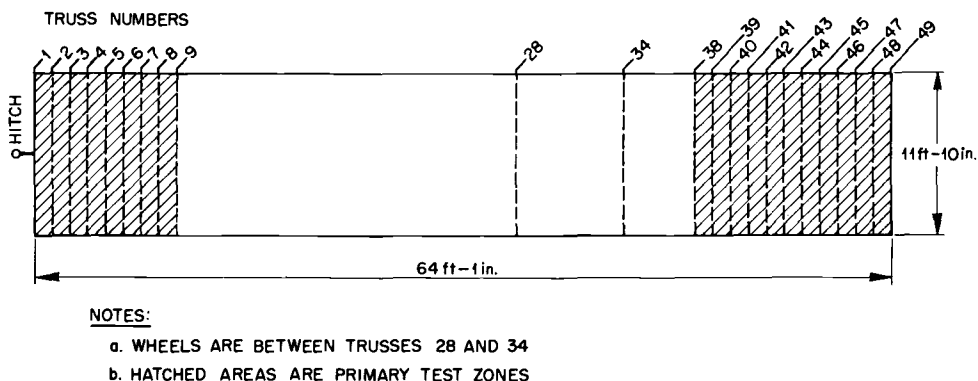


FIG. 1a—Top view of accessible part of attic (multiply feet by 0.3048 to obtain dimensions in metres).

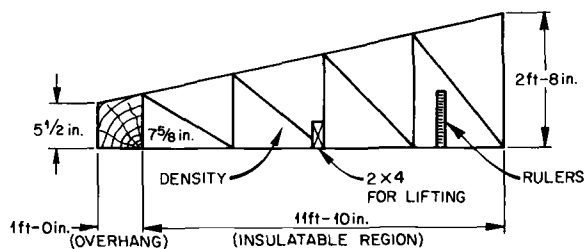


FIG. 1b—Side view of accessible part of attic (multiply feet by 0.3048 to obtain dimensions in metres).

gate and air settings were made by the rock wool manufacturer's area manager to ensure installation that was consistent with the product label. As a preliminary test of machine settings, approximately one bag of insulation was blown into a boxed-in area in the plant and two density determinations were made with a cylindrical cutter. Analysis of *in situ* loose-fill insulation density data indicates that the average measured density of 24.99 kg/m^3 (1.56 lb/ft^3) was satisfactory for the test. Attic application was done by the normal work crew with the exception of one third of Unit A in which the insulation was installed by the insulation manufacturer representative. Thirty-seven bags of insulation were installed in each unit on the basis of nominal dimensions of 19.51 by 3.658 m (64 by 12 ft). The insulation above the ceiling of a manufactured home is not of uniform thickness. As is the case with site-built homes there is also variation in insulation density. The agreement between mass of insulation installed and mass of insulation calculated from thickness and density measurements is generally poor unless a detailed determination of the density and thickness distribution is made. For this reason, repeated measurements were made within well-defined regions to reduce spatial variations. In this study the repeated measurements were made near the axis of the unit where the insulation is at full thickness. A complete distribution of thickness and density was not obtained.

In addition to the attic insulation, two 0.61 by 0.61 m (2 by 2 ft) boxes, each with an attached ruler, were filled to a depth of approximately 0.3048 m (12 in.) with the same product. One box was placed inside each unit to determine if floor vibration would produce settling different from that in the attics.

Results of the Test

After the insulation was installed, manila file folders with centered slots were slipped over the seven rulers in the accessible regions in each unit. The purpose of the folders was to provide a thickness average over an area and to define the ruler reading. In Unit B five density determinations were made with a cylindrical cutter. These were along the length of the unit, but only three were in the primary test areas shown in Figs. 1 and 2. The three in the test areas averaged 26.3

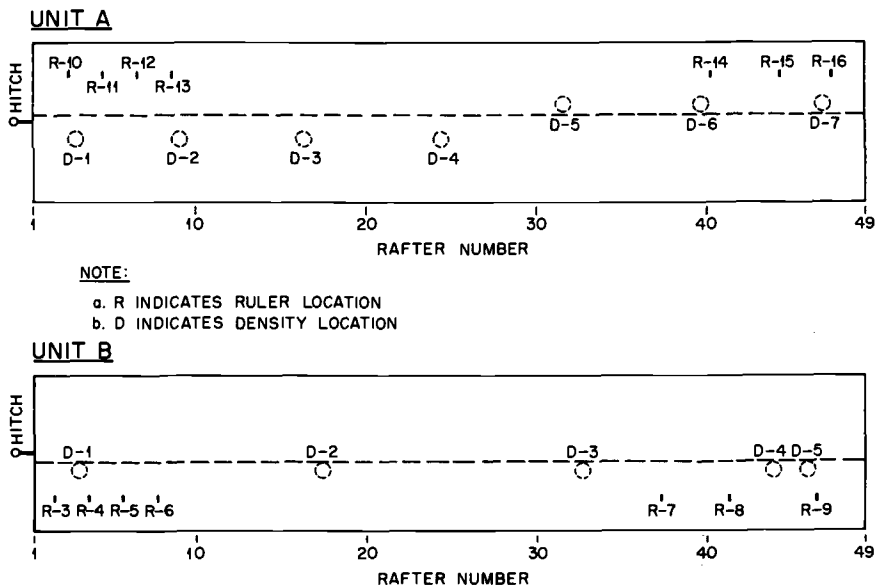


FIG. 2—Locations of thickness and density measurements.

kg/m³ (1.64 lb/ft³), which was very close to the label density of 27.2 kg/m³ (1.7 lb/ft³). The two densities in the center area were 33.3 and 41.0 kg/m³ (2.08 and 2.56 lb/ft³). An average thickness of 0.2583 m (10.17 in.) was derived from 22 end-section thickness measurements. The average density in the end sections of Unit A as determined with a cylindrical cutter was 28.4 kg/m³ (1.77 lb/ft³) at an average thickness of 0.2550 m (10.04 in.); the middle section had an average density of 39.9 kg/m³ (2.49 lb/ft³) at an average thickness of 0.2637 m (10.38 in.). Equations 1 and 2 were used to calculate the R-values corresponding to the insulation density and thickness measurements in the end sections and middle sections of the two test units:

$$R\text{-value} = \text{thickness/apparent thermal conductivity} \quad (1)$$

$$k_a = 7.551 \times 10^{-3} + 2.2130 \times 10^{-4} \rho + 0.9016/\rho \quad (2)$$

$$(k_a = 0.0524 + 0.0246 \rho + 0.3906/\rho)$$

Equation 2 was obtained from published data for loose-fill rock wool insulation [2] and gives k_a in W/m · K (Btu · in./ft² · h · °F) at a mean temperature of 23.89°C (75°F) with density, ρ , in kg/m³ (lb/ft³). The third term in the equation was adjusted to match the rock wool manufacturer's label information. Calculated end-section R-values as installed were 5.59 and 5.41 K · m²/W (31.7 and 30.7 ft² · h · °F/Btu) for Units A and B respectively. All results from tests of Units A and B are given in Tables 1 and 2 and summarized in Tables 3 and 4.

The manufacturing steps that follow the attic insulation installation induce considerable vi-

TABLE 1—Density (lb/ft³) and thickness (in.) measurements for Unit A.^a

Location ^b	Initial	At End of Manufacture	At Destination
Density (Thickness)^c			
3-4	1.863 (10.33)		
9-10	1.614 (9.12)		
39-40	1.742 (9.41)		
45-46	1.866 (11.02)		
Average	1.77		
16-17	2.578 (9.83)		
24-25	2.333 (11.21)		
32-33	2.571 (10.09)		
Thickness with Probes^c			
3-4		8.02	7.32
5-6		8.76	7.85
39-40		10.62	9.50
45-46		9.68	8.68
Thickness with Rulers			
3	9.06	8.50	8.00
5	10.00	8.75	7.25
7	10.00	9.00	8.00
9	10.56	10.00	9.50
41	10.25	9.25	8.12
44	10.62	10.25	9.00
47	11.06	10.25	8.75

^aData were recorded in inch-pound units.

^bSee Fig. 1 for truss numbering system.

^cThickness values are the average of five measurements.

TABLE 2—Density (lb/ft³) and thickness (in.) measurements for Unit B.^a

Location ^b	Initial	At End of Manufacture	At Destination
Density (Thickness)^c			
3-4	1.560 (8.86)		
43-44	1.644 (9.20)		
45-46	1.726 (12.59)		
Average	1.64		
17-18	2.077 (10.24)		
32-33	2.563 (10.50)		
Thickness with Probes^c			
3-4		8.64	8.27
6-7		9.83	8.92
39-40		10.33	9.24
48-49		10.16	8.68
Thickness with Rulers			
2	10.00	7.50	7.00
4	9.69	8.75	8.25
6	10.56	9.50	8.88
8	10.62	^d	
37	9.94	8.50	7.88
41	9.31	8.62	7.38
46	10.38	8.50	7.38

^aData were recorded in inch-pound units.^bSee Fig. 1 for truss numbering system.^cThickness values are the average of five measurements.^dRuler was damaged.

TABLE 3—Summary of density and thickness measurements.

Location	Initial Density, kg/m ³ (lb/ft ³)	Initial Thickness, cm (in.)	Thickness at End of Manufacturing, cm (in.)	Thickness at Destination, cm (in.)
Unit A				
End section	28.4 (1.77)	25.50 (10.04)	23.65 (9.31)	21.21 (8.35)
Mid-section	39.9 (2.49)	26.37 (10.38)		
Unit B				
End section	26.3 (1.64)	25.83 (10.17)	24.05 (9.47)	21.72 (8.55)
Mid-section	37.2 (2.32)	26.34 (10.37)		

bration in the structure. Consequently, the thicknesses indicated by the *in situ* rulers in the accessible end sections were observed at the end of manufacturing, and additional thickness measurements were made with probes as shown in Tables 1 and 2. Probes about 0.48 m (19 in.) long were fabricated from 0.00318 m (0.125 in.) diameter brass welding rods. The probes can be used with a finely graduated steel rule to determine thickness to about ± 0.0064 m (± 0.25 in.). Equation 3 was used to calculate the density, ρ_2 , after a change in thickness to t_2 giving the information needed for the calculation of R-value.

$$\rho_2 = \rho_1 t_1 / t_2 \quad (3)$$

TABLE 4—*Calculated thermal resistances.*

Location	Initial Value, K · m ² /W (ft ² · h · °F/Btu)	At End of Manufacturing, K · m ² /W (ft ² · h · °F/Btu)	At Destination, K · m ² /W (ft ² · h · °F/Btu)	Change in R-Value, %
Unit A				
End section	5.59 (31.7)	5.40 (30.6)	5.11 (29.0)	−8.5
Mid-section	6.77 (38.4)		5.94 (33.7) ^a	−12.2
Unit B				
End section	5.41 (30.7)	5.26 (29.8)	5.01 (28.4)	−7.5
Mid-section	6.58 (37.3)		5.87 (33.3) ^a	−10.7

^aCalculated by using percent decrease in thickness from end sections.

Six end-section rulers remained in place in Unit B at completion of construction, and seven end-section rulers remained in place in Unit A. The average end-section thickness in Unit A was 0.2365 m (9.31 in.); the average end-section thickness in Unit B was 0.2405 m (9.47 in.). The end-section R-values corresponding to the end-of-manufacture thicknesses are 5.39 and 5.26 K · m²/W (30.6 and 29.8 ft² · h · °F/Btu) for Units A and B, respectively.

The file folder at one location showed an indentation at the end of manufacturing, so the folders were removed to prevent compression due to folder movement. The insulation thicknesses determined in the end sections after removal of the folders represent a starting point for evaluating the effect of transport. The two units were towed 426.5 km (265 miles) primarily on interstate highways in 5 h for an average speed of 53 mph by the usual transport procedures.

Thicknesses in the accessible end sections of both units were determined after the 426.5 km (265 mile) trip. Unit A end-section thicknesses averaged 0.2121 m (8.35 in.) for an R-value of 5.11 K · m²/W (29.0 ft² · h · °F/Btu), and Unit B end-section thicknesses averaged 0.2172 m (8.55 in.) for an R-value of 5.03 K · m²/W (28.5 ft² · h · °F/Btu). The end sections of the manufactured units are believed to provide a severe test because movement results from wheel vibrations and flexing of the structure.

The insulation in boxes on the floors of the two units showed little settlement. The boxes in Units A and B were positioned 1.8 and 6.1 m (6 and 20 ft), respectively, from the hitch end. Average initial insulation thicknesses determined by ten probes and a fixed ruler in each box were 0.3190 and 0.3609 m (12.56 and 14.21 in.) in Units A and B, respectively. Similarly determined thicknesses in Units A and B after transport were 0.3086 and 0.3566 m (12.15 and 14.04 in.), respectively. A measurement at the end of the test showed that the insulation in the boxes was at a density of about 40.0 kg/m³ (2.5 lb/ft³).

The measurements completed after installation, end of construction, and after transport are summarized in Table 3 along with initial densities. Calculated R-values for the three examinations are listed in Table 4. The results in Tables 3 and 4 show a 16% decrease in the thickness of insulation in the test sections. The calculated decrease in R-value in the test sections was 8%. The higher-density material in the unit mid-sections should be less affected by vibration [3], and this was demonstrated by the boxed materials. If, however, mid-section R-values are reduced by the values derived for the ends and an overall R-value is obtained by averaging the end values and mid-section values, then Unit A has a final value of 5.53 K · m²/W (31.4 ft² · h · °F/Btu) and Unit B has a final value of 5.44 K · m²/W (30.9 ft² · h · °F/Btu). These averages are for the central region of the structure and do not include corrections for tapering of the insulation near the edges.

Conclusions

This test was limited to observations on two manufactured units, most of the measurements being made in the end sections. The thickness of the rock wool in the end sections decreased by about 16% between installation and delivery. Calculated thermal resistances in the end sections, however, decreased by about 8% after adjustments were made for increased density. The calculated R-values of the mid-sections of the units were initially greater than end-section R-values because of higher density and greater thickness. Final R-values for the mid-sections were calculated on the assumption that settling of the high-density insulation would not exceed that of the lower-density end-section insulation. Equal weighing of calculated end-section and mid-section R-values resulted in an average destination value exceeding $5.29 \text{ K} \cdot \text{m}^2/\text{W}$ ($30 \text{ ft}^2 \cdot \text{h} \cdot ^\circ\text{F}/\text{Btu}$) near the high point in the attic. The effect of reduced thickness along the edges of the attic space was not included in this analysis.

Recommendations

The results of this study indicate a need for additional data on thermal resistances present in manufactured housing units after transport to the consumer. The data base for loose-fill insulations in attic applications should be expanded to include all candidate materials installed to provide representative R-values. Future measurement plans should include provisions for repeated density and thickness measurements throughout the attic. Computer simulations and additional field data could provide thermal performance predictions for insulations installed at different thicknesses and densities because of the sometimes limited attic space.

Acknowledgments

The authors extend thanks to R. A. Sullivan and T. Hinson for coordinating this attic insulation test program and to R. L. Camp, Jr., for participating in the tests. The paper profited from reviews by D. L. McElroy and P. H. Shipp.

This research was sponsored by the Office of Buildings and Community Systems, U.S. Department of Energy, under Contract DE-AC05-84OR21400 with Martin Marietta Energy Systems, Inc.

References

- [1] *Federal Specification, Insulation Thermal (Loose-Fill for Pneumatic or Poured Application): Cellulosic or Wood Fiber*, Specification GSA HH-I-515D, 1979.
- [2] McElroy, D. L., Yarbrough, D. W., and Graves, R. S., "Thickness and Density of Loose-Fill Insulations after Installation in Residential Attics," in *Thermal Insulation: Materials and Systems, ASTM STP 922*, American Society for Testing and Materials, Philadelphia, 1987, pp. 493-505.
- [3] Yarbrough, D. W., Wright, J. H., McElroy, D. L., and Scanlan, T. F., "Settling of Loose-Fill Insulations Due to Vibration," in *Thermal Insulation, Materials and Systems for Energy Conservation in the '80s, ASTM STP 789*, F. A. Govan, D. M. Greason, and J. D. McAllister, Eds., American Society for Testing and Materials, Philadelphia, 1983, pp. 703-714.
- [4] McElroy, D. L., Yarbrough, D. W., and Graves, R. S., "An In-Situ Study of Attic Loose-Fill Thermal Insulation in Residential Applications," in *Thermal Performance of the Exterior Envelopes of Buildings II*, ASHRAE SP-38, American Society of Heating, Refrigerating and Air-Conditioning Engineers, New York, 1983, pp. 343-357.
- [5] Yarbrough, D. W., Graves, R. S., and McElroy, D. L., "Thickness and Density Measurements for Attic Loose-Fill Thermal Insulations in Eight Cities," ORNL/TM-10414, Oak Ridge National Laboratory, Oak Ridge, Tenn., Aug. 1987.
- [6] "Insulation in Mobile Homes—A Pacific Northwest Study," *Drexel Insulation Report*, Vol. 5, No. 5, Sept.-Oct. 1987.
- [7] "Mobile Home Test Begins This Fall," *Energy Use R/D*, TVA Office of Power, Oct. 1987.
- [8] National Mobile Home Construction and Safety Standards Act of 1974.

Apparent Thermal Conductivity versus Density as a Function of Blown Thickness for Pneumatically Applied Insulations: Continuing Studies

REFERENCE: Mathis, R. C. and Angleton, H. D., "Apparent Thermal Conductivity versus Density as a Function of Blown Thickness for Pneumatically Applied Insulations: Continuing Studies," *Insulation Materials, Testing, and Applications, ASTM STP 1030*, D. L. McElroy and J. F. Kimpflen, Eds., American Society for Testing and Materials, Philadelphia, 1990, pp. 244-252.

ABSTRACT: Seventy-three samples of pneumatically applied mineral fiber insulations were tested in a heat flow meter apparatus. The measured value of apparent thermal conductivity for these materials seems to be influenced negatively by the percentage of compression beyond the blown test sample thickness. The magnitude of this "compression effect" does not seem to be constant across the product and density spectrum. Implications for product evaluation and further test standardization are discussed.

KEY WORDS: blowing wool, heat flow meter device, lofting, apparent thermal conductivity, compression effect, ASTM C 687, thermal testing

Recent revisions in ASTM Practice for Determination of the Thermal Resistance of Loose-Fill Building Insulation (C 687) have necessitated re-evaluation of the "lofting" phenomenon in generating samples of pneumatically-applied insulation for thermal tests. The NAHB National Research Center studied the effect of blown thickness on the apparent thermal conductivities of samples of blown insulation. This study also compares the apparent thermal conductivities at various levels of sample compression to that of uncompressed samples blown to those densities, and replicates, with a larger sample, similar testing previously conducted by the Research Center [1] and related work by Bomberg et al. [2] and McCaa [3].

A total of 73 thermal specimens of four different products were evaluated. The products include unbonded glass fiber, two types of bonded glass fiber, and unbonded mineral fiber. All thermal specimens were prepared in accordance with ASTM C 687 and tested for apparent thermal conductivity in accordance with ASTM Steady-State Heat Flux Measurements and Thermal Transmission Properties by Means of the Heat Flow Meter Apparatus (C 518).

The Research Center conducts monthly samplings of a broad range of products as part of its ongoing programs of product performance certification for manufacturers and the homebuilding industry. This study was conducted to evaluate current practices of testing and to contribute to the further refinement of the applicable standards.

¹Research Scientist and Director of Laboratory Services, respectively, NAHB National Research Center, Upper Marlboro, MD 20772-8731.

Thermal Sample Preparation

All samples were prepared in the Research Center laboratory using a commercial blowing machine at each manufacturer's recommended machine settings. The blowing machine is a Meyer Model 1003 with an electric motor, four-gear transmission, dual by-pass valves, and adjustable gate with a 0.228 m (9 in.) maximum opening. The material was blown through 30.48 m (100 ft) of corrugated, flat wound plastic hose connected to 15.24 m (50 ft) of smooth rubber hose, each of 7.62 cm (3 in.) diameter.

The material was blown into a simulated attic with dimensions of 2.438 by 2.438 m (8 by 8 ft) in the center of which resides a square 0.61 by 0.61 m (2 by 2 ft) thermal specimen frame. This frame has a thin wood perimeter approximately 0.02 m (0.75 in.) thick and a height of 0.14 m (5.5 in.) to which a taut glass fiber screen is attached to its bottom edges. Material is blown into the attic and integral thermal specimen frame until the target weight of material at or near the target thickness is reached.

The same blowing machine settings were used for each sample of a given product. The only variable changed, to give densities both lesser and greater than the manufacturer's design density, was hose outlet angle. The lesser density samples were generated by angling the hose upward from the horizontal and allowing the material to "float" down into the attic and thermal specimen frame. Conversely, the greater density samples were produced by angling the hose downward toward the attic and test specimen frame. This downward angle slightly compacts the material, resulting in greater densities. After filling, the test specimen frame is removed for further test sample preparation.

The thermal test samples are then visually leveled by gently removing surface material with a small wire, pencil, or finger. Operator care is taken to minimize the impact on the balance of the sample during this process. The prepared leveled samples are then stored in a room temperature ($23 \pm 2^\circ\text{C}$) environment for at least 48 h.

Upon leveling, the thickness is determined using a technique similar to ASTM Methods for Thickness and Density of Blanket or Batt Thermal Insulations (C 167). The pin gage and a rule engineered to 0.254 mm (0.01 in.) are used to make material thickness measurements around the perimeter of the heat flow meter area. A transparent acrylic pin gage disk is used to determine the surface contact by visual means. Contact thickness is defined as "that thickness when approximately 50% of the acrylic surface is in contact with the material." The average of these four contact thickness readings is defined as the *blown thickness* (BT).

Subsequent test thicknesses are determined by taking percentages of the blown thickness. For example, BT/1.05 represents 5% compression beyond the blown thickness, BT/1.10 represents 10%, and so on. The minimum allowable test thickness with this specimen frame is 0.142 m (5.6 in.).

Thermal Testing

The prepared, level thermal test specimen is then placed in a heat flow meter (HFM) apparatus, in this case a Dynatech "R-Matic". The HFM has an adjustable height hot plate and a fixed position cold plate. The tests are conducted at $297.0 \pm 0.3\text{ K}$ ($75 \pm 0.5^\circ\text{F}$) mean temperature and a 22.2 K (40°F) temperature difference. Each thermal test specimen is placed in the HFM and is raised until the earlier determined blown thickness is reached. The HFM is located in a room maintained at $297.0 \pm 2.5\text{ K}$ ($75 \pm 4.5^\circ\text{F}$) and relative humidity controlled to $35 \pm 5\%$. The HFM is calibrated using low-density glass fiber Calibration Transfer Standards (CTS) from the National Bureau of Standards (NBS), with an estimated accuracy of $\pm 0.5\%$ and an estimated transferability of $\pm 2\%$. Recalibration with these CTS occurs monthly and has varied less than $\pm 0.1\%$ in two years. Each thermal specimen is allowed to reach thermal equilibrium before data acquisition. A minimum of 3 h at this first test thickness is allowed for each sample.

Longer time periods may be allowed if the heat flux has not stabilized within that period of time. The subsequent test thicknesses representing 5, 10, 15% compression and so on are each allowed a minimum of 1 h for restabilization of the heat flow. Once the heat flow is stabilized, an average of five readings each of hot plate, cold plate, millivolts (flux), thickness, and guard temperature variance are recorded. Upon completion of testing, the sample is removed from the HFM and the sample density is determined.

Density Determination

Following thermal testing, the meter area and whole box density at each test thickness are determined. A compression sampling device has been developed at the Research Center and is reported in detail in another paper [4]. This device allows for increased measurement accuracy and repeatability in the determination of meter area density, and significantly reduces the variable of operator judgement present in the current "cookie cutter" technique. After the sample is removed from the HFM, it is placed on a table where the compression sampling device uniformly compresses the entire specimen and delineates with knife blade edges the meter area of the HFM in the sample. This material is then removed from the thermal specimen frame and weighed to the nearest 0.01 g. This meter area weight is then used to determine the material density at each test thickness.

Analysis

After measuring the apparent thermal conductivity, k , and the meter area density, ρ , at each test thickness, x , for each sample, all data for a given product were then fit to a curve of the form

$$k_x = A + B \cdot \rho_x + C/\rho_x$$

where

k = apparent thermal conductivity at thickness x , W/m · K (Btu · in./h · ft² · °F),

ρ = density of material at thickness x , kg/m³ (lb/ft³), and

A, B, C = curve-fit coefficients.

Test Results

A total of 73 tests on four different loose fill insulation products were conducted. Table 1 shows the distribution of the number of tests per product.

Table 2 summarizes the measurement ranges of each product for blown thickness, density, compression percentage, and apparent thermal conductivity. This presentation format is for direct comparison to related work by Adams and Hust [5].

TABLE 1—Distribution of compression tests per product.

Product	Number of Tests	Total Number of Data Points
Product A	13	67
Product B	37	141
Product C	14	54
Product D	9	26
Four Total Products	73	288

TABLE 2—*Measurement ranges.^a*

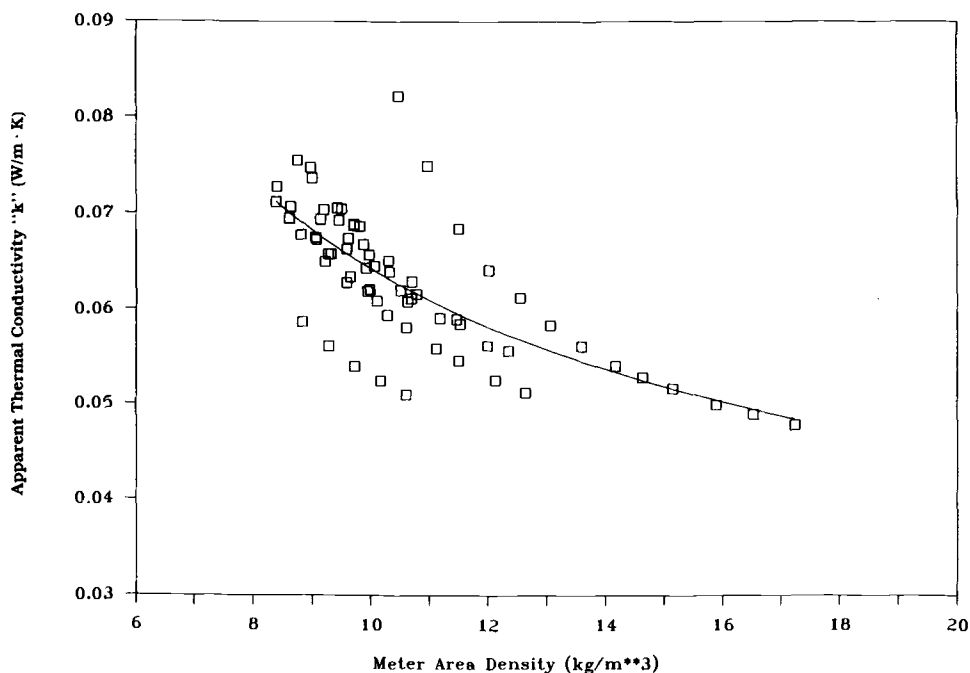
Material	Thickness (m)	Density (kg/m ³)	Compression (%)	Apparent Thermal Conductivity (W/m · K)
Product A	0.142–0.241 (5.6–9.49)	8.39–17.12 (0.524–1.07)	0–64.6	0.047–0.082 (0.333–0.569)
Product B	0.142–0.204 (5.6–8.03)	7.10–15.95 (0.444–0.997)	0–33.9	0.041–0.075 (0.285–0.521)
Product C	0.142–0.209 (5.6–8.23)	16.9–33.8 (1.06–2.11)	0–22.3	0.048–0.063 (0.333–0.438)
Product D	0.142–0.250 (5.6–9.84)	9.15–16.42 (0.572–1.03)	0–30.0	0.042–0.083 (0.292–0.576)

^aNumbers in parentheses are in the following English units: Thickness (inches); Density (lb/ft³); Apparent Thermal Conductivity (Btu · in./h · ft² · °F).

This discussion will focus on compression percentages from 0 to 15% of blown thickness, the range most typical in testing and defined by the 15% maximum excess thickness allowable in the current version of ASTM C 687.

Figures 1, 2, 3, and 4 illustrate the data and a curve of the previously mentioned form for Products A, B, C, and D, respectively.

Several conclusions are immediately apparent. First, even though the product specimens were generated by one technician in a single laboratory, and each specimen received the same sample conditioning and interpretation of standard procedures, there is still a wide scatter in

FIG. 1—*Apparent thermal conductivity versus density: Product A.*

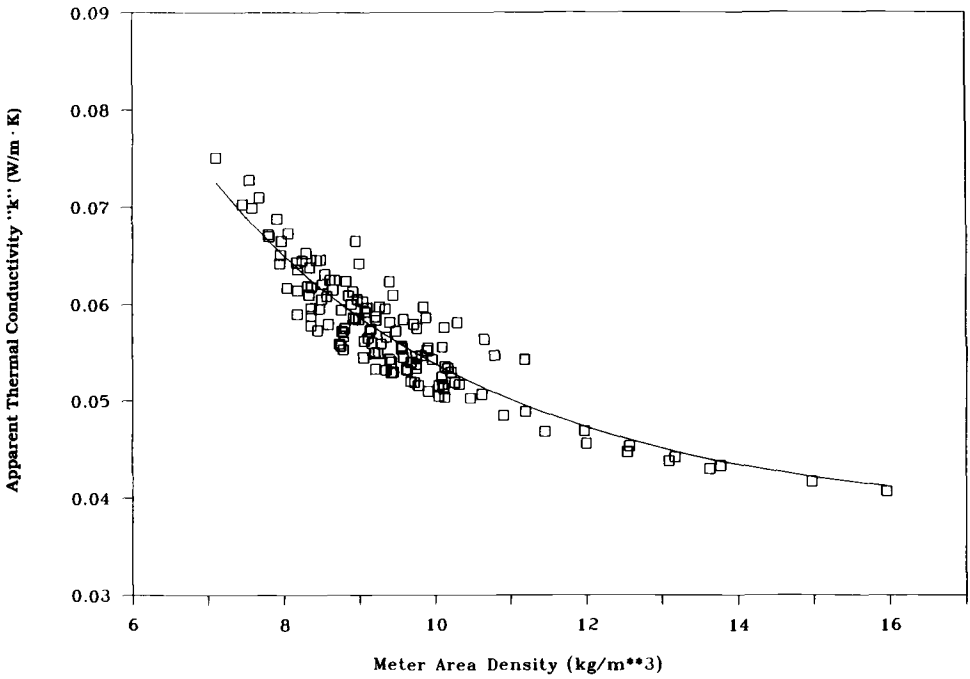


FIG. 2—Apparent thermal conductivity versus density: Product B.

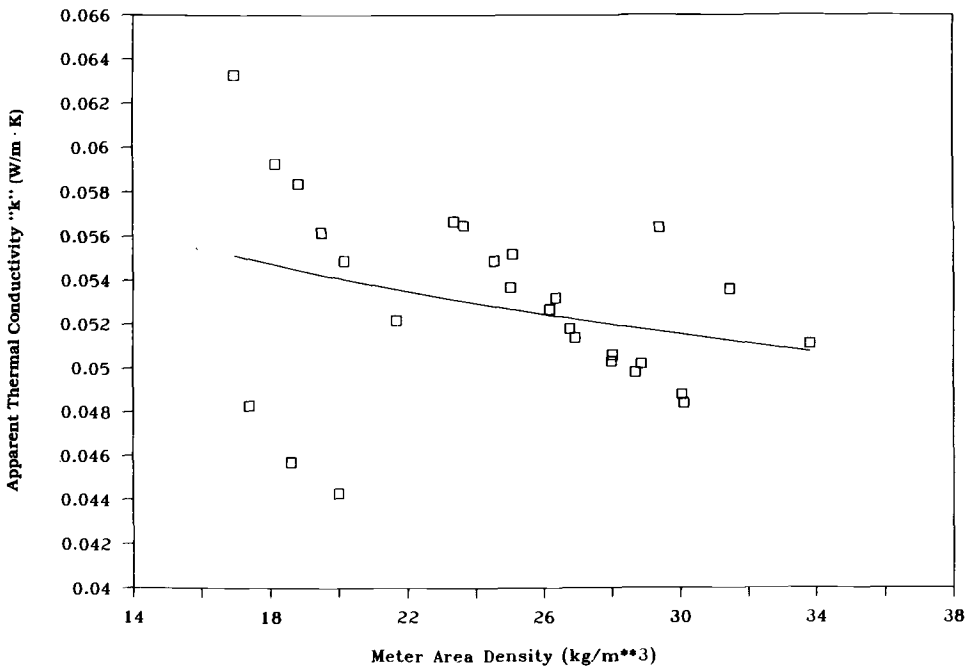


FIG. 3—Apparent thermal conductivity versus density: Product C.

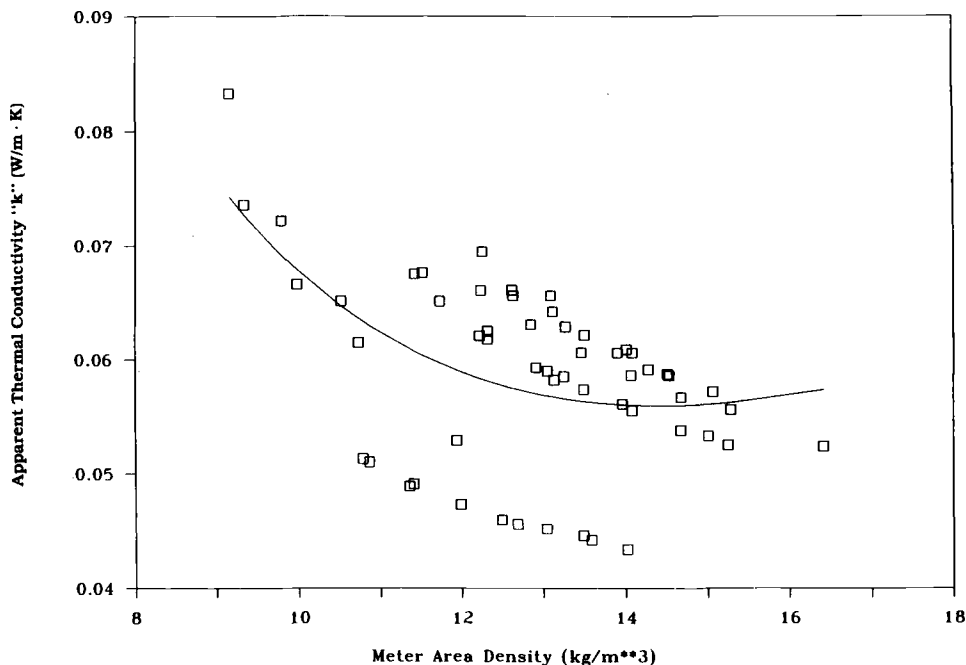


FIG. 4—Apparent thermal conductivity versus density: Product D.

the data. This scatter is not as great as that from the interlaboratory round-robin tests on a similar spectrum of products as referenced above [5]. However, the data still suggest several variables exist outside the current language of the standard which, when combined with the generally non-homogeneous materials in discussion, allow for substantial variance. Some of these variables are discussed in another paper [4].

Another conclusion from the inspection of all the data addresses the aforementioned homogeneity. Since, for a given product, the test material was not from a single production run or from a single plant, the scatter here is influenced further by manufacturing processes. Different production facilities for a given product may produce at opposite ends of the range of values implied by the labels. These data were not normalized by production facility or by product code or shift. This may also contribute to the data scatter. Other tests conducted by this laboratory on similar products of a single production run have exhibited much less scatter than presented here, though the process-dependent variability would still exist.

Figures 5 to 8 show regressions for test data at the blown thickness (0% compression) and for test data for 15% sample compression beyond the blown thickness. The dashed lines on each graph represent a 95% confidence interval.

These figures show that each of the four products tested exhibited a change in the apparent thermal conductivity between samples *blown* to various densities and samples *compressed* to various densities. This is illustrated by the change in the slope of the regressed curves. This change is not as evident among the samples of Product B (Fig. 6). It is thought that the plant and production variation in manufacturing may mask the compression effects. Other studies conducted by this laboratory on single production runs of this material have demonstrated changes in apparent thermal conductivities as a result of compression with similar magnitude as those changes exhibited by the other three products.

However, this limited amount of data, coupled with its variability by whatever the causes,

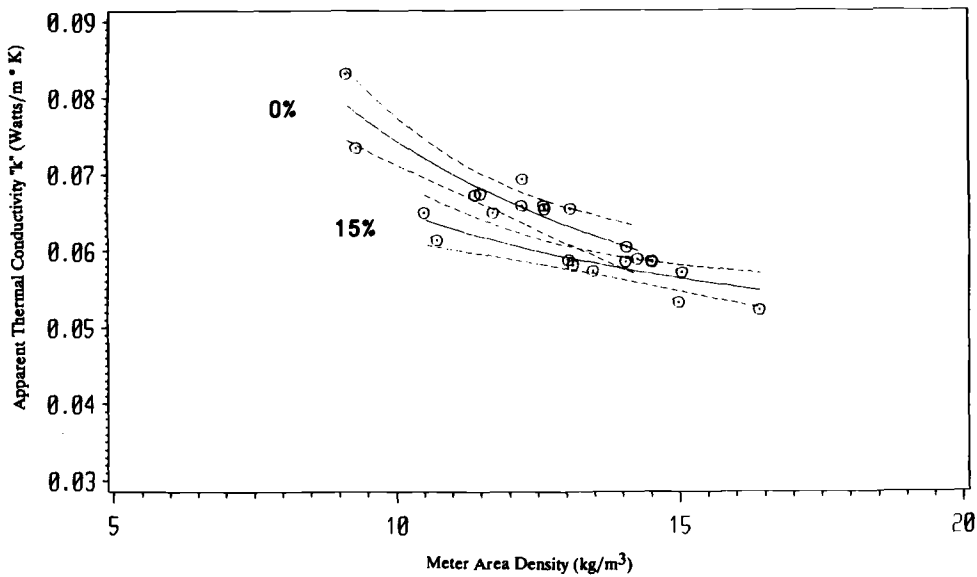


FIG. 5—Product A: 0 and 15% compression analysis.

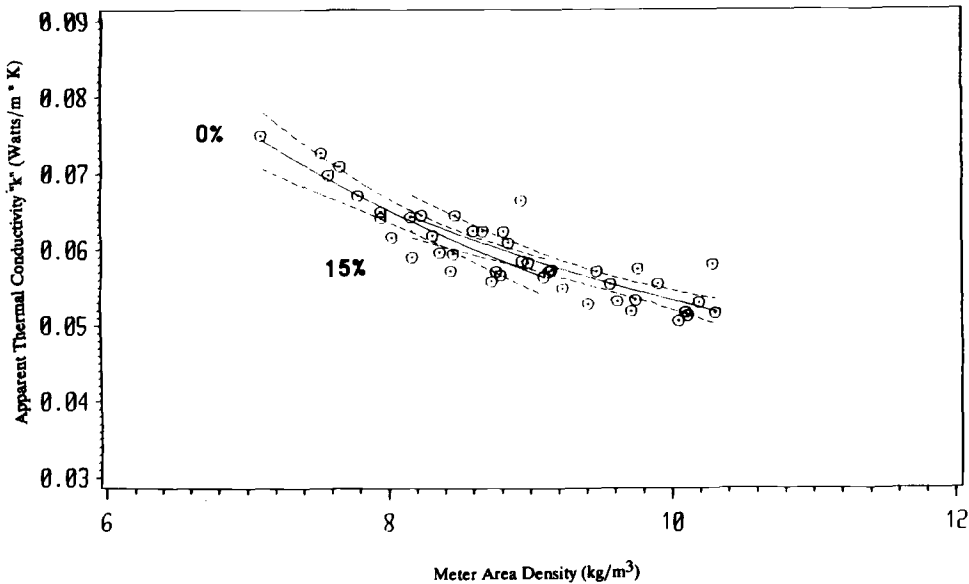


FIG. 6—Product B: 0 and 15% compression analysis.

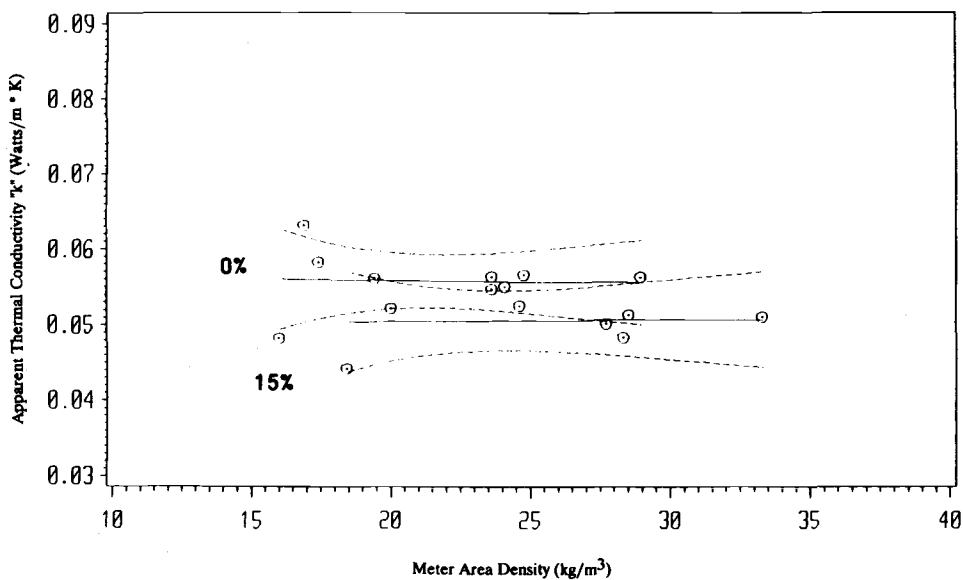


FIG. 7—Product C: 0 and 15% compression analysis.

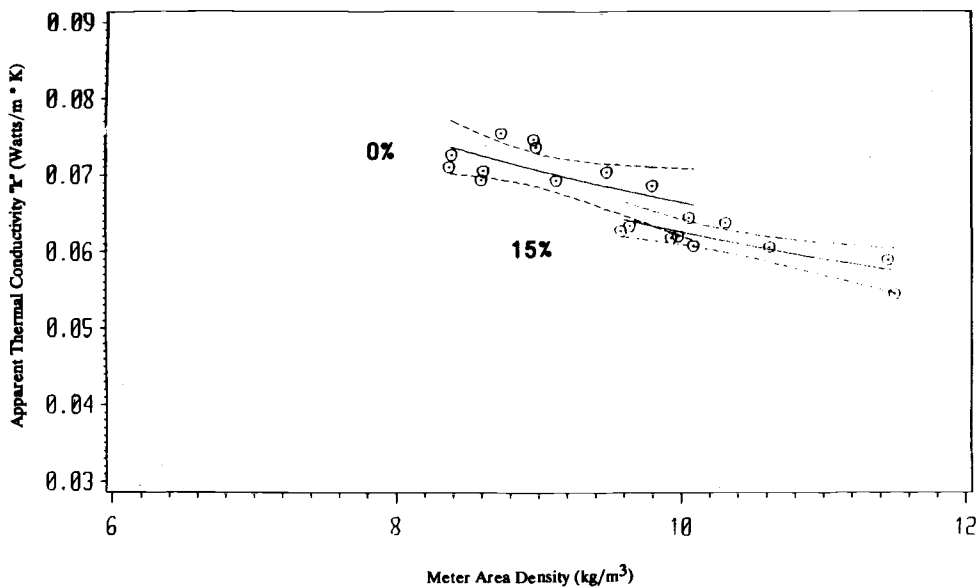


FIG. 8—Product D: 0 and 15% compression analysis.

precludes strong statistical conclusions regarding the magnitude of the "compression effect". It is apparent that, until more controlled experiments are conducted (which remove some of the manufacturing and other variables), sample compression should, at least, be minimized. Simultaneously, good HFM plate contact must be maintained.

Since these materials are not compressed in typical application, a more proper assessment of their potential performance should include minimum compression in the testing laboratory. This imposes several restrictions on current test protocols and suggests possible areas of further standardization.

One possible standardization approach might be to test each product at the blown thickness, as described herein, and measure the performance of a given sample at a single thickness and blown density. Product performance verification could then be conducted by measuring the sample's variance from an acknowledged product performance curve. This procedure is most applicable in a manufacturer's process control laboratory where close tracking of product and process performance is required. Another method may be to generate a product curve from a variety of samples tested at a single, uncompressed thickness. This procedure is probably most applicable for an independent laboratory conducting contract or quality assurance audit testing.

Summary

A total of 73 tests on four different loose fill insulation products were conducted at the NAHB National Research Center. These products were compressed during testing from 0 to 65% to evaluate the impact of compression on apparent thermal conductivity. The analysis here is limited to a maximum of 15% compression to match existing limits within the applicable standards. Though specific quantitative delineation of this compression effect is not achievable in this data sample, it is apparent that compression does affect the measured values. This effect is qualitatively similar to that found in other recent studies. Some materials may be more sensitive to this effect than others. Further refinement of existing standards may provide testing alternatives to minimize these effects. Test procedures which allow for evaluation of these products at conditions which more closely reflect typical field application are recommended.

Acknowledgments

The authors wish to acknowledge the assistance of S. K. Graves and F. D. Wilkerson in the preparation and testing of these products. Also acknowledged is C. P. Crall and L. M. Wesley for assistance in plot generation.

References

- [1] NAHBRF Report, "Thermal Conductivity versus Density as a Function of Blown Thickness for Pneumatically Applied Mineral Fiber Insulations," NAHB, Oct. 1983.
- [2] Bomberg and Solvason, Building Research Note 167, NRC, Canada, 1980.
- [3] McCaa, D., "Use of Heat Flow Meter Apparatus for Testing Loose-Fill Materials Prepared for Laboratory Testing," in *Guarded Hot Plate and Heat Flow Meter Methodology. ASTM STP 879*, American Society for Testing and Materials, Philadelphia, 1985, pp. 154-160.
- [4] Mathis, R. C. and Kenney, T. M., "New Developments Toward Accurate Assessment of Material Density for ASTM C 687 Testing of Pneumatically-Applied Insulations," this publication, pp. 253-262.
- [5] Adams, R. D. and Hust, J. G., "A Round Robin on Apparent Thermal Conductivity of Several Loose-Fill Insulations," this publication, pp. 263-289.

New Developments Toward Accurate Assessment of Material Density for ASTM C 687 Testing of Pneumatically Applied Insulations

REFERENCE: Mathis, R. C. and Kenney, T. M., "New Developments Toward Accurate Assessment of Material Density for ASTM C 687 Testing of Pneumatically Applied Insulations," *Insulation Materials, Testing, and Applications, ASTM STP 1030*, D. L. McElroy and J. F. Kimpflen, Eds., American Society for Testing and Materials, Philadelphia, 1990, pp. 253-262.

ABSTRACT: Quality measurements of the thermal performance of pneumatically applied mineral fiber insulations by use of a heat flow meter device require accurate assessment of the density of material in the specific area of the heat flow meter. Current standard methods to determine this density are inadequate. A compression sampling device/technique has been developed which increases the accuracy and repeatability of density determination. Operator judgement is also greatly reduced. This device, coupled with more detailed and standardized thermal specimen generation techniques, promotes reduced density variation within the test specimen. A $\pm 5\%$ density variation is achievable.

KEY WORDS: blowing wool, compression sampling, heat flow meter device, blown thickness, cookie cutter, density homogeneity, contact thickness

Current methods to assess material density in the area of the heat flow meter for testing in accordance with ASTM Practice for Determination of the Thermal Resistance of Loose-Fill Building Insulation (C 687) are inadequate. Parameters affecting the material density include test frame size, test frame edge thickness, blown insulation thickness, type of insulation, blowing machine type, settings and hoses, and the ratio of the meter area to the test frame area. Some of these parameters also affect the density distribution within the sample, as do blowing technique, operator experience, and blowing machine performance. Accurate assessment of the meter area density is imperative for correct thermal analysis.

A compression sampling device/technique has been developed at the NAHB National Research Center which increases the measurement accuracy and repeatability, and significantly decreases the variability in operator judgement present in the current technique. Procedures for more uniform density distribution within the thermal test specimen have also been developed.

A description of the compression sampler and its application, as well as a comparison of whole box versus meter area density, are included for four different loose fill insulation products. This study compares the compression sampling technique to the cylindrical cutter method displayed in ASTM C 687.

Recent ASTM round-robin test data [1] have shown that the density distributions over the entire test frame were very uneven, typically with the meter area density averaging between 5 to

¹Research Scientist and Mechanical Engineer, respectively, NAHB National Research Center, Upper Marlboro, MD 20772-8731.

10% higher than the whole box density. In this laboratory there has also been an observed relationship between the amount of variation in the whole box versus meter area density and total surface area blown. The data presented here show that achievable variance between meter area and whole box densities can be less than 5%.

Testing for Quality Assurance

The Research Center conducts monthly testing of a wide variety of products for the home-building industry including pneumatically applied loose fill insulation products. The Loose Fill Certification Program involves a variety of glass and mineral fiber products of varying design densities. As part of this ongoing quality assurance audit program, review and interpretation of applicable standards have resulted in development of several new testing procedures. These are presented here as a first step toward further refinement and specification of the language in ASTM C 687. Recent ASTM-sponsored interlaboratory round-robin testing demonstrated, and this document supports, the need for further standardization, particularly in the area of thermal specimen preparation and density analysis.

A discussion of some of the general parameters that influence thermal specimen preparation and analysis follows along with a specific description of the procedures used at the Research Center.

Influences on Thermal Specimens

The focus of this document is primarily on mineral and glass fiber loose-fill products. Some of the sample preparation items presented here may also be applicable for other pneumatically applied insulations such as cellulose.

Blowing Machines

Probably one of the single largest contributors to the variability in the conditioning of loose-fill insulation thermal specimens is the wide variety of equipment used in generating the samples. These blowing machines may range in size from material throughput of 3 kg/min (7 lb/min) to upwards of 13 kg/min (30 lb/min) with variable transmissions, blower speeds, and gate openings. The growth of the loose-fill insulation market in recent years has also precipitated the development of larger and faster throughput machines capable of properly applying a wide variety of products. Current practice is to generate samples at or near the manufacturer's design density for both thermal and coverage analysis. As the variety and age of machines available for this task increases, the potential for wider variability of test samples may also increase. A given manufacturer may be unable to determine "appropriate" settings for every possible machine used in field applications and for testing.

There are also specific machine parameters that, for a given blowing machine, may directly affect the quality and conditioning of the test specimens generated. Tracking blowing machine performance, in terms of transmission speeds, agitation, and throughput over time may positively facilitate the ongoing, proper evaluation of these materials. Outlet pressures, back-flow pressures, gear performance, and machine speeds may be checked on a periodic basis to assure consistent functioning.

Hoses

The length and diameter of hose for applying thermal test specimens is specified in ASTM C 687. However, the material conditioning can also be influenced by type of hose, whether smooth, corrugated, flat wound, or other, and by the specific configuration of the length. Configuration parameters that may influence material conditioning include: (1) the elevation of the

hose, with reference to both the machine and the specimen frame, (2) the straightness or tortuosity of path, and (3) the allowable number, shape, and diameter of hose coils.

Blowing Parameters

Several items in ASTM C 687 may influence specimen conditioning and performance: ratio of test specimen size to total blown area, rotation of the test specimen frame for even material distribution, type of frame construction, and application geometries. Whether the hose is held horizontal to the test frame plane or angled up or down, whether the outlet of the hose is allowed to "wash" over the thermal specimen from a single point at varying horizontal angles (like a car windshield wiper), or whether the horizontal hose outlet is moved linearly from side to side can influence the sample densities. Other factors which may influence the conditioning of the final test specimen include: temperature and relative humidity of the room in which the samples are being generated, total sample blown thickness, surface preparation and leveling techniques, and sample storage/movement procedures.

Area

The Research Center has developed some methods of thermal sample preparation which may allow for increased testing repeatability. One development focuses on the observed relationship between the total surface area blown during testing and the area of the thermal test specimen. Blowing a larger surface area than just the thermal specimen frame seems to reduce the "mounding" of material in the center of the frame. This directly affects the "quality" of the thermal test specimen with reference to the density homogeneity of the sample. The test area in which Research Center samples are generated is described below.

The thermal test specimen frame (Fig. 1) resides in a simulated attic with dimensions of 2.438 by 2.438 m (8 by 8 ft). The square thermal specimen frame is approximately 0.61 by 0.61 m (2 by 2 ft) and constructed of approximately 0.02 m (0.75 in.) thick and 0.14 m (5.5 in.) high wood (nominal 1 by 6). An open weave glass fiber screen is tautly attached to the bottom edge of the frame. Material is then blown into the attic and test specimen frame until the frame is at the proper weight to achieve the manufacturer's design density at 0.152 m (6 in.). This is the thickness at which the heat flow meter apparatus is calibrated and is the desired test thickness. The thermal specimen frame is then removed from the simulated attic and placed on an elevated table for sample preconditioning.

Preconditioning involves removing excess material from the perimeter of the frame and from the top of the sample until the correct weight of the material, at or near the design density, is reached and the thickness is within the test range desired. Then the sample is visually leveled by gently removing surface material with a small wire, pencil, or finger. Operator care is taken to minimize the impact of this leveling on the balance of the sample during this process.

Thickness Determination

Another important parameter affecting proper thermal analysis is the determination of the test thickness of the thermal test specimen. After leveling the thermal test specimen, the blown thickness is determined using a technique similar to ASTM Methods for Thickness and Density of Blanket or Batt Thermal Insulation (C 167). The pin gage and a rule engineered to 0.0254 cm (0.01 in.) are used to make material thickness readings around the perimeter of the heat flow meter area. A transparent acrylic pin gage disk is used to determine the surface contact by visual means. "Contact" thickness is defined as "that thickness when approximately 50 percent of the acrylic surface is in contact with the material." The average of these four thickness readings is defined as the *blown thickness* and is also the first test thickness.

Density Determination

The last and one of the most important components in the accurate measurement of the performance of loose-fill insulations is the determination of the material density in the area of the heat flow meter at each test thickness. The Research Center has developed a compression sampling device and technique which increases the measurement accuracy and repeatability and significantly reduces the variable of operator judgement present in the current technique. The compression device and its application are illustrated in Figs. 1 and 2. The prototype device is constructed primarily of readily available wood components, though it could be constructed from a number of other materials. These figures are intended to provide a conceptual understanding of the device and the process by which it is employed. Since its development, other laboratories have replicated this scheme, including such items as pneumatic controls and cutting.

Once heat flow meter (HFM) testing on a given specimen is completed, the specimen frame is removed from the apparatus and placed on a table. The compression device, encompassing the entire surface of the specimen, is lowered into the test frame and the material is uniformly compressed to the minimum possible, usually less than 0.02 m (0.75 in.). The compression device is locked into place with two clamps. The center 0.645 m² (100 in.²) of the compression plate is defined by four knife blade edges which define the actual heat flow meter area during testing. These knife edges cut and delineate material in the area of the heat flow meter from the perimeter within the thermal test specimen frame. The material in the meter area is then removed from the compressed sample and weighed on a gram scale to the nearest 0.01 g. The density at each test thickness is then determined by taking the weight of the material in the meter area and dividing by the volume of the test sample in the meter area at each test thickness.

There are several advantages of this technique over the cylindrical "cookie cutter" technique currently illustrated in the standard. The primary advantage is that the knife edges delineate much more precisely the actual meter area in the precise HFM geometry. Also, the variability of operator judgment as to what is "inside" versus "outside" the meter area for proper weight determination is reduced.

Test Results

A comparison of the two density determination techniques is presented in Figs. 3 to 8. The test data represent tests on over 100 samples of loose-fill insulation. The densities of these samples range up to 35 kg/m³ (2.2 lb/ft³). Each figure also includes a 45° line to illustrate what would be exact agreement between meter area and whole box density.

Figures 3 and 4 present the data for all samples tested. Figure 3 shows the data for the compression device/method, developed at the Research Center, and Fig. 4 shows the data for the cylindrical cookie-cutter. Figures 5 and 6 present only the data between 6 kg/m³ (0.38 lb/ft³) and 16 kg/m³ (1.01 lb/ft³). These figures illustrate, and statistical analysis of the data show, that both sampling methods result in density measurements closely distributed around the 45° exact fit. The quality of a linear fit through both the compression and cylindrical method data was high, with correlation coefficients of 0.993 and 0.965, respectively. This illustrates that both methods attest to the ability to generate test samples with a fairly uniform density distribution between the meter area and whole box. However, when viewing the standard error of estimate for each of the linear fits, the compression technique demonstrated less variability, 0.40 versus 1.46 for the cylindrical method.

One explanation for the greater dispersion in the cylindrical technique is that it requires greater operator judgment for determining what material is actually in the meter area. This is due to the difficulty in maintaining the cylinder perpendicular and parallel to the test material. Also, the "scalloped" edges of the cutter force the operator to "choose" what is in the meter

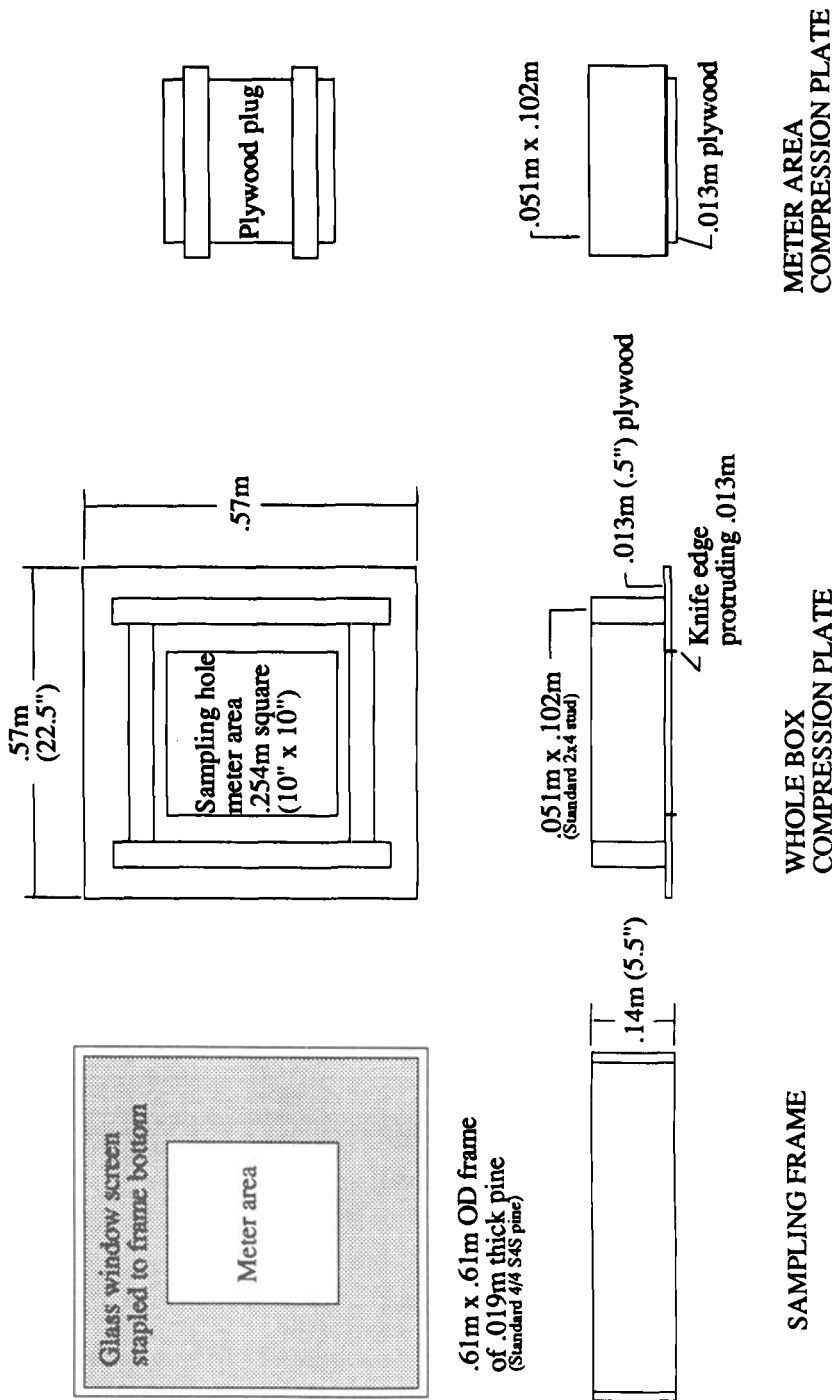
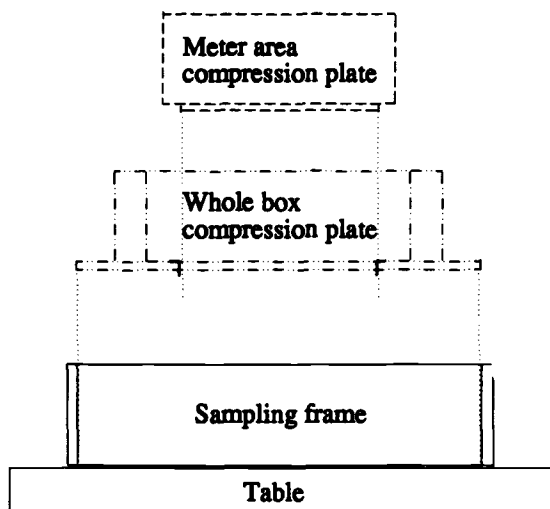
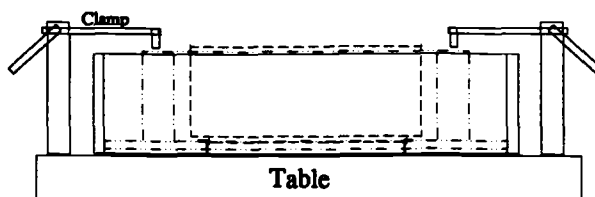


FIG. 1—Compression device schematic.



ASSEMBLY SEQUENCE



ASSEMBLED COMPRESSION SAMPLING DEVICE

FIG. 2—*Compression device application diagram.*

area under the edges of the “scallop”. Another contributor to this variation is that the cylinder does not reflect the square HFM area. Both data sets illustrate that these product specimens tend to be slightly more dense in the meter area. This may be due to the design of the thermal test frame. Current test frame designs are being reviewed to identify areas for further reduction in the variance between meter area and whole box density. Minimizing this variation is another potential candidate for standards modification.

The homogeneity of density within the thermal test specimen frame provides for an increased potential to assess these products near a specific target density, using weight as the first level of specimen evaluation. If the correct weight of material is present in the frame, and good sample preparation technique has been followed, testing near the target density is more nearly assured.

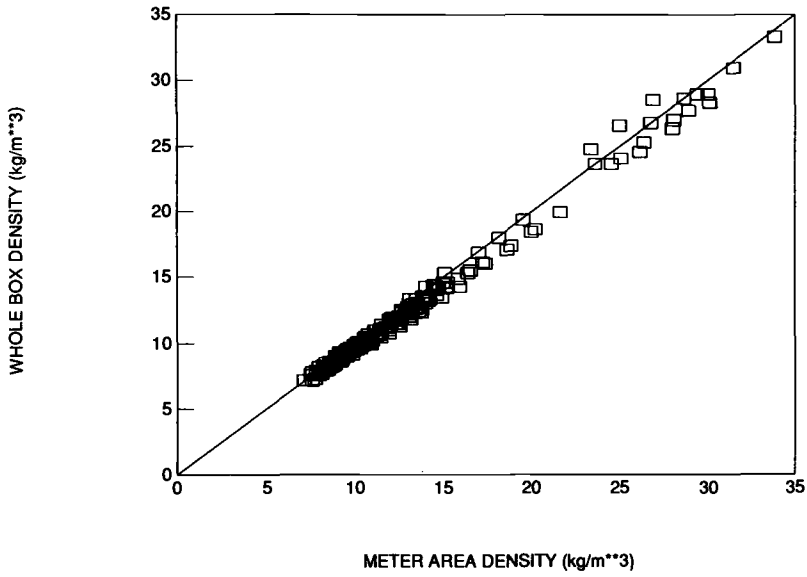


FIG. 3—Compression sampling technique (all samples).

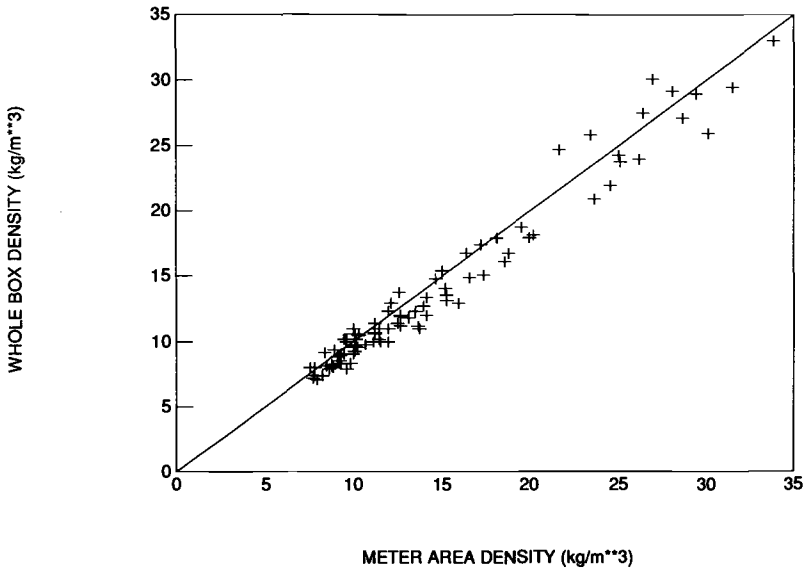


FIG. 4—Cylindrical sampling technique (all samples).

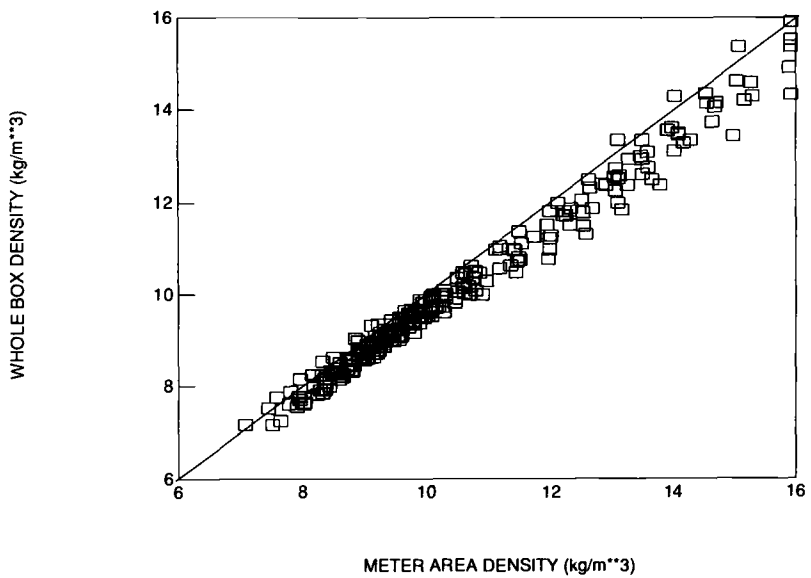


FIG. 5—Compression sampling technique (6 to 16 kg/m³).

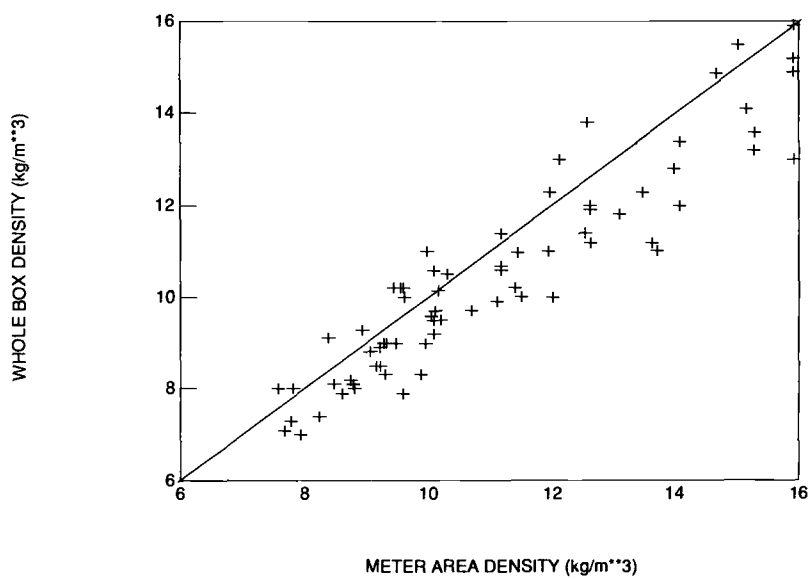


FIG. 6—Cylindrical sampling technique (6 to 16 kg/m³).

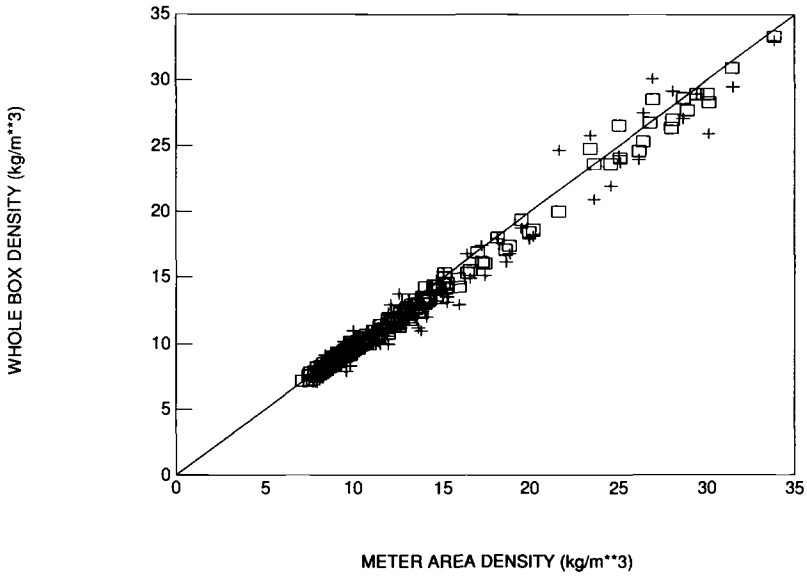


FIG. 7—Compression technique versus cylindrical technique (all samples). Compression data indicated by squares; cylindrical data indicated by pluses.

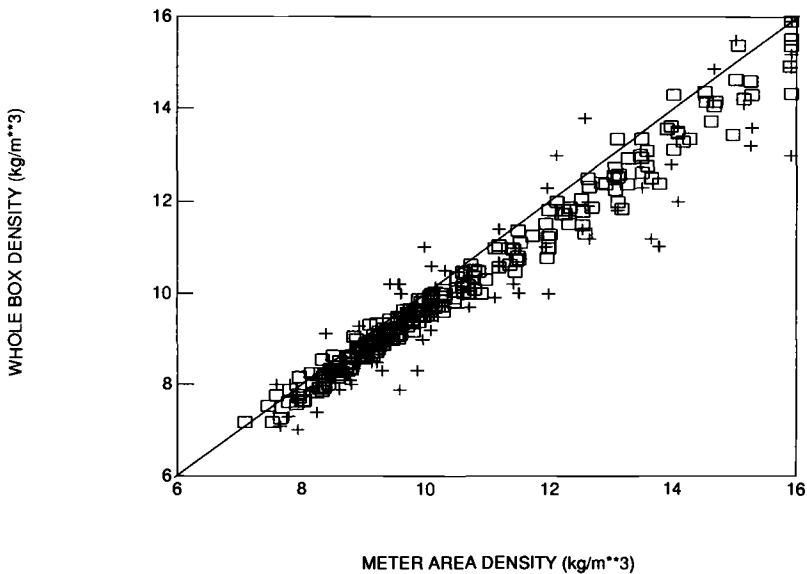


FIG. 8—Compression technique versus cylindrical technique (6 to 16 kg/m³). Compression data indicated by squares; cylindrical data indicated by pluses.

Summary

Several parameters, from blowing machine to meter area density measurement, influence the accuracy and repeatability of thermal testing of loose-fill insulation products in accordance with ASTM C 687. The Research Center has developed several test methods which reduce some of this variability including a compression device for determining meter area density. Many of these techniques and subjects are recommended for inclusion in standards documents. Further testing in each of these areas for standards delineation is encouraged.

Acknowledgments

The authors wish to acknowledge S. K. Graves and F. D. Wilkerson for their assistance in preparing and testing these thermal specimens.

Reference

- [1] Adams, R. D. and Hust, J. G., "A Round Robin on Apparent Thermal Conductivity of Several Loose-Fill Insulations," this publication, pp. 263-289.

A Round Robin on Apparent Thermal Conductivity of Several Loose-Fill Insulations

REFERENCE: Adams, R. D. and Hust, J. G., "A Round Robin on Apparent Thermal Conductivity of Several Loose-Fill Insulations," *Insulation Materials, Testing, and Applications, ASTM STP 1030*, D. L. McElroy and J. F. Kimpflen, Eds., American Society for Testing and Materials, Philadelphia, 1990, pp. 263-289.

ABSTRACT: The primary means of establishing the thermal performance of loose-fill insulation is ASTM Standard Practice C 687. To provide information for the development of a statement of precision and bias for this Standard Practice, a round robin was carried out by eleven laboratories measuring apparent thermal conductivity of four common loose-fill insulation products (cellulose, rock/slag wool, and bonded and unbonded glass fiber) and a glass fiber blanket.

The test results on the glass fiber blanket indicate that the measurement capability of the participants can be characterized by an imprecision of 3.0%, as measured by two standard deviations, and a negligible bias of the mean. The measurements on the loose-fill materials are characterized by an imprecision ranging from 21% for cellulose to 10% for the rock/slag wool. The increase in imprecision for the loose-fill materials is attributed primarily to inadequately defined procedures for preparing and conditioning the specimens.

KEY WORDS: bias, cellulose, glass fiber, loose-fill insulation, precision, apparent thermal conductivity, thermal insulation, rock/slag wool

During the last 10 to 15 years considerable progress has been made in the development of loose-fill building insulation materials and the techniques for the measurement of the thermal performance of these materials. The worldwide interest in energy conservation has resulted in increased efforts towards the production of improved and more cost-effective loose-fill building insulation products. As a result of the growing interest in energy conservation, loose-fill insulation products have grown in significance and share of market because of their low cost and ease of installation [1]. They also represent an attractive option for retrofit applications.

ASTM Standard Practice for Determination of the Thermal Resistance of Loose-Fill Building Insulation (C 687) was revised in 1985. Because ASTM requires that all Standard Practices contain precision and bias statements, a round-robin testing program was organized with the objective of providing experimental data for the development of a precision and bias statement for ASTM C 687.

ASTM C 687 accepts ASTM C 177, C 236, C 518, and C 976 as sources for suitable testing apparatus for these measurements. Due to cost and testing speed, the primary test apparatus used are the heat-flow-meter type based on ASTM C 518. A complete listing of the various sizes and configurations of test apparatus used by the round-robin participants is given in Table 1. One guarded hot plate based on ASTM C 177 and one thin-heater hot-plate test apparatus were used by participants in the round-robin test program.

¹Owens/Corning Fiberglas, Product Testing Laboratories, Granville, OH 43023.

²Chemical Engineering Science Division, National Bureau of Standards, Boulder, CO 80303-3328.

TABLE 1—*Round-robin test apparatus.*^a

Lab. Code	ASTM Apparatus Type	Plate Area, mm	Metered Area, mm	Symbols Used in Figures
1	C 518	610 × 610	254 × 254	0
2	C 518	914 × 914	457 × 457	△
	C 518	610 × 610	254 × 254	△
3	C 518	610 × 610	254 × 254	□
4	C 518	610 × 610	254 × 254	▽
5	THHP ^b	1092 × 1600	610 × 914	◇
6	C 518	610 × 610	254 × 254	+
7	C 518	610 × 610	254 × 254	X
8	C 518	914 × 914	305 × 305	⊕
9	C 518	914 × 914	305 × 305	⊗
10	C 177	1016 dia.	406 dia.	⊞
11	C 518	610 × 610	254 × 254	⊞

^aThe heat flows vertically and the specimens are oriented horizontally in each apparatus.

^bTHHP = Thin Heater Hot Plate (ASTM Test Method in development).

Scope

The round robin was begun following discussions at the October 1985 meeting of ASTM Committee C-16 on Thermal Insulation where the revised C 687 procedure was finalized. The round robin was designed to test samples of widely available material from four basic categories. The call for participants was circulated to all members of ASTM Subcommittee C16.30 on Thermal Measurement and to other interested parties. The eleven laboratories that volunteered to participate are listed below. Distribution of test samples was begun in July 1986, and the last set of test results was received in March 1987.

Test Materials

The test materials used in this round robin were rock/slag wool, cellulose, bonded glass fiber, unbonded glass fiber, and glass fiber blanket. They were selected as being representative of widely available loose-fill materials. The glass fiber blanket specimens, nominally 15 cm thick, were composed of six blankets, each having a nominal thickness of 2.54 cm.

Participants

The participants in the round robin were:

- Certainteed Corporation, Blue Bell, Pennsylvania
- Dynatech R/D Corporation, Cambridge, Massachusetts
- Fiberglas Canada, Incorporated, Sarnia, Ontario
- Manville Service Corporation, Denver, Colorado
- NAHB Research Foundation, Upper Marlboro, Maryland
- National Bureau of Standards, Gaithersburg, Maryland
- National Research Council of Canada, Ottawa, Ontario
- Oak Ridge National Laboratory, Oak Ridge, Tennessee
- Owens-Corning Fiberglas, Granville, Ohio
- Underwriters Laboratory, Incorporated, Northbrook, Illinois
- United States Gypsum, Libertyville, Illinois

Objectives

The primary objective of this round robin was to provide data for developing a precision and bias statement for ASTM C 687. Two secondary objectives were to provide additional information concerning the effect of compression and the procedure for determining density. The recommended density determination procedure was changed in the revised C 687 practice such that the metered area weight must be used to determine the specimen density, whereas the original method permitted the use of the weight of the entire test specimen to calculate density (also known as box density). Round-robin participants were requested to provide both densities for each test specimen.

Data illustrating the effect of compression were requested in order to show whether the thermal test results for specimens that are compressed to achieve design densities are significantly different from test results for specimens blown at the design density. Compression of the specimens beyond the test point at 0.9 times contact thickness was suggested as an option. The compression effect is addressed in the C 687-85 test procedure by limiting overblow on sample preparation to 15%.

A copy of the round-robin procedure is provided in Appendix A.

Experimental Data

Experimental data were reported in the customary English units and converted to SI units for analysis. Laboratory code numbers were randomly assigned and are used consistently throughout the report for intercomparing the data without identifying the source of each data set. In addition, the same symbol is used for each laboratory in the figures consistently throughout the paper (Table 1). The following comments pertain to all test materials.

The data include not only a range of density but also a slight range of temperature near 297 K. One laboratory (Lab 5) reported several data points for mean temperatures ranging from 304 to 324 K. The temperature dependencies, as reported by Lab 5, are linear in all cases (i.e., the slope is constant for each material). The temperature-dependent data reported by Lab 5 were extrapolated back to 297 K and are shown as single test points in the tables and figures. The data from the other participants are listed in the tables as reported but were corrected to 297 K for the analysis and the figures. The slopes of apparent thermal conductivity versus temperature in units of $\text{mW}/(\text{m} \cdot \text{K}^2)$ used for these corrections are given in Table 2. The statistical measure used to estimate the scatter of the data (imprecision) is two times the standard deviations of the percentage deviation between the test points and a reference curve. The reference curve chosen is of the form $k = a_1/(d + a_2) + a_3$, where k is apparent thermal conductivity and d is density.

TABLE 2—Measurement ranges.

Material	Thickness, cm	$\Delta K/\Delta T$, $\text{mW}/\text{m} \cdot \text{K}^2$	Density, kg/m^3	Compression, %	Apparent Thermal Conductivity, $\text{mW}/\text{m} \cdot \text{K}$
Glass fiber, blanket	14–18	0.3	11–16	0–28	38–51
Cellulose	11–18	0.4	32–70	0–35	39–56
Bonded glass fiber	11–18	0.6	6–18	0–40	43–78
Rock/slag wool	10–18	0.4	26–58	0–40	39–60
Unbonded glass fiber	11–18	0.4	6–21	0–45	38–68

The reference curves used in the analysis are based specifically on the test results of this round robin. They are not to be interpreted as product curves for these materials.

Table 2 provides the nominal ranges of the thickness, density, compression, and apparent thermal conductivity for each of the materials studied in the round robin. The percent compression data is with respect to the contact thickness.

Exceptions to the original round-robin plan are noted below. Two of the participants, Labs 8 and 9, did not measure the glass fiber blanket reference material. This omission could alter the determination of bias for the round robin. The test points of these two participants as shown in the figures do not represent outliers and therefore do not alter the conclusions significantly. In addition, one participant, Lab 2, provided significantly more test points for the loose-fill materials than did the other participants. The number of test points at 0.9 times contact thickness ranged from 3 to 38 for the various participants. The average number of test points reported is 13. The round-robin plan recommended a total of 12 points. Since the reference curves used in the analysis were based on the data, they were undoubtedly biased toward the results from those participants reporting the largest number of test points. However, in our opinion, this wide range of reported test points did not significantly alter the conclusions regarding the imprecision of the data. Lab 10 did not report the test densities because the specimens were needed for other measurements. Lab 3 did not report test densities for bonded glass fiber. For those data the box density was used in the analysis. Test densities were otherwise used in the plots of apparent thermal conductivity versus density in this paper.

Glass Fiber Blanket

The glass fiber blanket was used to assess the bias of the apparatus involved in the round robin. Nine laboratories reported 22 test points on glass fiber blanket. The data are given in Table 3 in SI units. The data are illustrated as a function of density in Fig. 1.

The imprecision of these data, as measured by two times the standard deviation ($2s$), is 3.0%. In addition, the mean deviation of these values from the values listed in the NBS certificate for SRM 1451 is 0.25%. Since the glass fiber blanket used in this round robin is basically the same material as SRM 1451, close agreement is expected. It is thus concluded that the bias of the mean value of these results at 297 K is negligible.

TABLE 3—Round-robin data for glass fiber blanket.

LAB CODE	TEST THICKNESS (cm)	TEST DENSITY (kg/m ³)	HOT TEMP. (K)	COLD TEMP. (K)	MEAN TEMP. (K)	THER. COND. (mW/m·K)	PCT. DEV. (OBS-CALC)
1	17.78	11.58	308.1	285.9	297.0	43.5	-.6
1	15.24	13.50	308.1	285.9	297.0	40.9	-1.0
1	15.24	13.50	308.1	285.9	297.0	40.8	-1.3
1	12.70	16.21	308.1	285.9	297.0	38.3	-1.6
1	15.24	13.50	308.1	286.0	297.0	40.9	-1.0
1	17.78	11.58	308.1	285.9	297.0	43.5	-.6
2	15.24	13.39	308.3	285.9	297.1	41.6	.4
2	15.24	13.39	308.8	285.9	297.3	41.4	-.4
3	15.24	13.10	310.9	283.2	297.0	41.9	.4
3	15.24	13.10	310.9	283.2	297.0	42.1	.7
4	18.29	11.98	308.2	285.8	297.0	43.3	.1
4	16.26	13.47	308.2	285.9	297.0	41.7	.9
4	15.24	14.38	308.2	285.8	297.0	40.6	.4
4	14.22	15.41	308.2	285.8	297.0	39.8	.6
5	15.24	13.33	299.8	294.3	297.0	43.1	3.6
5	15.24	13.29	299.8	294.3	297.0	42.8	2.9
6	15.24	13.78	312.2	284.5	298.4	42.2	2.0
7	15.24	13.29	308.2	286.4	297.3	40.9	-1.7
7	15.24	13.29	308.3	286.4	297.3	40.9	-1.7
10	15.23	13.65	311.0	283.1	297.0	40.6	-1.3
10	15.24	13.65	311.0	283.1	297.0	40.5	-1.7
11	15.24	13.29	311.1	283.4	297.3	42.2	1.4

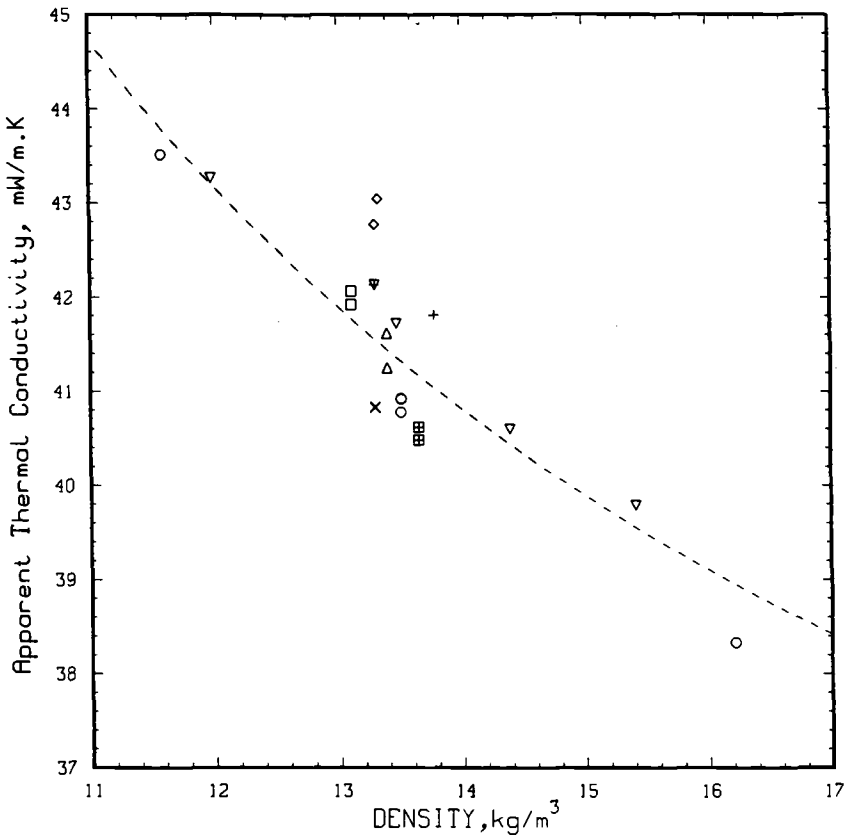


FIG. 1—Apparent thermal conductivity of glass fiber blanket versus test density at 297 K. Dashed line is obtained from the certified values for NBS SRM 1451. See Table 1 for symbol definitions.

Loose-Fill Results at 0.9 Times Contact Thickness

The principal objective of this round robin is to establish information for a precision and bias statement that can be used in ASTM C 687. The bias for the loose-fill test results is assumed to be the same as that for the glass fiber blanket results (i.e., less than 0.25%). However, each of the loose-fill materials has unique characteristics that may increase the bias above that for the well-studied glass fiber blanket (see, for example, Ref 2). Because many of the test points are not at exactly 0.9 times contact thickness, we arbitrarily selected the test points at 0.85 times contact thickness and above for the comparisons below.

Of the 65 test points reported by nine laboratories (Table 4) for cellulose, 37 of them were obtained at 0.9 times contact thickness and therefore are consistent with the round robin plan. These data are shown in Fig. 2. The dashed curve was used in calculating the imprecision ($2s$) value for cellulose, 21%.

Of the 75 test points reported by nine laboratories (Table 5) for bonded glass fiber loose-fill, 35 of them were obtained at approximately 0.9 times contact thickness. These data are shown in Fig. 3. The imprecision of these data is 14%.

Eight laboratories reported a total of 46 test points (Table 6) for rock/slag wool loose-fill. Of these, 25 of them were obtained at 0.9 times contact thickness. These data are illustrated in Fig. 4; the imprecision is 10%.

TABLE 4—Round-robin data for cellulose loose-fill.

LAB CODE	THICKNESS (cm)		TEST/CONTACT RATIO	DENSITY (kg/m ³)		BOX/TEST RATIO	HOT TEMP. (K)	COLD TEMP. (K)	MEAN TEMP. (K)	THER. COND. (mW/m.K)	PCT. DEV. (OBS-CALC)
1	18.10	16.51	.91	33.93	37.03	.92	308.3	286.0	297.2	56.1	19.5
1	18.10	15.24	.84	36.76	40.13		308.3	286.1	297.2	49.0	9.6
1	18.10	13.97	.77	40.09	43.78		308.3	286.1	297.2	45.8	5.1
1	18.67	17.78	.95	31.67	34.42	.92	308.3	286.0	297.1	52.9	13.2
1	18.67	15.24	.82	36.95	40.16		308.3	285.9	297.1	46.3	4.3
1	18.67	12.70	.68	44.35	48.18		308.2	285.7	296.9	35.2	-21.0
1	18.10	16.51	.91	34.37	38.28	.90	308.1	286.0	297.0	50.3	11.1
1	18.10	15.24	.84	37.24	41.47		308.1	285.9	297.0	46.3	5.0
1	18.10	13.97	.77	40.62	45.25		308.1	286.0	297.1	44.4	2.8
2	17.63	15.88	.90	40.37	42.93	.94	308.3	285.9	297.1	41.8	-4.4
2	17.63	14.10	.80	45.33	48.37		308.3	285.9	297.1	40.5	-5.2
2	17.63	12.34	.70	51.74	55.10		308.3	285.9	297.1	40.3	-3.0
2	17.63	11.46	.65	55.90	59.43		308.3	285.9	297.1	40.2	-2.1
2	17.63	10.67	.61	59.91	63.75		308.3	285.9	297.1	40.2	-.9
2	20.52	18.47	.90	42.29	46.61	.91	308.3	285.9	297.1	45.4	5.5
2	20.52	16.41	.80	47.57	52.38		308.3	285.9	297.1	42.9	2.3
2	20.52	14.38	.70	54.30	59.91		308.3	285.9	297.1	41.6	1.6
2	20.52	13.34	.65	58.63	64.55		308.3	285.9	297.1	41.5	2.4
2	20.52	12.32	.60	63.43	69.84		308.3	285.9	297.1	41.4	3.2
2	19.76	17.78	.90	43.25	46.45	.93	308.3	285.9	297.1	45.1	4.8
2	19.76	15.80	.80	48.69	52.22		308.3	285.9	297.1	40.9	-2.6
2	19.76	13.84	.70	55.58	59.59		308.3	285.9	297.1	40.3	-1.7
2	19.76	12.83	.65	60.07	64.39		308.3	285.9	297.1	40.3	-.4
2	19.76	11.86	.60	64.87	69.68		308.3	285.9	297.1	40.5	1.1
2	21.79	20.70	.95	35.56	40.05	.89	308.1	286.8	297.4	55.5	20.0
2	21.79	19.63	.90	37.48	42.29		308.0	286.7	297.3	45.8	4.3
2	21.79	18.95	.87	38.76	43.73		308.1	286.7	297.4	44.7	2.5
2	18.77	17.75	.95	36.36	40.85	.89	308.0	286.7	297.3	48.6	9.0
2	18.77	16.84	.90	38.28	43.09		308.0	286.7	297.3	46.5	6.1
2	18.77	16.28	.87	39.72	44.53		308.1	286.6	297.3	45.5	4.7
2	18.77	15.90	.85	40.69	45.65		308.1	286.6	297.5	42.8	-1.0
2	18.77	15.24	.81	42.45	47.57		308.1	286.7	297.4	41.6	-2.9
2	17.55	15.75	.90	37.64	42.61	.88	308.1	286.7	297.4	45.2	3.2
2	17.55	15.21	.87	38.92	44.05		308.0	286.6	297.3	44.4	2.0
2	17.55	14.83	.85	39.88	45.17		308.1	286.7	297.4	44.0	1.5
3	17.78	16.00	.90	35.08	32.36	1.08	310.9	283.2	297.0	41.1	-13.5
3	17.78	16.00	.90	35.08	33.80		310.9	283.2	297.0	40.9	-12.6
3	17.15	15.44	.90	36.36	34.12	1.07	310.9	283.2	297.0	40.2	-14.4
4	18.06	16.26	.90	35.16	41.17	.85	308.2	286.0	297.1	50.0	12.0
4	18.06	15.24	.84	37.50	43.92		308.2	286.0	297.1	48.0	9.5
4	18.06	14.22	.79	40.21	47.08		308.2	285.9	297.0	46.3	7.6
4	18.92	17.02	.90	32.44	35.64	.91	308.2	286.0	297.1	46.9	3.1
4	18.92	15.24	.81	36.23	39.80		308.2	285.9	297.0	44.8	1.0
4	18.92	14.22	.75	38.81	42.66		308.2	286.0	297.1	43.7	.0
4	18.80	16.92	.90	32.77	36.52	.90	308.2	286.0	297.1	53.7	15.8
4	18.80	15.23	.81	36.39	40.56		308.2	285.8	297.0	42.8	-3.0
4	18.80	14.23	.76	38.99	43.46		308.2	285.9	297.0	42.5	-2.3
5	15.91	14.26	.90	39.68	38.84	1.02	299.8	294.3	297.0	39.0	-14.2
5	17.17	15.44	.90	41.09	42.37	.97	299.8	294.3	297.0	39.4	-11.1
5	17.87	16.10	.90	40.27	42.56	.95	299.8	294.3	297.0	40.3	-8.3
6	16.51	15.01	.91	36.84	37.16	.99	312.2	284.5	298.3	42.2	-8.0
6	16.54	15.04	.91	36.84	34.92	1.06	312.3	284.9	298.6	43.1	-7.7
6	16.51	15.01	.91	36.84	36.52	1.01	312.2	284.7	298.5	42.8	-7.1
9	17.78	16.51	.93	39.56	37.80	1.05	311.1	283.0	297.1	42.5	-5.6
9	17.78	15.24	.86	42.77	41.01		311.1	283.0	297.0	40.3	-9.1
9	17.78	13.97	.79	46.77	44.69		311.0	282.9	297.0	39.9	-8.3
10	19.38	17.42	.90	42.29			310.9	283.1	297.0	40.5	-8.0
10	19.38	16.46	.85	44.69			310.9	283.1	297.0	40.1	-7.9
10	19.38	15.47	.80	44.69			310.9	283.1	297.0	39.6	-9.1
10	19.38	15.47	.80	47.73			310.9	283.1	297.0	39.3	-8.5
10	19.38	15.47	.80	47.73			310.9	283.1	297.0	39.5	-8.1
10	18.08	16.26	.90	44.85			310.9	283.1	297.0	40.1	-7.8
11	16.94	15.24	.90	34.76	37.64	.92	311.1	283.5	297.3	39.5	-14.0
11	16.94	15.24	.90	38.12	39.56		311.2	283.1	297.1	39.8	-11.7
11	16.94	15.24	.90	35.88	38.92		311.2	283.5	297.3	39.1	-14.4

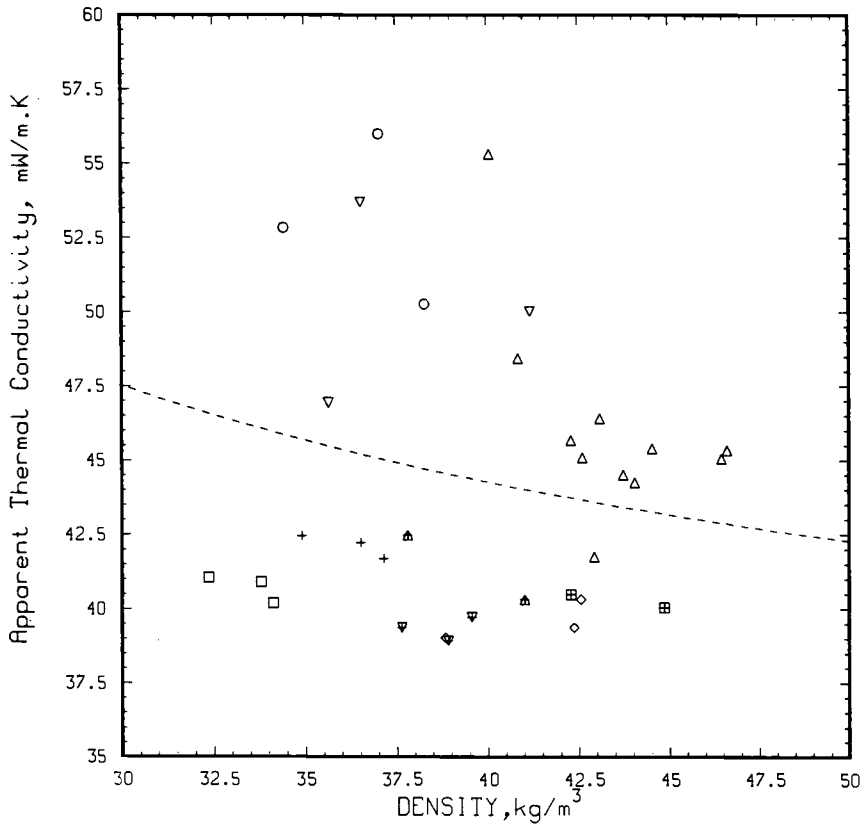


FIG. 2—Apparent thermal conductivity of cellulose loose-fill at 0.9 times contact thickness versus test density at 297 K. The dashed curve was used to calculate the 2s value of 21%. See Table 1 for symbol definition.

For unbonded glass fiber loose-fill nine laboratories reported 71 test points (Table 7). Forty-one of them were obtained at 0.9 times contact thickness. These data are shown in Fig. 5; the imprecision is 16%.

The imprecision of the loose-fill results is considerably greater than that for the glass fiber blanket calibration material (10 to 21% versus 3.0%). The reason for this is not clear, but it may be caused principally by inadequate standardization of the technique for preparing specimens.

Compression/Density Effect

A secondary objective of the round robin is to determine if the density dependence of apparent thermal conductivity with specimens at various blown densities is the same as that produced by compressing the specimens to various densities. Figures 6, 7, 8, and 9 show all the data obtained for the four loose-fill materials. The data obtained by compressing given specimens to various densities are interconnected with solid lines. These data sets are inherently more precise than the data for several specimens because the specimen preparation variability is not present.

Examination of Figs. 6 to 9 strongly suggests that the thermal conductivity decreases more rapidly with increasing density as a consequence of compressing given specimens versus blowing different specimens over the same density range. This difference appears to be most apparent at

TABLE 5—Round-robin data for bonded glass fiber loose-fill.

LAB CODE	THICKNESS (cm)		TEST/ CONTACT RATIO	DENSITY (kg/m ³)		BOX/ TEST RATIO	HOT TEMP. (K)	COLD TEMP. (K)	MEAN TEMP. (K)	THER. COND. (mW/m.K)	PCT. DEV. (OBS-CALC)
	CONTACT	TEST		BOX	TEST						
1	20.57	17.78	.86	7.26	8.12	.89	308.2	285.9	297.0	67.3	0
1	20.57	15.24	.74	8.47	9.48		308.2	285.9	297.0	58.2	-6.2
1	20.57	12.70	.62	10.16	11.37		308.1	285.9	297.0	52.2	-7.7
1	20.32	17.78	.88	7.72	8.28	.93	308.3	286.0	297.2	64.8	-2.8
1	20.32	15.24	.75	9.00	9.66		308.2	286.0	297.1	56.6	-8.2
1	20.32	12.70	.63	10.80	11.60		308.2	285.9	297.0	50.7	-9.7
1	21.27	17.78	.84	7.48	8.28		308.3	285.9	297.1	62.1	-7.3
1	21.27	15.24	.72	8.73	9.66		308.3	285.9	297.1	57.6	-6.3
1	21.27	12.70	.60	10.48	11.60		308.2	285.9	297.0	50.4	-10.3
2	17.58	15.82	.90		11.13		308.2	285.9	297.0	59.7	4.7
2	17.58	14.07	.80		12.53		308.2	285.9	297.0	54.3	1.5
2	17.58	12.29	.70		14.34		308.2	285.9	297.0	49.6	-1.0
2	17.58	11.43	.65		15.43		308.2	285.9	297.0	47.4	-2.0
2	17.58	10.54	.60		16.66		308.2	285.9	297.0	45.4	-2.8
2	18.80	16.92	.90		10.60		308.2	285.9	297.0	61.0	4.4
2	18.80	15.04	.80		11.93		308.2	285.9	297.0	55.8	1.7
2	18.80	13.16	.70		13.63		308.2	285.9	297.0	50.7	-1.1
2	18.80	12.22	.65		14.69		308.2	285.9	297.0	48.4	-2.2
2	18.80	11.28	.60		15.92		308.2	285.9	297.0	46.0	-3.6
2	18.49	16.64	.90		11.89		308.2	285.9	297.1	57.6	4.6
2	18.49	14.78	.80		13.39		308.2	285.9	297.1	52.6	1.6
2	18.49	12.95	.70		15.28		308.3	285.9	297.1	48.4	-4
2	18.49	12.01	.65		16.50		308.3	285.9	297.1	46.3	-1.4
2	18.49	11.10	.60		17.78		308.3	286.0	297.1	44.2	-2.5
2	18.42	16.59	.90	11.05	11.79	.94	308.3	285.9	297.1	58.6	5.9
2	18.42	14.73	.80	12.45	13.26		308.2	285.9	297.1	53.6	3.0
2	18.42	12.90	.70	14.21	15.15		308.2	285.9	297.1	49.0	.5
2	18.42	11.96	.65	15.33	16.34		308.2	285.9	297.1	47.0	-2
2	18.42	11.05	.60	16.66	17.78		308.2	285.9	297.1	44.8	-1.1
2	17.53	15.77	.90	11.87	12.27	.97	308.2	285.9	297.1	56.5	4.3
2	17.53	14.02	.80	13.36	13.81		308.2	285.9	297.1	51.7	1.4
2	17.53	12.27	.70	15.27	15.78		308.2	285.9	297.1	47.6	-6
2	17.53	11.40	.65	16.34	16.98		308.2	285.9	297.1	45.7	-1.3
2	17.53	10.52	.60	17.78	18.42		308.2	285.9	297.1	43.8	-1.8
2	18.42	16.59	.90	11.52	11.84	.97	308.3	285.9	297.1	59.4	7.2
2	18.42	14.73	.80	12.97	13.34		308.3	285.9	297.1	54.2	4.3
2	18.42	12.90	.70	14.80	15.22		308.3	285.9	297.1	49.4	1.5
2	18.42	11.96	.65	15.97	16.50		308.3	285.9	297.1	47.3	.8
2	18.42	11.05	.60	17.30	17.78		308.3	285.9	297.1	45.1	-5
2	17.40	15.62	.90	8.86	8.84	1.00	307.9	286.6	297.2	70.8	9.1
2	17.12	15.27	.89	8.94	9.23	.97	308.0	286.8	297.4	68.6	8.2
2	20.75	18.67	.90	9.75	10.49	.93	308.0	286.7	297.3	67.2	12.5
3	17.78	16.00	.90	6.41			310.9	283.2	297.0	71.8	-7.0
3	17.78	16.00	.90	5.91			310.9	283.2	297.0	77.4	-3.9
3	17.78	16.00	.90	6.09			310.9	283.2	297.0	76.2	-3.7
4	23.50	21.15	.90	6.92	7.83	.88	308.2	286.0	297.1	75.7	9.2
4	23.50	15.24	.65	9.61	10.88		308.2	285.9	297.0	55.8	-3.1
4	23.50	14.22	.61	10.30	11.65		308.2	285.9	297.1	53.0	-4.7
4	21.27	19.15	.90	7.59	8.15	.93	308.2	286.0	297.1	72.9	7.9
4	21.27	17.02	.80	8.54	9.18		308.2	286.0	297.1	64.4	2.2
4	21.27	14.90	.70	9.75	10.46		308.2	286.0	297.1	58.1	-1.1
4	20.42	18.38	.90	7.91	8.65	.91	308.2	286.0	297.1	70.5	7.7
4	20.42	16.33	.80	8.91	9.72		308.2	286.0	297.1	62.5	2.4
4	20.42	14.29	.70	10.19	11.12		308.2	286.0	297.1	56.5	-7
5	19.61	17.61	.90	9.16	9.58	.96	299.8	294.3	297.0	60.8	-1.2
5	19.48	17.50	.90	9.13	9.72	.94	299.8	294.3	297.0	62.5	2.4
5	18.37	16.52	.90	8.60	9.58	.90	299.8	294.3	297.0	62.1	1.0
7	16.92	15.27	.90	8.65	9.13	.95	307.9	286.4	297.2	65.7	3.8
7	17.27	14.99	.87	8.65	8.97	.96	307.9	286.4	297.2	65.3	2.3
7	17.37	14.99	.86	8.65	8.97	.96	307.9	286.4	297.1	65.3	2.3
8	15.29	15.29	1.00		9.13		308.9	285.5	297.2	59.4	-6.5
8	13.74	13.74	1.00		10.09		308.9	285.5	297.2	54.6	-9.8
8	15.27	15.27	1.00		9.13		308.9	285.5	297.2	61.2	-3.3
8	13.77	13.77	1.00		10.09		308.9	285.5	297.2	56.2	-6.7
8	15.29	15.29	1.00		9.13		308.9	285.5	297.2	57.4	-10.3
8	13.74	13.74	1.00		10.09		308.9	285.5	297.2	54.0	-11.0
9	17.78	16.51	.93	9.77	10.41	.94	310.8	283.3	297.1	54.0	-8.9
9	17.78	15.24	.86	10.73	11.21		310.8	283.2	297.0	51.2	-10.6
9	17.78	13.97	.79	11.69	12.17		310.8	283.0	296.9	48.6	-11.6
10	19.30	17.35	.90	10.48			310.9	283.2	297.0	54.0	-8.6
10	19.30	16.38	.85	11.12			310.9	283.2	297.0	52.2	-9.0
10	19.30	15.42	.80	11.84			310.9	283.2	297.0	50.1	-9.8
10	19.30	14.48	.75	12.64			310.9	283.2	297.0	48.3	-10.3
10	19.43	17.48	.90	10.65			311.0	283.0	297.0	54.5	-6.7
10	19.00	17.09	.90	10.88			310.9	283.1	297.0	53.3	-7.9

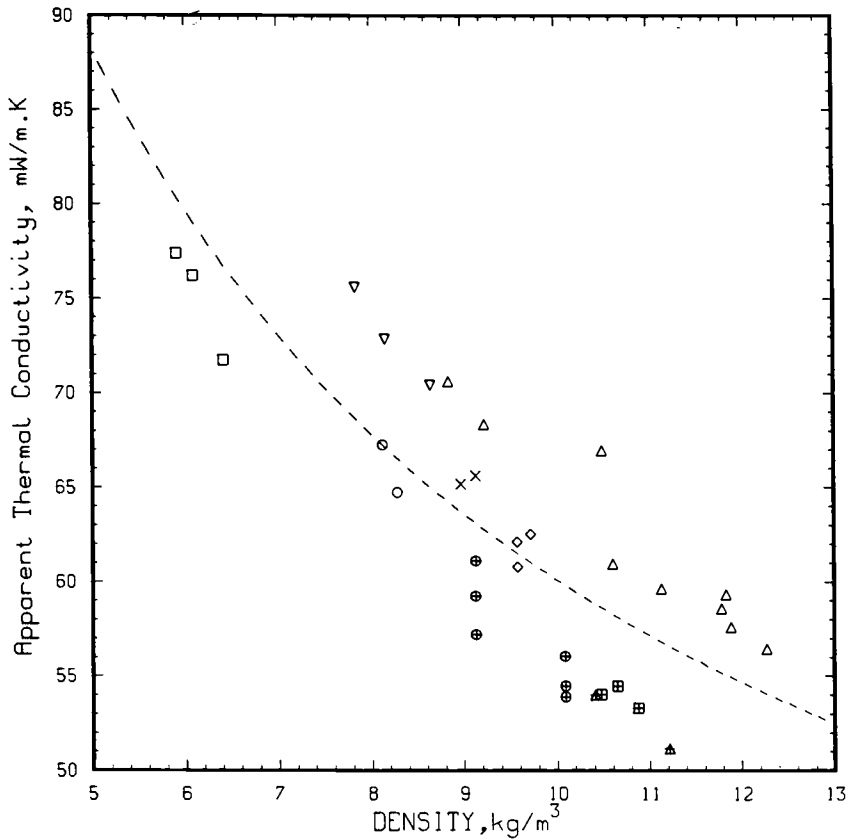


FIG. 3—Apparent thermal conductivity of bonded glass fiber loose-fill at 0.9 times contact thickness versus test density at 297 K. The dashed curve was used to calculate the 2s value of 14%. See Table 1 for symbol definition.

the lower densities. To quantify this difference, the following analysis was performed: The slope of the compression curves was graphically estimated at the lower densities. The slope of the reference curve was obtained in the same density range. The ratio of these slopes was calculated for each loose-fill material. The resulting ratios are 6.4 for cellulose, 1.5 for bonded glass fiber, 1.5 for rock/slag wool, and 2.0 for unbonded glass fiber.

It must be stressed that any conclusions drawn from these ratios are based on incomplete data sets of relatively high scatter and correspondingly high uncertainties in the slopes of the reference curves. The conclusions would be more clear if some of the specimens could have been blown at densities in the upper part of the range and if the lower-density specimens had been compressed to the upper part of the range. Bomberg and Solvason [3] have reported data on the compression effect with qualitatively similar conclusions.

Box Density versus Test Density

The final objective of this round robin was to determine if the density value as determined by weighing the entire specimens (box density) is different from the density values as determined by weighing only the test areas (test density). The latter densities are obtained with a "cookie cutter" or similar device.

TABLE 6—Round-robin data for rock/slag wool loose-fill.

LAB CODE	THICKNESS (cm)		TEST/CONTACT RATIO	DENSITY (kg/m ³)		BOX/TEST RATIO	HOT TEMP. (K)	COLD TEMP. (K)	MEAN TEMP. (K)	THER. COND. (mW/m.K)	PCT. DEV. (OBS-CALC)
	CONTACT	TEST		BOX	TEST						
1	16.51	15.88	.96	25.79	28.02	.92	308.2	286.0	297.1	55.2	7.1
1	16.51	14.61	.88	28.03	30.45		308.2	286.0	297.1	51.7	4.0
1	16.51	13.34	.81	30.71	34.95		308.1	286.0	297.1	48.7	2.9
1	17.78	16.51	.93	27.58	31.51	.88	308.2	286.0	297.1	52.5	6.5
1	17.78	15.24	.86	29.89	34.13		308.1	286.0	297.1	49.6	3.8
1	17.78	13.97	.79	32.61	37.24		308.1	286.0	297.1	47.3	2.1
1	15.56	15.24	.98	27.82	32.40	.86	308.2	286.0	297.1	53.3	8.9
1	15.56	13.97	.90	30.37	35.35		308.1	286.0	297.1	49.4	4.7
1	15.56	12.70	.82	33.40	38.89		308.1	286.0	297.1	47.8	4.6
2	15.90	14.30	.90	39.64	38.92	1.02	308.6	285.9	297.3	45.2	-1.0
2	15.90	13.51	.85	41.97	41.17		308.5	285.9	297.2	44.0	-2.2
2	15.90	12.73	.80	44.56	43.73		308.5	285.9	297.2	42.9	-2.7
2	15.90	11.13	.70	50.97	49.98		308.5	285.9	297.2	40.1	-6.0
2	15.90	10.34	.65	54.85	53.82		308.5	285.9	297.2	39.9	-4.3
2	16.76	15.09	.90	37.10	39.08	.95	308.5	285.9	297.2	47.0	2.8
2	16.76	13.41	.80	41.73	43.89		308.6	285.9	297.3	43.5	-1.2
2	16.76	11.73	.70	47.69	50.14		308.6	285.9	297.3	41.4	-2.6
2	16.76	10.40	.65	51.35	54.14		308.7	285.9	297.3	40.3	-3.0
2	17.17	15.44	.90	37.83	38.76	.98	308.7	285.9	297.3	46.7	1.9
2	17.17	13.74	.80	42.53	43.57		308.6	285.9	297.2	43.4	-1.8
2	17.17	12.01	.70	48.63	49.82		308.7	285.9	297.3	40.9	-3.9
2	17.17	11.10	.65	52.64	53.98		308.7	285.9	297.3	40.2	-3.5
2	17.17	10.41	.61	56.11	57.50		308.8	285.9	297.3	39.5	-3.8
3	19.05	15.93	.84	28.03	27.23		310.9	283.2	297.0	46.4	-11.7
3	17.78	16.00	.90	26.75	26.43	1.01	310.9	283.2	297.0	46.5	-12.6
3	17.15	15.44	.90	27.71	28.51	.97	310.9	283.2	297.0	45.7	-11.4
4	18.11	16.26	.90	19.94	26.43	.75	308.1	285.9	297.0	51.5	-1.8
4	18.11	15.24	.84	21.27	28.19		308.2	285.9	297.0	49.5	-3.2
4	18.11	14.22	.79	22.79	30.21		308.1	285.9	297.0	47.5	-4.9
4	18.44	16.59	.90	24.60	26.48	.93	308.2	286.0	297.1	50.9	-3.0
4	18.44	15.24	.83	26.78	28.83		308.2	286.0	297.1	48.5	-4.6
4	18.44	14.22	.77	28.69	30.90		308.2	285.9	297.0	46.6	-5.9
5	19.47	17.52	.90	26.08	28.94	.90	299.8	294.3	297.0	49.1	-3.0
5	18.61	16.73	.90	29.47	31.75	.93	299.8	294.3	297.0	48.4	-1.0
5	18.81	16.96	.90	25.63	26.77	.96	299.8	294.3	297.0	49.9	-4.6
7	16.89	15.32	.91	27.07	27.87	.97	308.1	286.4	297.2	52.5	2.0
7	16.56	15.06	.91	26.43	27.07	.98	308.1	286.4	297.2	52.0	.0
7	16.18	15.06	.93	28.99	28.67	1.01	308.1	286.4	297.2	52.7	3.6
9	17.78	16.51	.93	32.36	32.04	1.01	311.0	283.2	297.1	49.4	1.4
9	17.78	15.24	.86	35.08	34.60		311.0	283.0	297.0	46.7	-1.6
9	17.78	13.97	.79	38.28	37.80		311.0	283.0	297.0	44.7	-3.1
10	19.30	17.35	.90	30.75			310.9	283.1	297.0	48.8	-1.3
10	19.30	16.43	.85	32.52			310.9	283.1	297.0	47.3	-2.6
10	19.30	15.44	.80	34.60			310.9	283.1	297.0	45.7	-3.8
10	19.30	14.48	.75	37.00			310.9	283.2	297.0	44.2	-4.9
10	17.81	16.05	.90	33.48			311.0	283.0	297.0	46.0	-4.4

The reported box densities are plotted versus the reported test densities in Figs. 10, 11, 12, and 13. The solid line represents the ideal case where box density equals test density. The ratios of box density to test density were calculated for all the test specimens. The mean values of these ratios for each loose-fill material are shown in Table 8. In every case the mean value is less than the ideal case by about 5%; on the average the box densities are less than the test densities by about 5%. However, the imprecision ($2s$) of these ratios, given in Table 8, is greater than the mean ratio minus the ideal ratio of unity, indicating that any single measured box density can be greater than the measured test density. Values of two times the standard error of the mean, $2s \cdot n^{0.5}$, are also given in Table 8. These values indicate the imprecision of the mean values of the ratios. Since these values range from 1 to 3%, we conclude that the mean values of from 0.94 to 0.96 are statistically different from unity (i.e., average box densities are lower than average test densities).

Summary

The test results on the glass fiber blanket indicate that the measurement capability of the participants can be characterized by an imprecision, $2s$, of 3.0% and a negligible bias of the mean. The measurements on the loose-fill materials are characterized by an imprecision rang-

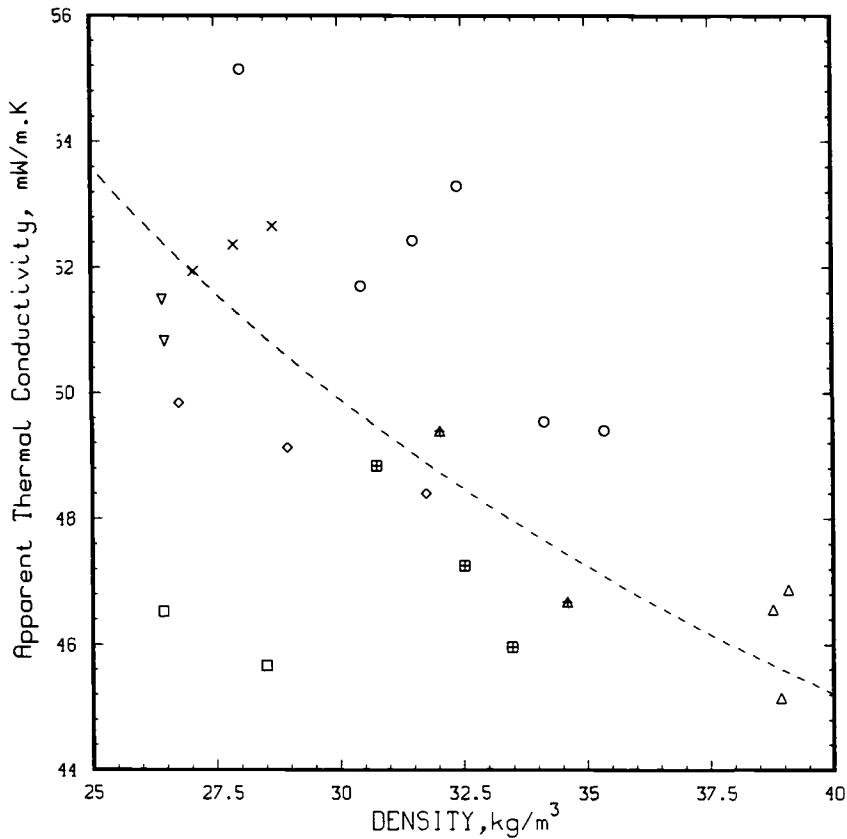


FIG. 4—Apparent thermal conductivity of rock/slag wool loose-fill at 0.9 times contact thickness versus test density at 297 K. The dashed curve was used to calculate the 2s value of 10%. See Table 1 for symbol definitions.

ing from 21% for cellulose to 10% for the rock/slag wool. The larger imprecision for the loose-fill materials is attributed primarily to inadequately defined procedures for preparing and conditioning specimens.

Five laboratories compressed material beyond 0.9 times contact thickness as indicated by the lines on Figs. 6, 7, 8, and 9. Since no specific procedure was established for the compression testing, separating the compression effect from the random variability of test results is difficult. However, it appears that a compression effect does exist. Additional data would be required in order to draw more quantitative conclusions concerning the compression effect.

The comparison of density determination techniques indicates that the test density is normally higher than the box density (Figs. 10, 11, 12, and 13). The discrepancy between these two measurements is probably due to the inability to produce homogeneous specimens of the loose-fill materials. Future efforts of the ASTM C 687 task group will be directed towards the improvement of procedures for preparing and conditioning specimens.

Recommendations

The test measurements made on the glass fiber blanket material indicate that the ASTM C 687 test apparatus are capable of significantly better precision than those reported here for the

TABLE 7—Round-robin data for unbonded glass fiber loose-fill.

LAB CODE	THICKNESS (cm)		TEST/ CONTACT RATIO	DENSITY (kg/m ³)		BOX/ TEST RATIO	HOT TEMP. (K)	COLD TEMP. (K)	MEAN TEMP. (K)	THER. COND. (mW/m ² ·K)	PCT. DEV. (OBS-CALC)
1	18.42	17.78	.97	8.11	8.79	.92	308.1	286.1	297.1	58.1	4.4
1	18.42	15.24	.83	9.45	10.25		308.1	286.0	297.1	52.0	-1.4
1	18.42	12.70	.69	11.34	12.32		308.1	286.0	297.0	46.1	-7.2
1	19.05	17.78	.93	7.91	8.01	.99	308.2	286.0	297.1	58.8	2.7
1	19.05	15.24	.80	9.23	9.35		308.2	286.1	297.1	52.7	-3.2
1	19.05	12.70	.67	11.07	11.23		308.1	286.0	297.1	46.4	-10.2
1	18.67	17.78	.95	8.03	8.47	.95	308.2	286.0	297.1	55.8	-8
1	18.67	15.24	.82	9.39	9.88		308.2	286.0	297.1	50.0	-6.8
1	18.67	12.70	.68	11.24	11.85		308.1	286.0	297.1	44.4	-13.0
2	19.81	18.29	.92	12.62	12.61	1.00	308.2	285.9	297.0	50.3	2.5
2	19.81	15.85	.80	14.56	14.54		308.2	285.9	297.0	45.8	-1.5
2	19.81	13.87	.70	16.66	16.66		308.2	285.9	297.0	42.5	-3.9
2	19.81	11.89	.60	19.38	19.38		308.2	285.9	297.0	39.5	-5.5
2	19.81	10.90	.55	21.14	21.14		308.2	285.9	297.0	38.3	-5.1
2	19.76	17.78	.90	12.25	12.78	.96	308.2	285.9	297.1	50.1	2.7
2	19.76	15.80	.80	13.78	14.38		308.2	285.9	297.0	46.4	-7
2	19.76	13.84	.70	15.73	16.42		308.2	285.9	297.1	43.1	-3.1
2	19.76	11.84	.60	18.42	19.22		308.2	285.9	297.0	39.9	-4.7
2	19.76	10.87	.55	20.02	20.90		308.2	285.9	297.0	38.9	-4.0
2	19.81	17.83	.90	13.10	13.04	1.00	308.3	285.9	297.1	49.1	1.4
2	19.81	15.85	.80	14.74	14.67		308.3	285.9	297.1	45.4	-2.2
2	19.81	13.87	.70	16.82	16.82		308.3	285.9	297.1	42.2	-4.3
2	19.81	11.89	.60	19.70	19.54		308.3	285.9	297.1	39.5	-5.3
2	19.81	10.90	.55	21.46	21.30		308.3	285.9	297.1	38.2	-5.2
2	18.80	16.87	.90	9.77	10.65	.92	308.0	286.8	297.4	60.4	13.6
2	18.80	16.31	.87	10.11	11.02		308.0	286.7	297.4	58.9	12.5
2	18.80	15.93	.85	10.33	11.28		308.0	286.7	297.3	57.9	11.7
2	18.80	14.99	.80	10.99	12.00		308.0	286.7	297.3	55.2	9.4
2	18.59	16.71	.90	9.92	10.65	.93	308.0	286.7	297.3	58.9	11.5
2	18.59	16.15	.87	10.25	11.18		308.1	286.7	297.4	57.6	11.0
2	18.59	15.77	.85	10.49	11.26		308.0	286.7	297.4	56.8	9.9
2	18.59	14.86	.80	11.15	11.98		308.0	286.7	297.3	54.5	8.1
2	18.64	16.74	.90	10.12	10.12	1.00	308.0	286.7	297.4	61.1	13.1
2	18.64	16.18	.87	10.48	10.48		308.0	286.7	297.3	59.5	11.9
2	18.64	15.82	.85	10.72	10.72		308.0	286.7	297.3	58.2	10.6
2	18.64	14.88	.80	11.39	11.39		308.0	286.7	297.4	55.3	7.9
3	17.78	16.00	.90	6.78	5.94	1.14	310.9	283.2	297.0	61.1	-2.1
3	17.78	16.00	.90	7.62	6.86		310.9	283.2	297.0	57.1	-5.0
3	17.78	16.00	.90		6.41		310.9	283.2	297.0	58.2	-4.9
4	19.05	17.15	.90	8.23	9.02	.91	308.2	286.0	297.1	53.7	-2.6
4	19.05	15.24	.80	9.26	10.16		308.2	286.0	297.1	49.8	-6.3
4	19.05	14.22	.75	9.92	10.88		308.2	285.9	297.0	47.8	-8.2
4	18.44	16.60	.90	8.33	8.89	.94	308.1	285.9	297.0	55.4	.2
4	18.44	15.24	.83	9.08	9.69		308.1	285.9	297.0	52.4	-2.6
4	18.44	14.22	.77	9.74	10.38		308.1	285.9	297.0	50.0	-4.9
4	18.77	16.91	.90	8.14	8.81	.92	308.1	286.0	297.1	57.4	3.3
4	18.77	15.04	.80	9.15	9.92		308.1	286.0	297.1	52.5	-1.6
4	18.77	14.10	.75	9.75	10.57		308.2	286.0	297.1	50.5	-3.4
5	17.25	15.51	.90	10.57	11.36	.93	299.8	294.3	297.0	52.9	3.8
5	17.10	15.39	.90	9.66	10.12	.95	299.8	294.3	297.0	55.3	4.3
5	17.27	15.60	.90	9.43	10.16	.93	299.8	294.3	297.0	55.2	4.1
7	16.54	14.96	.90	8.49	9.13	.93	308.0	286.4	297.2	56.8	3.3
7	16.51	14.99	.91	8.97	9.45	.95	308.1	286.4	297.2	55.6	2.4
7	16.79	15.27	.91	8.97	9.61	.93	308.1	286.4	297.2	55.9	3.5
8	15.21	15.21	1.00		9.13		309.0	285.4	297.2	50.6	-8.6
8	13.77	13.77	1.00		10.09		309.0	285.4	297.2	47.3	-12.4
8	15.21	15.21	1.00		9.13		309.0	285.4	297.2	50.9	-8.0
8	13.77	13.77	1.00		10.09		309.0	285.4	297.2	47.8	-11.0
8	15.21	15.21	1.00		9.13		309.0	285.4	297.2	49.6	-10.8
8	13.74	13.74	1.00		10.09		309.0	285.4	297.2	46.5	-14.1
8	15.21	15.21	1.00		9.13		309.0	285.4	297.2	52.2	-5.3
8	13.74	13.74	1.00		10.09		309.0	285.4	297.2	48.7	-9.1
9	17.78	16.51	.93	10.09	10.09	1.09	311.0	283.1	297.0	53.7	-1.4
9	17.78	15.24	.86	10.89	10.09		311.0	283.0	297.0	51.3	-3.3
9	17.78	13.97	.79	11.85	10.89		311.0	283.0	297.0	48.7	-6.0
10	19.38	17.40	.90	10.00			311.0	283.2	297.1	49.3	-8.0
10	19.38	16.46	.85	10.59			310.9	283.2	297.0	47.6	-9.7
10	19.38	15.49	.80	11.26			310.9	283.2	297.0	45.8	-11.4
10	19.38	14.50	.75	12.08			310.9	283.0	297.0	44.1	-12.9
10	17.98	16.08	.89	10.91			311.0	283.1	297.0	46.7	-10.6
10	18.06	16.21	.90	10.46			310.9	283.1	297.0	48.0	-9.1

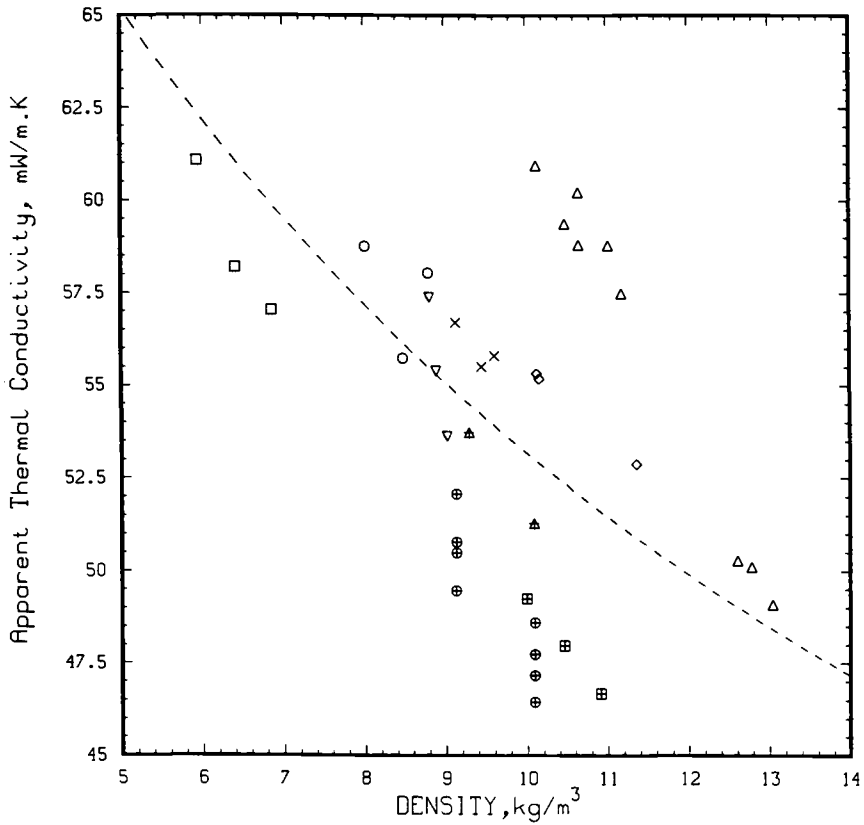


FIG. 5—Apparent thermal conductivity of unbonded glass fiber loose-fill at 0.9 times contact thickness versus test density at 297 K. The dashed curve was used to calculate the $2s$ value of 16%. See Table 1 for symbol definition.

TABLE 8—Mean values of the ratio of box density to test density, $2s$ values, and $2s \cdot n^{0.5}$ values.

	Ratio of Box Density to Test Density	$2s$	$2s \cdot n^{0.5}$
Cellulose	0.95	0.14	0.03
Bonded glass fiber	0.94	0.06	0.01
Rock/slag wool	0.94	0.14	0.03
Unbonded glass fiber	0.96	0.12	0.03

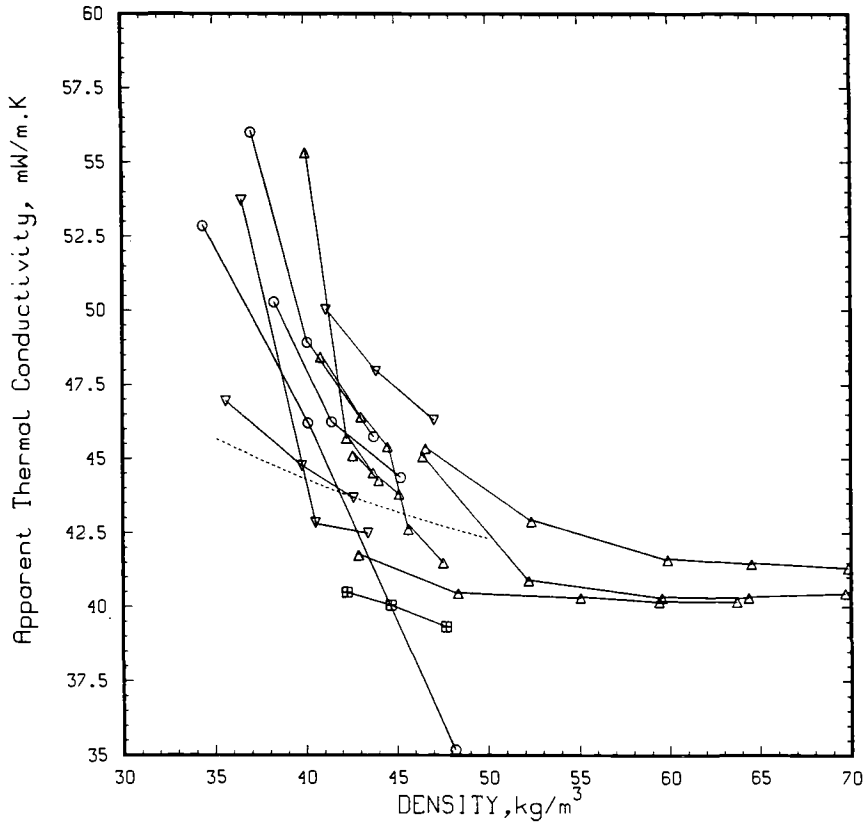


FIG. 6—Apparent thermal conductivity of cellulose loose-fill. The solid lines show the effect of compression on individual specimens.

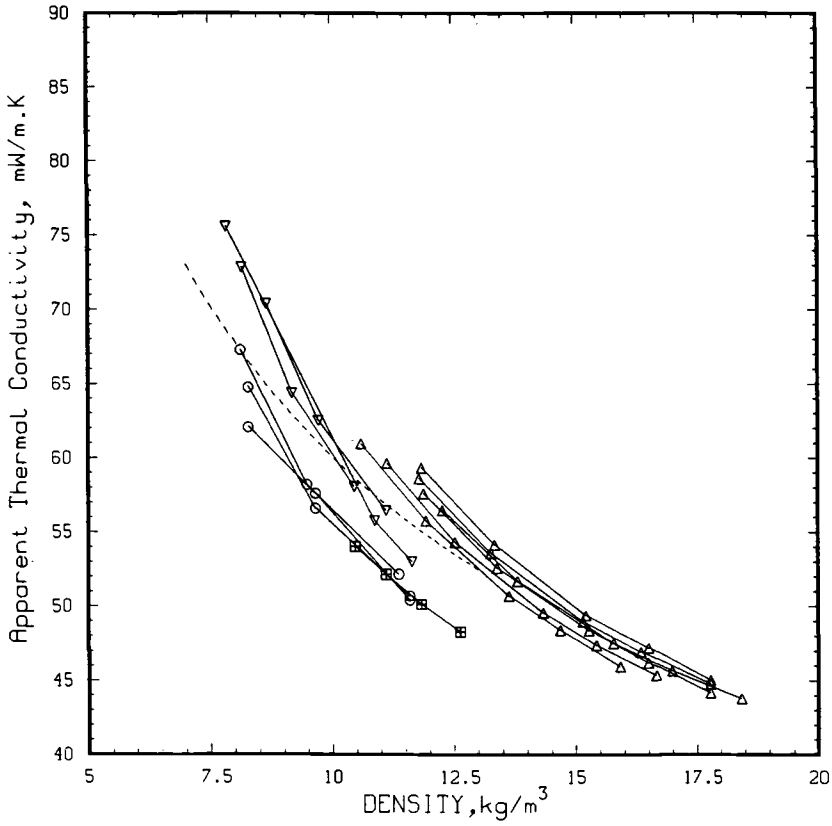


FIG. 7—Apparent thermal conductivity of bonded glass fiber loose-fill. The solid lines show the effect of compression on individual specimens.

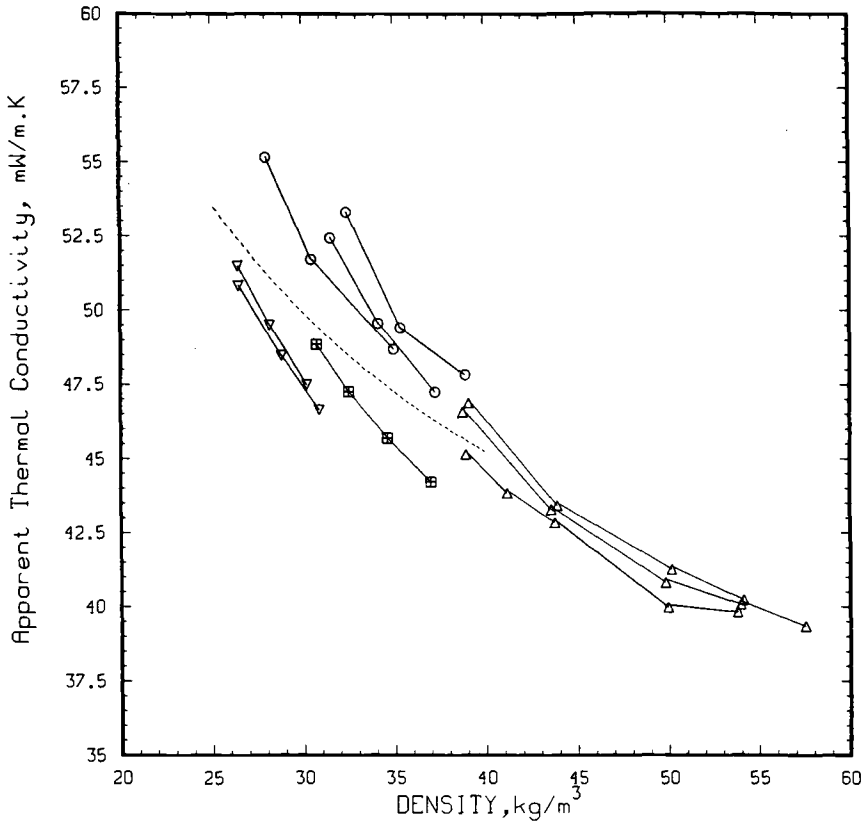


FIG. 8—Apparent thermal conductivity of rock/slag wool loose-fill. The solid lines show the effect of compression on individual specimens.

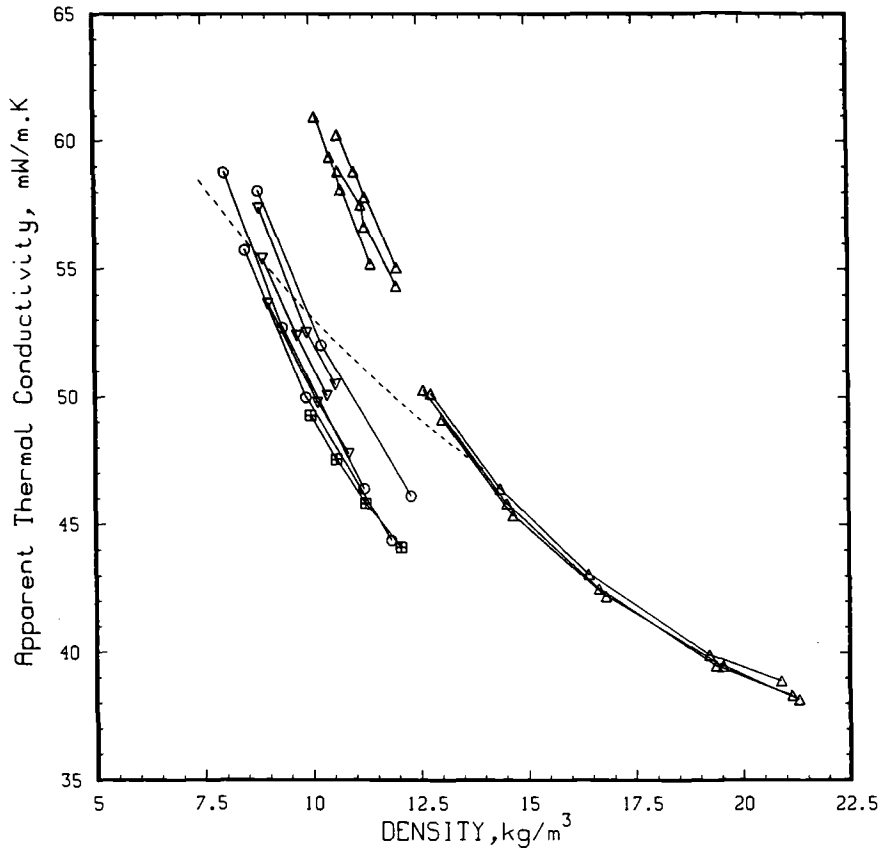


FIG. 9—Apparent thermal conductivity of unbonded glass fiber loose-fill. The solid lines show the effect of compression on individual specimens.

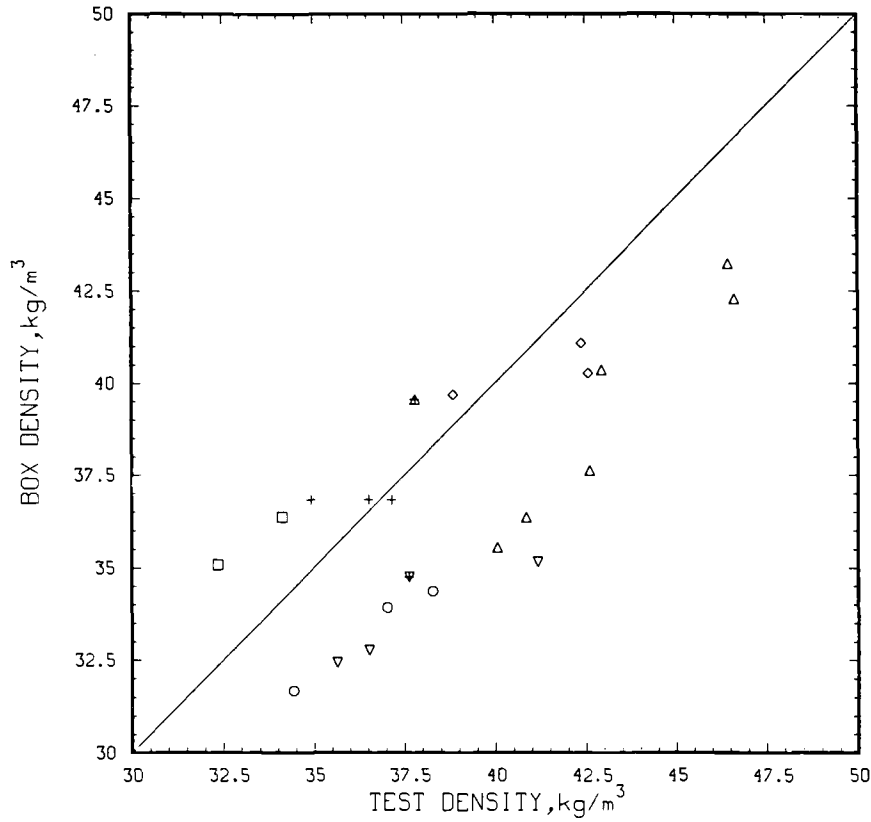


FIG. 10—Box density versus test density for cellulose loose-fill.

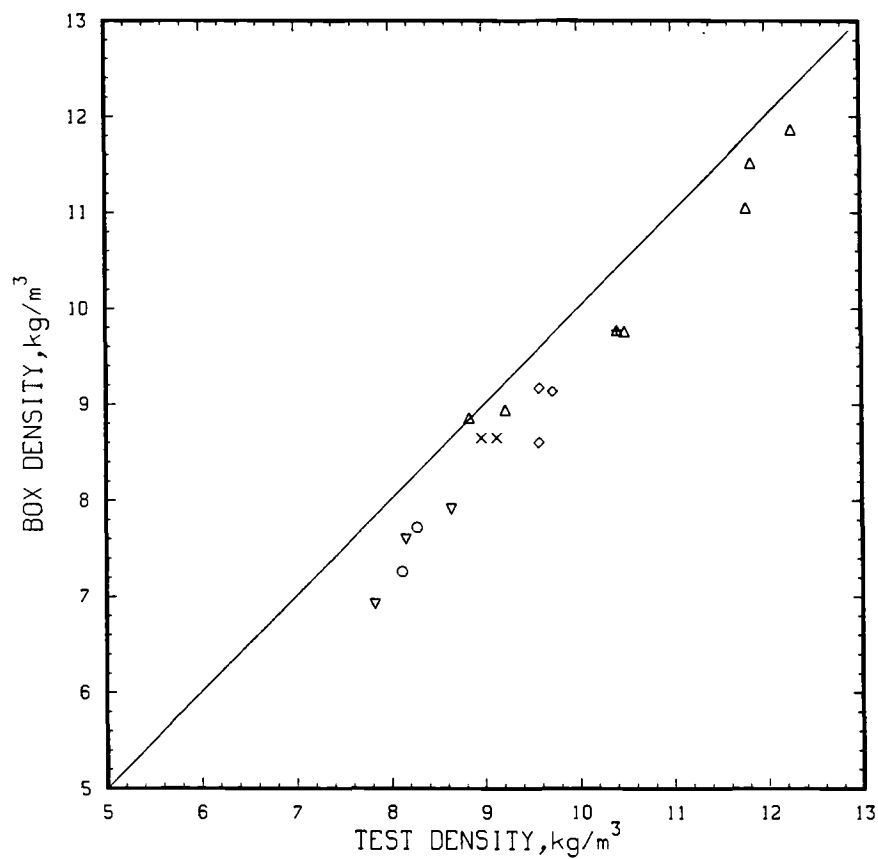


FIG. 11—Box density versus test density for bonded glass fiber loose-fill.

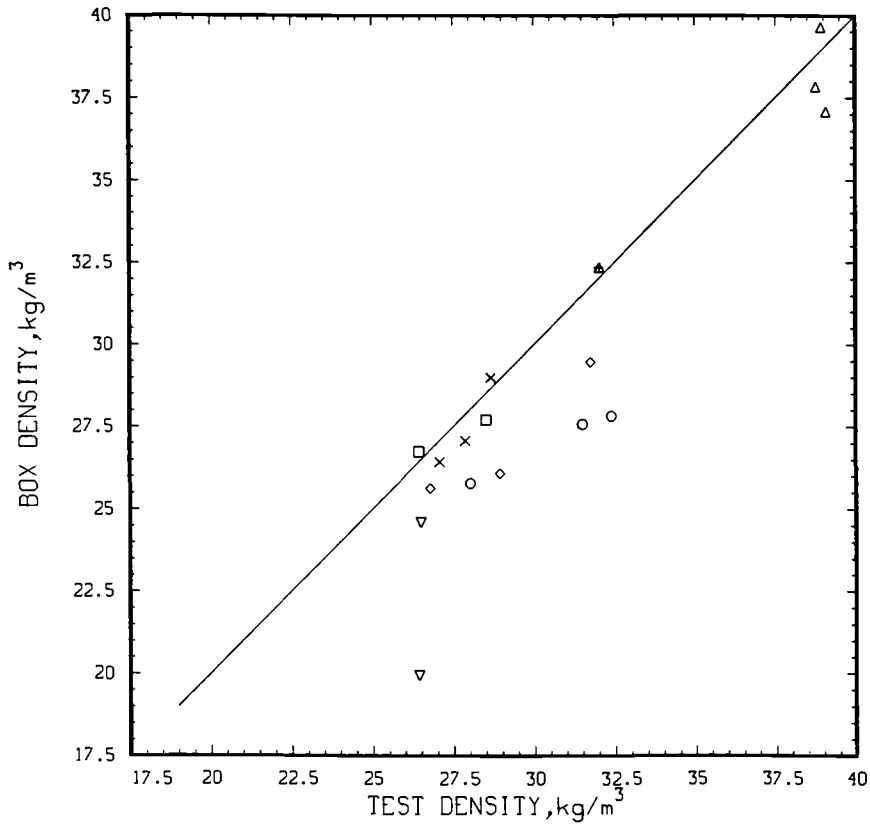


FIG. 12—Box density versus test density for rock/slag wool loose-fill.

four loose-fill materials. Importantly, the wide range of test results makes it difficult for system designers and consumers to make decisions concerning the benefits of loose-fill insulating materials. Therefore we recommend that the ASTM C 687 task group investigate specimen preparation and conditioning procedures that will reduce the imprecision in test results.

Acknowledgments

The authors wish to express their thanks to each of the participants for their concern and diligent efforts that made it possible to present this information. Appreciation is also expressed to those whose efforts were involved in the acquisition and shipment of the sample materials to each participant (G. Andrews of American Fiber Products, J. Hansen of U.S. Gypsum, D. McCaa of CertainTeed, C. Crall of Owens-Corning Fiberglas, and R. Troyer of Manville Service Corporation). The financial assistance of the Department of Energy, Oak Ridge National Laboratory is gratefully acknowledged. And finally, the authors wish to express their thanks to D. McElroy of Oak Ridge National Laboratory for his guidance and encouragement through this endeavor.

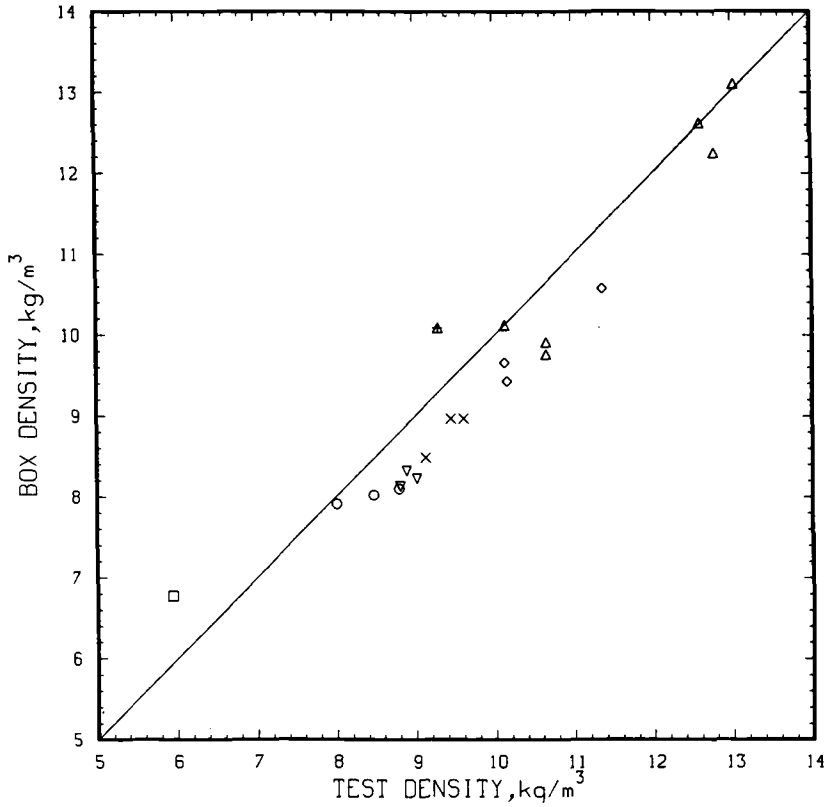


FIG. 13—Box density versus test density for unbonded glass fiber loose-fill.

References

- [1] "Annual Builder Practices Survey," NAHB, private communication.
- [2] Hust, J. G. and Pelanne, C. M., "Round Robins on the Apparent Thermal Conductivity of Low-Density Glass Fiber Insulations Using Guarded Hot Plate and Heat Flow Meter Apparatus," NBSIR 85-3026, 1985.
- [3] Bomberg, M. and Solvason, K. R., "How to Assure Good Thermal Performance of Blown Mineral Fibre Insulation in Horizontal and Vertical Installations," National Research Council Canada, Building Research Note No. 167, Dec. 1980.

APPENDIX A

ASTM C 687 ROUND ROBIN PLAN

The revised ASTM C-687 test method is available in print and a copy of the new standard is attached. The next task for C-687 is to develop a precision and bias statement through a round robin testing program. As the Task Force Chairman for C-687, I have been given the task of organizing the round robin program.

Since the San Diego ASTM meeting, I have had input and inquiries on some aspects of the round robin plan. To insure that the participants understand the testing plan, I have made a few minor revisions to the plan to accommodate these requests although the spirit of the plan remains the same.

In order to successfully use the data from the various laboratories participating in the round robin in an evaluation of C-687, it is imperative that the sample preparation techniques be as uniform as possible. To this end, each of the material suppliers has provided blowing machine settings for the pneumatic preparation of their material for the round robin where specific machine settings are necessary. If any participant is not sure of the procedure, they should contact the supplier for further instructions.

Jerry Hust of NBS has agreed to serve as co-author on the round robin with responsibility for coding the data as received and analyzing the results.

Please return all data sheets to Jerry - not me!

1. Materials

Materials selected must be widely available. Round robin samples will be selected from a single lot (i.e., consecutively produced).

Rockwool - USG Corporation

Cellulose - Fiber Products Corporation

Fiberglass - Bonded wool - OCF Thermacube

- Unbonded wool - Insulsafe III

- 6" R-19 batt from a characterized lot to be used as a reference standard - Manville Service Corp.

Testing Plan

Three samples of each material will be blown to product design density ($\pm 10\%$) and tested at a thickness of 6 inches (± 1 inch).

The data will be reported as listed on the attached data sheet.

Note: All samples must be conditioned for a minimum of 24 hours in laboratory environment prior to testing and estimates of nominal laboratory conditions (temperature and humidity with tolerances) are needed.

3. Test Thickness

In light of the compression issue, the test thickness will be set according to the procedure listed below.

3.1 Blow sample at manufacturer's design density.

3.2 Prepare sample such that a level uniform horizontal surface is established at a thickness between 5.5 and 7 inches (Note: It may be necessary to strike some material off the sample surface to obtain the required thickness).

3.3 Insert sample into test apparatus and bring plate into contact with sample surface.

Record as contact thickness.

Note: Contact thickness is defined as that thickness where there is no light transmission between the sample top surface and the plate of the test apparatus as demonstrated in the C-687 round robin videotape.

3.4 Compress sample such that Test Thickness = $0.9 \times$ Contact Thickness.

3.5 Run thermal test per standard testing procedure.

4. Sample Density

The metered area density must be measured in accordance with C-687 using the cookie cutter technique or an alternate method which conforms to the intent of the method. If an alternate method is used, a detailed description of the technique must be submitted with the test results. In addition, the density based on the entire sample area must be reported on the data sheet as "box density."

5. Coverage Tests (Optional)

For those participants which will be running coverage tests in conjunction with the round robin testing, it is suggested that all tests be run with two bags of material in the blowing machine hopper. Blow material for 10-15 seconds to ensure good machine flow and then begin to fill your coverage test frame.

Since this is not part of C-687, please supply appropriate data sheets describing your facility and procedures.

6. Timing

For those who were unable to attend the ASTM meetings, a videotape is available which demonstrates the sample preparation, contact thickness and cookie cutter density techniques. Please contact me at the number listed below or indicate on the participation form if you would like to borrow a video tape.

A preliminary report on the progress of the testing will be issued at the Fall 1986 meeting and the final draft prepared for the Spring 1987 meeting.

s/t/Ronald Adams

Ronald D. Adams

C 687 Task Force Chairman

614 587-7048

RDA/clm

Attachment

APPENDIX B

BLOWING MACHINE INFORMATION

Lab Code	Machine	Material	Blow Rate	Gear	Gate	Weights	Speed (RPM)
1	Meyers 1103F	Cellulose	NR	3	3-1/2"	16	NR
		Unbonded	NR	4	5-3/4"	3	NR
		Glass Fib. Bonded	NR	4	6"	6	NR
		Glass Fib. Rock/slag Wool	NR	3	3-1/2"	16	NR
2	Universal Volu-Matic E-5	Cellulose	NR	NR	NR	4	1000
		Unbonded	14.9	3	12"	1	1000
		Glass Fib. Bonded	10.7	3	12"	2	1000
		Glass Fib. Rock/Slag Wool	NR	2	7"	2	1000
3	Meyers Model 3000-S	No Information					
4	Meyers Model 1003-E	Cellulose	NR	3	5"	5	NR
		Unbonded	NR	2	5"	3	NR
		Glass Fib. Bonded	NR	4	10"	3	NR
		Glass Fib. Rock/Slag Wool	NR	3	9"	4	NR
5	Unisol Volumatic II 1804-E2MH	Cellulose	NR	3	12"	NR	NR
		Unbonded	NR	3	12"	NR	NR
		Glass Fib. Bonded	NR	3	15"	NR	NR
		Glass Fib. Rock/Slag Wool	NR	1	8"	NR	NR
6	Cyclone Blower	No Information					
7	Star Machine Works-Fiber Star Model 1412	Cellulose	Not Tested				
		Unbonded	12.1	NR	NR	NR	NR
		Glass Fib. Bonded	8.8	NR	NR	NR	NR
		Glass Fib. Rock/Slag Wool	12.8	NR	NR	NR	NR

A Theoretical and Experimental Study of Convective Effects in Loose-Fill Thermal Insulation

REFERENCE: Langlais, C., Arquis, E., and McCaa, D. J., "A Theoretical and Experimental Study of Convective Effects in Loose-Fill Thermal Insulation," *Insulation Materials, Testing, and Applications, ASTM STP 1030*, D. L. McElroy and J. F. Kimpflen, Eds., American Society for Testing and Materials, Philadelphia, 1990, pp. 290-318.

ABSTRACT: Experimental results obtained by guarded hot box testing of low density loose-fill insulations have been analyzed using convective models. Closed and open specimens have been studied in an attic configuration with heat flow up. Experiments were conducted with and without a transverse air flow across the top of the specimens. The occurrence of convective movements inside the insulation was investigated for different applied thermal gradients and air permeabilities of insulation. Comparisons between theoretical and experimental results are presented and discussed.

The study has shown that the boundary conditions at the open top surface of an attic insulation are the driving force in determining thermal performance. Both the model and the experiments have shown that a significant reduction in thermal performance for presently used glass fiber insulations can only occur under severe climatic conditions (i.e., where a temperature difference greater than 40°C will be present).

KEY WORDS: loose-fill insulation, convection, thermal conductivity, attics, model of convection, guarded hot box

Nomenclature

- a Thermal diffusivity
- A Aspect ratio
- B Height ratio
- c Specific heat
- Da Darcy number
- g Gravitational acceleration
- K' Periodicity
- K Permeability
- l Height
- L Length
- Nu Nusselt number
- p Pressure
- Pr Prandtl number
- Ra Rayleigh number
- T Temperature

¹Isover Saint-Gobain, Centre de Recherches Industrielles de Rantigny (CRIR), Rantigny, France.

²LEPT Ensam, Universite de Bordeaux, France.

³CertainTeed Corporation, Blue Bell, PA 19422.

t	Time
u	Horizontal velocity
v	Vertical velocity
V	Velocity vector
x	Horizontal coordinate
z	Vertical coordinate

Greek Symbols

α	Magnitude of top face temperature variations
β	Thermal expansion coefficient
λ	Thermal conductivity
Γ	Conductivity ratio
μ	Dynamic viscosity
ν	Kinematic viscosity
ρ	Density
φ	Heat flux density
ΔT	Temperature difference
χ	Fluid compressibility

Superscripts

-	Dimensionless
*	Quantities relative to porous medium
f	Quantities relative to fluid
—	Averaged values

Subscripts

c	Cold
eff	Effective
H	Hot
i	Interface
max	Maximum

Introduction

The introduction of new low-density permeable insulation materials in attics, with an open top surface, has raised questions about their thermal performance. This study addresses two questions related to convective effects:

1. When is it possible to have convection occur within the insulation?
2. Under what external conditions is it possible for air movements, above the top surface of the insulation, to penetrate into the insulation?

If either (1) or (2) occurs, the consequence is a reduction of the effective thermal resistance of the insulation.

The aim of the present study was to give some answers to the above questions by studying the general problem of convection in porous media. To achieve this goal, experiments were carried out while evaluating various theoretical models. Rather than start with a full-scale attic test, which is both difficult to realize and expensive to run, simpler geometries were studied using two different types of guarded hot boxes. Following a brief description of these geometries and

apparatus, the two main sections of this paper present theoretical and experimental results on the convective effects in closed (impermeable boundaries) porous media and open (permeable boundaries) porous media submitted to different boundary conditions. Finally, based on the relatively good agreement between behavior predicted by the models and behavior observed in the experiments, a theoretical approach for a model of a real attic configuration is discussed. Derivations of the main equations for this model are given in the Appendix.

Experimental Geometries

As mentioned in the Introduction, tests were run in configurations simpler than that of a full-scale attic. The tested geometries are shown in Figs. 1 and 2. As can be seen, we made measurements both on "closed" (Fig. 1) and "open" specimens (Fig. 2). In all cases, the bottom of the specimen was an impermeable layer and the heat flow was up. In closed configurations, the top of the sample was sealed with a polyethylene sheet. This top surface could then be:

- In contact with an impermeable "plate" (Fig. 1a).
- In contact with an "infinite" air space (attic) in natural or forced convection (Fig. 1b).
- In contact with a "finite" air layer in natural convection (Fig. 1c).

Open configurations involved similar geometries but with unsealed top surfaces.

All specimens were glass fiber products, either blankets or loose-fill. Their characteristics are given in Table 1.

Description of Apparatus

Guarded Hot Box

The guarded hot box, built by CertainTeed Corporation in the Levecque Technical Center, was used in a horizontal configuration with the metering box located below the specimen, with heat flow up. The specimen box, 1.21 by 1.21 by 0.254 m, was placed in a support frame 0.165

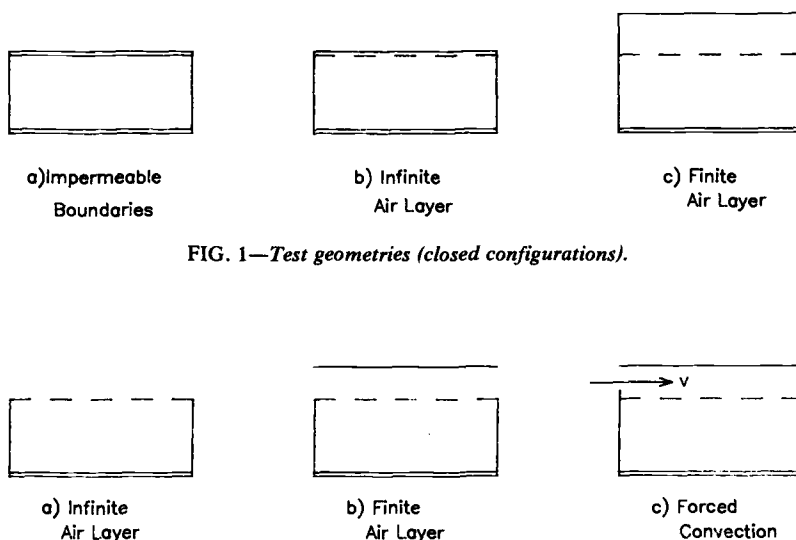


FIG. 1—Test geometries (closed configurations).

FIG. 2—Test geometries (open configurations).

TABLE 1—Physical properties of specimens.^a

• Apparatus 2 - Blanket: "Experimental Blanket"	
K^*	$= 5 \times 10^{-8} \text{ m}^2$
λ^*	$= 0.070 \text{ to } 0.080 \text{ W/m} \cdot \text{K at } 23^\circ\text{C}$
ℓ^*	$= 0.340 \text{ m}$
ρ^*	$= 6 \text{ to } 9 \text{ kg/m}^3$
• Apparatus 1 - Loose Fill: "Unbonded Fiberglass Insulation"	
K^*	$= 5 \times 10^{-8} \text{ m}^2$
λ^*	$= 0.060 \text{ to } 0.075 \text{ W/m} \cdot \text{K at } 23^\circ\text{C}$
ℓ^*	$= 0.254 \text{ or } 0.178 \text{ m}$
ρ^*	$= 6 \text{ to } 8 \text{ kg/m}^3$
• Apparatus 2 - Loose Fill: "Unbonded Fiberglass Insulation"	
K^*	$= 1.47 \times 10^{-8} \text{ m}^2$
λ^*	$= 0.0516 \text{ W/m} \cdot \text{K at } 23^\circ\text{C}$
ℓ^*	$= 0.310 \text{ m}$

^a K^* measured per ASTM C 522.

λ^* measured per ASTM C 236.

ℓ^* measured per ASTM C 167.

m thick which is filled with polystyrene foam that fills the entire 3 by 3 m area of the box. In the following sections this will be known as Apparatus 1.

On the upper side of the specimens, cooling was achieved by allowing liquid nitrogen to evaporate into the cold box with the flow of LN_2 controlled with a temperature controller and a solenoid in the LN_2 line. In addition, on the cold box side, an air diffuser was constructed which allowed the cold air (N_2) to be blown across the specimen for the forced convection studies.

The entire box is instrumented in accordance with ASTM Test for Steady-State Thermal Performance of Building Assemblies by Means of a Guarded Hot Box (C 236) using Type T thermocouples and d-c voltages to the fans and heaters. In operation a HP 9816 computer interfaces with a Fluke 2240 data logger to compute average temperatures and power levels which are then used to control the metering box and guard box heaters.

Horizontal Hot Box

The apparatus utilized for the studies at C.R.I.R. is a hybrid, using a bi-guarded hot plate as part of a guarded hot box (Fig. 3). In this case, the existing cooling system from the cold box was used but, instead of a metering box, the power to the single-sided hot plate was monitored and used to control the hot surface temperatures.

The box is 2.80 by 2.40 by 2.40 m, and the sample box formed by a polystyrene foam frame and the hot plate is 1.80 by 1.80 by 0.450 m. The hot plate itself measures 2.0 by 2.0 m with a metering area of 1.0 by 1.0 m. The metering area and the guard area of the hot plate are controlled separately, as is a bucking heater located below the main hot plate, which is used to ensure one-dimensional heat flow.

A plate (black aluminum sheet) can be installed above the test sample to create a finite air layer (Fig. 3a) or removed (Fig. 3b: infinite air space configuration). In both cases, the air above the specimen can be put in forced convection when desired (circulation fan on). Temperatures in the cold air, hot plate, and sample are measured with Type K thermocouples (total of 71). Power to the metering area is monitored, and all data are collected on a HP 3497A data logger and analyzed by a HP 85 computer. Temperatures are controlled by individual thermal controllers. In the following sections this will be referred to as Apparatus 2.

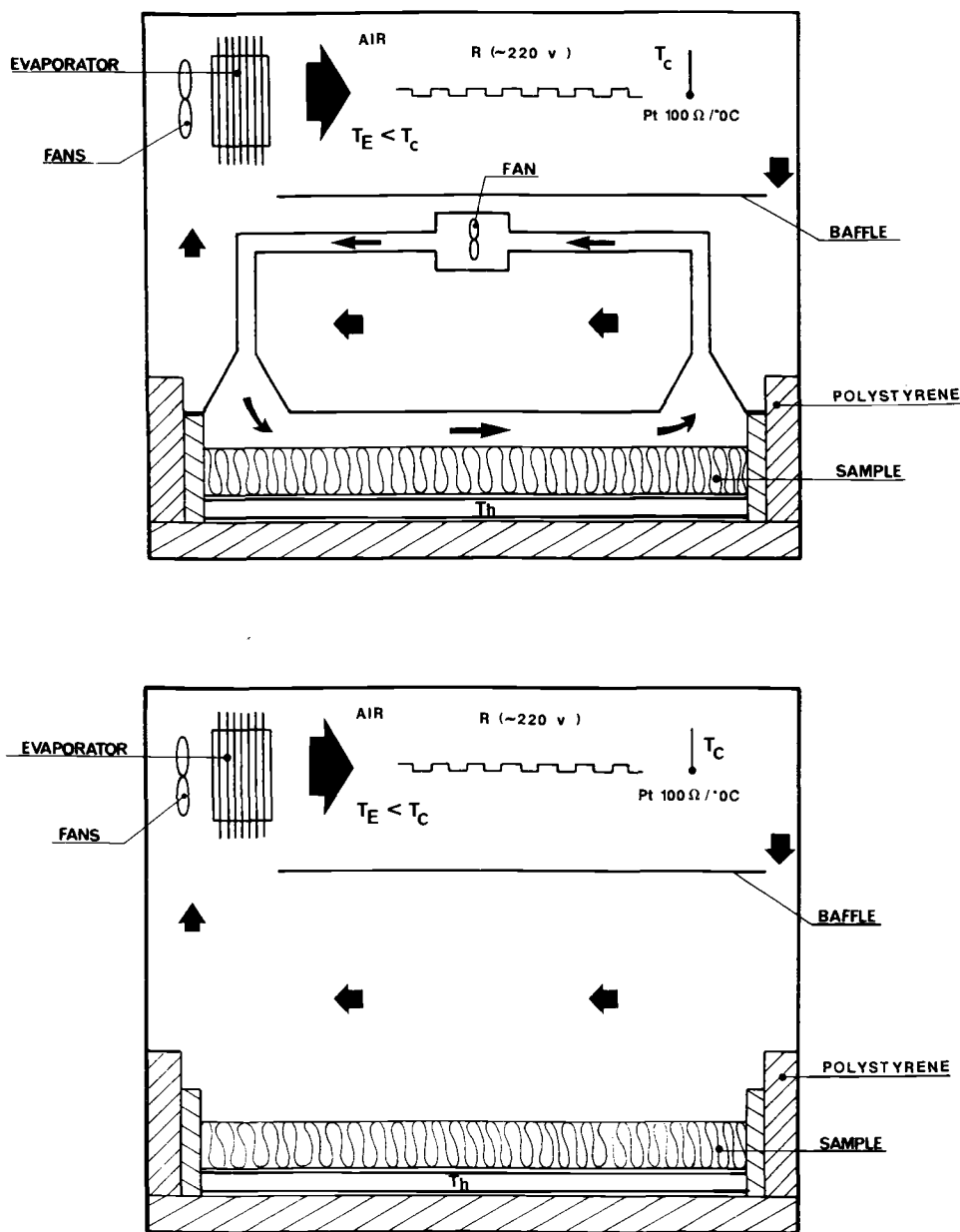


FIG. 3—Schematic of CRIR apparatus. (a) Finite air layer configuration. (b) Infinite air layer configuration.

Both of these apparatus have been tested previously, using homogeneous blanket materials, and have shown an accuracy of $\pm 3\%$ when compared to guarded hot plate results on the same specimens.

Closed Configuration

Previous Studies

The case of a horizontal porous medium (isotropic and finite) bounded by two impermeable, isothermal plates has been studied extensively [1-3]. It is well established that air convection within the medium can only occur if the bottom surface is the hot plate and heat flow is upward. In this case, the onset of natural convection cannot occur until a critical value of the porous Rayleigh number, Ra_c^* , is exceeded. As shown in Fig. 4, there is an abrupt change in Nusselt number (i.e., in apparent thermal conductivity) when $Ra^* > Ra_c^* = 4\pi^2$. For porous media exhibiting a marked anisotropy—both in thermal conductivity and permeability—(such as typical fibrous insulations) this critical Rayleigh number is still valid, provided that the definition of Ra^* is modified to take care of this anisotropy [4].

In addition, the $4\pi^2$ limit has been verified experimentally by several authors [5,6] by running tests in guarded hot plates in which the specimens were placed between two impermeable, isothermal plates (Fig. 1a).

Present Investigations

In order to relate the current studies to the real attic, it is necessary to investigate the applicability of the critical Rayleigh number ($4\pi^2$) to the case where the top surface, while still sealed, is no longer in contact with an isothermal plate but is in contact with a fluid layer considered "finite" (Fig. 1c) or "infinite" (Fig. 1b). The approach consisted of deriving a theoretical criti-

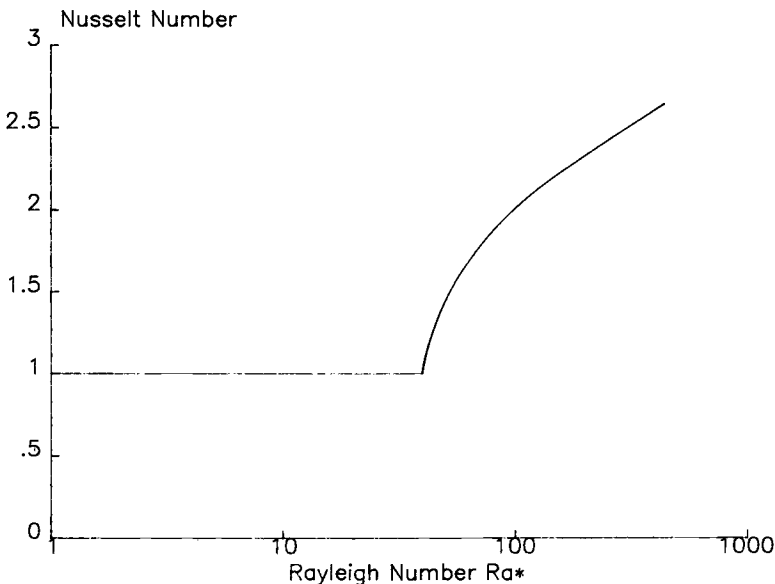


FIG. 4—Nusselt number versus Rayleigh number showing onset of convection at $Ra^* = 4\pi^2$ for closed configurations.

cal Rayleigh number for each configuration and then checking the model with several experiments.

Model—The system of equations to be solved for the model of the “finite fluid layer – porous medium” configuration (Fig. 1b) is given in the Appendix. The driving adimensional numbers affecting the solution are (see definitions in Appendix): the global Rayleigh number (Ra), the Darcy number (Da), the aspect ratios (A, B), and the global Nusselt number (Nu).

The theoretical curve $Nu = f(Ra)$ derived from stability analysis is plotted in Fig. 5 for fixed aspect ratios ($A = 2; B = 0.5$) and several porous medium permeabilities (or Darcy numbers). This plot shows several points of inflexion (B_i) for specific values of global Rayleigh numbers (Ra_i). The first point (B_0) corresponds to the onset of convection in the fluid layer itself ($Nu > 1$). It is of interest to convert the corresponding global critical Rayleigh number, Ra_0 , into a fluid critical Rayleigh number Ra_f (as defined in the Appendix). A value equal to 1650 is obtained in good agreement with the theoretical value of 1708 established for the onset of convection in a pure fluid layer confined between two impermeable and isothermal planes [7].

The next point of inflexion (B_1) corresponds to the onset of significant convection inside the porous medium itself. For increasing Rayleigh numbers, there exist several $Nu = f(Ra)$ curves depending on the Darcy numbers, Da_i . The curves are identical for Da_i and Da_{i+1} ($Da_{i+1} < Da_i$) as long as $Ra < Ra_i$ but differ once convection is started.

In this case it is interesting to convert the global critical Ra_i into critical porous media Rayleigh numbers, Ra_i^* , where (see the Appendix for notations):

$$Ra_i^* = Ra_i \times Da_i \times \frac{\ell^*}{\ell} \times \frac{\Delta T^*}{\Delta T} \quad (1)$$

To make this conversion, one needs to compute ΔT^* and therefore to evaluate the temperature, T_i , at the interface of the fluid with the porous medium. This temperature is a function of the convective movements within the fluid layer and non-uniform. Consequently, it is difficult (both experimentally and theoretically) to define a mean interface temperature. The problem is even more difficult for a loose-fill type insulation with a poorly defined top surface causing additional

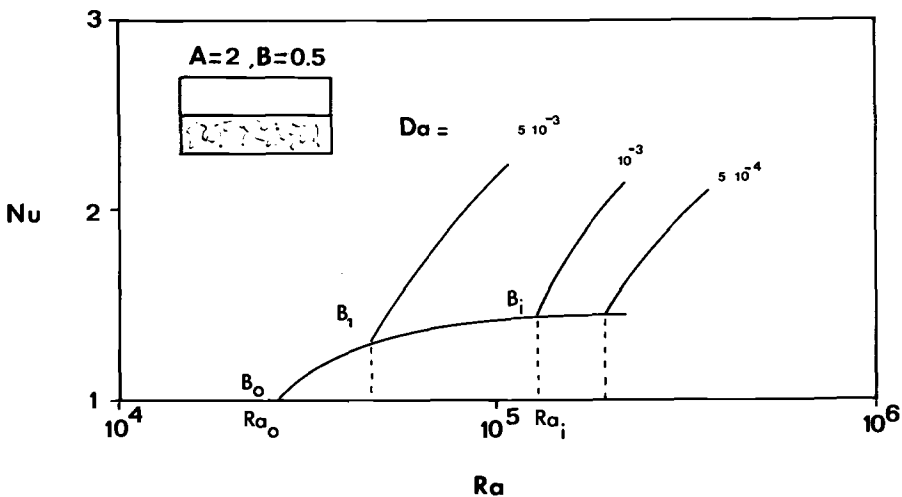


FIG. 5—Nusselt number versus Rayleigh number as a function of Darcy number, for a sealed specimen.

uncertainties (in both ℓ^* and T_i). This being said, it is theoretically possible, using the numerical data giving the distribution of temperatures at the interface and defining

$$T_i = \frac{1}{A} \int_0^A \bar{T}(\bar{x}, \bar{z} = 0.5) d\bar{x}, \quad (2)$$

to compute the following Rayleigh numbers:

Ra_i^*	Da_i
≈ 70	5×10^{-3}
≈ 50	1×10^{-3}
≈ 40	5×10^{-4}
≈ 40	5×10^{-4}

For all commercialized glass fiber products, the value of Darcy's number is always well below 10^{-5} . Therefore from the above table one sees that the critical value of $4\pi^2$ still holds in this case. However, this global approach (fluid layer, porous medium) remains rather approximate in the derivation of a critical porous Rayleigh number because of the uncertainty on the "mean" interface temperature previously mentioned.

To avoid this problem, it was of interest to model the closed porous medium alone, with the following temperature boundary conditions: (1) isothermal hot face, and (2) cold face temperature distribution such as

$$T_c = \bar{T}_c + \alpha \cos(K' \pi \chi / L) \quad (3)$$

in order to represent the effects of movements in the fluid layer above (finite or infinite).

With these boundary conditions, stability analysis allows one to plot the graph of $Nu^* = f(Ra^*)$, where the "mean" porous Rayleigh number is by convention defined as

$$\overline{Ra^*} = \frac{g\beta\Delta T\ell^*K^*}{\nu a^*f} \quad (4)$$

This plot is shown in Fig. 6 for a given aspect ratio ($A^* = 4$) and a fixed cold temperature amplitude ($\alpha = 0.2T_c$). The results are a function of the spatial periodicity, K' .

The dotted line in Fig. 6 represents the case $\alpha = 0$ (isothermal cold face) where of course one finds again a critical Rayleigh value of $4\pi^2$. In all other cases, one can see that the Nusselt number is never exactly equal to 1; convection starts as soon as $Ra^* > 0$ because of the horizontal temperature gradients induced by the non-isothermal cold face. However, this Nusselt increase is almost negligible up to a critical Ra^* depending on the K' value. The larger the variations of T_c (i.e., the smaller the K' value), the sooner the onset of convection.

The example illustrated here corresponds to an extreme case; in practice the fluid convective movements will tend to make the cold face temperature uniform. This is why, in the "global approach," the presence of significant convective movements within the porous medium were observed for a critical Rayleigh number close to 40. However, Fig. 6 is interesting because it shows the great influence of thermal boundary conditions which must be kept in mind when analyzing experimental results.

Experimental Results—Two types of specimens have been tested in the closed configuration. Their physical properties are given in Table 1.

The blanket material was especially fiberized for this study in order to achieve high permeability values favorable to convection. It was tested in Apparatus 2 with either a "finite" (Fig.

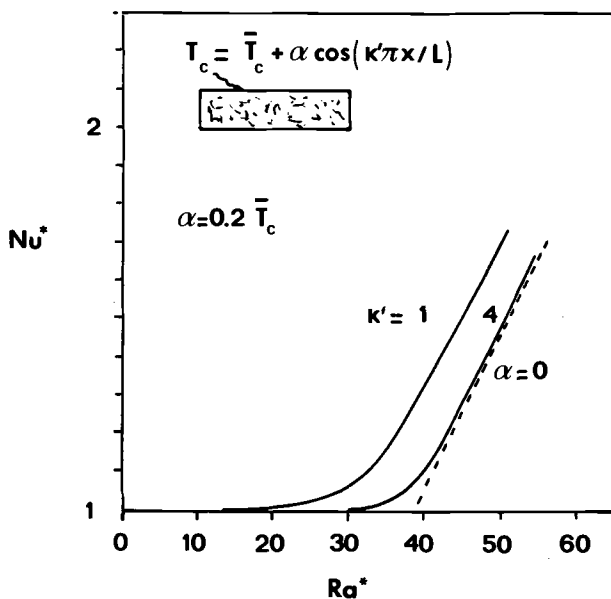


FIG. 6—Nusselt number as a function of Rayleigh number for a fixed aspect ratio and fixed $\alpha = 0.2 \bar{T}_c$, showing effect of cell size.

1c) or “infinite” (Fig. 1b) air layer above the specimen. The loose-fill insulation was tested in Apparatus 1 in the same configuration (Fig. 1b).

In all cases, the measured variables were power, temperature, specimen density and thickness, and temperature profiles in the test areas. From these hot box variables and sample properties, the apparent thermal conductivity and the porous Rayleigh numbers were calculated. It must be stated here that while all models used in this study neglected radiation, any radiative effects were included in the experimentally determined apparent λ -value.

Figure 7 plots the Nusselt number versus Ra^* for the loose-fill samples tested in Apparatus 1, while Fig. 8 shows the same plot for the blanket material tested in Apparatus 2. The data for these experiments are given in Table 2.

The foregoing theoretical analysis has shown that the interpretation of these experimental curves requires knowledge of the thermal boundary conditions. In the case of Apparatus 1, the expansion of liquid nitrogen into the cold box gives a relatively isothermal air layer. In Apparatus 2, tests were run under two different boundary conditions with either a forced air circulation above the sealed specimen (i.e., with the circulation fan of Fig. 3 on) or with no forced air circulation (fan off). The corresponding results are labelled respectively “forced convection” and “natural convection.” For Apparatus 1 and for Apparatus 2 in forced convection, one can consider that, more or less, isothermal boundary conditions existed. Experimental results indeed indicate that the Nusselt number increases above 1.0 only when the Rayleigh number exceeds the critical value of $Ra^* = 40$. In “natural convection,” one can assume that the temperature uniformity of the cold face was not as good, which explains the lower experimental critical Ra^* ($Ra_c^* \approx 32$).

These results clearly illustrate the difficulties inherent to this type of measurement that may lead to incorrect interpretation of experimental data. The same is true for the temperature profiles measured within the porous medium, once convection has started. Depending on the position of the thermocouples, the vertical profiles may be linear or observed with different curvatures (Fig. 9).

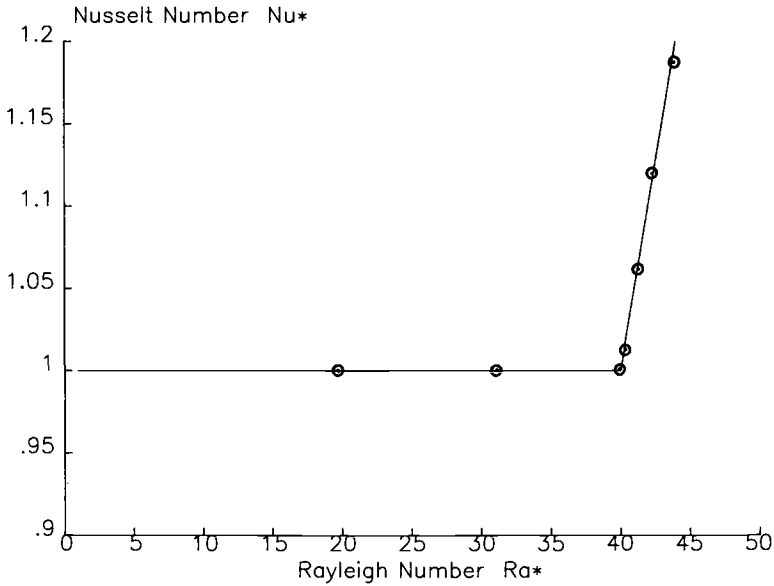


FIG. 7—Results from CertainTeed tests showing Nusselt number versus Rayleigh number for a sealed loose fill specimen with an infinite air layer.

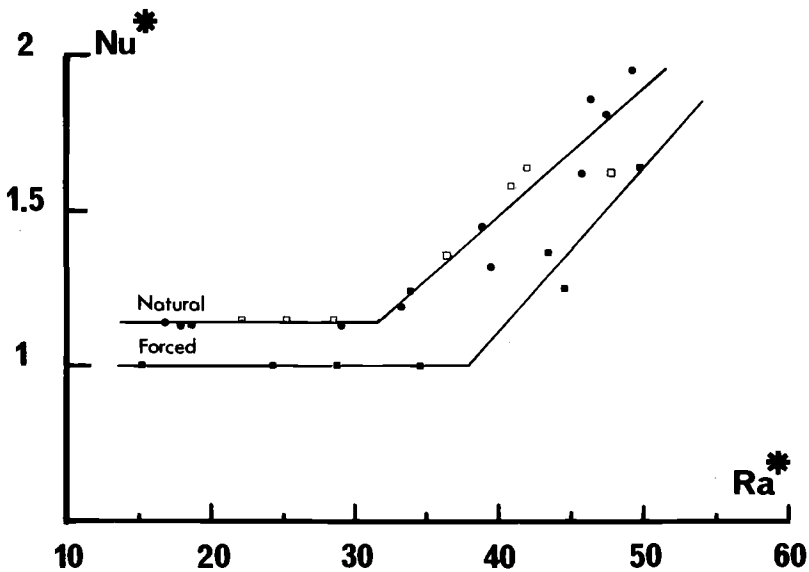


FIG. 8—Results from CRIR tests on blanket material in a closed configuration for forced and natural convection (\square , \blacksquare = infinite air layer, \bullet = finite air layer).

TABLE 2—Sealed specimen data.

T_{Hot} (°C)	T_{Cold} (°C)	ΔX (m)	λ (W/m · K)	$T\text{-Mean}$ (°C)	ΔT (°C)	Ra^*	Nu^*
9.90	-23.10	0.254	0.04096	-6.60	33	42.3	1.16
14.58	-22.42	0.254	0.04443	-3.92	37	42.0	1.09
19.14	-21.62	0.254	0.04759	-1.10	41	41.5	1.05
24.13	-20.63	0.254	0.05120	+1.67	45	40.6	1.02
29.44	-20.56	0.254	0.05481	+4.44	50	40.3	1.00
24.9	-3.1	0.340	0.0600	10.9	28.0	25.4	1.15
19.2	0.9	0.340	0.0855	10.1	18.3	16.8	1.14
30.3	-7.4	0.340	0.0924	11.5	37.7	33.9	1.24
32.6	-10.4	0.340	0.1087	11.1	43.0	38.9	1.45
32.1	-16.7	0.340	0.1391	7.7	48.8	46.4	1.86
36.3	-17.0	0.340	0.1455	9.7	53.3	49.2	1.95
22.7	-1.7	0.340	0.0857	10.5	24.4	22.3	1.15
25.6	-5.5	0.340	0.0856	10.1	31.1	28.6	1.15
28.7	-7.7	0.340	0.0888	10.5	36.4	33.2	1.19
31.6	-11.4	0.340	0.0983	10.1	43.0	39.5	1.32
35.4	-14.7	0.340	0.1213	10.4	50.1	95.8	1.62
38.3	-14.8	0.340	0.1354	11.8	53.1	47.5	1.81
18.7	-1.7	0.340	0.0845	8.8	19.9	18.6	1.13
18.7	-0.5	0.340	0.0897	9.1	19.2	17.9	1.13
23.6	-7.2	0.340	0.0845	8.2	30.8	29.1	1.13
28.7	-10.5	0.340	0.1013	9.1	39.2	36.5	1.36
33.7	-12.5	0.340	0.1226	10.6	46.2	42.1	1.64
31.7	-12.6	0.340	0.1183	9.6	44.3	41.0	1.58
31.5	-18.2	0.340	0.1209	6.6	49.5	47.9	1.48

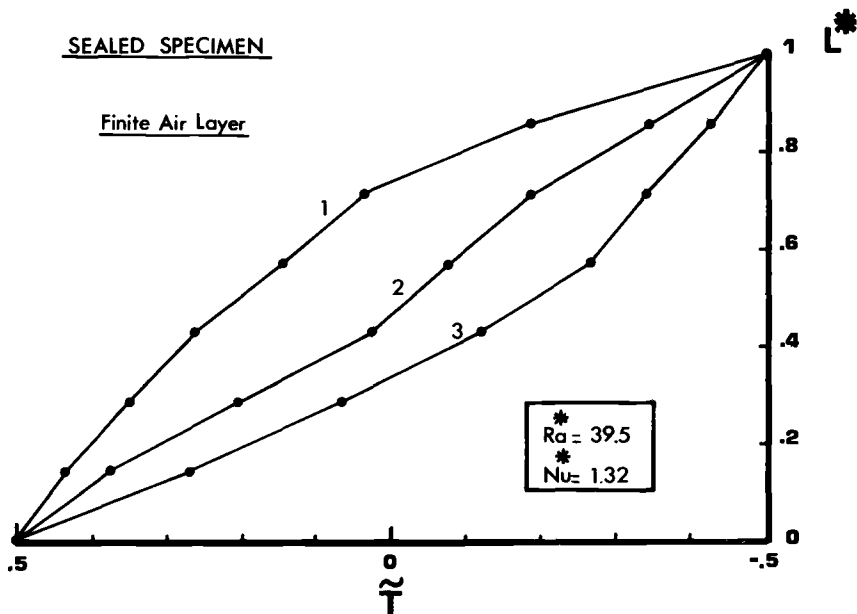


FIG. 9—Vertical temperature profiles at three locations in a sealed specimen. (1) Upper left corner. (2) Center. (3) Lower right corner.

The observed profiles can be a function of the location of the convective cells. A linear profile is not necessarily proof of the absence of convection.

Open Configuration

Previous Studies

A horizontal porous medium with an impermeable isothermal hot bottom face and a permeable isothermal cold top face has also been investigated [3,4]. In this case, stability analysis requires the knowledge of boundary conditions at the free surface. For the sake of simplicity, it is common to assume uniform temperature and pressure on this face or, in other words, to consider that the fluid above the porous medium is rigorously isothermal and still. This assumption is clearly unrealistic in practice and almost impossible to achieve experimentally, but it allows a simple numerical treatment of the governing equations. Stability analysis computations for these ideal boundary conditions give a critical porous Rayleigh number of 27.1 for the onset of convection. This value is valid for homogeneous isotropic media, but computations have also been extended to anisotropic cases [4].

This analysis, although interesting in principle, is not representative of real conditions of use. Taking the particular case of permeable insulation in an attic, the occurrence of convective movements within the attic air cannot be avoided. If one can reasonably assume that the condition of temperature uniformity still holds, the assumption of constant pressure is no longer valid, since the air convective cells will create a non-uniform pressure field on top of the porous medium. This reasoning led to the development of other models capable of taking into account more realistic boundary conditions.

Present Work

Consider two different configurations: (1) the effect of *natural* convective air movements on top of a permeable porous medium, and (2) the case of a *forced* air flow, parallel to the free surface of the medium. In both cases, theoretical and experimental results will be presented.

Natural Convection—As was done for the “closed porous medium” case, first consider the “finite fluid layer – porous medium” configuration, but this time with an open top surface (Fig. 2b). The permeable interface makes the writing of hydrodynamic boundary conditions difficult. It has been shown that in this case Brinkman’s formulation [8] is to be preferred to the classic Darcy model. The two models are recalled in the Appendix. The driving adimensional numbers affecting the solution are as given previously.

The theoretical curve $Nu = f(Ra)$ for given aspect ratio and different Da is plotted in Fig. 10. These results can be analyzed as previously done for Fig. 5. In particular, the conversion of the global critical Rayleigh numbers into critical porous media Rayleigh numbers gives values of Ra^* approximately equal to 30, for all Darcy numbers (rigorously lower than 10^{-4}) to be compared to 40 for the closed system. However, above this limit of 30, the model is not able to quantify how much of the increase in heat transfer is due to fluid penetration within the porous medium. Furthermore, the ranges of Darcy and of global Rayleigh numbers that can reasonably be treated numerically here are far from realistic values ($Ra \approx 10^8$ and $Da < 10^{-5}$). This led to work on another physical approach to the problem.

Second Model—Instead of a global approach (fluid and porous medium) consider here the porous medium alone, as the control volume of the model. The problem is then to derive realistic boundary conditions on the top permeable surface. In order to do so, consider the natural convective movements that develop within a horizontal fluid layer bounded by two impermeable and isothermal planes. It is known that these movements will induce a pressure field on both horizontal planes; a typical pressure distribution on the bottom plane is shown in Fig. 11. The amplitude of pressure variations depends on the magnitude of convective movements, while

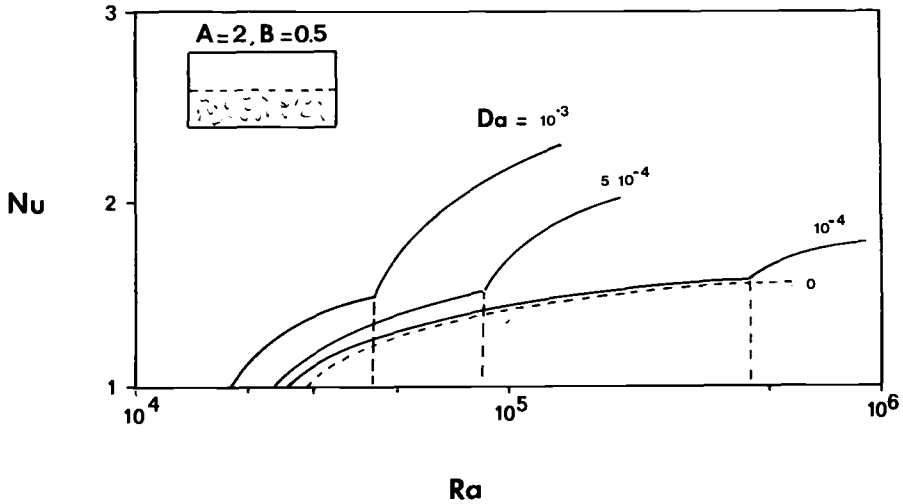


FIG. 10—Nusselt number versus Rayleigh number as a function of Darcy number for a finite air layer configuration.

their periodicity is a function of the observed “cellularization.” To a first approximation, one can therefore write

$$P = P_{\max} \cos(K' \pi x / L) \quad (5)$$

where K' is related to the width, L_c , of the convective cells ($K' = L/L_c$).

On the other hand, it is possible to derive a relationship between the maximum adimensional vertical velocity, \tilde{V}_z , and the fluid layer Rayleigh number, Ra_f . For the range of investigated Rayleigh numbers, computations gave

$$\tilde{V}_z = \alpha Ra_f^\beta = 0.06 Ra_f^{0.68} \quad (6)$$

This velocity can in turn be used for an estimation of the corresponding maximum pressure. If one makes the assumption of a perfect fluid (viscosity effects negligible relative to inertia), one can apply Bernouilli's theorem and write

$$\overline{P}_{\max} = \frac{1}{2} \rho V_{\max}^2 \quad (7)$$

Equations 5, 6, and 7 define a complete knowledge of the boundary conditions, and one can now solve the momentum and energy equations (see the Appendix).

The curves $Nu^* = f(K')$ for given values of \overline{P}_{\max} and Ra^* (and a fixed aspect ratio $A = 4$) are plotted in Fig. 12. One can see that Nu^* increases as the cell dimensions decrease (large K' values), the velocity of the air flowing through the porous medium being lower for a single convective cell than for several.

A maximum is observed for $K' = 3$ where $L_c A / K' = 1.33$; this value is almost equal to the cell dimensions observed within the porous medium after the critical value of $Ra^* = 27.1$. In other words, the external flow reinforces the natural movements if the convective modes are in phase. Inversely, the external flow may slow the development of internal convective movements. In this case, the Nusselt number may be larger when \overline{P}_{\max} is equal to 0 (i.e., no air flow) than

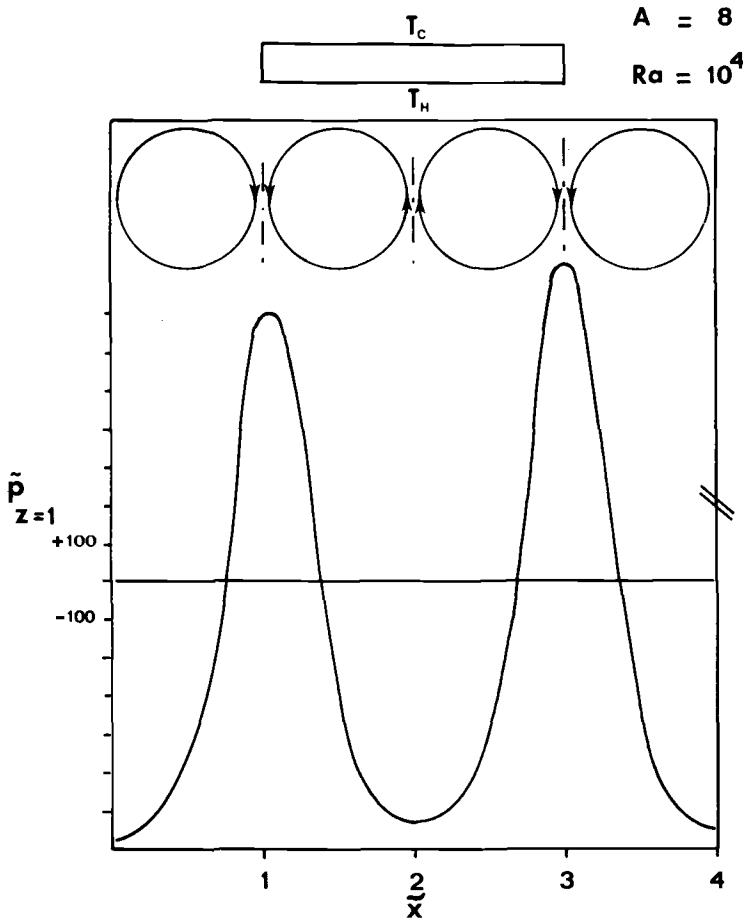


FIG. 11—Pressure distribution on the bottom plane of a porous specimen.

with air flow above. Figures 13a and 13b give the variations of Nu^* as a function of Ra^* for two different values of K' and several maximal pressures.

For $\overline{P}_{\max} = 0$, one logically finds again the critical Ra^* of 27.1, while for low values of $\overline{P}_{\max} < 0.1$ the Nusselt number becomes larger than 1 before 27.1. For large Ra^* , the curves $\overline{P}_{\max} = 0.1$ and $\overline{P}_{\max} = 0$ are close to each other as the external flow effect becomes negligible compared to the internal convective movements.

Open Specimen Experiments (Natural Convection)—Here only loose-fill samples were studied in both apparatuses. The infinite air layer configuration (Fig. 2a) was studied in Apparatus 1; the finite configuration (Fig. 2b) was studied in Apparatus 2. As was the case for the closed specimen configuration, but to a greater extent here, the theoretical analysis has shown evidence of the influence of the experimental boundary conditions, which makes the comparison between measurements and theory more difficult.

Infinite air layer (Apparatus 1)—As stated previously, the liquid nitrogen expansion within Apparatus 1 gives a rather isothermal air layer, leading to a configuration very close to the “ideal boundary conditions” of a still air layer above the product. Corresponding thermal data (Table 3) and plots of Nusselt number versus Rayleigh number (Fig. 14) indicate that the Nus-

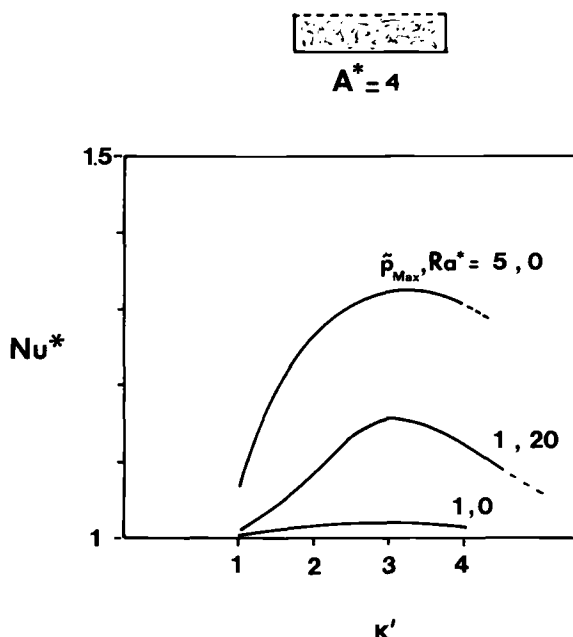


FIG. 12—Nusselt number as a function of periodicity for fixed values of P_{\max} and Rayleigh number.

selt number exceeds 1.0 only when $Ra^* > 30$; this is in good agreement with the theoretical critical value of 27.1.

Finite air layer (Apparatus 2)—Experiments have been conducted in the configuration shown in Fig. 2b for a constant mean temperature ($T = 10^\circ\text{C}$) for increasing differences of temperatures across the whole system. In order to compare the experimental results with the model, one needs to evaluate the pressure distribution in the fluid layer, maximum pressure (P_{\max}), and periodicity (K'), such as defined in Eq 5, which were not measured.

Even so, a direct comparison with Fig. 13a or 13b is not possible because P_{\max} varies with the applied temperature difference (i.e., one is not on a constant P_{\max} curve). One can, however, use the same approach and make computations for the experimental boundary conditions of each data point.

The temperature measurements of the hot and cold boundaries and of the fluid sample interface (average of 21 thermocouples) do make it possible to compute the effective Rayleigh numbers of the fluid layer (Appendix Eq A15) and of the porous medium (Appendix Eq A16). Using as a first approximation the correlation derived for a fluid flowing between two impermeable isothermal plates (Eq 6), one can derive from Ra_{eff}^f the maximum vertical velocity and finally estimate the corresponding maximum pressure (Eq 7). This pressure can be expressed adimensionally as (Appendix Eq A20)

$$\overline{P}_{\max}^* = \frac{K^*}{L_F^2} \cdot \Gamma \cdot \frac{(0.06 Ra_{\text{eff}}^f)^{0.68}}{2Pr} \quad (8)$$

The periodicity, K' , cannot be computed from our experimental data. However, one can draw different theoretical curves for various K' values and compare then with the measurement points. One can see in Fig. 15 that this gives a K' value lying between 4 and 5. This value, corresponding to a convective cell dimension equal to about the height of the porous medium, seems realistic.

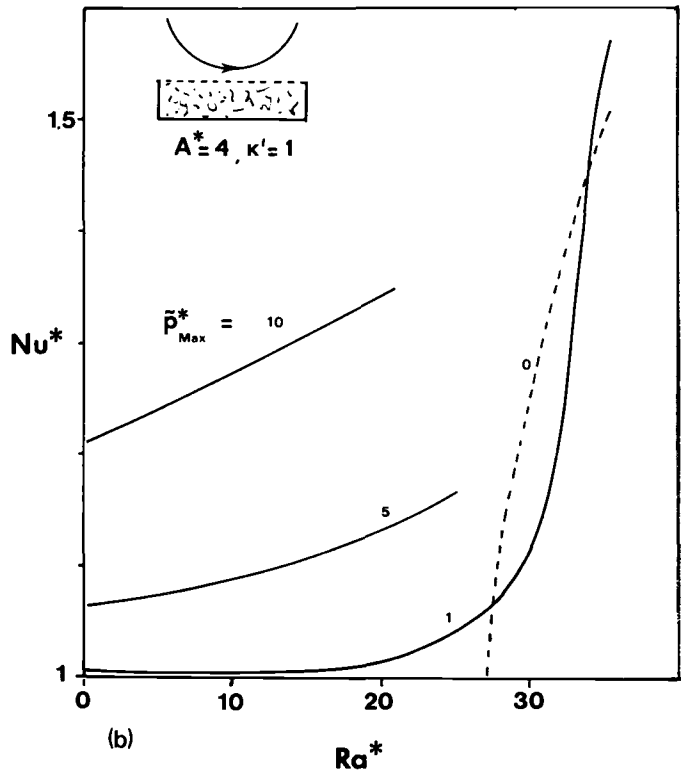
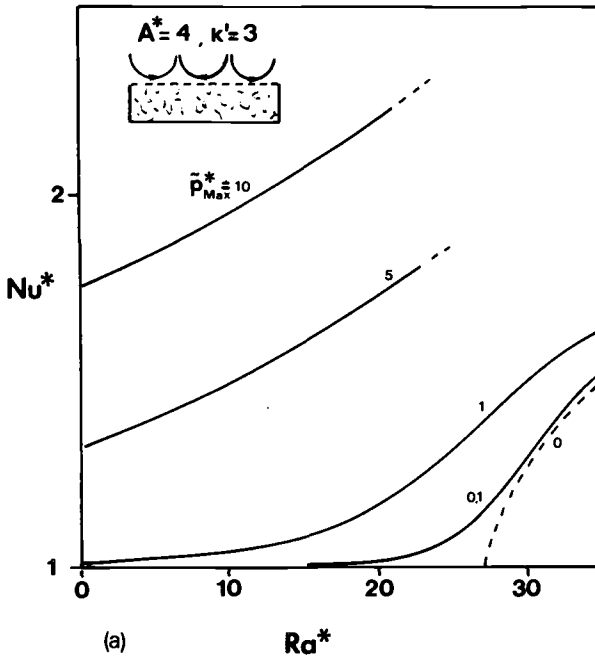


FIG. 13—Nusselt number as a function of Rayleigh number for various P_{max} . (a) For $K' = 3$. (b) For $K' = 1$.

TABLE 3—Open specimen data.

T_{Hot} (°C)	T_{Cold} (°C)	ΔX (m)	λ (W/m · K)	$T\text{-Mean}$ (°C)	ΔT (°C)	Ra^*	Nu^*
18.44	-30.66	0.254	0.04123	-6.11	49.1	62.1	1.15
19.10	-26.90	0.254	0.04442	-3.90	46.0	52.3	1.10
23.90	-21.40	0.254	0.04759	-1.10	45.0	44.5	1.07
24.67	-19.33	0.254	0.05120	1.67	42.0	39.3	1.03
24.44	-15.56	0.254	0.05481	4.44	40.0	32.5	1.01
26.22	-11.78	0.254	0.05848	7.22	38.0	27.8	1.00
20.8	-0.3	0.310	0.0516	10.3	21.1	6.9	1.00
23.3	-2.6	0.310	0.0516	10.4	25.9	8.5	1.00
25.8	-5.7	0.310	0.0516	10.1	31.5	10.4	1.00
26.8	-6.5	0.310	0.0516	10.2	33.3	11.0	1.00
29.8	-9.6	0.310	0.0524	10.1	39.9	13.0	1.01
31.4	-11.2	0.310	0.0528	10.1	42.6	24.0	1.02
34.8	-14.4	0.310	0.0546	10.2	49.2	16.2	1.06
36.8	-15.8	0.310	0.0558	10.5	52.6	17.2	1.08
38.9	-18.7	0.310	0.0588	10.1	57.6	19.0	1.14
41.4	-20.5	0.310	0.0617	10.5	61.9	20.3	1.20

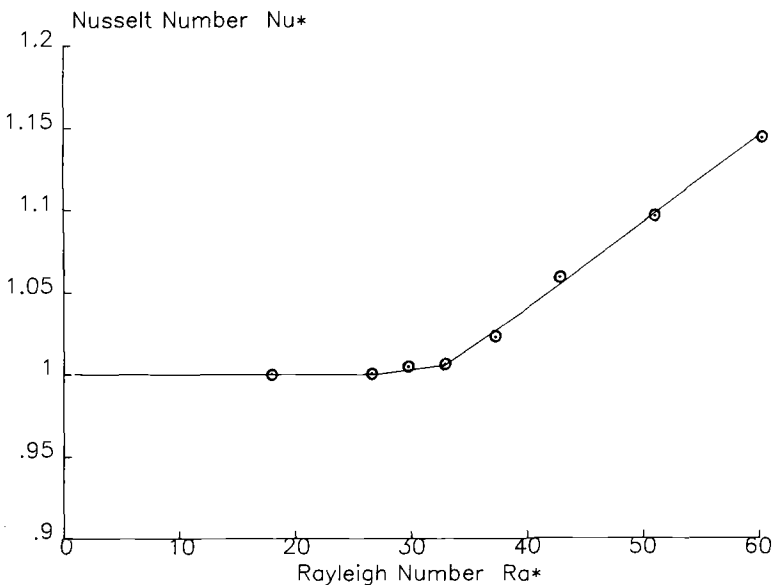


FIG. 14—Experimental results of Nusselt number versus Rayleigh number for an infinite air layer in CertainTeed hot box.

Considering the successive assumptions that were made, a perfect agreement between theory and experience is not possible. However, the comparative results shown in Fig. 15 can be considered as satisfactory. Another interesting comparison between theory and measurement can be made for the temperature profiles. Figure 16 gives, for a given Ra_{eff}^* , three vertical profiles computed at three different locations (a , b , and c) and compares them to measurements made in Position c . Once again the agreement is satisfactory. As in the closed configuration the shape

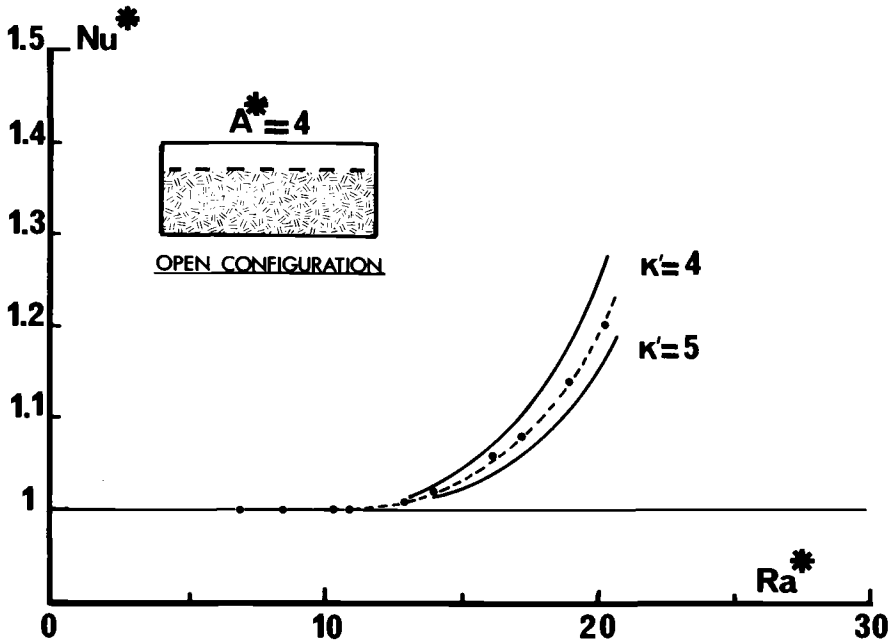


FIG. 15—Experimental data from CRIR apparatus used to estimate periodicity for an open configuration.

of the profile is a function of the vertical position and a single linear profile cannot be taken as evidence of no convection.

Forced Convection Experiments

Using Apparatus 1 an air diffuser was constructed that could direct a uniform flow of air across the specimen box. Two configurations (shown in Figs. 2b and 2c) were tested. For 2b the air was directed across the specimen above the polyethylene cover sheet. For configuration 2c, the polyethylene was raised 70 mm and the front and back of the sample box left open so that air flowed under the cover sheet.

In both configurations, tests were run with no air flow, then at two different air velocities. For configuration 2b the average velocities were 4.98 m/min and 16.78 m/min, while for configuration 2c they were 7.00 m/min and 22.89 m/min. Thermal data for the forced convection tests are shown in Table 4.

Figure 17 plots the observed heat flux as a function of average air flow velocity. Note that for the sealed test (Condition B) the increase in heat flux is at a constant rate. Initially the test with no air flow (Condition C) should be close to Condition B, but as soon as the airflow is started it shows a larger increase in heat flux. The fact that the heat flux for Condition C is essentially constant after the initial rise leads to the conclusion that the air flow is not penetrating the insulation.

From Table 4 one might conclude that the thermal performance deteriorated with increased air flows. For Case C it might be said that the air flow penetrated the loose-fill insulation. If one examines the temperature profiles within the insulation (Fig. 18), one can argue that this is not the case. Note that for Condition B, with a finite air gap, the profiles are independent of air flow velocity, but for Condition C the top surface of the insulation becomes colder with increased air

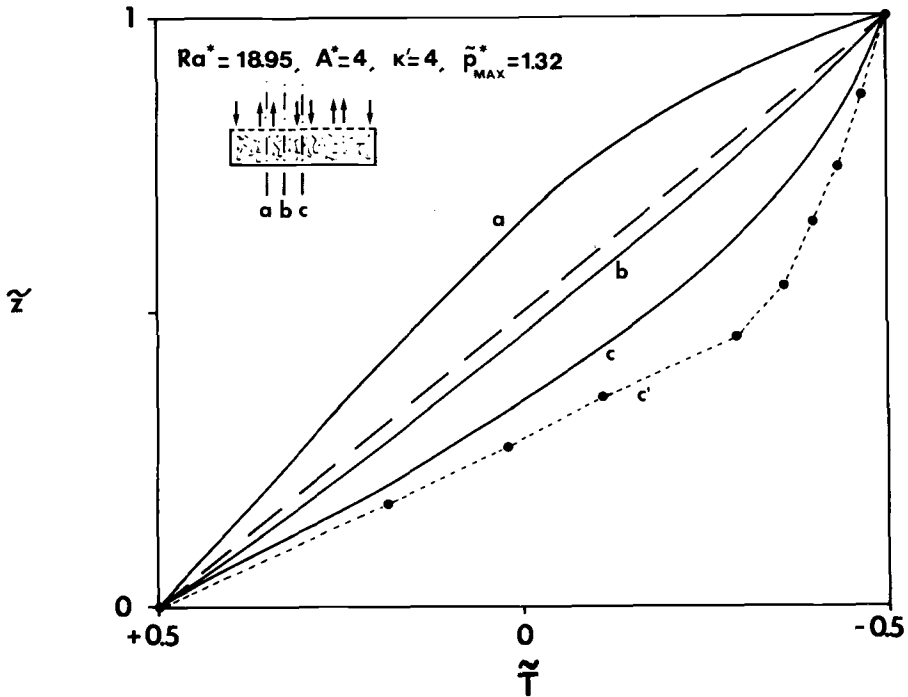


FIG. 16—Theoretical and experimental vertical temperature profiles for an open specimen at three locations.

TABLE 4—Forced convection studies.

Test Cond.	Average Air Flow (m/min)	T_{Hot} (°C)	T_{Cold} (°C)	ΔT (°C)	Heat Flux (W/m ²)	λ (W/m · K)	R -value (ft ² h °F/Btu)
B	0	27.85	−8.05	35.89	9.373	0.0485	21.76
	4.98	27.86	−8.18	36.04	9.668	0.0499	21.16
	16.78	27.79	−8.49	36.29	10.26	0.0526	20.07
C	0	26.75	−9.94	36.69	10.12	0.0513	20.58
	7.00	27.72	−10.02	37.74	11.63	0.0573	18.42
	22.89	27.81	−10.93	38.72	11.74	0.0564	18.71
$e = 0.340$ m “Blanket”							Ra^* Nu^*
		18.7	2.0	16.7		0.0746	15.3 1.00
		23.6	−3.0	26.6		0.0750	24.3 1.00
		26.7	−5.1	31.8		0.0748	28.9 1.00
		29.7	−8.3	38.0		0.0745	34.6 1.00
		34.6	−13.2	47.8		0.1026	43.5 1.37
		38.9	−18.6	54.9		0.1224	49.8 1.64
		34.4	−14.2	48.6		0.0939	44.6 1.25

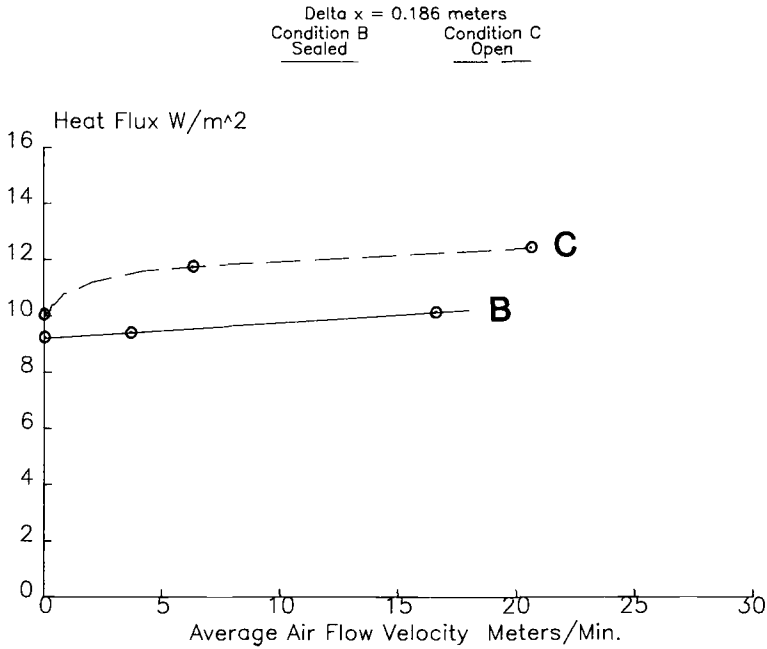


FIG. 17—Heat flux as a function of surface air velocity for sealed and open loose-fill specimens.

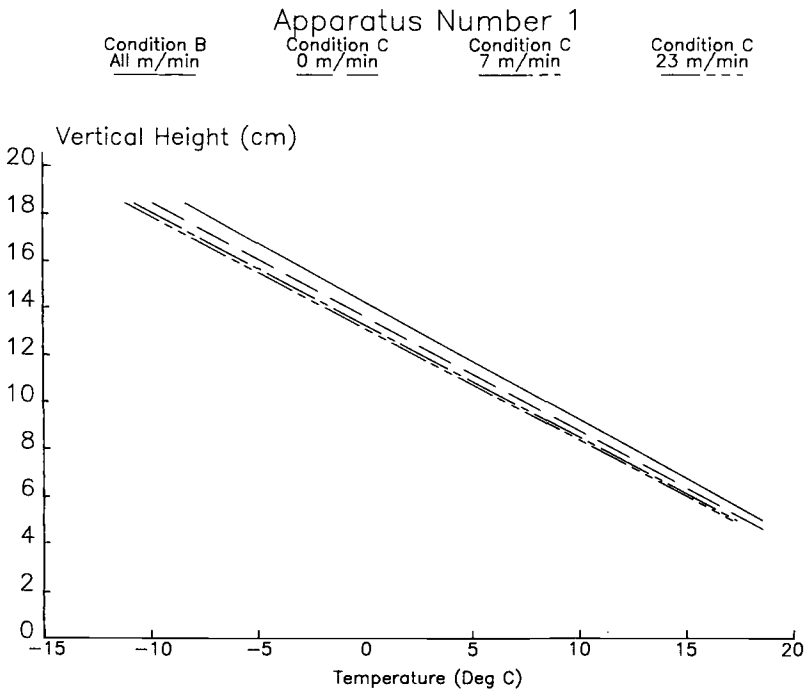


FIG. 18—Vertical temperature profiles of sealed and open loose-fill specimens under forced convection conditions.

flow. This is not surprising, since in Condition C the air is flowing directly across the insulation surface and therefore the surface will approach the cold air temperature. In fact, in Condition B the cold surface of the insulation was at -8°C while the cold air was at -10°C . In Condition C the insulation surface temperature was within 1°C of the cold air temperature.

Attic Configuration

It is now time to consider the initial question concerning the thermal performance of low density permeable insulation materials in attics. Attic configurations are clearly an open configuration, usually of the type designated as "infinite air layer" (Fig. 2a). In the previous section, a model for this configuration was experimentally validated. Thus one has a mathematical tool to predict the possible risks of penetration of the attic air into the insulation. But to use this tool, one needs to know the physical properties of the insulant together with the thermal and hydrodynamical boundary conditions at the open top interface.

Some recent work gives interesting information concerning the fluid dynamics in an attic. Poulikakos and Bejan [11] have proposed a model of an attic represented by a triangular or trapezoidal cavity up to relatively moderate fluid Rayleigh numbers ($Ra_f \leq 10^5$). They have shown in particular that the structure of the convective motion was of the classic Rayleigh-Benard type with contra-rotative cells. Higher Rayleigh numbers have also been studied but this time experimentally up to about 10^8 [12, 13]. For such a high value, the flow is then turbulent and one can only define a mean flow.

For $Ra = 10^8$, the order of magnitude of the maximum vertical velocities observed independently by Flack [12] and Kalache [13] is 0.2 m/s. More generally, the latter author reports that the maximum horizontal velocity (approximately equal to the maximum vertical velocity) is given by the following correlation:

$$|u_{\max}| \approx 0.2 \sqrt{g \cdot \rho^F \cdot \Delta T \cdot H} \quad (9)$$

where H is the largest height under the roof or in adimensional form:

$$|\overline{u}_{\max}| \approx 0.2 \sqrt{Ra \cdot Pr} \quad (10)$$

It is of interest to note that while these experimental results have been obtained on scale models, *in situ* measurements performed in attics in Great Britain [14] showed that the air speeds within the loft were mostly within the range 0 to 0.1 m/s (for external wind speeds up to 10 m/s).

This brief literature survey makes possible a first estimation of the pressure field at the open top surface of the insulant, which is needed for our model. Consider the following configuration:

- Attic geometry: $\begin{cases} H = 3 \text{ m} \\ L/2 = 6 \text{ m (half-length)} \end{cases}$
- Insulant: $\begin{cases} e^* = 0.3 \text{ m} \\ K^* = 3 \times 10^{-8} \text{ m}^2 \\ \lambda^* = 0.05 \text{ W/m} \cdot \text{k} \end{cases}$
- Attic air: $\begin{cases} u_{\max} = 0.2 \text{ m/s} \\ L_c = 2 \text{ m (characteristic dimension of convective cells [13])} \end{cases}$
(see Fig. 19)

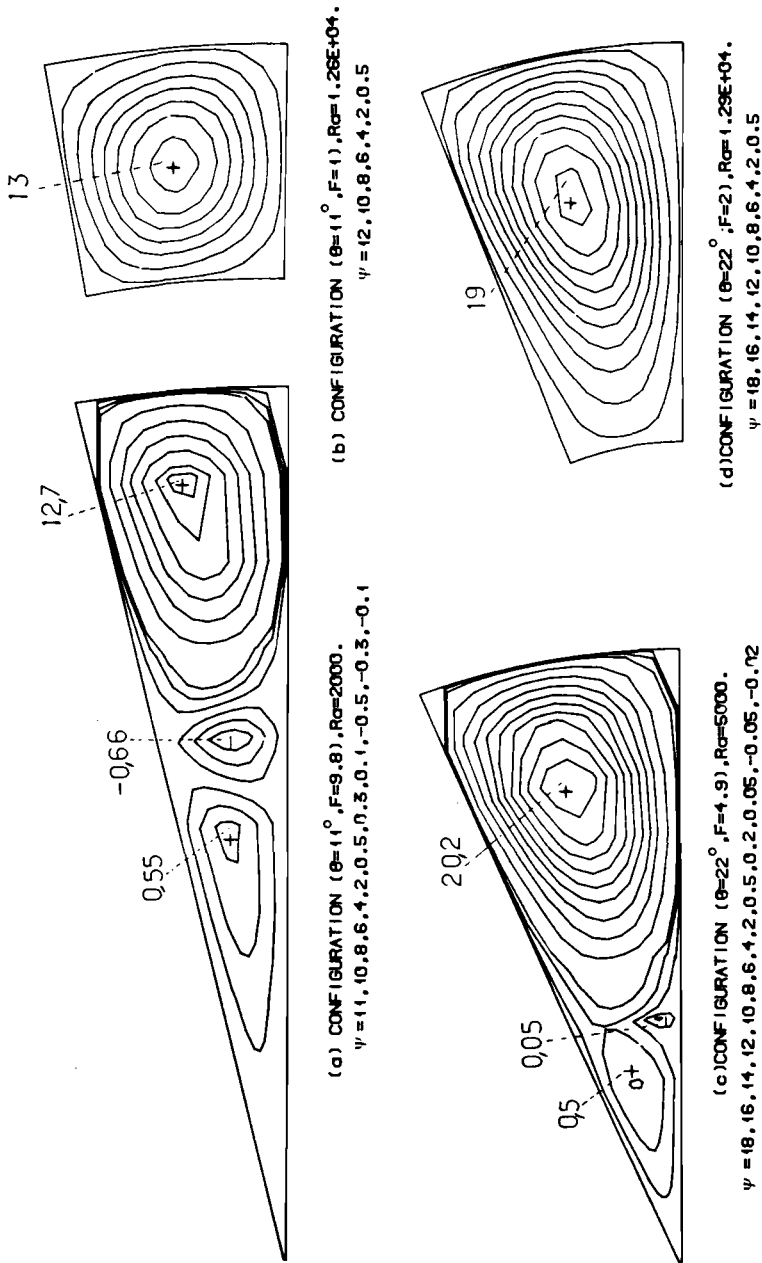


FIG. 19—Air flow patterns in an attic configuration (experimental results from Ref 13).

This gives (see definitions in the Appendix):

$$P_{\max}^* \approx 0.86$$

$$K' = L_c/L \approx 3$$

$$A^* = L/\ell^* \approx 20$$

In order to be consistent, consider the ratio A^*/K' and then estimate to a first approximation that one is close to a configuration of the type given in Fig. 13b ($A^* = 4$, $K' = 1$). From this figure, one can see that the risk of air penetration does not occur before a Ra^* of 20 and that the increase in heat transfer is relatively moderate (a few percent).

If one now considers the physical characteristics of the insulant taken in this example, one can see from Fig. 20 that a Rayleigh value of 20 can be achieved only in extreme climatic conditions ($T_c = -20^\circ\text{C}$). Although these computations are approximate and deliberately extreme conditions ($u = 0.2 \text{ m/s}$, $K^* = 3 \times 10^{-8} \text{ m}^2$) were used, it is possible to state that in most attic applications and for the range of permeabilities of existing *glass fiber* insulants, thermal performance is not affected by the air movements within the attic.

Conclusions

Onset of Convection Within Porous Media

Experience and theory clearly show the influence of boundary conditions on the onset of convection within porous media. The derivation of a critical Rayleigh number, Ra_c^* , is only possible for idealized boundary conditions:

- *In Closed Configuration* (the porous medium is bounded by two isothermal impermeable "plates," $Ra_c^* = 4\pi^2$)—When the cold top surface (still sealed) is in contact with either a finite

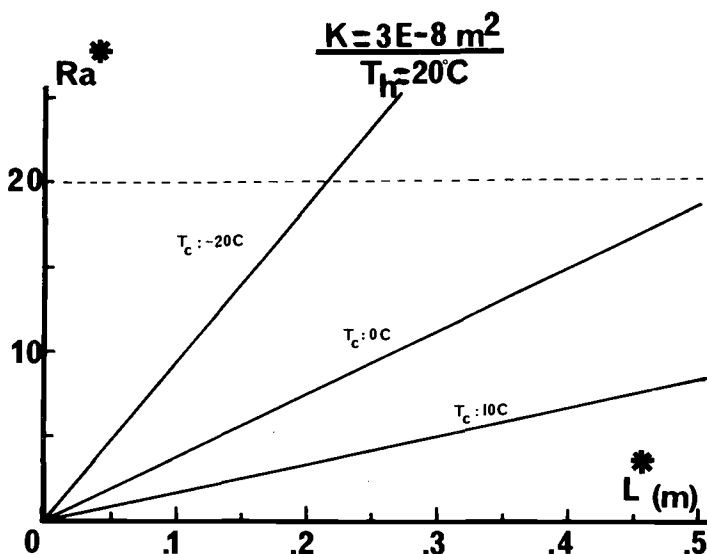


FIG. 20—Variation of the Rayleigh number as a function of thickness and cold face temperature for an isotropic porous medium of fixed air permeability, with a fixed hot face temperature.

or infinite air layer, the condition of isothermicity of this top surface can not always be fulfilled depending on the convective and radiative heat transfer processes within the air layer. In this configuration, it has been shown (experimentally and theoretically) that, depending on the extent of departure from true isothermicity, the onset of convection will occur as soon as the Rayleigh number is larger than 0 but becomes significant only for $Ra > 4\pi^2$. In most practical cases, this Rayleigh number will lie between 30 and 40.

- *In Open Configuration* (the fluid layer above the open cold top surface of the porous medium is rigorously isothermal and still $Ra_c^* = 27.1$)—When this condition is not fulfilled, the fluid penetration into the medium is responsible for an increase of the Nusselt number (i.e., of the total heat transfer). This penetration occurs before the onset of convection as such within the medium.

Penetration of External Air Flows into Porous Media

The occurrence of external fluid penetration is of course a function of the porous medium (in particular of its permeability) but is also strongly dependent on the magnitude of the convective movements within the external fluid. Starting from a known “convective pattern” of the fluid it is possible to establish theoretical correlations (confirmed by experiments) between the Nusselt and Rayleigh numbers of the porous medium. The approach to derive these correlations consisted of determining the pressure and temperature fields at the open top of the porous medium (needed as boundary conditions of the model) from the hydrodynamic conditions of the external fluid.

Attic Configuration

An important conclusion of this work has been to clearly show experimental and theoretical evidence that the boundary condition at the top of the porous layer influences the results. As a consequence, one has to be very careful when interpreting convection experiments. Moreover, the establishment of a unique correlation to predict the risk of heat transfer increase is impossible. This increase will be a function of the attic geometry and of the convective and radiative heat transfer within the attic air. Recent work on the fluid dynamics of an attic space has made it possible, however, to apply the model presented here in a “typical” attic situation and to show that the risk of attic air penetration into the insulant was not significant for Rayleigh values less than about 20. For existing glass fiber insulations, such high Rayleigh values can only be achieved in severe climatic conditions.

This research effort has shown the development of a useful model which can be used in the future to predict the convective effects in low density insulations. In order to use the model one needs to know, or accurately predict, the external fluid convective motions. Future developments await the availability of full-scale attic measurements or model predictions that can provide the data needed to define the parameters for use in the model.

Acknowledgments

The authors would like to thank Thierry Picard for his help in running the CRIR experiments and analyzing the data. We would also like to thank Carolyn Everhardt for typing this manuscript under very trying conditions.

APPENDIX

This Appendix describes both of the models discussed in the text and treats separately the modelling of the porous layer alone and the (fluid + porous) layers. The following equations have been solved numerically using the finite differences method (ADI scheme) [9]. Further details can be found in Ref 10.

Horizontal Porous Layer

Equations

The basic equations (conservation of mass, momentum, energy) for a horizontal porous medium (closed or open) within the classic assumptions (Darcy's formulation, Boussinesq approximation, isotropic medium) are:

$$\nabla \cdot \vec{V} = 0 \quad (11)$$

$$\frac{\mu f \vec{V}}{K^*} - \vec{\nabla} p - \rho^t g \vec{Z} = \rho^t \frac{\partial \vec{V}}{\partial t} \quad (12)$$

$$\nabla \cdot (\lambda^* \vec{\nabla} T) - (\rho c)^t \vec{V} \cdot \vec{\nabla} T = (\rho c)^* \frac{\partial T}{\partial t} \quad (13)$$

where

$$\rho^t = \rho_0(1 - \beta^t(T - T_0)) \quad (14)$$

Introducing the following adimensional variables:

$$\begin{aligned} \tilde{x}^* &= \frac{x}{\ell^*}; & \tilde{z}^* &= \frac{z}{\ell^*}; & \tilde{u} &= \frac{u \ell^*}{a^*}; & \tilde{v} &= \frac{v \ell^*}{a^*}; \\ \tilde{p}^* &= \frac{PK^*}{\mu^t a^*}; & \tilde{T}^* &= \frac{T - \tilde{T}^*}{\Delta T^*}; & A^* &= \frac{L}{\ell^*}; & \tilde{t} &= t; \\ Ra^* &= \frac{g \cdot \beta \cdot \Delta T^* \cdot K^* \cdot \ell^*}{\nu^t a^*} \end{aligned}$$

one can obtain either the stream function formulation

$$\nabla^2 \psi = -Ra^* \frac{\partial \tilde{T}}{\partial \tilde{x}} \quad (15)$$

with

$$\tilde{u} = \frac{\partial \psi}{\partial \tilde{z}}; \quad \tilde{v} = -\frac{\partial \psi}{\partial \tilde{x}}$$

or the pressure formulation

$$\nabla^2 \tilde{p}^* = Ra^* \frac{\partial \tilde{T}}{\partial \tilde{z}} \quad (16)$$

Boundary Conditions

Thermal Boundary Conditions

Thermal boundary conditions are identical for closed and open configurations:

$$\text{At } \bar{z}^* = 0: \quad \bar{T} = +0.5$$

$$\text{At } \bar{z}^* = 1: \quad \bar{T} = -0.5 + \alpha \cos(K' \pi \bar{x}/A^*)$$

$$\text{At } \bar{x} = 0, A^*: \quad \frac{\partial \bar{T}}{\partial \bar{x}} = 0$$

Hydrodynamic Boundary Conditions

Hydrodynamic boundary conditions are given below:

- Closed configuration:

$$\psi = 0 \text{ at all boundaries } (\bar{\mathbf{V}} \cdot \bar{\mathbf{n}} = 0)$$

- Open configuration:

$$\bar{p}^* = 0$$

if no fluid circulation in the upper fluid layer, and

$$\bar{P}^* = \bar{P}_{\max}^* \cos(K' \pi \bar{x}/A^*)$$

if cellular convection motion:

$$\text{At } \bar{z} = 0: \quad \frac{\partial \bar{p}}{\partial \bar{z}} = \text{Ra}^* \bar{T}$$

$$\text{At } \bar{x} = 0, A^*: \quad \frac{\partial \bar{p}}{\partial \bar{x}} = 0$$

Evaluation of Heat Transfer

The heat transfer through the porous medium is evaluated by the Nusselt number, defined as:

$$\text{Nu}^* = \frac{\frac{1}{L} \int_0^L \left(-\lambda^* \frac{\partial T}{\partial z} - (\rho c)^f \cdot \mathbf{v} \cdot T \right) dx}{\frac{-\Delta T}{\left(\frac{\ell^*}{\lambda^*} \right)}} \quad (17)$$

This number expresses the ratio of the effective heat transfer to the heat transfer in the absence of convection (if no convection, $\text{Nu}^* = 1$).

Superposed Fluid and Porous Layers

Equations

To obtain a single set of equations for both layers, one can use Brinkman's formulation:

$$\nabla \cdot \bar{\mathbf{V}} = 0 \quad (18)$$

$$\rho^f \nabla^2 \cdot \bar{\mathbf{V}} - \bar{\nabla} p - \frac{\mu^f \bar{\mathbf{V}}}{K(z)} = \rho^f \frac{\partial \bar{\mathbf{V}}}{\partial t} - \rho^f \bar{\mathbf{V}} \cdot \bar{\nabla} \bar{\mathbf{V}} \quad (19)$$

$$\nabla \cdot (\lambda(z) \nabla \bar{T}) - (\rho c)^f \bar{V} \cdot \nabla \bar{T} = (\rho c)^f \frac{\partial T}{\partial t} \quad (20)$$

with

$$\rho^f = \rho_0(1 - \beta^f(T - T_0)) \quad (21)$$

where $K(z) = K^*$ and $\lambda(z) = \lambda^*$ in the porous layer, and $K(z) = \infty$ and $\lambda(z) = \lambda^f$ in the fluid layer.

Introducing again adimensional variables:

$$\begin{aligned} \bar{x}^* &= \frac{x}{\ell^*}; & \bar{z}^* &= \frac{z}{\ell^*}; & \bar{u} &= \frac{u \ell}{a^f}; & \bar{v} &= \frac{v \ell}{a^f}; \\ \bar{p} &= \frac{P \ell^2}{\mu^f a^f}; & \bar{T} &= \frac{T - \bar{T}}{\Delta T}; & \text{Ra} &= \frac{g \cdot \beta \cdot \Delta T \cdot \ell^3}{\nu^f \cdot a^f}; \\ \text{Da} &= \frac{K^*}{\ell^2}; & \text{Pr} &= \frac{\nu^f}{a^f}; & \Gamma &= \frac{\lambda^*}{\lambda^f}; & A &= \frac{L}{\ell}; & B &= \frac{H}{\ell} \end{aligned}$$

the previous set of equations becomes

$$\frac{\partial \bar{p}}{\partial \bar{t}} = -\frac{1}{\chi} \nabla \bar{V} \quad (22)$$

$$\frac{1}{\text{Pr}} \left(\frac{\partial \bar{V}}{\partial \bar{t}} + \bar{v} \cdot \nabla \bar{V} \right) = \nabla^2 \bar{V} - \frac{\bar{K}(z) \bar{V}}{\text{Da}} + \text{Ra} \bar{T} \bar{z} - \nabla \bar{p} \quad (23)$$

$$\nabla \cdot (\bar{\lambda}(z) \nabla \bar{T}) - \bar{V} \cdot \nabla \bar{T} = \frac{\partial \bar{T}}{\partial \bar{t}} \quad (24)$$

with

$$\bar{K} = 0, \quad \bar{\lambda} = 1$$

in the fluid layer, and

$$\bar{K} = 1, \quad \bar{\lambda} = \Gamma$$

in the porous layer.

Note that Eq 18 has been transformed into a pressure equation. This method is known as the artificial compressibility (χ) method [9].

Boundary Conditions

The boundary conditions are given below:

$$\text{At } \bar{x} = 0, A \text{ and } \bar{z} = 0, 1: \quad \bar{u} = \bar{v} = 0$$

$$\text{At } \bar{z} = 0: \quad \bar{T} = 0.5$$

$$\text{At } \bar{z} = 1: \quad \bar{T} = -0.5$$

$$\text{At } \bar{x} = 0, A: \quad \frac{\partial \bar{T}}{\partial \bar{z}} = 0$$

Note that no condition is needed at the interface in Brinkman's formulation.

Effective Rayleigh Numbers

Effective individual Rayleigh numbers of the fluid and porous media can be computed if the mean temperature at the interface T_i is known:

$$Ra_{eff}^f = Ra B^3 \frac{\bar{T}_i - T_c}{T_H - T_c} \quad (25)$$

$$Ra_{eff}^* = Ra \cdot Da \left(\frac{1 - B}{\Gamma} \right) \cdot \frac{T_H - \bar{T}_c}{T_H - T_c} \quad (26)$$

Evaluation of Heat Transfer

The heat transfer is evaluated by the global Nusselt number:

$$\overline{Nu} = \frac{\frac{1}{L} \int_0^L \left(-\lambda(z) \frac{\partial T}{\partial z} + (\rho c)^t v T \right) dx}{\frac{-\Delta T}{\left(\frac{\ell^f}{\lambda^f} + \frac{\ell^*}{\lambda^*} \right)}} \quad (27)$$

or in adimensional form

$$\overline{Nu} = \frac{\frac{1}{A} \int_0^A \left(-\lambda(\bar{z}) \frac{\partial \bar{T}}{\partial \bar{z}} + \bar{v} \cdot \bar{T} \right) d\bar{x}}{\frac{\Gamma}{\Gamma \cdot B + (1 - B)}} \quad (28)$$

Again, one can define effective Nusselt numbers for both fluid (Nu^f) and porous layers (Nu^*):

$$Nu^f \left(\frac{\bar{T}_i - T_c}{T_H - T_c} \right) = Nu^* \left(\frac{T_H - \bar{T}_i}{T_H - T_c} \right) \Gamma \left(\frac{B}{1 - B} \right) = \frac{Nu \cdot B \cdot \Gamma}{(1 + B + B \cdot \Gamma)} \quad (29)$$

Pressures

Note that the dimensionless pressures are defined differently in the fluid and porous media:

$$\tilde{p}^f = \frac{p \ell^2}{\mu^f a^f}$$

$$\tilde{p}^* = \frac{p K^*}{\mu^f a^*}$$

and one has the relationship

$$\tilde{p}^* = \frac{K^*}{\ell^{f2}} \cdot \Gamma \cdot \tilde{p}^f \quad (30)$$

References

- [1] Bankvall, C. G., "Mechanisms of Heat Transfer in Permeable Insulation and Their Investigation in a Special Guarded Hot Plate," in *Heat Transmission Measurements in Thermal Insulations, ASTM STP 544*, American Society for Testing and Materials, Philadelphia, 1974, pp. 34-48.
- [2] Fournier, D. and Klarsfeld, S., "Some Recent Experimental Data on Glass Fiber Insulation Materials and Their Use for a Reliable Design of Insulations at Low Temperatures," in *Heat Transmission Measurements in Thermal Insulations, ASTM STP 544*, American Society for Testing and Materials, Philadelphia, 1974, pp. 223-242.
- [3] Nield, D. A., "Onset of Thermal Convection in a Porous Medium," *Water Resources Research*, Vol. 4, 1968, pp. 553-560.
- [4] MacKibbin, "Thermal Convection in a Porous Layer: Effects of Anisotropy and Surface Boundary Conditions," *Transport in Porous Media*, Vol. 1, No. 3, 1986, pp. 271-191.
- [5] Fournier, D. and Klarsfeld, S., "Utilisation d'un appareil orientable a plaque chaude garde pour la mise en evidence du transfert de chaleur par convection naturelle en milieux poreux dans des conditions simulees," in *Proceedings*, 13th International Congress of Refrigeration, Washington, D.C., Vol. 2, 1971, pp. 53-67.
- [6] Zehender, H., "Einfluss der freien Konvektion auf die Wärmeleitfähigkeit einer mineral-Fasermatte," *Kaltetechnik*, Vol. 10, 1964, pp. 308-311.
- [7] Nield, D. A., "Onset of Convection in a Fluid Layer Overlying a Layer of a Porous Medium," *Journal of Fluid Mechanics*, Vol. 81, Part 3, 1977, pp. 513-522.
- [8] Nield, D. A., "The Boundary Correction for the Rayleigh-Darcy Problem: Limitations of the Brinkman Equation," *Journal of Fluid Mechanics*, Vol. 128, 1983, pp. 39-46.
- [9] Teman, R., *Navier Stokes Equations*, North Holland, Amsterdam, 1977.
- [10] Arquis, E. and Caltagirone, J. P., "Interacting Convection Between Fluid and Open Porous Layers," presented to ASME Winter Meeting, Boston, 1987.
- [11] Poulikakos, D. and Bejan, A., "The Fluid Dynamics of an Attic Space," *Journal of Fluid Mechanics*, Vol. 131, 1983, pp. 251-269.
- [12] Flack, R. D., "The Experimental Measurement of Natural Convection Heat Transfer in Triangular Enclosures Heated or Cooled from Below," *ASME Journal of Heat Transfer*, Vol. 120, 1980, pp. 770-772.
- [13] Kalache, D., "Contribution a l'etude de la Convection Naturelle en Cavites Trapezoidales Chauffees par Dessous," These d'Etat Soutenue a Poitiers (France), Sept. 1987.
- [14] Anderson, R. R. and Wasrd, T. I., "Measurements of the Heat Loss Through an Insulated Roof," *Building Services Engineering Research & Technology*, Vol. 2, No. 2, 1981.

An Acoustic Technique for Evaluation of Thermal Insulation

REFERENCE: Flynn, D. R., Evans, D. J., and Bartel, T. W., "An Acoustic Technique for Evaluation of Thermal Insulation," *Insulation Materials, Testing, and Applications, ASTM STP 1030*, D. L. McElroy and J. F. Kimpflen, Eds., American Society for Testing and Materials, Philadelphia, 1990, pp. 319-342.

ABSTRACT: A laboratory apparatus has been constructed that enables rapid measurement of the sound insertion loss of a sample of insulation as a function of frequency. An extensive series of measurements of the sound insertion losses associated with blown samples of fiberglass, rockwool, and cellulose has been completed; the results of these acoustic measurements are highly correlated with coverage (mass per unit area) and thermal resistance (R-value). An investigation is planned to extend the acoustic techniques used in the laboratory apparatus to *in situ* determination of the sound transmission loss through thermal insulation installed in attics. Two possible approaches to such field measurements are described.

KEY WORDS: acoustics, attic insulation, heat flow, heat transfer, insulation, non-destructive evaluation, non-destructive testing, sound attenuation, sound propagation, thermal conductivity, thermal insulation, thermal resistance

There is convincing evidence that the customer may not always be getting his money's worth when he purchases blown-in-place attic insulation, either because the insulation is not applied properly or because the quantity of insulation delivered is less than that purchased. In 1982, for example, the Florida State Attorney's Office tested 639 houses and found that about 70% of the houses insulated by some contractors had less than 90% of the insulation claimed to have been installed. An investigation of an insulation certification program by the State of Georgia found that over two thirds of the "certified" homes actually had less than 90% of the required insulation. In addition to the customer being short-changed at the time of purchase, the failure to provide the specified amount of insulation leads to higher fuel bills over the life of the building. The overall economic implications of inadequate insulation of attics are believed to be very significant.

The present procedure for measuring the quantity of insulation installed in an attic is to send one or more workers into the attic to measure the thickness of the insulation, using a ruler, and to measure the density of the insulation, using a "cookie cutter" to acquire samples for weighing. This procedure is costly, in terms of the labor requirements, and destructive, in terms of disruption of the insulation.

Ideally, one would like to use a measurement technique that directly indicates the thermal performance of the installed insulation. Unfortunately, a review of possible thermal techniques for making such a measurement indicates that direct measurement of thermal performance poses several problems. Thermal resistance measurements inherently involve measurement of a heat flux. For large thicknesses of attic insulation, the heat fluxes are very small and difficult to measure accurately in the field. The problem is compounded by the difficulty of evaluating the

¹Supervisory Physicist, Mechanical Engineer, and Physicist, respectively, National Institute of Standards and Technology, Gaithersburg, MD 20899.

influence of heat flows—along the ceiling, through framing members, and, most importantly, to or from the attic space and to or from the rooms beneath the attic—that do not pass through the attic insulation. Furthermore, the time constants involved in direct measurement of the thermal resistance of installed attic insulation could be many hours.

In December 1984 the Mineral Insulation Manufacturers Association (MIMA) informed the National Bureau of Standards (NBS) (now the National Institute of Standards and Technology [NIST]) that:

. . . there is a national need to develop a field measurement technique to determine the installed loose fill R-values of thermal insulation. Other legal requirements such as the FTC Home Insulation Rule require a reliable measurement technique. The installer, builder, utility, code official and, most importantly, the consumer need a means to measure installed R-values. The technique should be accurate, fast, nondestructive and economical. Recent efforts in the industry, and elsewhere, to devise a measurement technique have not been satisfactory.

MIMA went on to ask NBS to address this measurement need.

Following meetings between MIMA and NBS technical personnel, a Workshop on New Methods to Measure the R-Value of Thermal Insulation was held in June 1985 at the National Association of Homebuilders in Washington, D.C., with approximately 70 people in attendance. There was extensive discussion of the nature of the problem and a general endorsement of the need for improved measurement procedures. NBS staff then described an acoustical technique for indirect measurement of either the coverage (mass per unit area) or the thermal resistance (R-value) of installed attic insulation by passing sound waves through a sample of material and measuring the sound insertion loss (i.e., the decrease in sound pressure level) caused by the insulation. A live demonstration of one simple implementation of this acoustical technique was given at the Workshop. NBS indicated that the development of such a technique as a practical field device would require considerable effort but that the preliminary analysis and results looked quite encouraging.

The present paper (1) describes the acoustic technique that was proposed in 1985 by NBS, (2) presents the results of an NBS pilot study (funded by MIMA, the U.S. Department of Energy, and NBS) that has been carried out to examine the feasibility of this acoustical technique for measurement of insulation coverage (or density) and thermal performance, and (3) indicates how this technique could be extended to enable practical field measurements of the adequacy of installed insulation.

General Technical Approach

When a sound wave passes through a porous material, such as loose-fill insulation, the sound wave undergoes both amplitude attenuation and a phase shift that depend on the nature of the material and on the frequency of the incident sound wave. For example, the sound attenuation characteristics of fibrous materials are dependent upon, in addition to the frequency of the sound wave, the type of fiber material, the distribution of fiber diameters, the surface condition of the fibers, the binder, the installed density, and the type and density of the gas filling the pores of the material. There is an extensive literature devoted to theoretical and empirical relationships between these factors and the sound attenuation characteristics of fibrous materials. The same factors which affect the propagation of sound in a fibrous material also affect thermal conductivity, and hence R-value.

The time-dependent sound pressure associated with an ideal plane acoustic wave traveling in the positive x -direction in a porous medium can be expressed as

$$p = p(x, t) = p(0, t)\exp(-\gamma x) \quad (1)$$

where $p(0, t)$ is the sound pressure that would exist, independent of the position, in the absence of attenuation; t is time; and γ is the complex propagation coefficient, which can be written as

$$\gamma = \alpha + j\beta \quad (2)$$

where the real part α is called the attenuation coefficient, the imaginary part β is the phase coefficient, and $j^2 = -1$. The attenuation coefficient, which is a property of the porous medium and of the frequency of the sound wave, determines the decay of the sound pressure with distance in the medium. The phase coefficient, which also is a property of the medium and the sound frequency, describes the speed of sound propagation through the medium.

Figure 1 illustrates the behavior described by Eq 1. The solid curve represents the sound pressure observed when an acoustic sine wave passed through air from a 40-kHz source to a receiving microphone. The curve designated by long dashes represents the received sound pressure when a sample of R-11 fiberglass insulation was interposed between the source and the receiving microphone, while the curve shown as short dashes illustrates the received sound pressure when two pieces of R-11 insulation were interposed. It is seen that as additional absorptive material is placed in the sound path, the amplitude of the sinusoidal sound wave decreases, the change being described by the attenuation coefficient (α), and the phase of the sine wave is shifted, by an amount described by the phase coefficient (β).

The mean-square sound pressure, which is independent of time, at the position x is given by

$$p^2 = p_0^2 \exp(-2\alpha x) \quad (3)$$

where p_0^2 is the time-averaged value of $p^2(0, t)$. The sound insertion loss, defined as the decrease in sound pressure level in decibels (with attenuation present) relative to the sound pressure level that would exist if there were no attenuation, is

$$D = -10 \log_{10}(p^2/p_0^2) = -10 \log_{10}[\exp(-2\alpha x)] = 8.686\alpha x \quad (4)$$

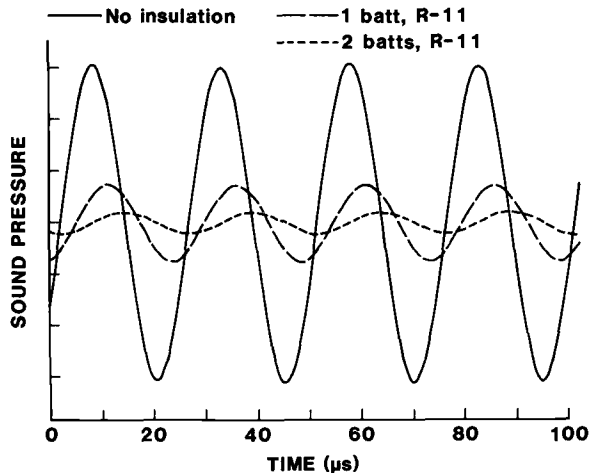


FIG. 1—Instantaneous sound pressure (arbitrary units) versus time for a 40-kHz sine wave. The solid line corresponds to propagation through air. The long-dash line illustrates the attenuation and the phase shift due to interposing a 9-cm-thick sample of fiberglass batt between the source and the receiver, while the short-dash line indicates the sound pressure with 18 cm of insulation in place.

Thus the sound insertion loss is proportional to the product of the attenuation coefficient and the sample thickness.

Delaney and Bazley [1] have developed empirical relationships expressing the attenuation and phase coefficients of fibrous absorbent materials as simple power-law functions of the ratio of the sound frequency divided by the specific flow resistance of the material. Bies [2] has presented an empirical relationship giving the specific flow resistance of fiberglass products in terms of the fiber diameter and the installed density of the material. Combining Delaney and Bazley's expressions with the Bies relationship enables us, for randomly oriented fibrous material, to express the attenuation and phase coefficients in terms of the installed density, ρ , of the insulation, the average fiber diameter, d , and the sound frequency, f . The resultant expression for the attenuation coefficient is

$$\alpha = \alpha_0 \cdot \left(\frac{\rho}{\rho_0}\right)^\mu \cdot \left(\frac{d_0}{d}\right)^\nu \cdot \left(\frac{f}{f_0}\right)^\xi \quad (5)$$

where α_0 is a reference attenuation coefficient corresponding to the values $\rho = \rho_0$, $d = d_0$, and $f = f_0$. The three exponents in Eq 5 have the approximate values $\mu \approx 0.9$, $\nu \approx 1.2$, and $\xi \approx 0.4$. These exponents vary somewhat for different materials. The phase coefficient will not be discussed further in the present paper.

Although there may be a considerable range of fiber diameters within a given batch of fibrous insulation, a representative fiber diameter may be determined. Since the sound frequency can be fixed experimentally, one can take $d = d_0$, $f = f_0$, and Eq 5 yields the following simple relationship between the attenuation coefficient and the installed density of the insulation:

$$\alpha = \alpha_0 \cdot \left(\frac{\rho}{\rho_0}\right)^\mu \quad (6)$$

Thus for a given material it is not necessary to know ν and ξ . The coverage, or mass per unit area, of installed insulation in an attic is given by $W = \rho\ell$, where ℓ is the thickness of the insulation. Combining this equation with Eqs 4 and 6, the coverage is related to the sound insertion loss by the expression

$$W = K \cdot D^\eta \ell^{1-\eta} \quad (7)$$

where $\eta = 1/\mu$ and K is a material-dependent proportionality constant. The parameter η will have a value not too different from unity so that the sample thickness, ℓ , need not be known very accurately in order to use Eq 7. For the special case where $\eta = 1$, Eq 7 reduces to simply $W = K \cdot D$ (i.e., the coverage is proportional to the sound insertion loss).

It is well known that the effective thermal conductivity of a given loose-fill insulating material depends upon the installed density of that material. For mineral fiber insulations, the effective thermal conductivity, λ , of relatively thick insulation can be represented in terms of the installed density, ρ , of the material by an equation of the form

$$\lambda = A + B\rho + C/\rho \quad (8)$$

where A , B , and C are constants, A representing the thermal conductivity of the gas (air) filling the insulation, $B\rho$ representing heat conduction through the fibers and the interaction of that conduction with the surrounding gas, and C/ρ representing the radiative heat transfer through the porous insulation.

The thermal resistance of the sample can be expressed as

$$R = \frac{\ell}{\lambda} = \frac{W}{A\rho + B\rho^2 + C} \quad (9)$$

If the density of the sample is constant, so is the denominator of Eq 9 and the thermal resistance of the sample is proportional to the coverage. Thus, by way of Eq 7, the thermal resistance can be expressed in terms of the sound insertion loss and the sample thickness. For the more general case where the installed density is variable and unknown, the density can be estimated from the sound insertion loss and the thickness. Dividing both sides of Eq 7 by ℓ yields

$$\rho = K \cdot (D/\ell)^n \quad (10)$$

This value of ρ can be used to compute the denominator of Eq 9. Thus, if the functional relationship between thermal conductivity and density is known (i.e., if A , B , and C are known for the example above), the thermal resistance can be obtained from the measured sound insertion loss and the approximate sample thickness.

Experimental Procedure

Acoustic Test Chamber

The apparatus designed and constructed for the acoustic measurements is conceptually somewhat similar to a guarded hot plate apparatus used for thermal resistance measurements. Ideally, as indicated in Fig. 2, a sound source projects a plane columnated sound wave upward through the sample to a receiver above. Measurement of the sound levels at the receiver with the sample present and with the sample absent enables calculation of the sound insertion loss (see Eq 4). This experimental configuration was achieved using the components illustrated in Fig. 3. The sound source consisted of a 25 mm dome loudspeaker located at the focal point of an upward-facing parabolic reflector used to collimate the sound. The sample of blown insulation was held in a wood-sided basket with a screen bottom to allow passage of the sound wave. The

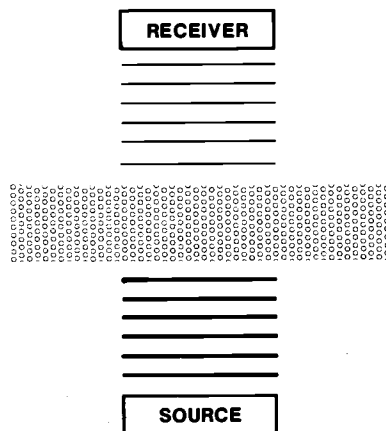


FIG. 2—Conceptual schematic of an acoustic plane wave traveling from a sound source through a porous insulation to a sound receiver.

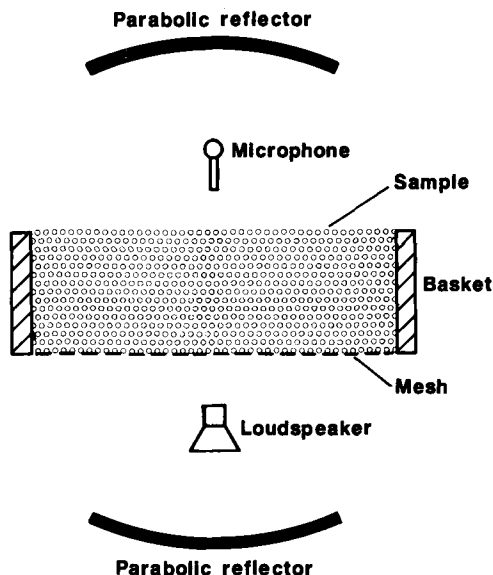


FIG. 3—Schematic drawing of a compact source projecting sound downward to a parabolic reflector, upward through the sample to another parabolic reflector, and then downward to a measuring microphone.

sound receiver consisted of a laboratory-grade condenser microphone located at the focal point of a downward-facing parabolic reflector.

The test chamber is shown on the right-hand side of Fig. 4. The two parabolic reflectors, the source transducer (loudspeaker), the measuring microphone, and a support shelf for the sample baskets were housed inside a cabinet approximately 0.9 m by 0.9 m by 2.1 m high. The interior walls of the cabinet were lined with 20 cm by 20 cm by 25 cm deep wedges constructed from fiberglass board (nominally of 50 kg/m³ density), except for a nominally 40 cm high section above the sample-basket support shelf (to allow room inside the enclosure for the insertion of a sample basket or baskets) and certain areas of the walls (e.g., corners) that were not completely covered by the wedges due to geometrical constraints—these portions were covered with a 5 or 15 cm thick layer of fiberglass board, as appropriate. The interiors of the floor and ceiling of the cabinet were covered with a 5 cm layer of fine-fiberglass aircraft insulation, which has a much higher sound attenuation coefficient than does the fiberglass board used for lining the rest of the cabinet.

The sample baskets, one of which is shown installed in the test chamber in Fig. 4, had nominal inside dimensions of 53 by 53 cm and nominal heights of 15 or 23 cm. The baskets were constructed from 1.3 cm thick unfinished plywood, were open at the top, and had nylon window screen stretched across the bottom to hold the material in the baskets (the baskets were transported with a piece of fiberboard underneath to prevent the screen from sagging in the center of the basket and thus possibly altering the distribution of material within the basket). The inside of each of the walls of the baskets was lined with 2.5 cm thick 50 kg/m³ fiberglass board insulation to reduce acoustic reflections within the baskets during testing. The sides of the baskets were held together with glue and metal finishing nails, and the nylon screen was attached to the outside of the walls of the baskets with metal staples and nylon tape.

Figure 5 is a close-up photograph of the lower half of the test chamber, showing the loudspeaker, the lower parabolic reflector, and a better view of the sound absorbing wedges used to minimize unwanted sound reflections inside the chamber. Figure 6 provides a view of the por-



FIG. 4—Photograph of the test chamber with a sample basket installed. The operator is measuring the thickness of another sample, which is resting on a digital balance.

tion of the test chamber where the sample baskets are installed in the region between the supporting wires and the height at which the absorbing wedges begin. The supporting wires prevent the nylon screen bottom of the sample basket from sagging. The measuring microphone can be seen near the top of the Fig. 6. The test results given in this paper are very insensitive to loudspeaker and microphone placement.

Instrumentation

The instrumentation used to make the acoustic measurements consisted primarily of a signal generator, filter, and amplifiers to provide the signal to the loudspeaker. A microphone preamplifier, measuring amplifier, and dynamic signal analyzer were used to measure the voltages produced by the signal generator and the measuring microphone.

The signal used to drive the loudspeaker was a highpass-filtered swept sine wave that was gated to produce a "chirp" of 1 ms duration. The chirp was repeated every 200 ms. The signal was gated such that the frequency sweeps at the output of the signal generator began and ended on a positive-going zero-crossing. A trigger circuit was used to synchronize the signal analyzer with the rest of the measurement instrumentation. The signal generator was comprised of two function generators. The first function generator produced a voltage ramp that was repeated every 200 ms and drove a voltage-controlled oscillator that was part of a second function generator. The second function generator was set to produce an integral number of cycles within each frequency sweep and then gate "off" until receiving the next trigger from the first function

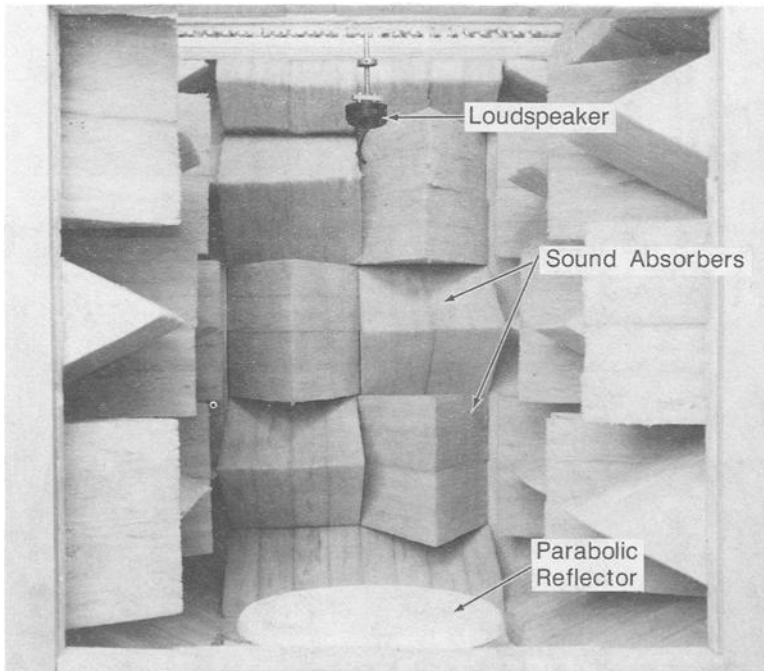


FIG. 5—Lower half of the test chamber showing the loudspeaker, the lower reflector, and the sound-absorbing wedges.

generator. The output of the second function generator was followed by a wide-band amplifier and high-pass filter to shape the spectrum of the “chirp.” The filtered waveform of the test signal was amplified by a power amplifier that drove the loudspeaker.

The output of the measuring microphone was coupled to a preamplifier, power supply, and measuring amplifier. The gain of the measuring amplifier was adjusted as needed to match the input sensitivity of the signal analyzer. The output signal of the measuring amplifier was time-gated by an electronic switch to prevent undesirable acoustic signals (e.g., delayed reflections) from occurring during a measurement period. The electronic switch was triggered by the output of a time-delay generator which was adjusted to provide the proper electronic delay to compensate for the acoustic delay in the test chamber.

The signal analyzer was used in a two-channel mode in which it obtained a transfer function, at 100 Hz intervals up to 25 kHz, for the measurement system between the output of the second function generator and the output of the electronic switch following the measuring microphone. The analyzer averaged the results from 100 chirps, or bursts of sound, obtained with and without the test sample being installed in the test chamber, and stored these results. The analyzer was later used to take the complex ratio of the transfer functions obtained with and without the sample present, thus compensating for the frequency response of the transducers and instrumentation. A desktop computer was used to calculate sound insertion loss, in decibels, and phase shift, in degrees, from the measurement results. A separate computer was used to combine the data so as to obtain the average sound insertion losses for the eleven $\frac{1}{3}$ -octave band frequencies centered at nominally 2.5, 3.15, 4, 5, 6.3, 8, 10, 12.5, 16, 20, and 25 kHz. Figure 7 shows a representative set of such data.

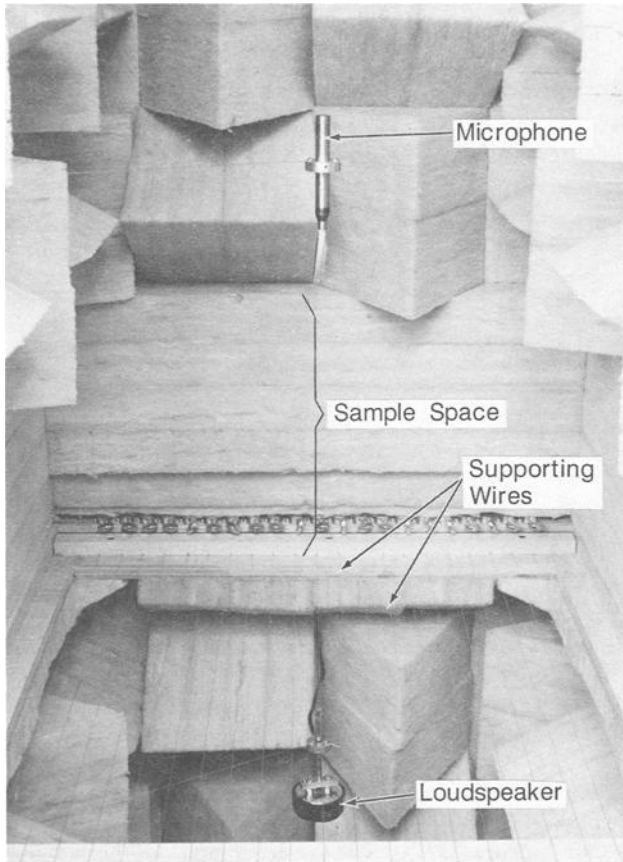


FIG. 6—Central portion of the test chamber showing the microphone, the region where the sample basket is installed, the wires that support the sample basket, and the top of the downward-facing loudspeaker.

Test Procedures

The test samples were blown into pre-weighed test baskets to the approximate desired test density using an “open blow machine” designed specifically for pneumatic application of the materials tested. The baskets of blown insulation were allowed to come to thermal and moisture equilibrium with the air in the laboratory module where the acoustic test apparatus was located. The weight of an empty basket was monitored to enable tracking the change in the tare weight of the baskets due to varying moisture content in the wooden sides of the baskets. Just prior to acoustic testing, the filled basket was weighed and the (adjusted) tare weight subtracted to obtain the mass of insulation material. Fiberglass blankets were tested without baskets and thus their weight was measured directly. The thickness of each test sample was measured at multiple locations using a pin and disk depth gage and steel rule in accordance with ASTM Test Methods for Thickness and Density of Blanket or Batt Thermal Insulations (C 167). The scientist shown in Fig. 4 is beginning to make a thickness measurement while the filled sample basket is located on the digital balance. The coverage (kg/m^2) and the installed density (kg/m^3) of each

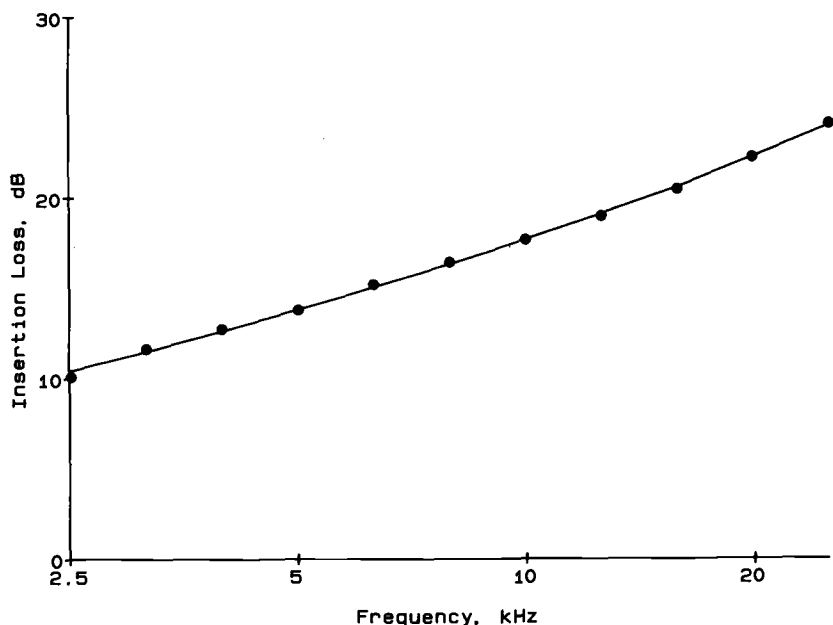


FIG. 7—An example data set of sound insertion loss versus frequency for the $1/3$ -octave bands with center frequencies from 2.5 to 25 kHz. The sample was blown bonded fiberglass with a coverage of 1.84 kg/m^2 .

test sample were computed from the mass and average thickness of the sample and the area of the interior of the basket.

After the mass and thickness measurements were completed, the sample was placed in the test chamber and the acoustic measurements carried out using the instrumentation and signal described above. The acoustic measurements required 20 s, of which only 0.1 s was used to acquire data, the rest of the time being used to assure that the signal captured corresponded to sound that made a single pass through the sample (i.e., contained negligible reflected energy) and to protect the source transducer from excessive power input.

Test Samples

This study benefitted greatly by being able to “piggyback” on the round-robin tests of the apparent thermal conductivity of several loose-fill insulations carried out recently under the auspices of the ASTM C16.30 Task Group on C 687 Loose-Fill Testing [3]. Materials from the same lots as those used for this round robin were made available to NBS for the acoustic tests described in the present paper. The test materials investigated were a fiberglass blanket (the only material not blown), a bonded fiberglass, an unbonded fiberglass, a rockwool, and a cellulose. The reader is referred to Ref 3 for more complete descriptions of these materials.

Samples were blown at densities within 10% of the target densities for the round-robin tests referenced above. Additional samples for this study were intentionally blown to smaller or larger densities than those specified in the round-robin instructions. For each of the four blown materials, at least one sample was tested at its as-blown density and then compressed and acoustically measured at two higher densities.

Table 1 gives the thickness, coverage, and density of the samples used for the acoustical mea-

TABLE 1—*Thickness, coverage, and density of test samples.*^a

Sample Material	Thickness, m	Coverage, kg/m ²	Density, kg/m ³
Fiberglass blanket	0.278	3.11	11.2
	0.248	2.78	11.2
	0.310	3.44	11.1
	0.184	2.11	11.5
Blown bonded glass wool	0.184	1.84	9.9
	0.186	1.87	10.1
	0.370†	3.70	10.0
	0.233	1.73	7.5
	0.183*	1.73	9.5
	0.128*	1.73	13.6
	0.188	1.37	7.3
	0.220	2.35	10.7
Blown unbonded glass wool	0.169	1.69	10.0
	0.168	1.75	10.4
	0.337†	3.44	10.2
	0.229	1.99	8.7
	0.178*	1.99	11.2
	0.119*	1.99	16.7
	0.191	1.52	7.9
	0.207	2.14	10.4
Blown rockwool	0.165	5.41	32.7
	0.225	5.44	24.2
	0.180*	5.44	30.2
	0.117*	5.44	46.3
	0.162	5.39	33.3
	0.189	6.47	34.3
	0.184	6.43	34.9
	0.173	3.69	21.3
Blown cellulose	0.169	3.64	21.5
	0.169	7.15	42.4
	0.199	8.04	40.3
	0.183	6.94	37.9
	0.188	7.79	41.4
	0.147*	7.79	52.9
	0.115*	7.79	67.6

^aSee text for explanation of reference marks.

surements reported in this paper. The entries with an asterisk following the sample thickness correspond to further compression of the preceding sample. The fiberglass blanket samples of different thicknesses were obtained by stacking individual blankets. The samples with a dagger following the thickness correspond to the two previous sample boxes being stacked one upon the other in the acoustic test chamber.

Experimental Results

Acoustic data were taken over the entire frequency range from 2.5 to 25 kHz. However, with the exception of the data on the direct effects of sample compression, shown in Figs. 12 to 15 below, only data at 10 kHz are included in the present paper. This frequency was selected to enable treating the various materials and thicknesses on a common basis.

Coverage

Figure 8 shows the measured values of coverage (mass per unit area in the test basket) plotted versus the measured sound insertion loss at 10 kHz for the samples of bonded fiberglass blanket and of blown bonded fiberglass. The straight lines drawn from the origin through the data are seen to fit the experimental data very well, and the slopes of the two lines only differ by 2.4%. Figure 9 shows the same quantities plotted for the blown unbonded fiberglass. The data are reasonably well fitted by the straight line but not so well as in the previous figure. The three data points for a coverage of 1.99 kg/m^2 (see Table 1) correspond to the same sample at three different thicknesses, obtained by further compression; the fact that the same coverage does not produce the same sound insertion loss indicates that the coverage is not simply proportional to the sound insertion loss so that, in Eq 7, η is not equal to one. It should also be noted that the slope of the line in Fig. 9 is very different from the slopes of the lines in Fig. 8. For a given coverage, the finer-fiber unbonded glass produces almost twice the sound attenuation produced by the larger-fiber bonded material.

Figure 10 is a plot of the coverage of blown rockwool plotted versus the measured sound insertion loss at 10 kHz. There is considerable scatter in the results, and the data deviate considerably from the straight line fitted to them. This scatter should not, however, be too surprising. Rockwool typically contains a significant percentage of "shot" and fused fibers that are too large to contribute to sound absorption but which may constitute up to 40% of the mass. One would expect to have statistical variations in the percentage of shot in different samples, even from the same lot of material. Furthermore, when samples of different density are produced by differences in blowing technique, one would expect systematic variations in shot content.

The coverage-versus-insertion loss data for cellulose are shown in Fig. 11. The sound insertion loss at 10 kHz for the highest density sample (the last entry in Table 1) was too high to be

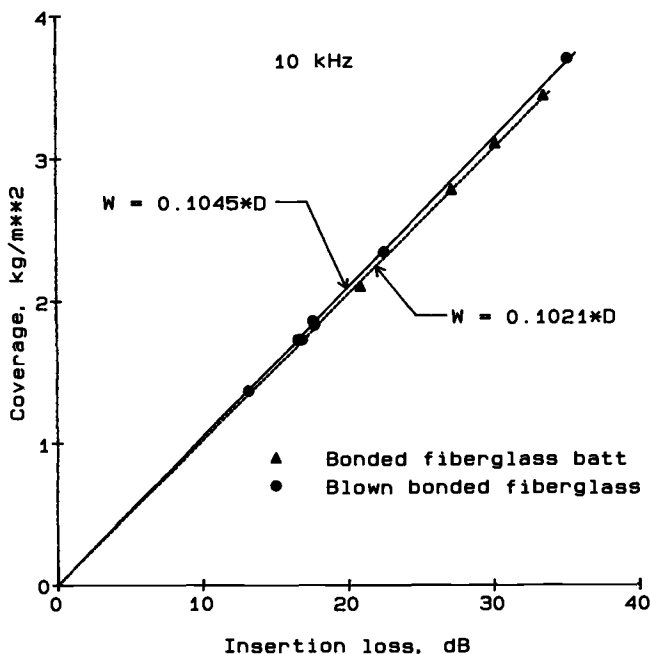


FIG. 8—Measured coverage versus sound insertion loss at 10 kHz for the bonded fiberglass samples (both the blanket and the blown materials). The equations define the least-squares straight lines fitted to the data and passing through the origin.

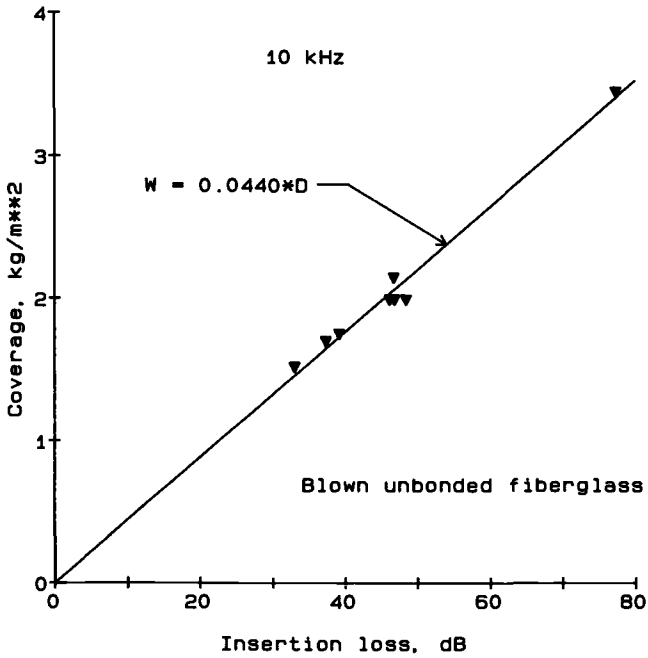


FIG. 9—Measured coverage versus sound insertion loss at 10 kHz for the blown unbonded fiberglass samples. The equation defines the least-squares straight line fitted to the data and passing through the origin.

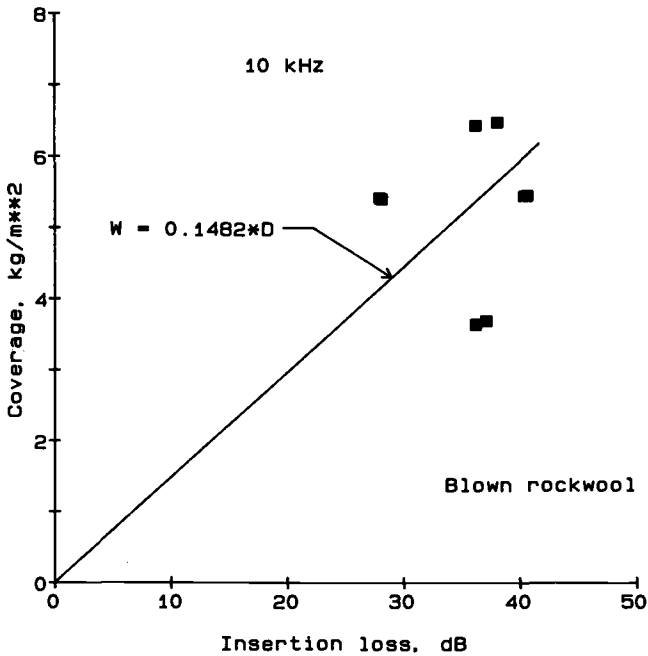


FIG. 10—Measured coverage versus sound insertion loss at 10 kHz for the blown rockwool samples. The equation defines the least-squares straight line fitted to the data and passing through the origin.

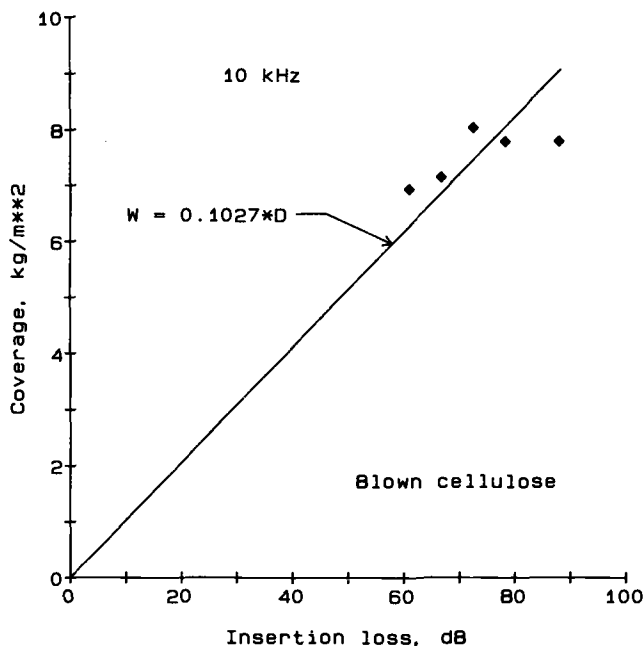


FIG. 11—Measured coverage versus sound insertion loss at 10 kHz for the blown cellulose samples. The equation defines the least-squares straight line fitted to the data and passing through the origin.

measured accurately and hence is not shown in Fig. 11. This fact, plus the observation that the two samples that have a coverage of 7.79 kg/m² have rather different insertion losses, indicates that η differs from unity for the cellulose samples as well.

The sound insertion loss data obtained with the same samples compressed to different thicknesses provide very useful information as to the values of the exponent η for the different materials at different sound frequencies. Figures 12 to 15 show the percentage change in insertion loss, versus frequency, for the four types of blown material. Restricting attention to the results at 10 kHz, it is seen that the blown bonded fiberglass and the blown rockwool samples exhibited very little dependency of insertion loss on thickness, indicating that for these samples the value of η appears to be very near to unity. For the finer-fiber unbonded glass material and, particularly, for the cellulose material which has a very small average pore size, the insertion loss increased as the sample was compressed, indicating a value for η that is significantly different from unity.

In order to further explore the effectiveness of using a value of η different from unity, a non-linear least squares software package was used to fit equations of the form of Eq 7 to the experimental data of coverage versus sound insertion loss and sample thickness for the various blown materials. For the two fiberglass materials, the proportionality constant, K , was forced to be the same but the bonded and unbonded materials were allowed to have different values for η . The measured coverage is plotted versus the predicted coverage in Fig. 16.

A similar procedure applied to the data for rockwool yielded the results plotted in Fig. 17. There is some improvement in comparison to the simple proportionality of Fig. 10, but the value obtained for η is not reasonable in terms of the results of the compression test (Fig. 14). In an attempt to predict coverage with less uncertainty, a number of equations with linear coefficients were fitted to the experimental data. One of the more successful equations was $W = K \cdot D(1 + bD + cD')$, where K , b , and c are constants to be determined and D' is the slope of the sound insertion loss versus the logarithm of sound frequency, evaluated at 10 kHz (see Fig. 7). The

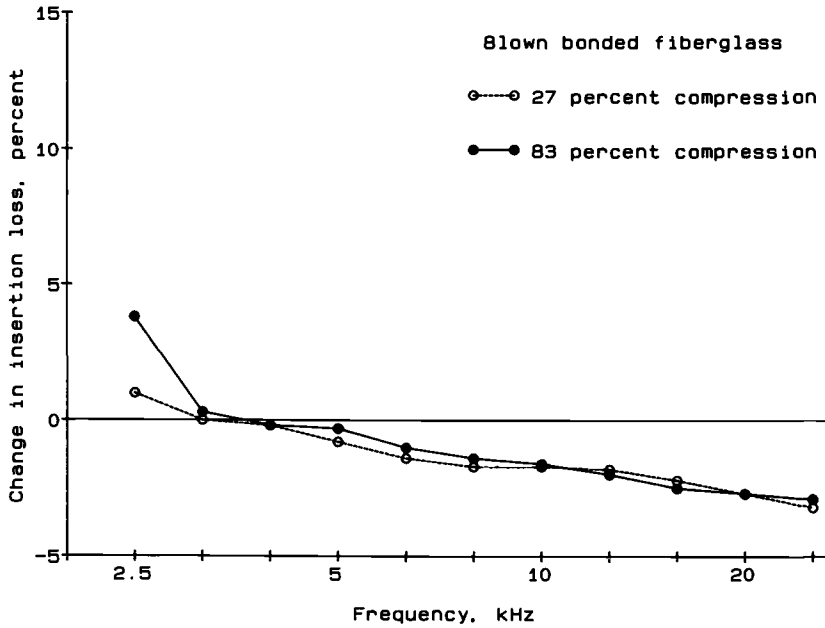


FIG. 12—Percentage change in insertion loss, plotted versus sound frequency, due to compressing a blown bonded fiberglass sample to two different thicknesses.

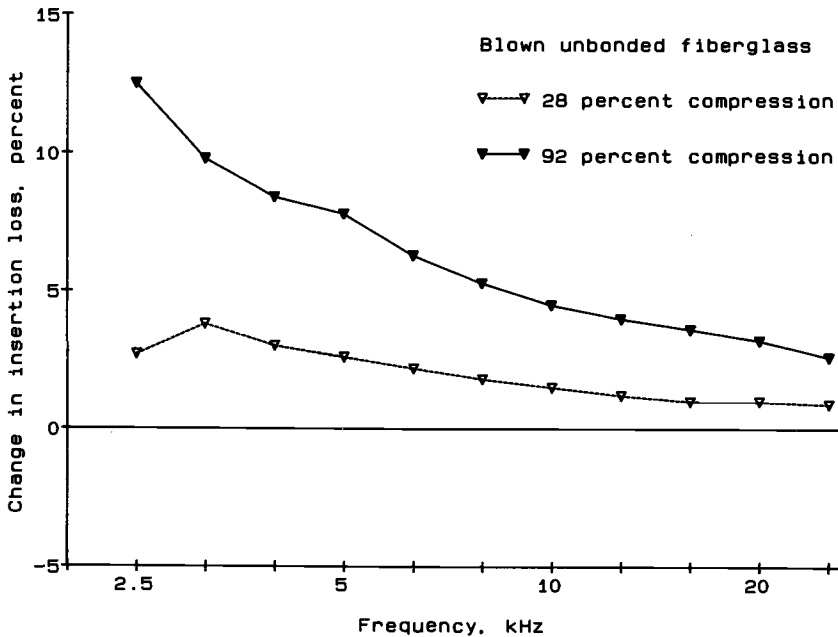


FIG. 13—Percentage change in insertion loss, plotted versus sound frequency, due to compressing a blown unbonded fiberglass sample to two different thicknesses.

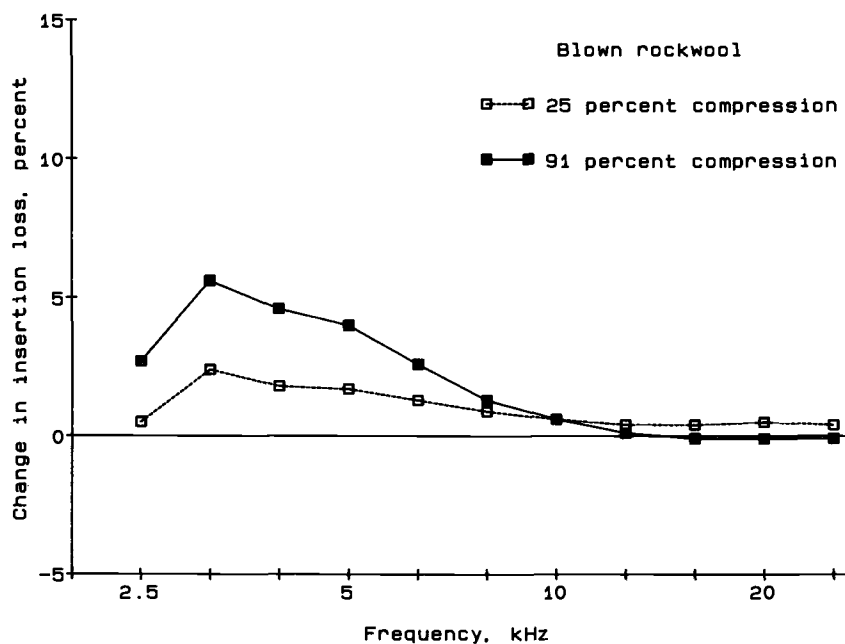


FIG. 14—Percentage change in insertion loss, plotted versus sound frequency, due to compressing a blown rockwool sample to two different thicknesses.

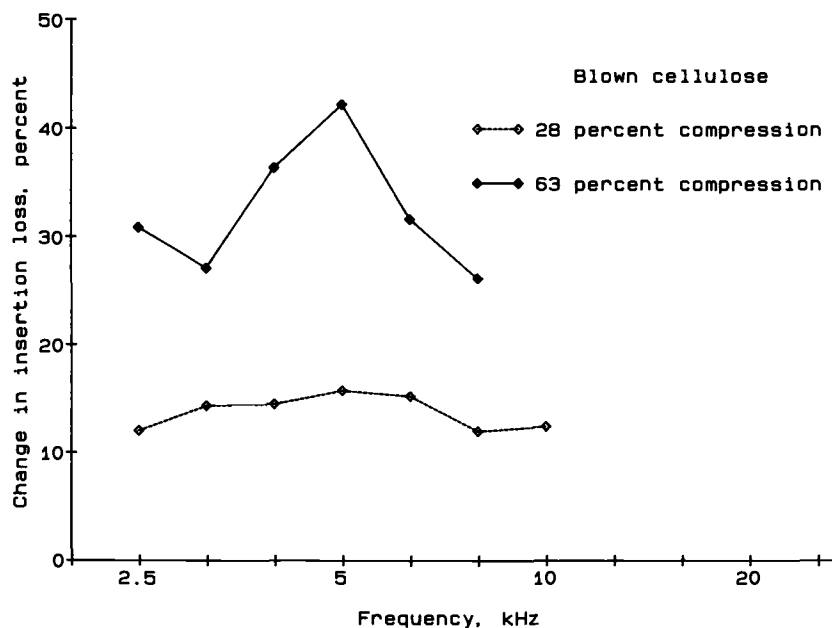


FIG. 15—Percentage change in insertion loss, plotted versus sound frequency, due to compressing a blown cellulose sample to two different thicknesses.

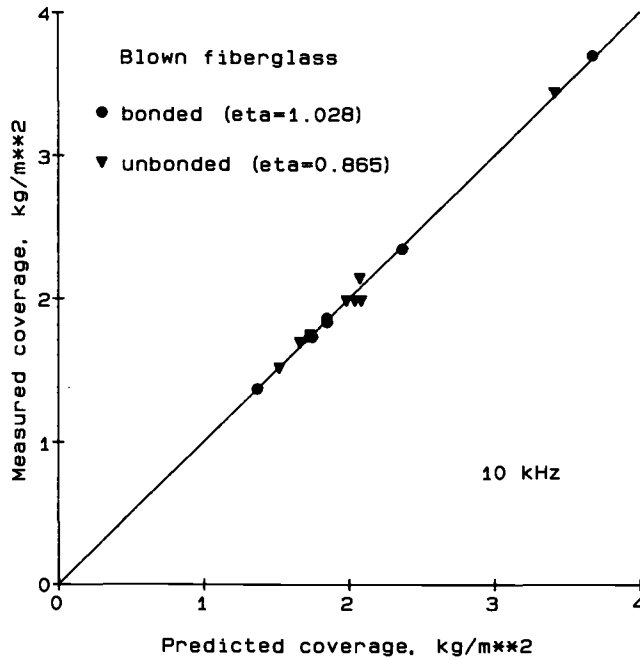


FIG. 16—Measured coverage plotted versus predicted coverage for the blown fiberglass samples, both bonded and unbonded. The prediction equations were of the form of Eq 7 with a fixed value of K but different values of η for the two types of material.

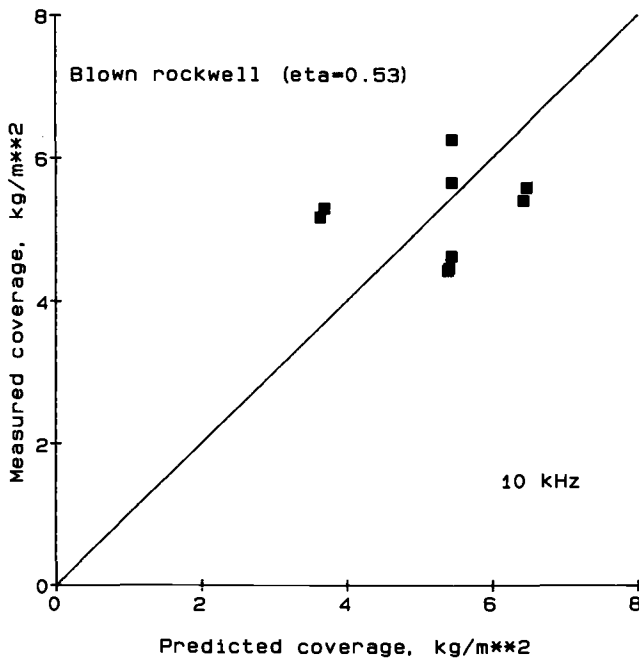


FIG. 17—Measured coverage plotted versus predicted coverage for the blown rockwool samples. The prediction equation was of the form of Eq 7.

results of this curve-fitting attempt are shown in Fig. 18. Clearly there is a marked improvement but at the expense of one more constant to be determined.

For future work of this nature, it is recommended that the value of η be determined directly by compression of a number of samples rather than just one of each material as was done here. It also would be very useful to measure the shot content of each sample after completion of the acoustic tests.

Thermal Resistance

The apparent thermal conductivities at 23.9°C for some samples of the round-robin materials were measured using the NBS 1-m line-heat-source guarded hot plate. The results of these measurements for the blown materials are illustrated in Figs. 19 and 20. The curves shown are of the form of Eq 8 and were fitted to the experimental data, yielding values for the constants A , B , and C . These equations were used to compute the thermal resistance of each acoustic test sample from its measured density and thickness.

As indicated following Eq 9, if the density of the material were constant, the thermal resistance would be simply proportional to the coverage, so that if the density were constant and η equal to unity, the thermal resistance would simply be proportional to the sound insertion loss. The limited usefulness of such a relationship is evidenced by the results shown in Figs. 21 and 22.

Figures 23, 24, and 25 show the thermal resistance (obtained, as described above, from density and thickness) plotted versus the predicted thermal resistance for blown fiberglass, rockwool, and cellulose, respectively. The predicted thermal resistance was obtained from the measured sound insertion loss and thickness using Eq 9, with W obtained by the best method of the previous section, ρ obtained from that value of W divided by the measured sample thickness, and A , B , and C being the values obtained for the curves in Figs. 19 and 20. The predictions are seen to be very good for fiberglass, not bad for cellulose, and only fair for rockwool. The agreement between observation and prediction for rockwool might be better if the density of the material were known exclusive of shot content for both the thermal and the acoustic measurements.

Prospects for Field Use

Based upon the results presented above, the use of sound insertion loss measurements to predict the coverage or the thermal resistance of loose-fill insulations appears promising, particularly for fiberglass materials. The extension of the aforementioned laboratory work to field conditions will be challenging but there do not appear to be any insurmountable difficulties. (It should be noted that regardless of whether a cookie-cutter, a thermal technique, or an acoustic technique is used, variations in installed thickness and coverage will require measurements at a large number of locations in order to achieve statistical reliability.)

Two different approaches appear feasible for using sound or ultrasound for *in situ* evaluation of attic insulation density and depth [4]. One approach, shown in Fig. 26, would be to position a transducer above the insulation and measure the (pulsed) signal that has passed downward through the insulation, reflected from the top of the ceiling, and passed upward through the insulation and back to the transducer. (The source/receiver shown in Fig. 26 could include a parabolic reflector, as used in the present study, or could simply be an extended transducer.) A second approach, illustrated conceptually in Fig. 27, would be to position a transmitter and a receiver a fixed distance apart within the insulation.

The technique of using a vertically oriented system such as depicted in Fig. 26, with the transducer in the attic space operating in a pulse-echo mode, would have the advantage of requiring no penetration holes in the ceiling. It has the disadvantage, however, of requiring access to the attic space, with the probe suspended from a "fishing pole" operated from the access hole or the

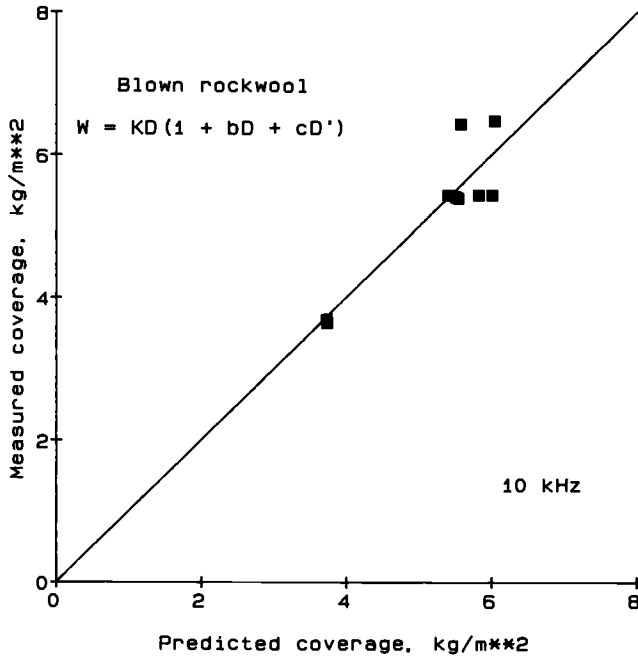


FIG. 18—Measured coverage plotted versus predicted coverage for the blown rockwool samples. The prediction equation is discussed in the text.

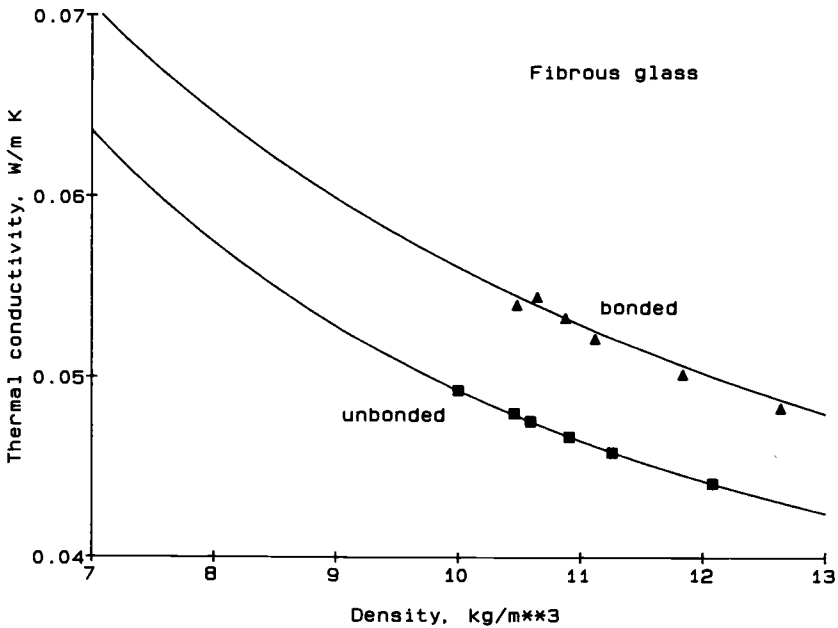


FIG. 19—Thermal conductivity versus installed density for the two types of blown fiberglass material. The data were obtained in the NBS 1-m line-heat-source guarded hot plate. The curves, of the form of Eq 8, were used to estimate, from measured densities, the thermal conductivities of the samples used in the acoustic tests.

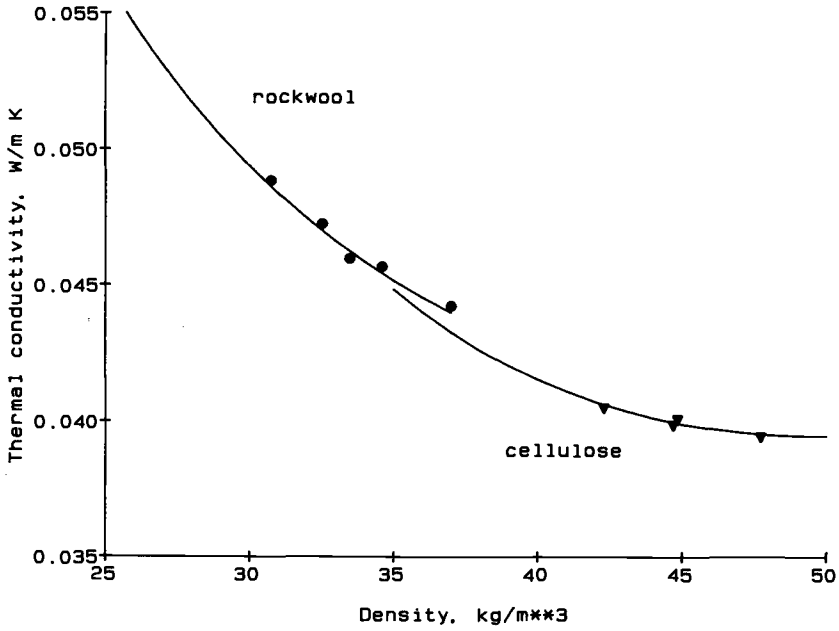


FIG. 20—Thermal conductivity versus installed density for blown rockwool and blown cellulose. The data were obtained in the NBS 1-m line-heat-source guarded hot plate. The curves, of the form of Eq 8, were used to estimate, from measured densities, the thermal conductivities of the samples used in the acoustic tests.

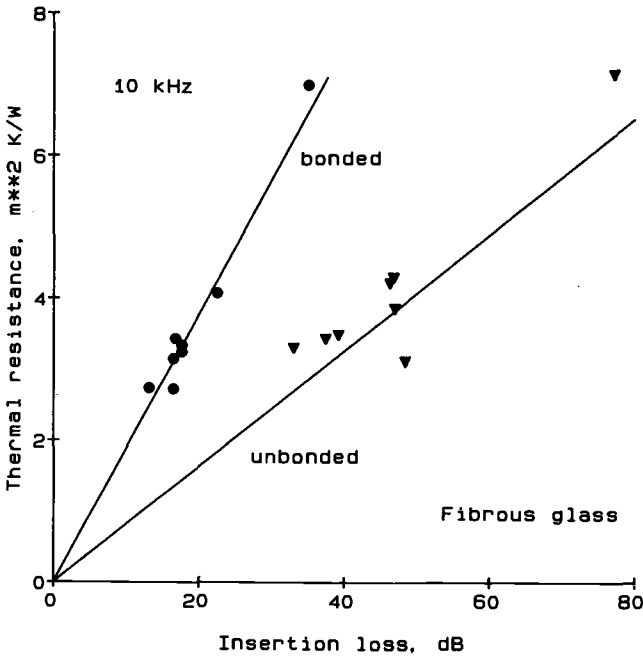


FIG. 21—Thermal resistance versus sound insertion loss, at 10 kHz, for the blown bonded and unbonded fiberglass samples. Each line fitted to the data represents the least-squares straight line passing through the origin.

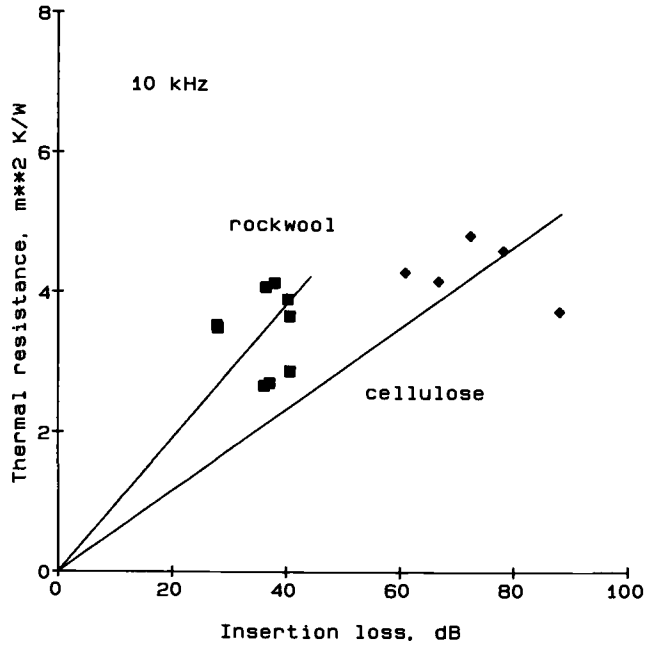


FIG. 22—Thermal resistance versus sound insertion loss, at 10 kHz, for the blown rockwool and cellulose samples. Each line fitted to the data represents the least-squares straight line passing through the origin.

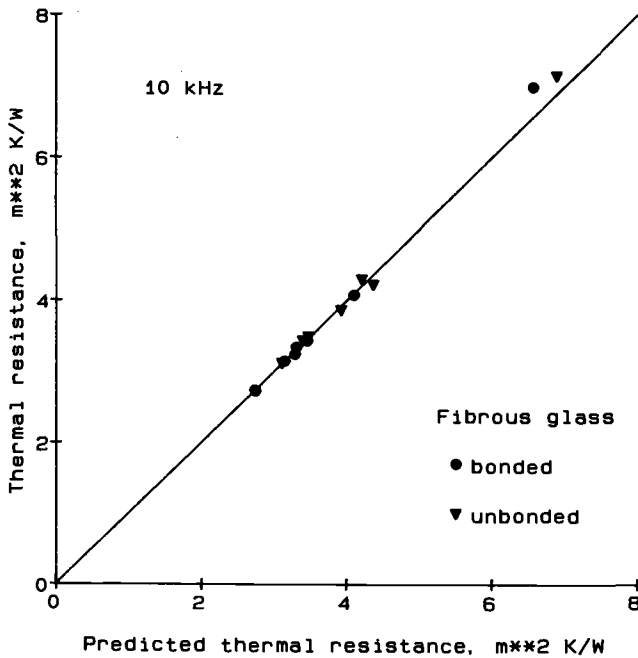


FIG. 23—Thermal resistance computed from density and thickness versus thermal resistance predicted from sound insertion loss and thickness for the blown bonded and unbonded fiberglass samples.

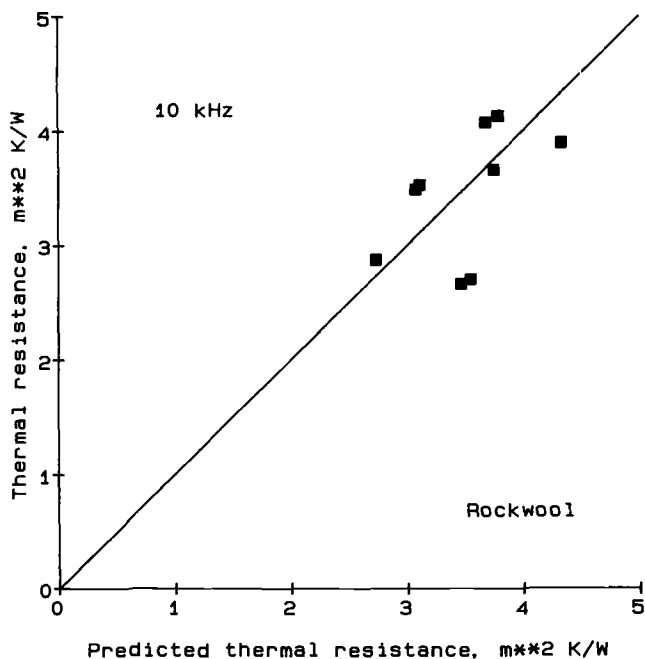


FIG. 24—Thermal resistance computed from density and thickness versus thermal resistance predicted from sound insertion loss and thickness for the blown rockwool samples.

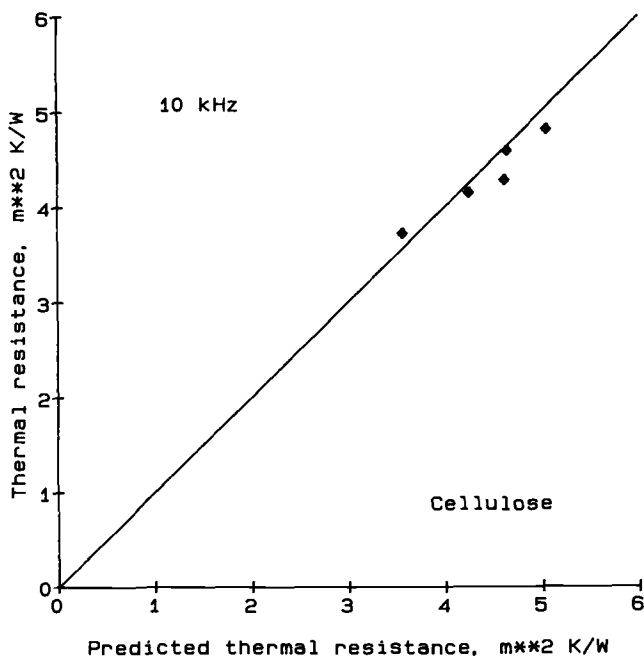


FIG. 25—Thermal resistance computed from density and thickness versus thermal resistance predicted from sound insertion loss and thickness for the blown cellulose samples.

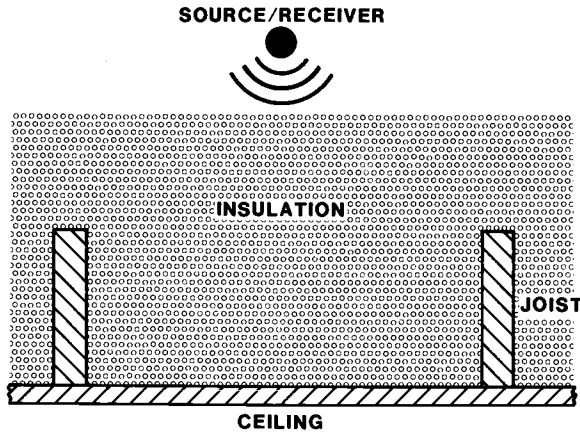


FIG. 26—Experimental configuration for field measurements of the coverage or thermal resistance of blown-in-place attic insulation. A pulse of sound from a transducer above the insulation passes downward through the insulation, reflects off the upper side of the ceiling, and returns through the insulation to the transducer.

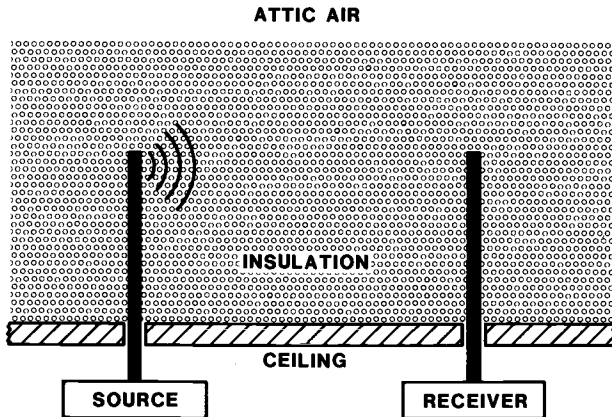


FIG. 27—Experimental configuration for field measurements of the density or thermal conductivity of blown-in-place attic insulation when it is not practical to enter the attic space. A sound source probe and a sound receiving probe are each inserted through small holes in the ceiling, and measurements are made as described in the text.

operator actually entering the attic. A further complication with this technique is the large attenuation associated with the sound passing twice through a large thickness of insulation; this difficulty can be dealt with by using sound of lower frequency than is reported in the present study.

The technique of using two probes inserted through small holes in the ceiling to the same height within the insulation, so that the sound waves travel parallel to the ceiling, has several advantages. It should be possible to determine the insulation depth by monitoring the signal as the probe pair is moved upward through the insulation layer. When the signal matched a pre-calibrated value established for an open air path, the boundary between the upper surface of the

insulation and the attic air would be determined. By measuring the signal as the probes are moved upward through the insulation, the insulation density as a function of elevation (depth) could be determined. This technique would have the disadvantage of requiring that two small holes be drilled through the ceiling at each location where the density profile and the depth of the insulation need to be ascertained. However, these holes would be very small and could easily be repaired upon completion of measurements.

It is important to reiterate the need to know the relationship between sound insertion loss and coverage for the particular material that is installed in an attic. If the insulation is, for example, a virgin glass wool of known origin, it should be possible to use "standard" parameters for that material. For unknown materials, or materials that exhibit considerable variability, the appropriate parameters should be determined for the particular lot of material.

Probably the easiest way to obtain the appropriate parameters, when access to the attic is possible, would be to measure the sound insertion loss at a few locations near the access hole to the attic, both with the insulation at its installed thickness and with the insulation compressed to, say, half its installed thickness. A cookie-cutter and depth gage could then be used to determine the coverage and thickness at the same locations where the acoustical measurements were made. From these data, the parameters K and η in Eq 7 could be obtained for the specific installed insulation.

The acoustic technique could then be used to map the sound insertion loss at a large number of locations in the attic. These data (plus the nominal thickness, since W is only weakly dependent upon ℓ) could then be used to compute the coverage at each location where sound insertion loss was measured. In this way the coverage could be mapped without the destructive effects of taking numerous cookie-cutter samples throughout the attic.

If it is desired to obtain the thermal resistance as well as the coverage, it would be necessary to know the relationship between thermal conductivity and density for the particular type of insulation. Usually such data should be available from the insulation manufacturer.

Acknowledgments

We thank H. G. Woten, President of Unisul Inc., for the loan of the blowing machine; R. S. Graves of Oak Ridge National Laboratory for sharing his experience in the use of the blowing machine; R. D. Adams of Owens Corning Fiberglas Corp. for arranging the availability of the ASTM round-robin materials and for providing us with data on fiber diameters; W. M. Edmunds of Owens Corning Fiberglas Corp. and J. F. Kimpflen of Certain-teed Corp. for arranging to provide guidance on blowing and handling of loose-fill insulations; T. A. Somers of the NIST Center for Building Technology (CBT) for carrying out the thermal conductivity measurements; and R. R. Zarr of CBT for supervising the thermal conductivity measurements and assisting with blowing the test samples.

References

- [1] Delany, M. E. and Bazley, E. N., "Acoustical Properties of Fibrous Absorbent Materials," *Applied Acoustics*, Vol. 3, 1970, pp. 105-116.
- [2] Bies, D. A., "Acoustical Properties of Porous Materials," in *Noise and Vibration Control*, L. L. Beranek, Ed., McGraw-Hill, New York, 1971, pp. 245-269.
- [3] Adams, R. D. and Hust, J. G., this publication, pp. 263-283.
- [4] Blessing, G. V. and Flynn, D. R., "Acoustic Evaluation of Thermal Insulation," U.S. Patent 4,672,851, 16 June 1987.

System Performance Testing

A Dynamic Test Method for Determining Transfer Function Coefficients for a Wall Specimen Using a Calibrated Hot Box

REFERENCE: Burch, D. M., Zarr, R. R., and Licitra, B. A., "A Dynamic Test Method for Determining Transfer Function Coefficients for a Wall Specimen Using a Calibrated Hot Box," *Insulation Materials, Testing, and Applications, ASTM STP 1030*, D. L. McElroy and J. F. Kimpflen, Eds., American Society for Testing and Materials, Philadelphia, 1990, pp. 345–361.

ABSTRACT: This paper describes a dynamic test method for determining transfer function coefficients (TFCs) for a wall specimen using a calibrated hot box (CHB). In this method, a wall specimen is installed between the climatic and metering chambers of a CHB. After a steady specimen heat transfer rate is attained, the air temperature in the climatic chamber is quickly ramped from an initial to a final temperature level in a linear manner. The final temperature level is maintained until a new steady specimen heat transfer rate is attained. The metering chamber is maintained at a steady indoor condition and is used as a calorimeter. The transient heat transfer rate at the inside surface of the wall specimen is determined at hourly time steps from an energy balance of the metering chamber. The poles and residues for a ramp analytical solution are derived by analyzing the measured specimen heat transfer response. The ramp analytical solution is subsequently used to form a triangular pulse from which TFCs are derived.

The dynamic test method was conducted on a masonry wall. Empirical TFCs derived by the test method predicted the diurnal performance of the wall specimen with good agreement. In fact, the results predicted by empirical TFCs tracked the measured results as closely as an analytical model.

KEY WORDS: calibrated hot box, dynamic thermal performance, heat conduction theory, empirical transfer function coefficients

Nomenclature

- A Surface area of specimen, ft² (m²)
- C_p Specific heat of air, Btu/lb · °F (J/kg · K)
- I Exfiltration rate for metering chamber, volume changes/h
- m Slope of ramp function, °F/h (°C/h)
- Q_{bl} Power delivered by the blower, Btu/h (W)
- Q_{box} Heat transfer rate at the inside walls of metering chamber, Btu/h (W)
- Q_c Rate of energy removed by the cooling coil, Btu/h (W)
- Q_{exf} Energy transfer rate due to air exfiltration, Btu/h (W)
- Q_f Final specimen heat transfer rate, Btu/h (W)
- Q_{fl} Flanking heat transfer rate, Btu/h (W)
- Q_h Power delivered by the electric heater, Btu/h (W)
- Q_i Initial specimen heat transfer rate, Btu/h (W)
- Q_{sp} Specimen heat transfer rate, Btu/h (W)
- Q_{stor} Total energy storage rate within the metering chamber, Btu/h (W)

¹National Institute of Standards and Technology, Gaithersburg, MD 20899.

QG	Rate of specimen heat gain, Btu/h (W)
t	Elapsed time, h
TI	Air temperature in metering chamber, °F (°C)
TL	Laboratory air temperature, °F (°C)
TO	Air temperature in climatic chamber, °F (°C)
U	Thermal transmittance, Btu/h · ft ² · °F (W/m ² · K)
V	Decrease in air temperature within climatic chamber, °F (°C)
V_m	Net volume inside the metering chamber, ft ³ (m ³)
y_i	Response factors at outside surface, Btu/h · ft ² · °F (W/m ² · K)
y_{int}	Vertical axis intercept
Y_i	Conduction transfer function coefficients at outside surface, Btu/h · ft ² · °F (W/m ² · K)

Greek Symbols

β_n^2	Poles of ramp solution, h ⁻¹
δ	Duration of ramp, h
Δ	Time interval of analysis, h
γ_n	Residues of ramp solution, h
γ_o	Sum of residues of ramp solution, h
λ	Common ratio
ρ	Density of air, lb/ft ³ (kg/m ³)
v	Transient solution, Btu/h (W)
v_r	Residual transient solution, Btu/h (W)
v_1	First exponential term of transient solution, Btu/h (W)

Introduction

Computer programs are widely used to perform hourly building energy simulation analyses. Building designers, architects, and building owners use these computer programs to size HVAC equipment, to predict peak demands, or to predict annual energy costs. Moreover, such programs are used to minimize annual energy costs by investigating trade-offs in the envelope design, selection of HVAC systems and equipment, and by analyzing various methods of building operation.

The transient heat transfer rate through a building envelope comprises an important portion of the total space heating and cooling loads. The mathematical algorithms of these computer programs predict the transient heat transfer rate through a building envelope by utilizing many simplifying approximations such as the assumption of one-dimensional heat transfer and constant heat transfer properties. Very little research has been conducted to measure the transient heat transfer rate through building envelope constructions and to compare these measurements with predictions using mathematical algorithms. Moreover, some walls are so complex that their dynamic thermal response can not be accurately predicted using analytical heat transfer theory. In this case, the only ways to obtain the dynamic thermal response are to measure it or to use complex numerical analysis methods.

A strong need exists to develop an experimental method for characterizing the dynamic thermal performance of wall systems in the laboratory using calibrated and guarded hot boxes. Such a method would permit the measured thermal response under one set of boundary conditions to be readily extended to different boundary conditions. ASTM is currently exploring the feasibility of developing a dynamic standard test method for calibrated and guarded hot boxes.

Stephenson et al. [1] of the National Research Council (NRC) of Canada have developed a ramp test method for guarded hot boxes (GHB) to determine transfer function coefficients (TFCs) for a wall specimen. In this method, a wall specimen is installed between the climatic

and metering chambers of a GHB. A "slow" ramp excitation function is generated in the climatic chamber. The metering chamber is maintained at an indoor condition and is used as a calorimeter. The transient heat transfer rate at the inside surface of the wall specimen is determined from an energy balance of the metering chamber. The poles and residues for a ramp analytical solution are determined by analyzing the measured specimen heat transfer response. This ramp analytical solution has been successfully analyzed by NRC to yield TFCs.

The National Institute of Standards and Technology (NIST) conducted the NRC "slow" ramp test method on a masonry wall in their calibrated hot box. Experimental difficulties arose due to the fact that the transient portion of the heat transfer response (i.e., the deviation of the measured response from the steady-state response) was very small and was the same order of magnitude as uncertainties in the measured data (± 2 W). This meant that the measured response could not be successfully analyzed to yield meaningful TFCs. The uncertainty in the measured response was believed to be due to random variations in the metering chamber air temperature of $\pm 0.05^\circ\text{F}$ ($\pm 0.03^\circ\text{C}$). The achievement of more precise control in CHBs is believed to be difficult because of the larger amount of interior mass and the presence of a flanking loss.

In an effort to resolve these experimental difficulties, NIST modified the NRC "slow" ramp test method. A "fast" instead of a "slow" ramp excitation function was generated in the climatic chamber. Here the advantage is that the transient portion of the heat transfer response is very large compared with uncertainties in the data. The modified dynamic test method is presented herein.

Description of Calibrated Hot Box

A schematic cross section of the NIST Calibrated Hot Box (CHB) is given in Fig. 1. It consists of three basic components: a metering chamber, a climatic chamber, and a specimen support frame.

The purpose of the climatic chamber is to generate an outdoor condition. It is a five-sided, highly insulated, rectangular enclosure. Air for the climatic chamber is conditioned by an external refrigeration system having a 21 kW electric-resistance heater and a nominal 5.8 ton (21

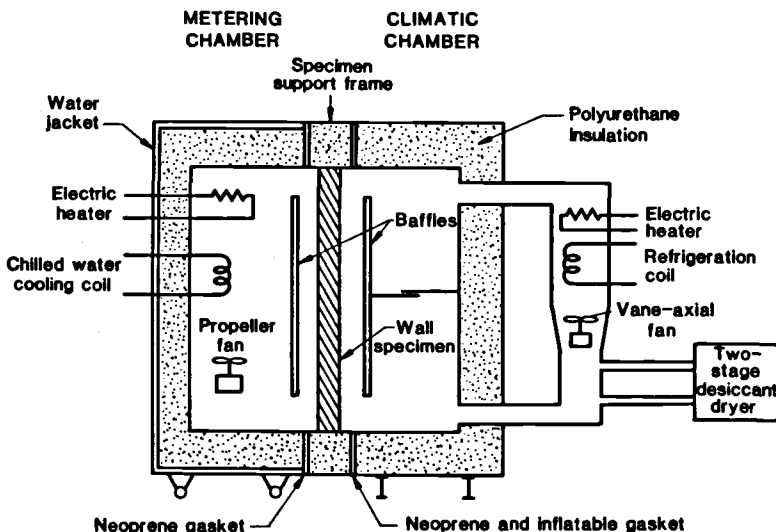


FIG. 1—Schematic cross section of calibrated hot box.

kW) refrigeration system. A portion of this air is diverted to a two-stage, rotating-drum, desiccant dryer that removes water vapor from the air and reduces the accumulation of frost on the refrigeration coil. Air is circulated to the climatic chamber by a vane-axial blower.

The purpose of the metering chamber is to maintain a steady indoor condition and to serve as a calorimeter. An energy balance of the metering chamber is used to determine the heat transfer rate at the inside surface of the wall specimen. Like the climatic chamber, the metering chamber is a five-sided, highly insulated, rectangular enclosure. Its exterior walls are comprised of 15 in. (0.38 m) polyurethane board insulation having a thermal resistance of $R-91 \text{ h} \cdot \text{ft}^2 \cdot \text{F/Btu}$ ($16 \text{ m}^2 \cdot \text{K/W}$). Surrounding the exterior surface of the metering chamber is a uniform-temperature water jacket guard, maintained at the same temperature as the air in the metering chamber.

A wall specimen is mounted in a 10 by 15 ft (3.0 by 4.6 m) support frame and sandwiched between the two aforementioned chambers. The specimen support frame consists of 18 in. (0.46 m) polyurethane board insulation covered with 0.067 in. (1.7 mm) fiberglass reinforced plastic (RFP) skin to provide structural support.

In both the climatic and metering chambers, conditioned air may be delivered to either the top or bottom of vertical plenums formed between a baffle and the opposite sides of the wall specimen. Conditioned air passes through air diffusers (not shown in the schematic cross section of Fig. 1) designed to deliver a uniform air curtain across the wall specimen. The speed of the air moving past the specimen can be varied by changing the rotational speed of the blower or by adjusting the position of the baffle.

For the tests described in the paper, the air speed was adjusted and maintained at 1.1 ft/s (0.34 m/s) in a downward direction at the interior surface and at 2.0 ft/s (0.61 m/s) in an upward direction at the exterior surface of the wall specimen. These air speeds provided a heat transfer coefficient (h_i) of $1.4 \text{ Btu/h} \cdot \text{ft}^2 \cdot ^\circ\text{F}$ ($7.9 \text{ W/m}^2 \cdot \text{K}$) at the inside surface and a value (h_o) of $2.0 \text{ Btu/h} \cdot \text{ft}^2 \cdot ^\circ\text{F}$ ($11.4 \text{ W/m}^2 \cdot \text{K}$) at the outside surface. The tests were carried out in compliance with the requirements of ASTM Test for Thermal Performance of Building Assemblies by Means of a Calibrated Hot Box (C 976) that are pertinent to dynamic testing.

Procedure for Dynamic Testing

This section describes an experimental procedure that uses a calibrated hot box to measure the transient heat transfer rate at the inside surface of a wall specimen. The procedure was originally presented in Ref 2.

For a dynamic test, a wall specimen is installed in the support frame and sandwiched between the climatic and metering chambers (Fig. 2). A time-dependent outdoor condition is generated in the climatic chamber. The air temperature within the metering chamber is maintained at a steady indoor condition by varying the heat output rate of an electric resistance heater within the metering chamber. Control was achieved by a proportional integral and derivative (PID) industrial controller. The temperature of the baffle facing the interior surface of the specimen was not controlled. The heat transfer rate (Q_{sp}) at the interior surface of the specimen is determined at hourly time steps from an energy balance of the metering chamber:

$$Q_{sp} = Q_h + Q_{bl} - Q_{fl} - Q_c - Q_{exf} - Q_{box} - Q_{stor} \quad (1)$$

Note that specimen heat transfer rate is positive under a condition of heat loss.

In Eq 1, all powers, heat transfer rates, and energy-storage rates are averaged over a 1-h period. The terms Q_h , Q_{bl} , Q_c , Q_{exf} , and Q_{box} are measured directly as described in the Instrumentation and Measurement Technique section. The flanking heat transfer rate (Q_{fl}) is predicted using a finite-difference computer program; the total energy storage rate (Q_{stor}) is predicted by a semi-empirical model using transfer function coefficients determined by a series of special calibration tests. The total energy storage rate (Q_{stor}) includes energy storage associated

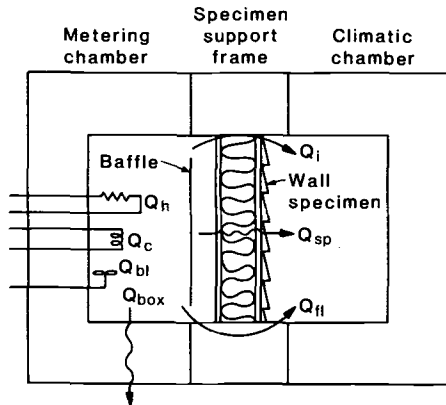


FIG. 2—Energy balance of metering chamber under dynamic conditions.

with the heater, energy storage at interior surfaces and equipment due to fluctuations in air temperature of the metering chamber, and energy storage at the baffle caused by radiation exchange with the wall specimen. The predictions of Q_{fl} and Q_{stor} are described in Ref 2.

This experimental procedure has been shown to provide closure of the energy balance of the metering chamber under dynamic conditions within an uncertainty of 4% [2].

Instrumentation and Measurement Technique

Energy Quantities

The direct current powers delivered to the heater (Q_h) and the blower (Q_{bl}) were determined by taking the product of the voltage and current supplied to each device. The current was obtained by measuring the voltage drop across a precision shunt resistor. The applied voltage was measured using a digital voltmeter that was part of the data acquisition equipment. The measurements of these d-c powers were uncertain by less than 0.1%.

During calibrated hot box tests, the pressure within the climatic chamber is maintained in slight suction with respect to the metering chamber and the laboratory. This prevents air from the climatic chamber from infiltrating into the metering chamber, which would significantly affect the energy balance of the metering chamber. Under test conditions, a small amount of air exfiltrates from the metering chamber into the climatic chamber. Exfiltration rates (I) for the metering chamber were measured using a sulfur-hexafluoride (SF_6) tracer-gas technique described in Ref 3. The energy transfer rate due to exfiltration (Q_{ext}) was determined from the relation:

$$Q_{ext} = \rho \cdot V_m \cdot I \cdot C_p \cdot (T_I - T_L) \quad (2)$$

The exfiltration rate (I) is typically quite small (i.e., less than 0.05 volume changes per hour). In the analysis of the dynamic tests, the exfiltration rate was treated as constant.

The heat transfer rate at the inside walls of the metering chamber (Q_{box}) was measured using an array of 28 heat-flux transducers installed at various locations under the interior RFP skin of the metering chamber. During the dynamic tests, Q_{box} is very small and comprises a small portion of the energy balance.

For the tests presented in this paper, the cooling coil was not operated. Therefore the rate of energy removed by the cooling coil (Q_c) was equal to zero.

Temperature Measurements

The specimen and air temperatures were measured in four vertical planes: the air stream 3 in. (75 mm) in front of the wall specimen in the metering chamber, the interior surface of the wall specimen, the exterior surface of the wall specimen, and the air stream 3 in. (75 mm) to the rear of the wall specimen in the climatic chamber. The two air stream measuring planes were located midway between the baffle and the wall specimen. Each temperature measurement was accomplished using a multi-junction thermopile between grid points in each plane and a uniform-temperature reference junction maintained at a similar temperature as the plane. Each thermopile consisted of 40 thermocouple pairs fabricated from 30-gage, premium-grade, copper-constantan thermocouple wire. The 40 junctions in each plane were arranged in a grid network of equal surface areas; the other 40 junctions were installed in the uniform-temperature reference junction. The temperature of the uniform-temperature reference junction was measured using a precision platinum-resistance thermometer having an uncertainty of $\pm 0.02^{\circ}\text{F}$ ($\pm 0.01\text{ K}$).

The temperature of the baffle in the metering chamber was measured using copper-constantan thermocouples taped to the front and rear surfaces of the baffle. The baffle temperature was taken to be equal to the average of the front and rear surfaces.

Further information on the measurement technique for the CHB is given in Ref 3.

Description of Wall Specimen

A multi-layer masonry wall without thermal bridges and anomalies was used as a wall specimen. Each of the layers consisted of a homogeneous material having known heat transfer properties.

The masonry wall was comprised of 4 in. (0.1 m) thick polystyrene insulation and 5.6 in. (0.14 m) thick solid concrete block having a density of 110 lb/ft^3 (1760 kg/m^3). It was installed in a 24 in. (0.61 m) wide support frame. The thermal conductivity of the polystyrene insulation was independently measured using the NBS Guarded Hot Plate; the thermal conductivity for the concrete block was taken from Ref 4; the thermal resistance for a narrow air space between the polystyrene insulation and the concrete block was determined from a steady-state calibrated-hot-box measurement. The densities of the materials were determined by weighing known volumes of material, and their specific heats were taken from Ref 5. Heat transfer properties for the wall specimen are given in Table 1.

Empirical Transfer Function Coefficients

Excitation Function and Heat Transfer Response

A steady air temperature 30°F (-1.1°C) was initially maintained in the climatic chamber. After a steady-state specimen heat transfer rate was attained, the air temperature in the cli-

TABLE 1—Heat transfer properties for wall specimens.

Material	Thickness, ft	Thermal Conductivity, $\text{Btu/h} \cdot \text{ft} \cdot ^{\circ}\text{F}$	Density, lb/ft^3	Specific Heat, $\text{Btu/lb} \cdot ^{\circ}\text{F}$	Thermal Resistance, $\text{h} \cdot \text{ft}^2 \cdot ^{\circ}\text{F/Btu}$
Concrete block	0.469	0.38	109.9	0.38	1.23
Air space	0.93
Polystyrene insulation	0.331	0.0194	1.51	0.290	17.06

matic chamber was quickly ramped down to a final temperature level of 10.2°F (−12.1°C). This final temperature level was maintained until a new steady-state specimen heat transfer rate was attained. The duration of the ramp (δ) was 0.42 h; the decrease (V) in the temperature level was 19.8°F (11.0°C). The excitation function is shown in Fig. 3a.

The measured specimen heat transfer response for the above excitation function is given in Fig. 3b. The difference between the final (Q_f) and the initial (Q_i) specimen heat transfer rate is equal to the product of the thermal transmittance (U), temperature decrease (V), and the surface area of the wall specimen (A).² Therefore the thermal transmittance of the wall specimen may be determined by the relation:

$$U = (Q_f - Q_i) / V \cdot A \quad (3)$$

From heat transfer theory, the specimen heat transfer rate (Q_{sp}) is given by the relation:

$$Q_{sp} - Q_i = A \cdot U \cdot V \left[1 + \sum_{n=1}^{\infty} \gamma_n \left(\frac{1 - e^{\beta_n^2 \delta}}{\delta} \right) e^{-\beta_n^2 t} \right] \quad (4)$$

The first term ($A \cdot U \cdot V$) is the steady-state solution. The second term is the transient solution (ϑ) labeled in the specimen heat transfer response given in Fig. 3b. The coefficients β_n^2 are the poles for the wall transfer function, and γ_n are the residues for a pure ramp excitation.

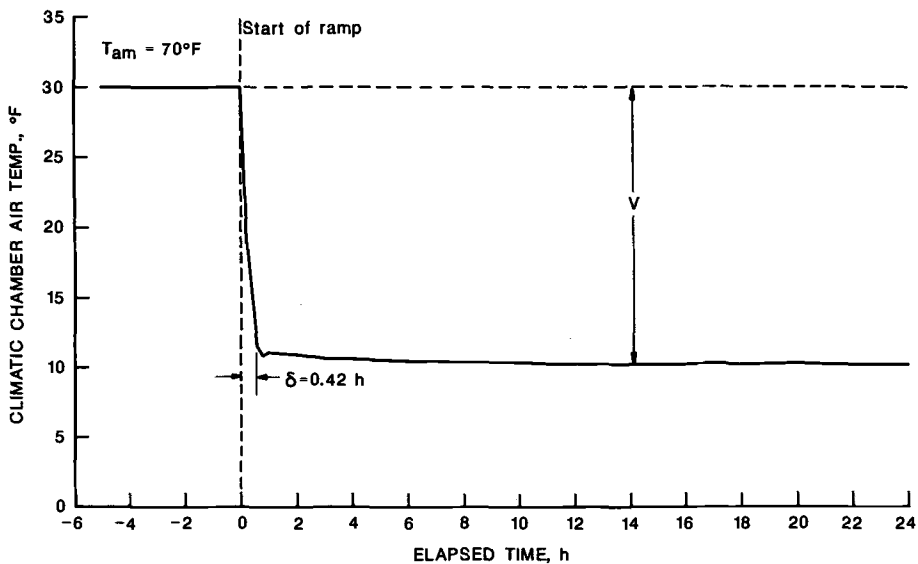


FIG. 3a—Excitation function generated in climatic chamber for fast ramp method.

²This analysis assumes that the air temperature decrease (V) is the driving force for specimen heat transfer response. During a dynamic test, the temperature of the baffles facing the wall specimen may be slightly different than the air temperature. Radiation exchange between the baffle and the wall specimen may cause the driving force for the specimen heat transfer response to be slightly different than the air temperature decrease (V).

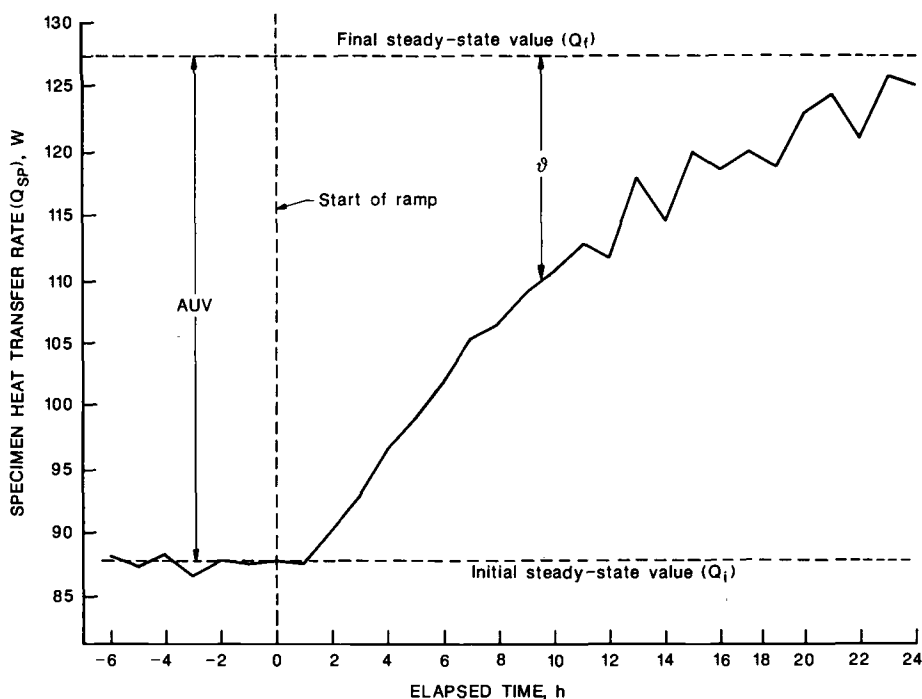


FIG. 3b—Specimen heat transfer response for fast ramp method.

Analysis of Poles and Residues

The transient solution (ϑ) may be expanded

$$\vartheta = A \cdot U \cdot V \left[\gamma_1 \left(\frac{1 - e^{\beta_1^2 \delta}}{\delta} \right) e^{-\beta_1^2 t} + \gamma_2 \left(\frac{1 - e^{\beta_2^2 \delta}}{\delta} \right) e^{-\beta_2^2 t} + \gamma_3 \left(\frac{1 - e^{\beta_3^2 \delta}}{\delta} \right) e^{-\beta_3^2 t} + \dots \right] \quad (5)$$

The second, third, and higher order terms contribute to the transient solution only during an initial period of the transient response. After this initial period, the transient solution becomes

$$\vartheta \approx \vartheta_1 = A \cdot U \cdot V \cdot \gamma_1 \left(\frac{1 - e^{\beta_1^2 \delta}}{\delta} \right) e^{-\beta_1^2 t} \quad \text{for } t \text{ large} \quad (6)$$

Taking the natural logarithm of Eq 6 gives

$$\ln(\vartheta) = \ln \left[A \cdot U \cdot V \cdot \gamma_1 \left(\frac{1 - e^{\beta_1^2 \delta}}{\delta} \right) \right] - \beta_1^2 \cdot t \quad (7)$$

Measured hourly values of $\ln(\vartheta)$ are plotted as a function of elapsed time (t) in Fig. 4a. Note that for t large, $\ln(\vartheta)$ follows a linear relationship. A least squares fit of data along the linear

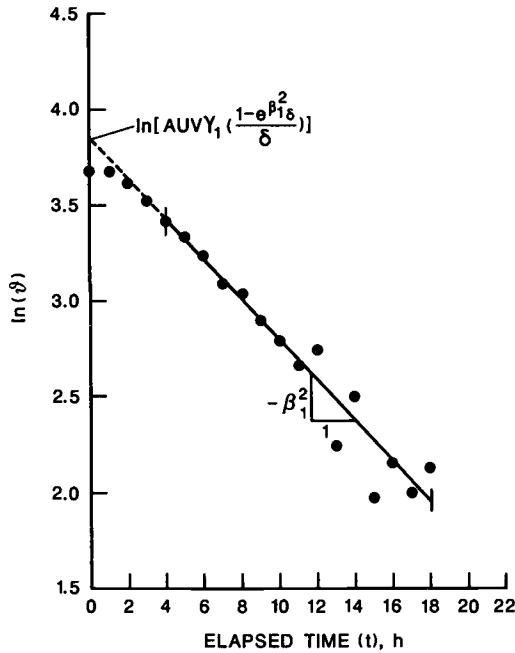


FIG. 4a—First pole and its residue.

portion of the data was obtained. From Eq 7, the slope of this straight line is equal to the first pole ($-\beta_1^2$), and an extrapolation of this line back to $t = 0$ will yield the intercept (y_{int}):

$$y_{\text{int}} = A \cdot U \cdot V \cdot \gamma_1 \left(\frac{1 - e^{\beta_1^2 \delta}}{\delta} \right) \quad (8)$$

The first residue (γ_1) was determined from Eq 8.

After the first pole (β_1^2) and its residue (γ_1) were determined, the first exponential term of Eq 5 was subtracted to give the residual transient solution (ϑ_r), or:

$$\vartheta_r = A \cdot U \cdot V \left[\gamma_2 \left(\frac{1 - e^{\beta_2^2 \delta}}{\delta} \right) e^{-\beta_2^2 t} + \gamma_3 \left(\frac{1 - e^{\beta_3^2 \delta}}{\delta} \right) e^{-\beta_3^2 t} + \dots \right] \quad (9)$$

The residual transient solution (ϑ_r) was analyzed in a similar fashion as ϑ to obtain the second pole (β_2^2) and its residue (γ_2) as shown in Fig. 4b. Insufficient transient data was present in the heat transfer response to permit the above procedure to be repeated a third time to yield a third pole (β_3^2) and its residue (γ_3).

It should be pointed out that uncertainties in the measured heat transfer response cause higher order poles and residues to be less certain than the first pole and its residue. However, the diurnal performance of most wall specimens is largely determined by the first pole and its residue.

The thermal transmittance (U) and the poles (β_n^2) and residues (γ_n) obtained from the above procedure are given in Table 2.

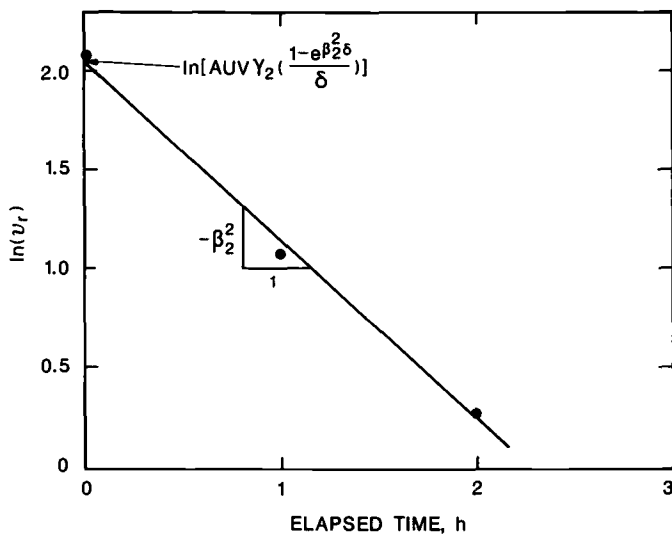


FIG. 4b—Second pole and its residue.

TABLE 2—Summary of poles and residues.

• Thermal transmittance, $U = 0.04912 \text{ Btu/h} \cdot \text{ft}^2 \cdot ^\circ\text{F}$	
• Poles, h^{-1}	
β_1^2	0.1066
β_2^2	0.8960
• Residues, h	
γ_1	11.00
γ_2	-0.1788

Stephenson *et al.* [1] have shown that the poles and residues must also satisfy the relation:

$$\sum_{n=1}^{\infty} \gamma_n \beta_n^2 = 1 \quad (10)$$

This equation is a good check on the validity of the empirical poles and residues. For the results of Table 2, the left-hand side of Eq 10 is equal 1.01, which is very nearly equal to 1.

Procedure for Obtaining Transfer Function Coefficients

From the above thermal transmittance, poles, and residues, the rate of heat gain (QG) at the inside surface of the wall specimen exposed to a ramp excitation function at its outside surface is given by

$$\text{QG} = A \cdot U \cdot m \left[t - \gamma_o + \sum_{n=1}^N \gamma_n e^{-\beta_n^2 t} \right] \quad (11)$$

where m is the slope of the ramp excitation function, and γ_o is the sum of the residues, or:

$$\gamma_o = \sum_{n=1}^N \gamma_n \quad (12)$$

Response factors (y_i) at the outside surface are the values of the rate of heat gain (QG) that occur in response to a positive triangular-pulse excitation function at the outside surface. A triangular-pulse excitation function was formed by summing three ramp functions with proper slope (m) and time delay as shown in Fig. 5a. The hourly values of the specimen heat transfer response factors (y_i), obtained by superimposing three ramp solutions (Eq 11), are plotted in Fig. 5b.

First-order conduction transfer coefficients (Y_i) may be found by the relations:

$$\begin{aligned} Y_o &= y_o \\ Y_i &= y_i - \lambda \cdot y_{i-1} \quad \text{for } i \geq 1 \end{aligned} \quad (13)$$

Here λ is the common ratio defined by the relation:

$$\lambda = e^{-\beta_1^2 \Delta} \quad (14)$$

where β_1^2 is the first pole, and Δ is the time interval for the analysis (i.e., 1 h). First-order transfer function coefficients are plotted in Fig. 5b and are summarized in Table 3.

Note that the first transfer function coefficient at the outside surface is a small negative value. Transfer function theory indicates that this value should be positive. This departure from theory is an artifact of the propagation of experimental uncertainty into the higher order poles and

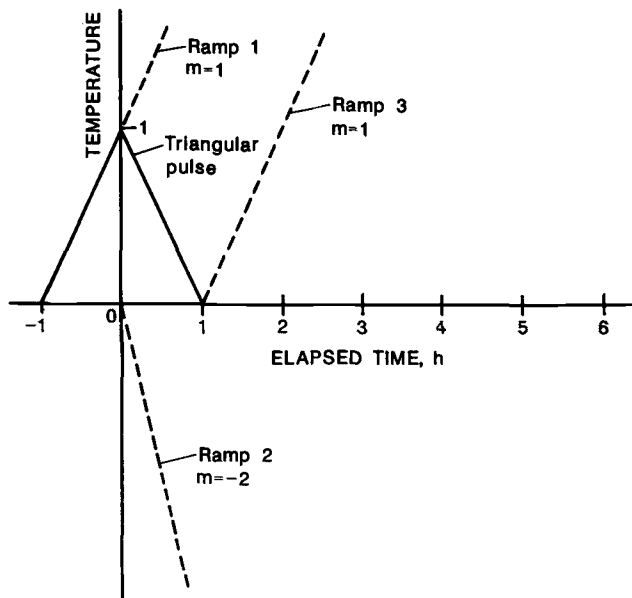


FIG. 5a—Superimposing three pure ramp functions to form a triangular pulse.

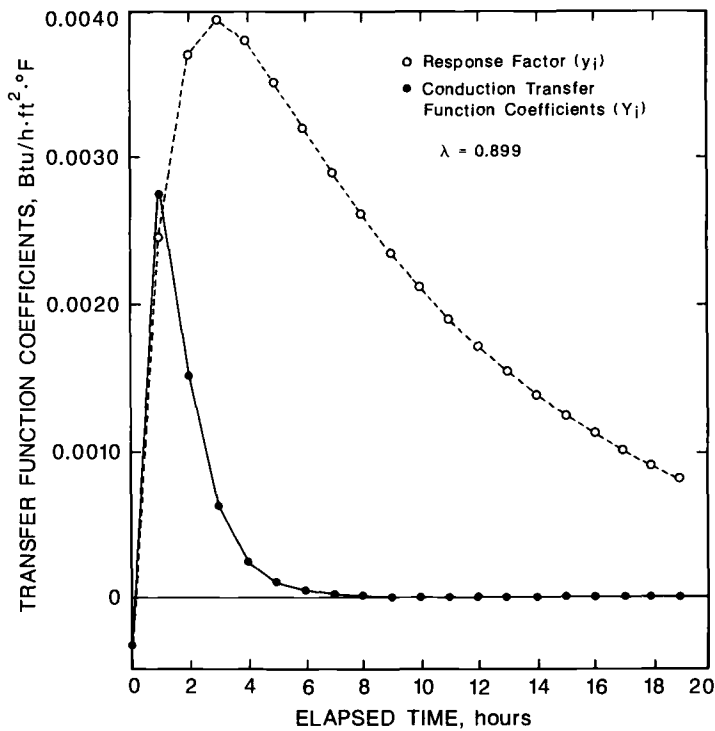


FIG. 5b—Transfer function coefficients as a function of time.

TABLE 3—Empirical TFCs by fast ramp method.^a

Y_0	-0.000332
Y_1	0.002749
Y_2	0.001509
Y_3	0.000617
Y_4	0.000253
Y_5	0.000102
Y_6	0.000041
.	.
.	.
.	.
.	.
.	.

^aThe Y TFCs are in Btu/h · ft² · °F.

residues. However, this experimental uncertainty does not significantly affect the diurnal performance of the wall specimen as shown later in the paper.

Using Empirical TFCS to Predict Heat Transfer Rate for Different Excitation Functions

The TFCs derived above were used in the transfer function equation:

$$\frac{Q_{sp,t}}{A} = U \cdot (1 - \lambda) \cdot T_{i,t} - Y_0 \cdot T_{O,t} - Y_1 \cdot T_{O,t-\Delta} - Y_2 \cdot T_{O,t-2\Delta} - \dots + \lambda \cdot \frac{Q_{sp,t-\Delta}}{A} \quad (15)$$

to predict the dynamic response of the wall specimen to three different excitation functions. The excitation functions included a sol-air diurnal cycle, a four-harmonic diurnal cycle, and a triangular pulse. The four-harmonic diurnal cycle consists of the sum of a fundamental 24-h sine wave and three harmonics each having reduced amplitude. The excitation functions are shown in Figs. 6a to 6c.

The specimen heat transfer rate measured by the CHB, that predicted using the empirical TFCs, and that predicted using an analytical model [6] for each of three dynamic tests are compared in Figs. 7a to 7c.

For each of the dynamic tests, the empirical TFCs successfully predict the specimen heat transfer rate. The maximum root-mean-square (RMS) difference between the measured and empirically predicted results was ± 2.2 W for the four-harmonic diurnal cycle test. Perhaps

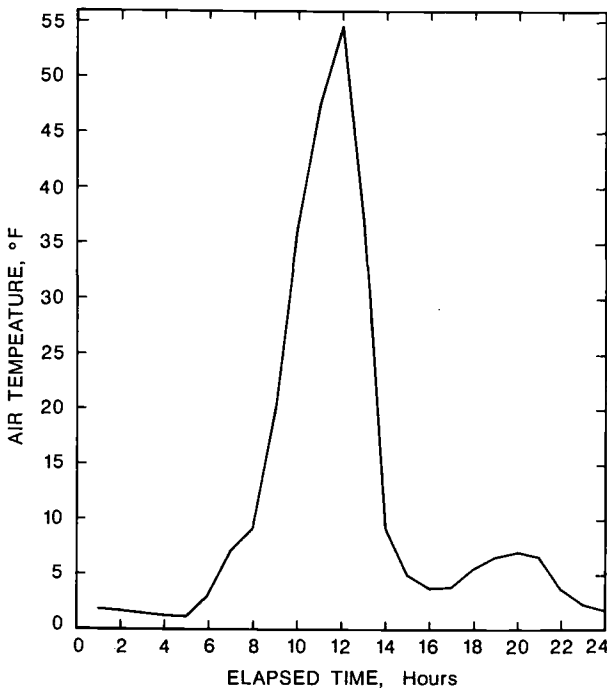


FIG. 6a—Sol-air diurnal cycle.

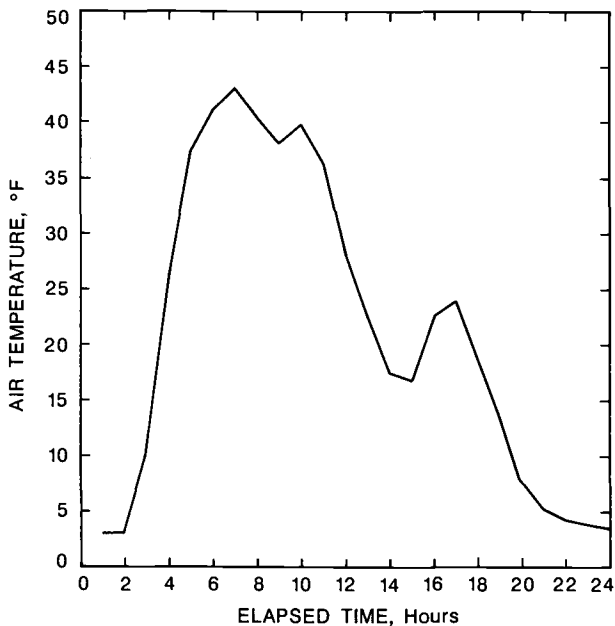


FIG. 6b—Four-harmonic diurnal cycle.

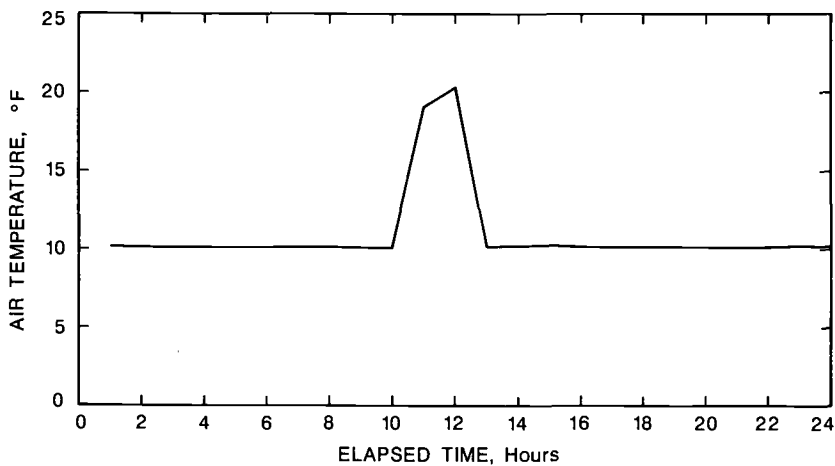


FIG. 6c—Triangular pulse.

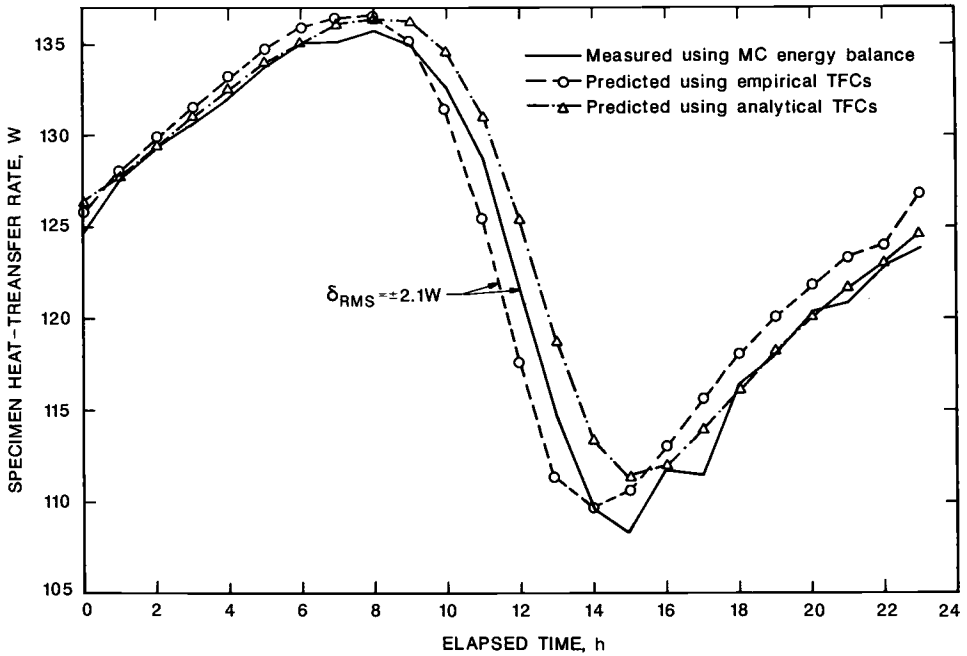


FIG. 7a—Sol-air diurnal cycle test comparison of specimen heat transfer rate measured by CHB, that predicted using empirical TFCs, and that predicted using an analytical model.

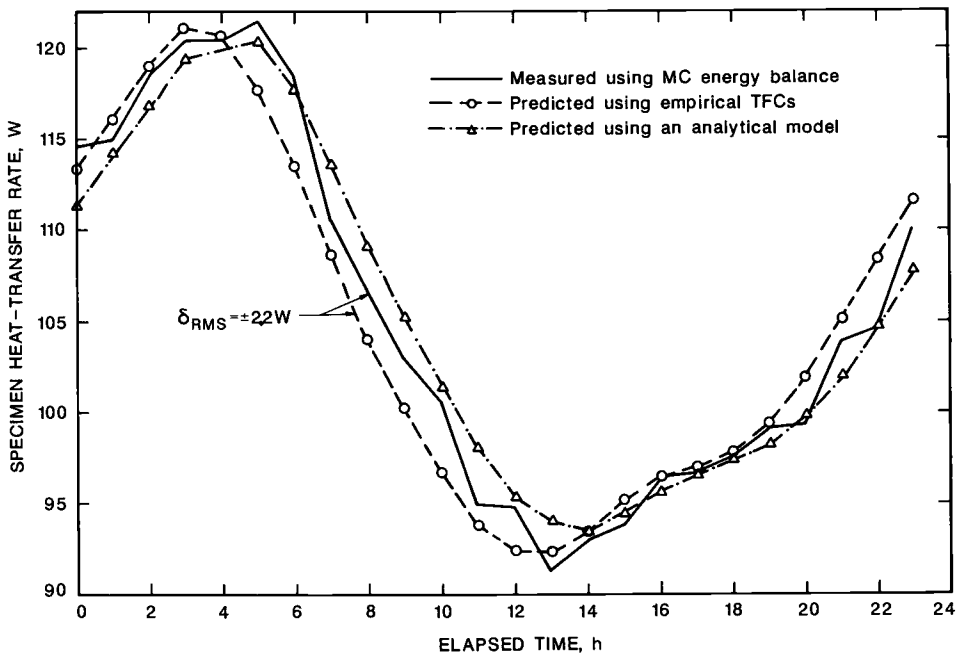


FIG. 7b—Four-harmonic diurnal cycle test comparison of specimen heat transfer rate measured by CHB, that predicted using empirical TFCs, and that predicted using an analytical model.

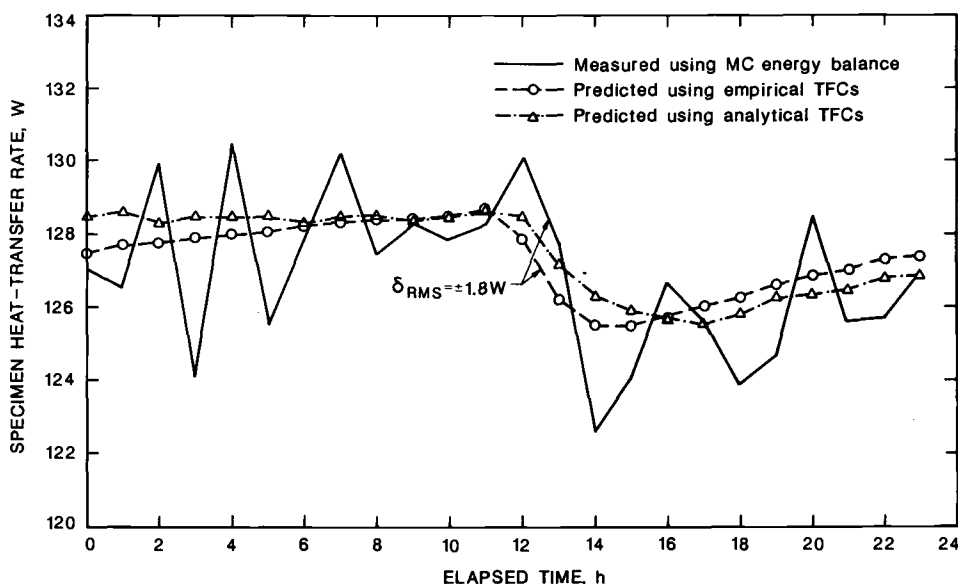


FIG. 7c—Triangular pulse test comparison of specimen heat transfer rate measured by CHB, that predicted using empirical TFCs, and that predicted using an analytical model.

even more interesting, the results predicted by empirical TFCs tracked the measured results as closely as the analytical model. The above agreement is comparable to the agreement achieved by using empirical TFCs derived by a curve fitting method [7].

The agreement was perceived as good in view of the fact that the RMS difference was very close to the measurement uncertainty for the calibrated hot box.

Summary and Conclusions

A dynamic test method was developed for using a calibrated hot box to characterize the dynamic thermal performance of a wall specimen. The method determined empirical transfer function coefficients that predicted with good agreement the diurnal performance of a masonry wall specimen. The results predicted by empirical TFCs tracked the measured results as closely as an analytical model.

Acknowledgments

The authors thank the Department of Energy for sponsoring this research.

References

- [1] Stephenson, D. G., Ouyand, K., and Brown, W. C., "A Procedure for Deriving Thermal Transfer Functions for Walls from Hot-Box Test Results," Internal Report No. 568, National Research Council Canada, May 1988.
- [2] Burch, D. M., Zarr, R. R., Faison, T. K., Licitra, B. A., and Arnold, C. E., "A Procedure for Measuring the Dynamic Thermal Performance of Wall Specimens Using a Calibrated Hot Box," *ASHRAE Transactions*, Vol. 93, 1987, Part 2.
- [3] Zarr, R. R., Burch, D. M., Faison, T. K., Arnold, C. E., and O'Connell, M. E., "Calibration of the NBS Calibrated Hot Box," *Journal of Testing and Evaluation*, Vol. 15, No. 3, May 1987, pp. 167-177.
- [4] Valore, R. C., Jr., "Calculation of U-Values of Hollow Concrete Masonry," *Concrete International*, Feb. 1980, pp. 40-63.

- [5] *ASHRAE Handbook of Fundamentals*, American Society of Heating, Refrigerating, and Air-Conditioning Engineers, New York, 1985.
- [6] Walton, G. N., "Thermal Analysis Research Program—Reference Manual," NBSIR 83-2655, National Bureau of Standards, Gaithersburg, Md., 1983.
- [7] Burch, D. M., Zarr, R. R., and Licitra, B. A., "A Method for Characterizing the Dynamic Performance of Wall Specimens Using A Calibrated Hot Box," *ASHRAE Transactions*, Vol. 94, 1988, Pt. 1.

DISCUSSION

*Martha G. Van Geem*¹ (*written discussion*)—Is the fast ramp adequate for determining properties of both high and low mass walls? Has NIST tested both high and low mass walls using the fast ramp?

D. M. Burch et al. (*authors' closure*)—NIST has tested only high mass walls using the fast ramp method. However, the fast ramp method should be modified for low mass walls by changing the time interval for data collection and analysis from 1 h to perhaps 15 min.

¹Construction Technology Laboratories, Inc., Skokie, IL 60077.

Thermal Resistances of Metal Frame Wall Constructions Incorporating Various Combinations of Insulating Materials

REFERENCE: Strzepek, W. R., "Thermal Resistances of Metal Frame Wall Constructions Incorporating Various Combinations of Insulating Materials," *Insulation Materials, Testing, and Applications, ASTM STP 1030*, D. L. McElroy and J. F. Kimpflen, Eds., American Society for Testing and Materials, Philadelphia, 1990, pp. 362-377.

ABSTRACT: Series of thermal transmission tests were conducted on large wall specimens, which measured 300 by 400 cm (118 by 157 in.), using a calibrated hot box test apparatus. The wall specimens were constructed with metal framing members and were insulated with various combinations of materials.

Wall constructions were tested with and without batt insulation in the wall cavity in an attempt to determine the effect of the metal framing members on the thermal performance of the batts. In addition, the same wall specimens incorporated either wood fiberboard or extruded, expanded polystyrene (XEPS) foam sheathing to examine the effect of the metal framing members on the thermal performance of the sheathing.

The resistance values for the various wall constructions were measured at four different mean temperatures. The test results indicated that the metal framing members significantly reduced the effectiveness of the batt insulation and, to a lesser extent, the effectiveness of the sheathing. However, the batt insulation installed was slightly undersized in the width dimension and did not fill the entire wall cavity. As a result, the effect of the metal framing members on the thermal performance of the batts could not be accurately determined. R-values were calculated for the metal frame wall constructions using several analytical procedures. Some of the calculated values were in reasonably good agreement with the measured values.

KEY WORDS: building envelope systems, calibrated hot box testing, cellular plastic, full-scale thermal testing, glass fiber insulation, heat transmission, insulation systems, performance of insulation, thermal insulation, thermal resistance

Over the years the building construction industry has taken an increasingly sophisticated approach to the issue of thermal transmission through the building envelope. Presently there is growing interest in the subject of building envelope thermal anomalies (BETAs). A BETA has been defined as a "material or configuration in a building which produces localized excessive heat flows from (or to) the building and a cold (or hot) area on the interior surface of the building" [1]. Similarly a thermal bridge is defined as a type of BETA that is caused solely by heat conduction [1]. Metal framing members certainly satisfy these criteria and therefore can be considered one of the most common types of thermal bridges incorporated in building envelope assemblies.

The impact of highly conductive steel framing elements on heat flow through envelopes has been well recognized. The American Society of Heating, Refrigerating, and Air-Conditioning Engineers (ASHRAE) has published information on heat flow through panels containing metal

¹Senior Development Engineer, Dow Chemical U.S.A., Granville, OH 43023.

in the Fundamentals Volume of the ASHRAE Handbook for many years and has advocated the use of the Zone Method [2] for calculating heat flows through constructions that contain highly conductive materials. Also, several other analytical procedures and numerical methods have been developed recently to investigate BETAs in more detail and with greater accuracy.

In 1983 the National Research Council of Canada published a document on measures for energy conservation in new buildings in which it is stated that thermal resistance values for the insulated portion of a building assembly incorporating metal framing elements should be increased 20% (above standard levels published in the document) to compensate for increased heat flows through these elements [3]. Similarly in the third public review draft of ANSI/IES/ASHRAE Standard 90.1P entitled "Energy Efficient Design of New Buildings Except Low-Rise Residential Buildings," the recommendation is made that for wall sections with metal studs the R-value of the cavity insulation should be discounted by 50% (in many cases) when calculating the total resistance of the envelope assembly [4].

In recent years many research papers and articles have been published on the subject of thermal anomalies in general and thermal bridges in particular. This paper represents an effort to further quantify the impact of metal framing members on thermal transmission through building envelopes. Measurements for four different metal frame wall constructions have been made in the laboratory using a calibrated hot box (CHB) test apparatus. The measurements have been compared with values calculated using several analytical procedures.

Test Apparatus and Experimental Procedure

Test Facility

The test facility and calibrated hot box test apparatus have been described in previous work [5-7]. As shown in Figures 1 and 2, the calibrated hot box was located in a controlled environment room. This room was maintained at the same temperature as the metering chamber. The testing was in compliance with the procedures and guidelines presented in ASTM Test for Thermal Performance of Building Assemblies by Means of a Calibrated Hot Box (C 976).

Test specimens measuring 300 by 400 cm (118 by 157 in.) were constructed in portable frames and instrumented with surface thermocouples in a general assembly area. Frames were transported into the test room and then positioned and sealed between the metering (hot) and climatic (cold) chambers. Temperature-controlled chilled air was circulated through insulated ducts to the climatic chamber from an external refrigeration evaporator coil.

Instrumentation and Control

The primary control system, which was located in the control room adjacent to the calibrated hot box, was used to control or monitor the following test parameters:

- (a) Hot and cold side air temperatures.
- (b) Hot and cold side wall surface temperatures.
- (c) Air infiltration mass flow.
- (d) Hot side relative humidity.
- (e) Energy consumption.

Transducer signals were monitored with a digital voltmeter and interfaced with the computer peripheral where data were collected for processing. Temperatures of both chambers were controlled with three-stage internal electric heaters. A small circulating fan was used to distribute air through the vaned plenum chamber on each side of the test wall and to maintain a uniform air flow along the surfaces of the test wall. As indicated in Fig. 2, the curtain of air flowed in the direction of natural convection, that is, down on the hot side and up on the cold. The high-

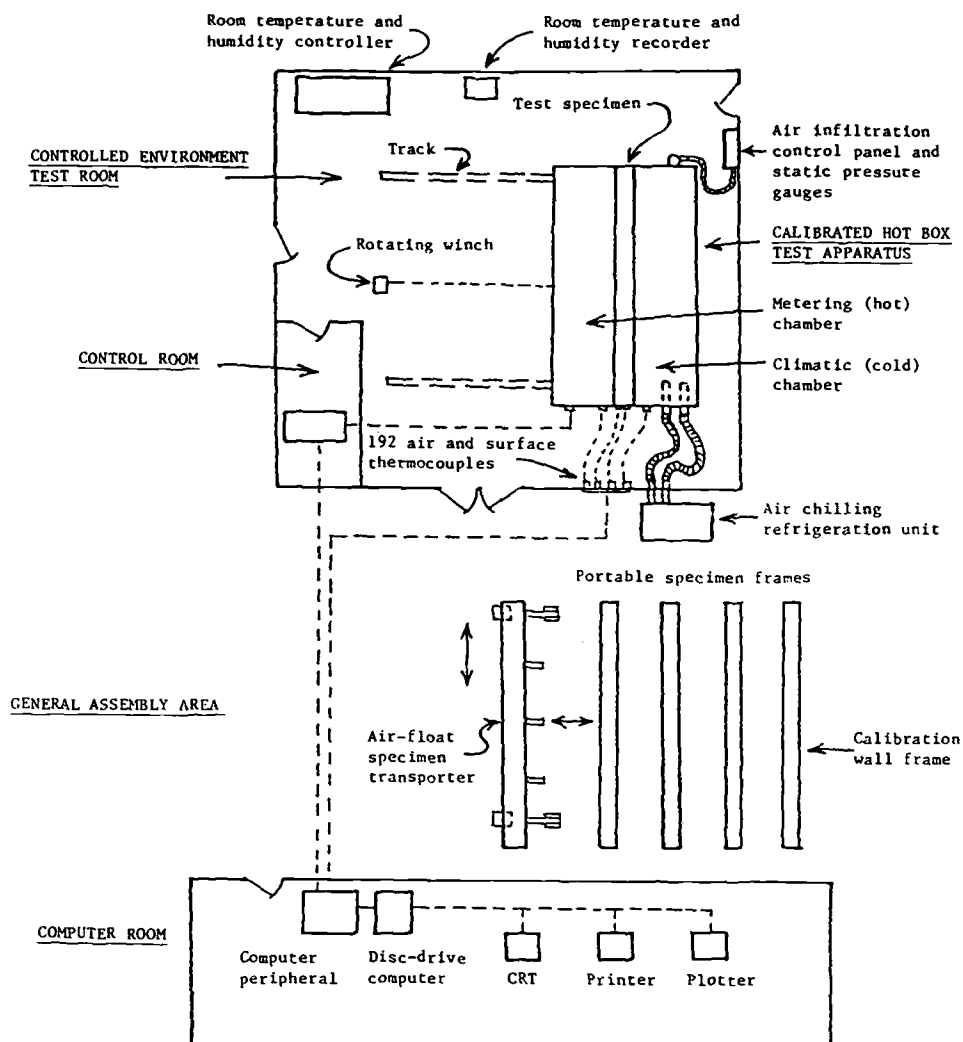


FIG. 1—Diagram of calibrated hot box facility.

emittance plenum panels on each side opposite the test wall were adjustable to control air velocity.

Temperatures were sensed with Type T copper-constantan thermocouples. Two sets of 42 thermocouples were distributed nonuniformly on the surface of the test walls in an effort to obtain representative surface temperatures. The effect that the highly conductive elements within the nonhomogeneous wall constructions could have on surface temperature readings was carefully considered in the placement of the thermocouples. Thermocouples were not placed in direct contact with fasteners. The same thermocouple-installation pattern was mirrored on both wall surfaces. Two sets of 48 thermocouples were uniformly distributed in the air curtains adjacent to the walls. Heat transfer through the metering chamber wall was sensed with nine pairs of differential thermocouples connected in series. The sensing thermocouples were located on the

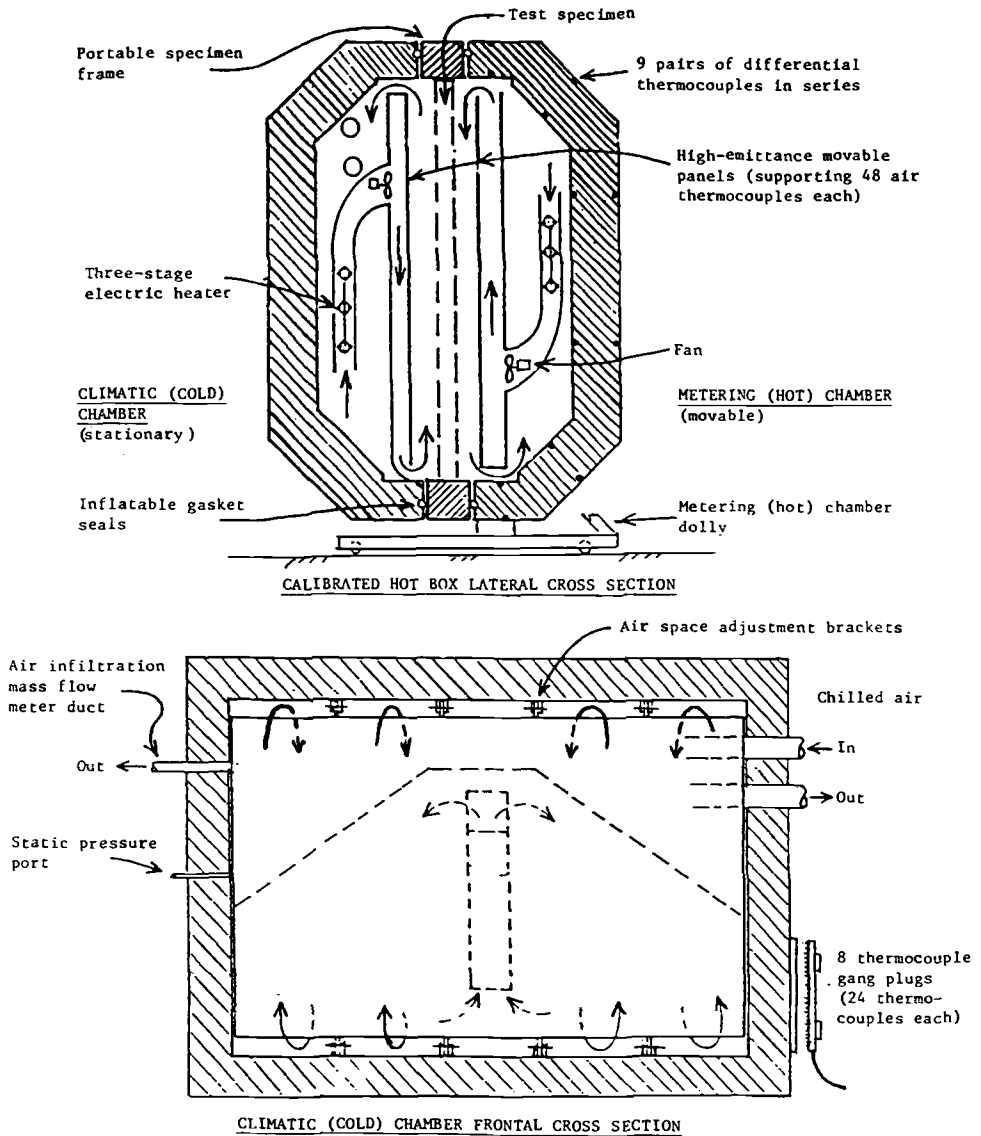


FIG. 2—Cross sections of calibrated hot box test apparatus.

inside and outside wall surfaces of the seven-sided chamber. Energy input to the metering chamber heaters and fan was measured with transducers that produce signals proportional to the watt-hours of energy used. One signal was equivalent to $0.125 \text{ W} \cdot \text{h}$ of energy consumed.

All the test data were collected and stored on magnetic computer disks. All test parameters, including 192 temperature points, were scanned at 15-min intervals and stored as data blocks. Each disk stored 940 data blocks, which was equivalent to 235 h of testing. Block data could be reviewed on a computer monitor or a hard copy could be printed. Computer programs were used to determine the test wall thermal transmission properties.

Metering Chamber Calibration

The metering chamber was calibrated so that the net heat flow through the test wall constructions and the insulated test frame could be determined. The calibration wall consisted of two plies of aged, high-density 2.54-cm (1.00-in.) extruded, expanded polystyrene thermal insulation covered with air-impervious aluminum sheet facings. The facings were painted with a high-emittance black paint.

After establishing a temperature difference across the calibration wall and reaching thermal equilibrium, all internal air and surface temperatures were maintained constant while the temperature outside the box was varied. Total power input to the metering chamber was plotted as a function of thermopile output, E , which reflected the temperature difference across the walls of the metering chamber. The slope of this line was used as the correction factor, M , in the expression

$$Q = Q_t - ME$$

where

Q = net heat flow rate (including flanking heat transfer), W, and

Q_t = total heater and fan input to the metering chamber, W.

Flanking heat transfer was considered to be the heat that did not pass through the metal frame wall constructions or through the walls of the metering chamber but through the insulated test frame.

Test Conditions and Data Reduction

The wall constructions were tested vertically in both heating and cooling modes. In the heating mode the gypsum wallboard interior finish was placed adjacent to the metering chamber, which was maintained at a high temperature relative to the climatic chamber, and the exterior system was positioned opposite the climatic chamber. In the cooling mode the interior finish was placed adjacent to the climatic chamber.

The designed operating temperature ranges for the metering chamber and climatic chamber were 0 to 60°C (32 to 140°F) and 25 to -40°C (77 to -40°F), respectively. In this study data were collected for mean temperatures of -1°C (30°F), 10°C (50°F), 21°C (70°F), and 32°C (90°F). To obtain these wall system mean temperatures, the metering chamber was maintained at temperatures of approximately 21°C (70°F), 21°C (70°F), 32°C (90°F), and 40°C (105°F), respectively; and the climatic chamber was maintained at temperatures of approximately -23°C (-10°F), -1°C (30°F), 10°C (50°F), and 24°C (75°F), respectively. Hence the temperature difference across the test wall specimens varied from 16 to 44 C (30 to 80 F) for the four different mean temperature conditions.

Velocities of the curtains of air that flowed along the surfaces of the test walls were controlled and normally ranged from 0.1 to 0.2 m/s (0.2 to 0.4 mph). The maximum variation in air temperature within both the hot and cold side air curtains was approximately 3 C (5 F). The variation in temperature of the hot or cold side wall surfaces ranged up to 8 C (14 F) for the test wall with the lowest insulation level when measured at a mean temperature of -1°C (30°F), which represented the largest temperature difference used in this study. The mean wall surface temperatures were determined by simply averaging the readings taken at the 42 thermocouple locations on each surface. The air pressure within the metering and climatic chambers was controlled to minimize the pressure differential across the wall constructions. As a result, the measured air infiltration mass flow rates through the wall specimens were negligible in all cases.

Some test parameters scanned at 0.25-h intervals for a 12-h period after a steady-state condition was attained are plotted in Fig. 3 for one of the wall constructions evaluated in this study.

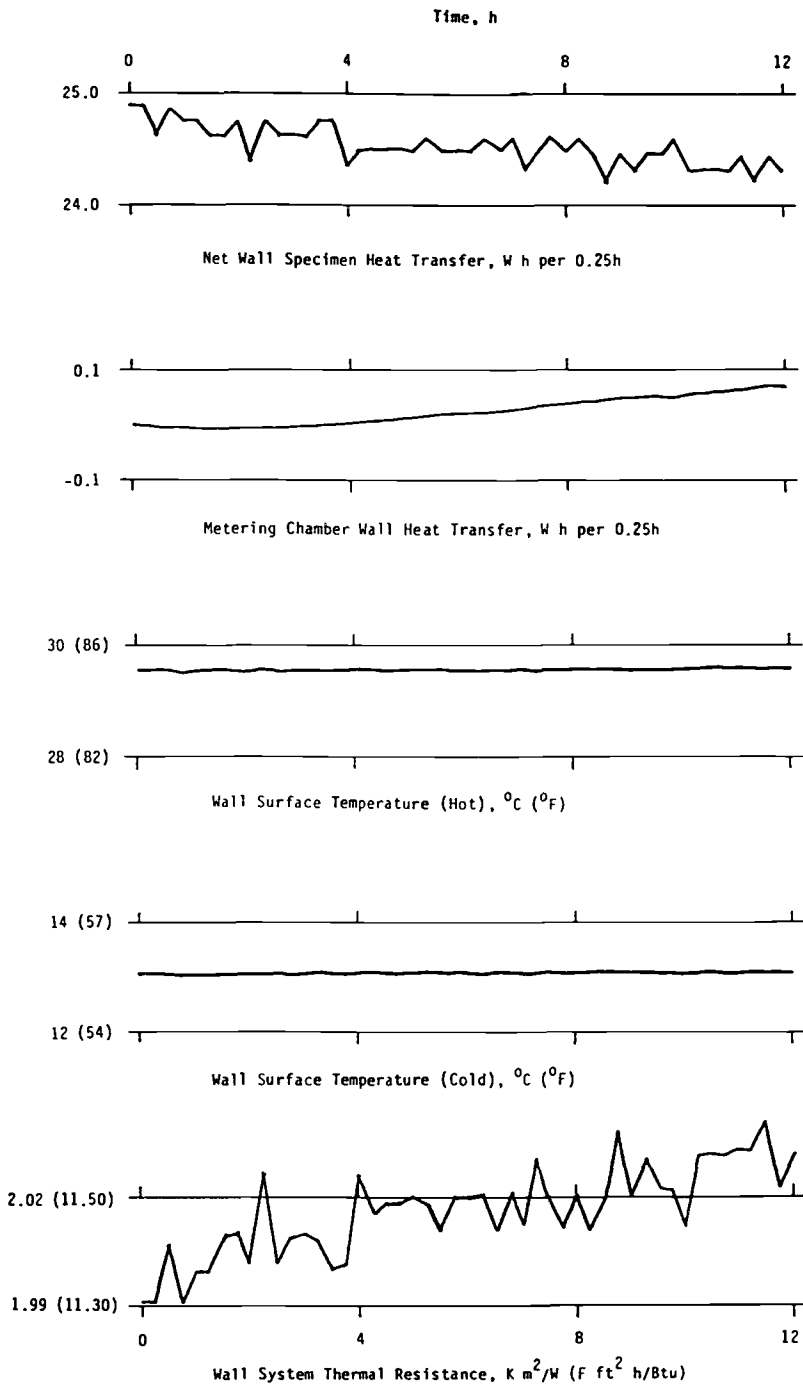


FIG. 3—Calibrated hot box performance parameters for the metal frame wall with XEPS sheathing and mineral fiber cavity insulation measured in the heating mode at a wall system mean temperature of 21°C (70°F).

The maximum percent change in energy transfer during successive 4-h periods was within the 1% tolerance recommended in ASTM C 976. At steady-state conditions the thermal resistance of a particular wall construction was calculated from

$$Q = Q_t - ME$$

$$R = (t_1 - t_2) A/Q$$

where

- Q = net heat flow rate (including flanking heat transfer), W,
- Q_t = total heater and fan input to the metering chamber, W,
- M = thermopile constant for the metering chamber walls (correction factor), W/V,
- E = thermopile output for metering chamber walls, V,
- t_1 = mean temperature of wall surface (hot), K,
- t_2 = mean temperature of wall surface (cold), K,
- A = area of wall construction normal to heat flow, m², and
- R = thermal resistance, K m²/W.

Wall Constructions

The metal frame wall evaluated consisted of steel studs with a gypsum wallboard interior finish and an exterior finish of reinforced stucco. The exterior sheathing was either wood fiberboard or extruded, expanded polystyrene (XEPS) foam sheathing, and the frame wall cavity contained mineral fiber batt insulation or remained empty. Four wall constructions with different combinations of insulating materials were tested. These four constructions are briefly described below:

1. Wood fiberboard sheathing with no cavity insulation.
2. Extruded polystyrene (XEPS) sheathing with no cavity insulation.
3. Wood fiberboard sheathing with mineral fiber cavity insulation.
4. Extruded polystyrene (XEPS) sheathing with mineral fiber cavity insulation.

The basic metal frame wall construction consisted of ten, C-shaped, galvanized steel studs. The studs were 18 gage, which represents a steel thickness of 1.21 mm (0.0478 in.). The Cee studs were approximately 300 cm (118 in.) in length and 9.21 cm (3.62 in.) in depth with 4.13-cm (1.62-in.) knurled flanges and a 1.27-cm (0.50 in.) return lip. The studs also were pre-punched with oval-shaped holes in the depth dimension. The Cee studs were erected vertically on 41-cm (16-in.) centers beginning approximately 15.2 cm (6.0 in.) from the edge of the test frame to minimize flanking heat loss. The studs were mounted in 18-gage, deep-leg, unpunched steel track with a 4.45-cm (1.75-in.) flange. The tracks were attached to the top and bottom of the test frame with a mastic adhesive and the studs were mechanically fastened to the tracks. Two self-tapping screw fasteners were used at each juncture—one on the exterior side of the track and the other on the interior—so a total of four screws was used per stud. The fasteners had diameters of 0.48 cm (0.19 in.) and lengths of 2.54 cm (1.00 in.). No lateral bridging was installed.

The interior finish for all the four wall constructions was nominal 1.27-cm (0.50-in.) gypsum wallboard. The drywall was installed vertically in sheets that measured approximately 122 by 300 cm (48 by 118 in.) and was mechanically attached to the steel studs with drywall screws fastened on roughly 61-cm (24-in.) centers on each stud. The self-tapping drywall screws had diameters of 0.38 cm (0.15 in.) and lengths of 2.54 cm (1.00 in.). The joints in the drywall were covered with a cotton-cloth, vinyl-coated adhesive tape, and the heads of the drywall screws were covered with small pieces of the same adhesive tape.

The exterior finish for all the constructions consisted of a metal-lath-reinforced, cement-based stucco. The stucco finish was applied in three coats for a total nominal thickness of 2.5 cm (1.0 in.). The 3.4 lb (per square yard) (1.9 kg/m²) galvanized, self-furring, expanded metal lath was installed horizontally over the exterior sheathing (which is discussed in the next paragraph) in sheets with nominal dimensions of 68 by 244 cm (27 by 96 in.). The expanded metal lath was installed so that adjacent sheets overlapped approximately 8 cm (3 in.). The metal lath was mechanically attached through the sheathing to the steel studs with self-tapping screws fastened on nominal 20-cm (8-in.) centers on each stud. The fasteners had diameters of 0.48 cm (0.19 in.) and lengths of 3.81 cm (1.50 in.) for wall constructions with wood fiberboard sheathing and 6.35 cm (2.50 in.) for wall constructions with extruded polystyrene (XEPS) foam sheathing.

The combination of insulating materials incorporated in the various wall constructions was varied. For two constructions, nominal 1.27-cm (0.50-in.) wood fiberboard was installed as the exterior sheathing. For the other two constructions, nominal 3.81-cm (1.50-in.) extruded polystyrene (XEPS) foam was used as the exterior sheathing. The products had nominal R-values of 0.23 K m²/W (1.32 F ft² h/Btu) and 1.32 K m²/W (7.50 F ft² h/Btu), respectively. In many geographic areas it is common to use exterior gypsum sheathing in metal frame wall construction either by itself or occasionally in combination with a rigid foam sheathing. In this study exterior gypsum sheathing was not evaluated. The wood fiberboard sheathing was installed vertically in 122 by 244 cm (48 by 96 in.) sheets and was mechanically fastened to the steel studs, using the same screws described in the preceding paragraph, on centers ranging from 30 to 60 cm (12 to 24 in.) on each stud. The extruded polystyrene (XEPS) foam sheathing was installed horizontally in 122 by 244 cm (48 by 96 in.) sheets and was mechanically fastened with the same screws used to attach the lath. Because the XEPS material was so light in weight, only two or three fasteners were used per board.

In two of the wall constructions—that is, one of the walls sheathed with wood fiberboard and one sheathed with XEPS foam—mineral fiber insulation was installed in the frame-wall cavity. In the other two wall constructions the wall cavity remained empty. The kraft-paper-faced batt was approximately 9.20 cm (3.62 in.) in thickness and had a nominal R-value of 2.29 K m²/W (13.0 F ft² h/Btu). The flange of the paper facing was taped to the outside surface of the stud flange. The batt was slightly undersized for the metal stud cavity because it was intended for use in wood frame construction. This is not typical of field practice. As a result, a small, vertical air space (approximately 2.5 cm [1.0 in.] in width) was created at each stud location. Each air space was contained within the open side of the C-shaped stud so that three of the four major surfaces of each air space were defined by the stud. The vertical air spaces represented additional thermal anomalies within the wall system that are not present if proper installation procedures are followed in the field. When changing from one wall construction to another (with the same exterior sheathing), the drywall was removed and the mineral fiber insulation installed. The stucco finish was not removed. Obviously, when the exterior sheathing was replaced, the stucco finish had to be reapplied.

Results

Thermal resistances for the four different metal frame wall constructions tested at three mean temperatures in the heating mode are presented in Table 1. Table 2 gives measured data for the same four wall specimens tested in the cooling mode at two of the same mean temperatures shown in Table 1 and one additional mean temperature. Figure 4 presents graphically the data included in Tables 1 and 2. As mentioned previously, in the heating mode the interior side of the wall specimen was maintained at a higher temperature than the exterior side. In the cooling mode the interior side was maintained at a lower temperature than the exterior. The thermal resistances shown represent surface-to-surface R-values. The values are for the wall only; air film resistances have not been included.

TABLE 1—*Thermal resistances^a of the metal frame wall incorporating various combinations of insulating materials in heating mode.*

Wall Description	Thermal Resistance, K m ² /W (F ft ² h/Btu), at Three Wall System Mean Temperatures		
	−1°C (30°F)	10°C (50°F)	21°C (70°F)
Wood fiberboard sheathing with no cavity insulation	0.49 (2.79)	0.47 (2.67)	0.46 (2.61)
Extruded polystyrene (XEPS) sheathing with no cavity insulation	1.29 (7.33)	1.21 (6.85)	1.16 (6.57)
Wood fiberboard sheathing with mineral fiber cavity insulation ^b	1.48 (8.42)	1.37 (7.79)	1.34 (7.59)
Extruded polystyrene (XEPS) sheathing with mineral fiber cavity insulation ^b	2.26 (12.84)	2.08 (11.82)	2.02 (11.46)

^aThermal resistances shown represent surface-to-surface R-values. Air film resistances are not included.

^bThe mineral fiber insulation installed in the wall cavity was slightly undersized in the width dimension, which is not typical of field practice. As a result, the thermal resistances are lower than values representative of proper installation.

TABLE 2—*Thermal resistances^a of the metal frame wall incorporating various combinations of insulating materials in cooling mode.*

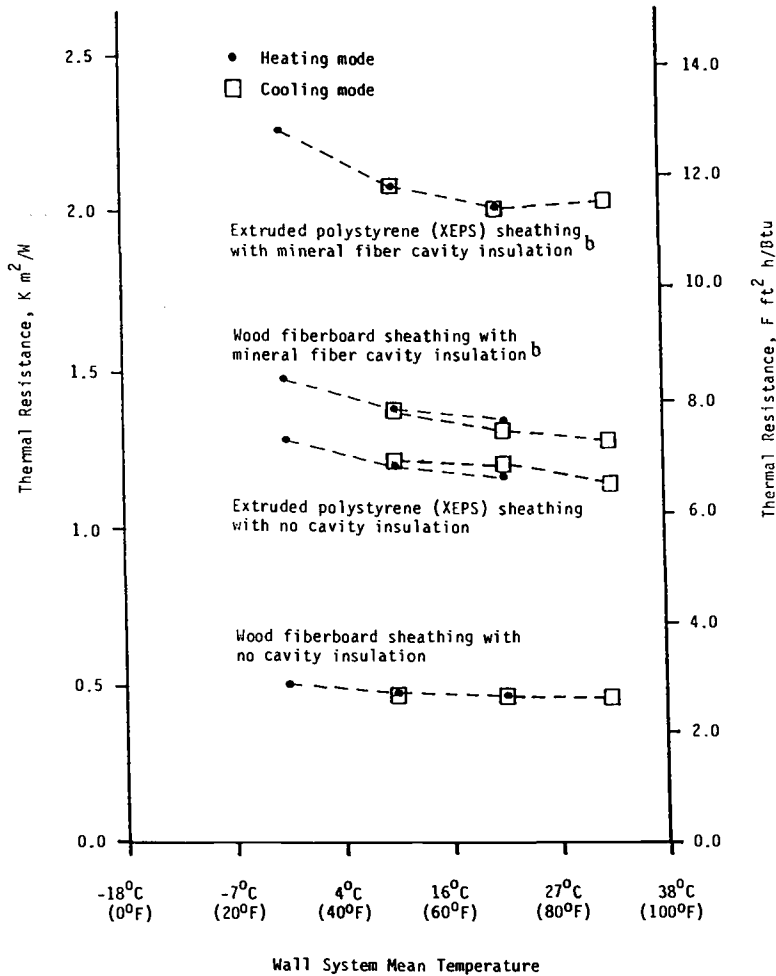
Wall Description	Thermal Resistance, K m ² /W (F ft ² h/Btu), at Three Wall System Mean Temperatures		
	0°C (50°F)	21°C (70°F)	32°C (90°F)
Wood fiberboard sheathing with no cavity insulation	0.46 (2.60)	0.45 (2.53)	0.45 (2.53)
Extruded polystyrene (XEPS) sheathing with no cavity insulation	1.22 (6.95)	1.18 (6.72)	1.14 (6.46)
Wood fiberboard sheathing with mineral fiber cavity insulation ^b	1.36 (7.75)	1.30 (7.37)	1.28 (7.25)
Extruded polystyrene (XEPS) sheathing with mineral fiber cavity insulation ^b	2.08 (11.82)	2.01 (11.41)	2.03 (11.55)

^aThermal resistances shown represent surface-to-surface R-values. Air film resistances are not included.

^bThe mineral fiber insulation installed in the wall cavity was slightly undersized in the width dimension, which is not typical of field practice. As a result, the thermal resistances are lower than values representative of proper installation.

In this study flanking heat transfer was not measured, although the apparent maximum flanking heat transfer was calculated to be less than 4% of the net heat flow rate, Q . Therefore the thermal resistances for the metal frame wall constructions presented in this paper are relative R-values in that comparison of the values indicates the differences in thermal performance between the systems. The R-values shown are not intended to be absolute values, since flanking heat transfer and measurement error associated with the test apparatus have not been included. The author feels that the relative thermal resistances presented are within 5% of the absolute R-values, but no data are included to substantiate this statement.

As expected the presence of the highly conductive metal framing members had a significant impact on the thermal performance of the wall specimens evaluated. The consequent reduction



^aThermal resistances shown represent surface-to-surface R-values. Air film resistances are not included.

^bThe mineral fiber insulation installed in the wall cavity was slightly undersized in the width dimension, which is not typical of field practice. As a result, the thermal resistances are lower than values representative of proper installation.

FIG. 4—Thermal resistance^a versus mean temperature for the metal frame wall incorporating various combinations of insulating materials in heating and cooling modes.

in thermal resistance was especially great for those wall constructions with high levels of insulation, whether the insulation was installed in the frame-wall cavity or as sheathing. The difference in R-values for the fiberboard-sheathed wall specimens with and without cavity insulation was only $0.88 K m^2/W$ ($4.98 F ft^2 h/Btu$) when tested in the heating mode at a mean temperature of $21^{\circ}C$ ($70^{\circ}F$). A difference of $0.86 K m^2/W$ ($4.89 F ft^2 h/Btu$) was observed for the foamed-sheathed specimens. There was a small air space adjacent to each stud (due to the use

of undersized batts), which is not present if proper installation practices are followed. The vertical air spaces made the BETA even more severe. Therefore the measured thermal resistances for the wall systems with batt insulations are lower than values representative of proper installation.

Similarly the differences in results for the specimens sheathed with wood fiberboard and extruded polystyrene (XEPS) foam were $0.70 \text{ K m}^2/\text{W}$ ($3.96 \text{ F ft}^2 \text{ h/Btu}$) with no cavity insulation and $0.68 \text{ K m}^2/\text{W}$ ($3.87 \text{ F ft}^2 \text{ h/Btu}$) with cavity insulation when measured in the heating mode at a 21°C (70°F) mean temperature. The large number of mechanical fasteners that were used to secure the expanded metal lath appeared to significantly reduce the effectiveness of the foam sheathing.

Hence for these specimens the apparent insulating value of the mineral fiber cavity insulation as installed in these test walls was approximately 40% of the estimated value based on published literature. The difference between the measured and estimated values was attributed to the steel studs and small vertical air spaces adjacent to the cavity insulation. Similarly, the effectiveness of the XEPS sheathing as installed in these wall constructions was roughly 60% of the estimated value based on published literature. In this case, the reduction in performance was due primarily to the mechanical fasteners used to secure the lath.

The thermal effect of the metal studs cannot be separated quantitatively from that of the vertical air spaces without some difficulty, and research has shown that the effect of air spaces on the thermal performance of insulation installed in wall cavities can be significant [8–10]. The work reported in Refs 8, 9, and 10, however, was based on wall constructions incorporating wood framing members. Vertical air spaces contained within metal studs similar to the spaces considered in this study were not specifically examined.

Data reported by Tye et al. [9] indicate that the reduction in thermal performance of the cavity insulation in wood frame walls due to air spaces of the size described in this paper could be as great as 30%. However, it is likely that air spaces within metal studs exhibit reduced convective flow compared with spaces of similar size and configuration in wood stud construction. Bankvall [11] has indicated that the conductive properties of the surfaces bounding air spaces can have an impact on convective air movement. Because of the impact of the highly conductive metal studs, it is likely that the temperature variation throughout the air spaces contained within the metal studs was reduced compared with similar air spaces in wood frame construction. Consequently, it is likely that convective heat transfer was reduced and the thermal anomaly mitigated to some degree.

Other researchers have measured metal stud wall constructions containing properly installed mineral fiber cavity insulation. Zarling et al. [12] tested two sets of frame walls: one set was constructed with metal framing and the other with wood framing. The metal frame walls consisted of 15.24-cm (6.00-in.) metal studs on 61-cm (24-in.) centers, and the wood frame walls consisted of 13.97-cm (5.50-in.) wood studs also on 61-cm (24-in.) centers. Each set included two test wall constructions. All walls were sheathed with 1.27-cm (0.50-in.) plywood, but for one wall in each set 5.08-cm (2.00-in.) extruded polystyrene foam insulation was installed over the plywood and covered with a second layer of 1.27 cm (0.50-in.) plywood. Fiberglass batt insulation was installed in the cavities of all four walls. In all cases the interior surface consisted of 0.95-cm (0.38-in.) plywood and a 0.15-mm (6-mil) polyethylene vapor retarder. The exterior surface was 1.59-cm (0.62-in.) textured plywood siding installed over nominal 15-lb (per 100 ft²) (0.73-kg/m²) roofing felt.

For the walls sheathed with plywood only, the surface-to-surface R-values (which do not include air films) were $3.05 \text{ K m}^2/\text{W}$ ($17.33 \text{ F ft}^2 \text{ h/Btu}$) for the wood frame wall and $2.04 \text{ K m}^2/\text{W}$ ($11.60 \text{ F ft}^2 \text{ h/Btu}$) for the metal frame wall when measured at a mean temperature of -7°C (20°F). The difference in R-value was $1.01 \text{ K m}^2/\text{W}$ ($5.73 \text{ F ft}^2 \text{ h/Btu}$). For walls sheathed with extruded polystyrene foam insulation and plywood, the surface-to-surface R-values measured at a mean temperature of -7°C (20°F) were $4.52 \text{ K m}^2/\text{W}$ ($25.70 \text{ F ft}^2 \text{ h/Btu}$) for the wood frame

wall and $3.77 \text{ K m}^2/\text{W}$ ($21.40 \text{ F ft}^2 \text{ h/Btu}$) for the metal frame wall. The difference in R-value was $0.75 \text{ K m}^2/\text{W}$ ($4.30 \text{ F ft}^2 \text{ h/Btu}$). Hence it is clear that the metal framing had a significantly greater impact on thermal performance than the wood framing.

In addition, Larson [13] measured the thermal resistance of a metal-frame wall consisting of 8.89-cm (3.50-in.) metal studs on 41-cm (16-in.) centers sheathed on both sides with 1.27-cm (0.50-in.) gypsum wallboard. The wall cavities were filled with foil-faced fiberglass batt insulation. The average surface-to-surface R-value reported for this wall was $1.16 \text{ K m}^2/\text{W}$ ($6.61 \text{ F ft}^2 \text{ h/Btu}$) when measured at a mean temperature of approximately 38°C (100°F). Again, the impact of metal studs is significant even in constructions where typical installation practices are followed.

In the study discussed in this paper, the thermal resistances for all the wall constructions were greater when tested at lower mean temperatures, as expected. This trend was more prominent in the wall specimens incorporating XEPS sheathing, which was anticipated because of the strong relationship between R-value and temperature that is characteristic of this material. Also, the values measured in the heating and cooling modes at the same mean temperatures agreed reasonably well. Conceivably the R-values obtained for the specimens incorporating extruded polystyrene foam sheathing in the cooling mode should have been slightly lower than those measured in the heating mode, especially in the case where cavity insulation was present, because the mean temperature of the foam would have been greater. However, this was not observed.

In addition, thermal resistances for the four different metal frame wall specimens were calculated using four analytical procedures. A wall system mean temperature of 21°C (70°F) was assumed. The results of these calculations are presented in Table 3. In the calculations nominal R-values of $0.035 \text{ K m}^2/\text{W}$ ($0.20 \text{ F ft}^2 \text{ h/Btu}$) and $0.079 \text{ K m}^2/\text{W}$ ($0.45 \text{ F ft}^2 \text{ h/Btu}$) were assumed for the stucco exterior finish and gypsum wallboard interior finish, respectively. Air film resistances were not included. Two of the calculations were based on the isothermal planes method. In one calculation the framing members were not considered, and in the second the steel studs were included using an approach suggested by Harold A. Trethowen of the Building Research Association of New Zealand (BRANZ).

In the Branz approach the area affected by the framing is assumed to be limited to the width of the stud flange. The R-value of the steel stud is determined as follows: (1) the width of the flange is divided by the thickness of the steel; (2) the R-value per inch of the steel is multiplied by the depth of the stud; and the two quantities defined in (1) and (2) are multiplied together. For this study the quantity defined by the R-value per inch of the steel multiplied by the stud depth was assumed to be $0.0021 \text{ K m}^2/\text{W}$ ($0.012 \text{ F ft}^2 \text{ h/Btu}$), and the calculated R-value of the thermal bridge was $0.072 \text{ K m}^2/\text{W}$ ($0.41 \text{ F ft}^2 \text{ h/Btu}$).

The parallel flow method used was based on the guidelines presented in the ISO Standard on Thermal Insulation – Calculation Methods – Part 2: Thermal Bridges of Rectangular Sections in Plane Structures (ISO 6946/2-1986 (E)), and wall section type “C” was selected for the analysis. An R-value of $0.0021 \text{ K m}^2/\text{W}$ ($0.012 \text{ F ft}^2 \text{ h/Btu}$) was used to calculate the U-factor for the thermal bridge, U_{TB} . The fourth calculation method used was the ASHRAE Zone Method, which is described in Ref 2.

To assess the accuracy of the various analytical procedures, ratios of measured and calculated thermal resistances were determined. These ratios are given in Table 4. Ratios less than one indicate that the procedure overestimated the measured performance; ratios greater than one indicate that the calculated values were less than the measured values. Without question the greatest source of error in the calculations was associated with the determination of the R-value of the thermal bridge and the size of the affected area. Generally speaking, better results were obtained by attempting to account for the BETA, which was especially true for those constructions with insulation in the frame wall cavity. For these test walls the ASHRAE Zone Method provided results closest to the measured values. However, the accuracy of any technique de-

TABLE 3—*Thermal resistances^a of the metal frame wall incorporating various combinations of insulating materials calculated using several analytical procedures.*

Wall Description	Thermal Resistance, $K \text{ m}^2/W$ ($F \text{ ft}^2 \text{ h/Btu}$)				
	Isothermal Planes Method (Framing Not Included)	Isothermal Planes Method	Parallel Flow Method	ASHRAE Zone Method	Measured Value (Heating Mode)
Wood fiberboard sheathing with no cavity insulation	0.50 (2.87)	0.48 (2.75)	0.48 (2.72)	0.48 (2.75)	0.46 (2.61)
Extruded polystyrene (XEPS) sheathing with no cavity insulation	1.59 (9.05)	1.57 (8.93)	1.57 (8.93)	1.57 (8.93)	1.16 (6.57)
Wood fiberboard sheathing with mineral fiber cavity insulation	2.63 (14.97)	0.81 (4.61)	1.43 (8.13)	1.18 (6.71) ^b	1.34 (7.59) ^b
Extruded polystyrene (XEPS) sheathing with mineral fiber cavity insulation	3.72 (21.15)	1.90 (10.79)	3.08 (17.51)	2.38 (13.51) ^b	2.02 (11.46) ^b

^aThermal resistances shown represent surface-to-surface R-values. Air film resistances are not included. Thermal resistances are for a wall system mean temperature of 21°C (70°F).

^bThe mineral fiber insulation installed in the wall cavity was slightly undersized in the width dimension, which is not typical of field practice. As a result, the thermal resistances are lower than values representative of proper installation.

TABLE 4—*Ratios of measured and calculated thermal resistances^a of the metal frame wall incorporating various combinations of insulating materials.*

Wall Description	Isothermal Planes Method (Framing Not Included)	Isothermal Planes Method	Parallel Flow Method	ASHRAE Zone Method
Wood fiberboard sheathing with no cavity insulation	0.92	0.95	0.95	0.95
Extruded polystyrene (XEPS) sheathing with no cavity insulation	0.73	0.74	0.74	0.74
Wood fiberboard sheathing with mineral fiber cavity insulation ^b	0.51	1.65	0.93	1.13
Extruded polystyrene (XEPS) sheathing with mineral fiber cavity insulation ^b	0.54	1.06	0.66	0.85

^aThermal resistances are for a wall system mean temperature of 21°C (70°F). Measured values used to determine the ratios are from tests run in the heating mode.

^bThe mineral fiber insulation installed in the wall cavity was slightly undersized in the width dimension, which is not typical field practice. As a result, the thermal resistances are lower than values representative of proper installation.

depends on the thermal and areal values assumed for the thermal bridge. Any of the more sophisticated analytical procedures can be used to generate accurate results, provided sound judgment is used in the selection of the aforementioned key parameters.

Conclusions

The detrimental effect that highly conductive steel framing elements can have on thermal performance of the building envelope is well recognized. The results of this study help to further quantify this effect. Specifically, laboratory measurements made on metal frame wall constructions incorporating various combinations of insulating materials indicate that the apparent insulating value of the mineral fiber cavity insulation as installed in these test walls is approximately 40% of the estimated value based on published literature. The difference between the measured and estimated values is attributed to the steel studs and small vertical air spaces adjacent to the cavity insulation. Similarly the apparent insulating value of the extruded polystyrene (XEPS) foam sheathing as installed is roughly 60% of the estimated value. In this case, the reduction in performance is due primarily to the mechanical fasteners used to secure the lath.

In addition, it can be difficult to calculate accurately the thermal resistance of wall constructions with thermal bridges such as steel studs. For the wall specimens considered in this study the ASHRAE Zone Method provided the best results compared with the other analytical procedures evaluated. However, the accuracy of any technique depends largely on the thermal and areal values assumed for the thermal bridge. Any of the more sophisticated analytical procedures can be used to generate results, provided sound judgment is used in the selection of these key parameters.

Acknowledgments

Daniel C. Kitts and Darrell W. Hollandsworth, both of Dow Chemical U.S.A., deserve special recognition for their efforts in designing the test program, constructing and testing the wall specimens, and collecting the data.

References

- [1] Brownell, D. L., Silvers, J. P., Smith, S. E., and Tye, R. P., "A Survey of Building Envelope Thermal Anomalies and Assessment of Thermal Break Materials for Anomaly Correction," ORNL/Sub/83-70376/1, Oak Ridge National Laboratory, July 1985.
- [2] *ASHRAE Handbook: 1985 Fundamentals Volume*, American Society of Heating, Refrigerating, and Air-Conditioning Engineers, Atlanta, 1985.
- [3] "Measures for Energy Conservation in New Buildings 1983," NRCC No. 22432, National Research Council of Canada, 1983.
- [4] "Energy Efficient Design of New Buildings Except Low-Rise Residential Buildings," ANSI/IES/ASHRAE Third Public Review Draft Standard 90.1P, American Society of Heating, Refrigerating, and Air-Conditioning Engineers, Atlanta, Sept. 1987.
- [5] Palfey, A. J., "Thermal Performance of Low Emittance Building Sheathing," *Journal of Thermal Insulation*, Vol. 3, Jan. 1980, pp. 129-141.
- [6] Contreras, A. G. and Palfey, A. J., "Thermal Resistances of Insulated Brick Veneer Walls with Reflective and Nonreflective Air Spaces," in *Thermal Insulation, Materials, and Systems for Energy Conservation in the '80s*, ASTM STP 789, F. A. Govan, D. M. Greason, and J. D. McAllister, Eds., American Society for Testing and Materials, Philadelphia, 1983, pp. 373-383.
- [7] Strzepek, W. R., "Thermal Resistance of Various Concrete Masonry Wall Constructions Incorporating Rigid Plastic Foam Insulation," in *Thermal Insulation: Materials and Systems*, ASTM STP 922, F. J. Powell and S. L. Matthews, Eds., American Society for Testing and Materials, Philadelphia, 1987, pp. 582-598.
- [8] Bankvall, C. G., "Forced Convection: Practical Thermal Conductivity in an Insulated Structure under the Influence of Workmanship and Wind," in *Thermal Transmission Measurements of Insulation*,

- ASTM STP 660*, R. P. Tye, Ed., American Society for Testing and Materials, Philadelphia, 1978, pp. 409-425.
- [9] Bourne, J. G., Desjarlais, A. O., Spinney, S. I., and Tye, R. P., "The Effective Thermal Performance of an Insulated Standard Stud Wall Containing Air Gaps," in *Proceedings, ASHRAE/DOE-ORNL Conference on Thermal Performance of Exterior Envelopes of Buildings*, ASHRAE SP 28, American Society of Heating, Refrigerating, and Air-conditioning Engineers, Atlanta, 1981, pp. 965-977.
 - [10] Verschoor, J. D. and Vinieratos, E. R., "Influence of Insulation Deficiencies on Heat Loss in Walls and Ceilings," in *Thermal Insulation Performance, ASTM STP 718*, D. L. McElroy and R. R. Tye, Eds., American Society for Testing and Materials, Philadelphia, 1980, pp. 142-159.
 - [11] Bankvall, C. G., "Natural Convective Heat Transfer in Permeable Insulation," in *Thermal Transmission Measurements of Insulation, ASTM STP 660*, R. P. Tye, Ed., American Society for Testing and Materials, Philadelphia, 1978, pp. 73-81.
 - [12] Bell, S. V., Braley, W. A., Strandberg, J. S., and Zarling, J. P., "Thermal Properties of Metal Stud Wall," Report AK-RD-85-05, State of Alaska Department of Transportation and Public Facilities, 1984.
 - [13] Larson, D. C., "Field Measurements of Steady-State Thermal Transfer Properties of Insulation Systems," in *Guarded Hot Plate and Heat Flow Meter Methodology, ASTM STP 879*, C. J. Shirliffe and R. P. Tye, Eds., American Society for Testing and Materials, Philadelphia, 1985, pp. 206-219.

DISCUSSION

*Richard J. Ray*¹ (*written discussion*)—The author reported that the efficiency of the material as stated thermal resistance to the system was 0.41 to 0.42 for the mineral fiber in the 16 in. wall cavity, and 0.63 to 0.64 for the extruded polystyrene sheathing. The reason for the low efficiency with the mineral fiber is that the wrong width was used for the mineral fiber. As metal C channel studs were used, 16 in. wide commercial insulation should have been used. Instead, 15 in. residential insulation was used. As a result, each cavity had a 1 in. gap the entire height of each stud space. This is an unacceptable application procedure and the reported results should state such.

William R. Strzepek (*author's closure*)—Richard Ray's comment is valid and well stated. Revisions have been included in the paper to address his concerns. It should be kept in mind, however, that the low efficiency of the mineral fiber batt insulation is not due solely to the small vertical air spaces. The metal framing members also have a substantial impact on thermal performance, as discussed in the paper.

¹Manville Sales Corporation, Denver, CO 80217.

R. Gerry Miller,¹ Debby S. Oscar,² Farrokh Seifaei,³ and William P. Goss⁴

Methods for Determining the Thermal Performance of Reflective Insulation Systems

REFERENCE: Miller, R. G., Oscar, D. S., Seifaei, F., and Goss, W. P., "Methods for Determining the Thermal Performance of Reflective Insulation Systems," *Insulation Materials, Testing, and Applications*, ASTM STP 1030, D. L. McElroy and J. F. Kimpflen, Eds., American Society for Testing and Materials, Philadelphia, 1990, pp. 378-396.

ABSTRACT: There has been no general agreement on how to perform, analyze, and report hot box tests on the thermal performance of reflective insulation systems which consist of a series of airspaces separated by reflective foils. This paper presents the results of experimental and analytical studies on the horizontal heat transfer through single- and multi-layer reflective insulations installed vertically. The multi-layer insulations were commercially available reflective insulation products. The experimental studies were carried out in a guarded hot plate and a calibrated hot box. The results showed the effect of aspect (height to width) ratio on the convective heat transfer in the air space. The experimental results were compared with a detailed three-dimensional finite element model of the conductive, convective, and radiative heat transfer which occurs in the reflective insulation system. The results were also compared with the original references used to determine the thermal resistance of plane reflective air spaces that are presented in the ASHRAE Fundamentals Handbook. These two analytical methods were also used to compare a wood and extruded polystyrene support structure for the reflective insulation product.

The results showed that the guarded hot plate did not adequately model the convective heat transfer, due to the low aspect ratio, and that a full-scale facility is needed to properly test a reflective insulation product. It was also indicated that the thermal performance of reflective insulation products are not comparable with the results for plane reflective airspaces in the ASHRAE Fundamentals Handbook due to the thermal bridges which characterize most reflective insulation products.

KEY WORDS: reflective insulation, multilayer insulation, thermal insulation, thermal resistance, R-value, calibrated hot box, guarded hot plate, finite element method, thermal performance

Nomenclature

- A Aspect ratio, H/L , nondimensional
- D Thermal diffusivity, $(\lambda/\rho c_p)$, m^2/s (ft^2/h)
- W Width of air space, m (ft)
- H Height of air space, m (ft)
- L Thickness of air space, m (ft)
- Q Heat transfer rate, W (Btu/h)
- Pr Prandtl number ($\text{Pr} = \nu/D$), nondimensional

¹Jim Walter Research Corp., St. Petersburg, FL 33716.

²Sandia National Laboratories, Albuquerque, NM 87185.

³Computer Simulations, Inc., Russellville, AR 72801.

⁴University of Massachusetts, Amherst, MA 01003.

- Gr Grashof number ($Gr = g\alpha (T_1 - T_2)L^3/\nu^2$), nondimensional
 Ra Rayleigh number ($Ra = Pr Gr = g\alpha (T_1 - T_2)L^3/\nu D$), nondimensional
 C_p Specific heat, J/kg K (Btu/lbm R)
 h Heat transfer coefficient, W/m² K (Btu/h ft² R)
 g Acceleration of gravity, 9.81 m/s² (32.174 ft/s²)
 T Temperature, °C (°F)
 ν Kinematic viscosity, m²/s (ft²/h)
 α Coefficient of thermal expansion, 1/K (1/R)
 λ Thermal conductivity, W/m K (Btu/h ft R)
 ρ Density, kg/m³ (lbm/ft³)

Subscripts

- C Cold
 c Convective
 H Hot
 r Radiative
 1 Hotter surface temperature of air space
 2 Colder surface temperature of air space

Introduction

The use of reflective surfaces to reduce the radiation component of the heat transfer across enclosed air spaces in buildings has been recognized and studied over the years. One problem with reflective insulation systems has been how to define a thermal performance parameter (such as R-value), so that they can be compared directly with mass insulation products.

As a result, experimental and analytical study of the thermal performance of reflective insulation products was performed. The experiments involved the use of a calibrated hot box (ASTM C 976, Thermal Performance of Building Assemblies by Means of a Calibrated Hot Box) and a guarded hot plate (ASTM C 177, Steady-State Heat Flux Measurements and Thermal Transmission Properties by Means of the Guarded-Hot-Plate Apparatus). The analytical models ranged from standard ASHRAE air space, one-dimensional calculations to three-dimensional finite element analysis of the basic equations of mass, momentum, and energy. The results presented in this paper should answer many of the questions regarding reflective insulation systems, so that they can be realistically compared with other commercially available insulation products.

Literature Review

Natural Convection in Enclosures

For reflective insulation systems, heat transfer may be by natural convection and radiation in the enclosure made up of one or more reflective surfaces and by conduction through the insulation system supporting structure and any thermal bridges inherent in the reflective insulation system itself. Examples of the latter are the flanges in multi-layer reflective building insulation and the spacers in metal reflective pipe and nuclear system insulation products. The conduction heat transfer which may occur is specific to the geometry of a particular insulation system and, while it cannot be generalized, it should be recognized and accounted for.

The other two modes of heat transfer can be generalized, and one of these, natural convection in the enclosure, will be discussed in this section, while radiation will be discussed in the next section. One reason they can be discussed separately is that for air (and some other gases),

which does not absorb far-infrared thermal radiation, the natural convection and radiation components of the net enclosure heat transfer do not physically interact with each other except through the effects they have on the boundary conditions. For example, if one of the sides of the enclosure is highly reflective, the radiation heat transfer will be significantly reduced in the enclosure. This will change the boundary condition (temperature gradient and thus temperature) which will then affect the natural convective heat transfer in the enclosure.

Natural convection in enclosures has been studied experimentally and analytically by a number of researchers over the years. Two good summaries of the literature in this area are presented in the recent books by Bejan [1] and Jaluria [2] and the literature reviews by Ostrach [3] and Catton [4]. This paper reviews the major results from these publications as they relate to reflective insulation systems.

Enclosures in building cavities can be categorized by the direction of heat transfer, each of which has a different natural convection situation. The reason for the difference is the effect of the gravitational forces on different temperature (and therefore density) fluid particles (in a macroscopic sense) in the enclosure.

For an enclosure in a vertical building wall, the gravitational force is in a downward direction, thus causing the more dense fluid particles near the colder surface to move downward and the lighter fluid particles near the warmer surface to move upward to create a circulation system within the enclosure (Fig. 1). It should be noted that Fig. 1 indicates a single convective loop or cell. Depending on conditions, multiple convective cells may exist.

For an enclosure in a horizontal building element, like a ceiling, flat roof, or floor, the direction of heat transfer is also important. In the case of a floor where the direction of heat transfer is downward, in the same direction as the gravitational force, the fluid becomes stratified (or thermally stable) whereby the warmer fluid is at the top of the enclosure and the cooler fluid is at the bottom. This results in no motion in the fluid (Fig. 2). In actual situations, some convective

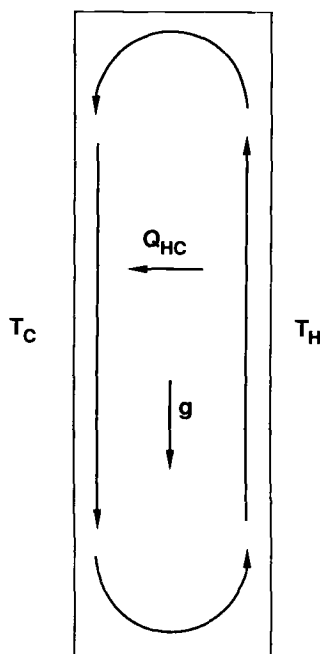


FIG. 1—Fluid motion in a typical vertical wall enclosure.

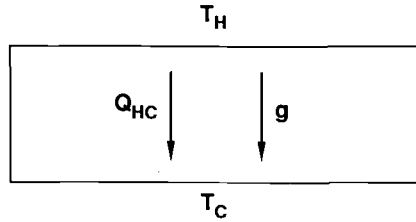


FIG. 2—No fluid motion in a typical horizontal floor enclosure.

motion may exist due to non-isothermal horizontal surfaces and non-adiabatic vertical edge surfaces. With no fluid motion, the natural convection becomes just pure conduction in the air. In the opposite situation, that of heat flow upward like in a ceiling or flat roof enclosure, with the heat transfer in a direction opposite that of the gravitational force, the fluid motion becomes more complex (Fig. 3). In this case the fluid is thermally unstable, the less dense warmer fluid being at the bottom of the enclosure and the more dense cooler fluid at the top. The gravitational force causes a cellular natural convective motion; these cells are called Benard cells and the flow is sometimes called Benard flow. Another, more complex, situation is when the fluid exists in a large non-enclosed cavity such as in an attic space with air infiltration from the heated or cooled portion of the building and attic ventilation from the outside environment which may be natural or forced.

This paper describes the results of several studies of the heat transfer of multi-air-space reflective insulation systems which can be installed in building wall, ceiling, and floor cavities as an alternative to mass insulation products such as mineral wool and fiberglass insulation. The scope is limited to reflective insulation systems installed in vertical wall cavities (horizontal heat flow), since this is the primary application of these products.

Vertical Air Spaces

The ASHRAE Fundamentals Handbook [5] tables entitled "Thermal Resistance of Plane Air Spaces" are the working reference for heat transfer through vertical and horizontal air spaces. The data presented in these tables are from two publications, Robinson and Powlitch [6] and Robinson et al. [7], which reported on guarded hot box experiments carried out at the National Bureau of Standards (NBS) in the 1950s. In the Analytical Methods section of this paper, the use and limitations of the ASHRAE air space tables will be presented. The work carried out at NBS and reported in the ASHRAE tables is well done and, if used in the appropriate situations, will result in accurate predictions of the thermal performance of plane air spaces. However, as will be illustrated subsequently, the inappropriate use of these tables can result in significant

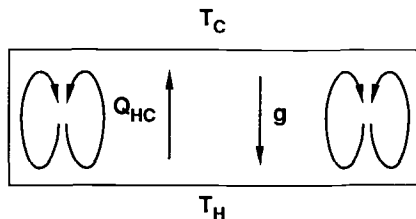


FIG. 3—Fluid motion in a typical horizontal flat roof or ceiling enclosure.

errors in predicting the thermal performance of reflective insulation systems which may not duplicate the plane air space configurations studied by NBS.

Good examples are provided by recent publications that reported on experiments performed on currently available reflective insulation system products. The first was a study by one reflective insulation manufacturer on several of its reflective insulation products using the guarded hot box at the Butler Manufacturing Company Research Center and reported in a Midwest Research Institute Report [8]. The study involved measuring the thermal performance of two reflective and one fiberglass insulation products installed in a 2.4 m (8 ft) high by 2.4 m (8 ft) wide by 14 cm (5½ in.) thick cavity without the usual wood stud support structure. The metering area of this hot box was 1.5 by 1.5 m (5 by 5 ft); however, no barriers were used to separate the guarded portion of the airspace from the metered portion. These reflective foil insulation products were tested without any wood stud support structure and therefore did not simulate any real reflective insulation system.

Subsequent to this work, the Mineral Insulation Manufacturers Association carried out its own study [9] of several reflective insulation products using the same Butler Manufacturing Company Research Center guarded hot box. This study measured the thermal performance of the same reflective insulation products installed in a similar 14 cm (5½ in.) thick cavity, but this time between wood studs. The results indicated that the same reflective insulation products had a significantly lower tested R-value when tested in an as-installed situation where wood studs exist. No physical explanation is given as to why these results occurred other than the suggestion of possible two- or three-dimensional heat transfer effects. No attempt was made to analytically model these multi-dimensional heat transfer effects. Part of the problem with the comparison between the tests reported in Refs 8 and 9 is the difference between a system R-value and a material R-value. This is discussed in more detail in the Results section of this paper.

At about the same time as the foregoing studies were being published, two other activities occurred regarding the thermal performance of reflective insulation systems. One was an ASHRAE symposium held in January 1983 on reflective insulations, and the second was a report of some work on reflective insulation carried out by the Oak Ridge National Laboratory (ORNL) for the Department of Energy.

At the ASHRAE symposium three papers were presented. The first, by Poppendiek et al. [10], was a study of the heat transfer in reflective insulation systems that was carried out for a reflective insulation manufacturer by Geoscience Ltd. using both a guarded hot box (ASTM C 236) and a guarded hot plate apparatus (ASTM C 177). The reflective insulation products were installed in a number of wood stud configurations of which the details were not presented in the paper. The experimental R-values were compared with a derived analytical model which assumed that the air space convective heat transfer coefficients were composed of two free convection boundary layer surface coefficients. The analytical results compared within -27% to +15% of the experimental results. It was stated that some of the differences may be due to the nonparallel reflective surface layers. It is difficult to compare these results with other studies due to a lack of detail in reporting the experimental configurations used, the data recorded, and the data analysis methods used. Also, since the reflective insulation surface emissivities were conservative (0.10 versus 0.03 for most noncoated reflective foil surfaces), the errors quoted were not indicative of what actually existed.

In the second symposium paper, Hollingsworth [11] reported on some experiments on the thermal performance of reflective insulation systems (reflective insulation products installed in wood stud walls appropriate for that reflective insulation product) that were performed with the Owens-Corning Fiberglas large calibrated hot box (ASTM C 976). The experimental configuration and data were presented in detail and the method of data analysis was described. The derived experimental insulation R-values were compared with calculated one-dimensional R-values obtained from the ASHRAE Air Space Resistance Tables using reflective surface emissivities of 0.05. The results showed good comparisons for a single nonreflective airspace and

significant differences for multiple airspace reflective insulation products. The ratio of the ASHRAE calculated-to-measured R-values ranged from 1.5 to 2.9. Hollingsworth concluded that the ASHRAE air space resistances should not be used for reflective insulation systems. No reasons were presented for these large discrepancies.

In the third paper presented at the ASHRAE symposium, Greason [12] reported on calibrated hot box studies at Dow Chemical on a number of building wall panels, some of which had reflective air spaces. Reflective insulation products were not studied, and the air spaces were singular. The experimental results were compared with ASHRAE one-dimensional calculations, and the comparisons were excellent except in the case for the wall panels with air spaces. For reflective air spaces the errors in the measured and ASHRAE air space R-values were significant. Greason concluded that the thermal resistances for typical reflective (surface emissivity of 0.03) and nonreflective air spaces were significantly lower than the ASHRAE "perfect" air space values. He recommended that the ASHRAE "perfect" air space thermal resistances not be used in design calculations.

In the study carried out for ORNL, Yarbrough [13] presented an excellent overview on the status of reflective insulation systems for buildings as of mid-1983. He also presented a one-dimensional model for calculating the thermal resistance of multiple reflective and nonreflective air spaces using the results from Robinson et al. [6]. The curves in Robinson et al. [6] were put into a very useful analytical form by deriving least square curve fit equations for the air space convective heat transfer coefficient as a function of the temperature difference across the air space, the air space width (or thickness), and the average airspace temperature. These correlation equations will probably be recommended as alternatives to the ASHRAE Air Space Resistance Tables in the 1989 ASHRAE Fundamentals Handbook. Using the one-dimensional model, Yarbrough [13] compared the analytical results with Hollingsworth's [11] ASHRAE calculations and experimental results and also with Yarbrough and Kim's [14] experimental results for the thermal resistance of reflective insulation systems using a vertical screen heater system. In both cases, the analytical results using the one-dimensional model based on the ASHRAE Tables predicted R-values which significantly overpredict the experimental values. In his recommendations, Yarbrough [13] concluded that one-dimensional models based on the ASHRAE Air Space Thermal Resistance Tables could not explain the much lower experimental R-value results and that multi-dimensional models were needed. In a subsequent study, Han, Yarbrough, and Han [15] developed a two-dimensional analytical model for the convective heat transfer in an enclosure and solved the model using finite difference methods. They concluded that their more detailed two-dimensional model could not explain the lower experimental reflective air space R-values reported in the literature.

In reviewing the literature, the authors of this paper recognized the need to have a detailed experimental and analytical research program on the thermal performance of building reflective insulation systems. The next two sections describe the experimental and analytical methods that were carried out.

Experimental Methods

Calibrated Hot Box

A rotatable calibrated hot box (ASTM C 976) at the University of Massachusetts [16] was used to study the thermal performance of full-scale thermal insulation products installed in a 2.43 by 2.43 m (8 by 8 ft) test specimen wall panel which, for a calibrated hot box, is also the metered area. The nominal 5 by 10 cm (2 by 4 in.) wood studs were installed vertically in the panel between 1.27 cm (1/2 in.) gypsum wallboard and 1.27 cm (1/2 in.) removable plywood panel, resulting in six standard size 9 cm (3.5 in.) wall cavities (Fig. 4). Full details of the experimental study are presented in the M.S. thesis of Oscar [17]. Three reflective insulation products and one mass insulation product (fiberglass batts) were carefully installed in the cavi-

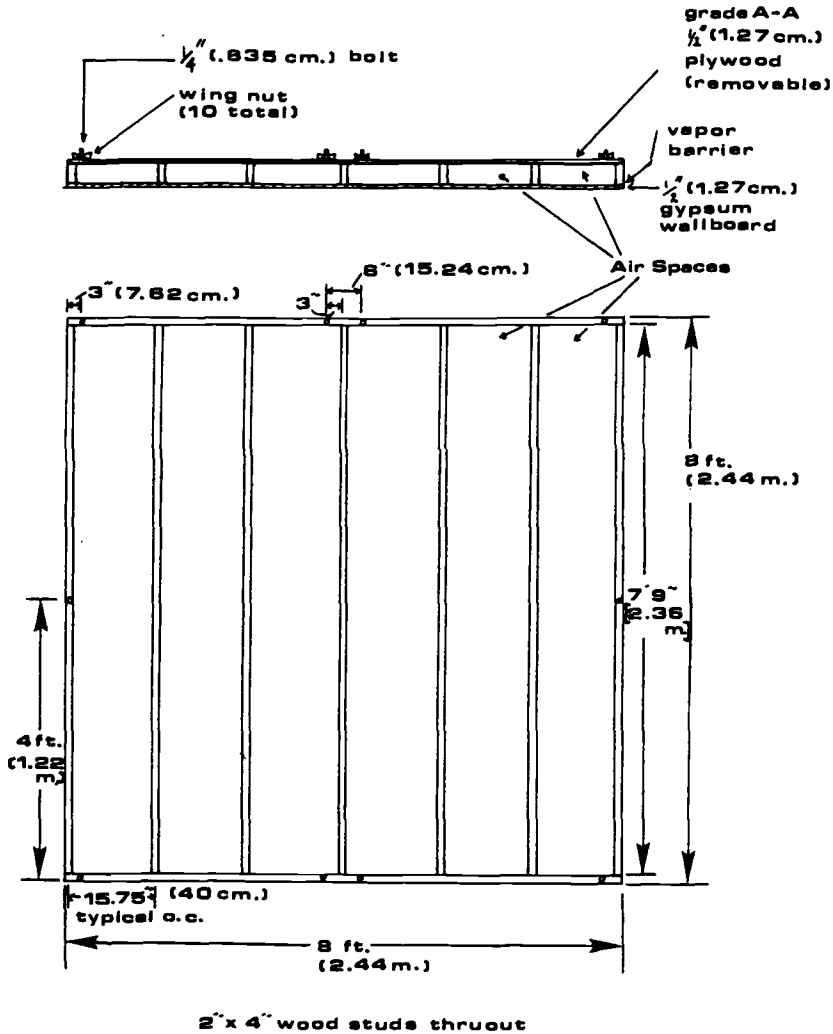


FIG. 4—Test specimen wall panel (calibrated hot box).

ties, and the thermal performance was measured over a range of environmental conditions. Details of the multilayer reflective insulation products studied are presented next.

Guarded Hot Plate

A vertically oriented guarded hot plate apparatus (ASTM C 177) was also used to determine the thermal performance of the reflective insulation systems. The size of the hot plate was 0.46 by 0.46 m (18 by 18 in.) with a 0.2 by 0.2 m (8 by 8 in.) meter area. Two 30-gage Type T thermocouples were installed in grooves in the metering area of the plates. The whole system was housed in an environmental chamber for temperature and humidity control. The guarded hot plate apparatus was used in a single-sided mode. The backflow specimen was a 5 cm (2 in.) unfaced foam material of known thermal resistance. It was installed on one side of the hot plate with the reflective insulation system on the other.

The reflective insulation test panel assembly was in the form of a cavity approximately 38 cm (15 in.) wide by 38 cm (15 in.) high by 9 cm (3.5 in.) thick. The basic assembly consisted of a nominal 5 by 10 cm (2 by 4 in.) wood frame enclosed by 1 cm ($\frac{3}{8}$ in.) plywood. The various types of reflective systems were installed in the cavity. Thermocouples were placed on the inner surfaces of the plywood to measure average surface temperatures of the bounding surfaces of the reflective insulation systems.

Seven systems were tested in the guarded hot plate apparatus at a mean temperature of 24°C (75°F):

1. 9 cm (3.5 in.) non-reflective air space.
2. Cavity filled with fiberglass batt insulation, $R1.9 \text{ Km}^2/\text{W}$ ($11 \text{ h ft}^2 \text{ }^\circ\text{F/Btu}$).
3. Aluminum foil (household type) attached to studs forming a 9 cm (3.5 in.) reflective air space; hemispherical emittance of foil 0.08 as measured by ASTM E 408 [18].
4. Aluminum foil (household type) placed in middle of cavity forming 2 reflective air spaces; hemispherical emittance of foil 0.08 as measured by ASTM E 408 [18].
5. Commercially available reflective insulation product; 3 layers forming 4 reflective air spaces; hemispherical emittance 0.03 as measured by ASTM E 408 [18].
6. Commercially available reflective insulation product; 4 layers forming 5 reflective air spaces; hemispherical emittance 0.03 as measured by ASTM E 408 [18].
7. Commercially available reflective insulation product; 5 layers forming 6 reflective air spaces; hemispherical emittance 0.03 as measured by ASTM E 408 [18].

Figure 5 illustrates the foil covered surfaces for the three commercially available reflective insulation products studied. The products were manufactured from foil-faced kraft paper. The foil is normally attached to one side of the kraft paper which is then attached to mounting flanges for attachment to the wood studs.

Analytical Methods

The heat transfer in an enclosed air space occurs by two modes of heat transfer: convection and radiation. In Fig. 6 the convective and radiative components are idealized to be in the horizontal direction only, with the two large vertical surfaces being isothermal and the other four smaller surfaces being adiabatic. In actuality, the heat transfer may be two- or three-dimensional and the vertical isothermal surfaces may be nearer to a constant heat transfer rate due to the convective and radiative boundary conditions with the surroundings. Also, the smaller end surfaces may not be adiabatic due to heat transfer to the surrounding support structure.

In the idealized situation, the horizontal heat transfer can be shown to be a function of several nondimensional variables. The important geometric variables are the vertical height of the air space, H , and the horizontal thickness (or cavity thickness in the direction of heat transfer) of the air space, L , which is nondimensionalized as the aspect ratio, A , which is the height-to-thickness ratio. The important hydrodynamic variable can be nondimensionalized as the Grashof number, Gr , which is the ratio of the gravitational effects to the viscous effects. The important property variables can be nondimensionalized as the Prandtl number, Pr , which is the ratio of the viscous to thermal diffusivities. These last two nondimensional variables can be combined by multiplication and the result is called the Rayleigh number, Ra . Finally, the important heat transfer variables can be nondimensionalized as the Nusselt number, Nu , which is the ratio of the convective to conductive heat transfer effects. The free convection heat transfer across the air space in the horizontal direction can usually be expressed in nondimensional form as the Nusselt number, which is a function of the Grashof number, the Prandtl number, and the aspect ratio.

With this in mind, there are several ways to predict the thermal performance of an enclosed air space or a system of enclosed air spaces, some of which may have surfaces that have a high

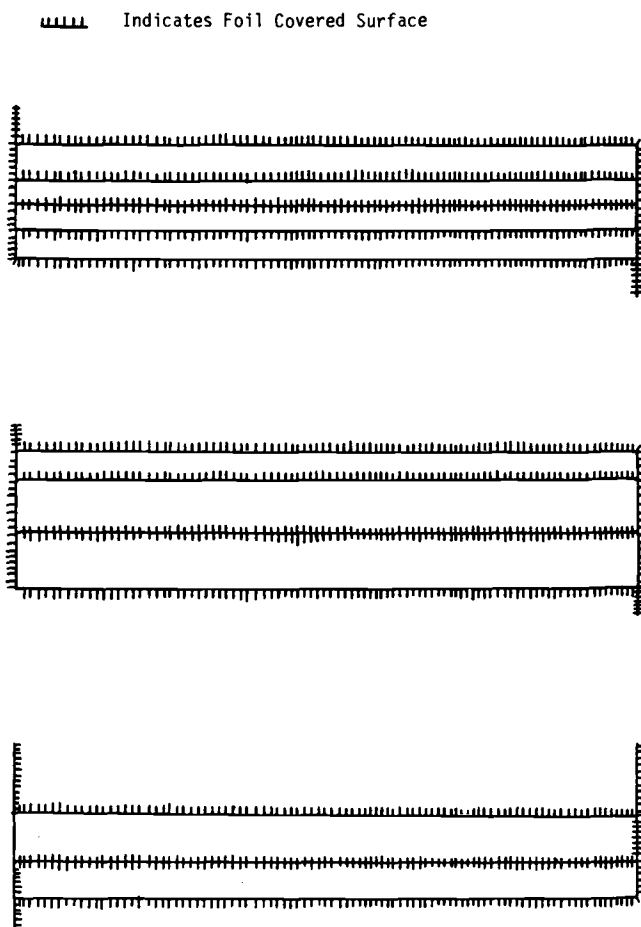


FIG. 5—*Reflective insulation products for installation between 2×4 studding members.*

reflectivity. In order of complexity, the following analytical methods can be used to calculate the overall (convective and radiative) thermal resistance of enclosed vertical air spaces. The first, and most often used, is based on the empirical air space resistances given in Tables 2A and 2B in Chapter 23 of the 1985 ASHRAE Fundamentals Handbook [5]. The main point is that the ASHRAE results are for several fixed air space height (H) to thickness (L) ratios (the aspect ratio) and are not generally applicable to all situations. The second analytical method is also based on experimental data but is less limited in nature in that the aspect ratio is also included in the empirical correlation for the convective heat transfer coefficient. This gives a convective heat transfer coefficient which is applicable for a wider range of air space geometries than the ASHRAE data. This method will be the subject of a subsequent paper. The third analytical method is the situation where the partial differential equations describing the hydrodynamic and heat transfer phenomena occurring in the air space are written out and solved numerically. The equations may be either in two- or three-dimensional form and can account for the two- or three-dimensional heat transfer effects which occur in the air space and the surrounding support structure. The convective heat transfer models can then be combined with the other mode of heat transfer, radiation, which occurs in parallel for a nonabsorbing fluid.

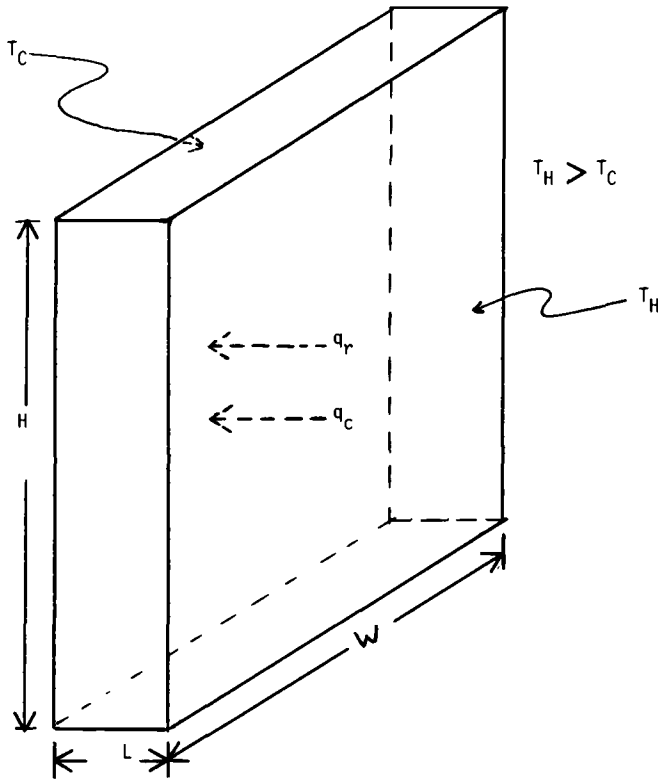


FIG. 6—Heat transfer in enclosed airspace.

ASHRAE Calculations

Table 2A in Chapter 23 of the 1985 ASHRAE Fundamentals Handbook [5] presents thermal resistance data for sealed, plane air spaces of uniform thicknesses. These data are based on guarded hot box tests conducted at the National Bureau of Standards in the mid-1950s [6, 7]. The tests were run in five different orientations on five different systems with aspect ratios (airspace height to thickness ratio) from 18 to 96. Table 1 summarizes the aspect ratios used. These values are less than those normally encountered in many reflective insulation systems and were governed by the size of the metering area of the NBS hot box. Even with the above limitations,

TABLE 1—Aspect ratios used in Ref 6.

Test Panel	Airspace Thickness (L), cm (in.)	Airspace Height (H), cm (in.)	Aspect Ratio (H/L)
1.1	1.6 ($5/8$)	152.4 (60)	96.0
1.2	2.2 ($7/8$)	152.4 (60)	68.6
1.3	3.8 ($1\frac{1}{2}$)	152.4 (60)	40.0
1.4	8.6 ($33/8$)	152.4 (60)	17.8
2.1	4.3 ($1\frac{11}{16}$)	152.4 (60)	35.6

the thermal resistance of a reflective insulation system is routinely estimated by using ASHRAE Table 2A.

The R-values in ASHRAE Table 2A are a combination of a radiation coefficient and a "convection-conduction" coefficient. The radiation coefficient is a function of the emittances, geometry, and absolute temperatures of the surfaces facing the reflective air space. The "convection-conduction" coefficient, in general, depends upon the aspect ratio, airspace orientation, direction of heat flow, air space thickness, mean temperature, and temperature difference across the reflective airspace. The "convection-conduction" coefficient is the free convection coefficient obtained by subtracting the radiation coefficient from the experimental total heat transfer coefficient. The direct use of ASHRAE Table 2A is limited to specific conditions (mean temperature, temperature difference, effective emittance, airspace thickness, position of airspace, and direction of heat flow). Interpolation is needed for most systems.

An alternative procedure is to use the graphs of the "convection-conduction" coefficient $(h_c)_{50}$ versus airspace thickness for the appropriate airspace orientation and heat flow direction in the original HRP 32 report [6]. In a multi-airspace system, this requires an estimation of the temperature difference across and mean temperature of each reflective airspace. An iterative calculation is then performed by matching

$$\frac{q}{A} = \frac{\Delta T}{R}$$

for each airspace, where R is the thermal resistance of the reflective airspace and includes both the "convection-conduction" and radiation heat transfer coefficients. For a multi-airspace reflective insulation system this iterative procedure may be quite time consuming. Yarbrough [13] has developed a correlation of the "convection-conduction" coefficient data in Ref 6. Using this correlation, the iteration procedure for determining R-values of multi-layer reflective insulations may be programmed on a computer as described in Yarbrough [13].

Multi-Dimensional Models

Since a number of researchers have concluded that the ASHRAE calculation method is not applicable to the reflective air spaces in commercially available reflective insulation systems, it was decided to develop a three-dimensional analytical model of the heat transfer which occurs within reflective insulation systems. This includes the conduction in the wood stud support structure and mounting flanges and radiation and free convection in the air spaces. The model is essentially the equations of mass, momentum, and energy written out in partial differential equation form and solved using finite element methods. Details of the model can be found in the Ph.D. dissertation of Seifaei [19] and in Seifaei and Goss [20].

Results

The experimental results presented here are from the guarded hot plate and calibrated hot box tests. The experimental uncertainties of these instruments, when used to measure homogeneous insulation products, are 2% for the guarded hot plate and 7% for the calibrated hot box. In the case of nonhomogeneous insulation products, the uncertainties are unknown. For the situation of the guarded hot plate measuring a reflective airspace larger than the metering area, the experimental uncertainty is probably much greater than 2% because of the neglect of the edge effects in the guard area. The same could be said for a guarded hot box (ASTM C 236) that does not have barriers installed in the airspace to correspond with the hot box metering area. The calibrated hot box does not have this problem.

The analytical results presented here are from the one-dimensional ASHRAE calculations and the three-dimensional finite element model. The thermal conductivities of the solid materi-

als were obtained from Table 3A in Chapter 23 of the 1985 ASHRAE Fundamentals Handbook. The reflective surface emittances used were those measured as described in the Experimental Methods section of this paper.

The results of the guarded hot plate and calibrated hot box tests are given in Tables 2 to 6. The data include the temperature difference across the cavity (DT), cavity or material mean temperature (T_m), the material or cavity R-value calculated using the ASHRAE tables and/or Ref 6 (R_{ASHRAE}), the experimentally determined material R-value (R_{exp}), the material R-value calculated by the three-dimensional finite element model (R_{FE}), and comparisons between measured and calculated R-values.

In the case of the guarded hot plate, R_{exp} was measured directly, in that no correction was needed for studs (none were in the metered area) and the temperatures of the surfaces bounding the cavity were measured. For the calibrated hot box, however, R_{exp} was calculated from the system R-value (insulation product plus wood studs and face panels) by the ASHRAE parallel path method [17]. The R-values of the face panels (plywood and gypsum wallboard) and wood studs were taken from Table 3A, Chapter 23, 1985 ASHRAE Fundamentals Handbook [5].

Table 2 presents the results for the single nonreflective airspace and for fiberglass batt installed in the cavity. One test at a mean temperature of about 24°C (75°F) was conducted in the guarded hot plate for both the nonreflective airspace and a nominal R1.9 Km²/W (11 h ft²F/Btu) fiberglass batt. Three tests were conducted in the calibrated hot box on the nonreflective airspace at mean temperatures of approximately 4.4°C (40°F), 24°C (75°F), and 43°C (110°F). One test on a nominal R2.3 Km²/W (13 h ft²F/Btu) fiberglass batt at a mean temperature of 6.8°C (44.3°F) was also conducted in the hot box.

With the guarded hot plate, agreement between R_{ASHRAE} and R_{exp} was about 12% for the nonreflective airspace and 3.5% when fiberglass was tested; or the ratio of experimental R-value to ASHRAE calculated R-value was 0.89 and 0.97, respectively. It is reasoned that the larger disagreement when testing the airspace was because of convective effects from the guard area to the meter area, since no barriers were used to separate these two areas in the guarded hot plate setup.

For the calibrated hot box, agreement between R_{ASHRAE} and R_{exp} , when testing the nonreflective airspace, was within $\pm 5\%$ for all three mean temperatures. The average ratio of R_{exp} to R_{ASHRAE} was 1.0. Agreement was even better, 2.9%, when testing the fiberglass batts. Table 2 also showed that the three-dimensional finite element model predicted the guarded hot plate nonreflective airspace experimental results better than the ASHRAE calculations. For the calibrated hot box nonreflective airspace experimental results, the finite element method slightly underpredicted the experimental results (average ratio of R_{exp} to R_{ASHRAE} was 1.06).

The results of the multilayer reflective airspace tests are presented in Tables 3 to 6. Table 7 gives the aspect ratios for the guarded hot plate and calibrated hot box when testing these multilayered products. In many of the tests, the aspect ratios were much different than those used in the NBS study [6] as shown earlier in Table 1.

Table 3 presents data from the guarded hot plate for a single and a double reflective airspace. The single airspace was 8.89 cm (3.5 in.) thick, whereas the double airspace contained two 4.4 cm (1.75 in.) reflective airspaces. In both cases, household aluminum foil was used to produce the reflective airspace. The emittance of the foil was 0.08 [18]. Comparing R_{exp} with the calculated R-values, we find that both analytical methods overpredicted the measured R-value. For these tests, R_{ASHRAE} yielded results closer to R_{exp} .

Tables 4 to 6 present the data on the three commercially available reflective insulation products. These products contained 3, 4, and 5 reflective layers forming 4, 5, and 6 reflective airspaces. Emittance of the foil surface was 0.03 [18].

In general, as the number of reflective airspaces increases, the R-value of the product increases. However, as the number of airspaces increased, the more difficult it was to install these products in the cavity and still maintain parallel and uniform airspaces. In some cases, even with the utmost care taken during installation, surfaces sometimes touched each other, causing

TABLE 2—Non-reflective air space and cavity mass insulation.

	DT		T _m		R _{ASHRAE}		R _{exp}		R _{FE}			
	°C	(°F)	°C	(°F)	Km ² /W	(F ft ² h/Btu)	R _{exp} /R _{ASHRAE}	Km ² /W	(F ft ² h/Btu)	Km ² /W	(F ft ² h/Btu)	R _{exp} /R _{FE}
Non-reflective air space (GHP)	13.7	(24.6)	23.0	(73.5)	0.15	(0.85)	0.89	0.13	(0.76)	0.14	(0.80)	0.95
Non-reflective air space (CHB)	9.2	(16.5)	5.7	(42.2)	0.18	(1.00)	0.96	0.17	(0.96)	0.17	(0.94)	1.02
	9.3	(16.7)	24.7	(76.5)	0.15	(0.84)	1.04	0.15	(0.87)	0.14	(0.80)	1.09
	8.1	(14.6)	44.4	(112.0)	0.13	(0.76)	1.01	0.14	(0.77)	0.12	(0.71)	1.08
R-11 fiberglass batt installed in cavity (GHP)	27.2	(49.0)	23.3	(73.9)	1.94	(11.00)	1.04	2.01	(11.40)
R-13 fiberglass batt installed in cavity (CHB)	29.9	(53.9)	6.8	(44.3)	2.29	(14.00)	0.97	2.39	(13.60)

TABLE 3—I and 2 reflective airspaces.

	DT		T _m		R _{ASHRAE}		R _{exp}		R _{FE}			
	°C	(°F)	°C	(°F)	Km ² /W (h ft ² °F/Btu)	R _{exp} /R _{ASHRAE}	Km ² /W (h ft ² °F/Btu)	R _{exp} /R _{FE}	Km ² /W (h ft ² °F/Btu)	R _{exp} /R _{FE}		
One 3.5-in. reflective air space (GHP)	19.5	(35.0)	23.2	(73.7)	0.41	(2.30)	0.78	0.32	(1.79)	0.43	(2.43)	0.74
Al foil installed in middle of cavity, two reflective air spaces (GHP)	24.9	(44.9)	24.6	(76.2)	0.89	(5.04)	0.88	0.78	(4.44)	1.07	(6.05)	0.73

TABLE 4—4 reflective airspaces.

	DT		T _m		R _{ASHRAE}		R _{exp}		R _{FE}			
	°C	(°F)	°C	(°F)	Km ² /W (h ft ² °F/Btu)	R _{exp} /R _{ASHRAE}	Km ² /W (h ft ² °F/Btu)	R _{exp} /R _{FE}				
3 sheets, 4 reflective air spaces (GHP)	25.9	(46.5)	23.4	(74.0)	2.76	(15.65)	0.52	1.44	(8.20)	1.27	(7.21)	1.14
	28.3	(50.9)	5.6	(42.0)	2.30	(13.04)	0.52	1.18	(6.72)	1.06	(6.02)	1.12
3 sheets, 4 reflective air spaces (CHB)	32.1	(57.7)	23.4	(74.0)	2.11	(11.96)	0.52	1.10	(6.22)	1.03	(5.87)	1.06
	29.4	(52.9)	41.5	(106.6)	2.03	(11.51)	0.53	1.08	(6.12)	0.97	(5.50)	1.11

TABLE 5—5 reflective airspaces.

	DT		T _m		R _{ASHRAE}		R _{exp}		R _{FE}			
	°C	(°F)	°C	(°F)	Km ² /W (h ft ² °F/Btu)	R _{exp} /R _{ASHRAE}	Km ² /W (h ft ² °F/Btu)	R _{exp} /R _{FE}				
4 sheets, 5 reflective air spaces (GHP)	27.4	(49.3)	23.9	(75.0)	2.84	(16.15)	0.47	1.34	(7.61)	1.38	(7.83)	0.97
	26.9	(48.4)	4.9	(40.8)	2.68	(15.19)	0.36	0.98	(5.54)	1.07	(6.05)	0.92
4 sheets, 5 reflective air spaces (CHB)	31.3	(56.3)	23.2	(73.7)	2.52	(14.30)	0.46	1.15	(6.54)	1.04	(5.90)	1.09
	28.3	(50.9)	42.1	(107.6)	2.44	(13.84)	0.41	0.99	(5.63)	1.02	(5.79)	0.97

TABLE 6—6 reflective airspaces.

	DT		T _m		R _{ASHRAE}		R _{exp}		R _{FE}		
	°C	(°F)	°C	(°F)	Km ² /W (h ft ² °F/Btu)	R _{ASHRAE}	Km ² /W (h ft ² °F/Btu)	R _{exp}	Km ² /W (h ft ² °F/Btu)	R _{exp} /R _{FE}	
5 sheets, 6 reflective airspace (GHP)	30.8	(55.6)	25.5	(77.9)	3.12	(17.73)	0.65	2.04	(11.59)	1.45 (8.26)	1.40
5 sheets, 6 reflective airspace (CHB)	25.5	(45.9)	5.0	(41.0)	3.08	(17.51)	0.24	0.75	(4.28)	1.07 (6.10)	0.70
	29.8	(53.5)	24.1	(75.3)	2.86	(16.24)	0.26	0.74	(4.21)	1.03 (5.85)	0.72
	26.7	(48.0)	41.8	(107.1)	2.68	(15.22)	0.36	0.97	(5.49)	1.00 (5.69)	0.96

TABLE 7—*Aspect ratios.*

System	Aspect Ratios	
	CHB Tests	GHP Tests
Single airspace	26.6	4.3
Double airspace	N.A.	8.6
3 sheet, 4 airspaces	120.9	17.1
4 sheets, 5 airspaces	133.9	21.4
5 sheets, 6 airspaces	165.3	25.7

thermal bridging or thermal short circuits. These problems accounted for some of the inconsistencies in the R-values measured on some of the multi-layered products and may also be the situation in actual usage. This can be seen by comparing the R_{exp} with the number of reflective airspaces. The 5 reflective airspace product tested low in the guarded hot plate due to installation difficulties. The same held true for the 6 reflective airspace product in the calibrated hot box.

Table 4 presents the results for the 4 reflective airspace (3 reflective layer) product. For both the guarded hot plate and calibrated hot box, the ASHRAE calculations greatly overpredicted the measured R-value (R_{exp}/R_{ASHRAE} ratio was 0.52 for both measuring devices). The three-dimensional finite element model slightly underpredicted the measured R-value (R_{exp}/R_{FE} ratio of 1.14 and an average ratio of 1.10 for guarded hot plate and calibrated hot box, respectively).

The results from the 5 reflective airspace (4 layer) product (Table 5) were similar to those of the 4 reflective airspace product. The ASHRAE calculated R-values were substantially above the measured R-values, while the finite element model calculated R-value was, on average, fairly close to the measured value. The ratio of measured R-value to calculated R-value for the guarded hot plate was 0.47 and 0.97 for the ASHRAE calculation and finite element model, respectively. For the calibrated hot box, the average ratios were 0.41 and 0.99 for the ASHRAE calculation and finite element model, respectively.

Table 6 presents the results of the 6 reflective airspace (5 layer) product. Again, the ASHRAE calculated R-values substantially overpredicted the measured R-value, with a measured R-value to calculated R-value ratio of 0.65 for the guarded hot plate and an average ratio of 0.29 for the calibrated hot box. The finite element model underpredicted the measured R-value for the guarded hot plate, but slightly overpredicted the calibrated hot box R-values. The average measured-to-calculated R-value ratios were 1.40 and 0.79, respectively. One reason for the larger discrepancies for the calibrated hot box tests was the difficulty in installing this product, resulting in airspaces which were not uniform, thus producing thermal shorts where the foil faced layers touched each other. The calibrated hot box measured R-value was less than the other two commercially available products, even though it had additional reflective layers.

In general, the guarded hot plate R-values were greater than the calibrated hot box R-values. As the test cavity for the guarded hot plate was 0.38 by 0.38 m (15 by 15 in.), the reflective insulation products were installed without any wood stud support structure in the metering area. Therefore any effects of the reflective insulation flange/wood stud were eliminated. In addition, since the guarded hot plate only measured the central 0.2 by 0.2 m (8 by 8 in.) area of the test cavity, any convective effects due to the flow reversals at either end of the cavity were neglected. These effects plus the different aspect ratio effect combined to consistently yield higher R-values than those measured in the calibrated hot box.

An overall comparison of the experimental data with the analytical data showed that the ASHRAE calculated R-values substantially overpredicted the experimental R-values. These results are consistent with the findings of Hollingsworth [9,11], Greason [12], and Yarbrough [13]. The three-dimensional finite element model, however, was able to better predict the exper-

imental R-values. The reason for this was the ability of the finite element model to predict the thermal bridge effects of the aluminum foil on the flange of the reflective insulation product. Since the flange is stapled to the side of the wood stud, the aluminum foil on its surface presents a direct thermal bridge through the airspace. Even though the aluminum foil is quite thin, it has a very high thermal conductivity and bridges the entire height of the airspace.

Table 8 presents a comparison between the three-dimensional finite element model calculated R-values (system and material) for a wood stud and an extruded polystyrene stud support structure. As the last column shows, if the calculation procedure is accurate, the choice of support structure material does not affect the R-value of the reflective insulation product.

Conclusions and Recommendations

Before getting into specific conclusions and recommendations, some comments are in order. While reflective insulation products are nonhomogeneous, the same basic heat transfer processes (radiation/convection in the gas portion and conduction in the solid portion) that occur in mass insulation products exist in reflective insulation products. The only differences are material geometries and properties such as surface emittance and thermal conductivity. Recognizing the above, it is then possible to define and measure the system R-value and to calculate the material R-value of reflective products.

Guarded hot boxes (ASTM C 236), while most are able to simulate a full-scale system, only measure the heat transfer through the center of a test panel containing reflective insulation products. As discussed for guarded hot plates, the R-values determined from these tests may be in error because of this. For the same reflective insulation products, the magnitude of this error should be less for a guarded hot box than for a guarded hot plate, since the aspect ratio should be closer to full scale.

Based on the experimental and analytical results presented, the following conclusions and recommendations may be stated:

1. Experiments should be full scale so as to simulate both the correct airspace thickness and height (i.e., aspect ratio).
2. Guarded hot plate (ASTM C 177) tests of reflective insulation products do not properly simulate the aspect ratio and only measure the heat transfer through the center of the nonhomogeneous cavity.
3. Calibrated hot boxes (ASTM C 976) are able to simulate full-scale systems and measure the total heat transfer through the complete test panel. Their use is recommended for determining the thermal performance of reflective insulation systems.
4. Thermal performance tests on reflective insulation products installed in test panels should include measurements of the thermal conductivity of the construction materials used and the emittance of all reflective surfaces in order to provide better comparisons with analytical results.
5. Before commencing with the reflective insulation system tests, it is recommended that the thermal performance of the empty nonreflective cavity test panels should be determined. This can provide a basis for comparison with other hot box tests and with the ASHRAE airspace resistance tables.
6. Use of the ASHRAE one-dimensional calculation methods along with the thermal resistance values for reflective airspaces [6] were found to overpredict the measured thermal performance of the reflective insulation products by about 90 to 300%. This procedure is not recommended for predicting the thermal performance of reflective insulation products.
7. Two- and three-dimensional analytical models can and should be used to predict the thermal performance of reflective insulation systems. They predicted the experimental results to within 8 to 40%. The larger differences were due to the 6 airspace reflective insulation product not having uniform noncontacting airspaces. The model should include thermal bridge effects like conduction through foil-faced mounting flanges and have good property data input.

TABLE 8—Comparison between wood studs and extruded polystyrene studs.

DT	°C	°F	R _{analytical system}		R _{analytical cavity}	
			T _m	R _{wood}	R _{sty}	R _{sty}
				Km ² /W (h ft ² °F/Btu)	Km ² /W (h ft ² °F/Btu)	Km ² /W (h ft ² °F/Btu)
27.8	7.2	(45)		1.24	1.33	1.09
27.8	23.9	(75)		1.21	1.27	1.06
27.8	40.6	(105)		1.15	1.23	0.99
				(7.02)	(7.56)	(6.21)
				(6.87)	(7.23)	(6.03)
				(6.51)	(6.97)	(5.60)
						1.09
						1.06
						0.99
						(6.20)
						(6.02)
						(5.62)

8. Future improvements for multidimensional analytical models are:

(a) Examine the effects of non-isothermal bounding surfaces. (Note: A constant heat flux boundary condition at the other panel surfaces may be more appropriate. Another alternative would be to assume constant hot and cold side air temperatures and variable surface heat transfer coefficients, rather than constant surface temperatures).

(b) Modification to handle non-parallel surface airspaces.

(c) Include air leakage effects due to rips, tears, and non-perfect fits with the top and bottom wood plates.

References

- [1] Bejan, A., *Convection Heat Transfer*, Wiley, New York, 1984.
- [2] Jaluria, Y., *Natural Convection Heat and Mass Transfer*, Pergamon Press, Oxford, 1980.
- [3] Ostrach, S., "Natural Convection in Enclosures," *Advances in Heat Transfer*, Vol. 8, 1977, pp. 161-227.
- [4] Catton, I., "Natural Convection in Enclosures," in *Proceedings*, GTU International Heat Transfer Conference, Toronto, Vol. 6, 1978, pp. 13-43.
- [5] *ASHRAE Fundamentals Handbook*, American Society of Heating, Refrigerating and Air Conditioning Engineers, Atlanta, Chapter 23, 1985.
- [6] Robinson, H. E., Powlitch, F. J., and Dill, R. S., "The Thermal Insulation Values of Airspaces," Housing Research Paper 32, National Bureau of Standards Project ME-12 for the Housing and Home Finance Agency, US GPO, 1954.
- [7] Robinson, H. E., Cosgrove, L. A., and Powell, F. J., "Thermal Resistance of Airspaces and Fibrous Insulations Bounded by Reflective Surfaces," Building Materials and Structures Report 151, National Bureau of Standards, 1957.
- [8] Butler Manufacturing Company, "Heat Transfer Measurements with Heat Flows Up, Horizontal and Down to Compare Foilpleat C-4R Aluminum Foil Insulation; Foilpleat B-3 Aluminum Foil Insulation; and Owens-Corning R-19, Kraft-Faced, Short-Fiber Batt Insulation," Midwest Research Institute, Project Report No. 3896-L (1), Kansas City, Mo., Jan. 1980.
- [9] Hollingsworth, M., "Thermal Testing of Reflective Insulations," in *Thermal Insulation: Materials and Systems*, ASTM STP 922, F. J. Powell and S. L. Matthews, Eds., American Society for Testing and Materials, Philadelphia, 1987, pp. 506-517.
- [10] Poppendiek, H. F., Connelly, D. J., and Fowler, E. W., "Some Remarks on Heat Transfer in Installed Foil Insulation Systems," *ASHRAE Transactions*, Vol. 89, Part 1B, 1983, pp. 559-567.
- [11] Hollingsworth, M., "Experimental Determination of the Thermal Resistance of Reflective Insulations," *ASHRAE Transactions*, Vol. 89, Part 1B, 1983, pp. 568-578.
- [12] Greason, D. M., "Calculated versus Measured Thermal Resistances of Simulated Building Walls Incorporating Airspaces," *ASHRAE Transactions*, Vol. 89, Part 1B, 1983, pp. 579-588.
- [13] Yarbrough, D. W., "Assessment of Reflective Insulations for Residential and Commercial Applications," Oak Ridge National Laboratory Report ORNL/TM-8891, Oct. 1983.
- [14] Yarbrough, D. W. and Kim, S. G., "Thermal Resistance of Reflective Insulations Installed in a Simulated Wall Cavity," in *Proceedings*, ASHRAE/DOE Conference on the Thermal Performance of the Exterior Envelopes of Buildings II, Las Vegas, ASHRAE SP 38, Dec. 1981, pp. 204-220.
- [15] Han, B. J., Yarbrough, D. W., and Han, S. M., "Thermal Resistance of Wall Cavities Containing Reflective Insulation," in *Proceedings*, 23rd National Heat Transfer Conference, AIChE/ASME, Denver, Aug. 1985, pp. 39-44.
- [16] Goss, W. P. and Olpak, A., "Design and Calibration of a Rotatable Thermal Test Facility," in *Thermal Insulation, Materials, and Systems for Energy Conservation in the 80's*, ASTM STP 789, American Society for Testing and Materials, Philadelphia, 1983, pp. 215-233.
- [17] Oscar, D., "Experimental Determination of the Thermal Resistance of Reflective Insulations," M.S. thesis, Mechanical Engineering Dept., University of Massachusetts, Sept. 1983, 112 pages.
- [18] Hardgrove, W. R., "Emittance of Nineteen Samples" for the Jim Walter Research Corporation, TRW Space and Technology Group, St. Petersburg, Fla., Oct. 1986.
- [19] Seifae, F., "Natural Convection in Reflective Building Insulation Systems," Ph.D. dissertation, Mechanical Engineering Dept., University of Massachusetts, Feb. 1986, 180 pages.
- [20] Seifae, F. and Goss, W. P., "A Finite Element Model for Predicting the Thermal Performance of Reflective Insulation Systems," to be published.

Influence of Natural Convection in an Insulated Cavity on the Thermal Performance of a Wall

REFERENCE: Lecompte, J. G. N., "Influence of Natural Convection in an Insulated Cavity on the Thermal Performance of a Wall," *Insulation Materials, Testing, and Applications, ASTM STP 1030*, D. L. McElroy and J. F. Kimpflen, Eds., American Society for Testing and Materials, Philadelphia, 1990, pp. 397-420.

ABSTRACT: The influence of the airtightness of the insulation layer in a partially filled cavity construction is discussed. In theory it is assumed that the insulation forms a continuous layer that is perfectly fixed against the inner wall of the cavity, leaving an air space between the outer wall and the insulation. However, in practice we frequently notice the presence of air gaps in the insulation layer, and of a second small cavity between the insulation and the inner wall. The influence of these inaccuracies on the heat transfer is studied by means of experimental research and computer simulations.

This paper presents the results of extensive measurements on a partially filled cavity wall (temperature profiles, heat loss), using a calibrated Hot Box-Cold Box. These results are compared with calculations of the temperature profiles and the overall heat transfer. A second series of measurements deals with the influence of the slope of the cavity.

KEY WORDS: thermal insulation, thermal transmittance, insulation in cavities, natural convection, calibrated Hot Box-Cold Box, airtightness, air leaks, workmanship, insulation in cavities, computer simulations

When thermal insulation is placed in the cavity of a wall, special attention must be paid to the airtightness of the insulation layer. Otherwise, a considerable increase of the heat transfer can be expected, due to air flows around and through the insulation layer, caused by the stack effect. The use of hard foam insulation boards (extruded or expanded polystyrene, polyurethane, etc.) introduces the problem of the joints between the boards themselves and between the boards and other construction parts (e.g., windows), coupled to the inevitable presence of small cavities on both sides of the insulation layer. The hard foam insulation boards can be considered as airtight (Fig. 1). Using mineral wool as insulation material leads to additional requirements concerning the minimal density in order to prevent air flows through the insulation (Fig. 2).

It must be stressed that these problems are directly coupled to workmanship in the application of insulating materials in partially filled cavity constructions, not to the materials themselves.

Experimental Study: A Partially Filled Cavity Wall

Test Wall

Test Wall Section—A layer of insulation is placed in a vertical cavity construction with an inner wall of cellular concrete, plastered on both sides, and an outer wall of plywood. Cellular

¹Assistant, Laboratory of Building Physics, Katholieke Universiteit Leuven, Kasteel van Arenberg, B 3030 Heverlee, Belgium.

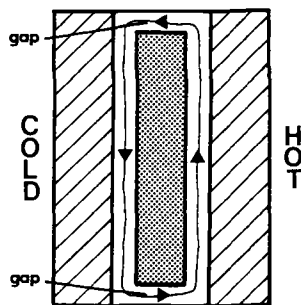


FIG. 1—Air flow around insulation.

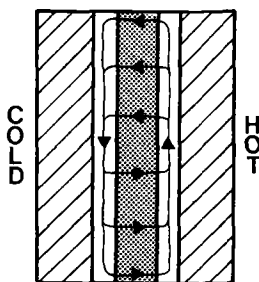


FIG. 2—Air flow through insulation.

concrete is used for a homogeneous inner wall, plywood for an outer wall that is easily removable to change the configuration of the insulation. The height of the wall is 2 m. See Fig. 3. This test wall simulates a cavity construction with an inner wall and an outer wall in brickwork, such as is commonly used in Belgium and The Netherlands. Measurement configurations 1, 2, and 3 deal with the influence of the width of the gaps and cavities; the insulation is airtight. There is an air gap at the top and at the bottom of the insulation; a cavity is created on both sides of the insulation. Measurement configurations 4, 5, 6, and 7 deal with the influence of the airtightness of mineral wool.

Measurement Points in the Test Wall—For temperature measurements, Cu/C thermocouples are used (0.25 mm diameter, absolute error on temperature differences $< 0.2^{\circ}\text{C}$). The local heat flux density is measured by means of circular heat flux transducers (Type WS 31, 85 mm diameter, TPD-TNO, Delft, The Netherlands) with an accuracy of 5%. See Fig. 4.

Thermal Conductivity of Materials—The drying of the cellular concrete results in a decreasing thermal conductivity of the inner wall during the measurements. The thermal conductivity is calculated from the moisture content of the cellular concrete. The relationship between thermal conductivity and moisture content is: $k = 0.18 + 6.6\text{E-}3 \cdot X$ (X = moisture content, % kg/kg) [1,2]. From Configuration 4 on, the thermal conductivity is taken constant, $k = 0.22 \text{ W}/(\text{m} \cdot \text{K})$. See Fig. 5.

The thermal conductivity of the other materials is determined in a heat flow apparatus. Mean temperature and moisture effects are not taken into account, since these are secondary effects in the problems studied.

- Plywood (Configuration 1) : $k = 0.145 \text{ W/(m} \cdot \text{K)}$
- Plywood (Configurations 2-7) : $k = 0.13 \text{ W/(m} \cdot \text{K)}$
- Gypsum rendering : $k = 0.26 \text{ W/(m} \cdot \text{K)}$
- Extruded polystyrene, $\rho = 25 \text{ kg/m}^3$
(Configurations 1-3) : $k = 0.029 \text{ W/(m} \cdot \text{K)}$
- Mineral wool, $\rho = 48 \text{ kg/m}^3$ (Configuration 4) : $k = 0.029 \text{ W/(m} \cdot \text{K)}$
- Mineral wool, $\rho = 23 \text{ kg/m}^3$ (Configuration 5) : $k = 0.034 \text{ W/(m} \cdot \text{K)}$
- Mineral wool, $\rho = 18 \text{ kg/m}^3$ (Configuration 6) : $k = 0.035 \text{ W/(m} \cdot \text{K)}$
- Mineral wool, $\rho = 18 \text{ kg/m}^3$ (Configuration 7) : $k = 0.036 \text{ W/(m} \cdot \text{K)}$

Airtightness of Insulation Materials—The extruded polystyrene boards used in Configurations 1 to 3 can be considered as airtight; the airtightness of the insulation layer is determined

Cavity wall : 2.4 m x 2.0 m (width x height)

Outside

- | | |
|----------------|--|
| 1 - outer wall | : 20 mm plywood (configuration 1)
12 mm plywood (configurations 2-7) |
| 2 - cavity C | : cavity on cold side of insulation |
| 3 - insulation | : 50 mm extruded polystyrene (configurations 1,2,3)
50 mm mineral wool (configurations 4,5)
60 mm mineral wool (configuration 6)
50 mm mineral wool with kraft paper
(configuration 7) |
| 4 - cavity H | : cavity on hot side of insulation |
| 5 - plastering | : 10 mm gypsum plastering |
| 6 - inner wall | : cellular concrete blocks (glued)
600 x 240 x 90 mm, $\rho = 600 \text{ kg/m}^3$ |
| 7 - plastering | : 15 mm gypsum plastering |

Inside

measuring points :

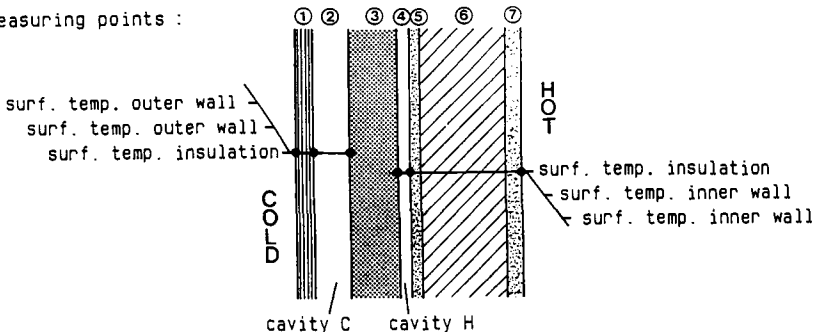


FIG. 3—Test wall section.

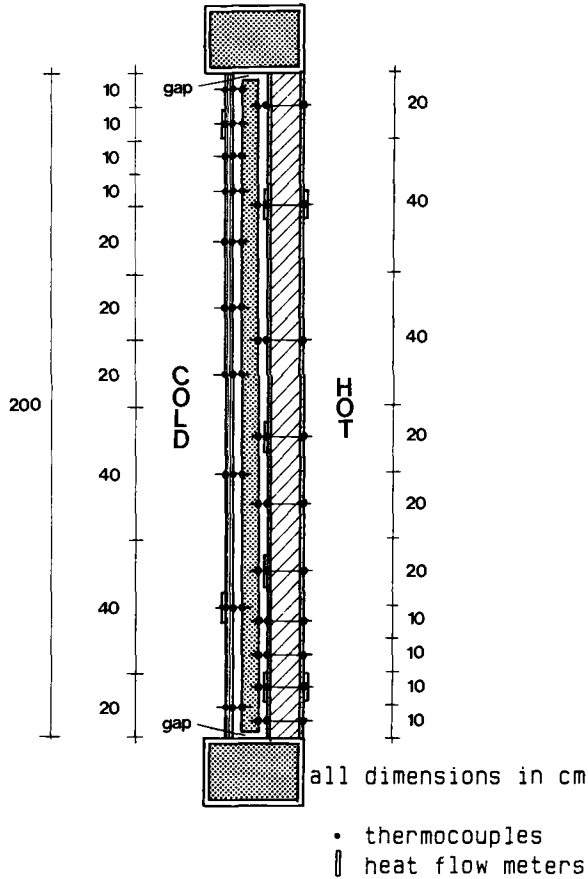


FIG. 4—Measuring points in test wall.

by the joints between the boards themselves and between the boards and other construction parts. Measurements have shown that a tongue and groove joint can not always guarantee sufficient airtightness, because the weakest points are not improved: (1) joints when boards must be cut to size, (2) joints in corners, (3) joints that are damaged because of bad handling, etc. [2]. The major problem, however, is the joints between the insulation boards and other construction parts (e.g., windows), whose width, in practice, can vary from a few millimetres to several centimetres. It is clear that this is mainly a problem of workmanship.

The airtightness of the mineral wool used in Configurations 4 to 7 was measured using a pressure box. More information on the method can be found in Ref 3. The air flow through the mineral wool is given as

$$q = a \cdot \Delta p$$

where

- q = air flow, $\text{m}^3/(\text{m}^2 \cdot \text{s})$,
- Δp = pressure difference, Pa,
- $a = 4.0\text{E-}4 \text{ m}^3/(\text{N} \cdot \text{s})$ (Configuration 4),
- $a = 15.0\text{E-}4 \text{ m}^3/(\text{N} \cdot \text{s})$ (Configuration 5), and
- $a = 25.0\text{E-}4 \text{ m}^3/(\text{N} \cdot \text{s})$ (Configuration 6).

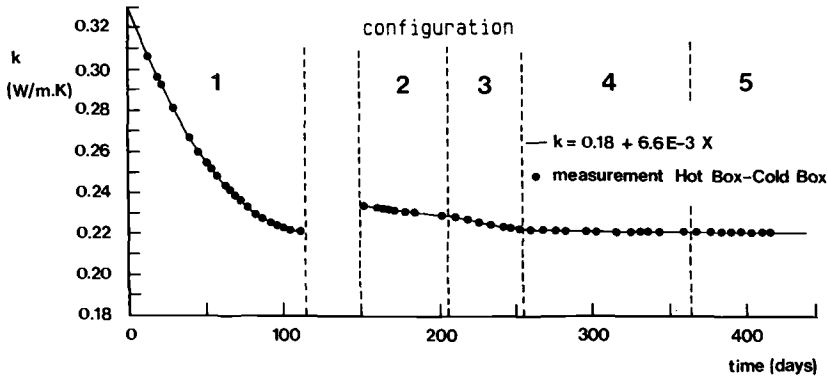


FIG. 5—Thermal conductivity of cellular concrete.

In the case of fibrous materials, a is a constant, independent of the pressure difference. Besides air flow through the mineral wool, the joints must be taken into account, as explained above. These joints are easier to close, however, due to the compressibility of the mineral wool. The mineral wool used in Configuration 7 is of a similar type as in Configuration 6, but with the addition of a kraft paper on one side. The joints between the kraft paper are not sealed during the measurements.

Note that the inner and outer walls are airtight.

Measurement Equipment

Hot Box-Cold Box—The test wall is placed in a calibrated Hot Box-Cold Box (Fig. 6). The Cold Box is equipped with a cooling radiator, coupled to an external cooling machine. Four fans assure a horizontal cold air stream along the outside of the test wall with a velocity of approximately 4 m/s, $h_e = 25 \text{ W}/(\text{m}^2 \cdot \text{K})$. The Hot Box is heated by two convectors coupled to a computer controlled d-c power source. Two fans assure forced convective heat transfer at the inside of the test wall, $h_i = 16 \text{ W}/(\text{m}^2 \cdot \text{K})$. A full description of this equipment can be found in Ref 1.

Measurement Points in Hot Box-Cold Box—The measurement points in the Hot Box and Cold Box are given below:

Hot Box:

- Air temperature at 8 points (8 quadrants).
- Mean radiant temperature at 3 points (Fig. 6: R1, R2, R3).
- Inner and outer surface temperatures of the different Hot Box walls, needed to calculate the heat losses to (or from) the laboratory.
- Heat flow through the upper and bottom walls of the Hot Box.
- Heating power of the convectors.

Cold Box:

- Air temperature at 5 points.

Data Acquisition—Data measuring, averaging, and recording is effectuated by a data acquisition/control Unit, coupled to a microcomputer. The results are the mean values of 144 measurements with intervals of 10 min (24 h) after steady-state conditions have been reached.

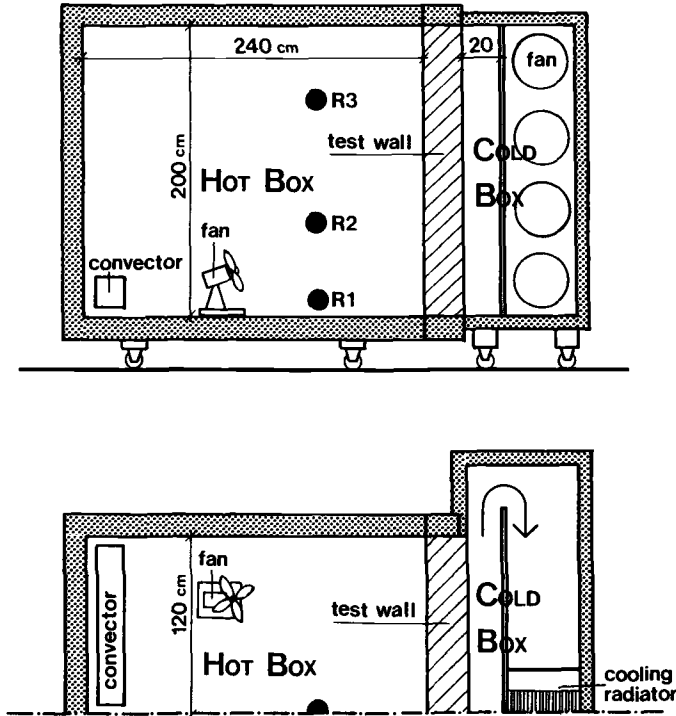


FIG. 6—Hot Box-Cold Box (side view and top view).

Calculation of Thermal Transmittance of Test Wall

Two different methods are used to calculate the thermal transmittance of the test wall (the effective U -value, $W/(m^2 \cdot K)$). Since both methods are independent, measurement errors can be detected and the accuracy improved.

The latent heat transfer due to the drying out of the inner wall had no measurable influence on the thermal transmittance of the test wall. This is illustrated in Measurements 9 and 33 (reference cases with no air leakage), where the measured and calculated U -values are in very good agreement. This is explained by the fact that most of the moisture that evaporates from the inner wall condenses against the cavity side of the outer wall, as was observed during the measurements.

Heat Balance of Hot Box—The thermal transmittance of the test wall, U_h ($W/(m^2 \cdot K)$), is calculated from the heat balance of the Hot Box:

$$U_h = \frac{W_1 + W_2 - Q_l - Q_e}{A \cdot (\theta_i - \theta_e)}$$

where

- W_1 = measured heating power of convectors, W ,
- W_2 = heating power dissipated by two small fans, W ,
- Q_l = conduction through walls of Hot Box, W ,

- Q_e = flanking heat transfer through the sample frame to the laboratory and Cold Box (calculated using the computer program KOBUR86 [4], W,
 A = area of test wall (= 4.8 m²),
 θ_i = measured radiant temperature R2 (difference between R1, R2, and R3 was less than 0.1°C), °C, and
 θ_e = measured air temperature in Cold Box (average of 5 points), °C.

Calculated Heat Flow Through Inner Wall—Out of the measured wall temperatures on both sides of the inner wall and the k -values given previously, the heat fluxes through the inner wall are calculated using the computer program KOBUR86 [4] for two-dimensional, steady-state heat transport. Taking into account the heat losses from the edges, the thermal transmittance of the test wall, U_i (W/(m² · K)), can be calculated. The measurement results of the heat flux transducers are used as an additional control on the calculated heat flux profiles.

Overview of Measurement Results

Tables 1 to 7 give the measured U -value of the test wall compared with the theoretical U -value, calculated from the thermal conductivities given previously, supposing no air flow. The calculated U -value, U_c , is the result of a computer simulation of the test wall.

Abbreviations used in Tables 1 to 7 are as follows:

- w_t = width of top gap, mm,
 w_l = width of lower gap, mm,
 Q_h = total heating power dissipated in Hot Box (= $W_1 + W_2$), W,
 θ_e = air temperature in Cold Box, °C,
 θ_i = radiant temperature in Hot Box, °C,
 U = theoretical U -value, W/(m² · K),
 U_i = effective U -value, W/(m² · K),
 U_h = effective U -value, W/(m² · K),
 d_e = (insulation thickness) - $(1/U - 1/U_h) \cdot (k\text{-insulation})$, mm; d_e is the effective insulation thickness (i.e., the thickness the insulation should have, where there is no air flow around the insulation, to obtain the same U -value as the measured effective U -value, U_h), and
 U_c = calculated U -value, W/(m² · K).

The results of measurements for Configurations 1 to 3 are valid for all insulation materials so far as the influence of air gaps is concerned. The results of measurements for Configurations 4 to 7 are specifically applicable to mineral wool.

The temperature profiles of the measurements marked with an asterisk in Tables 1 to 7 can be found in Figs. 7a to 7d. The figures give the measured surface temperatures on both sides of the outer wall, the insulation, and the inner wall as a function of height (for more information see Fig. 11). From Measurement 62 on, only the surface temperatures of the outer wall and inner wall are plotted.

Figures 7a to 7d clearly show the temperature gradients resulting from the air flows around the insulation layer: the inner wall is cooled down and the outer wall is heated up (compare, for example, Measurement 9 (reference case with no air leakage) with Measurement 27). This effect is more local in the case of small air gaps and/or small cavities (compare Measurements 45 and 48, Measurements 45 and 50). Remarkably the temperature gradient at the inner surface of the inner wall is very small compared to that at the cavity side of the inner wall. Thus it is very difficult to detect what happens in the cavity just by measuring surface temperatures at the inner surface of the cavity constructions. Only U -value measurements are suited for this purpose.

TABLE 1—Measurements for Configuration 1 (50 mm extruded polystyrene, Cavity C = 40 mm, Cavity H = 10 mm).^a

No.	w_i		w_i	Q_h	θ_e	θ_i	U_i	$W/(m^2 \cdot K)$		U	U_h/U	d_e	U_c	$U_c - U_h$
	mm	mm	mm	W	°C	°C					%	mm		$W/(m^2 \cdot K)$
* 9	0	0	0	48	1.5	21.3	0.36	0.35	0.35	100	100	50	0.35	0.00
33	0	0	0	48	1.1	21.0	0.34	0.33	0.33	101	101	49	0.33	0.00
*12	22	17	17	48	1.4	17.6	0.73	0.73	0.35	211	211	6	0.72	-0.01
15	22	17	17	93	1.6	23.0	0.75	0.76	0.35	220	220	4	0.76	0.00
13	22	17	17	138	1.4	25.7	0.80	0.80	0.35	230	230	3	0.79	-0.01
*17	11	8	8	48	1.7	17.8	0.70	0.70	0.34	208	208	6	0.68	-0.02
19	11	8	8	94	1.6	22.4	0.72	0.74	0.34	217	217	4	0.72	-0.02
18	11	8	8	137	1.6	26.6	0.76	0.77	0.34	225	225	3	0.75	-0.02
*20	7	3	3	48	0.8	19.1	0.59	0.60	0.34	175	175	14	0.59	-0.01
21	7	3	3	94	0.9	22.7	0.63	0.64	0.34	189	189	10	0.62	-0.02
24	7	3	3	137	0.9	26.8	0.65	0.67	0.34	198	198	8	0.65	-0.02
*27	2	2	3	48	0.8	20.0	0.49	0.48	0.34	142	142	25	0.49	+0.01
26	2	2	3	94	0.8	23.6	0.51	0.52	0.34	153	153	21	0.51	-0.01
25	2	3	3	138	0.8	27.6	0.54	0.54	0.34	159	159	18	0.53	-0.01
30	22	0	0	48	0.8	23.0	0.38	0.38	0.34	114	114	40
29	22	0	0	95	0.8	28.0	0.39	0.40	0.34	119	119	36
31	0	17	17	48	0.9	25.4	0.35	0.35	0.34	105	105	46
32	0	17	17	95	0.9	28.5	0.36	0.36	0.34	108	108	43
Test Wall Without Insulation														
*36	48	1.2	16.7	0.99	0.99	1.00	295 ^b	295 ^b	...	1.00	+0.01
35	95	1.0	20.7	1.00	1.00	1.00	297 ^b	297 ^b	...	1.00	0.00
34	138	1.1	23.9	1.00	1.00	1.00	299 ^b	299 ^b	...	1.00	0.00

^aSee text for key to abbreviations.
^bThe insulated test wall is taken as reference.

TABLE 2—Measurements for Configuration 2 (50 mm extruded polystyrene, Cavity $C = 25$ mm, Cavity $H = 25$ mm).^a

No.	w_i		Q_h	θ_e	θ_i	U_i		U	U_h/U	d_e	U_e	$U_e - U_h$
	mm	mm	W	°C	°C	$W/(m^2 \cdot K)$			%	mm		$W/(m^2 \cdot K)$
41	0	0	48	1.2	23.0	0.36	0.36	0.35	101	49	0.35	-0.01
*42	18	18	48	1.1	18.1	0.82	0.84	0.35	239	2	0.86	+0.02
43	18	18	137	1.0	26.7	0.87	0.90	0.35	256	0	0.90	0.00
*45	5	5	48	1.0	18.7	0.73	0.72	0.35	205	7	0.74	+0.02
46	5	5	94	0.9	24.0	0.76	0.77	0.35	222	5	0.78	+0.01
44	5	5	138	1.0	27.2	0.79	0.81	0.35	230	3	0.80	-0.01
*48	2	2	48	1.0	20.8	0.41	0.40	0.35	114	40	0.40	0.00
47	2	2	93	1.0	27.0	0.45	0.43	0.35	124	34	0.42	-0.01

^aSee text for key to abbreviations.TABLE 3—Measurements for Configuration 3 (50 mm extruded polystyrene, Cavity $C = 45$ mm, Cavity $H = 5$ mm).^a

No.	w_i		Q_h	θ_e	θ_i	U_i		U	U_h/U	d_e	U_e	$U_e - U_h$
	mm	mm	W	°C	°C	$W/(m^2 \cdot K)$			%	mm		$W/(m^2 \cdot K)$
56	0	0	48	1.0	19.7	0.34	0.35	0.35	102	48	0.35	0.00
*50	18	18	48	0.9	19.9	0.42	0.42	0.35	121	35	0.44	+0.02
51	18	18	94	1.0	25.5	0.45	0.45	0.35	130	31	0.46	+0.01
*53	5	5	48	0.9	19.1	0.41	0.42	0.35	121	35	0.42	0.00
52	5	5	94	0.9	24.7	0.43	0.44	0.35	128	32	0.44	0.00
*54	2	2	48	1.0	20.1	0.39	0.39	0.35	112	41	0.40	+0.01
55	2	2	93	1.0	23.7	0.41	0.42	0.35	120	36	0.41	-0.01

^aSee text for key to abbreviations.

TABLE 4—Measurements for Configuration 4 (50 mm mineral wool, $\rho = 48 \text{ kg/m}^3$).^a

No.	w_i	w_l	Q_h	θ_c	θ_l	U_i	U_h	U	U_h/U	d_c	U_c	$U_c - U_h$
	mm	mm	W	°C	°C	W/(m ² · K)			%	mm	W/(m ² · K)	
Cavity C = 50 mm, Cavity H = 0 mm												
*84	0	0	48	0.9	24.3	0.36	0.35	0.35	99	51	0.35	0.00
Cavity C = 30 mm, Cavity H = 20 mm												
*81	0	0	48	0.9	23.5	0.35	0.34	0.35	97	53	0.36	+0.02

^aSee text for key to abbreviations.

TABLE 5—Measurements for Configuration 5 (50 mm mineral wool, $\rho = 23 \text{ kg/m}^3$).^a

No.	w_i	w_l	Q_h	θ_c	θ_i	U_i	U_h	U	U_h/U	d_c	U_c	$U_c - U_h$
	mm	mm	W	°C	°C	W/(m ² · K)			%	mm	W/(m ² · K)	
Cavity C = 50 mm, Cavity H = 0 mm												
*64	0	0	48	1.1	20.5	0.38	0.39	0.39	102	48	0.39	0.00
65	13	13	48	1.0	20.9	0.38	0.40	0.39	102	48	0.39	-0.01
Cavity C = 40 mm, Cavity H = 10 mm												
*62 ^b	0	0	48	0.9	19.7	0.47	0.48	0.39	123	33	0.45	-0.03
63 ^b	13	13	48	1.1	18.7	0.67	0.65	0.39	167	15	0.67	+0.02
Cavity C = 30 mm, Cavity H = 20 mm												
*72	0	0	48	1.1	22.6	0.43	0.44	0.39	113	40	0.45	+0.01
70	10	90	48	1.1	17.1	0.81	0.78	0.39	202	6	0.79	+0.01
Cavity C = 40-50 mm, Cavity H = 0-10 mm												
67	10	10	48	1.0	20.0	0.47	0.48	0.39	123	34	0.39-0.53-	

^aSee text for key to abbreviations.

^bThere are small air gaps between several insulation boards due to damage at the corners of the boards.

TABLE 6—Measurements for Configuration 6 (60 mm mineral wool, $\rho = 16 \text{ kg/m}^3$).^a

No.	w_i mm	w_l mm	Q_h	θ_c °C	θ_i °C	U_i	U_h	U	U_h/U %	d_c mm	U_c	$U_c - U_h$ $W/(m^2 \cdot K)$
Cavity C = 40 mm, Cavity H = 0 mm												
*76	0	0	48	1.0	22.1	0.37	0.36	0.35	103	57	0.35	-0.01
Cavity C = 20 mm, Cavity H = 20 mm												
73	0	0	48	1.4	23.4	0.46	0.47	0.35	134	35	0.45	-0.02
*74	0	0	48	1.0	20.8	0.44	0.45	0.35	126	39	0.45	0.00
Cavity C = 20-40 mm, Cavity H = 0-20 mm												
75	0	0	48	1.0	19.4	0.43	0.42	0.35	120	43	0.35-0.45-	

^aSee text for key to abbreviations.TABLE 7—Measurements for Configuration 7 (50 mm mineral wool, $\rho = 18 \text{ kg/m}^3$, kraft paper on one side).^a

No.	w_i mm	w_l mm	Q_h	θ_c °C	θ_i °C	U_i	U_h	U	U_h/U %	d_c mm	U_c	$U_c - U_h$ $W/(m^2 \cdot K)$
Cavity C = 50 mm, Cavity H = 0 mm												
*83 ^b	0	0	48	1.1	24.4	0.39	0.39	0.40	98	52	0.40	+0.01
Cavity C = 30 mm, Cavity H = 20 mm												
*82 ^b	0	0	48	0.9	23.6	0.47	0.46	0.40	116	38	0.49	+0.03

^aSee text for key to abbreviations.^bThe joints between the kraft paper are not sealed.

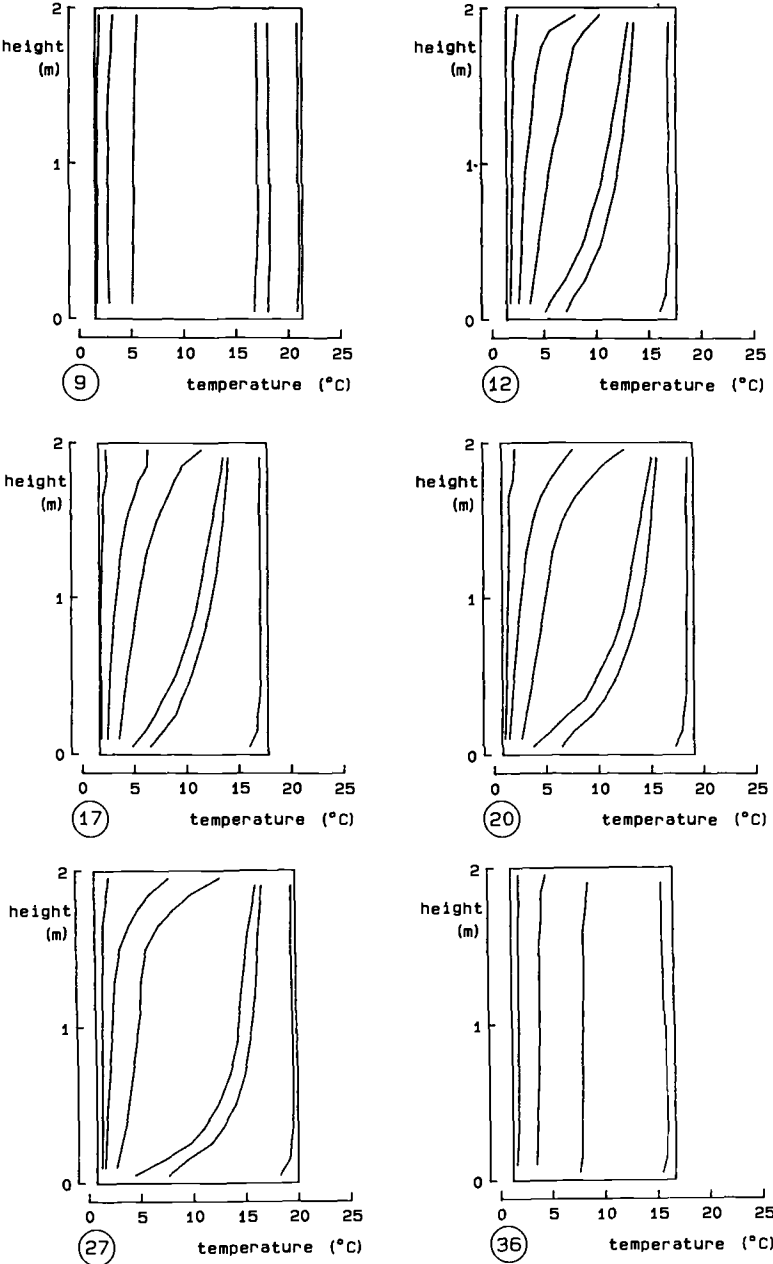


FIG. 7a—Temperature profiles.

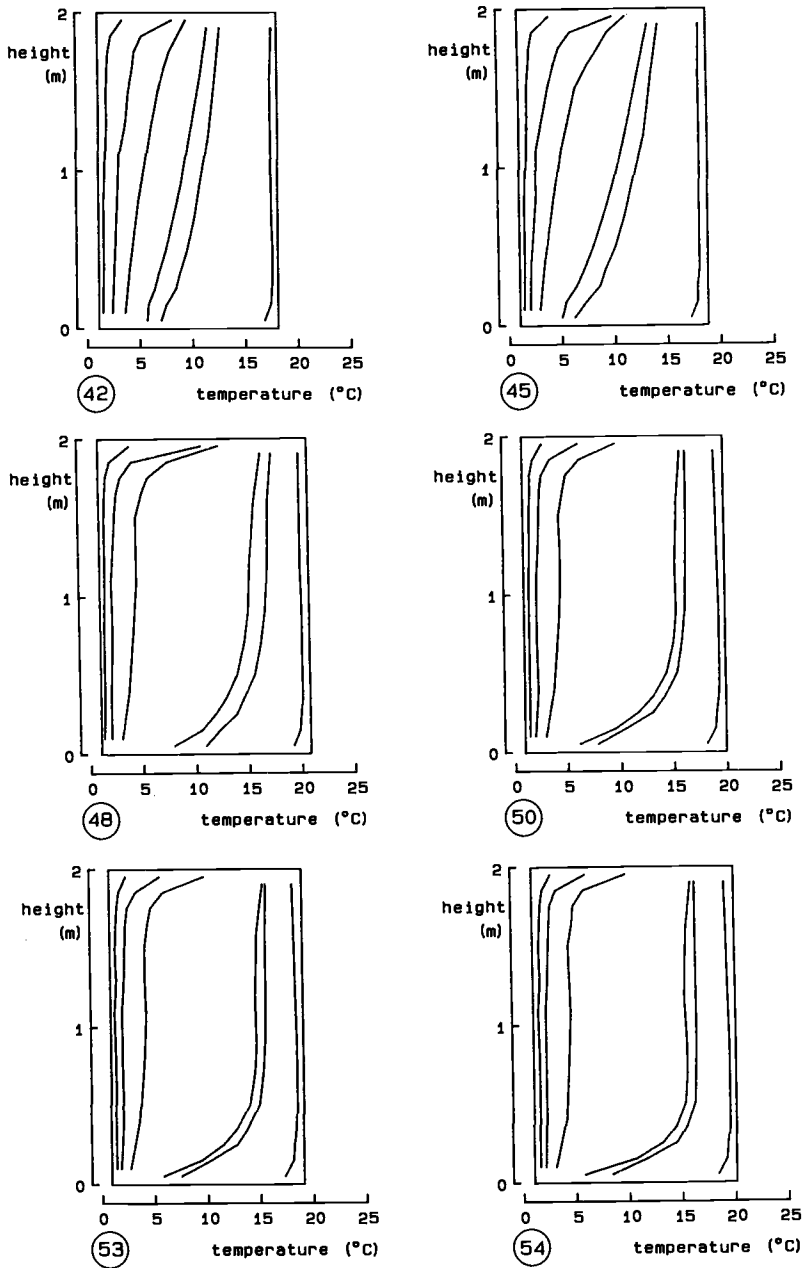


FIG. 7b—Temperature profiles.

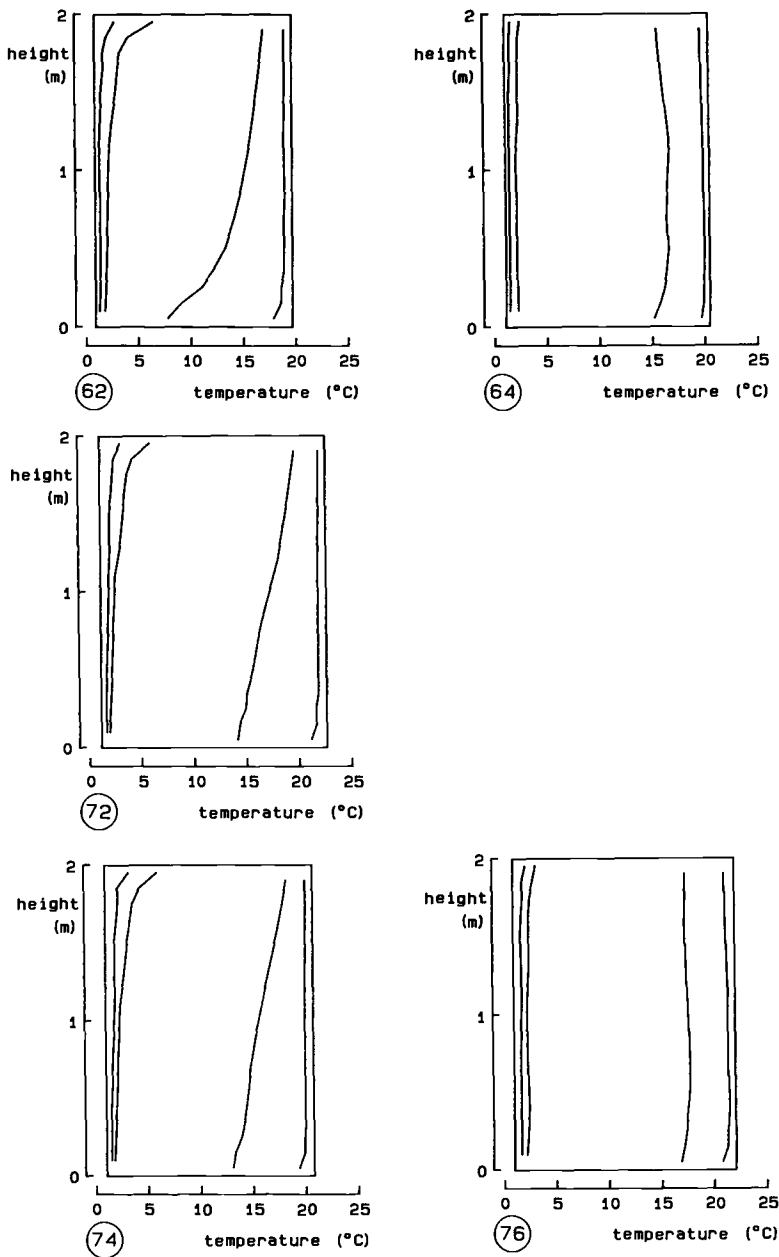


FIG. 7c—Temperature profiles.

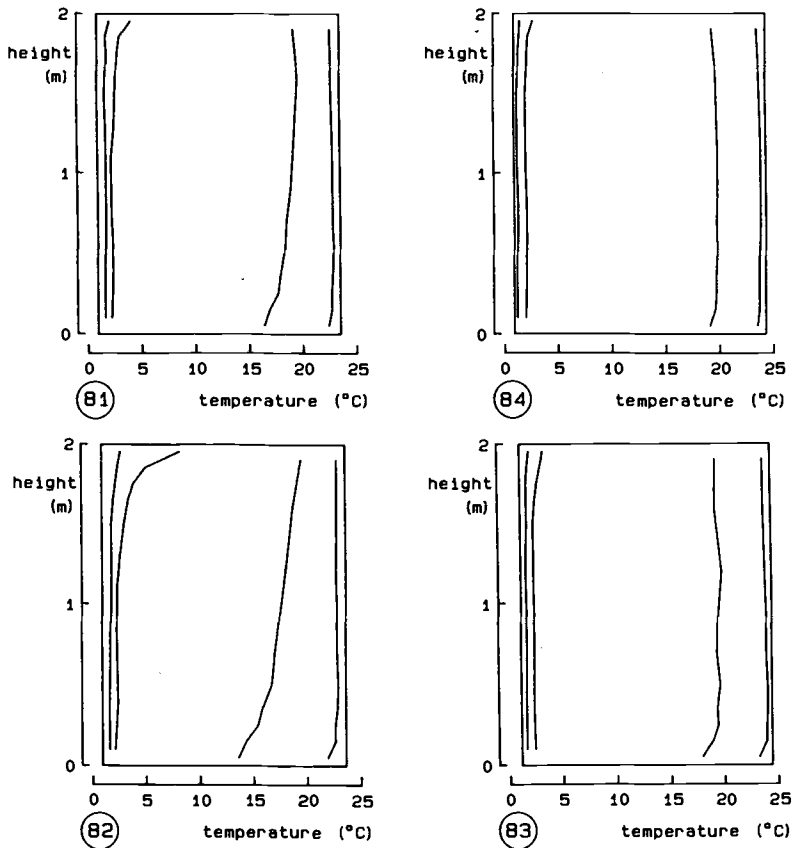


FIG. 7d—Temperature profiles.

Numerical Simulation

Calculation Model

For the calculation of the two-dimensional, steady-state air and heat transport, the method described in Refs 5 and 6 is used. A construction is transformed in a network of resistances, and in each node the laws of mass and energy conservation are applied. The two coupled sets of equations are iteratively solved. Natural convection is calculated as described in Ref 2. The difference in weight of the two air columns on both sides of the insulation is taken as the driving force for the air flow around and through the insulation layer. The major problem is the correct calculation of the convective heat transfer coefficients. Radiation through the cracks is not taken into account, since the total leakage area is very low in the presented examples (less than 2%).

The computer program offers the possibility of solving a general, two dimensional problem (Fig. 8). The air gaps in the insulation layer can be placed anywhere, the insulation can have a specified airtightness, and outer and inner wall are considered as airtight. The program calculates the temperature profiles and the overall heat transfer (the effective U -value). An overview of the results is given next.

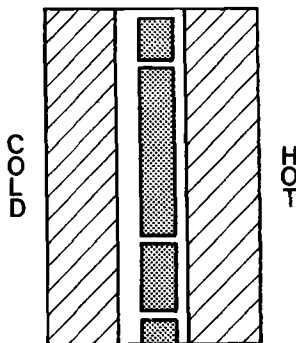


FIG. 8—General problem.

Sample Calculation

As an example, Measurement 20 is calculated as:

- Theoretical U -value : $U = 0.35 \text{ W}/(\text{m}^2 \cdot \text{K})$
- Effective U -value (Measured) : $U_i = 0.59 \text{ W}/(\text{m}^2 \cdot \text{K})$
 $U_h = 0.60 \text{ W}/(\text{m}^2 \cdot \text{K})$
 (Calculated) : $U_c = 0.59 \text{ W}/(\text{m}^2 \cdot \text{K})$

Figure 9 compares the measured and calculated temperature profiles (see also Figs. 7a to 7d).

Application 1: A Partially Filled Cavity Wall (Height = 2 m)

Table 8 gives the relevant data for a partially filled 2-m-high cavity wall. Figure 10 shows the ratio of the calculated effective U -value, U_c ($\text{W}/(\text{m}^2 \cdot \text{K})$), and the theoretical U -value ($U = 0.37 \text{ W}/(\text{m}^2 \cdot \text{K})$), as a function of the width of the top gap, W_t (mm) and the lower gap, W_l (mm); W_t and W_l are taken as equal. The widths of Cavity C and Cavity H are considered as parameters.

Application 2: Influence of Airtightness of Mineral Wool

The same cavity wall as above is taken, but 50 mm mineral wool is used as insulation material (thermal conductivity, $k = 0.035 \text{ W}/(\text{m} \cdot \text{K})$). Figure 11 shows the ratio of the calculated effective U -value, U_c ($\text{W}/(\text{m}^2 \cdot \text{K})$), and the theoretical U -value ($U = 0.44 \text{ W}/(\text{m}^2 \cdot \text{K})$), as a function of the airtightness of the mineral wool. The widths of Cavity C and Cavity H are considered as parameters. There are no gaps in the insulation layer.

From Fig. 11 and Configurations 4 to 7 it can be concluded that when mineral wool is used in a partially filled cavity and the insulation boards can not be fixed against a surface of the cavity (e.g., due to traditional workmanship in some specific applications), the use of mineral wool of higher density should be recommended, since density and airtightness are directly coupled. The relationship between the density and the airtightness of mineral wool can be approximated by the following expressions that are valid for air flow perpendicular to the fibers:

$$\begin{aligned} \text{glass wool: } a &= 3.6\text{E-}3 \cdot \rho^{-1.3}/d \text{ m}^3/(\text{N} \cdot \text{s}) \\ \text{rock wool: } a &= 1.7\text{E-}2 \cdot \rho^{-1.5}/d \text{ m}^3/(\text{N} \cdot \text{s}) \end{aligned}$$

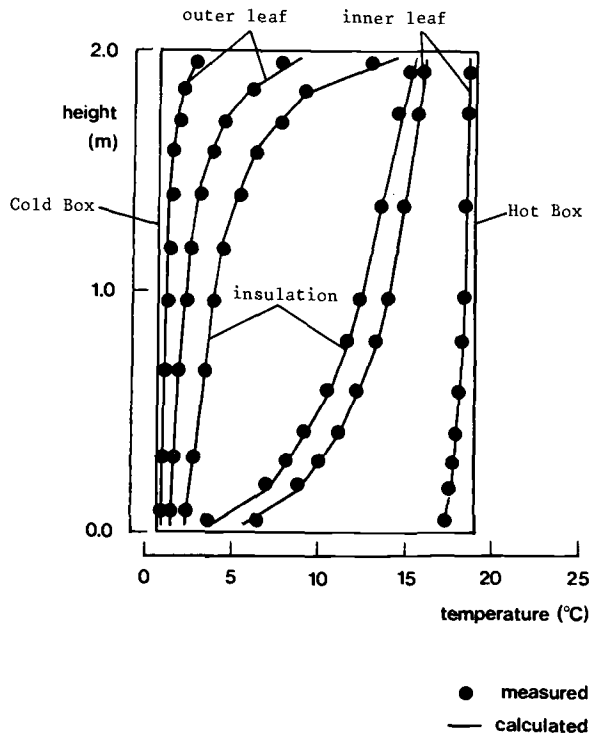


FIG. 9—Measured and calculated temperature profiles.

TABLE 8—Data for 2-m-high partially filled cavity wall (Application 1).

Section	Thickness, mm	k , W/(m · K)
Outside:		
Outer wall, brickwork	90	1
Cavity C		
Insulation (airtight)	50	0.029
Cavity H		
Inner wall, brickwork	140	0.7
Gypsum rendering	10	0.26
Inside:		
$\theta_e = 0^\circ\text{C}$	$h_e = 23 \text{ W}/(\text{m}^2 \cdot \text{K})$	
$\theta_i = 20^\circ\text{C}$	$h_i = 8 \text{ W}/(\text{m}^2 \cdot \text{K})$	

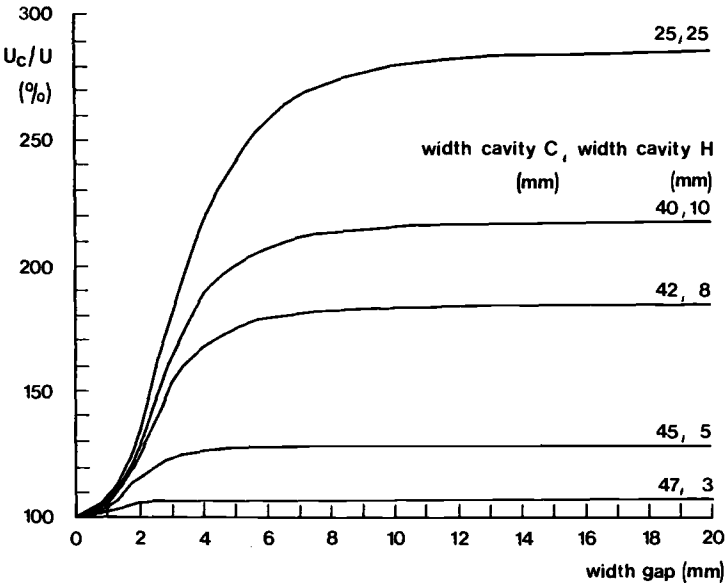


FIG. 10—Airtight insulation (50 mm).

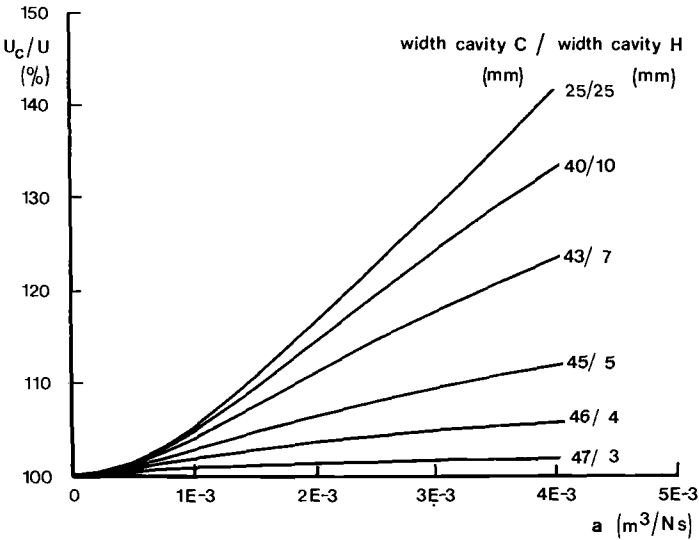


FIG. 11—Mineral wool (50 mm); no air leaks.

where

d = thickness of insulation, m, and
 ρ = density, kg/m³.

These relations are calculated from measurement results of Ref 7 and our own measurements. As an upper limit, $a = 5\text{E-}4 \text{ m}^3/(\text{N} \cdot \text{s})$ can be proposed. From this, and the expressions given above, the lower limit for the density of the mineral wool can be calculated as a function of insulation thickness. The results for glass wool and rock wool are shown in Fig. 12. These requirements are only applicable in cases where there are small cavities on both sides of the mineral wool insulation.

Experimental Study: Influence of Cavity Slope

Measurement Setup

A test cavity is placed between a hot plate and a cold plate (Figs. 13 and 14); these plates are coupled to external cooling and heating machines. The variation of the surface temperature over both plates was less than 0.2°C. Layers of 50 mm extruded polystyrene are placed between the test cavity and each plate. From the measured temperature difference across these insulation layers, the heat flow through the test cavity was calculated. The thermal conductivity, k (W/(m · K)), of the polystyrene as a function of temperature, θ (°C), is determined in the heat flow apparatus: $k = 0.0202 + 2.1\text{E-}4 \cdot \theta$. This expression is valid over the range 10 to 30°C. As insulation in the test cavity, 50 mm extruded polystyrene is used, $k = 0.024 \text{ W}/(\text{m} \cdot \text{K})$.

The whole measurement setup can be rotated. The slope can vary continuously from 0° (cold plate on top) over 90° (vertical) to 180° (hot plate on top).

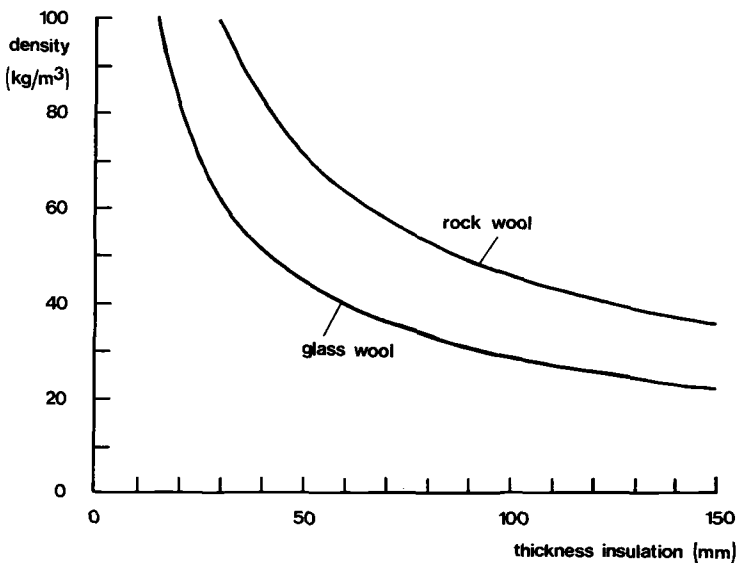


FIG. 12—Lower limit for density of mineral wool as function of insulation thickness.

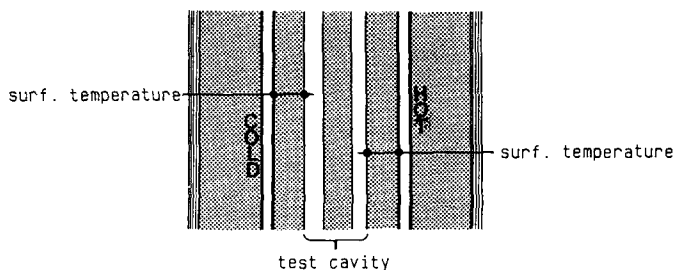


FIG. 13—*Test cavity.*

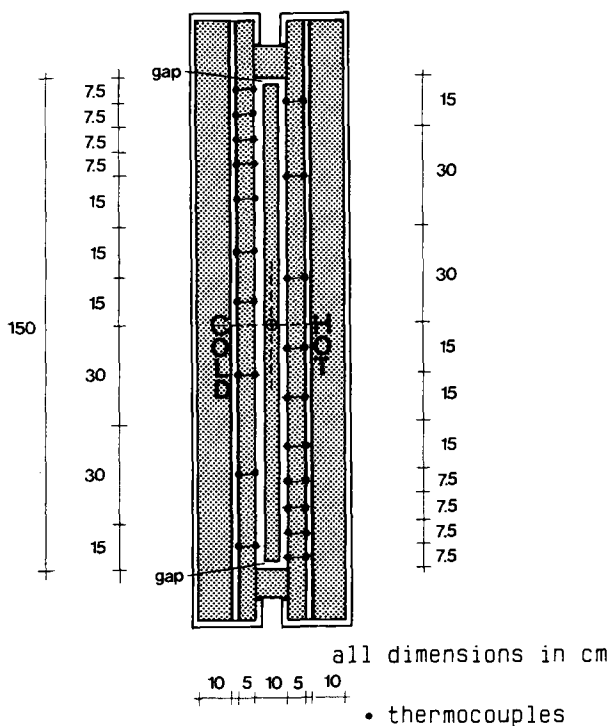


FIG. 14—Measurement setup.

Data Acquisition

Data measuring, averaging, and recording is effectuated by a data acquisition/control unit, coupled to a microcomputer. Cu/C thermocouples are used for the temperature measurements (0.25 mm diameter). The results are the mean values of 12 measurements with intervals of 5 min (1 h) after steady-state conditions have been reached.

Calculation of Heat Flow Through Test Cavity

The heat flow through the test cavity is calculated from the measured surface temperatures on both sides of the insulation against the cold plate, q_c (W/(m² · K)) and against the hot plate,

q_h ($\text{W}/(\text{m}^2 \cdot \text{K})$), using the computer program KOBUR86 [4]. Figure 15 shows the ratio of the effective heat loss, q_e ($\text{W}/(\text{m}^2 \cdot \text{K})$), and the theoretical heat loss, q ($\text{W}/(\text{m}^2 \cdot \text{K})$); q_e/q is calculated as

$$\frac{q_e}{q} = \frac{R}{R_e} = \frac{R_t - R_c - R_h}{2 \cdot \Delta\theta / (q_c + q_h) - R_c - R_h} = \frac{6.53 - 2.17 - 1.93}{38.6 / (q_c + q_h) - 2.17 - 1.93}$$

where

R = theoretical thermal resistance of test cavity ($= 2.43 \text{ (m}^2 \cdot \text{K)/W}$),

R_c = thermal resistance of insulation against cold plate,

R_h = thermal resistance of insulation against hot plate,

R_t = total thermal resistance of construction ($= R + R_c + R_h$),

R_e = effective thermal resistance of the test cavity (measured) ($= 2 \cdot \Delta\theta / (q_c + q_h) - R_c - R_h$, and

$\Delta\theta$ = temperature difference between hot and cold plate ($= 19.3^\circ\text{C}$).

Figure 16 shows the effective insulation thickness, d_e (mm):

$$d_e = (\text{insulation thickness}) - (R - R_e) \cdot (k\text{-insulation})$$

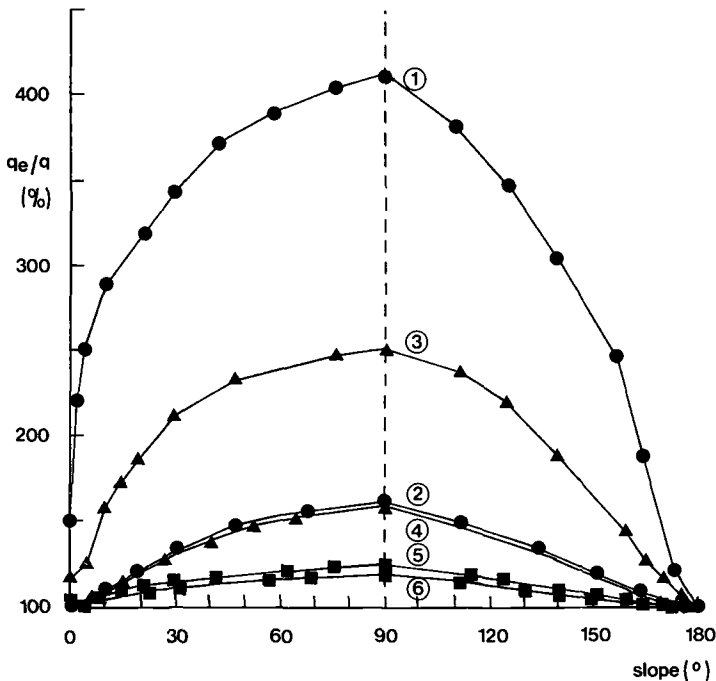


FIG. 15— q_e/q values for 50 mm extruded polystyrene.

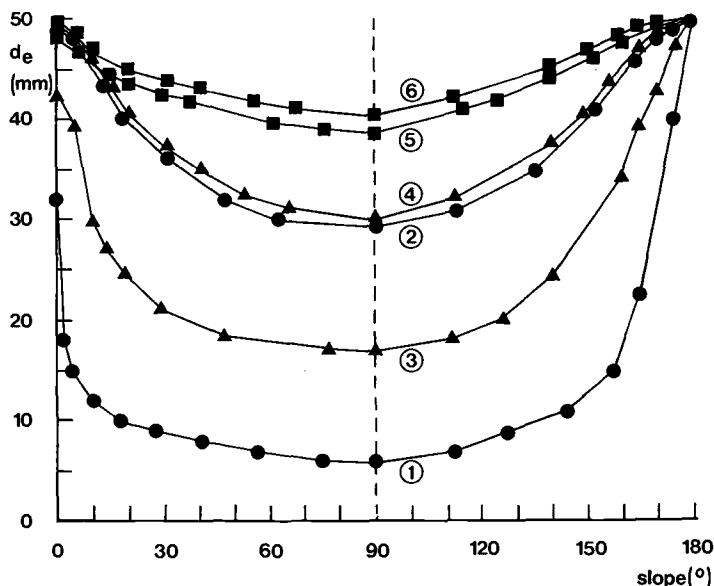


FIG. 16—Effective insulation thickness for 50 mm extruded polystyrene.

Overview of Results for 50 mm Extruded Polystyrene

The odd-numbered curves have gap widths of 14 mm for both the top gap and bottom gap; the even-numbered curves have gap widths of 3 mm.

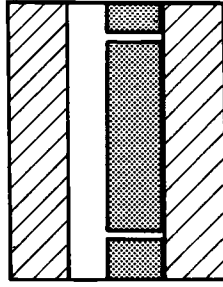
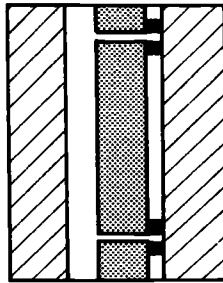
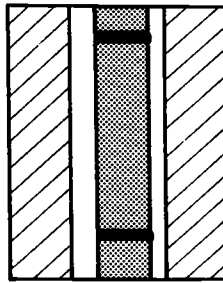
- Curves 1 and 2: width of Cavity C = 35 mm, Cavity H = 15 mm.
- Curves 3 and 4: width of Cavity C = 40 mm, Cavity H = 10 mm.
- Curves 5 and 6: width of Cavity C = 45 mm, Cavity H = 5 mm.

Conclusions

From this research it can be concluded that stringent requirements must be formulated concerning the correct application of insulation materials in constructions with insulated cavities, since even small air leaks can cause a substantial increase in heat loss. Not only are constructions with vertical cavities affected, but also those with small slopes (e.g., lightweight roofs). Where the insulation also has the function of vapor barrier in timber frame constructions (hard foam insulation, mineral wool with kraft paper), the air flows cause, aside from an increase of the heat transfer, an important increase of moisture transport towards the cold surface of the cavity. This may result in severe condensation problems due to the large amounts of moisture involved [8].

A first solution to the presented problems is the fixing of the insulation boards against one surface of the cavity in order to eliminate the cavity on one side of the insulation layer (Fig. 17). This is only possible if the surface of the cavity is very smooth or if the insulation is sufficiently compressible. A second solution is to seal the cavity on one side of the insulation (Fig. 18). A third solution is to seal the joints between the boards themselves and, especially, between the boards and other construction parts (Fig. 19). In the last two cases, when mineral wool is used, boards of higher density are recommended (Figs. 11 and 12).

It is clear that good workmanship is the major condition needed to obtain a construction of

FIG. 17—*Eliminating a cavity.*FIG. 18—*Sealing a cavity.*FIG. 19—*Sealing all joints.*

high thermal quality. Further research on this subject is at the appropriate solutions for the specific applications of cavity insulation (cavity wall, lightweight roof, . . .) in order to formulate practical guidelines for better workmanship.

There is good agreement between the measured and calculated temperature profiles and heat transfer. Consequently the computer model will be a helpful tool in further research and will be further developed to deal with constructions of a variable slope. A report on this calculation model is being prepared.

References 9 to 13 provide related information.

Acknowledgments

The author wishes to thank The Institute for the Encouragement of Scientific Research in Industry and Agriculture (I.W.O.N.L.), who gave me the opportunity to do this research.

References

- [1] Standaert, P., "Twee- en Driedimensionale Warmteoverdracht: Numerische Methoden, Experimentele Studie en Bouwfysische Toepassingen," Doktoraal Proefschrift, Laboratory of Building Physics, K. U. Leuven, Belgium, 1984.
- [2] Lecompte, J. G. N., "Invloed van Natuurlijke Konvektie op het Hygrothermisch Gedrag van Bouwelementen," Rapport Specialisatiebursaal I.W.O.N.L., Laboratory of Building Physics, K. U. Leuven, Belgium, Part 1: 1985, Part 2: 1986.
- [3] Lecompte, J. G. N., "Airtightness of Masonry Walls," presented to 8th AIVC Conference, Überlingen, FRG, 1987.
- [4] Standaert, P., "KOBUR86: Computer Program to Calculate Two-Dimensional Steady-State Heat Transfer in Objects, Described in a Rectangular Grid, Using the Energy Balance Technique," Belgium, 1986.
- [5] Kronvall, J., "Air Flows in Building Components," Report TVBH-1002, Division of Building Technology, Lund Institute of Technology, Sweden, 1982.
- [6] Vaes, F., "Hygrothermisch Gedrag van Lichte Hellende Daken," Laboratory of Building Physics, K. U. Leuven, Belgium, 1984.
- [7] Bankvall, C. G., "Natural Convective Heat Transfer in Insulated Structures," Report 38, Division of Building Technology, Lund Institute of Technology, Sweden, 1972.
- [8] Lecompte, J., "The Influence of Natural Convection on the Hygrothermal Quality of Insulated Cavity Constructions," in *Proceedings*, CIB Conference on Healthy Buildings '88, Stockholm, Sweden, Vol. 2, 1988, pp. 221-230.
- [9] Arquis, E. and Caltagirone, J. P., "Interacting Convection Between Fluid and Open Porous Layers," presented to ASME Annual Winter Meeting, Boston, 1987.
- [10] Arquis, E., Caltagirone, J. P., and Langlais, C., "Natural Convection in Cavities Partially Filled with Permeable Porous Materials," in *Proceedings*, 8th Heat Transfer Conference, San Francisco, Calif., Vol. 5, 1986, pp. 2653-2658.
- [11] Emery, A. F., "Exploratory Study of Free Convection Heat Transfer Through an Enclosed Vertical Liquid Layer with a Vertical Baffle," *Journal of Heat Transfer*, Vol. 91, 1969, pp. 163-165.
- [12] Kohonen, R., Kokko, E., Ojanen, T., and Virtanen, M., "Thermal Effects of Air Flows in Building Structures," Report 367, Technical Research Centre of Finland, Espoo, Finland, 1985.
- [13] Tye, R. P., Desjarlais, A. O., Bourne, J. C., and Spinney, S. C., "The Effective Thermal Performance of an Insulated Stud Wall Containing Air Gaps," presented to CIB W40 Meeting, Borås, Sweden, 1987.

A Survey of Window *U*-Value Measurements in Sweden (1977–1987)

REFERENCE: Staelens, P., "A Survey of Window *U*-Value Measurements in Sweden (1977–1987)," *Insulation Materials, Testing, and Evaluation, ASTM STP 1030*, D. L. McElroy and J. F. Kimpflen, Eds., American Society for Testing and Materials, Philadelphia, 1990, pp. 421–436.

ABSTRACT: At the Swedish National Testing Institute (SP) window thermal transmittance (*U*-value) measurements are carried out in a Guarded Hot Box (GHB). It is shown that the GHB meets the requirements of the relevant Swedish Standard (SS 024212, 13) and International Standard Draft Proposal (ISO/DP 8990). The SS 024213 measurement routines are discussed.

A survey of measurement results acquired during the last ten years shows the continuous improvement of the *U*-value of windows produced in Sweden as well as the increasing importance of additional panes and improved sealed glazing units.

By way of comparative Guarded Hot Plate (GHP) and GHB measurements on sealed glazing units it is shown that the GHP method should be examined thoroughly and its results handled with care in order to prevent misinterpretation by, for instance, the client. It is further noted that the GHB technique, although commonly used, is not completely investigated and that on the level of standardization much work is yet unfinished.

KEY WORDS: gasfilling, Guarded Hot Box, Guarded Hot Plate, low emissivity film, measurement, round robin, sealed glazing unit, standard, surface resistance, testing institute, thermal conductivity, thermal resistance, window

Measurements on windows have been carried out for more than ten years at the Division for Building Physics of the Swedish National Testing Institute (SP; 1977–1986). These measurements include thermal transmittance (*U*-value), air- and rain-tightness, wind load resistance, thermal load resistance of windows, aging of the sealing of the sealed glazing units, and condensation [1]. All of this research has provided considerable experience within the field of windows and glazing units.

This paper discusses *U*-value measurements of unaged windows and glazing units. The windows and glazing units are mainly produced in Sweden [2,3]. An overall survey of measurements carried out at SP therefore gives a clear picture of the evolution of what Swedish manufacturers have found important as well as of what is sold in Sweden. Because of the relative importance of the Swedish market within Scandinavia, it also pictures rather well the Nordic situation (Fig. 1).

The main reasons why manufacturers have their windows and glazing units tested at SP are:

- There has existed since 1975 a $2 \text{ W}/(\text{m}^2 \cdot \text{K})$ *U*-value requirement in the Swedish Building Code (SBN).
- In 1985 a supplementary $1.6 \text{ W}/(\text{m}^2 \cdot \text{K})$ *U*-value limit was introduced. This again was a government action in order to urge people to build low energy housing. Fulfillment of this requirement gives the principal a more advantageous building loan.

¹Research Engineer, Division for Building Physics, Swedish National Testing Institute, P.O. Box 857, 501 15 Borås, Sweden.

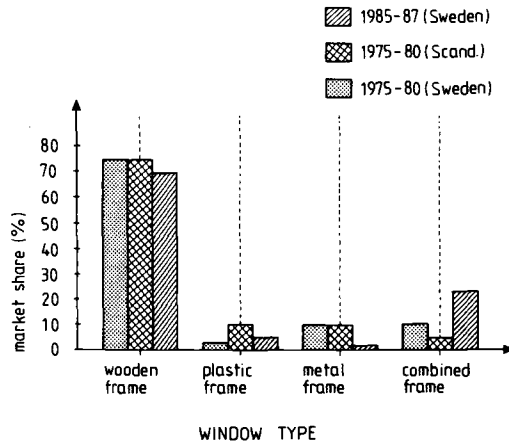


FIG. 1—Survey of Swedish and Scandinavian window market for the periods 1975-80 and 1985-87 [2,3].

The introduction of these requirements made it necessary to build up a quality control system including regular testing. It also made it important to manufacturers to intensify their R&D projects. This, in its turn, made testing at an impartial testing institute both interesting and indispensable.

The impact of the requirements mentioned above was that double and triple glazing are commonly used in Sweden, while in experimental housing quadruple glazing is mainly used now. The impact of the 1985 limit can be clearly pointed out by comparing the types of windows and glazing units tested during the 1977-81 period and those tested between 1982-86. From the surveys shown in Figs. 2a and 2b it can be seen that:

- The proportion of the different types of windows tested agrees well with data on the evolution of the Swedish market (Fig. 1).
- The less insulating, metal frame windows are now not as attractive as during 1977-81. Moreover, most of the metal frame windows tested between 1977-81 were tested in 1977. Some of the manufacturers still thought they could meet the $2 \text{ W}/(\text{m}^2 \cdot \text{K})$ requirement at that time.
- The importance of sealed glazing units with a gas-filling or a low emissivity coating, the so-called improved glazing units, has grown considerably.

Hot Box and Measurement Routines

Window and glazing unit U -value measurements are carried out at SP in a Guarded Hot Box (GHB) (Fig. 3). SP's GHB fulfils the requirements regarding measurement accuracy and overall error of the relevant Swedish Standard (SS 024212) as well as the International Standard Draft Proposal (ISO/DP 8990). A survey of the requirements is given in Table 1 [4]. The thermocouple gage requirement is not met; the thermocouples have a diameter of 0.4 mm instead. The reason is twofold:

- The stability of the air temperature in the rig is such that a 0.4 mm gage thermocouple still has a small time constant (τ) compared to the air temperature variations [5]; the effect on the boundary layer is negligible.
- The thermocouples are applied along the isotherms.

Practice showed that the repeatability of window and glazing unit U -value measurements is within 2%.

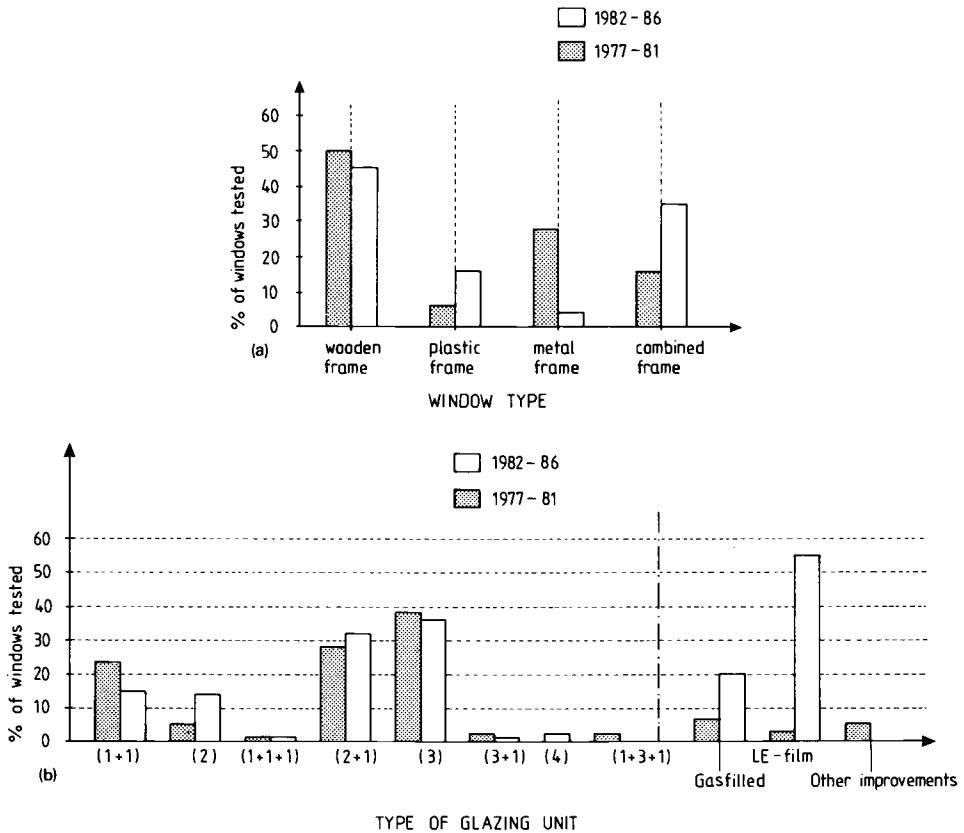


FIG. 2—Specimens tested at SP during the periods 1977-81 and 1982-86. (a) Survey with respect to window type. (b) Survey with respect to type of glazing unit.

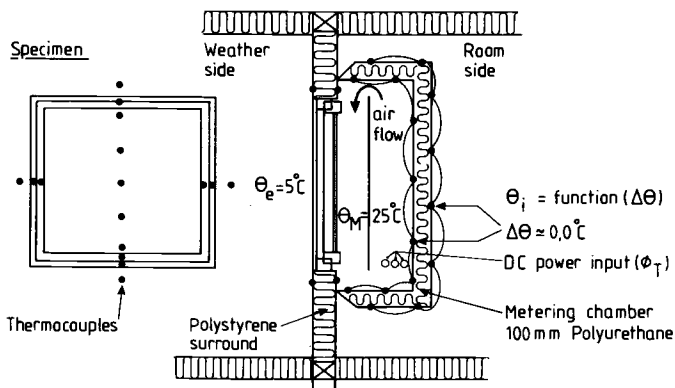


FIG. 3—Guarded Hot Box rig used at the Swedish National Testing Institute and measurement points on a window specimen (according to SS 024213).

TABLE 1—Comparison between SP's GHB and requirements of the Swedish standard (SS 024212, 13) and the ISO standard draft proposal (ISO/DP 8990).

Topic	SS 024212	ISO/DP 8990	SP's Hot Box
Overall Error			...
Temperature	±10%	±5%	
Indoor chamber			
Environmental chamber			298 K(+25°C) 268 K(-5°C) 283 K(+10°C)
Specimen's mean temperature	283 K(+10°C)	283 K(+10°C)	
Temperature Stability			
Metering chamber	±0.3 K	±0.3 K	±0.1 K
Indoor chamber	±0.3 K	±0.3 K	±0.3 K
Environmental chamber	±1.0 K	±0.3 K	±0.2 K
Temperature Gradient			
Vertical	...	<2 K/m	<1 K/m <2 K/m (windows)
Horizontal	...	<0.6 K	<0.5 K
Thermocouple gage	<0.5 mm	<0.25 mm	0.4 mm (*)
Accuracy			
Area	±2%	<0.5%	<±0.5%
Thickness	...	<1.0%	<±1.0 mm
Absolute temperatures	±0.2 K	±1.5 K	±0.1 K (**)
Differential temperatures	...	±0.3 K	±0.1 K (**)
Total power, Φ_T	±2%	<±1.5% Φ_1	±0.2%
Metering Chamber (flow through metering chamber's walls is denoted Φ_3)			
Thermal resistance	>1 (K · m ²)/W	<20 mm	5 (K · m ²)/W ≈10 mm
Gasket	...		

Thermopile ($m^2/\text{junction}$)	...	0.25	< 0.25 $< \pm 0.05 \text{ K}$ $< \pm 0.2 \text{ K (windows)}$...
Imbalance	...		
Error on flow, $\Delta\Phi_3$...		
Mask (flow through mask on account of two-dimensional effect is denoted Φ_2)	...	$< 0.5\% \Phi_1$	
Type	EPS without load-bearing elements
Surface Resistance	...		
Metering chamber (m_i)	$m_i \approx 0.13\text{--}0.18 \text{ (m}^2 \cdot \text{K)}/\text{W}$ (lower value for windows)
Environmental chamber (m_e)	...	$0.1 < v < 10 \text{ m/s}$	$m_e \approx 0.04\text{--}0.07 \text{ (m}^2 \cdot \text{K)}/\text{W}$
$m_i + m_e$	$0.25 \text{ (m}^2 \cdot \text{K)}/\text{W}$ $0.20 \text{ (m}^2 \cdot \text{K)}/\text{W}$ windows included in Φ_T		
Fans (error on power measurement)	...	$< 0.5\% \Phi_1$	Natural downward convection in metering chamber; forced downward convection in environmental chamber
Cooling Plenum	None
Ice Bath	...	$\pm 0.05 \text{ K}$	$< \pm 0.05 \text{ K}$
Measurement Period	3 h; maximum difference between two successive periods: 2%	1%	O K

(*) 0.4 mm gage thermocouples are used because they are placed on the isotherms and because of the stability of the rig (a slightly higher time constant is acceptable).

(**) After calibration of the whole data acquisition system.

Φ_1 (W) is the flow through the specimen.

EPS is expanded polystyrene.

Window U -value measurements are carried out according to Swedish Standard SS 024213. In SS 024213 it is left to the testing institute whether the U -value or the thermal resistance (R -value) of the specimen is measured. At SP R -value measurements are chosen. The U -value is then calculated using an overall standard surface resistance of $0.20 \text{ (m}^2 \cdot \text{K)/W}$ (according to SBN; from 1 July the overall surface resistance is $0.17 \text{ (m}^2 \cdot \text{K)/W}$). The specimens are made airtight at the warm side as well. In this way no heat loss is measured due to air flows through the specimen and no condensation occurs during the test.

If U -value measurements are carried out, it is evident that the surface resistances in the rig have to be equal to the standard values. The total surface resistance in SP's rig varies between 0.16 and $0.17 \text{ (m}^2 \cdot \text{K)/W}$ in the case of windows. The total surface resistance for wall specimens is approximately 0.20 to $0.25 \text{ (m}^2 \cdot \text{K)/W}$; these values are high compared with the standard values (SBN) because of the deliberate choice of not installing a fan in the metering chamber and thus having only natural convection.

U -values are measured using air temperatures and the average temperature of the mask. R -values are measured using an area weighted average surface temperature of the specimen. To this purpose the window is divided into representative areas, four at the most (Fig. 3): the window frame, the casement, a 0.04m wide area around the edge of the glazing unit, and the rest of the glazing unit. Four thermocouples are installed on the frame as well as on the casement, three on the middle part of the glazing unit, and two on the edge area. Measuring the surface temperature at the edge of the glazing unit has been introduced only recently in SS 024213. As a consequence the mean surface temperature difference becomes lower in comparison to previous measurements under the same conditions when it concerns windows with sealed glazing units; the R -value decreases approximately 2 to 3%. The impact on the U -value is an increase of approximately 3 to 5%. Thus it is seen that the way the panes of a sealed glazing unit are joined may strongly affect the heat loss.

Heat loss measurements on glazing units using the GHB are not included in any Swedish Standard. At SP measurements are carried out as described above. However, only two representative areas are involved: a 0.04 m wide area around the edge (with four thermocouples) and the rest of the glazing unit (with three thermocouples).

U -value measurements on frames have never been carried out at SP. There do not exist any general measurement routines in Scandinavia as, for instance, in Germany (in connection with German Standard DIN 52616) [6].

Overall Survey of Measurement Results

Survey of Different Window Types

Windows may be divided into four groups depending on the frame and the casement (if any): metal frame windows (in most cases aluminum), plastic frame windows (mainly PVC), wooden frame windows, and combined frame windows (in 95% of the cases a wooden frame at the inside and an aluminum finishing at the outside).

Measured U -values for these four types of windows are compared in Fig. 4, a separate survey being made for the periods 1977–81 and 1982–86. The comparison is made regardless of the type of glazing unit in the window. Ninety percent of the test results lie within the U -value ranges given.

The survey shows that:

- Window U -values, in general, have been reduced considerably.
- The spread of measured U -values for each type of window has become smaller.
- Practically no improvements have been made so far as the metal frame windows tested at SP are concerned.

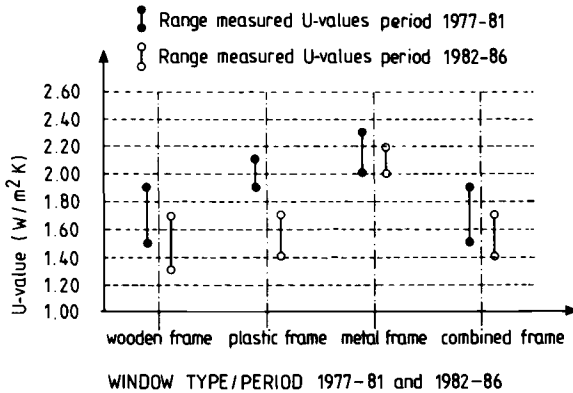


FIG. 4—Survey of measured U -values with respect to window type.

- All wooden frame and combined frame windows tested between 1977 and 1981 met the $2 \text{ W}/(\text{m}^2 \cdot \text{K})$ requirement.
- Most windows tested during the 1982-86 period even meet the $1.6 \text{ W}/(\text{m}^2 \cdot \text{K})$ limit. A more detailed survey would show that 85% of all nonmetal frame windows tested meet that limit.
- Metal frame windows generally do not meet any of the two U -value requirements. The importance of metal frame windows on the Swedish market therefore is very small.
- The U -value requirements are met equally well using plastic frame or combined frame windows as when using wooden frame windows.
- Heat losses through windows could be reduced more than 20%, (a) partially because the thermal resistance of the framing had been increased (plastic framing mainly), but (b) mostly because the glazing units used in the windows tested between 1982 and 1987 are almost without exception improved window panes or improved sealed glazing units. These have a higher thermal resistance than the glazing units used previously.

The result has been the considerable improvement of the U -value of the plastic frame windows tested; most of the (1982-86) test specimens had improved double or triple glazing instead of normal double glazing (1977-81).

The airtightness of windows, especially wooden windows, has become much better as well. This does not, however, affect the measured U -value because, during the test, windows are made airtight (in case of windows with sliding sash) and the joints between window and mask are sealed. In practice, the heat loss definitely is affected by the airtightness. It may be pointed out in this respect that plastic frame windows, generally taken, are less airtight than wooden frame windows [1].

Metal frame windows do not meet the $2 \text{ W}/(\text{m}^2 \cdot \text{K})$ requirement, although all specimens tested had triple glazing. The reason is the low thermal resistance of the frame. The thermal bridge effect of the metal frame becomes even more important the higher the glazing unit's thermal resistance. The U -value of metal frame windows can only be improved considerably by cross-cutting the frame and casement and by separating the inner and outer part by introducing a thermal break. This measure makes metal frame windows very expensive.

The differences between the U -values measured for plastic frame, wooden frame, and combined frame windows are in general small for the period 1982-86. The thermal resistance of these frames are almost equal to one another. It is of the same magnitude of triple glazing.

The lowest U -values have been measured for wooden frame windows, because it is easier to

experiment with, and to produce prototypes of, wooden frames than it is with plastic frames for instance. Moreover, wood is a very popular and commonly used building material in Sweden. In this respect only combined frame windows can compete with wooden frame windows. This alternative offers a wooden inside and has a more weather resistant outside when well designed.

The ranges of window U -values given in Fig. 4 do not only depend on the type of glazing unit but are dependent on the size of the window and on whether it concerns a window with fixed frame or a window with hinged frame:

- The larger the window the less important the impact of the edge of the glazing unit and frame on the U -value. This size effect is more important when low resistance glazing units are used. The overall area of the specimens varied from 0.9 to 1.4 m². The percentage glazed area of the total window area varied between 65 and 75%. It is difficult to point out an "area-thermal conductance" relation in general because the design of the frame is equally important.
- The U -value of windows with hinged frame is systematically 5 to 10% larger than the U -value of a fixed frame window of the same overall size.

Survey of Different Types of Glazing Units

The glazing units most frequently tested are: normal and improved (gasfilling and/or low emissivity film) double glazing (denoted (2)), normal and improved triple glazing (denoted (3)), normal and improved double glazing with an additional pane (denoted (1+2)), and single pane windows with an additional pane (denoted (1+1)). Windows with one of the last two types of glazing unit are also referred to as coupled windows.

Figure 5 gives a survey of measured U -values for different types of glazing units. No distinction is made between the different types of windows. Metal frame windows are mentioned separately because all metal frame windows tested had triple glazing. This would have led to a misinterpretation of the reported U -value ranges. Apart from this, no preferred combination of a type of window with a type of glazing unit can be indicated. Ninety percent of all U -values measured lie within the ranges given.

Besides what is deduced from Fig. 4, Fig. 5 shows that:

- The (1+1) glazing unit window is the only one of the glazing units currently used which does not meet the 1.6 W/(m² · K) limit.
- Only one third of the (2) glazing unit windows meet the 1.6 W/(m² · K) limit.
- During the period 1977–81 a number of measures were tried in order to reduce the U -value of the (1+1) glazing unit. The resulting window U -value was of the same magnitude as im-

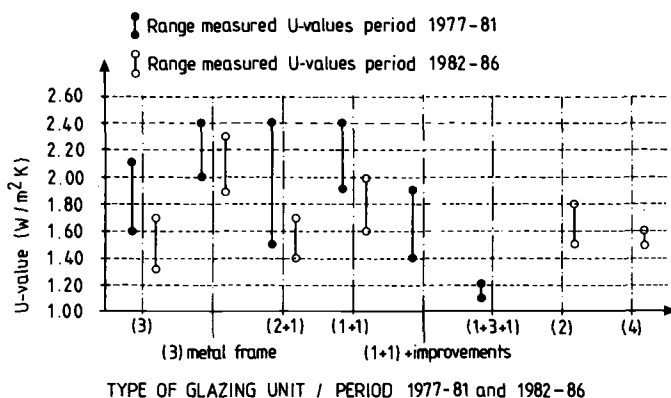


FIG. 5—Survey of measured U -values with respect to type of glazing unit.

proved double or even triple glazing. These measures included installing all kinds of reflective blinds in the air space or applying foils or fabrics on the inner window pane at the room side.

- A (1+3+1) glazing unit was experimented with as well between 1977 and 1981. This resulted in a very low *U*-value. This glazing unit, however, implies a very expensive frame.
- Quadruple glazing was not often tested and if so then only recently (between 1984 and 1987). The *U*-value is somewhat lower than the *U*-value of improved double glazing or triple glazing with a low emissivity film. Quadruple glazing is expensive (Table 2) and also implies large, expensive window frame sections. Quadruple glazing is therefore mainly used in experimental housing.

Manufacturers have been able to improve the window *U*-values by replacing the dry air in the cavities by other gases and/or by adding a low emissivity film on one of the window panes. Experiments of this kind had been done before, but the results were not as good as they are now. The importance of improved glazing has grown rapidly since 1983–84, 1984 being the year the $1.6 \text{ W}/(\text{m}^2 \cdot \text{K})$ limit was introduced.

The gases used to replace the dry air are argon and krypton, but mixtures of a number of different gases, unknown to the testing institute, may also be used. All these gases are heavier than air. In this way their thermal conductivity is lower than dry air.

There are two types of the low emissivity (LE) films used in Scandinavia [7,8]:

- A thick layer of a semi-conductor (for instance, doped SnO_2)
- A multilayer consisting of a noble metal (Ag, Cu, Au) between two oxide-layers (such as SnO_2 , TiO_2 , Al_2O_3).

The LE films are applied on the cavity side of the inner pane. The impact on the heat loss is, in principle, comparable to the impact of a reflective blind in a (1+1) glazing unit.

Eighty percent of all windows tested during 1982–87 had improved glazing. The exceptions were: metal frame windows, which only were manufactured with triple glazing, and (2+1) glazing unit windows of which only 50% of the tested specimens had improved glazing. The quadruple glazing units also were not improved. This is why their *U*-values are, in general, not lower than improved (gas and low emissivity film) double or improved (low emissivity film) triple glazing.

Figure 6 is a survey of GHB *U*-value measurements on sealed glazing units. Figure 7 shows *U*-values for a number of comparable wooden frame windows with different types of triple glazing. It can be seen from both figures that:

- Using other gases than air or using a low emissivity film is not a guarantee for *U*-values lower than $1.6 \text{ W}/(\text{m}^2 \cdot \text{K})$.
- Low emissivity films generally result in lower *U*-values than gas fillings.
- The combination of both generally gives very good results. The *U*-value of a glazing unit may be reduced by 20% or more.

Guarded Hot Plate Measurements on Sealed Glazing Units

The Guarded Hot Plate (GHP) apparatus is designed to measure the heat loss through mainly homogeneous insulation materials in laboratory. The method can be used to measure the heat loss through sealed glazing units as well. Glazing unit thermal resistance measurements of this kind are not described in any Swedish Standard. Therefore GHP measurements on glazing units are rarely carried out at SP. In other European countries, for instance in Germany, this method is generally accepted (DIN 52612).

SP uses a large GHP whose metering area can be chosen equal to 0.3 m^2 or 1.0 m^2 . During the test the glazing unit is placed between two thin fabrics. Temperatures are measured using 0.25 mm gage thermocouples. The fabric is used in order to avoid cavities between the plates and the specimen. The specimen usually is larger than the metering area but smaller than the overall

TABLE 2—Price (SEK) and thermal resistance ($m^2 \cdot K/W$) for a number of 1000 by 1000 mm glazing units.

Type of Glazing Unit (Glass Pane Thickness is 4 mm)	Price for a 1000 by 1000 mm Glazing Unit, Including Mounting (SEK) (*)	Thermal Resistance of Glazing Unit as Measured in a GHB ($m^2 \cdot K/W$) ($m_{1+c} = 0.17 (m^2 \cdot K/W)$)	Ratio: SEK/ $((m^2 \cdot K)/W)$ (Rounded Off to 100 SEK/ $((m^2 \cdot K)/W)$)
1	500:—	0.175	2900:—
1 + 1	1000:—	≈ 0.37	≈ 2700 :—
.. + 1	.. + 400:—	.. + (0.1—0.2)	.. + (4000:—
.. + (1 + (LE))	.. + 600:—	.. + (0.15—0.25) (**)	2000:—)
1 + (1 + (LE))	1200:—	≈ 0.51	.. + (4000:—
2	1480:—	0.330	2500:—)
2 + (LE)	1760:—	0.495	≈ 2400 :—
2 + (LE) + gasfilling	1840:—	0.570	4500:—
3	1890:—	0.480	3600:—
3 + (LE)	2170:—	0.645	3200:—
3 + (LE) + gasfilling	2280:—	0.745	3900:—
4	2440:—	0.585	3400:—
			3100:—
			4200:—

(*) 1 U.S. dollar ≈ 6.39 SEK; information acquired from the Swedish National Association of Glaziers.(**) The price includes the frame. The increase of thermal resistance is derived from window U -values. The improvement is dependent on branch, type of window, etc.

guard zone. Because of the inhomogeneity of the specimen the surface temperature is not a constant for the whole of the metering zone. This makes it difficult to control the temperature balance over the gap. Small imbalances may lead to considerable measurement errors on account of the high conductivity of the glass and/or the edge profile, depending on the placement of the specimen with respect to the guard zone. The edge insulation around the plates is thus very important. Because of the type of inhomogeneities of glazing units one can only use the concept of equivalent thermal resistance, not thermal resistance.

2. Another way to evaluate the heat loss through the glazing unit's edge uses two identical specimens placed symmetrically in the metering zone. This measurement cannot result in an equivalent thermal resistance but may be used to calculate the effect of the edge per meter run.

3. The fact that different measurement methods give different results also leads to practical problems as far as the client is concerned. He must be informed properly about which type of measurement results he gets. If it concerns a manufacturer, the testing institute must also see to it that the results are used in a technically correct way in the firm's public relations. Using GHP *R*-value results for calculating the glazing unit's *U*-value is not acceptable.

4. The correspondence between GHP and GHB measurements has to be studied as well. This problem has three aspects:

(a) The first aspect, namely the heat loss through the edge of the specimen, has been previously mentioned. The way the specimen is fixed in the mask during the GHB test should also correspond to the way it is placed in the GHP.

(b) The second aspect concerns the convective heat transfer in the glazing unit. Its share of the total heat transfer between the panes is affected by the direction of the heat flow:

(i) An upward flow results in lower equivalent resistances than a downward flow. The difference may be 20% or more.

(ii) It has also been ascertained that a horizontal flow results in equivalent thermal resistances comparable to a downward flow (Fig. 8). This differs from what would be expected and may actually be a consequence of measurement errors because convection in the vertical cavities (GHP in upright position) makes the gases leave the metering area. Because of this, energy may be transported out of or into the metering area.

(c) The third aspect regards the surface coefficients. The boundary conditions in the GHP being a constant surface temperature, not holding a constant air temperature may cause differences between the GHP and GHB results. It has been ascertained that differences exist between the measured thermal resistances in the case of homogeneous insulation materials as well.

Discussion of Hot Box Measurements on Windows

Although Hot Box measurements are common practice within the field of building physics, there are a number of problems yet unsolved. They concern the technique of measurement and the meaningfulness of the measured power and temperatures. Only problems specific to window *U*-value measurements will be discussed here.

Measuring the thermal resistance of a window or glazing unit using an area averaged mean surface temperature is not a very accurate method. The two-dimensional effects at the edge of the glazing unit, in the frame, and at the circumference of the window cannot be evaluated accurately in this way. This problem was illustrated when changing the measurement routine in the Swedish Standard. The introduction of two extra measuring points at the edge of the glazing unit changed the *U*-values; the magnitude of the change was of the same magnitude as the overall error mentioned in standards such as ISO/DP 8990, BS 874/III, and ASTM C 236.

An alternative to surface temperature measurements are air-to-air temperature measurements. Because the measured power takes into account the two-dimensional aspect of the heat loss through the window, accurately measured air temperatures would result in more correct *U*-values. It is difficult, however, to define the air temperature in the chambers. There is a considerable temperature gradient in the metering and environmental chamber. A similar gradient

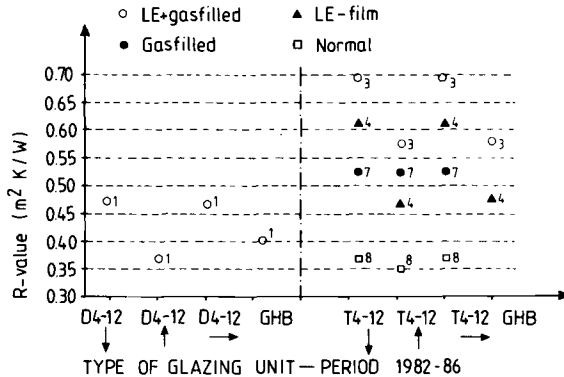


FIG. 8—GHP thermal resistances of eight types of glazing units compared with GHB results; the arrows give the direction of the heat flow.

can be ascertained on the baffle as well. This, and the fact that it does not concern a plane specimen, affects the surface resistances (m_e and m_i):

- The surface resistances for the mask differ from those for the specimen.
- The boundary layer at the surface of the specimen has a varying thickness because of the two-dimensional effects mentioned above. The air temperature sensors have to be situated out of it, because its air temperature is not a constant and differs from the bulk air temperature.

Moreover, if U -values are measured instead of equivalent R -values, it is indispensable that the surface resistances are standardized. This means that in all rigs the convective and radiative heat transfer in the chambers should be adjusted accordingly. The prescribed surface resistances may be deduced from *in situ* measurements. Measurements made on ground or second floor windows of a test house during an overcast night may be used. In this way the problem of a vertical temperature gradient may be, if not solved, at least related to reality and thus be partially justified.

The proportion of convective (m_c) to radiative transfer (m_r) may be important as well. Two measurements with identical surface coefficients on both sides of the window specimen would give different results depending on the ratio m_r/m_c . Calibration measurements, if any, would have to be made using the correct ratio.

Table 3 gives a survey of measurements carried out at three testing institutes (A, B, and SP) in Sweden and Norway some years ago. Window I is a wooden frame window, Window II a metal frame window. The results seem to be satisfactory; the difference between the measured U -values is 5% maximum. As to the equivalent R -value the maximum difference is twice as large. The results as the client gets them differ, however, from the ones used to compare the rigs used by A, B, and SP. The client who wants to use the results in his advertising is interested in the lower U -value. The testing institute with the lower U -values is, according to the client, the better institute. The differences are not only a consequence of differences in the test rigs. The equivalent R -values are not measured with the same routines; A used nine measuring points on the glazing unit while B and SP used three. This automatically results in a lower value. The surface resistances according to the respective standards differ as well. This clearly shows that standardization of the Hot Box method is necessary not only because of the technique of measurement but also in order to prevent misinterpretation or even abuse of the results by the client.

Another issue as to standardization concerns the overall error mentioned. Neither the Swedish nor other standards clearly state whether the promised accuracy regards the U -value or the

TABLE 3—Results of limited Nordic window round robin (1981).

	Institute A	Institute B	SP
<i>U</i> -value (Window I)	1.89	1.83	1.79
<i>U</i> -value (Window II)	2.18	2.22	2.15
Equivalent <i>R</i> -value (Window I)	0.330	0.345	0.360
Equivalent <i>R</i> -value (Window II)	0.255	0.250	0.265
Test results as the client gets them:			
<i>U</i> -value (Window I)	2.00	1.85	1.80
<i>U</i> -value (Window II)	2.40	2.20	2.15
Surface resistances according to standard	0.17	0.20	0.20
Surface coefficients during test	0.20	0.20	0.20
Error according to SS 024212:			
Δ in function of $\delta(U)$ (Window I)	± 0.19	± 0.18	± 0.18
Δ in function of $\delta(R)$ (Window I)	± 0.12	± 0.11	± 0.10

equivalent *R*-value. Again, from the client's point of view this is very important, since he wants his products to meet certain requirements or he wants the testing institute to measure the impact of measures carried out to improve the product's *U*-value. A *U*-value of 1.6 W/(m² · K) corresponds to an *R*-value of 0.425 (m² · K)/W according to SS 024213; the promised overall error (δ) is 10%.

If δ regards the *U*-value (δ_U), the absolute error on the *U*-value (Δ) becomes ± 0.16 W/(m² · K). If δ regards the equivalent *R*-value (δ_R), Δ becomes ± 0.10 W/(m² · K). This means that the latter interpretation gives the possibility of measuring smaller variations (Table 3).

Developments Regarding Measurement Routines

The latest change in Swedish Standard SS 024213 (i.e., the introduction of two extra measuring points on the glazing) has already been mentioned. Also, the Swedish Building Code (SBN) will be changed before long. The surface resistances used up to now (0.20 (m² · K)/W) will be decreased to 0.17 (m² · K)/W; m_i then becomes 0.13 (m² · K)/W and m_e becomes 0.04 (m² · K)/W. Both are part of a uniformization of Hot Box measurement routines in general within Scandinavia. The uniformization process was initiated by ISO.

The fact that the new surface coefficients correspond well with the surface coefficients during tests in SP's GHB gives SP the opportunity of measuring window *U*-values instead of equivalent window *R*-values.

R&D Program at SP

At SP a complete error analysis project of Hot Box measurements in general has been started. The project includes three major parts:

1. *Optimization of the Controlling System*—This part has been completed. It makes it possible to measure *U*-values larger than 0.25 W/(m² · K) without the use of a calibration curve.
2. *Checking the GHB Rig Against the Requirements in the Relevant Standards*—This check included the calibration of the temperature and power data acquiring system. The results of the check are given in Table 1.

3. *Analysis of U-Value Measurements on Homogeneous and Inhomogeneous Specimens (Mainly Windows)*—This part consists of three steps;

(a) A study of the specific boundary conditions in the Hot Box will be made. The conditions will be compared to GHP boundary conditions as well as their effect on the measurement results. In the case of windows and glazing units the radiative and convective part of the boundary heat transfer will be studied separately.

(b) The second step includes the mathematical modelling of leak flows and the way they are affected by surface coefficient variations. The work of the ISO 163 SC1/WG1 Workgroup on Hot Box Measurements will be very useful to this purpose.

(c) Parallel to Step (a), GHP measurements on glazing units will be studied. A secondary purpose is to acquire information in order to be able to determine future GHP measurement routines for glazing units. This is important for SP as a testing institute. If SP can offer a reliable method of quality control of glazing units, it will put an end to possible misinterpretations of measurement results on glazing units. Collaboration with other testing institutes within and outside Scandinavia will be necessary.

Conclusions

The *U*-value of windows produced in Sweden has been reduced, on an average, 10 to 20% during the latest decade because of keen *U*-value requirements. This reduction has been accomplished partially by improving the frames, but mainly by improving the glazing units and using additional panes.

Nonmetal frame windows with improved triple glazing or with improved double glazing and an additional pane are the only types of windows which meet the $1.6 \text{ W}/(\text{m}^2 \cdot \text{K})$ *U*-value requirement without difficulty.

The *U*-value measurement results the client obtains may differ depending on the testing institute. The reason often has nothing to do with measurement accuracy but with measurement routines and national standards. This is not a problem for the testing institutes themselves, but it causes misinterpretation and may lead to deliberate abuse when the client is concerned.

Uniformization of measurement routines thus seems indispensable. In order to find generally acceptable routines for windows and glazing units much research has to be completed. Some of the work has already been initiated by international workgroups.

As far as research and standardization are concerned, it is important to realize that the "dark" *U*-value as discussed is only as part of the total energy balance of buildings as a whole as well as of the window itself.

References

- [1] Brolin, H., "Air and Rain Tightness of Windows," Swedish Council for Building Research, Windows in Building Design and Maintenance Symposium, Gothenburg, Sweden, 13–15 June 1984.
- [2] "Den Svenska Fönstermarknaden 1985–1988; reviderad prognos (The Swedish Window Market 1985–1988; a revised prognosis)," Report 7/86, SIND Statens Industriverk, Oct. 1986.
- [3] *Kunststoff im Bau*, 16 Jahrgang 1981, Heft 4.
- [4] Staelens, P., "Hot-Box Measurements," in *Proceedings*, Scandinavian Symposium on Building Physics, Lund, 24–26 Aug. 1987, published by BFR, Stockholm, March 1988.
- [5] *Manual on the Use of Thermocouples in Temperature Measurements*, ASTM STP 470B, 3rd Ed., 1983, American Society for Testing and Materials, Philadelphia, pp. 112–250.
- [6] Hartmann, H.-J., Heinrich, R., and Schmid, J., "Wärmedurchgangskoeffizient *k* an Fenster (Thermal Transmittance of Windows)," *Fenster und Fassade*, Heft 2, 1978, pp. 46–52.
- [7] Ribbing, C.-G., "Selektiva Fönster; Möjligheter till Energibesparing genom Strålningskontroll (Selective Windows; A Possibility of Saving Energy by Controlling Radiative Heat Losses)," Swedish Council for Building Research, Report R127:1982, Stockholm, 1982.

- [8] Ribbing, C.-G. and Roos, A., "Semi-Conductor vs. Metal Based Multilayer Coatings on Energy Conserving Windows," Scandinavian Symposium on Building Physics, Lund, 24-26 Aug. 1987.
- [9] Jonsson, B., "Heat Transfer Through Windows—During the Hours of Darkness with the Effect of Infiltration Ignored," Swedish Council for Building Research, Document D13:1985, Stockholm, 1985.
- [10] Blomsterberg, Å., "K-värde hos fönster (Window U -values)," Nordtest Symposium, Stockholm, 1981.

Heat Transfer Characteristics of a Recently Developed Lightweight Structural Concrete

REFERENCE: Van Geem, M. G., "Heat Transfer Characteristics of a Recently Developed Lightweight Structural Concrete," *Insulation Materials, Testing, and Applications, ASTM STP 1030*, D. L. McElroy and J. F. Kimpflen, Eds., American Society for Testing and Materials, Philadelphia, 1990, pp. 437-463.

ABSTRACT: A lightweight structural concrete was developed for use in exterior walls of low-rise residential and commercial buildings. The lightweight concrete has a unit weight of 800 kg/m³ (50 pcf), a compressive strength of 13.8 MPa (2000 psi), and a thermal conductivity of 0.23 W/m · K (1.6 Btu · in./h · ft² · °F). Lightweight concretes have not been previously developed with this combination of low density and moderate strength. The most commonly used concrete, normal weight concrete, has a unit weight of approximately 2320 kg/m³ (145 pcf), a compressive strength in the range of 17 to 41 MPa (2500 to 6000 psi), and a thermal conductivity of 1.7 to 2.3 W/m · K (12 to 16 Btu · in./h · ft² · °F).

The portland cement concrete developed for this project can be used to combine structural, thermal insulation, and heat storage capacity functions of exterior walls in one element. For many climates this concrete can be used without additional insulation as a complete wall system in low-rise buildings.

Heat transfer characteristics of two 200-mm (8-in.)-thick, full-size wall assemblies were evaluated using a calibrated hot box (ASTM C 976). One test specimen, designated Wall L, was a 200-mm (8-in.)-thick wall constructed entirely of the newly developed lightweight structural concrete. The second specimen, designated Wall S, was the same as the first except for a 150-mm (6-in.)-high normal weight concrete strip running horizontally across the wall at midheight. The horizontal strip simulates a floor slab extending through an exterior wall.

Overall thermal resistances of Walls L and S, respectively, are 0.92 and 0.83 m² · K/W (5.2 and 4.7 h · ft² · °F/Btu) at 24°C (75°F). Thermal resistance of Wall S is 11% less than that for Wall L.

Tests under dynamic temperature conditions provide a measure of thermal response for selected temperature ranges. Dynamic response includes heat storage capacity as well as heat transmission characteristics of the wall assembly. Results from a 24-h period, sol-air temperature cycle showed that heat storage capacity of the low density concrete delayed heat flow through the test specimen. Average thermal lag for the 200-mm (8-in.)-thick lightweight concrete wall was 6 h.

Thermal and physical properties of the lightweight concrete were also measured on small-scale specimens. Concrete thermal conductivity, thermal diffusivity, specific heat, compressive strength, flexural strength, splitting tensile strength, shear strength, modulus of elasticity, drying shrinkage, and freeze/thaw resistance were determined.

Laboratory test results provide information on the thermal and physical performance of the new lightweight concrete.

KEY WORDS: calibrated hot box, energy, heat transmission, lightweight concrete, structural concrete, thermal conductivity, thermal mass, thermal resistance

This paper summarizes results from a project to develop portland cement concrete with sufficient thermal resistance and strength properties to serve as an effective thermal break in building envelopes.

¹Senior Research Engineer, Fire/Thermal Technology Section, Construction Technology Laboratories, Inc., Skokie, IL 60077.

A thermal break is an exterior building element made of a material with a high thermal resistance used in place of a material with a lower thermal resistance to reduce energy losses through a building envelope. A thermal break may range in size from a small plastic nail used in place of a metal nail, to a large sheet of insulation used to prevent energy losses through a building foundation. The term "structural" used as an adjective to "thermal break" implies that the material has load bearing capabilities.

A concrete was developed with an air-dry unit weight of 800 kg/m^3 (50 pcf), a compressive strength of approximately 13.8 MPa (2000 psi), and a thermal conductivity of $0.23 \text{ W/m} \cdot \text{K}$ ($1.6 \text{ Btu} \cdot \text{in.}/\text{h} \cdot \text{ft}^2 \cdot ^\circ\text{F}$). Although it is envisioned that concrete with these properties could be used for many building components, project emphasis is to evaluate the concrete for use in exterior walls for low-rise buildings.

The portland cement concrete developed for this project combines the structural, thermal insulation, and heat storage capacity functions of exterior walls in one element. For many climates this concrete can be used as a complete wall system in low-rise buildings without additional insulation.

Objectives and Scope

Project work is reported in Refs 1 to 3. Reference 1 is a feasibility study to identify uses for the proposed lightweight portland cement concrete in buildings. Reference 2 includes (1) selection of materials and mix designs for the lightweight portland cement and lightweight polymer concretes, (2) physical and thermal properties of candidate concretes, and (3) casting and surface finishing techniques for the most desirable mixes. Reference 3 describes heat transfer measurements of full-size wall assemblies constructed of the developed portland cement concrete.

Heat flow through two walls was measured in the calibrated hot box test facility (ASTM C 976) at Construction Technology Laboratories, Inc. (CTL). One test specimen, designated Wall L, was an 200-mm (8-in.)-thick wall constructed entirely of the newly developed lightweight structural concrete. The second specimen, designated Wall S, was the same as the first except for a 150-mm (6-in.)-high normal weight concrete strip running horizontally across the wall at midheight. The horizontal strip simulates a floor slab extending through an exterior wall.

Walls were tested for steady-state temperature conditions to obtain average heat transmission coefficients, including total thermal resistance (R_T) and thermal transmittance (U). A comparison of test results for the two walls shows the effect of the normal weight concrete strip.

Wall L, the homogeneous concrete wall, was also tested under dynamic temperature conditions. Dynamic tests provided a measure of thermal response for selected temperature ranges. A simulated sol-air dynamic cycle was selected to permit comparison of results with those obtained in previous investigations [4-6].

The program was conducted at Construction Technology Laboratories, Inc., (CTL). The project was sponsored jointly by the U.S. Department of Energy (DOE) Office of Buildings and Community Systems, and the Portland Cement Association. It is part of the Building Thermal Envelope Systems and Materials Program (BTESM), Energy Division, at Oak Ridge National Laboratory (ORNL).

Background

Concrete developed for this program will have lower heat transmission than concrete commonly used for low-rise building construction. A wall with low heat transmission will conserve energy.

Types of Concrete

Concrete is available in a wide range of weights and strengths. Normal weight concrete utilizes sand and gravel aggregate and is most commonly used for construction of structural con-

crete members. Normal weight concretes have a unit weight of approximately 2320 kg/m^3 (145 pcf), and compressive strengths of approximately 17 to 41 MPa (2500 to 6000 psi) are common. High-strength normal weight concretes have been developed with strengths exceeding 100 MPa (15 000 psi). Measured thermal conductivities of normal weight concretes range from 1.4 to $2.9 \text{ W/m} \cdot \text{K}$ (10 to $20 \text{ Btu} \cdot \text{in.}/\text{h} \cdot \text{ft}^2 \cdot ^\circ\text{F}$).

Concretes in the 1440 to 2080 kg/m^3 (90 to 130 pcf) range are known as structural lightweight concretes. These concretes have compressive strengths in the range of 17.2 to over 62.1 MPa (2500 to over 9000 psi), depending on materials, mix design, and other factors. Lightweight concretes typically have thermal conductivities ranging from 0.6 to $1.9 \text{ W/m} \cdot \text{K}$ (4 to $13 \text{ Btu} \cdot \text{in.}/\text{h} \cdot \text{ft}^2 \cdot ^\circ\text{F}$).

While normal weight and structural lightweight concretes have more than adequate strength for the proposed use, their thermal properties may be inadequate for external walls.

Concretes weighing 800 kg/m^3 (50 pcf) or less are called *insulating concretes*. Current technology limits the compressive strengths of these concretes to about 4.1 MPa (600 psi) [7]. These concretes typically have thermal conductivities of 0.07 to $0.22 \text{ W/m} \cdot \text{K}$ (0.5 to $1.5 \text{ Btu} \cdot \text{in.}/\text{h} \cdot \text{ft}^2 \cdot ^\circ\text{F}$).

A second category of lightweight concretes is in the weight range of 800 to about 1440 kg/m^3 (50 to about 90 pcf). These are usually called *fill concretes*. Concretes in this weight range have not been widely used and their development has been somewhat neglected. This is because of generally poor strength-weight relationships available with these concretes. However, it is at the lower limit of this category, in the range of 720 to 800 kg/m^3 (45 to 55 pcf) concrete, that an effort has been made to develop concrete which will meet strength and thermal resistance requirements desirable for external walls in low-rise buildings. Concretes with unit weights of 720 to 800 kg/m^3 (45 to 55 pcf) have thermal conductivities of approximately $0.22 \text{ W/m} \cdot \text{K}$ ($1.5 \text{ Btu} \cdot \text{in.}/\text{h} \cdot \text{ft}^2 \cdot ^\circ\text{F}$).

Thermal Properties of Concrete

Aggregates used to make concrete with a desired unit weight are available in a wide range of unit weights. Thermal conductivity of concrete is primarily dependent on its unit weight which is a function of the constituent aggregates used to make the concrete. To a lesser extent, thermal conductivity is dependent on the cement paste. Generally, concrete conductivity increases exponentially with unit weight. Concrete with a unit weight of 800 kg/m^3 (50 pcf) has a thermal conductivity of approximately $0.22 \text{ W/m} \cdot \text{K}$ ($1.5 \text{ Btu} \cdot \text{in.}/\text{h} \cdot \text{ft}^2 \cdot ^\circ\text{F}$), while concrete with a unit weight of 2240 kg/m^3 (140 pcf) has a thermal conductivity of approximately $2.3 \text{ W/m} \cdot \text{K}$ ($16 \text{ Btu} \cdot \text{in.}/\text{h} \cdot \text{ft}^2 \cdot ^\circ\text{F}$).

Heat flow through a homogeneous wall subjected to steady-state temperature conditions is linearly related to the thermal conductivity of the wall material and the temperature differential across the wall. For dynamic temperature conditions, heat flow is dependent on the storage capacity of the wall material in addition to its thermal conductivity.

Exterior building walls are seldom in a steady-state condition. Outdoor air temperatures and solar effects cause cyclic changes in outdoor surface temperatures.

A conditioned building with high mass walls will have less energy losses to the outdoor environment than an identical building with low mass walls of equivalent thermal resistance [1]. Energy savings are most significant for outdoor diurnal temperature cycles that cause reversals in heat flow through walls.

Optimally, the least heat will flow through a wall having high thermal resistance and high storage capacity. Heat transmission properties are more sensitive to changes in thermal resistance than to changes in storage capacity. The goal of this project is to develop a concrete with the highest thermal resistance and therefore the lowest unit weight. The concrete unit weight is limited by the need for sufficient structural capacity, because strength generally decreases with decreasing unit weight.

Concrete Mix Development

Portland Cement Concrete

Portland cement concrete consists, essentially, of portland cement, aggregates, and water. Relatively small quantities of other materials are frequently included to enhance certain properties which may be desirable for specific applications. Generally, aggregate is between 60 and 75% and cement, water, and air between 25 and 40% of the concrete volume. Since aggregate volume is so high, its specific gravity greatly influences the weight of the concrete. While cement has the highest specific gravity, it occupies a relatively small volume. Since cement is the strength-producing ingredient, the amount that it can be reduced is limited.

Based on the above, the investigative procedure consisted of locating the lightest available aggregates capable of producing concrete having sufficient structural capacity. With these aggregates, mixes had to be designed having the lowest cement contents (to lower weight) consistent with obtaining the required strength. Chemical and mineral admixtures were used to enhance the concrete's fresh properties and strength-to-weight relationship.²

Structural lightweight aggregates are available in all parts of the country. Many of these aggregates are capable of producing relatively high strength concrete in the weight range of 1400 to 1800 kg/m³ (90 to 115 pcf).

The aggregates used in this investigation were limited to those known by the principal investigator, by previous experience, to be capable of producing lower weight concretes with adequate strength, or those found in a search for additional desirable aggregates. Acceptance of an aggregate or concrete mix design was based on compressive strength and unit weight. Other properties were not determined on those mixes that did not meet the strength-to-weight criteria.

Preliminary Mix Development

Concrete mixes were made using seven aggregates, singly or in combination (Table 1). The number of mixes made with each aggregate varied from one to twelve, depending on the aggregate's potential for meeting the weight and strength objectives. Aggregate combinations were used in many cases in an attempt to take advantage of desirable properties found in fine or coarse sizes of certain aggregates.

The last column in Table 1 shows the average strength-to-weight ratio for mixes made with different aggregate combinations. Mixes utilizing 3M Macrolite³ had the highest strength-to-weight ratio and had the best chance of meeting the program objectives. Therefore mixes were made with this aggregate to optimize the strength-to-weight relationship and to provide test specimens for further testing.

Macrolite Ceramic Spheres (Fig. 1) is a recently developed ceramic supplied by the 3M Company of St. Paul, Minnesota. According to the company, arrangements are being made to produce this material commercially. A unique feature of this aggregate is that it has a relatively low water absorption of less than 0.5%. Most low-absorption lightweight aggregates have absorptions ranging from 6 to 14%. The aggregate was supplied in two sizes; 12.7 to 4.75 mm (1/2 in. to No. 4) and 4.75 mm to 300 μ m (No. 4 to No. 50).⁴

Fillite, furnished by Fillite USA, Inc. of Huntington, West Virginia, is described as hollow alumina silica microspheres. The particles are similar in size and chemical composition to fly ash. However, they are hollow and have a much lower specific gravity than most fly ash. The

²The strength-to-weight ratio is the ratio of the concrete's compressive strength to its unit weight.

³Product names used in this paper may be trademarked.

⁴Aggregate sizes are described by sieve opening sizes in accordance with ASTM Specification for Wire-Cloth Sieves for Testing Purposes (E 11).

TABLE 1—Portland cement concrete unit weights and compressive strengths.

Aggregate ⁽¹⁾	No. of Mixes	Unit Weight, kg/m ³ (pcf)		Compressive Strength, ⁽⁴⁾ MPa (psi)		Strength-to-Weight Ratio ⁽⁶⁾ , kPa/(kg/m ³), (psi/pcf)
		Fresh ⁽²⁾	28 day ⁽³⁾	7 day ⁽⁵⁾	28 day ⁽³⁾	
Project Objective	—	—	800 (50)	—	10.3 (1500)	12.9 (30.0)
Tufflite	1	1299 (81.2)	898 (56.1)	3.4 (490)	5.9 (850)	6.6 (15.2)
Tufflite & Filllite	1	1278 (79.9)	941 (58.8)	4.2 (610)	7.0 (1020)	7.4 (17.3)
Liapor	3	1005 (62.8)	898 (56.1)	5.4 (780)	8.0 (1160)	8.9 (20.7)
Liapor & Filllite	4	1064 (66.5)	962 (60.1)	8.2 (1190)	11.0 (1600)	11.4 (26.6)
Liapor, Filllite & PQ Microspheres	1	1010 (63.1)	896 (56.0)	8.5 (1230)	9.5 (1380)	10.6 (24.6)
Liapor, Filllite & 3 M Macrolite	2	896 (56.0)	829 (51.8)	10.7 (1550)	11.6 (1680)	14.0 (32.4)
Tufflite & Liapor	1	1107 (69.2)	1014 (63.4)	9.0 (1300)	11.0 (1590)	10.8 (25.1)
Livlite & Liapor	1	1117 (69.8)	997 (62.3)	8.1 (1170)	10.2 (1480)	10.2 (23.8)
Livlite	1	1275 (79.7)	1080 (67.5)	7.9 (1150)	15.0 (2170)	13.9 (32.1)
Livlite & Filllite	1	1213 (75.8)	970 (60.6)	4.0 (580)	10.3 (1500)	10.6 (24.8)
Leca	1	1062 (66.4)	941 (58.8)	4.1 (600)	6.8 (980)	7.2 (16.7)
3M Macrolite & Filllite	8	790 (49.4)	779 (48.7)	9.6 (1400)	12.3 (1780)	15.8 (36.6)

(1) Product names used in this paper may be trademarked.

(2) ASTM Designation: C 138, "Standard Test Method for Unit Weight, Yield, and Air Content (Gravimetric) of Concrete"

(3) Measured on 100x200-mm (4x8-in.) and 150x300-mm (6x12-in.) cylinders moist-cured 7 days at 23±1.7°C (73.4±3°F) and 100% RH, and then air-dried at 23±1.7°C (73.4±3°F) and 50±5% RH for the remaining 21 days.

(4) ASTM Designation: C 39, "Standard Test Method for Compressive Strength of Cylindrical Concrete Specimens"

(5) Measured on 100x200-mm (4x8-in.) and 150x300-mm (6x12-in.) cylinders moist-cured at 23±1.7°C (73.4±3°F) and 100% RH for 7 days.

(6) Ratio of 28-day compressive strength to 28-day air-dry unit weight.

Filllite size range was 30 to 300 μm . Filllite was used to provide a very fine lightweight material to those aggregates which were deficient in that size range.

Tufflite is a naturally occurring volcanic pumice aggregate. Livlite is an expanded clay aggregate. Liapor and Leca are expanded shale aggregates produced by grinding and pelletizing shales or clays and firing in a rotary kiln. Thus Liapor and Leca are spherical compared to Tufflite and Livlite which are irregularly shaped.

Most aggregates had relatively high water absorptions and were batched in a saturated condition to avoid rapid stiffening during mixing. However, the 3M Macrolite had an extremely low absorption and was batched in a dry condition.

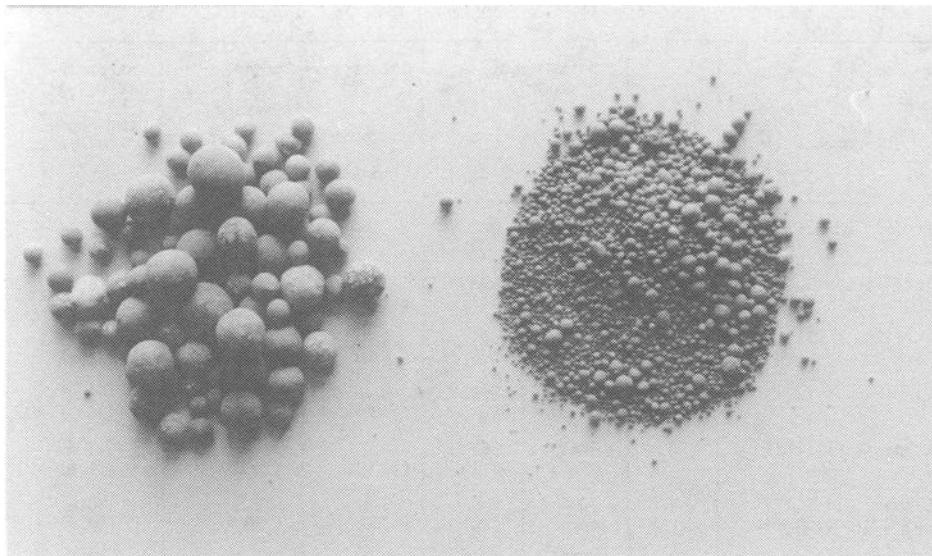


FIG. 1—3M Macrolite Ceramic Spheres.

Final Mix Design

The final mix design is shown in Table 2. It was used for determining various concrete physical and thermal properties and for casting two full-size wall panels, designated Walls L and S, for determination of thermal properties. The same volumetric mix design was used for both panels. However, aggregate weights varied because of the differences in specific gravities of aggregates from different shipments. The amount of vinsol resin air entraining agent was varied slightly to obtain a unit weight of about 800 kg/m^3 (50 pcf).

Physical and Thermal Properties of Small-Scale Specimens

Selected physical and thermal properties were measured on specimens cast from six concrete mixes using 3M Macrolite as aggregates. The six mixes are similar to those presented in Table 2. Test results are summarized in Table 3. Reference 2 gives details of specimen preparations and test procedures.

Reference 2 also compares properties of the newly developed concrete to properties of conventional normal weight and lightweight concretes.

Full-Size Test Specimens

Two lightweight structural concrete walls were constructed by CTL and subsequently tested in a calibrated hot box. Walls were cast horizontally and have overall nominal dimensions of 2.62 by 2.62 m (103 by 103 in.).

Wall Construction

Wall L is a lightweight structural concrete wall with an average thickness of 203 mm (8.00 in.). Wall S is similar to Wall L except for a 150-mm (6-in.)-high normal weight concrete strip running horizontally across the wall at midheight. Average thickness of Wall S is 206 mm (8.13 in.).

TABLE 2—Final portland cement concrete mix design.

Material	Quantities per 1.0 m ³ (Quantities per 1.0 cu yd)		
	Absolute Volume, m ³ (cu ft)	Weight, kg (lb)	
		Wall L	Wall S
Portland Cement	0.080 (2.16)	252 (425)	252 (425)
Silica Fume	0.012 (0.33)	26.1 (43)	26.1 (43)
Water	0.149 (4.01)	149 (250)	149 (250)
Air Content	0.060* (1.62)	--	--
3M Macrolite 12.7 to 4.75 mm (1/2" to #4)	0.342 (9.25)	174 (293)	195 (327)
4.75 to 0.30 mm (#4 to #50)	0.329 (8.88)	273 (459)	277 (466)
Fillite	0.028 (0.76)	20 (33)	20 (33)
Vincol Resin, 2% Solution	1670-1950 ml (1275-1488 ml)	1.7 (2.81)	2.0 (3.28)
WRDA, 4.55 ml/kg cement (7 oz/100 lb)	1160 ml (888 ml)	1.2 (1.96)	1.2 (1.96)

*Air content estimated at 6%.

The concrete mix for Walls L and S are presented in Table 2. Reinforcement representative of actual wall construction was placed within Walls L and S. Reinforcement consisted of a single layer of 13-mm (No. 4) bars spaced 305 mm (12 in.) center-to-center in each direction. The reinforcement was located at the walls' approximate midthickness.

Threaded concrete inserts were cast into the walls at midthickness to aid in transporting walls after concrete had attained the necessary strength.

Walls L and S were allowed to cure in the formwork for approximately two weeks. After removing from formwork, Wall L was allowed to air dry in the laboratory at a temperature of $18 \pm 6^\circ\text{C}$ ($65 \pm 10^\circ\text{F}$) for approximately three months. Wall S was air dried in the laboratory at a temperature of $21 \pm 6^\circ\text{C}$ ($70 \pm 10^\circ\text{F}$) for approximately four months.

Before testing, the faces of Walls L and S were coated with a cementitious waterproofing material to seal minor surface imperfections. A textured, noncementitious paint was subsequently used as a finish coat. These coatings provided a white, uniform surface for both faces of each wall. Wall edges were left uncoated.

Measured weights, thicknesses, surface areas, and estimated moisture contents of Walls L and S are summarized in Table 4. Wall weights immediately before and after calibrated hot box tests are presented.

Reference 3 more fully describes wall construction.

TABLE 3—Physical and thermal properties of hardened concrete.

Property	Test Method	Pre-Test Curing	Measured Value
Unit Weight 28-day	ASTM: C567, as applicable	7 days 100% RH, 21 days 50±5% RH	793 kg/cu m (49.5 pcf)
Compressive Strength 7-day 28-day	ASTM: C39	7 days 100% RH 7 days 100% RH, 21 days 50±5% RH	11.5 MPa (1670 psi) 13.8 MPa (2000 psi)
Splitting Tensile Strength 7-day 28-day	ASTM: C496	7 days 100% RH 7 days 100% RH, 21 days 50±5% RH	1.3 MPa (185 psi) 0.9 MPa (135 psi)
Modulus of Rupture (Flexural Strength) 7-day 28-day	ASTM: C78	7 days 100% RH 7 days 100% RH, 21 days 50±5% RH	1.8 MPa (260 psi) 1.7 MPa (250 psi)
Shear Strength 7-day 28-day	See Reference 2	7 days 100% RH 7 days 100% RH, 21 days 50±5% RH	2.0 MPa (290 psi) 1.8 MPa (260 psi)
Modulus of Elasticity 28-day	ASTM: C469	7 days 100% RH, 21 days 50±5% RH	6400 MPa (0.93x10 ⁶ psi)
Freezing and Thawing Resistance, relative dynamic modulus of elasticity	ASTM: C666, Procedure A (freezing in water)	7 days 100% RH, 21 days 50±5% RH, 24 hrs soaked in water	55% after 300 cycles
	See Reference 2 (freezing in air after 1/2 hr water soak)	14 days 100% RH, 14 days 50±5% RH	123% after 150 cycles
Drying Shrinkage @ 161 days @ 179 days @ 355 days	See Reference 2	7 days 100% RH, then 50±5% RH	0.088% 0.087% 0.093%
Thermal Conductivity	ASTM: C177* @ 75°F	7 days 100% RH, 58 to 70 days 45±15% RH, then oven dry	0.23 W/m·K (1.61 Btu·in./hr·sq ft·°F)
Specific Heat	US Army Corps of Engineers CRD-C124-73 (Ref. 8)	100% RH	1060 J/kg·K (0.25 Btu/lb·°F)
Saturated Surface Dry Air Dry			460 J/kg·K (0.11 Btu/lb·°F)
Thermal Diffusivity	US Army Corps of Engineers CRD-C36-73 (Ref. 8)	100% RH	0.00096 sq m/hr (0.0104 sq ft/hr)
Coefficient of Thermal Expansion	Similar to ASTM: E228	7 days 100% RH, 42 to 46 days 45±15% RH	64x10 ⁻⁶ mm/mm per °C (3.6x10 ⁻⁶ in./in. per °F)

* Thermocouples for measuring specimen surface temperatures embedded flush with specimen surface.

Instrumentation

Eighty 20-gage, Type T thermocouples, corresponding to ASTM Temperature-Electromotive Force (EMF) Tables for Standardized Thermocouples (E 230), were used to measure temperatures during thermal testing. For each test wall, 16 thermocouples were located in the air space on each side of the test specimen, 16 on each face of the test wall, and 16 at the approximate concrete midthickness. The 16 thermocouples in each plane were spaced 525 mm (20³/₈ in.) apart in a 4 × 4 grid over the wall area (Figs. 2 and 3).

An additional four thermocouples were located on each wall surface and at concrete mid-thickness along the centerline of the normal weight concrete strip of Wall S (Fig. 3).

TABLE 4—Summary of physical properties for Walls L and S.

Property	Measured Value	
	Wall L	Wall S
Weight of Wall, kg (lb)		
Before testing	1250 (2760)	1320 (2910)
After testing	1240 (2720)	1310 (2890)
Unit Weight of Wall,* kg/m ² (lb/ft ²)	182 (37.4)	--***
Unit Weight of Wall,* kg/m ³ (lb/ft ³)	898 (56.0)	--***
Average Wall Thickness, mm (in.)	203 (8.00)	207 (8.13)
Wall Area, m ² (ft ² ,)	6.86 (73.88)	6.87 (73.92)
Estimated Moisture Content**, % oven-dry weight	2	2

*Before calibrated hot box tests.

**Estimated from air dry and oven-dry weights of thermal conductivity specimens.

***Not calculated because Wall S is not homogeneous.

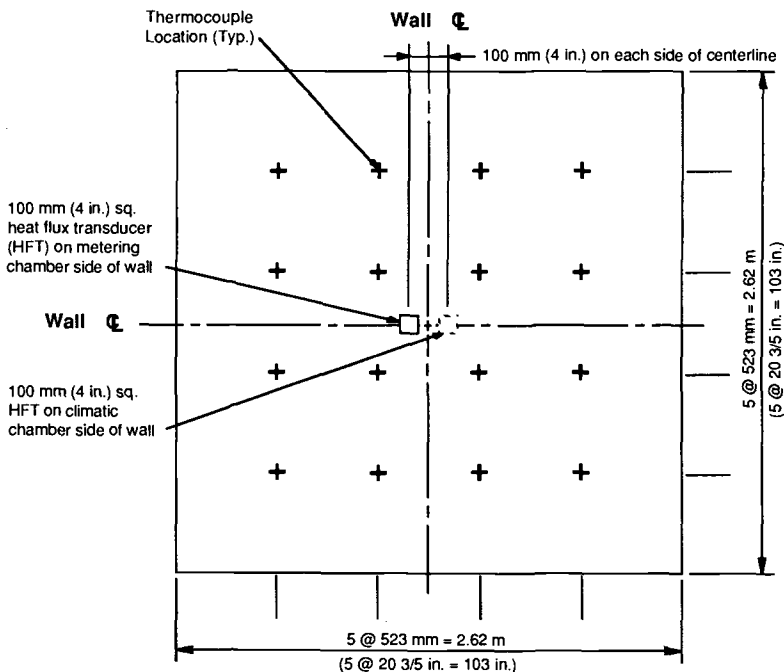


FIG. 2—Wall L air, surface, and internal thermocouple locations.

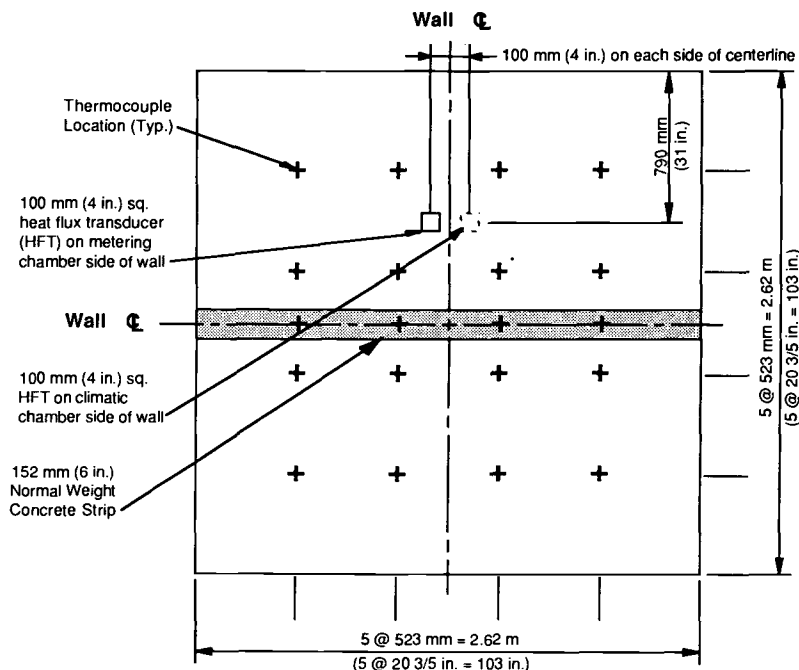


FIG. 3—Wall S air, surface, and internal thermocouple locations.

Thermocouples measuring temperatures in the air space of each chamber of the calibrated hot box were located approximately 75 mm (3 in.) from the face of the test wall.

Surface thermocouples were securely attached to the wall with duct tape for a length of approximately 100 mm (4 in.). The tape covering the sensors was painted the same color as the test wall surface.

During wall construction, internal thermocouples were placed at wall midthickness on top of the first 100-mm (4-in.) concrete layer. To secure their location, thermocouples were taped to reinforcement or suspended by wire between reinforcement. The thermocouple junction was not placed in contact with the reinforcement. This was done for all internal thermocouples to avoid any influence by internal heat flow through reinforcement. Thermocouples were wired to form a thermopile such that an electrical average of four thermocouple junctions, located along a horizontal line across the grid, was obtained. Wires for internal thermocouples were routed through side formwork before casting the second 100-mm (4-in.) concrete layer.

One heat flux transducer measuring 100 by 100 mm (4 by 4 in.) was mounted on each of the indoor and outdoor surfaces of the test walls. Sensors were located near the center of the walls (Figs. 2 and 3). The surface of the heat flux transducer in contact with a wall surface was coated with a thin layer of high-conductivity silicon grease. The silicon grease provided uniform contact between the heat flux transducer and wall surface. Duct tape was used to secure heat flux transducers to the wall surfaces. The duct tape was painted the same color as the test wall surface. Heat flux transducers were calibrated using results from steady-state calibrated hot box tests on Wall L.

Calibrated Hot Box Test Facility

Heat flow through Walls L and S was measured under steady-state and dynamic temperature conditions. Tests were conducted in the calibrated hot box facility shown in Figs. 4 and 5. Tests

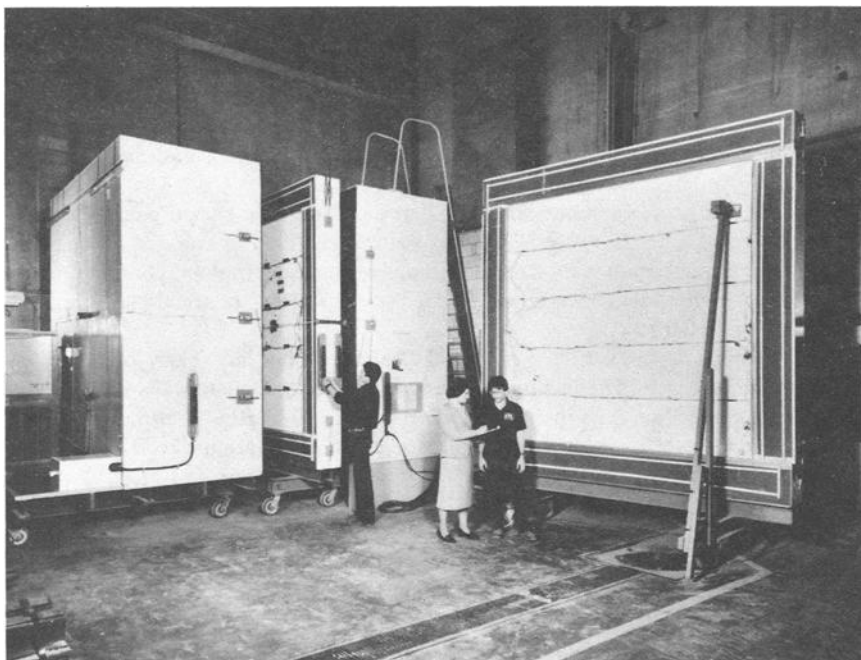


FIG. 4—Calibrated hot box test facility.

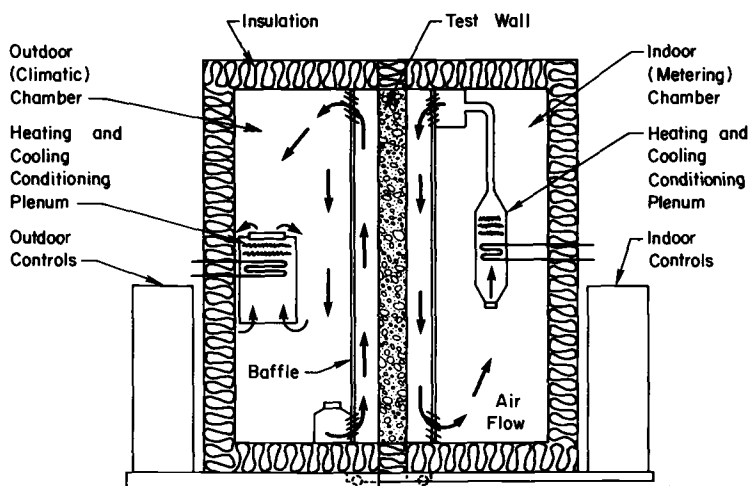


FIG. 5—Schematic of calibrated hot box.

were performed in accordance with ASTM Test for Thermal Performance of Building Assemblies by Means of a Calibrated Hot Box (C 976).

The following paragraphs give a brief description of the calibrated hot box. Instrumentation and calibration details are described in Refs 3 and 9.

The facility consists of two highly insulated chambers (Fig. 5). The walls, ceiling, and floors of each chamber are insulated with foamed urethane sheets to obtain a nominal thickness of 300 mm (12 in.). During tests, the chambers are clamped tightly against an insulating frame that surrounds the test wall. Air in each chamber is conditioned by heating and cooling equipment to obtain desired temperatures on each side of the test wall.

The climatic (outdoor) chamber can be held at a constant temperature or cycled within the range of -26 to 54°C (-15 to 130°F). Temperatures can be programmed for a 24-h cycle to obtain the desired temperature-time relationship. The metering (indoor) chamber, which simulates an indoor environment, can be maintained at a constant room temperature between 18 and 27°C (65 and 80°F).

The specimen is oriented vertically in the CTL calibrated hot box. Therefore heat flows horizontally through the wall. The facility was designed to accommodate walls with thermal resistance values ranging from 0.26 to $3.52 \text{ m}^2 \cdot \text{K/W}$ (1.5 to $20 \text{ h} \cdot \text{ft}^2 \cdot ^{\circ}\text{F/Btu}$).

The pressure in both the metering and climatic chambers is atmospheric.

Thermal Properties of Concrete for Steady-State Temperature Conditions

Thermal resistances of Walls L and S were measured using the calibrated hot box. Thermal conductivity of the lightweight concrete portion of Wall S was measured using heat flux transducers. Thermal conductivities of specimens made from concrete mixes used to make Walls L and S were measured using a guarded hot plate.

Calibrated Hot Box Test Results

Four calibrated hot box tests for steady-state temperature conditions were performed on each wall. Heat flow and temperature measurements were used to determine average overall thermal resistance (R_T) and thermal conductivity (k).

Test Procedures—Steady-state calibrated hot box tests were conducted by maintaining constant indoor and outdoor chamber temperatures. Results are calculated from data collected when specimen temperatures reach equilibrium and the rate of heat flow through the test wall is constant.

Hot box tests on Wall L were performed in April 1986. Tests on Wall S were performed in July and August 1986.

Test Results—Steady-state results from calibrated hot box tests on Walls L and S are summarized in Table 5. Data are averages for 16 consecutive hours of testing. Wall mean temperature, heat flow, and overall thermal resistance are listed for each steady-state test condition applied to the walls. Thermal conductivity is listed only for the homogeneous specimen, Wall L.

The first column of Table 5 lists the wall mean temperature during each steady-state test. Wall mean temperature is determined from the average of the metering and climatic wall surface temperatures. Average temperatures for Wall S, with the normal weight concrete strip, are the area-weighted averages of the lightweight and normal weight concrete temperatures. Table 5 presents metering and climatic chamber air temperatures and wall surface-to-surface temperature differentials.

Overall thermal resistances were calculated using heat flow measured by the calibrated hot box and standard surface resistance coefficients of $0.03 \text{ m}^2 \cdot \text{K/W}$ ($0.17 \text{ h} \cdot \text{ft}^2 \cdot ^{\circ}\text{F/Btu}$) for outdoor air and $0.12 \text{ m}^2 \cdot \text{K/W}$ ($0.68 \text{ h} \cdot \text{ft}^2 \cdot ^{\circ}\text{F/Btu}$) for indoor air [10].

Measured relative humidity within the metering and climatic chambers of the CTL calibrated hot box is also listed in Table 5. Metering chamber relative humidity is greater for Wall S tests

TABLE 5—Steady-state results from calibrated hot box tests.

Wall Designation	Wall Mean Temp., °C (°F)	t _c Climatic Chamber Temp., °C (°F)	t _m Metering Chamber Temp., °C (°F)	Δt Surface-to-Surface Temp. Diff., °C (°F)	q** Heat Flow, W/sq m (Btu/hr-sq ft)	Rt*** Thermal Resistance, sq m-K/W (hr-sq ft-°F/Btu)	k Thermal Conductivity, W/m-K (Btu-in./hr-sq ft-°F)	Relative Humidity		Laboratory Air Temperature	
								Metering Chamber, %	Climatic Chamber, %	Max., °C (°F)	Min., °C (°F)
L	2.7 (36.9)	-17.3 (0.9)	21.3 (70.4)	32.3 (58.2)	38.5 (12.2)	0.99 (5.6)	0.24 (1.68)	35	20	24 (75)	23 (74)
L	13.2 (55.7)	3.7 (38.6)	21.9 (71.4)	15.1 (27.1)	17.2 (5.5)	1.02 (5.8)	0.23 (1.61)	34	17	24 (75)	22 (72)
L	29.8 (85.6)	36.2 (97.2)	22.7 (72.8)	12.3 (22.2)	17.4 (5.5)	0.86 (4.9)	0.29 (1.99)	33	11	23 (74)	22 (72)
L	39.8 (103.7)	55.8 (132.5)	23.2 (73.7)	28.7 (51.6)	40.2 (12.7)	0.86 (4.9)	0.28 (1.97)	33	10	24 (75)	23 (73)
S	3.3 (37.9)	-15.9 (3.3)	21.5 (70.7)	31.3 (56.3)	44.9 (14.2)	0.85 (4.8)	—	55	21	23 (74)	23 (74)
S	13.7 (56.7)	4.6 (40.3)	22.0 (71.6)	14.4 (25.9)	21.6 (6.9)	0.81 (4.6)	—	53	18	23 (74)	23 (74)
S	30.6 (87.0)	37.5 (99.5)	23.0 (73.4)	12.4 (22.4)	18.1 (5.7)	0.85 (4.8)	—	51	12	26 (79)	24 (75)
S	40.6 (105.1)	56.8 (134.3)	23.7 (74.7)	28.3 (51.0)	43.8 (13.9)	0.79 (4.5)	—	51	10	27 (80)	26 (78)

* Average of metering and climatic wall surface temperatures.

** Heat flow through wall measured by calibrated hot box (ASTM Designation: C976).

*** Overall thermal resistance calculated using design surface coefficients of 0.15 sq m°K/W (0.85 hr-sq ft-°F/Btu) and measured values of heat flow.

than for Wall L tests because of a higher laboratory relative humidity when Wall S tests were started.

Maximum and minimum laboratory air temperatures obtained during each steady-state test are also listed in Table 5. The laboratory acts as a guard for the metering chamber during tests conducted in CTL's calibrated hot box.

Thermal conductivity of Wall L and thermal resistances of Walls L and S at a specimen mean temperature of 24°C (75°F) were interpolated from measured values. Thermal conductivity of Wall L is 0.27 W/m · K (1.86 Btu · in./h · ft² · °F) at 24°C (75°F). Overall thermal resistances of Walls L and S, respectively, are 0.92 and 0.83 m² · K/W (5.2 and 4.7 h · ft² · °F/Btu) at 24°C (75°F).

Thermal resistance of Wall S is 10% less than that for Wall L at 24°C (75°F). The normal weight concrete strip of Wall S is 5.8% of the total wall area.

Guarded Hot Plate Test Results

Thermal conductivities of specimens made from concrete mixes used to make Walls L and S were measured using a guarded hot plate. Tests were conducted at CTL in accordance with ASTM Test for Steady-State Heat Flux Measurements and Thermal Transmission Properties by Means of the Guarded-Hot-Plate Apparatus (C 177) and ASTM Practice for the Calculation of Thermal Transmission Properties from Steady-State Heat Flux Measurements (C 1045).

Test Specimens—Two specimens were tested from the lightweight concrete for Wall L, the lightweight concrete for Wall S, and the normal weight concrete for Wall S. Nominal specimen dimensions were 50 by 300 by 300 mm (2 by 12 by 12 in.). Specimens were moist-cured at 23 ± 1.7°C (73.4 ± 3°F) and 100% RH for seven days, then air-dried at 23 ± 3°F (73 ± 5°F) and 45 ± 15% RH. Specimens were oven-dried before testing to eliminate effects of moisture migration during testing. Measured specimen dimensions and unit weights are given in Table 6.

Test Procedure—Test specimen temperatures are measured by chromel/alumel thermocou-

TABLE 6—Measured properties of guarded hot plate test specimens.

Specimen		Overall Dimensions, mm (in.)	Average Thickness, mm (in.)	Oven-dry Unit Weight, kg/cu m (pcf)
Wall L Lightweight Concrete	Top	310 x 306 (12.2 x 12.1)	50 (1.98)	771 (48.1)
	Bottom	306 x 307 (12.1 x 12.1)	52 (2.03)	750 (46.8)
Wall S Lightweight Concrete	Top	305 x 305 (12.0 x 12.0)	51 (1.99)	805 (50.2)
	Bottom	305 x 305 (12.0 x 12.0)	50 (1.99)	801 (50.0)
Wall S Normal Weight Concrete	Top	305 x 305 (12.0 x 12.0)	51 (2.00)	2260 (141)
	Bottom	305 x 305 (12.0 x 12.0)	51 (2.02)	2270 (142)

ples embedded near the specimen surfaces. Thermocouples were placed in previously sawed grooves. Cement paste was used to fill the groove flush with the specimen surface and to secure thermocouples in place. Cement paste was also used to fill small holes in the specimen surface. The cement paste for lightweight concrete specimens had lightweight aggregate fines.

Embedded thermocouples reduce the effects of thermal contact resistance, which is due to the influence of any thin air gap between thermocouple wire and concrete. More information on embedding thermocouple wires and thermal contact resistance is given in Ref 11.

Test Results—Guarded hot plate test results are presented in Fig. 6 for Walls L and S lightweight concrete specimens and Fig. 7 for Wall S normal weight concrete specimens. Thermal conductivity is shown as a function of mean specimen temperature. Thermal conductivity increases with increasing mean temperature for lightweight concrete and decreases with increasing mean temperature for normal weight concrete.

Thermal conductivities at a specimen mean temperature of 24°C (75°F) were interpolated from measured guarded hot plate values. Thermal conductivities for Wall L, Wall S lightweight, and Wall S normal weight specimens, respectively, are 0.21, 0.21, and 1.82 W/m · K (1.43, 1.48, and 12.66 Btu · in./h · ft² · °F) at a specimen mean temperature of 24°C (75°F).

Average measured thermal conductivity of the lightweight concrete developed for this project is about one ninth that for normal weight concrete.

Heat Flux Transducer Test Results

Test Procedures—Two heat flux transducers (HFTs) were mounted on each wall specimen as shown in Figs. 2 and 3 and previously described in the Instrumentation section. Sensors were attached near the center of Wall L and on the lightweight concrete portion of Wall S.

Wall L calibrated hot box test results were used to calibrate the HFTs for Wall S. Heat flow through Wall S as measured by the HFT's was determined in accordance with ASTM Practice for In-Situ Measurement of Heat Flux and Temperature on Building Envelope Components (C 1046).

Test Results—Heat flux transducer test results for the lightweight concrete portion of Wall S are presented in Fig. 6. Results are averages for 16 consecutive hours of testing during steady-state temperature conditions. Data were collected during steady-state calibrated hot box tests.

Results are similar for the heat flux transducers mounted on the climatic chamber and metering chamber sides of the wall.

Thermal conductivity of Wall S lightweight concrete at a mean specimen temperature of 24°C (75°F), interpolated from measured values, is 0.26 W/m · K (1.8 Btu · in./h · ft² · °F).

Discussion of Results

Figure 6 presents thermal conductivities of the lightweight concrete measured by the calibrated hot box (ASTM C 976), the guarded hot plate (ASTM C 177), and heat flux transducers (ASTM C 1046). Thermal conductivities from calibrated hot box and HFT measurements are greater than those from guarded hot plate tests because guarded hot plate specimens were oven-dried to remove moisture, while the wall specimens were air-dried. An increase in specimen moisture content increases thermal conductivity.

Predicted thermal resistances of Walls L and S are presented in Table 7. Values are calculated using results from guarded hot plate tests on oven-dry specimens and measured wall thicknesses. Calculation procedures are from the *ASHRAE Handbook - 1985 Fundamentals* [10].

The predicted thermal resistance of Wall S is 17% less than that for Wall L. This compares to a 10% decrease in measured thermal resistance for Wall S compared to Wall L. A percent reduction comparison is used because predicted values are based on oven-dried specimens and measured values are based on air-dried specimens.

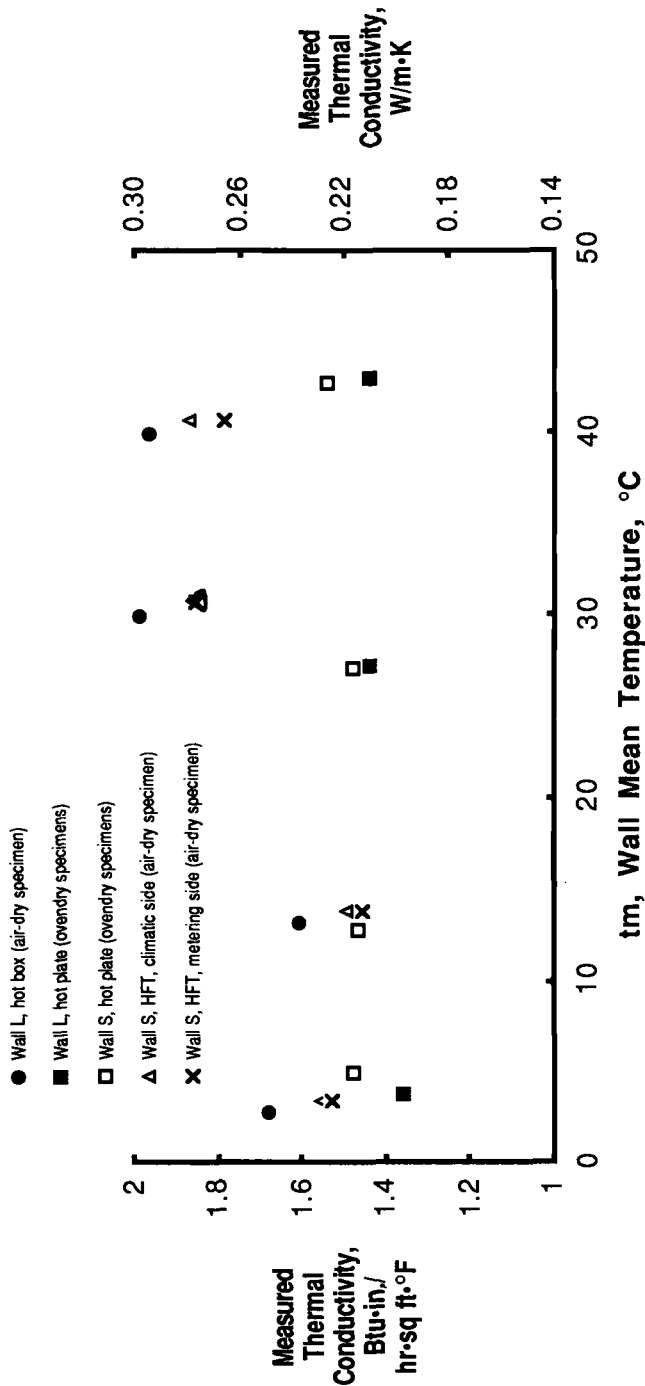


FIG. 6—Measured thermal conductivity of lightweight concrete.

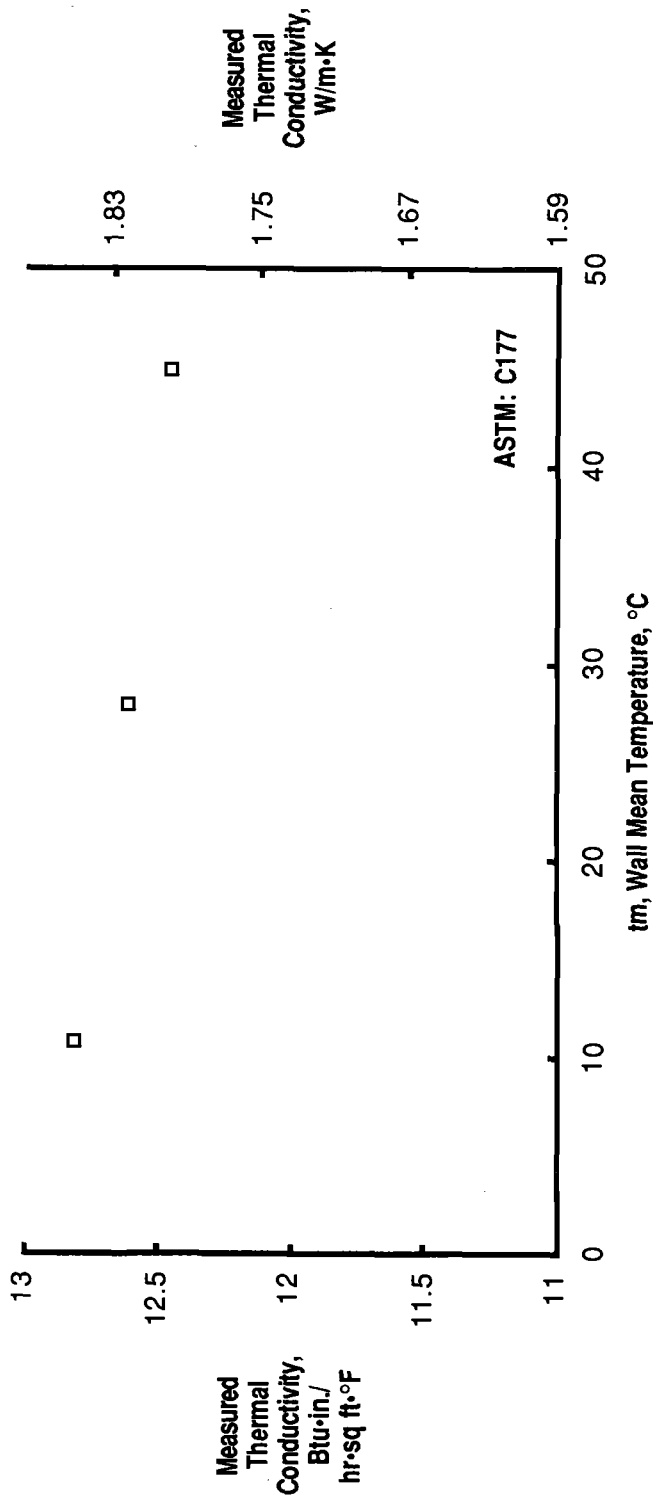


FIG. 7—Measured thermal conductivity of normal weight concrete.

TABLE 7—Predicted thermal resistance of Walls L and S.

Layer	R Thermal Resistance, sq m·K/W (hr·sq ft·°F/Btu)		
	Wall L	Wall S Lwt Concrete	Wall S NW Concrete
Outside Air Film	0.03 (0.17)	0.03 (0.17)	0.03 (0.17)
200 mm Thick Concrete Wall (8-in.)	0.98* (5.59)	0.97* (5.49)	0.11* (0.64)
Inside Air Film	0.12 (0.68)	0.12 (0.68)	0.12 (0.68)
Total R	1.13 (6.44)	1.12 (6.34)	0.26 (1.49)

* Calculated from guarded hot plate thermal conductivities of oven-dry specimens at 24°C (75°F) and measured wall thickness.

Wall S R-value calculated using ASHRAE parallel path method (Ref. 10):

$$\begin{aligned}
 U &= (1/1.49) + (6/103) + (1/6.34) + (97/103) \\
 &= 0.188 \text{ Btu/hr·sq ft·°F} \\
 &= 1.07 \text{ W/sq m·K}
 \end{aligned}$$

$$\begin{aligned}
 R &= 1/U = 5.33 \text{ hr·sq ft·°F/Btu} \\
 &= 0.94 \text{ sq m·K/W}
 \end{aligned}$$

Dynamic Calibrated Hot Box Tests

Exterior building walls are seldom subjected to steady-state thermal conditions. Outdoor air temperatures and solar effects cause cyclic changes in outdoor surface temperatures. Generally, indoor surface temperatures are relatively constant compared to outdoor surface temperatures.

Dynamic tests are a means of evaluating thermal response under controlled conditions that simulate temperature changes actually encountered in building envelopes. Heat flow through walls as a response to temperature changes is a function of both thermal resistance and thermal storage capacity.

Test Procedures

The lightweight concrete wall, designated Wall L, was subjected to four dynamic temperature cycles using the CTL calibrated hot box. For these tests, the calibrated hot box metering chamber air temperatures were held constant, while climatic chamber air temperatures were cycled over a pre-determined time versus temperature relationship. The rate of heat flow through a test specimen was determined from hourly averages of data.

Results for one cycle, denoted the NBS Temperature Cycle, are presented. Results for other test cycles are presented in Ref 3. The NBS Test Cycle has been applied to more than 25 walls in previous CTL calibrated hot box studies [12, 13]. This periodic cycle is based on a simulated sol-air⁵ cycle used by the National Bureau of Standards in their evaluation of dynamic thermal

⁵Sol-air temperature is that temperature of outdoor air that, in the absence of all radiation exchanges, would give the same rate of heat entry into the surface as would exist with the actual combination of incident solar radiation, radiant energy exchange, and convective heat exchange with outdoor air [10].

performance of an experimental masonry building [14]. It represents a large variation in outdoor temperature over a 24-h period. The mean climatic chamber temperature of the cycle is approximately equal to the mean metering chamber temperature.

A dynamic cycle is repeated until a condition of equilibrium is obtained. Equilibrium conditions were evaluated by consistency of applied temperatures and measured energy response. After an equilibrium condition was reached, the test was continued for a period of three days. Results are based on average readings for three consecutive 24-h cycles.

Test Results

Measured temperatures for the NBS Temperature Cycle applied to Wall L are presented in Fig. 8. Climatic chamber air (t_c), metering chamber air (t_m), climatic surface (t_{cs}), metering surface (t_{ms}), and internal wall (t_{md}) temperatures are average readings of 16 thermocouples placed as described in the Instrumentation section. The average climatic chamber air temperature was 20.2°C (68.3°F). The average metering chamber air temperature was 22.3°C (72.1°F).

Measured heat flow for the NBS Temperature Cycle applied to Wall L is presented in Fig. 9. Heat flow is designated positive when heat flows from the calibrated hot box climatic chamber to the metering chamber. Heat flow determined from calibrated hot box tests (ASTM C 976) is denoted q_w .

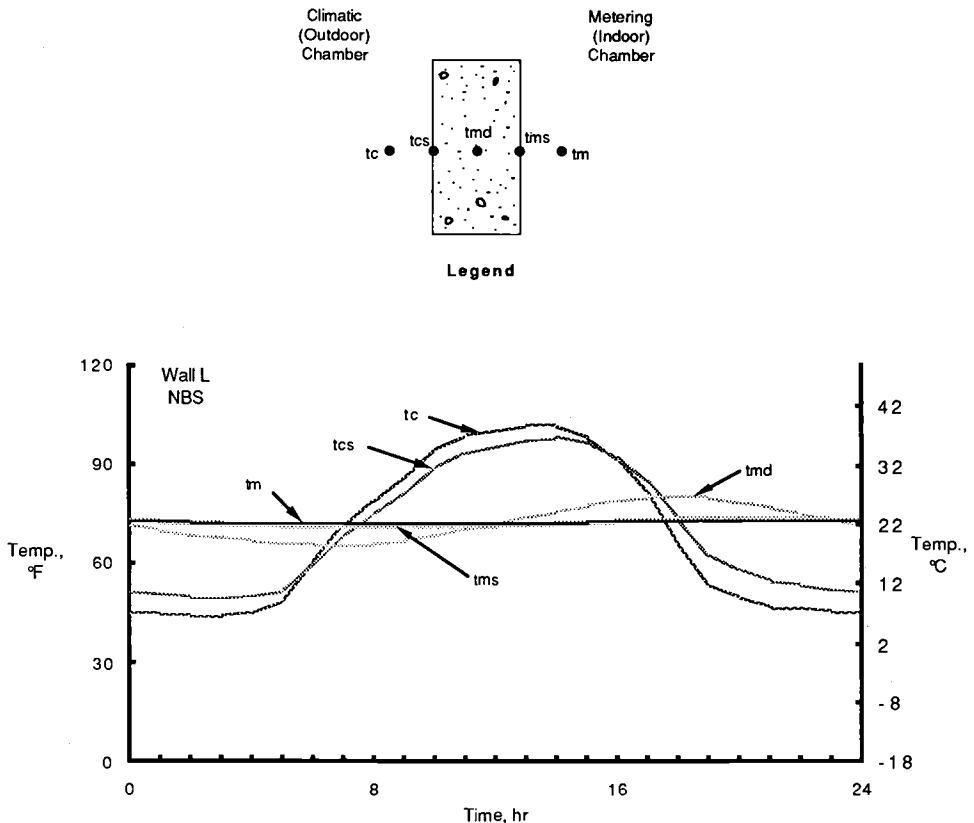


FIG. 8—Measured temperatures for NBS test cycle applied to Wall L.

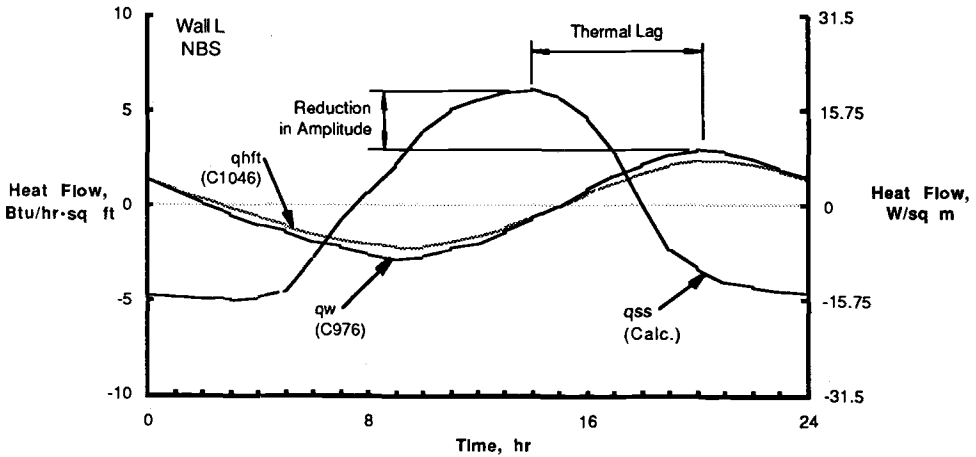


FIG. 9—Measured heat flow for NBS test cycle applied to Wall L.

Heat flow from the heat flux transducer (ASTM C 1046) located on the metering chamber side of the test specimen surface is denoted q_{hft} . Heat flux transducer data were calibrated using results from steady-state calibrated hot box tests on Wall L.

Heat flow predicted by steady-state analysis is denoted q_{ss} . Values were calculated on an hourly basis from wall surface temperatures using the equation

$$q_{ss} = (t_{ms} - t_{cs})/R \quad (1)$$

where

q_{ss} = heat flow through wall predicted by steady-state analysis, W/m^2 ($Btu/h \cdot ft^2$),

R = average thermal resistance, $m^2 \cdot K/W$ ($h \cdot ft^2 \cdot ^\circ F/Btu$),

t_{cs} = average temperature of wall surface, climatic chamber side, $^\circ C$ ($^\circ F$), and

t_{ms} = average temperature of wall surface, metering chamber side, $^\circ C$ ($^\circ F$).

Thermal resistances are dependent on wall mean temperature and were derived from steady-state calibrated hot box test results.

Measured heat flow curves, denoted q_w and q_{hft} , show significantly reduced and delayed peaks compared to calculated heat flow, denoted q_{ss} .

Thermal Lag

One measure of dynamic thermal performance is thermal lag. Thermal lag is a measure of the response of indoor surface temperatures and heat flow to fluctuations in outdoor air temperatures. Lag is dependent on thermal resistance and heat storage capacity of the test specimen, since both of these factors influence the rate of heat flow.

Calibrated hot box thermal lag is quantified by two methods. In one measure, lag is calculated as the time required for the maximum or minimum specimen surface temperature on the metering chamber side to be reached after the maximum or minimum climatic chamber air temperature is attained. In the second measure, lag is calculated as the time required for the maximum or minimum heat flow rate, q_w , or q_{hft} , to be reached after the maximum or minimum heat flow rate based on steady-state predictions, q_{ss} , is attained. The second measure is illustrated in Fig. 9 for the NBS Test Cycle applied to Wall L. Both measures give similar results.

Average thermal lag was 6.5 h for the NBS Test Cycle applied to Wall L. The value determined using heat flux transducer data is the same as that determined from calibrated hot box test results.

Lag times of 3 to 15 h are generally beneficial for exterior walls. Walls with these lag times delay peak afternoon heat loads until cooler night hours. Thermal lags as low as 3 h are beneficial in delaying peak afternoon loads until cooler evening hours. These lower lag times are especially beneficial in commercial and industrial buildings that are vacated in the evening hours. The "lag effect" is also beneficial for passive solar applications.

Reduction in Amplitude

Reduction in amplitude is a second measure of dynamic thermal performance. Reduction in amplitude, as well as thermal lag, is influenced by both wall thermal resistance and heat storage capacity. Reduction in amplitude is dependent on the temperature cycle applied to the test specimen.

Reduction in amplitude is defined as the percent reduction in peak heat flow when compared to peak heat flow calculated using steady-state theory. Reduction in amplitude is illustrated in Fig. 9. Values for reduction in amplitude were calculated using the equation

$$A = [1 - (q' - \bar{q}) / (q'_{ss} - \bar{q}_{ss})] \cdot 100 \quad (2)$$

where

A = reduction in amplitude, %,

q' = maximum or minimum heat flow through wall,

\bar{q} = mean heat flow through wall,

q'_{ss} = maximum or minimum heat flow through wall predicted by steady-state analysis, and

\bar{q}_{ss} = mean heat flow through wall predicted by steady-state analysis.

Average reduction in amplitude for heat flow measured by the calibrated hot box, q_w , is 47% for the NBS Temperature Cycle. Reduction in amplitude from heat flux transducer measurements is 58%.

Amplitudes for heat flux transducer data, q_{hft} , are generally not the same as those for calibrated hot box measurements, q_w [12, 13]. Heat flow amplitudes differ because of the physical presence of the instrument mounted on a wall. A wall's thermal properties are locally altered by the heat flux transducer. In addition, heat flux transducer calibration using steady-state hot box results may not fully correct for dynamic effects of the instrument location.

Actual maximum heat flow through a wall is important in determining the peak energy load for a building envelope. Test results show that anticipated peak energy demands based on actual heat flow are less than those based on steady-state predictions for walls with thermal storage capacity [1]. As expected, calculations based on steady-state analysis overestimate peak heat flow for the dynamic temperature cycle applied to Wall L.

Total Heat Flow

Results of dynamic tests are also compared using measures of total heat flow through a specimen for a 24-h temperature cycle. Figure 9 can be used to illustrate total measured heat flow. The curve marked " q_w " is heat flow through the test wall measured by the calibrated hot box. Areas enclosed by the measured heat flow curve and the line for zero heat flow are total heat flow through a wall. The sum of the areas above and below the horizontal axis is total measured heat flow for a 24-h period. A similar procedure is used to calculate total heat flow for a 24-h period from measured heat flux transducer data, q_{hft} , and predictions based on steady-state analysis, q_{ss} .

Total heat flows for a 24-h period measured by the calibrated hot box, measured by heat flux transducers, and predicted by steady-state analysis, respectively are 129, 107, and 294 W · h/m² (40.9, 33.8, and 93.3 Btu/ft²).

Total heat flow measured by the calibrated hot box is 44% of total heat flow calculated using steady-state analysis. The ratio of total measured heat flow to steady-state predictions, denoted the total heat flow ratio, depends on the climatic chamber air temperature cycle applied to the wall. Particularly for massive walls, greater reductions in actual heat flow, compared to steady-state predictions, occur for temperature cycles which produce heat flow reversals through a wall.

It should be noted that comparison of total measured heat flow values are limited to the specimen and dynamic cycle evaluated in this program. Results are for a particular diurnal test cycle and should not be arbitrarily assumed to represent annual heating and cooling loads. In addition, results are for an individual opaque wall assembly. As such, they are representative of only one component of the building envelope.

Comparisons with Other Concrete Walls

Dynamic heat transmission coefficients of thermal lag, reduction in amplitude, and total heat flow ratio are used to compare dynamic thermal response of alternative wall systems.

Thermal lag and reduction in amplitude are dependent on both thermal resistance, R , and heat storage capacity,

$$\rho cL$$

where

ρ = wall density, kg/m³ (pcf),

c = wall specific heat, J/kg · K (Btu/lb · °F), and

L = wall thickness, m (ft).

Mass, ρL , is the predominant factor in determining heat storage capacity of most building materials.

For homogeneous walls, thermal lag and reduction in amplitude increase with an increase in M [15]:

$$M = \left(\frac{L^2/\alpha}{P} \right)^{1/2} = \left(\frac{(R) \cdot (\rho cL)}{P} \right)^{1/2} \quad (3)$$

where

L = wall thickness, m (ft),

α = thermal diffusivity, $k/\rho c$, m²/s (ft²/h),

k = thermal conductivity of wall, W/m · K (Btu/h · ft · °F),

ρ = wall density, kg/m³ (pcf),

c = wall specific heat, J/kg · K (Btu/lb · °F),

R = wall resistance, m² · K/W (h · ft² · °F/Btu), and

P = period of dynamic cycle, h.

Table 8 presents values of M and dynamic heat transmission coefficients for Wall L and three other homogeneous concrete walls. Thermal lag, reduction in amplitude, and total heat flow ratio are for the NBS Temperature Cycle applied to each wall using the calibrated hot box. Thermal resistances used in Eq 3 to calculate M are for a wall mean temperature of 24°C (75°F) and are from measurements using CTL's calibrated hot box. Surface resistances are not included in resistances used in Eq 3.

TABLE 8—Concrete wall comparisons.

Wall Designation	Wall Type	Reference	Measured Properties							Calculated M	
			L Thickness, mm (in.)	Unit Weight, kg/cu m (pcf)	Estimated Moisture Content, % oven-dry wt.	R* Thermal Resistance, sq m ² /K/W (hr-sq ft ² °F/Btu)	c** Specific Heat, J/kg·K (Btu/lb·°F)	Thermal Lag,*** hr	Amplitude Reduction,*** %		Total Heat Flow Ratio,*** %
C1	Normal weight structural concrete with sand and gravel aggregate	7	211 (8.31)	2310 (144)	2	0.12 (0.71)	810 (0.19)	4.0	45	53	0.75
C2	Lightweight structural concrete with expanded shale aggregate	8	210 (8.28)	1630 (102)	9	0.31 (1.75)	960 (0.23)	5.5	54	48	1.09
L	Lightweight structural concrete with Macrolite™ aggregate	—	203 (8.00)	900 (56)	2	0.77 (4.4)	460 (0.11)	6.5	47	44	0.87
C3	Low density concrete with expanded perlite aggregate	9	216 (8.52)	740 (46)	10	1.00 (5.9)	750 (0.18)	8.5	61	39	1.20

* From calibrated hot box (ASTM C976) test results at a wall mean temperature of 24°C (75°F). Values do not include surface film resistances.

** Measured using U.S. Army Corps of Engineers Method CRD-C124-73.

*** Measured using the NBS Dynamic Temperature Cycle.

Specific heat values were measured using U.S. Army Corps of Engineers Method CRD-C124-73, "Method of Test for Specific Heat of Aggregates, Concrete, and Other Materials (Method of Mixtures)" [8].

The dynamic cycle period, P , is 24 h.

Figures 10 and 11, respectively, show that thermal lag and reduction in amplitude generally increase as M increases. Figure 12 shows that total heat flow ratio generally decreases with an increase in M .

Wall C3, low density concrete, has the greatest lag time, equal to 8.5 h. Concrete in Wall C3 has thermal mass as well as a higher resistance than most concrete and masonry materials. Equation 3 shows that thermal lag and M are dependent on both mass and resistance.

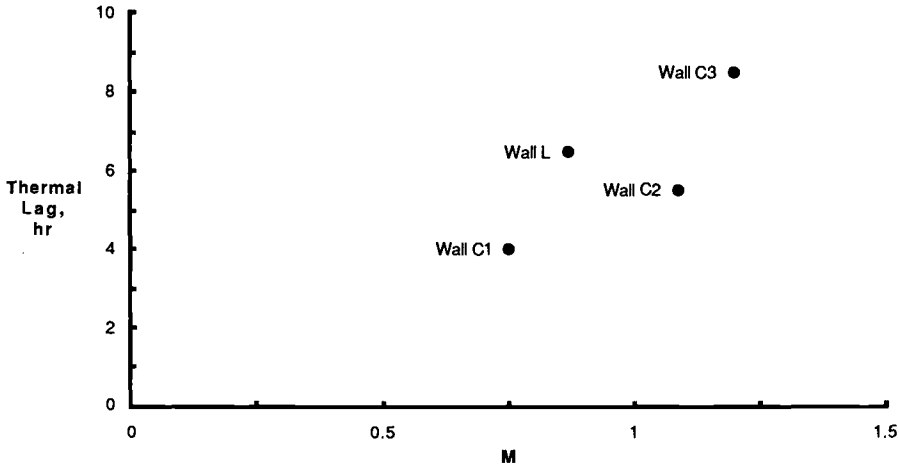


FIG. 10—Thermal lag and M values for the NBS test cycle applied to concrete walls.

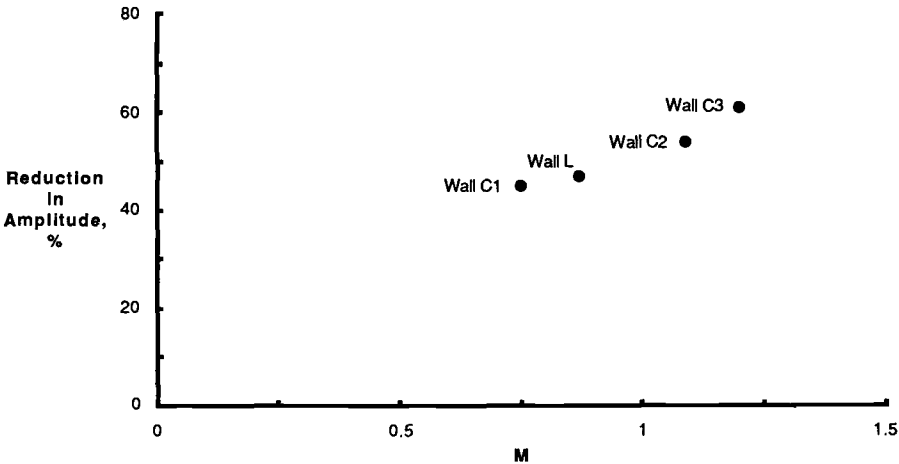


FIG. 11—Reduction in amplitude and M values for the NBS test cycle applied to concrete walls.

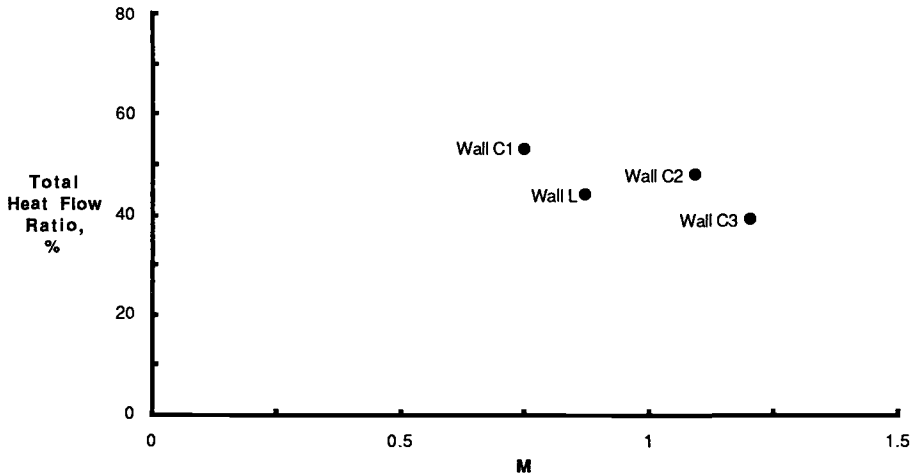


FIG. 12—Total heat flow ratio and M values for the NBS test cycle applied to concrete walls.

Compared to the low density concrete of Wall C3, the newly developed Wall L concrete has 80% the resistance, 80% of the thermal lag, but 230% the compressive strength. Twenty-eight day compressive strengths for Wall C3 and Wall L concretes, respectively, are 6.1 MPa (880 psi) [6] and 13.8 MPa (2000 psi). The concrete for Wall L can be used as a load-bearing wall, whereas the concrete for Wall C3 cannot.

Summary and Conclusions

This paper presents results of an investigation to develop a lightweight structural concrete with approximately one tenth the thermal conductivity of normal weight concrete. Concrete trial mixes were developed. Thermal and physical properties were measured on small-scale concrete specimens.

Heat transfer characteristics of two 200-mm (8-in.)-thick, full-size wall assemblies were evaluated using a calibrated hot box (ASTM C 976). One test specimen, designated Wall L, was a 200-mm (8-in.)-thick wall constructed entirely of the newly developed lightweight structural concrete. The second specimen, designated Wall S, was the same as the first except for a 150-mm (6-in.)-high normal weight concrete strip running horizontally across the wall at midheight. The horizontal strip simulates a floor slab extending through an exterior wall.

The following conclusions are based on results obtained in this investigation.

Concrete Mix Development

1. The concrete mix design with the highest strength-to-weight ratio utilized a new aggregate from the 3M Company designated as Macrolite Ceramic Spheres. Laboratory tests were conducted on concrete mixes utilizing this aggregate.
2. The newly developed concrete has a unit weight of 800 kg/m³ (50 pcf) and a 28-day compressive strength of 13.8 MPa (2000 psi).

Steady-State Temperature Conditions

1. Thermal conductivity of Wall L, the homogeneous lightweight concrete wall, measured by the calibrated hot box (ASTM C 976) is 0.27 W/m · K (1.86 Btu · in./h · ft² · °F). This value is

for a specimen mean temperature of 24°C (75°F) and was interpolated from steady-state test results.

2. Overall thermal resistances of Walls L and S, respectively, interpolated from values measured using the calibrated hot box, are 0.92 and 0.83 m² · K/W (5.2 and 4.7 h · ft² · °F/Btu) at 24°C (75°F). Thermal resistance of Wall S is 10% less than that for Wall L.

3. Thermal conductivities of small-scale lightweight and normal weight concrete specimens were measured using a guarded hot plate (ASTM C 177). Thermal conductivities for Wall L lightweight, Wall S lightweight, and Wall S normal weight specimens, respectively, are 0.21, 0.21, and 1.82 W/m · K (1.43, 1.48, and 12.66 Btu · in./h · ft² · °F) at a specimen mean temperature of 24°C (75°F). Thermal conductivities at a specimen mean temperature of 24°C (75°F) were interpolated from steady-state test results. Guarded hot plate specimens were oven-dried before testing.

4. Thermal conductivity of a lightweight concrete portion of Wall S determined from heat flux transducers (ASTM C 1046) was 0.26 W/m · K (1.8 Btu · in./h · ft² · °F). This value is for a specimen mean temperature of 24°C (75°F) and was interpolated from steady-state test results.

5. Predicted thermal resistances of Walls L and S were calculated using procedures from the *ASHRAE Handbook - 1985 Fundamentals* and measured thermal conductivities from guarded hot plate tests. Predicted thermal resistance of Wall S is 17% less than that for Wall L. This compares to a 10% decrease in measured thermal resistance for Wall S compared to Wall L. The reduction in R-value for Wall S is attributed to the normal weight concrete strip.

Dynamic Temperature Conditions

1. As indicated by thermal lag, heat storage capacity of the lightweight structural concrete wall delayed heat flow through the specimen. Average thermal lag for Wall L was 6.5 h.

2. As indicated by the damping effect, heat storage capacity of the wall reduced peak heat flows through the specimen for dynamic temperature conditions when compared to steady-state predictions. Reduction in amplitude was 47% for the NBS Temperature Cycle applied to Wall L.

3. For the diurnal temperature cycle applied to the Wall L, total heat flow for a 24-h period was less than would be predicted by steady-state analysis. Total measured heat flow for the 24-h NBS Temperature Cycle was 44% of that predicted by steady-state analysis. This reduction in total heat flow is attributed to wall storage capacity and reversals in heat flow.

Limitations

Calibrated hot box test results presented in this report are limited to the test specimen and temperature cycle used in this investigation. Results described in this report provide data on thermal response of a lightweight structural concrete wall subjected to steady-state and diurnal sol-air temperature cycles. A complete analysis of building energy requirements must include consideration of the entire building envelope, building orientation, building operation, and yearly weather conditions. Data developed in this experimental program provide a quantitative basis for modeling the building envelope, which is part of the overall energy analysis process.

References

- [1] Larson, S. C. and Van Geem, M. G., "Structural Thermal Break Systems for Buildings - Feasibility Study," Oak Ridge National Laboratory Report No. ORNL/Sub/84-21006/1, Construction Technology Laboratories, Inc., Skokie, Ill., 1987, 88 pages.
- [2] Litvin, A. and Van Geem, M. G., "Structural Thermal Break Systems for Buildings - Development and Properties of Lightweight Concrete Systems," Oak Ridge National Laboratory Report No. ORNL/Sub/84-21006/2, Construction Technology Laboratories, Inc., Skokie, Ill., 1988, 91 pages.

- [3] Van Geem, M. G., "Structural Thermal Break Systems for Buildings - Heat Transfer Characteristics of Lightweight Structural Concrete Walls," Oak Ridge National Laboratory Report No. ORNL/Sub/84-21006/3, Construction Technology Laboratories, Inc., Skokie, Ill., 1988, 143 pages.
- [4] Van Geem, M. G., Fiorato, A. E., and Julien, J. T., "Heat Transfer Characteristics of a Normal Weight Concrete Wall," Oak Ridge National Laboratory Report No. ORNL/Sub/79-42539/1, Construction Technology Laboratories, Portland Cement Association, Skokie, Ill., 1983, 89 pages.
- [5] Van Geem, M. G. and Fiorato, A. E., "Heat Transfer Characteristics of a Structural Lightweight Concrete Wall," Oak Ridge National Laboratory Report No. ORNL/Sub/79-42539/2, Construction Technology Laboratories, Portland Cement Association, Skokie, Ill., 1983, 88 pages.
- [6] Van Geem, M. G. and Fiorato, A. E., "Heat Transfer Characteristics of a Low Density Concrete Wall," Oak Ridge National Laboratory Report No. ORNL/Sub/79-42539/3, Construction Technology Laboratories, Portland Cement Association, Skokie, Ill., 1983, 89 pages.
- [7] "Guide for Cast-in-Place Low Density Concrete," ACI 523.1R-67, American Concrete Institute, Detroit, 1967.
- [8] *Handbook for Concrete and Cement*, U.S. Army Waterways Experimental Station, Vicksburg, Miss., 1988.
- [9] Fiorato, A. E., "Laboratory Tests of Thermal Performance of Exterior Walls," in *Proceedings, ASHRAE/DOE-ORNL Conference on Thermal Performance of the Exterior Envelopes of Buildings*, Orlando, Fla., Dec. 1979, ASHRAE SP28, Atlanta, 1981, pp. 221-236.
- [10] *ASHRAE Handbook - 1985 Fundamentals*, American Society of Heating, Refrigerating, and Air Conditioning Engineers, Atlanta, 1985, Chapter 23.
- [11] Larson, S. C. and Van Geem, M. G., "Surface Temperature Measurement Techniques for a Calibrated Hot Box Test Specimen," Report No. ORNL/Sub/79-42539/7, prepared for Oak Ridge National Laboratory, Construction Technology Laboratories, Portland Cement Association, Skokie, Ill., 1986, 78 pages.
- [12] Van Geem, M. G., "Calibrated Hot Box Test Results Data Manual - Volume I," Oak Ridge National Laboratory Report No. ORNL/Sub/79-42539/4, Construction Technology Laboratories, Portland Cement Association, Skokie, Ill., 1984, 336 pages.
- [13] Van Geem, M. G. and Larson, S. C., "Calibrated Hot Box Test Results Data Manual - Volume II," Oak Ridge National Laboratory Report No. ORNL/Sub/79-42539/5, Construction Technology Laboratories, Portland Cement Association, Skokie, Ill., 1985, 164 pages.
- [14] Peavy, B. A., Powell, F. J., and Burch, D. M., "Dynamic Thermal Performance of an Experimental Masonry Building," Building Science Series 45, U.S. Department of Commerce, National Bureau of Standards, Washington, D.C., 1973, 98 pages.
- [15] Childs, K. W., Courville, G. E., and Bales, E. L., "Thermal Mass Assessment," Oak Ridge National Laboratory for the U.S. Department of Energy, Oak Ridge, Tenn., 1983, 86 pages.

The Northwest Wall Moisture Study: A Field Study of Moisture in the Exterior Walls of New Northwest Energy-Efficient Homes

REFERENCE: Tsongas, G. A., "The Northwest Wall Moisture Study: A Field Study of Moisture in the Exterior Walls of New Northwest Energy-Efficient Homes," *Insulation Materials, Testing, and Applications*, ASTM STP 1030, D. L. McElroy and J. F. Kimpflen, Eds., American Society for Testing and Materials, Philadelphia, 1990, pp. 464-482.

ABSTRACT: The purpose of this study was to find out whether building the exterior walls of new homes to energy-efficient standards with more insulation (at least R-19) and an air/vapor barrier causes unacceptably high levels of moisture or related problems within walls. This was to be determined by field inspection of such homes and openings in their walls. An additional purpose of the study was to determine if any other type of moisture-related problems have occurred in the heavily-insulated, relatively airtight new homes. Fifty test homes were located in the Seattle-Olympia area, sixteen along the rainy Washington coast, and twenty in the cold Montana region. The exterior walls of the 86 newly constructed homes were opened between January and March 1987 under the worst expected conditions and inspected for signs of moisture, moisture accumulation, or moisture damage. Measurements of the moisture content of selected wood members within the wall cavities also were made. Over half of the test homes had at least one wall wood member with over 20% moisture content. Half of the mud (sill) plates and over one-third of the sheathing were equal to or above 20% moisture content. Whether the walls will dry out sufficiently during warmer weather in order to avoid wood decay and consequent structural damage is unresolved. In addition to the wall cavity moisture problems, numerous moisture-related problems were observed within the homes, primarily because of inadequate moisture control. The results and conclusions of the field study are described in detail. Future research needs also are discussed.

KEY WORDS: moisture, moisture damage, moisture control, wood decay, vapor barrier, wall, ventilation, energy-efficient, residential

Project Description and Purpose

Background

Concern about moisture accumulation and damage in conventional 2 × 4 walls retrofitted with insulation without a vapor barrier led to two separate field studies that measured the moisture levels within such walls [1,2]. Approximately 100 houses were examined in each of Portland, Oregon, and Spokane, Washington, during the winter months when moisture accumulation was expected to be greatest. In neither study was wall moisture concluded to pose a problem to the long-term structural integrity of the houses. It was assumed that comparably insulated walls with a vapor barrier would be even more immune to moisture problems.

In order to promote conservation in new houses built within the Pacific Northwest, the Northwest Power Planning Council developed the Model Conservation Standards (MCS) as an energy

¹Professor, Mechanical Engineering Department, Portland State University, Portland, OR 97207.

efficient building code. Electrically-heated houses built to the MCS are required to have walls insulated to at least R-19, and they must have a wall vapor barrier. Although the studies previously mentioned implied that the MCS houses should experience no wall moisture problems, some researchers and house builders expressed concern that the results of those studies should not be extrapolated to MCS walls. If the Bonneville Power Administration (BPA) is to actively promote the MCS for new construction in its service region, it is appropriate that the potential for wall moisture problems due to these construction techniques be identified prior to widespread adoption.

Project Objectives

Thus the purpose of this project was to measure the *in situ* moisture in actual MCS walls under the worst expected conditions. Such measurements would then determine whether building the exterior walls of homes to Model Conservation Standards causes unacceptably high levels of moisture or related problems within the walls. An additional goal of the study was to document any type of moisture-related problems that may have occurred in the heavily-insulated, relatively tightly constructed MCS homes.

Test Homes and Study Location

The pool of houses eligible for inclusion in this study was those built to the MCS. The age of the homes at the time of the openings ranged from brand new to a few years old.

The study was to span the climatic regions included within the BPA service region, which includes Washington, Oregon, Idaho, and western Montana. Tests were to be concentrated in two regions that experience climatic extremes to ensure that there would be the best chance of finding moisture damage, if it exists. In addition, another region with a major population concentration was selected. The following regions were to be studied:

1. *Coastal Region (10–20 homes)*—This region is characterized by relatively mild winters with high relative humidity, accompanied by frequent wind driven rains. The summers tend to be temperate with continuing high relative humidity, reducing the potential to dry moist wood. Grays Harbor County in central Washington had the only concentration of MCS homes large enough to obtain the required number of coastal homes.

2. *Cold Region (10–20 homes)*—The interior basins and mountains of the Northwest experience extremely cold winters. This climate condition leads to much greater condensation potential, even though the warm dry summers may cause substantial redrying. Homes in several Montana cities were to be solicited.

3. *Population Center (40–50 homes)*—Most of the people in the Northwest live in regions that are generally mild with high annual rainfall. Since most of the new houses are built in these regions, and because the potential for moisture accumulation definitely exists, a population center was to be studied. The test sample for this region was to be selected from MCS homes from the Seattle-Olympia area.

Study Work Plan and Schedule

The study was to be conducted in two sequential phases. The first phase, taking place during the fall of 1986, was aimed at identifying the pool of eligible houses. The requirements were that all homes be electrically heated and have a minimum nominal wall insulation R-value of 19. In addition, in each region an attempt was made to obtain a mix of vapor barrier types, including polyethylene (poly), interior foam, airtight drywall, and no vapor barrier as a control. Furthermore, it was planned to open as many as possible of those homes whose occupants had reported

on the returned questionnaires moisture-related problems such as window condensation or mold and mildew. The houses were then to be screened to select the specific houses to be included in the test sample. An effort was to be made to select worst case MCS houses from a moisture point of view.

The second phase of the study was to be undertaken during the winter months of 1987. It was to include an interview with an occupant of each proposed test house to determine pertinent lifestyle characteristics, a detailed inspection of each house, the actual measurement of moisture in the opened wall cavities of the specified houses, and the analysis of the results.

During the first phase, the houses with the required location and construction characteristics were to be identified through BPA data and through contact with state energy offices, local energy offices, or utilities. The occupants of the eligible houses were to be contacted to explain the motivation and individual benefit of the study, and to procure written permission to measure moisture in their houses. A list of the specific houses solicited was then to be compiled by location and included in a report to BPA. BPA personnel were then to evaluate whether the study included the proper distribution of houses to warrant execution of the second phase.

During the second phase, if conducted, the wood moisture content of the wall cavities of selected houses was to be physically measured during the winter months when the potential for condensation is greatest. Concurrently, a methodology for evaluating moisture problem houses was to be applied and modified as necessary. Upon completion of the field tests, the moisture content results were to be compiled and correlated to local climate and vapor barrier type. A final report was to be written to describe the results and recommendations.

Project Organization

The study was funded by Bonneville Power Administration in Portland Oregon. Seton, Johnson & Odell, Inc. of Washington (SJO) served as the prime contractor for this study. Dr. George Tsongas of Portland State University, working as a consultant to SJO, served as Project Manager with responsibility for overall direction of the study and writing of the final report. The remaining work force was divided into two main groups because of the need to solicit and open test homes in both Montana and Washington.

Identification and Selection of Test Homes

Four participating agencies identified potential test houses in their respective geographical area. Letters explaining the project were then sent to the occupants of 257 candidate single-family homes in the three regions. At the time of the study there were about 5000 single- and multi-family homes in the region. The occupants of 124 of the identified homes agreed to participate in the study, if selected.

In the Washington coastal region there were only 20 MCS homes and 18 signed up; 16 eventually were found to qualify and were selected for testing. In the cold region 75 letters were sent out and 38 agreed to participate; 20 were selected. In the metro region 155 letters were sent, of which 64 agreed to participate; from that group 50 were selected. In both the cold and metro regions, houses that were relatively large or only had one occupant were not used. Some others also were not used because of their inconvenient location. In those two regions most of the homes that had moisture problems as identified through the occupant questionnaire and later interview were selected. Of course, most of the occupants that had moisture problems wanted to participate. So while the homes tested were somewhat biased towards having moisture problems, it is nonetheless important to stress that almost half the occupants contacted at random within the three climatic regions had moisture-related problems in their MCS homes. Thus it is believed that the conclusions of this study are truly representative of the whole population of new energy-efficient MCS homes in the Northwest.

Field Test Methodology

Training

At the start of Phase II, the project director initiated training of all the personnel involved in the field work, including the occupant interviewers, engineer house inspectors, field opening engineers, and journeyman carpenters. There were two teams of field study personnel, one for the cold (Montana) region, and one that covered both the coastal and metro regions in the state of Washington. The training and consistent use of the same personnel resulted in an efficient and consistent interview and house inspection as well as wall opening data/sample collection procedure. The training of the two field teams was accomplished by having each team complete at least four occupant interviews, pre-opening house inspections, including locating the sites for wall openings, and wall openings. This was done on site at four test homes in each of the metro and cold regions under the direction of the project director.

Occupant Interviews and House Inspections

As the second step in Phase II, a project canvasser and an inspecting engineer visited each prequalified home in January 1987. The canvasser conducted an interview with an occupant to ascertain pertinent information on the lifestyle of the occupants as well as salient home characteristics. Simultaneously, the engineer verified the categorization of the house, inspected it carefully, identified relevant characteristics of the home, and located opening sites. The house inspection included the attic, crawl space, or basement, and a careful inspection of inner and outer wall surfaces for signs of leaks, moisture, or moisture damage. In addition, the ventilation and dehumidification systems were identified, inspected, and tested to see if they were working. The complete survey served as the final qualification of the home for field testing.

Determination of Opening Locations

One of the major tasks accomplished during the test home inspection was the determination of three locations for wall openings. The opening locations had to meet the following criteria:

- A. Quantity: A minimum of three openings in each house.
- B. Location within stud cavity:
 - 1. Two openings in the low cavity position.
 - 2. One opening in the high cavity position, in the same stud cavity as one of the low cavity positions.
- C. Location of stud cavities within the house, in order of descending priority:
 - 1. Areas with visible signs of wall moisture or moisture damage such as blistering paint, warped siding, discoloration, mold/mildew, and termite or dry rot damage.
 - 2. Areas that indicated high moisture content by the use of a noninvasive moisture meter.
 - 3. Exterior walls of kitchens, bathrooms, laundry rooms, closets.
 - 4. Walls containing electric outlets on interior surfaces.
 - 5. Walls that did not contain wall heaters or areas conducive to drying (such as south walls).

Usually there were no visible signs of high wall moisture or moisture damage because the houses were new and their wood siding typically was stained rather than painted. Thus it became clear that probing the moisture content of the wood sheathing behind the wood siding was a useful means of locating areas of high moisture content. The two small 25.4 mm (1 in.) long and 1.6 mm ($1/16$ in.) diameter pins of a hand-held moisture meter were driven through the

siding in numerous locations around the perimeter of the house. Using this technique enabled the field engineer to locate isolated sites with high sheathing moisture content that otherwise would not have been found except perhaps by chance. After careful examination of the inside and outside of the home, and with all the selection criteria in mind, including the sheathing moisture content determinations, the three best sites were selected.

Wall Openings

The walls of each test home were opened from the outside in the three locations selected during the initial house inspections or as a result of further probing the sheathing moisture content around the perimeter of the house. At each location an opening about 0.3 m (12 in.) high by about 0.4 or 0.6 m (16 or 24 in.) wide (one stud space) was made. Two openings were made near the floor line and one near the first story ceiling line directly above one of the other openings. The siding was carefully removed in whole pieces in order to avoid making unnecessary cuts in it. The carpenter then cut through the exterior rain and air barrier (typically 15# felt, or building paper, or Tyvek) and the sheathing (typically plywood or rigid foam board). The resultant opening exposed the cavity with wall insulation and normally extended down to the sill (mud) plate.

Data Collection and Recording

Immediately upon opening each hole, if exterior sheathing foam insulation was used, a sample of about 5 by 8 cm (2 by 3 in.) was cut out with a knife and sealed air tight in a 500 mL glass jar. The sample was removed quickly to avoid any change in its moisture content and treated carefully to avoid contamination with skin or other moisture sources. The samples were later gravimetrically analyzed in a laboratory for moisture content.

The next step was the measurement of the interior temperature of the wood in the hole opening. A small fine wire thermocouple probe with digital readout was used to determine the wood temperatures, which were required to correct the wood moisture content readings. As a result of previous careful testing during the Spokane Study [2], as well as testing during the training period for this study, it was noted that the temperatures of the various wood members never differed by more than a few degrees. Because the wood temperature correction on the moisture meter is not sensitive to such small differences, only the sole plate or top plate temperature as well as that for the warm side of the sheathing was recorded in order to save time. The temperature was determined in the wood member about one-quarter of its thickness from the outer surface (which is the location of the average moisture content). A nail was driven into the wood to form a hole in order to insert the thermocouple wire to the proper depth.

The wood moisture content of the sole plate, each stud, sheathing, rim joist (header), sub-flooring, and the mud (sill) plate was then measured using a penetrating resistivity-type probe with two insulated pins and a wood temperature correction setting. Measurements were made at one-quarter the member depth from the surface in order to determine the average moisture content. They were also made as close to the coldest outer surface as possible in order to measure the highest moisture content.

In addition to measuring the moisture content of the studs and plates near their outer edges adjacent to the exterior sheathing (wood or foam), measurements also were made near their inner edges. In addition, similar measurements were made in the second inner studs and plates of double stud walls. However, because the inner surfaces or inner studs were considerably drier, their values are not generally reported except to briefly comment on their differences. The wood temperatures also were measured in those inner locations to properly adjust the moisture meter.

For comparison with the moisture meter results, wood samples could be taken and their moisture contents determined gravimetrically in the laboratory. However, only a few such

checks were made because during the Portland Study [1] the moisture meter readings were found to compare quite closely with wood samples analyzed in the laboratory. Occasional wood samples were taken with a chisel. These samples of about 1/2 in. diameter or width and 1 in. length were stored in a sealed glass container and then sent to a laboratory for gravimetric analysis to check the moisture meter readings.

Samples of rigid foam board used as interior sheathing also were taken for gravimetric analysis of their moisture content. The procedure was the same as for the exterior foam sheathing. Whenever any polyethylene sheet air/vapor barrier was cut to provide access to interior sheathing or to measure double wall inner stud moisture contents, the air/vapor barrier was repaired and resealed using 3M sheathing tape or sometimes duct tape.

A careful visual inspection and photographic documentation of the conditions within the wall cavity was performed with the aid of a checklist to indicate factors such as discoloration, mold or mildew, liquid water or frost in the insulation, signs of rot, apparent condensation, etc. Any moisture or damage found was documented in writing and photographically. The existence of any corrosion on outlet boxes, wiring, or metal brads holding the wiring also was noted.

Laboratory Analysis

Sheathing Foam Insulation Sample Moisture Content Determination—One sample of foam insulation from each wall opening that had it either on the exterior or the interior of the wall was analyzed gravimetrically for moisture content by placing it in an oven and drying it to a constant weight. The percentage moisture content (MC) by weight of each sample was determined on a dry basis from the relation

$$MC = (W_w - W_d) \times 100/W_d \quad (1)$$

where W_w and W_d are the wet and dry weights of the material, respectively. The moisture content was determined to within 0.02% per 1 g sample. The minimum net sample weight was about 1 g. The samples were stored in an air-tight, metal-capped 500 mL glass jar prior to analysis in the laboratory. All sample jars were kept at room temperature (no less than 19°C [65°F]) for a minimum of 8 h prior to opening the jars for sample weighing and analysis; this was to prevent moisture in the sample from condensing on the jar inner wall surface prior to opening. Samples were weighed, dried at 52°C (125°F) for 24 h, then reweighed. The reason for using these drying conditions was to prevent outgassing of the foam material with subsequent weight loss. Weighing was completed within 1 min of exposure to air prior to drying and after drying and desiccating to prevent loss or gain of moisture from or to the sample.

Data Base

All the field data were entered into a microcomputer data base. A sample printout for one test home as well as a sample of all the field checklists is given in a more detailed report on this study [3].

Test Home and Occupant Characteristics

This section describes the salient characteristics of the 86 homes selected for study as well as pertinent lifestyle characteristics of their occupants. Selected house characteristics are presented in Table 1.

It is worth noting that the 178 m² (1915 ft²) average size of these new homes is relatively large in comparison to those older retrofit homes tested in the Portland study [1] (about 130 m² or 1400 ft²) and the Spokane study [2] (about 107 m² or 1150 ft²). On average, the cold region

TABLE 1—Selected test house characteristics.

	Cold	Coastal	Metro	All
No. of Test Houses	20	16	50	86
Living Space:				
Avg. (m ²)	207	155	173	178
Max. (m ²)	321	246	354	354
Min. (m ²)	111	69	64	64
Wall Air/Vapor Barrier Type:				
Interior Noncontinuous	0	8	9	17
Interior Poly, Walls Only	0	3	1	4
Interior Poly Wrap	19	2	29	50
Interior Foam Sheathing	1	1	10	12
Exterior Foam Sheathing	10	1	15	26
ADA	0	4	2	6
Exterior Tyvek	7	8	33	48
Sealed Receptacles	19	15	38	72
AAHX	20	10	43	73
Dehumidifier	1	6	7	14
Humidifier	3	0	4	7
Wall Insul. (Mean R)	33	20	22	24
Wall Insul. (Max. R)	42	25	30	42
Triple Glazing	13	7	24	44
Crawl Space	4	13	37	54
Electric Space Heat Type:				
Wall Heaters	1	5	39	45
Baseboard/Ceiling Cable	14	1	3	18
Heat Pump	1	6	2	9
Forced Air/Ducts Outside	0	2	5	7
Forced Air/Ducts Inside	0	2	5	3
Radiant Heaters	2	0	0	2
Hydronic	2	0	0	2

houses were the largest (typically split level or two stories). The smallest test house was a duplex.

There were a mix of wall vapor barrier types. Most of the cold region houses had a continuous poly air/vapor barrier, whereas most of the coastal houses did not. About 60% of the metro houses used an interior poly wrap; an additional 20% used interior foam sheathing. Exterior foam sheathing was used in almost one-third the test homes, but only in one home in the coastal region. Oftentimes, it was used in combination with interior poly.

All the cold region houses had an air-to-air heat exchanger (AAHX), whereas six coastal homes and seven metro houses used a dehumidifier to remove indoor moisture.

Most of the coastal houses used 2 × 6 single stud walls with R-19 batt wall insulation. The metro homes tended to use similar wall construction, except that half added external or internal rigid foam sheathing for additional insulation. The cold region houses utilized a wide variety of framing types, including single and double stud construction. Twelve of the 20 homes used external or internal rigid foam sheathing. The cold region houses had the highest average wall insulation R-value (foam sheathing plus batts or blow-in or spray-on insulation); they also had the highest maximum of R-42. Half of the test homes had triple-glazed windows.

There were a number of different heating system types. They all were electric because this study dealt only with electrically heated homes. Over half the homes were heated with fan-forced air wall heaters, while almost a quarter used baseboards or ceiling cable.

Heating season natural infiltration air change per hour (ach) values for 34 of the homes were obtained from previous blower door tests using LBL (Lawrence Berkeley Laboratory) methodol-

ogy. The mean values for the regions are: coastal, 0.22; cold, 0.30; metro, 0.27; all, 0.28. The range of values for all the test homes was very broad: from 0.05 to 0.86; the standard deviation for all the test homes was 0.17. There was only one coastal house tested, 16 of the 50 metro houses, and 17 of the 20 cold region homes with available air leakage rates. Thus the mean values may not be representative of all the houses in the metro and coastal regions. In part, given the lack of poly in half of the coastal houses, they are probably leakier than the one 0.22 ach value would suggest.

Occupant Lifestyle Characteristics

The average number of occupants per test home was 3.3. The date the houses were first occupied ranged from 15 January 1984 to 15 October 1986. Of those homes with an air-to-air heat exchanger, about 10% of the occupants do not use it. Moreover, of those who have a kitchen exhaust fan, about 40% do not use it. Surprisingly, 13% (or 11 out of 86) of the kitchen fans were the recirculating type that do not exhaust; that included 9 of the 50 metro homes. They were useless for moisture control. One third of the homes, including 15 of the 20 cold region homes, used a recirculating kitchen fan with an AAHX exhaust in the kitchen. However, oftentimes the AAHX was not on during cooking so that cooking moisture was not ventilated. About one quarter of the occupants do not use their bathroom exhaust fan.

The living room temperatures and relative humidities measured at the time of the house inspection are presented in Table 2. As can be seen, the living room relative humidities were lowest in the cold region and highest in the coastal region, as expected. The mean relative humidity for the coastal region homes was very similar to the 56% average measured in the Portland study homes [1]. The average value for all homes as well as for those homes in the metro region was almost identical to that for the Spokane study homes [2]. Relative humidities were oftentimes measured in other rooms, but they are not reported here. They are available in the data base. For the most part, they were very similar to the living room relative humidities. The highest RH value measured in this study was 85%; that occurred in a cold bedroom of a coastal house whose AAHX did not work properly. The highest values measured in this study point out the lack of proper moisture control in some of the homes. The high average for the coastal homes suggests a lack of sufficient moisture removal in many, if not most, of those homes.

The living room temperatures are also shown in Table 2. The average values were lower than expected, yet the homes were, for the most part, comfortable during the house inspection. This suggests a mean radiant temperature effect that allows occupants to be comfortable at lower indoor air temperatures because of the existence of well insulated walls, etc.

Results and Findings

This section is a summary of the results and findings of this study. Supporting details and documentation regarding all aspects of the study are presented in a separate report [3].

TABLE 2—*Living room temperatures and relative humidities.*

		Cold	Metro	Coastal	All
RH (%)	Avg.	40.4	47.4	53.3	46.9
	Max.	55	63	75	75
	Min.	23	32.7	39	23
Temp. (°C) [°F]	Avg.	19.9 [67.9]	18.8 [65.8]	19.6 [67.2]	19.2 [66.6]
	Max.	25 [77]	24 [75]	24 [75]	25 [77]
	Min.	14 [58]	12 [54]	12 [57]	12 [54]

Wood Moisture Content

Three wall openings were made from the outside in each of 86 MCS homes during January–March 1987. Twenty of the homes were located in Montana (the cold region); 16 were along the rainy, damp central Washington coast; and 50 were situated in the greater Seattle-Olympia metropolitan area. Two of the openings were at the floor level, and the other was at the ceiling level at the top of the stud cavity above one of the other holes. In each wall opening the wood moisture content was measured whenever possible at seven locations using a Delmhorst resistivity-type moisture meter. The seven measurement locations were: right stud, left stud, sole plate or top plate, sheathing (warm side), subflooring, rim joist (header), and mud (sill) plate. The locations are illustrated in Fig. 1. Wood member moisture contents were measured as close to the cold exterior surface of the wall as possible in order to determine the highest moisture content. They also were measured in other inner wall locations. The inner locations generally were much drier, so those results are not reported.

The field results are presented in Table 3. The overall mean moisture content of all 1244 outer wall temperature-corrected readings was 16.2%. The means for the sheathing, mud plates, and the subflooring were significantly higher, with the mean moisture content of 21.2% for the mud plates being the highest. Moreover, the maximum values measured for those three wood members were all over 50%. Those values found in newly-constructed MCS homes are substantially greater than the values found for corresponding wood members in older conventional homes during the Portland and Spokane studies [1,2]. Thus the wall moisture levels measured during this study in midwinter are of major concern. If those members do not dry out sufficiently during warm weather, wood decay and structural damage could occur.

Over half of the 86 test homes had at least one wall cavity wood member with over 20% moisture content. Anytime wood members have moisture contents over 20%, there is cause for concern. When moisture levels exceed 30%, there is major concern about the possibility of wood decay and structural damage [4]. All but one of the coastal homes had a moisture content

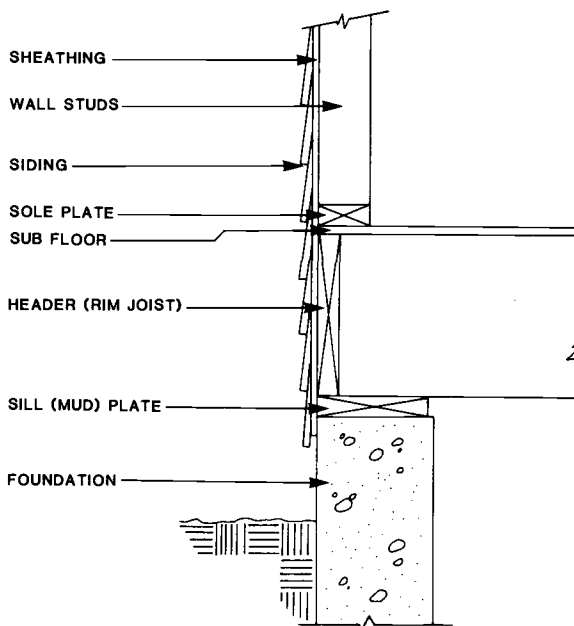


FIG. 1—Wall opening wood member locations of moisture content measurements.

TABLE 3—Moisture content in wall opening wood members.

Wood Member	Value	Cold	Coastal	Metro	All
Sole Plate	Count	38	31	90	159
	Avg. (%)	12.0	18.9	15.5	15.3
	Max. (%)	19.0	28.0	26.0	28.0
	Min. (%)	8.0	10.0	10.0	8.0
Top Plate	Count	17	15	48	80
	Avg. (%)	12.6	19.6	14.1	14.8
	Max. (%)	23.5	29.0	20.5	29.0
	Min. (%)	6.0	12.5	8.0	6.0
Left Stud	Count	57	48	150	255
	Avg. (%)	12.0	18.4	14.7	14.8
	Max. (%)	21.5	41	25.5	41.0
	Min. (%)	6.0	10.0	10.0	6.0
Right Stud	Count	57	48	150	255
	Avg. (%)	12.7	18.9	14.8	15.1
	Max. (%)	34.5	34.0	25.0	34.5
	Min. (%)	6.0	12.5	9.0	6.0
Rim Joist	Count	18	22	69	109
	Avg. (%)	12.4	17.7	15.9	15.7
	Max. (%)	21.5	26.0	20.5	26.0
	Min. (%)	8.5	11.0	11.0	8.5
Sheathing	Count	30	41	101	172
	Avg. (%)	15.5	20.6	18.1	18.3
	Max. (%)	50.0	32.0	52.0	52.0
	Min. (%)	8.0	9.0	9.0	8.0
Mud Plate	Count	5	29	59	93
	Avg. (%)	12.7	21.6	21.8	21.2
	Max. (%)	15.0	36.0	51.0	51.0
	Min. (%)	9.5	13.0	13.0	9.5
Subfloor	Count	20	28	73	121
	Avg. (%)	15.4	20.3	17.3	17.7
	Max. (%)	55.0	29.5	24.0	55.0
	Min. (%)	8.0	11.0	11.0	8.0
All	Count	242	262	740	1244
	Avg. (%)	13.0	19.4	16.2	16.2
	Max. (%)	55.0	41.0	52.0	55.0
	Min. (%)	6.0	9.0	8.0	6.0

of 20% or greater in at least one of the wall cavity wood members. One of the worst cases in this study was a coastal home in which all the wall cavity wood members were found to have moisture contents of 19.5% or above. Over half of the metro homes had at least one wood member at or above 20% moisture content, whereas two-fifths of the homes in the cold region had values of 20% and above.

Further examination of the test results revealed that about one-fifth of all the measured wood member moisture content readings were equal to or above 20%. While that finding is worrisome, perhaps of even greater interest is the fact that almost half of the readings in the coastal region were equal to or greater than 20%. That is of special concern because the coastal region climate is least conducive to drying.

Generally speaking, the highest moisture levels in the various wood members of the heavily-insulated, tightly-built wall cavities occurred in the sheathing and mud plates. About half of all the mud plate readings were equal to or above 20%. In the coastal region, almost three-quarters of them were that moist. On average, over one-third of the sheathing measurements were equal

to or above 20%. Based on these wintertime measurement results, there is a potential for a significant wall cavity moisture problem if these moist wood members do not dry out. That potential is greatest in the coastal region and least, but not negligible, in the cold region. Since mud plates are usually pressure-treated, any structural damage may only be noted over the very long term. However, high moisture content in mud plates can be transmitted to other wall cavity wood members.

It would appear that the moist mud plates were caused at least in part by moisture in the ground wicking up by capillary action through the crawl space foundation walls. Mud plates over basement foundation walls generally were satisfactorily dry, possibly because most of the basements were heated. The wet mud plates located in homes in the damp coastal region are of greatest concern because that region is least conducive to summer drying of the wall wood members.

Many of the cases of high sheathing moisture content have been tied directly to moist indoor air leaking out through the wall cavities. This was determined in part using infrared thermography and a blower door on one of the test homes in Helena, Montana, as part of an adjunct study known as the "Helena Thermography Study" [5]. Air leaks that caused high sheathing moisture contents occurred notably through electrical outlets and a variety of penetrations in the poly air/vapor barriers. Many of the leaks were the result of lack of proper sealing or poor workmanship and could have been avoided. It remains to be seen if sealing the leaks will reduce or eliminate the high sheathing moisture contents. If so, it may be necessary to blower door test all airtight houses to locate and seal air leaks at the time of construction.

As a separate but related part of this study, the sheathing moisture content of a two-story test home in Montana was measured high and low in every stud cavity of two walls by probing through the siding with the pin electrodes of a moisture meter. While sheathing moisture contents as high as 47% were measured in February 1987, when measurements were repeated two months later in the same locations, the highest sheathing moisture content was only 18%. There is no cause for concern when moisture levels are below 20%. Thus there is some hope that sheathing in the cold region will dry out sufficiently during warm weather. However, it is important to stress that this substantial drying was probably the result of the intervening period being unusually hot. It is not at all clear that such drying will always occur, especially in other climates such as the moist coastal region. Nor is it reasonable to expect similar drying in other regions in mud plates, since they should not be expected to dry anywhere near as fast. The degree and speed of drying during warm weather needs to be determined.

While the test results indicated that the climate or region seemed to make a considerable difference, further analysis of the results was undertaken to try and find out what other factors influenced the existence of high moisture levels in the wall cavities of the new MCS homes. Smaller houses were found to have higher wood member moisture contents, and there was a direct correlation of wood member moisture content with the measured relative humidity of the air in the living room. This suggests that if wall wood member moisture contents are high and found to be a problem, reducing the relative humidity of the indoor air may possibly help. Clearly, the indoor relative humidities in many of the homes were too high. There is an indication that the high indoor relative humidities and high wall wood member moisture contents were caused at least in part by lack of, or lack of use of, an air-to-air heat exchanger, dehumidifier, or other ventilation system components such as bathroom fans.

The influence of the type of wall air/vapor barrier on the high wall moisture levels also was examined. For the most part, the differences were small. Nor do they "explain" the high moisture contents found in this study. However, it would appear that the use of rigid foam sheathing, whether on the interior or the exterior, somewhat reduced all the wall member moisture contents. The exterior application was slightly better. Other investigations also have found that walls with exterior foam insulating sheathing added were dryer or no worse than with regular wood sheathing [7,8]. In addition, it is clear that those homes with an interior poly wrap had lower wall cavity moisture contents than those without a continuous air/vapor barrier. It is, of

course, not known if these results would be the same for other non-MCS houses or even MCS multi-family houses.

There was no obvious correlation of high moisture levels with the natural air change rate of the homes derived from blower door tests. However, the counts of homes and measured moisture content readings in any one range were small because only 34 of the 86 test homes were blower door tested. Only one of the 16 coastal homes and 16 of the 50 metro homes whose walls were so moist were blower door tested. It also may be that the natural air change rate is not particularly important, since the majority of the test houses had an air-to-air heat exchanger that provided an unknown but effectively greater air change rate. Nonetheless, the natural air change rate should indicate if there is a need to use the ventilation systems for moisture control.

Interestingly, even though the thermal resistance of the wall insulation in the test homes varied from R-19 to R-42, that factor did not seem to influence the wall cavity moisture content results. That result supports the previously suggested causes for the high moisture contents in sheathing and mud plates. It also says that building heavily-insulated walls does not by itself cause wall cavity moisture problems. That implies that the energy-efficient MCS insulation standards themselves are not the cause of the moisture problems.

Given that high wall cavity wood member moisture contents were found during this study, a key question was whether or not these high values were caused by the use of wet construction materials in walls that are relatively airtight and slow to dry out. Examination of the moisture content results based on the year when the houses were first occupied indicated that the age of the house was a partial factor. Older houses had lower overall average and sheathing moisture contents than newer houses, but the age of the house had no influence on the mud plate results. However, wet construction materials still quite possibly could be part of the mud plate problem if conditions exist such that the mud plates do not dry out or take many years to dry out after construction. One must view these results with caution because the homes in the coastal region were the wettest, and they all were relatively new. Nonetheless, there certainly is a suggestion that wet construction materials are at least part of the cause of the higher moisture contents of some, but not all, wood members. However, more testing is required to be sure.

A question that also should be asked is why the results of this study of new MCS houses are so different from those of the Portland and Spokane studies [1,2] that focused on older conventional houses. The walls of those older homes were quite dry by comparison. Two factors seem to be of critical importance. First of all, the new houses are much more airtight, probably on average by a factor of three or four. The mean air change rate of the 34 MCS test homes that were blower door tested was 0.28. At such levels it is absolutely imperative that moisture generated indoors be removed by a well controlled or correctly used ventilation or dehumidification system. Otherwise, very high indoor relative humidities can result [6], and that can lead to high wall cavity moisture levels. Yet based on observations of the ventilation system components, including their controls, as well as discussion with the occupants regarding their use habits, it is clear that the majority of the MCS test homes were not sufficiently ventilated from a moisture control standpoint.

The second contributing factor is that the new walls themselves are much tighter. In particular, the exteriors of those new walls are substantially more airtight. Thus any moisture that gets into the wall cavity will have a much more difficult time drying out. That is because of the prevalent use of panel siding and sheathing materials, such as plywood siding and plywood sheathing, as well as improved caulking and sealing. The older homes almost all used wooden board type sheathing and were subsequently much leakier on the outside. That is very likely a major part of the reason for the existence of high mud plate and sheathing moisture contents found in this study.

While the new houses and their walls are much more energy-efficient, they also are much less forgiving of construction errors. Keeping the moisture generated indoors from getting into the wall cavity in the first place becomes even more important. That will require even better sealing on the inside, which should not be too difficult. The effect of improved sealing on wall cavity

moisture contents needs to be examined. It is also extremely important to keep in mind one of the basic principles of wall construction: The exterior surface must be much less tight than the interior surface in order to avoid wall cavity moisture buildup. Thus it may be necessary to develop or utilize methods for making the exterior portion of MCS walls less airtight or more breathable.

A statistical analysis of the moisture content results and a number of key factors that were believed might influence those results was undertaken to try and find out what caused the high wall moisture levels. Unfortunately, no single factor "explained" the high results. Part of the reason is that there simply are too many variables influencing the conditions in the test houses. Moreover, the power of statistical analysis was severely limited in this study by the small size of the sample of test houses. While a number of factors were found to have an influence on the wall moisture levels, as already noted, in most cases it was difficult to decide which was the most important influence.

While inspecting the attics of the test homes, measurements were made of the moisture content of a roof joist and roof sheathing. The average for the sheathing was the highest at 15.8%. There were a few readings over 20%, but that was not thought to be a problem except for those few homes with an exhaust fan discharging into the attic directly at the roof sheathing instead of being properly vented to the outdoors.

During the wall openings, small samples were taken of interior and exterior rigid foam sheathing and then sent to a laboratory to be gravimetrically analyzed for moisture content. Generally speaking, both the isocyanurate and the polystyrene stayed relatively dry, although the polystyrene was considerably dryer than the isocyanurate in both interior and exterior applications. A few samples of asphalt-coated fiberboard had much higher moisture contents. They acted much like wood sheathing, and the coatings did not keep much moisture out.

Moisture Damage

In addition to measuring wood member moisture contents in wall openings, a further purpose of this study was to determine if any other moisture-related problems had occurred in the heavily-insulated, relatively airtight new homes. This was to be accomplished by a thorough inspection of each test house and its ventilation systems, by asking the occupants about previous and existing moisture-related problems, and by observing the conditions in and around each wall opening.

During the home inspections and interviews, a relatively large number of signs of possible moisture damage or moisture problems were observed. Window moisture problems were common. Almost three-quarters of the homes had condensation on window glass or frames, while one-third had mold and mildew on window frames and/or sills. One-quarter of the homes had moisture damage to window sills, and that is of concern. While some condensation, and even mold, is to be expected, the high frequency of occurrence of window problems was unexpected in these new homes that had improved window systems and presumably had well controlled interior conditions.

In addition, previous moisture or water leak problems were reported by 83% of the occupants. In part that reflects the fact that the test homes were selected because previous moisture-related problems had been noted by the occupants. Problems with ventilation and dehumidification equipment (notably air-to-air heat exchangers) were reported by over half the occupants. Mold and mildew was reported by just under half. That is not a particularly good record. Later observations by the inspecting engineers verified that numerous moisture problems were indeed in existence.

While the occurrence of water leak damage was not particularly extensive, the inspecting engineers observed a large number of nonleak associated moisture problems. About two-thirds of the homes had one kind or another. One-third of the homes had mold and mildew. That type of moisture damage in these MCS houses is not only a nuisance, it also causes additional main-

tenance and repair costs, such as for cleaning or repainting. That suggests that the ventilation systems were not doing an adequate job of removing excess moisture, and so relative humidities were too high. Reducing the incidence of mold and mildew will require lowering indoor relative humidities by improving moisture control.

The surprisingly large number of moisture and water leak problems reported in these new homes is disturbing. All these results suggest that moisture problems may be prevalent inside many MCS homes. Not enough attention had been paid to controlling excess moisture in the tight MCS homes, and there is a definite need to improve the moisture removal aspects of their ventilation systems. To not do so will result in continuing indoor moisture-related problems and possibly even long-term structural damage within walls.

A number of other checks also were made during the inspection of each hole and the nearby wall area while the wall was opened. There were hardly any observations of frost/ice or liquid condensation or wood decay in any of the wall cavities. In two cases condensation was observed in a few square inches area trapped on the warm side of a poly air/vapor barrier, but it was never observed in the insulation itself. Mold and mildew and water staining were observed in slightly more than 10% of the wall cavities, which is an indication that the wall cavities were moist in many cases. Yet, at the time of the wall openings, there were no indications of structural damage, although that certainly could occur if the wood members did not dry out sufficiently in warm weather.

Ventilation Systems

During the inspections of the test homes, all ventilation systems were observed, including air-to-air heat exchangers (AAHX), bathroom and kitchen exhaust fans, and any mechanical ventilation systems in other areas, as well as their controls. Dehumidifiers were also inspected. Simple checks of all systems were made to see if they were working. Moreover, indoor relative humidities were measured in each living room as well as other rooms. In addition, the use patterns of each system were determined during the occupant interview. Finally, the occupants were asked about previous ventilation and dehumidification problems.

The ventilation system observations were undertaken to provide information that might help explain the incidence of moisture-related problems within the test homes as well as the existence of high moisture contents or moisture damage within the opened wall cavities, if any. This aspect of the moisture study was not meant to be a thorough ventilation study. While it was observed during the course of the inspections that the ventilation systems often were not working properly, insufficient test data were collected to clearly determine the impact on moisture-related problems. Considerable additional work is needed to do that. Based on these findings, a thorough system study would appear to be in order and a major program need.

The relative humidity of the indoor air was measured in the living room of each test house as well as other rooms. The living room results were presented previously in Table 2. The average of 53% for the coastal homes seems high. Moreover, there were many individual homes whose indoor relative humidities were clearly too high, with values reaching as high as 85% in a cold bedroom. These high readings, along with the findings of interior moisture-related problems, directly indicated the lack of satisfactory moisture control in many of the test homes.

While 85% of the test homes had an AAHX, 11% of them were not used regularly. Moreover, another entirely different 11% of them did not work at all. While most systems did work, numerous design, installation, and operational problems resulted in them not being very effective from a moisture control point of view. Furthermore, the fact that they did not work or were not used was found from the statistical analysis of the results to lead to higher wall cavity moisture levels. In order to get the systems already installed in MCS homes working effectively, they need a thorough "house doctoring." However, a suitable test methodology and proper tools need to be developed for this purpose. If AAHX systems are to be installed in future MCS type homes, considerable thought and study must be given to their proper design, installation, and testing/

inspection. With that, the vast majority of the AAHX problems that are now so prevalent could be avoided.

It should be pointed out that air-to-air heat exchangers were installed in these MCS homes to provide ventilation that would mitigate any indoor air quality problems. They were not specifically designed for moisture control. Unfortunately, it is not clear if even the best, properly-used AAHX can satisfactorily remove moisture and control indoor relative humidities in the mild coastal and metro climates. That is because the outdoor air that "drys" the indoor air as a result of ventilation and air leakage is relatively moist during mild weather and less effective. It may be that even exhaust only ventilating systems (with or without passive intakes) will be inadequate for moisture removal and control. That certainly needs to be studied in detail, given the magnitude of the moisture problems found in this study. It may be that dehumidification should be considered as a major part of a moisture control strategy for coastal and metro homes.

There were numerous types of kitchen ventilation systems; 8% of them did not work. A number of the kitchen fans were of the non-exhausting, recirculating variety that provide no ventilation control of kitchen moisture. Some of the types that utilized the AAHX system often were not on when needed. Moreover, 40% of the occupants said they did not use the system when cooking, largely because they did not see the need. Many thought the major purpose was to get rid of cooking odors, and when there were no odors there was no need to use the system. There were numerous other problems that kept occupants from using the kitchen ventilation system. It would seem prudent to require that kitchen ventilation systems include dehumidistat control. In that way moisture would be exhausted automatically when necessary, and the occupants would not need to be relied upon to turn the system on at the appropriate times. The installation of range hood recirculating fans that do not exhaust to the outdoors should be prohibited.

About 8% of the homes did not have a bathroom exhaust fan. They were supposed to rely on opening the bathroom window for moisture control. That practice is inexcusable and should be prohibited. Of the homes that had a bathroom exhaust fan, 62% were connected to the AAHX. However, 20% of the bathroom exhausts connected to an AAHX did not work, and 9% of those systems with just an exhaust fan did not work. Yet these were brand new homes. It is believed that inadequate control and insufficient fan capacity coupled with long duct runs are the causes. While flow rates were not measured, they should be. It may be that the flow rates are too low because the houses are so airtight.

Moreover, 25% of the systems were not used often for showering or bathing. Control with a properly calibrated dehumidistat would automate the removal of moisture when humidity levels were too high. In that way, occupants would not need to remember to turn on the exhaust fan or even know that it was important to do so in order to remove moisture generated in the bathroom. Incidentally, such an approach should be especially effective in controlling moisture levels in homes because it would be removing moisture directly at its source.

A dehumidifier was used regularly in the wintertime to remove moisture in 16% of the homes. Use of a properly-selected dehumidifier could be one of the most effective methods of removing moisture for homes in the mild coastal and metro climates. Indoor relative humidities are highest when outdoor temperatures are mild because the outdoor air is relatively moist and ineffective at drying out the indoor air. Under those conditions, any mechanical ventilation system will be relatively ineffective for moisture control and dehumidification may be necessary.

An unanswered question is: What is the proper mix of dehumidification and ventilation, if any? Until recently, little has been known about the operation and wintertime performance of residential dehumidifiers. Recent research just being completed has provided some answers that show promise for effective moisture control using dehumidification [9]. However, additional research is still necessary.

Unfortunately, it is not certain whether the dehumidifiers used in this study were removing the moisture from indoor air effectively. In order to do that when indoor air is at typical indoor wintertime temperatures, it is necessary to use a dehumidifier that is oversized relative to those that are used primarily in the summer, and the unit should have a defrost control. Without the

defrost control the coil will frost or freeze up, and the water removal rate will drop or cease. Many commonly purchased dehumidifiers do not have a defrost control. Unfortunately, no check was made of the units for defrost control or high capacity. Surprisingly, 8% of the homes regularly used a humidifier, which in a few cases simply was a vaporizer.

The existence and use of fireplaces and wood stoves (or fireplace inserts) resulted in some unknown degree of ventilation and subsequent drying of the indoor air. Wood stoves or fireplace inserts were found in 42% of the test homes; 77% of those were used regularly. Numerous occupants commented about the "dry" heat from a wood stove.

Based upon first-hand conversations with the occupants, many do not really understand their house's ventilation systems, particularly with regard to how and why they should be operated. Seldom is there even an instruction manual, although there should be since these MCS homes really are different from conventional housing. In many cases, the occupants do not understand where moisture comes from, nor do they perceive the need to use exhaust fans or an AAHX to remove moisture in their airtight homes. Simply stated, there is a *huge* need to educate the occupants on how and why to operate their moisture control systems. It even may be necessary to install indoor relative humidity gages in each home so the occupants will be able to know whether their home is too moist.

Given the large percentage of the test homes that had ventilation system components that did not work at all or work properly, it is also evident that building code inspectors missed those basic ventilation system problems. They need to be trained to inspect ventilation systems and to understand their importance in tightly constructed homes that require proper moisture control.

Overall Moisture Study Conclusions

The major purpose of this moisture field study was to find out whether building the exterior walls of new homes to energy-efficient standards with more insulation (at least R-19) and an air/vapor barrier causes unacceptably high levels of moisture or related problems within walls. Previous studies of much older conventionally-constructed homes with blown-in insulation found a lack of such problems. As a result of measuring the moisture content of wood members within the opened wall cavities of 86 MCS newly-constructed electrically-heated homes in three distinctly different regions of the Northwest, unacceptably high moisture levels were found to exist in the walls of a surprisingly large percentage of those homes. However, it must be stressed that those measurements were made in the wintertime. Since wood decay only occurs during warmer weather, the question of whether the high moisture contents will lead to wood decay and subsequent structural damage is unresolved. There was essentially no decay within any of the wall cavities at the time of the wall openings. There is some evidence from one Montana test house that some wood members within the wall cavities may dry out sufficiently in warmer weather. Other wood members probably will not dry out, but that remains to be determined.

What also is unclear is whether similar results would occur in the walls of newly-constructed current practice homes in the region. There is reason to believe that those homes could be worse because they have similar insulation levels and are nearly as airtight, but they lack an AAHX or dehumidifier. Moreover, there is a good possibility that wall moisture levels will be as high, if not higher, in the many multi-family MCS homes already built in the region. That is because they are smaller, have less exposed exterior wall area, and generally have less expensive/effective ventilation systems. Thus the finding of moisture-related problems in this study of single family MCS homes may only be the tip of the iceberg.

An additional purpose of this study was to determine if any other types of moisture-related problems have occurred in the heavily-insulated, relatively airtight new homes. Based upon careful inspections of the test homes and their ventilation systems, as well as interviews with the occupants, numerous moisture-related problems and damage have been noted inside the MCS test homes. In fact, the widespread existence of so many different kinds of moisture problems

was much higher than expected. They appear to be directly related to the fact that their ventilation systems were not working properly or were not being used. That is especially disappointing since these homes were intended to include the best available ventilation systems that would result in well-controlled indoor conditions. Unfortunately, far too little attention was given to making the ventilation systems work properly and to educating the occupants in their proper use for moisture control.

Very likely the existence of high wall cavity moisture contents also is tied to the poor ventilation system performance. In order to partially remedy the overall moisture problem situation, the ventilation systems need to be "house doctored" to get them working properly. Educating the occupants will be an equally important component of the overall solution.

For future as well as existing energy-efficient airtight homes, moisture control must have a much higher priority in their design, construction, inspection and ongoing operation. That is a goal which appears achievable. It seems clear that this study is but the first in a series of studies and tests that are necessary to clarify and solve this potential moisture problem in MCS and perhaps all new energy-efficient residential housing in the Northwest.

Recommendations for Future Study

A number of important questions have been raised as a result of this Northwest Wall Moisture Study and the associated Helena Thermography Study [5]:

1. Given that the walls of many new energy-efficient homes in the Northwest have high moisture contents in the winter, will they dry out every summer such that wood decay will not occur, or will they remain moist enough (greater than 20%) during warm weather (greater than 10°C [50°F] continuously) to lead to wood decay?
2. For those homes with high moisture content levels in sheathing, will further house tightening and sealing of interior air leaks result in reduced moisture contents? If so, what level of air tightness is required to keep wall cavity wood members sufficiently dry (below 20% moisture content)? Are there measures other than interior wall air tightening that will reduce wall moisture levels, such as using a dehumidifier, or operating the mechanical ventilation systems properly or even continuously with the house slightly depressurized, or adding exterior insulating sheathing? What is the role of the tightness of the exterior portion of the wall cavity in maintaining sufficiently low moisture levels? Will it be necessary to make the exterior portion of wall cavities less airtight so the walls can dry out? If necessary, how can that be done? Should the use of panelized wood siding and wood sheathing be avoided?
3. Are there major factors other than air leakage that lead to high wall cavity wood member moisture contents, especially in the coastal and metro regions? For example, does wicking of moisture from the ground up through either basement or crawl space concrete foundation walls contribute to high wall cavity wood member moisture levels? If so, what can be done to prevent it? Are high wall cavity moisture contents due in part or entirely to high moisture levels in construction materials? In newly constructed tight houses, will the presumed drying of construction materials such as wet lumber and concrete take long enough that wood decay will have a chance to occur? How long does complete drying actually take? Does complete drying occur, or is there retention of enough moisture during the dryout period that drying is incomplete and moisture levels stay the same or get worse each year?
4. Can the finding of a correlation between air leakage and high sheathing moisture content be extrapolated to apply to other test homes?
5. Was the substantial and rapid drying noted over a two-month period in the Helena, Montana, test house typical or unusual and due to the abnormally warm weather?
6. Are individual rooms pressurized by the operation of an AAHX to such a degree that moisture is forced into and through walls, leading to high wall cavity wood member moisture levels?

7. Are the ventilation systems in the MCS houses really working effectively? If not, can they be fixed? Do they need to be run longer or even continuously? Can occupants be educated to use them more effectively? Is the use of air-to-air heat exchangers suitable as a moisture removal strategy in mild climates? Can simple and inexpensive dehumidistat controls installed on bathroom and kitchen exhaust fans effectively remove moisture generated at the source and result in proper and automatic control of indoor moisture levels? Can suitable dehumidifiers be effectively used to augment the necessary removal of moisture in new tight MCS homes where AAHX's are not used or where they may not work effectively for moisture control because of the mild outdoor conditions?

8. Are the high wall cavity moisture levels and moisture-related problems inside the MCS homes unique only to MCS homes, or are they common to newly-constructed current practice homes built in the Northwest? Are the current practice homes even worse? Are the multi-family homes in Tacoma experiencing the same or worse wall cavity and indoor moisture problems as the single family MCS homes tested in this study?

These questions need to be answered in order to conclusively determine if building homes with heavily-insulated walls, a continuous air/vapor barrier, and the need for mechanical ventilation with or without heat recovery leads to wall moisture damage. Even if it is found that present energy-efficient home construction practices cause wall or indoor moisture problems, remedial actions may be possible. Clearly, additional information is needed. Further study and testing are recommended in a number of areas.

Proposed Further Testing/Studies

1. Reopen the wettest walls in homes in all three regions in the summer to see if they have dried out sufficiently to avoid wood decay.
2. Continuously monitor over a full year or longer the variation in moisture content of selected wood members in a few homes that were found to have high moisture contents, as well as one brand new home in the coastal region where summer drying is least effective.
3. Given that air leakage was found to lead to high sheathing moisture contents in the Helena test home, determine the effect of leak sealing.
4. Repeat a thermography/blower door and moisture probing study on a coastal home with wet mud plates to examine wicking of ground moisture up through concrete foundation walls.
5. Initiate an AAHX and exhaust fan "house doctor" program to get all working properly. Develop consumer education information.
6. Repeat a similar moisture study on non-MCS current practice homes and MCS multi-family homes to see if they have similar or worse problems.
7. Test the effectiveness of dehumidistat controls on bathroom and kitchen exhaust fans at maintaining proper indoor moisture levels.
8. Test the effectiveness of dehumidification for moisture control in mild climates.
9. Test different exterior wall constructions in test huts under controlled conditions to determine the role of tightness of the exterior portion of walls.

Acknowledgments

Special thanks must go to the Bonneville Power Administration for recognizing the need for this study and for providing the necessary funding. Thanks also are gratefully extended to the owners and occupants of the test homes; their interest, support, and patience made this study possible.

References

- [1] Tsongas, G. A., "A Field Study of Moisture Damage in Walls Insulated Without a Vapor Barrier," in *Proceedings*, 1979 ASHRAE/DOE-ORNL Conference on the Thermal Performance of the Exterior Envelopes of Buildings, ASHRAE SP 28, 1980, pp. 801-815.
- [2] Tsongas, G. A., "The Spokane Wall Insulation Project: A Field Study of Moisture Damage in Walls Insulated Without a Vapor Barrier," in *Proceedings*, ASHRAE/DOE/BTECC Conference on Thermal Performance of the Exterior Envelopes of Buildings III, ASHRAE SP 49, 1986, pgs. 556-569; also Bonneville Power Administration, DOE/BP-541, Sept. 1985.
- [3] Tsongas, G. A., "The Northwest Wall Moisture Study: A Field Study of Moisture in the Exterior Walls of New Northwest Energy-Efficient Homes," Final Report for Bonneville Power Administration, Portland, Ore., Nov. 1987.
- [4] *Wood Handbook: Wood as an Engineering Material*, U.S.D.A. Forest Products Laboratory, Agriculture Handbook No. 72, 1974.
- [5] Tsongas, G. A., "Final Report on a Field Test for Correlation of Wall Air Leakage and Wall High Moisture Content Sites," Bonneville Power Administration, Portland, Ore., July 1987.
- [6] Tsongas, G. A., "The Effect of Building Air Leakage and Ventilation on Indoor Relative Humidity," in *Proceedings*, Building Thermal Envelope Coordinating Council (BTECC) Symposium on Air Infiltration, Ventilation and Moisture Transfer, Dec. 1987.
- [7] Burch, D. M., et al., "The Use of Low Permeability Insulation as an Exterior Retrofit System—A Condensation Study," *ASHRAE Transactions*, Vol. 85, Part 2, 1979, pp. 547-562.
- [8] Sherwood, G. E., "Condensation Potential in High Thermal Performance Walls—Cold Winter Climate," U.S. Dept. of Agriculture, Forest Products Laboratory Research Paper FPL 433, 1983.
- [9] Tsongas, G. A. and Wridge, R., "Field Monitoring of the Wintertime Performance of a Residential Dehumidifier," Final Report to Bonneville Power Administration, Portland, Ore., Dec. 1987; also in *ASHRAE Transactions*, Vol. 95, Part 1, 1989.

G. E. Courville,¹ P. W. Childs,¹ A. R. Moazed,² G. D. Derderian,²
G. D. Stewart,² and L. S. Shu²

A Comparison of Two Techniques for Monitoring the Field Thermal Performance of Roof Systems

REFERENCE: Courville, G. E., Childs, P. W., Moazed, A. R., Derderian, G. D., Stewart, G. D., and Shu, L. S., "A Comparison of Two Techniques for Monitoring the Field Thermal Performance of Roof Systems," *Insulation Materials, Testing, and Applications, ASTM STP 1030*, D. L. McElroy and J. F. Kimpflen, Eds., American Society for Testing and Materials, Philadelphia, 1990, pp. 483-495.

ABSTRACT: Two independent techniques, one intrusive and one non-intrusive, for monitoring the thermal performance of *in situ* roof systems are compared. The intrusive technique requires thermocouples on inside and outside surfaces of the roof system and a heat flux transducer (HFT) embedded in the system. The non-intrusive procedure has the same thermocouple placement and a series of HFTs on the inside surface of the deck. The crucial difference in the methods is in the HFT placement and the technique for HFT calibration. Results of a one-year field study using both methods on the same roof assembly are described. The roof assembly is a built-up roof with molded expanded polystyrene (EPS) insulation above a metal deck.

KEY WORDS: expanded polystyrene insulation, PROPOR, heat flux transducers, roof thermal research apparatus, thermal conductivity, thermal resistance, roof thermal performance, thermal drift

Field measurements of the thermal performance of building envelope components are important complements to laboratory testing. While there are several citations in the literature on techniques for field measurement of thermal performance [1-4], there are little data on the reliability of these techniques. This paper presents a comparison between two field techniques. One, developed by J. V. Beck of Michigan State University for Oak Ridge National Laboratory (ORNL), emphasizes the use of fairly sophisticated procedures and requires that sensors be placed within the component being tested (defined as "Exp. 1") [5]. The second, developed by W. R. Grace, features a procedure that requires only surface mounted sensors (defined as "Exp. 2") [6].

Apparatus

All field comparisons were conducted on a test specimen installed in the Roof Thermal Research Apparatus (RTRA) at Oak Ridge National Laboratory in Oak Ridge, TN. The RTRA (Fig. 1) is described more fully elsewhere [4, 7]. It is a 3 by 8.5 m conditioned building that can accommodate four 1.2 by 2.4 m test specimens as sections of its roof.

A cross section of the specimen used in this test is shown in Figs. 2a and 2b. The deck is 1.2-mm-thick galvanized steel. Next are four expanded polystyrene (EPS) boards having nominal

¹Oak Ridge National Laboratory, Oak Ridge, TN 37831-6097.

²W. R. Grace and Company, Cambridge, MA 02140.



FIG. 1—*Roof Thermal Research Apparatus. Roof specimens are instrumented for careful measurements and tested under field conditions.*

thicknesses of 3.2, 2.5, 2.5, and 3.2 cm, respectively. The top board is 1.1-cm-thick mineral fiberboard. In a separate laboratory test the installed total thickness of all four EPS boards was 11.8 cm. This is the value used in subsequent calculations.

The membrane is a three-ply asphalt built-up roof (BUR), and the top surface is an asphalt flood coat. The instrumentation for Exp. 1, as shown in Fig. 2a, is located near the center of the specimen. This consists of gage copper-constantan thermocouples between each layer of the specimen and a calibrated heat flux transducer between the middle two EPS layers. The heat flux transducer is a square thermopile disk, 5 cm on a side, and 0.32 cm thick. It is a standard item provided by Hy-Cal Engineering [8]. In Exp. 2 a total of 15 thermocouples are located on the inner and outer surfaces of the specimen and an array of 8 heat flux transducers which have been calibrated in place [2] on the inside surface of the deck. This configuration is shown in Fig. 2b.

The specimen was placed on the RTRA in November 1984 and has been in position continuously since that time. Data for this project were collected primarily during 1985 and 1986.

General Observations

Typical real-time summer and winter thermal data of this specimen are illustrated in Figs. 3 and 4. These are temperatures from thermocouples placed in the ambient air above the roof surface, under the flood coat, and 50.8 mm (2 in.) below the roof deck in the room. Figure 3 is for a week in August, and Fig. 4 for a week in January. Note that the interior temperature was

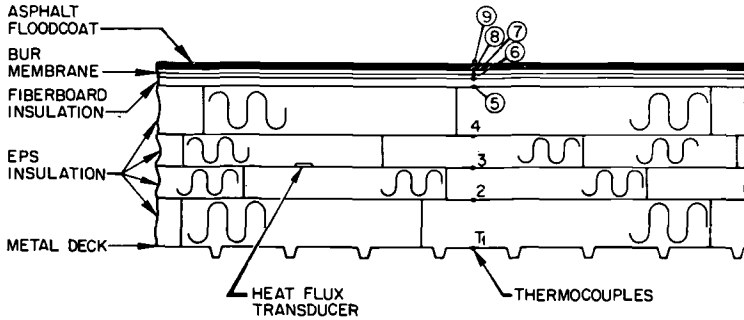


FIG. 2a—Schematic drawing of the EPS test specimen showing the location of sensors for Experiment 1.

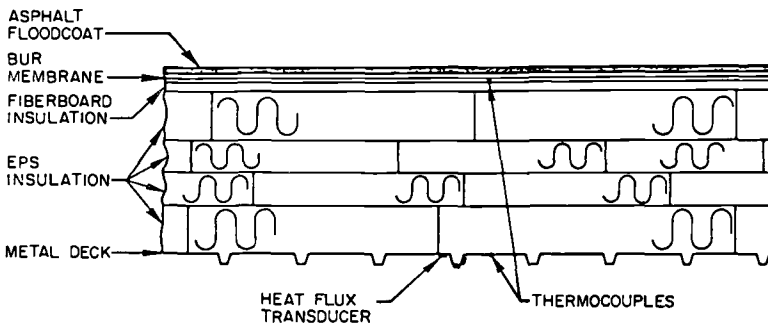


FIG. 2b—Schematic drawing of the EPS test specimen showing the location of sensors for Experiment 2.

held at different values for these two weeks, a feature that is possible in a controlled environment. While readings are specific to the roof conditions and weather at the moment, the general features of the data are typical. The strong influence of solar heating on a roof can be readily seen. Summer surface temperatures up to 80°C are common for black surfaces over well insulated roofs, and temperature differences over the surface boundary layer can reach 40 to 50°C on particularly hot and clear days. Even during the winter, daytime surface temperatures can be significantly above the ambient air temperature.

One fact that is relatively clear from these simple observations is that because of the big differences between air and surface temperatures due to solar radiation, ambient air temperature (either instantaneous or average) is not a reliable parameter to use alone for an estimate of roof heat transfer. Generally, it results in an underestimate of summer cooling requirements and an overestimate of winter heating requirements for the roof, which can be significant.

The strong temperature gradients in the boundary layer above the roof also suggest that this is a thermally unstable region, which can be significantly affected by small breezes and even seemingly negligible changes in sky cover. This helps explain why there is little symmetry between the daily surface temperature peaks. Figure 5, which gives plots of the temperature difference between ambient air and the roof surface explicitly for two one-week periods, shows even more clearly the strong variations in the boundary layer temperature gradient. It is also easier here to see the effects of nighttime radiative cooling of roof surfaces below the ambient air. Since this cooling is dependent upon sky cover, the maximum amounts are usually less in the summer than in the winter for this region because the summer air is more humid. Short-

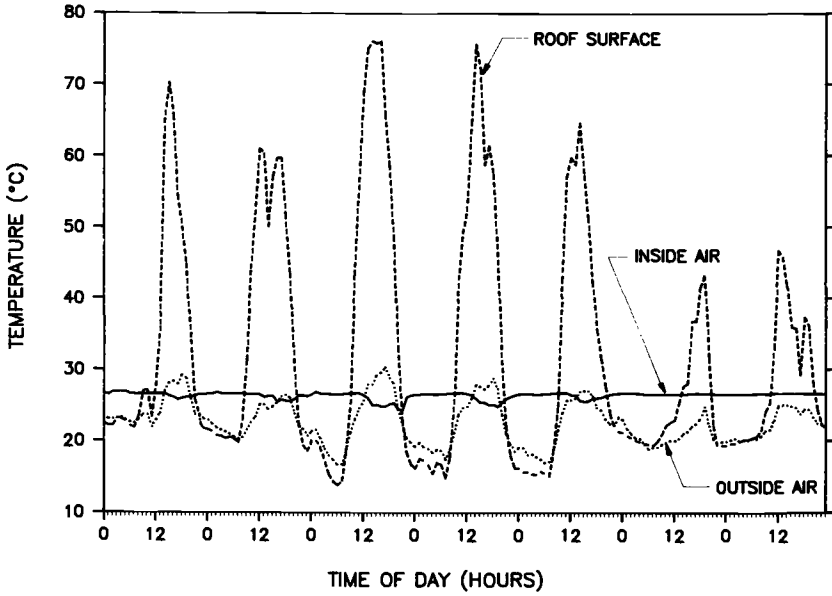


FIG. 3—Temperature variations on the EPS system for a week in August. Note that the surface temperature during the day is considerably greater than the ambient air temperature and that radiant cooling during the evening causes the surface temperature to be lower than the air temperature.

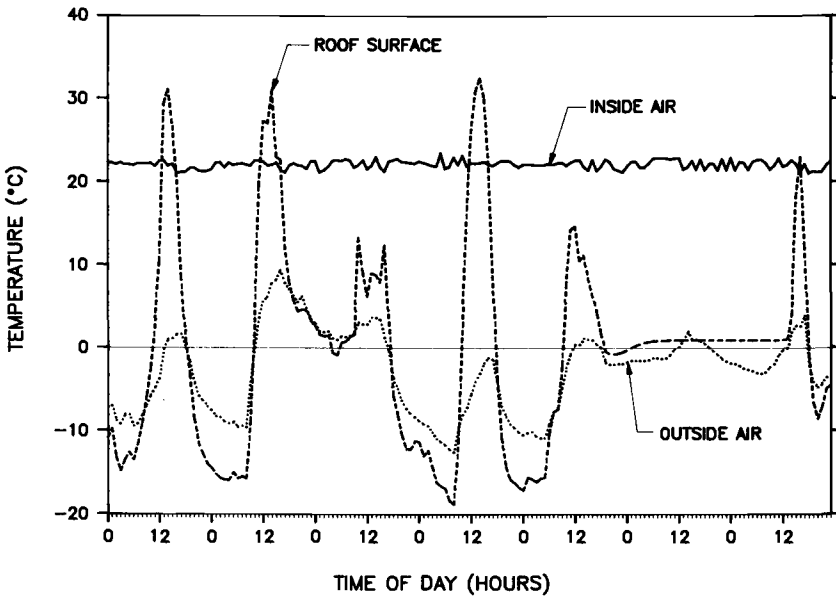


FIG. 4—Temperature variations on the EPS system for a week in January. The weather is much more variable than that in Fig. 3, but the same general comments are appropriate. Note that nighttime surface cooling is greater during the winter. This is because the outdoor humidity is less in winter, which increases the radiative losses to the night sky.

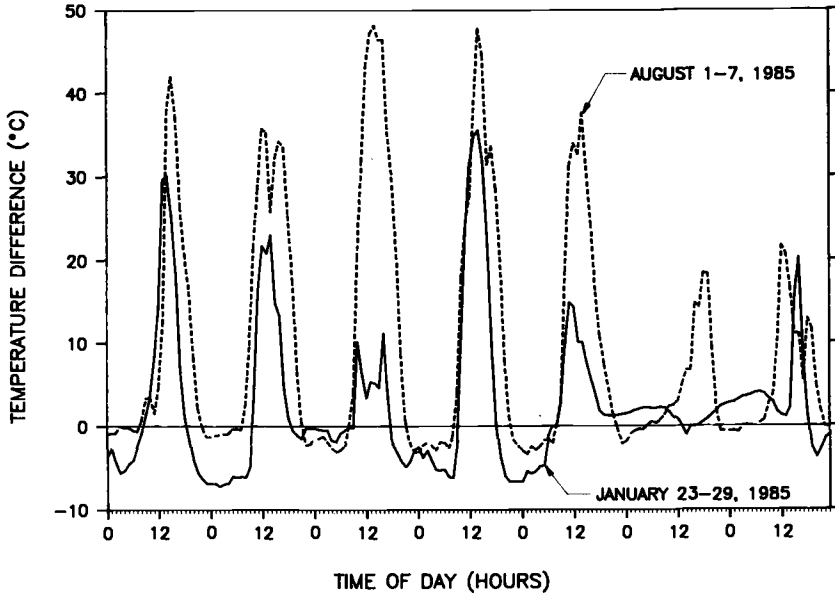


FIG. 5—Plot of the difference between the roof surface temperature and the ambient air temperature. The large daytime values illustrate the importance of daytime solar radiative heating, particularly during the summer.

term fluctuations in roof surface temperature have been verified by daytime infrared inspection. Here, small complex changes in surface temperature patterns in times of the order of minutes are often observed.

Experiment 1

Prior to installation on the RTRA, the EPS insulation was pre-tested in a steady-state laboratory apparatus. This apparatus has been shown to agree within 1% with Standard Reference Materials obtained from the National Bureau of Standards [9]. Two tests were carried out: one to determine the steady-state thermal conductivity of the 11.8 cm EPS stack and the second to give an *in situ* calibration of the heat flux transducer [10]. Following the pre-tests the sample was mounted in a test panel and installed on the RTRA.

Data were collected for five minutes before the hour, on the hour, and for five minutes after the hour. These readings were averaged and stored as the hourly values. Analysis was carried out on one-week (168 hours) blocks of experimental data. When variations over longer periods are needed, these one-week blocks can be combined or a series of one-week averages can be generated.

The principle results for the thermal performance of the EPS specimen have been obtained using the sensors shown in Fig. 2 and the computer program PROPOR. PROPOR is a FORTRAN program developed at Michigan State University [11] for estimating the thermal conductivity, λ , and the density specific heat product, $\rho \cdot c$, from transient heat flux and temperature measurements. PROPOR is a least-squares technique applied to measured and calculated temperatures and heat flows. In this experiment, the sums of squares to be minimized are

$$S(1) = \sum_{i=1}^{i=N} \sum_{j=1}^{j=J} (Y_{ji} - T_{ji})^2 \quad (1)$$

and

$$S(2) = \sum_{i=1}^N (X_i - q_i)^2 \quad (2)$$

where Y_{ji} and X_i are measured temperatures and heat flow at time t_i and location x_j , and T_{ji} and q_i are calculated temperatures and heat flow at the same time and location, N is the number of data points in a set ($N = 168$ for this study), and J is the number of thermocouple sites ($J = 3$ for this study because 3 thermocouples are located within the EPS sample). The T_{ji} and q_i values are calculated using Crank-Nicolson finite difference equations derived from the heat conduction equation

$$\frac{\partial}{\partial x} \left(\lambda \frac{\partial T}{\partial x} \right) = \rho \cdot c \frac{\partial T}{\partial t} \quad (3)$$

where λ is the thermal conductivity and $\rho \cdot c$ is the density-specific heat product.

For the geometry shown in Fig. 2a, the x -domain starts at the lower side of the EPS insulation and ends at the upper side of the EPS. The boundary conditions used in the calculation of T_{ji} and q_i are the temperatures at the lower and upper surfaces of the EPS (T_1 and T_5). The results of the finite difference analysis are the internal temperatures (T_2 , T_3 , and T_4 in Fig. 2a) and the heat flux. These are subsequently the inputs T_{ji} and q_i to the least-squares analysis.

As currently formulated, PROPOR is designed to accommodate two unknown parameters [12]. That is, Eqs 1 and 2, when differentiated and set equal to zero, have two adjustable parameters. This will always be some combination of $\lambda(T)$ and $\rho \cdot (T) \cdot c(T)$ evaluated at specified temperatures. Since one does not expect $\rho \cdot c$ to play a significant role in the thermal analysis of lightweight (low thermal storage) systems, it has been found most useful to use PROPOR first to determine the best values of constant λ and constant $\rho \cdot c$ for the full range of temperatures during the analysis period. Then, this value of $\rho \cdot c$ is re-entered into PROPOR as a constant and the program is used to estimate a temperature-dependent λ according to the model

$$\lambda = \lambda_a + \frac{k_b - k_a}{T_b - T_a} (T - T_a) \quad (4)$$

where λ_a and λ_b are the best-fit thermal conductivities at T_a and T_b respectively. If, for example, T_a and T_b are chosen to be just smaller and just larger than the smallest and largest temperatures in the analysis period, PROPOR gives the best-fit linear relation between λ and T over the temperature range covered by the analysis period.

Alternatively, the temperature range can be divided into several segments and T_a and T_b for each segment can be determined by an iterative procedure. The main criterion for selecting line segments is that a weekly data set has enough temperature data within each segment so that the analysis is statistically significant. In the present case three-line segments are considered; -18 to 18°C , 18 to 38°C , and 38 to 93°C . When there is adequate temperature data in all segments, the procedure is to estimate $\lambda(T)$ at $T = 38^\circ\text{C}$ and 93°C and use PROPOR to find $\lambda(T)$ at $T = -18^\circ\text{C}$ and 18°C . Then, $\lambda(T)$ for $T = -18^\circ\text{C}$ and 18°C is held at these values and $\lambda(T)$ at $T = 38^\circ\text{C}$ and 93°C is determined by PROPOR. This process is repeated until the calculated values converge on the estimated values.

This detailed procedure has been applied to seven one-week data sets selected at different times of the year in order to provide different temperature distributions. The PROPOR calculations are shown in Tables 1 and 2. In Table 1, T_{wm} is the weighted mean temperature for the insulation stack:

$$T_{wm} = \frac{\sum_{i=1}^N (T_{lj} - T_{sj}) \left(\frac{T_{lj} + T_{sj}}{2} \right)}{\sum_{i=1}^N (T_{lj} - T_{sj})} \quad (5)$$

which has been previously discussed [4] and $T(\text{range})$ is the range of temperatures recorded by all the thermocouples during the test period. $R(\text{constant})$ is the value of the thermal resistance of EPS for each weekly data set using PROPOR and the assumption that a constant value of thermal conductivity is adequate for the entire data set. Similarly, $R(\text{mean})$ is the value of the thermal resistance of EPS calculated at the weighted mean temperature for each weekly data set using PROPOR and the assumption that a single linear $\lambda(T)$ versus T curve is adequate for the entire data set. (See the discussion below Eq 4.)

The four columns for $\lambda(T)$ in Table 2 are thermal conductivities derived from the independent weekly data sets according to the procedure described earlier. $\lambda(\text{seg})$ is the average value of the thermal conductivity at each of the specified temperatures. Also shown is the standard deviation expressed as a percent of the average for each column of values. Finally, $R(\text{seg}) = l/\lambda(\text{seg})$

TABLE 1—Results of PROPOR calculations for $R(\text{constant})$ and $R(\text{mean})$.
(Quantities are defined in the text.)

Week of Test Set	Weighted Mean Temperature (T_{wm}), °C	$T(\text{range})$, °C	$R(\text{constant})$, m ² K/W	$R(\text{mean})$, m ² K/W
11-21-84	10.9	-1 to 39	3.29	3.33
12-01-84	9.8	-5 to 30	3.32	3.33
01-01-85	11.5	-1 to 30	3.29	3.35
04-10-85	25.4	0 to 51	2.99	3.14
05-14-85	34.8	3 to 72	2.82	2.96
08-01-85	36.4	19 to 61	2.82	2.96
08-09-85	42.8	21 to 76	2.76	2.84

TABLE 2—Results of PROPOR calculation for $R(\text{seg})$.
(Quantities are defined in the text.)

	Thermal Conductivity, W/mK			
	-18°C	18°C	38°C	93°C
	0.0359	0.0338	0.0403	...
	0.0348	0.0342	0.0425	...
	0.0362	0.0315	0.0386	...
	0.0361	0.0355	0.0387	0.0567
	...	0.0370	0.0389	0.0579
	...	0.0360	0.0388	0.0568
	...	0.0351	0.0387	0.0530
Average thermal conductivity $\lambda(\text{seg})$	0.0358	0.0351	0.0393	0.0561
Std. deviation (% of Average)	1.8%	3.3%	2.0%	3.4%
Thermal Resistance $R(\text{seg})$	3.19	3.25	2.91	2.04

is the thermal resistance of the EPS using the segmented λ versus T procedure, and $\ell = 0.118$ m is the measured full stack thickness of the insulation.

$R(\text{seg})$ should be viewed as the best data for the thermal resistance of EPS from Exp. 1 since $R(\text{constant})$ and $R(\text{mean})$ are both calculated with simpler assumptions for $\lambda(T)$. For a material with thermal conductivity actually constant, all three values should be identical; and for a material with a linear thermal conductivity over the range of temperatures in the test, $\lambda(\text{mean})$ and $\lambda(\text{seg})$ should be equal. Materials which satisfy these conditions have not been tested yet.

Results for $R(\text{seg})$, $R(\text{mean})$, and $R(\text{constant})$ are also plotted in Fig. 6. While the agreement between $R(\text{seg})$ and $R(\text{mean})$ is quite good, particularly at temperatures above about 16°C , there is a nearly constant difference of about 5% between $R(\text{constant})$ and $R(\text{seg})$ over this same range. The most unusual feature of the data is the strong change in slope of $R(\text{seg})$ below a temperature of about 15°C . (This curve shape has been verified by inserting additional line segments between -18 and 18°C .) We have not, as yet, found an adequate explanation for the change in slope for low temperature observed in our results. Additional tests are under way to determine if this feature is a material property or due to instrument error.

Experiment 2

This method of *in situ* measurement of thermal performance of roof decks by a non-intrusive method has been reported elsewhere [2]. It consists of *in situ* calibration, measurement, and analysis of data.

For the calibration, a 1.2 by 1.2 m calibrator unit with an inner metering area of 1 ft^2 was constructed. This unit, which replicates the underside of the roof deck, was attached just below the deck in the RTRA. This calibrator consisted of a heater, cooler, heat flow meter, insulation, and steel decking. The eight heat flux transducers were attached to the underside of the calibrator. The generated flux and output of the heat flux transducers were used to generate a series of calibration curves for different room temperatures. Curves for both heat flow in and out of the building were developed using the calibrator.

Because RTRA is a small room with an oversized heating/cooling system, significant fluctua-

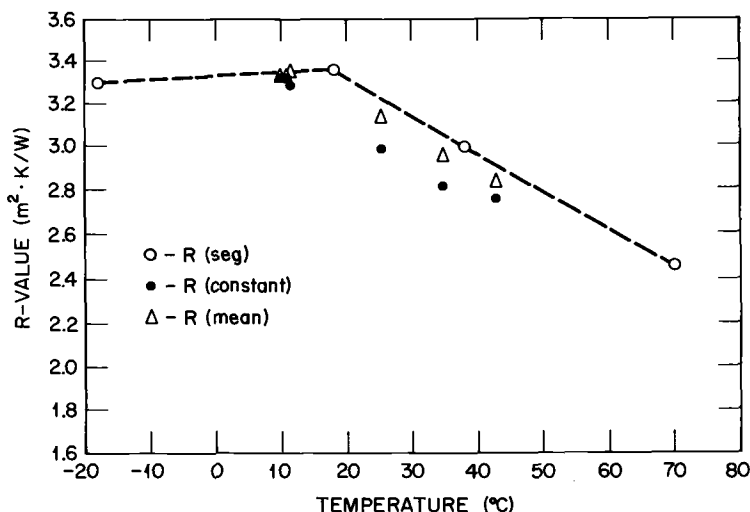


FIG. 6—R-value results from Experiment 1 using different assumptions for the variation of thermal conductivity with temperature. See text for discussion.

tions in room temperature were experienced. To interpret data accurately, the calibration was performed for the entire range of these temperatures.

Following this calibration, the heat flux transducers were removed from the calibrator and then mounted on the underside of the roof deck in the same configuration for which they were calibrated. Their outputs along with temperatures for the inside and outside surfaces of the roof system were scanned and recorded every 30 min. Typical data for Exp. 2 for a summer day are shown in Fig. 7.

The thermal performance of the system is characterized by the "dynamic R -value," which is defined as

$$\text{dynamic } R\text{-value} = \frac{n_+ R_+ + n_- R_-}{n} \quad (7)$$

where

$R_+ = \Sigma \Delta T_i / \Sigma q_i$ for all data within the sampling period for which both ΔT_i and q_i are positive,

$R_- = \Sigma \Delta T_i / \Sigma q_i$ for all data within the sampling period for which both ΔT_i and Σq_i are negative,

n_+ = number of hours in the sampling period for which both ΔT_i and q_i are positive,

n_- = number of hours in the sampling period for which both ΔT_i and q_i are negative, and

$n = n_+ + n_-$.

Weekly data files were combined using Eq 7 to arrive at seasonal dynamic- R -values for summer, fall, and winter seasons. These values are plotted in Fig. 8 as a function of roof weighted mean temperature, which is defined by Eq 5. Since the temperatures used in the calculation for Exp. 2 are those across the entire roof system, the dynamic R -value is also for the entire system.

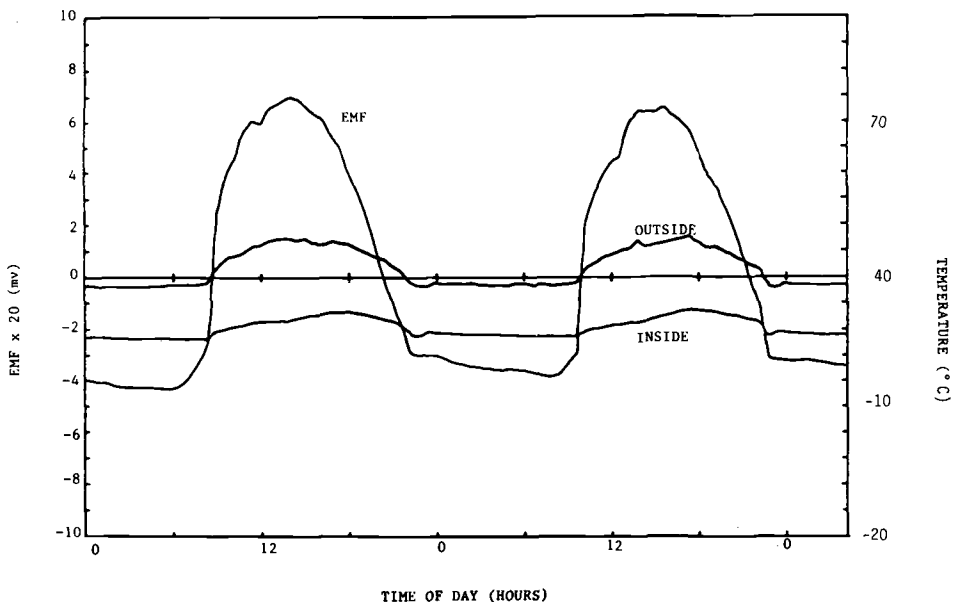


FIG. 7—Output data from Experiment 2 sensors for temperature and heat flux for a two-day period in July 1985.

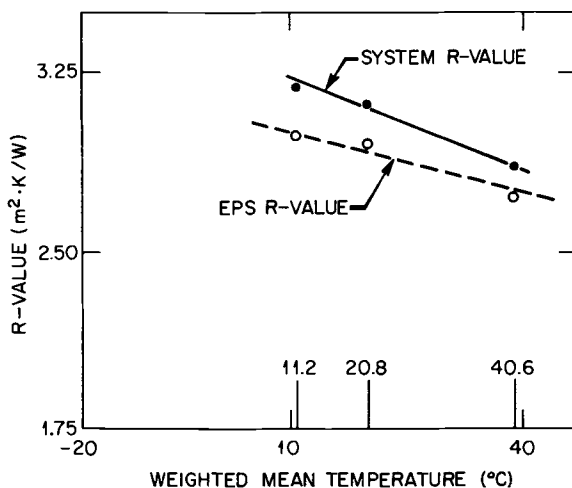


FIG. 8—*R-value results from Experiment 2. The upper curve is for the combined system of EPS and fiberboard. The lower curve is for the EPS alone.*

In order to make a comparison to field Exp. 1 and the laboratory results, which are for expanded polystyrene alone, it is necessary to subtract the R -value of the 1.1-cm-thick mineral fiberboard sheet, which is a function of temperature, from the Grace measurements. The Exp. 2 result for EPS, after this subtraction, is also shown in Fig. 8.

Differences in the Techniques

The paper discusses two different techniques for determining the thermal performance of insulated roof systems. Briefly, Exp. 1 is an intrusive technique in that sensors must either be installed during construction or the roof system must be opened to place them. Exp. 2 is non-intrusive. The heat flux transducer array is mounted on the underside of the deck and thermocouples are placed on inside and outside surfaces. The advantages of Exp. 1 are that the materials and construction of the roof will be well known and errors are more likely controllable. Exp. 2, on the other hand, is more portable, requiring mainly that the underside of the deck be available and that thermal conditions in the area of the underside of the deck not vary much.

The two methods also use different calibration procedures. In Exp. 1 the actual components destined for the roof, with sensors in place, are placed in a laboratory measuring device. Measured heat fluxes are used to calibrate the HFTs. In Exp. 2, a field calibration of heat flux transducers is carried out through the use of a replica of the roof deck with an insulation of known thermal resistance attached to its upper side. The calibration consists of correlating the transducer response with calculated heat flows for the calibrated insulation section.

Finally, the two techniques use different analysis procedures. PROPOR, for Exp. 1, is developed from a rigorous application of the one-dimensional transient heat conduction equation and involves the use of accepted elements of non-linear regression theory. The method for Exp. 2 is an empirical variation of the "Averaging Technique" [1,4], which allows one to extend its use to situations when the long-term system heat flow is near zero and when the system is experiencing significant heat flow reversals. Error analysis for the PROPOR method will be examined more rigorously in an upcoming report [13]. No detailed analysis of the Exp. 2 methodology is currently anticipated.

An important feature of both methods is that they, by design, are usable throughout the year. The only requirement on PROPOR, for example, is that there is significant variations in

monthly heat flows over the analysis period which is usually assured by diurnal solar fluxes. Figure 9 presents PROPOR results accumulated over a twelve month period. Here, weekly average R -values are plotted against the weighted mean temperatures for the week. During the winter the weighted mean temperature is low; during the spring and early summer it progressively increases to a maximum. Then as summer passes to fall and then to winter again the weighted mean temperature again decreases back to a minimum. Note that there is no unusual behavior in the results during any particular part of the year.

Discussion

The principle results of this work are shown in Fig. 10. Here we have plotted the results from the two field tests and have added laboratory steady-state data from three published sources [10,14,15]. The ORNL data [10] should be the most applicable of the steady-state results, because it was obtained for the same sample that was used in the field test.

At temperatures above about 10°C and within the range of measurement, the agreement between Exp. 1 and the ORNL steady-state laboratory data is within about 7%, although the slopes of the λ versus T lines are different. For Exp. 2, on the other hand, the difference is about 10% and the slopes are similar.

Except for the low temperature behavior noted in Exp. 1, the field data show approximately the same tendencies as the laboratory data. That is, R -values are high for low mean temperatures and lower for high mean temperatures. This would suggest that more attention should be given to performance variations in the R -value assigned to insulation in cold versus warm climates and in winter versus summer calculations.

The different slope at low temperatures for the curve from Exp. 1 is statistically significant. It is not known, however, if it is due to a material property, an instrument error, or a peculiarity of

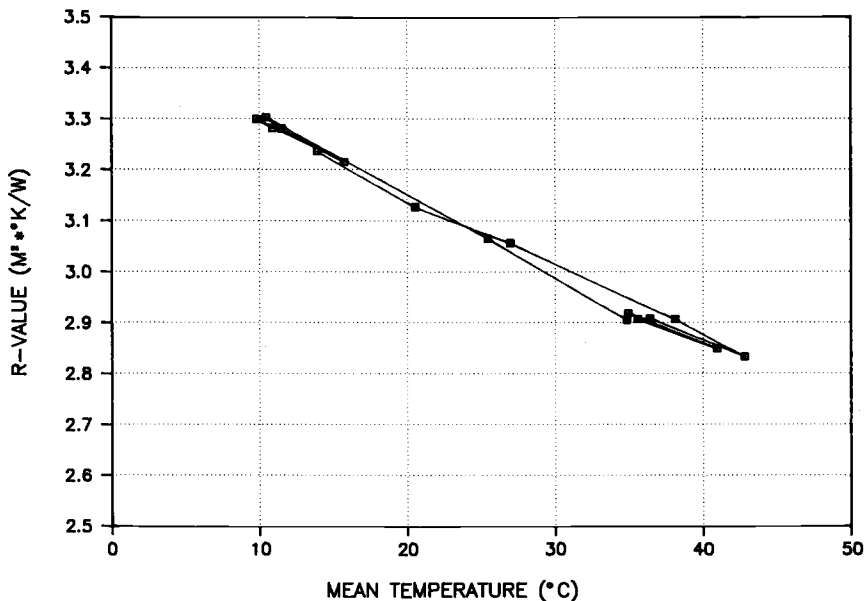


FIG. 9—Full thickness R -value results from PROPOR calculations. These results extend over one full year, from low mean temperature to high and back again to low. The sample is 0.118 m thick. The fact that the values tend to lie on a single line indicates no R -value drift over the year.

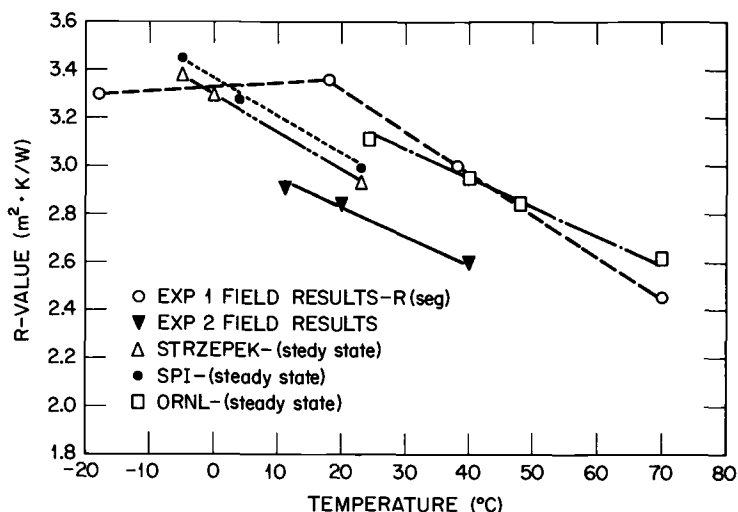


FIG. 10—Comparison of R -value results from the field tests (both Experiment 1 and Experiment 2) with results from laboratory steady-state tests.

PROPOR. This question is currently under study. Exp. 2 is not helpful in resolving this issue because of the limited availability of data.

The reasonableness of the agreement between field methods and between field and laboratory methods suggests that field methods, at least for lightweight roof systems, are acceptable methods for characterizing thermal performance of in-place systems. In particular, techniques similar to Exp. 2 that do not require penetration of the roof system can be quite valuable when it is necessary to determine the R -value of in-place systems.

Finally, referring to Fig. 9 again, the results illustrate the stability of thermal properties of expanded polystyrene insulation in the field. If there was a permanent R -value drift with time of any significance, the R -values for low mean temperatures (winter data) would not be bunched since they represent measurements taken a year apart. As one expects for expanded polystyrene, however, this does not occur.

Acknowledgments

This research was sponsored in part by the Office of Buildings and Community Systems, Building Systems Division, U.S. Department of Energy, under Contract DE-AC05-84OR21400 with Martin Marietta Energy Systems, Inc.

References

- [1] Flanders, S. N., "Time Constraints on Measuring Building R -Values," CRREL Report 80-15, U.S. Corps of Engineers, Cold Regions Research and Engineering Laboratory, Hanover, N.H., June 1980.
- [2] Orlandi, R. D., Shu, L. S., Derderian, G. D., and Siadat, B., "A Field Thermal Measurements Technique for Roofdeck Systems," Proceedings of the ASHRAE/DOE Conference, ASHRAE SP 38, 1982.
- [3] Grot, R. A., Fang, J. B., Courville, G. E., and Childs, K. W., "The Measurement and Quantification of Thermal Bridges in Four Office Buildings," Paper CH-85-11-4, ASHRAE Proceedings, Jan. 1985.
- [4] Courville, G. E., Childs, K. W., Walukas, D. J., Childs, P. W., and Griggs, E. I., "An Apparatus for Thermal Performance Measurements of Insulated Roof Systems," in *Thermal Insulation: Materials and Systems*, ASTM STP 922, American Society for Testing and Materials, Philadelphia, 1987, pp. 449-459.

- [5] Courville, G. E. and Beck, J. V., "Techniques for In Situ Determination of Thermal Resistance of Light Weight Board Insulations," 24th National Heat Transfer Conference, Pittsburgh, 9-12 Aug. 1987, ASME HTD-Vol. 78; also to be published in *ASME Journal*.
- [6] Orlandi, R. D., Derderian, G. D., Shu, L. S., Siadat, B., and Circignano, P. C., "In-Situ Thermal Performance Measurements of Some Roof Deck Systems," presented at ASTM C-16 Conference on Thermal Insulation: Materials and Systems, 2-6 Dec. 1984.
- [7] Courville, G. E., Sanders, J. P., and Childs, P. W., "Dynamic Thermal Performance of Insulated Metal Deck Roof Systems," ASHRAE/DOE/BTECC Thermal Performance of the Exterior Envelope of Buildings III, Clearwater Beach, Fla., 2-5 Dec. 1985, ASHRAE SP 49, 1986.
- [8] Hy-Cal Engineering, 9650 Tellstar, El Monte, CA 91713.
- [9] Yarbrough, D. W., McElroy, D. L., and Graves, R. S., "Thermal Resistance of Roof Panels and In Situ Calibration of Heat Flux Transducers," Thermal Performance of the Exterior Envelopes of Buildings III, ASHRAE SP 49, ASHRAE, Atlanta, 1986.
- [10] Graves, R. S. and McElroy, D. L., "Roof Panel Report—Polystyrene Boards," ORNL Internal Report, 1986.
- [11] Beck, J. V. and Arnold, K. J., *Parameter Estimation in Engineering and Science*, Wiley, New York, 1977.
- [12] Beck, J. V., "PROPOR: Determination of Material Properties from Field Data," to be published as an Oak Ridge National Laboratory Technical Report.
- [13] Beck, J. V. and Courville, G. E., "Analysis of Low-Slope Roof of Field Thermal Performance Data," to be presented at ASHRAE Symposium in June 1988.
- [14] Society of the Plastics Industry, "Expanded Polystyrene Insulation," Sweets Catalog File No. 7.15(d)So, McGraw-Hill, New York, 1983.
- [15] Strzepek, W. R., "Cellular Insulation," in *Handbook of Applied Thermal Design*, McGraw-Hill, New York, forthcoming.

A Comparison of Two Independent Techniques for the Determination of *In Situ* Thermal Performance

REFERENCE: Courville, G. E., Desjarlais, A. O., Tye, R. P., and McIntyre, C. R., "A Comparison of Two Independent Techniques for the Determination of *In Situ* Thermal Performance," *Insulation Materials, Testing, and Applications, ASTM STP 1030*, D. L. McElroy and J. F. Kimpflen, Eds., American Society for Testing and Materials, Philadelphia, 1990, pp. 496-509.

ABSTRACT: A parallel experiment has been performed on an insulated roof system installed in the Roof Thermal Research Apparatus at Oak Ridge National Laboratory. Separate sections of a 1.2 by 2.4 m test panel were evaluated for nine months using two different heat flux transducer (HFT) instrumentation packages, with the data being treated independently. The paper discusses the instrumentation packages, sensor calibration procedures, and data collection and analyses methods, highlighting the differences between the independent techniques. A comparison of the independently derived thermal performance results is presented. The comparison includes a discussion of the HFT test techniques for determining the *in situ* thermal performance of insulated building components. Limitations of these procedures are also detailed.

KEY WORDS: thermal performance, *in situ* testing, insulation, roofs, *R*-value, dynamic performance

The increased use of thermal insulation for energy conservation purposes in buildings has generated the need for understanding their thermal behavior under actual use conditions. The most widely used experimental technique for evaluating the thermal performance of insulation products and systems is to measure it under steady-state conditions in a laboratory using standardized experimental methods such as ASTM C 177, C 518, C 236, and C 976. In service, the insulation product is part of the building envelope system exposed to dynamic thermal conditions, and those products which are thermally sensitive or interact with other components of the system may behave differently in use than as predicted by laboratory testing. The development and validation of suitable analytical models used to predict building energy performance behavior require accurate measurements of field thermal performance; the application of laboratory derived data to actual installations needs investigation and verification.

ASTM Subcommittee C16.30 on Thermal Measurements has been active in generating documents to standardize the siting and application of instrumentation, the calibration of heat flux transducers (HFTs), and the collection and analysis of data from field experimentation. Two ASTM Standard Practices, *In-Situ Measurements of Heat Flux in Industrial Thermal Insulation Using Heat Flux Transducers* (C 1041) and *In-Situ Measurement of Heat Flux and Temperature on Building Envelope Components* (C 1046), are available, and two other Standard Practices are presently in draft form addressing various aspects of field experimentation.

Several researchers [1-6] have undertaken experiments to determine the thermal perfor-

¹Oak Ridge National Laboratory, Oak Ridge, TN 37381.

²Dynatech Scientific, Inc., Cambridge, MA 02139.

³Koppers Company, Pittsburgh, PA.

mance of building envelope components. Questions regarding the precision of these experiments have typically been addressed analytically or by comparison with laboratory derived data on similar products or building configurations. No direct comparisons between independently derived *in situ* data have been attempted.

A field experiment has been undertaken on the Roof Thermal Research Apparatus (RTRA) at Oak Ridge National Laboratory (ORNL). A test panel, simulating a low slope roof, has been instrumented with temperature sensors and heat flux transducers, monitored, and the generated data analyzed by two organizations using separately designed test plans. This series of concurrent experiments allows for the critical review of the individual phases of the *in situ* experiment and supplies the opportunity to directly examine the precision of the techniques employed.

Test Building and Panel Construction

The combined field experiment was undertaken on the Roof Thermal Research Apparatus (RTRA) [5] at ORNL. The RTRA (Fig. 1) is housed in a concrete block building approximately 2.4 m wide by 8 m long by 2.7 m high with a concrete slab-on-grade floor. The roof consists of a central fixed BUR roof sandwiched between two 1.2 by 2.4 m test sites on each side. The interior of the RTRA is temperature and humidity controlled. The test panel for this study was mounted into one of these test sites.

The test panel under study consisted of a metal deck, a 19 mm thick layer of perlite board, a

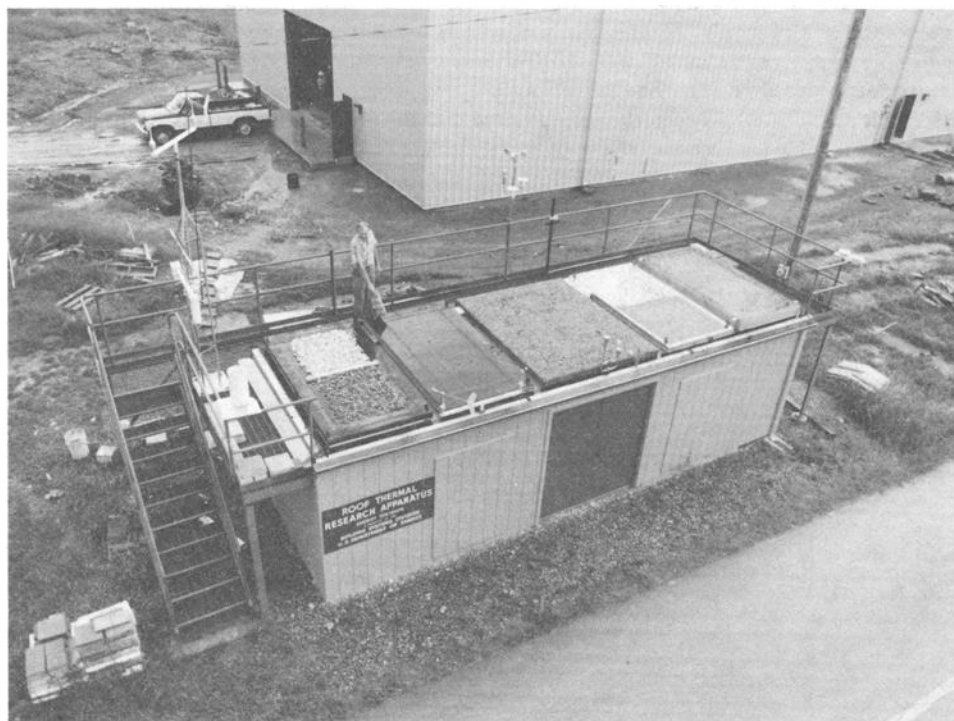


FIG. 1—Roof Thermal Research Apparatus at Oak Ridge National Laboratory. The test panel is located in the second test site from the left of the building.

51 mm thick layer of phenolic foam insulation, and a 13 mm thick layer of wood fiberboard. Wood nailers were mounted around the test panel; the panel was then placed into a steel frame to facilitate handling. A fully adhered EPDM membrane was laid over the entire panel. No vapor retarder was used in the construction. A schematic of the test panel is shown in Fig. 2.

Experimental Designs and Test Procedures

ORNL has performed a computer simulation of the test panel which indicates that the central 2.0 by 0.8 m portion is free of edge effects. The instrumentation package designed by Dynatech Scientific (No. 1) was mounted in one half of that isothermal zone of the test panel, while ORNL mounted their standard instrumentation package (No. 2) in the second half of the isothermal zone.

Instrumentation Package No. 1

The Dynatech Scientific instrumentation package and calibration procedure have been described previously [7]. Three large area HFTs [8] and nine 30-gage Type K Chromel/Alumel thermocouples were installed into the test panel for use by Instrumentation Package No. 1. Specifically, the HFTs are 300 mm square by 0.8 mm thick, have an active area that is 150 mm square, and have a sensitivity of approximately $0.06 \text{ mV}/(\text{W}/\text{m}^2)$ at 24°C . The HFTs were located between the metal deck and the perlite board, between the perlite board and the phenolic foam insulation, and between the phenolic foam insulation and the fiberboard, and were embedded into either the perlite board or the fiberboard in a staggered array. Thermocouples were also mounted at these locations within the test panel and on the interior and exterior surfaces of the roof assembly. Two temperature sensors were installed at each location. Each thermocouple array was "assigned" to a HFT, effectively allowing for three simultaneous series of independent measurements. For the purpose of this paper, discussions will be limited to the HFT that was located between the perlite board and the phenolic foam. This HFT location is the most desirable because the HFT is thermally isolated from exterior or interior environmental fluctuations. The HFTs mounted at the perlite board/metal deck and the fiberboard/phenolic foam interfaces are not discussed further. The reasons for these omissions are: (1) Instrumentation Package No. 2 did not include a HFT between the perlite board and metal deck, and (2) concerns about the data scanning procedures being representative of the rapidly changing thermal conditions at the phenolic foam/fiberboard interface. Information from these HFTs

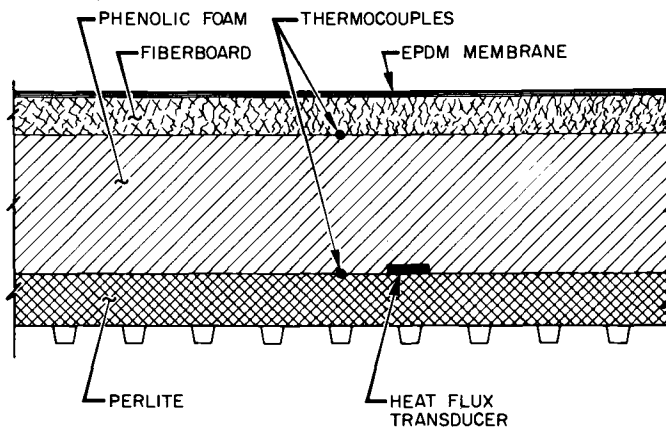


FIG. 2—Schematic drawing of roof test panel.

will be presented in a future paper and are only mentioned in this text to completely describe the instrumentation that was installed.

Before installation into the test panel, the heat flux transducers used for Instrumentation Package No. 1 were calibrated using a large heat flow meter apparatus [9] designed in accordance with ASTM C 518. The HFTs used in the test panel were embedded into 600 mm square sections of perlite board or fiberboard in an identical fashion to their test panel installation. The embedded HFTs were tested at three temperatures covering the anticipated temperature range of the field experiment (10, 24, and 38°C). The sensitivity of each HFT was determined by comparing its output to that of the instrument HFT. A least-squares linear regression was performed on the HFT sensitivity data as a function of temperature, and the coefficients of these regressions were written into the control program.

A meteorological station was set up outside the RTRA to monitor local weather conditions. A standard 3 m high tower was mounted on the RTRA and was equipped to measure wind speed and direction, temperature, dewpoint, and atmospheric pressure. A second wind vane and anemometer were installed approximately 0.3 m above the test panel to measure local surface conditions.

A digital data acquisition system (DDAS) was designed to collect temperature, heat flow, and weather data from the sensors located in, on, or near the test panel. The system consisted of a personal computer with a data acquisition/control unit connected through a general purpose interface bus. The data acquisition/control unit used in this instrumentation package was selected because its voltmeter has a high resolution (approximately 1 μV) which was needed with the large area, low sensitivity HFTs. A control program governed the functions of the DDAS during data accumulation, created data files, and reduced and stored the collected data. The sensors were scanned four times a minute over an 11 min period from 5 min before to 5 min after the hour (44 scans total per hour). These data were converted to engineering units, averaged, and the average stored as the data for that hour. This method of data collection was selected instead of gathering data over the entire hour at regular intervals because it emphasizes the data information at the prescribed time. This scanning protocol does not detect any thermal effects that occur during the remaining 49 min of each hourly interval. The data were analyzed in 5 day, 7 day, and monthly blocks, along with a total program summation. The thermal resistance (R) of the insulation material was determined by dividing the integrated temperature difference (dT) across the phenolic foam by the integrated heat flux (q) through the phenolic foam:

$$R = \frac{\sum_{i=1}^n dT_i}{\sum_{i=1}^n q_i} \quad (1)$$

where n is the number of data sets used in the summation. This "summation method" of calculation is similar to one of the proposed analysis techniques detailed in the draft ASTM Standard Practice for Determining Thermal Resistance of Building Envelope Components from In-Situ Data.

Instrumentation Package No. 2

The ORNL experimental package and analysis techniques have been described elsewhere [5]. Briefly, temperatures are measured by 30-gage copper-constantan thermocouples all cut from the same spool to minimize errors in temperature differences; heat flux transducers are thermopile disks, 50 by 50 mm in area and 3 mm thick,⁴ with a sensitivity of about 0.3 mV/(W/m²) at 24°C. The HFTs are calibrated *in situ* by assembling the entire insulation test panel into its final configuration and placing it into an unguarded hot screen laboratory steady-state thermal conductivity tester that has been shown to measure apparent thermal conductivity to within 1%

⁴Model BI-7-120-WP-T, Hy-Cal Engineering, El Monte, Calif.

of the National Bureau of Standards guarded hot plate [10]. Heat flows are established and measured in the screen tester; the transducer voltage/heat flux calibration equation is developed over the temperature range of the screen tester. In addition to the calibration of the heat flux transducers, the screen tester also provides a base line laboratory measurement of the temperature dependence of the thermal resistance of the test specimen. Data are collected from all sensors at eleven 1-min intervals from 5 min before to 5 min after the hour and averaged. These values are stored on computer disks as the hourly values. Typically, data are analyzed in seven day or 168 h blocks.

Although the summation method is also used, the principle technique used at ORNL for determining the thermal performance from *in situ* data is a least-squares procedure labeled PROPOR. This procedure has previously been described and compared to other methods [11]. This method of calculation is one of the proposed analysis techniques detailed in the draft ASTM Standard Practice for Determining Thermal Resistance of Building Envelope Components from In-Situ Data. The sum of squares to be minimized is

$$S = \sum_{i=1}^n (\hat{T}_i - T_i)^2 \quad (2)$$

where $\hat{T}_{(i)}$ is the experimental temperature at the i th hour at the interface between the perlite and the phenolic foam boards. $T_{(i)}$ is the temperature at the same location calculated using Crank-Nicolson difference equations derived from the one-dimensional transient heat conduction equation:

$$\frac{\partial T}{\partial t} = \frac{k}{pC} \frac{\partial^2 T}{\partial x^2}, \quad q = -kA \frac{\partial T}{\partial x}, \quad k = a + bT \quad (3)$$

with the measured temperature at the interface between the phenolic foam and the fiberboard insulation boards and the measured heat flux between the perlite and phenolic foam as the boundary conditions. The calculated values of T are functions of the apparent thermal conductivity, k , and the heat capacity, pC . For lightweight systems, pC is assumed constant and S in Eq 2 will vary as different values of k are tried. In this particular case, k is assumed to be linear with temperature and the $k(T)$ that gives a minimum value of S is taken as the result of the analysis for the data set analyzed.

Summation Method Mean Temperature

The summation method will yield a thermal performance result that is an average for the rapidly changing thermal conditions during the integration period. To compare these results with other techniques, it is necessary to attribute a "mean temperature" to the thermal performance result. Unlike the steady-state experiment, the temperatures measured in the field experiment will vary significantly. The heat flux will be changing accordingly, with a large percentage of heat flux occurring over the short periods of time when the temperature difference across the insulation product is maximized. A heat flux weighted mean temperature (T_w) calculation is used with Instrumentation Package No. 1 and is defined as

$$T_w = \frac{\int_0^t |q| (T_{\text{mean}}) dt}{\int_0^t |q| dt} \quad (4)$$

where t is time, $|q|$ is the absolute value of the heat flux, and T_{mean} is the arithmetic average temperature of the interior and exterior surfaces of the test panel.

Instrumentation Package No. 2 uses a similar calculation for determining the mean temperature for the data analyzed by the summation method by weighing the arithmetic mean with the temperature difference across the test panel [11]. Whenever temperature dependence of R -factors obtained by the summation method is discussed, the temperatures will be weighted means.

Laboratory Testing of Test Panel Components

Several spare boards of each material used to construct the test panel were saved for laboratory evaluation. The insulation products were analyzed for thermal resistance utilizing a large heat flow meter apparatus [9] in accordance with ASTM C 518. Before testing, the products were stored in an environmental room maintained at 24°C and 50% relative humidity. Specimens 600 mm square were prepared from the spare boards of each product and testing was undertaken in January and April 1986.

As discussed earlier, ORNL measures the panel thermal performance during their HFT calibration tests. Using Dynatech's thermal resistance data for the perlite board and the fiberboard, the thermal performance of the phenolic foam insulation was derived.

Figure 3 depicts the thermal resistance of the phenolic foam insulation as a function of temperature. Over the temperature range where the two data sets overlap, there is approximately a 6% average difference. About half of this difference is due to thickness differences in the laboratory test samples. When normalized to a constant thickness, the average variation in the laboratory-derived R -factor is 2.5%.

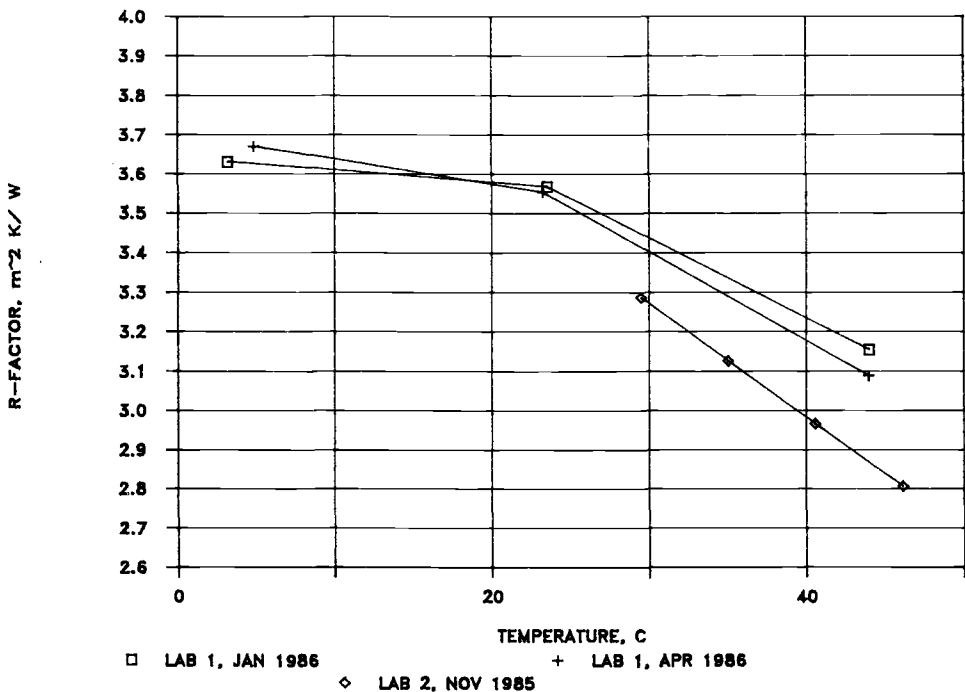


FIG. 3—Thermal resistance of the phenolic foam insulation measured in the laboratory. There is a 2.5% difference in the thickness of the specimens measured at the two laboratories.

Experimental Data

The *in situ* thermal performance experiment consists of two independent activities: (1) the accurate measurement of representative temperatures and heat fluxes over an extended time period, and (2) the processing of these data sets to calculate thermal performance. This combined experiment offers a unique opportunity to examine these activities separately.

Data collection with both instrumentation packages was initiated in late December 1985. A week (18–24 March 1986) was randomly selected to test the capability of the two sets of instrumentation to reproduce the basic measurements of temperature and heat flux. The selected week is average with respect to its heat flux for the nine months of data discussed in this paper. During this period of time, the monthly average heat flux ranges from -0.60 to 0.35 W/m^2 while the selected week has an average heat flux of -0.22 W/m^2 . Heat flow into the building is designated as positive.

Figure 4 depicts the temperatures of the interior and exterior surfaces of the phenolic foam as measured by the two instrumentation packages for the week. The average difference in the measurement of these temperatures between the two data sets is $+1.3$ and $+1.2^\circ\text{C}$ with standard deviations of 0.2 and 0.7°C respectively. Instrumentation Package No. 1 reports all temperatures at a lower level. A calibration check of a temperature sensor from each instrumentation package with an ice/water mixture has confirmed this magnitude of difference. This type of consistent discrepancy in temperature measurement can typically be traced to differences in electronic referencing devices. Fortunately, the measurement of absolute temperature does not directly impact the calculation of thermal performance other than alter the mean temperature ascribed to the *R*-factor.

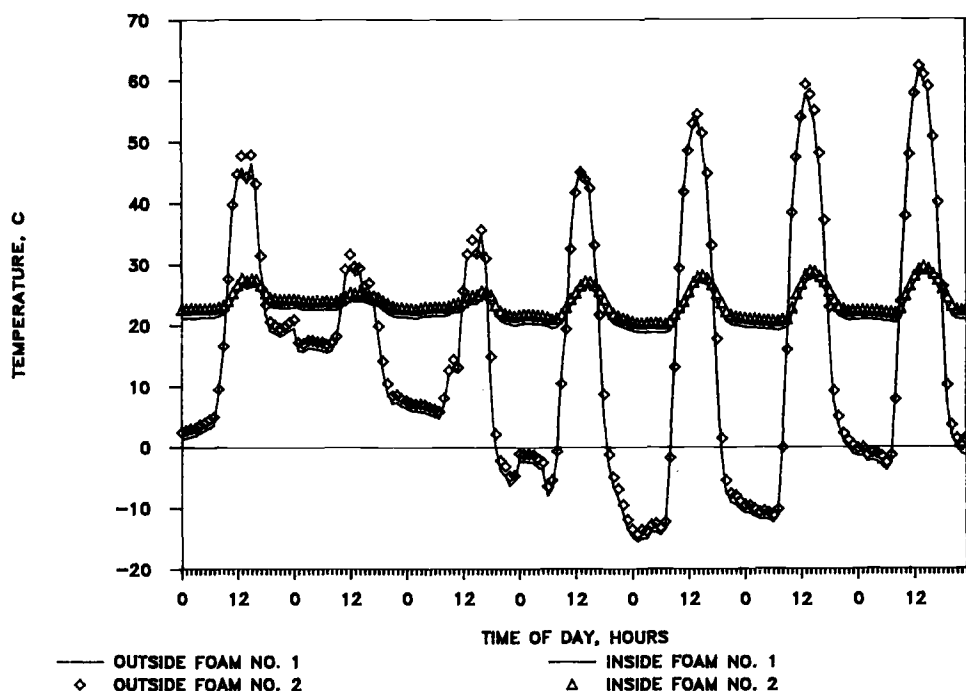


FIG. 4—Comparison of the absolute temperatures of the interior and exterior surfaces of the phenolic foam insulation as measured by the two instrumentation packages for the week of 18–24 March 1986. They measure differences of approximately 1.3°C ; the differences are consistent for different sensor sites.

The temperature difference (dT) between the exterior and interior surfaces of the phenolic foam as measured by the two instrumentation packages for the same time period is shown in Fig. 5. A positive temperature difference indicates that the exterior surface is at a higher temperature. The average temperature difference as measured by the two sets of instrumentation is -8.02 and -8.15°C , yielding a difference in dT of 0.13°C (1.6%) and a standard deviation of 0.68°C . Figure 6 depicts the difference in dT for the two data sets on an hourly basis. The large variations in temperature difference are typically at 9:00 and 18:00 hours or when there are some short-term fluctuations in dT due to changes in cloud cover or wind gusts. The aforementioned times represent periods when the temperature difference across the insulation will be changing at rates of 15 to 20°C/h . It is possible that these apparently large differences in the measurement of dT are simply due to different sampling times, since the clocks of the instrumentation packages were never synchronized.

Plots of heat flux as measured by the two instrumentation packages and the difference between those measurements are shown in Figs. 7 and 8 respectively. The average heat flux as measured by the two instrumentation packages is -0.222 and -0.226 W/m^2 . The integrated difference and the standard deviation between the two data sets is 0.0048 W/m^2 (2.1%) and 0.051 W/m^2 respectively. Although the agreement between the two data sets is excellent, it should be noted that Instrumentation Package No. 1 predicts lower absolute levels of heat flux in both heat flow directions.

By studying the difference in heat flux as a function of heat flux (Fig. 8), a systematic bias of approximately 8% exists between the two data sets. A second systematic bias may also account for the nonzero y -intercept. The most likely source of these biases is in the heat flux transducer

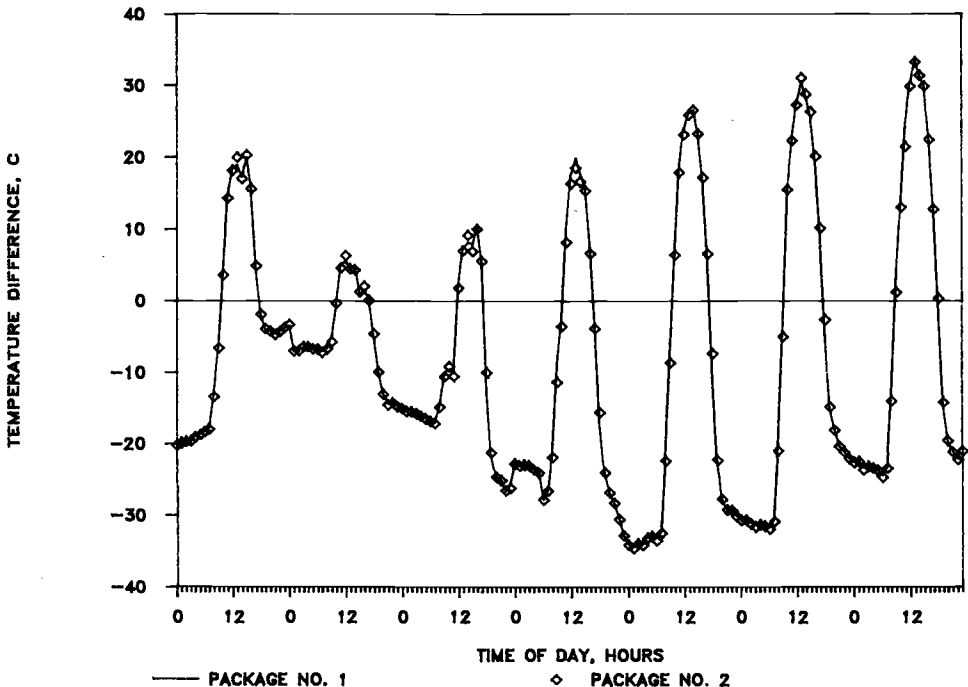


FIG. 5—Comparison of the temperature differences across the phenolic foam insulation as measured by the two instrumentation packages for the same time period as for Fig. 4. The average dT of the two data sets agreed to 0.13°C .

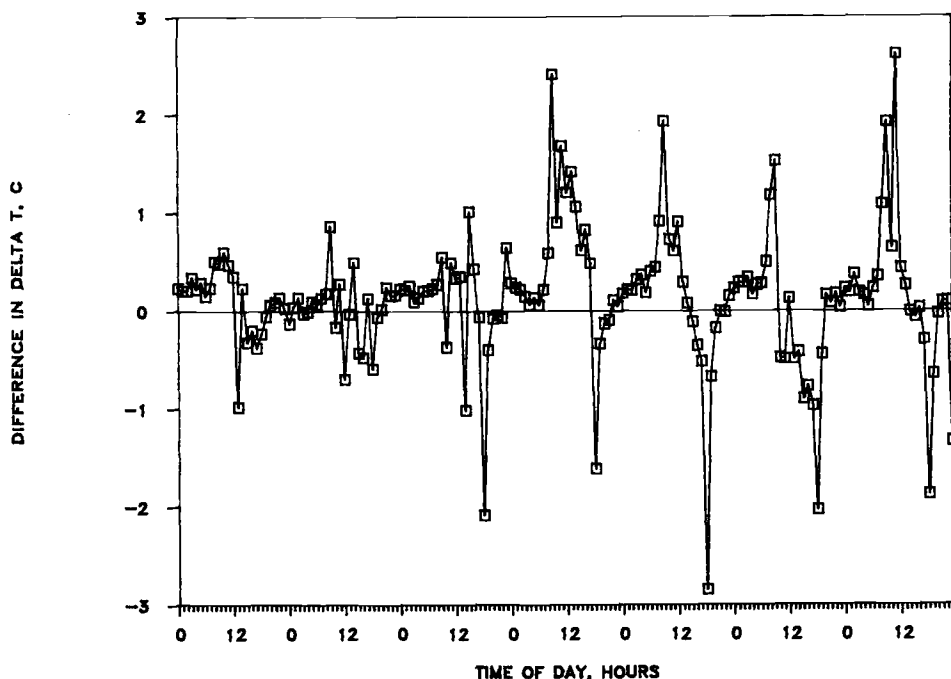


FIG. 6—Hourly temperature differences across the phenolic foam insulation as measured by the two instrumentation packages. Large discrepancies occur when there are rapid changes in thermal conditions. These differences may be due to the lack of clock synchronization.

calibration. The linear least-squares fit of this data predicts a difference in heat flux of 0.0044 W/m^2 for the heat flux level of the week being studied. The weekly data sets that are being discussed in this paper have integrated heat fluxes that coincidentally agree. The significant scatter in the data with positive heat fluxes is probably due to clock synchronization problems mentioned earlier, because virtually all these data points occur during rapidly changing thermal conditions.

Figure 9 depicts the R -factor of the phenolic foam as predicted by the two instrumentation packages using the summation method and by PROPOR using the Instrumentation Package No. 2 data set. The Summation Method integrates the temperature difference and heat flux data from the beginning of the data set (0:00 hours on 18 March 1986) to the hour of interest. Each successive data point represents the previous hour's summation plus the present hour's data. PROPOR utilizes the entire data set to determine the best levels of insulation thermal performance to fit the temperature and heat flux measurements. For this figure, the R -factor as a function of mean temperature predicted by PROPOR for the entire data set is calculated every hour based on the integrated mean temperature from the beginning of the data set to the hour in question. Although this is presented in a similar format as the summation method results, the only appropriate point of comparison is at the end of the seven day data set because this is the only point where both analysis techniques are working on an identical amount of data. The purpose for including the PROPOR R -factor results is to demonstrate the differences between the calculation techniques and to indicate on Fig. 9 the magnitude of the effect of mean temperature changes (if any) on R -factor for the time period being studied.

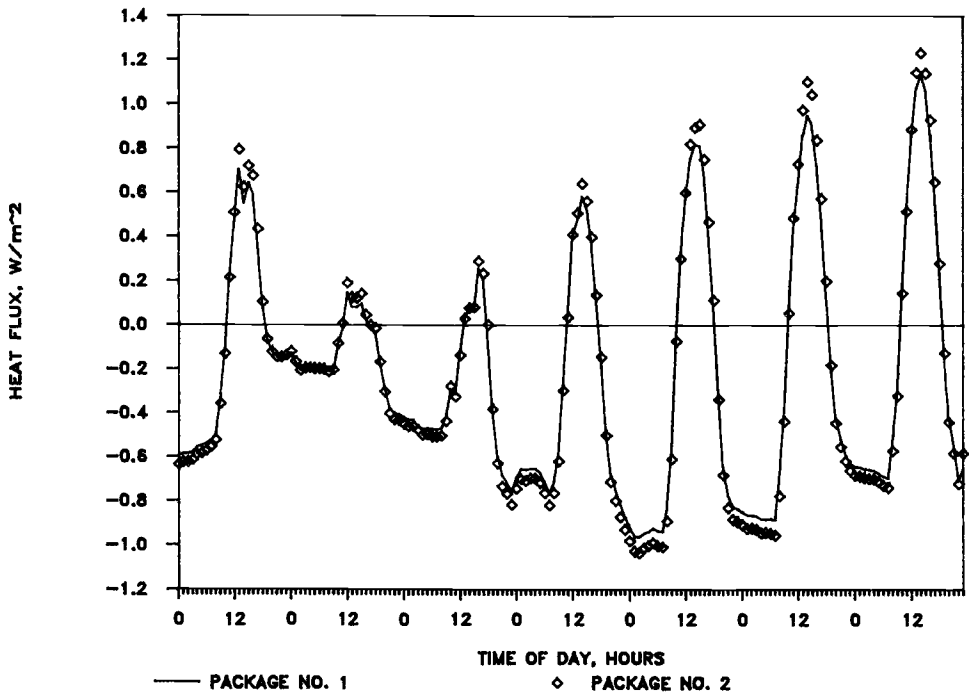


FIG. 7—Comparison of the heat flux measured by the two instrumentation packages for the same time period as for Fig. 4. Note that one data set predicts lower absolute levels of heat flux.

Given the agreement between the integrated values of temperature difference and heat flux, the R -factor predictions based on the two data sets using the summation method are excellent (better than 1%). The integrated R -factors calculated from each of the two data sets internally vary by $0.62 \text{ m}^2/\text{K} \cdot \text{W}$ (20%) during the first 24 h, $0.26 \text{ m}^2/\text{K} \cdot \text{W}$ (8%) during the fourth day, and $0.17 \text{ m}^2/\text{K} \cdot \text{W}$ (5%) during the seventh day. The summation method does not converge to an acceptable level for the test period being studied, and there is a 11% difference between the predictions of the summation and PROPOR methods. The cause of the upward drift in the summation method R -factors is unknown.

The impact of the variations in the heat flux measurements is clearly demonstrated in Fig. 9. Once the summation has developed a significant data base (after three days for this example), the R -factor predictions begin to diverge during the evening hours due to a constant difference in the integrated heat flux. Once the heat flux direction is reversed at 9:00 hours, the difference in the predicted R -factor decreases.

Figure 10 summarizes the test results for the nine months that are being reported in this paper. The data identified as Summation No. 1 are monthly integrations. The long integration period was selected to reduce the impact of the thermal capacitance of the system and to reduce the sensitivity of the calculation to short term fluctuations. The data identified as Summation No. 2 and PROPOR are weekly integrations and use the same input data sets. The R -factors predicted by the two different data sets by the summation method will indicate the reproducibility of the data collection process, while the comparison of the R -factors generated by the different analysis techniques on the same data set will measure the precision of the analysis techniques and the range of usability of the summation method.

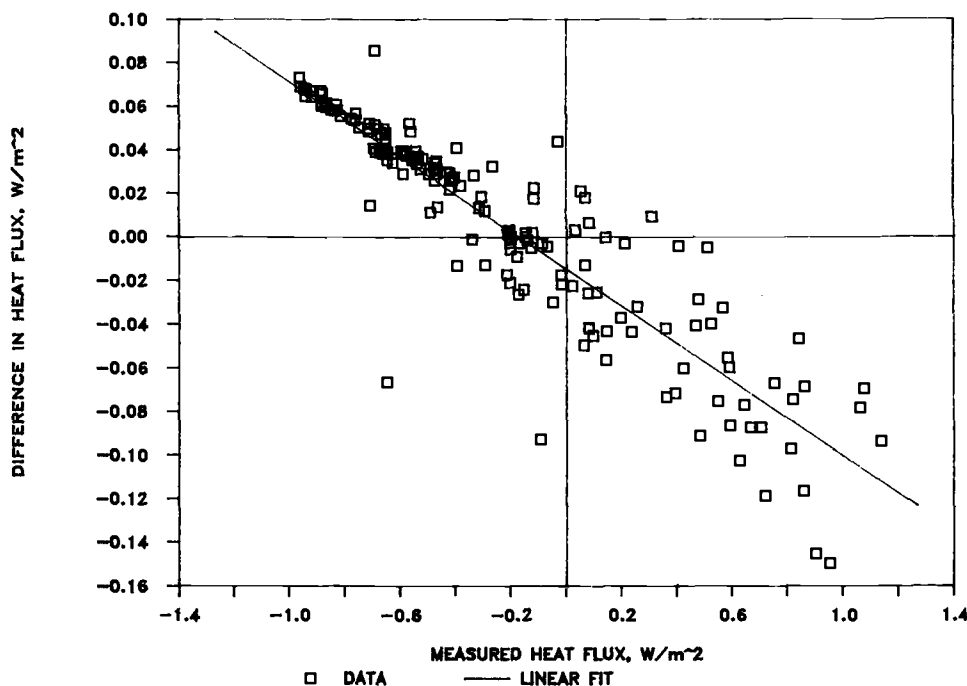


FIG. 8—Difference in heat flux as measured by the two instrumentation packages. A systematic bias of approximately 8% exists between the two data sets. The source of this bias is probably the heat flux transducer calibration.

In comparing the data predicted from the two summation methods, the temperature range is broken down into three segments. When the integrated heat flux approaches zero, the summation method breaks down [11]. For these data sets, there is a 10% or greater difference between the summation method and PROPOR in the weighted mean temperature range of 18 to 35°C. Comparisons of the variation of test results by the summation method in this temperature range are inconclusive due to the inconsistency of the data at low heat flux levels. The levels of heat flux for the test panel in this temperature range are approximately $\pm 0.15 \text{ W/m}^2$. Below 18°C and above 35°C, the summation data agree to approximately 5 and 15% respectively. This is consistent with the predicted variation in heat flux where differences of 6 and 13% would be expected over these temperature intervals.

The summation method and PROPOR agree to within 4 and 8% for the below 18°C and above 35°C temperature intervals when processing the same data set. It is unclear what the cause of the difference due to temperature interval is.

Conclusions

The comparison of two sets of field data allow for a first estimate of reproducibility in the measurement of temperatures and heat fluxes and a comparison of the calculation techniques employed in determining *in situ* thermal performance. Substantial care was taken by all parties in the selection, calibration, and installation of instrumentation. In addition, the test panel was

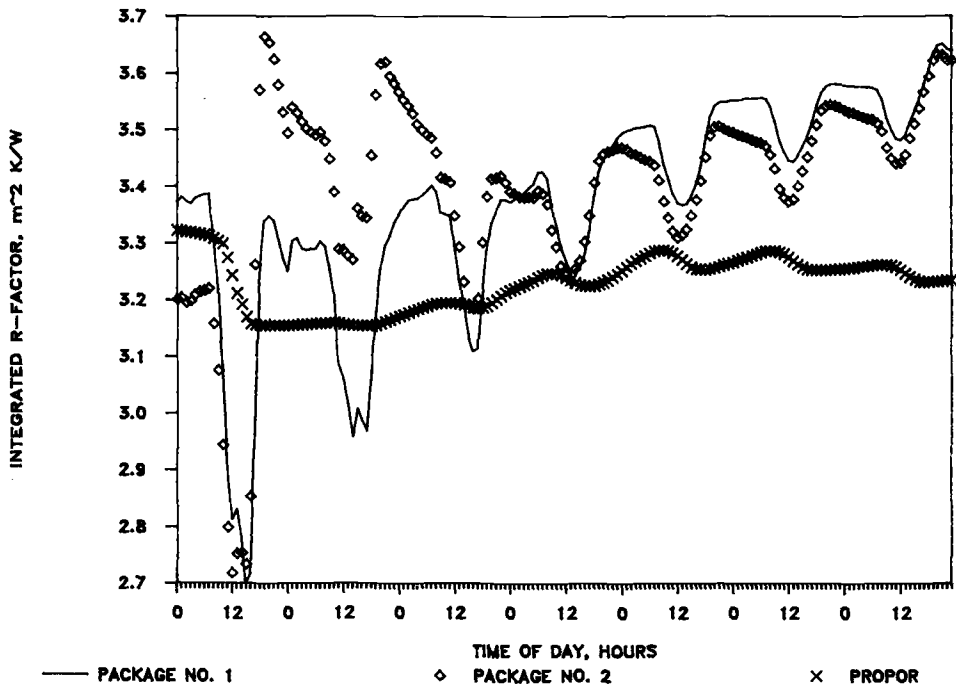


FIG. 9—Comparison of the R -factor as predicted by the two instrumentation packages for the same time period as for Fig. 4. Although the two summation method results agree, there is an 11% difference between the summation and PROPOR methods.

uniform in construction and had a relatively low mass and short time constant. This test program has yielded the following information. These results should not necessarily be attributed to all field experiments.

1. Differences in absolute temperature measurement were found to be on the order of $1.4^{\circ}C$ but were consistent within each data set. Temperature differences were measured to better than $0.15^{\circ}C$ and would have probably been better if the clocks of the data collection systems had been synchronized.
2. Although the data sets that were analyzed in this paper indicated close agreement in the measurement of heat flux, systematic biases on the order of 8% were discovered. The data also imply that these biases are temperature dependent, impacting the higher absolute temperature data to a greater extent. These biases are probably due to the HFT calibration and suggest that this aspect of the field experiment is not yet fully understood.
3. The reproducibility of the R -factor calculation is limited to the ability to measure heat flux. Differences in these calculations were approximately the same as the heat flux variations.
4. Significant differences (greater than 10%) in the R -factor calculated by the summation and PROPOR methods are noted in the weighted mean temperature range of 18 to $35^{\circ}C$. For this specific test panel, that temperature range coincides with heat fluxes of approximately $\pm 0.15 W/m^2$. Good agreement between the two methods of analysis is obtained when the measured heat flux is larger than $\pm 0.15 W/m^2$. In this heat flux range, the summation method can be used with confidence.

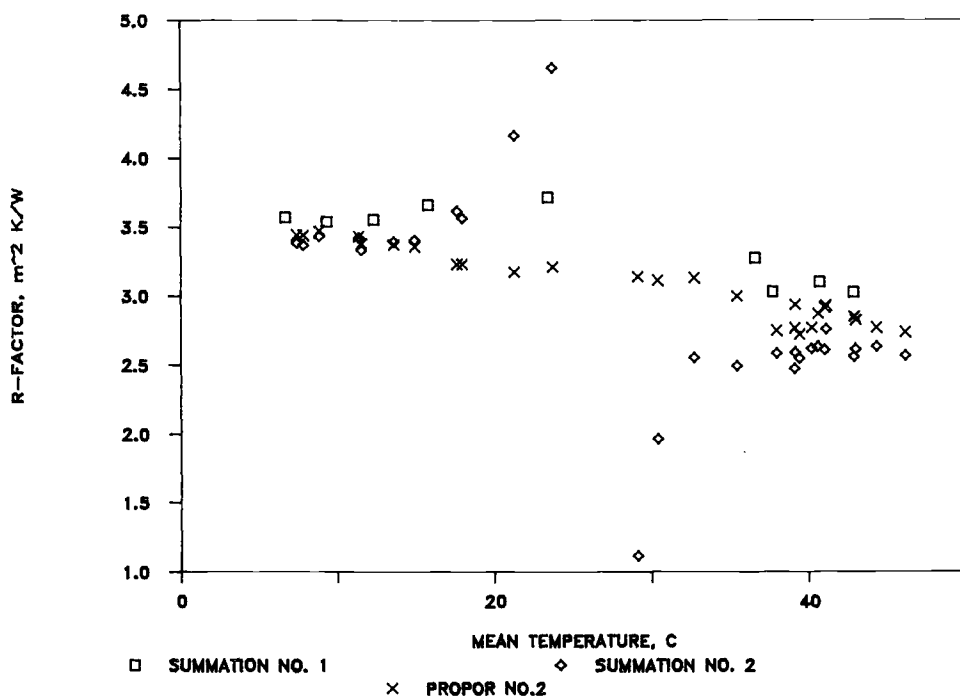


FIG. 10—Summary of the R-factors for the two summation and PROPOR methods for December 1985 to August 1986. Note that there is a weighted temperature window (18 to 35°C) where the summation method test results are not as reliable due to very low levels of heat flux.

References

- [1] Fang, J. B. and Grot, R. A., "In-Situ Measurement of the Thermal Resistance of Building Envelopes of Office Buildings," ASHRAE Paper No. CH-85-11 No. 3, 1985.
- [2] Flanders, S. N., "Confidence in Heat Flux Transducer Measurements of Buildings," ASHRAE Paper No. CH-85-11 No. 1, 1985.
- [3] Orlandi, R. D. et al., "A Field Thermal Measurements Technique for Roofdeck Systems," ASHRAE Paper No. SP-38-8 No. 4, 1982.
- [4] Modera, M. P., "Technical Description: The Thermal Envelope Thermal Test Unit," ASHRAE Paper No. CH-85-11 No. 2, 1985.
- [5] Courville, G. E., Childs, K. W., Walukas, D. J., and Childs, P. W., "Thermal Performance Measurements of Insulated Roof Systems," in *Proceedings, Second International Symposium on Roofing Technology*, Washington, D.C., 1985.
- [6] Roof Insulation Committee/Thermal Insulation Manufacturers Association, "Specifying and Installing Polyurethane, Polyisocyanurate Roof Insulations," *Roofer Magazine*, Vol. 6, No. 1, 1986, p. 21.
- [7] Desjarlais, A. O. and Tye, R. P., "Experimental Methods for Determining the Thermal Performance of Cellular Plastic Insulation Materials Used in Roofs," *Proceedings, 8th Conference on Roofing Technology*, Gaithersburg, Md., 1987.
- [8] Degenne, M. and Klarsfeld, S., "A New Type of Heat Flowmeter for Application and Study of Insulation and Systems," in *Building Applications of Heat Flux Transducers, ASTM STP 885*, E. Bales, M. Bomberg, and G. E. Courville, Eds., American Society for Testing and Materials, Philadelphia, 1985, pp. 163-171.
- [9] Tye, R. P., Coumou, K. G., Desjarlais, A. O., and Haines, D. M., "Historical Development of a Large Heat Flow Meter Apparatus for Measurements of Thermal Resistance of Insulations," in *Thermal Insulation: Materials and Systems, ASTM STP 922*, American Society for Testing and Materials, Philadelphia, 1987, pp. 651-664.
- [10] Graves, R. S., Yarbrough, D. W., and McElroy, D. L., "Apparent Thermal Conductivity Measure-

ments by an Unguarded Technique," in *Proceedings*, 18th International Conference of Thermal Conductivity, Rapid City, S.D., 1983.

- [11] Courville, G. E. and Beck, J. V., "Techniques for In Situ Determination of Thermal Resistance of Light Weight Board Insulations," in *Proceedings*, ASME 24th National Heat Transfer Conference, Pittsburgh, Pa., 1987.

DISCUSSION

*J. R. Hagan*¹ (*written discussion*)—(1) Were the data generated by these two independent techniques used to determine the aging characteristics of the phenolic foam panel? If so, what was the result of this data analysis?

(2) The test panel was a metal deck, a $\frac{3}{4}$ in. thick perlite board, a 2 in. thick phenolic foam insulation, a $\frac{1}{2}$ in. thick wood fiberboard, and a fully adhered EPDM membrane. Is this construction a standard industry roof configuration when installing a phenolic foam insulation?

G. E. Courville et al. (*authors' closure*)—(1) The purpose of the research that this paper describes was to attempt to measure the reproducibility of the *in situ* field experiment. To do so requires the measurement of the thermal performance of the insulation products used in the test panel over a period of time. These data will be presented separately as the subject of another paper.

(2) We do not think this is a standard configuration. The perlite board was added to the system so that the HFTs could be mounted on the interior side of the phenolic foam and not be in contact with the metal deck. At the time of installation, the EPDM manufacturer did not recommend direct application of the membrane to phenolic foam and recommended an "approved" cover sheet be installed over the phenolic foam prior to the application of the membrane.

¹Jim Walter Research Corporation, St. Petersburg, FL 33716.

Use of Two Heat Flow Transducers for Transient Thermal Measurements on Porous Insulating Materials

REFERENCE: Langlais, C. and Boulant, J., "Use of Two Heat Flow Transducers for Transient Thermal Measurements on Porous Insulating Materials," *Insulation Materials, Testing, and Applications, ASTM STP 1030*, D. L. McElroy and J. F. Kimpflen, Eds., American Society for Testing and Materials, Philadelphia, 1990, pp. 510-521.

ABSTRACT: A method for measuring the apparent thermal conductivity of fibrous insulating materials under non-steady-state conditions is presented. The apparatus comprises one specimen and two heat flow transducers.

Equations describing the variation of heat flow as a function of time and position are given. These equations are used to derive thermal transient properties from the heat flux measured on the cold and hot sides of the specimens.

Finally, measurements on a variety of fibrous insulating materials are presented. These measurements show good agreement between the apparent thermal conductivities measured under transient and steady-state conditions. A significant reduction in test times compared to classic measurements with a single heat flow transducer apparatus was obtained.

KEY WORDS: glass fibers, heat flow meter apparatus, heat flow transducer, heat transfer, thermal conductivity, thermal insulation, transient measurements

The most commonly used apparatus for the laboratory determination of thermal transmission properties of insulating materials are the guarded hot plate (GHP) and the heat flow meter (HFM). Classically, the GHP apparatus is used for the development of transfer standards and for research studies, while the HFM apparatus is usually preferred for routine thermal conductivity testing.

The HFM apparatus is present in many quality control laboratories of manufacturers of thermal insulating materials because of its shorter measuring time compared to the GHP apparatus. The need of taking into account a large number of measurements to characterize a given product (especially for low density fibrous materials) has led us to investigate possible means for a further reduction of HFM measuring time.

The aim of this paper is therefore to present the principle of a test method that we used on a large variety of mineral fiber products and that allows for such a reduction in measuring time. The emphasis is put on the principle of the method itself. Calibration problems inherent to the HFM apparatus are not discussed in detail.

Heat Flow Meter Method

General Background

The general principle of the HFM method will not be discussed here. As stated in International Standard ISO/DIS 8301 (Determination of Steady State Specific Thermal Resistance and Related Properties - Heat Flow Meter Method):

¹Isover Saint-Gobain, Centre De Recherches Industrielles de Rantigny, Rantigny, France.

The HFM tends to establish a unidirectional constant heat transfer rate density which simultaneously crosses the central metering area of one (or two) heat flow meter(s) and the central area of one (or two nearly identical) specimen(s) in the form of slab(s) when tested in steady-state conditions of constant mean temperature and constant temperature difference between one heating unit and one cooling unit bordering the assembly of the specimen(s) and heat flow meter(s).

This ISO standard gives different possible layouts of HFM configurations (Fig. 1). Several authors [1,2] have mentioned the advantages of the single-specimen symmetrical configuration (Fig. 1b), especially in terms of shorter measuring times. All work presented here has therefore been performed in this configuration.

Apparatus

Figure 2 shows the operating principle of the apparatus designed for this study. It uses one specimen with heat flowing from bottom to top. The hot plate (610 by 610 mm²) is a classic guarded hot plate (central area of 305 by 305 mm²), while the cold plate is a liquid cooled plate.

At ambient temperature, hot and cold plate temperature stabilities are better than $\pm 0.02^\circ\text{C}$ (steady-state conditions). The heat flux can be measured with two independent heat flow transducers placed respectively on the hot and cold plates. The structure and characteristics of these transducers (sensitive area of 305 by 305 mm²) are described in Ref 3.

Calibration of the heat flow transducers has been performed in accordance with ISO/DIS 8301 for plate temperatures of 14 and 34°C using two specimens of known thermal conductivities (heavy and low density fiberglass insulations measured in the reference GHP apparatus

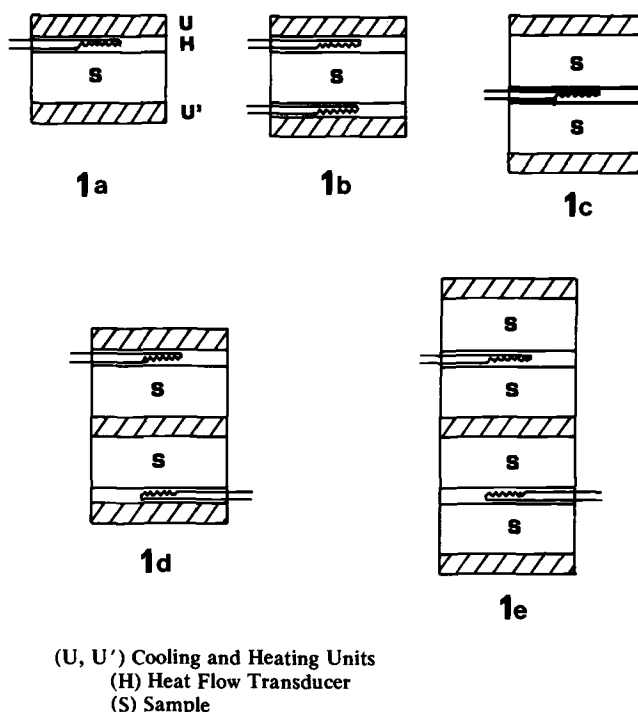
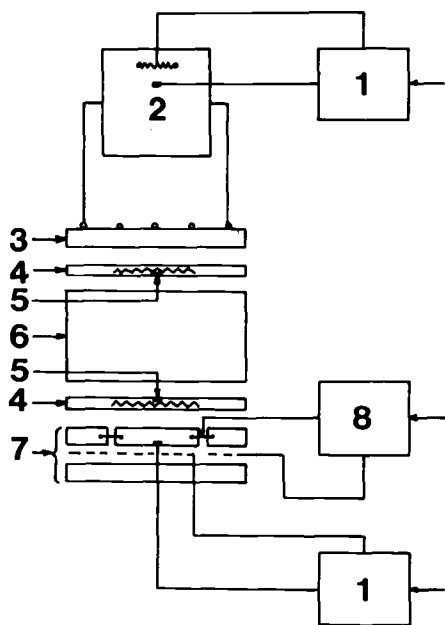


FIG. 1—Typical layouts of heat flow meter configurations.



- (1) Set Point Controller
- (2) Cooling Unit
- (3) Cold Plate
- (4) Heat Flow Transducer
- (5) Platinum Probe (Temperature Measurement)
- (6) Sample
- (7) Guarded Hot Plate
- (8) Guard Zero Balance Controller

FIG. 2—Operating principle of apparatus.

described in Ref 4). In addition, the whole plate assembly is in a temperature and humidity controlled atmosphere (ambient air regulation within the apparatus as described in Ref 4).

How Can We Decrease Measuring Time?

Heat Transfer Equations

Let us consider a slab of thickness e , placed between two plates at different initial temperatures. It is possible to derive from the heat conduction equation [1] the variation of the heat flux, φ , through this sample as a function of time, t , and height, h . With the following assumptions:

- Unidirectional heat flow (along h)
- At $t \geq 0$: $\theta(e) = \theta_C$
 $\theta(0) = \theta_H = \theta_C + \Delta\theta$

one can obtain the general equation

$$\varphi(h, t) = \lambda \frac{\Delta\theta}{e} \left(1 + 2 \sum_{n=1}^{+\infty} (-1)^n \cos\left(n \frac{\pi h}{e}\right) \exp\left(-a \frac{n^2 \pi^2}{e^2} t\right) \right) \quad (1)$$

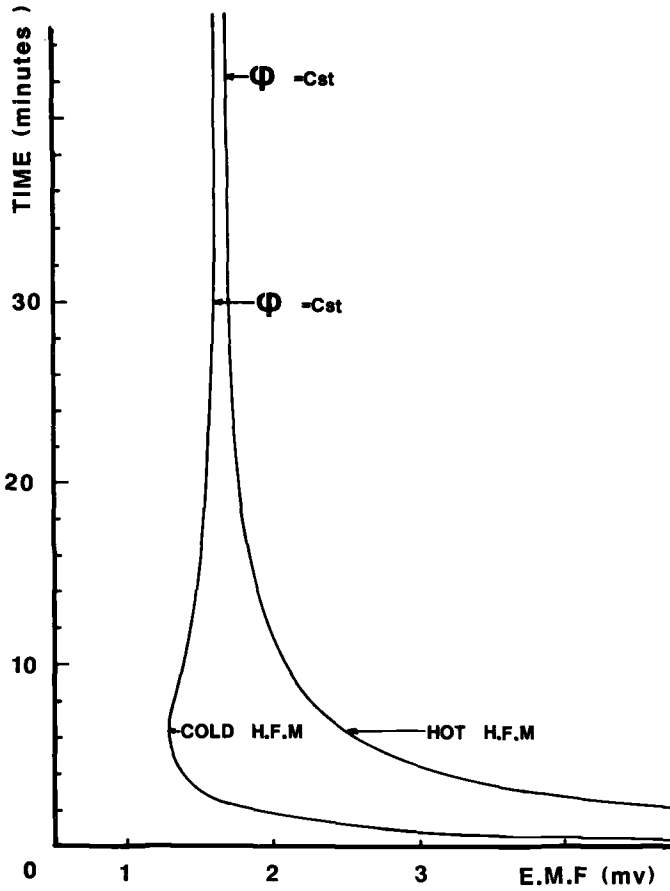


FIG. 3—Evolution of emf versus time for Sample 1 (first series of measurements).

where

λ = thermal conductivity of sample,

a = thermal diffusivity of sample,

φ = heat flux, and

θ = temperature.

A series expansion limited to the second derivative gives the expressions

$$\varphi_H = \varphi(0, t) = \lambda \frac{\Delta\theta}{e} \left\{ 1 + 2 \exp\left(-\frac{a\pi^2}{e^2} t\right) + 2 \exp\left(-\frac{4a\pi^2}{e^2} t\right) \right\} \quad (2)$$

$$\varphi_C = \varphi(e, t) = \lambda \frac{\Delta\theta}{e} \left\{ 1 - 2 \exp\left(-\frac{a\pi^2}{e^2} t\right) + 2 \exp\left(-\frac{4a\pi^2}{e^2} t\right) \right\} \quad (3)$$

$$\Sigma\varphi = \varphi_H + \varphi_C = 2\lambda \frac{\Delta\theta}{e} \left\{ 1 + 2 \exp\left(-\frac{4a\pi^2}{e^2} t\right) \right\} \quad (4)$$

For steady-state conditions:

$$\varphi_H = \varphi_C = \frac{\Sigma \varphi}{2} = \lambda \frac{\Delta \theta}{e} \quad (5)$$

Heat Transfer Measurements

After a verification of thermal equilibrium by observing the mean temperature, the temperature drop across the specimen, and the emf output of the heat flow transducers, the classic HFM test procedure consists of making observations at given time intervals until five successive observations yield a thermal resistance value agreeing to within 1% without changing monotonically in one direction.

One can see, by looking at the exponential terms of Eqs 2 to 5 that (within our assumptions): (1) φ_H and φ_C reach their final steady-state value *simultaneously*, and (2) $\Sigma \varphi$ reaches its final steady-state value *four times faster* than φ_H or φ_C . In other words, if one derives the thermal conductivity value from the sum of the outputs of the "hot" and "cold" heat flow transducers instead of from the individual outputs of each of them (as done classically), the measuring time can theoretically be reduced four times.

Initial Temperature Conditions

The foregoing equations are valid only if at time 0 the temperatures of the plates are constant and equal to their steady-state value. In practice, opening the HFM apparatus to change the test specimen is responsible for variations in plate temperatures. In general, for a mean test temperature of 24°C, at each opening, the plate temperature decreases on the hot side and increases (to a lesser extent) on the cold side.

The time needed to reach the final steady-state values varies with the sample and penalizes the total measuring time. To avoid this problem, we designed a system (see below) that minimizes the hot plate temperature variations at each opening. In what follows, we will present results of measurements performed without (1st series) and with (2nd series) this hot plate temperature control.

Measurements

Principle

The principle of our test method is based on the equations derived above. The test procedure is very similar to the classic procedure of the HFM method, the only difference being that the operator checks equilibrium by observing the sum of the emf outputs of the two heat flow transducers instead of the individual emf of a single one. In these tests, the calibration constants of the two heat flow transducers were very similar. This allowed us to add the emf values. If the calibration constants are different one may have to sum the calculated heat fluxes.

As explained previously, the sum ($\varphi_H + \varphi_C$) reaches its final steady-state value at time t_1 , before φ_H or φ_C (at time t_2). Therefore if we derive the thermal conductivity at time $t_1 < t_2$ from

$$\lambda = \frac{\varphi_H(t_1) + \varphi_C(t_1)}{2 \Delta T} \cdot e \quad (6)$$

we make a measurement before true steady state. Consequently, this method can be referred to as a "transient method", although it differs in principle from the classic transient measurements in which the temperature rise of one point of the tested sample due to a local sudden increase of electrical power is monitored as a function of time.

This is important, since some authors [5] have shown the problems raised by the use of transient methods for lightweight fiberglass insulation due to the simultaneous conduction and radiation transfer. The method proposed here eliminates these problems because we do not try to match a measured temperature rise with theory but simply use the fact that the sum ($\varphi_H + \varphi_C$) reaches its final steady-state value faster than either φ_H or φ_C .

Tested Products

We used our test method on seven different glass fiber products of various thicknesses and densities. Their characteristics are summarized in Table 1. Sample 6 was a loose-fill product, all others batts or panels. The values of thermal conductivity indicated in Table 1 were determined from standard measurements using only the hot side heat flow transducer.

In all the measurements presented hereafter we systematically compared the values of thermal conductivity derived in steady-state from Eq 5 (using the hot heat flow transducer output) and in non-steady-state from Eq 6. In all the cases studied, the two λ -values agreed with each other to within $\pm 1\%$, which is very satisfactory considering the limits of accuracy of the HFM method. In what follows the measured "transient values" are therefore not indicated, the emphasis being put on the possible reduction of measuring time.

First Series of Measurements

In this first series, we let the plate temperatures vary freely with each introduction of a sample and in some instances measured the corresponding temperature variation of the plates ($\Delta\theta$) as well as the time (Δt) needed to reach steady-state plate temperatures. The complete results are given in Table 2, which compares the time needed to reach steady-state values of φ_H , φ_C and $\Sigma\varphi$.

Analysis of the results of Table 2 indicates:

- A faster measuring time when monitoring φ_C instead of φ_H (Fig. 3)—this point is in apparent contradiction with theory (Eqs 2 and 3).
- A reduction of measuring time approximately equal to 15 min on all tested products when monitoring $\Sigma\varphi$ instead of φ_H (Fig. 4).
- A larger temperature perturbation on the hot plate than on the cold plate when introducing the specimen—this is due to a larger temperature difference between the sample and plate on the hot side ($\Delta\theta = 34 - 20 \approx 14^\circ\text{C}$) than on the cold side ($\Delta\theta = 20 - 14 \approx 6^\circ\text{C}$) (Fig. 5) and explains the observed differences between φ_H and φ_C for reaching steady state.

This first series of measurements showed clearly the influence of initial temperature conditions and led us to make a second series with more stable plate temperatures.

TABLE 1—Test specimens.

Specimen No.	Thickness (mm)	Density (kg/m ³)	Thermal Conductivity (W/mK)
1	50	53.2	0.032
2	50	25.4	0.0354
3	80	12.2	0.0439
4	120	11.4	0.045
5	160	11.4	0.046
6	140	8.7	0.0506
7	100	80	0.0356

TABLE 2—First series of measurements (no hot plate control).

Specimen No.	Time Needed (min) to Reach Steady-State Values of			Hot Plate		Cold Plate	
	φ_H	φ_C	$\Sigma\varphi$	$\Delta\theta$ (°C)	Δt (min)	$\Delta\theta$ (°C)	Δt (min)
1	44	32	28	-1.5	24	+1	6
2	30	22	18	-1.2	18	+0.7	8
3	30	NM ^a	15	NM	NM	NM	NM
4	35	NM	20	NM	NM	NM	NM
5	70	NM	45	NM	NM	NM	NM
6	40	NM	22	NM	NM	NM	NM
7	180	NM	NM	NM	NM	NM	NM

^aNM = Not Measured.

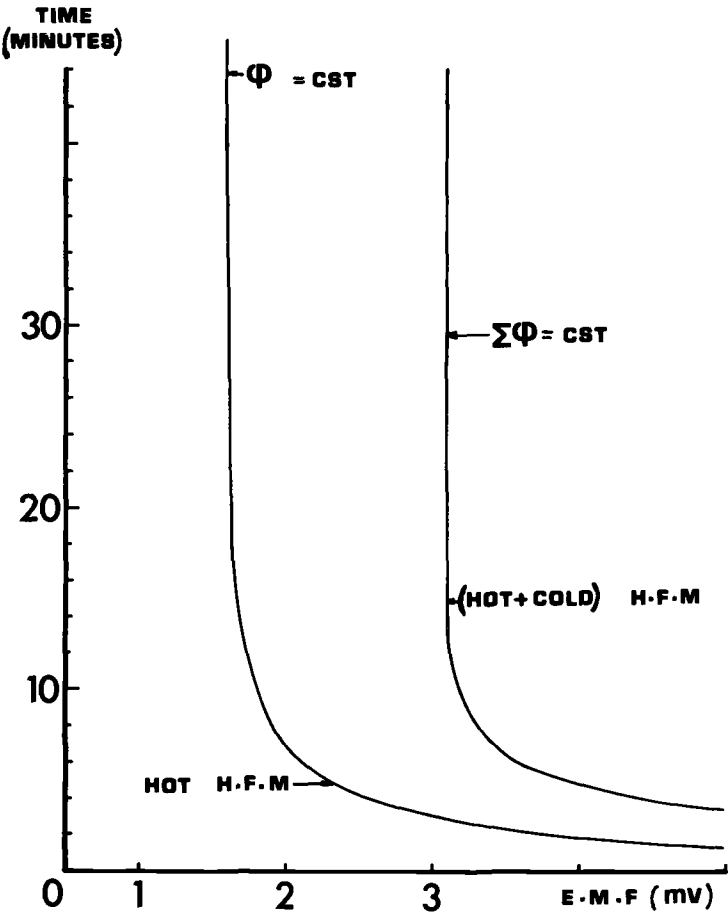


FIG. 4—Evolution of emf versus time for Sample 1 (first series of measurements).

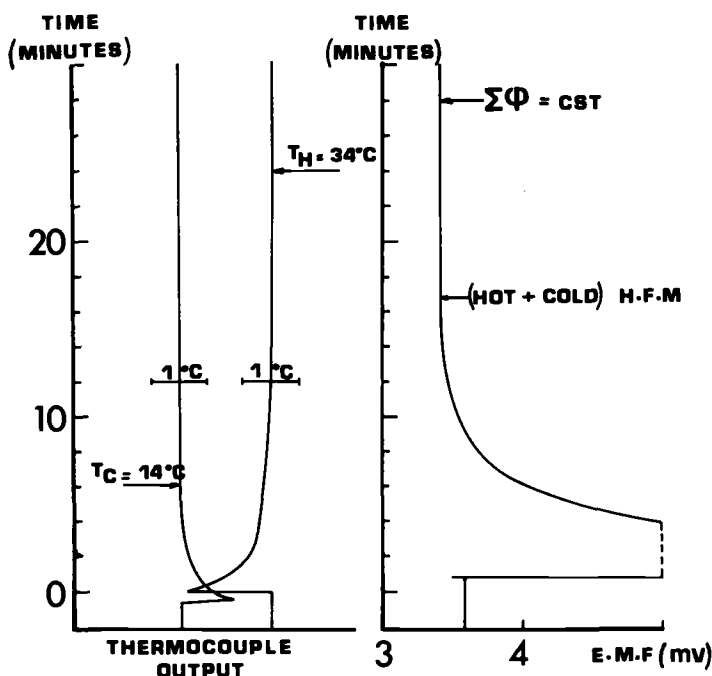


FIG. 5—Evolution of temperatures and emf versus time for Sample 1 (first series of measurements).

Second Series of Measurements

In this second series the hot plate was "overheated" at each opening of the apparatus. In order to do so without having to change the set point of the hot plate controller, we put an electrical resistance ($R = 12 \text{ k}\Omega$) in parallel with the control platinum resistance during each opening (Fig. 6).

This electrical circuit allows us to obtain an equivalent resistance about 1Ω lower than the platinum probe alone. Consequently, the controller "sees" a temperature 2 to 3°C lower than the set point and heats the plate. The whole system is operated by a simple switch, the only difficulty for the operator being to determine the time during which the plate must be overheated. This time is a function of the specimen and can be found by trial and error. One can see from Fig. 7 that the time needed to reach constant temperature plates is indeed decreased by this system (compare Fig. 5).

The complete set of results obtained from the samples is given in Table 3. The column labelled "Standard Measurement" (the second column from the right) gives the time needed to determine the thermal conductivity of the sample from φ_H only and with no "overheating" of the hot plate. Taking this measuring time as a reference value, Table 3 clearly shows the possible reduction in measuring time when monitoring $\Sigma\varphi$ instead of φ_H . As shown in Fig. 8, the slopes of the curves $\varphi = f(t)$ of the two heat flow transducers are identical but of opposite sign; this agrees with the heat transfer equations.

If we eliminate Sample 7, which is representative of a very seldom encountered product, the thermal conductivity measuring time is equal to 15 min or less, a reduction by a factor of 2 or more compared to "standard" measurements.

For a better illustration of this time reduction, we measured a series of eight samples (similar to Sample 1). The thermal conductivity data were obtained in 2 h elapsed time compared to the

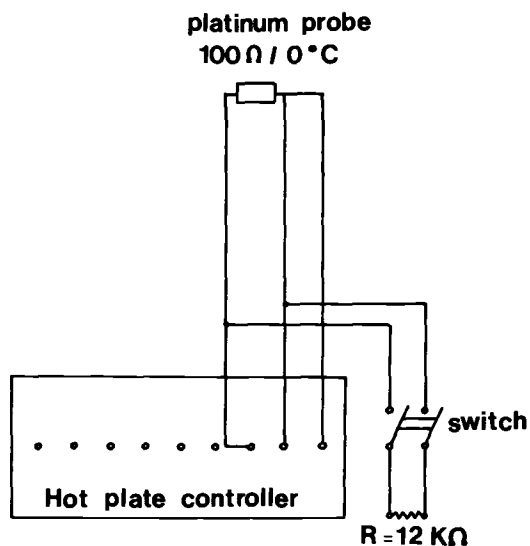


FIG. 6—Principle of hot plate temperature control (switch open: first series of measurements; switch closed: second series of measurements).

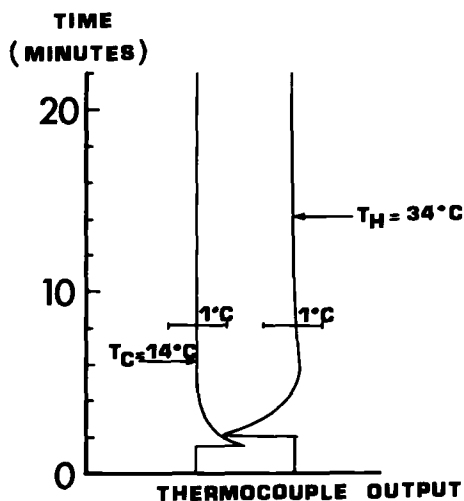


FIG. 7—Evolution of plate temperature when overheating hot plate for 15 s (Sample 2).

6 or 7 h usually needed. In this particular case, representative of quality control conditions, it was possible to fix the plate overheating time, since this time depends mainly on the type of tested product.

It is of interest to compare our experimental results with theory. From Eq 4, it can be seen that $\Sigma\varphi$ reaches its final value when

$$\exp\left(-\frac{4\lambda\pi^2}{\rho ce^2}t\right) \rightarrow 0$$

TABLE 3—*Second series of measurements (hot plate control).*

Specimen No.	Time Needed (min) to Reach Steady-State Values of			Measuring Time With "Standard" Measurement (min)	"Overheating" Time of Hot Plate (s)
	φ_H	φ_C	$\Sigma \varphi$		
1	32	32	12	44	55
2	8	30	15
3	10	30	15
4	12	35	22
5	12	70	48
6	12	40	20
7	60	180	15 min

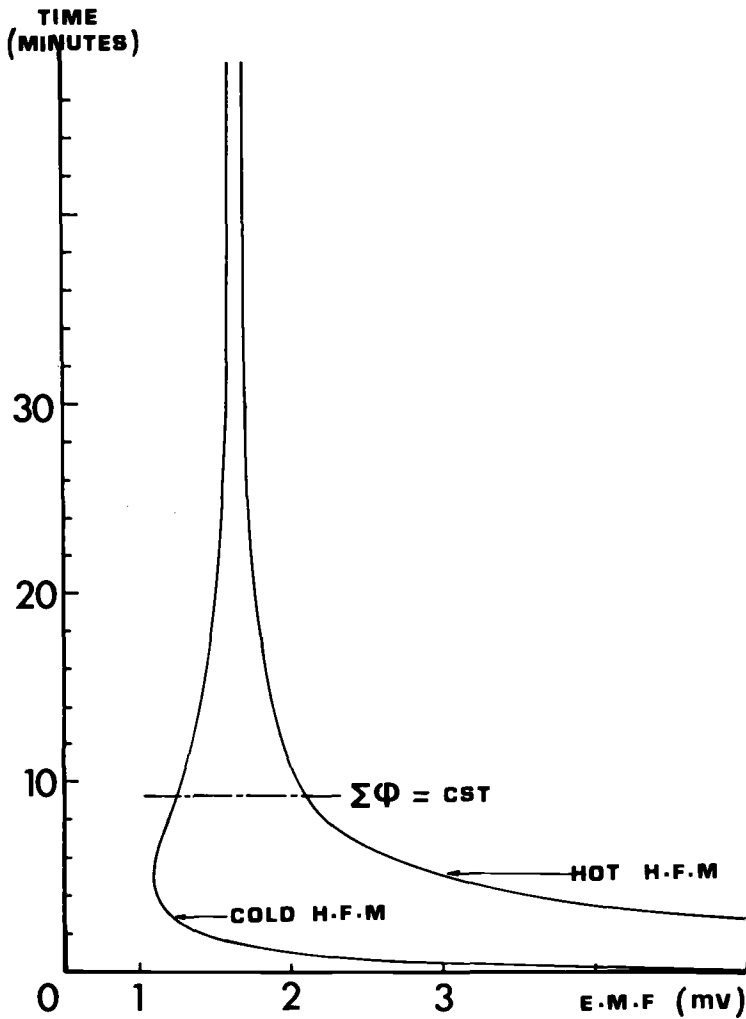


FIG. 8—*Evolution of emf versus time for Sample 1 (second series of measurements).*

In other words, measuring time increases when $\lambda/\rho e^2$ decreases. We therefore made computations of the exponential term for extreme and intermediate values of $\lambda/\rho e^2$ corresponding to Samples 7, 5, and 4. The results derived from Fig. 9 indicate approximate theoretical times for reaching steady state of 5 min for Sample 4, 15 min for Sample 5, and 60 min for Sample 7. These results are in relatively good agreement with our measurements.

Conclusions and Future Work

The results presented here can only be considered as preliminary. Additional measurements are needed for a further check of the accuracy and reproducibility of the proposed method. Despite the limited number of experimental data, we believe this method is very promising in terms of measuring time reduction. The purpose of this "early" paper is also to encourage other laboratories to investigate its possibilities.

The main advantage of our method is that it can be run on most existing single specimen apparatus once retrofitted by simply adding one heat flow transducer. The main drawback is the need to control the plate temperatures when introducing the samples in order to obtain a significant measuring time reduction.

The system of temperature control used here is somewhat difficult if one has to measure a large variety of samples but can be fixed when working on a given type of product. Another possibility may be the use of "liquid tanks" in place of electrically heated plates. Some authors [6] have reported good temperature stabilities simply by using liquid cooled and liquid heated plates well insulated on their peripheries. We plan to investigate this point in the future and also to make more systematic measurements on different types of insulating materials.

Finally, the possibility of monitoring the sum of the two heat flow transducer outputs as a function of time in order to derive thermal diffusivity will also be considered.

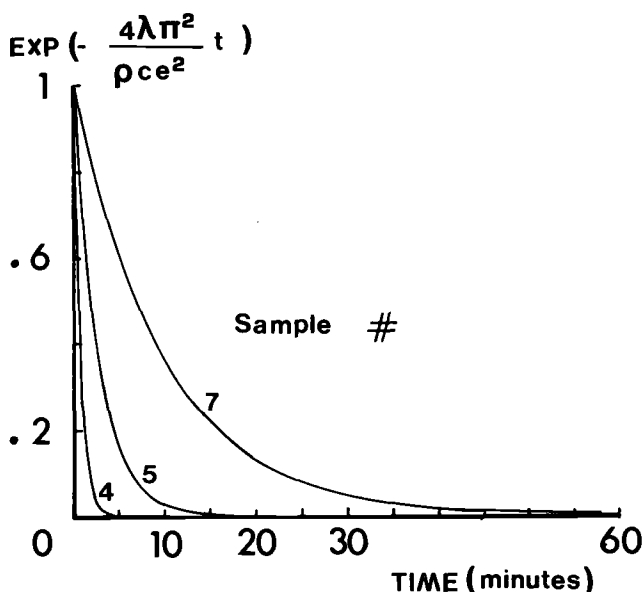


FIG. 9—Theoretical calculation of time required to reach steady state.

References

- [1] Devismes, J. M., "Conductivité et diffusivité thermiques simultanées par mesure de flux en régime non stationnaire," thèse de 3ème cycle, Université de Paris IV, Nov. 1973.
- [2] De Ponte, F. and Maccato, W., "The Calibration of Heat Flow Meters," in *Thermal Insulation Performance*, ASTM STP 718, American Society for Testing and Materials, Philadelphia, 1980, pp. 237-254.
- [3] Degenne, M. and Klarsfeld, S., "A New Type of Heat Flowmeter for Application and Study of Insulation and Systems," in *Building Applications of Heat Flux Transducers*, ASTM STP 885, American Society for Testing and Materials, Philadelphia, 1985, pp. 163-171.
- [4] De Ponte, F., Langlais, C., Boulant, J., and Klarsfeld, S., "Reference Guarded Hot Plate Apparatus for the Determination of Steady-State Thermal Transmission Properties in Agreement with the New International Standard ISO/DIS 8302," presented to 19th International Thermal Conductivity Conference, Cookeville, Tenn., Oct. 1985.
- [5] Tong, T. W., McElroy, D. L., and Yarbrough, D. W., "Transient Conduction and Radiation Heat Transfer in Porous Thermal Insulations," *Journal of Thermal Insulation*, Vol. 9, July 1985.
- [6] Centre Scientifique et Technique du Batiment, "Activités 1986," Cahiers du CSTB 2175-1, Sept. 1987, livraison 282.

Properties and Models

Modeling of Thermal Resistance Test Configurations That Use Thin Heaters

REFERENCE: Yarbrough, D. W., McElroy, D. L., and Graves, R. S., "Modeling of Thermal Resistance Test Configurations That Use Thin Heaters," *Insulation Materials, Testing, and Applications*, ASTM STP 1030, D. L. McElroy and J. F. Kimpflen, Eds., American Society for Testing and Materials, Philadelphia, 1990, pp. 525-536.

ABSTRACT: The usefulness of a large unguarded thin screen heater as an integral part of a thermal resistance measurement apparatus for insulations has been demonstrated. Thermal modeling of existing and proposed test configurations can be used to establish applicability. HEATING5, a general purpose conduction program, has been used to obtain the temperature distributions encountered in linear and radial heat flow testers with thin heaters.

Thermal simulations of the existing screen tester have been used to determine the effects of specimen thickness and thermal resistance on measurement errors. Simulation results were obtained for test configurations in order to provide a basis for design improvement (i.e., the effect of increasing levels of edge insulations on the apparent thermal conductivities obtained with the tester).

The extent to which limited edge guarding extends the operating range of a flat tester has been examined using HEATING5. A gradient guard along the edge of the specimen in the tester reduces the measurement errors due to edge heat loss. The improvement predicted by HEATING5 in measurement accuracy of a thin heater apparatus due to edge guarding that approximately matches the mean temperature on the edges with the mean temperature in the metering section has been examined experimentally.

KEY WORDS: thermal insulation, R-value, unguarded test, thin heater, edge loss, end loss, thermal modeling, thermal resistance, apparent thermal conductivity

The determination of material thermal resistances, R-values, for flat insulation specimens is routinely accomplished with guarded hot plates (ASTM C 177) and heat flux meters (ASTM C 518). The guarded hot plate (GHP) is referred to as an absolute method, since all the quantities needed to calculate apparent thermal conductivity, k_a , are directly measured. The heat flux meter (HFM), on the other hand, is comparative and requires calibration with a material of known k_a . In both cases the heat transfer process is assumed to be one-dimensional and k_a is obtained from Fourier's Law in rectangular coordinates.

A radial-heat-flow apparatus with end guards (ASTM C 335) is used to measure the thermal resistance of pipe insulation. If heat flows in the radial direction only, then k_a is obtained by applying Fourier's Law in cylindrical coordinates.

These three measurement techniques are based on one-dimensional heat flow equations, and ASTM C 177 and C 335 use guard heaters to reduce undesired heat flows. An "ideal" pipe insulation tester [1] or an "ideal" flat insulation tester could be realized with a very long radial-heat-flow measurement system or a very large rectangular system. For a sufficiently large separation between the "metering area" for a thermal measurement and test specimen ends or edges, one-dimensional heat flow can be realized. This idea combined with use of a thin heater

¹Building Materials Group, Metals and Ceramics Division, Oak Ridge National Laboratory, Oak Ridge, TN 37831.

of relatively low edgewise conductance led to the design and construction of a thermal measurement apparatus that uses an unguarded thin heater (Dynamic Insulation Efficiency Tester [DIET]). Figure 1 is a drawing of DIET.

DIET is used to measure the apparent thermal conductivity of 0.914 m (36 in.) by 1.524 m (60 in.) flat insulations having thicknesses from about 32 mm (1.25 in.) to about 165 mm (6.5 in.). The d-c powered Nichrome screen heat source is horizontally positioned between a pair of flat insulation specimens. Temperature-controlled copper plates positioned parallel to the screen heater are the cold boundaries for a thermal resistance measurement. The temperature difference that results in heat flow across the specimen is measured for a small central region of the rectangular test specimen. Figure 2 shows top and side views of the test section without support elements or external insulation. DIET can be used to measure k_a for a single flat specimen by matching the temperature of one bounding plate with the temperature of the central region of the screen. Test specimens smaller than 0.914 by 1.524 m have been tested by bordering the specimen with thermal insulation to cover the screen. The unguarded technique that is the basis for DIET has been discussed by Moore et al. [2]; the details of DIET have been presented by Graves et al. [3].

The validity of thermal resistance measurements obtained from DIET have been verified by results for identical specimens tested at the U.S. National Bureau of Standards (NBS). Thermal resistance measurements on NBS Standard Reference Material 1450 b by NBS and ORNL differ by less than 0.9%. A determinate error analysis [3] gives a 1.70% uncertainty for a 5°C temperature difference across a specimen and a 0.73% uncertainty when the temperature dif-

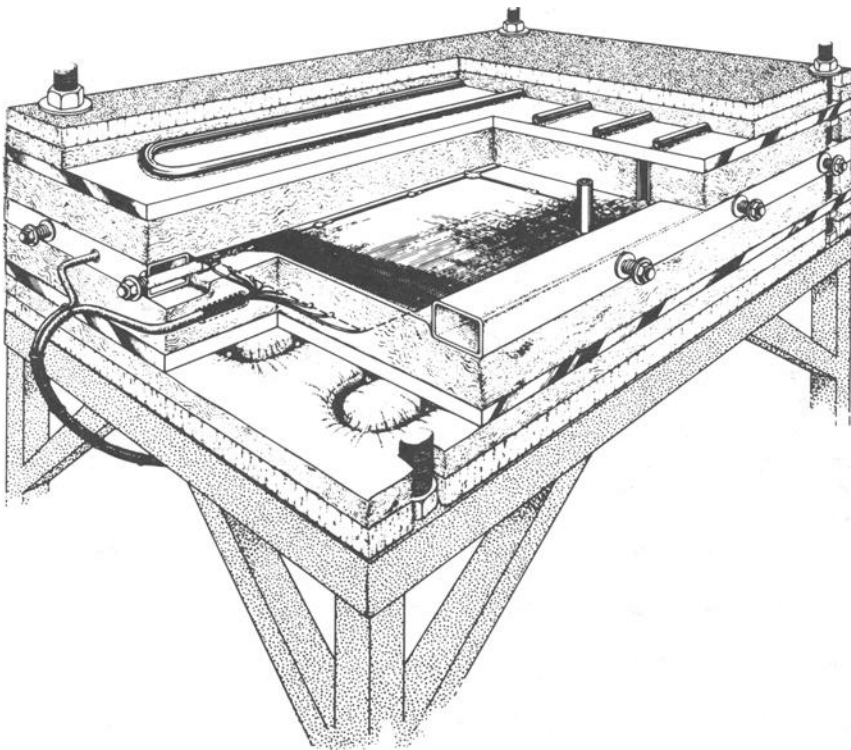


FIG. 1—Drawing of DIET, a thermal test apparatus that uses an unguarded heater made from Nichrome screen wire.

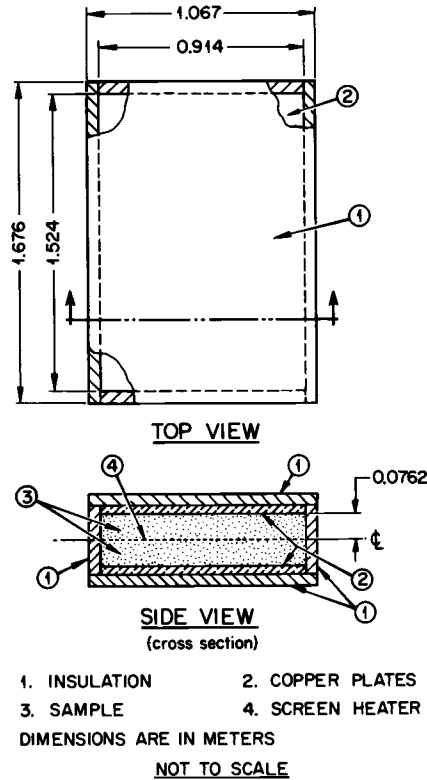


FIG. 2—Top and side views of thermal test section of DIET (dimensions in metres).

ference is 30°C. The corresponding most probable errors are 1.20% and 0.37%. In the absence of heat loss or gain from specimen edges DIET can provide accurate thermal resistance values.

Unguarded radial-heat-flow apparatuses that use thin walled tubular heaters have also been developed. The concept was discussed by Jury et al. [1]; specific apparatuses have been discussed by McElroy et al. [4] and Yarbrough et al. [5]. Figure 3 is a schematic of one of seven versions of this type of apparatus that have been used to measure the thermal resistance of fine powders. ORNL-4 is representative of the apparatuses that have been used.

Apparent thermal conductivities are obtained from either the longitudinal-heat-flow apparatus (DIET) or one of the radial-heat-flow apparatuses using a one-dimensional form of Fourier's Law:

$$k_a = Q \cdot \Delta x / A \cdot \Delta T \quad (\text{longitudinal}) \quad (1)$$

$$k_a = Q \cdot \ln(r_o/r_i) / 2\pi \Delta T \quad (\text{radial}) \quad (2)$$

In both cases k_a is proportional to the heat flow across a specimen and edge or end heat loss or gain affects Q . For the measurement systems analyzed, Q is taken to be equal to the d-c power dissipated in the heater, whereas the actual heat flux across the specimen can be changed by edge or end effects. If net edge or end heat losses are present, then $Q > Q_{\text{TRUE}}$ and the experimental value for k_a will be greater than the true value. Conversely, net edge or end heat gains will yield k_a values that are less than the true value. The experimental work done with DIET or

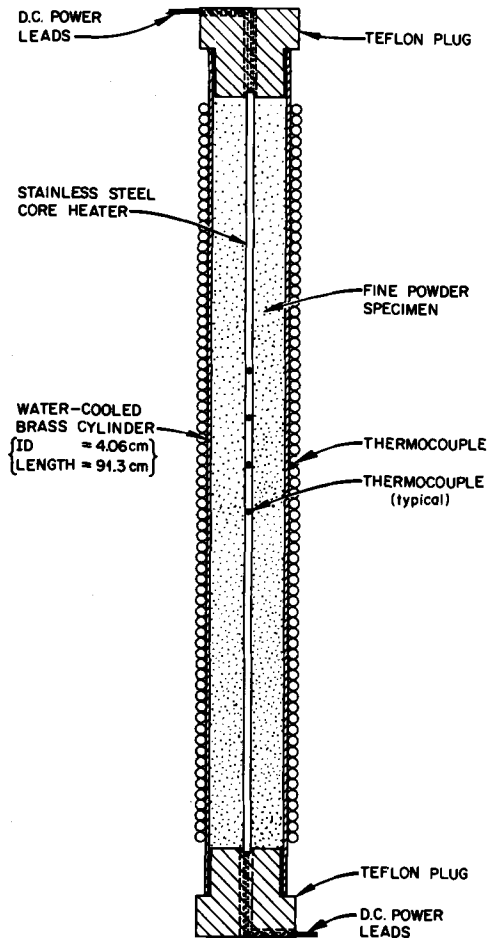


FIG. 3—Diagram of ORNL-4, an unguarded radial-heat-flow apparatus.

the radial-heat-flow equipment at ORNL has involved test specimen temperatures above the temperature of the surroundings and edge or end heat effects exist.

Thermal modeling can permit quantification of the edge or end heat loss effects. This is done by using mathematically generated temperature distributions obtained with known specimen properties and boundary conditions to calculate values for k_a using either Eq 1 or 2. The k_a calculated from a simulated temperature distribution can be compared with the k_a used to generate the temperature distribution and thus evaluate the one-dimensional heat flow assumption.

Modeling of Thermal Resistance Measurement Systems

Modeling of thermal resistance measurement systems has been done using a finite difference computer code entitled HEATING5 [6]. HEATING5 provides solutions for the heat conduction equation written for the geometry of interest and subject to user specified boundary conditions.

In the case of rectangular regions with constant k_a ; Eq 3 is solved for temperature with six boundary conditions specified for each rectangular region in the system:

$$\frac{\partial^2 T}{\partial x^2} + \frac{\partial^2 T}{\partial y^2} + \frac{\partial^2 T}{\partial z^2} = 0 \quad (3)$$

In the case of cylindrical regions with constant properties, no heat generation, and steady-state, the governing equation is

$$1/r(\partial/\partial r(r\partial T/\partial r)) + 1/r^2(\partial^2 T/\partial \theta^2) + \partial^2 T/\partial z^2 = 0 \quad (4)$$

Four boundary conditions must, in general, be specified for each cylindrical region of the system being modeled. The program input information includes the geometric definition of the regions in the system, the properties of the materials in each region, and heat generation or heat removal rates. The program can be used to analyze steady-state or dynamic heat transfer processes.

The present study was focused on the effect of three factors on the thermal test results obtained with either the longitudinal-heat-flow or radial-heat-flow apparatus. The effects of specimen thermal resistance, the thermal resistance of edge insulation, and the presence of specimen edge heaters have been studied.

Modeling of Radial-Heat-Flow Apparatuses

Figure 4 shows the ratio $k_a(\text{exp})/k_a(\text{true})$ for seven radial-heat-flow systems. The curves in Fig. 4 were calculated using HEATING5 results for configurations in which the cold boundary and the specimen ends are at the same temperature (Table 1). Temperature at the midpoint between the two ends will produce the most accurate $k_a(\text{exp})$ value; in this case, $k_a(\text{exp})$ is a

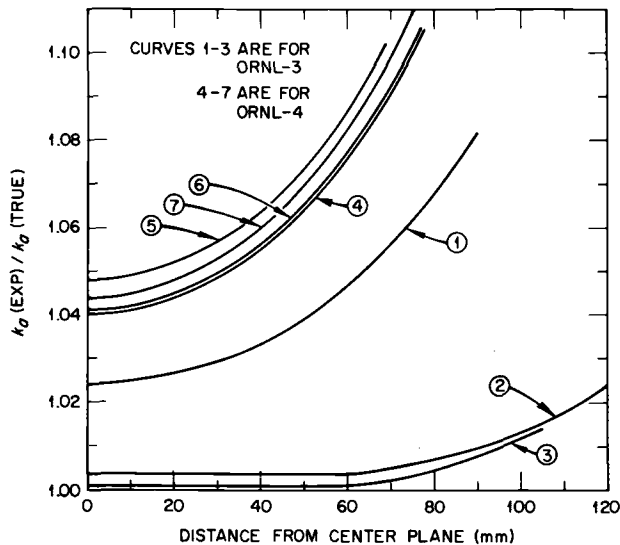


FIG. 4—Effect of end heat loss on experimentally determined k_a . The input data for the seven curves are given in Table 1.

TABLE 1—Physical property data input to HEATING5 to obtain the curves shown in Fig. 4.

Curve	Apparatus ^a	Thermal Conductivity, W/m · K		Maximum ΔT , K
		Sample	Heater End Plugs	
1	ORNL-3	0.007	...	17.50
2	ORNL-3	0.040	...	17.50
3	ORNL-3	0.040	...	3.06
4	ORNL-4	0.007	0.2	17.50
5	ORNL-4	0.007	0.4	35.00
6	ORNL-4	0.007	0.4	17.50
7	ORNL-4	0.007	0.2	35.00

^aORNL-3: Heater Tube, outer radius 2.62 mm; Specimen, outer radius 19.05 mm, half length 190.5 mm.

ORNL-4: Heater Tube, outer radius 3.05 mm; Specimen, outer radius 15.88 mm, half length 240 mm.

value calculated using HEATING5 results for the steady-state temperature distribution. End losses cause the ratio $k_a(\text{exp})/k_a(\text{true})$ to increase as the radial temperature difference decreases at locations displaced from the center.

Curves 1, 2, and 3 in Fig. 4 are for an apparatus identified as ORNL-3 that has a L/D value of about 10. Curves 2 and 3 are for a specimen with $k_a = 0.040$ W/m · K (R per inch = 3.6 ft² · h · °F/Btu), while Curve 1 is for a specimen with a $k_a = 0.007$ W/m · K (R per inch = 20.0 ft² · h · °F/Btu). These curves clearly show the shift in accuracy of the calculated k_a ($k_a(\text{exp})$) as the thermal resistance between the heater and cold boundary is increased.

The radial-heat-flow apparatus ORNL-3 was used to obtain k_a for powder specimens at reduced pressures. The end loss correction factor relationship shown in Fig. 5 was calculated for this apparatus. The factor C from Fig. 5 is multiplied by the k_a obtained from the one-dimensional heat flow equation (Eq 2) to correct for end loss.

Modeling of Longitudinal-Heat-Flow Apparatus

The longitudinal-heat-flow apparatus DIET has also been modeled using HEATING5. As in the case of the radial-heat-flow simulations results can be shown in terms of the ratio $k_a(\text{exp})/k_a(\text{true})$ which varies with the position in DIET where temperature difference is determined. The family of curves in Figure 6 shows the increasing effect of edge heat loss as test specimen thermal resistance increases. The vertical dashed lines in Figs. 6 and 7 locate the distance from the center for temperature measurements in DIET. For these results the HEATING5 calculations were done with a constant specimen thickness of 12.7 cm and a constant edge insulation thickness of 7.62 cm. The thermal resistance values were increased by decreasing the k_a values input to the computer program.

Figure 7 shows a family of curves for the ratio $k_a(\text{exp})/k_a(\text{true})$ versus position for increasing edge insulation thermal resistance. The results show that the ratio tends towards one as the edge insulation resistance increases, but that impractically large resistances are required to produce significant changes in the ratio.

A specimen edge heater can be used to reduce the temperature gradient perpendicular to the edge and thus reduce edge heat loss or gain. Figure 8 shows results of the thermal simulations of DIET with a heater along the entire specimen edge. The line in Fig. 8 shows that the error in the experimentally measured k_a due to edge loss can be significantly reduced by use of an edge heater. The figure also shows that overpowering of the edge heater can introduce an edge-gain error.

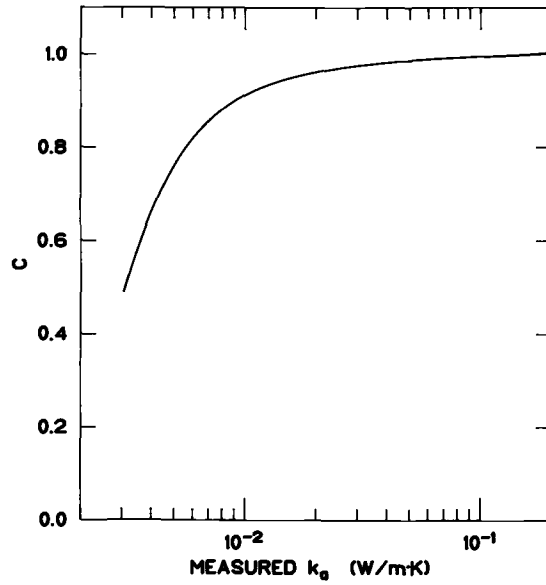


FIG. 5—Factor for the calculation of k_a (true) from k_a (measured) for ORNL-3; k_a (true) = $C \cdot k_a$ (measured).

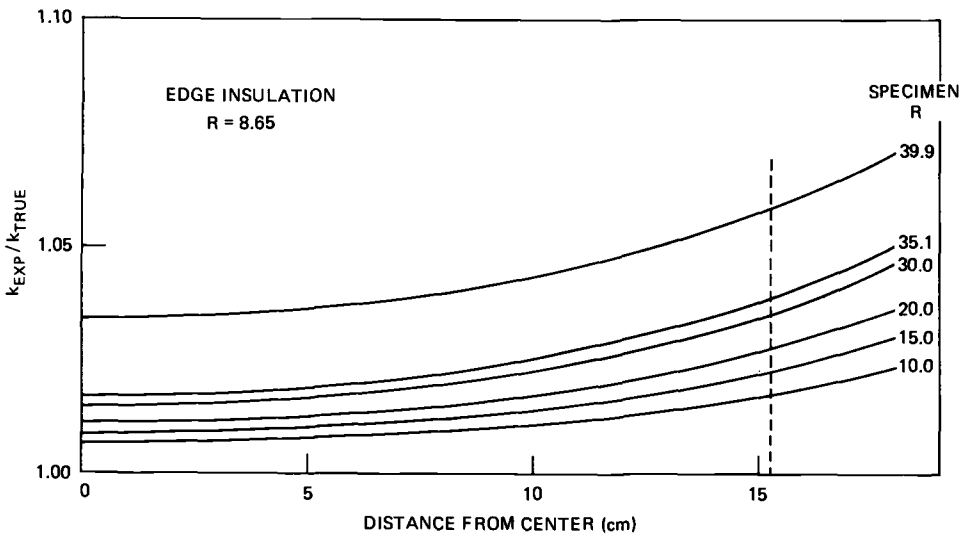


FIG. 6—Effect of specimen thermal resistance on the ratio k_{EXP}/k_{TRUE} for the longitudinal-heat-flow apparatus DIET.

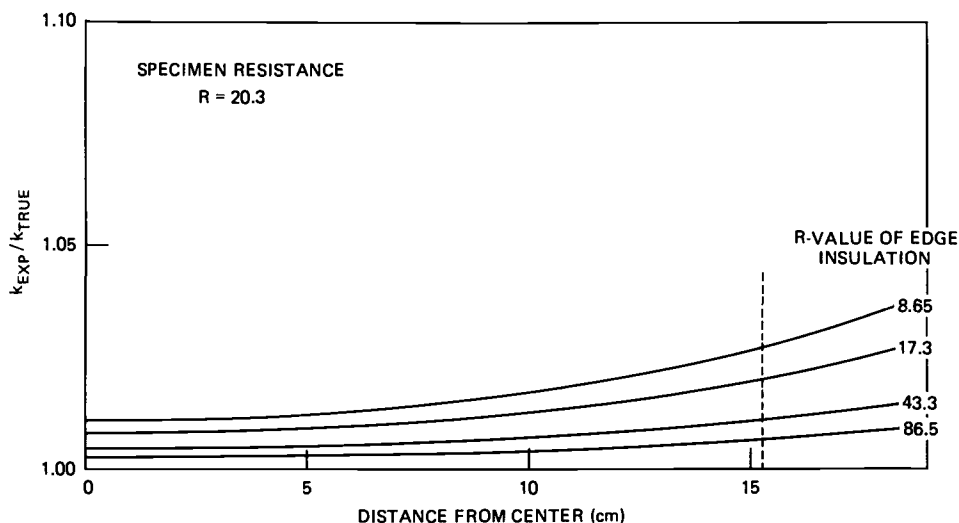


FIG. 7—Effect of edge insulation thermal resistance on the ratio $k(\text{exp})/k(\text{true})$ for the longitudinal-heat-flow apparatus DIET.

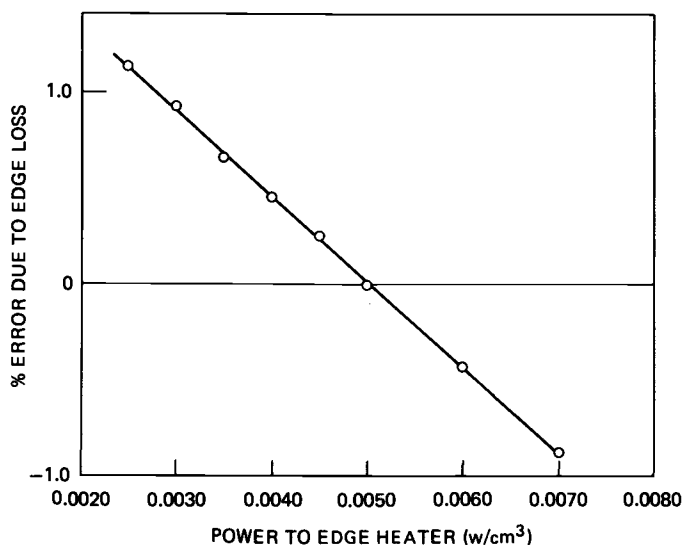


FIG. 8—Effect of a heater on the thermal test specimen edge as determined with HEATING5.

Figure 9 shows the percent error in k_a due to edge loss for a heater that covers part of the edge area. The simulations summarized in Fig. 9 are for an edge heater that is thermally connected to the cold plates. The effect of such an arrangement is a temperature profile along the edge of the test specimen that is an approximation of the temperature profile in the central part of the test specimen where temperature measurements are made. An exact match of these two temperature profiles would eliminate heat flow parallel to the screen and greatly reduce the error in the

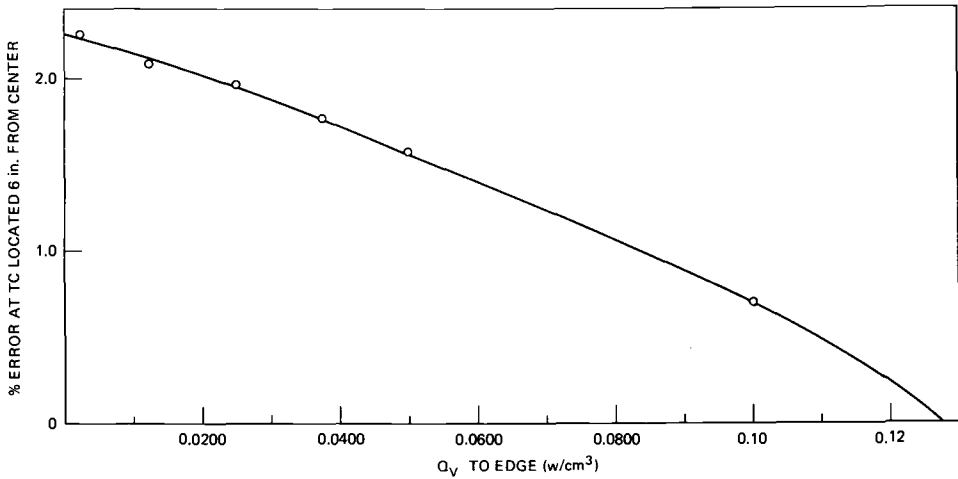


FIG. 9—Effect of a strip heater on the edge of a test specimen. The strip heater is attached to a stainless steel sheet that is bolted to the cold plates of DIET.

experimental k_a due to edge loss. The HEATING5 calculations show that a crude match between the two temperature profiles can significantly reduce the edge-loss effect.

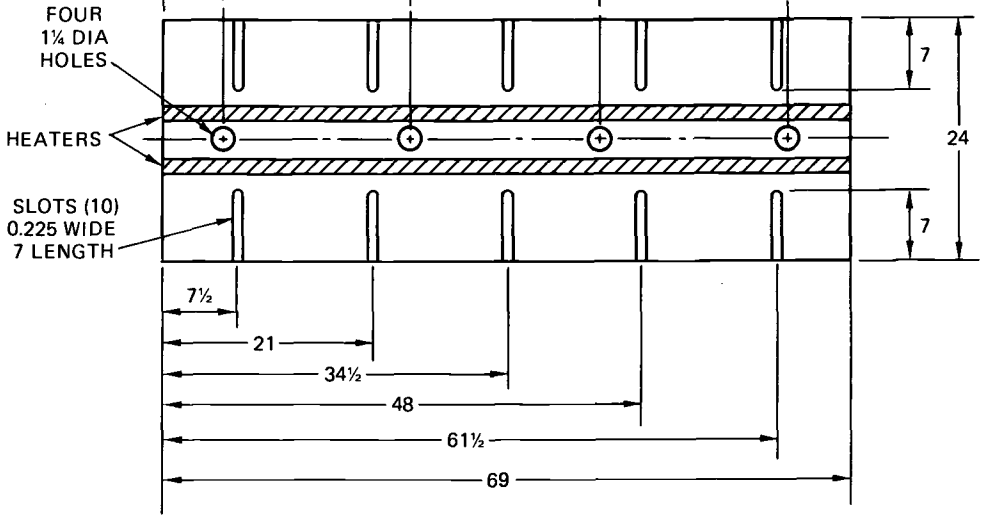
Experimental Study of Edge Heater Concept

The HEATING5 results shown in Fig. 9 were the motivation for a specimen edge heater design shown in Fig. 10. This edge heater consisted of four silicone rubber electrical resistance heaters bonded to a 1.59 mm (0.0625 in.) thick 304L stainless steel sheet at locations above and below the plane of the Nichrome screen heater. The stainless steel is attached to the temperature-controlled copper plates by bolts at ten locations. The steel is bolted to the copper plates at the slots, and this provides a way to accommodate test specimens of various thicknesses.

The objective of the experimental study was to compare an unguarded thermal resistance measurement for an insulation with thermal resistance near $7.05 \text{ m}^2 \cdot \text{K/W}$ ($40 \text{ ft}^2 \cdot \text{h} \cdot ^\circ\text{F/Btu}$) measured by DIET with the thermal resistance calculated from k_a and thickness where k_a was determined for test configurations with negligible edge loss. The introduction of the high R-value in a limited space required relatively high thermal resistance material. Fortunately, well-characterized isocyanurate foam boards were available to provide a high thermal resistance test specimen.

The k_a of isocyanurate insulation increases with time. The insulation used in the present study has been monitored for about 20 months and k_a as a function of age has been determined. Table 2 shows k_a as a function of age for isocyanurate boards with density of 33.6 kg/m^3 (2.1 lb/ft^3) and thickness of 48.3 mm (1.9 in.). These k_a data show a reduction in R-values from $1.28 \text{ m}^2 \cdot \text{K/W}$ for 25.4 mm ($7.25 \text{ ft}^2 \cdot \text{h} \cdot ^\circ\text{F/Btu}$ per inch) at age 103 days to $1.12 \text{ m}^2 \cdot \text{K/W}$ for 25.4 mm ($6.33 \text{ ft}^2 \cdot \text{h} \cdot ^\circ\text{F/Btu}$ per inch) at age 593 days. The rate of increase of k_a at age 593 days is much less than the initial rate of increase, but it is not zero. The test results used in the following analysis were obtained in time very close to the 593 day measurements.

A set of eight isocyanurate boards was milled flat to a thickness of about 40 mm (1.5 in.) to produce two stacks with thicknesses of about 158.8 mm (6.2 in.). Each stack of four milled boards was determined to have a thermal resistance of $6.78 \text{ m}^2 \cdot \text{K/W}$ ($38.5 \text{ ft}^2 \cdot \text{h} \cdot ^\circ\text{F/Btu}$) at 28.1°C (82.5°F) from k_a data. A two-sided DIET measurement of the thermal resistance of the stack with no edge heater in place yielded $6.70 \text{ m}^2 \cdot \text{K/W}$ ($38.1 \text{ ft}^2 \cdot \text{h} \cdot ^\circ\text{F/Btu}$) at 28.1°C



DIMENSIONS IN INCHES

FABRICATED FROM 1/16 INCH THICK STAINLESS STEEL

FIG. 10—Diagram of specimen edge heater used to reduce edge heat loss in DIET.

TABLE 2—Apparent thermal conductivity and thermal resistance at 23.9°C (75°F) for 33.6 kg/m³ (2.1 lb/ft³) isocyanate board as a function of age.

Age, days	k_a @ 23.9°C (75°F), W/m · K (Btu · in./ft ² · h · °F)	R per inch @ 23.9°C (75°F), ft ² · h · °F/Btu
103	0.0199 (0.1379)	7.25
155	0.0207 (0.1434)	6.97
327	0.0220 (0.1525)	6.56
469	0.0223 (0.1547)	6.46
593	0.0228 (0.1581)	6.33

(82.5°F). This measurement indicates an edge loss error in k_a of about 1.2%, less than the modeling prediction. These results indicate that the modeling provides a conservative estimate (upper bound) on the edge loss effect. This observation is of course limited to the configuration that was tested. Numerical results obtained with HEATING5 are dependent on the quality of the input data and the degree of correspondence between an actual apparatus and the model.

The measurement of the thermal resistance of the 158.8 mm thick stack of isocyanurate boards was repeated after the edge guard shown in Fig. 10 was installed along the long sides of DIET. The measured R-value was reduced to $6.68 \text{ m}^2 \cdot \text{K/W}$ ($37.9 \text{ ft}^2 \cdot \text{h} \cdot ^\circ\text{F/Btu}$) with no power applied to the edge heater. This small reduction in R-value from $6.70 \text{ m}^2 \cdot \text{K/W}$ to $6.68 \text{ m}^2 \cdot \text{K/W}$ ($37.9 \text{ ft}^2 \cdot \text{h} \cdot ^\circ\text{F/Btu}$) with no power applied is mostly likely attributable to a lowering

of the insulation edge temperature by the stainless steel guard connected to the cold boundaries.

Thermal measurements on the 158.8 mm thick stack were repeated with power applied to the edge heaters. Thermocouples installed on the edge guard permitted an evaluation of the temperature difference between the central region of the test specimen and the edge guard, $T(\text{guard})$. $T(\text{guard})$ was taken to be the average guard temperature, since a temperature gradient was present. Previous analysis [7] suggests that as these temperature differences tend to zero, the edge loss error will be greatly reduced. Results for a set of measurements at four edge heater power levels are shown in Table 3. The 0.1588 m (6.25 in.) thick specimen had a calculated thermal resistance of $6.78 \text{ m}^2 \cdot \text{K/W}$ ($38.5 \text{ ft}^2 \cdot \text{h} \cdot ^\circ\text{F/Btu}$) at 28.1°C (82.5°F) as determined from k_a obtained with 40 mm (1.5 in.) thick specimens. A thermal resistance measurement without an edge heater yielded $6.71 \text{ m}^2 \cdot \text{K/W}$ ($38.1 \text{ ft}^2 \cdot \text{h} \cdot ^\circ\text{F/Btu}$). The upper part of Table 3 shows the experimental R-value for the stack of isocyanurate boards as a function of the difference between the mean specimen temperature and the guard temperature. A least square fit to the four data points (Eq 5) shows a value for R of $6.78 \text{ m}^2 \cdot \text{K/W}$ ($38.5 \text{ ft}^2 \cdot \text{h} \cdot ^\circ\text{F/Btu}$) when the temperature difference is zero:

$$R(\text{m}^2 \cdot \text{K/W}) = 6.79 - 0.0266 (\bar{T}(\text{spec.}) - T(\text{guard}))^\circ\text{C} \quad (5a)$$

$$R(\text{ft}^2 \cdot \text{h} \cdot ^\circ\text{F/Btu}) = 38.5 - 0.0833 (\bar{T}(\text{spec.}) - T(\text{guard}))^\circ\text{F} \quad (5b)$$

The data in Table 3 further show that control of the temperature difference $\bar{T}(\text{specimen}) - T(\text{guard})$ to less than 2°C reduces the edge loss error in measured thermal resistance to less than 0.8%.

Summary

The thermal modeling of the radial-heat-flow thermal conductivity measurement apparatuses have shown that ORNL-3 with $L/D = 10$ can be used with specimens that have $k_a >$

TABLE 3—Thermal resistance measurements for a 0.1588 m (6.25 in.) thick isocyanurate specimen obtained with and without specimen edge heater.

Thermal Resistance Measured with Edge Heater (Guard) and Thermal Connection to Cold Plate		
$\bar{T}(\text{spec}) - T(\text{guard})$, °C (°F)		Experimental R-Value, $\text{m}^2 \cdot \text{K/W}$ ($\text{ft}^2 \cdot \text{h} \cdot ^\circ\text{F/Btu}$)
4.47 no power,	(8.05)	6.68 (37.9)
0.48	(0.86)	6.77 (38.4)
-4.86	(-8.75)	6.93 (39.3)
-10.45	(-18.81)	7.07 (40.1)
Percent Error in Experimental R-value Using $6.78 \text{ m}^2 \cdot \text{K/W}$ ($38.5 \text{ ft}^2 \cdot \text{h} \cdot ^\circ\text{F/Btu}$) as the "True" Value		
$\bar{T}(\text{spec}) - T(\text{guard})$, °C (°F)		% Error in R (Absolute Value)
-4	(-7.2)	1.6
-2	(-3.6)	0.8
0	(0.0)	0.0
2	(3.6)	0.8
4	(7.2)	1.6

$2.0 \times 10^{-2} \text{ W/m} \cdot \text{K}$ ($0.14 \text{ Btu} \cdot \text{in.}/\text{ft}^2 \cdot \text{h} \cdot ^\circ\text{F}$) to obtain a result with end-loss error of less than 5%. A radial-heat-flow apparatus with $L/D = 15$ can be used with specimens that have $k_a > 0.007 \text{ W/m} \cdot \text{K}$ ($0.05 \text{ ft}^2 \cdot \text{h} \cdot ^\circ\text{F}/\text{Btu}$) with end-loss error of less than 5%. In both cases the error due to end loss decreases as k_a of the test material becomes greater than the aforementioned limiting values.

Thermal modeling of DIET shows that thermal measurements on specimens up to a thermal resistance of $7.05 \text{ m}^2 \cdot \text{K}/\text{W}$ ($40 \text{ ft}^2 \cdot \text{h} \cdot ^\circ\text{F}/\text{Btu}$) with edge-loss error less than 5% can be achieved. A subsequent measurement with a specimen having a thermal resistance of $6.78 \text{ m}^2 \cdot \text{K}/\text{W}$ ($38.5 \text{ ft}^2 \cdot \text{h} \cdot ^\circ\text{F}/\text{Btu}$) yielded a value 1.2% less than the calculated value. This indicates that the modeling in this case provided a conservative estimate (upper bound) on the edge-loss effect.

HEATING5 calculations for DIET showed that increasing the thermal resistance of edge insulation reduces the edge loss effect, but that the amount of edge resistance required to make significant improvement may not be practical.

Thermal modeling showed that a heater along the edges of a test specimen can eliminate the edge-loss effect. Control of the edge heater to match the temperature of the guard to the mean specimen temperature reduced the edge-loss error to essentially zero. The test results that were obtained showed that controlling the difference between the mean specimen temperature and the guard temperature to 2°C reduced the edge-loss error of a $6.78 \text{ m}^2 \cdot \text{K}/\text{W}$ ($38.5 \text{ ft}^2 \cdot \text{h} \cdot ^\circ\text{F}/\text{Btu}$) specimen to less than 1%.

The analyses that have been presented show the value of an edge guard for testing of relatively high thermal resistance materials. It is recommended that edge guards be used in the testing of thick high thermal resistance specimens.

Acknowledgments

This research was sponsored by the Office of Buildings and Community Systems, Building Systems Division, U.S. Department of Energy, under Contract DE-AC05-84OR21400 with Martin Marietta Energy Systems, Inc.

References

- [1] Jury, S. H., McElroy, D. L., and Moore, J. P., "Pipe Insulation Testers," in *Thermal Transmission Measurements of Insulation*, ASTM STP 660, R. P. Tye, Ed., American Society for Testing and Materials, Philadelphia, 1978, pp. 310-326.
- [2] Moore, J. P., McElroy, D. L., and Jury, S. H., "A Technique for Measuring the Apparent Thermal Conductivity of Flat Insulations," ORNL/TM-6494, Oak Ridge National Laboratory, Oak Ridge, Tenn., 1979.
- [3] Graves, R. S., Yarbrough, D. W., and McElroy, D. L., "Apparent Thermal Conductivity Measurements by an Unguarded Technique," in *Thermal Conductivity 18*, T. Ashworth and D. R. Smith, Eds., Plenum Press, New York, 1985, pp. 339-355.
- [4] McElroy, D. L., Yarbrough, D. W., Copeland, G. L., Weaver, F. J., Graves, R. S., Tong, T. W., and Fine, H. A., "Development of Advanced Thermal Insulation for Appliances," ORNL/CON-159, Oak Ridge National Laboratory, Oak Ridge, Tenn., July 1984.
- [5] Yarbrough, D. W., Weaver, F. J., Graves, R. S., and McElroy, D. L., "Development of Advanced Thermal Insulation for Appliances, Progress Report for the period July 1984 through June 1985," ORNL/CON-199, Oak Ridge National Laboratory, Oak Ridge, Tenn., May 1986.
- [6] Turner, W. D., Elrod, D. L., and Siman-Tov, I. I., "HEATING5-An IBM 360 Heat Conduction Program," ORNL/CSD/TM-15, Oak Ridge National Laboratory, Oak Ridge, Tenn., March 1977 (HEATING: Heating Engineering And Transfer In Nine Geometries).
- [7] Bode, K. H., "Thermal Conductivity Measurements with the Plate Apparatus: Influence of the Guard Ring Width on the Accuracy of Measurements," in *Guarded Hot Plate and Heat Flow Meter Methodology*, ASTM STP 879, C. J. Shirliffe and R. P. Tye, Eds., American Society for Testing and Materials, Philadelphia, 1985, pp. 29-48.

Importance of Radiation in Transient Tests of Fibrous Insulations

REFERENCE: Thomas, J. R., Jr., "Importance of Radiation in Transient Tests of Fibrous Insulations," *Insulation Materials, Testing, and Applications, ASTM STP 1030*, D. L. McElroy and J. F. Kimpflen, Eds., American Society for Testing and Materials, Philadelphia, 1990, pp. 537-544.

ABSTRACT: Transient tests of fiberglass insulation were examined theoretically to determine effects of radiation heat transfer. It was found that radiation dominates the heat flow process during the first several minutes, and that waiting times on the order of 20 to 30 min are necessary to achieve results consistent with steady-state tests. This time could be reduced if samples are oven-dried before testing.

KEY WORDS: fiberglass, radiation, thermal conductivity, transient tests, insulation, moisture effects

Nomenclature

- c Heat capacity, J/(kg · K)
- I Radiation intensity, W/(m² · str)
- k Thermal conductivity, W/(m · K)
- ℓ Thickness of heating element, m
- p Scattering phase function
- \dot{q} Heat generation rate, W/m³
- q_r^- Radiative heat flux striking the heating element, W/m²
- t Time, s
- T Insulation temperature, K
- T_h Heating element temperature, K
- x Distance into insulation from heater, m

Greek Symbols

- α_h Radiation absorptivity of heater
- ϵ_h Emissivity of heater
- κ Radiation absorption coefficient, m⁻¹
- μ Direction cosine
- σ Stefan-Boltzmann constant, 5.669×10^{-8} W/(m² · K⁴)
- σ_s Radiation scattering coefficient, m⁻¹
- σ_e Extinction coefficient, $\sigma_s + \kappa$
- ρ_h Density of screen, kg/m³
- ρ_p Density of sample, kg/m³

¹Professor, Virginia Polytechnic Institute and State University, Blacksburg, VA 24061.

Introduction

The thermal resistance of insulation materials has traditionally been established with steady-state tests [1]. This is a reliable method, but has the disadvantage of requiring a considerable time investment to ensure that steady-state conditions are achieved in each test. Recently, transient methods have been introduced [2,3]. Although these methods appear attractive from the point of view of saving time, these methods raise some interesting and important questions relative to the analysis and interpretation of the resulting data. In particular, the role of radiation in such tests is not completely understood. Presumably, in this type of test the thermal properties of interest will be inferred from measurements made during the early phases of the transient. Since radiation propagates at the speed of light, will it dominate the early phases of a transient test, thereby leading to incorrect results for the thermal resistance of the insulation? How long must an experimenter wait to ensure that correct results are obtained? How important is the temperature dependence of specific heat? What is the effect of evaporation of entrained moisture as a specimen is heated?

The work reported here represents an attempt to answer these questions through development and use of an accurate theoretical model of unsteady heat transfer in fibrous insulations. The principal objective was to clarify the role of radiation in transient tests. The effects of temperature changes on the specific heat and effects of moisture removal were also investigated in trying to improve agreement between the predictions of the model and experimental data.

Theoretical Model

Theoretical modeling of combined radiation and conduction heat transfer in fibrous insulations is complicated by the coupling between the two modes and the anisotropic scattering of radiation by glass fibers. The coupling is caused by absorption and re-emission of thermal radiation, and leads to a highly nonlinear problem. Since a detailed description of the model used in this work is available elsewhere [4,5], only a summary will be given here. The system to be modeled is shown in Fig. 1. It consists of a thin heating element (hot boundary), the layer of insulation to be tested, and a thick, water-cooled, cold boundary which enforces isothermal conditions at the top of the specimen. Electrical current passing through the heating element produces energy generation by resistance heating at the rate \dot{q} , and the element loses heat to the

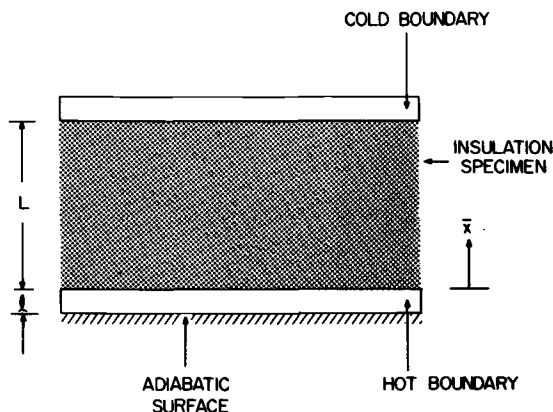


FIG. 1—System geometry.

insulation specimen by conduction and radiation, and receives heat from the specimen by radiation. Assuming a lumped capacitance model for the heating element leads to the equation [6]

$$\rho_h c_h \ell \frac{dT_h}{dt} = \dot{q} \ell + k \left. \frac{\partial T}{\partial x} \right|_{x=0} - \epsilon_h \sigma T_h^4 + \alpha_h q_r \quad (1)$$

The equation describing the temperature field in the presence of radiation is [7]

$$k \frac{\partial^2 T}{\partial x^2} - \frac{\partial q_r}{\partial x} = \rho_p C_p \frac{\partial T}{\partial t} \quad (2)$$

The radiative flux q_r is related to the radiation intensity $I(x, \mu)$ through the definition [7]

$$q_r(x, t) = 2\pi \int_{-1}^1 I(x, \mu) \mu d\mu \quad (3)$$

Finally, the radiation intensity must be obtained by solving the equation of radiative transfer [7]:

$$\mu \frac{\partial}{\partial x} I(x, \mu) + \sigma_e I(x, \mu) = \frac{\sigma_s}{2} \int_{-1}^1 p(\mu, \mu') I(x, \mu') d\mu' + \kappa \frac{\sigma}{\pi} T^4(x, t)$$

The symbols used in Eqs 1 to 4 are defined in the Nomenclature section. It is clear that Eqs 2 and 4 are coupled nonlinearly and must be solved simultaneously. They are also coupled to Eq 1 through the boundary conditions. The boundary conditions used for Eq 4 include emission of radiation from the boundaries and diffuse and specular reflection [4, 5].

Solution

The radiative transfer equation is solved by a high-order P_N method [8]; the energy equation is solved by the implicit finite difference technique. In the P_N method, the angular dependence of the radiation intensity is expanded in Legendre polynomials to degree N , and a set of ordinary differential equations are generated for the x -dependent expansion coefficients. The reader is referred to Ref 4 for details of the solution procedure, including a novel method for handling the coupling between the two equations.

Temperature dependence of the specific heat was modeled through a linear fit for dry fiberglass given by Hust et al. [9]:

$$C_p = 351.5 + 1.6376 T \quad (5)$$

and a correlation for moist samples deduced by McElroy [10] from the data of Hust et al. [9]:

$$C_p = -145 + 3.5 T \quad (6)$$

In these expressions T in Kelvin yields the specific heat in J/kg/K.

Results and Discussion

A typical experiment begins with the system in thermal equilibrium at temperature T_i . The current to the heating element is switched on, and the temperature of the element begins to

increase. This temperature is then recorded at intervals of 30 s until a new equilibrium is achieved, usually in about 1 h. Thus a set of data to be analyzed consists of a temperature history, along with known power input to the heater. Six data sets of this type for SRM 1451 low-density fiberglass were supplied to the author from experiments performed at the Oak Ridge National Laboratory (ORNL) [2]. The computer program based on the model described above predicts the screen temperature at the experimental points. Data for the thermal properties of SRM 1451 were taken from the report of Tong [6]; radiative property data were obtained from Schuetz [11].

Comparison between the data and the prediction of the model for a typical case is shown in Fig. 2, where Eq 6 is used for the temperature dependence of C_p . Using this correlation, agreement between model and experiment was achieved to within 1.2°C for all data points in all six data sets. When Eq 5 is used, the results shown in Fig. 3 are obtained. Since the predicted temperatures are so much in error, there is a clear suggestion that entrained moisture was a significant factor in the ORNL experiments. However, when this moisture is accounted for through Eq 6, the model is apparently sufficiently accurate to use as a tool to study the importance of radiation in these experiments. Note that accounting for the evaporation of moisture by modifying the specific heat term is not an exact treatment; the effect of moisture migration and vaporization should be modeled in a more fundamental way. This work is reserved for a future study.

It is important to realize that the relative contribution of radiative heat flow varies across the thickness of the insulation sample. Even in a steady-state test, the relative importance of radiation and conduction is different at every point, since the temperature profile is not linear in the presence of radiation. In the discussion which follows, the conductive heat flux is defined as the total temperature difference across the sample multiplied by the volume-weighted conductivity of insulation ($0.028 \text{ W}/(\text{m} \cdot \text{K})$) [6] divided by the sample thickness. For consistency, the radiative heat transfer reported is that at the midpoint of the sample.

To establish the maximum possible radiative heat transfer, it is instructive to calculate the radiative heat flux which would occur in a vacuum (or air) between the heating element and the cold boundary. Using emissivities of 0.75 for both surfaces and elementary equations for radiative transfer between parallel plates in vacuum [12], we find the radiative flux to be $107 \text{ W}/\text{m}^2$

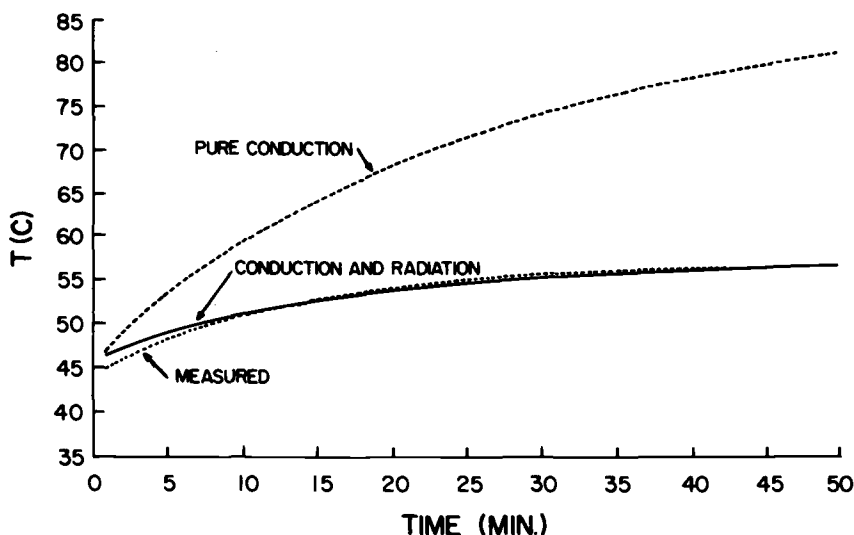


FIG. 2—Comparison of measured and calculated screen temperatures; C_p from Eq 6 (moist fibers).

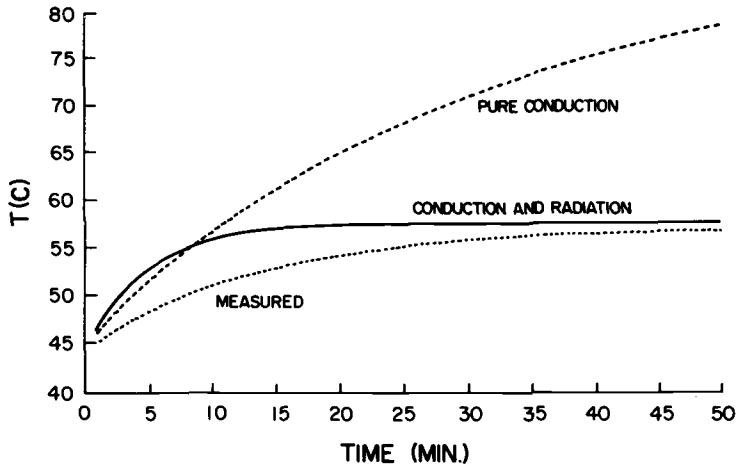


FIG. 3—Comparison of measured and calculated screen temperatures; C_p from Eq 5 (dry fibers).

for hot and cold boundary temperatures of 55°C and 30°C , respectively, which are typical final equilibrium temperatures for these experiments. The actual equilibrium values of the radiative and conductive heat fluxes for the six data sets provided by ORNL, computed from Eqs 1 to 4, are given in Table 1. The actual radiative heat transfer is less than 5% of the maximum possible, yet still accounts for about 40% of the total heat transfer. Thus a principal effect of insulation is the suppression of radiation.

The apparent thermal conductivity is defined as the value of the conductivity necessary to produce the actual total heat flux by conduction alone:

$$k = QL/\Delta T \quad (7)$$

This is the thermal conductivity which would be deduced from an experiment of the type modeled here. We are interested in the time dependence of the apparent conductivity. In particular, we would like to know how long after the beginning of the transient the measured conductivity is the same, within experimental uncertainty, as that which would be measured in a steady-state test. For purposes of comparison, the apparent conductivity for the final equilibrium state of each of the six ORNL experiments is given in Table 2. The temperature shown is the mean temperature of the insulation specimen. Note that the apparent conductivities are all substantially higher than the volume-averaged conductivity of $0.028 \text{ W}/(\text{m} \cdot \text{K})$ for SRM 1451.

TABLE 1—Steady-state radiation and conduction heat transfer for the equilibrium state of the ORNL data.

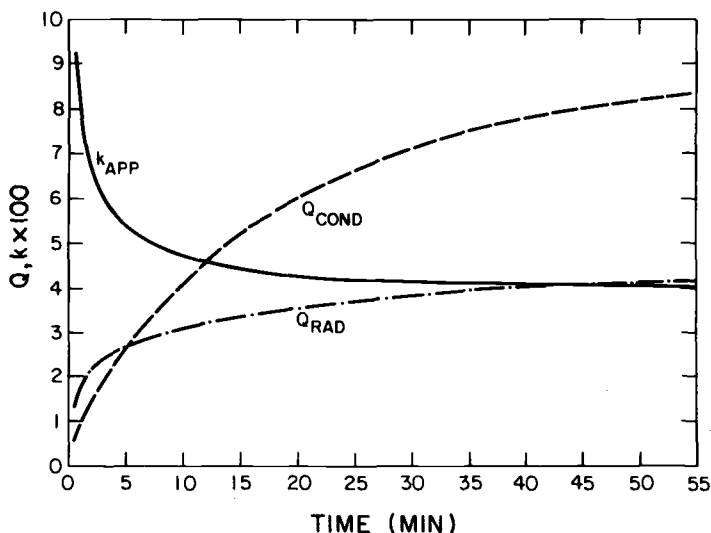
ΔT , $^{\circ}\text{C}$	T_H , $^{\circ}\text{C}$	T_c , $^{\circ}\text{C}$	Q_{rad} , W/m^2	Q_{cond} , W/m^2	Rad. Frac.	Exp. No.
11.9	37.4	25.5	2.32	4.45	0.34	F2
12.1	57.3	45.2	3.62	4.70	0.43	F5
13.8	59.1	45.3	3.97	5.29	0.43	F6
18.4	54.6	36.2	4.65	7.19	0.39	F4
18.6	54.9	36.3	4.63	7.34	0.39	F3
21.5	48.3	26.8	4.23	8.34	0.34	F1

TABLE 2—Steady-state values of apparent conductivity for the equilibrium state of the ORNL data.

ΔT , °C	Apparent Conductivity, W/(m · K)	Experiment No.
31.4	0.040	F2
36.9	0.041	F1
45.0	0.045	F3
45.6	0.043	F4
50.8	0.051	F5
51.7	0.049	F6

The effect of radiation on the transient heat flow can be deduced from Figs. 4 and 5. Shown in these figures are the radiative and total heat fluxes and the apparent conductivity computed from the simulation of the first experiment (data set F1). It is seen that the radiative flux exceeds the conductive flux for the first 5 min of the transient. The apparent conductivity is significantly different from the equilibrium value for the first 15 or 20 min of the test; it is within 5% of the equilibrium value after about 20 min.

The same quantities are plotted in Fig. 5, except here the calculation used the correlation given in Eq 6 for specific heat of dry SRM 1451. Clearly, the apparent conductivity reaches its equilibrium value within the first 5 min of the test. However, this simulation produced screen temperatures considerably in excess of the measured values, as seen in Fig. 3, so the plotted values for the radiative flux and apparent conductivity cannot be considered correct for this experiment. What these results do suggest, however, is that if the insulation sample is perfectly dry, a transient test can yield results equal to those from a steady-state test in a very short time.

FIG. 4—Time dependence of heat flow: C_p from Eq 5 (moist fibers).

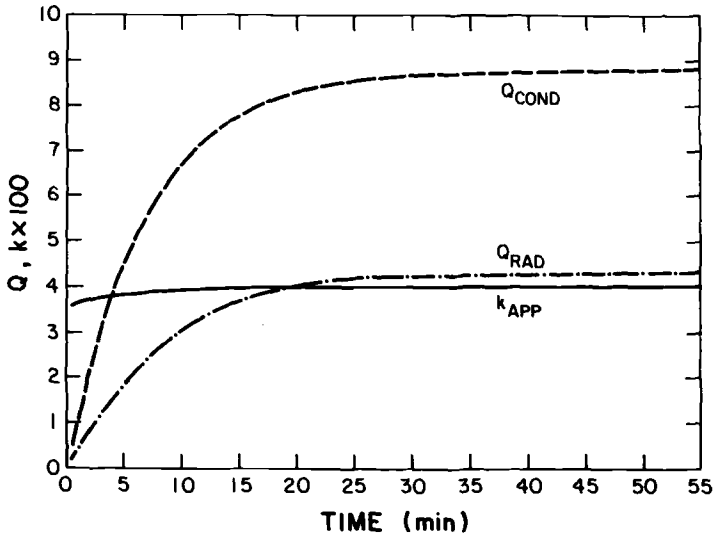


FIG. 5—Time dependence of heat flow; C_p from Eq 6 (dry fibers).

Conclusions

We may conclude from the predictions of the model discussed here that:

1. Radiation accounts for 30 to 40% of the total heat flow under steady conditions in low-density fiberglass insulation at temperatures in the range of 30 to 50°C.
2. Radiation is the dominant heat flow mode during the first few minutes of a transient test, and waiting times on the order of 20 min are necessary to obtain results equivalent to those obtained in steady-state tests.
3. Entrained moisture can substantially alter the results of a transient test during the first 30 min, and oven-drying samples to be tested could reduce the waiting time to 10 to 15 min for accurate results.

Acknowledgments

This research was sponsored by the U.S. Department of Energy as part of the National Program for Building Thermal Envelope Systems and Materials.

References

- [1] Fine, H. A., Jury, S. H., Yarbrough, D. W., and McElroy, D. L., "Analysis of Heat Transfer in Building Thermal Insulation," ORNL/TM-7481, Oak Ridge National Laboratory, Dec. 1980.
- [2] Yarbrough, D. W., McElroy, D. L., Tong, T. W., and Wood, J. K., III, "Analysis of Transient Thermal Measurements on Fibrous Insulations Obtained with an Unguarded Flat Tester," in *Proceedings*, 4th International Chemical Engineering Conference (CHEMPOR '85), Coimbra, Portugal, 1985.
- [3] Bae, S. C., "Transient Measurements of Insulation Materials," in *Proceedings*, 20th International Thermal Conductivity Conference, Blacksburg, Va., Oct. 1987.
- [4] Thomas, J. R., Jr., "Calculational Model Development for Fibrous Thermal Insulation Transient Test Procedures," ORNL/SUB-27494/1, Oak Ridge National Laboratory, 1988.
- [5] Thomas, J. R., Jr., "Modeling of Transient Tests of Combined Conductive and Radiative Heat Transfer in Fiberglass Insulations," in *Proceedings*, 20th International Thermal Conductivity Conference, Blacksburg, Va., Oct. 1987.

- [6] Tong, T. W., "Analysis of Transient Behavior and Radiation Measurements of Commercial Thermal Insulation," ORNL/SUB/83-43366/1, Oak Ridge National Laboratory, 1985.
- [7] Ozisik, M. N., *Radiative Transfer*, Wiley, New York, 1973, pp. 452-458.
- [8] Benassi, M., Cotta, R. M., and Siewert, C. E., "The P_N Method for Radiative Transfer Problems with Reflective Boundary Conditions," *Journal of Quantitative Spectroscopy and Radiative Transfer*, Vol. 30, 1983, p. 547.
- [9] Hust, J. G., Callahan, J. E., and Sullivan, S. A., "Specific Heat of Insulations," in *Thermal Conductivity*, Vol. 19 (in press).
- [10] McElroy, D. L., ORNL, private communication.
- [11] Schuetz, M. S., "Heat Transfer in Foam Insulation," M.S. thesis, Massachusetts Institute of Technology, Cambridge, 1982.
- [12] Incropera, F. P. and DeWitt, D. P., *Fundamentals of Heat and Mass Transfer*, 2nd ed., Wiley, New York, 1985, p. 646.

Transient Coupled Conduction and Radiation Heat Transfer Through Ceiling Fiberglass/Gypsum Board Composite

REFERENCE: Yeh, H. Y. and Roux, J. A., "Transient Coupled Conduction and Radiation Heat Transfer Through Ceiling Fiberglass/Gypsum Board Composite," *Insulation Materials, Testing, and Applications, ASTM STP 1030*, D. L. McElroy and J. F. Kimpflen, Eds., American Society for Testing and Materials, Philadelphia, 1990, pp. 545-560.

ABSTRACT: The heat transfer phenomenon in a fiberglass insulation and gypsum board (sheet-rock) composite was investigated numerically. Heat transfer through the fiberglass insulation was taken to occur by coupled conduction and volumetric radiation. The fiberglass insulation was considered as a radiatively absorbing, emitting, and scattering medium. Heat transfer within the gypsum board was taken to be by conduction only. Measured (transient) temperatures at the top of the fiberglass insulation and on the bottom of the gypsum board were used as boundary condition information in obtaining a numerical solution. These temperatures were measured in a residential attic for summer and winter climatic conditions. For purposes of minimizing heat loss in winter and heat gain in summer, two different configurations of fiberglass insulation were studied. One configuration was a standard R-19 [15 cm (6 in.) thick] fiberglass batt; the other configuration was a standard R-19 fiberglass batt with a foil radiant barrier installed on top of the insulation. It was found that the batt with the foil radiant barrier reduced the heat gain in summer by about 45% and reduced the heat loss in winter by about 13%.

KEY WORDS: transient heat transfer, fiberglass, attic, radiation, conduction, insulation

Nomenclature

- A_l l th coefficient of phase function Φ
- a_l l th Gaussian quadrature weight
- C_{pf} Specific heat of fiberglass
- C_{ps} Specific heat of gypsum board (sheetrock)
- I Radiative intensity, $W/m^2\text{-sr}$
- I_i Incident intensity
- k_f Thermal conductivity of fiberglass insulation, $W/m\text{-K}$
- k_s Thermal conductivity of gypsum board (sheetrock), $W/m\text{-K}$
- n Refractive index
- L Highest order of P_l as used in Eq 3
- M Number of Gaussian quadrature points
- P_l Legendre polynomial of l th order
- q Total heat flux, W/m^2
- q_c Conduction component of q
- q_r Radiation component of q
- T Temperature, K
- T_a Attic air temperature

¹University of Mississippi, University, MS 38677. Dr. Yeh is currently with EMRO, ITRI, Taiwan.

T_c	Ceiling temperature
T_i	Room air temperature
T_o	Fiberglass top temperature
T_r	Roof temperature
T_s	Fiberglass substrate temperature
t	Time, s
y	Spatial coordinate, cm
β	Extinction coefficient, $\sigma + \kappa$, cm^{-1}
γ_f	Fiberglass bulk density, kg/m^3
γ_s	Gypsum board (sheetrock) density, kg/m^3
ϵ	Emissivity
θ	Polar angle
λ_j	j th eigenvalue
μ	$\cos \theta$
μ_ℓ	ℓ th Gaussian quadrature point
ρ	Reflectivity
ρ_n	Reflectivity of fiberglass side of top interface
ρ_p	Reflectivity of air side of top interface
ρ_s	Specular reflectivity of substrate
τ	Local optical thickness, βy
τ_o	Total optical thickness
ω	Albedo

Introduction

Heat transfer in fibrous insulation materials has been theoretically and experimentally investigated by several authors [1-8], but none of these works have been done on the actual transient physical model. Recently Rish [9] numerically investigated heat transfer phenomena for a layer of attic fiberglass insulation; however, he did not include the ceiling board (gypsum board) in his study. It is more realistic to include both the gypsum board and the fiberglass insulation in an attic heat transfer investigation. The heat transfer problem studied in this work utilized temperature data [10] recorded in an actual Oxford, Mississippi, home.

Two configurations of insulation batts were investigated. One was the standard (R-19) fiberglass insulation batt on top of a gypsum board ceiling; the other was an R-19 batt on top of a gypsum board ceiling with a foil radiant barrier installed on top of the insulation. It was experimentally found by Fairey [11] that a radiant barrier mounted on the rafters can reduce the total heat transfer through the composite by about 42% during a summer's day. Fairey's work produced valuable experimental results but was costly and time consuming. This work provides an efficient numerical model to evaluate the total heat transfer through the fiberglass/gypsum board composite.

It has been found that only two heat transfer modes are important in fiberglass insulation. One is conduction through the gas; the other is thermal radiation which accounts for 30 to 50% of the total heat transfer in low density fibrous insulations. Inside the gypsum board, however, conduction is the only heat transfer mechanism. In this work, coupled conductive and radiative heat transfer was considered in the fiberglass insulation layer and only conductive heat transfer was modeled in the gypsum board.

Several techniques [12-19] are available for obtaining solutions of the radiative transport equation; here the method of discrete ordinates [12,15] was used. This work also used a control volume based implicit finite difference method [20] for numerically solving the transient energy equation.

A two-layer model of the fiberglass insulation and the gypsum board substrate (Fig. 1) was chosen for investigation of the heat transfer behavior as opposed to the single-layer (fiberglass)

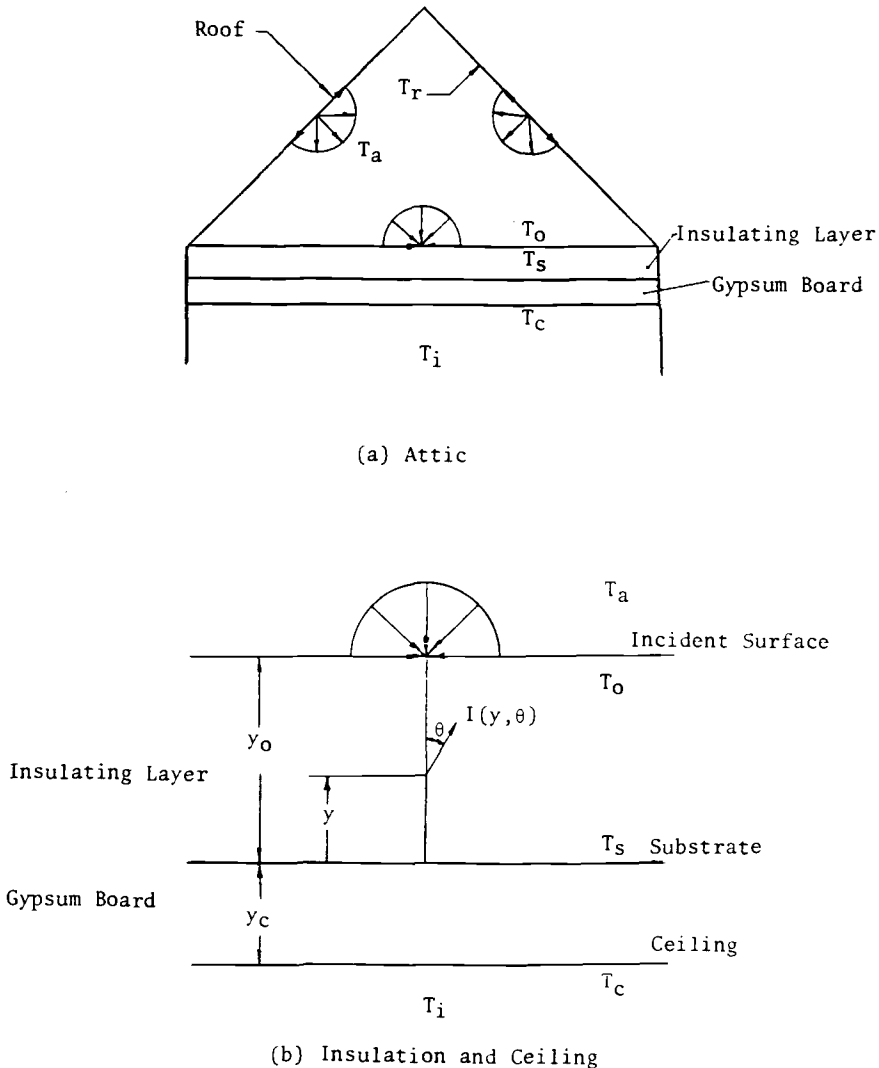


FIG. 1—Geometry and coordinate system.

model used by Rish [9]. The single-layer model cannot predict the influence of the sheetrock, which acts as a heat capacitor and hence can influence the transient heat-transfer behavior. The temperature profile near the top and bottom of the insulation batt was highly non-linear; therefore a fine spatial grid size was required to accurately describe the temperature profile. However, only a coarse spatial grid was required in the middle 90% of the fiberglass insulation and in the entire sheetrock region because of an essentially linear temperature profile occurring in these regions. The influence of the convergence criterion and of the number of temperature grid points on the total heat flux is presented in Ref 10. A 0.01% convergence criterion for temperature and the 22-point (17 in fiberglass and 5 in gypsum board) point irregular grid system [10] were found to be very efficient and accurate as compared to Rish's 98 uniformly spaced grid points [9].

The solution required an iterative procedure at each time step; the magnitude chosen for the

time step was 10 min. Results are shown for the total heat flux as a function of time for a 24-h period. The radiative properties used here were obtained in a previous work [10] which showed good agreement with steady-state heat transfer data. The results shown in this paper indicate that the application of a simple retrofit (foil radiant barrier) can result in significant improvement in the performance of attic insulation for summer and winter conditions.

Statement of Problem

The geometry for the physical attic insulation problem (Fig. 1a) depicts the typical attic of a residential home. The fiberglass insulation is bounded by air above and by the ceiling of gypsum board (sheetrock) below. The coordinate system for the insulation layer and ceiling board is shown in Fig. 1b. The origin of the coordinate y was chosen at the interface between the fiberglass insulation layer and the ceiling board. The positive y -direction was directed towards the top interface of the insulation layer. The polar angle, θ , is the angle between the positive y -direction and the direction of propagation of a radiant intensity beam.

The attic air and the top fiberglass-air interface were assumed to be totally transparent to the radiation. The heat transfer results were obtained for isotropic scattering. The thickness of the fiberglass insulation was about 15 cm (6 ± 0.25 in.). This is small compared to the length and width of the attic; thus the attic was treated as a one-dimensional heat-transfer problem. The batt thickness was measured before each 24-h test to be sure that the thickness was 15 ± 0.6 cm in a 40 by 40 cm area around the thermocouples. This yields a heat transfer error of about 4% due to thickness variation. The batt fiberglass is not prone to compression during a 24-h test period. The attic framing will cause some attic locations to have increased heat transfer. Hence the space-averaged heat transfer over the entire attic will be somewhat greater than the heat fluxes presented here. However, the computed heat fluxes compare favorably with experimental measurements [11,21]. Since convection in fiberglass insulation was effectively suppressed by the glass fibers, only conductive and radiative heat transfer modes were considered here.

In the fiberglass insulation, thermal radiation can be scattered, absorbed, and emitted; therefore volumetric radiative heat transfer was modeled. After each 30-min interval, the temperatures were measured with Type J thermocouples (0.500 mm diameter wire) at various locations (see Fig. 1). One location was an inner roof surface (T_r); next, the attic air (T_a); then, on top of the fiberglass insulation (T_o); the bottom of the gypsum board (T_c); fifth, on top of the gypsum board (T_s); and last, in the room air (T_i). The temperature accuracy on the thermocouples was better than $\pm 0.25^\circ\text{C}$, which yields an error in heat flux of about 2% for a 25°C temperature difference from the top of the insulation to the bottom of the gypsum board; for lower temperature differences the error could be greater than 2%. All thermocouples were mounted with 25 cm long horizontal-lead lengths to minimize conduction along the wires; also, the thermocouples were shielded.

Analysis

$$\frac{\partial}{\partial y} \left(k_t \frac{\partial T}{\partial y} \right) - \frac{\partial q_r}{\partial y} = \frac{\partial}{\partial t} (\gamma_t C_{pt} T) \quad (1a)$$

where k_t and C_{pt} are functions of the fiberglass temperature. Since there is no radiative transfer within the sheetrock, the corresponding energy equation for the sheetrock can be written as

$$\frac{\partial}{\partial y} \left(k_s \frac{\partial T}{\partial y} \right) = \frac{\partial}{\partial t} (\gamma_s C_{ps} T) \quad (1b)$$

where k_s , γ_s and C_{ps} are considered as constants. The boundary conditions corresponding to Eqs 1a and 1b are: at the ceiling-air surface

$$T = T_c(t) \quad \text{at} \quad y = -y_c, \quad y_c > 0 \quad (1c)$$

and at the top surface of the insulation,

$$T = T_o(t) \quad \text{at} \quad y = y_o, \quad y_o > 0 \quad (1d)$$

where T_c and T_o are functions of time as experimentally measured in an actual Oxford, Mississippi, home. At the interface between the fiberglass insulation and the sheetrock, an energy balance yields

$$-k_t \frac{\partial T}{\partial y} \Big|_{y=0} + q_r(0) = -k_s \frac{\partial T}{\partial y} \Big|_{y=0} \quad (1e)$$

Equations 1a to 1e were discretized by using a control-volume-based finite difference method [20]. The radiative heat-transfer component in Eqs 1a and 1e were obtained [10] by solving the radiative-transport equation, which can be written in discrete ordinates form as

$$\begin{aligned} \frac{dI(\tau, \mu_m)}{d\tau} = & -\frac{I(\tau, \mu_m)}{\mu_m} + \frac{\omega}{2\mu_m} \sum_{j=1}^M a_j I(\tau, \mu_j) \sum_{\ell=0}^L A_\ell P_\ell(\mu_m) P_\ell(\mu_j) \\ & + \frac{(1-\omega)n^2}{\mu_m} I_b(T(\tau)), \quad m = 1, 2, \dots, M \end{aligned} \quad (2a)$$

with boundary conditions

$$I(0, \mu_m) = \rho_s I(0, -\mu_m) + (1 - \rho_s) n^2 I_b(T_s), \quad \mu_m > 0, \quad m = 1, 2, \dots, M/2 \quad (2b)$$

$$I(\tau_o, -\mu_m) = \rho_n I(\tau_o, \mu_m) + (1 - \rho_n) n^2 I_i, \quad \mu_m > 0, \quad m = 1, 2, \dots, M/2 \quad (2c)$$

The quantity I_i can be characterized by the top insulation interface temperature or by the roof temperature, depending on whether or not a foil radiant barrier is employed at the top insulation interface. Finally the net radiative heat flux, q_r , obtained by integrating I spherically, is

$$\begin{aligned} q_r(\tau) = & -\frac{4\pi(1-\omega)}{\omega} \sum_{j=1}^{M/2} \frac{(1-\lambda_j \mu_j)}{\lambda_j} [C_j e^{\lambda_j \tau} - C_{M+1-j} e^{-\lambda_j \tau}] \\ & - \frac{4\pi(1-\omega)n^2}{\omega} \sum_{j=1}^{M/2} \frac{K_j}{\lambda_j} \left[\int_0^\tau I_b(t) e^{-\lambda_j(\tau-t)} dt - \int_\tau^{\tau_o} I_b(t) e^{-\lambda_j(t-\tau)} dt \right] \end{aligned} \quad (3)$$

The two integration terms appearing in Eq 3 can be approximately evaluated by two methods [9]. An iterative procedure was used to determine the temperature field within the insulation and sheetrock composite. The non-linear system of equations was solved by the following iterative procedure:

1. Guess the temperature field throughout the fiberglass insulation and sheetrock.
2. Insert the guessed temperature into Eq 3 to obtain the radiative heat-flux field.
3. Insert the radiative heat flux obtained in Step 2 into Eqs 1a and 1e and then solve for a new temperature field from Eqs 1a to 1e by the TriDiagonal Matrix Algorithm [20].

4. Use this new temperature field as an improved guess and return to Step 2 until the absolute errors for two consecutive temperature fields are within the convergence criterion.

The above iteration scheme was used at each time step of the transient problem. The computations were performed for a 24-h period by marching forward in 10-min steps. About 10 s of CPU time were required for modeling 24 h (145 time steps) of heat transfer using an AMDAHL 470 computer with an IBM VM 370 operating system. The radiative properties (extinction coefficient and albedo) [10] and other thermal properties (density, specific heat, and conductivity) used for calculating the heat transfer results are shown in Table 1.

Results and Conclusions

A computer model employing the analysis presented above was developed to perform heat transfer calculations. The experimentally measured temperatures presented in the lower portion of Figs. 2 to 5 were used as boundary condition information in the heat transfer analysis. These temperature data were recorded in an actual residence. For each figure, the upper portion contains the computed heat flux values at the ceiling and substrate (bottom of batt) surfaces corresponding to the experimentally measured temperatures (T_r , T_a , T_o , and T_c) shown in the lower portion of each figure. The boundary temperature histories of T_r , T_o , and T_c were used as boundary conditions for solving the energy equation (Eqs 1a to 1e). Ceiling heat fluxes, which are directly related to energy conservation, were predicted with the computer model.

The experimental temperature data presented in Figs. 2 to 5 were obtained for two different configurations of fiberglass batt (Table 2). One configuration was the standard (STD) insulation batt; the other has a foil radiant barrier (FRB) on top of the STD batt. The roof inner surface was taken to have an emissivity of 0.85 [14]. The FRB insulation batt had double-sided aluminum foil (shiny on both sides) placed on top. The double-sided foil was conservatively taken to have an infrared reflectivity of 0.95 on both sides. The FRB batt receives radiant heat from the foil radiant barrier instead of from the roof; hence the incident radiant heat flux for the FRB batt is much lower than that for the STD batt.

In Figs. 2 to 5, each even-numbered figure corresponds to a FRB batt and each odd-numbered figure corresponds to a STD batt; the foil radiant barriers were all horizontally mounted by placing the radiant barriers on top of the fiberglass batts. Figures 2 and 3 are for (winter) 12 January 1985; Figs. 4 and 5 correspond to (summer) 16 June 1985. The ceiling and roof temperatures for the FRB batt were identical to those for the STD batt. Due to thermostat control of the air conditioner/heat pump, the ceiling temperature only varied by about 2 K during the entire day. The time period when the ceiling temperature was lower than the batt top surface temperature is called the "heat gain period", for instance 9:00 A.M. to 9:30 P.M. on 16 June 1985. The time period when the ceiling temperature is greater than the batt top surface temperature is called the "heat loss period"; this corresponds to the entire days of 12 and 13 January

TABLE 1—Radiative and thermal properties.

γ_t , kg/m ³	C_{pt} , J/kg-K	k_t , W/m-K		
10.9	844.	$a + bT + 8.55374 \times 10^{-5} \gamma_t$ $a = 4.97576 \times 10^{-3}$ $b = 7.00025 \times 10^{-5}$		
γ_s , kg/m ³	C_{ps} , J/kg-K	k_s , W/m-K	β , cm ⁻¹	ω^a
880.0	1050.0	0.17	3.70	0.201

^aThese gray β and ω are the average values of non-gray isotropic scattering β and ω values from Ref 10.

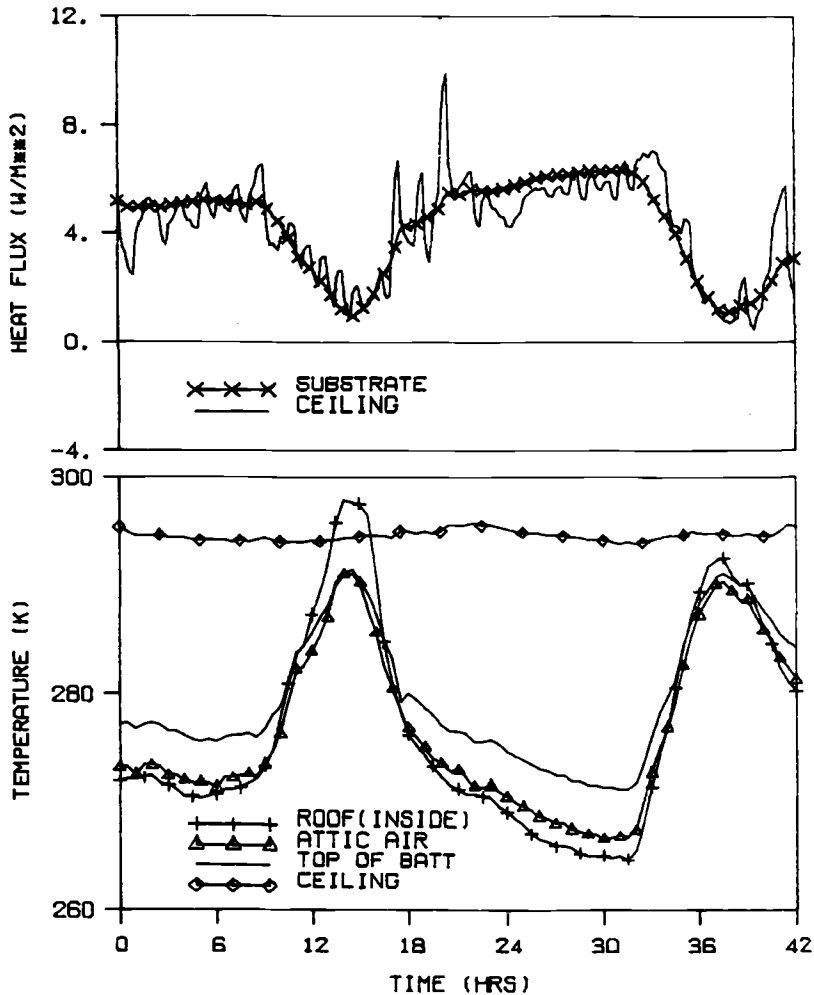


FIG. 2—Measured temperatures and predicted heat flux histories corresponding to the foil radiant barrier insulation batt for 12 January 1985.

1985 and also to the time periods 0:00 A.M. (midnight) to 9:00 A.M. and 9:30 P.M. to 12:00 midnight on 16 June 1985. The discussion of temperature and heat flux behavior will mainly focus on the "heat gain" and "heat loss" periods instead of night and day or winter and summer.

The roof temperature, which is strongly influenced by weather conditions and the incident solar heat flux, varied from 265 to 322 K in winter and from 290 to 345 K in summer (Figs. 2 to 5). It was found that the roof temperature increased from a minimum value at around 7:30 A.M. to a maximum value at around 2:00 P.M. for a winter day. During the summer, the minimum roof temperature occurred at about 6:00 A.M. and the maximum at around 3:30 P.M. Normally, the roof temperature was relatively steady at night but still slowly decreased until about 6:00 A.M. for hot summer days and decreased until about 7:30 A.M. for cold winter days. The roof inner surface was heated by the daily solar flux until reaching a maximum temperature. Then the roof temperature decreased as the solar heating diminished. The time histories of the

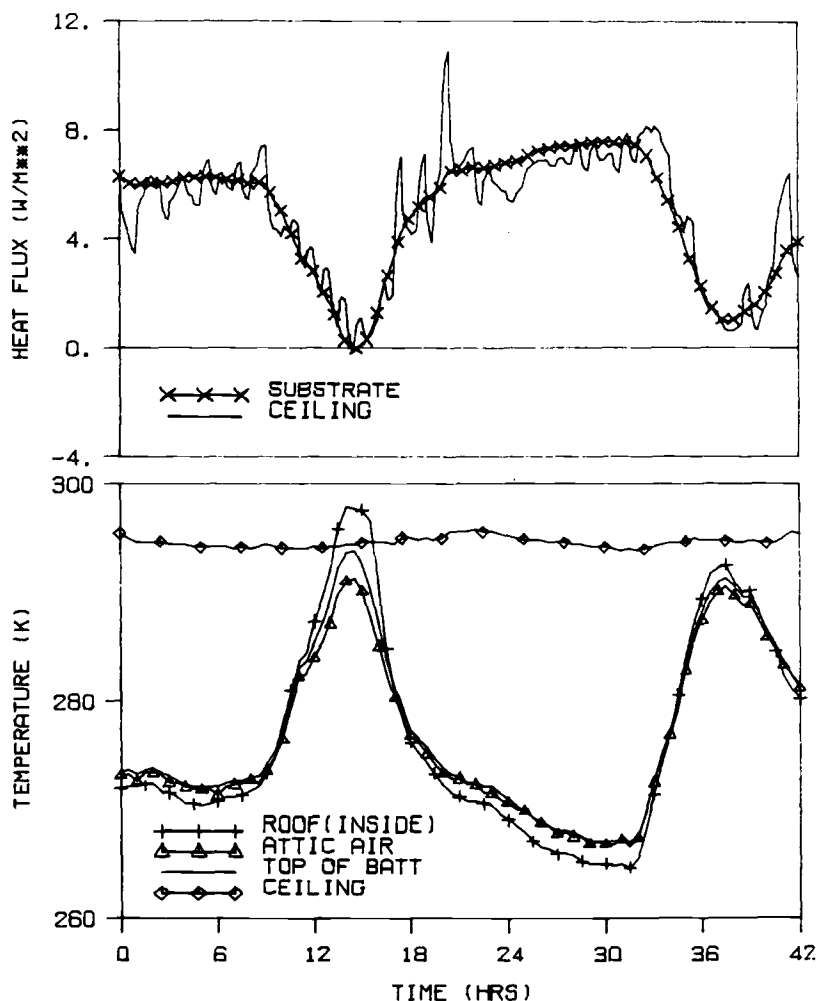


FIG. 3—Measured temperatures and predicted heat flux histories corresponding to the standard insulation batt for 12 January 1985.

batt top surface and attic air temperature followed the same pattern as the roof temperature history.

Since the temperatures for two different configurations were measured simultaneously in the same residence, the attic air temperatures for the FRB and STD batts were equal. The batt top surface temperature for the STD batt was significantly different from the FRB batt top surface temperature. During the “heat gain” period, the STD batt received a substantially higher roof radiant heat load than the FRB batt. Therefore the top surface temperature for the STD batt was significantly higher. For the STD batt, some of the absorbed radiant heat from the roof was lost by conduction out of the batt during the “heat gain” period (i.e., the attic air was actually heated by the batt). As seen in Figs. 3 and 5, the batt top surface temperature was higher than the attic air temperature during the “heat gain” period. During the “heat loss” period, the STD batt has a top surface temperature lower than the FRB batt because the foil radiant barrier resisted the flow of heat from the batt to the attic air.

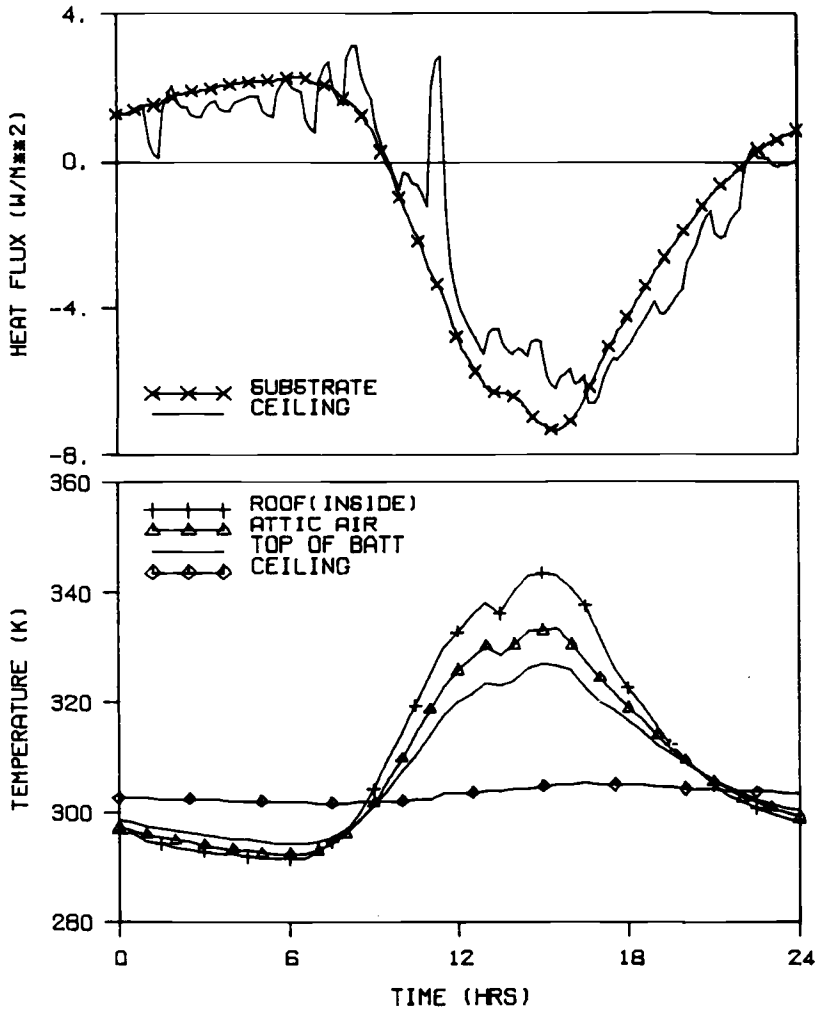


FIG. 4—Measured temperatures and predicted heat flux histories corresponding to the foil radiant barrier insulation batt for 16 June 1985.

Before proceeding with the discussion of the ceiling and substrate heat flux histories, the heat flux profiles within both the insulation and the sheetrock will be illustrated at specified times on January 12 and 13 and June 16. The positive y-coordinate in Figs. 6 to 9 corresponds to the region inside the fiberglass insulation; negative y-values correspond to the region inside the sheetrock layer (Fig. 1b). A positive value of heat flux means that heat is transferred in the positive y-direction or out of house; negative heat flux values correspond to heat transfer in the negative y-direction or into house. The temperature gradient in the insulation is relatively constant; hence the heat flux variation within the insulation is not very large because of its low heat capacity. When heat was transferred through the larger heat capacity material (sheetrock), a larger amount of heat was stored and a lesser amount of heat was transferred through the material. Thus a larger slope of the spatial heat flux profile occurred as shown in Figs. 6 to 9 for the larger heat capacitor, gypsum board.

As shown in Figs. 6 to 9, the temperature profile within the fiberglass insulation is essentially

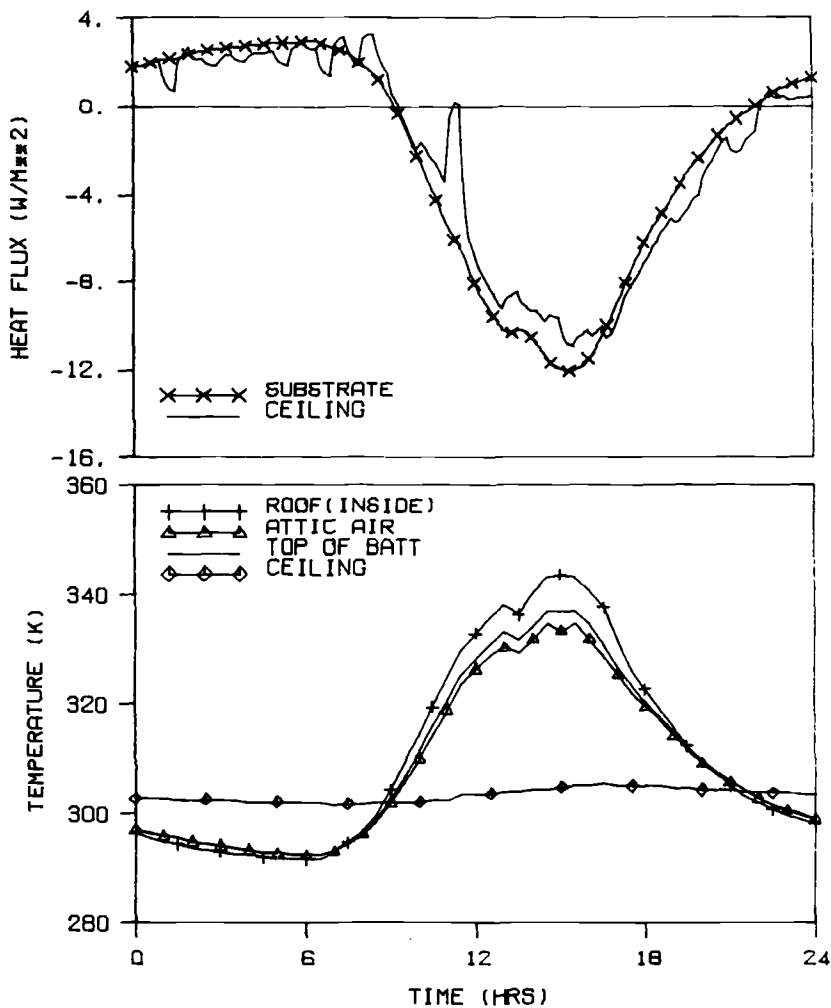


FIG. 5—Measured temperatures and predicted heat flux histories corresponding to the standard insulation batt for 16 June 1985.

TABLE 2—Configuration of the two different attic insulation batts (see Fig. 1).

Batt ^a Type	Top Boundary	Substrate Boundary	ρ_s	ρ_p	ρ_n	I_i
STD	air	gypsum board	0.07	0.00	0.15 ^b	$0.85\sigma T_i^4$
FRB	foil ^c	gypsum board	0.07	0.00	0.95	$0.05\sigma T_o^4$

^aInsulation batt thickness; $y_o = 0.152$ m; sheetrock thickness: $y_c = 0.0127$ m.

^bCharacterized by roof inner wood surface reflectivity.

^cDouble-sized aluminum foil.

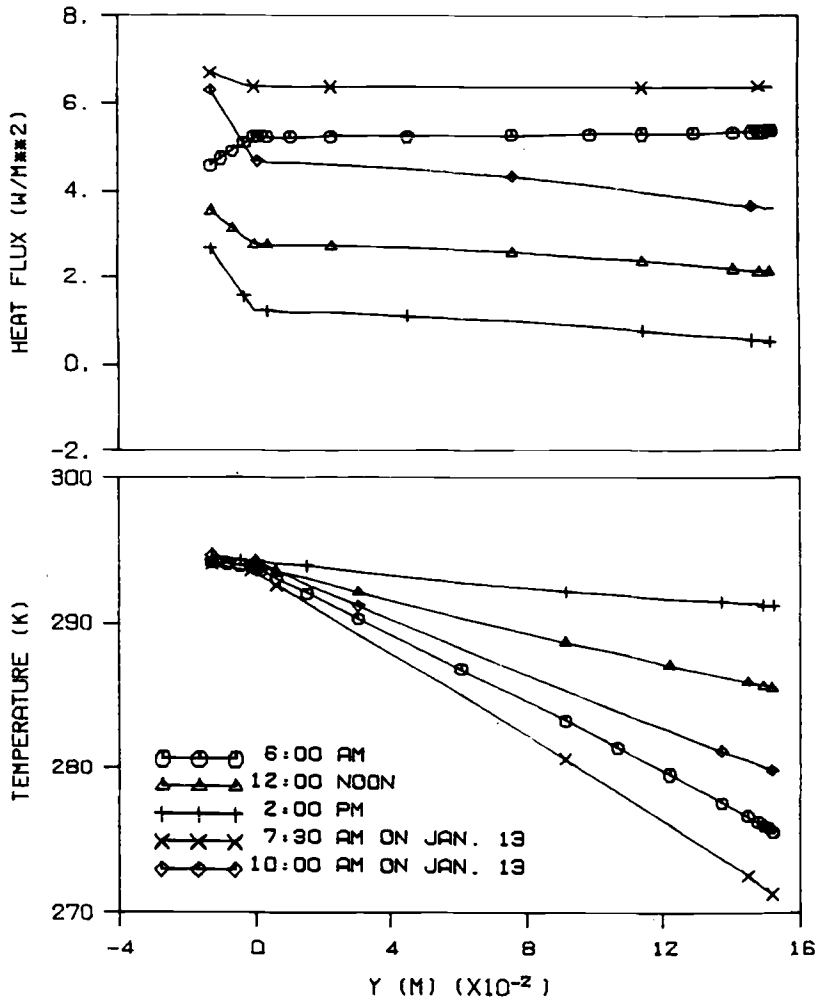


FIG. 6—Spatial heat flux and temperature profiles for 12 January 1985 (FRB batt).

linear except in a small region near the top of the STD batt at 11:00 A.M., 11:30 A.M., 3:00 P.M., 5:00 P.M., and 5:30 P.M. on 16 June 1985 (Fig. 9) and at 2:00 P.M. on 12 January 1985 (Fig. 7). At these times the radiative heat flux was identical to the total heat flux at a point "about" 3 mm below the top of the STD batt (i.e., the conductive heat flux and the spatial temperature gradient had a zero value at this location). A temperature maximum also occurs at this point. The temperature gradient at y -values beyond the maximum temperature point was negative; for y -values below the maximum temperature point the gradient was positive. The heat transfer phenomenon discussed above typically occurred when the roof temperature was greater than the batt top temperature (see Figs. 3 and 5).

The predicted heat flux history is presented above each corresponding temperature history as shown in Figs. 2 to 5. There are two types of data; one is summer-time data as shown in Figs. 4 and 5 for June 16 and the other one is winter-time data as shown in Figs. 2 and 3 for January 12. It can be seen from Figs. 2 and 3 (January 12) that heat was usually lost (positive value) from the house to the attic air; here the attic and roof were functioning as a heat sink. A heat gain oc-

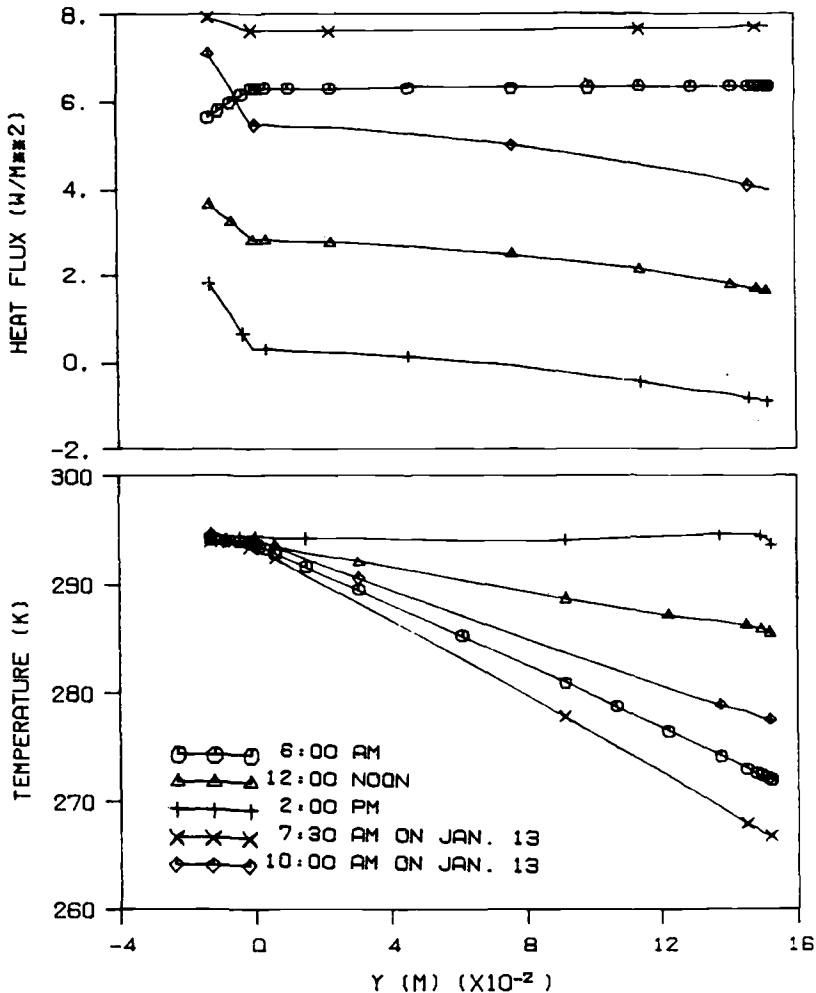


FIG. 7—Spatial heat flux and temperature profiles for 12 January 1985 (STD batt).

curred during the daytime for June 16 as shown on Figs. 4 and 5; here the roof functioned as a heat source. The heat loss (or heat gain) causes the heat pump (or air conditioner) to cycle on and off frequently; this is shown by the jagged curve corresponding to the ceiling heat flux history. The ceiling heat flux was very sensitive to local changes in the room flow field due to free convection currents, forced convection currents (generated by heat pump or air conditioner), and other disturbances. The substrate heat flux curve is seen to be smooth, since it is buffered by the ceiling gypsum board; the same type of ceiling and substrate heat flux behavior (i.e., noisy and smooth) was also observed by the Tennessee Valley Authority and the Florida Solar Energy Center.

At 2:00 P.M. on January 12, the peak in the roof temperature caused the STD batt to gain heat slightly; yet the FRB batt never gained heat during the entire day. The STD batt is more sensitive to changes in the roof temperature than the FRB batt; due to its high emissivity the roof can directly radiate heat to the STD batt. The FRB batt primarily receives heat from the attic air by heat conduction through the aluminum foil. Since the aluminum foil was double-

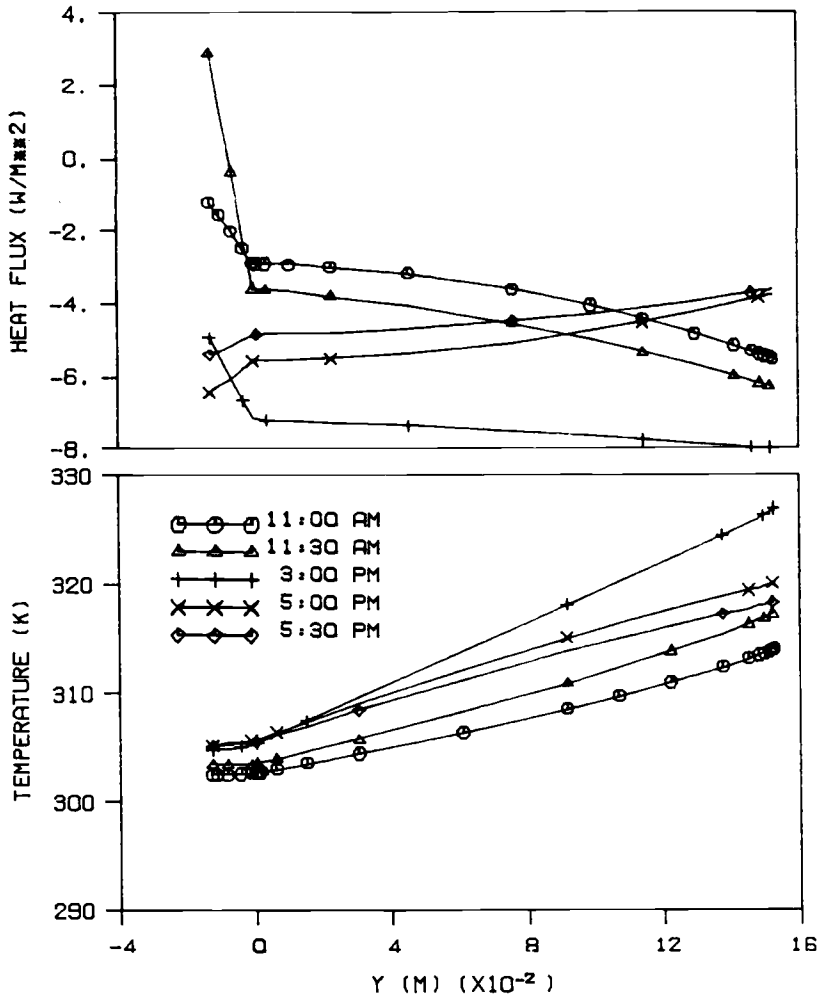


FIG. 8—Spatial heat flux and temperature profiles for 16 June 1985 (FRB batt).

sided, the foil radiant barrier not only acts as a high reflector to incoming radiant heat from the roof but also functions as a low emitter of radiant heat. Basically, the foil radiant barrier effectively reduces the heat loss from the fiberglass batt to the attic during a cold winter night and also retards heat gain during a hot summer day.

It can be seen in Figs. 4 and 5 that during the "heat gain" period, the sheetrock receives heat from the insulation batt. The sheetrock stores part of this heat and transfers the rest of it into the room. As shown in Figs. 4 and 5, the substrate heat flux was usually greater in magnitude than the ceiling heat flux during most of the "heat gain" period. However, the ceiling heat flux was usually greater than the substrate heat flux during the period of 5:00 P.M. to 10:00 P.M.; during this period the sheetrock releases the stored heat to the room. This behavior is a result of the sheetrock having a much higher heat capacity than does fiberglass insulation.

Total heat loss (or heat gain) for a 24-h period is shown in Table 3. A positive value means a heat loss (winter) and a negative value means a heat gain (summer). The winter day, January 12, had a net heat loss; the summer day, June 16, had a net heat gain. It was found that the FRB

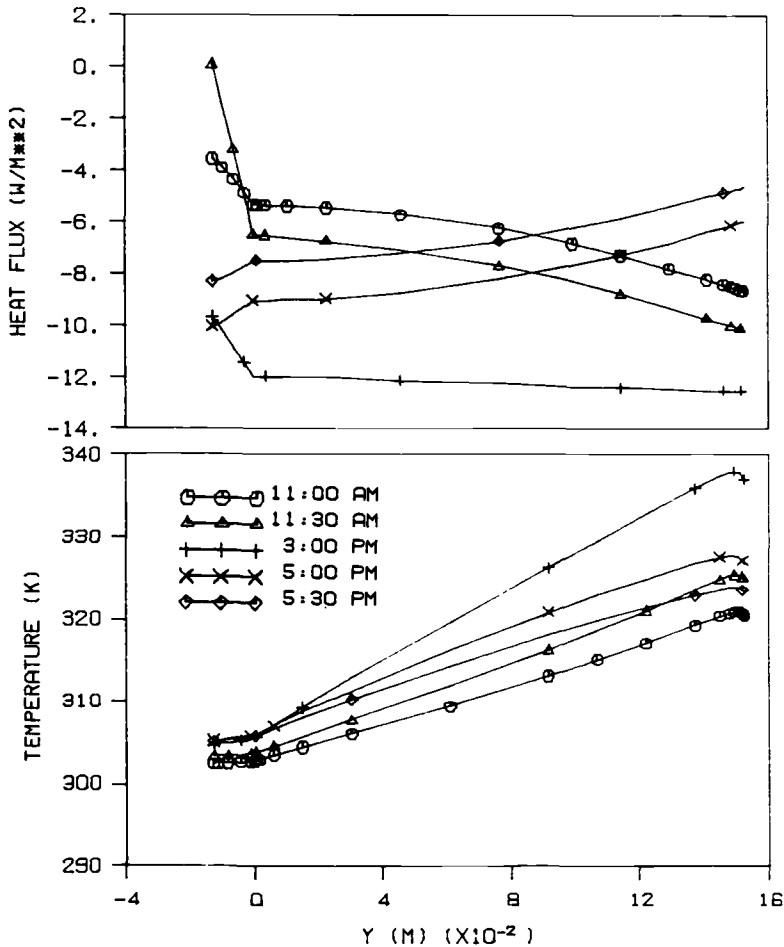


FIG. 9—Spatial heat flux and temperature profiles for 16 June 1985 (STD batt).

TABLE 3—Integrated (24 h) ceiling and substrate heat flux.^a

Date	STD Batt			FRB Batt			$Q_{cf} - Q_{cs}$	$Q_{cf} - Q_{cs}$
	Q_{cs} kJ/m ²	Q_{ss}	Q_r/Q_{ss} × 100%	Q_{cf} kJ/m ²	Q_{sf}	Q_r/Q_{sf} × 100%	Q_{cs} × 100%	Q_{ss} × 100%
1/12/85	417.	418.	29.0	364.	365.	27.6	-12.6	-12.6
6/16/85	-202.	-213.	30.9	-108.	-119.	29.5	-46.4	-44.0

^a Q_{cs} : Integrated ceiling heat flux on STD batt.
 Q_{cf} : Integrated ceiling heat flux on FRB batt.
 Q_{ss} : Integrated substrate heat flux on STD batt.
 Q_{sf} : Integrated substrate heat flux on FRB batt.
 Q_r : Integrated substrate radiation heat flux component.

batt can reduce heat transfer through the attic by about 45% in the summer and by about 13% in the winter over use of the STD batt. The integrated (24 h) heat loss or gain at the ceiling and at the substrate were almost identical for January 12 for the STD and FRB batts; however, the difference in the integrated ceiling and substrate heat gains for June 16 were 5% for the STD batt and 10% for the FRB batt (Table 3). The differences in the integrated heat fluxes between the ceiling and substrate can be due to the thermal capacitance of the gypsum board and the fact that this is an unsteady-state heat transfer problem. The integrated value of the radiative component of the total substrate heat flux was found to be about 29%; therefore the conduction component is about 2.5 times the radiation component. The configuration (FRB or STD) and season (winter and summer) only change the radiation to total heat transfer percentages by about 1 to 2%.

Summary

The purpose of this work was to calculate the ceiling and substrate heat fluxes in fiberglass attic insulation and sheetrock. The method of discrete ordinates was used for solving the radiative transport equation. The energy equation was solved by using Patankar's control volume method [20] with the radiative-transfer terms acting as a source term. The sheetrock thermal capacitance was found to influence the heat-transfer behavior of the attic insulation. The ceiling heat flux fluctuates about the substrate heat flux in response to forced convection currents caused by the heat pump or air conditioner. The integrated heat flux values for the ceiling and substrate differ by a maximum of 10%. It was also found that the FRB batt was able to reduce heat loss by about 13% in winter and to reduce heat gain in summer by about 45% as compared to the STD batt. These percentages compare favorably with the summer and winter measurements of Hall [21] and for the summer-time measurements of Fairey [11]. The radiant heat contributed to the substrate heat flux was about 29% for both the STD and FRB batts. The computation technique developed for this work was efficient for computation of heat transfer. The foil radiant barrier was found to be highly effective in improving conservation of energy.

Acknowledgments

This work was funded by the National Science Foundation under Grant MEA-8217974.

References

- [1] Verschoor, J. D., Greebler, P., and Manville, N. J., *Transactions of ASME*, Vol. 74, 1952, pp. 961-968.
- [2] Strong, H. M., Bundy, F. P., and Bovenkerk, H. P., *Journal of Applied Physics*, Vol. 31, No. 1, 1960, pp. 39-50.
- [3] Nathaniel, E. H. and Robin, C. S., *Journal of Applied Physics*, Vol. 38, No. 12, 1967, pp. 4663-4668.
- [4] Bankvall, C., *Journal of Testing and Evaluation*, Vol. 1, No. 3, May 1973, pp. 235-243.
- [5] Tong, T. W. and Tien, C. L., *Journal of Thermal Insulation*, Vol. 4, July 1980, pp. 27-44.
- [6] Tong, T. W. and Tien, C. L., *Journal of Heat Transfer*, Vol. 105, No. 1, 1983, pp. 70-75.
- [7] Tong, T. W., Yang, Q. S., and Tien, C. L., *Journal of Heat Transfer*, Vol. 105, No. 1, 1983, pp. 76-81.
- [8] Houston, R. L. and Korpela, S. A. in *Proceedings*, 7th International Heat Transfer Conference, Vol. 2, 1982, pp. 499-504.
- [9] Rish, J. W., III and Roux, J. A., *Journal of Thermophysics and Heat Transfer*, Vol. 1, No. 1, Jan. 1987, pp. 43-48.
- [10] Yeh, H. Y., "Radiative Properties and Heat Transfer Analysis of Fibrous Insulation," Ph.D. dissertation, University of Mississippi, University, 1986.
- [11] Fairey, P. W., "Effects of Infrared Radiation Barriers on the Effective Thermal Resistance of Building Envelopes," presented to ASHRAE/DOE Conference on Thermal Performance of the Exterior Envelopes of Buildings—II, Las Vegas, Nev., 1982.
- [12] Chandrasekhar, S., *Radiative Transfer*, Dover, New York, 1960.

- [13] Ozisik, M. N., *Radiative Transfer*, Wiley, New York, 1973.
- [14] Sparrow, E. M. and Cess, R. D., *Radiation Heat Transfer*, Hemisphere/McGraw-Hill, New York, 1978.
- [15] Roux, J. A., Smith, A. M., and Todd, D. C., *AIAA Journal*, Vol. 13, No. 9, Sept. 1975, pp. 1203-1211.
- [16] Hsia, H. M. and Love, T. J., *Journal of Heat Transfer*, Vol. 89, Aug. 1967, pp. 197-203.
- [17] Yuen, W. W. and Wong, L. W., *Journal of Heat Transfer*, Vol. 102, 1980, pp. 303-307.
- [18] Hottel, H. C., Sarofim, A. F., Evans, L. B., and Vasalos, I. A., *Journal of Heat Transfer*, Vol. 90, Feb. 1968, pp. 56-62.
- [19] Roux, J. A., Yeh, H. Y., Smith, A. M., and Wang, S. Y., *Journal of Energy*, Vol. 7, No. 6, Nov.-Dec. 1983, pp. 702-709.
- [20] Patankar, S. V., *Numerical Heat Transfer and Fluid Flow*, Hemisphere, Washington, D.C., 1980.
- [21] Hall, J. A., "Performance Testing of Radiant Barriers," presented at Symposium on Building Energy Efficiency in Hot and Humid Climates, Arlington, Tex., 17-19 Nov. 1986.

Spectral Radiative Properties and Apparent Thermal Conductivity of Expanded Polystyrene Foam Insulation

REFERENCE: Yajnik, S. J. and Roux, J. A., "Spectral Radiative Properties and Apparent Thermal Conductivity of Expanded Polystyrene Foam Insulation," *Insulation Materials, Testing, and Applications, ASTM STP 1030*, D. L. McElroy and J. F. Kimpflen, Eds., American Society for Testing and Materials, Philadelphia, 1990, pp. 561-574.

ABSTRACT: Heat transfer in foam insulations is primarily due to conduction and radiation. In order to predict the heat transfer in expanded polystyrene foams the determination of reliable spectral radiative properties is important since radiation accounts for up to 27% of the overall heat transfer at moderate temperatures (250 to 350 K). Most of the previous work done on the determination of the spectral radiative properties of foam insulations employed direct transmission measurements and Beer's law to invert the extinction coefficients. This paper utilizes directional-hemispherical reflectance data in the wavelength range from 4 to 20 μm to invert the spectral radiative properties of a standard reference material, namely 20.7 kg/m³ expanded polystyrene foam insulation. Apparent thermal conductivity values are predicted using the inverted radiative properties. The non-linear least squares method was used to invert the spectral radiative scattering and absorption coefficients from the experimental reflectance data and a numerical model.

KEY WORDS: radiative properties, apparent thermal conductivity, heat transfer, polystyrene foam, conduction, radiation

Heat transfer inside foam insulations can have three primary transport mechanisms: conduction, free convection, and volumetric radiation. Free convection in foams was shown to be effectively nonexistent [1,2] for cell sizes less than 1.5 mm, which would include most polystyrene and polyurethane foams. Hence heat transfer in foam insulations is due to coupled conduction and radiation. Schuetz [2], Sinofsky [3], and Glicksman et al. [4] have examined geometrical models of different foams, and the last two have determined upper and lower limits of foam true thermal conductivities.

It is imperative to accurately determine the spectral radiative properties of foam insulations since radiation accounts for up to 27% of the overall heat transfer at moderate temperatures. Since the albedo (ω) and extinction coefficient (β) (sum of the absorption, κ , and scattering, σ , coefficients) appear explicitly in the radiative transport equation, their determination is of primary importance. Amorebieta and Colussi [5] have computed the monochromatic extinction coefficient of polystyrene foams at 300 K using transmittance data in the wavelength range of 5 to 50 μm . Both Schuetz [2] and Sinofsky [3] have determined the extinction coefficient for various polyurethane foams using a "band model", in which the transmittance is taken as constant over various infrared wavelength ranges. All the above [2,3,5] used a Beer's law inversion technique to determine the extinction coefficient. Since Beer's law does not account for in-scattering and back-scattering, there can be considerable error involved depending on the extent of the

¹University of Mississippi, University, MS 38677.

non-isotropic nature of scattering in foams. For a 2.0 pcf ($\approx 32 \text{ kg/m}^3$) polyurethane foam the error was as high as 18% [2,3].

The present work [6] uses the non-linear least squares method to invert the radiative properties of a 20.7 kg/m³ expanded polystyrene foam (provided by Oak Ridge National Laboratory as prepared by W. R. Grace and Company; meets ASTM Specification C 5-78). Experimental directional-hemispherical reflectance (ρ_{dh}) data were used to invert the spectral scattering (σ) and absorption coefficient (κ) of the foam insulation. The spectral β and ω are then computed from the inverted σ and κ ($\beta = \sigma + \kappa$; $\omega = \sigma/(\sigma + \kappa)$). The one-dimensional radiative transport equation for both isotropic and anisotropic scattering [7] was solved by the discrete ordinates method [8,9].

Measurement Technique

The directional-hemispherical reflectance, ρ_{dh} , accounts for scattering both as an attenuation and augmentation process. For ρ_{dh} , the radiative transport is described as a collimated beam incident on the foam insulation top surface at a polar angle of 15 deg, with multiple scattering and absorption inside the foam. The reflected intensity was collected hemispherically to give the directional-hemispherical reflectance. The ρ_{dh} data covered a wavelength range of 4 to 20 μm . These data were obtained for ten different sample thicknesses (0.020 to 0.216 cm) of foam insulation. To obtain meaningful results, the foam samples were cut (sawed with a ISOMET cutting saw) as thin as possible without crumbling; the samples had rough surfaces after cutting was complete. The anisotropic radiative properties were also scaled to isotropic values using the scaling law according to Lee and Buckius [10]. These scaled isotropic properties were compared with the directly inverted isotropic radiative properties. The Planck mean values of ω and β were also computed from the spectral ω and β values.

Statement of Problem

The physical geometry of a single layer (bulk foam/cell matrix) of insulation is shown in Fig. 1, which depicts its one-dimensional heat transfer phenomenon. The coordinate system origin

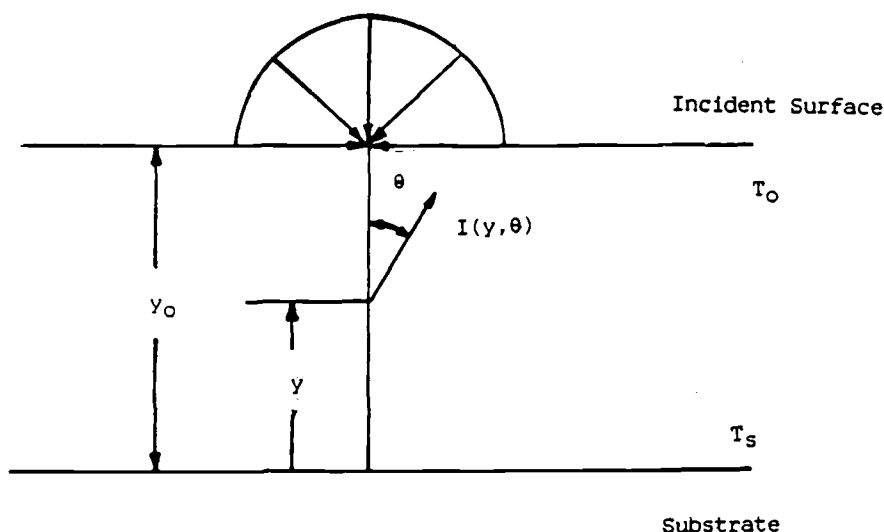


FIG. 1—Geometry of single layer of insulation with coordinate system.

was taken at the substrate (bottom) of the insulation. The angle between the positive y -direction and the propagated direction of a radiation ray defines the polar angle θ . The top interface temperature, T_o , and the substrate temperature, T_s , completely define the energy equation boundary conditions.

The single-layer, one-dimensional insulation problem is modeled to have coupled conductive and radiative heat transfer. Scattering and absorption account for radiation attenuation, while emission and scattering result in an augmentation process. The cell size and local variations in density account for scattering inside of foams. The anisotropic scattering phase function used was expressed as a series of Legendre polynomials. The first twelve coefficients of Sinofsky [3] were used for the foam scattering phase function; these coefficients are listed in Table 1.

The ρ_{dh} measurements were made in the 4 to 20 μm wavelength range with the Willey 318S FTS [7]. A collimated and modulated radiation beam, chopped at a frequency of 13 Hz, is incident on the top sample surface at an incidence angle of 15 deg. The detector signal corresponding to thermal emission was electronically filtered out by the modulator; the sample, therefore, may be treated as a non-emitting medium. Thus after undergoing multiple scattering and absorption in a non-emitting media, the collimated beam undergoes multiple reflections within a roughened gold coated integrating sphere; the radiation, finally, impinges on a detector. The detector signal is Fourier transformed to yield the spectral power distribution for the sample and reference (gold reference mirror) beams and these are ratioed at each wavelength.

With the ρ_{dh} reflectance data as input into the radiative properties computer program, the spectral absorption and scattering coefficients (extinction coefficient and albedo) were inverted in the wavelength range of 4 to 20 μm . The radiative properties were inverted both for the isotropic and the anisotropic scattering cases. A scaling law [10] was used to verify the isotropic and anisotropic radiative properties. Planck mean values were computed to give the weighted average (with respect to wavelength) radiative properties at different mean temperatures $[0.5(T_o + T_s)]$.

The computed gray radiative properties, together with the true thermal conductivity and the specific heat, were input into a heat transfer program to compare the steady-state heat transfer predictions with the experimental results provided by Oak Ridge National Laboratory (ORNL) for the expanded polystyrene foam insulation. The term "gray radiative properties" means that the spectral radiative properties were averaged over wavelength and then these averaged properties were used as constant values as if they were independent of wavelength.

TABLE 1—Coefficients used in Legendre polynomial expansion for the phase function [3]; sample thicknesses for expanded polystyrene foam.

Phase Function Coefficients		Thickness of Samples	
n	A_n	i	d_i (cm)
0	1.00000000	1	0.020
1	1.05164003	2	0.024
2	2.18705010	3	0.027
3	1.86943996	4	0.034
4	1.85876000	5	0.037
5	1.71955001	6	0.048
6	1.33608997	7	0.057
7	1.15337002	8	0.085 ^a
8	0.77673697	9	0.171
9	0.41531000	10	0.216
10	-0.03161620		
11	-0.36427799		

^aNot used for radiative properties inversion.

Experimental Measurements

Directional-hemispherical reflectance data were obtained for different thickness samples of the expanded polystyrene foam. The radiative properties were determined by placing the foam samples on an aluminum foil substrate. It was important to obtain high quality samples, since the inverted radiative properties depended strongly on the reflectance data. The expanded polystyrene sample thicknesses ranged from 0.020 to 0.216 cm. After the thicknesses were measured, the samples were weighed using the Mettler AE-50 digital balance. The weight divided by the cross-sectional area and the density of the foam ($=20.7 \text{ kg/m}^3$) gave the "calculated thickness". If the measured and calculated thicknesses did not match, the sample was discarded. The thicknesses of the ten expanded polystyrene foam samples prepared are listed in Table 1. Although ρ_{dh} measurements were obtained for all ten samples (Table 2), one sample was found to have "odd" reflectance values; this sample was not used for radiative properties inversion. The probable cause of the "odd" results was either a defective sample or a malfunction of the spectrometer. Table 2 gives the monochromatic ρ_{dh} values for all sample thicknesses. A representative plot of the reflectance values versus wavelength is given in Fig. 2. The reflectance data (most samples) from 2 to 4 μm and from 18.5 to 20 μm were noisy; hence the radiative properties were inverted from 4 to 18.5 μm .

Non-Linear Least Squares Method

The equations pertaining to the radiative properties and the solution for the heat transfer have not been included in this paper due to their involved nature [6, 7]. The non-linear least squares inversion method is briefly described below. The radiative properties (extinction coefficient, β , and albedo, ω) were determined via a coupling of the experimental reflectance data and a theoretical reflectance model. The theoretical reflectance is a function of β , ω , thickness (d), and incidence angle (θ):

$$\rho_{dh} = \rho_{dh}(\beta, \omega, d_i, \theta) \quad i = 1, 2, \dots, N \quad (1)$$

where ρ_{dh} is the reflectance for each sample of thickness d_i , and N is the total number of insulation samples ($N = 9$). Also, the incidence angle is known ($\theta = 15^\circ$). Hence in Eq 1 d_i and θ are known and the two unknowns are the radiative properties β and ω . The values of β and ω were found by solving for the β and ω values which minimize the error between the experimental data and the theory for all sample thicknesses at a fixed wavelength. This is accomplished by coupling the data and theory via the non-linear least squares method. In this method E ,

$$E = \sum_{i=1}^N [\rho_{dhi} - \rho_{dh}(\beta, \omega, d_i, \theta)]^2 \quad (2)$$

represents the magnitude of the error between the theory and the data, ρ_{dhi} is the experimental reflectance for the sample of thickness d_i , and $\rho_{dh}(\beta, \omega, d_i, \theta)$ is the theoretical reflectance obtained by solving the radiative transport equation. Since d_i and θ are known, the values of β and ω are determined which minimized E (makes E approach 0). This procedure was performed every 0.25 μm from 4 to 18.5 μm .

Results and Discussion

The non-linear least squares method was used to invert the radiative properties (β and ω) from ρ_{dh} data for expanded polystyrene foam insulation. The isotropic and anisotropic theoretical ρ_{dh} values were obtained by substituting the converged scattering coefficient, σ , and absorption coefficient, κ , into the radiative transport equation to compute ρ_{dh} ; the computed reflectance

tance values agreed very well with the experimental ρ_{dh} values (Figs. 3 and 4 for $\lambda = 9 \mu\text{m}$). The agreement shown in Figs. 3 and 4 was typical for all wavelengths. The extinction coefficients and albedo values were calculated from the converged σ and κ values. The extinction coefficients (β) and albedo (ω) values of the 20.7 kg/m^3 expanded polystyrene foam are presented as a function of the wavelength for the 4 to $18.5 \mu\text{m}$ range in Figs. 5 and 6 respectively. Both β and ω were found to be highly wavelength dependent; the anisotropic β and ω were found to be higher than the corresponding isotropic values. The foam κ values were found to be essentially independent of phase function; however, the σ values were found to depend strongly on phase function. Tables 3 and 4 give the spectral radiative properties in the wavelength range of 4 to $18.5 \mu\text{m}$ for isotropic and anisotropic scattering respectively.

The β and ω values obtained by scaling [10] from anisotropic to isotropic scattering compared well with the directly inverted isotropic values shown in Figs. 5 and 6. This implies that the heat transfer predictions obtained using an anisotropic scattering assumption should agree well with the heat transfer predictions obtained using isotropic scattering. (The isotropic gray radiative properties were used to predict heat transfer in foams in the present work.) Planck mean isotropic and anisotropic β and ω were determined in the temperature range of 100 to 500 K and are listed in Table 5. Both the Planck mean β and ω were found to increase monotonically in this temperature range. The isotropic Planck mean β ($=17.7 \text{ cm}^{-1}$) at 300 K was within 2% of the gray isotropic β ($=18.0 \text{ cm}^{-1}$) used for steady-state heat transfer predictions; the isotropic Planck mean ω ($=0.770$) was about 2.5% lower than the gray isotropic ω ($=0.787$). The anisotropic gray β ($=25.3 \text{ cm}^{-1}$) was about 1% different from the Planck mean β ($=25.6 \text{ cm}^{-1}$) at 300 K; the anisotropic gray albedo ($=0.834$) was less than 1% different from the Planck mean ω ($=0.840$).

The gray radiative properties listed in Table 6 were input into a heat transfer program which solved the energy equation for a one-dimensional plane insulation layer with coupled radiation and conduction. From these theoretical steady-state heat transfer values, the theoretical "apparent thermal conductivity" was computed. "Apparent thermal conductivity" is defined as

$$k_{app} = \frac{q \cdot d}{\Delta T} \quad (3)$$

where q is the steady-state heat flux in the one-dimensional plane insulation layer, d is the thickness of the layer, and ΔT is the temperature difference between the top and bottom surfaces of the insulation. It should be noted that k_{app} is proportional to the overall heat transfer; hence percentage changes in k_{app} and q are the same. The q value in Eq 3 was obtained by solution of the coupled conduction and radiative heat transfer problem [6] and using the properties in Table 6.

The theoretical "apparent thermal conductivity" predictions were compared to experimental "apparent thermal conductivity" values measured at Oak Ridge National Laboratory (ORNL) [11] and the National Bureau of Standards (NBS).

From experiments conducted at ORNL and NBS, k_{app} was measured as a function of temperature for various densities of the polystyrene foam. The experimental k_{app} as a function of temperature has been compared with the theoretical k_{app} for a foam density of 20.7 kg/m^3 ($\approx 1.3 \text{ pcf}$). The gray β , ω , and k_{true} used to compute the theoretical k_{app} have been listed in Table 6. As can be seen in Fig. 7, the theoretical k_{app} (dashed line) differed by about 4.5% from the experimental values. Two reasons have been attributed to this difference. Firstly, the expression for k_{true} used for foams was derived from the equation by Schuetz (as mentioned in Table 6), using typical values of the unknown parameters. The equation for k_{true} of foams is a function of the porosity of the foam, the percentage of struts in the solid foam [2,3], and the thermal conductivity (k_{solid}) of the solid polystyrene polymer. Secondly, the gray (average) isotropic β and ω ($=18.0 \text{ cm}^{-1}$ and 0.787 respectively) used in this work were determined from ρ_{dh} data in the wavelength range of 4 to $18.5 \mu\text{m}$. It is proposed that reflectance data be procured from 4 to 40

TABLE 2—Spectral ρ_{th} data for ten expanded polystyrene insulation samples.

d (cm)	0.020	0.024	0.027	0.034	0.037	0.048	0.057	0.085 ^a	0.171	0.216
λ (μm)										
2.25	0.951	0.984	0.980	0.917	0.938	0.909	0.948	0.859	0.878	0.824
2.75	0.998	0.981	0.963	0.962	0.953	0.927	0.918	0.823	0.771	0.743
3.00	0.995	0.989	0.921	0.984	0.990	0.881	0.936	0.857	0.853	0.789
3.48	0.668	0.619	0.591	0.551	0.482	0.429	0.420	0.346	0.344	0.317
3.75	0.965	0.949	0.938	0.916	0.897	0.848	0.840	0.739	0.709	0.662
4.00	0.990	0.977	0.962	0.952	0.949	0.918	0.893	0.815	0.763	0.731
4.50	1.000	0.993	0.986	0.981	0.980	0.948	0.940	0.885	0.839	0.817
4.98	0.967	0.953	0.941	0.931	0.924	0.885	0.862	0.776	0.728	0.697
5.49	0.904	0.876	0.866	0.831	0.818	0.751	0.716	0.584	0.532	0.512
6.00	0.922	0.901	0.868	0.876	0.853	0.814	0.806	0.681	0.629	0.575
6.48	0.872	0.840	0.829	0.802	0.782	0.722	0.697	0.549	0.497	0.478
6.75	0.734	0.686	0.659	0.624	0.563	0.503	0.490	0.367	0.330	0.307
6.97	0.849	0.807	0.772	0.752	0.712	0.648	0.644	0.507	0.463	0.416
7.45	0.804	0.754	0.725	0.686	0.660	0.575	0.535	0.380	0.347	0.318
8.00	0.871	0.824	0.814	0.793	0.741	0.678	0.666	0.534	0.473	0.428
8.53	0.866	0.832	0.811	0.787	0.733	0.669	0.656	0.516	0.449	0.429
8.76	0.897	0.862	0.835	0.825	0.779	0.719	0.713	0.570	0.514	0.474
8.88	0.876	0.832	0.817	0.787	0.747	0.675	0.667	0.502	0.444	0.408
9.00	0.850	0.807	0.791	0.756	0.709	0.640	0.624	0.447	0.396	0.363
9.39	0.824	0.788	0.766	0.723	0.677	0.607	0.583	0.409	0.353	0.318

9.53	0.791	0.750	0.720	0.668	0.635	0.553	0.521	0.357	0.305	0.273
9.82	0.838	0.795	0.782	0.728	0.697	0.624	0.584	0.411	0.352	0.321
9.97	0.871	0.836	0.820	0.776	0.751	0.673	0.643	0.461	0.389	0.362
10.12	0.873	0.832	0.811	0.772	0.747	0.670	0.643	0.447	0.377	0.349
10.45	0.905	0.866	0.855	0.808	0.775	0.703	0.672	0.479	0.412	0.380
10.62	0.914	0.881	0.871	0.843	0.811	0.731	0.704	0.518	0.432	0.400
10.80	0.891	0.860	0.834	0.818	0.787	0.692	0.665	0.474	0.404	0.370
11.17	0.894	0.878	0.846	0.830	0.801	0.740	0.714	0.534	0.470	0.440
11.37	0.855	0.850	0.838	0.810	0.784	0.729	0.675	0.513	0.398	0.407
11.78	0.777	0.742	0.691	0.729	0.698	0.643	0.591	0.475	0.292	0.309
12.00	0.719	0.660	0.620	0.655	0.622	0.566	0.518	0.486	0.202	0.224
12.46	0.483	0.413	0.385	0.357	0.344	0.236	0.135	0.017	0.000	0.027
12.71	0.388	0.315	0.291	0.250	0.253	0.149	0.074	0.045	0.011	0.020
13.50	0.700	0.662	0.640	0.613	0.569	0.500	0.456	0.268	0.195	0.173
14.09	0.496	0.459	0.422	0.407	0.385	0.323	0.276	0.172	0.149	0.134
14.40	0.754	0.713	0.678	0.666	0.640	0.566	0.533	0.356	0.309	0.285
15.07	0.900	0.884	0.858	0.854	0.824	0.785	0.749	0.583	0.500	0.450
15.43	0.906	0.872	0.857	0.844	0.821	0.783	0.741	0.562	0.465	0.414
16.20	0.893	0.855	0.836	0.832	0.794	0.749	0.694	0.489	0.405	0.351
16.62	0.875	0.833	0.806	0.801	0.780	0.708	0.628	0.428	0.358	0.316
17.51	0.740	0.699	0.622	0.629	0.604	0.482	0.378	0.211	0.146	0.196
18.00	0.679	0.663	0.568	0.569	0.522	0.408	0.289	0.174	0.146	0.182
18.51	0.703	0.677	0.658	0.610	0.557	0.515	0.349	0.198	0.229	0.200

*Not used for radiative properties inversion.

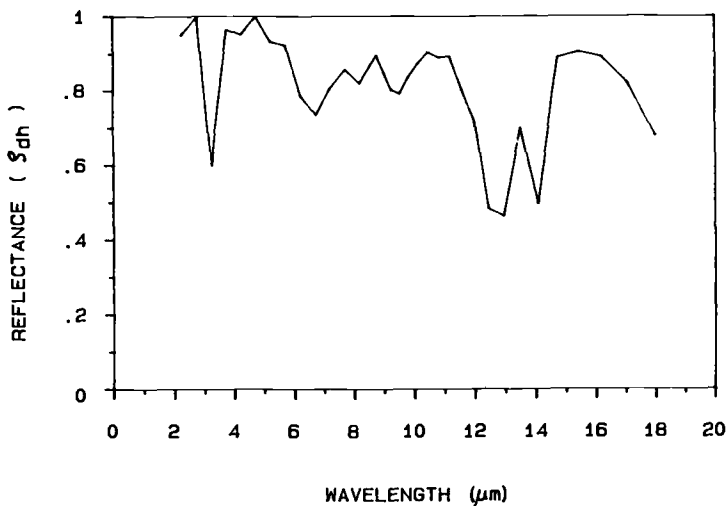


FIG. 2—Directional-hemispherical reflectance for expanded polystyrene foam for 0.020 cm sample thickness in the wavelength range of 2 to 20 μm .

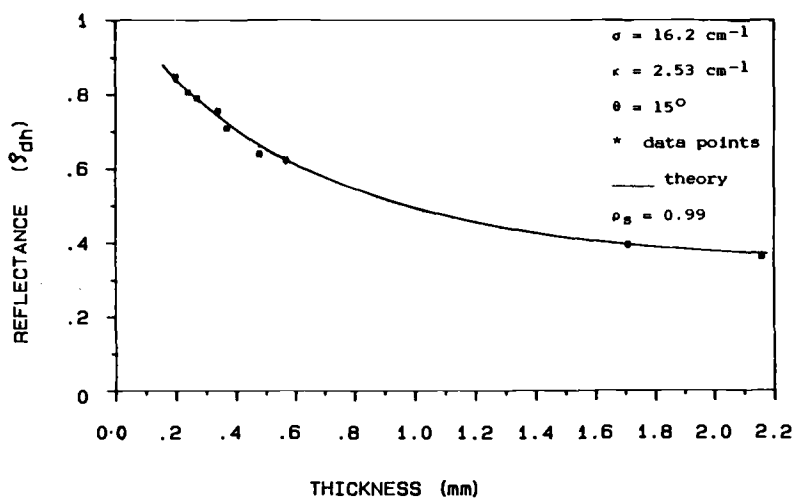


FIG. 3—Comparison of theoretical and experimental directional-hemispherical reflectance for isotropic scattering in expanded polystyrene foam using the inverted radiative properties at $\lambda = 9.00 \mu\text{m}$.

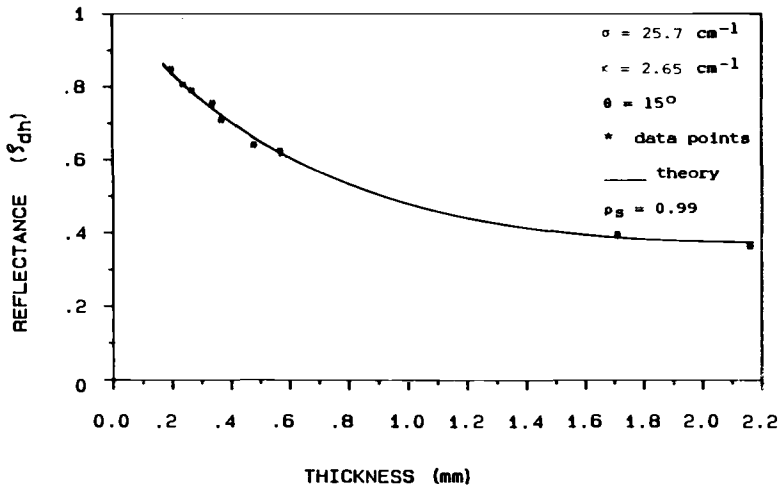


FIG. 4—Comparison of theoretical and experimental directional-hemispherical reflectance for anisotropic scattering in expanded polystyrene foam using the inverted radiative properties at $\lambda = 9.00 \mu\text{m}$.

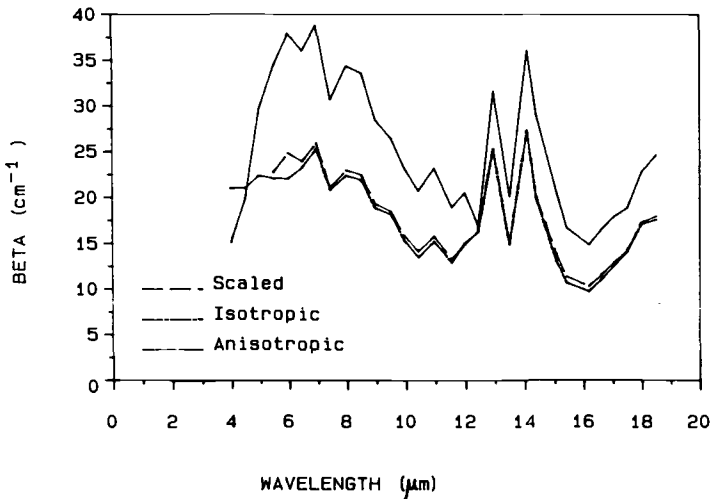


FIG. 5—Isotropic, anisotropic, and scaled extinction coefficient for expanded polystyrene foam inverted from directional-hemispherical reflectance in the wavelength range of 4 to 20 μm .

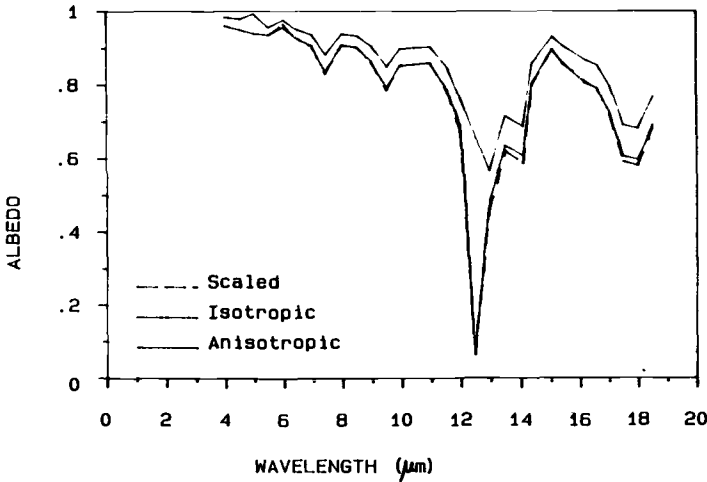


FIG. 6—Isotropic, anisotropic, and scaled albedo values for expanded polystyrene inverted from directional-hemispherical reflectance in the wavelength range of 4 to 20 μm .

TABLE 3—Radiative properties of expanded polystyrene foam using ρ_{dh} data for isotropic scattering.

λ (μm)	σ (cm^{-1})	κ (cm^{-1})	β^+ (cm^{-1})	ω^{++}
4.00	22.0	0.223	22.3	0.989
4.98	22.0	0.222	22.4	0.944
5.49	20.6	1.42	22.1	0.936
6.00	21.0	0.943	22.0	0.957
6.48	21.4	1.73	23.2	0.925
6.97	22.8	2.36	25.3	0.907
7.45	17.3	3.44	20.8	0.835
8.00	20.2	2.03	22.4	0.909
8.53	19.7	2.12	21.9	0.903
9.00	16.2	2.53	18.8	0.866
9.53	14.3	3.81	18.1	0.790
9.97	13.0	2.26	15.3	0.853
10.45	11.5	1.94	13.5	0.856
10.98	13.0	2.12	15.2	0.861
11.57	10.1	2.76	12.9	0.786
12.00	10.2	4.65	14.9	0.689
12.46	1.08	15.2	16.3	0.067
12.96	12.2	13.1	25.3	0.484
13.50	9.44	5.42	14.9	0.636
14.09	16.6	10.7	27.4	0.608
14.40	15.9	3.90	19.9	0.804
15.07	11.7	1.38	13.1	0.895
15.43	9.10	1.51	10.7	0.858
16.20	7.78	1.89	9.71	0.805
16.62	8.66	2.31	11.0	0.790
17.05	9.00	3.48	12.5	0.722
17.51	8.50	5.57	14.1	0.605
18.00	10.2	6.92	17.1	0.596
18.51	12.1	5.47	17.6	0.690
Gray	14.2	2.95	18.0	0.787

$^+\beta = \sigma + \kappa$.
 $^{++}\omega = \sigma/(\sigma + \kappa)$.

TABLE 4—Radiative properties of expanded polystyrene foam using ρ_{dh} data for anisotropic scattering.

λ (μm)	σ (cm^{-1})	κ (cm^{-1})	β^+ (cm^{-1})	ω^{++}
4.00	29.8	0.177	29.9	0.994
4.98	29.3	0.172	29.6	0.994
5.49	32.8	1.46	34.4	0.957
6.00	36.9	0.881	38.0	0.977
6.48	34.0	1.79	36.0	0.950
6.97	36.2	2.45	38.8	0.937
7.45	26.9	3.57	30.6	0.883
8.00	32.1	2.11	34.4	0.939
8.53	31.2	2.20	33.6	0.934
9.00	25.7	2.65	28.4	0.907
9.53	22.3	4.00	26.4	0.849
9.97	20.8	2.37	23.3	0.898
10.45	18.6	2.03	20.7	0.902
10.98	20.9	2.21	23.2	0.905
11.57	16.0	2.90	18.9	0.847
12.00	15.6	4.90	20.6	0.762
12.46	1.57	15.3	16.9	0.094
12.96	17.9	13.7	31.7	0.567
13.50	14.3	5.71	20.1	0.716
14.09	24.7	11.3	36.1	0.688
14.40	24.8	4.09	29.0	0.859
15.07	19.2	1.44	20.7	0.931
15.43	15.1	1.57	16.7	0.906
16.20	12.8	1.97	14.8	0.868
16.62	14.0	2.42	16.5	0.853
17.05	14.2	3.67	17.9	0.796
17.51	13.0	5.86	18.9	0.690
18.00	15.5	7.28	22.8	0.681
18.51	18.9	5.75	24.7	0.767
Gray	21.3	3.88	25.3	0.834

$$^+\beta = \sigma + \kappa.$$

$$^{++}\omega = \sigma/(\sigma + \kappa).$$

μm so that a more realistic wavelength average can be used to compute the steady-state heat transfer in foams. It is known that the β value in the wavelength range of 20 to 40 μm will be lower than in the wavelength range of 4 to 20 μm , because the specular reflectance measured at ORNL shows a monotonic increase in the wavelength range of 20 to 40 μm . In general, an increase in specular reflectance measurements means that β must decrease. A decrease in the gray β would result, thereby increasing k_{app} . This means that the k_{app} values (dashed line), shown in Fig. 7 to be about 4.5% lower than the experimental values, would increase and better agreement between the theoretical and experimental values would result.

The foam gray β and k_{true} values are increasing functions of the foam density [2]. Schuetz [2] has suggested a linear relation between polyurethane foam gray β and the density of polyurethane foam. Hence the isotropic gray β was assumed to be a linear increasing function of the polystyrene foam density, the straight line passing through the origin and the computed gray β ($=18.0 \text{ cm}^{-1}$) at 20.7 kg/m^3 . Using this linear variation of β and the equation for k_{true} (Table 6) for the expanded polystyrene foam, an optimization analysis was undertaken. The results of this analysis are shown in Fig. 8. A minimum k_{app} for expanded polystyrene foams was found to occur at a density of about 20 to 25 kg/m^3 . The theoretical optimum occurs close to the standard reference material (20.7 kg/m^3). The decrease in k_{app} from 10 to 20 kg/m^3 for the polysty-

TABLE 5—Planck mean radiative properties for expanded polystyrene foam using ρ_{dh} data.

T (K)	σ (cm^{-1})	κ (cm^{-1})	β (cm^{-1})	ω
Isotropic Scattering				
100.00	10.1	4.68	14.8	0.680
150.00	10.6	4.86	15.5	0.690
200.00	11.5	4.71	16.2	0.710
250.00	12.5	4.38	16.9	0.740
300.00	13.7	4.00	17.7	0.770
350.00	14.7	3.63	18.3	0.800
400.00	15.6	3.30	18.9	0.830
450.00	16.3	3.01	19.3	0.840
500.00	16.9	2.77	19.7	0.860
Gray ^a	14.2	3.95	18.0	0.787
Anisotropic Scattering				
100.00	15.9	4.90	20.8	0.760
150.00	16.7	5.07	21.8	0.770
200.00	18.1	4.91	23.0	0.790
250.00	19.8	4.57	24.3	0.810
300.00	21.5	4.17	25.6	0.840
350.00	22.9	3.80	26.6	0.860
400.00	24.0	3.44	27.5	0.870
450.00	24.8	3.15	28.0	0.890
500.00	25.4	2.90	28.3	0.900
Gray ^a	21.3	3.88	25.3	0.834

^aGray radiative properties inverted from ρ_{dh} data.

TABLE 6—Thermal and radiative properties used in the heat transfer program for expanded polystyrene foam.

- (1) Density of polystyrene foam (γ_f) = 20.7 kg/m³
- (2) True thermal conductivity (k_{true} for foam) [2]

$$= a + bT + 0.9(2/3 - P_s/300)(1 - \delta)k_s$$

$$a + bT = \text{thermal conductivity of air } (k_{\text{air}})$$

$$= 4.976 \times 10^{-3} + 7.000 \times 10^{-5}T$$

$$(k_{\text{true}} \text{ in W/m-K; } T \text{ in Kelvin})$$

$$P_s = \% \text{ struts in solids}$$

$$\delta = \text{porosity of foam} \approx 8 \times 10^{-4}\gamma_f$$

$$k_s = \text{thermal conductivity of solid polystyrene polymer}$$
 Present case [6]: $P_s = 0\%$; $k_s = 0.225 \text{ W/m-K}$
- (3) Gray β for foam insulation from ρ_{dh} data = 18.0 cm⁻¹
- (4) Gray ω for foam insulation from ρ_{dh} data = 0.787

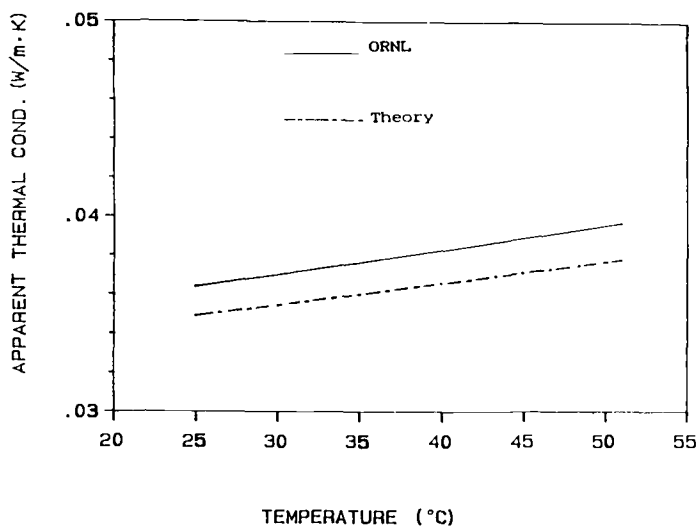


FIG. 7—Comparison of temperature dependence of theoretical and experimental apparent thermal conductivity for expanded polystyrene foam (density = 20.7 kg/m³).

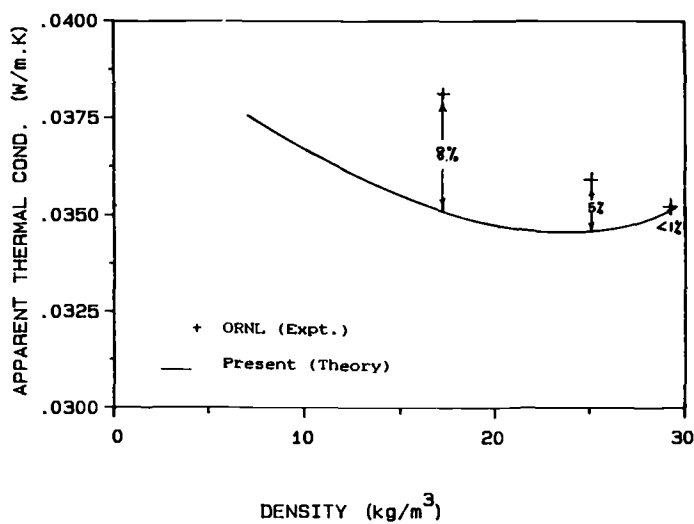


FIG. 8—Density dependence of theoretical apparent thermal conductivity for expanded polystyrene foam at 24°C.

rene foams was found to be about 7%. Also, the theoretical k_{app} values for the expanded polystyrene foam are shown to be lower than the ORNL experimental k_{app} values.

Conclusions and Recommendations

The spectral radiative properties of 20.7 kg/m³ expanded polystyrene foam have been determined. The agreement between the measured and predicted apparent thermal conductivity was fair. The properties were determined in the 4 to 18.5 μ m wavelength region.

It is proposed that reflectance data out to 40 μ m be obtained for the expanded polystyrene foam and also that different foam densities be explored in order to more completely characterize an optimum foam density.

Acknowledgments

This work was funded by the Department of Energy and the Oak Ridge National Laboratory under Contract 19X-55930C.

References

- [1] Tien, C. L. and Cunningham, G. R., "Cryogenic Insulation Heat Transfer," *Advances in Heat Transfer*, Vol. 9, 1973, p. 349.
- [2] Schuetz, M. A., "Heat Transfer in Foam Insulations," Master's thesis, Massachusetts Institute of Technology, Cambridge, Dec. 1982.
- [3] Sinofsky, M., "Property Measurement and Thermal Performance Prediction of Foam Insulations," Master's thesis, Massachusetts Institute of Technology, Cambridge, Jan. 1984.
- [4] Glicksman, L. R., Reitz, D. W., and Schuetz, M. A., *Journal of Cellular Plastics*, March/April 1984, pp. 104-113.
- [5] Amorebieta, V. T. and Colussi, A. J., "Radiation Scattering and Heat Transfer in Cellular Plastics: Thermal Conductivities from Infrared Spectra," *Latin American Journal of Heat and Mass Transfer*, Vol. 6, 1982, pp. 181-190.
- [6] Yajnik, S. and Roux, J. A., "Determination of Radiative Properties of Fiberglass and Foam Insulations," ORNL/Sub/86-55930/1, Dec. 1987.
- [7] Yeh, H. Y. and Roux, J. A., "Spectral Radiative Properties of Fiberglass Insulation," *Journal of Thermophysics and Heat Transfer*, Vol. 2, No. 1, 1988, pp. 75-81.
- [8] Chandrasekhar, S., *Radiative Transfer*, Dover, New York, 1960.
- [9] Roux, J. A., Todd, D. C., and Smith, A. M., *American Institute of Aeronautics and Astronautics Journal*, Vol. 10, No. 7, 1972, pp. 973-976.
- [10] Lee, H. and Buckius, B. O., *Journal of Heat Transfer*, Vol. 104, Feb. 1982, pp. 68-75.
- [11] McElroy, D. L., Graves, R. S., Yarbrough, D. W., and Moore, J. P., "A Flat Insulation Tester that Uses an Unguarded Nichrome Screen Wire Heater," in *Guarded Hot Plate and Heat Flow Meter Methodology*, ASTM STP 879, American Society for Testing and Materials, Philadelphia, 1985, pp. 121-139.

J. Fricke,¹ R. Caps,¹ E. Hümmer,¹ G. Döll,¹ M. C. Arduini,² and F. De Ponte²

Optically Thin Fibrous Insulations

REFERENCE: Fricke, J., Caps, R., Hümmer, E., Döll, G., Arduini, M. C., and De Ponte, F., "Optically Thin Fibrous Insulations," *Insulation Materials, Testing, and Applications, ASTM STP 1030*, D. L. McElroy and J. F. Kimpflen, Eds., American Society for Testing and Materials, Philadelphia, 1990, pp. 575–586.

ABSTRACT: The thermal conductivity of low density organic fiber boards has been measured using various guarded hot plate and heat flow meter apparatus. The data are analyzed with a three-flux representation for the radiative heat transfer and compared with extinction results from infrared optical measurements and scattering theory calculations.

KEY WORDS: thermal insulation, low-density fibrous insulation, guarded hot plate apparatus, radiative conductivity, three flux model, Mie theory

Low-density fiber materials are used to insulate house walls, air plane fuselages, and winter clothes. The density, ρ , of such materials is on the order of 10 kg/m^3 . Heat transport is governed by the thermal conduction of air and by infrared (IR) radiation; the solid conduction via the fiber skeleton contributes only marginally. As in such types of insulations the IR optical thickness, τ_0 , is on the order of 1, the photon diffusion approximation breaks down, and direct IR radiative communication between the insulation boundaries becomes possible. Thus the experimental evaluation, the interpretation as well as the systematic reduction of the loss coefficient, k , is no longer a trivial task. Especially for low boundary emissivity, ϵ , the measured total loss coefficient, k , in air is larger than the loss coefficient in vacuum, k_{vac} , plus the contribution from air conduction, k_{air} (in this case the total flux cannot be expressed as the sum of the individual heat transfer modes).

In order to understand the heat transfer in such insulation systems, we have studied low-density mineral and organic fiber mats in detail. Organic mats had larger fiber diameter and hence a larger heat transfer, which was easier to investigate. Only the results on organic fibers will be given here. Spectral transmission and reflection measurements between wavelengths $\Lambda = 2$ and $40 \text{ } \mu\text{m}$ as well as scattering calculations using the Mie theory allow us to derive a specific extinction coefficient for the fiber system. Extensive calorimetric measurements with different guarded hot plate and heat flow meter apparatus under variation of temperature T , boundary emissivity ϵ , density ρ , and thickness L in air as well as in vacuum allow us to study the contributions from IR radiation, gas conduction, and solid conduction.

Thermal Resistance Measurements

Guarded hot plate and heat flow meter devices basically measure the thermal resistance, $R (= k^{-1})$. Another quantity frequently quoted is the ratio of the specimen thickness, L , to the thermal resistance of the specimen. This quantity is termed the *thermal conductivity*. For low-

¹Physikalisches Institut der Universität, Am Hubland, D-8700 Würzburg, West Germany.

²Istituto di Fisica Tecnica, Università di Padova, Via F. Marzolo 9, I-35131 Padova, Italy.

density insulations, this quantity is not a material property and depends upon such parameters as specimen thickness ("thickness effect") and the surface emissivity of testing equipment; thus one could use the expression *pseudo-conductivity* or *apparent conductivity*. (In ISO Document 9288 the term *transfer factor* is used.) Our goal was to find an analytical expression including as many parameters as needed to describe thermal insulation performance within hot-plate accuracy (let us say 1%) and to derive these parameters experimentally with guarded hot plate or heat flow meter apparatus. Arduini and De Ponte [1,2] discussed a procedure to accurately measure apparatus emissivity, analytically described the pseudo-conductivity, and developed a detailed testing procedure, which is briefly described below.

The typical dependence of thermal resistance, R , from specimen thickness, L , in low-density materials is depicted in Fig. 1. Tests on the same material at different thicknesses give access to the parameters λ_∞ and R_0 . The parameter λ_∞ is the sum of λ_{SG} , the conduction in the gas and in the solid matrix of the fibers, and λ_r , the contribution from radiative heat transfer at infinite thickness. The parameter R_0 depends upon λ_r and λ_{SG} and, in addition, upon the albedo (ratio between scattering and extinction cross section) and the emissivity of the boundaries. The parameter λ_∞ is a material property that can be considered as the conductivity measured on specimens with very large thickness. (In ISO Document 9288 λ_∞ is called *transmissivity*.) It depends upon the density, ρ , according to the following approximate expressions (where C is a function of the extinction cross section and temperature):

$$\lambda_\infty(\rho) = \lambda_{SG}(\rho) + \lambda_r(\rho) = A + B \cdot \rho + C/\rho \quad (1)$$

Figure 2 shows how three specimens can be arranged for tests at different thicknesses to derive λ_∞ and R_0 and also at different densities to derive A , B and C .

These procedures had been applied to mineral and organic fibrous materials at the University of Padova. Data fitting, as shown later, gave very good results. Next the radiation parameters derived by calorimetric experiments had to be checked theoretically and experimentally. The mean test temperature varied between 285 and 305 K, the thickness of the organic fiber board between 33 and 100 mm, and its density between 8 and 25 kg/m³. Great care was devoted to obtaining accurate values for the density. The emissivity of boundary surfaces was 0.92, but tests were also repeated enclosing specimens in reflective foils with an emissivity close to 0.06. The special design and the calibration of the heat flow meter apparatus kept the experimental error on measured thermal resistances within 0.5% of the certified value of the reference material RM 64 issued by the Bureau Communautaire de Reference of the European Community. As the 95% confidence level for RM 64 is nearly 1.5%, the overall accuracy of measured data should be better than 2%. Table 1 is a compilation of some results.

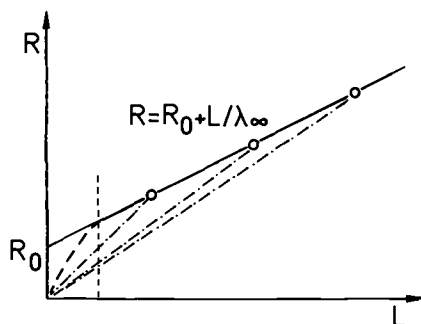


FIG. 1—Thermal resistance, R , of a layer of fibrous material as a function of its thickness, L (see also Eq 12).

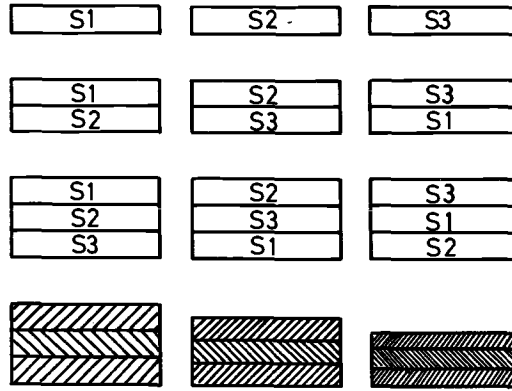


FIG. 2—Arrangements for testing fibrous insulation; the bottom row shows compressed triple stacks.

TABLE 1—Results of thermal pseudo-conductivity measurements with organic fiber boards in air; the last two columns give the percentage deviations of the least squares fit with respect to the experimental data using the gray (see Eq 10) and non-gray three-flux model; the characterization I + II + III indicates that three samples are stacked on top of each other.^a

Samples	ϵ	T_r , K	ρ , kg m ⁻³	L , mm	$\{(\lambda - \lambda_{nt})/\lambda\} \cdot 100$	
					Gray	Spectral
I + II + III	0.920	306.15	12.654	66.77	0.104	-0.244
I + II + III	0.920	306.19	25.273	33.43	0.233	0.047
II	0.920	306.21	8.379	33.43	-0.181	-0.138
II + III	0.920	306.21	8.484	66.77	0.225	0.009
I + II + III	0.920	306.18	8.441	100.10	0.535	0.126
I + II + III	0.920	296.18	12.654	66.77	0.234	0.081
I + II + III	0.920	296.17	25.273	33.43	0.107	0.070
II	0.920	296.19	8.379	33.43	-0.147	0.051
II + III	0.920	296.16	8.484	66.77	-0.132	-0.147
I + II + III	0.920	296.19	8.441	100.10	-0.019	-0.213
II	0.057	296.21	8.379	33.43	1.000	-0.697
II	0.057	296.19	8.848	66.77	-0.336	0.398
II	0.057	296.17	8.441	100.10	-1.025	0.010
I + II + III	0.920	285.75	12.654	66.77	0.149	0.145
I + II + III	0.920	285.77	25.273	33.43	-0.074	0.004
II	0.920	285.82	8.379	33.43	-0.096	0.222
II + III	0.920	285.79	8.484	66.77	-0.038	0.100
I + II + III	0.920	285.78	8.441	100.10	0.051	0.025

^a ϵ = emissivity of boundary, T_r = mean radiative temperature, ρ = density, L = thickness, λ = pseudo-conductivity.

Additional experiments with evacuated specimens have been performed with the guarded hot plate apparatus LOLA I and LOLA II at the University of Würzburg. The total pseudo-conductivity λ ($= L/R$) as a function of mean temperature, T_r , with highly reflective aluminum foil as boundaries for gas pressures below 10^{-3} mbar is depicted in Fig. 3. The derived values for λ are extremely small, since the radiative losses are restricted by the very low boundary emissivity. The solid conductivity, λ_s , via the fiber skeleton is estimated to be below 10^{-3} W/(m · K).

If the specimen filled with air, pseudo-conductivity rises from $\lambda \approx 5 \cdot 10^{-3}$ W/(m · K) to $60 \cdot 10^{-3}$ W/(m · K) at 300 K. The difference is far more than the air conductivity of $26 \cdot 10^{-3}$

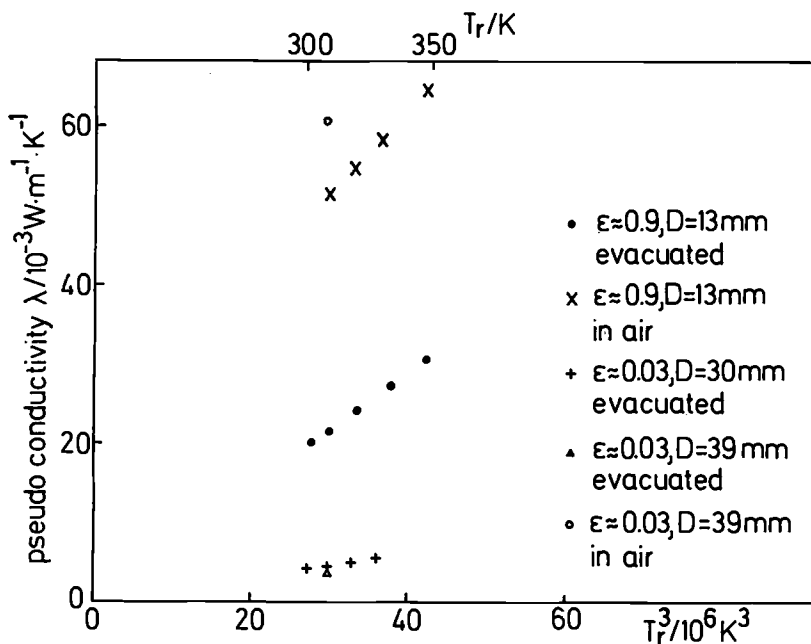


FIG. 3—Measured thermal (pseudo-) conductivity, λ , of organic fiber boards as function of cubed mean temperature, T_r .

$W/(m \cdot K)$. According to Viskanta and Grosh [3] this is due to the coupling between radiation and air/solid conduction heat transfer.

In the case of black boundaries ($\epsilon = 0.89$) the radiative heat flux mainly depends on the extinction properties of the fibers and less on the emissivity. The difference between air-filled and evacuated specimens is about $30 \cdot 10^{-3} W/(m \cdot K)$. The emissivity of the black surface (aluminum foil coated by commercial black paint) was determined from the heat transfer in the empty evacuated hot plate system.

Infrared Extinction Properties of Organic Fibers

Radiative Conductivity

The measured thermal resistances are closely connected to the IR extinction properties of the fibers, which scatter, absorb and emit thermal radiation. The mean free path, ℓ , of the IR radiation depends on the relative scattering and absorption cross sections of the fibers, Q_S and Q_A , respectively. The corresponding absorption, A , scattering, S , and total extinction coefficients, $E (= A + S)$, are related to the relative cross sections, Q , by, for example,

$$E = \frac{4}{\pi} \cdot \frac{\rho}{\rho_0} \cdot \frac{Q_E}{d} \quad (2)$$

where ρ_0 is the solid density of the fiber material and d is the fiber diameter. In the case of absorption and isotropic scattering the mean free path, ℓ , is equal to $1/E$. Note that the specific extinction $e = E/\rho$ is independent of the density of the insulation and thus is a characteristic quantity of the fiber material.

If the mean free path, ℓ , is far smaller than the distance, L , between the boundaries of the insulation, the radiative flux, q_r , can be described by the diffusion model (see, e.g., Hottel and Sarofim [4]):

$$q_r = -\frac{\ell}{3} \cdot \frac{c}{n} \cdot \text{grad}(u) \quad (3)$$

where c/n is the light velocity in the medium with index of refraction n and u is the energy density. In the case of a gray medium, where the mean free path, ℓ , is independent of wavelength, the energy density is

$$u = 4n^3 \cdot \sigma T^4 \quad (4)$$

where σ is the Stefan-Boltzmann constant. As the radiative flux, q_r , is proportional to the temperature gradient, the radiative conductivity, λ_r , becomes in the case of isotropic scattering where $\ell = 1/E$:

$$\lambda_r = \frac{16}{3} \cdot n^2 \cdot \frac{\sigma T^3}{E} \quad (5)$$

For non-gray media the extinction, E , varies with wavelength, Λ , and is replaced by the Rosseland mean, E_R , of the spectral extinction coefficient, $E(\Lambda)$ [4].

Scattering Theory

The cross sections Q and hence the extinction coefficients may be calculated from the optical properties of the fibers: the complex index of refraction, $m(\Lambda)$; the ratio α of fiber diameter, d , to wavelength, Λ ($\alpha = \pi \cdot d/\Lambda$); and the tilt angle, Φ , of the fibers relative to the impinging radiation. Most types of fibers used for thermal insulations show strong scattering in the forward direction. According to McKellar and Box [5] this behavior can be included in the diffusion model (Eq 3) if the extinction cross section, Q_E , is scaled with the anisotropy factor, g , of the intensity phase function, $p(\Omega)$, in the direction Ω , giving an effective cross section of

$$Q_E^* = Q_E \cdot (1 - g) \quad (6)$$

where

$$g = \frac{1}{4\pi} \cdot \int_{\Omega} p(\Omega) \cos \Theta \, d\Omega$$

and Θ is the scattering angle. In this paper the phase function, $p(\Omega)$, is normalized with respect to the albedo, ω_0 (the ratio between scattering and extinction cross section, Q_s/Q_E):

$$\frac{1}{4\pi} \cdot \int_{\Omega} p(\Omega) \, d\Omega = \omega_0 \quad (7)$$

The effective cross sections $Q_E^*(\alpha, m(\Lambda), \Phi)$ are calculated according to the theory of electromagnetic waves scattered off infinitely long cylinders illustrated by Kerker [6]. In lightweight insulations the fiber directions are usually random. Therefore the effective cross section, $Q_E^*(\Phi)$, written as a sum of the scattering coefficients a_{n1} , a_{n11} , b_{n1} , and b_{n11} [7,8], is integrated over all directions, giving the average effective cross section, $\langle Q_E^* \rangle$. The calculation of the scattering coefficients was performed on a PC using the program developed by Bohren and Huffman [9].

Figure 4 shows the wavelength-dependent specific extinction coefficient $e^* = E^*/\rho$ for randomly oriented organic fibers of $40\text{ }\mu\text{m}$ diameter. The index of refraction data, $m(\lambda)$, are taken from McKay et al. [7]. The IR absorption spectrum of the fibers varies strongly with wavelength. Therefore we performed the calculation mainly with values where absorption maxima and minima occur. The Rosseland mean, e_R , of the spectral specific extinction coefficient, $e^*(\lambda)$, is $15.7\text{ m}^2/\text{kg}$ at $T_r = 300\text{ K}$. As we find only a small variation of the relative cross section with fiber diameter between 30 and $50\text{ }\mu\text{m}$, the main error in the determination of the specific extinction ($e^* \propto Q^*/d$) is—besides the error by the limited number of spectral values used—caused by the uncertainty of the fiber diameter. Scanning electron microscopy of the organic fibers reveals increased diameters close to the fiber crossings. An exact determination of fiber thickness therefore is not possible. From measurements with a light microscope we estimate $d \approx 40 \pm 5\text{ }\mu\text{m}$.

Optical Methods

The effective specific extinction, e^* , of fibers can also be determined by optical methods. This technique is especially important if the complex index of refraction of the material is unknown. In the case of anisotropic scattering fibers we have to know the effective optical thickness, $\tau_0^* (= E^* \cdot L)$, of the sample for the calculation of the heat flux. In principle, $\tau_0^* = \tau_0 \cdot (1 - g)$ may be obtained from both the optical thickness, τ_0 , which is derived from the exponential decrease of the intensity with thickness, and the anisotropy factor, g . The determination of the anisotropy factor by measuring the angular variation of the scattered intensity, however, is extremely difficult in the IR, because the scattered intensities are very low and the angular measurement must be repeated for a large number of wavelengths. Thus we chose a different approach where the effective quantities are given directly (see Caps et al. [10]).

The hemispherical transmission, T , of a beam impinging perpendicularly onto the sample in general depends on the optical thickness, τ_0 , the albedo, ω_0 , and the scattering phase function $p(\Omega)$. If the radiative flux is conserved (i.e., in non-absorbing samples, $\omega_0 = 1$), it is possible to scale the optical thickness by the anisotropy factor, g , as in the diffusion model. Then one just has to solve the appropriate equation of transfer for isotropic scattering with $p(\Omega) \equiv \omega_0$. Caps et

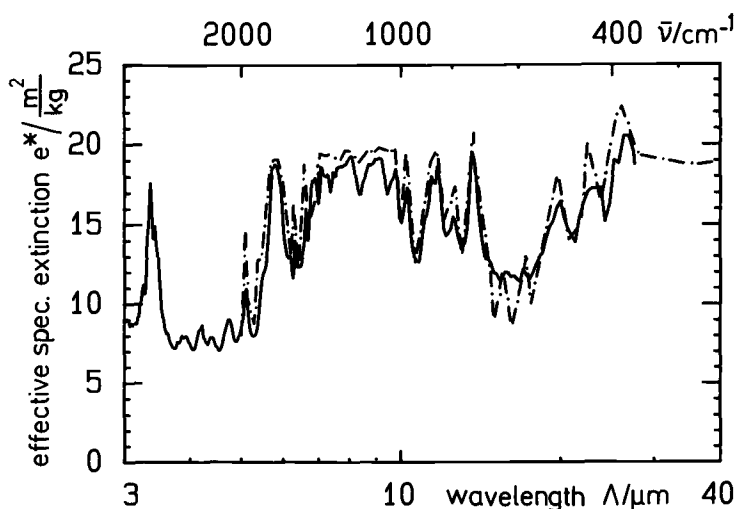


FIG. 4—Effective specific extinction, e^* , as a function of wavelength, λ , (and wave-number ν) calculated from scattering theory (dashed-dotted line, assuming a fiber diameter $d = 40\text{ }\mu\text{m}$) and derived from hemispherical reflection and transmission of organic fiber samples (solid line).

al. have shown [10] that in non-emitting, "cold" media with absorption and simultaneous strongly anisotropic scattering the scaling procedure gives quite accurate results for the hemispherical transmission, T . The equation of transfer again is solved for isotropic scattering, and the optical thicknesses, τ_0 , and albedo, ω_0 , are replaced by their scaled counterparts $\tau_0^* = \tau_0 \cdot (1 - g)$ and $\omega_0^* = (\omega_0 - g)/(1 - g)$; that is, $T = T(\tau_0^*, \omega_0^*, p(\Omega) \equiv \omega_0)$.

We determined the effective albedo, ω_0^* , from hemispherical reflection measurements of optically thick samples: $R_\infty = R_\infty(\omega_0^*)$. For the determination of T and R_∞ we used a three-flux approximation of the equation of transfer proposed by Kaganer [11]:

$$T(\tau_0, \omega_0) = \frac{5/9 p^2 - 5/4}{1 - p^2} \left[(e^{-\tau_0} - e^{-p\tau_0}) - 2/5 a \sinh(p\tau_0) \frac{e^{-\tau_0(1-p)} - 5a}{e^{2p\tau_0} - a^2} \right] + e^{-\tau_0} \quad (8a)$$

$$R_\infty(\omega_0) = \frac{1 - 2/3 p}{1 + p} \quad (8b)$$

where

$$a = \frac{1 - 2/3 p}{1 + 2/3 p}$$

and

$$p = 3/2 \cdot \left(\frac{1 - \omega_0}{1 - \frac{\omega_0}{4}} \right)^{1/2}$$

The hemispherical transmission and reflection measurements are performed with a 76-mm-diameter, gold-coated integrating sphere from Labsphere and a Perkin-Elmer Fourier-Transform IR Spectrometer 1700 for the wavelength range 2.3 to 45 μm . The pyroelectric deuterated-triglycin sulfate detector is mounted at the 90° port location. In the case of reflection measurements the 180° port is used as a sample holder. For transmission experiments the 180° port is closed by a diffuse reflecting gold-coated plug and the sample placed in the 0° port. The port hole diameter is 13 mm. A baffle at 45° prevents direct light from the sample hitting the detector.

Figure 5 shows the hemispherical effective albedo, $\omega_0^*(\lambda)$, of an organic fiber sample as derived from hemispherical reflection measurements in comparison with the scattering theory calculation for a fiber diameter $d = 40 \mu\text{m}$. Using the Rosseland mean the calculated albedo becomes 0.28. According to Eq 8a we get the specific extinction $e^* = \tau_0^*/m''$ with an additional hemispherical transmission measurement of a thin organic fiber sample of mass per area m'' . The measured values are in good agreement with the extinction e^* calculated from scattering theory in Fig. 4. Due to inhomogeneities of the organic samples and their relatively large fiber diameters, we estimate an error of the experimental extinction data on the order of 10%.

Heat Transport in Optically Thin Insulations

The optical thickness τ_0^* of a 40 mm thick organic board with 8 kg/m³ density is on the order of 4. In this case the radiative heat transfer can not be considered as a conduction process, which only depends on the local temperature gradient (Eq 3). The radiative flux, q_r , at a given location is also influenced by the emitted and scattered intensities further apart from this location and the boundaries. Here the appropriate equation of transfer for combined radiation and solid/gas conduction is derived by an integro-differential equation (see, e.g., Viskanta and

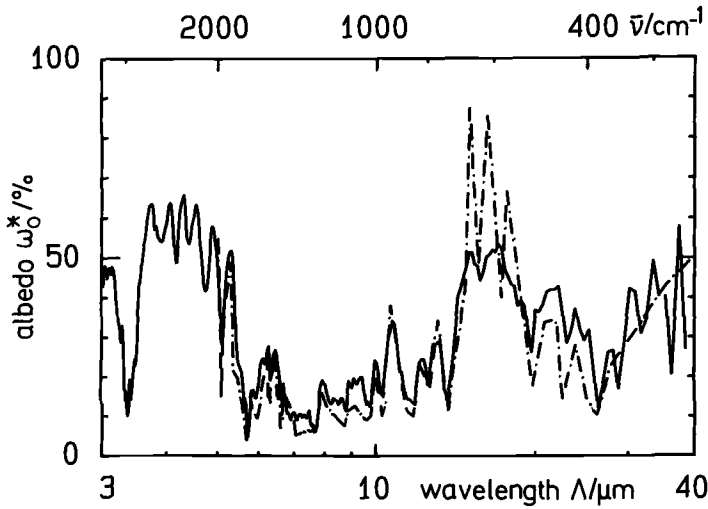


FIG. 5—Effective albedo, ω_0^* , as a function of wavelength, Λ (and wave-number ν) for 40 μm thick organic fibers as obtained from scattering theory (dashed-dotted line) and from hemispherical reflection measurements (solid line).

Grosh [3]), which in general can only be solved by iterative numerical techniques. The resulting total heat flux, q , depends on the boundary temperatures, T_1 , T_2 , and emissivities, ϵ_1 , ϵ_2 , the optical thickness, τ_0^* , albedo, ω_0^* , insulation thickness, L , and solid/gas conductivity, λ_{SG} .

The inverse problem, the determination of τ_0^* , ω_0^* , and λ_S from measured total heat flux, q , cannot be treated in this way. A least squares procedure that fits the above parameters to the measured values is tedious, because it needs a repeated evaluation of the total heat flux, q , for many different sets of parameters. Therefore we used an approximate representation of the combined conduction-radiation transfer problem.

Our approach starts from a three-flux representation (cosine directions μ_{-1} , μ_0 , μ_1) of the equation of transfer for isotropic scattering proposed by Kaganer [9], which includes the 90° sideward direction ($\mu_0 = \cos 90^\circ = 0$). The equations for the three intensities, I_i , are thus reduced to two differential equations plus an equation for the conservation of total flux:

$$\begin{aligned} \mu_1 \cdot \frac{dI_1}{d\tau} &= -\frac{1+\Omega}{2} \cdot I_1 + \frac{1-\Omega}{2} \cdot I_{-1} + 4\Omega \cdot \Theta - 3\Omega \\ \mu_{-1} \cdot \frac{dI_{-1}}{d\tau} &= \frac{1-\Omega}{2} \cdot I_1 - \frac{1+\Omega}{2} \cdot I_{-1} + 4\Omega \cdot \Theta - 3\Omega \\ N_r \cdot \frac{d^2\Theta}{d\tau^2} &= -\frac{a_1}{2} \Omega \cdot (I_1 + I_{-1}) + 4a_1 \cdot \Omega \cdot \Theta - 3a_1 \cdot \Omega \end{aligned} \quad (9)$$

where

$$\Theta = T/T_r$$

$$T_r^3 = (T_1^3 + T_2^3) \cdot (T_1 + T_2)/4$$

$$\Omega = (1 - \omega_0)/(1 - \omega_0 \cdot a_0/2)$$

$$\mu_1 = -\mu_{-1} = 2/3$$

$$a_1 = a_{-1} = 3/4$$

and

$$a_0 = 1/2$$

As we assume small temperature differences $T_1 - T_2$, the emission term has been linearized to $(\sigma T_r^4/\pi) \cdot (4\Theta - 3)$. The intensities, I_i , are expressed in units of $\sigma \cdot T_r^4/\pi$. Solving this system of linear differential equations and applying the appropriate boundary conditions, the following expression for the total heat flux, q , the loss coefficient, k , or the resistance, R , is obtained:

$$k = R^{-1} = \frac{q}{T_1 - T_2} = \frac{\frac{\lambda_\infty}{L}}{1 + \frac{4/3}{N_r \frac{p \tau_0}{2} \coth\left(\frac{p \tau_0}{2}\right) + \frac{\epsilon \tau_0}{2 - \epsilon} (3/4 N_r + 1)}} \quad (10)$$

where

$$p = 3/2 \left\{ \frac{1 - \omega_0}{1 - \frac{\omega_0}{4}} \cdot \left(1 + \frac{4}{3N_r} \right) \right\}^{1/2}$$

$$N_r = \frac{\lambda_{SG} \cdot E}{4\sigma n^2 T_r^3}$$

and

$$\lambda_\infty = 16/3 n^2 \frac{\sigma T_r^3}{E} + \lambda_{SG}$$

Anisotropic scattering again can be included by scaling the optical thickness, τ_0 , and the albedo, ω_0 . In principle this three-flux approximation may be extended to five- and n -flux equations if higher accuracy is needed. The same expression as Eq 10 was derived by McKay et al. [7] starting from the diffusion model, except that p is given by

$$p = \left\{ 3 \cdot (1 - \omega_0) \cdot \left(1 + \frac{4}{3N_r} \right) \right\}^{1/2} \quad (11)$$

Arduini and De Ponte [2] used a slightly modified form of Eq 10 to derive material parameters from measured hot plate and heat flow meter data, as explained in the Thermal Resistance Measurement section. If $p \cdot \tau_0/2 \geq 2$ holds, the coth term in Eq 10 can be neglected. The thermal resistance, R , is then a linear function of the thickness, L , as already depicted in Fig. 1:

$$R(L) = \frac{1}{E} \cdot \left(\frac{1}{\lambda_{SG}} - \frac{1}{\lambda_{\infty}} \right) \cdot \left\{ \frac{p}{2} + \frac{3}{4} \frac{\epsilon}{2 - \epsilon} \cdot \frac{\lambda_{\infty}}{\lambda_r} \right\}^{-1} + \frac{L}{\lambda_{\infty}} = R_0 + \frac{L}{\lambda_{\infty}} \quad (12)$$

A comparison between Eqs 10 and 11 and an exact solution of the equation of transfer for $\omega_0 = 0$ is given in Table 2 [12]. For the organic fiber insulation $N_r = 1$ and $\tau_0 = 5$ applies, for which the error of the diffusion and three-flux method is below 1%.

Analysis of Calorimetric Measurements

Equation 10 has been derived for a gray medium. If the spectral variation of the effective extinction cross section and albedo is not too large, we may interpret the unknown parameters τ_0^* and ω_0^* as the spectrally averaged values, and the gray solution is fitted to the experimental results of pseudo-conductivity measurements. The sum of the solid conduction part, λ_s , and the temperature-dependent conductivity of air gives

$$\lambda_{SG} = A(T_r) + B \cdot \rho = 0.025777 \cdot \{1 + 0.003047 \cdot (T_r - 293.2 \text{ K}) - 2.23 \cdot 10^{-6} \cdot (T_r - 293.2 \text{ K})^2\} + B \cdot \rho \quad (13)$$

where B is a free parameter, which will be adjusted by comparing the experimental data with Eq 10. Also the specific extinction coefficient, e^* , and the albedo, ω_0 , were chosen as free parameter for the fit. The square of the index of refraction, n^2 , was approximated by

$$n^2 = 1 + 1.4 \cdot \rho / \rho_0 \quad (14)$$

according to the Clausius-Mosotti formula with $n = 1.7$. Table 1 compares the results of the least squares fit procedure using Eq 10 with the experiment. We obtained $e^* = 13.5 \text{ m}^2/\text{kg}$, which is about 10% lower than the value obtained by Mie theory calculations and optical measurements. Furthermore, we derive $\omega_0^* = 0.54$ and $B = 80 \cdot 10^{-6} \text{ W m}^{-1} \text{ K}^{-1} \text{ kg}^{-1} \text{ m}^3$. The mean square deviation of the fit from the experiment is 0.4%. Another fit with a broader range of different samples gives about the same parameters with a least squares deviation of 0.7%.

TABLE 2—Deviation Δ of the normalized total heat flux $Q = q/\sigma T_2^4$ derived from the three-flux model (3fl) and the diffusion model (dif) according to Eqs 10 and 11 for $\omega_0 = 0$ and the flux Q_{num} from a numerical solution of the exact equation of transfer ($\Theta_2 = 1$, $\Theta_1 = 0.95$, $N_2 = \lambda_s \cdot E/(4n^2 \cdot \sigma T_2^3)$).

τ_0	N_2	1			0.1		
	ϵ	Q_{num}	$\Delta(3\text{fl}), \%$	$\Delta(\text{dif}), \%$	Q_{num}	$\Delta(3\text{fl}), \%$	$\Delta(\text{dif}), \%$
0.5	1.00	0.5413	0.97	1.63	0.1803	2.91	4.55
	0.05	0.4290	-0.69	0.83	0.0668	-3.85	4.20
1	1.00	0.3137	1.61	2.69	0.1312	3.59	5.21
	0.05	0.2415	-0.64	2.98	0.0539	-2.60	7.80
5	1.00	0.0814	0.99	1.47	0.0441	1.56	2.09
	0.05	0.0733	0.67	3.01	0.0295	-0.67	5.22
10	1.00	0.0426	0.56	0.81	0.0242	0.71	1.00
	0.05	0.0403	0.34	1.61	0.0192	-1.42	2.28

The derived albedo of 0.54 is higher than the aforementioned value 0.28. Therefore we tried to extend Eq 10 to the non-gray case by including the spectral values

$$e^*(\Lambda)/(m^2/kg) = (4/\pi) \cdot (1000/1.38) \cdot \langle Q_E^*(\Lambda) \rangle / (d/\mu m) \quad (15a)$$

$$\omega_0^*(\Lambda) = c \cdot \omega_0^*(\Lambda)_{\text{Mie}} \quad (15b)$$

We used $\langle Q_E^*(\Lambda) \rangle$ and $\omega_0^*(\Lambda)_{\text{Mie}}$ of the organic fibers from Mie scattering theory calculation (Figs. 4 and 5) and multiplied them by the free parameters $1/d$ and c . The flux, $q(\Lambda)$, is then integrated over the thermal spectrum with the Rosseland distribution as a weight function. Such a procedure has been employed quite successfully in the description of the radiative heat flux in silica aerogel, a light transparent low density insulation. According to Scheuerpflug et al. [13], the absorption coefficient in this material varies by a factor of up to 10 000 between $\Lambda = 2$ to $40 \mu m$.

The relative deviations of the spectrally fitted pseudo-conductivities from the experimental are shown in Table 1. The mean square deviation is now as low as 0.22%, and the fitted albedo agrees well with the calculated one, as the free parameter is $c = 1.04$. The best fit of extinction according to Eqs 15a and 15b corresponds to that of fibers with $d = 45.8 \mu m$ diameter; the solid conduction parameter, B , is again about $80 \cdot 10^{-6} W m^{-1} K^{-1} kg^{-1} m^3$. The same fit with an extended collection of experimental data shows no improvement of the accuracy compared to the "gray" fit. The main reason may be that the experimental errors (conductivity λ , density ρ , homogeneity) are not as low as for the data selected here, which mostly correspond to Sample II. If the parameter A of Eqs 1 and 13 is in addition left as a free parameter, its value reproduces the air conductivity (numerical part of Eq 13) to within 1%. This confirms the accuracy of the calorimetric measurements.

Conclusions

To conclude, data fitting by using Eq 10 and its modified forms has been shown to be quite successful. However, the extinction coefficient and the albedo obtained through optical and calorimetric methods agree only within about 10%. Here the accuracy needs to be improved. At the present stage of knowledge on theoretical analysis and experimental procedure, discrepancies can be caused by sample preparation, IR measurements, and simplified modelling of radiation heat transfer. Once the agreement of calorimetric and optical methods reaches an accuracy of a few percentage points, some of the long-lasting calorimetric tests with hot plate or heat flow meter apparatus could be replaced by faster IR optical methods.

Acknowledgments

This work was supported by the German Bundesministerium für Forschung und Technologie (BMFT).

References

- [1] Arduini, M. and De Ponte, F. in *Proceedings, 17th ICHMT Symposium on Heat and Mass Transfer in Refrigeration and Cryogenics*, Hemisphere Publishing, Washington, D.C., 1987.
- [2] Arduini, M. and De Ponte, F., *High Temperature-High Pressure*, Vol. 19, 1987.
- [3] Viskanta, R. and Grosh, R. J., *International Journal of Heat and Mass Transfer*, Vol. 5, 1962, p. 729.
- [4] Hottel, H. C. and Sarofim, A. F., *Radiative Transfer*, McGraw-Hill, New York, 1967.
- [5] McKellar, B. H. J. and Box, M. A., *Journal of Atmospheric Sciences*, Vol. 38, 1981, p. 1063.
- [6] Kerker, M., *The Scattering of Light*, Academic Press, New York, 1965.

- [7] McKay, N. L., Timusk, T., and Farnworth, B., *Journal of Applied Physics*, Vol. 55, 1984, p. 4064.
- [8] Caps, R., Fricke, J., and Reiss, H., *High Temperature-High Pressure*, Vol. 17, 1985, p. 303.
- [9] Bohren, C. F. and Huffman, D. R., *Absorption and Scattering of Light by Small Particles*, Wiley, New York, 1983.
- [10] Caps, R., Baumeister, K., and Fricke, J., *High Temperature-High Pressure*, Vol. 18, 1986, p. 589.
- [11] Kaganer, M. G., translated from *Optika and Spektroskopika*, Vol. 26, 1969, p. 443.
- [12] Döll, G., Diplom. thesis, Report E12-0987-1, 1987, Physikalisches Institut der Universität, Würzburg, West Germany (unpublished).
- [13] Scheuerpflug, P., Caps, R., Büttner, D., and Fricke, J., *International Journal of Heat and Mass Transfer*, Vol. 28, 1985, p. 2299.

Minimum Life-Cycle Cost Analysis of Residential Buildings for PC-Based Energy Conservation Standards

REFERENCE: Tuluca, A. and Heidell, J., "Minimum Life-Cycle Cost Analysis of Residential Buildings for PC-Based Energy Conservation Standards," *Insulation Materials, Testing, and Applications, ASTM STP 1030*, D. L. McElroy and J. F. Kimpflen, Eds., American Society for Testing and Materials, Philadelphia, 1990, pp. 587-596.

ABSTRACT: The proposed "Energy Conservation Standards for New Federal Residential Buildings" are embodied in an interactive computer program which analyzes over 400 Energy Conservation Options (ECOs) for 9 housing types and 5 fuels across 1000 U.S. climate zones. The program uses Life-Cycle Cost (LCC) economic analyses in a two-step procedure to derive a result close to the "economic optimum": (1) an initial Savings-to-Investment Ratio (SIR) ranking, followed by (2) a series of Net Benefit (NB) iterations. Consideration is given to the interaction between the set of envelope and the set of mechanical equipment ECOs.

The distinctive feature of the LCC algorithm is that it simultaneously evaluates these two sets of ECO types, and in doing so it keeps active the *entire* list of energy conservation measures throughout the NB calculations. Envelope ECOs found to be ineffective at a certain combination of heating/cooling mechanical equipment efficiencies are re-examined every time equipment efficiencies change. In a new context of efficiencies, these envelope ECOs may become cost-effective. Similarly, envelope ECOs which were before cost-effective may lose this status. The same process applies to the LCC evaluation of equipment ECOs within a changing loads context.

KEY WORDS: standards, life-cycle cost, energy conservation, energy conservation option, housing, residences, optimization

The performance-based "Energy Conservation Standards for New Federal Residential Buildings" apply to housing built by the Federal Government. The Standards were incorporated in a computer program with the goal of providing a flexible tool that is responsive to the wide range of climate and economic conditions encountered in the United States. This computer program—COSTSAFR—calculates the "optimum" mix of energy conservation options for a variety of residential building prototypes (ranch, two-story, etc.) based on location-specific variables. The variables include local weather, construction cost, mechanical equipment cost, and energy cost. In the compliance section, the user has over 400 Energy Conservation Options (ECOs) to select from in order to achieve an energy consumption lower than or equal to the "optimum" prototype.

The computer program addresses both site-built and HUD-code manufactured housing (formerly known as "mobile homes"). The analyzed ECOs are based upon two energy use and three cost data bases. The site-built energy data base [1] includes seven prototypes: ranch house, split-level house, mid and end town houses, mid and end apartment houses, and two-story house. The HUD-code manufactured housing energy use data base [2] contains two prototypes: a single and a double section manufactured home. These energy use data bases include the

¹Steven Winter Associates, Inc., New York, NY 10001.

²Synergic Resources Corporation, Seattle, WA 98103.

condensed results of over 20 000 DOE-2.1 simulations (in general, DOE-2.1A for insulation and infiltration ECOs, and DOE-2.1C for glazing and thermal mass ECOs). The cost data bases include current construction and equipment costs for single-section manufactured housing, for double-section manufactured housing, and for site-built houses.

The Life-Cycle Cost (LCC) method described in this paper employs algorithms which were developed to provide accurate ECO selection through an analysis of the *combined* effect of these ECOs on energy usage. These algorithms are applicable to any automated ECO selection procedure, but are believed not to be practical for manual calculations due to their iterative nature.

Description of COSTSAFR Program

The COSTSAFR program (Conservation Optimization Standards for Savings in Federal Residences) is written in C and runs on a PC compatible computer with a minimum of 256K of memory. The program is in the public domain and comes with a user's manual [3]. In addition, there is extensive documentation in the technical support document [4].

The data are entered into the program through a series of screen menus that check the input for valid ranges. The user selects the housing prototypes and HVAC equipment/fuel combinations. The building location is extracted from a list of over 1000 U.S. climate zones. Local fuel costs are also entered at this time. Finally, the user can constrain the optimization program by defining minimum levels for the thermal integrity of the building shell components, or minimum efficiencies for the HVAC equipment. The input can be saved and recalled for future use and/or modification.

Modifications are also performed using menus. First costs can be adjusted either individually, or globally with regional multipliers. Inflation factors are based on U.S. Department of Energy estimates and can be updated.

The program performs an LCC analysis and outputs a point system, customized according to climate and economic parameters.

Approach to Life-Cycle Cost Minimization

The economic analysis is based upon LCC calculations. The LCC approach is logical for government construction [5], since it incorporates all costs associated with an investment: initial investment costs, salvage values, non-fuel operations and maintenance costs, replacement costs, fuel costs, and cost of money.

Two LCC calculation procedures are used in the Standards: Savings-to-Investment Ratio (SIR) and Net Benefit (NB). The SIR divides the energy savings over the life of the project under analysis by the associated project costs. An SIR greater than 1 indicates that the project is cost-effective. The NB procedure calculates the difference between the LCC of a building with and without a given energy conservation option (ECO). If the NB is positive, then the ECO is cost-effective.

The SIR ranking is performed first, since the order in which ECOs are analyzed may affect the final solution. (This is because the optimization procedure does not analyze every permutation of the hundreds of ECOs.) Based on the SIR ranking, options with the highest return per dollar invested are considered first by the computer program in its NB calculations. If Net Benefits were used instead for the initial ranking, options with higher absolute savings but a lower return per dollar invested might have been considered first.

In the second procedure, calculations ensure that ECOs which yield the lowest LCC are selected in the final set of "optimum" energy conservation measures. During this second test ECOs with lower and lower SIRs are examined and their Net Benefits calculated. If the Net Benefit is positive, the ECO examined is added to the list of "optimum" ECOs. The process continues until the most cost-effective ECOs are selected. Detailed algorithm description is provided in the following sections.

Dependence and Independence of ECOs

Before reviewing the logic of the optimization procedure it is necessary to examine the interaction of the hundreds of alternative ECOs. The energy consumption data bases derived from DOE-2.1 computer simulations have the underlying assumption that "base" ECOs affecting the building envelope are all independent [6]. "Base" envelope ECOs are ceiling insulation, wall insulation, foundation, insulation, infiltration, and certain window attributes (namely, number of panes, sash type, air gap, and window area). The independence assumption is approximate, so the computer simulations were specifically designed to minimize the errors. One of the means to minimize the approximations was to simulate realistic combinations of ECOs. For example, when investigating the effectiveness of changing the wall R-values from R-11 to R-13, the floor and roof were assigned moderate insulation levels too (R-11 and R-19 respectively). However, the overall thermal integrity of the house was much higher when calculating the energy savings resulting from the upgrade of an R-19 wall to an R-24 wall (R-30 in the floor and R-38 in the roof).

Additional envelope ECOs are included in the energy data base as "modifiers" which interact with the "base" building envelope ECOs. There are five sets of modifiers: roof color, movable insulation, heat reflective glass, sun spaces, and passive solar design. In the LCC analysis each (ceiling insulation)/(roof color) ECO combination is treated separately. A level of ceiling insulation with light color roof constitutes one ECO, while the same level of insulation with a dark color roof constitutes another ECO. Movable insulation, heat reflective glass, and heat absorbing glass are combined with the "base" window attributes. There is a separate ECO for each combination of movable insulation, window area, type of glass (clear, heat absorptive, heat reflective), number of panes of glass, air gap, and sash type. This represents a significant increase in the number of window ECOs to be considered in the optimization process. However, it is necessary to consider all window ECO combinations since they are mutually exclusive; that is, they cannot exist at the same time.

Heating and cooling equipment performance affects envelope ECO performance and vice versa. The cost-effectiveness of heating and cooling equipment is a function of building loads. Likewise, the cost-effectiveness of each building envelope option is a function of the efficiency of the heating and cooling equipment. Consequently all "envelope" type ECOs are inter-dependent with all ECOs of "equipment" type.

General Description of Economics Algorithm

An algorithm which identifies a list of cost-effective ECOs was developed to incorporate the previous assumptions about independence and exclusiveness. This algorithm is conceptually illustrated in Fig. 1 and explained in Steps 1 to 19 of the Detailed Description of Economics Algorithm section. References to these steps are made below. The basic economic analysis approach consists of two procedures:

(1) *Savings-to-Investment Ratio Calculations:*

(a) The SIRs for all mutually exclusive ECOs are calculated using marginal savings and marginal costs (Steps 1 and 2).

(b) ECOs with $0 < \text{SIR} < 1$ are eliminated from further consideration. Remaining ECOs are ranked in descending order by their SIRs (Steps 3, 4, and 5).

(2) *Net Benefit Calculations:*

(a) The computer keeps track of the latest adopted ECOs by incorporating them into the Current Building Description (CBD). Within the CBD, ECOs are grouped in categories (e.g., wall insulation, floor insulation, glazings, oil heating equipment efficiencies) and are also tagged as "envelope type" or "equipment type" as shown in Step 6. Starting initially with the ECO with the highest SIR, the Net Benefit of each ECO is examined (Step 7). *ECOs with posi-*

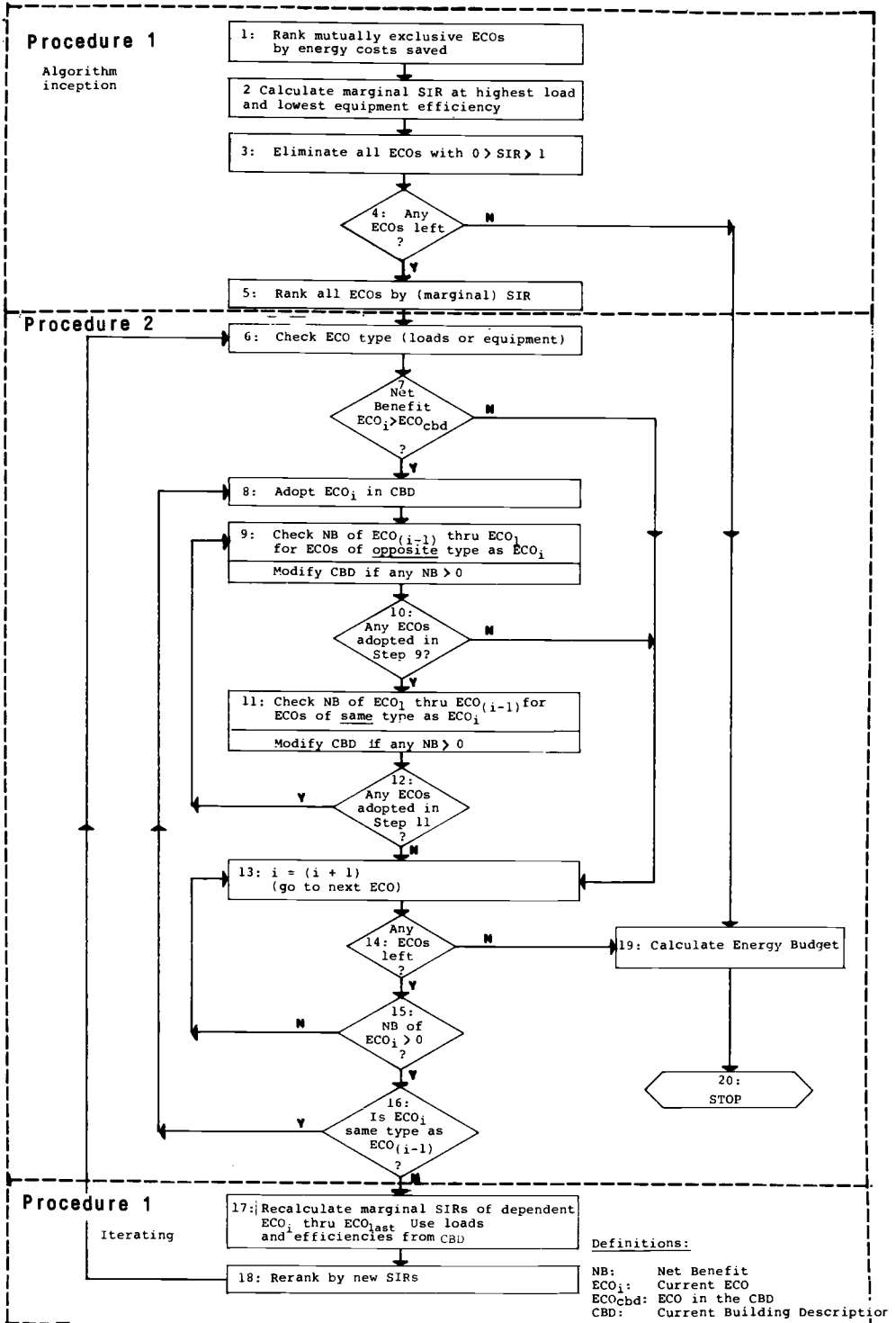


FIG. 1—Logical flow chart.

tive Net Benefits are adopted. ECOs with negative Net Benefits are rejected for the moment, but are not eliminated from the ECO list (Step 8). These ECOs, as well as those adopted previously, are subject to being reconsidered repeatedly during the "optimization" process. It is here that the COSTSAFR algorithms depart from the Life-Cycle Cost procedures of the Federal Energy Management Program (FEMP) [5], because FEMP procedures do not reconsider an ECO once it is eliminated.

The approach taken in COSTSAFR was to increase the accuracy of the FEMP procedures by examining the merit of every ECO in more than one context. That is, the cost-effectiveness of envelope ECOs is examined at several equipment efficiencies, and the cost-effectiveness of equipment ECOs is examined at different space conditioning loads. As loads change, equipment ECOs previously examined are checked again. Similarly, as equipment efficiencies change, the envelope ECOs are rechecked (see Part 2b). In order to achieve this, no ECO which was retained after the completion of the SIR procedure is discarded during the NB procedure.

(b) The computer program performs a test to determine whether the adoption of the latest ECO will change the status of any of the previously examined interdependent ECOs (Step 9). (Remember that envelope ECOs are inter-dependent with mechanical equipment ECOs.) This test is necessary because a reduction in total loads due to the incorporation of an envelope ECO may result in a substantial reduction in the energy savings associated with the equipment ECO currently in the "optimum" list (in the CBD). Consequently, the cost-effectiveness of this equipment ECO may be negated, leading to its exclusion from the list and to the adoption of a previously rejected equipment ECO. Likewise, incorporation of an equipment ECO may result in the rejection of an envelope ECO currently in the CBD and in the adoption of a previously rejected envelope ECO. The program iterates in Steps 10 to 12 until no further changes are made to the Current Building Description.

(c) A new ECO is then examined in Steps 14 and 15, using the positive NB criterion. If $NB > 0$, the program checks whether the ECO is interdependent (i.e., has a different type from the previous one adopted in Steps 8 to 11). This check is performed in Step 16. If the last adopted measure was of "equipment" type, a newly adopted "envelope" ECO signifies a change in type and vice versa. When a dependent measure is adopted, the *remaining ECOs* are recalculated using marginal SIRs, then ranked again (Steps 17–18). The SIRs for remaining envelope measures are calculated at current equipment efficiency. Likewise, remaining equipment measures are evaluated at current heating and cooling loads.

The key term in this description is "remaining ECOs". For example, if a new equipment efficiency was adopted, all remaining envelope ECO energy savings, and therefore all associated SIRs, are recalculated. Theoretically, *all* envelope ECOs, both remaining and already examined, need to be rechecked. This would result in checking *all* ECOs combinations, an impossible task. By checking all the *remaining* ECOs, an approximation may be incurred. The approximation is, however, mitigated by the fact that the entire list of ECOs was initially ranked based on SIRs, thereby decreasing the possibility of substantial ranking misplacements. Furthermore, the process of continuously checking the Net Benefits of all ECOs previously examined (Part 2b) provides another degree of safety. The partial SIR ranking thus devised increases the accuracy of the algorithm without rendering it unwieldy.

(d) After re-ranking, the program loops to Part 2a.

(e) When all ECOs have been examined, the program calculates in Step 19 the energy consumption of the "optimum" house (i.e., the house which is most cost-effective over its useful life).

Detailed Description of Economics Algorithm

The preceding section describes the general procedures for calculating marginal SIRs and includes a brief overview of the optimization process. This section provides additional details about the 19 steps shown in Fig. 1.

Step 1: Rank Mutually Exclusive ECOs by Energy Costs Saved

The mutually exclusive Energy Conservation Options (ECOs) are ranked within each ECO Category (e.g., wall insulation, floor insulation, fenestration, efficiency of oil furnaces and boilers, efficiency of gas furnaces and boilers). The ranking is performed in increasing order of the combined heating and cooling fuel cost savings of these ECOs. All savings are calculated at their maximum possible value: savings of envelope ECOs are calculated at the lowest heating and cooling equipment efficiencies, and savings of equipment ECOs at the highest heating and cooling loads.

In order to facilitate the illustration of the program's algorithms, each ranked ECO Category is described as having the ECO with highest energy cost (least stringent) at the "top", and the ECO with lowest energy cost (most stringent) at the "bottom". In this context, an ECO is "above" another one if it has a higher energy cost. This step is necessary in order to correctly calculate the marginal (incremental) SIRs in Step 2.

Step 2: Calculate Marginal SIRs at Highest Load and Lowest Equipment Efficiency

The SIRs are calculated separately, and marginally, within each ECO category. For example, within the Wall Insulation ECO Category, all wall insulation alternatives are mutually exclusive (i.e., they cannot exist simultaneously). If the ranking of wall insulation by stringency (STEP 1) is R-7, R-11, R-13, then both savings and costs for R-11 are calculated relative to R-7. Similarly, for R-13, savings and costs are calculated relative to R-11.

The SIRs of the initial list of ECOs are calculated at their highest possible values. Equipment options are calculated at the highest possible load, and building envelope options are calculated at the lowest possible equipment efficiency. This procedure ensures that SIRs can only decrease when interactions between envelope and equipment are taken into account. As a result, options that are economically ineffective at this stage (SIRs between 0 and 1) will be ineffective for any other equipment/envelope configuration.

Step 3: Eliminate All ECOs with $0 < SIR < 1$

The ECOs with SIRs in the range $0 < SIR < 1$ are eliminated from further consideration since they are not, and could not be under any circumstances, cost-effective.

An $SIR < 0$ for a given ECO indicates that the dollar energy savings criterion is insufficient to properly rank that particular ECO. To correct this situation, the SIR for the ECO under examination is recalculated in reference to the mutually exclusive ECO two levels "above" it (as defined in Step 1).

Assume that in the Wall ECO Category the measures are ranked R-7, R-11, R-13, R-19, and R-13 plus R-5 sheathing, from highest to lowest energy cost. Further assume that due to local circumstances the wall with R-13 insulation and R-5 sheathing costs less than the R-19 wall. (This may be due to the difference in cost of 2×6 framing versus 2×4 framing, to more expensive window and door jambs in a $5\frac{1}{2}$ in. wall, and to the need of structural metal straps in the unsheathed 2×6 wall). In this case, the R-13 wall with R-5 sheathing has a negative SIR, since it saves both energy and dollars when compared to the R-19 wall. The calculation has to be performed again, this time in reference to the ECO two levels "above" it (i.e., R-11).

Step 4: Check Whether Any ECO Passed the SIR Screening

If all ECOs are eliminated in Step 3, then the "base case" building is the most cost-effective and the program skips directly to Step 19, where the energy budget is calculated. If ECOs remain after the purging in Step 3, the LCC procedure continues.

Step 5: Rank the ECOs By SIRs

All ECOs, regardless of whether they are mutually exclusive or not, are ranked in descending order by their SIRs, within a single list.

Step 6: Check ECO Types (Envelope or Equipment)

There are two generic types of ECOs: those which improve the thermal integrity of the building envelope and those which augment the HVAC equipment efficiency. The energy savings of ECOs within each type are independent, while the energy savings of ECOs of different types are inter-dependent. In order to correctly account for interactions between inter-dependent ECOs, the program must know whether any given ECO affects the envelope or the equipment. At this step a flag is set to determine whether the ECO type is "envelope" or "equipment".

Step 7: Calculate the Net Benefit of the ECO under Analysis

The Net Benefit of the ECO under analysis is calculated relative to the mutually exclusive ECO in the Current Building Description (CBD). The CBD contains the list of all energy conservation features found to be cost-effective at a given time. Envelope and equipment efficiencies from the CBD are used for calculating the energy savings of both ECO types. If the Net Benefit is positive, the program proceeds to Step 8. If the Net Benefit is zero *and* the ECO under consideration yields greater energy savings than the one in the CBD, the program also proceeds to Step 8. Otherwise, the program branches to Step 13.

Step 8: Adopt the ECO in the Current Building Description

As noted above, the CBD contains the list of all energy conservation features found to be cost-effective at a given time. The ECO evaluated in Step 7 is included in the Current Building Description by replacing the prior mutually exclusive ECO. For example, if the CBD contains a wall insulation of R-11, and if the R-13 wall is found to be cost-effective in Step 7, then the R-13 wall replaces the R-11 wall in the CBD.

Step 9: Check the Net Benefit of Those Previously Examined ECOs Which Are of the Opposite Type from the Latest Adopted ECO

The ECO adopted in Step 8 is either of the "envelope" or "equipment" type. When an envelope ECO is adopted in Step 8, all equipment ECOs previously examined in the NB procedure must be re-examined. For example, assume that a heat-reflective window is selected in Step 8 and that it replaced a clear-glass window in the Current Building Description. Further, assume that a high efficiency furnace was previously rejected as not cost-effective. Under the new circumstances, the heat-reflective window might increase the heating load sufficiently to make the adoption of the high efficiency furnace cost-effective. Conversely, when an equipment option is adopted, envelope ECOs previously examined must be rechecked.

The rechecking refers to *all* previously examined ECOs of opposite type, whether they were judged to be cost-effective or not. This is because ECOs which were effective in a context may become ineffective in a different set of circumstances. Going back to the example with the heat-reflective window, a high-efficiency air conditioner that had a positive Net Benefit for clear glass might get a negative Net Benefit at the lower cooling load engendered by the heat-reflective film.

Measures are adopted if, with the new building description, the Net Benefit is positive, or if it is zero provided that it yields greater energy savings than the mutually exclusive option in the CBD.

Step 10: Determine if Step 9 Resulted in Modifying the CBD

If Step 9 did not result in any changes to Current Building Description, the program examines the next ECO in Step 13. Otherwise the program proceeds to Step 11.

Step 11: Check Prior ECOs of Same Type with the One Adopted in Step 8

If Step 9 resulted in modifications to the CBD, it is necessary to recheck those ECOs which (1) were previously examined in the NB procedure of Step 7, and which (2) are of the same type with the ECO adopted in Step 8.

For example, if an ECO examined in Step 7 is of "envelope" type, and if this ECO gets adopted in the CBD in Step 8, then the loads of the building have changed and prior equipment ECOs are re-examined in Step 9. If any of the previously rejected "equipment" type ECOs are now adopted in Step 9, the efficiencies of the mechanical equipment in the CBD have been altered. Different equipment efficiencies modify the energy savings of the envelope ECOs. Consequently, the status of envelope ECOs previously examined and adopted or rejected might now change. Step 11 will recheck the Net Benefits of these "envelope" type ECOs previously examined in Step 7.

Step 12: Determine if Step 11 Resulted in Changing the CBD

If the list of ECOs in the CBD has changed as a result of the calculations in Step 11, then it is necessary to reiterate through the procedure (go back to Step 9) until no further changes occur.

Step 13: Locate Next ECO on the List

The program looks for the next ECO in the list established in Step 5 (the first execution of the algorithm) or in Step 18 (subsequent iterations).

Step 14: Check if There Are Any ECOs Left To Be Examined

If there are no more ECOs in the list, the program calculates the building energy budget in Step 19. Otherwise, the program proceeds to Step 15.

Step 15: Calculate the Net Benefit of the ECO under Analysis

The Net Benefit of the new ECO is calculated with respect to the mutually exclusive option it would replace (identical to Step 7). The Net Benefit calculation is based upon the new envelope and new equipment efficiencies calculated in Steps 7 to 12.

If the $NB > 0$, or if $NB = 0$ and yields greater energy savings than the mutually exclusive ECO in the CBD, the ECO is further examined in Step 16. (Note that the ECO under analysis is not yet adopted in the CBD.) If neither of the above conditions is met, the program proceeds to the next ECO in the SIR-ranked list (Step 13).

Step 16: Has the ECO Type Changed?

The type (envelope or equipment) of the ECO which passed the NB test of Step 15 is examined. If the type has not changed (i.e., if it is of same type as the one previously adopted in Step 8), and if the Current Building Description did not change in Steps 9 or 11, then the ECO is adopted in Step 8. For example, assume that COSTSAFR has examined an "equipment type" ECO and has adopted it in the Current Building Description (Step 8). Further, assume that no changes to the CBD are made in Steps 9 and 11, and that the next ECO with positive Net

Benefits (Step 15) is also of "equipment type", as determined in Step 16. Since there is no interaction (dependency) between the two ECOs, the last ECO is simply "sent" for adoption in Step 8. However, if the ECO type is different from the one previously adopted in Step 8, or if the CBD did change in Steps 9 or 11, the program proceeds to Step 17. Continuing the preceding example, assume that after adopting two equipment ECOs the program calculates positive Net Benefits for an envelope ECO. Now that envelope ECOs are considered, the program addresses the *order* in which they are considered by recalculating their SIRs in Step 17 and by re-ranking them in Step 18.

Step 17: Recalculate Remaining Dependent SIRs

The marginal SIRs of the dependent ECOs left in the list are recalculated when the ECO under analysis yields a positive Net Benefit or a zero Net Benefit with greater energy savings (Step 15), *and* when it is of different type from the latest ECO adopted in the CBD (Step 16). For example, assume that the ECO under consideration is of envelope type, has positive Net Benefits, and follows after the adoption in the CBD of an "equipment type" ECO. The program will recalculate the SIRs of all "envelope type" ECOs which are "down" in the list (see definition of list "top" and list "bottom" at preceding Step 1 description).

Recalculating the SIRs consists of two steps: (1) re-ranking mutually exclusive ECOs in each category by energy dollars saved, and (2) recalculating marginal SIRs. Current CBD equipment efficiencies and envelope components are used.

Step 18: Re-Rank By SIR

The ECOs, starting with the one currently under analysis (Step 15) through the last ECO in the list, are re-ranked by their SIRs. The procedure differs from Step 2 in that ECOs with $0 < \text{SIR} < 1$ are not eliminated. These ECOs might be eventually adopted in the CBD as a result of iterations in Steps 9 to 11. The program loops back to Step 6.

Step 19: Calculate Energy Budget

The ECOs adopted in the Current Building Description as a result of the optimization are used to calculate total annual energy consumption.

Conclusions

The economic analysis method in the "Energy Conservation Standards for New Federal Residential Buildings" uses an iterative procedure to examine the impact of ECO dependencies and approaches the mathematical LCC minimum. By accounting for the interaction between envelope and mechanical equipment ECOs, this method is more accurate than the simplified LCC calculations of FEMP [5]. However, in some cases the minimum LCC may not be achieved, since not all permutations of envelope and equipment ECOs are investigated. The deviation from the minimum is likely to be insignificant, since the initial ranking by SIRs allows the examination of a large number of combinations. In the second procedure, examination of the Net Benefits of ECOs, an algorithm was developed to insure that each time a new ECO is adopted all inter-dependent ECOs are re-examined.

An alternative approach of calculating the minimum LCC through a formal optimization procedure would have required the curve-fitting of cost and energy data points. In calculating the optimal combination of ECOs, it should be recognized that there is considerable uncertainty in energy cost predictions and that there are quite large variations in "typical" cost data. Therefore a mathematically exact solution is not necessarily more accurate. However, no error analysis has been performed to ascertain the deviation of results from the mathematical minimum.

The COSTSAFR computer program, and its underlying computerized LCC method, can be used for accurate investigations of economic scenarios for residential construction by both governmental and private users.

Acknowledgments

This research was sponsored by the U.S. Department of Energy as part of the Building Systems Integration Program at Pacific Northwest Laboratory. Special recognition is extended to William Wright of Wright Associates for the coding of the computer program described in this paper.

References

- [1] "Affordable Housing Through Energy Conservation, Data Base for Simplified Energy Analysis," DOE/SF/00098-2, Energy Analysis Program, Lawrence Berkeley Laboratory, Berkeley, Calif./U.S. Department of Energy, Washington, D.C., June 1983.
- [2] Tuluca, A. and Levy, M., "Affordable Manufactured Housing Through Energy Conservation, Energy Data Base," Steven Winter Associates, Inc., New York, N.Y./U.S. Department of Energy, Washington, D.C., Nov. 1983.
- [3] Tuluca, A., Mitnick, P., Boschen, R., Lee, A., Pratt, R., and Heidell, J., "COSTSAFR—User's Manual (Conservation Optimization Standards for Savings in Federal Residences)," U.S. Department of Energy, Washington, D.C., July 1986.
- [4] Tuluca, A., Mitnick, P., Boschen, R., Lee, A., Pratt, R., and Heidell, J., "Proposed Interim Energy Conservation Standards for New Federal Residential Buildings," Technical Support Document, U.S. Department of Energy, July 1986.
- [5] Ruegg, R., "Life-Cycle Costing Manual for the Federal Energy Management Programs," National Bureau of Standards, Washington, D.C., Dec. 1980.
- [6] Cleary, P. and Levine, M., "An Analysis of the Accuracy of a Proposed Energy Rating System for New Houses," Lawrence Berkeley Laboratory, Berkeley, Calif., Sept. 1982.

Building Applications and User Interests

Computer Modeling of Climates

REFERENCE: Cash, C. G., "Computer Modeling of Climates," *Insulation Materials, Testing, and Applications, ASTM STP 1030*, D. L. McElroy and J. F. Kimpflen, Eds., American Society for Testing and Materials, Philadelphia, 1990, pp. 599-611.

ABSTRACT: The mathematical study of many dynamic responses of building materials and constructions to climatic variations has been hampered by the lack of a suitable way to model climatic components such as temperature, precipitation, humidity, wind, solar radiation, and cloud cover. It was noticed by the author that a curve called the "companion to the cycloid" seems to be similar in shape to ambient temperature versus time plots. This was the start of the work reported in this paper because, if a successful model of the temperature cycles could be developed, we would have a powerful tool to help us in our understanding of the thermal behavior of materials and systems.

This paper presents methods for the mathematical modeling of the ambient air temperature at any location where statistical atmospheric data are available. The model was checked by comparing the calculated air temperatures with the actual air temperature data at six diverse locations in the continental United States. In addition, the actual hourly air temperatures (recorded at three-hour intervals) were compared with the calculated hourly air temperatures from the model for a six-year period at one location.

The model was expanded, with data from the literature, to model the temperature of white, gray, and black roof surfaces. These calculated surface temperatures are used to illustrate the utility of the model in estimating the sliding potential of several bituminous roofs.

The usefulness of the minimum temperature and the temperature loading parts of the model has been demonstrated by the work reported in this paper. The validity of the surface temperature part of the work is yet to be established.

Finding the proper curve shape for the thermal model opens up many lines of investigation for studying building materials as dynamic components. Other studies currently being performed include the migration of bitumen through the felts within the roofing membrane and the displacement of one-ply systems in response to the normal thermal cycles. Future studies are not limited to roofing; the model can be applied wherever the effects of temperature cycles are important.

The preliminary look at the sliding potential of bituminous built-up roofing membranes reported in this paper may be the start of a study to provide rational limits for the maximum slope that should be permitted for each class of bitumen, instead of using timeworn standards that may not be appropriate.

KEY WORDS: air temperature, surface temperature, roofing, sliding, viscosity, climatic temperature variation

The mathematical study of many dynamic responses of building materials and constructions to climatic variations has been hampered by the lack of a suitable way to model climatic components such as temperature, precipitation, humidity, wind, solar radiation, and cloud cover. Of this abbreviated list of climatic factors, temperature cycles greatly influence the performance of our building materials, since thermal changes cause dimensional dislocations, moisture vapor migrations, and a host of other effects that influence the durability of the materials and systems.

While searching for a formula in a handbook on mathematics, I saw a curve called the "companion to the cycloid" [1] that seemed to be similar in shape to ambient temperature versus time

¹Principal, Simpson Gumpertz & Heger Inc., Arlington, MA 02174.

plots that I had previously reviewed. This was the start of the work reported in this paper, because I realized that if a successful model of the temperature cycles could be developed, we would all have a powerful tool to help us in our understanding of the thermal behavior of materials and systems.

This paper presents methods for the mathematical modeling of the ambient air temperature at any location where statistical atmospheric data are available. I checked the model by comparing the calculated daily mean minimum monthly air temperatures with the actual daily mean minimum monthly ambient air temperature data at six diverse locations in the continental United States [2]. In addition, I compared the actual hourly air temperatures (recorded in three-hour intervals) with the calculated hourly air temperatures from the model for a six-year period at one location.

I expanded the model, with data from the literature, to model the temperature of white, gray, and black roof surfaces. These calculated surface temperatures are used to illustrate the utility of the model in estimating the sliding potential of several different bituminous roofs at various geographic locations.

Theoretical Development

If one examines the graph of ambient air temperature versus time, one sees at least three components to the plotted data: minimum annual temperature, seasonal variation in the minimum daily temperatures, and diurnal temperature variation. The annual minimum daily temperature (I used the mean minimum monthly temperature for January) can easily be obtained from the weather records for any recording location. This value forms the base, the floor (Fig. 1), for the remainder of the model.

The remainder of the ambient temperature model uses the companion to the cycloid curve, the sinusoidal curve shown in Fig. 2, to add the seasonal and the diurnal cycles.

The ordinate of the curve at any point is:

$$y = a(1 - \cos \phi) \quad (1)$$

where

y = ordinate or amplitude,

a = radius of the circle used to generate the cycloid, and

ϕ = angle between the vertical line from the center of the circle and the rotating reference radius, rad.

The abscissa of the curve at any point is

$$x = a\phi \quad (2)$$

where x , a time unit, is the horizontal component.

The sinusoidal period is

$$p = 2\pi a \quad (3)$$

where p is the cyclic period.

We are interested in obtaining the fraction of the maximum amplitude on the curve for the various values during the cyclic period. In addition, the first (the lowest) value in each cycle must be expressed so that the incremental amplitude equals zero. The equations below are derived from Eqs 1 to 3 and the cycles of interest:

$$a = p/2\pi \quad \text{and} \quad \phi = x/a - 2\pi x/p \quad (4)$$

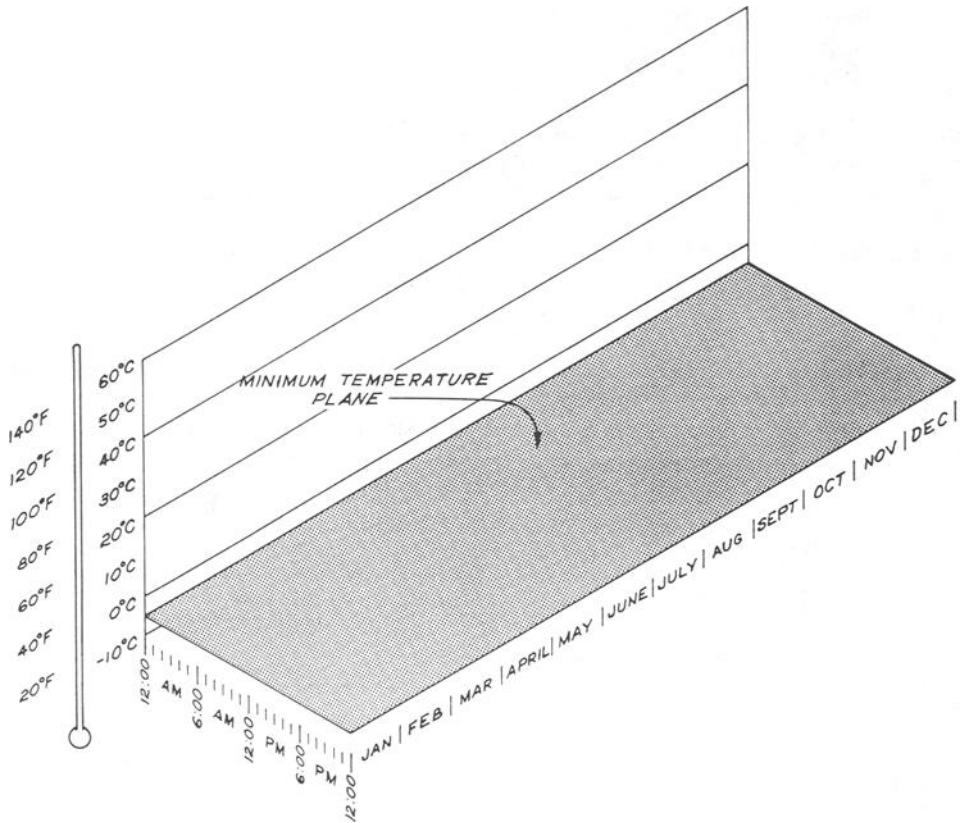


FIG. 1—Minimum daily temperatures.

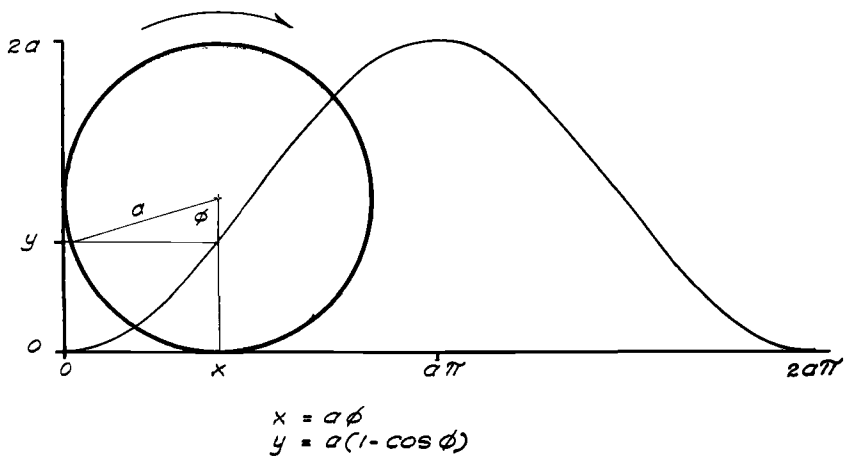


FIG. 2—Companion to the cycloid curve.

Therefore

$$y = p/2\pi(1 - \cos(2\pi x/p)) \quad (5)$$

where y is temperature and x is units of time in the cyclic period p . Also

$$y(\text{maximum}) = 2a = 2p/2\pi = p/\pi \quad (6)$$

Therefore the fraction yf of $y(\text{maximum})$ at any point in time x in the cyclic period is

$$yf = (p/2\pi)(\pi/p)(1 - \cos(2\pi x/p)) = 0.5(1 - \cos(2x/p)) \quad (7)$$

where x varies from 1 to p (i.e., 1 equals the first hour of the day, the first month of the year, or the first day of the year depending on the cycle considered). At the minima, the incremental value must be equal to zero. Thus the correct expression for the incremental value is

$$yf = 0.5(1 - \cos(2\pi(x - 1)/p)) \quad (8)$$

When we apply this equation to the annual cycle, the fraction is

$$yf = 0.5(11 - \cos(2\pi(m - 1)/12)) = 0.5(1 - \cos(\pi(m - 1)/6)) \quad (9)$$

for the 12 month seasonal cycle (m = the number of the month, 1 to 12); and

$$yf = 0.5(1 - \cos(2\pi(n - 1)/365)) \quad (10)$$

for the 365-day seasonal cycle, where n = the day of the year, 1 to 365; and

$$yf = 0.5(1 - \cos(2\pi(n - 1)/366)) = 0.5(1 - \cos(\pi(n - 1)/183)) \quad (11)$$

for the 366 day leap year seasonal cycle; and

$$yf = 0.5(1 - \cos(2\pi(h - 1)/24)) = 0.5(1 - \cos(\pi(h - 1)/12)) \quad (12)$$

for the 24-h diurnal cycle, where h equals the hour of the day, 1 to 24.

The following general equation adds the minimum temperature, the seasonal cycle, and the diurnal cycle:

$$T = A + 0.5B\{1 - \cos[2\pi(n - 1)/365]\} + 0.5C\{1 - \cos[\pi(h - 1)/12]\} \quad (13)$$

where

T = calculated temperature,

A = mean minimum daily January temperature (1941–1970 data),

B = difference between July and January mean monthly minimum daily temperatures, and

C = difference between mean maximum and mean minimum daily temperatures during the month under consideration.

The sequential addition of the seasonal and diurnal cycles to the minimum base temperature (Fig. 1) is shown in Figs. 3 and 4 respectively. These model data are for Logan Airport in Boston, Massachusetts.

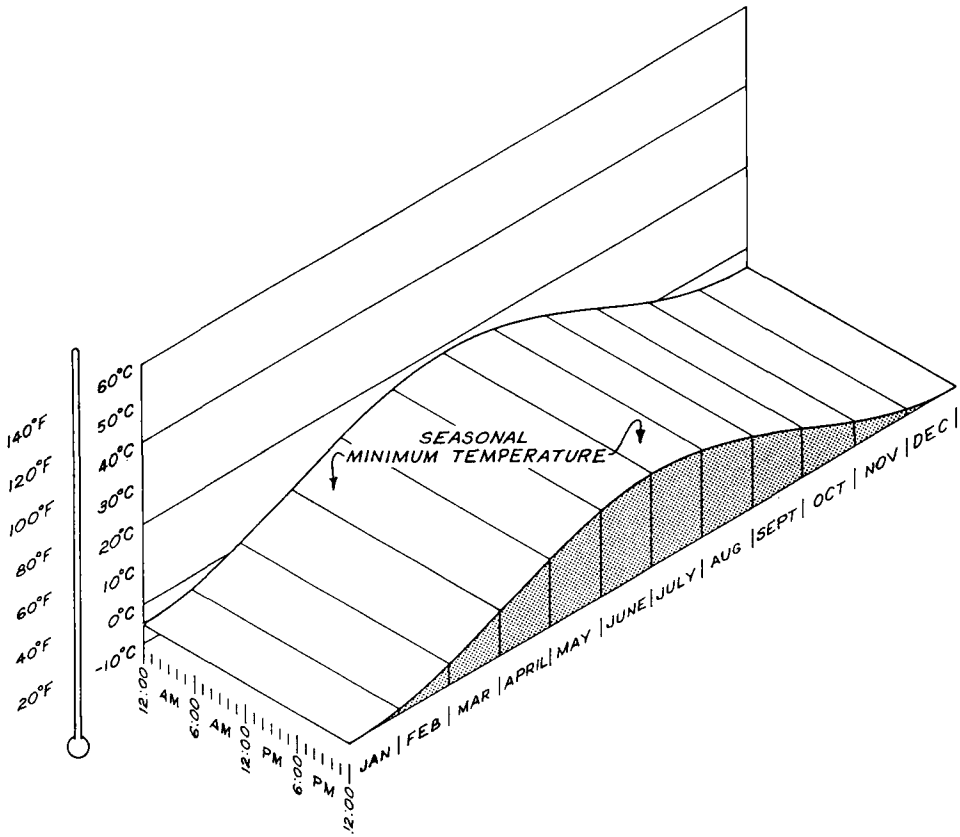


FIG. 3—Sequential addition of seasonal cycles to minimum base temperature.

Model Validation

Any mathematical model is an approximation of reality and must be tested to see how close the calculated values are to the measured values. The seasonal part of the model was checked by calculating monthly mean minimum temperatures at six locations and comparing them with the actual values reported in the weather records. The equation used is:

$$T = A + 0.5B\{1 - \cos[\pi(m - 1)/6]\} \quad (14)$$

Table 1 shows the name, latitude, longitude, and elevation for each weather station selected for this study, together with the least squares coefficient of correlation between the calculated and actual monthly data for the mean (1941–1970) minimum monthly temperature. The portion of the model that includes the minimum temperature and the seasonal cycle is quite accurate, as shown by the very high coefficient of correlation in every case tested.

A co-op student performed the more substantial test of the model. He used Eq 13 to calculate the hourly temperatures, in three-hour increments (the increments used for the actual temperature data), for temperatures in Boston. The calculated temperatures were compared with six years of the actual temperatures (1975–1979 & 1981), in least squares fit of paired data, to determine the ability of the model to predict the actual temperature. This also checked the

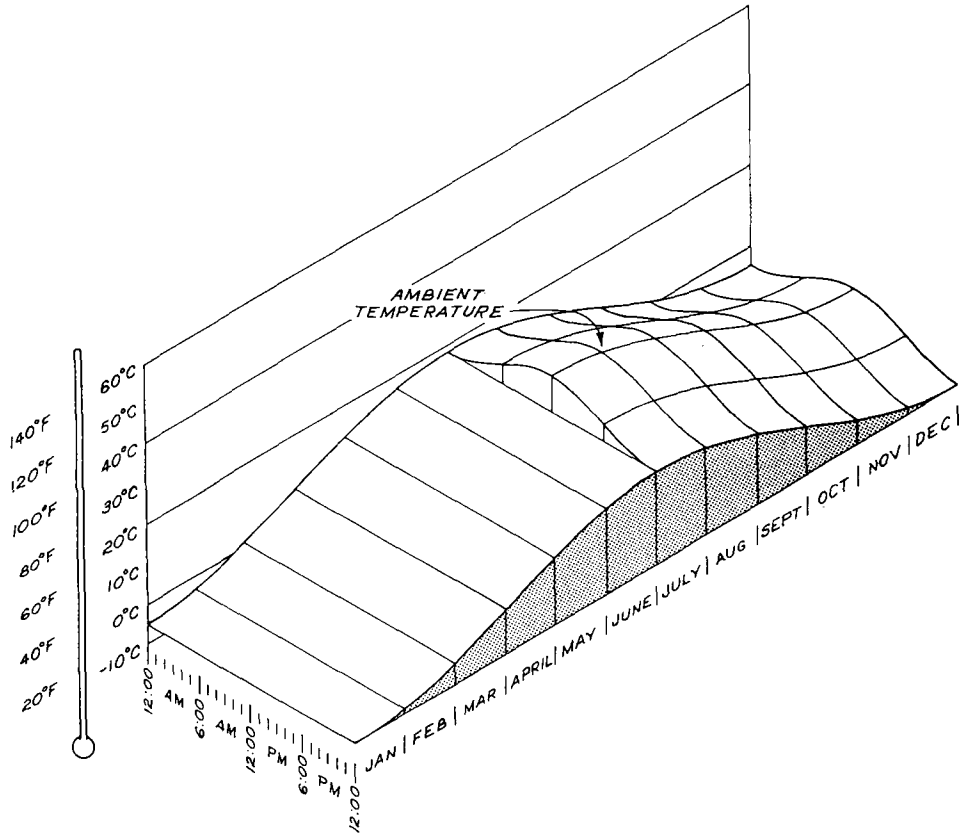


FIG. 4—Sequential addition of diurnal cycles to minimum base temperature.

TABLE 1—Location of weather stations and coefficient of correlation of calculated and actual mean temperatures.

City, State	Latitude	Longitude	Altitude	Coef. of Correlation
Boston, Mass.	42°22' N	71°02' W	5 m (15 ft)	0.98
Denver, Colo.	39°45' N	104°52' W	1610 m (5283 ft)	0.99
Dubuque, Iowa	42°24' N	90°42' W	322 m (1056 ft)	0.99
Miami, Fla.	25°48' N	80°16' W	2 m (7 ft)	0.97
New Orleans, La.	29°59' N	90°15' W	1 m (4 ft)	0.99
Presque Isle, Me.	46°39' N	68°00' W	183 m (599 ft)	0.98

ability to understand and use the model by someone other than the author. Also, the sum of the calculated temperatures was compared with the sum of the actual temperatures to determine the accuracy of the temperature loading (the time-temperature loading); that is probably more significant for the use of the model than, for example, predicting the precise temperature at 2 p.m. on August 23.

The coefficient of correlation between the calculated and actual temperatures is 0.827, which is quite good considering factors such as precipitation and cloud cover that are not represented fully in the model.

The temperature loading (the area under the temperature curve) from the model is 99.3% of the actual temperature loading. This ratio varied from 99.2 to 101.3 in the years studied and tended to approach 100% as the length of time increased.

These data show that the model is of only limited use in predicting the temperature at one specific hour on one specific day, but is very useful in predicting the longer term temperature loading at a specific location.

Surface Temperatures

The estimate of the ambient air temperature at a specific location has some utility, but for most roofing applications the surface temperature of the roof is of greater interest, since bitumen viscosity and other physical properties, such as tensile strength and thermal expansion or contraction, are dependent on the temperature of the membrane rather than the ambient air temperature. The temperatures calculated in this paper are for horizontal roofs only.

I expanded the ambient air temperature model using published data [3,4] without further qualifications.

From Eq 13 it is obvious that the maximum ambient air temperature in the year (in July) is

$$T_{\max} = A + B + C \quad (15)$$

The minimum July ambient air temperature, on clear nights, is

$$T_{\min} = A - R_c + B \quad (16)$$

where $R_c = 10^\circ\text{C}$ (18°F) decline in the lowest ambient air temperature represents the radiative cooling that is relatively independent of the color of the surface [3].

The surface temperature during daylight hours (assuming full sunlight on a clear day) is strongly dependent on the color of the surface [5]. The ratio of the maximum horizontal surface temperature to the maximum ambient air temperature is 1.51 for roofs with white surfaces, 1.74 for roofs with gray surfaces, and 1.97 for roofs with black surfaces. These ratios enable the substitution of new coefficients in the basic equation (13) to generate the estimated surface temperature of the roofing on clear days and nights. The new coefficients are

$$A' = A - R_c \quad (17)$$

where $A' =$ the modified minimum value; and

$$C' = (0.51A + 0.51B + 1.51C + R_c) \quad (\text{for white roof surfaces}) \quad (18)$$

where $C' =$ the modified diurnal coefficient; and

$$C' = (0.74A + 0.74B + 1.74C + R_c) \quad (\text{for gray roof surfaces}) \quad (19)$$

and

$$C' = (0.97A + 0.97B + 1.97C + R_c) \quad (\text{for black roofs}) \quad (20)$$

and

$$B' = B \quad (21)$$

where the seasonal coefficient is unchanged.

Figure 5 shows the roof surface temperatures from the extended model, for white, gray, and black roofs in Boston, superimposed on the three-dimensional graph that is Fig. 4.

The previous coefficients are for full sunshine and must be adjusted to reflect the local cloud cover that varies at each location. Fortunately, the weather data also provide the normal number of days that are clear, partly cloudy, and cloudy each month, at many locations. For the purposes of this model, the degree of cloud cover is assumed to influence on the diurnal coefficient for each month at each location, as shown by the equation

$$C'' = ccC + cpc(C + C')/2 + ccrC' \quad (22)$$

where

C'' = normal diurnal coefficient for each month, at each location,

cc = fraction of days that are cloudy,

cpc = fraction of days that are partly cloudy,

ccr = fraction of days that are clear, and

C' = full sun diurnal coefficient.

The equation used to generate hourly temperatures for the balance of this paper is

$$T = A' + 0.5B\{1 - \cos[2\pi(n - 1)/365]\} + 0.5C''\{1 - \cos[\pi(h - 1)/12]\} \quad (23)$$

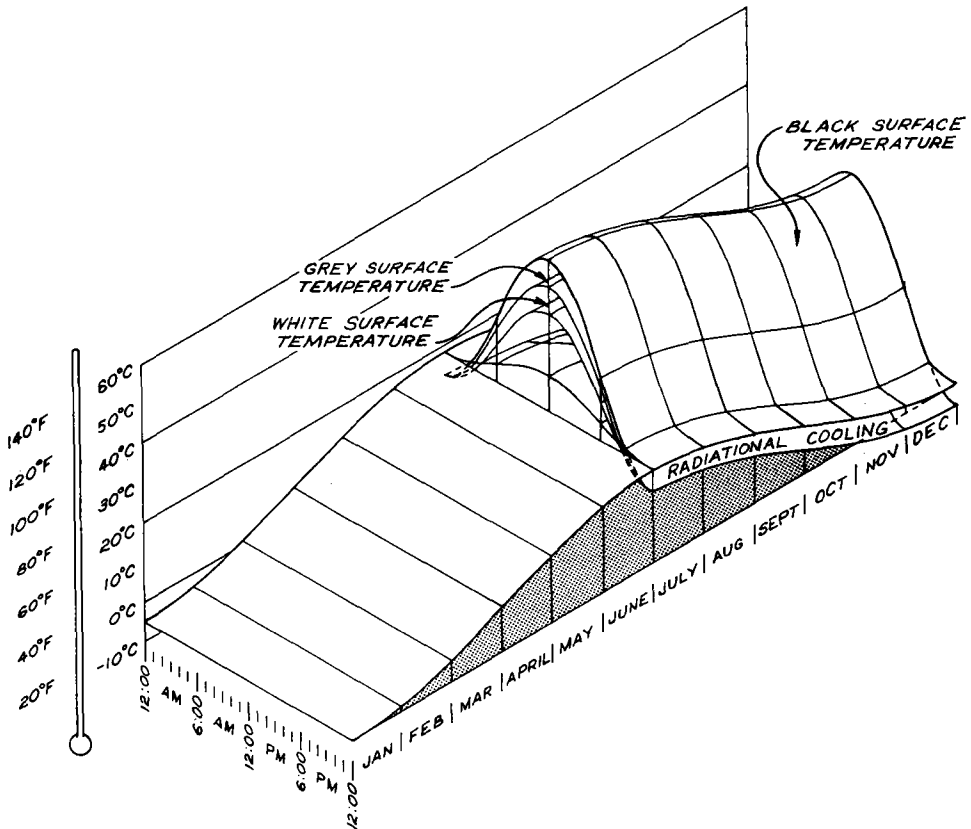


FIG. 5—Roof surface temperatures.

Sliding Potential of Bituminous Built-Up Roofing Membranes

The sliding potential of bituminous built-up roofing membranes is calculated using the methods set forth by Cramp, Cullen and Tryon at the National Bureau of Standards [4]. The 1-h displacement in sliding of a bituminous membrane with one slip plane is given by

$$D = 980tdWs/vA \quad (24)$$

where

- D = lateral hourly down slope displacement, cm,
- 980 = acceleration due to gravity, cm g/s²,
- t = time, s (= 3600 in this model [1 h]),
- d = interply bitumen thickness, cm,
- W = mass over the slip plane, g,
- s = slope factor = rise/(rise² + run²)^{0.5},
- v = viscosity of the bitumen, P, and
- A = area, cm².

Where more than one slip plane exists, such as in a typical built-up roofing membrane, the mass W is the sum of the masses over each slip plane in the system and must be used to calculate the overall sliding potential. Figure 6 shows a typical built-up roofing assembly before and after displacement.

The hourly displacement of a typical four ply built-up roofing membrane is given by

$$D = 980tds(W1 + W2 + W3)/vA \quad (25)$$

where

- $W1$ = the mass above the first slip plane, g,
- $W2$ = the mass above the second slip plane, g, and
- $W3$ = the mass above the third slip plane, g.

The hourly displacement D is identical to the displacement velocity expressed in centimeters per hour.

The log-log of viscosity of any bitumen can usually be represented as linear relationship to temperature. Thus

$$v = \text{antilog}(\text{antilog}(\alpha - \beta T)) \quad (26)$$

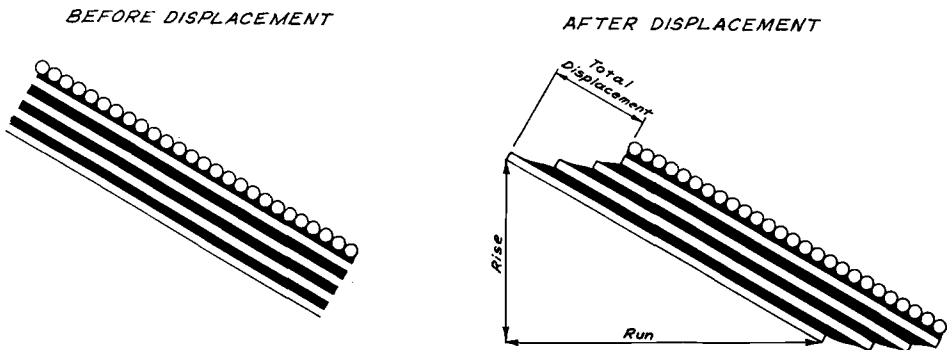


FIG. 6—Typical built-up roofing assembly before and after displacement.

where

α = viscosity curve-ordinate intercept,
 β = slope of viscosity curve, and
 T = temperature calculated using Eq 23.

The total annual displacement is

$$D(\text{total}) = \int_0^{8760} D \delta t' \quad (27)$$

or

$$D(\text{total}) = \int_0^{8760} [3,528,000sd(\Sigma W)/A(\text{antilog}(\text{antilog}(\alpha - \beta T)))] \delta t' \quad (28)$$

where t' = time (hours).

The total calculated displacements of built-up roofing membranes is the sum of the displacements each hour for a year at the specific location. The membrane is composed of gravel surfacing (grey color), four plies of asphalt-organic felt (ASTM D 226, Type 1), and built-up roofing asphalts (ASTM D 312, Types 1, 2, and 3) (Table 2).

Similar roofing systems, exposed at five other locations, have the calculated displacements shown in Tables 3 to 7.

The usefulness of this model of sliding potential is not limited to built-up roofing membranes composed of asphalt and asphalt-organic felts. For example, Table 8 shows the sliding potential of various asphalt and coal-tar pitch membranes made with glass fiber and organic felts exposed in Denver.

Conclusions

The utility of the minimum temperature and the temperature loading parts of the model have been demonstrated by the work reported in this paper. The validity of the roofing membrane temperature part of the work is yet to be established.

Finding the proper curve shape for the thermal model opens up many lines of investigation for studying building materials as dynamic components. Other studies currently being performed include the migration of bitumen through the felts within the roofing membrane and the displacement of one-ply systems in response to the normal thermal cycles. Future studies are

TABLE 2—Displacement at various slopes with three types of asphalt at Boston, Massachusetts.

Slope, % (in./ft)	Slope Factor	Total Displacement Per Year, mm		
		Type 1 Asphalt	Type 2 Asphalt	Type 3 Asphalt
1.042 (1/8)	0.010416	19.41	0.70	0.04
2.083 (1/4)	0.020828	38.82	1.40	0.08
4.167 (1/2)	0.041630	...	2.79	0.16
8.333 (1)	0.083045	...	5.56	0.32
16.667 (2)	0.164398	...	11.01	0.64
33.333 (4)	0.316227	...	21.18	1.23
66.667 (8)	0.554700	...	37.16	2.17

TABLE 3—Displacement at various slopes with three types of asphalt at Denver, Colorado.

Slope, % (in./ft)	Slope Factor	Total Displacement Per Year, mm		
		Type 1 Asphalt	Type 2 Asphalt	Type 3 Asphalt
1.042 (1/8)	0.010416	137.52	3.93	0.17
2.083 (1/4)	0.020828	...	7.85	0.35
4.167 (1/2)	0.041630	...	15.70	0.70
8.333 (1)	0.083045	...	31.31	1.39
16.667 (2)	0.164398	2.76
33.333 (4)	0.316227	5.31
66.667 (8)	0.554700	9.31

TABLE 4—Displacement at various slopes with three types of asphalt at Dubuque, Iowa.

Slope, % (in./ft)	Slope Factor	Total Displacement Per Year, mm		
		Type 1 Asphalt	Type 2 Asphalt	Type 3 Asphalt
1.042 (1/8)	0.010416	19.26	0.73	0.04
2.083 (1/4)	0.020828	38.52	1.45	0.08
4.167 (1/2)	0.041630	...	2.90	0.16
8.333 (1)	0.083045	...	5.79	0.33
16.667 (2)	0.164398	...	11.46	0.65
33.333 (4)	0.316227	...	22.04	1.24
66.667 (8)	0.554700	...	38.66	2.18

TABLE 5—Displacement at various slopes with three types of asphalt at Miami, Florida.

Slope, % (in./ft)	Slope Factor	Total Displacement Per Year, mm		
		Type 1 Asphalt	Type 2 Asphalt	Type 3 Asphalt
1.042 (1/8)	0.010416	243.94	7.39	0.31
2.083 (1/4)	0.020828	...	14.77	0.62
4.167 (1/2)	0.041630	...	29.53	1.23
8.333 (1)	0.083045	2.46
16.667 (2)	0.164398	4.87
33.333 (4)	0.316227	9.37
66.667 (8)	0.554700	16.44

not limited to roofing; the model can be applied wherever the effects of temperature cycles are important.

The preliminary look at the sliding potential of bituminous built-up roofing membranes reported in this paper may be the start of a study to provide rational limits for the maximum slope that should be permitted for each class of bitumen. The sliding values reported in this preliminary study are comparable to each other, but should be taken *cum grano salis* until the work is completed and validated by experiment. Some additional work needs to be done to accurately determine the effective viscosity of bitumens in the temperature range involved. The parallel plate viscosity, the basis of this work, needs more careful study.

TABLE 6—Displacement at various slopes with three types of asphalt at New Orleans, Louisiana.

Slope, % (in./ft)	Slope Factor	Total Displacement Per Year, mm		
		Type 1 Asphalt	Type 2 Asphalt	Type 3 Asphalt
1.042 (1/8)	0.010416	394.03	10.63	0.44
2.083 (1/4)	0.020828	...	21.26	0.88
4.167 (1/2)	0.041630	...	42.48	1.76
8.333 (1)	0.083045	3.51
16.667 (2)	0.164398	6.94
33.333 (4)	0.316227	13.36
66.667 (8)	0.554700	23.43

TABLE 7—Displacement at various slopes with three types of asphalt at Presque Isle, Maine.

Slope, % (in./ft)	Slope Factor	Total Displacement Per Year, mm		
		Type 1 Asphalt	Type 2 Asphalt	Type 3 Asphalt
1.042 (1/8)	0.010416	59.34	1.83	0.09
2.083 (1/4)	0.020828	...	3.67	0.18
4.167 (1/2)	0.041630	...	7.33	0.36
8.333 (1)	0.083045	...	14.62	0.72
16.667 (2)	0.164398	...	28.94	1.42
33.333 (4)	0.316227	2.73
66.667 (8)	0.554700	4.79

TABLE 8—Displacement of various roofing membranes at various slopes at Denver, Colorado.

Surface Color	gravel grey	gravel grey	gravel grey	gravel grey	smooth black
Felt Type, Plies	glass, 4	cto, 4	glass, 4	glass, 3	glass, 4
Bitumen Type	coal-tar pitch	coal-tar pitch	Type 3 asphalt	Type 3 asphalt	Type 3 asphalt
Nd. of Slip Planes	3	3	3	2	3
Slope % (in./ft)	Total Displacement Per Year, mm				
1.042 (1/8)	16.33	14.68	0.01	0.01	0.00
2.082 (1/4)	32.65	29.34	0.02	0.01	0.00
4.167 (1/2)	0.04	0.02	0.01
8.333 (1)	0.07	0.04	0.02
16.667 (2)	0.14	0.09	0.04
33.333 (4)	0.27	0.17	0.08
66.667 (8)	(cto = coal-tar organic)	...	0.48	0.30	0.15

Acknowledgments

The work reported in this paper was supported by the Principals and Associates of Simpson Gumpertz & Heger Inc. Special thanks are due Robert F. MacDonald, the co-op student who made many of the fundamental computer calculations.

References

- [1] Selby, S. M., *Standard Mathematical Tables*, CRC Press, Cleveland, Ohio, 1973, p. 388.
- [2] Climatography of the United States," Report 60, National Ocean and Atmospheric Administration, Environmental Data Service, Asheville, N.C., 1976.
- [3] Cullen, W. C., "Solar Heating, Radiative Cooling, and Thermal Movement: Their Effects on Built-Up Roofing," Technical Note 231, National Bureau of Standards, Washington, D.C., 1963.
- [4] Cramp, A. P., Cullen, W. C., and Tryon, M., "Slippage of Built-Up Roof Membranes: Causes and Prevention," Report 10950, National Bureau of Standards, Washington, D.C., 1972.
- [5] Rossiter, W. J. and Mathey, R. G., "Effects of Insulation on the Surface Temperature of Roof Membranes," NBSIR 76-987, National Bureau of Standards, Washington, D.C., 1976.

Factors Influencing Consumer Insulation Activities

REFERENCE: Meeks, C. B., "Factors Influencing Consumer Insulation Activities," *Insulation Materials, Testing, and Applications, ASTM STP 1030*, D. L. McElroy and J. F. Kimpflen, Eds., American Society for Testing and Materials, Philadelphia, 1990, pp. 612-625.

ABSTRACT: Using a sample of 37 687 single family homeowners from the 1980 Annual Housing Survey, this study applied discriminant analysis to determine which variables influence presence, addition, and cost of insulation. Housing units with insulation were more likely to have storm doors or windows, be newer, more expensive, be located in the Northcentral region rather than the South, and have an attached fan and electric or oil heat rather than natural gas. An increase in the age of the head and presence of a child under 6 years old as well as length of occupancy were more highly associated with housing without insulation.

The addition of insulation was more likely in older homes, homes located in regions other than the South, homes heated with oil, liquid petroleum gas, or wood rather than natural gas, and homes with storm doors or windows and an attached fan. While presence of a child under 6 years old increased the probability, length of occupancy had a negative impact.

Using these variables as discriminators, 74.2% of the households with insulation were correctly classified, while 60.5% of the households who added insulation were correctly classified. Expenditures on insulation varied with region, length of occupancy, age and value of the house, and presence of an attached fan. Thus this study provides a base for identifying households which will undertake insulation activities.

KEY WORDS: energy conservation, insulation, consumers, residences

Residential structures account for about 20% of the energy consumption in the United States; about 57% percent of this is used for space heating and 7% percent for air conditioning [1]. Cost-effective opportunities exist to reduce energy consumption in housing [2].

Many conservation measures exist which can enhance energy efficiency such as addition of insulation, energy-saving appliances, and clock thermostats as well as simpler measures such as caulking and weather-stripping. New construction can make use of passive and active solar design as well as earth sheltering more easily than adding these items to existing structures. Diffusion of such measures has been slow [3]. Lack of information, beliefs about discomfort, potential energy savings, and expense all influenced adoption [3].

Much has been written about the need to improve energy conservation [4-6]. However, few studies using a national sample were located that focused on adoption of energy conservation measures [7-9]. A major DOE effort focused on factors that influence energy consumption [10].

This paper focuses on insulation, since many conservation programs encourage insulation activities. It helps reduce consumption in heating and cooling, the largest users of energy in the home. Depending on the package of conservation activities compared, it may have a relatively high first cost. Further, GAO [11] reported that 86% of single family homes could be considered less than fully insulated and while there was a nominal increase in the percentage of hous-

¹Associate Professor, University of Georgia, Athens, GA 30602.

ing units that had a particular conservation item, none of the increases between 1978 and 1984 were statistically significant.

This paper examines the factors which influence the use and addition of thermal insulation in owner-occupied single-family detached residences. The sample of 37 687 home owners was obtained from the 1980 Annual Housing Survey (AHS) tapes. In 1980, AHS reported 51% of owner-occupied units were single-family detached structures, while another 10% were attached units or mobile homes [12]. The data were collected from mid-August 1980 through December 1980 by the Bureau of the Census for the Department of Housing and Urban Development. A survey instrument was used by interviewers to collect the data. Energy data were not collected on mobile homes.

Only home owners were selected for study, since tenants are not likely to undertake insulation energy conservation activities in which the benefits would be generally received by the landlord. However, tenants who directly pay their utility bills and expect to remain in the unit for a long time may be a topic of further interest.

Analysis Plan

Discriminant analysis is used to determine which household or housing characteristics influence: (1) the presence of insulation in a house, and (2) the addition of insulation to the attic, walls, or floor in the 12 months prior to the survey. Both of these variables are measured as either 0 (no insulation or none added) or 1 (insulation or insulation added).

Discriminant analysis is also used to determine differences in the cost of insulation added; both because the data were collected by categories and not exact dollar amounts and to enable comparisons across analyses. Three categories are used for cost: less than \$100, \$100 to \$399, and \$400 or more.

Discriminant analysis is a statistical technique which may be used to classify cases into a particular group based on the information carried by the discriminating variables [13]. The discriminant function can be expressed as

$$C = b_0 + b_1 x_1 + b_2 x_2 + \dots + b_k x_k$$

where

x_1, x_2, \dots, x_k = the values of the predictor variables,

b_1, b_2, \dots, b_k = the weights associated with each of the respective predictor variables, and

C = the discriminant score.

The variable coefficient represents the amount of change in a households' position on that function if its score on the corresponding variable changed by one unit. To determine where any individual household would be classified, their raw score on each predictor variable is multiplied by the associated classification function coefficient. These products are summed and added to the constant.

For the discriminant analysis, the sample was split randomly. One group, the developmental sample ($N = 35\ 802$), containing 95% of the households was used to obtain the discriminators that were significant. The results from this analysis were then validated on the other 5% of the sample ($N = 1884$) to see how well they discriminated.

The analysis was thus performed in three stages. (1) A stepwise procedure was used with all the variables discussed below as discriminators. This produces an optimal set of discriminating variables [13]. A variable had to be statistically significant at the 0.05 level to both enter and remain in the model. With a smaller sample size, a more moderate level of significance would have been chosen, since the overall probability of rejecting at least one true null hypothesis is

much larger than 5%. (2) From the stepwise model, a smaller list of discriminators was then entered into a discriminant analysis model using the developmental sample. The results from this were then (3) tested on the validation sample.

The following sections describe the household and housing characteristics selected for use as discriminators, the reasons for their selection, and how the variables are measured.

Household Characteristics

Household characteristics examined include: household income, education and age of the head, family size, and length of occupancy. Although Gladhart [14] reported that family characteristics have little relation to conservation, other research as indicated below suggests that household characteristics may be useful as discriminators.

Income—Researchers [15, 16] seem to agree that income is a strong predictor of energy consumption and energy conservation. Dillman et al. [17] found that lower income households adjusted to higher energy prices by purchasing less of other items or making temporary adjustments, such as changing the temperature of the room. On the other hand, higher income households invested in more permanent conservation activities. Thus the housing of lower income families is less energy efficient [18, 19].

Thompson [20] reported that: "There is a large difference in average energy consumption and expenditures among households with different incomes. The highest income households use about 70% more energy than the lowest income group . . ." Their houses are about twice the size of the lowest income group and they have more appliances. However, for three years (1978, 1979, and 1980) higher income households lowered their energy consumption more than lower income households. Although lower income families tend to use less energy than higher income families, Newman and Day found that they spend a greater percentage of their income on energy [19].

Income in the present study is total household income from earnings as well as assets. Transfer payments such as social security, welfare, or alimony are also included. The discriminant analysis coefficient for income is reported in \$10 units rather than \$1.

Education—Previous studies suggest that education is negatively related to conservation behavior [21] but positively related to consumption [22]. Although better educated household heads have higher earnings and can thus afford larger houses and energy-consuming appliances, it is hypothesized in this study, despite Heberlein and Warriner [21], that better educated household heads will undertake energy conservation activities.

Five levels of education were examined: (1) less than high school education, (2) a high school graduate, (3) some college, (4) a college graduate, and (5) post college or graduate work. These were entered in the stepwise discriminant analysis as 0, 1 with the group of high school graduates used as the omitted variable.

Age—Tyler et al. [23] found that the homes of the elderly were energy efficient, while Eichner and Morris [18] found no relationship between age of the household head and energy conservation features. However, Brown and Rollinson [24] reported that elderly home owners consume residential energy more inefficiently than others because of characteristics of their homes, their stock of appliances, and their behavior. Johnson-Carroll et al. [25] reported that the older the respondent the less likely was there to be a propensity for conservation alterations. Berry and Brown [26] also found that the elderly have low participation rates in conservation programs.

Two measures related to age are included in the present study: age of the head of the household and presence of a person 65 years of age or older. In addition, the presence of a child under 6 years old was included on the basis that a household with young children would consume more energy and thus have a higher demand for conservation. Douthitt [27] found that the presence of preschool children increases energy consumption.

Length of Occupancy—The number of years the current household head had lived in the

house was thought to be an influence on current conservation behavior. Gladhart [14] reported that families work at conservation year after year and as a group get more efficient and effective in conserving.

Household Size—Although Latta [28] reported that the larger the household the greater the use of energy, Eichner and Morris [18] found no relationship between size of household and energy conservation features. Johnson-Carroll et al. [25] found that the larger the household size, the more energy-saving features were added to the house. In this paper, household size is measured as the number of persons living in the house.

Housing Characteristics

Characteristics of the housing unit which were thought to influence energy conservation include: age, size, and value of the house, type of heating fuel, utility costs, presence of other energy saving features, and region of the country in which the house was located.

Age of House—Age is measured in years. It was thought that older houses would be less energy efficient than newer homes.

Size of House—Size of the housing unit has been related to energy consumption [29] and energy conservation [25]. The measure of house size used in this study is number of rooms. Total square feet would obviously be more precise, but this was not available on the data tape.

Value—Value of the house is the respondent's estimate of how much the property (house and lot) would sell for if it were for sale. It is expected that higher valued homes would use more energy; whether their owners would then opt for more energy conservation measures is unknown.

Heating Fuel—A study of natural gas (NG) and liquid petroleum gas (LPG) users provides an indication of how households respond to price increases and the role that type of heating fuel could play in energy conservation. When the price of LP gas doubled and natural gas changed little, LPG households adopted and maintained energy conservation activities such as closing off a room and turning down the thermostat. Furthermore, they were more likely to make permanent changes such as attic and wall insulation, adding storm windows and doors, caulking, and weather-stripping. Ogus [30] concluded that a substantial economic incentive is required to create a significant and sustained energy conservation response. Latta [28] reported that households that use liquid petroleum gas tend to use less energy than households with the same characteristics that use natural gas.

Thus the type of heating fuel may contribute to different energy conservation behavior. Types of heat considered here are: electricity, oil, gas, wood and liquid petroleum gas. Since gas was the fuel used in the largest number of households, it was omitted as a discriminator. The other variables were entered as 0, 1 in the model with 1 being presence of that type of fuel.

Utility Costs—It was thought that households with higher utility costs would be more likely to install insulation and less likely to already have insulation in place. Three kinds of utility costs were included: average monthly costs for (1) gas and (2) electricity and (3) the average annual cost of oil, coal, or kerosene. Cost for owners who did not use a given fuel were entered as zero.

Energy-Saving Features—Households with other energy-saving features were thought to be more likely to have insulation and less likely to add more insulation. Several energy savings features were considered: (1) whether a household had a ceiling or attic fan, (2) whether a household used a window or portable fan rather than air conditioning, and (3) presence of storm doors and windows.

Region—Region of the country in which the house is located was used to measure variance in climatic conditions. Region was coded as 0 not in a given region or 1 in the region. The Northeast, Northcentral, and Western regions were included, while the South was omitted. Obviously a more specific variable such as heating and cooling degree days would give precise rather than general results obtained by using region, but such data were unavailable for this sample.

Sample Description

The 37 687 homeowners in this study had a mean income of \$21 481 (Table 1). Most were married (76.1%). About one third had less than a high school education, one third had a high school education, and one third had at least some college. Most of the heads of household were male (80.9%) and white (91.8%). Age was fairly evenly distributed among the categories from 30 to 69 years with only 8.9% of the heads under 30 and 14.6% over 70. A person 65 years or older was present in 25.2% of the households and a child under 6 years in 15.8%.

The housing units had an average of 6 rooms (Table 2). Twenty-two percent of the housing units were 10 years old or less, 20.2% were 11 to 19 years old, another 28.4% were 20 to 40 years old, and the remaining 28.6% of the units were over 40 years old. House value was fairly evenly

TABLE 1—Household characteristics.

Characteristic	N	%
Presence of Child <6 years	5 967	15.8
Presence of a Person 65+ years	9 503	25.2
Age of Head		
< 29 years	3 365	8.9
30-39 years	8 222	21.8
40-49 years	7 041	18.7
50-59 years	7 251	19.3
60-69 years	6 316	16.8
70-79 years	4 024	10.7
80+ years	1 468	3.9
Race of Head		
Black & other	3 090	8.2
White	34 597	91.8
Education of Head		
<8 years	6 526	17.3
9-11 years	5 039	13.4
High school graduate	12 939	34.3
Some college	5 787	15.4
College graduate	3 818	10.1
Post graduate	3 578	9.5
Sex of Head		
Female	7 187	19.1
Male	30 500	80.9
Marital Status of Head		
Married	28 695	76.1
Widowed	4 850	12.9
Divorced	2 102	5.6
Separated	607	1.6
Never married	1 433	3.8
Length of Occupancy		
< 1	1 722	4.6
1-5	12 646	33.6
6-10	6 093	16.2
11-20	8 500	22.5
Over 20	8 726	23.2
	Mean	S.D.
Household Income	\$21 481	\$13 649
(N = 37 687)		
Household Size	3.04	1.6

TABLE 2—*Housing characteristics.*

Characteristic	N	%
Age of House		
< 1 year	327	0.9
1-5 years	4 614	12.2
6-10 years	3 663	9.7
11-19 years	7 606	20.2
20-40 years	10 701	28.4
Over 40 years	10 766	28.6
Type of Heat		
Electric	6 570	17.4
Gas	19 556	51.9
LP gas	2 664	7.1
Oil	7 311	19.4
Wood	1 023	2.7
Value (\$)		
< 25,000	4 299	13.5
25-34,999	4 134	12.9
35-44,999	5 038	15.9
50-54,999	4 524	14.3
55-64,999	3 455	10.8
65-74,999	2 866	9.0
75-89,999	2 878	9.1
90-99,999	1 123	3.5
100,000+	3 426	10.9
	Mean	S.D.
Number of Rooms (N = 37 687)	6.1	1.6

distributed among the categories. Natural gas heat was the dominant fuel for 51.9% of the units, followed by oil for 19.4% and electricity for 17.4%.

Storm doors and windows were the most frequent energy-saving feature present for the housing units studied (Fig. 1). Slightly over half of all households had storm doors and windows on every door or window in the house. In addition, 11.2% had storm windows on some of the windows, while 13.3% had storm doors on some of the doors. In declining order of importance, 7.6% of the sample used a window or portable fan (detached fan), 6.4% a ceiling or attic fan (attached fan), 5.7% awnings, and 2.8% a dehumidifier to save energy.

Cost for utilities is reported in two ways (Table 3). Actual reported electric bills averaged \$50.04 per month, gas \$37.82 per month, and oil, coal, or kerosene \$537 per year. In order to reduce the problem of missing data, costs were recalculated with nonusers or households not reporting a cost for that utility as zero. This obviously led to a lowering of the mean values. In the final discriminant analyses, utility costs were not used because of concern for the quality of the data.

The Southern region contained 35.7% of the units, followed by the Northcentral region with 28.9% and by the Northeast with 19.8% and West with 15.6%.

Conservation Activities

In the 37 687 households studied, 30 605 (81.2%) reported having some insulation, 4661 (12.4%) reported having no insulation, while the remaining 2421 (6.4%) did not know whether they had insulation in their houses.

In the 12 months prior to the survey, 20.6% of the sample added insulation in the following

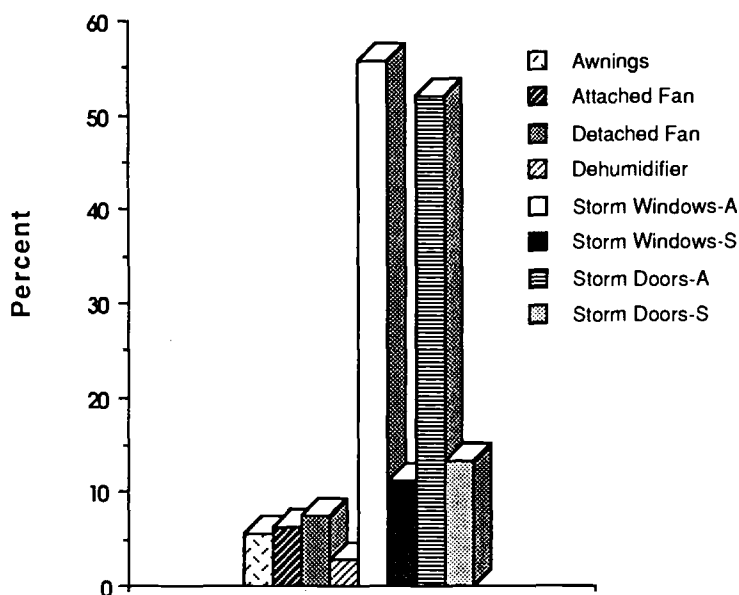


FIG. 1—Presence of energy-saving items.

TABLE 3—Energy costs.^a

Utility	Time	N	Mean	S.D.
Actual Users				
Electricity	Monthly	31 714	50.04	32.54
Gas	Monthly	22 238	37.82	23.76
Oil, coal, or kerosene	Annually	8 662	537.09	414.52
Total Sample				
Electricity	Monthly	37 687	42.11	35.00
Gas	Monthly	37 687	22.32	26.06
Oil, coal, or kerosene	Annually	37 687	123.45	300.92

^aNon-users and households with missing data are included in calculation of utility costs as zero.

areas: 3.1% floor, 5.6% walls, 7.6% attic, and 4.7% water heater (Fig. 2). (Addition of the individual percents slightly exceed 20.6, since households could have added insulation in more than one area.) Other energy-saving improvements added included storm windows (4.7%), storm doors (5.0%), and weather-stripping (19.1%).

Cost of insulation added was listed in three categories: 12.9% of the total sample spent less than \$100, 8.6% spent between \$100 and \$400, and 3.3% spent \$400 or more for insulation. For the 7766 households in the developmental sample who actually reported expenditures on insulation, 52.4% spent less than \$100, 34% spent between \$100 and \$399, and 13.6% spent \$400 or more.

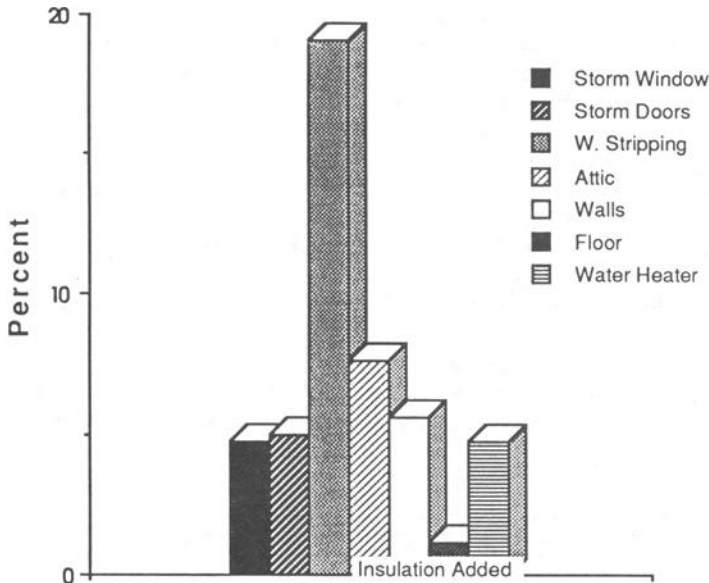


FIG. 2—Energy-saving improvements added in last 12 months.

Discriminant Analysis

SAS computer programs were used for the discriminant analyses [31]. As presented here, the variables entered into the stepwise discriminant analyses were:

- Age of head.
- Presence of a child under 6 years.
- Household income.
- Length of occupancy.
- Age of house.
- Value of house.
- Region.
- Presence of storm doors or windows.
- Presence of a ceiling or attic fan.
- Type of heating fuel.

Multicollinearity among the predictors could influence the results by contributing to the unreliability of the estimated coefficients [34]. According to Kmenta [34], little can be done about multicollinearity if all available information is used. One possible way of increasing information is to increase the sample size. The sample size in the present study is very large for most social science research. However, the sample size also influences the discriminant function. Although a large sample size may improve the function, a smaller sample seems to improve correct classification functions [33].

Quality of Predictions

Of key importance is how well the variables selected as discriminators predict behavior of households. Results are reported for both the developmental and validation samples.

Presence of Insulation—In the developmental sample, the discriminating variables correctly classified 75.9% of the households without insulation and 74.2% of those with insulation (Table 4). In the validation sample, 56.5% of the households without insulation were correctly classified, whereas 76.1% of those with insulation were correctly classified. This suggests the variables are somewhat less successful in classifying household without insulation. Since this is a key group to target for energy conservation education and sales, more work is needed to improve the prediction ability of the model. For some households data on insulation were missing, these were classified as indicated in (Table 4).

Addition of Insulation—In the developmental sample, the discriminating variables correctly classified 60.5% of the sample who did not add insulation and 61.6% who added insulation (Table 5). In the validation sample, 59.6% were correctly classified as not adding insulation and 63.7% as adding insulation.

Cost of Insulation—The model developed for expenditures on insulation accurately predicted expenditures of less than \$100 for 46.0% of the households and predicted expenditures of \$400 or more for 42.6% of the households in the developmental sample (Table 6). However, for the

TABLE 4—*Predicted versus actual presence of insulation.*

Actual	Predicted				Totals	
	Had Insulation		No Insulation			
	<i>N</i>	%	<i>N</i>	%	<i>N</i>	%
Developmental Sample						
Had insulation	18 993	74.23	6593	25.77	25 586	100.0
No insulation	880	24.10	2772	75.90	3 652	100.0
Missing	555	57.51	410	42.49	965	100.0
Totals	20 283	67.16	9920	32.84	30 203	100.0
Validation Sample						
Had insulation	999	76.14	313	23.86	1 312	100.0
No insulation	80	43.48	104	56.52	184	100.0
Missing	18	40.91	26	59.09	44	100.0
Totals	1 097	71.23	443	28.77	1 540	100.0

TABLE 5—*Predicted versus actual addition of insulation.*

Actual	Predicted				Totals	
	Added Insulation		No Insulation Added			
	N	%	N	%	N	%
Developmental Sample						
Added insulation	2600	61.60	1 621	38.40	4 221	100.0
No insulation added	2497	39.51	19 135	60.49	31 632	100.0
Totals	5097	42.11	20 756	57.89	35 853	100.0
Validation Sample						
Added insulation	142	63.68	81	36.32	223	100.0
No insulation added	651	40.41	960	59.59	1 611	100.0
Totals	793	43.24	1 041	56.76	1 834	100.0

TABLE 6—*Predicted versus actual expenditures on insulation by categories.^a*

Actual	Predicted							
	\$100		\$100 to \$399		\$400+		Totals	
	N	%	N	%	N	%	N	%
Developmental Sample								
< \$100	1 872	46.03	919	22.60	1 276	31.37	4 067	100.0
\$100 to \$399	989	37.48	682	25.84	968	36.68	2 639	100.0
\$400+	359	33.87	249	23.49	452	42.64	1 060	100.0
Missing	8 825	39.33	6259	27.90	7 353	32.77	22 437	100.0
Totals	12 045	39.88	8109	26.85	10 049	33.27	30 203	100.0
Validation Sample								
< \$100	111	48.26	53	23.04	66	28.70	230	100.0
\$100 to \$399	45	35.16	36	28.13	47	36.72	128	100.0
\$400+	19	36.54	9	17.31	24	46.15	52	100.0
Missing	466	41.24	294	26.02	370	32.74	1 130	100.0
Totals	641	41.62	392	25.45	507	32.92	1 540	100.0

^aAll households that did not make expenditures on insulation are included here.

middle group, only 25.8% were classified correctly less than would be expected by chance. Results were somewhat better on the validation sample for all three groups, indicating that the variables identified are important. Thus the models works fairly well in identifying households who spend a small amount and households who make major expenditures but not very well for the others.

Predictor Variables

In addition to knowing how well the discriminant function differentiates between members of the groups studied, the contribution of the individual predictor variables to that success is also important. Variables found to discriminate between housing units with insulation and those without are reported and the direction of the influence noted (Table 7). As expected, housing units that were insulated were more likely to have storm doors or windows, be newer, more expensive, be located in the Northcentral region as opposed to the South, and have an attached fan. Electric or oil heat rather than natural gas also influenced presence of insulation. Households with an older head and a child under 6 were more likely to live in units with no insulation than with insulation. Brown and Rollinson [24] reported that the homes of the elderly were less weatherized. However, households with a child under 6 were more likely to have insulation in their homes than those without a child under 6, and age of households head contributed positively to having insulation. The longer a household had lived in the house the less likely they were to have insulation. This may indicate that movers have been educated to consider the energy efficiency of a house.

Variables which were found to discriminate between those households which added insulation and those that did not are reported in Table 8. As found by Johnson-Carroll et al. [25], elderly households were less likely to add insulation, this being indicated by the size of the coefficient. Berry and Brown [26] suggested the need for marketing strategies targeted specifically for the elderly based on their low participation rates in conservation programs. The presence of child under 6 increases the probability of adding insulation, while length of occupancy had a negative impact in contrast to what was expected based on Gladhart's work [14]. The addition of insulation was more likely in older homes, homes located in regions other than the

TABLE 7—*Discriminant analysis coefficients for presence of insulation*
(N = 29 238).

Variable	Coefficient	
	Insulation	No Insulation
Constant	-15.271	-14.511
Age of house	0.212	0.256
Northeast	-0.499	-0.488
Northcentral	0.718	0.074
West	0.246	0.499
Age of head	0.991	1.020
Household income	0.001	0.001
Presence of child under 6	5.477	5.608
Length of occupancy	-0.061	-0.056
Value of house	0.665	0.588
Storm doors and windows	3.480	1.959
Attached fan	0.395	0.044
Electric heat	4.468	4.005
Oil heat	0.937	0.613
LP gas heat	4.856	5.441
Wood heat	5.954	6.288

TABLE 8—*Discriminant analysis coefficients for addition of insulation*
(N = 35 853).

Variable	Coefficient	
	Insulation Added	No Insulation Added
Constant	-10.234	-9.804
Age of house	0.139	0.122
Northeast	0.826	0.620
Northcentral	1.003	0.884
West	3.423	3.212
Age of head	1.007	1.069
Household income	0.002	0.002
Presence of child under 6	5.779	5.577
Length of occupancy	-0.110	-0.085
Storm doors and windows	3.655	3.182
Attached fan	2.359	1.901
Oil heat	0.481	0.257
LP gas heat	2.341	2.133
Wood heat	3.643	2.989

South, homes heated with oil, LP gas, or wood as opposed to natural gas, and homes with storm doors or windows and an attached fan.

Fewer variables were retained in the stepwise discriminant analysis for the categories on expenditures on insulation. In order of declining importance the significant variables are: location in the Northcentral region, length of occupancy, house value, presence of attached fan, presence of storm doors and windows, age of house, and presence of a child under 6 years. Table 9 contains the coefficients for each of the expenditure categories.

TABLE 9—*Discriminant analysis coefficients for expenditures on insulation (N = 7766).*

Variable	Coefficient		
	< \$100	\$100–\$399	\$400 +
Constant	–9.930	–9.804	–10.411
Northcentral	2.115	1.697	1.493
Northeast	1.021	0.879	0.949
West	0.358	0.174	0.072
Length of occupancy	0.078	0.064	0.063
Attached fan	0.500	0.628	0.899
Age of house	0.208	0.211	0.221
Value of house	0.818	0.827	0.851

Implications

The present study can be used to identify households that live in housing units with no insulation as well as households who are likely to add insulation. Once targeted, an array of incentives may be applied to increase energy conservation activity.

The elderly are low participators in conservation programs but growing in number in the population. Berry and Brown [26] suggest several approaches to stimulating conservation activities by the elderly: door-to-door canvassing, use of existing community groups, peer services, and rebate programs. Similarly contacts with parents of young children could be made through nursery schools and day-care programs.

Energy standards in building codes and utility programs have had some success in increasing energy of efficiency as indicated by the age of house variable. Improvement in locations with weaker requirements is needed as well as maintenance of requirements in other areas.

Older neighborhoods of existing housing units could be targeted for specific assistance. Local governments could provide incentives such as a property tax credit for energy-saving improvements undertaken. Free installation would also be an incentive for many.

Since the presence and addition of insulation were more likely in housing units with other energy-saving features, coordination of sales approaches and marketing materials would assist all suppliers as well as enable consumers to make an informed choice. Williams and Braun [7] indicate success with educational efforts directed towards limited resource households. Johnson-Carroll et al. [25] note that educational programs aimed at encouraging energy conservation through belief in the energy problem are not recommended.

Policy makers can segment programs to financially assist those most likely to undertake insulation conservation action and conversely to educate those least likely to undertake insulation activities on the benefits of such activities.

Caution should be used in applying the results of this study in that the data were collected in 1980 and, as with much research, could be refined and improved, especially in measurement of the variables. However, the study can provide a meaningful base for program planning, educational efforts, and sales targeting.

Acknowledgments

Special thanks are due Dr. Glenn O. Ware for his advice on the discriminant analysis and to three anonymous reviewers for their helpful suggestions.

References

- [1] *Consequences of Energy Conservation Policies for Western Region Households*, jointly sponsored by Agricultural Experiment Stations, June 1986.
- [2] Dillman, J. J., Tremblay, K. R., Jr., and Dillman, D. A., "Energy Policies Directed at the Home: Which Ones Will People Accept?" *Housing Educators Journal*, Vol. 4, No. 2, 1977, pp. 2-13.
- [3] Brown, M. A., "Change Mechanisms in the Diffusion of Residential Energy Conservation Practices: An Empirical Study," *Technological Forecasting and Social Change*, Vol. 25, 1984, pp. 123-138.
- [4] Dillman et al., "A Western State's Perspective on Public Policy for Household Energy Conservation," *Housing and Society*, Vol. 8, No. 2, 1981, pp. 80-92.
- [5] Laquatra, J., "Energy Efficient Housing and Extension Specialist," in *Proceedings*, American Association of Housing Educators, Oct. 1986, pp. 88-98.
- [6] Hanna, S., "Evaluation of Energy Saving Investments," *Journal of Consumer Affairs*, Vol. 12, No. 1, 1978, pp. 63-75.
- [7] Williams, S., Lauener, N., and Braun, B., "Adoption of Energy Conservation Practices by Selected Oklahoma Families," in *Proceedings*, American Association of Housing Educators, 1979, pp. 91-97.
- [8] Tremblay, K. R., McCray, J. W., and Navin, J. L., "Impact of Economic and Energy Variables on Housing Preferences," in *Proceedings*, American Association of Housing Educators, 1984, pp. 203-213.
- [9] Niemeyer, S. M. and Morris, E. W., "Economic and Psychological Constraints in Household Energy Conservation," *Housing and Society*, Vol. 13, No. 1, 1986, pp. 44-55.
- [10] Latta, R. B., *Regression Analysis of Energy Consumption by End Use*, U.S. Department of Energy, Washington, D.C., Oct. 1983.
- [11] *Energy Conservation*, U.S. General Accounting Office, Washington, D.C., Dec. 1986.
- [12] *Annual Housing Survey: 1980*, Part A, General Housing Characteristics, U.S. Department of Commerce and U.S. Department of HUD, 1982.
- [13] Klecka, W. R., *Discriminant Analysis*, Sage Publications, Newbury Park, Calif., 1980.
- [14] Gladhart, P. M., "Interactions of Prices and Household Characteristics and Residential Energy Conservation," *Housing and Society*, Vol. 11, No. 3, 1984, pp. 149-167.
- [15] Cunningham, W. and Lopreato, S. C., *Energy Use and Conservation Incentives*, Praeger, New York, 1977.
- [16] Newman, D. and Day, D., *The America Energy Consumer: A Report to the Energy Policy Project of the Ford Foundation*, Ballinger, Cambridge, Mass., 1975.
- [17] Dillman, D. A., Rosa, E. A., and Dillman, J. J., "Lifestyle and Home Energy Conservation in the United States: The Poor Accept Lifestyle Cutbacks Which the Rich Invest in Conservation," *Journal of Economic Psychology*, Vol. 4, pp. 299-315.
- [18] Eichner, M. M. and Morris, E. W., "Energy Conservation, Air Quality, Health, and Housing Satisfaction," *Housing and Society*, Vol. 11, No. 1, 1984, pp. 1-15.
- [19] Trienda, M. and Aboramph, O., "Energy-Related Adaptions in Low-Income Non-metropolitan Wisconsin Counties," *Journal of Consumer Research*, Vol. 8, 1981, pp. 265-270.
- [20] Thompson, W., *Consumption and Expenditures, April 1981 through March 1982*, U.S. Dept. of Energy, Washington, D.C., Sept. 1983.
- [21] Heberlein, T. A. and Warriner, G. K., *Attitude, Motive, Ability and Knowledge Factors Affecting Household Peak Load Reductions in Consumption of Electricity*, Department of Sociology, University of Wisconsin, Madison, 1980.
- [22] Cramer, J. C. et al., *The Determinants of Residential Energy Use: A Physical-Social Causal Model of Summer Electricity Use*, paper presented at the Energy Crisis and Families Conference, Michigan State University, East Lansing, Oct. 1983.
- [23] Tyler, L. L., Lovingood, R. P., Bowen, S. P., and Tyler, R. F., "Energy-Related Characteristics of Low-Income Urban Tenants," *Housing and Society*, Vol. 9, No. 3, 1982, pp. 9-15.
- [24] Brown, M. A. and Rollinson, P. A., "Residential Energy Consumption in Low-Income and Elderly Households: How Nondiscretionary Is It?" *Energy Systems and Policy*, Vol. 9, No. 3, 1985, pp. 271-301.
- [25] Johnson-Carroll, K. J. A., Brandt, J. A., and Olson, G. I., "Factors That Influence Energy-Conservation Alternatives in Oregon Households," *Housing and Society*, Vol. 14, No. 2, 1987, pp. 111-129.
- [26] Berry, L. G. and Brown, M. A., "Participation of the Elderly in Residential Conservation Programs," *Energy Policy*, forthcoming.
- [27] Douthitt, R. A., "The Demand for Residential Space and Water Heating Fuel by Energy Conserving Households," *Journal of Consumer Affairs*, Vol. 20, No. 2, Winter 1986, pp. 231-248.
- [28] Latta, R. B., "The National Interim Energy Consumption Survey: Exploring the Variability in Energy Consumption—A Supplement," U.S. Department of Energy, Washington, D.C., Oct. 1981.
- [29] Morrison, B. M., Gladhart, P. M., Zuiches, J. J., Keith, J. G., Keefe, D., and Long, B. R., "Energy and Families: The Crisis and the Response," *Journal of Home Economics*, Vol. 70, 1978, pp. 19-21.

- [30] Ogus, M. R., "Residential Energy Conservation and Price Response," Report to ERS, USDA, Washington, D.C., 1980.
- [31] *SAS Users' Guide: Statistics Version*, 5th ed., SAS Institute, Cary, N.C., 1985.
- [32] Kmenta, J., *Elements of Econometrics*, Macmillan, New York, 1971.
- [33] Lachenbruch, P. A., *Discriminant Analysis and Applications*, T. Cacoullos, Ed., Academic Press, New York, 1973.

Implementing Thermal Insulation Product Standards

REFERENCE: Nelson, B. D., "Implementing Thermal Insulation Product Standards," *Insulation Materials, Testing, and Applications, ASTM STP 1030*, D. L. McElroy and J. F. Kimpflen, Eds., American Society for Testing and Materials, Philadelphia, 1990, pp. 626-633.

ABSTRACT: Product standards for residential thermal insulation were authorized by the Minnesota Legislature in response to the marketing of substandard insulation. In 1985 administrative rules established minimum standards for all residential insulation products sold or installed in the State. When possible, these requirements were based on industry consensus standards. The rules require manufacturers to file annual reports with the State, indicating that their products have been tested and meet the minimum standards. Manufacturers must also provide installation instructions to purchasers. Special testing provisions and installation instructions are required for insulations intended for use exterior below ground.

Manufacturers of insulation marketed in the State have been notified of this regulation. Filings of products are acknowledged by the State as being complete, or incomplete, with explanations as necessary. The State has published lists including products of 36 companies with completed filings and of those with filings in preparation.

Four areas have been particularly difficult in the design and implementation of this program. The first is deciding on equitable quality assurance requirements for manufacturers of insulation. A second is determining what products are acceptable for exterior foundation wall applications. Third is how consumers can identify which insulation products meet the standards. Finally, and probably most important, is how the installation of material can be improved so as to realize its full potential energy saving benefits.

The insulation manufacturing industry has been very supportive of this program. In the first two years of its existence, the program has benefited both consumers and industry.

KEY WORDS: thermal insulation, design standards, quality assurance, quality control, residential buildings, building materials, materials testing

Thermal insulation product standards were authorized by the Minnesota Legislature in 1978 in response to speculation that the rising demand for insulation would lead to the production of insulation materials of marginal quality or that poor installation would be practiced. The Minnesota Division of Energy, Department of Public Service, has been implementing the standards since they became effective in November 1985. The State of California and the Bonneville Power Administration (BPA) have the only other known public agency programs in the country that list thermal insulation products as meeting established performance criteria.

Manufacturers of insulation sold in Minnesota are required to demonstrate that their products meet applicable ASTM standards. No fee is imposed, although an annual filing to demonstrate conformance with the requirements is required. The department published the first list of products with completed filings in October 1986.

Most of the insulation industry has been pleased with this regulatory program. However, a major complaint for some manufacturers outside the State, for which Minnesota is a small part of their market, is that the cost of the required testing is not justified by the amount of product they sell here.

¹Minnesota Department of Public Service, St. Paul, MN 55101.

A program aimed at regulating quality is difficult. A comprehensive quality assurance program cannot be based on a once-a-year or one-time test. Recommendations for improving this situation include requiring third-party follow-up service, manufacturer quality assurance programs, and random testing of products by the State.

Program Purpose

In 1979, when the first draft of Minnesota thermal insulation standards rules was developed, the need for standards was immediate. Following the oil embargo and energy crisis of 1973, rapidly rising prices for residential customers had made either new or additional insulation an economic necessity. In addition, federal, state, and local governments were calling for energy conservation, which convinced many Minnesota citizens to purchase increased amounts of insulation and installation services. It was speculated that the rising demand for insulation would lead to both new products and increased production, which may result in the production of insulation materials of marginal quality, or that poor installation would be practiced, resulting in ineffective performance of the insulation. These concerns led the Minnesota Legislature to authorize the adoption of standards.

The years between 1979 and 1985 were filled with a rise and fall of substantial federal regulation. When the Minnesota Insulation Standards Program rules were proposed in 1985, there was a perception that regulation of insulation at the federal level had nearly disappeared. California was first in adopting state insulation standards in 1982. Additional incentives for regulation came from the urea-formaldehyde controversy and a 1983 experience with a Minnesota cellulose manufacturer selling a product which was misrepresented and did not meet federal flammability specifications [1].

By 1985, the insulation industry was very competitive, with no supply shortages. Although no immediate emergency existed, many of the concerns were the same as in 1979. The next energy crisis could once again trigger a run on insulation. But, also, new uses of insulation are emerging which were previously overlooked. Regardless of energy availability, the purpose of the rules is to provide a legal basis to mandating compliance of these products with industry standards.

The materials included under the Minnesota rules are limited to those used in residential structures. The Department of Public Service believed that limiting regulation to the residential sector is a course that carries out the legislature's intent, and which is reasonable and workable.

When the Minnesota rules were enacted, federal specifications existed for the quality and safety of thermal insulation. However, the federal specifications were enforced on a complaint basis only. Small consumers of residential products would have few resources to monitor and test products to determine whether they indeed met the specifications. In addition, standard practices for the installation of insulation materials had not been established. The Department believes that regulation of product quality, labeling, and installation services must reasonably and effectively be accomplished at the State level if problems are to be addressed. With these rules in place, recourse is available within the State to deal with product quality.

Legislative Authority

The authority for adopting rules governing the manufacture, labeling, and installation of thermal insulation materials arises directly from legislative mandate. Minnesota Statutes Chapters 325F.20 and 320F.21 provide that:

The (Department of Public Service) shall adopt rules . . . regarding quality, information and product safety specifications for the manufacture, labeling, installation and thermography of insulation. . . . All insulation used or offered for sale in Minnesota shall be tested in accordance with testing procedures required under those specifications by a laboratory qualified to test thermal insulation.

Administrative Rules

In accordance with the State's Administrative Procedures Act, meetings were held with industry representatives to solicit ideas for draft rules, proposed rules were published, a public hearing was held, and the recommendations of the administrative law judge were followed in adopting the final rule.

On 30 November 1985 the State of Minnesota adopted administrative rules establishing standards governing the manufacture of all thermal insulation for residential buildings that is offered for sale. "Residential" includes single family and multifamily buildings three stories or less in height.

The rules set requirements for the manufacture, sale, and installation of insulation products. The requirements apply to manufacturers, distributors, retailers, and installers, although the program to date has primarily affected manufacturers.

The rules contain three basic requirements for manufacturers: test requirements, product labeling and installation instructions, and reporting requirements. These are explained fully below.

Test Requirements

All products within the scope of this regulation must be tested and shown to meet specified standards. Generally, these standards are ASTM Standard Specifications for specific insulation types. Insulation types which are not specifically described in the rules are designated "Other." These types must be tested for thermal resistance, fire performance, and moisture absorption, and the manufacturer must present evidence that the product is safe and effective.

Tests must have been performed since 1985. Tests performed in 1986 and later must be done by a laboratory accredited for the specific test by the National Voluntary Laboratory Accreditation Program of the U.S. Bureau of Standards (NVLAP).

The rule imposes additional testing requirements for insulation products intended for exterior below ground use, including an "in-service" test to demonstrate the product's effectiveness in cold climate conditions. While no standard for this in-service test exists, the rules state that "the testing environment must reflect the extremes of weather, moisture and soil conditions."

Product Labeling and Installation Instructions

The Minnesota rules make reference to the Federal Trade Commission (FTC) "R-value Rule" [2]. These requirements call for R-value testing and specify the labeling that is required. The State rules also specify that the manufacturer must provide installation instructions for products. These instructions must include the product's intended uses, installation procedures, and recommended or required safety measures. Additional installation instructions are required for insulation products intended for exterior below ground use.

The rules further require that insulation be installed in accordance with the manufacturer's instructions.

Reporting Requirements

Manufacturers must submit reports with the Department before the product is sold, and report on an annual basis thereafter. The reports must document the test results and show the installation instructions provided to insulation purchasers. The annual report has been a valuable tool to determine whether a product is still for sale in the State and to identify new product lines.

Aside from the costs which may be incurred by the manufacturer by the testing and follow-up services, the State imposes no charge for participating in the program.

Program Implementation

Deadlines

The first filing deadline for reports from manufacturers was 30 June 1986. The Department published the first list of products with complete filings on 28 October 1986, with only 30 manufacturers having completed filings for insulation products. Currently there are 66 manufacturers with products filed or filings under preparation. The number of manufacturers selling in the state is probably not much different now than it was on 30 June 1986. A major task, which is continuing today, has been to identify insulations marketed in the State and to ensure that manufacturers complete their filings. The rules did not anticipate this difficulty with completing filings. The rules essentially state, "If the filing for a product is not complete, it can't be sold in the state." The department has attempted to deal with this issue as described below.

Approved Products

Once a filing is submitted, the Department decides whether the product filing is complete or incomplete. The words "approved" and "disapproved" are avoided. A completed filing for a product is analogous to issuance of an International Council of Building Officials (ICBO) evaluation report in that test data are verified. The word "approved" connotes approved for a specific installation, as approval would be granted by a building official for the installation of a product which has an ICBO evaluation report. The Department only determines if the filing meets specified requirements.

Due to the time required to find and notify manufacturers, and then to have them complete the required testing, it became apparent that a category of products whose filing was in process was necessary. Although the rules had established no criteria for this category, we indicated that we would not take action against a manufacturer which was moving ahead in a good faith effort to complete a filing.

What is Insulation?

Another issue we did not anticipate was ambiguity over precisely what products were considered to be insulation materials. This question first arose while considering submissions for "siding backer" extruded polystyrene material from two manufacturers. One manufacturer advertised the material as insulation, the other did not. Since the Minnesota rules define thermal insulation as any material "advertised" as having an *R*-value, the characteristics of the material do not necessarily make it insulation; rather it is how the manufacturer promotes the product. We concluded that any material labeled as "insulation" or advertised as saving energy by virtue of its low conductivity or low emissivity has been interpreted as insulation. Products *not* considered insulation are those for which the *R*-value is listed only for information or those sold only for air leakage reduction.

A related problem is determining which insulation products of a given manufacturer are different enough to require separate complete testing of all characteristics. For example, different design densities of polystyrene or thicknesses of mineral fiber batts of one manufacturer will result in different *R*-values for the product. However, a different design density of cellulose may be associated with a different formulation which should be tested in total. Similar distinctions are being made for spray-applied products which may be of different chemical nature or different densities.

What is a Manufacturer?

Even more unexpected was uncertainty over what company should be designated the manufacturer of a particular product. We did not at first anticipate that many insulation products

were repackaged under different trade names. However, we discovered that this practice is especially prevalent with pipe insulation, duct wrap, and water heater blankets. We decided to allow the company whose name appears on the package to decide if they would prefer to be listed as the manufacturer or have their product name listed with the products produced by the original manufacturer. Companies have chosen both routes. In all cases, the manufacturer is required to assemble evidence of the required testing and file the requisite reports with the Department.

The manufacturer is also difficult to identify for products for which the manufacturing process is not completed until application at the job site. These include urethane spray, spray-applied mineral fiber or cellulose, or any insulation which is modified just prior to application. In each of these cases to date, companies supplying products to installers have chosen to be named the manufacturer. In doing this, they have performed the required tests based on the product as produced using their installation instructions. They have also trained, and in some cases certified, installers who are the only persons able to obtain the product and install it.

Problems with Filings

Although it has taken considerable time to notify manufacturers and then to have them complete their filings, relatively few problems were found in the submitted filings. We did encounter the kinds of problems given below.

Tests by Approved Laboratories

All manufacturers do some testing in-house. Manufacturers were willing to provide these test results, but sometimes balked at our requirement that the tests be conducted by a laboratory accredited by a NVLAP for each test. The additional cost for testing by NVLAP-accredited laboratory was too much for some companies whose sales volume in Minnesota market was small. As a result, some companies are considering not selling their products in the State.

Products Not Meeting Standard Specifications

As might be expected, very few test failures were reported. A flame spread of 775 for one type of pipe insulation was reported, which exceeds the maximum allowed by the Minnesota Building Code. The manufacturer voluntarily withdrew the product from the market until a suitable flame retardant could be found.

Insulation Systems for Exterior Foundation Walls

Manufacturers of most insulation types, including expanded polystyrene, polyisocyanurate, and spray-applied urethane, have stated that their insulation was appropriate for insulating the exterior of foundation walls. This is a very controversial issue, and the filings did not magically resolve the controversy. Manufacturers were often asked to explain why a particular material characteristic (moisture absorption, for example) made the material suitable for this application. The required in-service test is the most difficult for manufacturers to complete and for the Department to determine if the criteria in the rules had been satisfied. The Department has accepted reports on single samples of products taken from below ground applications in Minnesota as well as published research reports on below ground performance of insulation materials as meeting the requirement for an in-service test.

Installation Instructions

To date, the Minnesota program has focused on material standards, while realizing that installation is also very important. Installation instructions and other manufacturer's literature

are reviewed for FTC-required notices and charts as applicable. We sometimes find that installation instruction do not contain prescribed safety measures as required by the Minnesota rules. This was always readily corrected once pointed out to the manufacturer.

Another deficiency sometimes found is inadequate instructions on how to achieve system *R*-values. This has particularly been a problem with reflective (low emissivity) insulation products.

We examine installation instructions for exterior foundation wall insulation with particular care. A review of relevant literature [3] indicated that drainage was a critical need. The Expanded Polystyrene Committee of the Society of Plastics Industry has put much effort into a set of model installation instructions for this material.

Program Benefits

Many manufacturers have expressed appreciation for the Minnesota Insulation Standards Program, saying that it helps keep the manufacturing quality on an equal basis. On several occasions, manufacturers have also found the State a handy complaint bureau. They can voice grievances with some anonymity to the State, and have us follow up on a possible defective product.

Because consumers generally cannot evaluate differences between insulation products, the Department's role is critical in ensuring that all products are safe and effective. Retailers, building officials, and builders have used the Department's list of products with completed filings as a basis to accept or reject various products or product applications. For example, a local building official can use the list of products to ensure that only products with completed filings for below ground use are used for exterior foundation wall insulation applications.

Also, our program should help prevent reintroduction of hazardous products such as an untreated sawdust product installed in some Minnesota attics as recently as the late 1970s.

Program Challenges

Implementing a State standards program for thermal insulation materials has had some success. However, fundamental difficulties with this type of program remain.

Can Manufacturing Quality Assurance Be Legislated?

The Minnesota rules initially tried to accomplish manufacturing quality by mandating complete annual testing of one sample of product. Such a test simply proves that the manufacturer has the *capability* of producing a quality product. It does not ensure that with routine production, products would satisfy the requirements of the standard.

Further complicating the question of quality assurance for all insulations is an implicit requirement to equitably treat manufacturers of different insulation types. Although the manufacturing processes differ dramatically, the level of quality assurance required should be reasonably similar in order that the products be competitive in the same market.

One option would be to require a follow-up service by a third-party laboratory, including unannounced inspections of manufacturing facilities. Some large manufacturers object to this proposal because of the lack of standards for follow-up services and a lack of a choice (or no choice) of laboratories for certain insulation types. Even more important to large companies is a contention that their internal quality assurance programs preclude the need for a third-party follow-up service. For small businesses there is the problem of being able to afford a follow-up service.

Another solution would be to require manufacturers to have in place an in-plant quality assurance program. However, the department would have great difficulty evaluating the ade-

quacy of such programs. ANSI/ASQC Standard Z-1.15-1979, Generic Guidelines for Quality Systems, warns against possible misuse of the standard:

There exists the danger that a standard providing generic guidelines for a quality system will be used as a "shopping list," in which systems analysis consists of checking off items on a list, and quality assurance degrades into nothing more than a way to verify compliance with a set of procedures.

The State might require an independent review of manufacturers' quality assurance programs.

A program of State sampling and testing of products from the marketplace may be an essential follow-up to whatever regulatory approach is taken. The California and BPA programs have funded such an effort, and Minnesota will soon commence a limited scale test program of its own.

Insulation product quality can be improved by State requirements, but there are burdens of time and cost for the State and manufacturers with any system chosen.

What Criteria Should Below-Ground Insulation Meet?

There currently exist no standards for either testing or specifying insulation for use below ground. The criteria established by the Minnesota rules are a partial solution to this question. There is a great need for industry standards on (1) testing the performance of exterior foundation wall insulation systems and (2) materials or systems used as exterior foundation wall insulation. This is a critical and major challenge as more states adopt codes requiring foundation walls to be insulated. Without minimum standards, products and systems may be installed which may not retain their effectiveness as thermal insulation with weathering and aging.

How Can Complying Products Be Identified?

Our initial method of identifying products that comply has been to distribute lists of products filed to the insulation manufacturing industry, insulation contractors, material suppliers, building officials, and builder.² Probably the most useful distribution was to the material suppliers (i.e., lumber yards, hardware wholesalers, etc.). Some of the material suppliers responded by informing us of other products that were not found on the lists.

Product labeling is an alternative prescribed by California's program. Laboratories performing follow-up services allow, but do not require, their label to appear on covered products.

How Can Insulation Installation Be Improved?

Proper installation of insulation is extremely important. Building officials who enforce installation quality in the field consider many variables and have inadequate time. Education of contractors as to the importance of careful installation, and the efforts being taken to assure quality products are delivered to the jobsite, may help to ensure quality installation.

Material and installation quality of products whose manufacture is completed at the job site could be more assured if a requirement were in place that product manufacturers train and annually certify all installers.

The Future

Minnesota's objective with its insulation standards program is to assure quality products for its citizens. A good quality assurance program in all manufacturing plants is critical to this end.

²A free copy of the most recent listing of products filed may be obtained by calling the Minnesota Energy Information Center at 612/296-5175.

We have learned that to achieve this objective there must be a balance struck between over-regulation and under-regulation.

An insulation standards program would be much more cost-effective for manufacturers if more states had standards. However, these state standards must be identical. In this light, there is a similarity between appliance standards and insulation standards. Perhaps a national program to assure insulation material quality is needed.

References

- [1] State of Minnesota v. Omega Insulation Corporation, Hennepin County (Minnesota) District Court, File number 83-09607.
- [2] Federal Trade Commission, "Trade Regulations: Labeling and Advertising of Home Insulation," *16 Code of Federal Regulations*, Part 460.
- [3] Sterling, R. L., "Moisture Absorption and Its Effect on the Thermal Properties of EPS Insulation for Foundation Applications," Report to Society of Plastics Industry, Expanded Polystyrene Division, 1986.

Corrosiveness of Residential Thermal Insulation Materials under Simulated Service Conditions

REFERENCE: Sheppard, K., Weil, R., and Desjarlais, A., "Corrosiveness of Residential Thermal Insulation Materials under Simulated Service Conditions," *Insulation Materials, Testing, and Applications, ASTM STP 1030*, D. L. McElroy and J. F. Kimpflen, Eds., American Society for Testing and Materials, Philadelphia, 1990, pp. 634-654.

ABSTRACT: The corrosiveness of various residential thermal insulation materials was tested under simulated field conditions in a test wall structure. The test was conducted under controlled conditions typical of winter in the absence of a vapor barrier to create relatively severe moisture transport and possible condensation. The house-wall simulation was achieved by constructing a test panel containing 50 compartments into which various insulation materials were installed. The panel was located in an environmental chamber. The test samples included various cellulosic, glass fiber and rockwool insulations as well as sterile cotton as a control. Steel and copper coupons together with water-cooled copper pipes were embedded in the insulation and exposed for six months. It was found that moisture absorption by the insulation was the primary factor in causing corrosion but required that chemical activity from insulation components also be present. No corrosion occurred in the absence of insulation or in rockwool and glassfiber insulation. All cellulose insulations caused some corrosion; mostly this was minimal, but in a few cases severe pitting resulted. Such behavior of the cellulose did not correspond to previous laboratory test results in saturated insulation or leachants made from the insulation. However, laboratory testing of leachants made from some of the cellulose after the simulated wall test showed a change in pitting tendency, suggesting that time and/or exposure to moisture can change the corrosiveness. This should be further explored.

KEY WORDS: corrosion, corrosiveness, cellulose, glass fiber, rockwool, mineral wool, wall simulation, moisture, condensation, steel, copper, pipes

A task group of ASTM Subcommittee C16.31 has been developing a uniform corrosiveness test procedure that would be applicable to all types of residential insulation. To support their efforts, data have been obtained and provided to the task group by Stevens Institute of Technology under sponsorship of the Department of Energy through Oak Ridge National Laboratory. Some results of this work have been previously reported [1-5].

It is clearly desirable that any new laboratory test procedure produce results that reflect the corrosiveness of thermal insulation under service conditions. It is also desirable to be able to discriminate between corrosiveness and corrosion. It is possible for the latter to occur even with an inert insulation material because of the insulation's ability to trap or draw moisture to a metallic surface without taking part in aggravating the corrosion that could subsequently occur. One major weakness of existing test procedures is that they were developed without the benefit of field performance data. The reason for this is the almost complete absence of published field

¹Department of Materials and Metallurgical Engineering, Stevens Institute of Technology, Hoboken, NJ 07030.

²Thermotest Division, Holometrix Inc., Cambridge, MA 02139.

performance data on the corrosiveness of residential insulation. The few published field studies [6, 7] containing data on corrosion were not specifically designed to investigate corrosion. The investigators did not deliberately examine metal components in the buildings under study; in fact, generally such locations were avoided. One of the reports [7], in fact, called for "a more rigorous examination of the potential for corrosion." The availability of reliable field data has been limited by the cost and difficulty associated with gaining access to metal components in the walls of houses and by problems with obtaining adequate environmental histories at each location. Some limited field testing in attics of residential buildings at various geographical locations was previously carried out [3], but no significant corrosion was found.

Corrosion requires the presence of moisture. House wall cavities are more probable sites for moisture accumulation, that could potentially lead to corrosion, than are attics. Aside from leakage (e.g., from bathrooms), condensation is possible under severe conditions when a vapor barrier is not present or is compromised. The presence of cold-water pipes can also cause condensation of moisture.

Background

One of the field studies previously mentioned [6] found that 12.5% of a sample of 96 houses had suffered water leakage into the wall cavity. This figure does not include numerous other leaks that were found but not further investigated by opening the wall. Clearly, leakage is an important source of moisture and the potential for corrosion cannot be ignored; however, the present work concentrates on moisture originating from condensation. In the previously cited study the authors calculated that on average over the winter of their study the opportunity for condensation existed from 40 to 80% of the time in insulated walls.

Wang [8] has reported that in two test houses studied during a winter in Michigan condensation occurred in the wall cavity. Outdoor conditions were 0 to 7°C, indoor conditions 21 to 24°C. The condensation occurred with both medium (30 to 35% RH) and high (50 to 55% RH) interior humidity settings. At the medium humidity value a Kraft paper vapor barrier prevented condensation but did not at the high humidity value. However, it should be noted that Wang also reports that field inspections of over 70 houses in the United States and Canada having a variety of constructions, insulations, vapor barriers, sidings, etc., did not reveal evidence of condensation.

It is against this background that a simulation was constructed to determine the potential corrosiveness of various residential thermal insulation materials under relatively severe conditions, conducive to moisture transport and possibly condensation, that might be experienced by an insulated house wall cavity without a vapor barrier during a winter condition.

Experimental Procedure

The house-wall simulation was achieved by constructing a test panel containing 50 compartments into which various insulation materials were installed. The panel was located in an environmental chamber. The chamber was constructed such that the environmental conditions (temperature and relative humidity) on both sides of the test panel could be independently controlled. The panel was conditioned for 190 days (this being a nominal six-month period) with the environmental conditions maintained at approximately 22°C and 45% relative humidity on the interior (hot) side and 3°C and 95% relative humidity on the exterior (cold) side. This would be expected to produce a vapor pressure differential of 6.19 mm Hg (0.12 psi). These conditions, although relatively severe in terms of vapor pressure drop, are within those to be expected during a winter in the United States (see, for example, the study by Wang [8] cited above).

Test Panel Configuration

The test panel used in this program was 210 cm long by 150 cm high by 11.5 cm thick and was constructed with standard 2 by 4 studs around the perimeter of the test panel and 1.25 cm thick gypsum board sheathing to represent the interior side of the wall. The exterior side was sheathed with two different products: 1.25 cm thick plywood and 1.25 cm thick aluminum foil-faced polyisocyanurate foam board. The left half (Cells 1–4, 11–15, 21–25, 31–35, and 41–45) of the test panel was sheathed with plywood, while the right half (all remaining cells) of the test panel was sheathed with the foam board. The purpose of using two different sheathings was to demonstrate the effect of the water vapor permeability of the exterior sheathing on the potential for corrosion. The panel was designed so that there would be as far as possible pairs of cells with identical insulation materials with the only variable being the sheathing material. The panel was mounted vertically.

The interior of the test panel was divided into 50 identically sized cells laid out in an array 10 cells wide by 5 cells high. The cells were numbered 1 to 50 with Cell 1 being the upper left corner, Cell 10 the upper right corner and Cell 50 the lower right corner when viewed from the interior side. The walls of the cells were fabricated from 1.25 cm thick extruded polystyrene foam glued with silicone cement to seal the cells from each other. The resulting cell size was 29 cm high, 20 cm wide and 9 cm deep.

The insulation materials employed in the test were identified as Cellulose 1, Cellulose 2, Cellulose 3, Cellulose 4, Cellulose 6, Cellulose 527G, Rockwool, Glass Fiber B, Glass Fiber O, Glass Fiber T, and sterile cotton wool as a control. For this test no degreasing was used on the cotton. The presence of natural oils in the cotton may have resulted in less moisture absorption and thus possibly reduced corrosion compared to degreased cotton. However, the choice of cotton, whether degreased or not, as an inert control is arbitrary. In previous tests at Stevens Institute [3] Celluloses 1, 2, 3, 4, and 6 all passed the federally mandated HH-I-515D corrosiveness test which is equivalent to that in ASTM Specification for Cellulosic Fiber (Wood-Base) Loose-Fill Thermal Insulation (C 739). Cellulose 527G failed this test. No ASTM Specification for Mineral-Fiber Blanket Thermal Insulation for Light Frame Construction and Manufactured Housing (C 665) corrosiveness test data were available to us for the glass fiber and rockwool insulations, but in various other corrosiveness tests at Stevens, Rockwool and Glassfiber B produced low corrosion levels, less than a distilled water control [3]. Glass Fiber O and T were not part of those tests and were purchased from retail outlets. The other insulations were supplied by the manufacturers. More information on these materials is given in Table 1. In addition, some cells were left without insulation. Figure 1 details which insulating materials were installed in each cell. The loose-fill materials were applied based on manufacturers' values for applied density (Table 2). Applied densities rather than settled densities were used because the former had been specified by the ASTM C16.31 Corrosiveness Task Group for the laboratory testing at Stevens and we wished to maintain consistency. It might be anticipated that some small differences in moisture absorption within each cell might have resulted if settled rather than applied densities had been used. The batt materials were cut to size and placed into the cells. To the extent possible, it was desired to test all the insulating materials used in previous laboratory tests at Stevens and to include steel and copper coupons which could not be located together in the same cell because of the possibility of galvanic corrosion. The same insulation materials were placed in the two corresponding cells with different exterior sheathings. Due to the limited number of cells it was not possible in all cases to test both copper and steel in each insulation with each of the outer sheathings.

Metal coupons (5.08 by 2.54 by 0.3 cm) were inserted into the insulation materials installed in Cells 1 to 40. The coupons were either AISI 1010 steel or Cabra 110 tough-pitch copper. Before installation the coupons were abraded to a 600-grit finish on silicon carbide abrasive paper, washed in distilled water and ultrasonically degreased with 1,1,1-trichloroethane. They were then accurately weighed. The coupons were centered in the cell at midthickness of the insula-

TABLE 1—*Materials included in test.*

Cellulose 1	1 part borax (5 mol); 2 parts boric acid, 25% chemical content
Cellulose 2	2 parts borax; 1 part boric acid, 25% chemical content
Cellulose 3	1 part borax; 1 part boric acid; 1 part aluminum trihydrate, 25% chemical content
Cellulose 4	1 part borax; 4 parts ammonium sulfate, 30% chemical content
Cellulose 6	2 parts borax; 2 parts boric acid; 1 part aluminum sulfate, 25% chemical content
Cellulose 527G	Ammonium sulfate, 19% chemical content
Rockwool	Loose fill
Glass Fiber B	1/2 in. appliance type
Glass Fiber O ^a	3 1/2 in. batts
Glass Fiber T ^a	3 1/2 in. batts

^aPurchased retail; all other insulations were those previously employed in the test program at Stevens and were supplied by manufacturers.

tion with the large faces of the coupons parallel to the sheathing. When there was no insulation in the cell, the coupon and pipe sections (copper) were suspended in the center of the cell with a nylon thread.

Corrosometer (Rohrback Industries) probes [3] were installed in Cells 11 to 20 along with test coupons. These probes allow monitoring of corrosion during the test by changes in electrical resistance of one of the probe elements. The probe contains two identical steel sheet elements, one of which is protected from the environment. The two elements are connected in a bridge circuit. Changes in resistance of the exposed element can therefore be determined and converted to a corrosion rate by assuming uniform loss in thickness due to general corrosion. The probe material was AISI 1010 steel. Care was taken to ensure a reasonable separation between these probes and the steel coupons mounted into the same cell. Small holes were cut into the gypsum board sheathing to allow the probe cables to exit the test panel. These openings were sealed with duct tape as were the edges of the inner and outer sheathings.

Sections of copper pipe cleaned on the outside in the manner described above and weighed were installed in Cells 1, 6, and 41 to 50. The individual sections of pipe in Cells 41 to 50 were connected together with Tygon tubing, and the ends of the tubing exiting Cells 41 and 50 were attached to a refrigerated circulation bath in order to simulate the presence of cold water pipes in the insulation. The Tygon tubing allowed electrical isolation of the pipe sections in each cell, preventing possible galvanic corrosion effects between sections in different cells. Cells 41 to 50 were those at the bottom of the test wall when mounted in the conditioning chamber.

Test Chamber Description

A test chamber was constructed to accommodate the test panel and create the required environmental conditions. The inside dimensions of the chamber were 210 cm long by 172 cm high by 50 cm deep. It was constructed from plywood on a framework of 5.08 by 15.24 cm (2 by 6 in.) studs spaced 60 cm on center. All the walls were insulated with R-19 glass-fiber batts. One of the 210 by 150 cm walls was removable to gain access to the chamber interior. All the joints inside the chamber were reinforced with glass fiber cloth, and the interior surfaces of the chamber were waterproofed with epoxy.

Heat exchangers of similar surface dimensions as the test panel were mounted to the chamber such that, with the test panel in place, the heat exchangers would be 7.5 cm from each surface of the test panel. The heat exchangers were constructed from 9 mm thick anodized aluminum plates with 1.25 cm rigid copper tubing attached to the back side. The copper tubes were spaced 7.5 cm apart and connected in a parallel configuration to minimize the pressure drop across the heat exchanger. The heat exchangers were connected to temperature-controlled recirculating

PLYWOOD SHEATHING					POLYISOCYANURATE BOARD SHEATHING				
1 Copper in air (no insulation)	2 Steel in Cellulose 1	3 Steel in Glassfiber T	4 Steel in Cellulose 3	5 Steel in Cellulose 6	6 Copper in air (no insulation)	7 Steel in Cellulose 1	8 Steel in Glassfiber T	9 Steel in Cellulose 3	10 Steel in Cellulose 6
11 Steel in Cellulose 4	12 Steel in Cellulose 527G	13 Steel in Cellulose 2	14 Steel in Glassfiber B	15 Steel in Rockwool	16 Steel in Cellulose 4	17 Steel in Cellulose 527G	18 Steel in Cellulose 2	19 Steel in Glassfiber B	20 Steel in Rockwool
21 Steel in Cellulose 527G	22 Steel in Fiberglass 0	23 Steel in Fiberglass T	24 Steel in Cellulose 4	25 Steel in Cellulose 2	26 Steel in Cellulose 527G	27 Steel in Glassfiber 0	28 Steel in Glassfiber T	29 Steel in Cellulose 4	30 Steel in Cellulose 2
31 Copper in Glassfiber B	32 Copper in Cellulose 2	33 Copper in Rockwool	34 Copper in Cellulose 527G	35 Steel in Sterile Cotton	36 Copper in Glassfiber B	37 Copper in Cellulose 2	38 Copper in Glassfiber 0	39 Copper in Cellulose 527G	40 Steel in Sterile Cotton
41	42	43	44	45	46	47	48	49	50
Copper in air (no insulation)	Copper in Cellulose 2	Copper in Cellulose 527G	Copper in Sterile Cotton	Copper in Glassfiber T	Copper in air (no insulation)	Copper in Cellulose 2	Copper in Cellulose 527G	Copper in Glassfiber 0	Copper in Glassfiber T

FIG. 1—Location of cells in test wall and their contents.

baths; the exterior and interior baths had cooling capacities of 2400 W and 366 W at 0°C, respectively. A series of fans were also mounted on each side of the test panel to circulate air across the surfaces of the test panel and maintain uniform environmental conditions.

Each side of the test panel was outfitted with a saturated salt bath to maintain the required levels of humidity. The salt baths were connected to distilled water level controllers which would maintain a continuous supply of water to the baths without opening the chamber. The salts used in the exterior and interior baths were zinc sulfate and magnesium nitrate, respectively.

Ten thermocouple temperature sensors and a lithium-chloride type humidity detector were installed on each side of the test panel to monitor the environmental conditions during the course of the experiment.

The environmental chamber is shown in Fig. 2 with one of the heat exchanger plates lifted to reveal the space where the test wall was installed. A schematic for the test chamber is shown in Fig. 3.

TABLE 2—Data summary.

CELL NO.	MATERIAL	DENSITY, PCF	INSULATION WEIGHT, GRAMS			COUPON WEIGHT, GRAMS				
			INSTALLED	FINAL	% CHANGE	COUPON	INSTALLED	FINAL	CHANGE	% CHANGE
1	NONE	---	---	---	---	Cu 1	38.756	38.756	0.000	0.00
		---	---	---	---	Cu PIPE 1	26.000	25.993	0.007	0.03
2	CELLULOSE 1	3.14	220.07	270.42	22.88	Fe 21	27.935	27.905	0.030	0.11
3	GLASSFIBER T	0.568	39.79	40.52	1.83	Fe 22	29.192	29.142	0.050	0.17
4	CELLULOSE 3	3.12	218.50	304.43	39.33	Fe 1	29.345	29.274	0.071	0.24
5	CELLULOSE 6	2.91	203.39	228.69	12.44	Fe 2	28.495	28.493	0.002	0.01
6	NONE	---	---	---	---	Cu 2	38.292	38.241	0.051	0.13
		---	---	---	---	Cu PIPE 6	25.760	25.764	-0.004	-0.02
7	CELLULOSE 1	3.14	220.07	231.09	5.01	Fe 3	28.770	28.767	0.003	0.01
8	GLASSFIBER T	0.534	37.39	37.78	1.04	Fe 4	29.047	29.047	0.000	0.00
9	CELLULOSE 3	3.12	218.50	265.98	21.73	Fe 5	28.722	28.722	0.000	0.00
10	CELLULOSE 6	2.91	203.39	276.99	36.19	Fe 6	28.808	28.791	0.017	0.06
11	CELLULOSE 4	3.17	221.99	269.10	21.22	Fe 7	28.969	28.967	0.002	0.01
						PROBE 11	---	---	---	---
12	CELLULOSE 527G	3.12	218.33	278.39	27.51	Fe 8	28.583	28.576	0.007	0.02
						PROBE 12	---	---	---	---
13	CELLULOSE 2	3.24	226.84	342.49	50.98	Fe 9	29.218	29.197	0.021	0.07
						PROBE 13	---	---	---	---
14	GLASSFIBER B	0.491	34.36	36.26	5.53	Fe 19	29.067	29.068	-0.001	0.00
						PROBE 14	---	---	---	---
15	ROCKWOOL	2.78	194.80	191.03	-1.94	Fe 10	28.957	28.958	-0.001	0.00
						PROBE 15	---	---	---	---
16	CELLULOSE 4	3.17	221.99	235.90	6.27	Fe 11	28.790	28.785	0.005	0.02
						PROBE 16	---	---	---	---
17	CELLULOSE 527G	3.12	218.33	250.23	14.61	Fe 12	28.708	28.698	0.010	0.03
						PROBE 17	---	---	---	---
18	CELLULOSE 2	3.24	226.84	236.02	4.05	Fe 13	28.631	28.623	0.008	0.03
						PROBE 18	---	---	---	---
19	GLASSFIBER B	0.498	34.86	35.16	0.86	Fe 20	28.683	28.685	-0.002	-0.01
						PROBE 19	---	---	---	---
20	ROCKWOOL	2.78	194.80	190.69	-2.11	Fe 14	28.911	28.750	0.161	0.56
						PROBE 20	---	---	---	---
21	CELLULOSE 527G	3.12	218.33	358.32	64.12	Fe 15	28.255	28.263	-0.008	-0.03
22	GLASSFIBER O	0.615	43.02	43.09	0.16	Fe 28	25.927	25.926	0.001	0.00
23	GLASSFIBER T	0.443	31.01	32.10	3.51	Fe 16	28.811	28.814	-0.003	-0.01
24	CELLULOSE 4	3.17	221.99	274.35	23.59	Fe 17	28.878	28.880	-0.002	-0.01
25	CELLULOSE 2	3.24	226.84	454.16	100.21	Fe 30	25.764	25.660	0.104	0.40
26	CELLULOSE 527G	3.12	218.33	257.16	17.79	Fe 18	28.045	28.040	0.005	0.02
27	GLASSFIBER O	0.633	44.26	44.73	1.06	Fe 29	25.812	25.812	0.000	0.00

TABLE 2—(continued)

CELL NO.	MATERIAL	DENSITY, PCF	INSULATION WEIGHT, GRAMS			COUPON	COUPON WEIGHT, GRAMS			
			INSTALLED	FINAL	% CHANGE		INSTALLED	FINAL	CHANGE	% CHANGE
28	GLASSFIBER T	0.483	33.77	33.86	0.27	Fe 24	25.575	25.575	0.000	0.00
29	CELLULOSE 4	5.17	221.99	248.32	11.86	Fe 25	25.793	25.760	0.033	0.13
30	CELLULOSE 2	3.24	226.84	250.93	10.62	Fe 26	25.756	25.750	0.006	0.02
31	GLASSFIBER B	0.524	36.67	38.72	5.59	Cu 3	39.861	39.812	0.049	0.12
32	CELLULOSE 2	3.24	226.84	526.32	132.02	Cu 4	38.297	38.283	0.014	0.04
33	ROCKWOOL	2.78	194.80	191.95	-1.46	Cu 5	38.995	38.998	-0.003	-0.01
34	CELLULOSE 527G	3.12	218.33	308.73	41.41	Cu 6	38.267	38.265	0.002	0.01
35	STERILE COTTON	1.3	90.77	94.71	4.34	Fe 23	25.083	25.082	0.001	0.00
36	GLASSFIBER	0.512	35.86	36.18	0.89	Cu 7	39.145	39.148	-0.003	-0.01
37	CELLULOSE 2	3.24	226.84	255.05	12.44	Cu 8	38.542	38.526	0.016	0.04
38	GLASSFIBER O	0.505	35.35	35.37	0.06	Cu 10	38.506	38.508	-0.002	-0.01
39	CELLULOSE 527G	3.12	218.33	267.12	22.35	Cu 9	38.564	38.562	0.002	0.01
40	STERILE COTTON	1.35	94.54	95.89	1.43	Fe 27	25.983	25.984	-0.001	0.00
41	NONE	---	---	---	---	Cu PIPE 41	55.970	55.950	0.020	0.04
42	CELLULOSE 2	3.24	226.84	558.65	146.27	Cu PIPE 42	57.950	57.885	0.065	0.11
43	CELLULOSE 527G	3.12	218.33	636.00	191.30	Cu PIPE 43	59.490	59.315	0.175	0.29
44	STERILE COTTON	1.31	91.62	164.08	79.09	Cu PIPE 44	58.440	58.431	0.009	0.02
45	GLASSFIBER T	0.558	39.08	40.06	2.51	Cu PIPE 45	58.350	58.325	0.025	0.04
46	NONE	---	---	---	---	Cu PIPE 46	59.430	59.399	0.031	0.05
47	CELLULOSE 2	3.24	226.84	335.57	47.93	Cu PIPE 47	58.010	57.997	0.013	0.02
48	CELLULOSE 527G	3.12	218.33	479.23	119.50	Cu PIPE 48	60.580	60.529	0.051	0.08
49	GLASSFIBER O	0.577	40.38	44.48	10.15	Cu PIPE 49	57.740	57.697	0.043	0.07
50	GLASSFIBER T	0.434	30.34	30.49	0.49	Cu PIPE 50	57.280	57.246	0.034	0.06

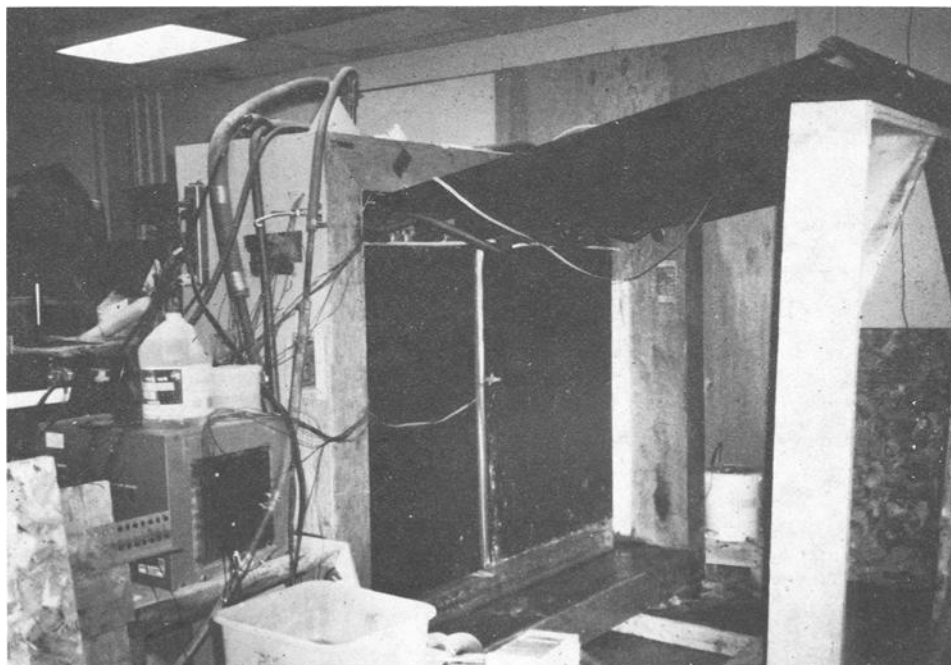


FIG. 2—Environmental chamber with one of the heat-exchanger plates lifted.

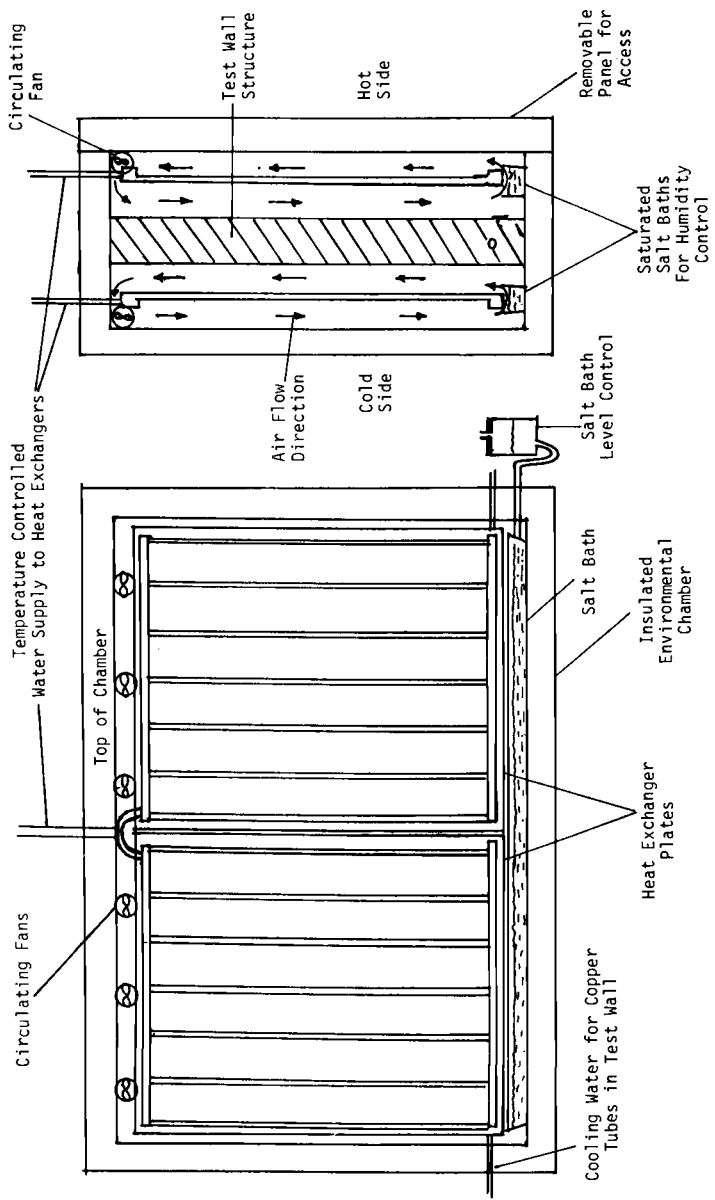


FIG. 3—Schematic of environmental chamber.

Conditioning Procedure

Periodically, the output from the temperature sensors and the humidity detectors were scanned to verify the performance of the temperature and humidity control equipment. The outputs of the ten corrosimeters were monitored at the same frequency. The environmental conditions for the duration of the exposure are shown graphically in Figs. 4 and 5. The hot side averaged 21.6°C (70.8°F) and 44.3% RH, while the cold side averaged 3.3°C (38.0°F) and 95.4% RH.

The conditioning equipment was maintained for 190 days. During this time, there was one 6-h period when one of the refrigerated circulators required maintenance and was off-line.

The refrigerated circulator attached to the copper pipes in Cells 41 to 50 was operated daily for 8 h. The temperature of the coolant in this loop was 10°C (50°F).

The likelihood of condensation under the conditions of the test was evaluated using the estimated temperature and vapor pressure profiles obtained by the method described in the *ASHRAE Handbook* [10]. This approximate calculation placed the condensation plane inside the wall cavity for both types of outer sheathing, being 1.4 cm and 0.8 cm from the inside surface of the plywood and foam board, respectively. Assuming condensation actually occurred at the inside surface of the outer sheathing, the vapor pressure profile was recalculated and a moisture accumulation rate estimated. Moisture accumulation was found to be approximately twice as high with the plywood as with the foam sheathing.

Test Panel Disassembly

Upon completion of the 190-day conditioning exposure period, the test panel was opened and the metal coupons, copper pipes, and corrosimeters were removed from the cells. The insulation materials were carefully removed from each of the cells and weighed to determine their moisture gain during the test. These results are presented in Table 2. The weights of the cou-

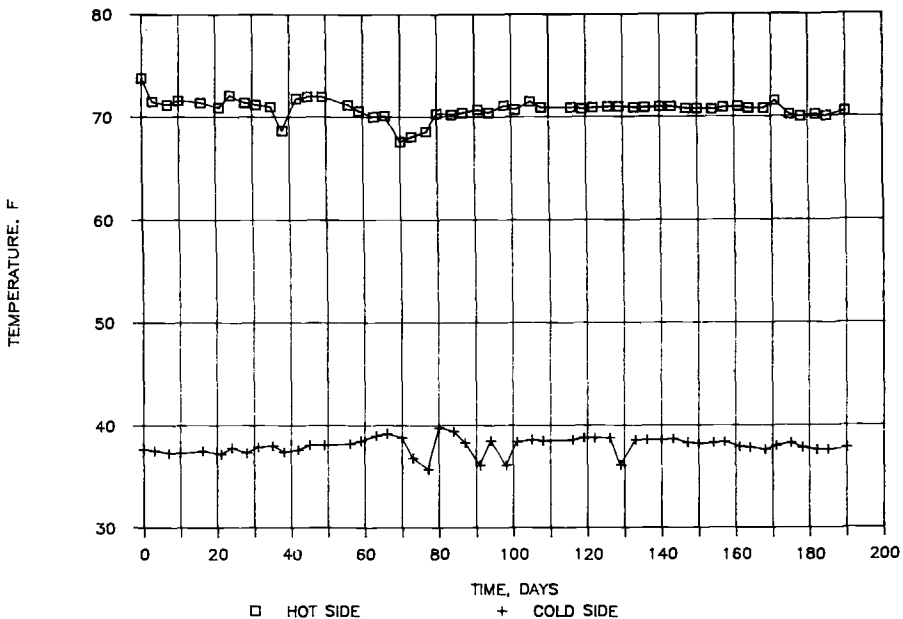


FIG. 4—Environmental chamber temperature levels.

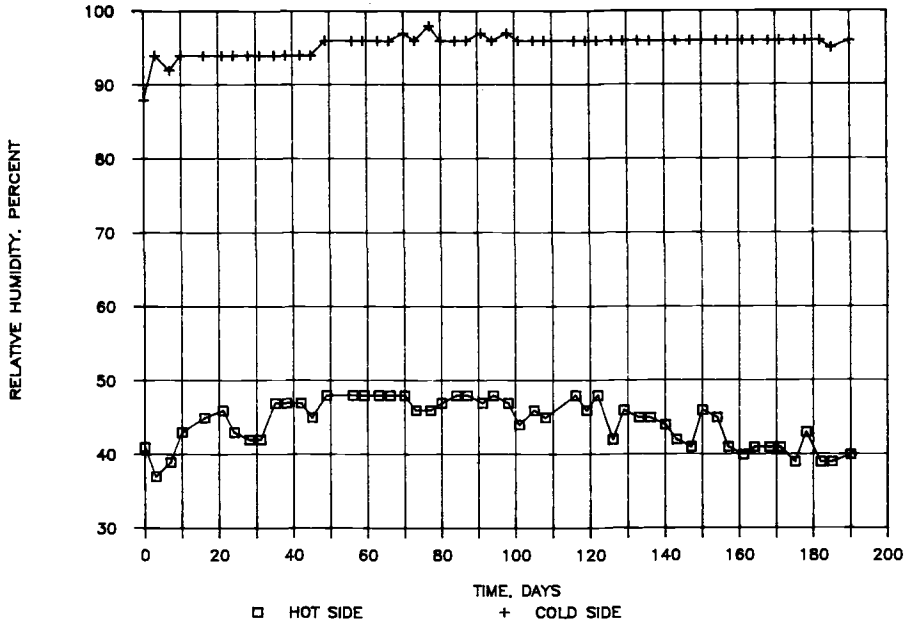


FIG. 5—Environmental chamber relative humidity levels.

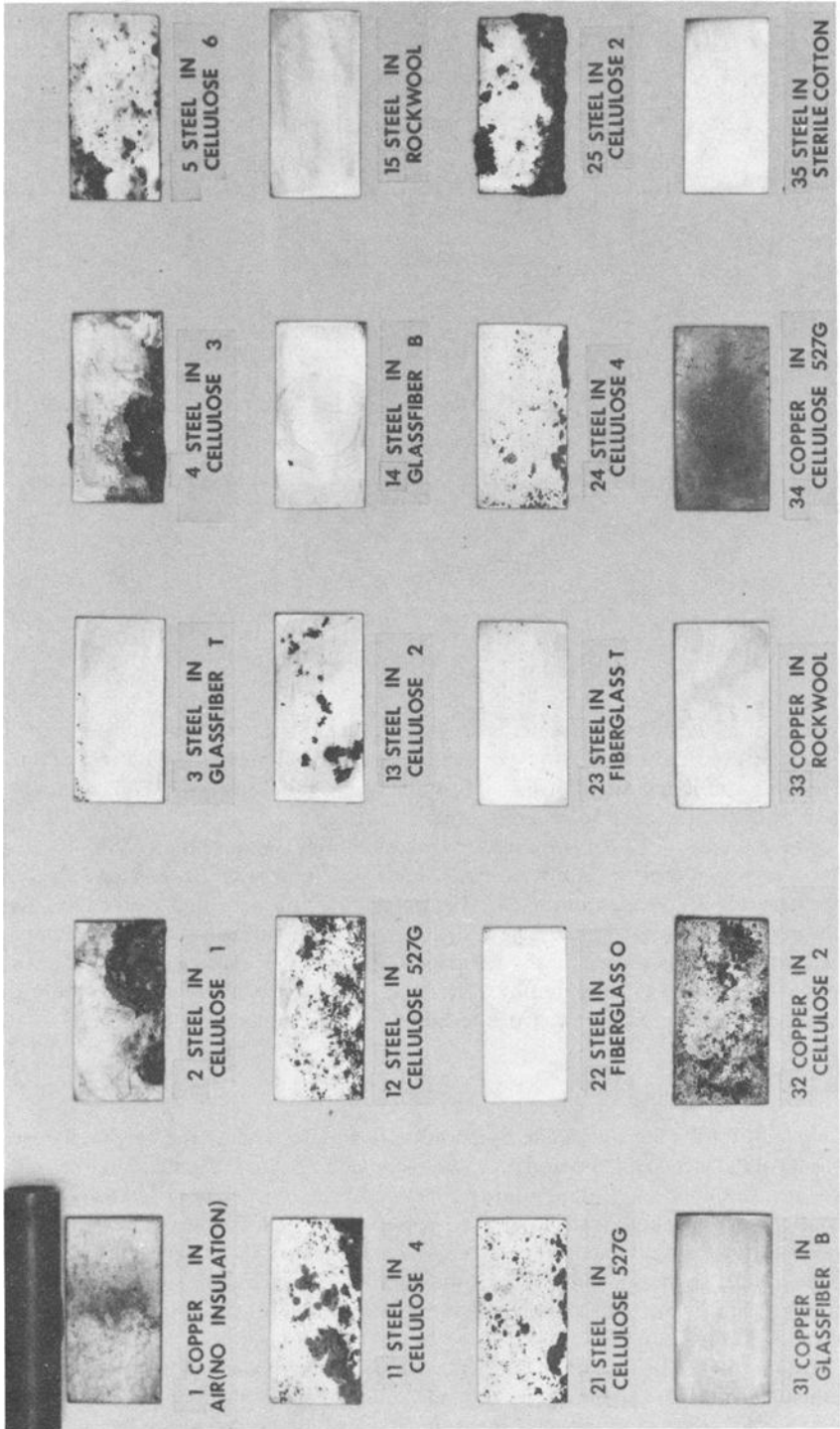
pons and pipes are shown before testing and after post-exposure cleaning also in Table 2. The cleaning procedure to remove corrosion products followed ASTM Practice for Preparing, Cleaning and Evaluating Corrosion Test Specimens (G 1), using Clarke's solution for the steel and hydrochloric/sulfuric acid mixture for the copper.

Weight losses were not converted to corrosion rates, because that would have assumed uniform corrosion over the entire specimen surface. Visual observation showed that this was not the case for the corroded specimens. The weight loss data were able to give a relative measure of the severity of attack if one treated them with caution and considered them along with visual observations. In addition, for those coupons and pipes that showed observable pitting, the maximum pit depth was measured by differential focussing at high magnification with an optical metallograph. The accuracy of this technique was estimated at $\pm 2 \mu\text{m}$.

Results and Discussion

Results for the moisture gains of the insulation materials and the weight changes due to corrosion of the metal coupons and pipes are recorded in Table 2. Figures 6 to 9 are photographs of the metal coupons and pipes after completion of the test but prior to cleaning and weighing. The photographs are arranged to show both faces of each coupon (i.e., that toward the high-temperature side and that toward the cold side) for each of the two types of outer sheathing. The copper pipes are only included in one photograph from each outer sheathing pair, since orientation was not important. The maximum pit depth data for those samples showing pitting are given in Table 3.

Due to the limited number of cells available, it was not possible to have a complete set of matching metal/insulation pairs located behind the two sheathing types and this, unfortunately, reduced the number of direct comparisons based on sheathing permeability. However, the following observations can be made from the photographs and data.



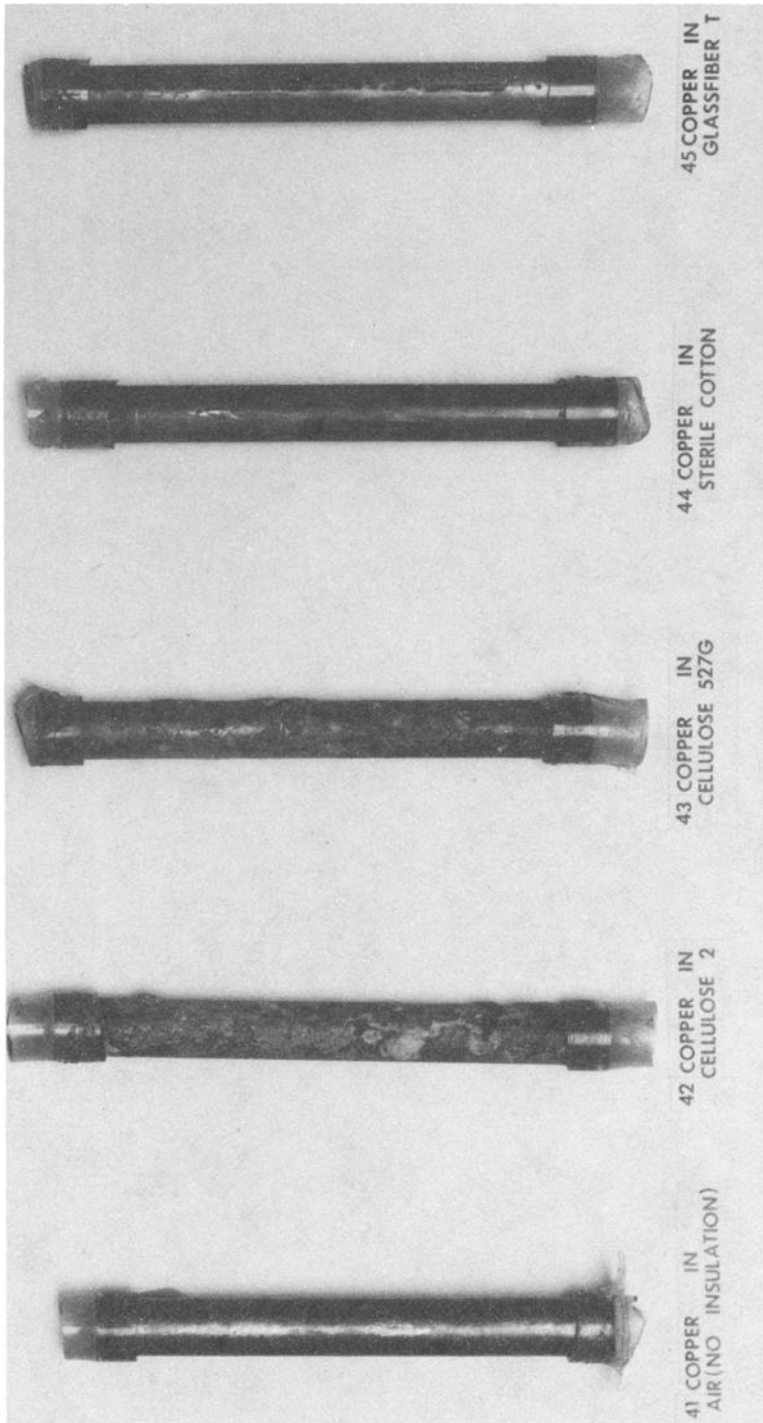


FIG. 6—Metal specimens after six months' exposure in cells sheathed with plywood (high permeability), showing faces of coupons toward warm side of wall.

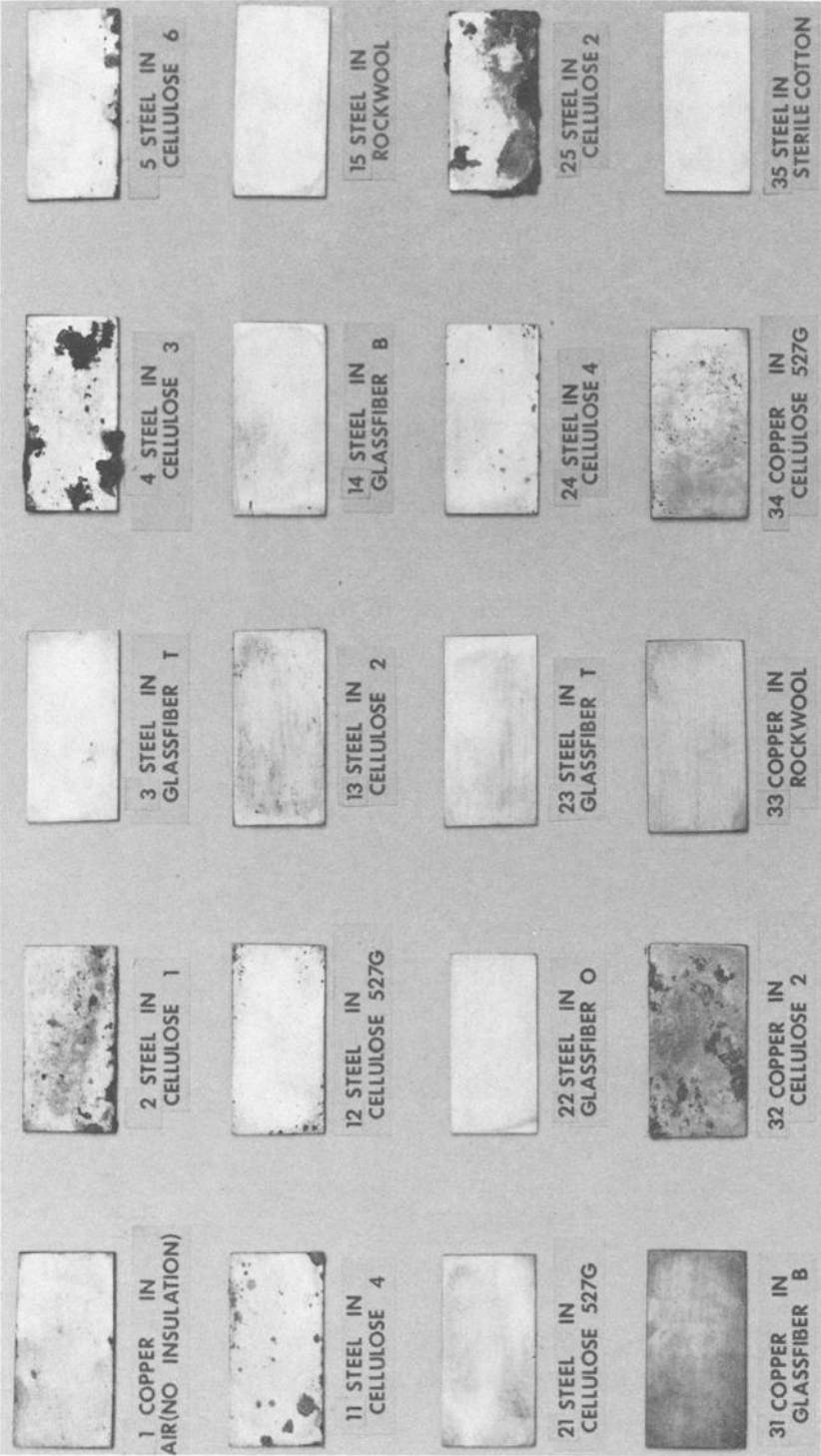


FIG. 7—As Fig. 6, except showing coupon faces toward the cold side of wall.

Coupon Corrosion

In no case was corrosion observed to be uniform over the entire coupon surface. Even those coupons with the most corrosion showed attack in patches or localized pitting. On coupons where corrosion was observed, it was found, in general, that more attack occurred on the faces toward the high temperature side of the wall. This was true for both types of sheathing. This result is probably due to the direction of water vapor transport being from the hot to the cold side.

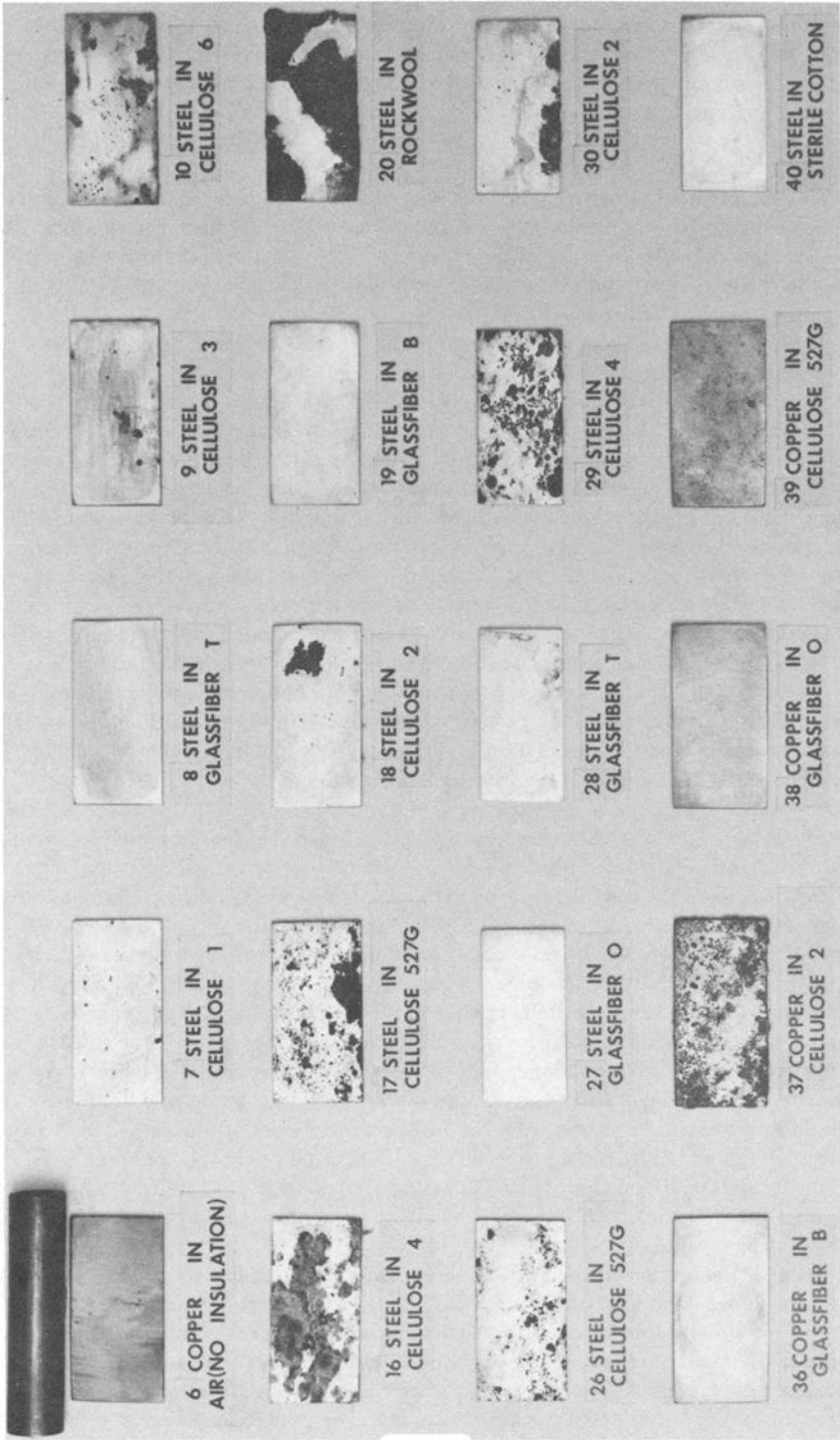
No Insulation—Copper coupons that were exposed in cells with no insulation were not corroded, indicating that condensation did not occur in the absence of insulation. This is to be expected as the absence of insulation would result in a less severe drop in saturation pressure within the wall cavity than if insulation were present and less probability that the dew point would be reached within the wall.

Sterile Cotton—Steel coupons exposed in the cells containing the sterile cotton control material were not corroded. This is probably due to the low moisture gains in these cells, 4% when there was plywood sheathing and 1% when the sheathing was foam.

Glass Fiber and Rockwool—No corrosion occurred on any of the steel and copper coupons embedded in the glass fiber and rockwool insulation samples for both types of outer sheathing. One exception, a steel coupon (Cell 20) in rockwool, had corrosion on its high temperature facing side but no corrosion on its other face. The weight loss for this coupon of 0.56% was the largest observed of any in this experiment. This cell was in the foam sheathed half of the wall. The equivalent coupon in the plywood half of the wall was not corroded. The copper coupon in rockwool also showed no corrosion. There does not appear to be an obvious explanation as there was no weight gain of the insulation due to moisture pickup for any of the three cells containing rockwool. In fact, each experienced a slight weight loss during the test. It may be that the rockwool in Cell 20 had some local contamination. We therefore consider this result anomalous; however, it does illustrate that product contamination could easily influence corrosiveness. The lack of corrosion for coupons in the glass fiber and rockwool insulations appears to be due to the very low moisture gains of these materials during the test, the maximum being 6% for Glass Fiber B in the plywood sheathed part of the wall. These results are also consistent with our previous laboratory corrosiveness testing [3–5] in which the glass fiber and rockwool insulation samples consistently proved of low corrosiveness relative to a distilled water control.

Cellulose—All the coupons embedded in cellulosic insulation displayed some corrosion; however, in most cases it was minor surface staining with no significant loss of metal. The weight gains due to moisture for the cellulosic insulation samples was generally very much greater than for the glass fiber and rockwool, with gains from 4 to 100%. With one exception (Cell 10), moisture gains were substantially greater in the cells with the plywood sheathing which had a higher permeability than the foam sheathing. This correlates with the previously discussed estimates of moisture accumulation. Many of the coupons were corroded more where the moisture content was higher, but there were exceptions, notably the coupons in Celluloses 4 and 527G. In the former case, the coupons from the foam sheathed part of the wall (Cells 16 and 29) were corroded more than from the plywood side (Cells 11 and 24) in spite of lower moisture contents in the insulation. The coupons in 527G were corroded about the same in both halves of the wall (Cells 12, 16, 31, 26), although again moisture contents were much higher in the cells on the plywood side.

While in many cases the weight loss data correlate with visual observations of corrosion, there are exceptions. Coupons from Cells 36, 29 and 31 had large weight losses compared to those typically found for the other coupons. These results did not correlate to the visual evidence. It is possible that error may have been introduced as a result of the cleaning procedure or from the weighing process itself. The before-and-after weighings were done many months apart and the weight losses involved were typically very small. The probability of error is therefore high and



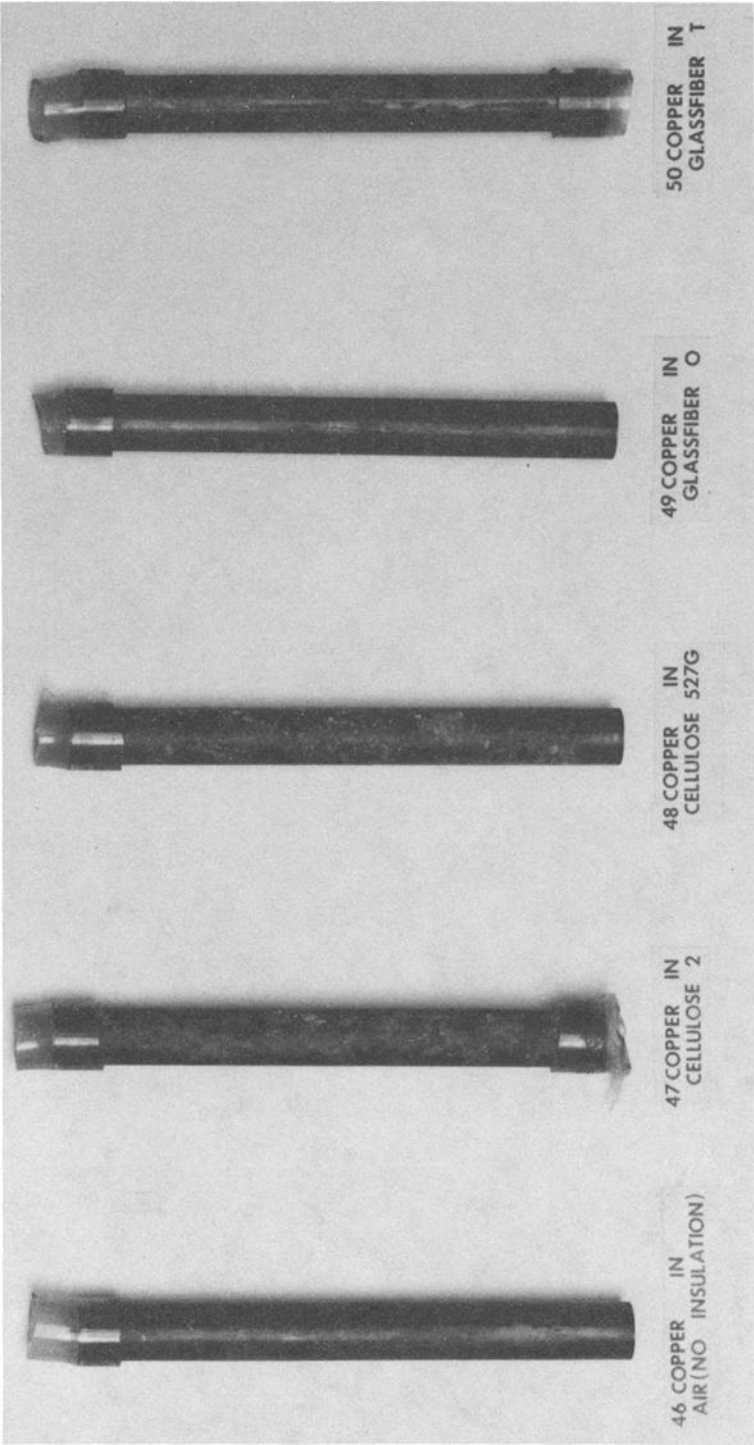


FIG. 8—Metal specimens after six months' exposure in cells sheathed with polyisocyanurate foam (low permeability). Faces of coupons toward the warm side of wall.

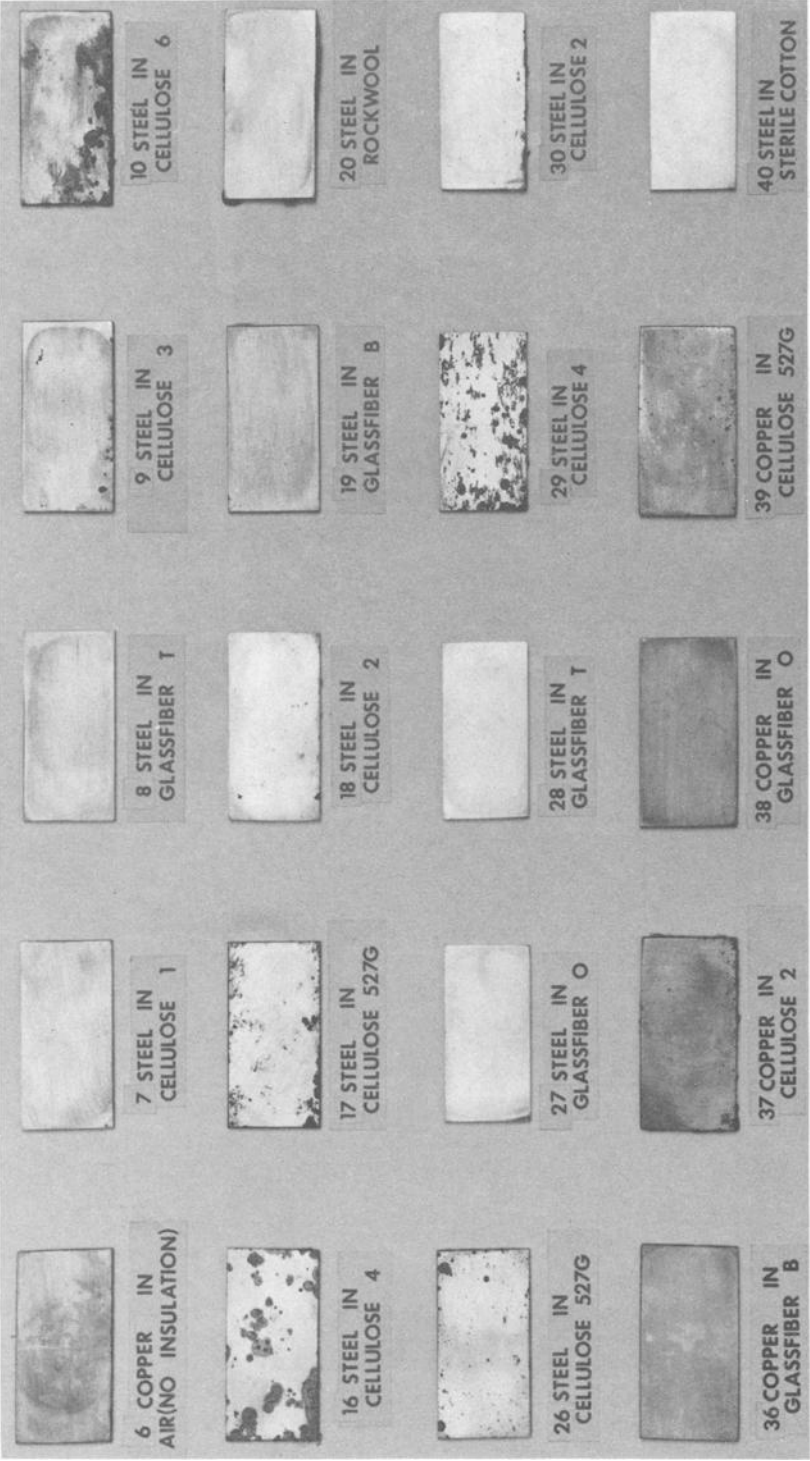


FIG. 9—As Fig. 8, except showing coupon faces toward the cold side of wall.

TABLE 3—*Maximum pit depth for metal specimens that exhibited pitting corrosion.^a*

Cell	Metal	Insulation	Max. Pit Depth, μm
2 HP	Fe coupon	Cellulose 1	104
4 HP	Fe coupon	Cellulose 3	580
5 HP	Fe coupon	Cellulose 6	96
13 HP	Fe coupon	Cellulose 2	648
16 LP	Fe coupon	Cellulose 4	54
18 LP	Fe coupon	Cellulose 2	196
25 HP	Fe coupon	Cellulose 2	616
32 HP	Cu coupon	Cellulose 2	86
37 LP	Cu pipe	Cellulose 2	36
42 HP	Cu pipe (cooled)	Cellulose 2	94
43 HP	Cu pipe (cooled)	Cellulose 527G	40

^aHP = high permeability plywood sheathing.

LP = low permeability foam sheathing.

For comparison a pit penetration of 150 μm in six months (the test period) would extrapolate to penetration of 0.159 cm ($1/16$ in.) in approximately five years assuming a constant rate.

the weight loss data should be treated with appropriate caution. We are also concerned about the reliability of the ASTM G 1 cleaning procedure, which we plan to investigate further.

For Celluloses 2, 4, and 527G it was possible to examine the reproducibility of corrosion for cells that had nominally the same conditions. Samples of Cellulose 2 which were located in Cells 18 and 30 in the foam-sheathed part of the wall give similar visual and weight loss results. The samples in Cells 13 and 25 on the plywood-sheathed side had different results. The coupons from Cell 25 appeared to be much more corroded and had a larger weight loss. There was also a large difference in moisture gain. The insulation in Cell 13 gained 51% while that in Cell 25 gained 100%. No obvious reason for these results is apparent. Possibly the chemical loading was greater for the sample of the cellulose insulation in Cell 25. Moisture gain has previously been shown to be a function of the type of additive and its concentration in the insulation [9].

The samples in Cellulose 4 located in Cells 11, 16, 25 and 29 exhibited reasonably good reproducibility when comparing visual evidence of corrosion, weight loss (except for an anomalously high result for Cell 29) and moisture gain. Similarly for Cellulose 527G (Cells 12, 17, 21, 26), the corrosion was about the same in each cell as was weight loss even though the moisture gain in Cell 21 was twice that in Cell 17. Apart from the exception (Cell 29) mentioned, reproducibility was reasonable between similar cells in the wall.

Although most of the corrosion in the cellulose insulation was limited to surface staining, samples were pitted. The maximum pit depths shown in Table 3 show that the pitting was quite deep in some cases. It should be noted, however, that pit distribution on the sample surfaces was limited. Most of the pitting was in the plywood sheathed half of the wall. It can be seen that Celluloses 1, 2, 3, 4 and 6 all caused pitting of the steel, the most being in Cellulose 3 and in particular in Cellulose 2. Cellulose 527G did not cause pitting. These results are surprising in view of our previous laboratory test results with these materials [3]. In those tests Cellulose 2 which contained borax and boric acid consistently showed the least corrosiveness of the Cellulose samples, with minor pitting tendency, and Cellulose 527G containing ammonium sulfate the most producing general corrosion rather than pitting. On completion of the test, samples of Cellulose 2 that had caused severe pitting were re-examined for pitting tendency using a voltammetric test [5] in the insulation leachant. This showed a pitting tendency that had not been observed in the earlier experiments and suggested that the corrosiveness of the insulation may have changed with time and/or exposure to high moisture levels. Alternatively a sample con-

taining less borax may have been used in the test, suggesting poor additive distribution in the material supplied. One may speculate that chemical additives in the laboratory tests dissolve and the solution uniformly distributes across the metal surface allowing inhibiting chemicals to work effectively. In the test wall, hygroscopic particles of additives may have absorbed moisture and the resulting droplets in contact with the metal could form isolated localized cells. In these cells the outer part of the droplet, with more oxygen access, would become cathodic to the inner part (as in atmospheric corrosion by water droplets), resulting in a localized corrosion. If the borax, for example, which normally provides a corrosion-inhibiting effect for cellulose, was not sufficiently well distributed to dissolve in all moisture droplets, it could not provide its effective inhibiting role typically obtained in the more uniform coverage of the laboratory tests done with leachants. Settling or lack of sufficient milling during manufacture could produce this non-uniform distribution. However, this explanation does not explain why the ammonium sulfate in Cellulose 527G did not cause pitting. Corrosion of copper in Cellulose 527G was barely visible and was reflected in the low weight losses. The moisture gain in the 527G insulation was 41% with the plywood and 22% with the foam sheathings. This was approximately in the middle of the range for the various cellulose-containing cells and does not appear to have been a critical variable in the amount of corrosion given that a minimum moisture level was present.

Copper coupons in Cellulose 2 showed significant localized corrosion, the only pitting of copper coupons being in Cells 32 and 37. On the high-temperature sides of the coupons the corrosion was about the same. On the low-temperature side there was no corrosion in Cell 37, but there was a reasonable amount in Cell 32 which had the plywood sheathing. The moisture pickup in Cell 32 was 132%, which was the highest recorded, but it was only 12% in Cell 37. Therefore variation in moisture content does not appear to have had a significant influence on the corrosion rate of copper coupons assuming that a minimum threshold was attained to initiate corrosion. That threshold appears to be equal to or less than the minimum 12% pickup found in these cells. For the steel coupons the threshold appears to have been as low as 4% (Cellulose 2, Cell 18) and 6% (Cellulose 4, Cell 16) to cause corrosion in certain of the cellulose insulation. There was apparently not enough moisture absorbed by the glass fiber and rockwool insulation to reach the threshold. The cellulosic insulation apparently absorbed enough moisture to cause corrosion. The differences in behavior is then explained by the differing efficacies of chemicals in the cellulose in inhibiting or aggravating the corrosion that would have occurred solely due to the significant moisture pickup of this type of material. From the consideration of the vapor pressure and saturation pressure profiles previously discussed, condensation within the wall cavity was a strong possibility, if not in the insulation, than on the inside sheathing surface.

Copper Pipe Corrosion

Corrosion did not occur on the water-cooled copper pipes in cells without insulation, or on cells containing glass fiber types O and T or cells with sterile cotton control. Insufficient material and limited cell locations precluded embedding the pipes in rockwool and Glass Fiber B samples. The moisture gains were quite low for the glass fibers (2.5% and 1% for Glass Fiber T, 10% for Glass Fiber O). The sterile cotton increased in weight by 79% without causing corrosion.

Copper pipes embedded in Cellulose 2 and 527G showed significant visual evidence of corrosion. Corrosion was more pronounced in the cells that had the plywood sheathing. Moisture gain in the four cellulose-containing cells was high, the larger increases being in cells that had the plywood sheathing. The gain for Cellulose 527G was higher, being 192% in Cell 43 and 120% in Cell 48, than for Cellulose 2, which was 146% in Cell 42 and 48% in Cell 47. The two figures for each insulation are for the two types of sheathing. The weight loss data for the pipes does not match well with the visual evidence. The pipes from Cells 42 and 43 which appeared the most corroded had the highest weight losses. However, based on weight loss it would not

have been possible to differentiate between the other pipes which had losses between 0.02 and 0.08%. Yet the pipes from Cells 47 and 48 had evidence of corrosion while the others did not. It would again appear that the weight loss data are questionable for the reasons previously cited, and it is also unknown how much corrosion occurred inside the pipe. The corrosion on the pipe in Cellulose 2 (Cell 42) appeared more extensive than on the copper coupon in the same insulation (Cell 32); however, they have similar maximum pit depths. These cells had similar moisture gains (146% and 132%, respectively). Pit depth for Cellulose 527G (Cell 43) was less than half that for the Cellulose 2 (Cell 42), a result again surprising given the laboratory test results discussed above.

Electrical Resistance Probes

The outputs of the electrical resistance probes, although showing some fluctuations, were relatively unchanged during the test period. These results indicated little corrosion occurred (the slope of the output versus time is proportional to corrosion rate). This was confirmed on examination of the probes following the test. One reason for the results, given that some of the cellulose samples had produced corrosion of coupons, is that the sensing surfaces of the probes had faced the cold side of the wall. It had not been predicted before the test that facing the hot side would have been a more severe corrosion site.

Conclusions

1. Moisture absorption appears to be the primary, but not only, factor in causing corrosion by insulating materials. Sterile cotton which exhibited a high moisture absorption in contact with a cooled copper pipe did not produce corrosion. It therefore appears that other factors, most probably the activity of chemicals from the insulation, are required for corrosion, even if their role is just to increase the conductivity of the solution. They may also contribute aggressive species.

2. No corrosion occurred in the absence of insulation even on the cooled copper pipes.

3. No corrosion occurred on steel coupons, copper coupons or cooled copper pipes embedded in glass fiber or rockwool (except for one anomalous specimen) insulations in this simulation. This appears to be due to the low moisture absorption by these materials.

4. All the cellulosic insulation materials produced corrosion of steel and copper. For many cases this corrosion was very minor, being in patches and resulting only in surface staining. However, in some materials a few deep pits were produced. In the worst cases, if they propagated at the same rate as in this test, they would result in penetration of a 0.159 cm ($1/16$ in.) thickness in as little as 18 months (steel coupons in Cellulose 2). It is not known, however, if this penetration rate would be maintained in a large exposure.

5. Cellulosic insulations, in particular Cellulose 2, that had relatively low corrosiveness in previous laboratory testing produced significant pitting in the test wall. It is postulated that this is due to formation of localized cells of concentrated additive solutions that promoted local corrosion. This occurred without the mediating effect of borax inhibitor additive that was kept separated from the aggressive additive due to lack of saturation conditions. In the laboratory testing, use of saturated insulation or leachant allowed the inhibitor to be effective. Additionally it is possible that changes in corrosiveness occur with time and/or moist air exposure due to changes in the chemical additives.

6. Corrosion was generally more severe on the sides of coupons which faced the warmer side of the test wall and were first in the path of moisture diffusing through the wall.

7. The plywood sheathing material generally resulted in a greater moisture gain in the insulation than the less permeable foam sheathing. This was anticipated from calculated accumulation rates. While the amount of moisture gain did not always correlate with the amount of corrosion in the cellulosic materials, there did appear to be a moisture-gain threshold below

which corrosion was not significant and in this respect sheathing permeability could be an important factor.

Recommendations

1. Clearly it would be desirable to obtain information over a longer period. One must be very cautious in extrapolating the results of the six months' simulation reported here. Corrosion rates vary with time (e.g., as corrosion product films limit additional attack). It would also be desirable to test the effect of diurnal temperature and humidity fluctuations as well as other types of insulation.
2. The results suggest that further study is required on the effects of moisture saturation levels and aging on the corrosiveness of cellulosic insulations and the implications for development of a uniform accelerated laboratory testing procedure for all types of residential thermal insulation materials.
3. Pitting appears to be the primary form of corrosion and this should be reflected in accelerated laboratory test procedures, with an appropriate quantitative measure. Coupon weight loss is not appropriate. Pit depth measurements or the presence and size of a hysteresis loop in potentiodynamic electrochemical analysis are possible indices and are currently being pursued by us.
4. The effect on moisture gain by the insulation due to the absorptivity of the sheathing was not specifically addressed in this study. It may warrant further study.

Acknowledgments

This work was supported under the National Program for Building Thermal Envelope Systems and Materials of the U.S. Department of Energy through Sub-contract 19X-07556C for the Oak Ridge National Laboratory.

References

- [1] Weil, R. and Graviano, A., "Assessment of the Corrosiveness of Cellulosic Insulating Materials," Technical Report ORNL/Sub-7556/1, Oak Ridge National Laboratory, Oak Ridge, Tenn., June 1979.
- [2] Weil, R., Graviano, A., and Sheppard, K., "Corrosion Testing of Urea-Formaldehyde Foam Insulating Materials," Technical Report ORNL/Sub-7556/2, Oak Ridge National Laboratory, Oak Ridge, Tenn., Sept. 1980.
- [3] Sheppard, K. and Weil, R., "Corrosiveness Testing of Thermal-Insulating Materials," Technical Report ORNL/Sub-78-7556/3, Oak Ridge National Laboratory, Oak Ridge, Tenn., Aug. 1984.
- [4] Sheppard, K. and Weil, R., "Aspects of Corrosion Testing of Thermal Insulating Materials," in *Thermal Insulation, Materials and Systems for Energy Conservation in the 80's*, ASTM STP 789, F. A. Govan, D. M. Greason, and J. C. McAllister, Eds., American Society for Testing and Materials, Philadelphia, 1982, pp. 114-132.
- [5] Sheppard, K., Patel, S., Taneja, M., and Weil, R., "Comparison of Several Accelerated Corrosiveness Test Methods for Thermal Insulating Materials," in *Corrosion of Metals under Thermal Insulation*, ASTM STP 880, W. Pollock and J. Barnhart, Eds., American Society for Testing and Materials, Philadelphia, 1985, pp. 220-230.
- [6] Seton, Johnson and Odell, Inc., G. Tsongas and Applied Social Research, Inc., "A Field Study of Moisture Damage in Walls Insulated Without a Vapor Barrier," Technical Report ORNL/Sub-78/977261/1, Oak Ridge National Laboratory, Oak Ridge, Tenn., May 1980.
- [7] "Minnesota Retrofit Insulation In-Situ Program," Technical Report HCP/W 2843-91, Department of Energy, Washington, D.C., 1978.
- [8] Wang, F. S., "Comparative Studies of Vapor Condensation Potentials in Wood-Framed Walls," ASHRAE/DOE Conference on Thermal Performance of the Exterior Envelopes of Buildings, Orlando, Fla., Dec. 1979.
- [9] Anderson, R. W. and Wilkes, P., "Survey of Cellulosic Insulation Materials," Technical Report ERDA 77-23, Energy Research and Development Administration, Washington, D.C., 1977.
- [10] *ASHRAE Handbook: Fundamentals*, American Society of Heating, Refrigeration and Airconditioning Engineers, New York, 1977, Chapter 21.

The Most Needed Building Foundations Research Products

REFERENCE: Christian, J., "The Most Needed Building Foundations Research Products," *Insulation Materials, Testing, and Applications, ASTM STP 1030*, D. L. McElroy and J. F. Kimpflen, Eds., American Society for Testing and Materials, Philadelphia, 1990, pp. 655-662.

ABSTRACT: This paper describes a research program targeted towards the significant potential for energy savings from improved residential building foundations design. A recent study at the University of Minnesota estimates that less than 5% of foundations in the present building stock are optimally insulated. In addition, this study indicates that the potential national savings from upgraded basements, crawl spaces, and slab-on-grade foundation systems in residential and small commercial buildings is about 0.5 quads/year (0.523×10^{18} J/year).

This research program is based upon a research needs assessment developed by the Building Foundations Research Review Panel. This panel was established by the U.S. Department of Energy (DOE) and Oak Ridge National Laboratory to assist in the formulation of DOE foundations research policy and the development of a technology transfer strategy to get this research to the marketplace. Half of the panel members are from private industry.

One of the first tasks the panel addressed was to formulate a prioritized list of building foundation research needs.

Building foundations research needs include: widescale dissemination of existing information on good practices for energy-efficient construction and retrofit, accurate characterization of the thermal properties of soils, validated foundation heat and mass transfer algorithms coupled into whole-building simulation models, an experimental data base from one or more well-characterized test sites, and design tools to effectively transfer the results of research into practice.

KEY WORDS: heat transfer, foundations, research planning, energy savings, foundation insulation, modeling, thermal performance

Introduction

A recently completed assessment of energy savings potential of thermally upgrading building foundations found that 0.5×10^{15} Btu/year (0.523×10^{18} J/year) of energy could be saved by broad application of foundation wall and slab-edge insulation in the United States [1]. The total energy currently being saved by foundation insulation in one year's worth of new housing starts in the U.S. (1.7×10^6) is estimated at 9.6×10^{12} Btu/year (0.01×10^{18} J/year) [2]. The total potential energy savings from the use of cost-effective insulation in one year's worth of new housing starts is more than double the current realized savings, 23×10^{12} Btu/year (0.024×10^{18} J/year) [2]. These estimates are based on the use of optimized levels of readily available insulation. If less expensive insulation systems were installed, the cost-effective energy savings potential could be even greater. What research could lead to the attainment of this savings? The Department of Energy (DOE) and the Oak Ridge National Laboratory enlisted a group of about 30 individuals with strong interests in building foundations to form a Building Foundations

¹Energy Division, Oak Ridge National Laboratory, Oak Ridge, TN 37831.

Research Review Panel and address this question. About half of the members are from private industry. The long term objective of this Panel is to help formulate and guide building foundations research which will help fulfill DOE's mission of enhanced energy efficiency in the building sector.

A secondary objective is to accelerate technology transfer. The first task the panel addressed was to formulate a prioritized list of building foundation research needs. The research needs consist of: techniques for accurate soil characterization to select inputs for calculating foundation heat loss, a validated foundation heat and mass transfer algorithm coupled with a whole-building simulation model, an experimental data base from one or more well-characterized test sites, and design tools.

Scope

The research products are primarily applicable to new residential construction with focus on masonry foundations. This construction includes slab-on-grade, crawl space, and basement systems. Other systems considered include retrofit applications, pressure-treated wood systems, and small commercial buildings.

Research Needs

Over the course of one year the panel met three times: first to identify research needs to be addressed by a cooperative industry/government national program; secondly to describe research projects which could fulfill each of the broadly defined research needs; and thirdly to prioritize the research areas as to their importance towards improving the energy efficiency of building foundations.

At the first meeting, the panel generated a list of 21 broadly defined, significant research areas. This list is shown in Table 1. To allow systematic analyses of these issues, specific research projects were identified for each issue on the list, which included the objectives, significance, technical approach, and anticipated products. Panel members were then to provide an "importance ranking" for each issue based on titles only. The information on the issues was assembled, and the first ranking survey was conducted by mail ballot in May 1985. Detailed information on research issues identified by the panel is provided in the ORNL Report, "Building Foundations Research Agenda" [3]. The issues in Table 1 are ordered according to their importance as determined by a second panel vote, taken after the full research project descriptions were assembled for each. Numbers in parentheses in Table 1 are the averages of all votes. Panel members were asked to assign a number between 1 and 5, with 5 being "most important." The first ranking was based on broad titles only, without the benefit of detailed research descriptions. Average values and rankings compiled after the first vote are shown in Table 1 under the column titled "Old Ranking." After the first draft of the Building Foundations Research Agenda was prepared, complete with a clear statement of objectives that included the whole foundation system performance and initial composite ranking by about 10 panel members, a second vote was taken in January 1986. The values in the column titled "New Ranking" show the average numerical value of 15 panel members after the second vote.

Foundations handbooks took an even stronger first place, and the need for well-characterized test site data and development of energy-efficient foundation systems that reduce the risk of high radon infiltration moved up in the ranking. A brief description of each of these research needs is given below:

1. *Foundations Handbooks*—Instructive handbooks for builders and designers need to be prepared. While emphasizing energy-efficient practices, these handbooks should also address impacts of other foundation performance factors such as moisture, structural integrity, and indoor air quality. Special attention should be given to optimization and trade-off issues.

TABLE 1—*Building Foundations Research Review Panel's importance ranking of foundations research needs.*

Research Area	May 1985 (Old Ranking) ^a	January 1986 (New Ranking) ^a
Foundations Handbooks	1 (4.5)	1 (4.54)
Simplified Tools	2 (4.2)	2 (4.04)
Benchmark Research Models	4 (4.0)	3 (3.95)
Well-Characterized Test Sites	9 (3.8)	4 (3.95)
Integration of Earth Contact Algorithms into Whole Building Models	3 (4.2)	5 (3.91)
Indoor Air Quality and Radon Mitigation	14 (3.2)	6 (3.88)
Shallow Insulated Foundations	^b	7 (3.88)
Warm Climate Efficient Foundations	7 (3.9)	8 (3.5)
Foundation Thermal Mass and Energy Storage	10 (3.8)	9 (3.5)
Soil Characterization	13 (3.5)	10 (3.38)
Insulation Constraints	11 (3.7)	11 (3.38)
Moisture, Mold and Mildew in Foundations	16 (3.1)	12 (3.36)
Foundation Material Performance Degradation	12 (3.6)	13 (3.32)
Assessment of Foundation Failures	8 (3.9)	14 (3.29)
Crawl Space Heat and Mass Transfer Analysis	5 (4.0)	15 (3.27)
Foundation Thermal Anomalies	15 (3.2)	16 (3.18)
Soil Measurements	6 (3.9)	17 (3.04)
Performance of Heated Slabs	^b	18 (2.46)
Block Wall Convection	17 (2.6)	19 (2.32)
Mixed-Composition Backfills	18 (2.6)	20 (2.27)
Integrally Insulated Foundation Construction Unit	^c	21 ^c

^aNumbers in parentheses are the averages of the panel members' votes on importance rankings (a number between 1 and 5, with 5 being highest).

^bThis issue was added to the list after the first balloting.

^cThis issue was added to the list after the second balloting.

Guidelines are needed for both new construction and retrofit. The first handbook for designers has been completed and has been available since the summer of 1988 [4].

2. *Simplified Tools*—Simplified tools (e.g., charts, nomographs, or programs for personal computers) that are directly useful to builders and designers need to be developed. These tools should clearly show the energy savings and the economic impact of design decisions. To the greatest extent possible, they should also show the impact of different designs on other performance factors. A systematic procedure was developed to recommend foundation insulation levels for ASHRAE Standard 90.2P, "Energy Efficient Design of New, Low-Rise Residential Buildings" [5].

3. *Benchmark Research Models*—The possibility that a single mathematical model can be general enough, yet not too unwieldy, to handle all energy-related issues for all typical foundations needs to be explored. If such a model were available and were generally acceptable in the buildings community, validation research could be focused and, eventually, this "benchmark" model could provide the simulation data for development of simplified tools.

4. *Well-Characterized Test Sites*—Frequently, laboratory or in-service building field data are not adequate for model validation and problem analysis. Test sites could provide the opportunity to look at specific foundation systems under specific environmental conditions. Individual parameters (e.g., heat transfer, freeze/thaw, moisture migration, or gas infiltration) could be isolated for study.

5. *Integration of Earth Contact Algorithms into Whole Building Models*—Current techniques for inputting foundation performance into whole-building models are not accurate and/

or are difficult to use. Improved equations coupling the earth to the foundation and the foundation to the building are needed, as are more accurate values for soil and foundation parameters. Attention must be given to the coupling of intrinsic three-dimensional foundation equations to typical one-dimensional whole-building models.

6. *Indoor Air Quality Issues in Foundation Systems*—The mechanics of radon entry into buildings through foundations and mitigation techniques needs to be studied. In addition, general characteristics of air quality in foundation systems must be examined more systematically because basements, while increasingly being used as conditioned living space, typically lack good, natural ventilation.

7. *Shallow Foundations for Northern Climates*—Almost every building code in the United States requires the footings to be located below the maximum frost penetration depth. This requirement may not be necessary, provided the foundation wall is properly insulated and drained on the exterior side. Insulation extending out from the foundation wall a distance below grade will allow the footings to remain isolated from the potential frost-heave danger at shallow depths. This concept is commonly used in Scandinavian countries. The major appeal of shallow foundations is significantly lower first cost of housing (estimated as high as \$1300 per house) [6]. Analytical and experimental evidence must be generated to substantiate any proposed changes to the building codes in this country.

8. *Southern Climate (Slab-on-Grade and Crawl Space) Foundation Systems*—A better data base for determining near-surface soil properties based on solar impacts and other environmental driving conditions and for shallow foundations systems in warm climates is needed to validate thermal performance models.

9. *Foundation Thermal Mass and Energy Storage*—Few data are available on the effect of mass in below-grade components on building thermal performance. Adequate mathematical models are not available, and whole-building testing has proved to be very difficult.

10. *Soil Properties Data Base*—The data base on soil properties is inadequate in terms of the data on individual soils, their variability with climate, and the range of soil types considered. Improved instrumentation, systematic data collection, and more thorough analysis are needed to strengthen the soils data base. An indexing system should be developed and validated for correlating soil thermal and physical properties. The properties should be made available as a function of soil type, moisture content, density, and temperature.

11. *Barriers to Foundation Thermal Performance Enhancements*—Studies indicate that energy-efficient foundations are cost effective, and the materials and skills are available. Yet, foundation insulation is not always a routine element in new construction. Barriers, real and perceived, must be identified and addressed in order to realize the energy savings potential of thermally efficient foundation systems for new and existing structures. This issue is partially addressed by compiling the design handbooks described in Issue 1 above.

12. *Moisture, Mold, and Mildew in Foundations*—Key factors for organic growth are temperature distributions and moisture concentrations. Data on long-term, *in-situ* behavior of these parameters are limited. Modeling is difficult because it requires the use of combined heat and mass transfer techniques, which are only now being slowly introduced by building science researchers.

13. *Long-Term Performance Degradation of in-situ Foundation Materials, Particularly Insulations*—Perimeter insulation on foundations is subjected to a range of stresses unlike those in above-grade applications. Long-term water exposure can lead to deteriorating effects such as water absorption dimensional instability, chemical attack, and fungus growth. Laboratory and field testing protocols and studies are needed to analyze these effects and suggest priorities for specific product and construction changes.

14. *Assessment of Foundation Failures*—Failure analysis, if carried out systematically, can be useful in identifying critical foundation issues. There is a need to establish a central recipient for these data and, as data become available, to start searching for correlations between system characteristics and failure mechanisms.

15. *Crawl Space Heat and Mass Transfer Analysis*—The energy and economic benefits of various crawl space insulation systems need to be determined. Mathematical relations that couple the crawl space with conditioned space, with the ground, and with the outside ambient air are needed. Moisture phenomena must also be included.

16. *Foundation Thermal Anomalies*—Thermal anomalies are localized regions of unusually high heat transfer in buildings. They can influence foundation performance by decreasing thermal efficiency and by acting as condensation sites leading to subsequent moisture deterioration. Anomalies need to be systematically identified and analyzed to assess the cost effectiveness of design changes or retrofits.

17. *Moisture, Conductivity, and Heat Flow Measurements in Soils*—Instruments for reliable soil measurements are needed. When available, they could provide data concerning the variation of soil parameters with geographic region and with time. The effects of underground water table levels and water flow below ground are examples of moisture movements which impact foundations heat flow.

18. *Performance of Heated Slabs*—Foundation slabs are occasionally integrated into the heating, ventilating, and air conditioning (HVAC) system by utilizing the concrete constructions as the distribution system and/or active thermal storage. An insulation strategy entirely different from that used on conventional slab-on-grade foundations is required. There are no readily available analytical tools for evaluating the thermal performance of these integrated foundation designs and, therefore, no guidance for optimal insulation.

19. *Heat Transfer in Masonry Block Walls*—Heat transfer in hollow-core masonry block walls involves combined conduction, convection, and radiation mechanisms. High lateral conductivity reduces the usefulness of one-dimensional modeling. Together, these effects create a formidable mathematical problem.

20. *Mixed Composition Backfills*—The flow of heat from a building foundation can be very dependent upon the soil properties of the surrounding backfill soil. Reducing the thermal conductivity and altering the drainage characteristics of the backfill by utilizing a mixed composition has the potential to limit heat loss cost effectively. Mixed-composition backfills can have an additional value of reducing the risk of structural damage caused by expansive clays.

21. *Integrally Insulated Foundation Construction Units*—Foundation insulation levels of 0.88 and 1.76 m² · C/W (R-5 to R-10 h · ft² · °F/Btu) are justifiable throughout most of the United States. Foundation construction units with integral insulation, air barriers, and vapor retarders have cost-saving and performance-enhancing implications. The design of an optimal prefabricated basement-wall construction unit should be pursued with the aid of a detailed, finite-difference model coupled with a whole house model for initial optimization, followed by fabrication and testing of a prototypical system and model validation.

These issues were grouped into the more general categories of experimental, testing, modeling, and analysis. This was the starting point for development of the foundations research agenda described in Ref 3.

Research Products

A list of the research products that should result from the completion of the research activities described in this paper is shown below. The major products will be those involving model development and validation, supported with well-characterized test sites that highlight the model's sensitivity, integration of the detailed foundation algorithm into a whole-building model, and then the production of handbooks for designers and builders to provide convincing evidence to builders that energy-efficient foundations are cost effective.

- Builder's and Designer's Handbooks
 - Effect of foundation mass on building loads

- Construction techniques to minimize anomalies
- How to optimize foundation systems
- Comprehensive Technical Data Base for Future Model-Validation Systems
 - Slabs-on-grade
 - Crawl spaces
 - Basements
 - Earth modified systems
- Soils
 - Measurement techniques
 - Comprehensive data base
 - Soil thermal properties estimation model
- Enhanced Foundation Thermal Performance Research Tools
 - Heat and mass transfer
 - Foundation infiltration
- Building Foundation Optimization Design Tools
 - Hand calculations
 - Personal computer software: compatible, analytical
- High-Efficiency Foundation Systems
 - Radon mitigating
 - Non-CFC-containing materials
 - Optimally insulated
 - Earth modified
 - Reduced material costs
 - Variable-R foundations
 - Variable mass foundations
 - Integrally insulated foundations
- Information to Aid in the Development of ASHRAE and ASTM Standards
- National Building Foundations Systems User Facility

Foundation Insulation in the Future

A host of recent events are likely to impact the way building foundations will be insulated in the future. First, ASHRAE Standard 90.2 will likely become the new residential building energy standard some time in the early 1990s. ASHRAE 90.2P utilized a systematic procedure based on consumer economics that leads to increases in foundation insulation beyond typical practice in many areas of the country [5].

Secondly, the heightened awareness of radon penetration will lead to tighter-waterproofed foundations with better exterior subdrainage. One method of protecting exterior waterproofing is with board insulation. Exterior insulation can also contribute to crack minimization by reducing foundation material expansion and contraction, and it can aid in initial concrete curing by eliminating the need for an interior vapor retarder.

Thirdly, the research findings that document the large heat losses from properly insulated and sealed HVAC ducts in unconditioned basements, coupled with the desire to increase living space, will result in more building owners conditioning the basement [7]. More conditioned basements will lead to more basement wall insulation.

A fourth event which may affect how builders insulate foundation walls is the growing understanding of moisture movement and building damage potential. Research is needed to test the hypotheses that (1) exterior foundation wall insulation reduces the risk of moisture damage compared to interior insulation, and (2) interior insulation can be installed with acceptable risk of moisture damage.

Another significant event which impacts the future use of foundation insulation is the suspension of the use of the termiticides chlordane and heptachlor by the EPA. The increased public

awareness of human health risks and cost of termite treatments could result in more dependence on visual inspection of termite tunnels. If reliable mechanical termite barriers and periodic visual inspection methods are not developed, tested, and demonstrated to the public, some potential exists that a negative impact on foundation insulation positioned on either the inside or the outside may result. Recognition of this issue should lead to foundation system development, which includes both properly installed termite shields and foundation insulation.

Since compiling the building foundation research agenda, the chlorofluorocarbon (CFC) restriction issue has developed rapidly. Potential restrictions on the future availability and increasing price of CFC-11 and CFC-12, which are currently used in the manufacturing of many cellular plastic insulations, should accelerate the initiation of more foundation research activities to minimize the impact of the restrictions on the goal of improving the energy efficiency of building foundations. A very popular and effective way to insulate foundations in on the exterior in contact with the earth, and one of the commonly used insulating products for this application is extruded polystyrene, which is currently blown with mostly CFC-12. Since CFCs could be a major contributor to anticipated future ozone depletion, some restrictions are likely or other insulating products will replace CFC blown foam products. Without an accelerated research effort it is estimated that twelve years would be needed to bring a non-CFC extruded polystyrene to market [8]. The role a federal research program can play in shortening this development time is currently being determined.

Conclusions and Summary

This paper begins to outline the needs and issues for defining a broad research program targeted at accelerating the trend towards more energy-efficient building foundations. There seem to be many factors among designers, builders, and building owners that make them reluctant to insulate foundations. By addressing the interactions of foundation thermal performance, structural integrity, indoor air quality, waterproofing, drainage, and moisture migration, methodologies for optimizing foundation construction will surface.

A series of handbooks has been selected as the technology transfer path for implementing results of this research program. The first handbook has been available since the summer of 1988. The release of the new ASHRAE Standard 90.2, "Energy Efficient Design of New Low-Rise Residential Structures," is expected in the early 1990s. The economic methodology based on cost effectiveness that was used to develop the recommended foundation insulation levels shown in this standard indicate that almost all housing in the United States should have at least some foundation insulation. With less than 5% of the 1985 building stock having such insulation and a potential energy savings of 0.5 quads/year (0.523×10^{18} J/year), it is clear that we have a long way to go and that the results of this research will be most timely.

If CFC-12 is contributing to the deterioration of the ozone layer, then alternatives must be found for insulating foundations as well as currently available extruded polystyrene. An accelerated research effort should be initiated to develop and demonstrate alternatives and/or verify systems using other available insulating materials with equivalent or superior performance compared with insulated basement wall, crawl space wall, and slab-on-grade systems incorporating extruded polystyrene installed on the exterior. The research should employ a set of well-characterized test facilities in which moisture conditions are controllable on both the inside surfaces and in the adjacent soil. The industry needs independent verification of benefits of foundation insulation with foam, mineral wool, EPS, fiberglass, or other products.

Thermal durability and moisture damage potential in well-characterized foundation system applications, including the rim joist, should be measured. These measurements should include condensation, mold, mildew, wood moisture content resulting from different insulation, and vapor retarder placement. All three types of insulated foundation types should be tested: basements, slabs, and crawl spaces. The insulation types which should be tested include: extruded polystyrene with alternative blowing agents, molded expanded polystyrene (MEPS), fiberglass

insulation-drainage board, MEPS drainage board, interior insulation, evacuated panels, and other innovative materials.

Acknowledgments

This research was sponsored by the Office of Buildings and Community Systems, Building Systems Division, U.S. Department of Energy, under Contract DE-AC05-84OR21400 with Martin Marietta Energy Systems, Inc.

References

- [1] Sterling, R., Meixel, G., Shen, L., Labs, K., and Bligh, T., "Assessment of the Energy Savings Potential of Building Foundation Research," ORNL/Sub/84-00240/1, Oak Ridge National Laboratory, Oak Ridge, Tenn., Jan. 1985.
- [2] Christian, J. E., "Impact of CFC Restrictions on U.S. Building Foundation Thermal Performance," ORNL/CON-245, Oak Ridge National Laboratory, Oak Ridge, Tenn., Sept. 1987, Draft.
- [3] Christian, J. E., "Building Foundations Research Agenda," ORNL/CON-222, Oak Ridge National Laboratory, Oak Ridge, Tenn., Dec. 1986.
- [4] Labs, K., Carmody, J., Sterling, R., Shen, L., Huang, Y. J., and Parker, P., "Energy-Efficient Building Foundation Design Handbook," ORNL/Sub/86-72143/1, May 1988.
- [5] Christian, J. E. and Strzepek, W. R., "Procedure for Determining the Optimum Foundation Insulation Levels for New, Low-Rise Residential Buildings," *ASHRAE Transactions*, Vol. 93, Pt. 1, 1987.
- [6] Morris, R., "Insulated Shallow Foundation Technology Workshop," National Association of Home Builders Research Foundation, Rockville, Md., 21 May 1986.
- [7] Jakob, F. E., Jacklin, D. W., Fischer, R. D., Flanigan, L. J., and Cudnik, R. A., "SP43 Evaluation of System Options for Residential Forced-Air Heating," *ASHRAE Transactions*, Vol. 92, Pt. 2, 1986.
- [8] Radian, "Draft Report: Central Technology Overview Report on Emission from Rigid Foam Manufacturing," EPA Contract 68-02-3994, June 1987.

Industrial Applications and Tests

Case Histories of Underground Heat Distribution Systems: 1959–1986

REFERENCE: Govan, F. A. and Bahnfleth, D. R., “Case Histories of Underground Heat Distribution Systems: 1959–1986,” *Insulation Materials, Testing, and Evaluation, ASTM STP 1030*, D. L. McElroy and J. F. Kimpflen, Eds., American Society for Testing and Materials, Philadelphia, 1990, pp. 665–674.

ABSTRACT: Since 1959 the authors have been involved in the design and system evaluation of underground insulated piping systems that distribute chilled water, steam, and high temperature water. As of the date of this paper, 272 various systems have been field inspected by excavation and physical examination, participation as expert witnesses for legal action in failure cases, and evaluation of systems.

In 1959 the failure rate in federal installations of these systems exceeded 50%. Some, such as at an Air Force base in upper New York State, were catastrophic failures. Some, such as at a Naval facility in California, were progressive over a short period of time. As a result, design criteria and prequalification test procedures were prepared that now form the basis of present day federal specifications. In response to these new criteria, manufacturers have developed new systems, modified old systems, and improved installation methods and procedures. Therefore the original design criteria need to be kept up to date as new materials, designs, and installation procedures are developed. This report reflects 27 years of inspection and evaluation of these systems and the maintenance of rigorous design criteria to provide a minimum 20-year system life.

This paper summarizes 272 evaluations of eight major types of systems. It reports the causes of failure and the importance of following clear design criteria. Rigorous enforcement of design criteria has become more important due to the resurgence in interest by municipalities in these systems. Already the authors have seen a partial return to the “low bid” concept *without* clear drawings and specifications to make sure that the finished system will provide a long-term life. It is hoped that the reporting of actual results of system installation will help to maintain the quality of work now prevalent in the United States.

KEY WORDS: underground insulated pipe systems, design criteria, standards enforcement, design installation procedures

The United States Government, through various federal agencies, is the largest purchaser of underground insulated piping systems. Since World War II, many installations have been made to serve various federal facilities. The initial investment was considerable. During the 1950s, system failures became a matter of major concern. Therefore a Federal Construction Council (FCC) task group was formed in 1957 to determine the reasons for the failures and to develop design and installation criteria that would produce more reliable systems. Nicholas M. Deme-troulis was the Corps of Engineers (U.S. Army) Engineering Representative and Francis A. Govan was Project Manager.

The National Academy of Sciences/National Research Council published the findings and recommendations of the FCC task group in 1958 as Technical Report No. 30, “Underground Heat Distribution Systems.” This report was revised and updated three times, most recently in 1975. FCC Technical Report No. 39, “Evaluation of Components for Underground Heat Distri-

¹Executive Vice President and President, respectively, ZBA, Inc., Cincinnati, OH 45202.

bution Systems," which outlined test procedures for prequalification of systems, was issued in 1960 and revised in 1964.

These reports provided the basis for the construction specifications of various federal agencies. In 1964 the first interagency specification based on the work of the FCC was published. This was the Tri-Service Specification, still used with modifications by the Army, Navy, and Air Force. In 1963 FCC Technical Report No. 47, "Field Investigation of Underground Heat Distribution Systems," was issued. This covered 121 field investigations of 15 different types of buried, insulated heat distribution systems. Both prefabricated and field-fabricated systems were covered. The age of these installations ranged from 2 to 46 years.

These specification criteria developed through the efforts of the FCC reversed the failure trend of the early post World War II period. To take advantage of new developments in material technology, however, and to reduce costs where lower temperatures and pressure might be safely handled with materials other than steel, another FCC group was formed to prepare underground heat distribution system design and evaluation criteria based upon current technology and the experience gained through use of the criteria developed previously. The recommendations of the task group may be found in TCC Technical Report No. 66, "Criteria for Underground Heat Distribution Systems," published in 1974.

An FCC Guide Specification, Section 15705, "Underground Heat Distribution Systems (Prefabricated or Pre-engineered Type)," is used by members of the Federal Interagency Group (which has superseded the Tri-Service Committee) that currently consists of the three armed services, the General Services Administration, and the Veterans Administration. The criteria are based on the premise that, sometime during a 20-year service life, water will get into any system. Therefore the system must be designed so that insulation in hot systems will withstand boiling and, after drying, be restored to within 10% of its original insulating condition.

Preliminary Design Considerations

Many factors must be considered when selecting an underground insulating piping system. Among the most important is knowledge of soil conditions along the proposed route with respect to soil type(s), ground water conditions, corrosivity, soil stability, alkalinity, and drainage patterns. All have a major bearing upon what types of systems should be considered for a specific installation.

FCC Technical Report No. 66 goes into considerable detail on soil types, their relation to ground water conditions, and corrosiveness. Four ground water classifications are set forth in the document: Severe, Bad, Moderate, and Mild. Briefly, these classifications are based on the frequency that the water table will or will not be above the bottom of the insulated piping system combined with the length of time that accumulated surface water will remain in the soil around the pipe. Table 1 shows the relationship of these two criteria with the four classifications. The Tri-Service specification allows only drainable and dryable pressure-testable systems to be used

TABLE 1—Ground water classification.^a

Classification	Water Table Above Bottom of Systems	Duration that Surface Accumulation Remains in Soil
Severe	Frequent or occasional	Long
Bad	Occasional or never	Long
Moderate	Never	Short
Mild	Never	Not expected to remain

^aThis table is based on criteria set forth in Ref 7. Additional information regarding soil types encountered with above classifications, precipitation, and irrigation practices may be found therein.

with the Severe classification. Both these systems and the water-spread limiting system are considered suitable for Bad and Moderate classifications, while the Mild classification encompasses many systems.

A soil survey should be made to determine the conditions along the pipeline route. The survey should include the water table level, the percolation characteristics of the soil, and the determination of soil pH since the acidity or the alkalinity of the soil may adversely affect some materials. For example, asbestos-cement may be harmed by soils having a pH less than 5.5.

Soil corrosivity is most commonly determined by the soil resistivity test. This measures the electrical resistance of the soil: the lower the resistance, the higher the corrosivity. Wet soils, organic soils, and soils having a high soluble salt content generally are corrosive.

Ground water level is not so great a concern for drainable and dryable pressure-testable conduits or water-spread limiting conduits as it is with some other types of systems. Some types of soil will retain surface water for an extended period. Also, the trench in which the pipe is installed may disrupt normal drainage patterns and become a catch basin for surface water. Therefore installation of drain tile along the route may be necessary to assure satisfactory performance of insulating envelopes and most types of field-fabricated conduit systems.

The most satisfactory insulation based on a series of National Bureau of Standards boiling tests should be specified for all pipes, valves, and other appurtenances in heat distribution manholes. The insulation was premolded calcium silicate. The insulation should be covered with jacketing to prevent mechanical damage. In steam and hot water systems, manholes should also be vented. Excessive manhole temperatures are a major cause of inadequate inspection and maintenance of underground heat distribution systems.

Drainable and dryable systems should be sloped so that water will drain from the entire length of conduits, concrete trenches, etc. Provisions should be made for water removal from manholes should a major infiltration occur.

Great care must be taken in the design of the entire system. Manholes are made of concrete or prefabricated coated steel. They must be vented and drained. Water removal by pump or ejector is a requirement in almost all systems.

Pipe expansion can be handled with expansion loops, expansion joints, and ball joints. Prefabricated expansion loop assemblies are available for pressure-testable and nonpressure-testable conduit systems. An expansion chamber may be designed into the encasement at corners and loops of insulating concrete installations as a movement absorber. Expansion loops may be used with various types of loose-fill insulation, usually with some limitation on the amount of lateral movement that may be accommodated.

Expansion loops are the preferred method of accommodating expansion. Expansion joints, where used because of space limitations, should be internally and externally guided.

There has been a recent trend towards the use of underdrainage channels in the bed upon which the conduit is set. In view of the damage that standing water can cause, this is a step forward.

Installation

All piping should be installed in accordance with applicable codes and industry standards. The conduit or pipe should be firmly supported along its entire length by virgin earth, compacted sand, or insulating fill so as to minimize the possibility of excessive strain due to ground subsidence and the possibility of washouts that could remove protective fill from around the pipe. Inspect all piping when received to assure quality meets specifications. Check for cracked lining, damaged pipe ends, damaged insulation jackets, and other defects that may occur in manufacture or delivery.

Pipe laid in poured-in-place insulating materials should not rest on anything porous such as bricks, timbers, etc. These provide a moisture path to the pipe, and severe concentration cell corrosion may occur. Additionally, all poured-in-place insulation installations must be installed

to the proper depth, backfilled, and the backfill compacted in accordance with manufacturer's requirements. Care must be taken to avoid contaminating the backfill with stone or other construction debris. In all cases, except for extremely dry soils, poured-in-place insulation systems should be underdrained.

Insulating concrete should be permitted to dry before covering with a waterproof membrane and backfilling. Internally vented and drained systems have been successful in maintaining their service performance.

Any damage to protective coatings incurred during shipping or construction must be repaired in accordance with methods compatible with the original coating. The three major causes of coating damage are improper transportation techniques, use of chain lifts for handling pipe sections, and improper storing at the job site.

All welding should be done in accordance with the ASME B31.1 Code for Pressure Piping. Manufacturer's requirements for joining coupled pipe should be followed to avoid leaks on low pressure lines and damage to high pressure systems.

All lines should be tested for tightness before complete backfilling. All joints and fitting should remain exposed until the test is completed. Pressure should not be put on lines before concrete anchors and thrust blocks have cured sufficiently to withstand the stress. Care should be taken during backfilling to prevent damage to protective coatings, conduits, and vapor sealing membranes.

System Classifications

Many insulated underground piping system concepts are in use. They may be classified in various ways, such as prefabricated, pre-engineered, and field fabricated.

Thermal distribution systems also may be classified by temperature. Three ranges are generally accepted: above 250°F, steam and high temperature hot water; 180 to 250°F, steam and low temperature hot water; and 35 to 180°F, chilled water and dual temperature water ($t_{\text{°C}} = (t_{\text{°F}} - 32)/1.8$). A number of piping materials are in use that are restricted by allowable pressure ratings to applications with the lowest or the two lower temperature ranges.

Systems also can be classified by their construction:

- Pressure-testable conduit systems.
- Nonpressure-testable conduit systems.
- Insulating envelope systems.
- Concrete trench and tunnel systems.

Because moisture in the form of ground water or pipe leakage has been the major cause of insulation and pipe failure (by corrosion), emphasis today for systems above 250°F is on the development and use of systems that are either drainable and dryable or that are capable of confining water spread to a limited section of the conduit.

Pressure-Testable Systems

Pressure-testable systems, sometimes referred to as *air gap systems*, are drainable and dryable when properly installed. They consist of a carrier pipe, pipe insulation, spacers, and an outer casing pipe or conduit. An annular air space between the insulation and casing provides added resistance to heat flow and also provides the means to leak test the conduit (with pressurized air). It also permits the conduit to be drained if the conduit or pipe develops leaks without wetting the insulation.

The outer casing may be of steel, galvanized steel, fiber-glass-reinforced polyester, cement-asbestos pipe, or cast iron. The steel and galvanized steel conduits are generally covered with either a glass-reinforced coal tar enamel having an outer wrap of glass-fiber-reinforced pipeline felt or with a glass-fiber-reinforced epoxy resin. Cast-iron casings are not coated.

Pipe insulation is usually calcium silicate. The choice of calcium silicate as the best preformed insulation was based on an extensive test program conducted by the National Bureau of Standards in 1960–1961. The results are discussed in the Insulating Envelope Systems section of this paper. The systems can be designed to handle fluid temperatures ranging from 200 to 800°F. Premolded mineral wool insert was also available.

The carrier pipes are joined by welding, and the joints are covered with split preformed insulation sections. Steel conduits are joined by welding also. Cast-iron conduits are connected by sleeves (plain end conduits), bolted together (flanged end conduits), or connected with mechanical joint fittings (mechanical joint conduit).

Steel conduit assemblies are available in 20 and 39 ft lengths (1 ft = 0.3048 m). Cast-iron assemblies come in 13 and 18½ ft lengths.

Pressurized monitoring alarm systems are available that maintain the conduit at a pressure above atmospheric—typically, 2 to 5 psig. The unit signals any loss in pressure if a leak develops or if the casing is accidentally ruptured. In the case of pinhole leaks, the pressure source can maintain pressure and prevent ground water from entering the conduit. Either an air compressor or compressed nitrogen gas may be used as the pressure source.

Nonpressure-Testable Systems

Nonpressure-testable systems are available in a variety of material combinations to meet the requirements of many applications. Some conduits are factory fabricated and consist of carrier pipe surrounded insulation that in turn is enclosed in an outer nonmetallic casing. The area between the carrier pipe and outer casing is completely filled with insulation; generally the ends of the insulation are sealed with a watertight enclosure that limits the spread of water if the pipe or outer cover fails.

Some nonpressure-testable conduits are field fabricated. These may be a factory engineered system consisting of components specifically manufactured for underground heat distribution components, or they may be concrete trenches or other nonproprietary designs.

Prefabricated water-limiting conduits can be obtained with a variety of components. Carrier pipes may be made of copper, carbon steel, stainless steel, polyvinyl chloride (PVC), fiber-glass-reinforced polyester (FRP), or epoxy-lined asbestos-cement. Outer casings generally are PVC, FRP, or asbestos-cement. Insulations commonly use include calcium silicate and premolded mineral wool for applications above 250°F, and both plastic foam and preformed cellular glass for applications below 250°F.

Copper, FRP, and epoxy-lined cement carrier pipe are commonly used below 250°F. Copper may be used with fluid temperatures up to 250°F. FRP pipe generally is not used above 225°F, and some carry a maximum rating of 150°F. Asbestos-cement pipe has an allowable operating temperature range of 35 to 210°F. Steel pipe is used exclusively on hot water and steam installations operating above 250°F because of the pressures and temperatures encountered.

The insulation selected for prefabricated insulated conduits depends primarily upon the operating temperature of the pipe. Foamed polyurethane insulation may be used in applications between –50 to 250°F. Polyurethane resists water penetration. Nevertheless, it must be covered with a vapor barrier of some type. Ground water under a sufficient head may rupture the cells. Damage during construction or pipe flexing due to ground settling after installation may cause cracks to develop in the foam. Also, if the pipe is used for chilled water service without a vapor barrier, the difference in vapor pressure resulting from a pipe temperature lower than the ground water temperature may draw moisture to the pipe. The major limitation of foamed polyurethane insulation is temperature, since around 250°F the material softens and loses thermal efficiency.

Composite insulations, consisting of an insulation suitable for higher temperature service next to the pipe, which in turn is covered with a lower temperature rated insulation, are also used. Calcium silicate on premolded mineral wool covers the pipe and in turn is surrounded by

polyurethane or other insulating materials. Pipe systems having this insulation construction are rated for temperature to 450°F and a maximum operating pressure of 500 psig. There is still concern that, in case of a leak, the urethane will collapse due to high temperatures.

Formed cellular glass insulation is also used with prefabricated pipe construction. The insulation itself will withstand temperatures between -450 and 800°F. Prefabricated piping with sufficient insulation thickness to protect the outer jacket is available for this temperature range. Foamed glass has not been widely used by the federal government in applications above 250°F due to its fragility and susceptibility to damage due to boiling action. Experience has shown that sudden temperature differential shocks will fracture the cellular structure and lead to subsequent total failure.

Prefabricated insulated pipe lengths vary with manufacturer, carrier pipe materials, and pipe size. Typical lengths are 20 ft for copper, steel, PVC, and FRP carrier pipe sizes up to 12 in. Asbestos-cement carrier pipe sections typically come in 10 and 13 ft lengths with carrier pipe sizes ranging from 4 to 16 in. One manufacturer offers 55 ft lengths with carrier pipe diameters (steel) up to 36 in.

Field-Fabricated Systems

Field-fabricated pipe conduits are nonpressure testable and may or may not have an air space around the pipe. They may be pre-engineered in that the conduit consists of an assembly specifically designed to house underground insulated pipelines. One type consists of a poured concrete structure formed so that it has a trough for water (either ground water or pipe leakage) to collect and be drained away. Cast-iron pipe supports, rollers, etc., are mounted on the base. Vitrified clay side pieces and half-round covers cemented together complete the conduit. The cemented joints are covered with a waterproof mastic to seal the conduit.

Concrete trenches are also applied. These may be considered mini-tunnels, since they are similar to walk-through tunnel systems. The bottom and sides are formed and poured. The top consists of concrete slabs. After the pipes are installed, insulated, and jacketed in the trench, the top is set in place. Coal tar or other sealing material is used to provide a barrier to ground or surface water entrance at the joints. The top of the trench often is at grade level and serves as a walkway. This facilitates access to the pipe, because the ground does not have to be dug up when checking for leaks, adding a line, replacing a line, etc. It is recommended that the bottom of the trench be set on a vapor barrier and the sides be coated with a mastic material to provide greater resistance to moisture penetration. The success rate of today's concrete trench has improved markedly due to four factors: preformed pipe insulation with a surrounding air space, a built-in drain channel to keep water out of the bottom of the trench, underdrainage, and improved jointing material.

Vitrified clay tile and concrete sewer tile also are sometimes used to construct pipe conduits. These and other field fabricated conduits may serve well where drainage is good and the system is installed above the water level.

Years ago, concrete trenches and field fabricated conduits sometimes were completely filled with insulation. However, examination of these systems after they were in operation revealed that it was not unusual for the insulation to be wet and the pipes corroded. Good practice today is to insulate the pipe and cover the insulation with a moisture barrier. The air space around the pipe permits water to drain from the system, and the heat from the line can dry the insulation if it becomes wet.

Insulating Envelope Systems

Insulating envelope systems are pre-engineered systems designed to surround the pipe with a poured-in-place insulating media, which may be any of the following:

- Insulating concrete.
- Granular hydrocarbon fill (noncuring and heat-curing types are available).
- Treated calcium carbonate fill.
- Insulating granular perlite fill.
- Field-installed polyurethane foam.

Insulating concretes are available with two types of aggregates: vermiculite or expanded polystyrene beads. It is the aggregate that provides the insulating value to the concrete.

A structural concrete base pad is poured to the desired grade. Precast insulating blocks and drain vents are set on a waterproof membrane that covers the structural slab and lines the trench or forms. The pipes rest on top of the insulating blocks, and the insulating concrete is poured over the slab, pipes, and internal drains. The waterproof membrane is wrapped around the top of the concrete and sealed.

If required, cathodic protection can be achieved by the installation of a continuous ribbon zinc anode parallel to the pipes inside of the concrete. Internal electrical sensors can be installed inside the internal drain channels to detect and locate leaks. Additional drainage can be had by installing an external drain tile. In addition to providing thermal insulation, insulating concrete provides continuous support and alignment of the piping and resists heavy loads.

Granular hydrocarbon insulations are installed in an open trench. A bed of the material is placed on the bottom of the trench. The pipe is installed and more insulation is placed around and over the pipe. The material is then compacted to the proper density. The materials resist wetting; however, installation of drain tiles along the pipe path may be required, depending on the natural drainage characteristics of the earth and ground water conditions, to avoid buildup of hydrostatic heads that would penetrate the fill.

Natural and artificial hydrocarbon mineral material do not have to be heat cured. They are suitable for temperatures between 35 to 500°F.

Heat-cured granular insulations are derived from petroleum residuals and by coating materials such as perlite. These are available for various temperature ranges between 150 to 520°F. An asphaltic binder in the fill melts and bonds to the pipe during the curing process. Surrounding the pipe and binder is a sintered zone, and the outer layer of the fill is unaffected by the curing process. Heat-cured systems are rarely used today due to their dismal performance record. Since these materials are used with metal piping systems, cathodic protection should be installed whenever material selection and soil conditions dictate.

Powdered calcium carbonate, which is treated to resist water penetration, is another insulating material. It is rated for temperatures up to 480°F. Side forms in the trench are required. The material is installed around and below the pipe to the proper dimensions, compacted, and covered on the top with a plastic film. The manufacturer states that due to the hydrophobic properties of the material and its high electrical resistivity cathodic protection is not required.

Expanded perlite particles are also used as a buried insulation. Powdered perlite is heated to a high temperature, causing it to pop or burst into granular air-celled particles. These particles are mixed in the field with an asphalt binder. A base pad, consisting of the insulating material and binder, is poured in a formed trench. The pipes are laid on the base, tested as required, then the pad and pipes are primed with a corrosion resisting compound. The installation is then completed by pouring more material over the pipes to the depth of the forms. Operating temperatures range from 15 to 800°F; the material is said to have a high electrical resistivity.

Polyurethane foam may be poured or blown around pipes in the field. The systems are ready to be backfilled within an hour after the foam has been placed around the pipes. Forms are required for the froth-pour type of insulation, and a vapor barrier liner and covering generally are used to seal off ground moisture. The direct spray method does not require side forms. Again, vapor barriers are recommended. They may be used up to 250°F.

TABLE 2—*Condition of insulation in various types of underground insulated piping systems.^a*

System Type	Number Inspected	Wet	Deteriorated
Concrete Trench:	31		
Loose fill (drained or not)	11	11	11
Preformed (not drained)	8	5	5
Preformed (drained)	12	2	0
Clay Tile:	12		
Loose fill	7	7	7
Preformed (drained)	5	2	2
Prefab Steel (Nonpressure Type):	23		
No air space	16	11	7
Air space	7	2	2
Prefab Steel (Pressuretight):	68		
Precriteria (1959)	31	13	9
FCC criteria (to date)	37	4	2
Insulating Concrete:	34		
Envelope	29	26	13
Vented (drained)	5	4	0
Poured-in-Place:	70		
Hydrocarbon (cured)	31	5	21
Hydrocarbon (uncured)	14	4	5
Hydrophobic	25	7	9
Closed Glass Cell	8	3	5
Foamed Plastic:	55		
Foamed-in-place	12	2	10
Preformed in rigid conduit	29	4	9
Preformed in flexible jacket	14	6	7
Total Inspected or Reported (1959-1986)	301	118	124

^aThese data are based on actual excavation and examination, personal letter reports from users, and reported litigation data.

Tunnel and Trench Systems

Buried walk-through tunnels generally are the most expensive way to house underground piping. However, they greatly facilitate piping maintenance, future modifications, and, when properly drained and ventilated, they greatly minimize the development of corrosion on pipe and appurtenances.

Concrete tunnels constructed by forming and pouring are the most expensive. To reduce the cost of tunnels, prefabricated steel and concrete tunnels have been developed. These are complete with pipe racks and hangers. The sections are dropped into the excavation and joined together. The steel is factory coated and cathodic protection can be applied to provide additional protection against corrosion.

Large diameter concrete sewer pipe has also been successfully used to construct tunnels. The joints must be sealed and caulked, and, as with other tunnel systems, provisions for drainage should be made as job conditions require.

System Maintenance

Careful inspection and regular maintenance will reduce the likelihood of premature failure of buried lines. Procedures include:

1. Monitoring of steam pressures or water temperatures at points of send out and use. This will warn of excess heat loss caused by damaged or wet insulation.
2. Periodic patrolling of the line. Burned grass over the route, water or steam coming to the surface, and melted snow indicate problems.
3. Periodic inspection of manholes and vaults. Water in the vault or signs of moisture in insulation or in the ends of conduits are other signs of problems.
4. Maintaining a regular program of checking the performance of cathodic protection systems. This includes taking anode readings, monitoring rectifier installations, and checking all electrical insulating fittings.

Central heating/cooling plants offer many advantages. They are more efficient in the use of resources than individual building heating/cooling plants. They provide a means of alleviating the solid waste disposal problem by disposing of combustible trash. And it is easier to control air pollution at a large central installation than at many small ones.

Underground insulated piping systems are an integral part of the central plant concept. Sometimes they have been the weakest link. With the vast amount of experience to draw from, however, and present technology, buried heating and cooling distribution systems can be in-

TABLE 3—*Causes of failure.*

	Soil Conditions	Casing or Insulation	Workman- ship	Corrosion or Drainage	Design
Concrete Trench:					
Loose fill (drained or not)	6	14	3	6	...
Preformed (not drained)	3	7	...
Preformed (drained)	2
Clay/Concrete Tile:					
Loose fill	3	3	1	8	1
Preformed (drained)	2	1	...
Prefab Steel (Nonpressure):					
No air space	9	19	8	13	7
Air space	1	3	1	2	1
Prefab Steel (Pressure-tight):					
Precriteria	5	18	9	16	9
FCC criteria	1	3	2	3	1
Insulating Concrete:					
Envelope	16	43	17	28	2
Vented (drained)	4	3	1	2	...
Poured-in-Place:					
Hydrocarbon (cured)	16	40	19	30	11
Hydrocarbon (uncured)	3	3	...	6	2
Hydrophobic	8	3	...	9	2
Closed Cell Glass	3	5	2	4	1
Foamed Plastic:					
Foamed-in-place	2	5	...	5	2
Preformed in rigid conduit	3	8	2	8	3
Preformed in flexible conduit	4	11	6	7	4
Total	91	181	71	156	46

stalled that will give reliable, economical service for any application that is not beyond the limitations of the system itself.

Case Histories

The criteria discussed previously have been based on careful study and examination of actual systems and components while they are in service. Since the original survey of users in 1957, the authors have continued their interest in these underground insulated piping systems. Thus, since 1964, when the last major FCC field study was completed, the authors have taken every opportunity to field inspect systems, follow-up on systems designed by the firm, collect data from court cases of failures, visit installations designed by other firms, and obtain information from other firms.

The authors are dedicated to maintaining the high level of performance that has been attained by professional engineers in the United States. We are concerned that technology based on readily available materials and standards, rather than on proper design concepts of selecting the optimum technical and economic systems, will result in a significant failure rate and return underground insulated piping systems to the sad reputation they had before the federal studies and design criteria. The historical and case history portion of this paper should serve as a warning to us to carefully evaluate today's new products.

Tables 2 and 3 describe the types of systems, success or failure rate, and the reasons for failure. Included are systems from 2 to 46 years old.

References 1 to 11 provide further background information.

References

- [1] Irvin, L. V., Jr., "Federal Agency Specification for Underground Heat Distribution Systems," Underground Heat and Chilled Water Distribution Systems, NBS Building Science Series 66, U.S. Department of Commerce, National Bureau of Standards, Washington, D.C., 1975, pp. 73-77.
- [2] "Underground Heat Distribution Systems," FCC Technical Report No. 3OR-64, National Academy of Sciences - National Research Council (Pub. 1186), Washington, D.C., 1964.
- [3] "Field Investigation of Underground Heat Distribution Systems," FCC Technical Report No. 47, National Academy of Sciences - National Research Council (Pub. 1144), Washington, D.C., 1963.
- [4] "Criteria for Underground Heat Distribution Systems," FCC Technical Report No. 66, National Academy of Sciences, Washington, D.C., 1975.
- [5] "ASHRAE Handbook & Product Directory - Systems Volume," American Society of Heating, Refrigerating, and Air-Conditioning Engineers, New York, 1976, Chapter 14, p. 2.
- [6] "Criteria for Underground Heat Distribution Systems," FCC Technical Report No. 66, National Academy of Sciences, Washington D.C., 1975, p. 17.
- [7] "Criteria for Underground Heat Distribution Systems," FCC Technical Report No. 66, National Academy of Sciences, Washington, D.C., 1975, pp. 4-5, 49-51.
- [8] "Field Investigation of Underground Heat Distribution Systems," FCC Technical Report No. 47, National Academy of Sciences, Washington, D.C., 1975, p. 3.
- [9] Govan, F. A., "A Case History of an Underground Piping System Failure," North American District Heating and Cooling Institute, 1986.
- [10] Kasuda, T. et al., "A Method for Measuring Heat Loss from Underground Heat Distribution Systems," in *Thermal Insulation: Materials and Systems*, ASTM STP 922, American Society for Testing and Materials, Philadelphia, 1987, pp. 52-68.
- [11] Govan, F. A. and Demetroulis, N. M., "Design Criteria for Underground Insulated Piping Systems," in *Thermal Insulation: Materials and Systems*, ASTM STP 922, American Society for Testing and Materials, Philadelphia, 1987, pp. 43-51.

Review of ASTM Guide for Removable Insulation Covers (C 1094)

REFERENCE: Hart, G., "Review of ASTM Guide for Removable Insulation Covers (C 1094)," *Insulation Materials, Testing, and Applications, ASTM STP 1030*, D. L. McElroy and J. F. Kimpflen, Eds., American Society for Testing and Materials, Philadelphia, 1990, pp. 675-687.

ABSTRACT: With a need for periodic inspection or access to many hot insulated surfaces, removable/reuseable insulation covers have been found to be a good solution. These covers reduce the heat loss on surfaces such as valves, flanges, pumps, compressors, and piping where otherwise a permanent, non-reuseable type of insulation might be added. The use of removable covers can reduce the long-term cost of gaining access to the hot surfaces that need periodic inspection.

There are a number of different performance requirements encountered by removable insulation covers on hot surfaces. In general, the covers should insulate effectively, be capable of being easily removed and replaced, and last a certain period of time. An impediment to their durability is the conditions to which the blankets are exposed: high service temperature, leaking chemicals, sun and rain, physical abuse, and fire, among others. The selection of appropriate materials to meet the performance requirements of a particular job can be a difficult and complex task. Such a selection is generally addressed with specifications.

As a first step in developing removable insulation specifications, ASTM Committee C-16 on Thermal Insulation formed a task group to develop a standard guide. This document, which was balloted before Committee C-16 in late 1987 and received Society approval as ASTM C 1094 in 1988, identifies the performance issues faced by removable covers and their constituent materials. Being a guide, it does not recommend particular materials or even performance values. Rather, it recommends appropriate test methods, as well as general design and construction issues, that should be addressed by a specification. The use of ASTM C 1094 in developing removable cover specifications should ultimately improve the performance and quality of those covers.

KEY WORDS: removable/reuseable thermal insulation covers, exposure, inspection, maintenance, heat loss, ASTM C 1094, specification, fabric

Removable and reuseable insulation covers are typically custom designed and manufactured to insulate hot surfaces that require periodic inspection or maintenance. These surfaces generally are piping system components, such as valves or flanges, or equipment such as pumps and compressors. With the two simultaneous needs of insulating the hot surfaces against the loss of heat and of allowing easy access to those surfaces, properly designed and manufactured removable insulation covers are an ideal solution to insulating those surfaces.

There are a number of variables which affect the performance and durability of these covers. Service temperature, chemical exposure, and degree of vibration are examples of a few of these. Due to the wide range of these variables, it has become recognized that there is now a need for a specification for removable covers. ASTM, in addressing this need, decided, as a first step, to develop a standard guide. With a standard guide in place, a structure is established for developing standard specifications.

¹Performance Contracting, Inc., Shawnee Mission, KS 66201.

Philosophy Behind the Standard Guide (ASTM C 1094)

Generally, removable insulation covers are fabricated from an insulating material covered with fabric, as mesh, or both, held together at the seams with metal staples or sewing thread, and attached around the hot surface with wire, belts, or hook-and-loop fasteners. It has been the practice of users of these covers to specify the individual materials to be used. Typically, this might include the type and weight of fabrics, the type of sewing thread and spacing of stitches, and the type of spacing of wires and rings to hold the covers in place. The type of fabric typically may change with the specific service temperature.

Many of these type specifications have been successful for limited applications. However, in other cases, fabrics become corroded from leaking chemicals, seams become broken so as to expose the insulating media, or the insulating media becomes saturated with leaking chemicals. If these sorts of failures occur before the expected life of the blankets, the application cannot be considered a success.

To address these and other issues, ASTM Committee C-16 on Thermal Insulation decided to examine the performance issues involved in removable covers. Rather than specify particular materials or even particular performance criteria, a Committee C-16 task group identified performance issues and test methods that could be used to evaluate those criteria. This is the philosophy behind the standard guide (approved by the Society in 1988 as ASTM C 1094): identify the performance issues, recommend specific test methods for evaluating that performance, and allow the user the freedom of selecting his own performance criteria. Such criteria would allow for the screening of various systems and selecting the one(s) that meet the requirements of the application.

Performance Issues for Covers

What are the performance issues for insulation covers and for cover materials? In general, the user should expect that the cover will fit snugly and effectively insulate the surfaces that are intended to be insulated. Gaps, areas of reduced thickness, and improper fits will compromise the thermal effectiveness of the covers. The user should expect that the covers will install easily and quickly with no special tools. Likewise, they should be easy to remove and reinstall. The user is paying a premium for removability and reusability, so it is reasonable for him to expect the covers to withstand a large number of removals and reinstallations. This is where the need for performance specifications arises.

If the user expects to remove and reinstall each blanket a certain number of times, then that should be stated in his specification. Whatever the number of cycles he expects, he can set a performance criteria. If the covers are to be used outdoors, then weatherproofness is a performance issue to be addressed. If resistance to the ingress of oils or dirt is expected, this issue should be addressed. Of course, the maximum service temperature should be identified. The user of the cover should be able to expect that the cover materials will not disintegrate, melt, or significantly lose durability when exposed to the service temperature.

From here, the list of possible performance issues grows. If the cover is expected to resist deterioration from certain leaking chemicals, that should be stated. Issues of flammability, fire resistance, weather resistance, and sound-absorbing characteristics must be identified, as should the thermal performance. For ease of handling, the user should be concerned with the total cover weight. To achieve these, certain component material properties must be known. These are discussed in the next section.

Performance Requirements for Cover Materials

To assure the performance of the entire insulation cover, the user must first direct his attention to the insulation media. For a removable/reuseable cover, this is probably a fibrous mate-

rial such as fibrous glass, rock wool, or ceramic fiber. Regardless, the user and manufacturer of the cover should identify certain properties and the retention of those properties after exposure to a hot surface with the service temperature. The insulation media properties have been identified in the Standard Guide as the following:

1. Density (per ASTM C 167).
2. Thickness and thickness recovery (per ASTM C 165).
3. Compressive strength (per ASTM C 165).
4. Flexibility (per ASTM C 553).
5. Flammability (per ASTM E 84).
6. Thermal conductivity (at certain mean temperatures) (per ASTM C 177).

Basically, knowing these insulation media properties are necessary for predicting the performance of the insulation blanket as a whole. Since these properties may change with temperature, it should be emphasized that the insulation should be tested for these properties *before and after* temperature exposure.

The fabric or mesh is typically the jacketing for the insulation media and is the barrier between it and the environment. This jacketing is the most important component in making insulation covers removable/reuseable. Therefore, the integrity of this jacketing is critical to the durability of the insulation. This jacketing integrity includes that of the fabric or mesh as well as that of the seams joining pieces of fabric or mesh.

In ASTM C 1094 several fabric properties are identified:

1. Breaking load (per ASTM D 1682).
2. Tear strength (per ASTM D 1117).
3. Burst strength (per ASTM D 751).
4. Folding endurance (per ASTM D 2176).
5. Abrasion resistance (per ASTM D 4157).
6. Flammability (per ASTM E 84).
7. Water resistance (per AATCC 35-1980).

Furthermore, for high temperature exposure or for chemical exposure, it is suggested that these properties be evaluated after the exposure. The use of test results which measure the above properties can be used to evaluate the capability of a fabric to withstand the conditions of actual use. For example, an abrasion resistance test subjects a fabric to a vibration type of wear, such as a removable cover may experience on a vibrating valve. A folding endurance test subjects a fabric to the type of wear it may experience with a number of removals and reinstallations. Both of these tests are particularly significant for fabric which has been subjected to a high temperature such as 538°C (1000°F). Most fabrics lose a large percentage of their original strength after high temperature exposure.

The issue of chemical exposure is quite complex. ASTM C 1094 does not suggest how to perform such a test but only how to evaluate its properties after exposure. Corrosive chemicals are more corrosive at higher temperatures. Therefore, the specific chemical and specific temperature should be addressed by the user. Failure to address them could result in severe and widespread fabric failure.

Fire resistance insulation covers are a special case that is addressed by ASTM C 1094. In many applications, such as a cover for an oil well head valve, the blanket only insulates in the event of a catastrophic fire; the valve must be able to be remotely shut off some specified period of time after the start of the fire. Therefore, the cover must fit tightly, be weatherproof, insulate effectively up to the fire temperature, and, of course, not fall off the valve during a catastrophic fire. Such an insulation cover is truly a high performance one whose construction must be evaluated and specified carefully.

An acoustical insulation cover is also a special case that is addressed by ASTM C 1094. Such a cover is designated as a sound barrier. It is placed over a noisy apparatus, such as a compres-

sor, to significantly reduce the noise level released to the environment by that compressor. Usually, this cover must not only need a certain thickness of fibrous insulation but also have a solid barrier, called a septum, contained within.

Converting ASTM C 1094 to a Specification

ASTM C 1094 can be the framework for building a specification. It identifies performance issues to be evaluated in specifying materials and construction for a durable, effective insulation cover. With specific values given for performance criteria, this Standard Guide can be converted to a specification.

Once the user, or a cover fabricator, has selected specific performance values to insert into ASTM C 1094, he must then select materials based on available test data. Presumably, these test data would be supplied by manufacturers of insulation media, fabrics, attachment systems, etc. For example, if the user has established a performance criteria for insulation media to have a compressive strength greater than or equal to 479 Pa (10 lb/ft²) after exposure (on a hot plate) to 260°C (500°F), then he must have these data available to him from the insulation media manufacturer. Likewise, if he needs a hot side fabric for continuous use at 388°C (750°F), he may decide to specify an abrasion resistance of a certain number of cycles, maybe 20 cycles, under a particular weight. Such criteria would be used to select certain fabrics and reject others.

There are other issues which ASTM C 1094 suggests that the user address for his specification. For example, if leaking chemicals are expected to flow onto the outer jacketing, then those chemicals must be specifically identified and included in the specification. This may result in the exclusion of certain coated fabrics and the selection of others. Exposures of test samples would need to have been performed, followed afterwards by exposure strength tests.

The Appendix is a draft of a sample specification that the author developed with ASTM C 1094. The test values were selected based on experience and available data. Other values could be substituted, but the values given are those recommended by the author for the particular applications cited in the specification.

To demonstrate the usefulness of ASTM C 1094, a number of silicone-coated fiberglass fabrics were subjected to some of the recommended tests. These samples are commercially available and have an appearance similar to one another. Tests were conducted on fabric samples first exposed for 96 h at 260°C (500°F), the maximum temperature rating of this category of fabric. Table 1 gives the test results. It is obvious that there is a wide variation of performance. Sample C, in particular, performed much better than the others, yet it was significantly heavier. With this type of data, the user can decide whether it is worthwhile to pay the expense of the additional weight. Even among the other fabrics, however, that have roughly the same weight as one another, there is significant variation of performance. For example, for the abrasion resistance test, which is the number of cycles for a piece of Grade 3 emery cloth to wear through the coating to the woven glass fibers, the maximum test result was 308 cycles and the lowest was 19 cycles when excluding Sample C. It is significant that all these fabrics, except Sample C, had a gray color and were fairly similar in appearance. If someone were to specify simply a silicone-coated fiberglass fabric weighing between 474 and 575 g/m² (14 and 17 oz/yd²), he could get a wide variety of qualities of fabric.

Conclusion

ASTM Committee C-16 has recently developed a Standard Guide for Removable Insulation Covers (ASTM C 1094). Due to the need for specifications for this type of insulation, Committee C-16 decided, as a first step, to write a Standard Guide; this can then be used as a framework from which to develop specifications. ASTM C 1094 identifies the significant performance is-

TABLE 1—Summary of test results on nine commercially available silicone-coated fiberglass fabrics (by the test procedures recommended in ASTM C 1094).

Sample	Weight/Area, g/m ² (oz/yd ²)	Tear Strength, N (lb) (ASTM D 1117) ^a	Folding Endurance Cycles (ASTM D 2176) ^b	Abrasion Resistance Cycles (ASTM D 4157) ^c
A	508 (15.0)	178 (40)	33	19
B	525 (15.5)	401 (90)	257	308
C	684 (20.2)	1482 (333)	342	3333
D	559 (16.5)	125 (28)	47	167
E	525 (15.5)	71 (16)	44	175
F	474 (14.0)	89 (20)	64	217
G	508 (15.0)	129 (29)	175	158
H	572 (16.9)	125 (28)	56	83
I	565 (16.7)	129 (29)	166	242

^aThese test results are for fabric samples that have been exposed at 260°C (500°F) for 96 h. In each case, five samples were tested in the warp direction and five samples in the fill direction. From these, average warp and fill test values were determined. The low of the two is reported in this table.

^bThis is the M.I.T. Folding Endurance Test run on 13 mm (1/2 in.) wide samples, an 18 N (4 lb) load, and a 36 N (8 lb) spring.

^cThis is the Wyzenbeek Abrasion Resistance Test run with a 9 N (2 lb) load and a 9 N (2 lb) tension with medium-grit emery cloth as the abradent. Specimens were run until the silicone coating was abraded sufficiently to expose the bare fiberglass fabric.

sues for removable covers. In particular, tests are recommended for insulation media and for fabric jacketing that can be used to compare materials.

To develop a specification, the user must determine criteria for each of the tests that he feels is relevant to his needs. He can then use these to either develop a performance specification or a material specification. By requesting test data from the insulation media and fabric suppliers, he can select the appropriate materials and screen out those that do not meet his criteria. Or, he may request that the removable cover fabricator supply data to demonstrate that the covers meet the specifications.

ASTM C 1094 is a first step in the development of performance-oriented specifications for removable covers. Because it limits itself to being a guide, users can customize their own specifications by using ASTM C 1094 as a framework.

APPENDIX

SAMPLE
PERFORMANCE SPECIFICATIONS FOR
REMOVABLE/REUSEABLE INSULATION COVERS
(Adopted from the Proposed ASTM Standard Guide)

1. Scope

- 1.1 This guide recommends the criteria to be considered in specifying removable/reuseable insulation covers for surfaces operating in air at temperatures above ambient. Typical applications are in industrial plants and refineries.
- 1.2 A removable insulation cover is fabricated from a batt of fibrous insulation material encased in a tailored fabric and/or wire mesh enclosure. The fabric seams are held together with either sewn seams, metal rings, and/or staples. These covers must be designed and fabricated to allow a close fit with tight joints over piping, elbows, flanges, valves, and tanks. They are intended to be easily removed and replaced to allow for periodic access to surfaces they cover.

In addition to thermal performance, there are other performance categories of removable covers. These may include, but are not limited to, the following:

1. temperature exposure
 2. chemical and weather exposure
 3. acoustical
 4. fire endurance.
- 1.3 The materials of which the cover is made may include, but are not limited to, the following:
- o insulation media
 - o fabric, metal mesh enclosure, and/or foil enclosure
 - o seam materials (sewing thread, metal hooks, etc.)
 - o attachment system (hook and loop attachment, straps, wire, etc.)
- 1.4 The shape, size, and physical design of the cover will vary depending on the object to be covered. The cover may consist of more than one piece. Pipes, valves, pumps, and flanges are typical objects to be covered. On-site measurements should be made to ensure an acceptable fit.

- 1.5 Units of Measurement - The Inch-Pound (I-P) units shall be used.

2. Applicable Documents

2.1 ASTM Standard specifications:

- | | |
|------|---|
| C553 | Mineral Fiber Blanket and Felt Insulation (Industrial Type) |
| C795 | Wicking Type Thermal Insulation for Use Over Austenitic Stainless Steel |
| C892 | High Temperature Fiber Blanket Thermal Insulation |

2.2 ASTM Standard Test Methods:

- | | |
|------|---|
| C165 | Method for Measuring Compressive Properties of Thermal Insulation |
|------|---|
-

C167	Test Methods for Thickness and Density of Blanket or Batt Thermal Insulation
C177	Test Method for Steady-State Thermal Transmission Properties by Means of the Guarded Hot Plate
C335	Test Method for Steady-State Heat Transfer Properties of Horizontal Pipe Insulation
C411	Test Method for Hot Surface Performance of High Temperature Thermal Insulation
C423	Test Method for Sound Absorption and Sound Absorption Coefficients by the Reverberation Room Method
C692	Method of Evaluating the Influence of Wicking-Type Thermal Insulations on Stress Corrosion Cracking Austenitic Stainless Steel
C871	Methods for Chemical Analysis of Thermal Insulation Materials for Leachable Chloride, Fluoride, Silicate and Sodium Ions
D471	Test Method for Rubber Property - Effect of Liquids
D751	Standard Method of Testing Coated Fabrics
D1117	Methods of Testing Nonwoven Fabrics
D1682	Test Methods for Breaking Load and Elongation of Textile Fabrics
D1683	Test Method for Failure in Sewn Seams of Woven Fabrics
D1894	Test Method of Static and Kinetic Coefficients of Friction of Plastic Film and Sheeting
D2176	Test Method for Folding Endurance of Paper by the M.I.T. Tester
D4157	Test Method for Abrasion Resistance of Textile Fabrics (Oscillatory Cylinder Method)
E84	Test Methods for Surface Burning Characteristics of Building Materials
E119	Fire Tests of Building Construction and Materials
E596	Laboratory Measurements of Noise Reduction of Sound-Isolating Enclosures
G26	Recommended Practice for Operating Light-Exposure Apparatus With and Without Water for Exposure of Nonmetallic Materials (Weathering Test)

2.3 Other Test Methods

American Association of Textile Chemists and Colorists (AATCC)
Method 35-1980, Water Resistance - Scrim Test

National Fire Protection Association (NFPA) 701 - Standard Method
for Fire Test for Flame-Resistant Textiles and films

Underwriters' Laboratory (UL) 1709 - Fire Resistance Test for
Petrochemical Facility Standard elements

3. Physical and Chemical Properties

3.1 Several areas of performance may be considered:

- a. general physical and chemical properties
- b. resistance to temperature
- c. chemical resistance
- d. weather resistance
- e. fire endurance
- f. acoustical performance
- g. service life

3.2 Physical Properties of the Insulation Media:

3.2.1 Acceptable requirements:

3.2.1.1 Thermal Conductivity of insulation - not to exceed in units of W/m-°C (Btu-in/hr-sq ft. -F)

0.504 (0.35) at 38°C (100°F) Mean Temperature
.0720 (0.50) at 149°C (300°F) Mean Temperature
.1080 (0.75) at 260°C (500°F) Mean Temperature
.1080 (0.75) at 371°C (700°F) Mean Temperature
.1296 (0.90) at 482°C (900°F) Mean Temperature

Per ASTM C177 (up to the temperature limitation of the particular insulation).

3.2.1.2 Insulation Density - not to exceed 192 kg/m³ (12 pcf), per ASTM C167.

3.2.1.3 Insulation Thickness - as received thickness tolerance: +15 percent, -5 percent. per ASTM C165.

3.2.1.4 Insulation Thickness Recovery - to at least 85 percent after compression to 50 percent of original thickness, per ASTM C165.

3.2.1.5 Insulation Flexibility - wool will test as "flexible", per ASTM C553.

3.2.1.6 Temperature Limits - after exposure on a hot surface to _____ degrees for 96 hours, the insulation material shall maintain the specifications required above for unexposed material.

3.3 Physical properties of the fabric enclosure system:

3.3.1 Acceptable criteria:

3.3.1.1 Tear Strength - At least 89 Newtons (20 lbs.) per ASTM D1117, speed at 305 mm/min. (12 inches/min.).

3.3.1.2 Flexibility - At least 20 cycles, with a 18 Newton (4 pound) load, before failure, per ASTM D2176, 13 mm (1/2 inch) specimen.

3.3.1.3 Abrasion Resistance -

- (a) Woven fabrics, no rubber coating: After exposure to 250 cycles with zero emery, 9 N (2 lb.) load, 9 N (2 lb.) tension, per ASTM D4157, fabric will have a tensile strength of at least 4.38 N/mm (25 lbs/in.), per ASTM D1682-1E.
-

- (b) Woven fabrics with a rubber coating: Using a medium grit emery, a 9 N (2 lb.) load, and 9 N (2 lb.) tension per ASTM D4157, the fabric should withstand at least 200 cycles without the rubber coating wearing to the point that the fabric threads are exposed.

3.3.1.4 Surface Coefficient of Friction - Not to exceed 0.75, per ASTM D1894-78.

3.3.1.5 Water Resistance (if required) - No more than 0.1 gram of water will pass through with a 9 kPa (3 foot) head in 5 minutes, per AATCC Method 35-1980.

3.4 Physical Properties of the Assembled Cover

3.4.1 Acceptable assembled cover performance criteria:

3.4.1.1 Thermal Conductance: The thermal conductance of the cover, when tested per ASTM C335 with 51mm (2 in.) cover thickness, shall not exceed the following values in units of W/M²-°C at an ambient temperature = 24 C): (in units of Btu/hr-sq.ft.-°F at an ambient temperatures = 75°F)

PIPE TEMPERATURE, °C (°F) MAX THERMAL CONDUCTANCE

93 (200)	0.114 (0.020)
204 (400)	0.136 (0.024)
316 (600)	0.159 (0.028)
427 (800)	0.182 (0.032)
538 (1,000)	0.227 (0.040)
649 (1,200)	0.227 (0.040)
760 (1,400)	0.233 (0.041)
871 (1,600)	0.256 (0.045)

up to the temperature limitation of the particular materials

3.4.1.2 Weight: No cover shall weigh more than 23 kg. (50 pounds).

3.4.1.3 Attachment System: The attachment system shall allow easy removal and reinstallation of the cover. These systems can consist of hook and loop fasteners, SS wires and lacing hooks, or belts with loops, depending on the strength requirements.

3.4.1.4 Stress Corrosion: If the covers are to be used to insulate austenitic stainless steel surfaces, they shall meet the minimum requirements for stress corrosion cracking, per ASTM C692, and for concentrations of leachable chlorides, fluorides, silicate, and sodium ions, per ASTM C871.

3.5 Physical Properties of Seams and Closure System:

3.5.1 Minimum acceptable seam and closure system strengths:

3.5.1.1 Sewing Thread Tensile Strength - at least 71 Newtons (16 pounds), per ASTM D 578.

3.5.1.2 Seam Breaking Load - at least 89 Newtons (20 pounds), per ASTM D1683.

- 3.5.1.3 Fastener System Tensile Strength - at least 89 Newtons (20 pounds), 102mm (4 inch) width, per ASTM D1683.
- 3.5.1.4 Hook and Loop Fastener Width-wise Shear Strength - at least 34.5 kPa (5.0 psi), per Velcro test procedure.
- 3.5.1.5 Hook and Loop Fastener Tension Effect - at least 10.3 kPa (1.5 psi), per Velcro test procedure

3.6 Temperature Endurance

- 3.6.1 The Acceptable properties of the assembled cover and of its components after exposure to the highest expected temperature difference and service temperature for 96 hours on either a flat plate or a pipe:

- 3.6.1.1 The minimum fabric properties, when tested by the same test procedures given in Section 3.3, shall be the same as for unexposed fabrics. For coated or impregnated fabrics, no delamination or severe stiffening shall occur. The coating shall not discolor with temperature exposure.

- 3.6.1.2 The insulation media, when tested by the same test procedures given in Section 3.2, shall be as follows:

Thermal Conductivity - same as for unexposed insulation

Density - not to exceed 192 kg/m³ (12 pcf)

Thickness - not to change by more than 15% of the unexposed thickness

Thickness Recovery - same as for unexposed insulation

Flexibility - will test as "flexible"

- 3.6.1.3 The cover seams, when tested by the same test procedures given in Section 3.5, shall be the same as for the unexposed samples.

3.7 Fire Endurance Cover (if required)

- 3.7.1 This category of insulation cover is designed to reduce the transfer of heat during a hydrocarbon fire. The goal is to keep the temperature of the covered equipment below a prescribed level for a prescribed time period. This type of blanket is particularly applicable for use in petrochemical plants and refineries.
 - 3.7.2 Test Procedure: UL 1709 - the outer insulation surface on a nominal 3-inch N.P.S. insulated pipe is exposed in a furnace with a high-rise temperature. This procedure simulates the condition that would occur under an actual hydrocarbon fire. The furnace is to have a temperature capability of at least 1093°C (2000°F) within 5 minutes from the start of the test.
 - 3.7.3 Cover Performance: There are three criteria from which to choose for an acceptable fire endurance blanket. Each
-

involves the maximum temperature of the surface inside of the insulation; it is to remain below:

1. 121°C (250°F) after 20 minutes,
2. 343°C (650°F) after 60 minutes, or
3. 538°C (1000°F) after 60 minutes.

During the fire, the attachment systems will remain in place so that the blanket still is positively attached to the pipe. In addition, the seams of the jacket holding the blanket together will remain intact. The blanket does not, however, need to be capable of being reused. Therefore, weather protective jacketing is not expected to remain intact.

- 3.7.4 Material Performance: Fabrics, insulation materials, and seams are expected to meet the standard performance requirements for all covers. If the blanket is to be used outdoors, a weather protective jacket is required.

3.8 Chemical Resistance (if required)

- 3.8.1 A cover of this category is designed to withstand exposure to acids, bases, or solvents without significant degradation of physical properties.
- 3.8.2 For the best evaluation, the covers' fabric should be exposed to the actual chemicals, at the actual temperature, that it will see in the field. The period of time of exposure should be agreed upon by the cover fabricator and the customers.
- 3.8.3 In general, if leaks are expected, the fabric enclosure should resist the ingress of liquid chemicals so that the insulation materials do not absorb the liquid. Below 260°C (500°F) service temperatures, this is generally achieved with a coated fabric on the hot side. For service temperatures above 260°C (500°F), this may require either a foil laminated fabric or separate stainless steel jacketing placed between the cover and the hot surface.
- 3.8.4 Acceptable values of seam break strength and fastener tensile strengths after weathering exposure may be established.
- 3.8.4.1 For coated, hot side fabrics where leaks are expected, seams are to be sewn to avoid puncturing of the fabric. Penetration of the coated fabric by hog rings, staples, or metal attachment pins shall be avoided.
- 3.8.5 Laboratory chemical exposure testing on fabrics should be in conformance to ASTM D471 for 96 hours at room temperature. After exposure, the fabrics shall meet the minimum strength criteria in Section 3.3.
- 3.8.6 Field chemical exposure testing should be conducted by placing a small insulation cover sample over a leaking surface which is operating at the temperature of concern.
- 3.8.7 Weathering: Any fabrics which are chemically resistant shall be weather resistant.

3.9 Acoustical Cover (if required)

- 3.9.1 This category of insulation cover can serve as a thermal insulating cover while simultaneously serving as a noise
-

barrier and sound absorber. This noise may be generated by a motor, compressor, or other mechanical device.

- 3.9.2 To be an effective acoustical cover, a removable cover must contain a high density septum. This septum is to be included in the cover.
- 3.9.3 Testing: Tests are to be performed by a qualified laboratory, per ASTM E-413, on a flat sample measuring at least 762 mm (30 in.) on each side.
- 3.9.4 Performance: The establishment of a single number rating for acoustical barrier/absorber covers can be misleading. Instead, the barrier should be evaluated on an individual frequency basis. The insulation losses for individual frequencies shall not be less than the following:

<u>FREQUENCY, HZ</u>	<u>INSERTION LOSS, dB</u>
125	9
250	9
500	21
1000	33
2000	38
4000	41
8000	54

4. Workmanship, Finish and Appearance

- 4.1 The purpose for having a well designed, well fabricated insulation cover is (1) to restrict the flow of heat and/or reduce the transfer of sound, to some specified level, (2) to be removable and replaceable with relative ease, and/or (3) to provide personnel protection from hot surfaces.
- 4.2 It is important that covers be fabricated so that gaps are minimized at the closure points or between adjacent insulation. Such gaps can severely compromise thermal effectiveness. It is also important that the minimum designed cover thickness be maintained over most of the entire surface. It is advisable to overlap seams so that water or other liquids will flow away, not into, seams.
- 4.3 The quality of the covers should be such that the appearance is uniform. Attention may need to be paid to lots of fabric, attachment materials, other visible cover materials, and the insulation media.
- 4.4 Covers should be fabricated and installed in such a way that adjacent covers should form a tight butt joint. The bare hot surface should not show and the full thickness of the insulation should be maintained. Cements, loose fibers, and mastics should not be exposed.
- 4.5 Where possible, on site measurements should be made to assure correct fit of the covers on the surfaces to be insulated.

5. Product Marking and Design Drawings

- 5.1 The cover shall be permanently marked or labeled with tags to identify the part for the purpose of proper relocation after removal and for reordering. Also, each insulation cover should be labeled with the name of the project and an identity code number traceable to its exact location to ensure proper installation and reinstallation as agreed upon by the supplier and purchaser.

- 5.2 Location of sections insulated with the covers should be labeled on drawings. Identification numbers for the individual covers should be referenced on the drawings.

6. Shipping, Storage, and Handling

- 6.1 The covers shall be packed in sealed 2 mil thick polyethylene bags and cardboard boxes for shipping and handling. Containers should be labeled with the cover designation if such labeling is being used.
- 6.2 The blankets should be visibly clean on arrival at the job site. This may require a pre-shipping inspection and a final inspection of the covers.

7. References

- C692 Mineral Fiber Blanket Insulation and Blanket-Type Pipe Insulation (Metal-Mesh covered) (Industrial Type).
- C871 Chemical Analysis of Thermal Insulation Materials for Leachable Chloride, Silicate, and Sodium Ions.
- C612 Mineral Fiber Block and Board Thermal Insulation.

8. Sample Preparation

Each group interested in bidding on removable covers, described by this specification, shall provide one (1) sample blanket to be reimbursed at normal market price. This cover will be 51 mm (2 inches) thick and be designed to insulate an 8" NPS, ANSI Class 150 gate valve with appropriate materials for the chemical and temperature exposure. If the contract is awarded for those covers, this sample will be used as the standard for workmanship for all others delivered under the contract.

Thomas E. Whitaker,¹ Kenneth M. Whorlow,¹ and
Francis B. Hutto, Jr.¹

New Developments in Test Technology for ASTM C 692 (Preproduction Corrosion Test for Insulation To Be Used on Austenitic Stainless Steel)

REFERENCE: Whitaker, T. E., Whorlow, K. M., and Hutto, F. B., Jr., "New Developments in Test Technology for ASTM C 692 (Preproduction Corrosion Test for Insulation To Be Used on Austenitic Stainless Steel)," *Insulation Materials, Testing, and Applications, ASTM STP 1030*, D. L. McElroy and J. F. Kimpflen, Eds., American Society for Testing and Materials, Philadelphia, 1990, pp. 688-698.

ABSTRACT: Significant improvements have been made in the test procedures used in ASTM C 692 which deal with preproduction testing of wicking-type insulation for use on austenitic stainless steel. A drip procedure which literally turns the apparatus upside down has been found to be more reproducible as well as more realistic in terms of how insulation is actually contaminated in a real-use situation. The new procedure employs a steam-heated pipe to heat the coupons and thus provides far greater temperature uniformity than previously. The drip method controls the amount of liquid applied to each coupon to $\pm 10\%$, a much closer control than was possible with the previous wicking method. Correlations between the old and new procedures are provided. In addition to improvements in the test protocol, procedures for the metal qualification test have been vastly improved.

KEY WORDS: preproduction corrosion test, ASTM C 692, external stress corrosion cracking, chloride

External stress corrosion cracking (ESCC) [1] has plagued the process industries for a long time, but the problem really became "epidemic" in the mid-1950s. Some excellent detective work by A. W. Dana [2] of Du Pont, and others, established the fact that leachable chloride in insulating materials can induce ESCC, given the proper environmental conditions for the phenomenon to take place:

1. The austenitic stainless steel must be stressed.
2. Moisture must be present.
3. The temperature of the stainless steel must be in the 50 to 200°C (122 to 392°F) range [1].
4. Oxygen must be present [3].
5. Chlorides (or other ESCC promoters) must be present.

While it was early recognized that chlorides from the plant environment were as much or even more responsible for ESCC [2], it was established that chlorides in the insulation, as received, could and must be monitored and controlled to minimize ESCC. Other contaminants, such as alkalis, sulfites, sulfides, and sulfates, have been found to cause ESCC, but chlorides are the principal concern in insulating materials.

¹Pabco Insulation Division, Fibreboard Corporation, Fruita, CO 81521.

It was also discovered early on that the presence of significant quantities of leachable sodium silicate could offset the effects of modest amounts of chloride found in the insulation or even chloride introduced from the environment.

The Dana Test

ASTM Bulletin No. 225 [2], written by A. W. Dana, Jr., and issued in October 1957, was the foundation for ASTM Method of Evaluating the Influence of Wicking-Type Thermal Insulations on the Stress Corrosion Cracking Tendency of Austenitic Stainless Steel (C 692). The test coupon was designated to be made from 16 gal (61 L) Type 304 stainless steel, cut 2 by 7 in. (50.8 by 177.8 mm), and bent into a horseshoe shape around a 1 in. (25.4 mm) radius. The mathematics involved in determining the proper amount of post-stressing after the bending process remains unchanged, as does the size and shape of the insulation test block used for wicking water up to the coupon-insulation interface where chlorides may accumulate and possibly cause ESCC to occur.

While the original Dana test procedure called for heating the test coupons with a strip heater mounted on the inside of the bend of the coupon, ASTM C 692-77 calls for heating the coupons by connecting several in electrical series and resistance-heating by applying a low-voltage/high-amperage current. Figure 1 shows the basic setup for the ASTM C 692-77 Dana Test.

When set up as shown in Fig. 1 and operated with distilled water in the crystallizing dish and the test coupon heated to the range of the boiling point, wicking-type insulations that contain sufficient amounts of leachable chlorides, not offset by leachable sodium silicate, will cause ESCC to occur in 28 days.

If chlorides are present, and the test is run long enough, ESCC will eventually happen in most cases. Based on an analysis of available data, it was agreed that if ESCC did not occur in 28 days of ASTM C 692 test conditions, the risk of ESCC with the particular insulation sample was acceptable.

Acceptability Curve

Since the Dana test is not an absolute, and failure is dependent not only on chloride concentration but on offsetting sodium silicate, Karnes [4] correlated his own data and those of others to show the effect of the relationship between chloride and sodium + silicates and failure rate on a 28-day test. The Karnes test differed from the Dana test physically but brought effectively the same test conditions to the stressed stainless steel coupon. Figure 2 (from Karnes' paper) shows the arbitrary line that may be drawn through the data to separate most of the "passes" from the "failures".

When incorporated into Nuclear Regulatory Guide 1.36 [5], the acceptability curve was modified as shown in Fig. 3 with a maximum allowable chloride *plus fluoride* concentration of 600 ppm. Research into the origin of the fluoride requirement [6] revealed that it was added because of the chemical similarity and normally greater chemical aggressiveness of the fluoride. It was assumed that: "If chloride is bad, then fluoride must be worse!" When Military Standard MIL-I-24244 was issued on 12 February 1974, it contained the same acceptability curve (Fig. 3) but without the fluoride requirement. A subsequent revision of MIL-I-24244 added the fluoride requirement, presumably to come into line with Regulatory Guide 1.36.

ASTM C 795, which covers the same basic requirements as Regulatory Guide 1.36 and MIL-I-24244, does not contain the fluoride requirement. Efforts to add fluoride to ASTM C 795 have met with resistance and a demand that the corrosiveness of fluoride be documented before it is added. More will be said on this later in this paper.

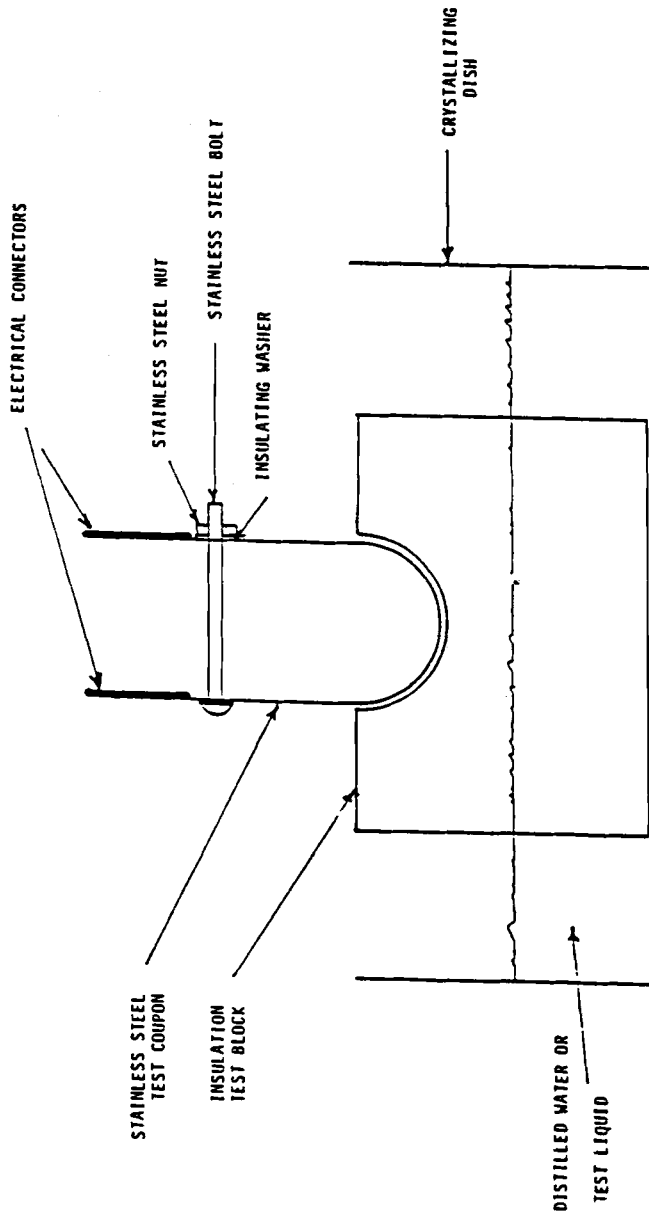


FIG. 1—Basic setup of ASTM C 692-77 Dana Test.

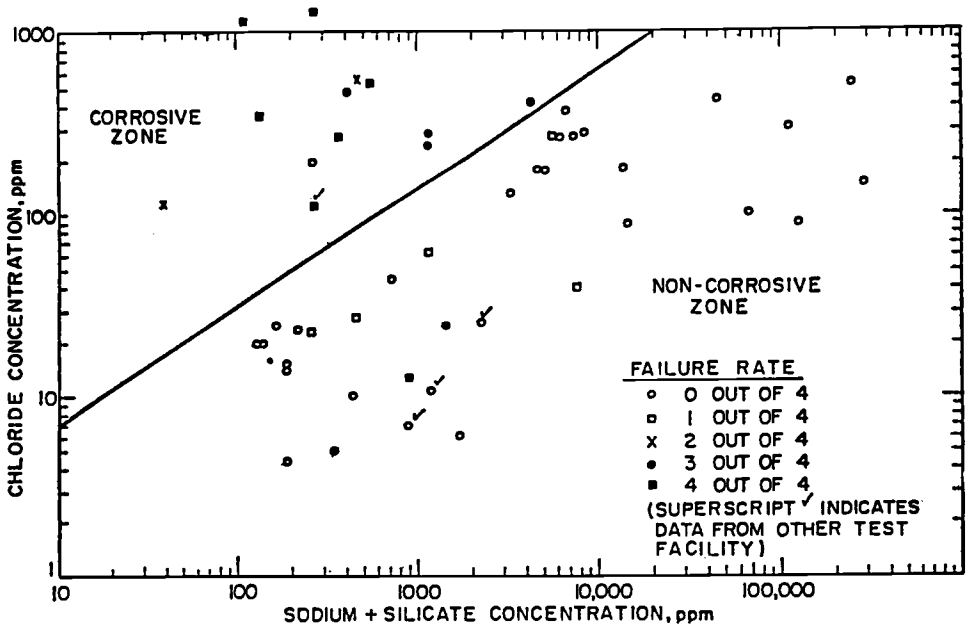


FIG. 2—Arbitrary line drawn through the data to separate most of the “passes” from the “failures” [4].

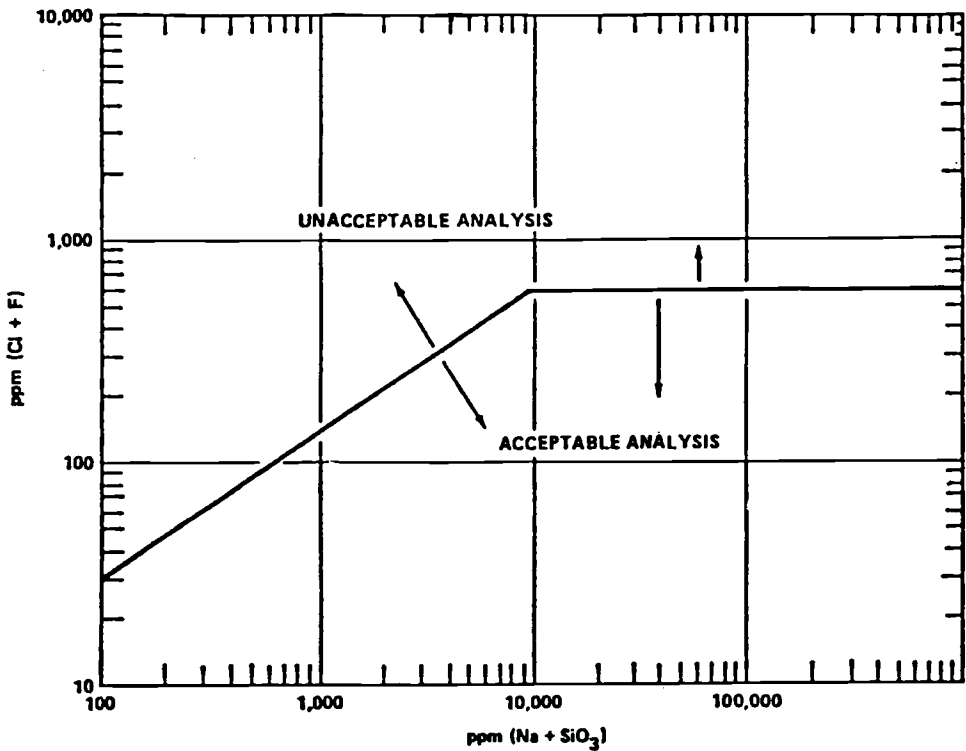


FIG. 3—Acceptability curve.

Accelerated Dana Test

While the 28-day test with distilled water shows what can happen when chloride in the insulation is wicked up through to the stainless steel, substituting a 1500 ppm (mg/L) chloride solution for the distilled water causes failure in a much shorter time period as well as provides information as to whether or not the insulation might give some protection from chlorides introduced from the environment (rather than from the insulation itself). Work at Du Pont showed that a 7-day accelerated test using 1500 ppm (mg/L) chloride solution is equivalent to a 28-day test with distilled water. Several companies and regulating agencies have required that insulation pass the accelerated Dana test to be acceptable. Attempts to add the accelerated Dana test to ASTM C 795 (and ASTM C 692) were unsuccessful.

ASTM C 692-77 Update

As discussed in Hutto et al. [7], ASTM C 692-77 is beset with many problems. When revision was begun in 1980, efforts were expended in an attempt to incorporate the accelerated Dana Test (described above) as an alternative. A new round robin was run to help put an updated version of ASTM C 692-77 on the books. The first problem encountered was in finding a material that could be shown to "pass" while another "failed". No failing material could be found. Attempts to "spike" one calcium silicate product with chloride to make it fail were not successful. Spiking a second product produced a test material that marginally failed. Test data from this round robin are shown in Appendix I.

Metal Qualification Test

ASTM C 692 requires that metal used for making test coupons be qualified by running a three-day neutral wick test with 1500 ppm (mg/L) chloride. Under such conditions, four out of four test specimens must crack in order to qualify the lot of metal for test purposes. Over the past several years, the Pabco R&D Laboratory had observed that cracks in qualifying coupons were less and less distinct but nevertheless present. When two other laboratories (new at running ASTM C 692-77) tried to run the qualification test, they failed. In discussing the matter with the other laboratories, it was obvious that Pabco was carefully controlling conditions that were not spelled out in detail in ASTM C 692-77. Further experimentation by Pabco showed that a more repeatable qualification test could be made by using a neutral wick in the form of a 1½ in. (38 mm) diameter plug cut from an 8 pcf (128 kg/m³) ceramic wool blanket. Both the neutral wick test and the regular ASTM C 692 test showed cracks better when the apparatus was left open to air rather than covered up with glass plates, as suggested in ASTM C 692-77. The need for oxygen to participate in the ESCC process is in line with the data given by White et al. [3]. With some coaching by Pabco, one of the other laboratories managed to obtain a successful qualification test, while the second gave up in despair.

Qualified Metal

ASTM C 692 states that the metal used must be Type 304 stainless steel that meets the composition requirements of ASTM A 240 and that has been sensitized in argon at 1200°F (649°C) for 3 h and has passed the stated qualification test. MIL-I-24244B states only that the coupons be cut from 16 gage AISI Type 304 stainless steel which has been sensitized in argon at 1200°F (649°C) for 3 h. With the difficulties in qualifying metal discussed above, it would appear that a qualification under MIL-I-24244B might not necessarily be valid.

In reviewing the mounting difficulties with the qualification test and data on the stainless

steel and by the Pabco R&D Laboratory, it would appear that Type 304 stainless steel is getting better! The ASTM specification (ASTM A 240) for Type 304 allows 0.08% carbon, while Type 304L allows 0.03. Several years ago, domestic Type 304 typically had 0.06% C, while today most, if not all, of the Type 304 sheet available comes from overseas and runs 0.04 to 0.05% C, which is closer to Type 304L! Additionally, recent lots of Type 304 are running 0.9 to 1.4% manganese as opposed to a previous 1.5% typical with a 2.0% specification maximum. The effect of this change in manganese content is unknown, but it may be significant.

Sensitization

The Pabco R&D Laboratory also experimented with sensitization and found that Type 304 stainless steel sensitized in air for 7 h, as suggested by White et al. [3], also passed the qualification test. While ASTM C 692-77 calls for sanding after sensitization, White et al. [3] state that removing the tarnish film reduces susceptibility to stress corrosion cracking. Pabco found that both presanded and postsanded coupons passed the qualification test, but it appears that pre-sanding might be preferred since excessive postsanding might remove all of the sensitized layer and thus cause misleading results. While air sensitization might be preferable from a cost standpoint, argon sensitization would maintain better continuity with the past and MIL-I-24244B.

C692X

As described in Hutto et al. [7] in seeking to overcome the acknowledged shortcomings of ASTM C 692-77, a new apparatus and test method designated as C692X was developed in the Pabco R&D Laboratory. C692X incorporates the steam-heated pipe approach of MIL-I-24244B to achieve maximum temperature uniformity while retaining the larger coupon of ASTM C 692 for greater test area and greater likelihood of developing cracks. In addition, the drip method of Ashbaugh [1] has been used because it more nearly simulates a real-life situation than the wicking methods. If insulation is installed in a "puddle", it is a misapplication that would draw sharp objections from any insulation manufacturer!

Figure 4 shows a schematic of the apparatus used in C692X. Since the development of the apparatus and test procedure was discussed in detail in Hutto et al. [7], the description here shall be brief. In essence, however, C692X brings the same test conditions to bear on the test coupon as do ASTM C 692 and MIL-I-24244B.

A 20-channel peristaltic pump delivers 250 ± 25 mL/day to each test sample from its separate, calibrated, 1-L reservoir. Thus each channel can be separately monitored for precision of delivery and adjusted if necessary. Reservoirs need be filled only every four days, making three-day weekends easy to handle.

C692X requires that all insulation samples be heat treated at $400 \pm 10^\circ\text{F}$ ($205 \pm 6^\circ\text{C}$) overnight before testing. This heat treatment makes all samples wet readily so that the test water penetrates down to the stainless steel in a uniform, reproducible manner. Thus it is possible to test fiberglass, perlite, ASTM C 449 insulating cements, ASTM C 195 insulating cements, and other configurations that would be difficult or impossible to test in strict accordance with ASTM C 692-77 or MIL-I-24244B.

Sample size has been reduced to $1\frac{1}{2}$ in. (38 mm) width from 2 in. (50.8 mm) width. The narrower sample gives more coupon-air-sample interface and thus greater likelihood of cracking, since this is the usual location of most cracks.

Cleaning the coupons after a test is always a problem, particularly if fiberglass samples have been run. The use of spray-type oven cleaner helps this situation somewhat.

Additional suggestions and allowances are made for detecting cracks in tested coupons.

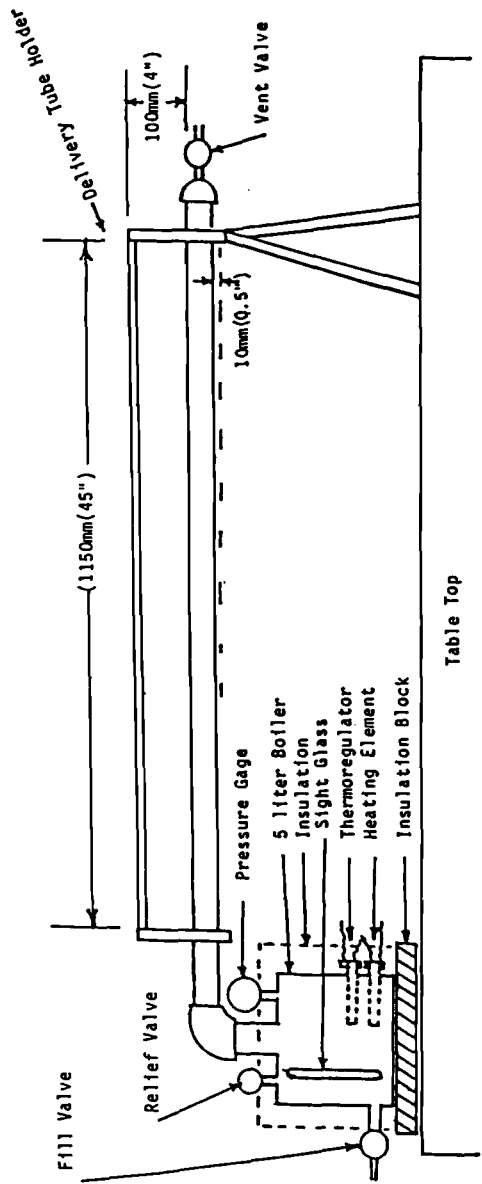


FIG. 4—Apparatus used in C692X.

Other Halide Investigation

To shed more light on whether or not fluoride, bromide, or iodide acts in the same manner as chloride in the ESCC phenomenon, four coupons each were exposed to 1500 ppm (mg/L) fluoride, bromide, or iodide solution for two months on the C692X apparatus. There were no cracks whatsoever. Switching to 1500 ppm (mg/L) chloride for three days resulted in cracks in all coupons.

ASTM C 692-77 Round Robin

Appendix I shows round robin data on four insulation samples run by two different laboratories on C 692-77 (Rev.) plus a comparison with C692X. Paragraph 13.1 indicates that when two laboratories ran ASTM C 692 on the samples (A, B, C, D) shown on the acceptability graph of Fig. 6 (not shown), the only failures found were on Samples B and C (one each by one laboratory; none by the other). No failures were found on Samples A and D. While the chemical analyses show that Sample A should not cause cracking, Sample D should have. The fact that there were no failures in Sample D gives further credibility to the premise that fluoride does not cause ESCC, since the "Cl + F" in Sample D was 2 ppm (mg/L) chloride and 494 ppm (mg/L) fluoride.

C692X (13.2), on the other hand, found no cracks out of 8 coupons on Sample A (expected), 6 cracked coupons out of 8 on Sample B (expected), 7 cracked coupons out of 8 on Sample C (expected), and no cracks out of 8 coupons on Sample D (not expected by chemical tests but explained in the paragraph above).

Conclusions

1. C692X is demonstrably more capable than ASTM C 692 of correlating pre-production corrosion test data with chemical test data developed in accordance with ASTM C 871 as required in ASTM C 795.
2. Chloride ions, under certain conditions, can induce external stress corrosion cracking (ESCC) in austenitic stainless steel.
3. 1500 ppm (mg/L) chloride ions, under the conditions of the C692X metal qualification test, produce cracks in three days or less in coupons of Type 304 stainless steel meeting the standards of ASTM A 240, sensitized in argon or air.
4. 1500 ppm (mg/L) fluoride ions, under the conditions of the C692X metal qualification test, did not produce cracks in any of four test coupons in 60 days.
5. 1500 ppm (mg/L) bromide ions, under the conditions of the C692X metal qualification test, did not produce cracks in any of four test coupons in 60 days.
6. 1500 ppm (mg/L) iodide ions, under the conditions of the C692X metal qualification test, did not produce cracks in any of four test coupons in 60 days.
7. Air sensitization, as suggested by White et al. [3], is equivalent to argon sensitization for C692X.
8. Type 304 stainless steel, as available today, contains less carbon than formerly and hence is harder to crack under the conditions of ASTM C 692-77, making the more precise control of C692X a necessity for preproduction corrosion testing as required in ASTM C 795.

Recommendations

1. That ASTM C 692-77 be replaced with C692X.
2. That efforts be made for the acceptance of C692X by NAVSEA and others using MIL-I-24244B.
3. That research on C692X be included in the ASTM Committee C-16 research agenda.

References

- [1] Ashbaugh, W. G., "ESCC of Stainless Steel under Thermal Insulation," *Materials Protection*, May 1965, pp. 18-23.
- [2] Dana, A. W., Jr., "Stress-Corrosion Cracking of Insulated Austenitic Stainless Steel," ASTM Bulletin No. 225, American Society for Testing and Materials, Philadelphia, Oct. 1957.
- [3] White, E. L., Berry, W. E., and Boyd, W. K., "Stress Corrosion Cracking of Sensitized Stainless Steel in Oxygenated High Temperature Water," Battelle Report BMI-1927, Battelle Columbus Laboratories, Columbus, Ohio.
- [4] Karnes, H. F., "The Corrosive Potential of Wetted Thermal Insulation," presented at the 57th National Meeting of the American Institute of Chemical Engineers, Minneapolis, Minn., 26-29 Sept. 1965.
- [5] Nuclear Regulatory Guide 1.36, dated 23 Feb. 1973.
- [6] Private communication from H. F. Karnes, General Electric Company, Knolls Atomic Power Laboratory, Schenectady, N.Y.
- [7] Hutto, F. B., Jr., Tissot, R. G., Jr., and Whitaker, T. E., "A New Apparatus and Test Procedure for Running ASTM C 692 Stress Corrosion Cracking Tests," in *Corrosion of Metals under Thermal Insulation*, ASTM STP 880, American Society for Testing and Materials, Philadelphia, 1985, pp. 211-219.

Appendix

PRECISION AND BIAS STATEMENT FROM C692X, DRAFT 3, 11/4/87

(Not truly a P&B statement but a statement representing all the available interlaboratory data.)

13.0 PRECISION AND BIAS

13.1 The following samples were available from a C692 round robin in which one of the two participating labs found no cracks at all while the other found only two coupons cracked in 22 samples of B and C tested and none at all in samples A and D.

13.1.1	<u>Sample</u>	<u>Na* + SiO₂*</u>	<u>Cl* + F*</u>
	A	5845	123
	B	6561	638
	C	7609	656
	D	3611	496**

*ppm(mg/l) as determined by ASTM C871

**2 chloride + 494 fluoride

13.1.2 Figure 6 shows that based on the chemical analysis, samples B,C, and D should cause ESCC.

13.2 A single laboratory ran C692X tests in quadruplicate - twice, with the following results:

<u>Cracks out of 4 in</u>	<u>Run 1</u>	<u>Run 2</u>
Sample A	0	0
Sample B	4	2
Sample C	4	3
Sample D	0	0

13.3 Based on the pass-fail criterion of C795(no cracks allowed), samples A and D would pass. Samples B and C would fail.

13.4 The absence of cracks with insulation D is understandable since practically all of the "chloride + fluoride" was fluoride. It has been shown elsewhere that 60 days' exposure to 1500 ppm(mg/l) fluoride in a C692X qualification test, does not cause ESCC.

High-Temperature Calorimeter Performance Variable Study

REFERENCE: Troyer, R. L., "High-Temperature Calorimeter Performance Variable Study," *Insulation Materials, Testing, and Applications, ASTM STP 1030*, D. L. McElroy and J. F. Kimpflen, Eds., American Society for Testing and Materials, Philadelphia, 1990, pp. 699-709.

ABSTRACT: Oak Ridge National Laboratory with funding supplied by the Department of Energy sponsored the evaluation of a water calorimeter for thermal transmission testing of refractory fiber insulation using a ruggedness test. A round robin conducted on the calorimeter indicated that differences between laboratories are significant. The water calorimeter has several design characteristics that differ from other test methods. The energy transfer is measured by the increase in temperature of a constant water flow so the calorimeter is on the cold side and never exposed to high temperatures. With this test method the temperature difference across the sample is very large compared to some other instruments. In order to improve the test method a series of experiments was performed within a single laboratory to evaluate the sensitivity of the test method to deviations in standard practices. This experimental method is a ruggedness test, which is a statistical method of evaluating step changes while making multiple changes each test. Since this method is used for testing materials at different temperatures, essentially an independent ruggedness test was conducted at three temperatures. The factors evaluated included (1) emissivity of cold surface, (2) calorimeter to guard balance, (3) calorimeter to room temperature balance, (4) calorimeter water flow rate, (5) perimeter insulation, (6) type of hot side thermocouple, and (7) type of cold side thermocouple. Different factors were significant at different temperatures. Short and long term recommendations are given for improving the operation of the calorimeter.

KEY WORDS: calorimeter, ruggedness test, thermal conductivity, refractory fiber, emissivity

High temperature insulations such as brick and refractory fibers that are widely used by industry are often tested for thermal conductivity by a water calorimeter (ASTM C 182, C 201, C 202, and C 417). Presently only a refractory brick test method has been approved, but a new test method for refractory fibers is pending ASTM approval. A round robin between the four U.S. laboratories known to have calorimeters has shown great variability in interlaboratory results [1].

A "ruggedness" test was sponsored by Oak Ridge National Laboratory with funding by the U.S. Department of Energy because of a concern by ASTM Committees C-8 and C-16 about accuracy. The "ruggedness" test is one step in determining how much variation in calorimeter testing is due to laboratory practices and what these factors are.

Principles of a Calorimeter

The water calorimeter used for measuring thermal conductivity of refractory products was designed almost 40 years ago and has remained essentially unchanged. Figure 1 is a cross section of the apparatus. The bottom of the test area of the calorimeter is copper and is sectioned into four distinct areas with each area water cooled. Water flows through the center test area in

¹Section Manager of Research, Material Performance Evaluation, Manville Technology Section, Manville Corporation, Denver, CO 80217.

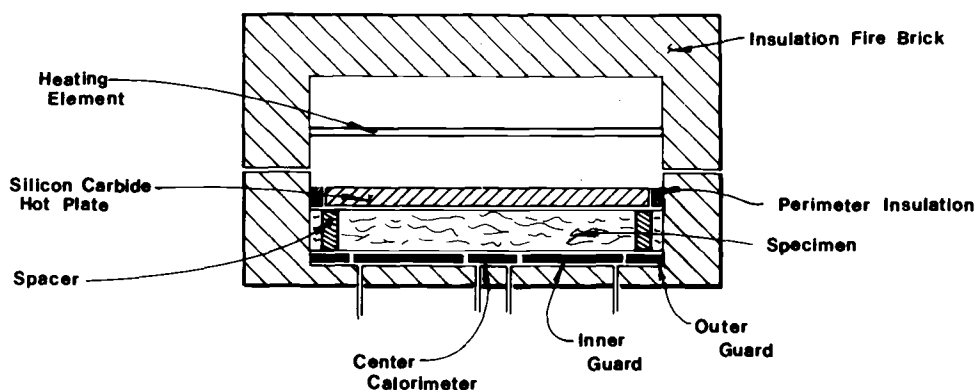


FIG. 1—Cross section of calorimeter apparatus.

a square double helix. On two sides the outside channel carries incoming water. On the other two sides, the outside channel carries outgoing water. The water is controlled at a constant pressure which results in a constant flow rate. The increase in water temperature is measured with a thermopile. The energy through the specimen is then calculated from the flow rate, increase in water temperature, and heat capacity of the water. This assumes an energy balance between calorimeter and guards and calorimeter and room. The balance between the center calorimeter and guards is measured by using two thermopiles as shown in cross section A-A of Fig. 2.

Water flows through two inner guards. The temperature of one guard is controlled by a thermopile which measures the temperature difference from the calorimeter to the guard. The second inner guard's temperature is controlled by another thermopile from the first guard. The specimens used for this ruggedness test were fibrous insulation with a density of approximately 0.4 kg/m^3 . This density was selected so that heat radiation would be a significant component of the total heat thickness.

Principles of a Ruggedness Test

Before a thorough evaluation can be made of an interlaboratory round robin, an experiment must be done within a single laboratory to evaluate the sensitivity of the test method to small deviations in standard practices. Often, a test method works well within a single laboratory with good repeatability and sensitivity but does very poorly when used in a number of laboratories.

A method of evaluation has been derived by Youden and Yates, who studied the power of statistics to resolve the problem [2-4]. The effectiveness of the ruggedness test was introduced to ASTM Committee C-8 on Refractories by Dr. Grant Wernimont [5,6].

Ruggedness Test Design

Seven factors were chosen to be tested in this ruggedness project. Each factor is evaluated at two levels. The fractional factorial design requires eight tests.

1. *Emissivity of Copper Plate*—The cold plate of a calorimeter is copper. Fibrous insulations have a radiation component of heat transfer so the plate surface emittance may affect test results.

2. *Calorimeter to Inner Guard Balance*—In order to obtain an accurate test the heat transfer between the calorimeter and guard must be very low. The calorimeter is surrounded by two

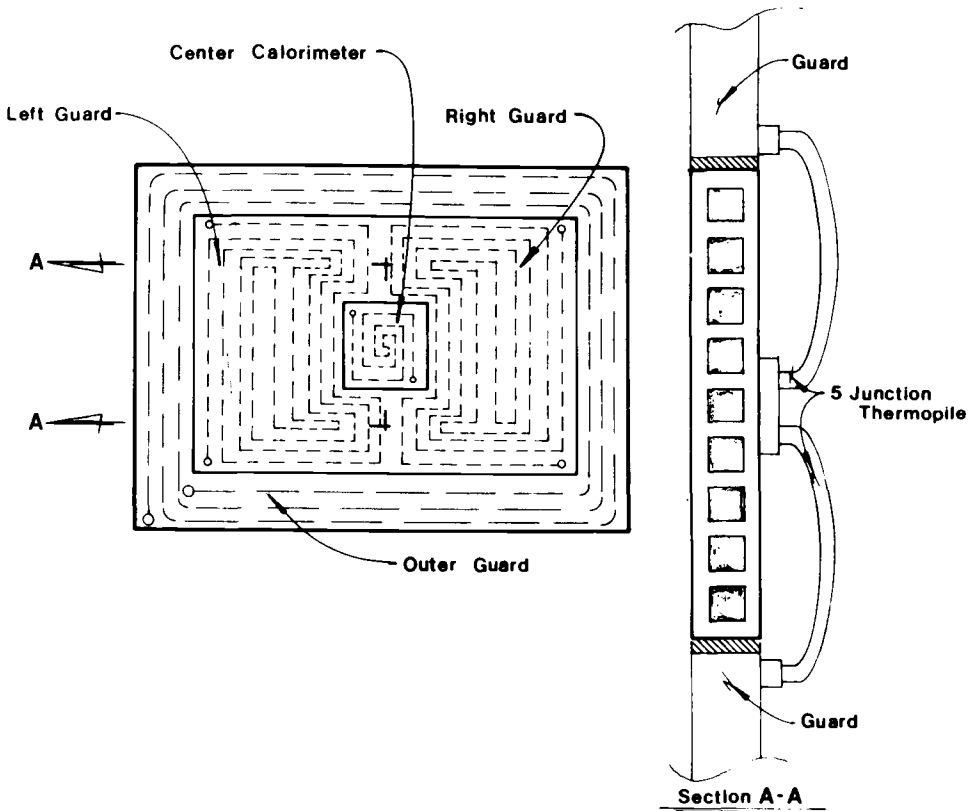


FIG. 2—Layout of calorimeter and guard.

guards. Because it is never possible to get the calorimeter to an exact balance, for the balanced condition a ΔT within ± 0.03 K was considered balanced and 0.3 K for unbalanced.

3. *Calorimeter Water Temperature to Room Temperature Balance*—With this particular instrument the room temperature acts as a guard to the calorimeter. The calorimeter is insulated with 25 mm thick fibrous insulation to reduce the energy flow to or from the room. For this ruggedness test, the room was maintained at a nominal 6 K above the calorimeter temperature for the unbalanced condition. For the balanced condition, the room temperature was maintained at ± 2 K to calorimeter temperature.

4. *Calorimeter Water Flow Rate*—For this trial the two levels of water flow rate were 80 and 200 cm³/min. The flow rate is an important factor that affects the accuracy of the test. If it is too low, flow rate measurements will be inaccurate. If flow rate is too high, the water temperature will be small and inaccuracies will result.

5. *Perimeter Insulation*—There is insulation around the edges of the silicon carbide plate to improve the temperature uniformity. The two levels used were 12.7 and 50.8 mm thick insulation.

6. *Hot Side Thermocouple*—The thermocouple on the hot side can be buried in the plate or laid between the insulation and plate.

7. *Cold Side Thermocouple*—Two methods of measuring the cold side temperature are to use a bead thermocouple laid between the plate and specimen or to glue a thin foil thermocouple to the cold plate.

The schedule of the ruggedness test is shown in Table 1 as designed by ASTM Committee C-8. Note that there are seven variables listed on the left side of the table as previously discussed, and eight trials are listed across the top of the table.

For the first trial, all parameters are upper case level. For the second trial, four factors are changed to the lower case level. For each succeeding trial, four factors are changed each time.

Each factor is at the upper case level four times and the lower case level four times. When a factor is in the upper case level, all other factors are upper case level twice and lower case level twice.

When a factor is at the lower case level, all other factors are at an upper case level twice and lower case level twice. As an example, look at the copper emissivity factor since it is at the top and easiest to follow. The first four trials are at upper case level or shiny copper. The meter is balanced twice in this condition and unbalanced twice. Likewise when the calorimeter is black the meter is balanced twice and unbalanced twice. By this arrangement the meter balance should not affect the results of the emissivity of the calorimeter unless there is an interaction. Each factor follows in likewise manner.

Ruggedness Test Results

The ruggedness test was conducted at three different hot side temperatures of nominally 588, 922, and 1366 K, with a repeat of the 922 K point. Table 2 is a compilation of the results. The numbers in the large box are the tested apparent thermal conductivity results in $W/(m \cdot K)$ for a specific set of test conditions. For example: the 0.0506 is the thermal conductivity at 588 K hot side with copper plate, meter balance of 0.1 MV, water room balance of $+6$ K, water flow rate of $200 \text{ cm}^3/\text{min}$, edge insulation thickness of 50.8 mm, hot side thermocouple in groove, and cold side thermocouple is attached foil.

By looking at the data, it is impossible to see easily what are the significant variables. The bottom half of Table 2 is a determination of significance at the 922 K point [5,6]. The average and difference are merely the average and difference of the first and repeat test at 922 K. S_1 is

TABLE 1—*Ruggedness test design.*

Variable	Level	Trial No.							
		1	2	3	4	5	6	7	8
1. Cu Emissivity	A = Shiny Copper a = Black	A	A	A	A	a	a	a	a
2. Meter Balance	B = 0.1 MV b = 0.01 MV	B	B	b	b	B	B	b	b
3. Water/Room Temp. Bal.	C = $+6$ K c = ± 2 K	C	c	C	c	C	c	C	c
4. Water Flow Rate	D = $200 \text{ cm}^3/\text{min}$ d = $80 \text{ cm}^3/\text{min}$	D	D	d	d	d	d	D	D
5. Edge Ins. Thick	E = 50.8 mm e = 12.7 mm	E	e	E	e	e	E	e	E
6. TC Position Carbide	F = Plate Groove f = Bead on Sample	F	f	f	F	F	f	f	F
7. TC Type on Cu Plate	G = Foil Attached g = Bead	G	g	g	G	g	G	G	g

TABLE 2—Summary of ruggedness results.^a

Hot Side Temp- erature, K	Thermal Conductivity at Trial No.								Average and Std. Deviation
	1	2	3	4	5	6	7	8	
(A) 588	0.0506	0.0528	0.0477	0.0469	0.0198	0.0469	0.0414	0.0479	$\left\{ \begin{array}{l} X = 0.0485 \\ S = 0.0039 \text{ (7.9\%)} \\ X = 0.0830 \\ S = 0.0033 \text{ (3.8\%)} \\ X = 0.164 \\ S = 0.0053 \text{ (3.2\%)} \end{array} \right.$
(B) 922	0.0862	0.0895	0.818	0.0805	0.0819	0.0803	0.0805	0.0842	
(C) 1366	0.169	0.171	0.160	0.163	0.162	0.154	0.162	0.167	
(D) 922	0.0855	0.0874	0.0800	0.0828	0.0833	0.0792	0.0822	0.0856	
(Repeat)									
For 922 K Only									
Average Difference	0.0859	0.0885	0.0809	0.0822	0.0826	0.0797	0.0813	0.0846	
	0.007	0.0021	0.0017	0.0023	0.0014	0.0011	0.0017	0.0014	
$S_1 = \sqrt{\frac{D^2}{2N}} = 0.0012$									
$S_D = S_1^2/4 = 0.00058$									
$X_1 \pm (3.36 \times S_D) = 0.0020 \text{ (99\% confidence)}$									
$N = \text{number of trials} - 8.$									

^aAll numbers except temperatures and percents are in W/(m · K).

the standard deviation on individual results within a batch which is equal to 0.0012. S_D is the standard error for differences between averages of the eight results, which is 0.00058. At the 99% confidence interval for judging differences, any number higher than 0.0020 would be considered significant. Note that this confidence interval is valid only for the 922 K point. Repeating the test for the other temperatures would have extended the scope of this project significantly. The standard deviations at 588 and 1366 K are on the same order of magnitude as at 922 K but somewhat larger in absolute values. For this report 0.0020 will be used as the test confidence interval for all temperatures.

The results at nominally 588 K hot side are shown in Table 3, at 922 K in Table 4, and at 1366 K in Table 5.

The assumption has previously been made that any number greater than 0.0020 is significant. As previously discussed, the results are averages for the test conditions. As an example, the 0.0495 for copper emissivity is the average of the first four trials, while the 0.0474 for black emissivity is the average of the last four trials. For each factor, all other values are at an upper

TABLE 3—*Ruggedness test results at 588 K.*

Factor	Level	Thermal Conductivity, W/(m · K)	Thermal Conductivity Difference
1. Copper Emissivity	Copper	0.0495	0.0021
	Black	0.0474	
2. Meter Balance	0.1 MV	0.0509	0.0049
	0.01 MV	0.0460	
3. Water/Room Balance	±2 K	0.0486	0.0003
	+6 K	0.0483	
4. Flow Rate	200 cm ³ /min	0.0482	0.0005
	80 cm ³ /min	0.0487	
5. Edge Insulation	50.8 mm	0.0483	0.0003
	12.7 mm	0.0486	
6. Hot Side TC	Plate	0.0497	0.0025
	Sample	0.0472	
7. Cold Side TC	Foil	0.0464	0.0041
	Bead	0.0505	

TABLE 4—*Ruggedness test results at 922 K.*

Factor	Level	Thermal Conductivity, W/(m · K)	Thermal Conductivity Difference
1. Copper Emissivity	Copper	0.0845	0.0027
	Black	0.0818	
2. Meter Balance	0.1 MV	0.0845	0.0027
	0.01 MV	0.0818	
3. Water/Room Balance	±2 K	0.0836	0.0010
	+6 K	0.0826	
4. Flow Rate	200 cm ³ /min	0.0851	0.0039
	80 cm ³ /min	0.0812	
5. Edge Insulation	50.8 mm	0.0832	0.0001
	12.7 mm	0.0831	
6. Hot Side TC	Plate	0.0832	0.0001
	Sample	0.0831	
7. Cold Side TC	Foil	0.0819	0.0025
	Bead	0.0844	

TABLE 5—*Ruggedness test results at 1366 K.*

Factor	Level	Conductivity, W/(m · K)	Conductivity Difference
1. Copper Emissivity	Copper	0.1655	0.0041
	Black	0.1614	
2. Meter Balance	0.1 MV	0.1640	0.0011
	0.01 MV	0.1629	
3. Water/Room Balance	±2 K	0.1635	0.0001
	+6 K	0.1634	
4. Flow Rate	200 cm ³ /min	0.1671	0.0073
	80 cm ³ /min	0.1598	
5. Edge Insulation	50.8 mm	0.1627	0.0015
	12.7 mm	0.1642	
6. Hot Side TC	Plate	0.1653	0.0035
	Sample	0.1618	
7. Cold Side TC	Foil	0.1618	0.0035
	Bead	0.1653	

case level and a lower case level an equal number of times. We can then come to the conclusion at 588 K hot side that water/room balance, flow rate, and edge insulation are not significant, while all others are significant. This conclusion is valid only at 588 K hot side since, at other temperatures, different factors may be significant.

One may have observed that at 922 K there is a different set of significant factors. Water/room balance, edge insulation, and hot side thermocouple are not significant, while all other factors are significant. There will be a table later comparing the results at all three temperatures.

One may have observed that at 1366 K there is again a different set of significant factors: meter balance, water/room balance, and edge insulation are not significant, while all remaining factors are significant.

To better understand how the factors change with temperature, see the results in Table 6. Each factor will be reviewed separately.

1. *Copper Emissivity*—The emissivity of the cold plate is a significant factor at all temperatures. This is not surprising, since the product was chosen to be low in density so that there would be a significant radiation component of energy transfer. However, there is a contradiction with the results in that the conductivity is higher with a copper plate than with a black

TABLE 6—*Comparison of results at different temperatures.*

Factor	Conductivity ^a Difference @588 K	Conductivity ^a Difference @922 K	Conductivity ^a Difference @1366 K
1. Copper Emissivity	0.0021	0.0027	0.0041
2. Meter Balance	0.0049	0.0027	0.0011
3. Water/Room Balance	0.0003	0.0010	0.0001
4. Flow Rate	0.0005	0.0039	0.0073
5. Edge Insulation	0.0003	0.0001	0.0015
6. Hot Side TC	0.0025	0.0001	0.0035
7. Cold Side TC	0.0041	0.0025	0.0035

^aW/(m · K).

plate. All accepted theory indicates that conductivity must be higher with the black cold surface. This knowledge prompted a review of the data to see if the reason could be determined.

For this ruggedness test all the thermocouples were in place for all the trials and the appropriate thermocouples were attached to the data logging equipment which was in turn interfaced to a computer. The results are thus calculated for only the parameters as specified in the ruggedness test.

The cold side measured temperatures are shown in Table 7 for the 1366 K trial.

It is obvious that at 1366 K hot side there is a temperature measurement problem when comparing a high emissivity surface to a shiny copper surface. Keep in mind that in all cases the exit water temperature was in the 300 K range. When the surface is copper, the foil thermocouple and bead thermocouple are 2 to 6 K different. This variation may be somewhat dependent on other factors. When the surface is painted black there is 40 to 48 K difference. The difference in temperature when the surface is black results in approximately 4% difference in calculated conductivity. The difference in conductivity when the cold surface is painted black versus shiny copper is approximately 3 1/2%, so it is obvious that the major reason for the difference is a temperature measurement problem. The same trend follows at lower temperatures except to a smaller degree.

2. Meter Balance—The meter balance appears to be a very significant factor at 588 K but decreases until it is not a significant factor at 1366 K. The ruggedness test was run with one level of 0.1 MV unbalanced and the second level as close to balanced as possible. When unbalanced at the 0.1 MV level, the energy that flows from the metering area to the guard is approximately independent of the heat flow through the specimen. If one assumes a conductivity of 0.14 W/(M · K) for the filler between the meter and guard, a gap width of 0.8 mm, and a ΔT of 0.3 K, then the heat flow from meter to guard is about 0.09 W. This rough calculation is within 20% of the results obtained in the ruggedness test. At 588 K hot side, the heat flow from meter to guard is 10% of the heat flow through the specimen; this drops to 2 1/2% at 922 K and 1/2% at 1366 K.

3. Water/Room Balance—This factor was not significant for any temperature. We concluded that, if a calorimeter is reasonably well insulated and the room temperature kept within the ASTM specification, then heat exchange with the room is insignificant.

4. Flow Rate—The ruggedness test was conducted with water flow rates of 80 and 200 cm³/min. The water flow rate is under the 99% confidence interval for 588 K, but for 922 K it is definitely significant, and at 1366 K it is the largest factor for the whole ruggedness test.

To understand why flow rate is such a significant factor one must go back to the design of the flow pattern of the test area (Fig. 3). The design of the calorimeter can be described as a square double helix. The temperature along two sides is primarily controlled by the temperature of the inlet water temperature; the temperature of the other two sides is primarily controlled by the water temperature of the outlet water temperature. Keep in mind that the temperature balance is controlled by two thermopiles with five junctions each, but that they read the temperature at

TABLE 7—Cold side measured temperatures with 1366 K hot side.^a

	Copper Surface				Black Surface			
	Trial 1	Trial 2	Trial 3	Trial 4	Trial 5	Trial 6	Trial 7	Trial 8
Bead	342.5	345.4	348.5	351.0	349.2	355.8	356.7	356.4
Foil	349.2	350.3	351.7	352.7	309.0	307.8	308.7	308.8
Diff.	-6.7	-4.9	-3.2	-1.7	40.2	48.0	48.0	47.6

^aAll temperatures are in Kelvin.

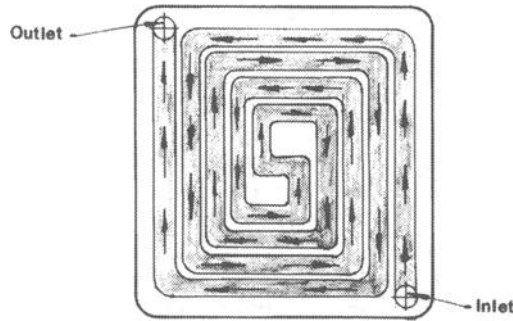


FIG. 3—Water flow pattern of calorimeter.

only two locations. The thermopiles are located on the bottom of the calorimeter and guard (Fig. 2). At a 1366 K hot surface there is a significant temperature increase, especially at low water flow rates. At 1366 K the increase in water temperature would be about 4.4 K, so the energy balance is sensitive to where the balance thermopile is placed.

5. *Edge Insulation*—The edge insulation here refers to the insulation above the specimen and around the silicon carbide plate perimeter. The thickness of edge insulation was not significant for the specimen thickness tested.

6. *Hot Side Thermocouple*—The hot side for this apparatus can be as high as 1813 K, so the thermocouples commonly used are platinum-platinum 10% rhodium. For the ruggedness test the two levels are the thermocouple buried in the silicon carbide plate and the thermocouple sandwiched between the specimen and plate. The ruggedness test showed significance at 588 and 1366 K but not at 922 K.

7. *Cold Side Thermocouple*—The two levels for this trial were a welded 26-gage Type T thermocouple or a foil-type T thermocouple. The latter was 0.01 mm foil attached to a plastic base and was attached directly to the calorimeter with adhesive, while the bead thermocouple was laid between the cold plate and specimen. The type of thermocouple is significant at all temperatures but, again, it is unaccountably at a lower level at 922 K. The cold side thermocouple temperature was previously discussed. When the cold surface is painted black, there is a large difference between the measurements with different types of thermocouples. Standardization is obviously needed on cold side thermocouples, and several recommendations will be made later in the report.

Recommendations and Conclusions

The calorimeter is a good method of measuring heat flow with several inherent advantages over other methods. Firstly, the energy measuring calorimeter is on the cold side of the apparatus, which makes maintenance much easier than the guarded hot plate where the energy measuring device is necessarily on the hot side. Secondly, the calorimeter measures heat flow with a large ΔT , which is information needed for many applications. Most other types of apparatus have a limited ΔT that can be tested.

The round robin sponsored by ASTM Committee C-8 showed considerable differences between laboratories [1]. This ruggedness test shows that a number of factors contribute to error in the calorimeter.

The factors that definitely affect the test results are:

1. Meter balance.
2. Flow rate.

3. Method of measuring hot side temperature.
4. Method of measuring cold side temperature.

Other factors may affect the results, but the differences are not large enough to be statistically significant.

1. *Copper Emissivity*—The ruggedness test indicates that emissivity is a factor but that conductivity changes in the opposite direction from that expected. This was also reported by Chaille and Wahle [7]. In this particular test, the evidence points toward a temperature difference rather than an actual difference in conductivity. In the same report by Chaille and Wahle the theoretical difference would be approximately 2%. A 2% change is on the threshold of detection for this ruggedness test. The recommendation is that the cold surface be painted black with an emittance of ≥ 0.8 to eliminate any doubt.

2. *Meter Balance*—The meter was unbalanced significantly outside of specification and caused a very large error when unbalanced. The specification in the standard test method must be rigidly followed.

3. *Water/Room Balance*—For the ruggedness test the temperature of the center calorimeter was maintained as close to room temperature as possible for one level and the room was maintained at 6 K above the calorimeter for the other level. The change in room temperature did not have a significant effect on results, so the present standard is satisfactory.

4. *Flow Rate*—This parameter had a large impact on the results. At high temperatures and low flow rate the increase in water temperature was significant, which could easily cause error due to heat exchange. Short and long term recommendations are as follows:

- (a) Replace the bakelite with a better insulator as proposed by ASTM Committee C-8.
- (b) Have a specification to control the flow rate.
- (c) Design the edges of the calorimeter to guard with a notched gap as is frequently used in guarded hot plates (Fig. 4).
- (d) Change the design of the water flow so that it is easier to balance the edges (Fig. 5). This design has the advantage of having all of the outside at approximately the temperature of the inlet water. Since the outside edge of the calorimeter is of more uniform temperature, balance would be improved.
- (e) Use multiple distributed thermocouples to determine balance rather than two thermopiles at two points.

5. *Edge Insulation*—Edge insulation level is probably not significant.

6. *Hot Side Thermocouple*—There is a significant difference in how the hot side temperatures are measured. The ASTM Committee C-8 has recommended burying the thermocouple on the hot side.

7. *Cold Side Thermocouple*—There is a significant difference in how the cold side temperatures are measured. This ruggedness test showed a large difference between bead and foil thermocouples. There are some indications that even the foil thermocouple, which has the best surface contact, has some problems. This whole area needs further study. As a short term solu-

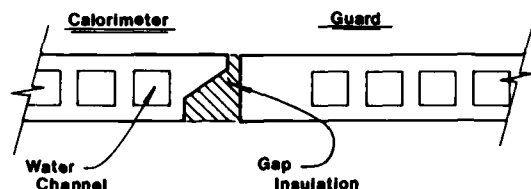


FIG. 4—Cross section of possible gap configuration.

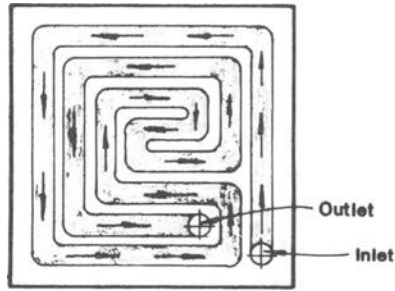


FIG. 5—Possible pattern of calorimeter.

tion, a foil thermocouple glued to the cold surface should be specified. In the long term burying the thermocouples in the copper should be considered.

References

- [1] Ober, D. G., "Final Report on ASTM Committee C-8 Thermal Conductivity Ceramic Fiber Round Robin," in *Thermal Insulation: Materials and Systems*, ASTM STP 922, American Society for Testing and Materials, Philadelphia, 1988, pp. 685-703.
- [2] Yates, F., "Complex Experiments," *Royal Statistical Society, Supplement*, Vol. 2, 1935, p. 181.
- [3] Youden, W. J., "Designs for Multifactor Experimentation," *Industrial and Engineering Chemistry*, Vol. 51, No. 10, Oct. 1959, pp. 79-80.
- [4] Youden, W. J., "Experimental Design and ASTM Committees," *Materials Research and Standards*, Vol. 1, Nov. 1961, pp. 862-867.
- [5] Wernimont, G., "Ruggedness Evaluation of Test Procedures," *ASTM Standardization News*, Vol. 5, March 1977, pp. 13-16.
- [6] Wernimont, G., "Development and Evaluation of Standard Test Methods: The Role of Statistical Design of Experiments," *Materials Research and Standards*, Vol. 9, Sept. 1969, pp. 8-20.
- [7] Chaille, C. E. and Wahle, H. W., "Evaluation of ASTM C 201 Apparatus for Measuring the Thermal Conductance of Ceramic Fiber Insulation," in *Thermal Insulation Performance*, ASTM STP 718, D. L. McElroy and R. P. Tye, Eds., American Society for Testing and Materials, Philadelphia, 1980, pp. 208-224.

Jerome G. Hust,¹ B. James Filla,¹ James A. Hurley,¹ and David R. Smith¹

An Automated High-Temperature Guarded-Hot-Plate Apparatus for Measuring Apparent Thermal Conductivity of Insulations Between 300 and 750 K

REFERENCE: Hust, J. G., Filla, B. J., Hurley, J. A., and Smith, D. R., "An Automated High-Temperature Guarded-Hot-Plate Apparatus for Measuring Apparent Thermal Conductivity of Insulations Between 300 and 750 K," *Insulation Materials, Testing, and Applications, ASTM STP 1030*, D. L. McElroy and J. F. Kimpflen, Eds., American Society for Testing and Materials, Philadelphia, 1990, pp. 710-722.

ABSTRACT: An automated guarded-hot-plate apparatus was designed and built to meet the requirements of ASTM standard test method C 177 for measuring the thermal transmission properties of thermal insulation. The apparatus is controlled by a scientific desktop computer. Measurements with this apparatus can be performed at temperatures from 300 to 750 K in environments of different gases at pressures ranging from atmospheric pressure to roughing-pump vacuum. A novel design for a thermocouple device is used; this device more accurately senses the average temperature over the surface of each heater plate. An improved algorithm for the control sequence provides more stable heater powers and specimen temperatures. Initially the algorithm brings the system rapidly to a temperature setpoint with minimal overshoot. It also permits highly sensitive control of the plate temperatures in later phases of the measurement sequence when thermal stability of the specimen boundaries is very important in measuring the thermal conductivity with high precision. Overall uncertainties of thermal conductivities at atmospheric pressure are 2% at 300 K and 3% at 750 K.

KEY WORDS: automated control system, guarded-hot-plate apparatus, high temperature, mean-temperature sensor, thermal conductivity, thermal insulation, thermocouple device

Nomenclature

k	Thermal Conductivity
A	Area of Metered Section
DVM	Digital Voltmeter
emf	Electromotive Force (Potential Difference)
GHP	Guarded Hot Plate
I	Electric Current

¹Chemical Engineering Science Division, National Engineering Laboratory, National Institute of Standards and Technology, U.S. Department of Commerce, Boulder, CO 80303-3328. Direct all correspondence to Dr. Smith.

MH	Main Heater
PID	Proportional, Integral, and Derivative
PRT	Platinum Resistance Thermometer
Q	Heater Power
R	Resistance
RTD	Resistive Temperature Detector (Thermometer)
SRM	Standard Reference Material
$\Delta T_1, \Delta T_2$	Temperature Difference Across Each Specimen
T_C	Temperature of Cold Surface of Specimen
T_H	Temperature of Hot Surface of Specimen
TC	Thermocouple
V	Potential Difference
ΔX	Specimen Thickness

Introduction

The U.S. National Institute of Standards and Technology (NIST) establishes Standard Reference Materials (SRMs) needed to improve accuracy in the measurement of physical properties. During the past ten years the Center for Chemical Engineering (CCE) within NIST has helped establish SRM-1450b and SRM-1451 for thermal insulation at temperatures from 100 to 330 K [1-6]. The low-temperature data for certifying these SRMs from CCE were obtained with a guarded-hot-plate (GHP) apparatus [7] designed to be used at ambient and low temperatures.

Both industry and NIST have for several years recognized the need for thermal insulation SRMs for use at higher temperatures. Several years ago CCE began to design and construct a high-temperature GHP apparatus capable of measuring thermal conductivity to temperatures of at least 750 K. This apparatus has been completed and tested to establish its precision and bias. The tests include measurement of the thermal resistance of SRM 1450b at temperatures from 300 to 350 K and of two candidate SRMs from 320 to 750 K. These measurements use environments of different gases, double-sided as well as single-sided heat flow, small and large temperature gradients, runs with temperature offsets on the primary and secondary guards, and investigations of the effect of drift of the specimen temperature. The results of these measurements, along with comparisons to previously published data, are used to assess the precision and bias of the new GHP apparatus.

The initial design of the high-temperature GHP apparatus was guided by the following criteria: (a) the size of the hot plate should be typical of those commonly in use, (b) the temperature range of the apparatus should be large enough to satisfy a significant need but not so large as to delay its timely completion, and (c) the apparatus should be totally automated. A logical extension of item (c) was to construct the system for control and data acquisition in such a way that it could also be used to operate the previously described low-temperature GHP system [7]. This has been done.

This paper is a synopsis of a more complete report [8], which can be obtained from DRS.

Apparatus Elements

This GHP apparatus is consistent with the specifications of ASTM Test for Steady-State Heat Flux Measurements and Thermal Transmission Properties by Means of the Guarded-Hot-Plate Apparatus (C 177). It differs from the low-temperature GHP apparatus only in the diameter of

its measurement "stack" and in the materials used in its construction. The stack elements of the apparatus are illustrated in Fig. 1 with the associated environmental-control components. A block diagram of the electronic system for control and data acquisition is shown in Fig. 2. The entire computer software package that completes the automation of the system is listed in an appendix of Ref 8.

Stack and Environmental Control Elements

The stack is surrounded by a cylindrical secondary or outer guard. Alumina, with its high melting point and relatively high thermal conductivity for an insulating material, was chosen as the material for the outer guard and heater plates. Each copper cold plate (6 mm thick) and

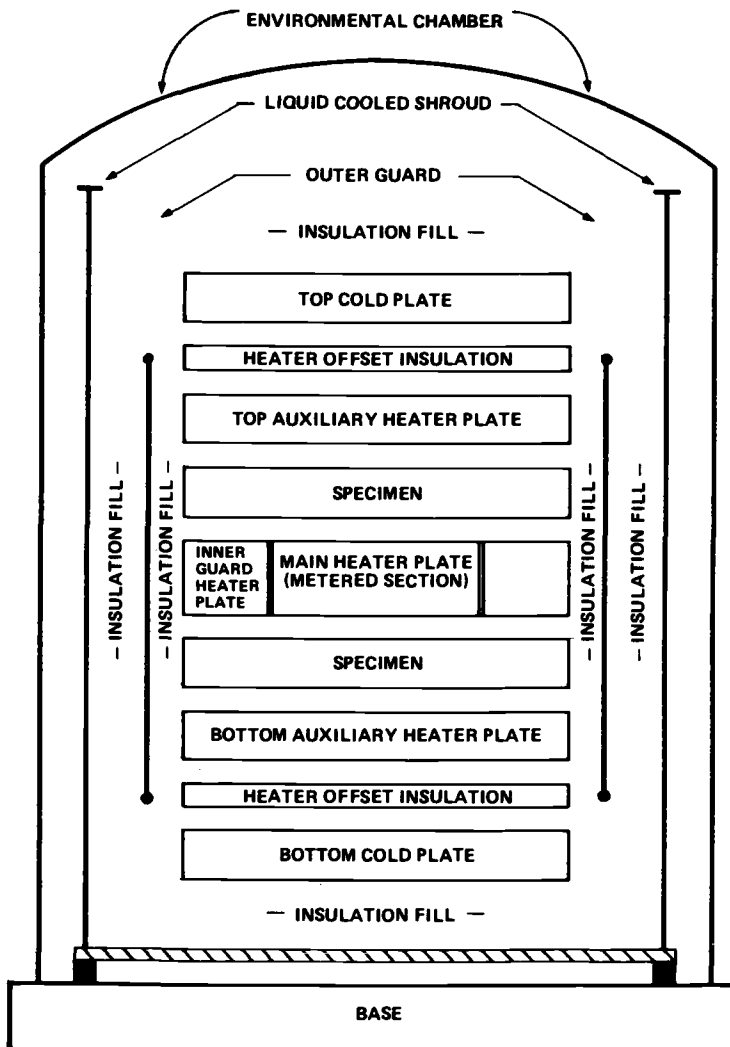


FIG. 1—Layout of thermal conductivity stack, guards, shroud, and environmental chamber of the NIST high-temperature guarded-hot-plate apparatus.

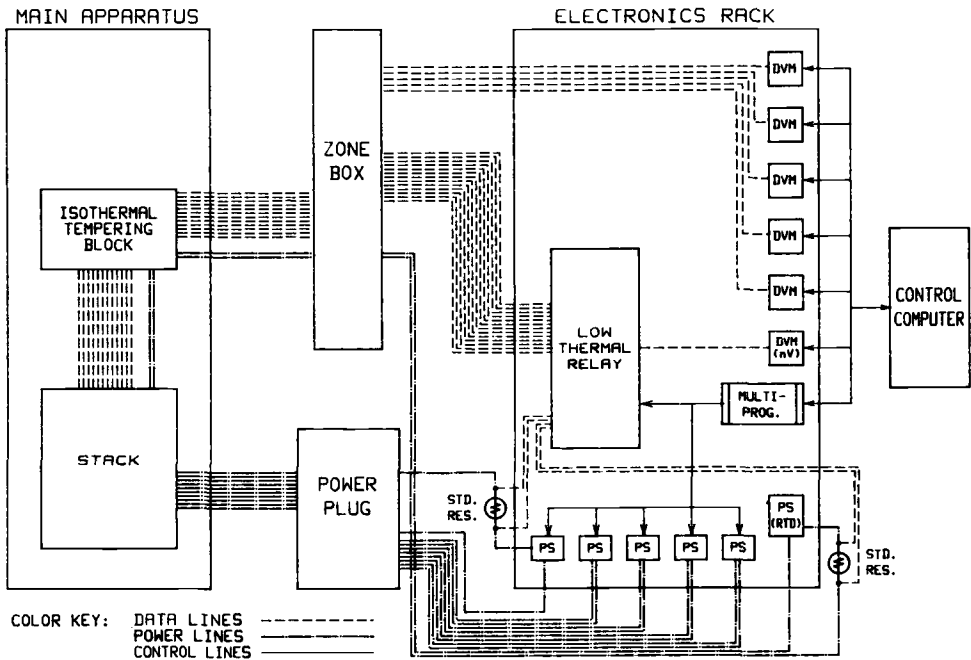


FIG. 2—Block diagram of electronic system for control of temperature and acquisition of data.

each sintered-alumina heater plate (25 mm thick and 3.2 kg mass) is a circular disk 25.4 cm (10.0 in.) in diameter. A 25 mm thickness of calcium silicate heater-offset insulation permits the use of a wide range of specimen temperature differences within the limitations of the power supplies.

Nisil/Nicrosil thermocouples,² resistant to the effects of high temperatures, are used to sense the temperatures of the heater surfaces. Type-K thermocouples, for example, have greater sensitivity but deteriorate ("green rot") at high temperatures. Sensitive control of each heater or guard is achieved by mounting platinum resistance thermometers (PRTs) on them.

Each cold plate comprises two copper disks soldered together. Two symmetric spiral grooves are machined next to each other in the inner surface of each disk and are connected at the center. These form a counterflow heat exchanger for the entering and exiting streams of coolant and minimize the temperature differences within the cold plates induced by the temperature difference between the two streams.

Each stack heater plate (main, top, and bottom) was constructed from two alumina disks, one of which was grooved. The grooves were cast as two adjacent spirals connected at the center of the plate. This design is a convenient way to distribute the heating power uniformly over the heater area. Platinum heater wire was held within the grooves with refractory cement, which also held the two plates together. The heater wire in the grooves lies in the plane midway between the top and bottom surfaces of the assembled heater plate.

To make the plate for the main heater and inner guard, the centers of two plates, identical to those used for the auxiliary heaters, were cut out with diameters half of that of the whole plate. The central core became the main heater, and the annulus, the inner guard.

²Trade names, given purely for identification, do not imply endorsement by NIST. Similar products of other manufacturers may work as well or better.

The outer guard is a 4.6 kg circular cylinder of cast alumina with a thickness of 6 mm, a length of 20 cm, and an outer diameter of 31 cm, surrounding the stack from the bottom auxiliary heater plate to the top auxiliary heater plate. An aluminum shroud surrounds the stack and contains the loose-fill insulation, which limits the loss of heat from the stack.

Surrounding the entire stack-shroud assembly is a stainless steel environmental-control chamber which allows us to introduce different gases or to evacuate the space around the stack.

Mounting of Thermocouples and PRTs

Thermocouples are used at the centers of the heater plate surfaces to sense the absolute temperature needed to obtain the thermal conductivity, with minimum distortion of the isotherms and heat flux lines within the specimens. Four-lead PRTs are used as sensors in the control circuits to control the desired plate temperatures.

One PRT was cemented into the periphery of each auxiliary heater plate. Another PRT was similarly mounted on the metered (main) plate within the gap between it and the inner guard. The PRT for the outer guard was cemented to its outside surface.

A unique three-lead thermocouple combination was designed to measure accurately the average temperature over the surface of each heater plate. This three-lead device results in significantly more accurate measurements of the average temperature of a surface than those obtained with a single thermocouple. See Ref 9 for a more detailed discussion of the theoretical basis, construction, and comparative performance of this device.

The temperature difference across the gap between the metered plate and the inner guard is controlled with a 20-element thermopile. Ten thermopile elements lie on the top surface of the plate; the other ten are on the bottom. Control is exercised using the whole thermopile, but a third lead is connected to the junction between the two halves so that the top and bottom thermopiles can be monitored separately. The thermopile junctions are uniformly placed along the circumference of the gap at locations alternating between its opposite sides, 4 mm from the edges of the gap.

System for Data Acquisition and Control

The system for acquiring data and controlling temperature and power is composed of two principal parts: (a) the computer and (b) the power supplies and digital voltmeters (DVMs). The schematic arrangement of these components is shown in Fig. 2. The DVMs used to read the thermocouple emfs or potential differences across the PRTs have precisions of at least $5\frac{1}{2}$ digits. The computer selects each thermocouple emf or potential difference to be read through the use of two switching-relay modules having low parasitic thermal emfs.

The core of the control system is a modified digital proportional-integral-derivative (PID) controller of novel design based in software residing in the computer. Its algorithm for PID control of the power supplied to the heater plates provides for vigorous heating and rapid approach to the desired temperature when the controlled temperature is far from the setpoint, yet gives very sensitive control when the controlled temperature is near the setpoint. The control gains vary as Gaussian error functions. At the setpoint, the integral gain peaks, the derivative gain vanishes, and the proportional gain has a non-zero minimum. The algorithm is described in greater detail in Ref 10.

Specimen Thickness Spacers

Some specimens compress under the weight of the overlying stack plates. The thickness of the specimens then varies with time, due to creep. To slightly compress these specimens and

thereby assure good thermal contact between heater plates and specimens, the plates are held apart with rigid spacers. They are made with lengths shorter than the specimen thickness by about 0.2 mm. Three equally spaced notches are cut into the outer periphery of each specimen to hold the thin-walled, tubular stainless-steel spacers between the outer edges of the inner guard and auxiliary heater plates. These spacers are filled with fibrous refractory insulation to reduce the possibility that radiative and convective heat transfer within their interiors would shunt the conductive heat transfer through the specimens.

Operation

After the specimens have been prepared and installed, the computer program is started. During the initial part of the run the computer prompts the operator for detailed information on the characteristics of the particular specimens and run. The operator may choose whether the system should be controlled at constant temperature or at constant power.

After the operator has keyed in the required information, the computer begins an automatic sequence of control of the experimental conditions and acquisition of data. During this automated sequence, the operator may view on the computer monitor various plots illustrating the behavior of any of the controlled heaters, and in addition may change setpoint temperatures and other control parameters during the run.

Each measurement sequence is divided into three phases. In Phase I, the desired temperatures are established at the surfaces of the heater plates facing the specimens. When these temperatures and the main heater power have stabilized within preset limits, the sequence enters Phase II.

During this second phase thermal conductivity is computed every 3 min. After the first 30 min of Phase II the main heater power and the calculated thermal conductivity are examined for stability within specified limits, allowing entry into Phase III if the stability criteria are met.

In this last phase the operator is allowed to make a permanent printed record of the history of the various plate temperatures, the power to the metered heater, or the thermal conductivity calculated as successive 3-min time averages. Then, if the operator does not intervene, the computer automatically averages the last 30 min of data for storage on disk. Data from any longer interval may be averaged if the operator so chooses. All the data from Phase II are saved to disk for later re-analysis as desired.

At the end of a typical experimental sequence a summary of the conditions of the experiment is printed out. Also included are final values of measured temperatures and temperature differences, heater power, and thermal conductivity for the experiment. Statistical measures of the random variations of these quantities, averaged over the interval of stability at the end of the run, are listed.

Both Phase I and Phase II have predetermined maximum time limits, which force the run to be completed after a definite time interval in cases where the stability requirements are too stringent in the control software.

Typical graphical outputs that may be viewed during the measurement sequence and printed at the end of the run are given in Figs. 3 to 6. Figure 3 shows the initial approach to equilibrium of the main heater plate under control of the automated system. Figure 4 depicts typical behavior of the final temperature of the main heater plate during stable operation at the setpoint. The amplitude of these temperature fluctuations is about ± 5 mK.

Figure 5 shows that the power fluctuation amplitude has decayed to relatively small values (± 10 mW), a direct result of the PID control algorithm, when the control system operates in the constant-temperature mode. The data illustrated in Figure 6, averaged every 3 min over the last 60 min of the run, gave a value for thermal conductivity of $22.07 \text{ mW}/(\text{m} \cdot \text{K})$, with a standard deviation of $0.028 \text{ mW}/(\text{m} \cdot \text{K})$. This represents a relative deviation of 0.13%, which is typical behavior for most temperatures of operation.

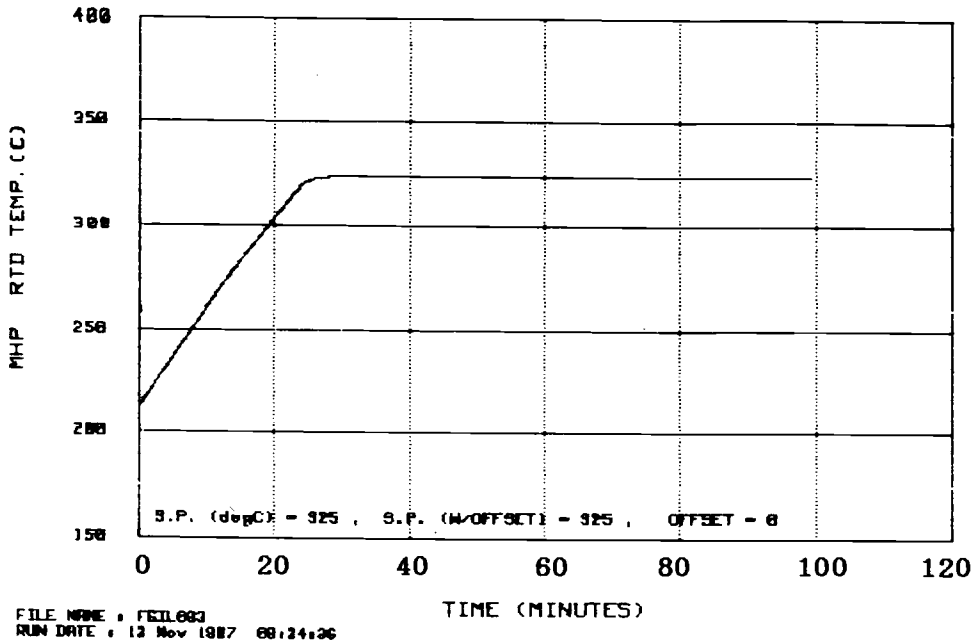


FIG. 3—Temperature of main heater plate, measured by resistance thermometer, versus time: behavior during initial approach to set-point.

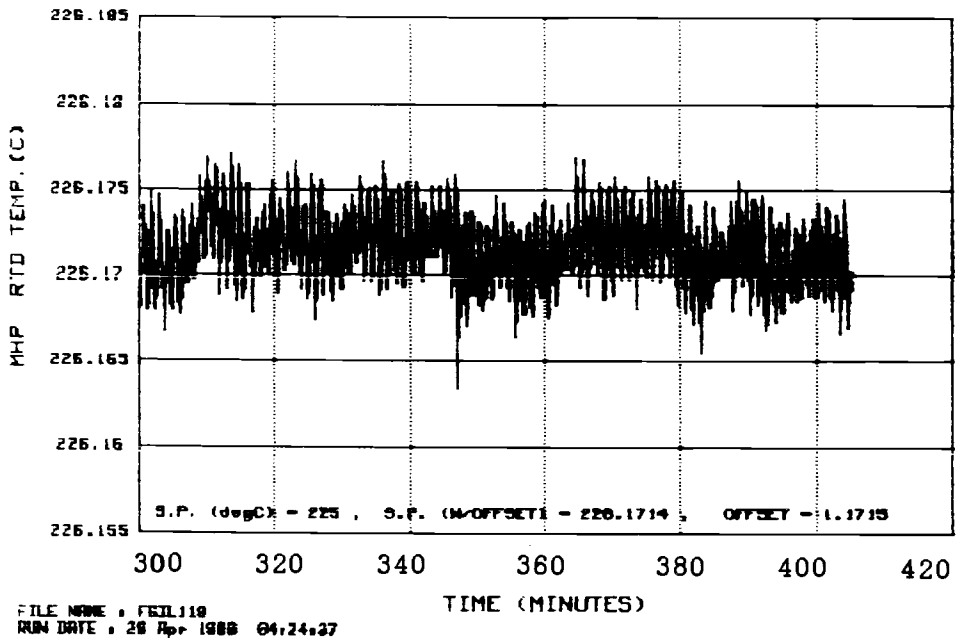


FIG. 4—Temperature of main heater plate, measured by resistance thermometer, versus time: behavior during stable operation at set-point.

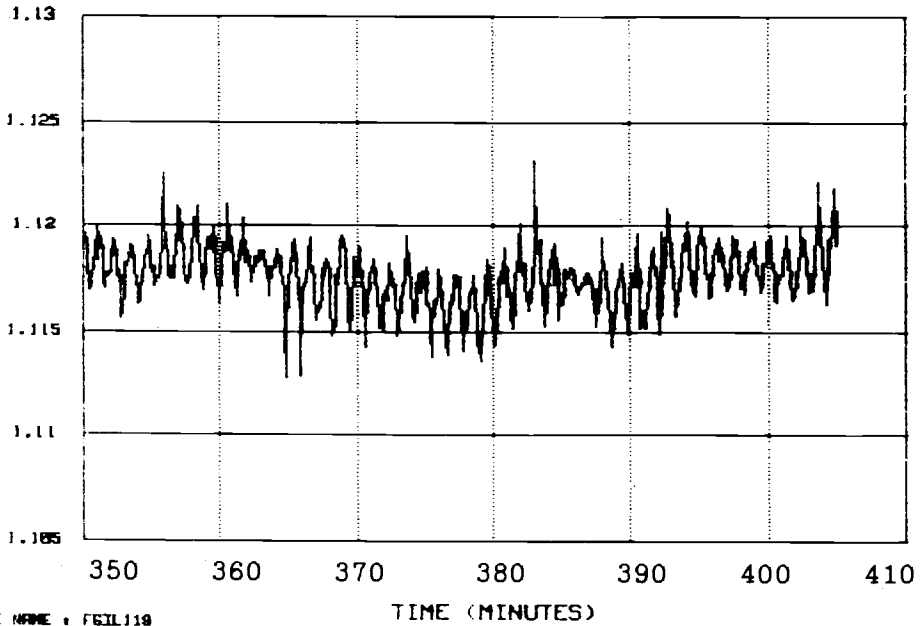


FIG. 5—Main heater power versus time: behavior during stable operation at set-point.

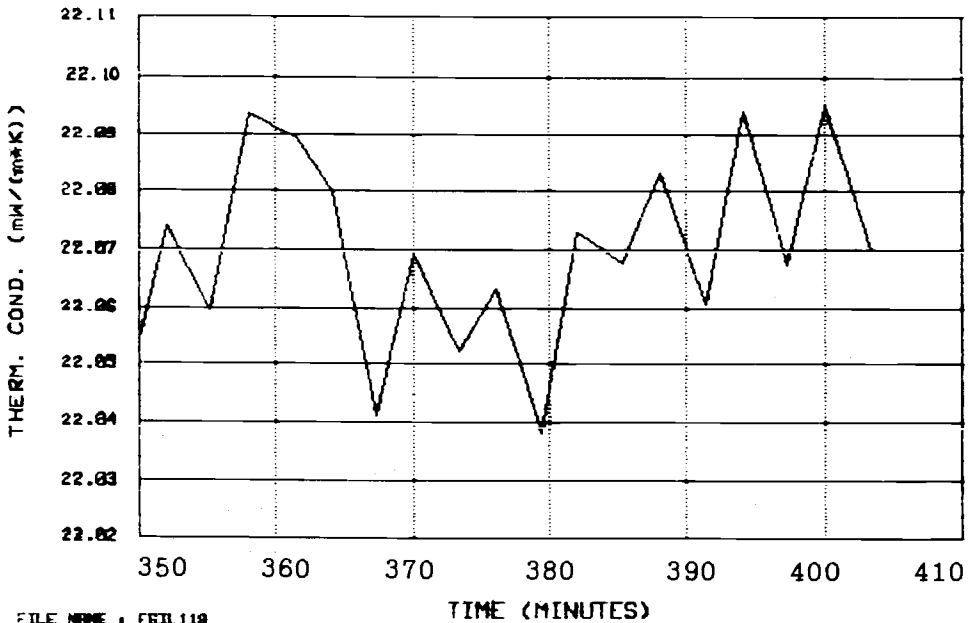


FIG. 6—Experimental thermal conductivity, calculated from main heater power, specimen area, and temperature gradient, versus time: behavior during stable operation at set-point.

Primary Measurements

The normal mode of operation of the GHP apparatus is referred to as the "double-sided" mode and results in an average value of k for two specimens. Alternatively we can adjust the temperature of one of the auxiliary heaters to match that of the main heater, thus minimizing the flow of heat through the specimen in that direction. This is referred to as the "one-sided" mode of operation and results in the k value for the other specimen, through which most of the heat flows. To accommodate both modes of operation, the relation

$$k = Q \Delta X / (A(\Delta T_1 + \Delta T_2)) \quad (1)$$

is used to calculate thermal conductivity, where Q is the rate of flow of heat through the metered portion of the specimen, ΔX is the average thickness of the specimen, A is the metered area (including one half of the gap area), and ΔT_1 and ΔT_2 are respectively the temperature differences across the two specimens. For the one-sided mode either ΔT_1 or ΔT_2 is small, but this small value can be either positive or negative.

The term *average thermal conductivity* has been used here to denote two types of averaging. First, in the double-sided mode the arithmetic average value of k for the two specimens is obtained. No information on either specimen individually can be calculated from measurements in this mode. Second, the value of k averaged with respect to temperature from the cold-face temperature, T_C , to the hot-face temperature, T_H , is obtained in either the single- or double-sided mode. As a rule of thumb, if this temperature difference ΔT between the two faces is less than 10% of the absolute mean temperature of the specimen, $(T_C + T_H)/2$, the value of k can be assigned to the mean temperature with negligible error. If ΔT is significantly larger, the k value obtained may be measurably different from the true k value corresponding to that mean temperature. In such cases, the integral method of analysis as described by Hust and Lankford [11] is used to obtain k as a function of temperature.

There is also a third type of averaging involved in the calculation of k using this apparatus: an average over time. Time-averaging is done to reduce the effect of the imprecision of the individual readings. The minimum time interval for this averaging process, occurring in Phase II, is 30 min. During this period values of temperature are obtained every 3 min; thus the time-averaged value of T involves a minimum of 10 readings. The values of potential difference and current needed to obtain the power are read every 5 s; thus the time-averaged value of power involves a minimum of 360 readings.

Analysis of Precision and Bias

The imprecision and bias of this apparatus were analyzed by two methods: (a) from analysis of the propagation of error due to the imprecision and bias inherent in measurements of primary variables, and (b) from the measurement of standard reference specimens. Only uncertainties in experimental control and measurement were considered.

Experimental Reproducibility

Thermal conductivities were repeatedly measured for a clay-bonded fibrous alumina-silica thermal insulation board being considered for adoption as a high-temperature SRM. The imprecision of these results with removal and re-installation of the specimens in new orientations is 0.5%.

Measurements on a Fibrous Glass Insulation SRM

One series of comparison measurements of thermal conductivity was made on a pair of specimens of SRM 1450b fibrous glass insulation board from a lot certified in 1982 [1]. The experi-

mental data obtained for thermal conductivity as a function of temperature were compared with values obtained from the polynomial published in the SRM certification document. Figure 7 shows thermal conductivity data obtained with the high-temperature GHP for temperatures from 300 to 345 K, compared with the certification function. The deviation plot for these data (Fig. 8) reveals a slight systematic bias between the data points and the thermal conductivity function, but the agreement is better than 1.8%. This is approximately the same as the imprecision estimated from the error-propagation analysis, namely, 1%.

Other studies of experimental precision and bias were performed. Deliberate offsets of the setpoint of the inner and outer guard indicated the error in measured thermal conductivity due to errors in control of these guards; runs controlled for zero temperature gradient gave a conductivity from which a power is calculated to indicate the presence of any heat leaks to or from the stack at different temperatures of operation; and participation in interlaboratory comparative measurement programs allowed estimates of the accuracy of this apparatus. The resulting estimates of imprecision and bias, justified in Ref 8, are given in Table 1.

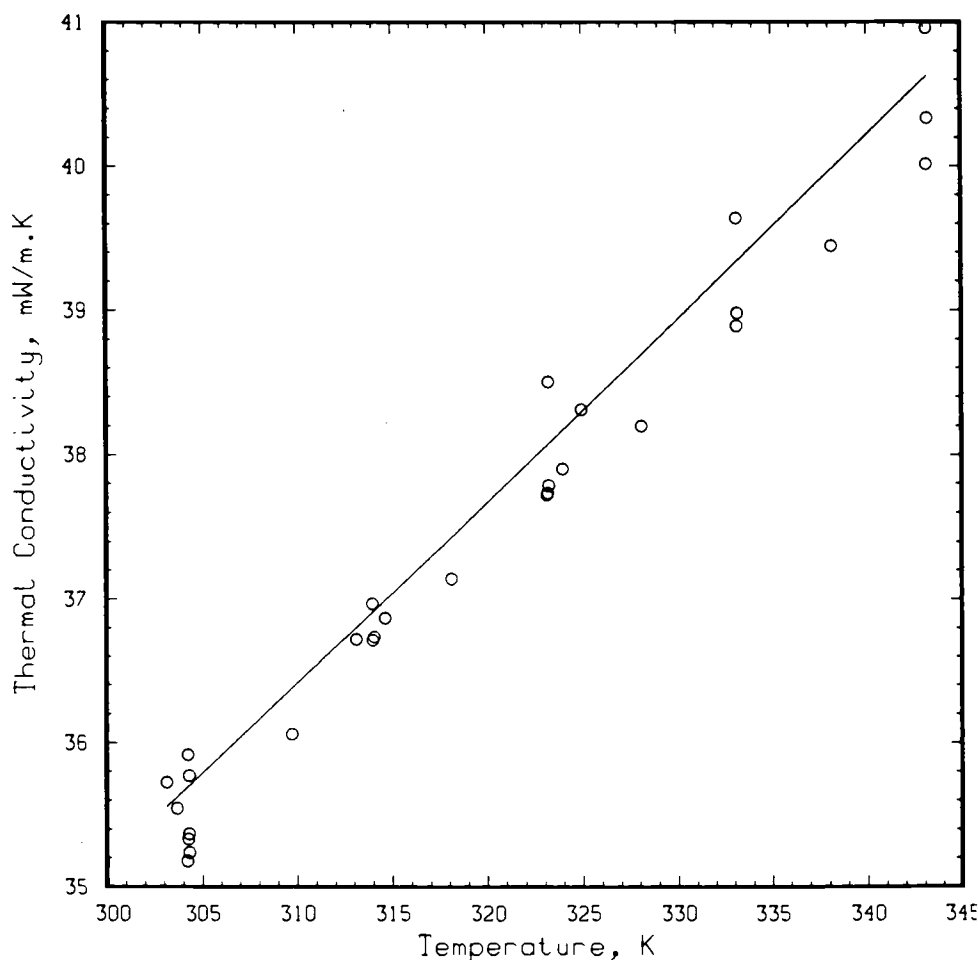


FIG. 7—Thermal conductivity of fibrous glass insulation SRM 1450b compared with certification function for $k(T)$ (solid line).

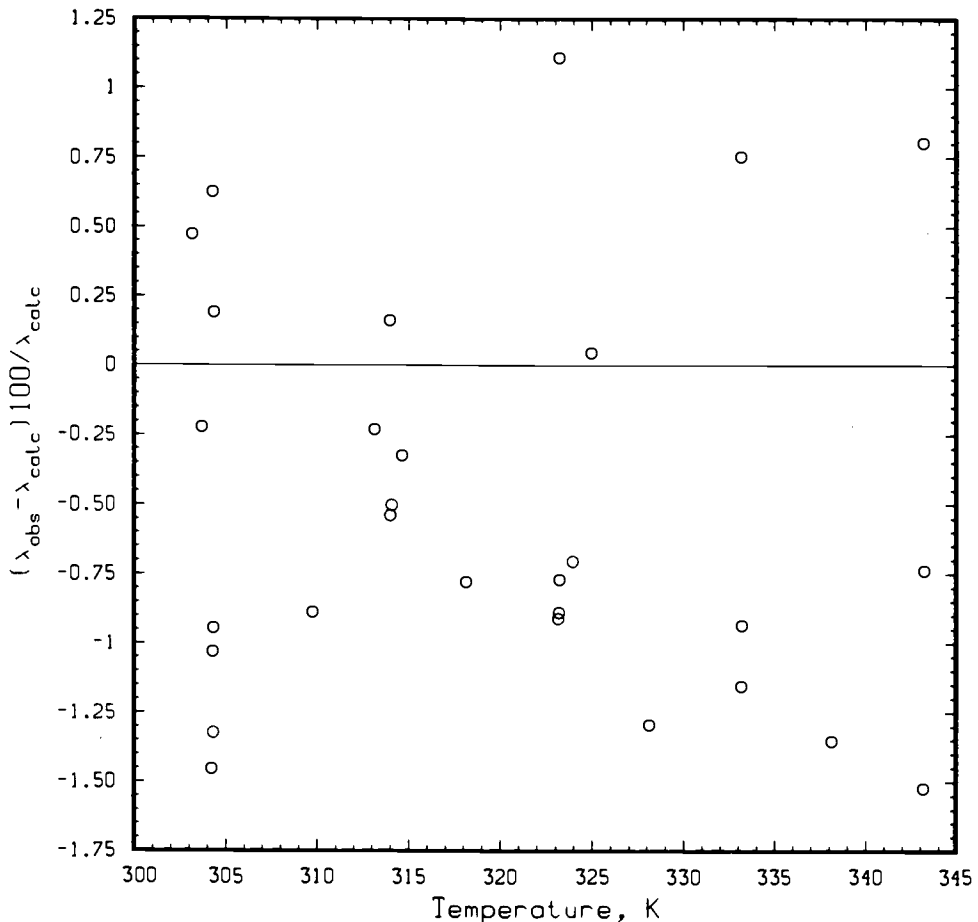


FIG. 8—Relative deviations of thermal conductivity of fibrous glass insulation SRM 1450b compared with certification function for $k(T)$.

Summary

This report describes the design and performance of an automated GHP apparatus built to meet the requirements of ASTM C 177 for measuring the thermal conductance of thermal insulation. The apparatus can measure apparent thermal conductivity over a range of temperatures from ambient to 750 K.

Important features of the design and construction of this apparatus are as follows:

1. An improved algorithm for the control sequence leading to stable heater powers and specimen temperatures was developed. Initially the apparatus rapidly approaches the temperature set point with minimal overshoot. The algorithm also permits highly sensitive control of the plate temperatures in later phases of the measurement sequence when thermal stability of the specimen boundaries is very important in measuring the thermal conductivity with high precision. The high precision of control leads to very good reproducibility of measurements under the same nominal conditions, as has been verified experimentally.

2. A novel thermocouple design provides more accurate sensing of the average temperature over the surface of each heater plate in the apparatus. This design provides greater accuracy

TABLE 1—*Estimates of random variations and systematic uncertainties in measured quantities at room temperature.*

Primary Variable	Value	Uncertainty	Imprecision	Bias
Measurements at 325 K (52°C) ($R_H = 3.73 \Omega$; TC sensitivity: $29 \mu\text{V/K}$)				
V	2.38 V	$10 \mu\text{V}$	$10^{-3} \%$	0.1 %
I	0.63 A	$1 \mu\text{A}$	$10^{-3} \%$	$10^{-3} \%$
TC emf	$836.0 \mu\text{V}$	$1 \mu\text{V}$	0.1 %	0.9 %
Q	1.50 W	0.07 W	0.5 %	0.1 %
A	129.1 cm^2	1 cm^2	0.0 %	0.8 %
ΔX	2.61 cm	0.01 cm	0.0 %	0.3 %
ΔT	29.00 K	0.005 K	0.02 %	0.9 %
T	325.00 K	0.05 K	0.02 %	0.9 %
k	$52.6 \text{ mW}/(\text{m} \cdot \text{K})$	$0.25 \text{ mW}/(\text{m} \cdot \text{K})$	0.5 %	1.5 %
Measurements at 750 K (477°C) ($R_H = 5.71 \Omega$; TC sensitivity: $38.4 \mu\text{V/K}$)				
V	6.48 V	$10 \mu\text{V}$	$10^{-3} \%$	0.1 %
I	1.14 A	$10 \mu\text{A}$	$10^{-3} \%$	$10^{-3} \%$
TC emf	15.9 mV	$1 \mu\text{V}$	0.01 %	0.02 %
Q	7.40 W	0.05 W	0.7 %	2 %
A	129.1 cm^2	1 cm^2	0.0 %	0.8 %
ΔX	2.61 cm	0.01 cm	0.0 %	0.3 %
ΔT	75.00 K	0.015 K	0.02 %	0.9 %
T	750.00 K	0.15 K	0.02 %	0.9 %
k	$100.0 \text{ mW}/(\text{m} \cdot \text{K})$	$0.7 \text{ mW}/(\text{m} \cdot \text{K})$	0.7 %	2.5 %

because more points of the surface are sampled. This yields more accurate control of the absolute temperature of the plate surfaces and of the adjoining surfaces of the specimens. Consequently the measurement of thermal conductivity with this instrument is also more accurate. The arrangement also offers greater precision in measurement of temperature because the design incorporates a thermopile arrangement which multiplies the effect of any temperature differences across the area sampled by the sensor.

Measurements are described which help to assess the precision and bias of the apparatus. Data from this apparatus are compared with measurements on similar materials reported in the literature.

Error-propagation analysis suggests the estimated imprecision in measurement of thermal conductivity is 0.5% at room temperature and 0.7% at 750 K. The experimentally observed imprecision under dynamic control of the automated system is 1% near room temperature. The estimated bias is 2% at room temperature, rising to 2.5% at the upper end of the temperature range. The experimentally observed reproducibility of the apparatus is about 1.2%.

Acknowledgments

This work was funded in part by DoE/ORNL under Contract ORNL/IA-21428.

References

- [1] Siu, M. C. I. and Hust, J. G., "Standard Reference Material 1450b, Thermal Resistance-Fibrous Glass Board," National Bureau of Standards Certificate (Office of Standard Reference Materials, NIST, Gaithersburg, Md., 1982).
- [2] Siu, M. C. I., "Fibrous Glass Board as a Standard Reference Material for Thermal Resistance Mea-

- surement Systems," in *Symposium on Thermal Insulation Performance, ASTM STP 718*, American Society for Testing and Materials, pp. 343-360 (ASTM, Philadelphia, 1980).
- [3] Smith, D. R. and Hust, J. G., "Effective Thermal Conductivity of Glass-Fiber Board and Blanket Standard Reference Materials," in *Thermal Conductivity 17: Proceedings of the 17th International Conference on Thermal Conductivity*, J. G. Hust, Ed., pp. 408-410 (Plenum, NY, 1980).
 - [4] Smith, D. R. and Hust, J. G., "Effective Thermal Conductivity of a Glass Fiber-Board Standard Reference Material," NBSIR 81-1639, National Institute of Standards and Technology, 1981.
 - [5] Hust, J. G., "Standard Reference Materials: Glass Fiberboard SRM for Thermal Resistance," Special Publication 260-98, National Institute of Standards and Technology, Aug. 1985.
 - [6] Hust, J. G., "Standard Reference Materials: Glass Fiberblanket SRM for Thermal Resistance," Special Publication 260-103 National Institute of Standards and Technology, Sept. 1985.
 - [7] Smith, D. R., Hust, J. G., and Van Poolen, L. J., "A Guarded-Hot-Plate Apparatus for Measuring Effective Thermal Conductivity of Insulations between 80 K and 360 K," NBSIR 81-1657, National Institute of Standards and Technology, 1982.
 - [8] Hust, J. G. and Smith D. R., "An Automated High-Temperature Guarded-Hot-Plate Apparatus for Measuring Apparent Thermal Conductivity of Insulations Between 300 K and 750 K," NBSIR 88-3089, National Institute of Standards and Technology, May 1988.
 - [9] Hust, J. G. and Smith, D. R., "A Thermocouple Device for Determination of Average Surface Temperature," *Journal of Thermal Insulation*, Vol. 11, Oct. 1987, pp. 96-101.
 - [10] Hust, J. G., Filla, B. J., and Smith, D. R., "A Modified Digital PID Temperature Controller for Thermal Properties Measurements," *Journal of Thermal Insulation*, Vol. 11, Oct. 1987, pp. 102-107.
 - [11] Hust, J. G. and Lankford, A. B., "Comments on the Measurement of Thermal Conductivity and Presentation of a Thermal Conductivity Integral Method," *International Journal of Thermophysics*, Vol. 3, No. 1, 1982, pp. 67-77.

On the Thermal Insulation of Outdoor Electronic Cabinets

REFERENCE: Guglielmini, G. and Milano, G., "On the Thermal Insulation of Outdoor Electronic Cabinets," *Insulation Materials, Testing, and Applications, ASTM STP 1030*, D. L. McElroy and J. F. Kimpflen, Eds., American Society for Testing and Materials, Philadelphia, 1990, pp. 723-740.

ABSTRACT: The thermal behavior of electronic cabinets for outdoor installation is analyzed. As the correct working condition of circuit boards requires a temperature-conditioned housing, the thermal design of the cabinet structure must be carefully foreseen from both the insulating and cooling point of view.

After a short review of some technical solutions for passively conditioned cabinets, an approximate physical model is presented that is able to simulate with a sufficient degree of generality the transient thermal behavior of the structure as a whole. Several examples of numerical solutions are reported relating to different kinds of cabinets with or without natural air ventilation. The effect of thermal storage inside the cabinet is analyzed, too.

The numerical simulations show that for this kind of application any thermal calculation procedure must take into account the transient effect in all structural components.

KEY WORDS: electronic cabinets, shelter, passive conditioning, thermal insulation, thermal storage, natural cooling, solar radiation, thermal transient, physical model, thermal design

Nomenclature

Symbols

- $a_{i,k}$ Thermal diffusivity of the i th layer of the k th wall (m^2/s)
- A Total surface area of the cabinet (m^2)
- A_o Surface area of the opening (mm^2)
- A_k Surface area of the k th wall (m^2)
- A_M Surface area of the inner heat capacity (m^2)
- A_s Surface area of the thermal energy storage (m^2)
- C_a Specific heat of air ($\text{kJ/kg}^\circ\text{C}$)
- C_R Dimensional coefficient in the air flow resistance factor ($\text{mmH}_2\text{O} \cdot \text{mm}^2/(\text{L}/\text{min})^2$)
- D Average side dimension of the cabinet rectangular cross section (m)
- f Frequency of temperature fluctuation (s^{-1})
- G_a Volumetric air flow rate (L/min)
- \bar{h}_i Inner mean heat transfer coefficient ($\text{W}/\text{m}^2^\circ\text{C}$)
- $\bar{h}_{i,k}$ Inner heat transfer coefficient of the k th wall ($\text{W}/\text{m}^2^\circ\text{C}$)
- \bar{h}_e Outer mean heat transfer coefficient ($\text{W}/\text{m}^2^\circ\text{C}$)
- $\bar{h}_{e,k}$ Outer heat transfer coefficient of the k th wall ($\text{W}/\text{m}^2^\circ\text{C}$)
- \bar{h}_M Mean heat transfer coefficient of the inner heat capacity ($\text{W}/\text{m}^2^\circ\text{C}$)
- \bar{h}_s Mean heat transfer coefficient of the thermal energy storage ($\text{W}/\text{m}^2^\circ\text{C}$)

¹Professor, Energy Engineering Department, University of Genoa, Via all'Opera Pia, 15A, I 16145 Genoa, Italy.

h_{sf}	Latent heat of the fluid contained in the thermal energy storage (kJ/kg)
H	Cabinet height (m)
m_s	Mass of the fluid in the thermal energy storage (kg)
M	Mean value of the heat capacity of electronic equipment (kJ/°C)
N	Number of walls
N_k	Number of layers of the k th wall
P	Thermal power dissipated by circuitry (W)
q_a	Total heat flux transferred to inner ambient air (W)
$q_{r,k}''$	Solar specific heat flux component for the k th wall (W/m ²)
q_s''	Specific heat flux exchanged through the south wall of the cabinet (W/m ²)
R	Air flow resistance coefficient (mmH ₂ O/(L/min) ²)
$S_{i,k}$	Thickness of the i th layer of the k th wall (m)
T	Temperature (°C)
T_{ai}	Inner air temperature (°C)
T_{ae}	Outer air temperature (°C)
$T_{i,k}$	Temperature of the i th layer of the k th wall (°C)
T_c	Temperature of a cold surface of the cabinet (°C)
T_H	Temperature of a hot surface of the cabinet (°C)
T_M	Temperature of the inner heat capacity (°C)
T_s	Temperature of change of phase (°C)
T_{sa}	Equivalent sol-air temperature for the cabinet (°C)
$T_{sa,k}$	Equivalent sol-air temperature of the k th wall (°C)
u	Wind speed (m/s)
$x_{i,k}$	Space variable of the i th layer of the k th wall (m)
X	Mixture quality of the fluid in the thermal energy storage (%)
W	Cabinet width (m)

Greek Symbols

α	Dimensional coefficient in the air flow equation (7) (m ³ /kJ)
β	Dimensional coefficient in the air flow equation (7) (m ³ /kJ)
ϵ	Emissivity of the external surfaces of the cabinet
ϵ_k	Emissivity of the external k th wall of the cabinet
ΔH	Vertical distance between the openings (m)
$\lambda_{i,k}$	Thermal conductivity of the i th layer of the k th wall (W/m°C)
ρ_a	Air density (kg/m ³)
ρ_{H_2O}	Water density (kg/m ³)
σ	Amplitude reduction factor
τ	Time (h)
τ_0	Initial time of the thermal transient (h)

Suffixes

∂	Partial derivative
d	Total derivative
Δ	Variation

Superscript

$-$	Mean value
-----	------------

Subscripts

- a* Ambient air value
- e* External value
- i* Internal value, layer index
- k* Wall index
- M* Inner heat capacity index
- o* Opening index
- r* Radiative index
- s* Thermal energy storage index

Introduction

Over the last few years the tendency to install electronic equipment for telecommunications in outdoor loop plants has increased considerably. The circuit boards are typically arranged in simple metal cabinets or in more sophisticated "shelters" according to the size and power of the electronic apparatus. In order to assure a correct working condition for circuit boards, the inner air temperature cannot exceed certain limit values, depending upon the kind and class of the electronic components. If standard civil circuitry is utilized, for example, the maximum allowable temperature excursion of the inner air must be limited to the range from -5 to $+45^{\circ}\text{C}$, while the external air temperature can vary in the extreme (reference range from -40 to $+45^{\circ}\text{C}$) and several exterior surfaces of the cabinet can be subjected to direct solar heating.

As the telecommunications stations are commonly placed in remote, unattended sites, in which the aforementioned severe climates can occur, there is a need for temperature-conditioned housing. In these cases it has been recognized that the most economic and reliable temperature conditioning system is entirely passive (i.e., has no moving parts and requires no power consumption). Some technical options for 100% passive conditioning of cabinets and shelters, having different sizes and power dissipated by internal equipment, are shown in Fig. 1.

For powers ranging from 10 to 50 W in warm climates (or up to 500 W in cold climates), for relatively small-sized electronic equipment, an "RC" structure of the cabinet may be sufficient. The temperature variation during the day is almost entirely damped by a proper combination of the insulating (R) and capacitance (C) effects of the cabinet walls and of the thermal masses present in the interior.

In cold climates the power dissipated inside the insulated cabinet is used to shift upward by a proper amount ΔT , the internal air temperature. Conversely, in warm climates, the mean external air temperature, added to the same temperature interval ΔT , must not exceed the maximum allowable inner temperature. Thus a proper compromise must be selected, and a careful thermal design of the structure as a whole is required.

In the case of electronic equipment dissipating more than 50 W in warm climates or when the seasonal temperature variations are large, the "RTC" structure is more appropriate. The cabinet, of intermediate size, is insulated, as in the previous case, by proper thermal resistance (R) and capacitance (C). Additionally, a proper fluid circuit is present having a transistor (T) function (i.e., it is able to collect, when certain temperature values are reached, the heat dissipated inside and carry it outside, but not vice versa). As shown in Fig. 1, the selective cooling effect can be simply obtained by a system of openings which allows a natural ventilation of air in warm climates only when a certain maximum inner temperature is exceeded.

An efficient transistor function can be also obtained by a thermosyphon loop, based on the fact that a warm liquid rises and a cold one sinks. By choosing an appropriate mixture of liquids for the thermosyphon (e.g., water and Glicol), the temperature-dependent viscosity can be varied so as to make the thermosyphon more efficient when it gets hotter and to stop it when a certain lower temperature limit is reached.

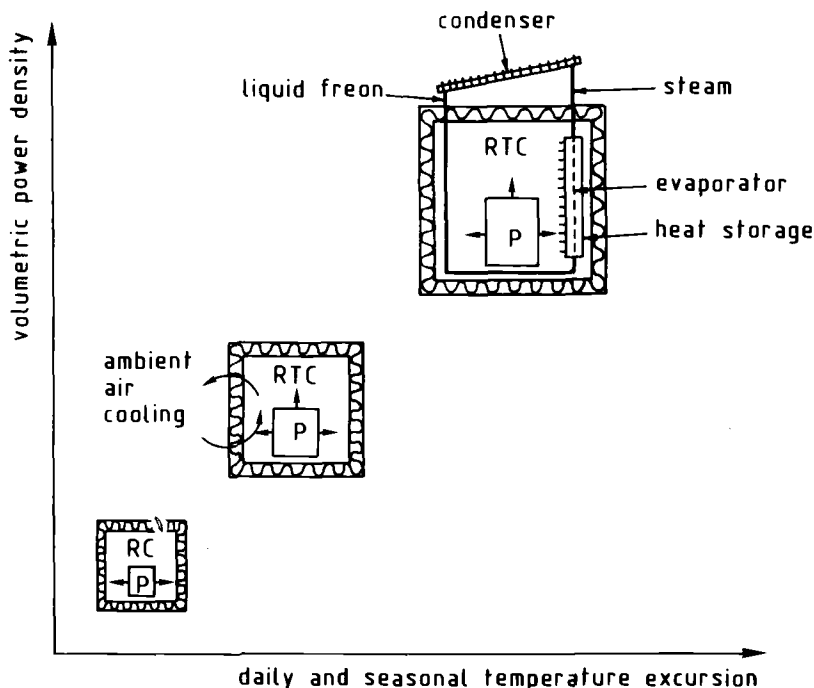


FIG. 1—Sketch of some technical options utilized for passive conditioning of electronic cabinets and shelters for outdoor installation.

For dissipated powers on the order of several kilowatts and for corresponding equipment of relatively large size, more sophisticated passively-cooled shelters must be utilized. In this case the "RTC" structure, often provided with solar shields, operates in conjunction with large internal heat storage, and the thermosyphon loop is composed of one or two evaporator-condenser systems in which Freon circulates.

This short review of some existing options for passive conditioning systems of electronic cabinets or shelters shows that, regardless of the different technical solutions, some important thermal problems occur in all cases. Of great importance are the insulating characteristics of the walls, with or without solar shields, and the need to design the walls in conjunction with the effect of internal heat dissipation and local climate conditions. Moreover, due to the typical temperature fluctuations characterizing the passively conditioned systems, any thermal design procedure must take into account the transient effect in all the components. We note, in fact, that the response time of a well-insulated cabin, containing a large amount of internal masses, is not negligible in respect to the daily sol-air temperature variation.

Although many kinds of cabinets for outdoor installation have been available for some years [1-3], to the authors' knowledge no general thermal calculation procedures seem to have been published for this application. In Ref 4, for instance, the thermal analysis is limited to the steady-state regime and is valid therefore only for cabinets having small time constant compared with the time scale of the sol-air waveform. On the other hand, the standard computer codes set up for the transient thermal analysis of buildings cannot easily be fit to the case of electronic cabinets due to their remarkable structural and functional differences.

In a previous work [5] an attempt was made to formulate an approximate physical model able to reproduce with a sufficient degree of generality the transient thermal behavior of electronic cabinets or shelters. In this work the physical model is extended to the more general case of a

system composed of an arbitrary number of walls, each made of an arbitrary number of layers of different materials. An improved version of the computer code, based on a finite difference solution of the transient energy balance equations, is developed and several examples of numerical simulation are reported.

Physical Model

As shown in Fig. 2, the cabinet or shelter is schematized by a generic enclosure composed of N walls which delineates the external ambient air at variable temperature $T_{ae}(\tau)$ from the internal air at variable temperature $T_{ai}(\tau)$. Each wall, having a surface area A_k ($k = 1, 2, \dots, N$), may be made in turn of N_k layers and, for simplicity, an ideal thermal contact is supposed between the different materials of the layers.

The external ($\bar{h}_{e,k}$) and internal ($\bar{h}_{i,k}$) surface heat transfer coefficients control the heat exchanges between the generic k th wall and the surrounding air; these coefficients can be different for each wall but are constant with temperature. Moreover, each external layer of the walls may absorb a fraction ϵ_k of the solar radiation component $q''_{r,k}(\tau)$ and, with the usual assumptions, an equivalent sol-air temperature $T_{sa,k}(\tau)$ for each wall can be defined:

$$T_{sa,k}(\tau) = T_{ae}(\tau) + q''_{r,k}(\tau) \frac{\epsilon_k}{\bar{h}_{e,k}}$$

The heat conduction through the cabinet walls is assumed one dimensional, neglecting all thermal gradients except that normal to the wall itself. All inner circuit boards and their metal supports are considered as a lumped heat capacity M having a surface area A_M and a mean heat transfer coefficient \bar{h}_M , whose temperature $T_M(\tau)$ varies in time only. The thermal power P dissipated by circuitry is assumed uniformly distributed in the lumped heat capacity M . The heat capacity of the inner air is considered negligible in respect to that of solid materials.

In warm climates a natural air cooling circulation may be foreseen, making some openings in the cabinet walls. The volumetric flow rate of ventilating air $G_a(\tau)$ depends upon the actual

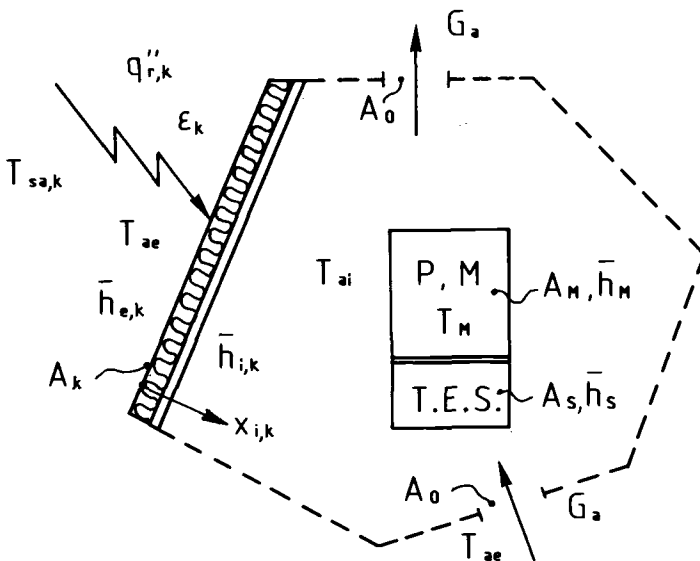


FIG. 2—Schematic drawing of the energy exchanges in a passively cooled electronic cabinet.

difference between the inner and outer air temperature, the vertical distance ΔH between the lower and upper opening, the area A_o of the opening itself, the concentrated and distributed air flow resistance R inside the cabinet, and the total amount $q_a(\tau)$ of heat transferred to the inner air.

Finally, in order to increase the cabinet capacitance a thermal energy storage (TES) can be added to the internal heat capacity. This last contains a mass m_s of fluid that, in absence of change of phase, undergoes, for assumption, the same temperature variations $T_M(\tau)$ as the other internal masses. When the temperature of change of phase T_s is reached, the thermal energy storage is able to exchange with the inner ambient air large quantities of heat of constant temperature.

Taking into account the aforesaid simplifications and assuming also all thermophysical properties constant with temperature, the governing heat transfer equations and the corresponding boundary conditions can be written as follows:

$$\frac{\partial^2 T_{i,k}}{\partial x_{i,k}^2} = \frac{1}{a_{i,k}} \frac{\partial T_{i,k}}{\partial \tau} \quad \text{for } k = 1, \dots, N \quad \text{and } i = 1, \dots, N_k \quad (1)$$

$$T_{i,k}(x_{i,k}, 0) = T_{i,k}^0(x_{i,k}) \quad \text{for } k = 1, \dots, N \quad \text{and } i = 1, \dots, N_k \quad (1a)$$

$$T_M(o) = T_M^0$$

$$\lambda_{1,k} \frac{\partial T_{1,k}(0, \tau)}{\partial x_{1,k}} - \bar{h}_{e,k} [T_{1,k}(0, \tau) - T_{sa,k}(\tau)] = 0 \quad \text{for } k = 1, \dots, N \quad (1b)$$

$$\lambda_{N_k,k} \frac{\partial T_{N_k,k}(S_{N_k,k}, \tau)}{\partial x_{N_k,k}} + \bar{h}_{i,k} [T_{N_k,k}(S_{N_k,k}, \tau) - T_{ai}(\tau)] = 0 \quad \text{for } k = 1, \dots, N \quad (1c)$$

$$\lambda_{i,k} \left. \frac{\partial T_{i,k}}{\partial x_{i,k}} \right|_{\text{int}} = \lambda_{i+1,k} \left. \frac{\partial T_{i+1,k}}{\partial x_{i+1,k}} \right|_{\text{int}} \quad \text{for } k = 1, \dots, N \quad \text{and } i = 2, \dots, N_k^{-1} \quad (1d)$$

$$T_{i,k}|_{\text{int}} = T_{i+1,k}|_{\text{int}} \quad \text{for } k = 1, \dots, N \quad \text{and } i = 2, \dots, N_k^{-1} \quad (1e)$$

$$\sum_{k=1}^N \{ \bar{h}_{i,k} A_k [T_{N_k,k}(S_{N_k,k}, \tau) - T_{ai}(\tau)] \} + \bar{h}_M A_M [T_M(\tau) - T_{ai}(\tau)] + \rho_a G_a(\tau) C_a [T_{ae}(\tau) - T_{ai}(\tau)] = 0 \quad (2)$$

$$G_a = G_a \{ [T_{ai}(\tau) - T_{ae}(\tau)], \Delta H, A_o, R, q_a(\tau) \} \quad (3)$$

$$P - \bar{h}_M A_M [T_M(\tau) - T_{ai}(\tau)] = M \frac{dT_M(\tau)}{d\tau} \quad (4)$$

$$\bar{h}_s A_s [T_{ai}(\tau) - T_s] = m_s h_{sf} \frac{dX(\tau)}{d\tau} \quad (5)$$

where τ is time and $T_{i,k}$, $x_{i,k}$, $S_{i,k}$, $\lambda_{i,k}$, and $a_{i,k}$ represent respectively the temperature, space variable, thickness, thermal conductivity, and thermal diffusivity of the generic i th layer of the k th wall; h_s and A_s are the mean surface heat transfer coefficient and the surface area of the thermal energy storage; and m_s , h_{sf} , and $X(\tau)$ are respectively the mass, the latent heat, and the

time-dependent mixture quality (liquid-solid) of the fluid contained in the thermal storage. For the meaning of the other symbols see the Nomenclature section.

Equation 1 is the one-dimensional (1-D) heat conduction equation applied to all the N_k layers composing the N walls. Equations 1a, 1b, and 1c are the initial and boundary conditions for Eqs 1 and 4, while the interfacial conditions between the different materials composing the layers are expressed by Eqs 1d and 1e.

Equation 2 represents the energy balance equation for inner air, taking into account the effect of natural ventilation which can give rise through lower and upper openings.

The volumetric flow rate of ventilating air depends upon several factors as shown by Eq 3 and can be obtained iteratively using the appropriate correlations reported, for example, in Ref 6.

Equations 4 and 5 represent respectively the energy balance for the lumped heat capacity M and, with the usual approximations, for the thermal energy storage. As long as $T_M(\tau)$ is different from the value T_S corresponding to the change of phase, Eq 5 is dropped and the fluid heat capacity is simply added to the other internal masses.

Numerical Solution

The unknown functions of the problem are: the temperatures $T_{i,k}(x_{i,k}, \tau)$ for $k = 1, \dots, N$ and $i = 1, \dots, N_k$; the inner air temperature $T_{ai}(\tau)$; the lumped capacity temperature $T_M(\tau)$; the volumetric air flow rate $G_a(\tau)$ if there is natural ventilation; and the quality mixture variation $X(\tau)$ if a thermal energy storage is present and acts.

The complete set of equations (1, 2, 3, 4, 5) with the initial and boundary conditions (1a, 1b, 1c, 1d, 1e) is solved numerically by a finite difference procedure. An unconditionally stable, fully implicit scheme is adopted, and if natural air ventilation is present an iterative process is activated with automatic control of the convergence.

If the cabinet's walls are made of different materials or have different thicknesses, or when the surface heat transfer coefficients $\bar{h}_{i,k}$ and $\bar{h}_{e,k}$ take different values for $k = 1, \dots, N$, the matrix of the unknown coefficients that arises from the discretization of the complete set of equations is not symmetrical. In this case standard methods of solution for the system of linear algebraic equations at each time instant must be used, depending upon the matrix size. However, in the rather frequent case in which all walls are made of the same materials, have the same thickness and emissivity, and the external and internal surface coefficients assume the same two values ($\bar{h}_{i,k} = \bar{h}_i$ and $\bar{h}_{e,k} = \bar{h}_e$), the matrix of unknown coefficients can be reduced to a tridiagonal form giving rise to a large savings of time and memory occupation in the computer solution. In fact, when the aforesaid conditions are verified only one heat conduction equation need be considered ($k = 1$), and an equivalent sol-air temperature $T_{sa}(\tau)$ for the external surface of the cabinets as a whole can be defined:

$$T_{sa}(\tau) = T_{ae}(\tau) + \frac{\epsilon}{\bar{h}_e} \frac{\sum_{k=1}^N q_{r,k}''(\tau) A_k}{\sum_{k=1}^N A_k} \quad (6)$$

Moreover, in Eq 2 only one term of the summations is present and the inner air temperature $T_{ai}(\tau)$ can be expressed as a function of temperature $T_M(\tau)$ by means of Eq 4, reducing the unknown functions to $T_M(\tau)$ and $T_{N_1}(S_{N_1}, \tau)$. A similar substitution can be made in the boundary condition (1c) using Eq 2.

We note that the unknown temperature $T_{ai}(\tau)$ can be considered as not a primary variable due to the assumption that the inner ambient air behaves as a pure thermal resistance. In this way not more than three adjacent coefficients compare in each one of the discretized equations, and the problem is reduced to a typical implicit formulation of a parabolic diffusion equation.

Among the different technical solutions which allow a passive cooling of the cabinet by means of circulating fluids, only natural air ventilation cooling is considered in the present version of the computer code. An extension to the passive cooling by a thermosyphon loop is in progress, however.

The volumetric flow rate $G_a(\tau)$ of cooling air is evaluated iteratively, at each time instant, using the following approximate equation proposed in Ref 6,

$$G_a^3(\tau) \cdot R \cdot (T_{ae}(\tau) + 273.15) + \alpha G_a^2(\tau) \cdot R \cdot q_a(\tau) \cdot (T_{ai}(\tau) + 273.15) - \beta \Delta H q_a(\tau) \cdot (T_{ai}(\tau) + 273.15) = 0 \quad (7)$$

where α and β are two-dimensional coefficients which depend upon the thermophysical properties of air evaluated at the temperature $T_{ae}(\tau)$:

$$\alpha = \frac{1}{2C_a \rho_a T_{ae}}; \quad \beta = \alpha \frac{\rho_a}{\rho_{H_2O}}$$

where C_a and ρ_a are the specific heat and density of air, respectively, and ρ_{H_2O} is the density of water.

Here $q_a(\tau)$ represents the total heat flux transferred from the cabinet to the inner air:

$$q_a(\tau) = \sum_{k=1}^N \{ \bar{h}_{i,k} A_k [T_{N_{k,k}}(x_{N_{k,k}} \tau) - T_{ai}(\tau)] \} + \bar{h}_M A_M [T_M(\tau) - T_{ai}(\tau)]$$

and R is the air flow resistance coefficient (concentrated and distributed) which can be expressed by

$$R = \frac{C_R}{A_o^2}$$

where A_o is the surface area of one opening and C_R is a proper dimensional coefficient.

If we adopt the following units for the main variables:

$$G_a \text{ (L/min); } A_o \text{ (mm}^2\text{); } q_a \text{ (W); } \Delta H \text{ (m); } R \text{ (mmH}_2\text{O/(L/min)}^2\text{)}$$

then the numerical values of the coefficients α and β at the reference temperature $T_{ai} = 20^\circ\text{C}$ are

$$\alpha = 0.0849 \text{ (m}^3\text{/kJ); } \beta = 1.019 \cdot 10^{-4} \text{ (m}^3\text{/kJ)}$$

The real, positive solution of the cubic algebraic equation (7) gives the volumetric air flow rate $G_a(\tau)$ circulating inside the cabinet at a generic instant τ . Equation 7, which represents the explicit form of Eq 3, is coupled to the remaining set of equations by an iterative procedure. At each instant the system of equations (1, 1a, 1b, 1c, 1d, 1e, 2, 4) is solved using the value $G_a(\tau)$ obtained in the previous iteration. The new set of temperature allows a new evaluation of $G_a(\tau)$ by means of Eq 7, and the iteration loop at the same instant is repeated until the desired convergence is reached.

In spite of the several approximations contained in Eq 7 it has been shown [7] that it provides reasonable agreement with experimental results in the case of air natural cooling of electronic cabinets.

Finally, when the fluid contained in the thermal energy storage undergoes a change of phase

at temperature T_s , the heat flux component $Q_s = \bar{h}_s A_s [T_s - T_{ai}(\tau)]$ is added to the left-hand side of Eq 2 and Eq 5 is integrated with the initial condition:

$$X(\tau_0) = 100\% \text{ at the instant } \tau_0, \text{ when } T_M(\tau_0) = T_s$$

We note that Eq 5 assumes the temperature T_s uniformly distributed in the fluid during the change of phase. In addition, the inner thermal resistance of the thermal storage is neglected and the latent heat is considered to be transferred only to the surrounding air. With these assumptions Eq 5 is uncoupled and can be integrated directly without iteration loop.

Examples of Numerical Simulations

The examples of numerical simulations reported in this work refer to an electronic cabinet for outdoor installation having the same external dimensions (length \times width \times height) of $0.8 \times 0.4 \times 1.4$ m but different types of wall. The geometrical and thermophysical characteristics of the cabinet's walls are summarized in Table 1.

A typical Italian climate is selected as a reference for outdoor sol-air temperature waveform (Fig. 3). The mean warmest day occurs in Messina (August) and the mean coldest day in Plateau Rosa (January). Concerning the values of external and internal convective heat transfer coefficients several empirical relationships are available. For example, assuming a random wind direction, the mean convective heat transfer coefficient for the external (horizontal and vertical) surfaces [4, 8, 9] is approximately given by

$$\bar{h}_e = 4 \left(\frac{u}{D} \right)^{0.5} \quad (8)$$

where u (m/s) is wind speed and D (m) is the average side dimension of the cabinet's rectangular cross section.

For the inner surfaces of the cabinet the heat transfer coefficient by natural convection can be evaluated [4, 10] using the empirical relationship

$$\bar{h}_i = 0.9 W^{0.11} H^{-0.36} (T_H - T_c)^{0.25} \quad (9)$$

where W (m) is the cabinet width, H (m) the cabinet height and T_H ($^{\circ}\text{C}$) and T_c ($^{\circ}\text{C}$) are some hot and cold wall temperatures.

For electronic equipment dissipating thermal power and cooled by natural convection of air, the mean heat transfer coefficient can be predicted using a class of empirical relations developed in Ref 11 and valid for a wide range of thermal conditions.


We note that the contribution of long wave radiation heat transfer must be added to the pure convective coefficients defined by the previous relationships in order to obtain the effective surface heat transfer coefficient. Since the examples here reported tend to show the effects of the main thermal parameters rather than the specific behavior of a particular type of cabinet, the following standard values of surface coefficients are assumed:

$$\bar{h}_e = 20 \text{ (W/m}^2\text{K)} \quad \text{and} \quad \bar{h}_i = 10 \text{ (W/m}^2\text{K)}$$

For simplicity the coefficients \bar{h}_M and \bar{h}_s are set equal to \bar{h}_i .

Several tests of the computer solutions are reported here. Figure 4 shows the thermal frequency response of cabinets having different wall composition and thickness. Numerical results are compared with analytical results obtained with a solution method valid only for the steady

TABLE 1—Geometrical and thermophysical properties of cabinet walls analyzed in numerical examples.

Type	Material	thickness S (m)	thermal conductivity λ (W/mK)	thermal diffusivity a (m ² s ⁻¹)
1	 iron	0.002	63	$1.86 \cdot 10^{-5}$
2A	a) iron	0.002	63	$1.86 \cdot 10^{-5}$
	b) polyurethane foam	0.015	0.03	$3.8 \cdot 10^{-7}$
	c) capacitative layer	0.01	1.0	$7.6 \cdot 10^{-7}$
2B	a) iron	0.002	63	$1.86 \cdot 10^{-5}$
	b) polyurethane foam	0.05	0.003	$3.8 \cdot 10^{-7}$
	c) capacitative layer	0.01	1.0	$7.6 \cdot 10^{-7}$
2C	a) iron	0.002	63	$1.86 \cdot 10^{-5}$
	b) polyurethane foam	0.10	0.03	$3.8 \cdot 10^{-7}$
	c) capacitative layer	0.01	1.0	$7.6 \cdot 10^{-7}$
3	a) iron	0.002	63	$1.86 \cdot 10^{-5}$
	b) capacitative layer	0.01	1.0	$7.6 \cdot 10^{-7}$
	c) polyurethane foam	0.015	0.03	$3.8 \cdot 10^{-7}$
4	a) iron	0.002	63	$1.86 \cdot 10^{-7}$
	b) polyurethane foam	0.015	0.03	$3.8 \cdot 10^{-7}$
<p>NOTE: In all calculations the following values of thermal parameters are assumed: $\bar{h}_e = 20$ (W/m²K), $\bar{h}_i = \bar{h}_M = \bar{h}_s = 10$ (W/m²K), $A = 4$ m², $A_M = 2.6$ m², $A_S = 1.0$ m², $A_O = 18,000$ mm², $M = 48 \cdot 4$ (kJ/K), $p = 70$ (W).</p>				

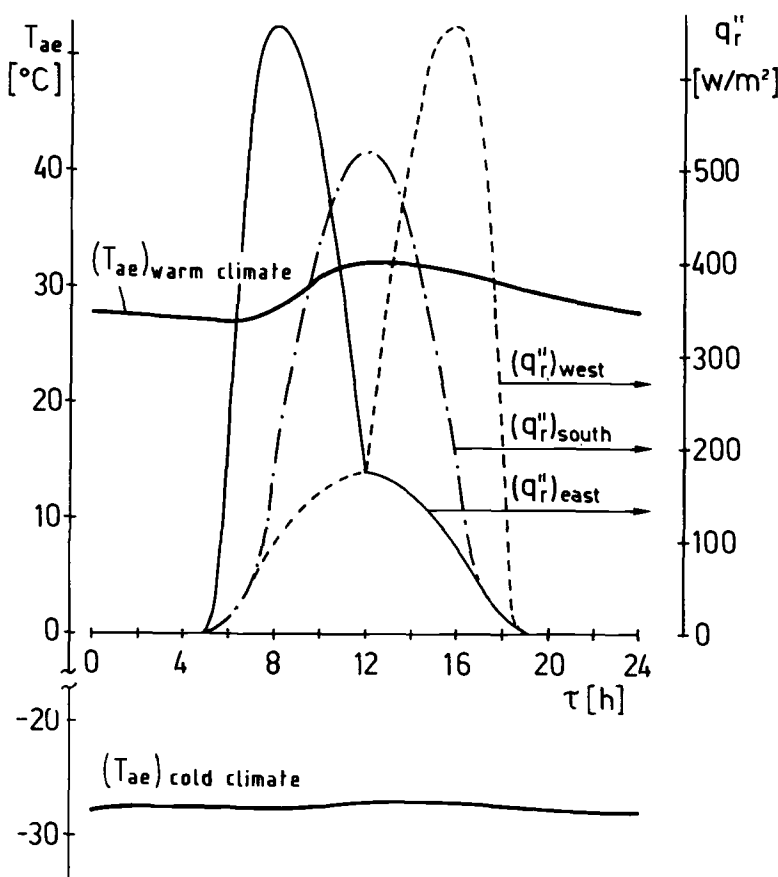


FIG. 3—Air temperature variations and solar heat flux waveforms representative of the extreme warm and cold climate in Italy.

periodic regime and proposed in Ref 12. Good agreement in all tests has been observed, with the error not greater than $\pm 1\%$. Figure 4 shows that the amplitude reduction factor σ is far from unity in the typical frequency range of sol-air temperature variation. In these cases the cabinet time constant cannot be considered negligible and the thermal behavior of the structure must be analyzed in the transient regime. Furthermore, it can be deduced that a capacitive layer properly placed in respect to the external excitation can greatly reduce the damping factor σ .

Figure 5 makes further comparisons with the analytical solution in the steady periodic regime concerning a cabinet cooled by an air forced ventilation at constant flow rate and with the same temperature fluctuation as the external ambient air. Figure 5 shows the well-known effect of an increase of σ increasing the volumetric flow rate G_a .

Figures 6 and 7 analyze the thermal behavior of an uninsulated and a partially insulated cabinet dissipating a power of $P = 70$ (W). In this case the cabinet is covered with a double roof and placed with the back surface facing the wall of a building so that only three surfaces are subjected, during clear days, to direct solar heating. The inner air temperature $T_{ai}(\tau)$ (Fig. 6) and the specific heat flux component q_s'' (Fig. 7) exchanged through the south wall are reported as a function of time during a typical day in warm climate. Only the three walls (south, west, east) subjected to direct solar radiation are insulated with different thicknesses of the insulating

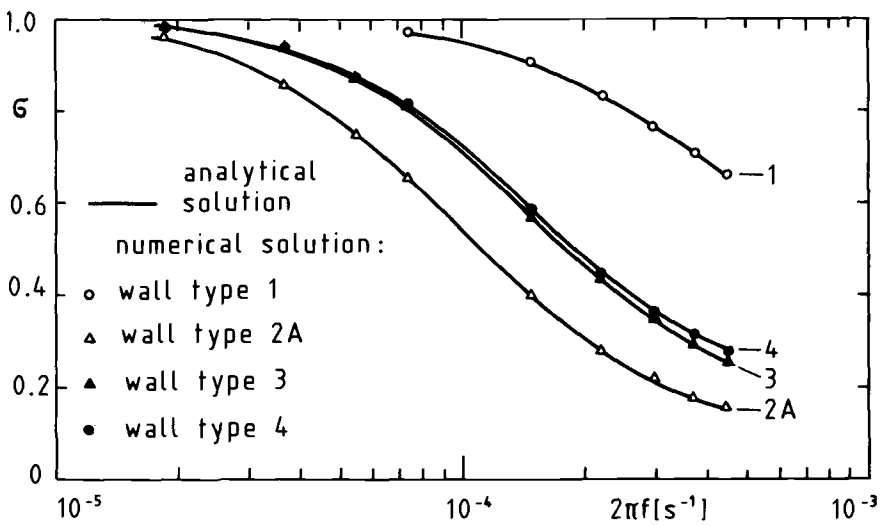


FIG. 4—Thermal frequency response for different types of cabinets without ventilation.

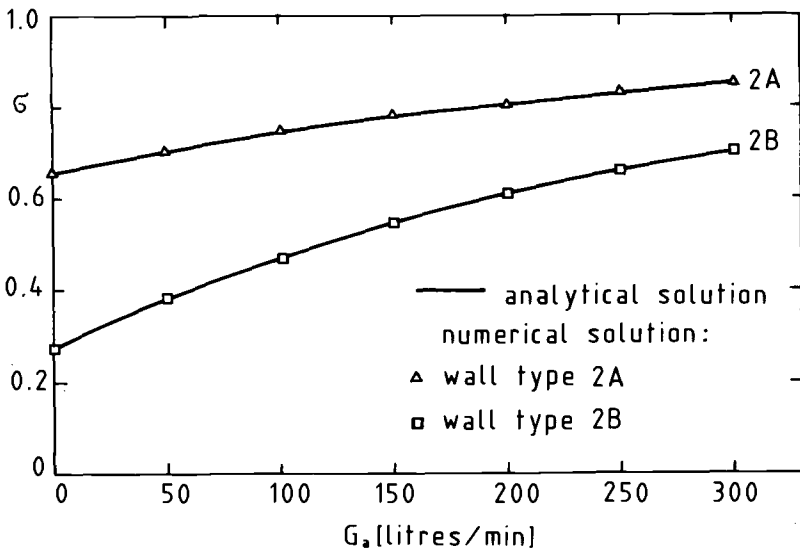


FIG. 5—Amplitude reduction factor for different types of cabinets as a function of volumetric air flow rate.

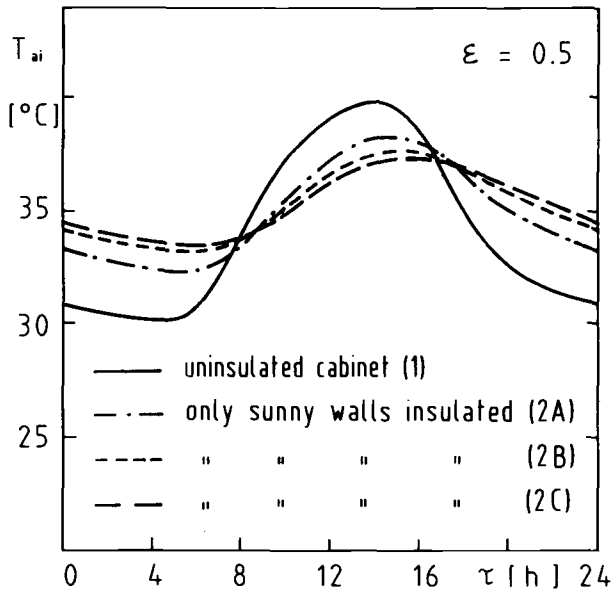


FIG. 6—Comparison of inner air temperature fluctuations of uninsulated and partially insulated cabinets.

layer. Figure 6 shows the favorable effect of the partial insulation in reducing the peak of inner air temperature in respect to the fully uninsulated cabinet.

The effect of insulation is to reduce the peak of radiation transmitted by the sunny walls, whereas the internal heat dissipation is transferred outside chiefly through the shaded walls. Obviously any insulating layer applied on each of the six walls improves the thermal behavior in cold climate.

The influence of the emissivity ϵ of the external surface is shown in Figs. 8 and 9. In Fig. 8 the walls are uninsulated, while in Fig. 9 the cabinet is fully insulated. As in the previous cases only three lateral surfaces are subjected to direct solar radiation but, owing to the same geometrical and thermophysical characteristics of the walls, an equivalent sol-air temperature defined by Eq 6 can be introduced. The results show that by using external paints with low ϵ values in the solar spectrum (e.g., a white finish with $\epsilon = 0.2$), the inner air temperature of the cabinet under examination keeps below the maximum allowable temperature (45°C), even if all the walls are insulated. The only disadvantage of using a white surface as the principal protection from solar radiation is that it may require regular maintenance, otherwise its emissivity may increase with time. In fact, some measurements of total normal emissivity performed in the range of solar wavelength on surfaces aged and covered with dust led to an increase of ϵ up to 0.8.

If a dark external finish is essential, as for military purposes, an efficient protection from solar radiation can only be achieved using solar shields. Some cautions, however, are necessary in the design of solar shields [13] in order to allow heat to be removed from the cabinet by convection and re-radiation at long wavelength.

If the seasonal temperature excursion is large, a cabinet with an RTC structure is more appropriate. In this case the insulating layer can be selected as fairly thick in order to satisfy the cold climate, while a natural fluid circulation is foreseen in warm climates.

Figure 10 presents some numerical simulations concerning a cabinet cooled in a warm climate by natural air ventilation. Three values of total air flow resistance coefficient R are considered; the value $R = \infty$ represents the situation in which no air ventilation flow is allowed.

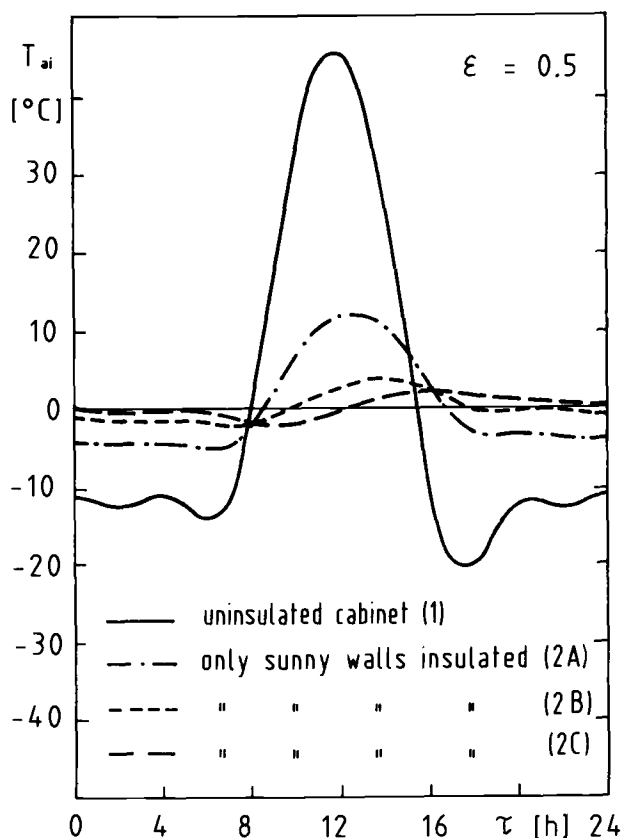


FIG. 7—Comparison of specific heat fluxes exchanged through the south wall of uninsulated and partially insulated cabinets.

If the electronic equipment is directly cooled by ambient air ventilation (Fig. 10), the cooling is quite efficient but appropriate filters must be placed near the openings in order to reduce the presence of dust and pollutants inside the cabinet. The filters may, however, introduce large resistance flow values and require regular maintenance. Another solution adopted by some makers consists in confining the electronic circuitry inside an inner dustproof cabinet placed in an outer insulated cover that protects it against rain, snow, and direct sunlight. The space between the inner cabinet and the cover allows a natural ventilation in warm climates only. Using this solution the cooling of circuitry is less efficient and a higher temperature level of the air inside the inner airtight cabinet must be accepted.

Finally in Figs. 11 and 12 some results of the thermal transient of an insulated cabinet in cold climates are reported. In this case the thickness of the insulating layer is supposed insufficient to maintain the inner air temperature within the allowable limit and the cabinet is provided with an auxiliary heat source. During an accidental breakoff of the main power supply, the contribution of the auxiliary heat source fails and only the heat dissipated by the electronic equipment acts because it is supplied by means of autonomous batteries having a certain operating time.

If the aforesaid event occurs, the problem is to avoid a too rapid decrease of inner air temperature and to maintain it above the limit value at least for a period corresponding to the operating time of the batteries (e.g., 8 h). Figure 11 shows that if no additional heat capacity or thermal energy storage is placed inside the cabinet the temperature decrease is much too rapid. An

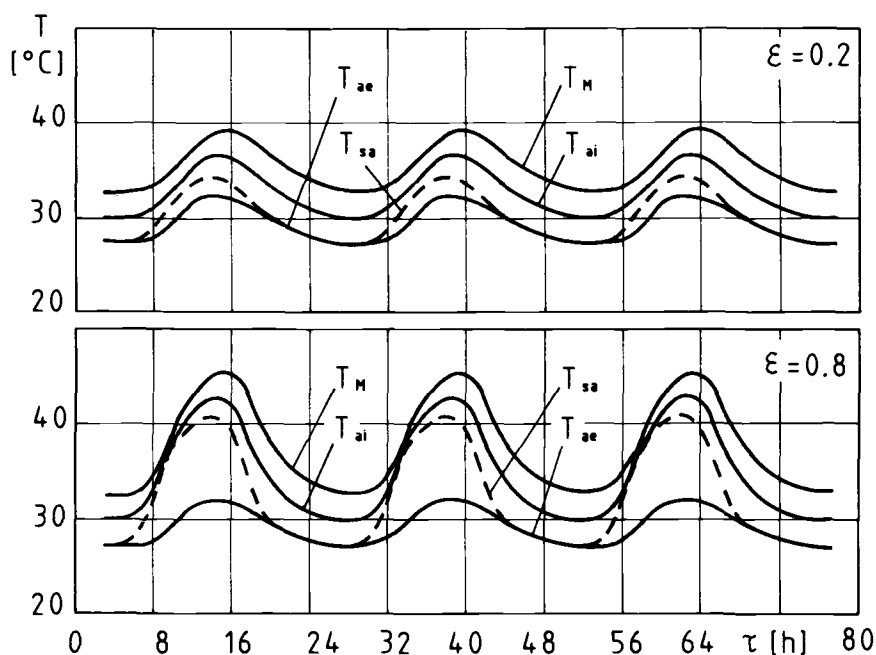


FIG. 8—Transient thermal behavior of uninsulated cabinet with natural ventilation, in warm climate, for $\epsilon = 0.2$ and 0.8 .

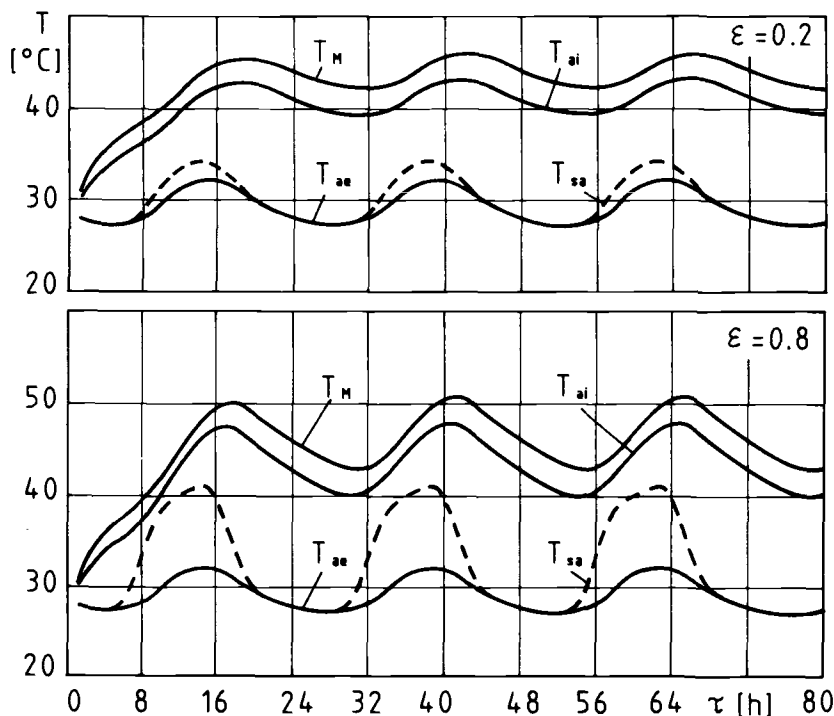


FIG. 9—Transient thermal behavior of insulated cabinet (wall type 2A), without ventilation, in warm climate, for $\epsilon = 0.2$ and 0.8 .

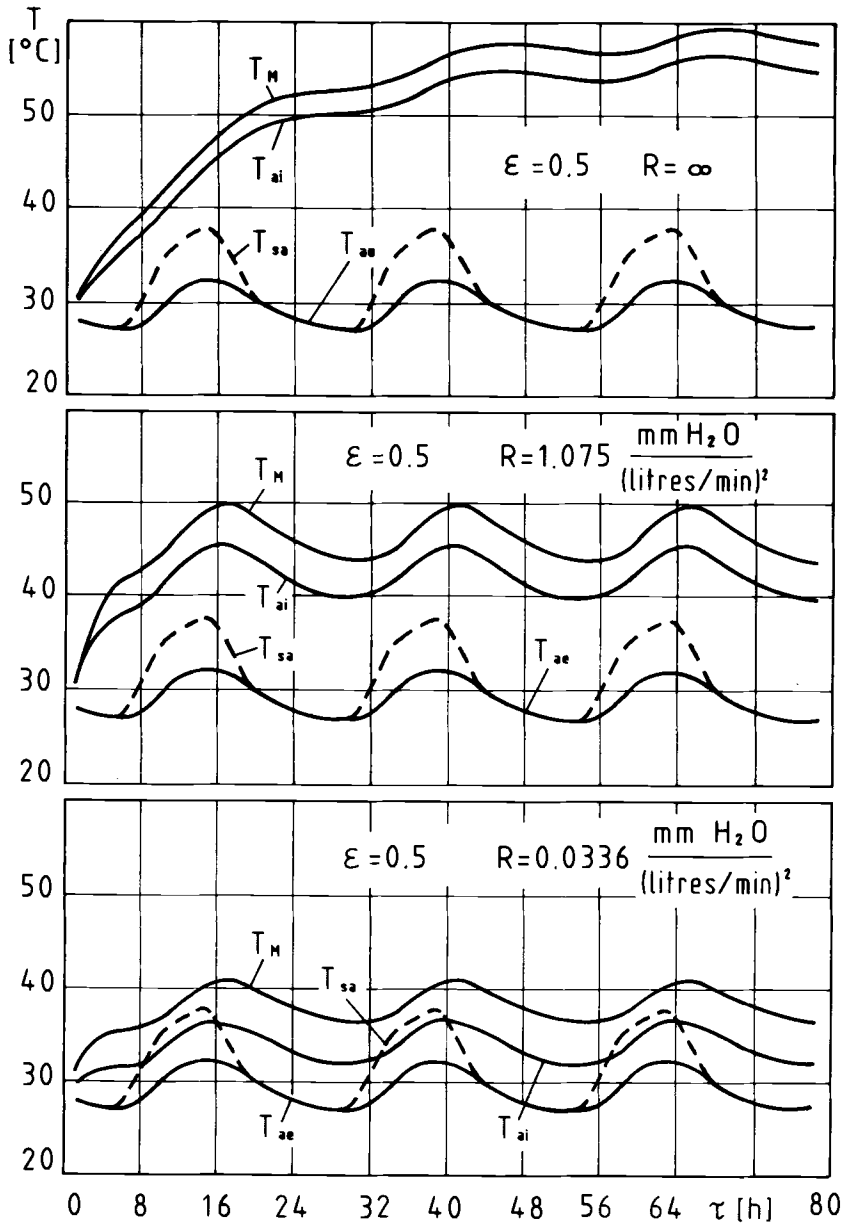


FIG. 10—Transient thermal behavior of fully insulated cabinet with natural ventilation; $\epsilon = 0.5$; $R = 0.0336, 1.075, \infty$ ($\text{mmH}_2\text{O}/(\text{L}/\text{min})^2$).

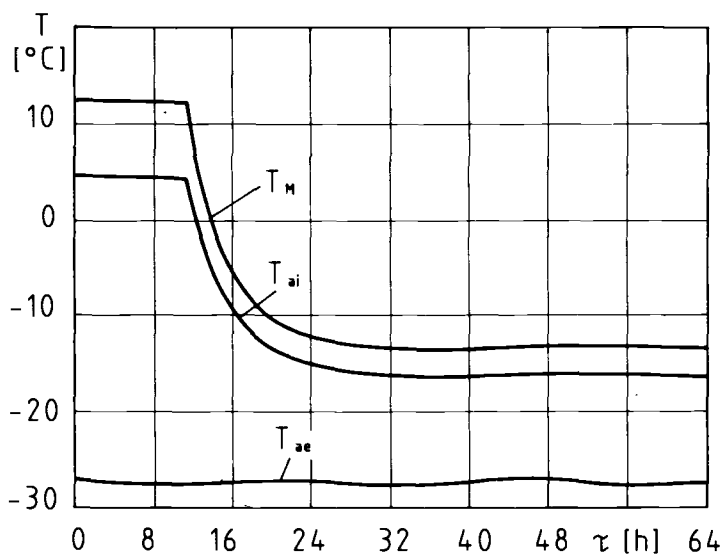


FIG. 11—Transient behavior of insulated cabinet (wall type 2A) during a main power breakoff in cold climate.

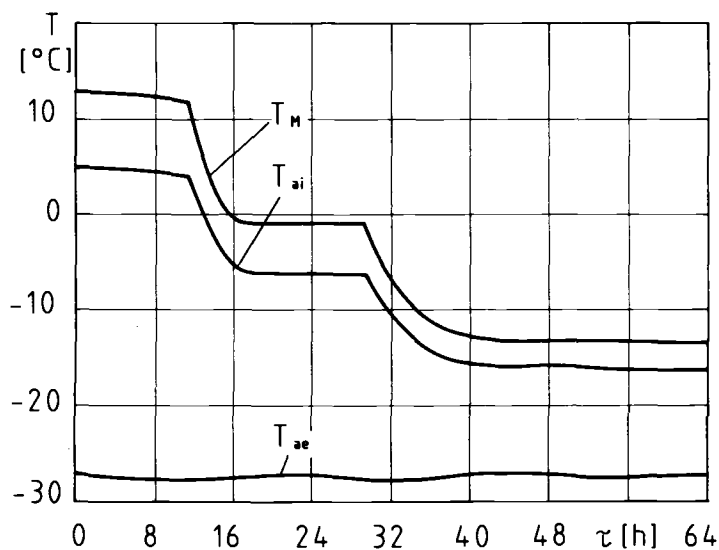


FIG. 12—Effect of thermal energy storage on transient behavior of insulated cabinet (wall type 2A) during a main power breakoff in cold climate.

addition of 10 L of water is more than enough to satisfy the thermal constraints (Fig. 12). Obviously many other kinds of fluids having a different temperature T_i of change of phase and latent heat can be selected according to the specific requirements.

Conclusions

The prediction of thermal behavior in the transient regime of electronic cabinets for outdoor installation is necessary to the thermal design. Due to the peculiarity of the heat transfer problems involved, a computer code developed for this application seems to be appropriate. An approximate numerical approach and a corresponding computer code proposed in this work is sufficiently general to deal with thermal analysis in the transient state. The high degree of accuracy required and the wide variety of technical options in the field of passively cooled cabinets and shelters suggest the need for further improvements and generalizations. An effort in this direction is in progress.

Acknowledgments

The authors wish to thank Marconi Italiana S.p.A. for its contributions to this study.

References

- [1] Scheepstra, J. and Siebers, G. H., *Philips Telecommunication Review*, Vol. 42, No. 1, April 1984, pp. 28-34.
- [2] Alexandersson, R., Junborg, A., and Vesterberg, H. J., *Ericsson Review*, No. 3, 1984, pp. 128-131.
- [3] "Passive Conditioned Shelters," DSDP Reports 8304/B and C, Defense Engineering Systems, Milan, April 1983.
- [4] Coyne, J. C., *Bell Systems Technical Journal*, Vol. 61, No. 2, Feb. 1982, pp. 227-246.
- [5] Guglielmini, G. and Milano, G. in *Proceedings*, 17th International Congress of Refrigeration, Vol. B, Wien, Aug. 1987, pp. 84-91.
- [6] Ellison, G. N., *Thermal Computation for Electronic Equipment*, Van Nostrand Reynolds, New York, 1984, pp. 166-170.
- [7] Guglielmini, G., Milano, G., and Misale, M., "Electronic Cooling by Natural Convection in Partially Confined Enclosures," *Heat and Technology*, Vol. 3, No. 3,4, 1985, pp. 43-57.
- [8] Grober, H. and Erk, S., *Fundamentals of Heat Transfer*, McGraw-Hill, New York, 1961, p. 216.
- [9] Kutateladze, S. S. and Borishanskii, V. M., *A Concise Encyclopaedia of Heat Transfer*, Pergamon Press, Elmsford, N.Y., 1966, pp. 140-143.
- [10] Seki, N., Fukusako, S., and Inoba, H., *Journal of Fluid Mechanics*, Vol. 84, Part 4, 1978, pp. 695-704.
- [11] Bar-Cohen, A. and Rohsenow, W. M., *Journal of Heat Transfer, Transactions of ASME*, Vol. 106, Feb. 1984, pp. 116-123.
- [12] Guglielmini, G., Magrini, U., and Nannei, E., *Journal of Thermal Insulation*, Vol. 5, Oct. 1981, pp. 59-72.
- [13] Finch, D. J., "The Use of Simple Low Cost Solar Shields for the Protection of Communication Equipment," Marconi Research Centre, ITM Report 85/62, May 1985.

Heat-Insulating, High-Temperature Materials on Cenosphere Base

REFERENCE: Ignaszak, Z., Baranowski, A., Hycnar, J., and Żak, M., "Heat-Insulating, High-Temperature Materials on Cenosphere Base," *Insulation Materials, Testing, and Applications, ASTM STP 1030*, D. L. McElroy and J. F. Kimpflen, Eds., American Society for Testing and Materials, Philadelphia, 1990, pp. 741-747.

ABSTRACT: Cenospheres (microspheres) are silica-alumina fly ash lightweight fractions obtained from burning pulverized coal. These fractions are characterized by spherical particle shapes of 40 to 400 μm diameter (apparent bulk density 400 kg/m^3). The thermal-insulation properties of microspheres are useful. A binder that ensures good strength and improves thermal-insulation properties of bonded materials is hydrated sodium silicate. These microsphere materials are characterized by: (a) apparent bulk density in the compressed state from 400 to 500 kg/m^3 , (b) compressive strength up to 6 MPa, (c) average mean heat capacity of 500 $\text{kJ}/\text{m}^3\text{K}$ at temperatures from 298 to 993 K, and (d) thermal conductivity in the range 0.13 to 0.38 W/mK at temperatures from 298 to 1273 K. The investigation made it possible to optimize the material composition for particular applications. Microsphere materials with silicate binders can be used in the building industry, in heating equipment, and in metallurgical and foundry work.

KEY WORDS: aluminosilicate materials, cenospheres, compressive strength, fly ash, heat transmission, microspheres, mean specific heat, silicate binder, thermal conductivity, thermal insulation

According to the mineralogical and chemical composition of coal mineral components and conditions of its burning in boiler furnaces, a great diversity of fly ash and slag products can be obtained. An increase in the aluminum oxide content of coal causes a rise in its softening and melting temperature, but in many cases an increase in iron oxide content leads to a decrease in its thermal conductivity. These facts were used to investigate fly ash as a raw material to produce stable heat-insulating materials. The occurrence of fly ash ball-shaped grains, filled with gas (the so-called cenospheres) was one result of these investigations.

Microspheres, separated from fly ashes derived from bituminous coal, are a light-grey to dark-grey powder. They consist morphologically of spherical grains of various degrees of filling with an aluminosilicate glaze. The spherical grains, composed of an aluminosilicate envelope, usually contain an inert gas consisting mainly of nitrogen and carbon dioxide. The peculiar structure of microspheres determines their low apparent bulk density and low thermal conductivity [1,2]. Table 1 shows the physical chemical characteristics of microspheres produced on a commercial scale in Poland; Fig. 1 shows their appearance. In spite of good heat-insulating properties, microspheres in the natural state are very seldom used as an insulant. The basic obstacle is their occurrence as powders. In practice the microspheres are mixed with binders which enable them to be sprayed on or formed. The mixture may require an additional heat treatment, and even burning. The insulating properties of the material will depend mainly on its structure and on the binder used. The highest insulating power is shown by materials of

¹Poznań Technical University, Piotrowo 5, 60-965 Poznań, Poland.

²Power Research Establishment Energopomiar, Bocheńskiego 64, 40-816 Katowice, Poland.

TABLE 1—Physical chemical properties of microspheres produced in Poland.^a

Definition	Microspheres MS, MZ, and MM ^b in Dry State
Apparent density, kg/m ³	250 to 400
Density, kg/m ³	400 to 600
Thermal conductivity, W/mK	0.07 to 0.10 ^c
Content of grains, % by mass.	
60 μ m	5 to 20
60 to 400 μ m	80 to 95
Content of particles	
sunk in water, % by mass	0.1 to 6.7
Content of compounds, % by mass	
Of silicon (as SiO ₂)	49 to 61
Of aluminum (as Al ₂ O ₃)	26 to 30
Of iron (as Fe ₂ O ₃)	4 to 10

^aProducer: Power Research and Testing Establishment, Katowice, Poland.

^bMicrospheres MS: 0.5 \pm 0.2% moisture.

Microspheres MZ: 15 \pm 5% moisture.

Microspheres MM: 30 \pm 5% moisture.

^cAt room temperature.

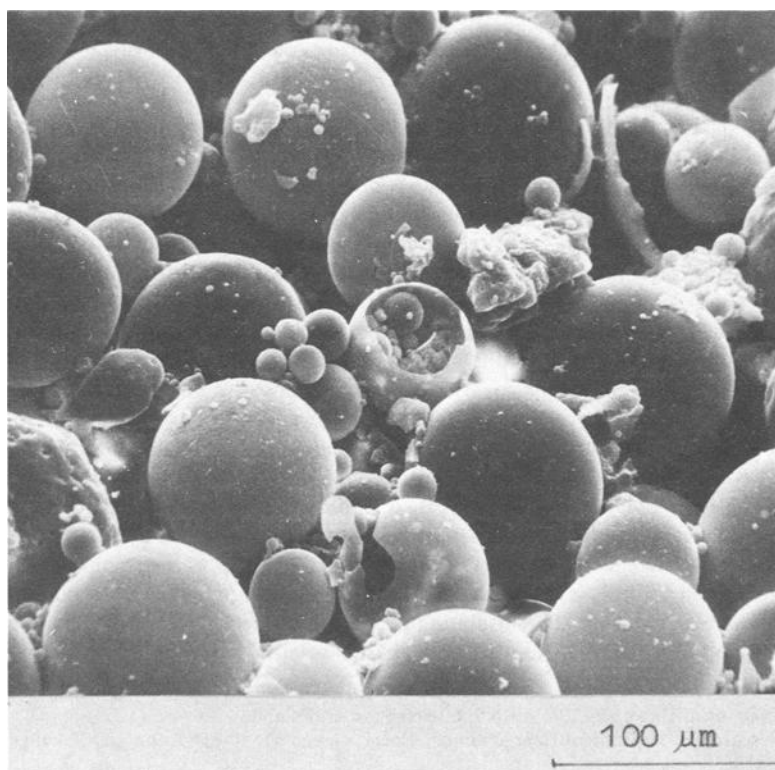


FIG. 1—Microspheres.

cavernous structure; these are formed by large-grained monofractional microspheres where the binder joins grains only at their contact points. On the other hand, the poorest insulating power is shown by materials of compact structure in which the space between the microsphere grains is completely filled by the binder. The insulating power of the material decreases with an increase in binder volume, but there is a simultaneous increase in the mechanical strength of the material.

Other investigations have described heat-insulating materials by binding microspheres with Portland and aluminate cements [3,4], phosphate binders [3], synthetic resins [2,3,5], etc. Some of these solutions have been put into practice in industry [2,6].

This paper describes results of investigations of the heat-insulating material obtained by binding microspheres with silicate binder [7-13].

Scope of Testing

Tests were carried out using sodium silicate $m\text{Na}_2\text{O} \cdot n\text{SiO}_2 \cdot p\text{H}_2\text{O}$, with a $\text{SiO}_2:\text{Na}_2\text{O}$ moles ratio of 2.5, and dry lightweight microspheres. The process of binding microsphere grains with sodium silicate takes place automatically at ambient temperature without any activating agents. Five mixtures of diversified content of sodium silicate (M1, M2, M3, M4, M5) were selected. Their compressive strength and gas permeability were evaluated, and they were cured for 1, 2, 3, 4, 7, 10, 14, 21, 28, and 90 days.

Thermal properties of the mixtures were characterized by two parameters: thermal conductivity (tested versus temperature $\lambda = f/T$) and mean thermal capacity (C) as a product of mean specific heat (c) and apparent density [8,10,14].

Table 2 and Figs. 2 and 3 show the results of investigations on five microsphere mixtures with the silicate binder.

Material Properties

The compressive strength of the microsphere material increases with increasing silicate binder volume and with the cure period (Table 2, Figs. 2 and 4). It was found that the increase in strength, as a function of sodium silicate content, is linear. Independently of the binder content, the strength of microsphere materials increases together with the cure period at least to 28 days; this is due to the curing process advancing deep inside the samples. Maximum strength was achieved after 7 to 14 days. The drop in material strength (10 to 20% in relation to the maximum values R_c) was also recorded. It must be mentioned as well that the R_c strength values, determined immediately after sample consolidation, are inversely proportional to the silicate binder content.

In order to compare the strength of cube samples, R_c strength has also been tested after 28 days. It was found that it was lower than the R_c strength of cylindrical samples. This decrease is due to an incomplete curing of the whole volume of the samples, because access of air to the surface of the samples was not controlled. The process of sample curing under the conditions of free access of air depends on the volume of mixture per area unit of contact with the atmospheric air and on the gaseous permeability (p) of mixture. This fact indicated the absence of the solid or gaseous phase in the composition of microspheres, which would initiate or speed up the process of self-curing.

The thermal conductivity has been determined for Mixtures M1, M3, and M5. For each of them, about 150 values of λ were obtained, after which statistical calculations enabled us to establish the equation of the regression curve and to estimate the correlation coefficient. On assuming, for the highest order of the approximating multinomial

$$\lambda = \sum_{i=0}^n a_i \cdot T^i \quad (1)$$

TABLE 2—*Characteristics of microsphere materials with silicate binder.^a*

Mixture	Apparent Density, kg/m ³		Mean Specific Heat, J/kgK, in the Temperature Range of 273 to 993 K	Thermal Conductivity, W/mK, at			Compressive Strength, MPa, at Day					Gas Permeability, m ⁴ /Ns
	p_w	p_d		300 K	1273 K	at	0	1	14	28	90	
M1	458	429	1119	0.13	0.37	...	0.017	...	2.59	2.06	2.05	$75 \cdot 10^{-8}$
M2	501	461	1095	0.014	0.82	3.80	4.01	3.63	$66 \cdot 10^{-8}$
M3	537	479	1104	0.012	1.03	4.39	4.18	...	$70 \cdot 10^{-8}$
M4	571	498	1099	0.010	0.70	5.12	5.04	3.97	$64 \cdot 10^{-8}$
M5	601	512	1114	0.16	0.38	...	0.009	0.84	6.01	5.58	4.84	$58 \cdot 10^{-8}$

^a p_w is density of mixtures in moist state. p_d is density of mixtures after drying at 383 K.

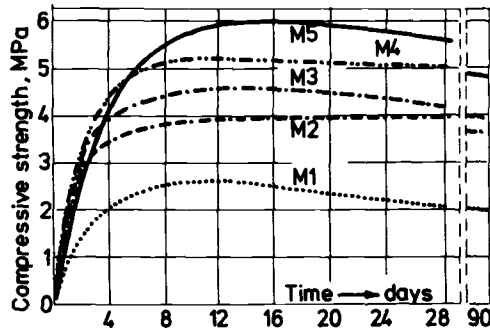


FIG. 2—Compressive strength of the microsphere material versus the volume of the silicate binder and seasoning period of the material.

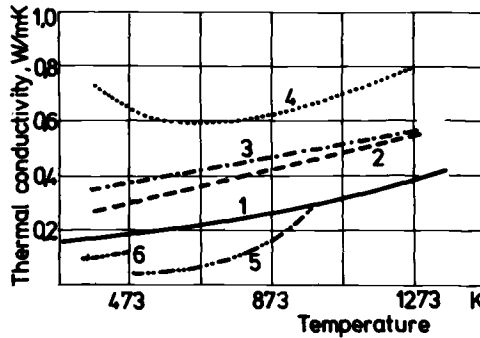


FIG. 3—Thermal conductivity of microsphere material compared with that of heat-insulating materials versus temperature. (1) Microsphere material with silicate binder. (2) Material based on keramzite matrix. (3) Material based on diatomite matrix. (4) Material based on high silica sand. (5) Asbestos material. (6) Vitreous fiber.

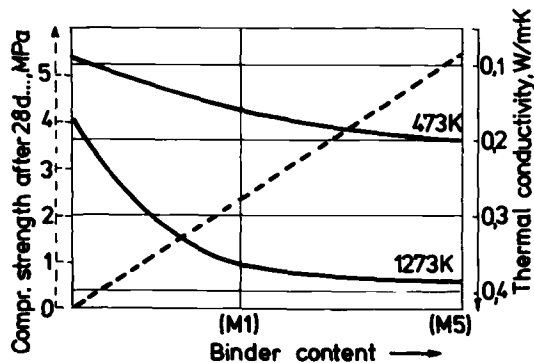


FIG. 4—Thermal conductivity and compressive strength of microsphere material versus silicate binder content.

the significance level coefficient $\alpha = 0.05$, the multinomial dependence of the second order was obtained for all three mixtures in the form

$$\lambda = a_0 + a_1T + a_2T^2 \quad (2)$$

with a high value of curvilinear correlation coefficient R^2 .

The measured quantities λ and the calculated function $\lambda = f/T$ for particular mixtures are given in the analysis. After setting them together, it was found that the increase in the silicate binder content results in an increase in the thermal conductivity coefficient by about 0.025 W/mK (i.e., on average, 10%), which is equal to the value of the maximum square error, calculated for the determination method used to find λ . Practically identical values of the function $\lambda = f/T$ have been obtained for M3 and M5 mixtures in the tested interval of temperatures; thus the space between the M1 and M5 diagrams averaged 10%. In connection with this, the above statistical calculations were repeated, setting together all values of λ for the M1, M3, and M5 mixtures. Thus the final multinomial dependence $\lambda = f/T$ for microsphere mixtures containing the silicate binder was obtained, where T is in degrees Kelvin:

$$\lambda = 0.1252 + 0.8119 \cdot 10^{-4}T + 0.0928 \cdot 10^{-6}T^2; \quad R^2 = 0.87 \quad (3)$$

The analysis of the results of mean specific heat determination (Table 2) has not shown its dependence on the binder content. Thus the average value c is equal to 1106 J/kgK in the temperature range of 273 to 993 K and is to be accepted as the representative value.

Heat storage capacity of the microsphere mixtures in this temperature range, being a product of c and λ , depends mainly on density, changing with temperature (Table 2). The effect of temperature on the microsphere material with the silicate binder was evaluated in the temperature range of 293 to 1373 K. The material does not show any changes in its structure or color up to 923 K. An increase in temperature to 923 to 1123 K results only in the change in color of the material from grey to orange. A further increase in temperature up to 1323 K results in structural changes; at temperatures of 1323 to 1373 K the material starts melting at the side of the heat source.

Potential Utilization

Simple production technology, high mechanical strength, good insulating properties, low density, and high thermal resistance make the microsphere material a good heat-insulating material, suitable for use at low and high temperatures. A comparison of microsphere material properties with those of the material obtained from silica sand (molding sand used in metal foundry engineering) shows that the microsphere material is characterized by good mechanical strength (with binder content at least such as in M3). Gaseous permeability of the material is, however, less advantageous, since it is two to three times lower than that of materials obtained from sand. Thermal conductivity of the microsphere material, in the entire tested temperature range, is on the average 2.5 times lower than λ of sand-based materials such as a standard high-silica sand (Fig. 3). The value obtained for the mean specific heat (c) of the microsphere material is close to that obtained from the high-silica sand, but thermal capacity is, on average, 3 times lower (1695 kJ/m³K) [7]. Microsphere mixtures with the silicate binder have thus shown better insulating properties than those of conventional high-silica material with the same binder.

The applicability of these materials in ferroalloy foundries [15] has been confirmed by obtaining improvement in the quality of castings and by the reduction of production costs in Polish foundries.

A comparison of the obtained microsphere material bound by silicate binder with many building materials (brick, aggregate concrete, cement, and gypsum mortars) shows that its in-

insulating power is 1.5 to 3 times higher and its apparent density about twice lower. These qualities and the forming facility of the material indicate that it is advisable to use it for the production of multi-layer protective walls, claddings, and insulating plates.

Conclusions

From among many heat-insulating materials particular attention should be paid to microsphere materials with silicate binder, because:

1. It is characterized by low heat conductivity and is resistant to high temperatures (to 1300 K).
2. It is characterized by considerable mechanical strength and low gas permeability.
3. After having been mixed with the binder, it can be molded or sprayed by various processes.

Microsphere materials with silicate binder have been partly applied in foundry, metallurgical, building, and power engineering, and as a heat-insulating material.

References

- [1] Raask, E., "Cenospheres in Pulverized Fuel Ash," *Journal of the Institute of Fuel*, No. 9, 1968.
- [2] Hycnar, J., "Microspheres—New Insulating Material," *Gospodarka Paliwami i Energią* [Fuel and Energy Economics], No. 1-4, April 1982, pp. 9-13.
- [3] Pawłowski, W., Hycnar, J., and Serkowski, S., "Ein neuartiger Rohstoffe zur Herstellung von Wärmedämmstoffen," *Silikattechnik*, No. 11, Nov. 1982.
- [4] Matyszewski, T. et al., "Properties of Insulating-Structural Concrete Based on Microspheres and Fly Ash," presented at Second International Conference on the Use of Fly Ash, Madrid, April 1986.
- [5] Hycnar, J., "Application Power Station Ashes in the Production of Plastics," *Chemik* [Chemist], No. 2, Feb. 1985.
- [6] Hycnar, J., "Insulating Material Based on the Microspheres," Certificate of Building Technic Institute, No. 456, Warsaw, 1982.
- [7] Ignaszak, Z. and Baranowski, A., "Specific Heat of Various Insulating Mold Sands," Technical Report No. 22-094, Poznań Technical University, Poznań, Poland, 1981 and 1982.
- [8] Ignaszak, A. and Baranowski, A., "Evaluation of Microsphere Mixtures as Insulating Material," Technical Report No. 22-539, Poznań Technical University, Poznań, Poland, 1983.
- [9] Hycnar, J., Żak, M., and Troszka, A., "Optimization of Production Methods of the Fillers, Carriers and Modified Ashes," Technical Report No. 8.2.4, Power Research Establishment, Katowice, Poland, 1983.
- [10] Ignaszak, Z., Hycnar, J., Baranowski, A., and Żak, M., "Thermophysical Properties of the Microsphere Materials," *Gospodarka Paliwami i Energią* [Fuel and Energy Economics], No. 11, Nov. 1984.
- [11] Ignaszak, Z., Hycnar, J., Baranowski, A., and Żak, M., "Cenosphere Material with Silicate Binder," presented at Second International Conference on the Use of Fly Ash, Madrid, April 1986.
- [12] Ignaszak, Z. et al., "Heat-Insulating Mixture to Insulating Elements," Polish Patent No. 136,546, Sept. 1987.
- [13] Ignaszak, Z., "Investigations of the Thermal Conductivity of the Mold Materials," *Prace z Inżynierii Materiałowej* [Works in Material Engineering], Poznań Technical University, Poznań, Poland, June 1982, pp. 162-171.
- [14] Ignaszak, Z., "Thermal Conductivity of Mold Sands," *Krzepnięcie Metali i Stopów* [Solidification of Metals and Alloys], No. 3, Polish Academy of Science, KatowiceGliwice, Poland, 1980, pp. 264-268.
- [15] Ignaszak, Z. et al., "Microsphere Mixtures and Their Application in Riser Heat Insulation," in *Proceedings*, Symposium on Materials for Foundry Molds and Core Materials, Częstochowa, Poland, Sept. 1986, pp. 26-37.

Author Index

A

Adams, R. D., 263
Angleton, H. D., 244
Arduini, M. C., 575
Arquis, E., 290

B

Bahnfleth, D. R., 665
Baranowski, A., 741
Bartel, T. W., 319
Bomberg, M., 156
Boulant, J., 510
Brandreth, D. A., 156
Burch, D. M., 345
Brown, P. W., 38
Buttner, D., 66

C

Caps, R., 66, 575
Cash, C. G., 599
Childs, P. W., 483
Christian, J. E., 655
Courville, G. E., 483, 496

D

Damont, G. H., 221
Dent, R. W., 79
De Ponte, F., 575
Derderian, G. D., 483
Desjarlais, A., 634
Desjarlais, A. O., 496
Döll, G., 575
Donovan, J. G., 79

E

Evans, D. J., 319

F

Faison, T. K., 3
Filla, B. J., 710
Flynn, D. R., 319
Fricke, J., 66, 575

G

Glicksman, L. R., 109
Goss, W. P., 378
Govan, F. A., 665
Graves, R. S., 52, 237, 525
Gross, J., 66
Guglielmini, G., 723

H

Hagan, J. R., 205
Hart, G., 675
Heidell, J., 587
Hillier, R. L., 221
Hümmer, E., 575
Hurley, J. A., 710
Hust, J. G., 263, 710
Hutto, F. B., Jr., 688
Hycnar, J., 741

I

Ignaszak, Z., 741

K

Kenney, T. M., 253

L

Langlais, C., 290, 510
Lecompte, J. G. N., 397
Licitra, B. A., 345

M

Mathey, R. G., 15
Mathis, R. C., 244, 253
McCaa, D. J., 290
McElroy, D. L., 52, 525
McIntyre, C. R., 496
Meeks, C. B., 612
Milano, G., 723
Miller, R. G., 205, 378
Moazed, A. R., 483

N

Needles, H. L., 221
Nelson, B. D., 626
Nilsson, O., 66

O

Oscar, D. S., 378
Ostrogorsky, A. G., 109

R

Rennex, B. G., 3
Rossiter, W. J., Jr., 15, 38
Roux, J. A., 545, 561

S

Sandberg, P. I., 197
Seiface, F., 378
Shankland, I. R., 174
Sheppard, K., 634
Shu, L. S., 483
Siddiqui, S. A., 221
Skelton, J., 79
Smith, D. R., 710
Somers, T. A., 3
Staelens, P., 421
Stewart, G. D., 483
Strzepek, W. R., 121, 362
Svennerstedt, B., 231

T

Thomas, J. R., Jr., 537
Troyer, R. L., 699
Tsongas, G. A., 464
Tuluca, A., 587
Tye, R. P., 141, 496

V

Van Geem, M. G., 437

W

Weaver, F. J., 52
Weil, R., 634
Whitaker, T. E., 688
Whorlow, K. M., 688

Y

Yajnik, S. J., 561
Yarbrough, D. W., 52, 237, 525
Yeh, H. Y., 545

Z

Zak, M., 741
Zarr, R. R., 3, 345
Zwolinski, L. M., 189

Subject Index

A

AATCC. *See* American Association of Textile Chemists and Colorists.

Absorption, 82–87, 132, 133(table), 134(fig)

Accelerated aging test, 110

Acoustical insulation covers, 677–678

Acoustics

evaluation of thermal insulation, 319–342

Aerated concrete, 15–37

Ageing. *See* Aging.

Aging

cellular thermal insulations, 121, 124–125
closed-cell foam insulation, 110, 116–119(figs)

extruded polystyrene, 201

foam insulation, 189–196

gas diffusion in closed-cell foams, 174–186

gas-filled foams, 156–173, 159–163(tables,figs)

rigid insulating foams, 205–217

test procedure, 170

Aging acceleration, 199, 200(figs)

Aging tests

gas-filled foams, 156–173

rigid insulating foams, 205–217

Air quality, indoor—building foundations
research and design, 658

Air temperature

calibrated hot box—transfer function coefficients, 347

computer modeling of climate, 599–611

outdoor electronic cabinets, 735–736, 737–739(figs)

Airtightness, 397, 412, 426

ALC. *See* Autoclaved aerated concrete.

Alumina fleece

elasto-mechanical behavior, 71–73(figs)

ultrasonic investigations, 71–77(figs)

Aluminosilicate materials, 741

American Association of Textile Chemists and Colorists (AATCC)

AATCC-M35-1980, 677, 681

American Society of Heating, Refrigerating, and Air-Conditioning Engineers (ASHRAE)

Standards

ANSI/IES/ASHRAE standard, 90, 365

ASHRAE air space resistance tables, 382

ASHRAE air space thermal resistance tables, 383

ASHRAE fundamentals handbook, 381, 386–387

ASHRAE handbook—1985 fundamentals, 451

ASHRAE handbook, 365

ASHRAE standard 90.2, 660–661

Analytical design—insulation of outdoor electronic cabinets, 723–740

Analysis

magnesium oxychloride-based foam, 41–50

Apparatus and technique

gas diffusion measurement, 177–179(figs)

Appliance insulation

material properties, 52–65

ASHRAE. *See* American Society of Heating, Refrigerating and Air-conditioning Engineers—Standards

ASTM Standards

See also Standards—International, Building codes

A-240, 692

Bulletin no. 225, 689

C-39, 444(table)

C-78, 444(table)

C-165, 677, 680

C-167, 255, 677, 680

C-177, 163, 164, 170, 194, 217, 263, 382, 384, 444(table), 450, 451, 462, 496, 525, 677, 680, 710, 711, 720

C-182, 699

C-195, 693

C-202, 699

C-236, 164, 205, 208, 263, 382, 496

C-335, 525, 681

C-411, 681

C-417, 699

C-423, 681

C-449, 693

C-469, 444(table)

ASTM Standards (*cont.*)

- C-496, 444(table)
 - C-518, 3, 163, 164, 170, 194, 208, 217, 244, 263, 496, 518
 - C-553, 677, 680
 - C-567, 444(table)
 - C-665, 636
 - C-666, 444(table)
 - C-687, 244, 253, 254, 255, 262, 263, 264, 265, 267
 - C-692, 681, 688–698
 - C-739, 222, 636
 - C-795, 680, 689
 - C-871, 681
 - C-892, 680
 - C-945, 143
 - C-976, 163, 263, 382, 383, 437, 448, 451, 461, 518
 - C-1029, 143
 - C-1041, 496
 - C-1046, 451, 462, 496
 - C-1094, 675–687
 - D-226, 608
 - D-312, 608
 - D-XXX (in preparation), 143
 - D-471, 681
 - D-751, 677, 681
 - D-1117, 677, 679, 681
 - D-1434, 184
 - D-1682, 677, 681
 - D-1683, 681
 - D-1894, 681
 - D-2176, 677, 679, 681
 - D-4157, 677, 679, 681
 - E-84, 677, 681
 - E-108, 144
 - E-119, 681
 - E-228, 444(table)
 - E-230, 444
 - E-408, 385
 - E-596, 681
 - G-1, 651
 - G-26, 681
- Attics**
- acoustics for evaluation of thermal insulation, 319–342
 - insulation, 548
 - loose-fill thermal insulation, 231, 290–318
 - loose-fill rock wool insulation, 237–243
 - radiation heat transfer, 545–560
- Austenitic stainless steel—corrosion testing, 688**
- Autoclaved aerated concrete, 15–37**
- Autoclaved lightweight concrete. *See* Autoclaved aerated concrete.**
- Automated control system—high temperature apparatus, 714**

B

- Barometric pressure, 9(fig)
- Blocks, 20
- Blowing, 254–255
- Bond strength, 28–29
- Building codes
 - BOCA, 144
 - ICBO, 144
 - SBCCI, 144
 - Underwriters Laboratory, UL 790, 144
- Building envelope
 - cellular plastics applications, 141–155
 - lightweight structural concrete, 438
 - metal frame walls—insulating materials, 362–377
 - reflective insulation systems, 378–396
 - roof systems—thermal performance, 483–495, 496–509
- Building Foundations Research Review Panel, 657(table)
- Building foundations—research and design, 655–662
- Building materials, thermal insulation, 626

C

- Calibrated hot box
 - insulated cavity wall, 397
 - test method for transfer function coefficients, 347(fig), 348
 - thermal resistance testing, 363, 364–365(figs), 383–384, 389, 393–394
- California, State of, thermal insulation program, 221–230
- Calorimeter—performance test methods, 699–709
- Calorimetric measurements, 584
- Capillarity, 22
- Cavity wall
 - test wall, 397–400(figs)
- Ceiling heat flux
 - attic insulation, 545–560
- Cellular concrete
 - thermal conductivity, 401(fig)
- Cellular glass, 123
- Cellular plastics
 - building envelope applications, 141–155
 - gas-filled foams, 156–173
- Cellular thermal insulations, 121–140
- Cellulose—corrosiveness testing, 636–640, 651–652
- Cellulose loose fill, 268(table), 269(fig)
- Cement-based foam, 39
- Cenosphere, 741
- Central heating/cooling plants, 672–673

Chlorofluorocarbons
 foam insulation aging, 189–196
 in closed-cell foams, 174–175
 in foundations, 661
 thermal testing for rigid insulating foams, 205–217

Classification—Sweden
 thermal insulation materials, 197

Climate
 computer modeling, 599–611
 foundations data base, 658

Closed-cell foam insulation
 physical properties, 109–120

Coatings
 foam-in-place insulation, 147

Coefficient of thermal expansion, 23

Combustion
 cellular thermal insulation, 138

Compression sampling, 253

Compressive strength, 27(fig), 741

Computer modeling of climate, 599–611

Concrete, aerated, 15–37

Concrete—lightweight
 heat transfer, 438–439
 physical and thermal properties, 444(table)
 Portland cement, 440–443

Condensation, 635

Conduction heat transfer
 in attic ceiling fiberglass composite, 545–560
 in fibrous insulation, 538–539
 polystyrene foam insulation, 561–574

Conduction program—HEATING5, 525–536

Conductivity
 closed-cell foam insulation, 110–112, 115–120(figs)

Conduit. *See* Piping.

Conservation activities—homeowners
 household/housing characteristics, 616–617

Construction material, 17

Consumers, 612

Convection
 loose-fill thermal insulation, 290–318
 reflective insulation systems, 378–396
 thermal performance of insulated wall cavity, 397–420

Copper—corrosiveness testing, 639–640(table)

Copper pipe corrosion, 652–653

Corrosion, 635

Corrosion testing, 688–698

Corrosiveness study—test methods
 residential thermal insulation materials, 635–664

Costs
 foam-in-place insulation, 145, 146(table)
 residential buildings—energy conservation standards, 587

COSTSAVR computer program, 587–588

Covers. *See* Insulation covers.

Cracking, 23

Creep, 23

Cylinders
 electromagnetic radiation, 95, 105

D

Dana test—corrosion, 689

Data acquisition and control, 714

Data base—foundations research and design, 657–659

Degradation—foundation materials
 research and design, 658

Density
 autoclaved aerated concrete, 23, 27(fig)
 cellular insulation, 130
 foam insulation, 40–42
 loose-fill insulations, 263–289
 loose-fill rock wool, 239–242
 mineral fiber insulations, 244–252
 pneumatically applied insulations, 246–251(figs), 253–262

Design considerations
 autoclaved aerated concrete, 21–22
 outdoor electronic cabinets—thermal insulation, 723–740
 standards—thermal insulation, 626–633
 underground heat systems, 666–668

Deterioration resistance, 23

DIET. *See* Dynamic insulation efficiency tester.

Diffusion
 closed-cell foam insulation, 111–112, 113(tables), 114, 174–186

Dynamic insulation efficiency tester (DIET), 526–536

Dynamic thermal performance, 345

E

Economic considerations, 10–11

Elasticity, 27(table)

Elasto-mechanical measurements
 fibrous insulations, 70, 71(figs)

Electric radiant panel
 flammability testing, 221, 225–229

Electrical resistance probes, 653

Electromagnetic radiation by cylinders, 105

Electronic cabinets, outdoor—thermal insulation, 723–740

Electronic equipment—outdoor shelters, 725–727
 Emissivity, 699, 700, 704–705(tables), 708, 735
 Energy conservation, 612
 Energy conservation standards
 HUD manufactured housing, 587
 Energy considerations—autoclaved concrete, 32–33
 Energy-efficient homes
 cost analysis, 587
 foundations—design, 655–662
 wall moisture study, 464–482
 Energy simulation analyses, 346
 Environmental chamber for corrosion tests, 641–643(figs)
 Excitation function, 350–351, 357
 Expansion, moisture, 25

F

Failure studies—underground heating systems, 673–674
 Fiberglass insulation, 66–78, 537–544, 548
 Fibrous assemblies, 79–105
 Fibrous insulation, 575
 Fire resistance, 24
 Fire resistance insulation covers, 677
 Flammability testing
 loose-fill cellulose insulation, 221–230
 Fly ash, 741
 Foam aging. *See* Aging.
 Foam-in-place cellular plastics
 building envelope applications, 141–155
 methods of applications, 141
 roof applications, 144
 walls, 144–145
 Foam insulation
 cellular thermal, 121–140
 closed-cell, 109–120
 foam-in-place cellular plastics, 141–155
 gas-filled foams, 156–173
 manufacturing process, 39–40, 158–160
 rigid insulating foams, thermal testing, 205–217
 Foil-faced polyisocyanurate.
 See Polyisocyanurate.
 Foundation walls, 630
 Foundations—insulation, 660–661
 Foundations—research and design energy savings potential, 655–662
 Frost resistance, 25
 Fumed-silica insulation, 3–14

G

Gas diffusion measurement
 in closed-cell foams, 174–186

Gas-filled foams, 156–173
 Gas radiant panel
 flammability testing, 222–225
 Gasbeton. *See* Autoclaved aerated concrete.
 Glass
 use in cellular thermal insulation, 121
 Glass fiber, 266(table), 267(fig), 274(table), 275(fig)
 Glass fiber—corrosiveness testing, 637–640
 Ground water, 666
 Guarded hot box, 292–293, 384–385, 389, 393–394
 Guarded hot plate measurement
 concrete mixes, 450–451
 fibrous insulations, 575
 thermal conductivity—high temperature apparatus, 710–715, 716–717(figs), 718–721
 windows, 429–431

H

Health and safety
 cellular thermal insulations, 138–139
 Heat conduction theory, 345
 Heat flow
 evaluation of attic insulation, 319–342
 transducers, 510–521
 Heat flow apparatus, 52–65, 530–531(figs)
 Heat flow measurement
 calorimeter, 707
 Heat-flux devices, 3
 Heat, specific, 26
 Heat transfer
 attic insulation, 336, 548–550
 building foundations, 655–662
 calibrated hot box, 346–347, 350(table), 351–355(figs)
 cenosphere base, 741
 closed-cell foam insulation, 110, 114
 extruded polystyrene, 203–204
 fiberglass/gypsum composite, 546–560
 fibrous insulation materials, 546–548
 insulated wall cavity, 402–403, 404–407(tables), 408–411(figs)
 lightweight structural concrete, 437–463
 low density insulators, 80–81
 polystyrene foam insulation, 561–574
 reflective insulation systems, 385
 windows, 421–436
 Heat transfer equations, 512–514
 Heat transfer measurements, 514–519
 Heat transmission. *See* Heat transfer.
 Heat treatment tests, 10–11
 HEATING5 conduction program, 525–536
 High temperature conditioning, 11(table)

High temperature measurement, guarded-hot-plate apparatus, 710
 Homeowners—conservation/energy activities, 616–619
 Horizontal hot box, 293–295(figs)
 Hot box-cold box, 401, 402(fig), 432–433, 446–450, 454–455
 Humidity effects, 11

I

In situ thermal performance, 496–509
 Infrared properties, 578
 Injection methods for foam-in-place cellular plastics, 142
 Insulated pipe, 665
 Insulating concrete, 15–37
 Insulating gases, 191–194
 Insulation
 See also Thermal conductivity, Thermal insulation
 cavity wall, 397–420
 ceiling fiberglass/gypsum composite, 545–560
 cellular thermal, 121–140
 closed-cell foam, 109–120, 174–187
 consumer activities, 612–623
 design standards, 626–633
 fiberglass, 537–544
 fibrous assemblies, 79–105
 for appliances, 52–65
 foundations—energy saving potential, 655–662
 gas-filled foams, 156–173
 handling, 4
 loose-fill cellulose insulation, 221–230, 231
 magnesium oxychloride-based foam, 38–51
 polystyrene insulation, 483, 561–574
 porous materials, 510–521
 residential, 635
 roofs, 496–509
 underground piping systems, 672(table)
 Insulation corrosion testing, 688–698
 Insulation covers—removable/reusable, 675
 International Union of Testing and Research Laboratories for Materials and Structures (RILEM), 33

K

Karnes test—corrosion, 689

L

Labeling, 628

Life-cycle cost analysis of residential buildings, 587
 Lightweight aerated concrete, 15–37
 Lightweight structural concrete. *See* Concrete.
 Linear heat flow apparatus, 56, 57(fig)
 Lofting, 244
 Loose-fill insulation
 apparent thermal conductivity, 263–289
 blowing, 254
 convective effects, 291
 flammability testing, 221–230
 settling, 231
 Low-density insulators, 80–81

M

Magnesium oxychloride-based foam
 manufacture, 39–40
 physical properties, 40–41
 Manufacture and production
 autoclaved aerated concrete, 18, 19(fig)
 cellular insulations, 122–123
 magnesium oxychloride-based foam, 38–51
 Masonry foundations—design, 656
 Material density, 8(fig)
 Material handling
 fumed-silica insulation
 Material properties of appliance insulation, 52–65
 Material stability, 9
 Materials testing, thermal insulation, 626
 Mean specific heat, 741
 Mean temperature sensor, 711, 718, 720–721
 Measurement technique
 energy-calibrated hot box tests, 349
 for evaluating attic insulations, 320–324
 Mechanical properties
 cellular thermal insulations, 121
 foam-in-place urethanes, 152
 Microspheres, 741, 742(tables), 743–746(figs, tables)
 Mie theory, 575
 Mineral wool—airtightness/density, 412, 413–414(figs)
 Mineral wool—corrosiveness testing, 637–640
 Modeling of aging process
 gas-filled foams, 164–168
 Models
 See also Physical model
 building foundations research and design, 655–658
 computer modeling of climate, 603
 Moisture content
 autoclaved aerated concrete, 22

Moisture content (*cont.*)

- cellular thermal insulations, 121, 132, 133(table)
 - extruded polystyrene, 201–204
 - magnesium oxychloride-based foam, 40–42
 - walls, 464–482
- Moisture effects
- condensation, 635
 - corrosiveness testing, 653–654
 - fibrous insulations, 537–544
 - foundations—research and design, 659
 - wall moisture study, 476–477
 - water leakage in walls, 635
- Moisture expansion and shrinkage, 25
- Moisture migration, 25

N

- National Fire Protection Association (NFPA) Standards
- NFPA 701, 681
- Natural cooling, 723

O

- Optical methods, 580–581

P

- Panels, 20
- Passive conditioning, 723
- Percolation theory, 68
- Performance standards—insulation covers, 676–677
- Permeability
- autoclaved, aerated concrete, 25
 - cellular insulation, 132
 - closed-cell foam insulation, 109–120, 178–185
- Permeable insulation materials in attics, 310–313
- Phenolic, 123
- Physical model
- thermal insulation—outdoor electronic cabinets, 723, 727–728
- Physical properties
- cellular thermal insulations, 121, 124–125, 126–127(table), 130–140
 - closed-cell foam insulation, 109–120
 - foam-in-place urethane, 148–152, 149(table)
 - fumed silica material, 5(table), 7(table)
 - hardened concrete, 444(table)
 - magnesium oxychloride-based foam, 40–48
- Pipes—corrosiveness testing, 639–640(table)

- Piping—underground heating systems, 667–673

Plastic foams. *See* Foam insulation, Insulation.

- Pneumatically applied insulations, 244–252, 253–262

Polycarbanilide, 141

Polyisocyanurate, 122, 141, 205

Polystyrene, 122, 197–204

Polystyrene foam insulation

- thermal conductivity, 561–574

Polyurethane

- aging, 189–196
- aging study for rigid insulating foams, 205–217

- building envelope applications, 141

- gas-filled foams, 158–159

- physical properties, 122–123

Porosities, 29, 30–31(figs)

Porous insulating materials

- thermal measurements, 510–521

Production—autoclaved aerated concrete, 17(table, fig)

Properties

- autoclaved aerated concrete, 22–31

PROPOR (computer program for estimating thermal conductivity), 483, 504–506

Protective coatings

- foam-in-place insulation, 147–148

Q

Quality assurance, 254, 626, 630

Quality control—Sweden

- extruded polystyrene, 197–204

R

Radial heat flow apparatus, 54, 55(fig), 529–530(table)

Radiant heat transfer

- fibrous low-density insulators, 79–105

Radiant panels

- for flammability testing, 221–230

Radiation

- fiberglass insulation, 537–544, 545–560

Radiation transfer, 86–87

Radiative heat transfer

- insulation material, 99, 575

- modeling, 540

- organic fibers, 578

Refractive index of polymeric materials, 86–87

Refractory fiber, 699

Reproducibility, 718, 720

Research needs—building foundations, 656–661

Residences
 consumer insulation activities, 612
 Residential buildings—design standards,
 626–633
 Residential insulation—test methods, 634–
 654
 RILEM (International Union of Testing and
 Research Laboratories), 33
 Rock/slag wool, 272(table), 273(fig)
 Rockwool—corrosiveness testing, 637–640
 Roof systems
 thermal performance, 483–495, 496–509
 Roofing membranes—sliding
 climatic effects, 599, 607–610
 Round robin on ASTM C-687 loose-fill in-
 sulations, 284–289
 Round robin on calorimeter performance,
 699
 Round robin on Nordic window *U*-value
 measurements, 434
 Ruggedness test—calorimeter, 700–702,
 703–705(tables)

S

Safety
 cellular thermal insulations, 138–139
 Sampling for thermal testing, 208, 209(fig)
 Scanning electron microscopy, 45
 Scattering theory, 82–87, 88–93(figs), 105,
 579
 Settling—loose-fill insulation in attics, 232–
 233, 234–235(figs)
 Shaping and working, 26
 Shear and bond strength, 28–29
 Shelter—outdoor electronic cabinets—insu-
 lation, 723–740
 Shrinkage, moisture, 25, 40–42
 Silica aerogel composite
 sample description, 4
 Silica powder
 thermal resistance, 52–65
 Silicate binder, 745(figs)
 Soil properties data base, 658
 Soil studies, 666–667
 Solar radiation, 723
 Solid conduction, 67–68
 Sound absorption, 26
 Specific heat, 26
 Spraying method for foam-in-place cellular
 plastics, 142
 Stainless steel—test methods for corrosion,
 688–698
 Standard reference material, 3–14
 Standards—International
See also ASTM, Building codes
 AATCC 35-1980, 677

ANSI/ASQC standard Z-1.15-1979
 ANSI/IES/ASHRAE standard 90, 365
 ASME B31.1 Code for pressure piping
 Federal Construction Council Technical
 reports
 30-Underground heat distribution sys-
 tems, 665
 39-. . . components for underground
 heat distribution systems, 665–666
 47-Field investigation—underground
 heat distribution systems, 666
 66-Underground heat distribution sys-
 tems, 666
 German standard DION 52612, 428
 German standard DIN 52616, 426
 ISO/DIS 8301, 510, 511
 ISO/DIS 8873, 143
 ISO/DOC. 9288, 576
 ISO/DP 8990, 421
 MIL-I-24244, 689, 692–693
 Minnesota Statutes chapters 325F.20 and
 320F.21, 627
 NSB standard reference material
 #1450b, 217, 526, 711
 #1451, 711
 #1470, 184–185
 NFPA-701, 681
 Nuclear regulatory guide, 1.36, 689
 Swedish standard
 SS 024212, 421
 SS 024213, 421, 426
 UL-1709, 681
 US Army Corps of Engineers, CRD-36-
 73, 444(table)
 US Army Corps of Engineers, CRD-C124-
 73, 444(table), 460
 US fed std HH-I-515D, 636
 Steel—corrosiveness testing, 639–640(table)
 Stocking and shipping—autoclaved aerated
 concrete
 quality assurance tests, 20
 Strength
 autoclaved aerated concrete, 26,
 27(table), 28–29
 cellular thermal insulations, 134,
 136(table)
 foam-in-place urethanes, 152
 Structure of autoclaved aerated concrete, 29
 Surface temperature
 computer modeling of climate, 599–611
 Sweden
 window *U*-value measurements, 421–436

T

Temperature
 computer modeling of climate, 599–611

- Temperature measurement
 - calibrated hot box, 350
- Temperature resistance
 - autoclaved aerated concrete, 31
 - cellular insulation, 130, 131(fig)
- Tensile strength, 28
- Termite shields, 661
- Test house characteristics
 - wall moisture study, 470(table)
- Test methods
 - acoustic technique for measuring attic insulations, 327–333, 334–335(figs)
 - calorimeter performance, 699–709
 - corrosion— austenitic stainless steel, 688–698
 - fumed-silica specimens, 6
 - gas-filled foams, 156–173, 194–195
 - in situ* thermal performance—roofs, 496–509
 - guarded-hot-plate apparatus—thermal conductivity measurement, 710–722
 - insulated cavity walls, 397–420
 - lightweight structural concrete, 446–451
 - pneumatically applied insulations, 245–246
 - radiant panels, gas and electric, 222–228
 - ramp test, 347
 - residential insulation, 635–654
 - rigid insulating foams, 207–217
 - thermal resistance
 - metal frame wall construction—insulating materials, 366–369
 - modeling, 525
 - thin fibrous insulations, 576
 - transfer function coefficients for calibrated hot box, 348–349
 - wall moisture study, 464–482
 - window *U*-value measurements, 421–436
- Thermal conductivity
 - autoclaved aerated concrete, 31
 - calorimeter performance study, 699–709
 - cenosphere, 745
 - closed-cell foam insulation, 115–119(figs), 174–186
 - extruded polystyrene, 197–204
 - fibrous insulations, 66–78, 537–544
 - fine powders, 60(table), 61–62(figs)
 - foam-in-place urethane, 148, 149–151(tables)
 - foam insulation aging, 189–196
 - fumed-silica insulation, 8–13
 - gas-filled foams, 156–173, 159(fig)
 - insulated cavity walls, 398
 - loose-fill insulations, 263–289
 - magnesium oxychloride-based foam, 40–44
 - measurement, calorimeter performance, 699
 - measurement, guarded-hot-plate apparatus, 710–722
 - pneumatically applied insulations, 244–252
 - polystyrene foam insulation, 561–574
 - PROPOR computer program for estimating, 487–489, 492, 494
 - thin heaters, 526–527
- Thermal conductivity—calorimeter performance study, 699–709
- Thermal conductivity standard reference materials (SRMs), 3
- Thermal insulation
 - cavity wall, 397–420
 - cenosphere, 741
 - conductivity. *See* Thermal conductivity.
 - extruded polystyrene, 197–204
 - flammability testing of loose-fill cellulose, 221–230
 - low-density fiber materials, 575
 - outdoor electronic cabinets, 723–740
 - reflective insulation systems, 378–396
 - residential, 634–635
 - settling of loose-fill in attics, 231–236
 - settling of rock wool insulation in attics, 237–243
 - standards, 626–633
- Thermal insulation covers—removable/reusable, 675–687
- Thermal measurements, 70–77(figs), 510–521
- Thermal modeling, 56(table), 528–529
- Thermal performance
 - cavity wall, 397–420
 - metal frame wall constructions—insulating materials, 376
 - reflective insulation systems, 378
 - roof systems, 483–495
 - transfer function coefficients for calibrated hot box, 345
- Thermal properties—hardened concrete, 444(table), 448–462
- Thermal resistance
 - attic insulations, 336, 338–341(figs)
 - fine powders, 52–65
 - gas-filled foams, 156–173
 - loose-fill rock wool, 242
 - metal frame wall constructions—insulating materials, 362–369, 370(tables), 371–373, 374–375(tables)
 - modeling—on thin heaters, 526
 - reflective insulation systems, 378–396
- Thermal resistance measurements systems, 526–529, 575–576

Thermal resistance tests
 gas-filled foams, 163–168
 thin heaters, 525–536
 Thermal test apparatus, 526–527
 Thermal testing
 calibrated hot box, 345–361
 pneumatically applied insulations, 244–252
 rigid insulating foams, 205–217
 Thermal transmission
 cellular thermal insulations, 124, 128–129(table, fig)
 window *U*-value, 421–436
 Thermocouple device, 701, 714
 Thermogravimetric analysis, 46–47, 48(table)
 Thermophysical properties—outdoor electronic cabinets, 732(table)
 Thin heaters
 thermal modeling, 525–536
 Toxicity
 cellular thermal insulation, 138
 Transducers, heat flow, 510
 Transfer function coefficients
 calibrated hot box, 350–351(table, fig), 350(table), 351–357(figs)
 Transient heat transfer tests, 537–544, 545–560

U

Ultrasonic investigation
 fibrous insulations, 71–77(figs)
 Underground insulated pipe systems, 665–674

Underwriters' Laboratory (UL), UL-701, 681
 Urea-formaldehyde, 123
 Urethane raw material production—US, 146(table)

V

Ventilation
 wall moisture study, 477–479
 Viscosity, 115

W

Wall constructions—thermal resistance
 insulated cavity, 397
 metal frame with insulating materials, 362–377
 moisture study, 464–482
 Wall simulation—test methods for corrosiveness study, 635–643
 Walls—water leakage, 635
 Water calorimeter, 699, 700(fig)
 Water leakage. *See* Moisture
 Water solubility, 26
 Water vapor permeability, 132, 134(fig), 152
 Windows—thermal transmission, 421–436
 Wood moisture content, 472–476

X

X-ray diffraction, 44

ISBN 0-8031-1278-5